A Comprehensive Assessment of the Influence of Oxygenated Volatile Organic Compounds on the Atmospheric Composition

Inaugural – Dissertation
zur
Erlangung des Doktorgrades
der Mathematisch–Naturwissenschaftlichen Fakultät
der Universität zu Köln

vorgelegt von

Simon Henrik Rosanka

aus Solingen

Jülich, 2021

Berichterstatter: Prof. Dr. Dr. h.c. Andreas Wahner
Prof. Dr. Susanne Crewell

Tag der mündlichen Prüfung: 26.01.2021

Failure is not an option!

A quote attributed to
Eugene Francis "Gene" Kranz
[1933 – present]

Abstract

Global atmospheric chemical models are an important tool to improve our understanding of the Earth's atmospheric processes and to address the influence of anthropogenic activities on the Earth's climate. In this context, one of the most important greenhouse gases is ozone (O_3), whose photochemical production in the troposphere is fueled by volatile organic compounds (VOCs). An important sub-group of VOCs are oxygenated VOCs (OVOCs), which are photolabile and water soluble. Thus, a realistic simulation of tropospheric O_3 in global atmospheric models also relies on the realistic representation of OVOCs. The overall objective of this thesis is to provide a comprehensive assessment of the influences of OVOCs on the atmospheric composition, by addressing three important aspects and their model representation. These aspects are: OVOCs' photochemistry in the gas-phase, their uptake and transformations in the aqueous phase, and their emissions.

With this aim, five studies are performed. Gas- and aqueous-phase mechanisms are built from chemical kinetic data, which are obtained from experiments, quantum chemical and theoretical kinetic calculations, or the literature. In order to investigate the importance of each mechanism on the atmospheric composition, they are implemented into the global ECHAM/MESSy Atmospheric Chemistry (EMAC) model. For analysing the impact of VOC emissions from biomass burning, a combination of the developed mechanisms is applied.

The first study shows that EMAC underestimates gas-phase OVOC and hydroxyl radical (OH) concentrations, when ignoring isomerization reactions of isoprene peroxy radicals under low-NO_x (NO_x=NO+NO_2) conditions. The second study demonstrates that in case of isocyanic acid (HNCO), its heterogeneous loss is far more important than its gas-phase chemical loss. In the third and fourth study, the development of the Jülich Aqueous-phase Mechanism of Organic Chemistry (JAMOC) allows to address the importance of in-cloud OVOC oxidation on tropospheric oxidants. This process leads to a significant reduction in gas-phase concentrations of OVOCs and HO_x (HO_x=OH+HO_2). Elevated in-cloud $HO_{2(aq)}$ concentrations introduce an enhanced destruction in $O_{3(aq)}$ resulting in reduced gas-phase O_3 concentrations. Thus, EMAC's bias towards too high tropospheric O_3 concentrations is diminished. Finally in the fifth study, the investigation of the 2015 Indonesian peatland fires reveals the significant impact of biomass burning VOC emissions on the regional tropospheric oxidation capacity. At the same time, enhanced phenol concentrations are predicted in the lower stratosphere leading to an enhanced destruction of O_3 by phenoxy radicals, potentially contributing to the variability of O_3 observed in satellite retrievals.

The complete assessment demonstrates that a comprehensive and explicit representation of all OVOC fluxes and transformations in global models is one key to guide the activities solving humanity's current and upcoming challenges related to climate change and air pollution. Especially, the development of JAMOC shows great potential to investigate the influence of aqueous-phase OVOC oxidation on acids and secondary organic aerosols (SOA) in future studies.

Contents

List of Figures

Chapter 2

Chapter 3

Chapter 4

Chapter 5

Chapter 6

Chapter 7

Appendix A

Appendix B

List of Tables

Chapter 7

Chapter 8

Appendix A

Appendix B

Appendix C

List of Abbreviations

General Abbreviations

ANNI	Artificial Neural Network for IASI
ASMA	Asian Monsoon Anticyclone
CLEPS	CLoud Explicit Physico-chemical Scheme
ECHAM5	Global circulation model: 'EC' from ECMWF and 'HAM' from HAMburg, version 5
ECMWF	European Centre for Medium-Range Weather Forecasts
EF	Emission Factor
ESM	Earth System Model
GCM	Global Circulation Model
GFAS	Global Fire Assimilation System
GHG	GreenHouse Gas
HOVOC	Highly Oxidised Volatile Organic Compound
HPC	High-Performance Computing
IASI	Infrared Atmospheric Sounding Interferometer
ITCZ	InterTropical Convergence Zone
IUPAC	International Union of Pure and Applied Chemistry
JAMOC	Jülich Aqueous-phase Mechanism of Organic Chemistry
JPL	Jet Propulsion Laboratory
JSC	Jülich Supercomputing Centre
JURECA	Jülich Research on Exascale Cluster Architectures
JUWELS	Jülich Wizard for European Leadership Science
KP^4	KPP Post Processor
KPP	Kinetic Pre-Processor
LAI	Leaf Area Index
LWC	Liquid Water Content
MCM	Master Chemical Mechanism
MIM2	Mainz Isoprene Mechanism 2
MIME	Mainz Isoprene Mechanism Extended
MODIS	MODerate resolution Imaging Spectroradiometer
MOM	Mainz Isoprene Mechanism
MOZART	Model of OZone And Related Tracers
NMVOC	NonMethane Volatile Organic Compound
ODE	Ordinary Differential Equations
OVOC	Oxygenated Volatile Organic Compound

PBL	Planetary Boundary Layer
PFT	Plant Functional Type
RF	Radiative Forcing
SAPHIR	Simulation of Atmospheric PHotochemistry In a large Reaction chamber
SAR	Structure–Activity Relationship
SEMIDEP	Simplified EMIssion and DEPosition
SOA	Secondary Organic Aerosol
STE	Stratospheric Tropospheric Exchange
TST	Transition State Theory
UTLS	Upper Troposphere/Lower Stratosphere
VOC	Volatile Organic Compound

MESSy Abbreviations

BMIL	Base Model Interface Layer
BML	Base Model Layer
CAABA	Chemistry As A Boxmodel Application
EMAC	ECHAM/MESSy Atmospheric Chemistry
MESSy	Modular Earth Submodel System
QCTM mode	Quasi Chemistry-Transport Model mode
SMCL	SubModel Core Layer
SMIL	SubModel Interface Layer

MESSy Submodels

AEROPT	Aerosol optical depth
AIRSEA	Air-sea exchange of trace gases
CH4	Methane oxidation feedback to the hydrological cycle
CLOUD	ECHAM5 cloud scheme as MESSy submodel
CLOUDOPT	Calculation of cloud optical properties
CONVECT	Convection parameterisations
DDEP	Dry deposition of trace gases and aerosols
GWAVE	Hines non-orographic gravity wave routines from ECHAM5
JVAL	Photolysis rates
LNOX	Lightning NO_x production
MECCA	Module Efficiently Calculating the Chemistry of the Atmosphere
MEGAN	Model of Emissions of Gases and Aerosols from Nature
MSBM	Multi-phase stratospheric box model
OFFEMIS	Prescribed emissions of trace gases and aerosols
ONEMIS	On-line calculated emissions of trace gases and aerosols
ORBIT	Calculation of orbital parameters of the Earth orbit
OROGW	Orographic gravity wave forcing
PTRAC	Prognostic tracers
QBO	Newtonian relaxation of quasi-biennial oscillation

RAD	ECHAM5 radiation code
S4D	Sampling in 4 dimensions
SCAV	SCAVenging submodel
SEDI	Sedimentation of aerosol particles
SORBIT	Sampling along sun-synchronous satellite orbits
SURFACE	ECHAM5 subroutines SURF, LAKE, LICETEMP and SICETEMP
TNUDGE	Newtonian relaxation of species as pseudo-emissions
TREXP	Tracer release experiments from point sources
TROPOP	Tropopause and other diagnostics
VERTEX	Represents land-atmosphere exchange (except for tracers) and vertical diffusion

Chemical Species

O_2^-	Superoxide Anion
Br	Bromine Atom
C_4H_8	*n*-Butene
C_5H_8	Isoprene
$C_6H_5NO_4$	Nitrocatechol
$C_6H_5O_2$	Phenyl Peroxy Radical
CH_3O_2	Methylperoxy Radical
CH_3OH	Methanol
CH_3OOH	Methyl Hydroperoxide
CH_4	Methane
Cl	Chlorine Atom
CO_2	Carbon Dioxide
CO	Carbon Monoxide
Fe	Iron
H_2O_2	Hydrogen Peroxide
H_2O	Water
HAMC	3-Hydroxy-2-Methyl-Acrolein
HCHO	Formaldehyde
HCN	Hydrogen Cyanide
HNCO	Isocyanic Acid
HO_2	Hydroperoxyl Radical
HO_x	Hydrogen Oxide Radicals (HO_x=OH+HO_2)
HONO	Nitrous acid
HPALD	Hydroperoxy Aldehydes
HVMK	Hydroxy Vinyl Methyl Ketone
MACR	Methacrolein
MVK	Methyl Vinyl Ketone
N_2	Dinitrogen
NO_2	Nitrogen Dioxide

NO_3	Nitrate Radical
NO_x	Nitrogen Oxides (NO_x=NO+NO_2)
NO	Nitrogen Monoxide
$O(^1D)$	Singlet oxygen
$O(^3P)$	Atomic oxygen
O_2	Oxygen
O_3	Ozone
O_x	Odd Oxygen
OH	Hydroxyl Radical
PAN	Peroxyacyl Nitrates
RO_2NO_2	Peroxy Nitrates
RO_2	Peroxy Radicals
$RONO_2$	Alkyl Nitrate
RO	Alkoxy Radicals
SO_2	Sulfur Dioxide
S	Sulfur Atom
di-HPCARP-RO_2	Di-hydroperoxy carbonyl peroxy radicals

Chapter 1

Introduction

In the past decades, global atmospheric models have been established as a key tool to improve our understanding of the Earth's atmospheric processes and to address the influence of anthropogenic activities on the Earth's climate. Especially, the proper modelling of atmospheric chemistry is an important aspect to tackle humanity's current and upcoming challenges related to climate change and air pollution.

One well known tropospheric greenhouse gas (GHG) is ozone (O_3). In the troposphere, O_3 is of special interest since close to the ground (i.e. the planetary boundary layer, PBL), it is a pollutant that directly impacts human health (e.g. respiratory problems, Fowler et al., 2008) and the ecosystem's productivity (Fowler et al., 2009). Additionally, O_3 absorbs radiation and, therefore, has a direct climate impact. It is the third largest GHG contributor to radiative forcing (RF) since pre-industrial times (Myhre et al., 2014). At the same time, O_3 is the main tropospheric source of hydroxyl radicals (OH) and thus has an indirect climate impact by controlling the lifetime of GHGs like methane (CH_4). O_3 is not directly emitted and its tropospheric abundance depends on its main budget terms: the influx by stratospheric tropospheric exchange (STE), chemical losses, deposition, and its chemical production (Young et al., 2018). The latter strongly depends on O_3 precursor emissions, like carbon monoxide (CO), nitrogen oxides (NO_x=NO+NO_2), and volatile organic compounds (VOCs) (Seinfeld and Pandis, 2016). Oxygenated VOCs (OVOCs) form an important sub-group of VOCs, which comprise ketones, aldehydes, and alcohols. Among other aspects, a realistic simulation of tropospheric O_3 in global atmospheric models thus relies on the realistic representation of OVOCs. Therefore, this thesis aims to provide a comprehensive assessment of the influence of OVOCs on the atmospheric composition and their representation in the global ECHAM/MESSy Atmospheric Chemistry model (EMAC, Jöckel et al., 2010).

In the following sections, insights to sources and sinks of OVOCs and O_3 in the atmosphere are provided. In order to understand their relation and the deficits and consequences of their representation in global models, their most relevant reactions and processes are described, before addressing the overall research objective of this thesis.

1.1 Oxygenated volatile organic compounds in the atmosphere

Opposite to O_3, the direct effect of OVOCs on climate is minimal. Most of their lifetimes are rather short and typically range from hours to weeks (except for a few halogenated OVOCs) and their radiation absorption is relatively weak. Therefore, the contribution of OVOCs to RF is negligible. However, their degradation leads to the formation of secondary organic aerosols (SOA) and radicals that influence the oxidation capacity of the troposphere on a regional and global scale, resulting in an indirect effect on climate (Mellouki et al., 2015).

In the atmosphere, VOCs (including OVOCs) are directly emitted by biogenic, biomass burning, and anthropogenic activities, of which biogenic emissions contribute the most. Table 1.1 gives an overview of the total biogenic VOC emissions estimated for the year 2000 (Guenther et al., 2012). Here, isoprene (C_5H_8) emissions are the strongest VOC emissions, which accounts for almost half of the total biogenic emissions (535 Tg a^{-1}). Isoprene emissions are biologically important for plants since they protect plants from heat stress (Sharkey and Singsaas, 1995) and O_3 damages (Loreto et al., 2001; Loreto and Velikova, 2001). Table 1.1 also shows that biogenic OVOC emissions are substantially lower compared to isoprene emissions, with the highest emissions of methanol (about 100 Tg a^{-1}), followed by acetone, ethanol, and acetaldehyde. CH_4, the simplest hydrocarbon, is the VOC that is emitted the most by anthropogenic activities. Prather et al. (2012) estimate that anthropogenic activities contributed about 352 Tg a^{-1} to the total CH_4 emissions of 554 Tg a^{-1} in 2010. Additionally, Huang et al. (2017) estimated that anthropogenic activities emitted about 169 Tg a^{-1} of non-methane VOCs (NMVOCs). Further, biomass burning events emit about 400 Tg NMVOCs per year (Akagi et al., 2011).

Even though OVOC emissions contribute significantly to tropospheric OVOC concentrations, by far most OVOCs are chemically produced from hydrocarbon oxidation (Mellouki et al., 2015). For example, CH_4 reacts initially with OH, which results in the formation of formaldehyde (HCHO) and methyl hydroperoxide (CH_3OOH) (Seinfeld and Pandis, 2016). These products further oxidise, forming carbon monoxide (CO), which ultimately leads to carbon dioxide (CO_2). A more complex example is the oxidation of *n*-butene (C_4H_8). Calvert et al. (2011) propose that its oxidation leads to the formation of about 60 OVOCs including alcohols, aldehydes, carboxylic- and percarboxylic acids, and organic- and peroxyacyl nitrates (PAN). When isoprene oxidises under low NO_x conditions, isomerization reactions of peroxy radicals (RO_2) become important, leading to a high variety of OVOCs. Under high-NO_x conditions, RO_2 mainly reacts with NO, leading to the formation of the stable products methacrolein (MACR) and methyl vinyl ketone (MVK) (Wennberg et al., 2018).

In the atmosphere, OVOCs mainly undergo chemical and physical processes, resulting in their transformation or removal from the atmosphere. During daytime, the degradation of OVOCs in the gas-phase is mainly initiated by their reaction with OH. The degradation by photolysis plays a significant role for carbonyls (e.g.

Table 1.1: A selection of global biogenic VOC emissions for the year 2000. Estimates based on Guenther et al. (2012).

Species	Tg a^{-1}	Species	Tg a^{-1}	Species	Tg a^{-1}
Hydrocarbons					
Isoprene	535.0	α-pinene	66.1	Ethene	26.9
Trans-β-ocimene	19.4	β-pinene	18.9	Propene	15.8
Limonene	11.4	Sabinene	9.0	Myrcene	8.7
Butene	8.0	β-caryophyllene	7.4		
OVOCs					
Methanol	99.6	Acetone	43.7	Ethanol	20.7
Acetaldehyde	20.7				
Total biogenic VOC emissions: 1007.4 Tg a^{-1}					

aldehydes, ketones). In addition, reactions with O_3 may initiate the degradation of these OVOCs. At nighttime, OH concentrations are low and reactions with the nitrate radical (NO_3) become important, which are insignificant during daytime since NO_3 is rapidly photolysed. The tropospheric degradation of OVOCs leads to the formation of a large range of PAN, SOA, highly oxidised VOCs (HOVOCs), and O_3.

Many OVOCs are highly soluble and partition into the aqueous-phase (Sander, 2015). Aqueous-phase chemistry in cloud droplets differs significantly from gas-phase chemistry, mainly due to photolysis enhanced by scattering effects within cloud droplets (Bott and Zdunkowski, 1987; Mayer and Madronich, 2004), faster reaction rates, and chemical reactions that do not occur in the gas-phase (Herrmann, 2003; Epstein and Nizkorodov, 2012). The in-cloud degradation of OVOCs is mainly initiated by OH during daytime and by NO_3 during nighttime (Herrmann et al., 2015). The in-cloud oligomerisation of OVOCs (e.g. from glyoxal and methylglyoxal) leads to the formation of SOA (Blando and Turpin, 2000; Ervens et al., 2011; Ervens, 2015). Ervens et al. (2011) suggest that in-cloud processes might even contribute in the same order to SOA formation as gas-phase processes. In the lower troposphere, OVOCs are additionally removed by dry deposition due to their high solubility.

1.2 A short review of tropospheric ozone

The abundance of tropospheric O_3 ranges from less than 10 ppb over remote tropical oceans to 100 ppb in the upper troposphere. Downwind of polluted urban regions, 100 ppb are frequently exceeded (Myhre et al., 2014). Based on satellite observations, the tropospheric O_3 burden is estimated to be 324 Tg (Young et al., 2018). Tropospheric O_3 levels increased in most parts of the world in the past decades (Cooper et al., 2014) and it is expected that they will further increase in the next decades (Young et al., 2013).

The tropospheric O_3 abundance depends on its main sources and sinks. About

500 Tg a^{-1} of O_3 enter the atmosphere as stratospheric influx (Young et al., 2018). Based on a recent multi-model estimate by Young et al. (2018), the total tropospheric chemical production is estimated to be about 4950 Tg a^{-1}. In the troposphere, O_3 is produced as a result of chemical reactions involving NO_x and VOCs. In absence of VOCs, O_3 and NO_x establish a fast photo-chemical null cycle (Seinfeld and Pandis, 2016):

$$NO_2 + h\nu\ (\lambda \leq 424\,\text{nm}) \rightarrow NO + O(^3P) \quad \text{(R 1.1)}$$

$$O_2 + O(^3P) + M \rightarrow O_3 + M \quad \text{(R 1.2)}$$

$$NO + O_3 \rightarrow NO_2 + O_2 \quad \text{(R 1.3)}$$

A net O_3 formation in the troposphere is only possible when NO-to-NO_2 conversion occurs by peroxy radicals (HO_2 and RO_2) without O_3 consumption as in Reaction R 1.3 (Crutzen, 1973). This is done by VOC oxidation that is mainly initiated by OH, following the scheme of Seinfeld and Pandis (2016):

$$RH + OH \rightarrow R + H_2O \quad \text{(R 1.4)}$$

$$R + O_2 + M \rightarrow RO_2 + M \quad \text{(R 1.5)}$$

$$RO_2 + NO \rightarrow RO + NO_2 \quad \text{(R 1.6)}$$

$$RO + O_2 \rightarrow R'CHO + HO_2 \quad \text{(R 1.7)}$$

$$HO_2 + NO \rightarrow OH + NO_2 \quad \text{(R 1.8)}$$

The net production of O_3 is thus dependent on the available NO_x and VOC concentrations, on which it depends in a non-linear manner. In the free troposphere, the formation of O_3 is mainly initiated by the oxidation of CO and CH_4, whereas over urban and vegetated regions, the oxidation of VOCs drives the O_3 formation. At low NO_x concentration levels with sufficiently available VOCs, the production of O_3 is NO_x-limited. Increasing the NO_x concentration leads to an enhanced O_3 formation. Eventually, the O_3 production reaches a local maximum and a further increase of NO_x leads to a reduced production of O_3 because of the NO_x radical terminating reaction:

$$OH + NO_2 + M \rightarrow HNO_3 + M \quad \text{(R 1.9)}$$

If NO_x concentrations are sufficiently high but VOC concentrations are low, the O_3 production becomes VOC-limited (Sillman, 1999).

At the same time, tropospheric O_3 is destroyed mainly by its own photolysis yielding singlet oxygen ($O(^1D)$):

$$O_3 + h\nu\ (\lambda \leq 319\,\text{nm}) \rightarrow O(^1D) + O_2 \quad \text{(R 1.10)}$$

However, effective O_3 destruction is only possible in the presence of water:

$$O(^1D) + H_2O \rightarrow OH + OH \quad \text{(R 1.11)}$$

since $O(^1D)$ is efficiently converted to atomic oxygen ($O(^3P)$), and thus to O_3 (Reaction R 1.2) by reacting with N_2 and O_2:

$$O(^1D) + N_2 \rightarrow O(^3P) + N_2 \quad \text{(R 1.12)}$$

$$O(^1D) + O_2 \rightarrow O(^3P) + O_2 \quad \text{(R 1.13)}$$

Additionally, O_3 is destroyed by reactions with HO_2, OH, and most VOCs with carbon double bonds. The total chemical O_3 loss is estimated to be about 4500 Tg a^{-1} and additional 950 Tg a^{-1} are lost by dry deposition (Young et al., 2018).

In general, O_3 is rather insoluble in water but it is still taken up by warm (liquid) cloud droplets, which act as a significant O_3 sink. Within cloud droplets, the dissolved ozone ($O_{3(aq)}$) is mainly destroyed via (Staehelin et al., 1984):

$$O_{3(aq)} + O^-_{2(aq)} \rightarrow O^-_{3(aq)} + O_{2(aq)} \quad \text{(R 1.14)}$$
$$O^-_{3(aq)} + H^+_{(aq)} \rightarrow OH_{(aq)} + O_{2(aq)} \quad \text{(R 1.15)}$$

where the superoxide anion ($O^-_{2(aq)}$) is in equilibrium with its conjugated base hydroperoxyl radical ($HO_{2(aq)}$):

$$HO_{2(aq)} \rightleftharpoons O^-_{2(aq)} + H^+_{(aq)} \quad \text{(R 1.16)}$$

Here, $HO_{2(aq)}$ is either taken up into or produced by photo-oxidation within the cloud droplet (e.g. by in-cloud OVOC oxidation). The realistic representation of clouds as O_3 sinks in models is thus sensitive to a proper representation of $HO_{2(aq)}$ and OVOC oxidation in cloud droplets.

1.3 Current modelling status and process representation

In general, atmospheric models vary in their complexity ranging from simple box-models, representing a single air parcel, to complex global atmospheric chemistry models. A comprehensive assessment of the influence of OVOCs on the atmospheric composition needs to address three important aspects: the OVOCs' photochemistry in the gas-phase, their uptake and transformations in the aqueous phase, and their surface-atmosphere exchanges. The model representation of all three aspects must be accordingly evaluated.

In the core of global models, atmospheric gas-phase chemistry is represented by a set of reactions. The oxidation of isoprene, the most abundant VOC, is represented for example by the highly explicit Master Chemical Mechanism (MCM, Jenkin et al., 2015). However, due to its complexity, the MCM is not suitable for global model applications and reduced mechanisms, which vary in their complexity, are used instead. Example mechanisms for global models comprise the Model of OZone And Related Tracers (MOZART, Emmons et al., 2010), the Mainz Isoprene Mechanism 2 (MIM2, Taraborrelli et al., 2009), and the Mainz Organic Mechanism (MOM, Sander et al., 2019, further details in Sect. 2.1.1). Uncertainties originating from mechanism reduction may introduce significant inaccuracies into the representation of atmospheric chemistry in global models (Whitehouse et al., 2004a,b).

Herrmann et al. (2015) showed that the partitioning and oxidation of OVOCs in cloud droplets significantly influence the OH budget. Thus, the detailed representation of aqueous-phase chemistry is important to properly predict the atmospheric concentrations of VOCs and oxidants. However, most global models only include the uptake of a few soluble compounds, their acid-base equilibria, and the oxidation of sulfur dioxide (SO_2) via O_3 and hydrogen peroxide (H_2O_2) (Ervens, 2015, Table 1). The explicit oxidation of OVOCs is currently not considered in any global model with one exception, though limited to species containing one carbon atom (Tost et al., 2006a). It is thus expected that the missing in-cloud OVOC oxidation leads to too low in-cloud $HO_{2(aq)}$ concentrations, resulting in an underprediction of clouds as O_3 sinks (Reaction R 1.14).

In global models, biomass burning emissions are represented based on a combination of satellite observations and emission coefficients (Kaiser et al., 2012). The latter mainly differ for each emitted species and the primary biomass type burned (Akagi et al., 2011). Recently, multiple studies found substantial differences between multiple biomass burning emission inventories (Shi and Matsunaga, 2017; Pan et al., 2020; Liu et al., 2020). As biomass burning releases a significant amount of VOCs into the atmosphere, the representation of OVOCs in global models also depends on the representation of the biomass burning inventory used. Additionally, the chemical mechanisms of global models do not represent all OVOCs emitted by biomass burning and their importance can thus not be addressed. One example of such OVOCs is isocyanic acid (HNCO), which is strongly emitted by biomass burning and inadvertently released by NO_x mitigation measures in flue gas treatments. Its chemical lifetime in the gas phase is expected to be in the order of years, since the reaction with its main chemical reactant (OH) is estimated to be slow (Leslie et al., 2019). Therefore, heterogeneous losses are expected to be its major sinks, resulting in an estimated atmospheric lifetime of about a month (Young et al., 2012). HNCO is linked to protein carbamylation if ambient concentrations exceed 1 ppb, which causes adverse health effects for humans (Wang et al., 2007; Roberts et al., 2011; Leslie et al., 2019). Currently, HNCO is not represented in EMAC but with increasing biomass burning and more widespread usage of catalytic converters in car engines its representation is desirable.

1.4 Scientific approach and thesis structure

This thesis aims to provide a comprehensive assessment of the influence of OVOCs on the atmospheric composition. The focus is on the importance of the representation of OVOCs in EMAC and associated uncertainties, in order to improve EMACs capabilities in representing air pollution and climate change related processes. The assessment is achieved by investigating the formation and degradation of OVOCs in the gas-phase, their relevance for aqueous-phase chemistry, and the representation of VOC emissions from biomass burning. In this scope, five individual studies are conducted, which can be grouped according to their focus on the importance of:

- **Gas-phase chemistry of OVOCs**:
  1. Novelli et al. (2020) (here Chapter 3) quantify the OH regeneration in isoprene oxidation and address the importance of the isomerization reactions of isoprene peroxy radicals by using a combination of chamber experiments, quantum chemical and theoretical kinetic calculations, box-model studies, and EMAC simulations.
  2. Rosanka et al. (2020) (here Chapter 4) investigate the importance of atmospheric loss processes of HNCO by combining a theoretical kinetic study and EMAC simulations.
- **Aqueous-phase chemistry of OVOCs**:
  3. Rosanka et al. (2021a) (here Chapter 5) develop the in-cloud oxidation scheme Jülich Aqueous-phase Mechanism of Organic Chemistry (JAMOC), which is suitable for global model applications, and implement it into the Module Efficiently Calculating the Chemistry of the Atmosphere (MECCA).
  4. Rosanka et al. (2021b) (here Chapter 6) apply JAMOC in EMAC and address the importance of in-cloud OVOC oxidation on tropospheric oxidants (OVOCs, HO_x, and O_3).
- **Biomass burning emissions of VOCs**:
  5. Rosanka et al. (2021c) (here Chapter 7) illustrate the influence of biomass burning VOC emissions on the troposphere and lower stratosphere by analysing the impact from Indonesian peatland fires in 2015.

The thesis is organised as follows: in the subsequent Chapter 2 the atmospheric chemistry models used in the performed studies are reviewed. Here, the main focus is on the representation of gas- and aqueous-phase chemistry in these models as well as other important physical processes connected to VOCs. In the follow up chapters (Chapter 3-7), each individual study is presented as published in the respective journal in the order listed above. In Chapter 8, all studies are summarised and discussed in the context of this thesis. Final conclusions are drawn in Chapter 9, including an outlook for upcoming research projects.

Chapter 2

Modelling systems

In order to address the research objectives of this thesis, the chemical mechanism used in the global model ECHAM/MESSy Atmospheric Chemistry (EMAC, Jöckel et al., 2010) has been further developed. Figure 2.1 gives an overview on the general approach used during this development process. In a first step, the mechanism is derived and developed based on chemical kinetic data, which are obtained from the literature or quantum chemical and theoretical kinetic calculations. Afterwards, the resulting mechanism is implemented into a box-model (e.g. Chemistry As A Boxmodel Application (CAABA), Sander et al., 2019) and its simulation results are compared to measurements or reviewed using earlier studies. Once the mechanism properly represents the added chemistry, it is optimised with respect to its computational costs and implemented into EMAC. This allows to investigate the global implications of the new chemical mechanism. The gas- and aqueous-phase chemistry mechanisms, which are used across all studies, are introduced in Sect. 2.1. Afterwards, an introduction of the two modelling systems, mainly used in this thesis, is provided (Sect. 2.2 and 2.3), focusing on the physical aspects most relevant to this thesis.

In Novelli et al. (2020) (here Chapter 3) and Rosanka et al. (2020) (here Chapter 4), additional methodologies are used, which are not directly related to global modelling. These techniques mainly concern measurement techniques and theoretical chemistry modelling. For further details on these techniques, please refer to the main manuscripts (Chapter 3 and 4) and their supplemental material (Appendix A and B).

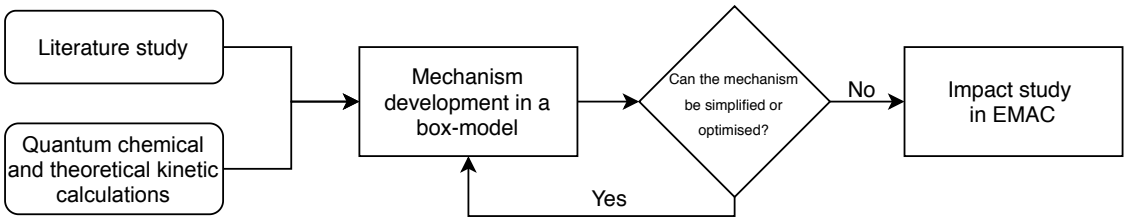

Figure 2.1: General mechanism development strategy used in this thesis.

2.1 Base chemical mechanisms

All developments in this thesis are based on the same original chemical mechanism, which is spilt in a gas- and an aqueous-phase mechanism. The base gas-phase mechanism is the Mainz Organic Mechanism (MOM, Sander et al., 2019), which includes the most complex VOC oxidation scheme currently available in EMAC. The base aqueous-phase mechanism is EMAC's standard aqueous-phase mechanism. In the following, both are shortly introduced.

2.1.1 The gas-phase Mainz Organic Mechanism (MOM)

In general, MOM contains the basic HO_x, NO_x, CH_4, NMVOCs, halogen (Cl, Br), and sulfur (S) chemistry and represents a large variety of VOCs. Figure 2.2 shows this variety by providing an overview on the chemical structure and the classification of the 43 primarily emitted VOCs. In total, MOM represents more than 600 species and 1600 reactions (Sander et al., 2019). The following paragraphs focus on the treatment of isoprene, terpenes, aromatics, and peroxy radicals (RO_2).

Oxidation of isoprene

The oxidation scheme of isoprene (C_5H_8) is based on the Mainz Isoprene Mechanism Extended (MIME, Nölscher et al., 2014). It has been originally derived from the Master Chemical Mechanism (MCM, v3.1, Jenkin et al., 1997; Saunders et al., 2003)[1] as described by Taraborrelli et al. (2009) and subsequently extended by Taraborrelli et al. (2012). Figure 2.3 gives an overview of the OH addition pathway as represented in MIME. In MIME the OH addition to isoprene occurs mostly at position 1 and 4 and to much lesser extent (7 %) at position 2 and 3. In MIME, 93 % of the reaction flux results in four alkyl radicals. These undergo O_2-addition/elimination with 6 peroxy radicals, which in turn then react with HO_2, NO, NO_3, and RO_2. In MOM for each OH-addition position, the two alkyl radical isomers and associated three RO_2 are lumped together.

The representation of isoprene in MOM includes: (1) the 1,6-H-shift for Z-1,4- and Z-4,1-ISOPO2 isomers following Peeters et al. (2009) using the rate coefficients estimated by Taraborrelli et al. (2012) and the isoprene-derived hydroperoxy aldehydes (HPALDs) yield from Nölscher et al. (2014), (2) a simplified mechanism of the non-HPALD-yielding channel according to Peeters et al. (2014) and Jenkin et al. (2015), (3) the OH addition of the unsaturated isoprene hydroperoxides following Paulot et al. (2009) yielding epoxydiols and OH, and (4) the degradation of methacrolein (MACR) following Orlando et al. (1999) using the MACR peroxy radical 1,4 H-shift reaction rate as proposed by Crounse et al. (2012). In MOM, the isoprene related photolysis is implemented for: (1) carbonyl nitrates according to Barnes et al.

[1] Rickard, A. and Pascoe, S.: The Master Chemical Mechanism (MCM), available at: `http://mcm.leeds.ac.uk/MCMv3.1/` (last access: 6 September 2020)

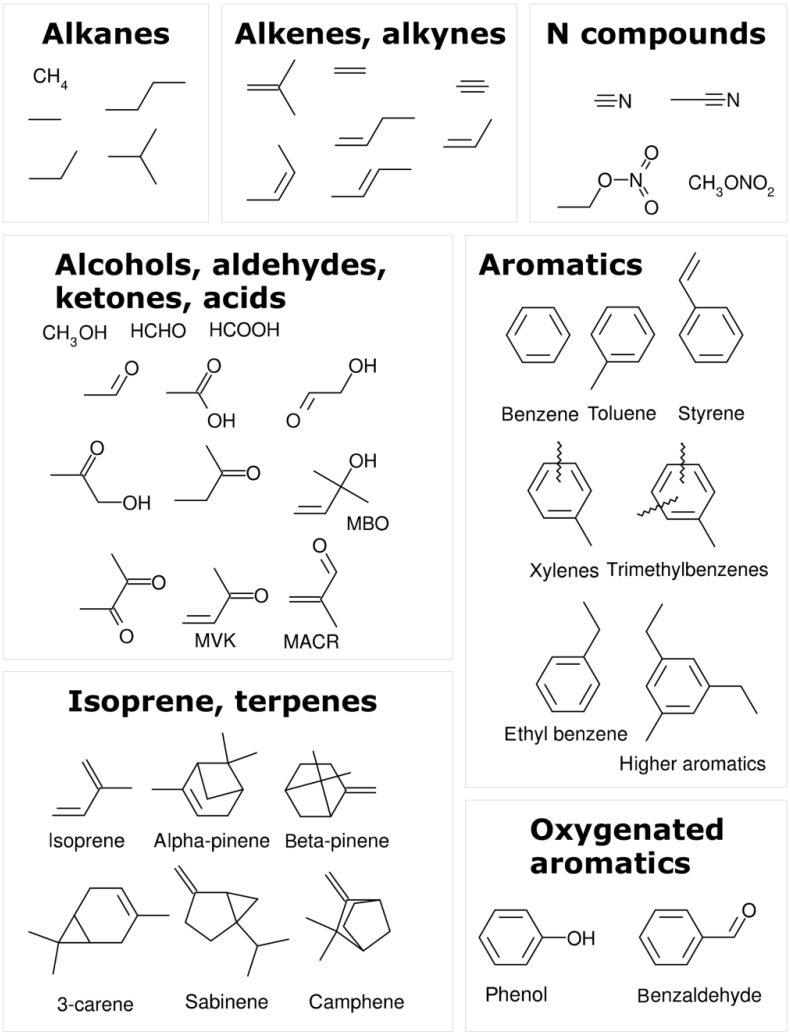

Figure 2.2: Overview of the 43 primarily emitted VOCs treated in MOM (obtained from Sander et al., 2019)

(1993) and Müller et al. (2014), (2) HPALDs following Peeters et al. (2014) and Jenkin et al. (2015), and (3) hydroxy vinyl methyl ketone (HVMK) and 3-hydroxy-2-methyl-acrolein (HAMC) following Nakanishi et al. (1977) and Messaadia et al. (2015).

Oxidation of terpenes

The oxidation of the two terpenes with the highest biogenical emission rates (α-pinene and β-pinene, see Table 1.1) is based on the MCM implementation as proposed by Jenkin et al. (2000). In general, the oxidation of both terpenes is initialised by O_3 addition to the double bond. This forms an ozonide, which quickly decomposes by two possible channels. Each leads to the formation of a Criegee intermediate, which either decomposes yielding an organic radical and OH or stabilises by collision. This mechanism is modified to include developments from Vereecken et al. (2007),

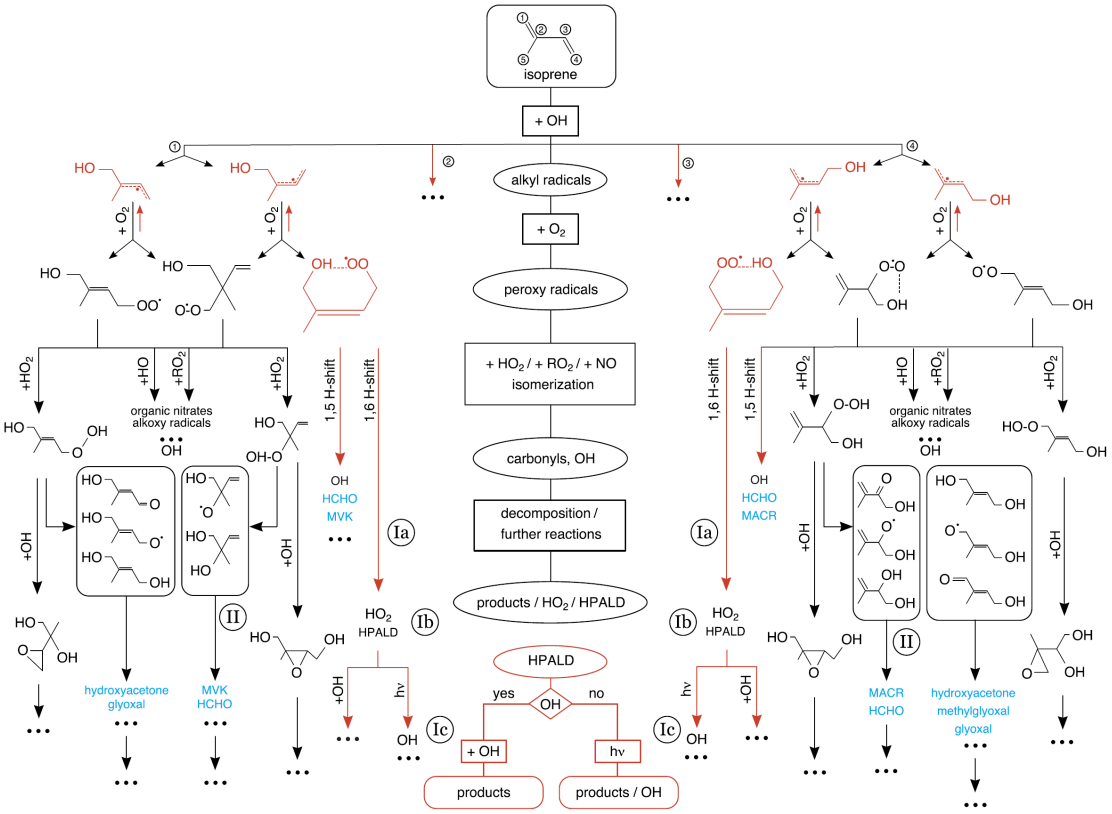

Figure 2.3: The isoprene OH-addition pathway as represented in MIME, which has been reduced to MOM. The species and reactions in red are the ones proposed originally by Peeters et al. (2009) (obtained from Nölscher et al., 2014).

Nguyen et al. (2009), Vereecken and Peeters (2012), and Capouet et al. (2008). The modifications obtained from these theoretical works are simplified, neglecting minor O_3 and OH initiated oxidation channels.

Oxidation of aromatics

The oxidation of aromatics (e.g. benzene, toluene, xylenes) is implemented following Cabrera-Perez et al. (2016), which is a reduction of the aromatics mechanism used in MCM (v3.2, Jenkin et al., 2003; Bloss et al., 2005)[2]. Here, the mechanisms for benzene and toluene are directly taken from MCM, due to their high abundance in the atmosphere. The first oxidation step of all other aromatics, except for xylenes and trimethylbenzenes, follows the implementation of MCM. The second oxidation step of these aromatics is linked to the one of toluene. Xylenes and trimethylbenzenes are lumped with equal proportion. Products with a lifetime shorter than 1 s are not explicitly represented and replaced by their respective products. The re-

[2]Rickard, A., Young, J. and Pascoe, S.: The Master Chemical Mechanism (MCM), available at: `http://mcm.leeds.ac.uk/MCMv3.2/` (last access: 6 September 2020)

action of NO_2 with phenyl peroxy radicals ($C_6H_5O_2$) yielding NO_3 is implemented following Jagiella and Zabel (2007). Additionally, the representation of nitrophenols is expanded to include their photolysis reactions according to Bejan et al. (2006) and Chen et al. (2011). The non-HONO formation channel from nitrophenol photolysis, which does not destroy the aromatic ring and reforms phenoxy radicals (Cheng et al., 2009; Vereecken et al., 2016) is neglected in MOM.

VOC oxidation by OH, NO_3, and O_3

OH is the major daytime oxidant, which reacts with VOCs by either H-abstraction or OH addition. When available, measured rate coefficients are used, while most coefficients are taken from the International Union of Pure and Applied Chemistry (IUPAC) kinetic data evaluation (Atkinson et al., 2006)[3]. Rate coefficients are estimated if no measured values are available. For species containing up to five carbon atoms, the rate coefficients are estimated using a structure–activity relationship (SAR) based on Atkinson (1987) and Kwok and Atkinson (1995). The rate coefficients for closed-shell species (containing five- to eleven-carbon atoms) are taken from MCM. The OH addition is represented using the rate coefficients from Peeters et al. (2007). In order to take the effect of neighbouring groups into account, substituent factors are used, which are differentiated by the neighbouring functional group. In MOM, the NO_3 and O_3 initiated VOC oxidation follows the MCM implementation.

Peroxy radicals (RO_2)

Under polluted conditions, peroxy radicals (RO_2) formed from VOC oxidation predominantly react with NO. For this reaction, two reaction channels are considered, resulting either in the formation of the corresponding alkoxy radical (RO) and NO_2 or in alkyl nitrate ($RONO_2$). The yields for the formation of alkyl nitrates are mainly obtained from Arey et al. (2001). The formation and decomposition of peroxy nitrates (RO_2NO_2) are implemented following the MCM implementation using the kinetic data from the Jet Propulsion Laboratory (JPL)[4]. Reactions of RO_2 with NO_3 produce the corresponding RO and NO_2. For the reaction of RO_2 with HO_2, three possible channels are considered:

$$\mathrm{RO_2 + HO_2} \rightarrow \mathrm{RO + OH + O_2} \quad \text{(R 2.1)}$$

$$\rightarrow \mathrm{ROOH + O_2} \quad \text{(R 2.2)}$$

$$\rightarrow \mathrm{ROH + O_3} \quad \text{(R 2.3)}$$

[3]Wallington, T. J., Ammann, M., Cox, R. A., Crowley, J. N., Herrmann, H., Jenkin, M. E., McNeill, V., Mellouki, A., Rossi,M. J., and Troe, J.: IUPAC Task group on atmospheric chemical kinetic data evaluation: Evaluated kinetic data, available at: `http://iupac.pole-ether.fr` (last access: 6 September 2020)

[4]Chemical Kinetics and Photochemical Data for Use in Atmospheric Studies, Evaluation No. 19, available at: `http://jpldataeval.jpl.nasa.gov` (last access: 6 September 2020)

Additionally, self- and cross-reactions of each RO_2 are taken into account using the permutation reaction formalism from MCM (Jenkin et al., 1997). Here, the methylperoxy radical (CH_3O_2) is assumed to be the main co-reactant of each RO_2 following Madronich and Calvert (1990). The resulting pseudo-first-order reaction rate coefficient is represented as:

$$k^{1st} = 2 \times \sqrt{k_{RO_2} \times k_{CH_3O_2}} \times [RO_2] \tag{2.1}$$

where, k_{RO_2} is the second-order rate coefficient of the self-reaction of the respective RO_2, $k_{CH_3O_2}$ is the second-order rate coefficient of CH_3O_2, and $[RO_2]$ represents the concentration sum of all organic peroxy radicals.

2.1.2 The aqueous-phase mechanism

Most global atmospheric chemistry models only include very limited representations of in-cloud chemistry (Ervens, 2015). Both models used within this study (see Sect. 2.2 and 2.3) allow to include an advanced aqueous-phase mechanism. It represents more than 150 reactions (Tost et al., 2007a; Jöckel et al., 2016) including phase transfer, acid dissociation equilibria, oxidation-reduction reactions, heterogeneous reactions on droplet surfaces, and photolysis reactions. This mechanism can be considered to be the current standard mechanism used in EMAC. Similar to other global model aqueous-phase mechanisms, it includes the oxidation of sulfur dioxide ($SO_{2(aq)}$) via $O_{3(aq)}$ and hydrogen peroxide ($H_2O_{2(aq)}$). Opposite to other global model mechanisms, it considers the uptake of radicals like HO_2 into cloud droplets, which leads to an active destruction of O_3, following the Reactions R 1.14 and R 1.16. In addition, it includes a simplified degradation scheme of methane oxidation products.

2.2 The box-model CABBA

When implementing advancements in chemical mechanisms, box-models provide an easy infrastructure to develop these changes and to understand their fundamental atmospheric implications. In Rosanka et al. (2021a) (here Chapter 5) and Rosanka et al. (2021b) (here Chapter 6), the Chemistry As A Boxmodel Application (CAABA, Sander et al., 2019) is used for this purpose. CAABA represents a single air parcel (i.e. a box) in the atmosphere under predefined conditions (e.g. temperature, humidity). The gas- and aqueous-phase chemistry mechanisms are represented using the multi-purpose Module Efficiently Calculating the Chemistry of the Atmosphere (MECCA), using one aerosol size bin with a constant radius and liquid water content (LWC). MECCA is capable to integrate the defined multiphase chemical mechanism as one single system of Ordinary Differential Equations (ODEs) with appropriate phase-transfer reactions (Sander, 1999; Kerkweg et al., 2007), using the Kinetic Pre-Processor (KPP version 2.2.3, Sandu and Sander, 2006). In addition

to chemical processes, CAABA considers physical processes like emissions, deposition, entrainment, and detrainment by using the submodel Simplified EMIssion and DEPosition (SEMIDEP). Due to the 0-dimensional nature of box-models, no differences exist between physical processes like emissions and entrainment, as they can be represented as fluxes into the box, whereas deposition and detrainment are represented as fluxes out of the box. Concentration changes due to emissions or entrainment fluxes and changes due to deposition or detrainment are calculated using the representations described by Kerkweg et al. (2006b) and Kerkweg et al. (2006a), respectively. Photolysis rate coefficients are calculated using the submodel JVAL (Jöckel et al., 2005; Sander et al., 2014), which applies the method of Landgraf and Crutzen (1998). Here, the rate coefficients for photolysis reactions are calculated for eight predefined wavelength bands using the spectral actinic flux, the quantum yield, and absorption cross section.

2.3 The global model EMAC

The global chemistry climate model EMAC is employed to investigate the global influence of the expanded chemistry mechanism, which are developed in this thesis. It consists of the Modular Earth Submodel System (MESSy, Jöckel et al., 2010) infrastructure applying the 5$^{\text{th}}$ generation European Centre Hamburg general circulation model (ECHAM5, Roeckner et al., 2006) as the base model. Within this section, the major aspects of EMAC are discussed, including an introduction to the MESSy infrastructure (Sect. 2.3.1) and the base model ECHAM5 (Sect. 2.3.2). Physical processes most relevant for this thesis and one key diagnostic method are presented in Sect. 2.3.3 to 2.3.8.

2.3.1 The MESSy interface

The Modular Earth Submodel System (MESSy)[5] is a software providing the framework for the bottom up implementation of Earth System Model components. MESSy is coded in so-called submodels, i.e. each process or functionality is coded as a submodel. Each submodel consists of a 'core', which is independent of all other model components, and an interface managing the communication between this specific and all other model components (submodels). These submodels may represent infrastructure components (e.g. input/output), physical process descriptions (e.g. gas-phase chemistry), or diagnostics (e.g. sampling along satellite orbits). Technically, this is achieved by using four different layers: (1) the base model layer (BML), which in this study is ECHAM5, (2) the base model interface layer (BMIL), which acts as socket that connects all submodels, (3) the submodel interface layer (SMIL), which connects the processes described in each submodel with the BMIL, and (4) the submodel core layer (SMCL), in which the submodel's process is described (e.g.

[5]The highly structured Modular Earth Submodel System (MESSy), available at: `https://www.messy-interface.org/` (last accessed: 9 September 2020)

Table 2.1: MESSy submodels used within all studies.

Name	Function	Reference
AEROPT	Aerosol optical depth	Jöckel et al. (2006)
AIRSEA	Air-sea exchange of trace gases	Pozzer et al. (2006)
BIOBURN	Biomass burning emissions (see Sect. 2.3.7)	Cabrera Perez (2017)
CH4	Oxidation of CH_4 by OH, $O(^1D)$, Cl. Feedback to the hydrological cycle.	*
CLOUD	ECHAM5 cloud scheme as MESSy submodel	Roeckner et al. (2006)
CLOUDOPT	Calculation of cloud optical properties	Dietmüller et al. (2016)
CONVECT	Convection parameterisations	Tost et al. (2006b)
CVTRANS	Convective tracer transport	Tost (2006)
DDEP	Dry deposition of trace gases and aerosols (see Sect. 2.3.5)	Kerkweg et al. (2006a)
GWAVE	Hines non-orographic gravity wave routines from ECHAM5	*
JVAL	Photolysis rates	Jöckel et al. (2005)
LNOX	Lightning NO_x production	Tost et al. (2007b)
MECCA	Atmospheric chemistry (see Sect. 2.3.3)	Sander et al. (2019)
MEGAN	Model of Emissions of Gases and Aerosols from Nature (see Sect. 2.3.6)	Guenther et al. (2006)
MSBM	Multi-phase stratospheric box model	Jöckel et al. (2010)
OFFEMIS	Prescribed emissions of trace gases and aerosols	Kerkweg et al. (2006b)
ONEMIS	On-line calculated emissions of trace gases and aerosols	Kerkweg et al. (2006b)
ORBIT	Calculation of orbital parameters of the Earth orbit	Dietmüller et al. (2016)
OROGW	Parameterisation of subgrid scale orography (SSO) drag due to low level SSO blocking and orographic gravity wave forcing	*
PTRAC	Define additional prognostic tracers via namelist	Jöckel et al. (2008)
QBO	Newtonian relaxation of quasi-biennial oscillation	Jöckel et al. (2006)
RAD	Implementation of the ECHAM5 radiation code	Dietmüller et al. (2016)
S4D	Sampling in 4 dimensions (e.g. flight tracks)	Jöckel et al. (2010)

Table 2.1: MESSy submodels used within all studies (... continued).

Name	Function	Reference
SCAV	Scavenging and wet deposition of trace gases and aerosol (see Sect. 2.3.4)	Tost et al. (2006a)
SEDI	Sedimentation of aerosol particles	Kerkweg et al. (2006a)
SORBIT	Sampling along sun-synchronous satellite orbits (see Sect. 2.3.8)	Jöckel et al. (2010)
SURFACE	The SURFACE submodel is the modularised version of the ECHAM5 subroutines SURF, LAKE, LICETEMP and SICETEMP	*
TNUDGE	Newtonian relaxation of species as pseudo-emissions	Kerkweg et al. (2006b)
TREXP	Tracer release experiments from point sources	Jöckel et al. (2010)
TROPOP	Tropopause and other diagnostics	Jöckel et al. (2006)
VERTEX	Represents land-atmosphere exchange (except for tracers) and vertical diffusion	*

* Modular Earth Submodel System (MESSy) - MESSy Submodels, available at: `https://www.messy-interface.org/current/auto/messy_submodels.html` (last accessed: 9 September 2020)

gas-phase chemistry). One important aspect of MESSy is its infrastructure, which builds the middleware between the base model and all regular submodels. The MESSy submodels building the infrastructure (e.g., TRACER, TIMER, IMPORT) are called generic submodels. By providing standardised interface routines, the submodel CHANNEL allows different submodels to access data generated by another submodel using pointers and avoiding usage of variables throughout the code (Jöckel et al., 2010). For example, the data object for the atmospheric concentration of O_3 can be accessed by the gas- and aqueous-phase chemistry and the dry deposition submodels. Table 2.1 provides an overview of all non-generic submodels used in this thesis including their main references.

2.3.2 ECHAM5: EMAC's dynamical core

ECHAM5 ('EC' from ECMWF and 'HAM' from HAMburg, version 5) is a global circulation model (GCM) providing the dynamical core for EMAC. It is based on the global weather forecast model developed at the European Centre for Medium-Range Weather Forecasts (ECMWF) and includes additional physical parameterisations developed at the Max-Plank Institute for Meteorology in Hamburg. A detailed description of the model is provided by Roeckner et al. (2003). The four prognostic variables temperature, vorticity, divergence, and the logarithm of the surface pressure are defined in spectral space by a truncated series of spherical harmonics. The

Table 2.2: Summary of the different EMAC grid resolutions used in this thesis.

Resolution	# of longitudes	# of latitudes	Approximated box width	Vertical levels	Model top height [hPa]	Time step [s]
T42L90	128	64	2.81°/313 km	90	0.01	720
T63L90	192	96	1.87°/209 km	90	0.01	600
T106L31	320	160	1.12°/125 km	31	10	360
T106L90	320	160	1.12°/125 km	90	0.01	300

tracer transport is based on a semi-Lagrangian approach (Lin and Rood, 1996).

Within this thesis, EMAC is used at different horizontal resolutions corresponding to different spherical truncations (T42, T63, and T106) and vertical resolutions with hybrid pressure levels up to 10 hPa (31 levels) and 0.01 hPa (90 levels), respectively. Table 2.2 provides an overview of all resolutions used, including approximations for the different grid box sizes. All simulations performed in this thesis use the Quasi Chemistry-Transport Model mode (QCTM mode, Deckert et al., 2011). This means that chemistry and dynamics are decoupled, e.g. fixed tracer mixing rations are used as input for the radiation scheme instead of the prognostic chemical tracers. In this way, the meteorology is the same for all simulations enabling the investigation of the implications of different chemical mechanisms.

2.3.3 Representation of the gas-phase chemistry

In EMAC, MECCA is used to represent chemical processes in the troposphere and the stratosphere. Differently to CAABA, gas- and aqueous-phase chemistry are calculated by two different submodels in EMAC. In this thesis, gas-phase chemical processes are represented by MECCA, using the gas-phase mechanism MOM described in Sect. 2.1.1. Additionally, MECCA applies the KPP Post Processor (KP^4) when coupled to EMAC, in order to improve computation efficiency for three dimensional models (Jöckel et al., 2010). MECCA employs a tagging system that allows to obtain reaction rates from multiple reactions and to combine them into a single tracer (Gromov et al., 2010). In this thesis, this tagging system is mainly used to calculate detailed gas-phase chemical budgets, focusing on odd oxygen (O_x) and HO_x.

2.3.4 Representation of the aqueous-phase chemistry

Aqueous-phase chemistry in clouds and wet deposition are represented by using the SCAVenging submodel (SCAV, Tost et al., 2006a). It simulates the removal of trace gases and aerosol particles by clouds and precipitation. The phase transfer of species is described by Schwartz (1986) (see Sander, 1999; Tost et al., 2006a). In this approach, the outgassing depends on Henry's law constants. In addition to the phase transfer, SCAV calculates acid dissociation equilibria, oxidation-reduction reactions,

heterogeneous reactions on droplet surfaces, and aqueous-phase photolysis reactions using the aqueous-phase mechanisms presented in Sect. 2.1.2. Wet deposition is calculated from the in-cloud and in-precipitation chemical concentrations for both, large-scale and convective clouds. SCAV also employs a rudimental tagging system, which allows to budget the in-cloud chemical production and losses of selected species. Similarly to MECCA, SCAV represents the aqueous-phase mechanism as an ODE system, which is solved by applying KPP (version 1). The ODE systems resulting from the combination of gas-phase and in-cloud aqueous-phase suffer from a higher stiffness due to fast acid-base equilibria and phase-transfer reactions and a load imbalance on High-Performance Computing (HPC) systems due to the sparsity of clouds. Thus, the increase in computational demand per added aqueous-phase reaction is expected to be higher compared to gas-phase reactions (i.e. reactions added to MOM in MECCA).

2.3.5 Representation of dry deposition

The removal of trace gases (e.g. O_3 and many VOCs) by dry deposition is an important atmospheric sink. For example, dry deposition of O_3 accounts for about 20 % of the total O_3 loss (Young et al., 2018). In EMAC, this process is represented by the submodel Dry DEPosition (DDEP, Kerkweg et al., 2006a). It calculates the dry deposition of trace gases to vegetation using the multiple resistance model by Wesely (1989). Compared to Wesely (1989), DDEP only considers a reduced number of surface types. Since the dry deposition velocities of O_3 and SO_2 are relatively well known, the dry deposition velocities of other trace gases are scaled to these two species, using their solubility and reactivity. The so called 'one big-leaf approach' is applied, in which the vegetation canopy is represented as a single system in each grid box, neglecting detailed plant structures and characteristics. Therefore, it is assumed that the leaf density is vertically uniformly distributed and that leaves are horizontally oriented (Sellers, 1985).

2.3.6 Representation of biogenic emissions

The strongest atmospheric sources of hydrocarbons are the emissions from biogenic activities (see Table 1.1). The MESSy submodel Model of Emissions of Gases and Aerosols from Nature (MEGAN, Guenther et al., 2006) is used in EMAC to represent these sources. In general, biogenic emissions are driven by the density of plants (leaf area index, LAI), the plant type (plant functional type, PFT), weather conditions (i.e. solar radiation, temperature, and moisture), and the atmospheric chemical composition. In EMAC, global biogenic VOC emissions are dependent on the grid resolution. In order to allow the comparability of model results across different resolutions, the global biogenic emissions of important VOCs (e.g. isoprene) are scaled to the same best estimate.

2.3.7 Representation of biomass burning events

The second strongest atmospheric source of VOCs is biomass burning (Akagi et al., 2011). In EMAC, biomass burning emission fluxes are determined by the submodel BIOBURN (Cabrera Perez, 2017). These fluxes are calculated by using biomass burning emission factors (EF) and dry matter combustion rates. For the latter, Global Fire Assimilation System (GFAS, Heil et al., 2010) data are used, which are based on satellite observations of fire radiative power obtained from the Moderate Resolution Imaging Spectroradiometer (MODIS, Kaufman et al., 1998) satellite instruments (Kaiser et al., 2012). In general, the biomass burning emission factors for VOCs are based on Akagi et al. (2011) and vary for the dominant fire type of each biomass burning event. The latter depends on the main vegetation in the area of each fire. In BIOBURN, these vegetation types are categorised into extratropical forest with organic soil, tropical forest, savanna, and peatland.

2.3.8 Comparison with satellite retrievals

Satellite retrievals provide the unique possibility to compare the global distribution of important atmospheric species. In Rosanka et al. (2021b) (here Chapter 6) and Rosanka et al. (2021c) (here Chapter 7), the modelling results are compared to satellite observations obtained from the Infrared Atmospheric Sounding Interferometer (IASI, Clerbaux et al., 2009) onboard the Metop-A (IASI-A) and Metop-B (IASI-B) satellites. This is achieved by using the submodel SORBIT (Jöckel et al., 2010), which samples the model's output along sun-synchronous satellite orbits at the time of the satellite overpass. In particular, the Fast Optimal Retrievals on Layers for IASI Ozone (FORLI-O_3, version 20151001; see Hurtmans et al. (2012), for a description of the retrievals) is used for comparison of tropospheric O_3 columns in Rosanka et al. (2021b) (here Chapter 6). The evaluation of simulation results against global observational datasets of VOC abundance can be performed for only a few species. In particular, VOC total columns have been retrieved globally from IASI, using the neural network-based approach Artificial Neural Network for IASI (ANNI, Franco et al., 2018). In Rosanka et al. (2021b) (here Chapter 6) and Rosanka et al. (2021c) (here Chapter 7), the modelled columns of methanol (CH_3OH) are compared to these retrievals. In addition, ANNI hydrogen cyanide (HCN) columns are used for the model evaluation in Rosanka et al. (2021c) (here Chapter 7). Due to the limited information on the vertical distribution of most VOCs that are contained in the IASI spectra, only total columns are available for the model evaluation. Since the neural network-based retrievals do not rely on scene-dependent a priori information, no averaging kernels are produced. The retrieved total columns can directly be compared to the model data such that SORBIT is not used when analysing CH_3OH and HCN.

Chapter 3

Importance of isomerization reactions for OH radical regeneration from the photo-oxidation of isoprene investigated in the atmospheric simulation chamber SAPHIR

Novelli, A., Vereecken, L., Bohn, B., Dorn, H.-P., Gkatzelis, G. I., Hofzumahaus, A., Holland, F., Reimer, D., Rohrer, F., Rosanka, S., Taraborrelli, D., Tillmann, R., Wegener, R., Yu, Z., Kiendler-Scharr, A., Wahner, A., and Fuchs, H.: Importance of isomerization reactions for OH radical regeneration from the photo-oxidation of isoprene investigated in the atmospheric simulation chamber SAPHIR, Atmospheric Chemistry and Physics, 20, 3333–3355, https://doi.org/10.5194/acp-20-3333-2020, 2020

General information:
The manuscript has been submitted on 4 September 2019 and it has been published on 20 March 2020. The supplemental material of this manuscript is presented in Appendix A.

Importance for this thesis and the author's contribution:
In this study, the importance of the isomerization reactions of isoprene peroxy radicals on the OH regeneration and gas-phase OVOC production is addressed. It therefore contributes to the assessment of the representation of gas-phase OVOC chemistry in global models. This is further discussed in Sect. 8.1.

I implemented the developed chemical mechanism into the global model EMAC and designed, performed, and analysed the global model simulations. I created all figures related to the global model results and wrote the global model description and parts of the model result section. Additionally, I contributed to the general discussion and proofread the manuscript. Further information and the contributions of all co-authors are available in the manuscript's 'Author contributions' section.

[1] `https://creativecommons.org/licenses/by/4.0/` (last access: 6 September 2020)

Atmos. Chem. Phys., 20, 3333–3355, 2020
https://doi.org/10.5194/acp-20-3333-2020

Atmospheric Chemistry and Physics Open Access EGU

Importance of isomerization reactions for OH radical regeneration from the photo-oxidation of isoprene investigated in the atmospheric simulation chamber SAPHIR

Anna Novelli[1], Luc Vereecken[1], Birger Bohn[1], Hans-Peter Dorn[1], Georgios I. Gkatzelis[1,a,b], Andreas Hofzumahaus[1], Frank Holland[1], David Reimer[1], Franz Rohrer[1], Simon Rosanka[1], Domenico Taraborrelli[1], Ralf Tillmann[1], Robert Wegener[1], Zhujun Yu[1,c], Astrid Kiendler-Scharr[1], Andreas Wahner[1], and Hendrik Fuchs[1]

[1]Forschungszentrum Jülich, Institute for Energy and Climate Research: Troposphere (IEK-8), 52425 Jülich, Germany
[a]now at: NOAA Earth Systems Research Laboratory, Boulder, Colorado 80305, USA
[b]now at: Cooperative Institute for Research in Environmental Sciences, Boulder, Colorado 80309, USA
[c]now at: Institute of Mass Spectrometry and Atmospheric Environment, Jinan University, Guangzhou 510632, China

Correspondence: Anna Novelli (a.novelli@fz-juelich.de)

Received: 4 September 2019 – Discussion started: 21 October 2019
Revised: 10 February 2020 – Accepted: 16 February 2020 – Published: 20 March 2020

Abstract. Theoretical, laboratory, and chamber studies have shown fast regeneration of the hydroxyl radical (OH) in the photochemistry of isoprene, largely due to unimolecular reactions which were previously thought not to be important under atmospheric conditions. Based on early field measurements, nearly complete regeneration was hypothesized for a wide range of tropospheric conditions, including areas such as the rainforest where slow regeneration of OH radicals is expected due to low concentrations of nitric oxide (NO). In this work the OH regeneration in isoprene oxidation is directly quantified for the first time through experiments covering a wide range of atmospherically relevant NO levels (between 0.15 and 2 ppbv – parts per billion by volume) in the atmospheric simulation chamber SAPHIR. These conditions cover remote areas partially influenced by anthropogenic NO emissions, giving a regeneration efficiency of OH close to 1, and areas like the Amazonian rainforest with very low NO, resulting in a surprisingly high regeneration efficiency of 0.5, i.e. a factor of 2 to 3 higher than explainable in the absence of unimolecular reactions. The measured radical concentrations were compared to model calculations, and the best agreement was observed when at least 50 % of the total loss of isoprene peroxy radicals conformers (weighted by their abundance) occurs via isomerization reactions for NO lower than 0.2 ppbv. For these levels of NO, up to 50 % of the OH radicals are regenerated from the products of the 1,6 α-hydroxy-hydrogen shift (1,6-H shift) of Z-δ-RO_2 radicals through the photolysis of an unsaturated hydroperoxy aldehyde (HPALD) and/or through the fast aldehydic hydrogen shift (rate constant $\sim 10\,s^{-1}$ at 300 K) in di-hydroperoxy carbonyl peroxy radicals (di-HPCARP-RO_2), depending on their relative yield. The agreement between all measured and modelled trace gases (hydroxyl, hydroperoxy, and organic peroxy radicals, carbon monoxide, and the sum of methyl vinyl ketone, methacrolein, and hydroxyl hydroperoxides) is nearly independent of the adopted yield of HPALD and di-HPCARP-RO_2 as both degrade relatively fast (< 1 h), forming the OH radical and CO among other products. Taking into consideration this and earlier isoprene studies, considerable uncertainties remain on the distribution of oxygenated products, which affect radical levels and organic aerosol downwind of unpolluted isoprene-dominated regions.

1 Introduction

The hydroxyl radical (OH) is the main daytime oxidant controlling the removal and transformation of gaseous pollutants in the atmosphere (Levy, 1974). Its high efficiency in the oxidation of trace gases is based on the effective regeneration of OH by radical chain reactions, in which nitric oxide (NO) is oxidized to nitrogen dioxide (NO_2), linking the OH chem-

istry to the formation of tropospheric pollutant ozone (O_3). Because high levels of OH radicals were observed in field experiments in mainly forested environments with large concentrations of isoprene (Tan et al., 2001; Ren et al., 2008; Hofzumahaus et al., 2009; Kubistin et al., 2010; Whalley et al., 2011), a large number of investigations over the last decade focused on OH-initiated isoprene chemistry, including laboratory and chamber studies (Crounse et al., 2011; Berndt, 2012; Wolfe et al., 2012; Fuchs et al., 2013; Teng et al., 2017; Berndt et al., 2019), theoretical calculations (Peeters et al., 2009, 2014; Da Silva et al., 2010; Peeters and Müller, 2010; 2014; Wang et al., 2018; Møller et al., 2019), and global model impact (Lelieveld et al., 2008; Taraborrelli et al., 2012; Bates and Jacob, 2019; Møller et al., 2019; Müller et al., 2019). The observed OH levels could only be explained if an OH radical regeneration mechanism exists independently of NO and thus without the formation of O_3. It is now widely accepted that unimolecular isomerization reactions of peroxy radicals (RO_2) formed during the oxidation of organic compounds can contribute to the regeneration of radicals, in particular if they become competitive against RO_2 radical losses via NO (Praske et al., 2018).

In OH-initiated isoprene oxidation, the first reaction step comprises the formation of six isoprene-RO_2 conformers from the addition of the OH radical to the terminal carbon atoms (C1 and C4, 0.91 total yield; Fig. 1), which are in equilibrium and can quickly inter-convert as first suggested in the Leuven isoprene mechanism (LIM) (Peeters et al., 2009) (Fig. 1). The concentration of the different conformers, which is affected by both their losses (unimolecular decomposition and reaction with NO and the hydroxyl and RO_2 radicals) and their re-equilibration, can have a large impact on the OH radical concentration. There are three different sets of reaction rate coefficients currently in use in the literature for equilibrium reactions between the isoprene-RO_2 conformers (Table 1), differing in the individual rate coefficients by up to a factor of 35. One set is from theoretical calculations in the LIM1 study (Peeters et al., 2014). A second set is currently in use within the Master Chemical Mechanism version 3.3.1 (MCMv3.3.1; Jenkin et al., 2015), whereby the rate coefficients are as described in LIM1 but all increased by a factor of 5. This change was prompted by preliminary results from Caltech (Crounse et al., 2014) and the review by one of the LIM1 authors (Peeters, 2015). Finally, Wennberg et al. (2018), in their recent review paper on the mechanism of isoprene degradation (Caltech mechanism), applied their experimentally optimized parameters, as reported by Teng et al. (2017) (Table 2).

Four of the six isoprene-RO_2 conformers can undergo atmospherically relevant isomerization reactions (Fig. 2). The β-RO_2 radicals directly reform OH radicals, together with the oxygenated organic products methacrolein (MACR), methyl vinyl ketone (MVK), and formaldehyde (HCHO), after a 1,5 hydroxy-hydrogen shift (1,5-H shift) (Da Silva et al., 2010) with a slow reaction rate constant (1.1×10^{-3} and $0.7 \times 10^{-3}\,s^{-1}$ at 298 K for OH addition on C4 and C1, respectively) (Peeters et al., 2014), making this reaction competitive only in the presence of exceptionally low NO levels (< 10 pptv).

Table 1. The rate coefficients for the addition of O_2 to OH-isoprene adducts and for the re-dissociation of isoprene-RO_2 (Fig. 1). The rate coefficients for the oxygen additions (kf; $cm^3\,s^{-1}$) are typically temperature-independent or provided at 298.15 K. The rate coefficients for the re-dissociations (kr; s^{-1}) are provided at 298.15 K. The temperature-dependent rate coefficients are given in Table S8.

	LIM1[a]	MCMv3.3.1[b]	Caltech[c]
kf1	0.1×10^{-12}	0.5×10^{-12}	0.4×10^{-12}
kf2	0.6×10^{-12}	3.0×10^{-12}	0.8×10^{-12}
kf3	0.6×10^{-12}	3.0×10^{-12}	0.8×10^{-12}
kf4	0.7×10^{-12}	3.5×10^{-12}	0.1×10^{-12}
kf5	0.4×10^{-12}	2.0×10^{-12}	0.2×10^{-12}
kf6	0.7×10^{-12}	3.5×10^{-12}	0.7×10^{-12}
kf7	0.7×10^{-12}	3.5×10^{-12}	0.7×10^{-12}
kf8	0.1×10^{-12}	0.5×10^{-12}	0.5×10^{-12}
kr1	4.0	20	18
kr2	0.4	2.0	1.8
kr3	0.05	0.3	0.3
kr4	5.0	24	25
kr5	0.7	3.6	11
kr6	0.2	0.1	0.2
kr7	0.03	0.2	0.3
kr8	0.1	0.6	4.3

[a] Peeters et al. (2014), [b] Jenkin et al. (2015), [c] Wennberg et al. (2018).

The most relevant isomerization reaction, the 1,6 α-hydroxy-hydrogen shift (1,6-H shift), occurs for the Z-δ-RO_2 radicals with a fast reaction rate coefficient (measured at 3.6 and $0.4\,s^{-1}$ at 298 K for OH addition on C4 and C1, respectively, by Teng et al. (2017). These experimental values are used directly within the Caltech mechanism and are in good agreement with the calculated rates in LIM1 (Peeters et al., 2014) (within 40 %). The MCMv3.3.1 is currently using rate coefficients slower by a factor of ~ 5 (Table 2). This change was suggested by one of the LIM1 authors (Peeters, 2015) to keep the phenomenological bulk isomerization rate in agreement with previous experimental results on the unsaturated hydroperoxy aldehyde (HAPLD; Fig. 2) formation (Crounse et al., 2011). Following the definition by Peeters et al. (2014), these phenomenological bulk isomerization rates (k(bulk 1,6-H)) are equal to the sum of the isomer-specific 1,6-H shift rate multiplied by its steady-state fraction weighted by their OH addition branching ratio.

One of the predicted (Peeters et al., 2009, 2014) and measured (Crounse et al., 2011; Berndt, 2012; Teng et al., 2017; Berndt et al., 2019) products following the 1,6-H shift is HPALD, which can photolyse, producing OH radicals (Peeters and Müller, 2010; Wolfe et al., 2012; Liu et al.,

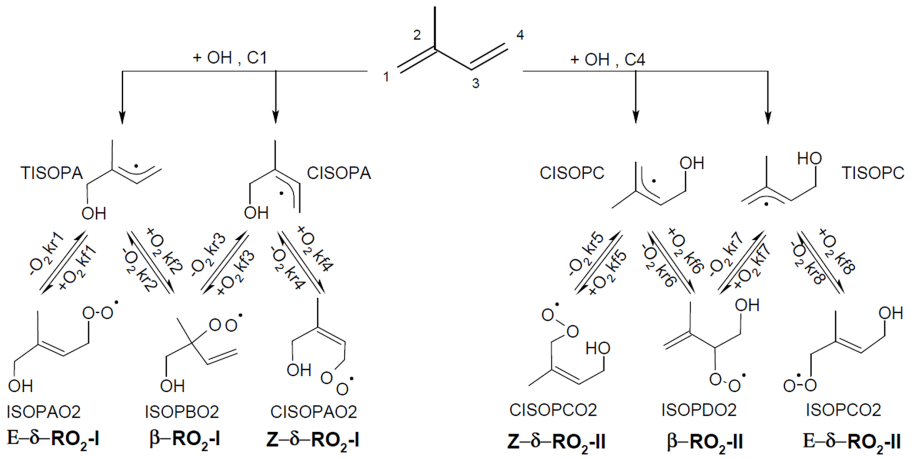

Figure 1. Schematic of the equilibrium reactions between OH-isoprene adducts and isoprene-RO_2 conformers, as well as their formation reactions. The names used for the different molecules are as in the MCMv3.3.1 (regular text) and in the LIM1 study (bold). The model-specific rate coefficients for each reaction are summarized in Table 1.

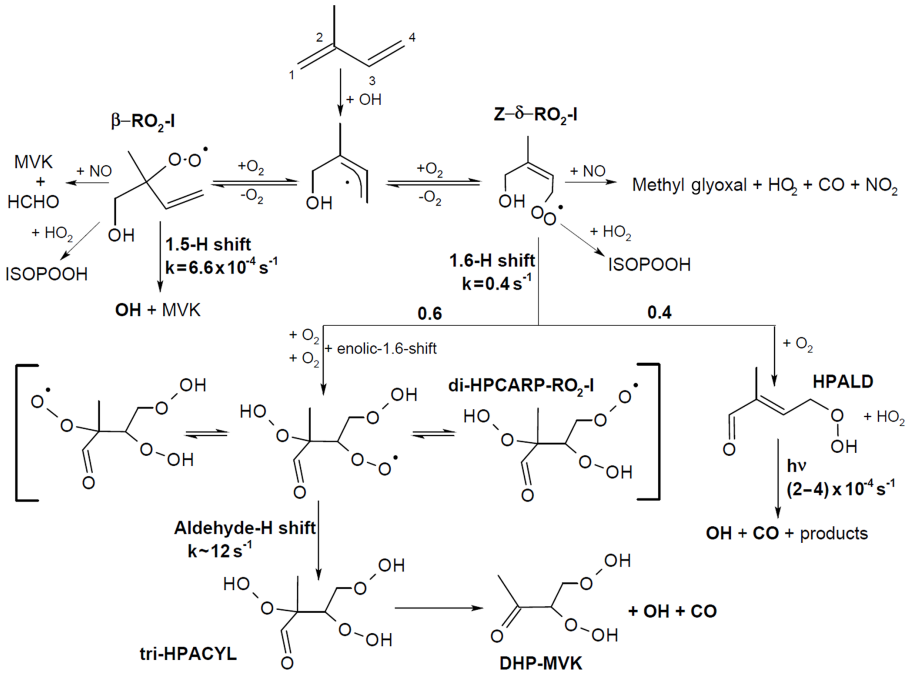

Figure 2. Simplified reaction schematic following OH addition to isoprene on the carbon C1. Only the most relevant reaction paths for OH radical formation are shown; the implemented mechanism includes all six isoprene-RO_2 isomers. The schematic illustrates the RO_2 unimolecular H shift reactions (1,5-, 1,6-, and aldehyde-H shifts), but all RO_2 species undergo competing reactions with NO, HO_2, and RO_2 radicals (not shown), and the reaction steps shown can represent multiple fast, sequential elementary reactions. The rate coefficients and yields shown are obtained from the theoretical work from this study and from recent experimental and theoretical studies. The same yields for the product of the 1,6-H shift, rate coefficient of the aldehyde-H shift, and photolysis frequencies for HPALD are applied to the chemistry following the OH addition on C4. All rate coefficients are shown for 298 K and a 30° solar zenith angle.

Table 2. Summary of the relevant differences for assessing the 1,6-H shift impact between available chemical models. All model versions within this work are based on the MCMv3.3.1 (accounting for chamber properties) with only specific rates and yields included in the table adapted from different studies. They also include the follow-up chemistry of di-HPCARP-RO_2 as theoretically investigated within this study.

Mechanism	$R + O_2 \rightleftarrows RO_2$	k 1,6-H shift (298 K)[a]	HPALD : di-HPCARP-RO_2 yield	k(bulk 1,6-H)[d] s^{-1}
LIM1	LIM1	0.5 (C1), 5.8 (C4)	0.5 : 0.5	0.008
MCMv3.3.1	LIM1 ×5	0.1 (C1), 1.2 (C4)[b]	0.5 : 0.5	0.002
Caltech	From Teng et al. (2017)	0.4 (C1), 3.6 (C4)	0.4 : 0.6	0.002
This work				
M0		No isomerization		n/a
M1	Caltech	Caltech	Caltech	0.002
M2	MCMv3.3.1	Caltech	Caltech	0.006
M3	MCMv3.3.1	Caltech	0.75 : 0.25[c]	0.006

[a] s^{-1}. [b] The same rate coefficient as in LIM1 reduced by a factor of 5. [c] Adapted from Berndt et al. (2019). [d] For the experimental concentration as observed in Fig. 4. n/a – not applicable

2017; Müller et al., 2019) (atmospheric lifetime of ~ 1 h). In addition, the formation of a di-hydroperoxy carbonyl peroxy radical (di-HPCARP-RO_2, Fig. 2) was predicted by theoretical calculations (Peeters et al., 2014) and inferred in a recent experimental study (Teng et al., 2017). Its fate is a fast unimolecular decomposition ($\sim 1\,s^{-1}$) with the formation of an OH radical (Wang et al., 2018; Møller et al., 2019) and suggested subsequent elimination of CO, as well as the formation of a di-hydroperoxy carbonyl compound (Peeters et al., 2014; Møller et al., 2019). Large uncertainties remain on the yield of these two products. One earlier experimental study proposes a yield for HPALD of the order of 0.04 with a factor of 2 uncertainty (Berndt, 2012). A more recent experimental study (Teng et al., 2017) suggests a total yield of HPALD of 0.4, distinguishing between β- (0.25) and δ-HPALD (0.15) with large uncertainties in the assignment of the latter; the remainder, 0.6, is assigned to di-HPCARP-RO_2 LIM0 (Peeters and Müller, 2010) and LIM1 (Peeters et al., 2014); both proposed a yield of ~ 0.5 for HPALD and di-HPCARP-RO_2. In contrast, a recent experimental study by Berndt et al. (2019) sets a lower limit of 0.75, with a recent addition (Müller et al., 2019) to the theoretical work within the LIM1 also rationalizing a much higher yield of HPALD (0.74) than previously reported in LIM1. In addition to the above products, both experimental (Berndt et al., 2019) and theoretical (Müller et al., 2019) studies suggest the formation of an hydroperoxy-epoxy-carbonyl compound (~ 0.15).

Both currently available explicit isoprene oxidation mechanisms, i.e. the Master Chemical Mechanism (MCMv3.3.1) (Jenkin et al., 2015) and the Caltech mechanism (Wennberg et al., 2018), use a yield of 0.5 and 0.4, respectively, for HPALD, with the Caltech mechanism distinguishing between β- (0.15) and δ-HPALD (0.25). In both models, the only other product formed from the 1,6-H shift is di-HPCARP-RO_2.

To summarize, recent experimental and theoretical studies agree that the most relevant isomerization reaction of isoprene peroxy radicals is the 1,6-H shift of Z-δ-RO_2. The following kinetic aspects control the impact of the 1,6-H shift of Z-δ-RO_2 on the regeneration of OH radicals and the production of oxygenated products:

- the equilibrium between the isoprene-RO_2 conformers, which determines the fraction of Z-δ-RO_2 radicals that can undergo fast 1,6-H shift isomerization;
- the temperature-dependent rate coefficient for the 1,6-H shift itself;
- the relative yields of HPALD and di-HPCARP-RO_2 formed following the 1,6-H shift; and
- the follow-up chemistry of HPALD and di-HPCARP-RO_2.

Despite intensive research as detailed above, there are significant differences between current chemical mechanisms (Table 2); i.e. different sets of rate coefficients are used for the equilibrium reactions, rate coefficients for the 1,6-H shift differ by up to a factor of 5, and the measured yield of HPALD ranges from 0.4 to 0.75.

In this work, new chamber experiments have been performed to test our understanding of the photo-oxidation of isoprene. The experiments are used to test the ability of the explicit mechanisms in MCMv3.3.1 to predict OH radical regeneration from isoprene oxidation over a wide range of NO concentrations (0.15 to 2 ppbv). The chemistry of di-HPCARP-RO_2 has been investigated (Novelli et al., 2018a) with high levels of theory, in particular to confirm the role of these radicals in OH radical formation. Model sensitivity studies are applied to identify the isoprene-RO_2 conformer equilibrium constants, the 1,6-H shift rate constant, and the HPALD/di-HPCARP-RO_2 branching ratio that provide the best description of the observed radical and trace gas concentrations. The global impact of the optimized isoprene mechanism on the OH radical concentration is shown.

2 Methods

2.1 Quantum chemical and theoretical kinetic calculations

The reactants, transition states, and products in the studied mechanistic branches of the isoprene chemistry were characterized at the M06-2X and CCSD(T) levels of theory. The conformer space for each of these structures was characterized at the M06-2X/cc-pVDZ level of theory (Dunning, 1989; Zhao and Truhlar, 2008; Alecu et al., 2010; Bao et al., 2017), locating ∼ 24 000 distinguishable structures from ∼ 60 000 systematically generated starting geometries. The most relevant conformers (∼ 850 structures across all reactions examined) were then fully re-optimized at the M06-2X/aug-cc-pVTZ level of theory (Dunning, 1989). The number of conformers re-optimized at this higher level of theory differs per structure (see Table S1 in the Supplement), but enough were included to cover over ∼ 80 % of the thermal population at 300 K. Intrinsic reaction coordinate (IRC) calculations were performed on the lowest transition state (TS) to verify the nature of the transition state and to provide the energies used for Eckart tunnelling corrections. Finally, single-point energy calculations at the CCSD(T)/aug-cc-pVTZ level of theory (Purvis and Bartlett, 1982) were performed on the energetically lowest-lying geometries of each structure to further refine the energy barrier estimates. The thermal rate coefficients were then obtained using multi-conformer transition state theory (MC-TST) incorporating the energetic and rovibrational characteristics of all conformers (Vereecken and Peeters, 2003). Temperature-dependent rate coefficients are derived for the temperature range between 200 and 400 K, and both isomer-specific and bulk phenomenological rate coefficients are provided; the latter incorporate the effect of fast H scrambling in the hydroperoxide-peroxy radical isomers. See the Supplement for a more detailed description of the methodologies involved.

2.2 Atmospheric simulation chamber SAPHIR and experimental procedure

The experiments were conducted in the atmospheric simulation chamber SAPHIR at Forschungszentrum Jülich, Germany. The SAPHIR chamber is designed for the investigation of oxidation processes under atmospheric conditions in a controlled environment. SAPHIR is made of a double-wall Teflon (FEP) film that is inert, has a high transmittance for solar radiation (Bohn and Zilken, 2005), and is equipped with a shutter system that is opened during photolysis experiments, allowing solar radiation to penetrate the chamber. The synthetic air provided to the chamber is mixed from ultra-pure nitrogen and oxygen (Linde, > 99.99990 %). Two fans in the chamber ensure complete mixing of trace gases within 2 min. The pressure in the chamber is slightly higher than ambient (∼ 30 Pa) to avoid external air penetrating the chamber. Due to small leakages and air consumption by instruments, trace gases are diluted at a rate of $\sim 6\,\%\,h^{-1}$ due to the replenishment flow. More details regarding the chamber can be found elsewhere (Rohrer et al., 2005; Poppe et al., 2007; Schlosser et al., 2007).

The chamber was cleaned before the experiments by exchanging the chamber air 8 to 10 times with pure synthetic air. Evaporated Milli-Q® water was then introduced into the dark chamber by a carrier flow of synthetic air until a concentration of $\sim 5 \times 10^{17}$ cm^{-3} of water vapour was reached. In order to keep the concentration of NO as small as possible after the opening of the shutters, ozone produced by a silent discharge ozonizer (O3onia) was added in the chamber to reach ozone mixing ratios up to 100 ppbv. For experiments at higher concentrations of NO, NO was injected from a gas mixture (Linde, 500 ppm NO in N_2) into the chamber by a mass flow controller. After opening the shutter system of the chamber, nitrous acid (HONO) was photochemically formed on the Teflon surface and released into the chamber (Rohrer et al., 2005), and its subsequent photolysis produced OH radicals and NO. Afterwards, isoprene was injected three times at intervals of about 2 h directly from the liquid (99 % purity, Sigma Aldrich). The aim was to reach ∼ 6 ppbv of isoprene in the chamber after each injection (which corresponds to an OH reactivity between 12 and 15 s^{-1}). Experiments were designed such that chamber-specific sinks (dilution and wall loss of trace gases), and sources of trace gases that are formed in the sunlit chamber, except for nitrous acid, did not influence the results.

2.3 Instrumentation

Table 4 summarizes the instruments available during the experiment, giving time resolution, accuracy, and precision for each instrument. The concentrations of OH, HO_2, and RO_2 radicals were measured with the laser-induced fluorescence (LIF) instrument permanently in use at the SAPHIR chamber and described previously (Holland et al., 2003; Fuchs et al., 2011). Several studies have been recently published showing the presence of an interference in OH radical detection with the LIF for ambient measurements in some environments (Mao et al., 2012; Novelli et al., 2014; Rickly and Stevens, 2018). The interference depends on the chemical conditions of the sampled air and on the geometry of the different instruments. A laboratory study performed with this LIF instrument (Fuchs et al., 2016) showed only interferences for high ozone concentrations (300–900 ppbv) together with biogenic volatile organic compound (BVOC) concentrations up to 450 ppbv, which are far beyond any condition encountered in this study. Therefore, the OH radical concentration measured by the LIF instrument in this study is considered free from interferences. In addition, OH was measured by differential optical absorption spectroscopy (DOAS) (Dorn et al., 1995) for some of the experiments shown within this study. Numerous inter-comparisons between the LIF and the DOAS

Table 3. Stereospecific rate coefficients (s^{-1}) at 300 K for the relevant reactions of di-HPCARP-RO_2-I. The temperature dependence is given as a Kooij expression, $k(T) = A \cdot T^n \cdot \exp(-E_a/T)$, for the temperature range 200–400 K. The effective bulk rates of reactions are also given, accounting for hydroperoxide H-atom scrambling and aldehyde H migration across all channels. The bottom expression averages the stereospecific rate coefficients for use in simplified models.

Reaction	k (300 K)	A (s^{-1})	n	E_a (K)
(2R,3R)-2-Me-3,4-diOOH-butanal-2-peroxyl (A)				
1,4-aldehyde-H migration to D	1.15×10^{0}	1.21×10^{-83}	30.69	−4811
1,4-α-OOH-H migration	1.18×10^{-5}	4.59×10^{-82}	28.94	−3276
1,5-α-OOH-H migration	4.88×10^{-3}	2.87×10^{-35}	15.11	3586
1,6-OOH-H migration to B	1.84×10^{4}	7.26×10^{-40}	15.39	−3656
1,7-OOH-H migration to C	6.29×10^{4}	2.75×10^{-25}	10.85	−1725
HO_2 elimination	$\leq 1 \times 10^{-7}$			
(2R,3R)-2-Me-2,4-diOOH-butanal-3-peroxyl (B)				
1,5-aldehyde-H migration to D	3.34×10^{1}	1.12×10^{-67}	25.15	−4273
1,6-OOH-H migration to A	2.97×10^{4}	1.36×10^{-38}	14.73	−4035
1,6-OOH-H migration to C	1.88×10^{4}	1.17×10^{-34}	13.27	−3683
(2R,3R)-2-Me-2,3-diOOH-butanal-4-peroxyl (C)				
1,6-aldehyde-H migration to D	2.28×10^{0}	3.57×10^{-41}	16.93	788
1,7-OOH-H migration to A	2.35×10^{3}	3.06×10^{-33}	13.03	−2486
1,6-OOH-H migration to B	1.27×10^{4}	1.35×10^{-22}	9.96	−906
(2R,3S)-2-Me-3,4-diOOH-butanal-2-peroxyl (A′)				
1,4-aldehyde-H migration to D′	3.71×10^{0}	7.07×10^{-75}	27.88	3914
1,4-α-OOH-H migration	8.44×10^{-5}	2.52×10^{-68}	24.59	−18.17
1,5-α-OOH-H migration	5.02×10^{-2}	8.69×10^{-27}	12.33	3989
1,6-OOH-H migration to B′	6.34×10^{4}	7.94×10^{-17}	7.46	−1680
1,7-OOH-H migration to C′	6.20×10^{4}	4.02×10^{-20}	9.43	−579
HO_2 elimination	$\leq 1 \times 10^{-7}$			
(2R,3S)-2-Me-2,4-diOOH-butanal-3-peroxyl (B′)				
1,5-aldehyde-H migration to D′	3.05×10^{-1}	4.28×10^{-75}	28.30	−25.89
1,6-OOH-H migration to A′	2.07×10^{3}	7.58×10^{-19}	7.91	−1277
1,6-OOH-H migration to C′	1.32×10^{3}	4.40×10^{-22}	9.34	−926
(2R,3S)-2-Me-2,3-diOOH-butanal-4-peroxyl (C′)				
1,6-aldehyde-H migration to D′	4.86×10^{1}	6.99×10^{-37}	15.20	−133
1,7-OOH-H migration to A′	9.89×10^{2}	7.65×10^{-28}	11.39	−1308
1,6-OOH-H migration to B′	1.52×10^{3}	6.68×10^{-28}	11.93	−558
(2R,3R)-2-Me-2,3,4-diOOH-1-oxo-1-butyl (D)				
CO elimination	1.40×10^{8}	1.02×10^{13}	0.38	4004
(2R,3S)-2-Me-2,3,4-diOOH-1-oxo-1-butyl (D′)				
CO elimination	2.40×10^{8}	3.63×10^{15}	−0.41	4261
(2R,3R)-2-Me-diOOH-butanalperoxyl (A+B+C)				
Effective aldehyde H migration to D	5.03×10^{0}	8.43×10^{-71}	26.62	−3342
(2R,3S)-2-Me-diOOH-butanalperoxyl (A′ + B′ + C′)				
Effective aldehyde H migration to D′	2.76×10^{1}	5.04×10^{-35}	14.43	3
2-Me-diOOH-butanalperoxyl aldehyde H migration*	11.8	6.52×10^{-53}	20.52	−1669

* Average of the data for (2R,3R) and (2R,3S) conformers.

instrument in the SAPHIR chamber (Schlosser et al., 2007, 2009; Fuchs et al., 2012) showed very good agreement between these two instruments, giving high reliability to the OH radical measurements performed in the chamber. For the experiments within this study, a slope of 1.1 for the scatter plot of DOAS OH vs. LIF OH was obtained, with a correlation coefficient, R^2, of 0.94.

Several studies have proven that RO_2 radicals can cause an interference signal in the HO_2 radicals measured by conversion to OH after reaction with an excess of NO (Fuchs et al., 2011; Hornbrook et al., 2011; Whalley et al., 2013; Lew et al., 2018). It was shown that a reasonable approach for avoiding the interference is to lower the concentration of NO reacting with the sampled air inside the instrument. During this study, the NO concentration used was low ($\sim 2.5 \times 10^{13}$ cm^{-3}) to minimize the possibility of an interference as described in Fuchs et al. (2011). Still, as the RO_2 radicals which originate from the oxidation of isoprene by OH radicals are those able to quickly convert, despite the low NO used, interference from RO_2 radicals was still observed. Tests performed on the LIF instrument used for this study showed that, for the conditions the instrument was used in during the experiments, an interference of $\sim 30\,\%$ was observed for isoprene-RO_2. As such, the HO_2 radical measurement was defined as HO_2^* to indicate the presence of interference from RO_2 radicals. As the measured RO_2 concentration is obtained from the difference between measured RO_x (OH+HO_2+RO_2) and HO_2 radicals, the obtained RO_2 radicals are also underestimated due to the interference observed in the HO_2 measurement and will be marked as RO_2^*. The OH reactivity (k_{OH}), the inverse lifetime of OH, was measured by a pump-and-probe technique coupled with a time-resolved detection of OH by LIF (Lou et al., 2010; Fuchs et al., 2017). Isoprene and the sum of MVK and MACR were measured by a proton-transfer-reaction time-of-flight mass spectrometer (PTR-TOF-MS; Lindinger et al., 1998; Jordan et al., 2009) and a gas chromatography system (GC; Wegener et al., 2007). As the PTR-TOF-MS and the GC were calibrated only for the species listed in Table 4, concentrations for other species were not available. Carbon monoxide (CO), carbon dioxide (CO_2), methane (CH_4), and water vapour were measured by an instrument applying cavity ring-down spectroscopy (CRDS; Picarro). NO and nitrogen dioxide (NO_2) were measured by chemiluminescence (CL; Ridley et al., 1992) and O_3 by UV absorption (Ansyco). Photolysis frequencies were calculated from measurements of solar actinic radiation by a spectroradiometer (Bohn et al., 2005; Bohn and Zilken, 2005).

2.4 Model calculations

The measured radicals and trace gases were modelled with a zero-dimensional box model using chemical mechanistic information from the Master Chemical Mechanism downloaded via the following website: http://mcm.leeds.ac.uk/MCM (last access: November 2019). The MCMv3.3.1 was released in 2015 with newly updated isoprene chemistry in line with LIM1 chemistry, updated and/or optimized to recent experimental results, as described in Jenkin et al. (2015). The most relevant changes for this study are the inclusion of the equilibrium reactions between the OH-isoprene adducts and isoprene-RO_2 (Fig. 1) and the inclusion of isomerization reactions for isoprene-RO_2 radicals (Table 2). Further, the OH addition to central carbon atoms (C2 and C3, Fig. 1) and following chemistry was implemented.

Several chamber-specific properties were implemented in the model. First, a dilution rate was applied to all the trace gases present in the model to account for dilution from the replenishing flow of the chamber. The background production of HONO and HCHO known to occur in the sunlit chamber (Rohrer et al., 2005; Karl et al., 2006) was parameterized by an empirical function that depends on temperature, relative humidity, and solar radiation. For the experiments shown in this study, the background OH reactivity in the chamber was at most 1 s^{-1} and was parameterized with a co-reactant Y added to the model, which converts OH to HO_2 in the same way as CO does (Fuchs et al., 2012, 2014; Kaminski et al., 2017). The concentration of Y was adjusted to match the observed OH reactivity during the zero-air phase of the experiment and was kept constant throughout the experiment. As shown in a previous study (Novelli et al., 2018b), the unknown chemical nature of the background reactivity that dominates the loss of OH radicals for the zero-air phase of the experiment has a negligible impact once the main reactant, in this case isoprene, is added, with total OH reactivity as high as 20 s^{-1}.

Photolysis frequencies for O_3, NO_2, HONO, hydrogen peroxide (H_2O_2), formaldehyde (HCHO), acetone, glyoxal, MVK, and MACR were constrained to values calculated from the measured actinic flux. For HPALD and peroxy acid aldehyde (PACALD), photolysis frequencies of MACR scaled up by a factor of 100 and 2, respectively, were used (Fuchs et al., 2013). All the other photolysis frequencies present in the model were first calculated for clear-sky conditions according to the MCMv3.3.1 and then scaled by the ratio of measured to calculated $j(NO_2)$ to account for clouds and transmission of the chamber film. The model was constrained to measured chamber pressure (ambient pressure) and temperature, as well as water vapour, NO, NO_2, and O_3 concentrations. Model values were re-initiated at 1 min intervals. Isoprene injections were implemented in the model by applying an isoprene source only active at the time of the injection, adjusted in strength to reproduce the observed change in OH reactivity at the injection time. The modelled OH reactivity used for comparison against the measurement is the total modelled OH reactivity excluding the reactivity of isoprene hydroxy hydroperoxides (ISOPOOHs) (Fig. 2), as for these compounds the OH radicals are recycled at a timescale much shorter than the OH lifetime observed in the k_{OH} instrument, negating their measurable OH reactiv-

Table 4. Instrumentation for radical and trace gas quantification during the oxidation experiment.

	Technique	Time resolution	1σ precision	1σ accuracy
OH	LIF	47 s	0.3×10^6 cm^{-3}	13 %
OH	DOAS	200 s	0.8×10^6 cm^{-3}	6.5 %
HO_2^* and RO2*	LIF	47 s	1.5×10^7 cm^{-3}	16 %
k_{OH}	Laser photolysis + LIF	180 s	0.3 s^{-1}	10 %
NO	Chemiluminescence	180 s	4 pptv	5 %
NO_2	Chemiluminescence	180 s	2 pptv	5 %
O_3	UV absorption	10 s	1 ppbv	5 %
Isoprene, MVK+MACR	PTR-TOF-MS	30 s	> 15 pptv	< 14 %
Isoprene, MVK+MACR	GC	30 min	4 %–8 %	5 %
CO	CRDS	60 s	1.5 ppbv	1 %
Photolysis frequencies	Spectroradiometer	60 s	10 %	10 %

ity. Measurements of MVK and MACR by PTRMS and GC are affected by interferences from ISOPOOHs (Rivera-Rios et al., 2014). For this reason the measured data are compared with the sum of MVK and MACR together with ISOPOOHs (all isomers); the same sensitivity for MVK, MACR, and ISOPOOHs is assumed. Due to RO_2 interference in the HO_2 measurement, modelled HO_2 concentrations increased by a small fraction of modelled RO_2 (30 % of RO_2 radicals from isoprene and 10 % of RO_2 radicals from MVK and MACR; Fuchs et al., 2013). Likewise, the measured RO_2^* values are compared against the difference between modelled RO_x and HO_2^*, rather than the uncorrected RO_2 concentrations, to account for this interference.

The chemistry of di-HPCARP-RO_2-I and di-HPCARP-RO_2-II, originating from the addition of the OH radical on C1 and C4, respectively, is implemented in the model based on our explicit study of the di-HPCARP-RO_2-I reactions, and the chemistry for di-HPCARP-RO_2-II could thus need refining in future work (see also below).

This model (MCMv3.3.1, Table 2) served as the basis of all model calculations done in this work, with variations as defined below. Table 2 summarizes the additional model runs performed.

- M0 was constructed by removing all isomerization reactions (no isomerization, Table 2) from the MCMv3.3.1 model (see the Supplement and Table S2).

- M1 (Caltech, Table 2) was built by using the rate coefficients for the reversible addition of O_2 to OH-isoprene adducts, the rate coefficient for the 1,6-H shift of Z-δ-RO_2 radicals, and the relative yield of HPALD/di-HPCARP-RO_2, as applied in the Caltech mechanism (Table S3).

- M2 is the same as M1 but using the rate coefficients for the reversible addition reactions of O_2 to OH-isoprene adducts as applied in the MCMv3.3.1 (Tables 2 and S4).

- M3 is identical to M2 but using a relative yield of HPALD/di-HPCARP-RO_2 of 0.75 : 0.25 adapted from Berndt et al. (2019) (Tables 2 and S5).

Within this study only δ-HPALD (called HPALD) and its following chemistry are included in the different models. For M1 and M2 the sum of the δ- and β-HPALD yield is used as HPALD (Table S4). The identification of β-HPALD and its following chemistry is uncertain, but within the Caltech mechanism it will form the same products as formed from δ-HPALD, albeit with large uncertainties on the yields and rate coefficients (Wennberg et al., 2018) and without an experimentally accessible way to distinguish between the two within this study. Following the same reasoning, within the M3 model, we do not include the hydroperoxy-epoxy-carbonyl compound; as its chemistry cannot be univocally probed, its yield is comparatively small ($\sim$ 15 %, see above), and it has little influence on the topics investigated in this work.

2.5 Global model

The ECHAM–MESSy Atmospheric Chemistry (EMAC) model is a numerical chemistry and climate simulation system that includes submodels describing tropospheric and middle atmosphere processes and their interaction with oceans, land, and human influences (Jöckel et al., 2010). It uses the second version of the Modular Earth Submodel System (MESSy2) to link multi-institutional computer codes. The core atmospheric model is the fifth-generation European Centre Hamburg general circulation model (ECHAM5) (Roeckner et al., 2006). For the present study we applied EMAC (ECHAM5 version 5.3.02, MESSy version 2.53.0) in the T106L31ECMWF resolution, i.e. with a spherical truncation of T106 (corresponding to a quadratic Gaussian grid of approximately 1.1 by 1.1° in latitude and longitude) with 31 vertical hybrid pressure levels up to 10 hPa. The applied model setup comprised the submodel MECCA (Module Efficiently Calculating the Chemistry of the Atmosphere) to calculate atmospheric chemistry using the Mainz Organic

Mechanism (MOM) (Sander et al., 2011). The mechanism was adapted to the changes proposed in this study (Table S7). In addition, the submodel MEGAN (Model of Emissions of Gases and Aerosols from Nature) was used to simulate biogenic emissions of tracers, including isoprene (Guenther et al., 2006). Global isoprene emissions were scaled to 595 Tg yr^{-1}, which is the best estimate by Sindelarova et al. (2014). The model was run for 1.5 years (summer 2011–2012), during which the first half-year was used as spin-up and 2012 was used for analysis.

3 Theoretical work on isoprene di-HPCARP-RO_2-I

3.1 Kinetics of the di-HPCARP-RO_2 H-migration reactions

The di-HPCARP-RO_2 chemistry was studied in more detail compared to earlier published work (Wang et al., 2018; Møller et al., 2019), with more reliable kinetic methodologies, to obtain the isomer-specific rate coefficients, the phenomenological (bulk) rate coefficients, and the subsequent chemistry. Table 3 lists the rate coefficients at 300 K and the Kooij expressions for the key reactions in the di-HPCARP-RO_2-I reaction system for the temperature range 200–400 K. As expected from the higher energy barriers and entropic considerations, the migration of non-aldehyde H atoms is not competitive, nor is HO_2 elimination. The fastest reactions are, for all di-HPCARP-RO_2-I intermediates, the hydroperoxide-H scrambling across all peroxyl sites. This result is anticipated, as fast scrambling has been known for several years (Miyoshi, 2011; Jorgensen et al., 2016; Knap and Jorgensen, 2017; Møller et al., 2019; Praske et al., 2019). Given that these reactions outrun the next fastest reaction by over an order of magnitude, it can be assumed that the different di-HPCARP-RO_2-I isomers are in steady-state equilibrium and can be considered a unified pool of reactants in atmospheric models for the purpose of unimolecular reactivity. The 1,4-aldehyde-H-migration reaction is comparatively slow owing to its higher energy barrier (see Table S1, Fig. 3), and the formation of the tri-hydroperoxide acyl radical tri-HPACYL will thus occur mostly by 1,5- and 1,6-H migration in the di-HPCARP-RO_2-I reactant pool. Table 3 lists the rate coefficients of the elementary processes, but for atmospheric modelling the more relevant numbers are the bulk $k(T)$ expressions that account for the H scrambling and the combined flux across the 1,4-, 1,5-, and 1,6-H migrations listed at the bottom of the table. The stereospecific rate coefficients are not all that different and can be expressed within a factor of 2 to 3 as a single Kooij expression across the temperature range 200–400 K as follows (see also Fig. S1 in the Supplement):

$$k(T) = 6.5 \times 10^{-53} T^{20.5} \exp\left(\frac{1700\,\mathrm{K}}{T}\right). \quad (1)$$

The effective rate of acyl radical formation by aldehyde-H migration, i.e. accounting for the rapid re-equilibration across the di-HPCARP-RO_2-I isomers and the different H shift channels, is then of the order of 10 s^{-1} at 300 K. For the (2R, 3R) and (2S, 3S) stereoisomers, 63 % of the reaction flux at 300 K passes through the 1,5-aldehyde-H migration, with 35 % undergoing a 1,6-H migration. For the (2R, 3S) and (2S, 3R) isomers, 1,6-aldehyde-H migration constitutes over 99 % of the acyl radical formation. The estimated uncertainty on the rate coefficient is about a factor of 5, mostly due to the current use of non-conformer-specific tunnelling.

3.2 Elimination of CO from tri-hydroperoxy acyl radicals

It has been assumed in most models in the literature (Peeters et al., 2009, 2014; Jenkin et al., 2015; Wennberg et al., 2018) that the tri-hydroperoxy acyl radical formed, tri-HPACYL, will eliminate CO, followed by OH elimination and the formation of a di-hydroperoxy carbonyl compound, DHP-MVK (Fig. 3). All these models seem to be based ultimately on an estimate by Peeters et al. (2014), who predicted that the reaction would proceed via a 1,4-H shift, forming tri-HPACYL intermediates with an internal energy of the order of 22–25 kcal mol^{-1}, rapidly losing CO with a barrier $\leq$ 7 kcal mol^{-1}. This work, however, shows that these predicates do not represent the chemistry accurately, and the fate of tri-HPACYL must be examined in more detail.

The lower energy barriers of the effective aldehyde-H-migration processes imply that the acyl radical tri-HPACYL is formed with a significantly lower energy content, 17–19 kcal mol^{-1}, than estimated by Peeters et al. (2014), reducing the likelihood of chemically activated decomposition. Note that the H-migration reactions are typically found to be in the high-pressure limit (Miyoshi, 2012; Peeters et al., 2014; Xing et al., 2018; Møller et al., 2019), and multi-step chemical activation does not contribute significantly. Furthermore, we found that the CO elimination barrier in tri-HPACYL-I, $\sim$ 8 kcal mol^{-1} (see Table S1), is higher than estimated by Peeters et al. (2014) ($\leq$ 7 kcal mol^{-1}), further hampering prompt decomposition. With only $\sim$ 10 kcal mol^{-1} excess internal energy, as opposed to 15–18 kcal mol^{-1} as proposed by Peeters et al. (2014), a significant fraction of the nascent acyl radical tri-HPACYL could be thermalized, and the resulting slower decomposition process could potentially allow for O_2 addition on the acyl radical site. However, based on MC-TST calculations incorporating all conformers, we found that thermal decomposition of the tri-HPACYL-I acyl radicals is still sufficiently fast to dominate over O_2 addition; i.e. even when assuming a Boltzmann energy distribution, the predicted rate coefficient of $\sim 2 \times 10^8$ s^{-1} at 300 K (see Table 3) is significantly higher than the effective O_2 addition rate for acyl radicals, experimentally measured at $\leq\sim 3 \times 10^7$ s^{-1} in atmospheric conditions (Sehested et al., 1998; Blitz et al., 2002; Park et al.,

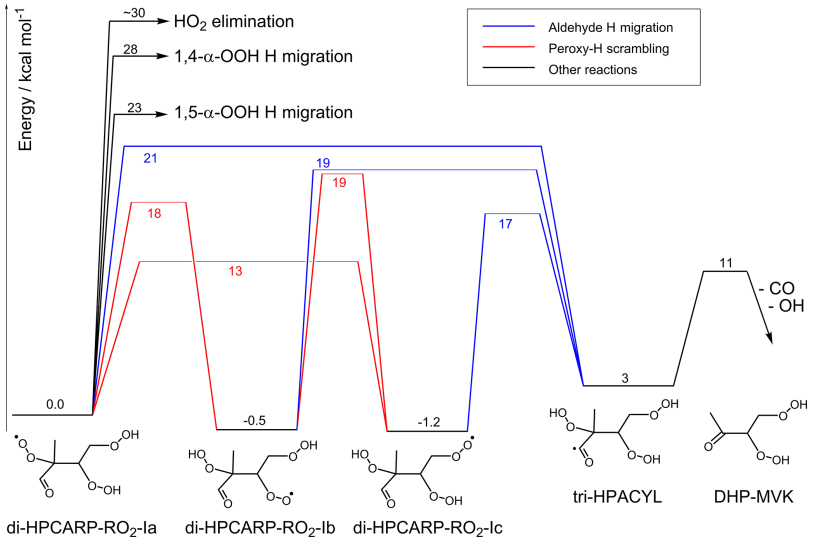

Figure 3. Potential energy surface for the aldehyde-H shift reaction showing the multiple competing reactions. A set of fast H-migration reactions ultimately leads to the formation of a tri-hydroperoxy acyl radical, tri-HPACYL. The main fate of this radical is shown by explicit theoretical calculations to be CO elimination, forming DHP-MVK; O_2 addition to a tri-hydroperoxy acylperoxy radical has only a minor contribution.

2004; Baulch et al., 2005; Atkinson et al., 2006; Carr et al., 2011). One could counter that the presence of –OOH groups might stabilize the acylperoxy radicals formed in the O_2 addition (e.g. by H bonding), thus increasing the addition rate coefficient above those reported for the smaller acyl radicals in the literature. Sample calculations on a smaller proxy with substituted acetyl radicals (see Table S1) revealed no evidence that a hydroperoxide group interacts with the oxygen atom moiety in a way that reduces the entrance energy barrier (thus increasing the capture rate coefficient) or stabilizes the adduct (thus reducing re-dissociation). From these results, we conclude that CO elimination will be the dominant fate at 300 K for the tri-HPACYL-I acyl radicals formed in aldehyde-H migration, with O_2 addition as a minor channel. Whether CO elimination occurs promptly or in a thermal reaction is then a moot issue.

Based on a preliminary version of our results (Novelli et al., 2018a), Peeters and coworkers (Müller et al., 2019) now suggest that tri-HPACYL-II acyl radicals (differing from the case I acyl radical by the position of the methyl group) would not eliminate CO due to a higher CO elimination energy barrier (Méreau et al., 2001) compared to the tri-HPACYL-I acyl radicals we explicitly characterized above. We have as yet been unable to dedicate the required significant computational resources for an explicit study of di-HPCARP-RO_2-II and tri-HPACYL-II, so this issue cannot be resolved at this time. We can, however, estimate the tri-HPACYL-II thermal CO elimination rate by assuming that case I and case II reactions are entropically similar and increasing the barrier for tri-HPACYL-II by the difference between a tertiary (case I) and secondary (case II) product radical as calculated by Méreau et al. (2001). The obtained rate coefficients at 298 K ($\sim 6 \times 10^6\ s^{-1}$ for the (R, R) and (S, S) stereoisomers; $\sim 1 \times 10^7\ s^{-1}$ for the (R, S) and (S, R) stereoisomers) remain competitive against O_2 addition. Though these channels appear no longer truly dominant thermally, CO elimination from tri-HPACYL-II can clearly not be discounted with any degree of confidence based on such estimates, especially as any chemical activation afforded by the preceding H migration would further shift the subtle competition towards higher CO yields. Quantifying this yield theoretically would be a very committed effort, as it requires explicit calculation of the full conformation space, with chemical activation depending on the energy-specific state density, conformer-specific tunnelling, and collisional energy transfer across the thousands of di-HPCARP-RO_2-II and tri-HPACYL-II conformers; this is beyond the scope of the current paper. Therefore, to keep the model simple and for lack of better information, the same aldehyde-H shift is implemented for both HPCARP-RO_2 isomers, both followed by the formation of CO, OH radicals, and DHP compounds.

3.3 Comparison to literature theoretical work

Two earlier studies examined the di-HPCARP-RO_2 chemistry theoretically. A first study by Wang et al. (2018) was based on a partial characterization of the conformational

space. While some of the provided rate coefficients are comparable to our values, these predictions carry a larger uncertainty due to the limited number of conformers examined, and differences of over an order of magnitude are found compared to our predictions, leading to qualitative changes in the predicted fate of the intermediates. The methodology of the second study, by Møller et al. (2019), is more comparable to that used in our work, with the main difference being the methodology used to screen the conformational space and select the conformers included in the rate calculations. As discussed in more detail in the Supplement, we find that this study only incorporates half or less of the population in the kinetic predictions, relying on the cancellation of error to a far greater extent than our more rigorous population description. Though for most reactions the differences in the predicted rate coefficient at 298 K are small, we find some values that differ by about an order of magnitude. We surmise that this is mostly due to the impact of the population truncation in the Møller et al. (2019) study compared to the full population used our work (e.g. 11 conformers versus ~ 1500 conformers included), making our predictions more robust in this respect. Improved conformer screening methodologies, balancing completeness and accuracy against computational cost, will help to converge the results of the two similar methodologies; this is discussed briefly in the Supplement.

4 Comparison of measured trace gases with model calculations

Figure 4 shows the evolution of trace gas concentrations for an experiment with three separate injections of isoprene and for which the NO concentration was below 0.15 ppbv for the entire duration of the experiment. For all three isoprene injections it is possible to observe large discrepancies between measured trace gases and model calculations when using the MCMv3.3.1 or the M1 model. Both models underestimate the measured OH radical concentration with a ratio of measured to model data of 0.7 ± 0.07 and overestimate the measured sum or MVK, MACR, and hydroxyl hydroperoxides (ISOPOOHs; Fig. 2) by almost a factor of 2. The similarity between the two models, despite M1 including a factor of 3 faster 1,6-H shift, is due to the different distribution of the isoprene-RO_2 conformers. Specifically, a much smaller fraction of Z-δ-RO_2 radicals for M1, ~ 0.004, is formed compared with 0.015 for the MCMv3.3.1 model, thus reducing the contribution of the 1,6-H shift. Although a larger fraction of Z-δ-RO_2 radicals are formed within the MCMv3.3.1 model, the slow 1,6-H shift used also results in an underestimation of the OH radical concentrations. For both models, for conditions under which the NO concentration is lower than 0.2 ppbv, i.e. under which isomerization reactions should become more relevant, $\sim 30\,\%$ of the total loss of isoprene-RO_2 conformers (weighted by their abundance) occurs via isomerization reactions. Compared with a simulation without isomerization reactions (M0) there is an improvement in the reproduction of the measured trace gases, but still the importance of the isomerization reactions is underestimated. The best agreement between measured and modelled trace gases was achieved when the equilibrium reactions between the isoprene-RO_2 conformers providing a larger fraction of Z-δ-RO_2 radicals in combination with the faster 1,6-H shift were used (M2, Fig. 5). Ratios of measured to modelled data of 0.97 ± 0.10 and 0.98 ± 0.07 for the OH radicals and of the sum of the oxidation products MVK, MACR, and ISOPOOHs, respectively, are found. Also, the increase in the carbon monoxide (CO) concentration, of which nearly one-quarter is explained by the CO elimination of di-HPCARP-RO_2, is well captured by the model calculations (ratio of measured to modelled data of 0.98 ± 0.05). In comparison with MCMv3.3.1 and M1 model runs, $\sim 50\,\%$ of the total loss of isoprene-RO_2 conformers proceeds via isomerization reactions. In addition, both the MCMv3.3.1 and M1 models predict a larger concentration of ISOPOOHs compared to the optimized model M2 due to the different distribution of isoprene-RO_2 conformers. This will cause a larger expected concentration of new particles formed during the oxidation of isoprene due to the subsequent degradation products of ISOPOOHs, which includes epoxides (St. Clair et al., 2016).

The yields of the chemical compounds formed following the 1,6-H shift of Z-δ-RO_2 radicals carry a large uncertainty as summarized in the Introduction. Two HPALD yields are currently described in the literature: one in the range of 0.4 to 0.5, used within the Caltech mechanism and the MCMv3.3.1, and the other exceeding 0.75 based on the most recent literature. To quantify the impact of the uncertainty on the HPALD yield, a sensitivity model run was performed by changing the yield of HPALD from 0.4 to 0.75, with the yield of di-HPCARP-RO_2 set to 0.25 (M3, Table 2). As can be seen in Fig. 5, increasing the yield of HPALD by almost a factor of 2 does not have a large impact on model reproduction of the measured trace gases. The degradation of HPALD and di-HPCARP-RO_2 is followed by the formation of OH radicals and CO. On the timescale of the experiments in the chamber, it is not possible to distinguish between the relatively slow formation of OH radicals from the photolysis of HPALD (~ 1 h) from their formation from the fast aldehyde-H shift of di-HPCARP-RO_2 (~ 0.1 s). This is not entirely true for the CO, for which the measurement indicates a faster formation rate, better agreeing with the model and including a larger yield towards di-HPCARP-RO_2 (M2 model). A better agreement is, however, observed between measured and modelled HO_2^* radicals for the HPALD 0.75 model, although this remains within the uncertainty of the measurement, due to the formation of HO_2 radicals together with HPALD following the 1,6-H shift.

For experiments transitioning from high (1.5 ppbv) to low (0.2 ppbv) NO (Fig. 6) all the models are able to reproduce (within 10 %) the measured trace gases and the OH reactivity for the first injection of isoprene when the NO concentration

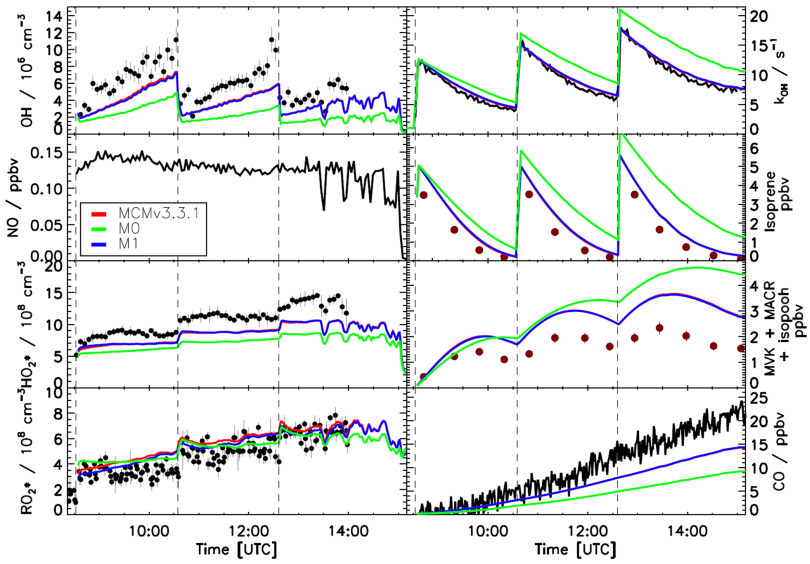

Figure 4. Comparison of modelled and measured trace gases for an experiment with NO < 0.2 ppbv. Measured time series of radicals and OH reactivity (LIF), isoprene and MVK+MACR+ISOPOOHs (GC), and CO (Picarro) are compared to model calculations. Vertical dashed lines indicate the times when isoprene was injected. No good agreement is observed when using the MCMv3.3.1 or a modified version (M1, Table 2) including isoprene-RO_2 conformer equilibrium reactions as included in the Caltech mechanism. Error bars represent 1σ standard deviation.

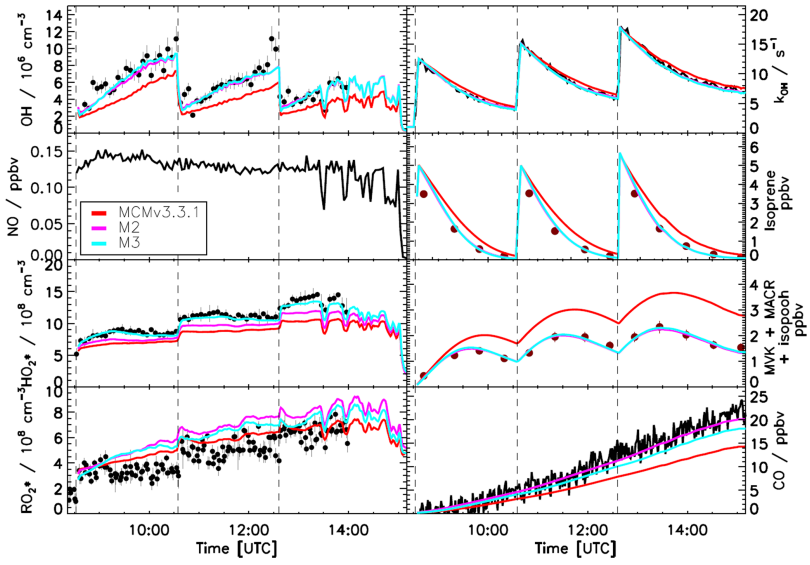

Figure 5. Comparison of modelled and measured trace gases for an experiment with NO < 0.2 ppbv. Measured time series of radicals and OH reactivity (LIF), isoprene and MVK+MACR+ISOPOOHs (GC), and CO (Picarro) are compared to model calculations. Vertical dashed lines indicate the times when isoprene was injected. Good agreement is observed when using M2 or M3 (Table 2), which use a different yield for HPALD of 0.40 and 0.75, respectively. Within both models, ~ 50 % of isoprene-RO_2 radicals (weighted by their abundance) are lost via isomerization reactions. Error bars represent 1σ standard deviation.

is above 0.5 ppbv. At this NO level, the OH production is mainly controlled by the reaction between HO_2 radicals and NO; therefore, the impact of the isomerization reactions on the OH radical production is marginal. As soon as the concentration of NO decreases below this threshold, larger discrepancies between the model calculations and the measured trace gases can be observed.

One additional model run (Fig. S5) was performed by re-implementing the original LIM1 within the MCMv3.3.1 model (Table 2), which includes a factor 5 slower equilibrium reactions between the isoprene-RO_2 conformers and a factor of 5 faster 1,6-H shift. Despite the large reduction in the equilibrium reactions between the isoprene-RO_2 conformers the LIM1 model run can reproduce the measured data as well as M2 and M3 for all concentrations of NO investigated in this study, as a change of only 5 % in the fraction of Z-δ-RO_2 radicals formed is observed.

When comparing the phenomenological bulk isomerization rate among the different models tested within this study calculated for the low NO experiment (Table 2) a similar value is observed for both the MCMv3.3.1 and M1 models. This is to be expected as both models are optimized to reproduce the phenomenological bulk isomerization rate as measured from the formation rate of HPALD (Crounse et al., 2011). In addition, in a study by Jenkin et al. (2019), the MCMv3.3.1 and M1 models are compared for different NO values and show no significant differences, as also observed within this study. On the other hand, the value obtained from this study is in good agreement with the LIM1 theoretical calculations and is needed to bring measurements and model results into agreement. Between these two groups of models, the bulk rate differs by a factor of 3 to 4.

5 Modelled contributions to the measured OH radical regeneration efficiency

The extensive range of NO concentrations in the experimental studies, reaching up to 2.0 ppbv, allowed for the exploration of the ability of the models to reproduce the measured data and to quantify the efficiency of the regeneration of OH radicals across a wide range of atmospheric conditions (Fig. 7) by drastically changing the competition between the isomerization reactions of RO_2 and the RO_2 + NO reactions.

The efficiency of OH regeneration, noted RE henceforward, is defined as the number of OH radicals that are produced after one OH radical has reacted with isoprene. It is calculated as the ratio of the OH regeneration rate R and the OH loss rate L. The modelled R quantifies the OH production via radical chain reactions (HO_2+NO, HO_2+O_3 and isomerization of isoprene-RO_2) and the photolysis of HPALD as produced in the isomerization reactions. It also includes the OH regenerated from the direct products of HPALD photolysis and the aldehyde-H shift of di-HPCARP-RO_2 and following products as well as the OH regenerated from the aldehyde-H shift of the MACR-RO_2 (Table S6). L represents the OH loss by reaction with isoprene and its products. As such, the model values for the OH regeneration efficiency represent a lower limit. The measured RE is obtained from the difference between the total OH loss rate and the primary OH production rate (ozone and nitrous acid photolysis) divided by the total OH loss rate.

$$\mathrm{RE} = \frac{R}{L} = \frac{\left(k_{\mathrm{OH}} \times [\mathrm{OH}] - ([\mathrm{O_3}] \times j\mathrm{O}(^1\mathrm{D}) \times y + [\mathrm{HONO}] \times j\mathrm{HONO})\right)}{k_{\mathrm{OH}} \times [\mathrm{OH}]} \quad (2)$$

Here, most values used ([OH], k_{OH}, [O_3], [H_2O], jO(^{1}D), jHONO) are experimentally measured quantities. Only the HONO concentration was not measured but taken from the model; y is the fraction of O(^{1}D) reacting with water vapour multiplied by the OH yield of the O(^{1}D) + H_2O reaction.

Good agreement is found between measured and modelled OH regeneration efficiency at all values of NO within the uncertainty of the measurements when using either M2 or M3 (Fig. 7), suggesting that all relevant OH production pathways are included.

In environments influenced by anthropogenic emissions, with NO values higher than 0.2 ppbv, 75 % of OH radicals are regenerated by the reaction of HO_2 radicals with NO. In contrast, at the lowest NO values representative of rainforest conditions, only 10 % of OH radicals reacting with isoprene are reformed by the HO_2 + NO reaction. This decrease in the OH RE from radical reactions with NO is partly compensated for by an increased contribution of regeneration from RO_2 isomerization reactions such that the total OH RE is still approximately 0.5 at the lowest NO concentration investigated. Though contributions of isomerization reactions to the OH RE diminish with increasing NO concentrations, their reaction rate coefficients are high enough to still constitute a competitive loss path for Z-δ-RO_2 radicals even at 2 ppbv of NO, with 10 % of the OH radicals consumed still regenerated by RO_2 isomerization reactions. The differences in the contribution of the isomerization reactions to the OH RE found for [NO] above 0.3 ppbv are mainly due to differences in ambient temperature impacting the isomerization rate coefficient. Although no experiments are available for levels of NO lower than 0.15 ppbv, a model simulation for the OH RE for up to 0.005 ppbv of NO indicates that the value of OH RE remains constant at around 0.5.

Among the isomerization reactions, the 1,5-H shift contributes less than 5 % to OH radical regeneration, with the large majority of the OH radical regenerated by the products following the 1,6-H shift. This is not surprising as the 1,5-H shift rate coefficient is $\sim$ 2 orders of magnitude slower than the 1,6-H shift. A more detailed analysis of the contribution of HPALD vs. Di-HPCARP-RO_2 and its products to OH regeneration is hindered by the uncertainty on their relative yield. Anyway, it is interesting to see that when a larger yield for di-HPCARP-RO_2 (0.6, M2) is applied, the largest frac-

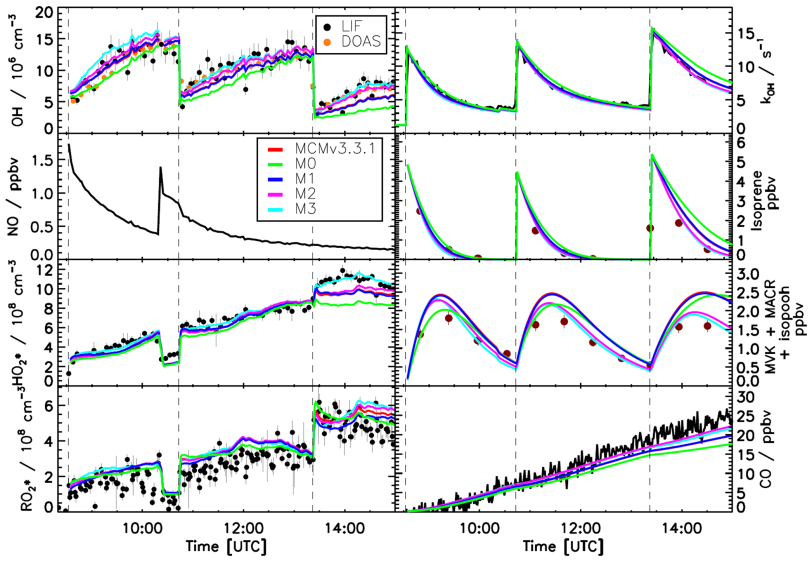

Figure 6. Comparison of modelled and measured trace gases for an experiment with variable NO concentrations, 1.5 > NO > 0.2 ppbv. Measured time series of radicals and OH reactivity (LIF), isoprene and MVK+MACR+ISOPOOHs (GC), and CO (Picarro) are compared to model calculations. Vertical dashed lines indicate the times when isoprene was injected. All models are able to reproduce the observed trace gases within their uncertainties for NO > 0.2 ppbv.

tion of the OH radical is regenerated via the aldehyde-H shift of di-HPCARP-RO_2 and its direct di-hydroperoxy carbonyl products ($\sim$ 70 %; Fig. 7a). When using a yield of HPALD of 0.75 (Fig. 7b) the photolysis of HPALD and the following direct products increase their contribution from 12 % to 60 %. Still, despite a much smaller yield (0.25) compared to HPALD, di-HPCARP-RO_2 and direct products contribute up to 30 % to OH radical regeneration due to the fast aldehyde-H shift.

The magnitude of the OH RE observed in this study, however, remains much lower than anticipated from OH concentration measurements in field campaigns under similar conditions, requiring an OH RE of nearly 1 to reproduce the observations (Rohrer et al., 2014). The reason for the discrepancy is still not fully understood. On the one hand, the experiments in the chamber refer only to isoprene chemistry, while the field studies, although performed in areas with large emissions of isoprene, include several different organic compounds which could contribute to the OH concentration. On the other hand, it could be that part of the measured OH radical concentrations in field campaigns was due to an interference. However, an LIF instrument with the same design as that used in this study was deployed in several field campaigns in China with the addition of a chemical titration device to separate ambient OH radicals from interferences, showing at maximum an interference of 10 % during daytime (Tan et al., 2017, 2018, 2019).

6 Global impact

Results from the simulation chamber experiments are used to investigate the impact on the global distribution of the OH regeneration efficiency due to either radical reactions with NO or isomerization reactions by implementing the detailed isoprene chemistry as derived in this study within the M2 model (Table S7). The global atmospheric chemistry model EMAC (Jöckel et al., 2010) was applied, including a modified version of the Mainz Organic Mechanism (MOM) (Sander et al., 2019) that represents an advanced isoprene oxidation mechanism with a complexity comparable to the MCM.

In regions with low NO concentrations, OH regeneration by HO_2 + NO is suppressed but compensated for by the OH regenerated from RO_2 radical isomerization reactions. These reactions globally have the largest impact in the tropics due to high isoprene concentrations and high temperatures (Peeters et al., 2014). The inclusion of OH regeneration routes gives an OH regeneration efficiency that is at least 60 % globally over all land masses covered with vegetation (Fig. 8). As a consequence, in areas where isoprene is the most important reactant for the OH radicals, the concentration at the surface is enhanced by more than a factor of 3 compared to model predictions neglecting RO_2 isomerization reactions (Fig. S3). Several studies showing the global impact of isomerization reactions were performed (Bates and Jacob, 2019; Møller et al., 2019; Müller et al., 2019), all showing, similarly to the results within this study, an enhanced concentration of the

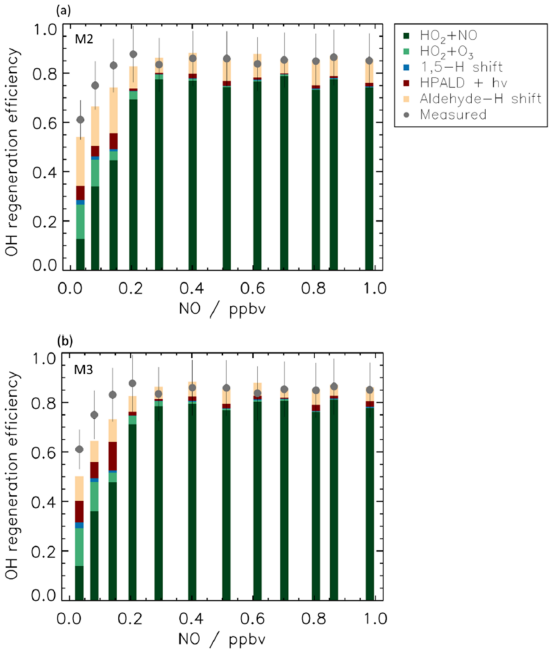

Figure 7. OH regeneration efficiency at different NO concentrations. The experimental OH regeneration efficiency (RE) is compared with the modelled one (M2, panel **a**; M3, panel **b**) for different NO values. The modelled OH RE is colour-coded by its main contributors (see Table S6 for more details). The RE is sustained at low levels of NO by the contribution from isomerization reactions, in particular by the aldehyde-H shift and its products. For [NO] higher than 0.3 ppbv, most of the OH recycling originates from the reaction of HO_2 with NO, but, although to a small extent, isomerization reactions still contribute up to 2 ppbv NO as the 1,6-H shift is still a competitive loss path for Z-δ-RO_2 radicals. The relatively large contribution to RE by the reaction between HO_2 radicals and O_3 at low NO is due to the large concentration of O_3 (90 ppbv) needed in the simulation chamber to maintain low values of NO, and it is not representative of ambient conditions. Error bars (1σ) for the measured OH regeneration efficiency include the accuracy of the measurements.

OH radical, in particular at the tropics where high concentrations of isoprene and high temperatures can be observed. A detailed comparison between the different models is not straightforward as they all contain different sets of reactions and are performed with different model parameters (e.g. NO_x and isoprene emissions). Three published studies are based on the isoprene Caltech mechanism (Table 2), which underestimates the measured OH radical concentration from this study due to a low yield of the formation of the Z-δ-RO_2 radical (Fig. 4). In addition, the model used in the study by Müller et al. (2019) includes large yields towards HPALD (0.75) as suggested from the study by Berndt et al. (2019), which is different from the other models. Thus, one additional global model test run within this work was performed with a yield of HPALD of 0.75 and of di-HPCARP-RO_2 of 0.25 (comparable to M3) to verify if the alternative branching ratio would result in significant differences. However, no change in the expected OH radical concentration was observed, in agreement with the model runs for the chamber experiments. However, for small oxygenated volatile organic compounds (OVOCs) like formaldehyde, formic acid, methanol, glyoxal, methyl glyoxal, hydroxyacetone, and peroxy acetyl nitrate, a change of up to 30 % was found at the ground level in isoprene-dominated regions. In the same regions, the change in the CO concentration was less than 5 %.

7 Remaining uncertainties

7.1 Yield of di-HPCARP-RO_2 versus HPALD

The LIM1 mechanism by Peeters et al. (2014) proposed a low ratio of HPALD to di-HPCARP-RO_2 formation, in agreement with the Teng et al. (2017) experiments. Since then, the experimental study of Berndt et al. (2019) found a much higher HPALD yield, with small contributions only of di-HPCARP-RO_2. The HPALD to di-HPCARP-RO_2 ratio is governed by the chemistry of the HOO-hydroxy-allyl radicals formed after the dominant 1,6-H shift in the Z-δ-1,4-ISOPOO radicals (Fig. S4). The Müller et al. (2019) rationalization of the high HPALD yield by Berndt et al. (2019) is based mostly on the stereoselectivity of the Z-δ-1,4-ISOPOO H migration and the subsequent O_2 addition, in connection with which new theoretical work (Müller et al., 2019) showed a comparatively high barrier for internal rotation of the HOC•H–C=C moiety in the HOO-hydroxy-allyl radicals due to the partial double bond. The nascent stereospecificity (Z, E′ versus Z, Z′; see Fig. S4 box A) then remains essentially unchanged throughout the subsequent chemistry of the HOO-hydroxy-allyl radicals; this is contrary to earlier assumptions in Peeters et al. (2014). HPALD can be formed rapidly from both stereoisomers by O_2 addition on the HOC•H– radical carbon (Fig. S4 box D), followed by fast HO_2 elimination. Di-HPCARP-RO_2 is formed only from the Z, Z′-HOO-hydroxy-allyl radicals (Fig. S4 box E), as the fast enol H migration requires the geometric proximity of the –OH and –OO• groups.

Müller et al. (2019) suggest, based on the stereospecific chemistry, that the E′-enol-peroxy radicals formed from O_2 addition on C4 of the Z, E′-HOO-hydroxy-allyl radicals (Fig. S4 box B) will solely undergo re-dissociation, as well as the subsequent re-addition of O_2 on either of the radical sites of the Z, E′-HOO-hydroxy-allyl radical, until "indirect" (Müller et al., 2019) HPALD is formed. Thus, the high yield of HPALD is explained based on its formation from all Z, E′-HOO-hydroxy-allyl radicals and part of the Z, Z′-

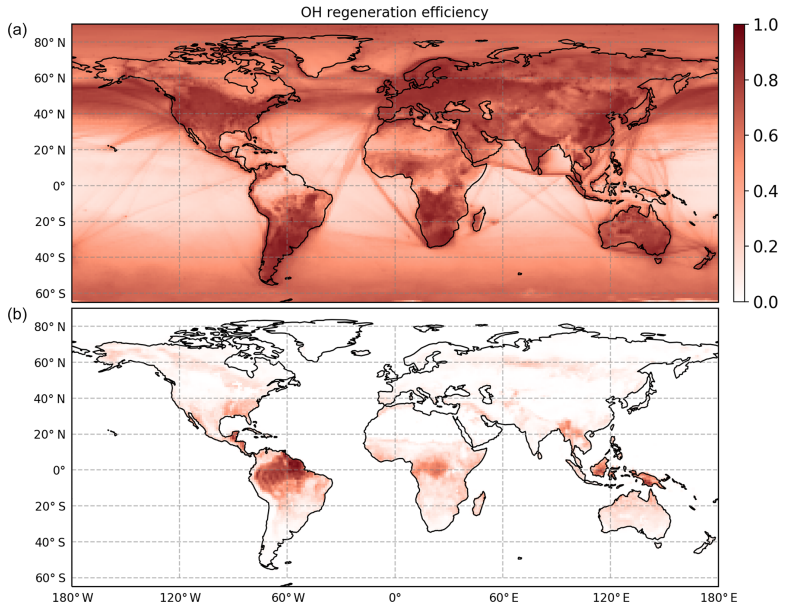

Figure 8. Global model of the OH regeneration efficiency at the surface (M2). **(a)** The OH regeneration efficiency when considering only the reaction between HO_2 radicals with NO and with O_3. **(b)** Including the remaining contributions by isomerization reactions and the photolysis of HPALD. Isomerization reactions are very efficient in recycling the OH radicals and thus maintaining the oxidation capacity of the atmosphere in environments characterized by high isoprene and low NO.

HOO-hydroxy-allyl radicals, whereas di-HPCARP-RO_2 is only formed from part of the Z, Z' radicals.

While this mechanism can indeed lead to numerical agreement with the Berndt et al. yields, the argumentation is not based on actual quantitative theoretical work on each reaction step and may thus be unable to discriminate between alternative mechanisms or yields in this subtle, complex chemistry; in this paragraph, we briefly examine a few aspects of the mechanism that warrant further investigation. Different yields would be obtained if the stereospecific yields (determined based on minimum energy pathways) are affected by non-statistical dynamics induced by chemical activation or post-barrier energy release. Likewise, the site specificity of O_2 addition, based on radical spin densities as a first-order approximation rather than on characterizations of the addition TS, carries a large uncertainty. The rate of re-dissociation of the HOO-enol-peroxy adducts is suggested by Müller et al. (2019) to be very similar to the initial Z- and E-δ-OH-peroxy radicals from isoprene. However, H scrambling between the –OOH and –OO• groups (see Fig. S4 box C) is expected to be orders of magnitude faster (Miyoshi, 2011), leading to an equilibrated population in which the terminal peroxy radical has no access to a rapid re-dissociation channel, leading to lower overall phenomenological rate coefficients for re-dissociation. Without characterization of the impact of the terminal peroxy radical in the bulk rate coefficient it is difficult to assess whether sufficient re-dissociation and/or re-addition events can occur on the experimental timescale to ensure complete reconversion to HPALD. H scrambling also allows access to enol reaction pathways ignored by Müller et al. (2019). We examined ring closure and H-migration reactions for the $HOCH{=}C(CH_3)CH_2CH_2OO\bullet$ proxy molecule, predicting a ring closure rate coefficient of $\sim 1 \times 10^3\ s^{-1}$ (see Fig. S2) that dominates re-dissociation. The impact of the additional –OOH group in $HOCH{=}C(CH_3)CH(OOH)CH_2OO\bullet$ on the ring closure rate is hard to estimate without computational work, and these proxy results may thus not be applicable to the isoprene chemistry. At the very least, one expects significant differences between the case I and II rate coefficients. However, even a slower rate of ring closure would disrupt the reaction flow as laid out by Müller et al. (2019) and affect the predicted HPALD yield.

At this moment, there are contradictory experimental data on the HPALD vs. di-HPCARP-RO_2 yield (Berndt, 2012; Teng et al., 2017; Berndt et al., 2019). The authors acknowledge that the reasons behind the disagreement are not clear. The earlier mechanism by Peeters et al. (2014) was used to rationalize the low HPALD observations of Teng et al. (2017) but did not appropriately account for stereospecificity. The Müller et al. (2019) mechanism is compatible with the high HPALD yield by Berndt et al. (2019), but it is based par-

tially on mechanistic argumentations that may not be compatible with new and existing quantitative theoretical work despite the excellent apparent numerical agreement with experiments. We must stress that none of the aforementioned considerations listed here on the Müller et al. (2019) reaction scheme have the strength by themselves to invalidate the proposed mechanism and are mostly indications that caveats apply when implementing this scheme in chemical models. In this complex chemistry, with subtle competition between many channels, we feel there is as yet not enough quantitative theoretical work to claim theory-based support for either experimental yield.

It is therefore not possible from this study to unequivocally determine the correct yield of HPALD versus di-HPCARP-RO_2, highlighting the need for further studies measuring their degradation products to pinpoint their yield of formation.

7.2 Fate of HPALD and di-hydroperoxy carbonyl compounds

HPALD is assumed to photolyse at a relatively fast rate ($\sim 2 \times 10^{-4}\,s^{-1}$ at a 30° solar zenith angle), producing CO and OH radicals among other trace gases (Wolfe et al., 2012; Liu et al., 2017). In addition to photolysis it will react with OH radicals, for which MCMv3.3.1 includes three site-specific reactions with a total rate of $5.2 \times 10^{-11}\,cm^3\,s^{-1}$ (Wolfe et al., 2012). This reaction can compete with photolysis when OH radical concentrations reach $4 \times 10^6\,cm^{-3}$ ($\sim 2 \times 10^{-4}\,s^{-1}$), but the product distribution has not yet been measured. The fate of the di-hydroperoxy carbonyl compounds (DHPMEK and DHPMPAL in the MCMv3.3.1 and MVK3OOH4OOH and MACR2OOH3OOH in the Caltech mechanism), formed from the aldehyde shift of the di-HPCARP-RO_2, is more uncertain and within the M2 model they are predicted in relatively large concentrations ($\sim 10^{10}\,cm^{-3}$). In the MCMv3.3.1 model, the two di-hydroperoxy carbonyl compounds degrade either by reacting with OH radicals, regenerating the OH radical, or by photolysis. Only two of the possible five site-specific reactions (Jenkin et al., 2018) are included, with a total rate coefficient of the order of $\sim 3.3 \times 10^{-11}\,cm^3\,s^{-1}$. Within the MCMv3.3.1 this is the main loss path for these species as photolysis is slower than $1.3 \times 10^{-5}\,s^{-1}$ and does not compete with the pseudo-first-order rate coefficient for the ambient concentration of OH radicals. A recent theoretical study by Liu et al. (2018) suggests, based on a calculation for the proxy molecule 2-hydroperoxypropanal, a much faster rate for the photolysis (~ 1 to $5 \times 10^{-4}\,s^{-1}$ at a 30° solar zenith angle) with a yield of $\sim 20\,\%$ OH radicals. At an ambient concentration of OH radicals lower than $4 \times 10^6\,cm^{-3}$, photolysis would then become the dominant path. The Caltech mechanism, based on Liu et al. (2018), then has photolysis as the only degradation path for the di-hydroperoxy carbonyl compounds. As long as the yield of HPALD remains uncertain, it is difficult to assess the importance of these reactions. This underlines the need for additional studies on the degradation of di-hydroperoxy carbonyl compounds and HPALD as they can have, locally, a large impact on the type of oxygenated products obtained.

8 Summary and conclusion

Photo-oxidation experiments on isoprene, the globally dominant biogenic volatile organic compound emitted, were performed in the atmospheric simulation chamber SAPHIR for a range of NO mixing ratios to explore the importance of the isomerization reaction for OH radical regeneration. Measurements of OH reactivity, OH, HO_2^* and RO_2^* radical concentrations, and other important trace gases were compared to results from different model calculations all based on a state-of-the-art chemical mechanistic model (MCMv3.3.1) (Jenkin et al., 2015).

It was found that the MCMv3.3.1 for isoprene degradation initiated by OH radicals is not able to reproduce the measured trace gas concentrations in the experiments despite the inclusion of the isomerization reaction for isoprene-RO_2 following the LIM1 mechanism for NO mixing ratios < 0.2 ppbv. Large discrepancies are observed, in particular for OH radicals, with a ratio of modelled to measured OH of 0.7 ± 0.07 and of almost a factor of 2 for the sum of MVK, MACR, and ISOPOOHs (all isomers).

Summarizing the theoretical analysis, we find that the main fate of di-HPCARP-RO_2-I is migration of the aldehyde H atom followed by rapid CO loss, leading to an unstable α-OOH alkyl radical that will eliminate an OH radical (Vereecken et al., 2004), forming DHP-MVK. The rate-limiting reaction is the aldehyde H migration, with an effective rate coefficient $k(300\,K) = \sim 10\,s^{-1}$. Alternative reaction channels are found to be uncompetitive. The mechanism leading to these results is significantly more complex than originally proposed (Peeters et al., 2014), with a rate coefficient significantly higher than the original $0.1\,s^{-1}$ estimate and possibly a contribution of thermalized reactions of the tri-HPACYL intermediate. However, the nett product formation remains identical to that incorporated in the mechanisms by Peeters et al. (2014) and Wennberg et al. (2018) and implemented in e.g. the Master Chemical Mechanism v3.3.1 (Jenkin et al., 2015). Extrapolating these results to the di-HPCARP-RO_2-II radicals by accounting for the expected barrier difference due to the different position of the methyl group, we find there is competition between CO elimination versus O_2 addition in the tri-HPACYL-II radicals formed, especially when assuming the absence of chemical activation.

The kinetic aspects controlling the impact of the 1,6-H shift of Z-δ-RO_2 on the regeneration of OH radicals and the production of oxygenated products were carefully checked based on what is available in the literature (Table 2). It was found that the best agreement between measured and mod-

elled trace gases is observed when up to 50 % of the isoprene-RO_2 conformers (weighted by their abundance) are isomerized. This is achieved when including within the MCMv3.3.1 a faster rate coefficient (3.6 and 0.4 s^{-1} at 298 K for OH addition on C4 and C1, respectively; Fig. 1) for the 1,6-H shift of the Z-δ-RO_2 radical based on a recent experimental study (Teng et al., 2017). These changes result in a phenomenological bulk isomerization rate in agreement with what can be obtained from the LIM1 study by Peeters et al. (2014). Large uncertainties remain regarding the relative yield of HPALD and di-HPCARP-RO_2 following the 1,6-H shift of Z-δ-RO_2 radicals. Within this study, no meaningful differences between the results of different model calculations could be observed when the yield of HPALD was varied from 0.4 to 0.75. Both HPALD and di-HPCARP-RO_2 produce OH radicals and CO in a relatively short timescale (less than 1 h). Therefore, as long as the 1,6-H shift is fast and there are sufficient Z-δ-RO_2 radicals undergoing isomerization, the measurements from this study are not sensitive to the HPALD to di-HPCARP-RO_2 ratio.

A detailed study of the path contribution to the OH radical regeneration highlights how, for NO mixing ratios $<$ 0.2 ppbv, $\sim$ 50 % of the OH radical is regenerated from the products following the 1,6-H shift: the photolysis of HPALD and aldehyde shift of the di-HPCARP-RO_2. These processes help maintain the OH radical regeneration efficiency up to 0.5 in environments with low NO mixing ratios wherein regeneration via the reaction of HO_2 with NO becomes less important. For environments in which the NO concentration is higher, regeneration via HO_2 plus NO dominates ($>$ 75 %), and even models not including isomerization reactions are able to reproduce the measured trace gases. The observed OH radical regeneration efficiency in this chamber study at low NO mixing ratios study is, however, lower than what is observed and needed in the field to explain the measured OH radical concentrations in isoprene-dominated environments (Rohrer et al., 2014).

A semi-explicit global model which includes the chemistry highlighted in this study shows how isomerization helps maintain an OH regeneration efficiency up to 0.6 globally. In the Amazon at the ground level, the inclusion of isomerization reactions increases the OH radical concentrations up to a factor of 3, although this has no relevant impact on the global budget of methane or CO.

Code and data availability. The data from the experiments in the SAPHIR chamber used in this work are available on the EUROCHAMP data home page (https://data.eurochamp.org/, last access: 1 October 2019, EUROCHAMP, 2019).

Supplement. The supplement related to this article is available online at: https://doi.org/10.5194/acp-20-3333-2020-supplement.

Author contributions. HF and AH designed the experiments. AN analysed the data, performed the box model simulations, and wrote the paper together with HF. LV did the theoretical calculations. SR and DT performed the global model simulations. All other co-authors participated in data collection and experiment operations, and all co-authors participated in paper discussion.

Competing interests. The authors declare that they have no conflict of interest.

Special issue statement. This article is part of the special issue "Simulation chambers as tools in atmospheric research (AMT/ACP/GMD inter-journal SI)". It is not associated with a conference.

Acknowledgements. This project has received funding from the European Research Council (ERC) under the European Union's Horizon 2020 research and innovation programme (SARLEP grant agreement no. 681529). The authors gratefully acknowledge the computing time granted through JARA-HPC on the supercomputer JURECA at Forschungszentrum Jülich Centre, 2018.

Financial support. This research has been supported by the European Research Council (SARLEP (grant no. 681529)), the European Commission, and the H2020 Research Infrastructures (EUROCHAMP-2020 (grant no. 730997)).

The article processing charges for this open-access publication were covered by a Research Centre of the Helmholtz Association.

Review statement. This paper was edited by Dwayne Heard and reviewed by three anonymous referees.

References

Alecu, I. M., Zheng, J., Zhao, Y., and Truhlar, D. G.: Computational Thermochemistry: Scale Factor Databases and Scale Factors for Vibrational Frequencies Obtained from Electronic Model Chemistries, J. Chem. Theory Comput., 6, 2872–2887, https://doi.org/10.1021/ct100326h, 2010.

Atkinson, R., Baulch, D. L., Cox, R. A., Crowley, J. N., Hampson, R. F., Hynes, R. G., Jenkin, M. E., Rossi, M. J., Troe, J., and IUPAC Subcommittee: Evaluated kinetic and photochemical data for atmospheric chemistry: Volume II – gas phase reactions of organic species, Atmos. Chem. Phys., 6, 3625–4055, https://doi.org/10.5194/acp-6-3625-2006, 2006.

Bao, J. L., Zheng, J., Alecu, I. M., Lynch, B. J., Zhao, Y., and Truhlar, D. G.: DDatabase of Frequency Scale Factors for Electronic Model Chemistries (Version 3 Beta 2), available at: http://comp.chem.umn.edu/freqscale/index.html (last access: June 2018), 2017.

Bates, K. H. and Jacob, D. J.: A new model mechanism for atmospheric oxidation of isoprene: global effects on oxidants, nitrogen oxides, organic products, and secondary organic aerosol, Atmos. Chem. Phys., 19, 9613–9640, https://doi.org/10.5194/acp-19-9613-2019, 2019.

Baulch, D. L., Bowman, C. T., Cobos, C. J., Cox, R. A., Just, T., Kerr, J. A., Pilling, M. J., Stocker, D., Troe, J., Tsang, W., Walker, R. W., and Warnatz, J.: Evaluated Kinetic Data for Combustion Modeling: Supplement II, J. Phys. Chem. Ref. Data, 34, p. 757, https://doi.org/10.1063/1.1748524, 2005.

Berndt, T.: Formation of carbonyls and hydroperoxyenals (HPALDs) from the OH radical reaction of isoprene for low-NO_x conditions: influence of temperature and water vapour content, J. Atmos. Chem., 69, 253–272, https://doi.org/10.1007/s10874-012-9245-2, 2012.

Berndt, T., Hyttinen, N., Herrmann, H., and Hansel, A.: First oxidation products from the reaction of hydroxyl radicals with isoprene for pristine environmental conditions, Comm. Chem., 2, p. 21, https://doi.org/10.1038/s42004-019-0120-9, 2019.

Blitz, M. A., Heard, D. E., and Pilling, M. J.: OH formation from $CH_3CO + O_2$: a convenient experimental marker for the acetyl radical, Chem. Phys. Lett., 365, 374–379, https://doi.org/10.1016/S0009-2614(02)01484-7, 2002.

Bohn, B. and Zilken, H.: Model-aided radiometric determination of photolysis frequencies in a sunlit atmosphere simulation chamber, Atmos. Chem. Phys., 5, 191–206, https://doi.org/10.5194/acp-5-191-2005, 2005.

Bohn, B., Rohrer, F., Brauers, T., and Wahner, A.: Actinometric measurements of NO_2 photolysis frequencies in the atmosphere simulation chamber SAPHIR, Atmos. Chem. Phys., 5, 493–503, https://doi.org/10.5194/acp-5-493-2005, 2005.

Carr, S. A., Glowacki, D. R., Liang, C.-H., Baeza-Romero, M. T., Blitz, M. A., Pilling, M. J., and Seakins, P. W.: Experimental and Modeling Studies of the Pressure and Temperature Dependences of the Kinetics and the OH Yields in the Acetyl + O_2 Reaction, J. Phys. Chem. A, 115, 1069–1085, https://doi.org/10.1021/jp1099199, 2011.

Crounse, J. D., Teng, A., and Wennberg, P. O.: Experimental constrains on the distribution and fate of peroxy radicals formed in the reactions of isoprene + OH + O_2 presented at the Atmospheric Chemical Mechanisms: Simple Models – Real world Complexities, Universtiy of California, Davis, USA, 10–12 December 2014.

Crounse, J. D., Paulot, F., Kjaergaard, H. G., and Wennberg, P. O.: Peroxy radical isomerization in the oxidation of isoprene, Phys. Chem. Chem. Phys., 13, 13607–13613, https://doi.org/10.1039/c1cp21330j, 2011.

Da Silva, G., Graham, C., and Wang, Z.-F.: Unimolecular β-hydroxyperoxy radical decomposition with OH recycling in the photochemical oxidation of isoprene, Environ. Sci. Technol., 44, 250–256, https://doi.org/10.1021/es900924d, 2010.

Dorn, H.-P., Brandenburger, U., Brauers, T., and Hausmann, M.: A New In Situ Laser Long-Path Absorption Instrument for the Measurement of Tropospheric OH Radicals, J. Atmos. Sci., 52, 3373–3380, https://doi.org/10.1175/1520-0469(1995)052<3373:anisll>2.0.co;2, 1995.

Dunning, T. H.: Gaussian basis sets for use in correlated molecular calculations. I. The atoms boron through neon and hydrogen, J. Chem. Phys., 90, 1007–1023, https://doi.org/10.1063/1.456153, 1989.

EUROCHAMP: EUROCHAMP Data Centre, https://data.eurochamp.org/, last access: 1 October 2019.

Fuchs, H., Bohn, B., Hofzumahaus, A., Holland, F., Lu, K. D., Nehr, S., Rohrer, F., and Wahner, A.: Detection of HO_2 by laser-induced fluorescence: calibration and interferences from RO_2 radicals, Atmos. Meas. Tech., 4, 1209–1225, https://doi.org/10.5194/amt-4-1209-2011, 2011.

Fuchs, H., Dorn, H.-P., Bachner, M., Bohn, B., Brauers, T., Gomm, S., Hofzumahaus, A., Holland, F., Nehr, S., Rohrer, F., Tillmann, R., and Wahner, A.: Comparison of OH concentration measurements by DOAS and LIF during SAPHIR chamber experiments at high OH reactivity and low NO concentration, Atmos. Meas. Tech., 5, 1611–1626, https://doi.org/10.5194/amt-5-1611-2012, 2012.

Fuchs, H., Hofzumahaus, A., Rohrer, F., Bohn, B., Brauers, T., Dorn, H. P., Haseler, R., Holland, F., Kaminski, M., Li, X., Lu, K., Nehr, S., Tillmann, R., Wegener, R., and Wahner, A.: Experimental evidence for efficient hydroxyl radical regeneration in isoprene oxidation, Nat. Geosci., 6, 1023–1026, https://doi.org/10.1038/Ngeo1964, 2013.

Fuchs, H., Acir, I.-H., Bohn, B., Brauers, T., Dorn, H.-P., Häseler, R., Hofzumahaus, A., Holland, F., Kaminski, M., Li, X., Lu, K., Lutz, A., Nehr, S., Rohrer, F., Tillmann, R., Wegener, R., and Wahner, A.: OH regeneration from methacrolein oxidation investigated in the atmosphere simulation chamber SAPHIR, Atmos. Chem. Phys., 14, 7895–7908, https://doi.org/10.5194/acp-14-7895-2014, 2014.

Fuchs, H., Tan, Z., Hofzumahaus, A., Broch, S., Dorn, H.-P., Holland, F., Künstler, C., Gomm, S., Rohrer, F., Schrade, S., Tillmann, R., and Wahner, A.: Investigation of potential interferences in the detection of atmospheric RO_x radicals by laser-induced fluorescence under dark conditions, Atmos. Meas. Tech., 9, 1431–1447, https://doi.org/10.5194/amt-9-1431-2016, 2016.

Fuchs, H., Novelli, A., Rolletter, M., Hofzumahaus, A., Pfannerstill, E. Y., Kessel, S., Edtbauer, A., Williams, J., Michoud, V., Dusanter, S., Locoge, N., Zannoni, N., Gros, V., Truong, F., Sarda-Esteve, R., Cryer, D. R., Brumby, C. A., Whalley, L. K., Stone, D., Seakins, P. W., Heard, D. E., Schoemaecker, C., Blocquet, M., Coudert, S., Batut, S., Fittschen, C., Thames, A. B., Brune, W. H., Ernest, C., Harder, H., Muller, J. B. A., Elste, T., Kubistin, D., Andres, S., Bohn, B., Hohaus, T., Holland, F., Li, X., Rohrer, F., Kiendler-Scharr, A., Tillmann, R., Wegener, R., Yu, Z., Zou, Q., and Wahner, A.: Comparison of OH reactivity measurements in the atmospheric simulation chamber SAPHIR, Atmos. Meas. Tech., 10, 4023–4053, https://doi.org/10.5194/amt-10-4023-2017, 2017.

Guenther, A., Karl, T., Harley, P., Wiedinmyer, C., Palmer, P. I., and Geron, C.: Estimates of global terrestrial isoprene emissions using MEGAN (Model of Emissions of Gases and Aerosols from Nature), Atmos. Chem. Phys., 6, 3181–3210, https://doi.org/10.5194/acp-6-3181-2006, 2006.

Hofzumahaus, A., Rohrer, F., Lu, K., Bohn, B., Brauers, T., Chang, C.-C., Fuchs, H., Holland, F., Kita, K., Kondo, Y., Li, X., Lou, S., Shao, M., Zeng, L., Wahner, A., and Zhang, Y.: Amplified trace gas removal in the troposphere, Science, 324, 1702–1704, https://doi.org/10.1126/science.1164566, 2009.

Holland, F., Hofzumahaus, A., Schafer, R., Kraus, A., and Patz, H. W.: Measurements of OH and HO_2 radical concentrations and photolysis frequencies during BERLIOZ, J. Geophys. Res.-Atmos., 108, 8246, https://doi.org/10.1029/2001jd001393, 2003.

Hornbrook, R. S., Crawford, J. H., Edwards, G. D., Goyea, O., Mauldin III, R. L., Olson, J. S., and Cantrell, C. A.: Measurements of tropospheric HO_2 and RO_2 by oxygen dilution modulation and chemical ionization mass spectrometry, Atmos. Meas. Tech., 4, 735–756, https://doi.org/10.5194/amt-4-735-2011, 2011.

Jenkin, M. E., Young, J. C., and Rickard, A. R.: The MCM v3.3.1 degradation scheme for isoprene, Atmos. Chem. Phys., 15, 11433–11459, https://doi.org/10.5194/acp-15-11433-2015, 2015.

Jenkin, M. E., Valorso, R., Aumont, B., Rickard, A. R., and Wallington, T. J.: Estimation of rate coefficients and branching ratios for gas-phase reactions of OH with aliphatic organic compounds for use in automated mechanism construction, Atmos. Chem. Phys., 18, 9297–9328, https://doi.org/10.5194/acp-18-9297-2018, 2018.

Jenkin, M. E., Khan, M. A. H., Shallcross, D. E., Bergström, R., Simpson, D., Murphy, K. L. C., and Rickard, A. R.: The CRI v2.2 reduced degradation scheme for isoprene, Atmos. Environ., 212, 172–182, https://doi.org/10.1016/j.atmosenv.2019.05.055, 2019.

Jöckel, P., Kerkweg, A., Pozzer, A., Sander, R., Tost, H., Riede, H., Baumgaertner, A., Gromov, S., and Kern, B.: Development cycle 2 of the Modular Earth Submodel System (MESSy2), Geosci. Model Dev., 3, 717–752, https://doi.org/10.5194/gmd-3-717-2010, 2010.

Jordan, A., Haidacher, S., Hanel, G., Hartungen, E., Mark, L., Seehauser, H., Schottkowsky, R., Sulzer, P., and Mark, T. D.: A high resolution and high sensitivity proton-transfer-reaction time-of-flight mass spectrometer (PTR-TOF-MS), Int. J. Mass Spectrom., 286, 122–128, https://doi.org/10.1016/j.ijms.2009.07.005, 2009.

Jorgensen, S., Knap, H. C., Otkjaer, R. V., Jensen, A. M., Kjeldsen, M. L. H., Wennberg, P. O., and Kjaergaard, H. G.: Rapid Hydrogen Shift Scrambling in Hydroperoxy-Substituted Organic Peroxy Radicals, J. Phys. Chem. A, 120, 266–275, https://doi.org/10.1021/acs.jpca.5b067613, 2016.

Kaminski, M., Fuchs, H., Acir, I.-H., Bohn, B., Brauers, T., Dorn, H.-P., Häseler, R., Hofzumahaus, A., Li, X., Lutz, A., Nehr, S., Rohrer, F., Tillmann, R., Vereecken, L., Wegener, R., and Wahner, A.: Investigation of the β-pinene photooxidation by OH in the atmosphere simulation chamber SAPHIR, Atmos. Chem. Phys., 17, 6631–6650, https://doi.org/10.5194/acp-17-6631-2017, 2017.

Karl, M., Dorn, H.-P., Holland, F., Koppmann, R., Poppe, D., Rupp, L., Schaub, A., and Wahner, A.: Product study of the reaction of OH radicals with isoprene in the atmosphere simulation chamber SAPHIR, J. Atmos. Chem., 55, 167–187, https://doi.org/10.1007/s10874-006-9034-x, 2006.

Knap, H. C. and Jorgensen, S.: Rapid Hydrogen Shift Reactions in Acyl Peroxy Radicals, J. Phys. Chem. A, 121, 1470–1479, https://doi.org/10.1021/acs.jpca.6b12787, 2017.

Kubistin, D., Harder, H., Martinez, M., Rudolf, M., Sander, R., Bozem, H., Eerdekens, G., Fischer, H., Gurk, C., Klüpfel, T., Königstedt, R., Parchatka, U., Schiller, C. L., Stickler, A., Taraborrelli, D., Williams, J., and Lelieveld, J.: Hydroxyl radicals in the tropical troposphere over the Suriname rainforest: comparison of measurements with the box model MECCA, Atmos. Chem. Phys., 10, 9705–9728, https://doi.org/10.5194/acp-10-9705-2010, 2010.

Lelieveld, J., Butler, T. M., Crowley, J. N., Dillon, T. J., Fischer, H., Ganzeveld, L., Harder, H., Lawrence, M. G., Martinez, M., Taraborrelli, D., and Williams, J.: Atmospheric oxidation capacity sustained by a tropical forest, Nature, 452, 737–740, https://doi.org/10.1038/nature06870, 2008.

Levy, H.: Photochemistry of the Troposphere, in: Advances in Photochemistry, John Wiley & Sons, Inc., 369–524, 1974.

Lew, M. M., Dusanter, S., and Stevens, P. S.: Measurement of interferences associated with the detection of the hydroperoxy radical in the atmosphere using laser-induced fluorescence, Atmos. Meas. Tech., 11, 95–109, https://doi.org/10.5194/amt-11-95-2018, 2018.

Lindinger, W., Hansel, A., and Jordan, A.: On-line monitoring of volatile organic compounds at pptv levels by means of proton-transfer-reaction mass spectrometry (PTR-MS) – Medical applications, food control and environmental research, Int. J. Mass. Spectrom., 173, 191–241, https://doi.org/10.1016/S0168-1176(97)00281-4, 1998.

Liu, Z., Nguyen, V. S., Harvey, J., Müller, J.-F., and Peeters, J.: Theoretically derived mechanisms of HPALD photolysis in isoprene oxidation, Phys. Chem. Chem. Phys., 19, 9096–9106, https://doi.org/10.1039/C7CP00288B, 2017.

Liu, Z., Nguyen, V. S., Harvey, J., Muller, J.-F., and Peeters, J.: The photolysis of [small alpha]-hydroperoxycarbonyls, Phys. Chem. Chem. Phys., 20, 6970–6979, https://doi.org/10.1039/C7CP08421H, 2018.

Lou, S., Holland, F., Rohrer, F., Lu, K., Bohn, B., Brauers, T., Chang, C. C., Fuchs, H., Häseler, R., Kita, K., Kondo, Y., Li, X., Shao, M., Zeng, L., Wahner, A., Zhang, Y., Wang, W., and Hofzumahaus, A.: Atmospheric OH reactivities in the Pearl River Delta – China in summer 2006: measurement and model results, Atmos. Chem. Phys., 10, 11243–11260, https://doi.org/10.5194/acp-10-11243-2010, 2010.

Mao, J., Ren, X., Zhang, L., Van Duin, D. M., Cohen, R. C., Park, J.-H., Goldstein, A. H., Paulot, F., Beaver, M. R., Crounse, J. D., Wennberg, P. O., DiGangi, J. P., Henry, S. B., Keutsch, F. N., Park, C., Schade, G. W., Wolfe, G. M., Thornton, J. A., and Brune, W. H.: Insights into hydroxyl measurements and atmospheric oxidation in a California forest, Atmos. Chem. Phys., 12, 8009–8020, https://doi.org/10.5194/acp-12-8009-2012, 2012.

Méreau, R., Rayez, M.-T., Rayez, J.-C., Caralp, F., and Lesclaux, R.: Theoretical study on the atmospheric fate of carbonyl radicals: kinetics of decomposition reactions, Phys. Chem. Chem. Phys., 3, 4712–4717, https://doi.org/10.1039/B105824J, 2001.

Miyoshi, A.: Systematic computational study on the unimolecular reactions of alkylperoxy (RO_2), hydroperoxyalkyl (QOOH), and hydroperoxyalkylperoxy (O_2QOOH) radicals, J. Phys. Chem. A, 115, 3301–3325, https://doi.org/10.1021/jp112152n, 2011.

Miyoshi, A.: Molecular size dependent falloff rate constants for the recombination reactions of alkyl radicals with O_2 and implications for simplified kinetics of alkylperoxy radicals, Int. J. Chem. Kinet., 44, 59–74, https://doi.org/10.1002/kin.20623, 2012.

Møller, K. H., Bates, K. H., and Kjaergaard, H. G.: The importance of peroxy radical hydrogen-shift reactions in atmo-

spheric isoprene oxidation, J. Phys. Chem. A, 123, 920–932, https://doi.org/10.1021/acs.jpca.8b10432, 2019.

Müller, J.-F., Stavrakou, T., and Peeters, J.: Chemistry and deposition in the Model of Atmospheric composition at Global and Regional scales using Inversion Techniques for Trace gas Emissions (MAGRITTE v1.1) – Part 1: Chemical mechanism, Geosci. Model Dev., 12, 2307–2356, https://doi.org/10.5194/gmd-12-2307-2019, 2019.

Novelli, A., Hens, K., Tatum Ernest, C., Kubistin, D., Regelin, E., Elste, T., Plass-Dülmer, C., Martinez, M., Lelieveld, J., and Harder, H.: Characterisation of an inlet pre-injector laser-induced fluorescence instrument for the measurement of atmospheric hydroxyl radicals, Atmos. Meas. Tech., 7, 3413–3430, https://doi.org/10.5194/amt-7-3413-2014, 2014.

Novelli, A., Bohn, B., Dorn, H.-P., Hofzumahaus, A., Holland, F., Li, X., Kaminski, M., Yu, Z., Rosanka, S., Reimer, D., Gkatzelis, G. I., Taraborrelli, D., Vereecken, L., Rohrer, F., Tillmann, R., Wegener, R., Kiendler-Scharr, A., Wahner, A., and Fuchs, H.: The atmosphere of a tropical forest simulated in a chamber: experiments, theory and global significance of OH regeneration in isoprene oxidation, iCACGP-IGAC 2018 Conference, 25–29 September 2018, Takamatsu, Japan, 2018a.

Novelli, A., Kaminski, M., Rolletter, M., Acir, I.-H., Bohn, B., Dorn, H.-P., Li, X., Lutz, A., Nehr, S., Rohrer, F., Tillmann, R., Wegener, R., Holland, F., Hofzumahaus, A., Kiendler-Scharr, A., Wahner, A., and Fuchs, H.: Evaluation of OH and HO_2 concentrations and their budgets during photooxidation of 2-methyl-3-butene-2-ol (MBO) in the atmospheric simulation chamber SAPHIR, Atmos. Chem. Phys., 18, 11409–11422, https://doi.org/10.5194/acp-18-11409-2018, 2018b.

Park, J., Jongsma, C. G., Zhang, R., and North, S. W.: OH/OD Initiated Oxidation of Isoprene in the Presence of O_2 and NO, J. Phys. Chem. A, 108, 10688–10697, https://doi.org/10.1021/jp040421t, 2004.

Peeters, J.: Interactive comment on "The MCM v3.3. degradation scheme for isoprene" by M. E. Jenkin et al., Atmos. Chem. Phys. Discuss., 15, C2486–C2486, 2015.

Peeters, J. and Müller, J.-F.: HO_x radical regeneration in isoprene oxidation via peroxy radical isomerisations. II: experimental evidence and global impact, Phys. Chem. Chem. Phys., 12, 14227–14235, https://doi.org/10.1039/c0cp00811g, 2010.

Peeters, J., Nguyen, T. L., and Vereecken, L.: HO_x radical regeneration in the oxidation of isoprene, Phys. Chem. Chem. Phys., 11, 5935–5939, https://doi.org/10.1039/b908511d, 2009.

Peeters, J., Müller, J.-F., Stavrakou, T., and Nguyen, V. S.: Hydroxyl radical recycling in isoprene oxidation driven by hydrogen bonding and hydrogen tunneling: the upgraded LIM1 mechanism, J. Phys. Chem. A, 118, 8625–8643 https://doi.org/10.1021/jp5033146, 2014.

Poppe, D., Brauers, T., Dorn, H.-P., Karl, M., Mentel, T., Schlosser, E., Tillmann, R., Wegener, R., and Wahner, A.: OH-initiated degradation of several hydrocarbons in the atmosphere simulation chamber SAPHIR, J. Atmos. Chem., 57, 203–214, https://doi.org/10.1007/s10874-007-9065-y, 2007.

Praske, E., Otkjær, R. V., Crounse, J. D., Hethcox, J. C., Stoltz, B. M., Kjaergaard, H. G., and Wennberg, P. O.: Atmospheric autoxidation is increasingly important in urban and suburban North America, P. Natl. Acad. Sci. USA, 115, 64–69, https://doi.org/10.1073/pnas.1715540115, 2018.

Praske, E., Otkjær, R. V., Crounse, J. D., Hethcox, J. C., Stoltz, B. M., Kjaergaard, H. G., and Wennberg, P. O.: Intramolecular Hydrogen Shift Chemistry of Hydroperoxy-Substituted Peroxy Radicals, J. Phys. Chem. A, 123, 590–600, https://doi.org/10.1021/acs.jpca.8b09745, 2019.

Purvis, G. D. and Bartlett, R. J.: A full coupled-cluster singles and doubles model: The inclusion of disconnected triples, J. Chem. Phys., 76, 1910, https://doi.org/10.1063/1.443164, 1982.

Ren, X., Olson, J. R., Crawford, J. H., Brune, W. H., Mao, J., Long, R. B., Chen, Z., Chen, G., Avery, M. A., Sachse, G. W., Barrick, J. D., Diskin, G. S., Huey, L. G., Fried, A., Cohen, R. C., Heikes, B., Wennberg, P. O., Singh, H. B., Blake, D. R., and Shetter, R. E.: HO_x chemistry during INTEX-A 2004: Observation, model calculation, and comparison with previous studies, J. Geophys. Res.-Atmos., 113, D05310, https://doi.org/10.1029/2007jd009166, 2008.

Rickly, P. and Stevens, P. S.: Measurements of a potential interference with laser-induced fluorescence measurements of ambient OH from the ozonolysis of biogenic alkenes, Atmos. Meas. Tech., 11, 1–16, https://doi.org/10.5194/amt-11-1-2018, 2018.

Ridley, B. A., Grahek, F. E., and Walega, J. G.: A small, high-sensitivity, medium-response ozone detector suitable for measurements from light aircraft, J. Atmos. Ocean. Tech., 9, 142–148, https://doi.org/10.1175/1520-0426(1992)009, 1992.

Rivera-Rios, J. C., Nguyen, T. B., Crounse, J. D., Jud, W., St. Clair, J. M., Mikoviny, T., Gilman, J. B., Lerner, B. M., Kaiser, J. B., de Gouw, J., Wisthaler, A., Hansel, A., Wennberg, P. O., Seinfeld, J. H., and Keutsch, F. N.: Conversion of hydroperoxides to carbonyls in field and laboratory instrumentation: observational bias in diagnosing pristine versus anthropogenically-controlled atmospheric chemistry, Geophys. Res. Lett., 41, 8645–8651, https://doi.org/10.1002/2014gl061919, 2014.

Roeckner, E., Brokopf, R., Esch, M., Giorgetta, M., Hagemann, S., Kornblueh, L., Manzini, E., Schlese, U., and Schulzweida, U.: Sensitivity of Simulated Climate to Horizontal and Vertical Resolution in the ECHAM5 Atmosphere Model, J. Climate, 19, 3771–3791, https://doi.org/10.1175/jcli3824.1, 2006.

Rohrer, F., Bohn, B., Brauers, T., Brüning, D., Johnen, F.-J., Wahner, A., and Kleffmann, J.: Characterisation of the photolytic HONO-source in the atmosphere simulation chamber SAPHIR, Atmos. Chem. Phys., 5, 2189–2201, https://doi.org/10.5194/acp-5-2189-2005, 2005.

Rohrer, F., Lu, K., Hofzumahaus, A., Bohn, B., Brauers, T., Chang, C.-C., Fuchs, H., Häseler, R., Holland, F., Hu, M., Kita, K., Kondo, Y., Li, X., Lou, S., Oebel, A., Shao, M., Zeng, L., Zhu, T., Zhang, Y., and Wahner, A.: Maximum efficiency in the hydroxyl-radical-based self-cleansing of the troposphere, Nat. Geosci., 7, 559, https://doi.org/10.1038/ngeo2199, 2014.

Sander, R., Baumgaertner, A., Gromov, S., Harder, H., Jöckel, P., Kerkweg, A., Kubistin, D., Regelin, E., Riede, H., Sandu, A., Taraborrelli, D., Tost, H., and Xie, Z.-Q.: The atmospheric chemistry box model CAABA/MECCA-3.0, Geosci. Model Dev., 4, 373–380, https://doi.org/10.5194/gmd-4-373-2011, 2011.

Sander, R., Baumgaertner, A., Cabrera-Perez, D., Frank, F., Gromov, S., Grooß, J.-U., Harder, H., Huijnen, V., Jöckel, P., Karydis, V. A., Niemeyer, K. E., Pozzer, A., Riede, H., Schultz, M. G., Taraborrelli, D., and Tauer, S.: The community atmospheric chemistry box model CAABA/MECCA-4.0, Geosci.

Model Dev., 12, 1365–1385, https://doi.org/10.5194/gmd-12-1365-2019, 2019.

Schlosser, E., Bohn, B., Brauers, T., Dorn, H.-P., Fuchs, H., Häseler, R., Hofzumahaus, A., Holland, F., Rohrer, F., Rupp, L., Siese, M., Tillmann, R., and Wahner, A.: Intercomparison of two hydroxyl radical measurement techniques at the atmosphere simulation chamber SAPHIR, J. Atmos. Chem., 56, 187–205, https://doi.org/10.1007/s10874-006-9049-3, 2007.

Schlosser, E., Brauers, T., Dorn, H.-P., Fuchs, H., Häseler, R., Hofzumahaus, A., Holland, F., Wahner, A., Kanaya, Y., Kajii, Y., Miyamoto, K., Nishida, S., Watanabe, K., Yoshino, A., Kubistin, D., Martinez, M., Rudolf, M., Harder, H., Berresheim, H., Elste, T., Plass-Dülmer, C., Stange, G., and Schurath, U.: Technical Note: Formal blind intercomparison of OH measurements: results from the international campaign HOxComp, Atmos. Chem. Phys., 9, 7923–7948, https://doi.org/10.5194/acp-9-7923-2009, 2009.

Sehested, J., Christensen, L. K., Nielsen, O. J., and Wallington, T. J.: Absolute rate constants for F + CH_3CHO and CH_3CHO + O_2, relative rate study of CH_3CHO + NO, and the product distribution of the F + CH_3CHO reaction, Int. J. Chem. Kinet., 30, 913–921, https://doi.org/10.1002/(SICI)1097-4601(1998)30:12<913::AID-KIN6>3.0.CO;2-5, 1998.

Sindelarova, K., Granier, C., Bouarar, I., Guenther, A., Tilmes, S., Stavrakou, T., Müller, J.-F., Kuhn, U., Stefani, P., and Knorr, W.: Global data set of biogenic VOC emissions calculated by the MEGAN model over the last 30 years, Atmos. Chem. Phys., 14, 9317–9341, https://doi.org/10.5194/acp-14-9317-2014, 2014.

St. Clair, J. M., Rivera-Rios, J. C., Crounse, J. D., Knap, H. C., Bates, K. H., Teng, A. P., Jørgensen, S., Kjaergaard, H. G., Keutsch, F. N., and Wennberg, P. O.: Kinetics and Products of the Reaction of the First-Generation Isoprene Hydroxy Hydroperoxide (ISOPOOH) with OH, The J. Phys. Chem. A, 120, 1441–1451, https://doi.org/10.1021/acs.jpca.5b06532, 2016.

Tan, D., Faloona, I., Simpas, J. B., Brune, W., Shepson, P. B., Couch, T. L., Sumner, A. L., Carroll, M. A., Thornberry, T., Apel, E., Riemer, D., and Stockwell, W.: HO_x budgets in a deciduous forest: Results from the PROPHET summer 1998 campaign, J. Geophys. Res., 106, 24407–24427, https://doi.org/10.1029/2001jd900016, 2001.

Tan, Z., Fuchs, H., Lu, K., Hofzumahaus, A., Bohn, B., Broch, S., Dong, H., Gomm, S., Häseler, R., He, L., Holland, F., Li, X., Liu, Y., Lu, S., Rohrer, F., Shao, M., Wang, B., Wang, M., Wu, Y., Zeng, L., Zhang, Y., Wahner, A., and Zhang, Y.: Radical chemistry at a rural site (Wangdu) in the North China Plain: observation and model calculations of OH, HO_2 and RO_2 radicals, Atmos. Chem. Phys., 17, 663–690, https://doi.org/10.5194/acp-17-663-2017, 2017.

Tan, Z., Rohrer, F., Lu, K., Ma, X., Bohn, B., Broch, S., Dong, H., Fuchs, H., Gkatzelis, G. I., Hofzumahaus, A., Holland, F., Li, X., Liu, Y., Liu, Y., Novelli, A., Shao, M., Wang, H., Wu, Y., Zeng, L., Hu, M., Kiendler-Scharr, A., Wahner, A., and Zhang, Y.: Wintertime photochemistry in Beijing: observations of RO_x radical concentrations in the North China Plain during the BEST-ONE campaign, Atmos. Chem. Phys., 18, 12391–12411, https://doi.org/10.5194/acp-18-12391-2018, 2018.

Tan, Z., Lu, K., Hofzumahaus, A., Fuchs, H., Bohn, B., Holland, F., Liu, Y., Rohrer, F., Shao, M., Sun, K., Wu, Y., Zeng, L., Zhang, Y., Zou, Q., Kiendler-Scharr, A., Wahner, A., and Zhang, Y.: Experimental budgets of OH, HO_2, and RO_2 radicals and implications for ozone formation in the Pearl River Delta in China 2014, Atmos. Chem. Phys., 19, 7129–7150, https://doi.org/10.5194/acp-19-7129-2019, 2019.

Taraborrelli, D., Lawrence, M. G., Crowley, J. N., Dillon, T. J., Gromov, S., Groß, C. B. M., Vereecken, L., and Lelieveld, J.: Hydroxyl radical buffered by isoprene oxidation over tropical forests, Nat. Geosci., 5, 190–193, 2012.

Teng, A. P., Crounse, J. D., and Wennberg, P. O.: Isoprene peroxy radical dynamics, J. Am. Chem. Soc., 139, 5367–5377, https://doi.org/10.1021/jacs.6b12838, 2017.

Vereecken, L. and Peeters, J.: The 1,5-H-shift in 1-butoxy: A case study in the rigorous implementation of transition state theory for a multirotamer system, J. Chem. Phys., 119, 5159–5170, https://doi.org/10.1063/1.1597479, 2003.

Vereecken, L., Nguyen, T. L., Hermans, I., and Peeters, J.: Computational study of the stability of α-hydroperoxyl- or α-alkylperoxyl substituted alkyl radicals, Chem. Phys. Lett., 393, 432–436, https://doi.org/10.1016/j.cplett.2004.06.076, 2004.

Wang, S., Riva, M., Yan, C., Ehn, M., and Wang, L.: Primary formation of highly oxidized multifunctional products in the OH-Initiated oxidation of Isoprene: a combined theoretical and experimental study, Environ. Sci. Technol., 52, 12255–12264, https://doi.org/10.1021/acs.est.8b02783, 2018.

Wegener, R., Brauers, T., Koppmann, R., Rodríguez Bares, S., Rohrer, F., Tillmann, R., Wahner, A., Hansel, A., and Wisthaler, A.: Simulation chamber investigation of the reactions of ozone with short-chained alkenes, J. Geophys. Res.-Atmos., 112, D13301, https://doi.org/10.1029/2006JD007531, 2007.

Wennberg, P. O., Bates, K. H., Crounse, J. D., Dodson, L. G., McVay, R. C., Mertens, L. A., Nguyen, T. B., Praske, E., Schwantes, R. H., Smarte, M. D., St Clair, J. M., Teng, A. P., Zhang, X., and Seinfeld, J. H.: Gas-phase reactions of isoprene and its major oxidation products, Chem. Rev., 118, 3337–3390, https://doi.org/10.1021/acs.chemrev.7b00439, 2018.

Whalley, L. K., Edwards, P. M., Furneaux, K. L., Goddard, A., Ingham, T., Evans, M. J., Stone, D., Hopkins, J. R., Jones, C. E., Karunaharan, A., Lee, J. D., Lewis, A. C., Monks, P. S., Moller, S. J., and Heard, D. E.: Quantifying the magnitude of a missing hydroxyl radical source in a tropical rainforest, Atmos. Chem. Phys., 11, 7223–7233, https://doi.org/10.5194/acp-11-7223-2011, 2011.

Whalley, L. K., Blitz, M. A., Desservettaz, M., Seakins, P. W., and Heard, D. E.: Reporting the sensitivity of laser-induced fluorescence instruments used for HO_2 detection to an interference from RO_2 radicals and introducing a novel approach that enables HO_2 and certain RO_2 types to be selectively measured, Atmos. Meas. Tech., 6, 3425–3440, https://doi.org/10.5194/amt-6-3425-2013, 2013.

Wolfe, G. M., Crounse, J. D., Parrish, J. D., St. Clair, J. M., Beaver, M. R., Paulot, F., Yoon, T. P., Wennberg, P. O., and Keutsch, F. N.: Photolysis, OH reactivity and ozone reactivity of a proxy for isoprene-derived hydroperoxyenals (HPALDs), Phys. Chem. Chem. Phys., 14, 7276–7286, https://doi.org/10.1039/C2CP40388A, 2012.

Xing, L., Lucas, J., Wang, Z., Wang, X., and Truhlar, D. G.: Hydrogen shift isomerizations in the kinetics of the second oxidation mechanism of alkane combustion, Reactions of the hydroper-

oxypentylperoxy OOQOOH radical, Combust. Flame, 197, 88–101, https://doi.org/10.1016/j.combustflame.2018.07.013, 2018.

Zhao, Y. and Truhlar, D. G.: The M06 suite of density functionals for main group thermochemistry, thermochemical kinetics, noncovalent interactions, excited states, and transition elements: two new functionals and systematic testing of four M06-class functionals and 12 other functionals, Theor. Chem. Acc., 120, 215–241, https://doi.org/10.1007/s00214-007-0310-x, 2008.

Chapter 4

Atmospheric chemical loss processes of isocyanic acid (HNCO): a combined theoretical kinetic and global modelling study

Rosanka, S., Vu, G. H. T., Nguyen, H. M. T., Pham, T. V., Javed, U., Taraborrelli, D., and Vereecken, L.: Atmospheric chemical loss processes of isocyanic acid (HNCO): a combined theoretical kinetic and global modelling study, Atmospheric Chemistry and Physics, 20, 6671–6686, https://doi.org/10.5194/acp-20-6671-2020, 2020

General information:
The manuscript has been submitted on 11 December 2019 and it has been published on 8 June 2020. The supplemental material of this manuscript is presented in Appendix B.

Importance for this thesis and the author's contribution:
In this study, the importance of atmospheric loss processes (gas-, aqueous-phase, and deposition) of HNCO is addressed. It contributes to the assessment of the representation of gas- and aqueous-phase OVOC chemistry. Additionally, the influence of varying biomass burning emission factors is addressed. Further details are discussed in Sect. 8.2.

I developed and implemented the gas- and aqueous-phase mechanism into the global model EMAC. Afterwards, I performed and analysed the global model simulations. I created the figures related to the global model analysis and wrote the global model description, the global model result section, and parts of the introduction. Additionally, I contributed to the general discussion and contributed to other parts of the manuscript. Further information and the contributions of all co-authors are available in the manuscript's 'Author contributions' section.

[1] `https://creativecommons.org/licenses/by/4.0/` (last access: 6 September 2020)

Atmos. Chem. Phys., 20, 6671–6686, 2020
https://doi.org/10.5194/acp-20-6671-2020

Atmospheric Chemistry and Physics Open Access EGU

Atmospheric chemical loss processes of isocyanic acid (HNCO): a combined theoretical kinetic and global modelling study

Simon Rosanka[1], Giang H. T. Vu[2], Hue M. T. Nguyen[2], Tien V. Pham[3], Umar Javed[1], Domenico Taraborrelli[1], and Luc Vereecken[1]

[1]Institute for energy and climate research, Forschungszentrum Jülich GmbH, Jülich, Germany
[2]Faculty of Chemistry and Center for Computational Science, Hanoi National University of Education, Hanoi, Vietnam
[3]School of Chemical Engineering, Hanoi University of Science and Technology, Hanoi, Vietnam

Correspondence: Hue M. T. Nguyen (hue.nguyen@hnue.edu.vn) and Domenico Taraborrelli (d.taraborrelli@fz-juelich.de)

Received: 11 December 2019 – Discussion started: 3 February 2020
Revised: 4 May 2020 – Accepted: 6 May 2020 – Published: 8 June 2020

Abstract. Isocyanic acid (HNCO) is a chemical constituent suspected to be harmful to humans if ambient concentrations exceed ~ 1 ppbv. HNCO is mainly emitted by combustion processes but is also inadvertently released by NO_x mitigation measures in flue gas treatments. With increasing biomass burning and more widespread usage of catalytic converters in car engines, good prediction of HNCO atmospheric levels with global models is desirable. Little is known directly about the chemical loss processes of HNCO, which limits the implementation in global Earth system models. This study aims to close this knowledge gap by combining a theoretical kinetic study on the major oxidants reacting with HNCO with a global modelling study. The potential energy surfaces of the reactions of HNCO with OH and NO_3 radicals, Cl atoms, and ozone were studied using high-level CCSD(T)/CBS(DTQ)//M06-2X/aug-cc-pVTZ quantum chemical methodologies, followed by transition state theory (TST) theoretical kinetic predictions of the rate coefficients at temperatures of 200–3000 K. It was found that the reactions are all slow in atmospheric conditions, with $k(300\,\mathrm{K}) \leq 7 \times 10^{-16}\,\mathrm{cm^3\,molecule^{-1}\,s^{-1}}$, and that product formation occurs predominantly by H abstraction; the predictions are in good agreement with earlier experimental work, where available. The reverse reactions of NCO radicals with H_2O, HNO_3, and HCl, of importance mostly in combustion, were also examined briefly.

The findings are implemented into the atmospheric model EMAC (ECHAM/MESSy Atmospheric Chemistry) to estimate the importance of each chemical loss process on a global scale. The EMAC predictions confirm that the gas-phase chemical loss of HNCO is a negligible process, contributing less than 1 % and leaving heterogeneous losses as the major sinks. The removal of HNCO by clouds and precipitation contributes about 10 % of the total loss, while globally dry deposition is the main sink, accounting for ~ 90 %. The global simulation also shows that due to its long chemical lifetime in the free troposphere, HNCO can be efficiently transported into the UTLS by deep convection events. Daily-average mixing ratios of ground-level HNCO are found to regularly exceed 1 ppbv in regions dominated by biomass burning events, but rarely exceed levels above 10 ppt in other areas of the troposphere, though locally instantaneous toxic levels are expected.

1 Introduction

The existence of isocyanic acid (HNCO) in the atmosphere has been established only recently (Roberts et al., 2011; Wentzell et al., 2013) despite its molecular structure and chemical synthesis being first discovered in the 19th century (Liebig and Wöhler, 1830). HNCO can form H-bonded clusters (Zabardasti et al., 2009, 2010; Zabardasti and Solimannejad, 2007) and in pure form appreciably polymerizes to other species (Belson and Strachan, 1982) but becomes relatively stable in the gaseous phase (ppm level) under ambient temperature conditions (Roberts et al., 2010). It is thus near-exclusively present as a monomer in the gaseous phase under ambient temperature conditions (Fischer et al., 2002; Roberts et al., 2010). The background ambient mixing ratios

of HNCO as determined by Young et al. (2012) using a global chemistry transport model vary in the range of a few parts per trillion by volume (pptv) over the ocean and remote Southern Hemisphere to tens of pptv over land. In urban regions, HNCO mixing ratio increases from tens of pptv to hundreds of pptv (Roberts et al., 2014; Wentzell et al., 2013). Peak levels can reach up to a few parts per billion by volume under the conditions impacted by direct emissions (Chandra and Sinha, 2016).

HNCO has been linked to adverse health effects such as cataracts, cardiovascular disease, and rheumatoid arthritis via a process called protein carbamylation (see Leslie et al., 2019; Roberts et al., 2011; Suarez-Bertoa and Astorga, 2016; SUVA, 2016; Wang et al., 2007, and references therein). To our knowledge, no past studies have been performed to provide a direct link between inhalation exposure and related adverse health effects. However, human exposure to HNCO concentrations of 1 ppbv is estimated to be potentially sufficient to start the process of protein carbamylation (Roberts et al., 2011). Unfortunately, an air quality standard for HNCO does not exist in most of the countries, whereas an occupational exposure limit has been established by law in only a few countries, including the Swedish Work Environment Authority (SWEA, 2011) and the Swiss National Accident Insurance Fund (SUVA, 2016). For example, the Swedish Work Environment Authority sets the level limit value (LLV) for HNCO at about $0.018\,\mathrm{mg\,m^{-3}}$, i.e. 10 ppbv (SWEA, 2011). The potential negative impact on health makes it important to assess the atmospheric sources and sinks of HNCO to determine its fate and lifetime.

HNCO emission into the atmosphere is driven primarily by combustion processes based on both natural and anthropogenic activities (see Leslie et al., 2019, and references therein), where the pyrolysis of nitrogen-containing biomass materials during the events of wildfires and agricultural fires leads to the emission of HNCO into the atmosphere. The presence of HNCO in cigarette smoke has been established via the pyrolysis of urea used as a cigarette additive (Baker and Bishop, 2004), oxidation of nicotine (Borduas et al., 2016a), and oxidation of formamide (Barnes et al., 2010; Borduas et al., 2015; Bunkan et al., 2015). Even the combustion of almost all sorts of common household materials, including fibre glass, rubber, wood, PVC-based carpet, and cables (Blomqvist et al., 2003), and polyurethane-based foam (Blomqvist et al., 2003; Jankowski et al., 2014), leads to HNCO emissions along with other isocyanates (Leslie et al., 2019). HNCO emissions from traffic are originating mainly from usage of recent catalytic converters in the exhaust systems of gasoline-based (Brady et al., 2014) and diesel-based (Heeb et al., 2011) vehicles. These converters are implemented to control the emission of primary pollutants such as hydrocarbons, carbon monoxide, particulate matter, and nitrogen oxides. However, these implementations have promoted (Suarez-Bertoa and Astorga, 2016) the formation and emissions of HNCO via surface-bound chain reactions at different stages of the flue gas exhaust and additionally due to emission of unreacted HNCO in the most commonly used urea-based SCR (selective catalytic reduction) system (Heeb et al., 2011). The usages of catalytic converters in modern vehicles potentially give rise to the emission of HNCO especially in urban regions with a growing density of vehicles. A few studies also reported a direct formation of HNCO in the diesel engines during fuel combustion without any aftertreatments (Heeb et al., 2011; Jathar et al., 2017). A tabular overview of past studies for HNCO emissions related to gasoline or diesel exhausts can be found in Wren et al. (2018) and Leslie et al. (2019). HNCO emissions via fossil fuel usage are not limited to on-road activity. Off-road fossil fuel activities (e.g. tar sands) also contribute to significant HNCO emissions on regional scales (Liggio et al., 2017). Finally, secondary HNCO formation in the atmosphere is also known through the oxidation of amines and amides (e.g. Borduas et al., 2016a; Parandaman et al., 2017).

The number of studies examining HNCO gas-phase chemistry is limited and mostly focused on its role in the chemistry in NO_x mitigation strategies in combustion systems. The scarce data suggest that HNCO destruction in the atmosphere by typical pathways such as reactions with oxidizing agents or by photolysis is ineffective. We give a short overview here to supplement a recent review (Leslie et al., 2019). The reaction of HNCO with the hydroxyl radical (OH), the most important daytime oxidizing agent, has only been studied experimentally at temperatures between 620 and 2500 K (Baulch et al., 2005; Mertens et al., 1992; Tsang, 1992; Tully et al., 1989; Wooldridge et al., 1996), where the extrapolated rate expressions lead to an estimated rate coefficient of 5–$12 \times 10^{-16}\,\mathrm{cm^3\,molecule^{-1}\,s^{-1}}$ at 298 K, i.e. a HNCO lifetime towards OH of over 25 years when assuming a typical OH concentration of $1 \times 10^6\,\mathrm{molecule\,cm^{-3}}$. Early theoretical work by Sengupta and Nguyen (1997) at temperatures ≥ 500 K showed that the mechanism proceeds predominantly by H abstraction, forming $NCO+H_2O$, with an energy barrier of $\sim 6\,\mathrm{kcal\,mol^{-1}}$. Wooldridge et al. (1996) determined an upper limit of ≤ 0.1 for the fraction of $CO_2 + NH_2$ formation. To our knowledge, no experimental or theoretical data are available on HNCO reactions with other dominant atmospheric oxidants, including the nitrate radicals (NO_3), chlorine atoms (Cl), or ozone (O_3). Some data are available for H- and O-atom co-reactants of importance in combustion, as well as estimates for HCO and CN (Baulch et al., 2005; Tsang, 1992), but these are not reviewed here. There is no direct measurement for the dry deposition of HNCO. In a global chemical-transport-model-based study, the deposition velocity was considered to be similar to formic acid, yielding a HNCO lifetime of 1–3 d (over the ocean) to 1–2 weeks (over vegetation) (Young et al., 2012). The UV absorption for HNCO is only reported at wavelengths < 262 nm, and photolysis is mostly reported for energies at wavelengths below 240 nm by excitation to the first singlet excited states, forming $H + NCO$ or $NH + CO$ (Keller-

Rudek et al., 2013; Okabe, 1970; Spiglanin et al., 1987; Spiglanin and Chandler, 1987; Uno et al., 1990; Vatsa and Volpp, 2001). In the troposphere photolysis occurs only at the UV absorption wavelength band > 290 nm due to filtering of shorter-wavelength radiation (Hofzumahaus et al., 2002). DrozGeorget et al. (1997) have reported the photolysis of HNCO forming $NH(a^1\Delta) + CO(X^1\sum^+)$ at 332.4 nm, but the HNCO absorption cross section at this wavelength would lead to a lifetime of months (Roberts et al., 2011). Therefore, HNCO loss due to photo-dissociation appears to be negligible in the lower atmosphere. HNCO has absorption bands in the infrared (Sharpe et al., 2004), but at these wavelengths the photon energy is generally too limited for photo-dissociation (Hofzumahaus et al., 2002). The main atmospheric loss processes are considered to be the transfer to the liquid phase, followed by hydrolysis, and deposition. This process depends on the varying atmospheric liquid water contents, relevant temperatures, and pH of cloud droplets. Therefore, the gas-to-liquid partitioning, in the varying atmospheric properties, i.e. water content, temperature, and pH of cloud droplets, becomes important to determine the atmospheric fate of HNCO (Leslie et al., 2019). The gas-to-liquid partitioning has been described by the Henry's law coefficient K_H (ranging from 20 to 26 ± 2 M atm^{-1}) and related parameters by a handful of studies (Borduas et al., 2016b; Roberts et al., 2011; Roberts and Liu, 2019). Based on a recent study (Barth et al., 2013), the lifetime of HNCO due to heterogeneous processes is known to be of the order of a few hours (in-cloud reactions) to weeks (aerosol deposition).

The emissions and sources of HNCO have been focused on by many past studies, but there remain large uncertainties in our understanding of HNCO removal processes, especially in gas-phase chemistry. This missing information on HNCO removal processes limits global models to predict HNCO with confidence. To alleviate the dearth of direct data and therefore improve the representation of HNCO in global models, we first provide a theoretical analysis of the chemical reactions of HNCO with the dominant atmospheric oxidants: OH and NO_3 radicals, Cl atoms, and O_3 molecules, including the prediction of each rate coefficient at atmospheric conditions. In a second step, these results are included in a global numerical chemistry and climate model to assess the impact of chemical loss of HNCO in competition against hydrolysis within cloud droplets and against deposition to the Earth's surface. Additionally, the model is used to provide an estimate of the relative importance of primary and secondary HNCO sources.

2 Methodologies

2.1 Theoretical methodologies

The potential energy surfaces of the initiation reactions of all four reaction systems were characterized at the M06-2X/aug-cc-pVTZ level of theory (Dunning, 1989; Zhao and Truhlar, 2008), optimizing the geometries and rovibrational characteristics of all minima and transition states. The relative energy of the critical points was further refined at the CCSD(T) level of theory in a set of single-point energy calculations using a systematic series of basis sets, aug-cc-pVxZ ($x = D$, T, Q) (Dunning, 1989; Purvis and Bartlett, 1982). These energies were extrapolated to the complete basis set (CBS) limit using the aug-Schwartz6(DTQ) scheme as proposed by Martin (1996). The rate coefficients were then obtained by transition state theory (Truhlar et al., 1996) in a rigid rotor, harmonic oscillator approximation, applying a scaling factor of 0.971 to the vibrational wavenumbers (Alecu et al., 2010; Bao et al., 2017). The spin–orbit splitting of the OH radicals of 27.95 cm^{-1} was taken into account (Huber and Herzberg, 1979). Tunnelling was incorporated using an asymmetric Eckart correction (Johnston and Heicklen, 1962).

To further complete our knowledge on some of the reactions beyond their initiation steps, the full potential energy surfaces of the $HNCO + Cl$ and $HNCO + O_3$ reactants were characterized at the M06-2X/aug-cc-pVTZ or B3LYP/aug-cc-pVTZ level of theory (Becke, 1993; Dunning, 1989; Lee et al., 1988), combined with CCSD(T)/aug-cc-pVTZ single-point energy calculations. To our knowledge, these are the first characterizations of these surfaces. At atmospheric temperatures, most of the reaction channels are negligible, and a detailed kinetic analysis is not performed at this time.

The expected uncertainty of the rate predictions at room temperature is of a factor of 4, based on an estimated uncertainty on the barrier height of at least 0.5 kcal mol^{-1}, and on the tunnelling correction of a factor of 1.5. Though the level of theory used is robust, there are some aspects that are not treated with the highest possible precision. For example, post-CCSD(T)/CBS calculations could refine the predicted energies but are not expected to change our values by more than a few tenths of a kilocalorie per mole (kcal mol^{-1}). The calculation of the state densities could be improved for internal rotation (especially at temperatures outside the atmospheric range), for the notoriously complex rovibronic structure of the NO_3 radical (Stanton, 2007, 2009; Stanton and Okumura, 2009), or by treating the transition states (micro)variationally to better characterize the energy-specific kinetic bottleneck. Another aspect is the effect of redissociation of chemically activated adducts, which decreases the effective rate of HNCO loss. Finally, tunnelling corrections for the H-abstraction reactions could benefit from higher-dimensional (curvature and corner-cutting) corrections. The tunnelling corrections are currently predicted to be smaller than a factor of 15 at room temperature due to the low and broad energy barriers, except for a factor of ~ 40 for the $HNCO + NO_3$ H abstraction with a somewhat higher barrier. Incorporating any of the aforementioned improvements in the theoretical predictions, however, has a high to very high computational burden with strongly diminished return, as none are expected to change the rate coefficient by a fac-

tor large enough to affect the conclusions of our calculations; i.e. that the reactions are negligibly slow by many orders of magnitude compared to other HNCO loss processes (see further text). This is also illustrated in Fig. 2. We refer to Vereecken and Francisco (2012), Vereecken et al. (2015), and Papajak and Truhlar (2012) for further information on theoretical methodologies in atmospheric chemistry.

2.2 Global modelling

The ECHAM/MESSy Atmospheric Chemistry (EMAC) model is a numerical chemistry and climate simulation system that includes submodels describing tropospheric and middle-atmosphere processes and their interaction with oceans, land, and human influences (Jöckel et al., 2010). It uses the second version of the Modular Earth Submodel System (MESSy2) to link multi-institutional computer codes. The core atmospheric model is the fifth-generation European Centre Hamburg general circulation model (ECHAM5) (Roeckner et al., 2006). A hierarchal diagram of EMAC is given in Jöckel et al. (2005). Additionally, Jöckel et al. (2010) provide an update on all modelling components used. For the present study, we applied EMAC (ECHAM5 version 5.3.02, MESSy version 2.54.0) in the T63L90MA resolution, i.e. with a spherical truncation of T63 (corresponding to a quadratic Gaussian grid of approximately 1.875° by 1.875° in latitude and longitude) with 90 vertical hybrid pressure levels up to 0.01 hPa. By using this horizontal resolution, assessing the global impact is still feasible while at the same time being of a computationally reasonable cost. The 90 vertical layers used (focusing on the lower and middle atmosphere) represent tropospheric and stratospheric transport processes reasonable well (Jöckel et al., 2010) such that the tropospheric impact and the impact on the UTLS (upper troposphere/lower stratosphere) can be addressed. The applied model setup comprised the submodel MECCA (Module Efficiently Calculating the Chemistry of the Atmosphere) to calculate atmospheric chemistry using parts of the Mainz Organic Mechanism (MOM) (Sander et al., 2011). Within MOM, aromatics and terpenes were excluded to reduce the computational demand of all simulations performed; this chemistry has no relevant impact on HNCO. The mechanism was extended to include the proposed changes of this study: formamide as an additional chemical source of HNCO (Bunkan et al., 2016) and chemical mechanisms for nitromethane (Calvert, 2008; Taylor et al., 1980), methylamine, dimethylamine, and trimethylamine (Nielsen et al., 2012). The reaction rates used for the latter three are average values of the measured values reported in Nielsen et al. (2012). The product yields reported in the same source are simplified to suit a global model application. The submodel SCAV (SCAVenging submodel) was used to simulate the physical and chemical removal of trace gases and aerosol particles by clouds and precipitation (Tost et al., 2006). The aqueous-phase mechanism was extended to include the HNCO and formamide mechanism proposed by Borduas et al. (2016b), Barnes et al. (2010), and Behar (1974). These lead to the formation to ammonia in the aqueous phase, which was before limited to the acid–base equilibrium in cloud droplets. The representation of cyanide was improved based on Buechler et al. (1976). Tables S1 and S2 in the Supplement summarize all additional changes to the chemical mechanism in gas and aqueous phases, respectively. The submodel DDEP (Dry DEPosition) is used to simulate the dry deposition of HNCO using the default scheme, where non-stomatal uptake is effectively disabled by using a large and constant resistance (Kerkweg et al., 2006a). The effective Henry's law coefficient (H^*) is used, as proposed by Borduas et al. (2016b), modified to a pH of 7. Differently from Young et al. (2012), the same H^* over the ocean is used. This approximation is reasonable since the levels of HNCO in the marine boundary layer are expected to be minor. In a global context, the major sources of HNCO and formamide are biomass burning emissions. From literature, two emission factors are available, which differ substantially: $0.53\,\mathrm{g\,kg^{-1}}$ (Koss et al., 2018) versus $0.2\,\mathrm{g\,kg^{-1}}$ (Kumar et al., 2018). Thus two simulations are performed to quantify the uncertainty due to those emission factors. The MESSy submodel BIOBURN is used to calculate biomass burning fluxes based on the selected emission factor and Global Fire Assimilation System (GFAS) data. GFAS data are calculated based on fire radiative power observations from the Moderate Resolution Imaging Spectroradiometer (MODIS) satellite instruments, which are used to calculate the dry-matter combustion rates (Kaiser et al., 2012). The biomass burning emission fluxes are then obtained by combining these dry-matter combustion rates with the defined biomass burning emission factors per unit of dry matter burned. The MESSy submodel OFFEMIS (OFFline EMISsions) then calculates the resulting concentration changes for each tracer due to the biomass burning emissions (Kerkweg et al., 2006b). Anthropogenic HNCO emissions from diesel cars are scaled to ammonia EDGAR (Crippa et al., 2016) road emissions by 15 % (Heeb et al., 2011). Other known sources of HNCO (e.g. cigarette smoke) were not taken into account due to the resolution of the spatial grid used. The model was run for 2 years (2010–2011) in which the first year was used as spin-up and 2011 for analysis. In 2010, the biomass burning emissions were particularly high (Kaiser et al., 2012), providing higher background HNCO concentrations during spin-up and improving the representation of HNCO, which allows for a more representative comparison in 2011.

3 Loss processes by chemical oxidants

3.1 HNCO + OH

The reaction of HNCO with OH can proceed by four distinct pathways: H abstraction or OH addition on the

carbon, nitrogen, or oxygen atom of HNCO; a potential energy surface is shown in Fig. 1. Formation of the HN=C•OOH and HN(OH)C•=O adducts through OH addition on the oxygen or nitrogen atom is highly endothermic by 20 kcal mol^{-1} or more, and it is not competitive at any temperature. The two remaining pathways are exothermic, with HN•C(=O)OH being the most stable nascent product, 19.8 kcal mol^{-1} below the reactants, followed by H_2O + •N=C=O, at 7.5 kcal mol^{-1} exoergicity. Despite the higher energy of the products, we predict this last reaction to have a lower barrier, 6.0 kcal mol^{-1}, compared to the addition process, 8.7 kcal mol^{-1}, in agreement with the theoretical predictions of Sengupta and Nguyen (1997). Furthermore, the H-abstraction process allows for faster tunnelling, making this process the fastest reaction channel, while addition contributes less than 0.5 % of product formation at temperatures below 400 K. From these data, we derive the following rate coefficient expressions (see also Fig. 2):

$$k_{OH}(298\,K) = 7.03 \times 10^{-16}\,cm^3\,molecule^{-1}\,s^{-1},$$
$$k_{OH}(200-450\,K) = 3.27 \times 10^{-34} T^{7.01} \exp(685\,K/T)\,cm^3\,molecule^{-1}\,s^{-1},$$
$$k_{OH}(300-3000\,K) = 1.79 \times 10^{-23} T^{3.48} \exp(-733\,K/T)\,cm^3\,molecule^{-1}\,s^{-1}.$$

Our predictions are in very good agreement between 624 and 875 K, when compared with experimental data from Tully et al. (1989), which served as the basis for the recommendation of Tsang (1992); our predictions reproduce the rate coefficients within a factor of 1.7, comparable to the experimental uncertainty of a factor of 1.5 (see Fig. 2). Likewise, our predictions agree within a factor of 1.7 with the experimental determination by Wooldridge et al. (1996) over the entire 620–1860 K temperature range. Our predictions overshoot the upper limit estimated by Mertens et al. (1992) by a factor of up to 4 at the upper end of the temperature range (2120 to 2500 K). At these elevated temperatures, it is expected that our theoretical kinetic calculations are less accurate since anharmonicity, internal rotation, and possibly pressure effects are not fully accounted for. At this time, we choose not to invest the computational cost to improve the predictions at these temperatures. The predicted rate at room temperature is within a factor of 2 of the extrapolation of the recommended expression derived by Tsang (1992), $k(298\,K) \approx 1.24 \times 10^{-15}$ cm^3 molecule^{-1} s^{-1} and very close to the extrapolation of the expression by Wooldridge et al. (1996), which is 7.2×10^{-16} cm^3 molecule^{-1} s^{-1}. The good agreement of our rate coefficient with the experimental data extrapolated to room temperature is mainly due to the curvature predicted in the temperature dependence (see Fig. 2), as our calculations have a slightly steeper temperature dependence than the experiments in the high-temperature range. Though negligible at low temperature, we find that OH addition on the C atom of HNCO accounts for 7 % to 8 % of the reaction rate between 2000 and 3000 K, with other non-H-abstraction channels remaining negligible (< 0.1 %). The addition channel is the likely origin of $CO_2 + NH_2$ products (Sengupta and Nguyen, 1997), for which Wooldridge et al. (1996) experimentally determined an upper limit of ≤ 0.1 over the temperature range 1250–1860 K, corroborating our predictions to its low contribution.

Typical concentrations of the OH radical during daytime are measured at $\sim 10^6$ molecule cm^{-3} (Stone et al., 2012), leading to a pseudo-first order rate coefficient for HNCO loss by OH radicals of $k(298\,K) = 7 \times 10^{-10}$ s^{-1}, i.e. suggesting an atmospheric chemical lifetime of decades to several centuries, depending on local temperature and OH concentration, negligible compared to other loss processes like scavenging. Even in extremely dry conditions, where aqueous uptake is slow, heterogeneous loss processes will dominate, or alternatively atmospheric mixing processes will transport HNCO to more humid environments where it will hydrolyze.

3.2 HNCO + Cl

From the potential energy surface (PES) shown in Fig. 1, we see that the reaction between HNCO and the Cl atom can occur by abstraction of the H atom from HNCO or by addition of the Cl atom on the C, N, or O atoms. Contrary to the OH reaction, all entrance reactions are endothermic, with formation of the HN•C(Cl)=O alkoxy radical nearly energy neutral (see Fig. 1). Formation of this latter product, proceeding by the addition of a Cl atom to the carbon atom of HNCO, also has the lowest energy barrier, which is 7.3 kcal mol^{-1} above the reactants. The hydrogen abstraction, forming HCl and •NCO, requires passing a higher barrier of 11.2 kcal mol^{-1}, whereas additions on the N and O atoms have very high barriers exceeding 34 kcal mol^{-1}. The product energy difference between addition and H abstraction is much smaller compared to the HNCO + OH reaction. Despite this reduced reaction energy, the addition barrier remains 4 kcal mol^{-1} below the H-abstraction barrier, making the HNCO + Cl reaction the only reaction studied here where H abstraction is not dominant. For the HNCO + Cl reaction, we then obtain the following rate coefficients (see also Fig. 3):

$$k_{Cl}(298\,K) = 3.19 \times 10^{-17}\,cm^3\,molecule^{-1}\,s^{-1},$$
$$k_{Cl}(200-450\,K) = 1.11 \times 10^{-17} T^{1.97} \exp(-3031\,K/T)\,cm^3\,molecule^{-1}\,s^{-1}.$$

We find that the overall rate coefficient of the HNCO + Cl reaction is almost 1 order of magnitude below that for the OH radical. The HN•C(Cl)=O radical formed, however, has a weak C−Cl bond requiring only 5.4 kcal mol^{-1} to redissociate. The rate coefficient of 8×10^8 s^{-1} for dissociation at room temperature ($k(T) = 8.3 \times 10^{12} \exp(-2760/T)$ s^{-1}) is over an order of magnitude faster than O_2 addition under atmospheric conditions, assuming the latter is equally fast as for H_2C•CH=O vinoxy radicals, i.e. $k(298\,K, 0.2\,atm\,O_2) \leq$

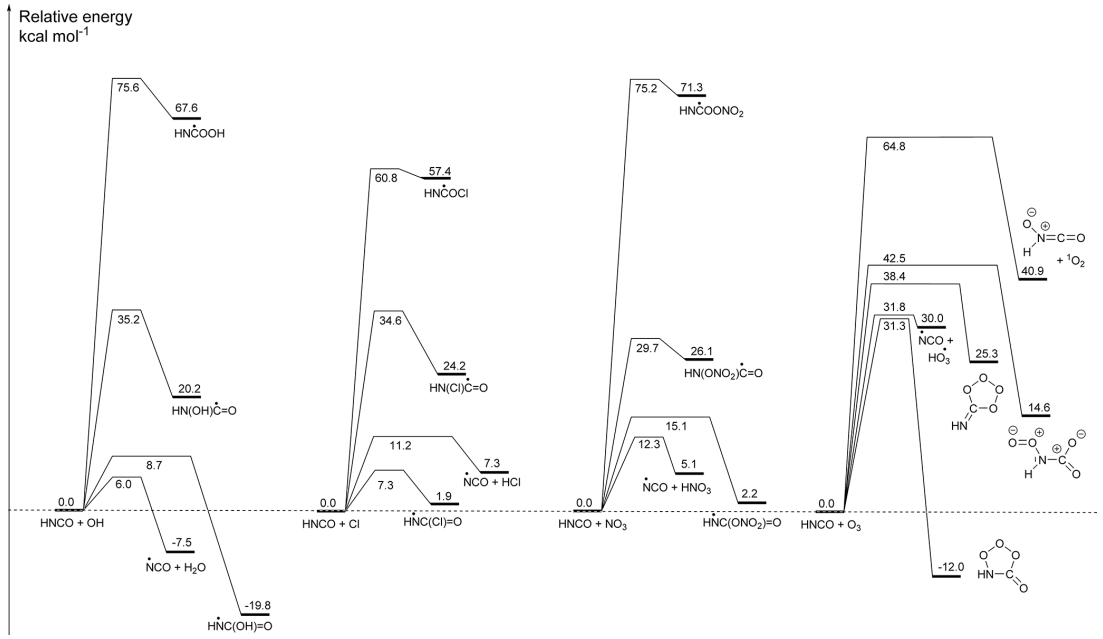

Figure 1. Potential energy surfaces for the initiation reactions of HNCO with OH radicals, Cl atoms, NO_3 radicals, and ozone, showing CCSD(T)/CBS(DTQ) energies (kcal mol^{-1}) based on M06-2X/aug-cc-pVTZ geometries. The pre-reactive complexes are omitted as they do not influence the kinetics; similarly, the subsequent reactions of the products are not shown. The Supplement has additional energetic and rovibrational data, more complete potential energy surfaces for some of the reactions, and three-dimensional representations of the molecular structures with bond lengths and angles.

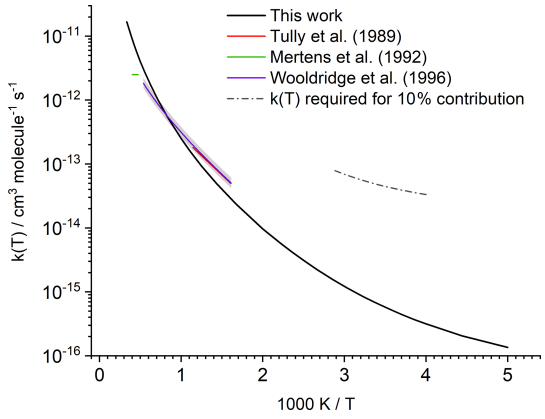

Figure 2. Predicted rate coefficient $k(T)$ for the reaction of HNCO + OH compared against experimental data. The shaded area indicates the experimental uncertainty reported by Wooldridge et al. (1996). The dashed line estimates the 298 K rate coefficient that would be needed to remove 10 % of the atmospheric HNCO by reaction with OH (see text).

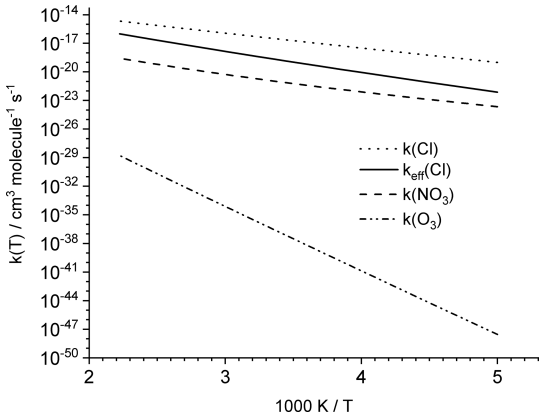

Figure 3. Total rate coefficient predictions for the reaction of HNCO with NO_3, Cl, and O_3. The addition of Cl atoms on HNCO leads to the formation of a very short-lived adduct, which rapidly redissociates to the reactants; the effective rate coefficient for HNCO loss by Cl atoms, k_{eff} (Cl), is thus equal to the H-abstraction rate forming HCl + NCO (see text).

$10^7\,s^{-1}$ (IUPAC Subcommittee on Atmospheric Chemical Kinetic Data Evaluation, 2017). This makes redissociation to the reactants the most likely fate of the HN•C(Cl)=O adduct. Addition is thus an ineffective channel for HNCO removal, and the effective reaction with Cl atoms is dominated by the H-abstraction reaction, forming HCl + •NCO, with the following rate coefficient (see also Fig. 3):

$$k_{Cl,eff}(298\,K) = 2.23 \times 10^{-19}\,cm^3\,molecule^{-1}\,s^{-1},$$
$$k_{Cl,eff}(200-450\,K) = 1.01 \times 10^{-24} T^{4.40} \exp(-3799\,K/T)\,cm^3\,molecule^{-1}\,s^{-1}.$$

Globally, Cl atoms have a lower concentration, about 5×10^3 atom cm^{-3}, compared to OH radicals (Finlayson-Pitts and Pitts, 1999). Under such conditions, lifetimes estimated for HNCO towards Cl atoms are about 3×10^7 years, which is much longer than towards the OH radial. Therefore, HNCO loss by Cl radicals is negligible.

The supporting information provides information on the extended potential energy surface of the HNCO+Cl reaction, with information on nine intermediates, 19 transition states, and 16 products.

3.3 HNCO + NO_3

The reaction of NO_3 with HNCO shows the same four radical mechanisms found for OH and Cl, i.e. H abstraction and addition on the three heavy atoms. As for Cl atoms, none of the reactions are exothermic, and the energy difference between the two most stable products is reduced to 3 kcal mol^{-1}, indicating that NO_3 addition is even less favourable than Cl addition. Formation of HNO_3 + •NCO is more favourable than HCl + NCO formation by about 2 kcal mol^{-1}. The barrier for H abstraction, however, is larger compared to abstraction by both OH and Cl and exceeds 12 kcal mol^{-1}. The most favourable addition process, forming HN•C(=O)NO_3, has a barrier of 15.1 kcal mol^{-1}, but it contributes less than 0.01 % to the reaction rate at room temperature. The overall reaction thus proceeds nearly exclusively by H abstraction forming HNO_3 + •NCO for which we derived the following rate coefficients (see also Fig. 3):

$$k_{NO_3}(298\,K) = 1.11 \times 10^{-21}\,cm^3\,molecule^{-1}\,s^{-1},$$
$$k_{NO_3}(200-450\,K) = 8.87 \times 10^{-42} T^{9.06} \exp(-1585\,K/T)\,cm^3\,molecule^{-1}\,s^{-1}.$$

While this rate coefficient is almost 5 orders of magnitude below that of the OH radical, the nitrate radical is known to be present in higher concentrations during night-time, reaching concentrations as high as 10^9 molecule cm^{-3} (Finlayson-Pitts and Pitts, 1999). The effective rate of the NO_3 reaction at night-time is similar to the reaction with OH at daytime. The NO_3 radical is thus likewise considered to be ineffective for atmospheric removal of HNCO, compared to heterogeneous loss processes.

3.4 HNCO + O_3

The chemistry of ozone with organic compounds is drastically different from radicals, where O_3 typically reacts by cycloaddition on double bonds in unsaturated compounds. For HNCO, cycloaddition pathways have been characterized for both double bonds (HN=C=O). Only cycloaddition on the N=C bond leads to an exothermic reaction, with the oxo-ozonide product being 12 kcal mol^{-1} more stable than the reactants (see Fig. 1). In addition to the traditional cycloaddition channels, three further channels were found, corresponding to H abstraction, forming HO_3 + NCO; oxygen transfer to the N atom, forming ON(H)CO + $^1O_2$; and addition on the C and N atoms, forming HN(OO)C(O)O. The HO_3 product radical is known to be only weakly bonded by 2.94 kcal mol^{-1}, falling apart to OH + O_2 (Bartlett et al., 2019; Le Picard et al., 2010; Varandas, 2014).

The cyclo-addition channels on the hetero-atom double bonds have high-energy barriers, exceeding 30 kcal mol^{-1}, significantly larger than typical barriers for C=C bonds with aliphatic substitutions. Surprisingly, this allows H abstraction to become competitive to cycloaddition, with a comparable barrier of 32 kcal mol^{-1}. For the overall reaction, we obtain the following rate coefficients (see also Fig. 3):

$$k_{O_3}(298\,K) = 2.95 \times 10^{-37}\,cm^3\,molecule^{-1}\,s^{-1},$$
$$k_{O_3}(200-450\,K) = 3.72 \times 10^{-23} T^{2.96} \exp(-14700\,K/T)\,cm^3\,molecule^{-1}\,s^{-1}.$$

At room temperature, H abstraction contributes 80 % to the total reaction and cycloaddition on the N=C bond the remaining 20 %. All other channels are negligible. The rate coefficient is exceedingly low, $\sim 10^{-37}$ cm^3 $molecule^{-1}$ s^{-1}, such that even in areas with very high ozone concentrations of 100 ppbv the loss by ozonolysis is expected to be negligible.

The Supplement provides information on the extended potential energy surface of the HNCO + O_3 reaction, with information on 10 intermediates, 30 transition states, and 15 products. The lowest-energy unimolecular product channel leads to formation of CO_2 + HNOO by breaking of the cyclic primary ozonide (see Fig. 1) following the traditional Criegee mechanism (Criegee, 1975).

4 H-abstraction reactions by NCO radicals

The radical reactions characterized above proceed by H abstraction, forming the NCO radical with an H_2O, HNO_3, or HCl co-product. Likewise, the ozonolysis reaction proceeds for a large part by H abstraction, forming NCO with a HO_3 co-product that readily dissociates to OH + O_2. Though NCO radical formation through these reactions is found to be negligibly slow in atmospheric conditions, this radical remains of interest in other environments. Examples include combustion chemistry, where it can be formed di-

rectly from nitrogen-containing fuels and where it is a critical radical intermediate in, for example, the RAPRENOx (RAPid REmoval of nitrogen oxides) NO_x mitigation strategy which employs HNCO introduced in the combustion mixture through $(HOCN)_3$ (cyanuric acid) injection (Fenimore, 1971; Gardiner, 2000). The NCO radical has also been observed in space (Marcelino et al., 2018). There is extensive experimental and theoretical information on the reactions of NCO radicals, e.g. tabulated in Tsang (1992), Baulch et al. (2005), and other works. To our knowledge, the rate coefficients of the reactions of NCO radicals with H_2O, HNO_3, and HCl have not been determined before, but Tsang (1992) has estimated a rate coefficient $k(\mathrm{NCO}+\mathrm{H_2O}) = 3.9\times10^{-19}T^{2.1}\exp(-3046\,\mathrm{K}/T)\,\mathrm{cm^3\,molecule^{-1}\,s^{-1}}$ based on the equilibrium constant and rate coefficient of the HNCO + OH reaction. Since the H–N bond in HNCO is quite strong, with a bond energy of $\sim 110\,\mathrm{kcal\,mol^{-1}}$ (Ruscic, 2014; Ruscic and Bross, 2019), it is expected that NCO can readily abstract a hydrogen atom from most hydrogen-bearing species to produce HNCO, and that H abstraction is the main reaction channel. Hence, despite that our potential energy surfaces do not include an exhaustive search of all possible reaction channels in the NCO radical chemistry, we expect that the single-channel H-abstraction rate predictions for NCO from H_2O, HNO_3, and HCl are sufficiently dominant that these rates are fair estimates of the total rate coefficients including all possible channels for each of these reactions.

The energy barriers for the NCO radical reactions with H_2O, HNO_3, and HCl, being 14, 7, and $4\,\mathrm{kcal\,mol^{-1}}$, respectively (see Fig. 1), follow the bond strength trend in these reactants, with $D_0(\mathrm{H-OH}) = 118\,\mathrm{kcal\,mol^{-1}}$, $D_0(\mathrm{H-NO_3}) = 104\,\mathrm{kcal\,mol^{-1}}$, and $D_0(\mathrm{H-Cl}) = 103\,\mathrm{kcal\,mol^{-1}}$ (Luo, 2007; Ruscic et al., 2002). Figure 1 also shows that the $\mathrm{NCO}+\mathrm{H_2O}$ reaction is endothermic by $8\,\mathrm{kcal\,mol^{-1}}$, while the HNO_3 and HCl paths are exothermic by -5 and $-7\,\mathrm{kcal\,mol^{-1}}$, respectively. The predicted rate coefficients are then the following:

$$k_{\mathrm{NCO+H_2O}}(300\,\mathrm{K}) = 1.36\times10^{-21}\,\mathrm{cm^3\,molecule^{-1}\,s^{-1}},$$
$$k_{\mathrm{NCO+HNO_3}}(300\,\mathrm{K}) = 3.37\times10^{-17}\,\mathrm{cm^3\,molecule^{-1}\,s^{-1}},$$
$$k_{\mathrm{NCO+HCl}}(300\,\mathrm{K}) = 1.39\times10^{-14}\,\mathrm{cm^3\,molecule^{-1}\,s^{-1}},$$
$$k_{\mathrm{NCO+H_2O}}(300-3000\,\mathrm{K}) = 4.59\times10^{-24}T^{3.63}\exp(-4530\,\mathrm{K}/T)\,\mathrm{cm^3\,molecule^{-1}\,s^{-1}},$$
$$k_{\mathrm{NCO+HNO_3}}(300-3000\,\mathrm{K}) = 7.18\times10^{-26}T^{4.21}\exp(-1273\,\mathrm{K}/T)\,\mathrm{cm^3\,molecule^{-1}\,s^{-1}},$$
$$k_{\mathrm{NCO+HCl}}(300-3000\,\mathrm{K}) = 3.73\times10^{-20}T^{2.63}\exp(-662\,\mathrm{K}/T)\,\mathrm{cm^3\,molecule^{-1}\,s^{-1}}.$$

The indirect estimate of Tsang (1992) compares well to our prediction for $\mathrm{NCO}+\mathrm{H_2O}$, reproducing our values within a factor of 15 at 1000 K and a factor of 3 at 2000 K, i.e. within the stated uncertainties. An analysis of the impact of the NCO reactions in combustion or non-terrestrial environments is well outside the scope of this paper, and reactions with other co-reactants not discussed in this paper are likely to be of higher importance, e.g. H abstraction from organic compounds or recombination with other radicals. In atmospheric conditions, the fate of the NCO radical is likely recombination with an O_2 molecule, with a rate coefficient of $k(298\,\mathrm{K}) = 1.3\times10^{-12}\,\mathrm{cm^3\,molecule^{-1}\,s^{-1}}$ (Manion et al., 2020; Schacke et al., 1974), leaving H_2O, HNO_3, and HCl as negligible co-reactants. Hence, the NCO radical will not affect the atmospheric fate of any of these compounds to any extent. Subsequent chemistry of the $^{\bullet}$OONCO radical is assumed to be conversion to an $^{\bullet}$ONCO alkoxy radical through reactions with NO, HO_2, or RO_2, followed by dissociation to NO + CO.

5 Global impact

Global atmospheric simulations allow us to gain insights into the significance of the chemical loss processes of HNCO and its distribution. Table 1 shows the corresponding HNCO budget for both performed simulations. The full kinetic model including our theoretically predicted gas-phase chemical reactions of HNCO is detailed in Tables S1 and S2 of the Supplement. Figure 4 shows the mean seasonal surface mixing ratio of HNCO using the biomass burning emission factors by Koss et al. (2018). It can be observed that high levels persist in each season. In general, high HNCO levels occur in regions associated with frequent biomass burning activities. Regions with no biomass burning activities have low HNCO concentrations, mainly caused by free tropospheric entrainment from regions with higher concentrations. The global vertical profile of HNCO is well illustrated by that for January as given in Fig. 5, showing that the free troposphere contains about 81 % of the total HNCO mass. The gas-phase production via formamide differs greatly depending on the biomass burning emissions used. In the case of Kumar et al. (2018), significantly more formamide is emitted, leading to a higher production of HNCO in the gas phase. The hydrolysis of HNCO produces $\sim 120\,\mathrm{Tg\,yr^{-1}}$ of ammonia and thus contributing little to the global ammonia budget. Our estimate is a factor of 5–6 lower than the upper limit estimated by Leslie et al. (2019).

The model predictions for local OH radical concentrations range from 1.15×10^{0} to $1.56\times10^{7}\,\mathrm{molecule\,cm^{-3}}$, with a weighted atmospheric global average of $1.14\times10^{6}\,\mathrm{molecule\,cm^{-3}}$; in the air parcel where the highest OH concentration is found this leads to a HNCO lifetime towards OH of more than 500 years when accounting for the temperature-dependent rate coefficient (~ 276 K). In the planetary boundary layer, the highest OH concentration predicted is $7.6\times10^{6}\,\mathrm{molecule\,cm^{-3}}$ at a temperature of 297.8 K, leading to a HNCO lifetime to OH of

Table 1. Yearly global HNCO budget in 2011 for both biomass burning emission datasets by Kumar et al. (2018) and Koss et al. (2018). Additionally, the HNCO budget from Young et al. (2012) is given for comparison.

	Simulations in this study based on emission factors		Comparable literature
	Koss et al. (2018)	Kumar et al. (2018)	Young et al. (2012)
Emissions ($Gg\,yr^{-1}$)			
Biomass burning (HNCO)	2160	815	661
Anthropogenic (HNCO)	177	177	828
Gas-phase production ($Gg\,yr^{-1}$)			
$NH_2CHO + OH$	482[a]	2370[b]	–
Gas-phase loss ($Gg\,yr^{-1}$)			
$HNCO + OH$	4.0	5.4	~ 6.0
$HNCO + O_3$	1.9×10^{-16}	2.4×10^{-16}	–
$HNCO + NO_3$	1.1×10^{-4}	1.4×10^{-4}	–
$HNCO + Cl$	1.0×10^{-7}	1.4×10^{-7}	–
Heterogeneous losses ($Gg\,yr^{-1}$)			
Dry deposition	250	2890	~ 1420
Over land	1170	1090	–
Over ocean	1340	1810	–
Scavenging	275	377	–
Wet deposition	0.13	0.16	~ 67
Yearly-mean burden (Gg)	201	272	~ 150
Atmospheric lifetime (d)	26	30	37

[a] of which 51 $Gg\,yr^{-1}$ is NH_2CHO biomass burning emissions (Koss et al., 2018)
[b] of which 2340 $Gg\,yr^{-1}$ is NH_2CHO biomass burning emissions (Kumar et al., 2018)

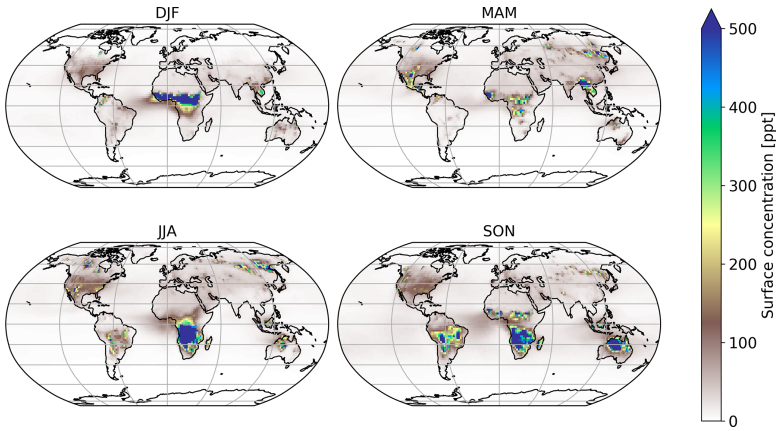

Figure 4. Mean seasonal surface concentration of HNCO using Koss et al. (2018) biomass burning emission factors.

~ 6 years in that air parcel. The calculated average OH concentration of 1.2×10^6 molecule cm^{-3} in the boundary layer leads to lifetimes towards OH of about 40 years near the surface. For O_3, Cl, and NO_3 – with maximum oxidant concentrations of 1.0×10^{13}, 7.8×10^5, 1.5×10^9 molecule cm^{-3} and atmospheric average concentrations of 1.0×10^{12}, 2.0×10^3, and 1.1×10^7 molecule cm^{-3}, respectively – even longer temperature-dependent lifetimes are found, exceeding 5000 years even in the air parcels with the most favourable co-reactant concentration and temperature.

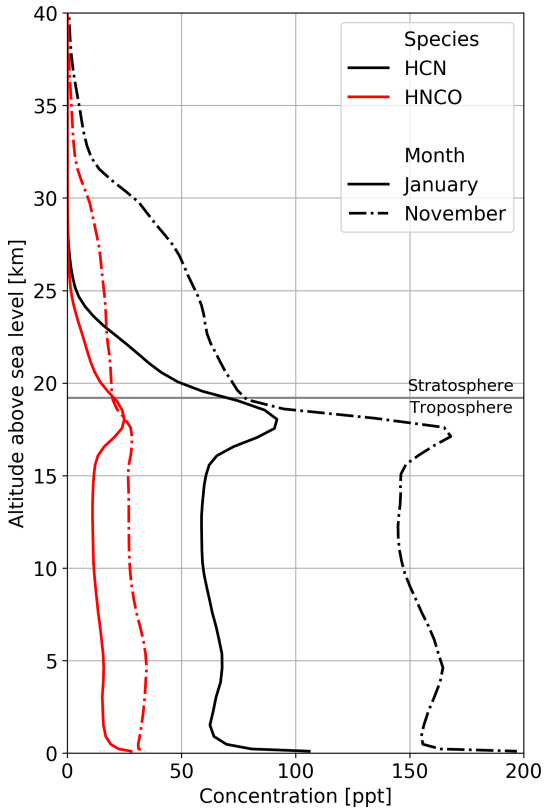

Figure 5. Mean vertical profiles of HCN (black) and HNCO (red) for January (solid lines) and November (dashed-dotted lines) over South East Asia. Biomass burning emission factors are based on Koss et al. (2018).

The relative contributions of the different co-reactants varies locally and temporally, and shorter lifetimes might occur locally when co-reactant concentration and temperature are at their most favourable, but it is clear that gas-phase chemical losses of HNCO are small. Only the reaction of HNCO with OH leads to some destruction of HNCO, while the other chemical sinks (O_3, NO_3, and Cl) are negligible. When compared to the major loss processes, however, all these loss processes are negligible on a global scale (see Table 1). Young et al. (2012) have a somewhat higher chemical loss via OH compared to our result, which is due to the higher rate constant used. Figure 2 shows the rate coefficient that would be required to allow for the gas-phase loss of HNCO by reaction with OH radicals to contribute 10 % of the total atmospheric sink, which is well outside the expected uncertainty of the theoretical kinetic rate predictions. It can therefore be robustly concluded that the gas-phase chemical sinks predicted and assessed in this study (OH, Cl, NO_3, O_3) are insignificant when compared to heterogeneous loss processes, confirming earlier assumptions. This is independent of the high uncertainty in the available biomass burning emission factors or missing road emission datasets.

As seen in Table 1 the major sinks are dry deposition and scavenging (heterogeneous losses), where the former contributes between 2520 and 2890 Gg yr^{-1} and the latter from 274 to 377 Gg yr^{-1}, when using the emission factors by Koss et al. (2018) and Kumar et al. (2018), respectively. The results in this study are in a similar range as the modelling study by Young et al. (2012). These authors had lower total HNCO emissions and did not include formamide as a secondary source of HNCO. The lower total HNCO emissions could be explained by a different year simulated in that study and different biomass burning emission model approaches used. Young et al. (2012) also scaled their HNCO emissions to the HCN emissions by a factor of 0.3, whereas in this study actual measured emission factors are used. In our study, formamide contributes between 17 % and 70 % of the total HNCO emissions when using the biomass burning emission factors by Koss et al. (2018) and Kumar et al. (2018) respectively. Young et al. (2012) find a higher HNCO lifetime due to generally lower total heterogeneous loss terms (dry and wet deposition). The total dry deposition varies slightly depending on the biomass burning emission factor used (see Table 1). In both scenarios, most HNCO is deposited over the ocean. For biomass burning emission factors from Koss et al. (2018), this contribution 53 %, is significantly lower when compared to the simulation using emission factors from Kumar et al. (2018), where about 62 % of the total HNCO deposition is deposited over the ocean. The larger fraction of computed HNCO deposition over the ocean is a consequence of the much larger secondary HNCO production from formamide far from its source regions (continents). Young et al. (2012) found that the importance of both heterogeneous loss processes depends on the cloud pH. In the SCAV submodel, as used in this work, cloud droplet pH is calculated online and includes an explicit hydrolysis scheme for HNCO, whereas Young et al. (2012) used a simplified approach. The relative importance of dry deposition is higher in the simulation in which Young et al. (2012) calculated pH online, when compared to the findings in this study.

The atmospheric lifetime of HNCO is dominated by its heterogeneous loss processes, leading to an atmospheric lifetime of multiple weeks when accounting for all HNCO losses (chemical and heterogeneous), as opposed to a gas-phase lifetime in the free troposphere of about 50 years when calculated solely based on the chemical losses towards the four chemical oxidants described in this study. This long gas-phase lifetime and the fact that mainly surface sources are relevant indicate that atmospheric HNCO distribution is significantly affected by transport processes. Our simulations even show that HNCO is transported from the surface into the UTLS and that about 10 % of the total atmospheric HNCO mass is located in the stratosphere (see Fig. 5), with mod-

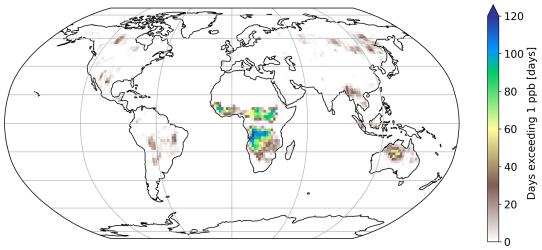

Figure 6. Number of days exceeding 1 ppb of HNCO at the surface. Biomass burning emission factors are based on Koss et al. (2018).

elled concentrations of HNCO in the lower stratosphere of typically tens of parts per trillion by volume but reaching up to hundreds of parts per trillion by volume in tropical regions. In the chemical model, photolysis in the stratosphere was not taken into account. Thus, OH is the only significant stratospheric sink included, resulting in a stratospheric lifetime of more than 330 years. During the monsoon period, the total stratospheric HNCO mass increases from 15 Gg before to 20 Gg at the end of the monsoon season. Pumphrey et al. (2018) demonstrated that in 2015 and 2016, elevated levels of stratospheric hydrogen cyanide (HCN) can be linked to biomass burning emissions from Indonesian fires. Figure 5 shows the vertical profiles of HCN and HNCO over South East Asia well before (January) and after (November) the Indian monsoon. It becomes evident that, similar to HNCO in our simulations, tropospheric and stratospheric concentrations of HCN increase during the Indian monsoon period. In the performed simulations, the ratio between stratospheric HCN and HNCO is very similar throughout the year, indicating that HCN and HNCO are similarly affected by transport processes within this period. The combination of strong biomass burning events and strong vertical transport during the monsoon period leads to high HNCO concentrations in the UTLS, indicating that pollutants from biomass burning events could potentially influence stratospheric chemistry.

Figure 6 shows the number of days exceeding a daily mean HNCO concentration of 1 ppbv. Mainly regions impacted by biomass burning events have frequent concentrations above this threshold. When using 10 ppbv as a limit for toxic concentrations of HNCO, as proposed by the Swedish Work Environment Authority (SWEA, 2011), only a few days can be observed in which this limit is exceeded. The maximum number of days exceeding 10 ppbv is 10 d over Africa, compared to 120 d above 1 ppbv. It is important to take into account that this analysis is limited by the computational output available in this study, which has only daily averages. Therefore, it is expected that areas which frequently exceed daily averages of 1 ppbv are potentially areas in which peak HNCO can be observed above 10 ppbv throughout the day.

No correlation exists between the number of days exceeding 1 or 10 ppbv and road traffic emissions. This becomes evident since typical areas of high road traffic activities (i.e. USA and Europe) do not exceed daily averages of 1 ppbv (see Fig. 6). Road traffic activities occur on a smaller spatial scale than biomass burning events. The EMAC model used is not capable of representing, for example, inner-city road traffic activities, due to the spatial resolution of the model used (1.875° by 1.875° in latitude and longitude). Therefore, we are not capable of drawing any conclusion if 10 ppbv is exceeded regionally in densely populated areas, impacted by high traffic emissions.

6 Conclusions

The isocyanic acid molecule, HNCO, is found to be chemically unreactive towards the dominant atmospheric gas-phase oxidants, i.e. OH and NO_3 radicals, Cl atoms, and O_3 molecules. The reactions all remove HNCO predominantly by H abstraction and have low rates of reactions with $k(298\,\mathrm{K}) \leq 7 \times 10^{-16}\,\mathrm{cm^3\,molecule^{-1}\,s^{-1}}$, leading to chemical gas-phase lifetimes of decades to centuries. Yearly loss of HNCO towards these reactants is only $\sim 5\,\mathrm{Gg\,yr^{-1}}$ out of $\sim 3000\,\mathrm{Gg\,yr^{-1}}$ total losses. Removal of HNCO by clouds and precipitation ("scavenging"), with hydrolysis to ammonia, is also implemented in the global model and was found to contribute significantly more, $\sim 300\,\mathrm{Gg\,yr^{-1}}$, than the gas-phase loss processes. Still, these combined processes are overwhelmed by the loss of HNCO by dry deposition, which is removing $\sim 2700\,\mathrm{Gg\,yr^{-1}}$. These conclusions are robust against modifications of the emission scenarios, where two distinct sets of emission factors were used, incorporating HNCO formation from biomass burning, as well as anthropogenic sources such as formamide oxidation and road traffic. The inefficiency of gas-phase chemical loss processes confirms earlier assumptions; inclusion of the gas-phase chemical loss processes in kinetic models appears superfluous except in specific experimental conditions with very high co-reactant concentrations. The long gas-phase chemical lifetime (multiple decades to centuries) allows HNCO to be transported efficiently into the upper troposphere lower stratosphere (UTLS) demonstrating that surface emissions may impact the upper troposphere. Further research is necessary to identify the importance of strong biomass burning events coupled to strong vertical transport processes (i.e. monsoon systems) on the chemical composition of the UTLS.

On a global scale, the daily-average concentrations of HNCO rarely exceed 10 ppbv, which is the threshold assumed here for toxicity; the exceedances are mainly located in regions with strong biomass burning emissions. Average daily concentrations of the order of 1 ppbv are encountered more frequently, with about one-third of the year exceeding this limit. This suggests that local concentrations might peak to much higher values, e.g. in urban environments where road traffic emissions are highest, or in the downwind plume of

biomass burning events, and could impact regional air quality. Such regional effects were not studied in the current work, as the resolution of the global model used here is not sufficiently fine grained.

Though not important for the atmosphere, we briefly examined the reactions of the NCO radical formed in the chemical reactions studied. The rate coefficients of the H-abstraction reactions with H_2O, HNO_3, and HCl suggest that these reactions might contribute in high-temperature environments, such as combustion processes.

Data availability. The simulation results are archived at the Jülich Supercomputing Centre (JSC) and are available on request from Domenico Taraborrelli (d.taraborrelli@fz-juelich.de).

Supplement. The supplement related to this article contains extended information on the chemical model and the quantum chemical characterizations (geometric, energetic, and entropic data). The supplement related to this article is available online at: https://doi.org/10.5194/acp-20-6671-2020-supplement.

Author contributions. The quantum chemical calculations were performed by HMTN, GHTV, and TVP, while LV performed the theoretical kinetic calculations. UJ, SR, and DT collected the literature data on HNCO sources and sinks and implemented these in the kinetic model; the model runs were performed by SR and DT. All authors contributed significantly to the writing of the article.

Competing interests. The authors declare that they have no conflict of interest.

Acknowledgements. Hue M. T. Nguyen, Giang H. T. Vu, and Tien V. Pham thank the National Foundation for Science and Technology Development (Nafosted), Vietnam, for sponsoring this work under project number 104.06-2015.85. Simon Rosanka and Domenico Taraborrelli gratefully acknowledge the Earth System Modelling Project (ESM) for funding this work by providing computing time on the ESM partition of the supercomputer JUWELS at the Jülich Supercomputing Centre (Forschungszentrum Jülich, 2019).

Financial support. This research has been supported by the National Foundation for Science and Technology Development (Nafosted), Vietnam (grant no. 104.06-2015.85).

The article processing charges for this open-access publication were covered by a Research Centre of the Helmholtz Association.

Review statement. This paper was edited by James Roberts and reviewed by two anonymous referees.

References

Alecu, I. M., Zheng, J., Zhao, Y., and Truhlar, D. G.: Computational Thermochemistry: Scale Factor Databases and Scale Factors for Vibrational Frequencies Obtained from Electronic Model Chemistries, J. Chem. Theory Comput., 6, 2872–2887, https://doi.org/10.1021/ct100326h, 2010.

Baker, R. R. and Bishop, L. J.: The pyrolysis of tobacco ingredients, J. Anal. Appl. Pyrolysis, 71, 223–311, https://doi.org/10.1016/S0165-2370(03)00090-1, 2004.

Bao, J. L., Zheng, J., Alecu, I. M., Lynch, B. J., Zhao, Y., and Truhlar, D. G.: Database of Frequency Scale Factors for Electronic Model Chemistries (Version 3 Beta 2), available at: http://comp.chem.umn.edu/freqscale/index.html (last access: 29 May 2020), 2017.

Barnes, I., Solignac, G., Mellouki, A., and Becker, K. H.: Aspects of the Atmospheric Chemistry of Amides, Chemphyschem, 11, 3844–3857, https://doi.org/10.1002/cphc.201000374, 2010.

Barth, M. C., Cochran, A. K., Fiddler, M. N., Roberts, J. M., and Bililign, S.: Numerical modeling of cloud chemistry effects on isocyanic acid (HNCO), J. Geophys. Res.-Atmos., 118, 8688–8701, https://doi.org/10.1002/jgrd.50661, 2013.

Bartlett, M. A., Kazez, A. H., Schaefer, H. F., and Allen, W. D.: Riddles of the structure and vibrational dynamics of HO_3 resolved near the ab initio limit, J. Chem. Phys., 151, 094304, https://doi.org/10.1063/1.5110291, 2019.

Baulch, D. L., Bowman, C. T., Cobos, C. J., Cox, R. A., Just, Th., Kerr, J. A., Pilling, M. J., Stocker, D., Troe, J., Tsang, W., Walker, R. W., and Warnatz, J.: Evaluated Kinetic Data for Combustion Modeling: Supplement II, J. Phys. Chem. Ref. Data, 34, 757, https://doi.org/10.1063/1.1748524, 2005.

Becke, A. D.: A New Mixing of Hartree-Fock and Local Density-Functional Theories, J. Chem. Phys., 98, 1372–1377, https://doi.org/10.1063/1.464304, 1993.

Behar, D.: Pulse-Radiolysis Study of Aqueous Hydrogen-Cyanide and Cyanide Solutions, J. Phys. Chem., 78, 2660–2663, https://doi.org/10.1021/j100619a005, 1974.

Belson, D. J. and Strachan, A. N.: Preparation and Properties of Isocyanic Acid, Chem. Soc. Rev., 11, 41–56, https://doi.org/10.1039/cs9821100041, 1982.

Blomqvist, P., Hertzberg, T., Dalene, M., and Skarping, G.: Isocyanates, aminoisocyanates and amines from fires – a screening of common materials found in buildings, Fire Mater., 27, 275–294, https://doi.org/10.1002/fam.836, 2003.

Borduas, N., da Silva, G., Murphy, J. G., and Abbatt, J. P. D.: Experimental and Theoretical Understanding of the Gas Phase Oxidation of Atmospheric Amides with OH Radicals: Kinetics, Products, and Mechanisms, J. Phys. Chem. A, 119, 4298–4308, https://doi.org/10.1021/jp503759f, 2015.

Borduas, N., Murphy, J. G., Wang, C., da Silva, G., and Abbatt, J. P. D.: Gas Phase Oxidation of Nicotine by OH Radicals: Kinetics, Mechanisms, and Formation of HNCO, Environ. Sci. Technol. Lett., 3, 327–331, https://doi.org/10.1021/acs.estlett.6b00231, 2016a.

Borduas, N., Place, B., Wentworth, G. R., Abbatt, J. P. D., and Murphy, J. G.: Solubility and reactivity of HNCO in water: insights into HNCO's fate in the atmosphere, Atmos. Chem. Phys., 16, 703–714, https://doi.org/10.5194/acp-16-703-2016, 2016b.

Brady, J. M., Crisp, T. A., Collier, S., Kuwayama, T., Forestieri, S. D., Perraud, V., Zhang, Q., Kleeman, M. J., Cappa, C. D., and Bertram, T. H.: Real-Time Emission Factor Measurements of Isocyanic Acid from Light Duty Gasoline Vehicles, Environ. Sci. Technol., 48, 11405–11412, https://doi.org/10.1021/es504354p, 2014.

Büchler, H., Bühler, R. E., and Cooper, R.: Pulse radiolysis of aqueous cyanide solutions. Kinetics of the transient hydroxyl radical and hydrogen atom adducts and subsequent rearrangements, J. Phys. Chem., 80, 1549–1553, https://doi.org/10.1021/j100555a006, 1976.

Bunkan, A. J. C., Hetzler, J., Mikoviny, T., Wisthaler, A., Nielsen, C. J., and Olzmann, M.: The reactions of N-methylformamide and N,N-dimethylformamide with OH and their photo-oxidation under atmospheric conditions: experimental and theoretical studies, Phys. Chem. Chem. Phys., 17, 7046–7059, https://doi.org/10.1039/c4cp05805d, 2015.

Bunkan, A. J. C., Mikoviny, T., Nielsen, C. J., Wisthaler, A., and Zhu, L.: Experimental and Theoretical Study of the OH-Initiated Photo-oxidation of Formamide, J. Phys. Chem. A, 120, 1222–1230, https://doi.org/10.1021/acs.jpca.6b00032, 2016.

Calvert, J. G.: Mechanisms of atmospheric oxidation of the alkanes, Oxford University Press, Oxford, New York, 2008.

Chandra, B. P. and Sinha, V.: Contribution of post-harvest agricultural paddy residue fires in the NW Indo-Gangetic Plain to ambient carcinogenic benzenoids, toxic isocyanic acid and carbon monoxide, Environ. Int., 88, 187–197, https://doi.org/10.1016/j.envint.2015.12.025, 2016.

Criegee, R.: Mechanism of Ozonolysis, Angew. Chem. Int. Ed. Engl., 14, 745–752, https://doi.org/10.1002/anie.197507451, 1975.

Crippa, M., Janssens-Maenhout, G., Dentener, F., Guizzardi, D., Sindelarova, K., Muntean, M., Van Dingenen, R., and Granier, C.: Forty years of improvements in European air quality: regional policy-industry interactions with global impacts, Atmos. Chem. Phys., 16, 3825–3841, https://doi.org/10.5194/acp-16-3825-2016, 2016.

DrozGeorget, T., Zyrianov, M., Reisler, H., and Chandler, D. W.: Correlated distributions in the photodissociation of HNCO to NH(X-3 Sigma(-),a(1)Delta)+CO(X-1 Sigma(+)) near the barrier on S-1, Chem. Phys. Lett., 276, 316–324, https://doi.org/10.1016/S0009-2614(97)00804-X, 1997.

Dunning, T. H.: Gaussian basis sets for use in correlated molecular calculations. I. The atoms boron through neon and hydrogen, J. Chem. Phys., 90, 1007–1023, https://doi.org/10.1063/1.456153, 1989.

Fenimore, C. P.: Formation of nitric oxide in premixed hydrocarbon flames, Proc. Combust. Inst., 13, 373–380, 1971.

Finlayson-Pitts, B. J. and Pitts, J. N.: Chemistry of the Upper and Lower Atmosphere: Theory, Experiments, and Applications, Academic Press, San Diego, 1999.

Fischer, G., Geith, J., Klapotke, T. M., and Krumm, B.: Synthesis, properties and dimerization study of isocyanic acid, Z. Naturforschung Sect. B-J. Chem. Sci., 57, 19–24, 2002.

Forschungszentrum Jülich: JUWELS: Modular Tier-0/1 Supercomputer at Jülich Supercomputing Centre, J. Large-Scale Res. Facil., 5, A135, https://doi.org/10.17815/jlsrf-5-171, 2019.

Gardiner, W. C. (Ed.): Gas-phase combustion chemistry, Springer, New York, 2000.

Heeb, N. V., Zimmerli, Y., Czerwinski, J., Schmid, P., Zennegg, M., Haag, R., Seiler, C., Wichser, A., Ulrich, A., Honegger, P., Zeyer, K., Emmenegger, L., Mosimann, T., Kasper, M., and Mayer, A.: Reactive nitrogen compounds (RNCs) in exhaust of advanced PM-NOx abatement technologies for future diesel applications, Atmos. Environ., 45, 3203–3209, https://doi.org/10.1016/j.atmosenv.2011.02.013, 2011.

Hofzumahaus, A., Kraus, A., Kylling, A., and Zerefos, C. S.: Solar actinic radiation (280–420 nm) in the cloud-free troposphere between ground and 12 km altitude: Measurements and model results, J. Geophys. Res.-Atmos., 107, D18, https://doi.org/10.1029/2001jd900142, 2002.

Huber, K.-P. and Herzberg, G.: Molecular Spectra and Molecular Structure IV. Constants of diatomic molecules, Van Nostrand Reinhold, New York, 1979.

IUPAC Subcommittee on Atmospheric Chemical Kinetic Data Evaluation: Evaluated Kinetic Data, English, IUPAC, available at: http://iupac.pole-ether.fr/index.html (last access: 29 May 2020), 2017.

Jankowski, M. J., Olsen, R., Nielsen, C. J., Thomassen, Y., and Molander, P.: The applicability of proton transfer reaction-mass spectrometry (PTR-MS) for determination of isocyanic acid (ICA) in work room atmospheres, Environ. Sci.-Process. Impacts, 16, 2423–2431, https://doi.org/10.1039/c4em00363b, 2014.

Jathar, S. H., Heppding, C., Link, M. F., Farmer, D. K., Akherati, A., Kleeman, M. J., de Gouw, J. A., Veres, P. R., and Roberts, J. M.: Investigating diesel engines as an atmospheric source of isocyanic acid in urban areas, Atmos. Chem. Phys., 17, 8959–8970, https://doi.org/10.5194/acp-17-8959-2017, 2017.

Jöckel, P., Sander, R., Kerkweg, A., Tost, H., and Lelieveld, J.: Technical Note: The Modular Earth Submodel System (MESSy) – a new approach towards Earth System Modeling, Atmos. Chem. Phys., 5, 433–444, https://doi.org/10.5194/acp-5-433-2005, 2005.

Jöckel, P., Kerkweg, A., Pozzer, A., Sander, R., Tost, H., Riede, H., Baumgaertner, A., Gromov, S., and Kern, B.: Development cycle 2 of the Modular Earth Submodel System (MESSy2), Geosci. Model Dev., 3, 717–752, https://doi.org/10.5194/gmd-3-717-2010, 2010.

Johnston, H. S. and Heicklen, J.: Tunneling corrections for unsymmetrical Eckart potential energy barriers, J. Phys. Chem., 66, 532–533, https://doi.org/10.1021/j100809a040, 1962.

Kaiser, J. W., Heil, A., Andreae, M. O., Benedetti, A., Chubarova, N., Jones, L., Morcrette, J.-J., Razinger, M., Schultz, M. G., Suttie, M., and van der Werf, G. R.: Biomass burning emissions estimated with a global fire assimilation system based on observed fire radiative power, Biogeosciences, 9, 527–554, https://doi.org/10.5194/bg-9-527-2012, 2012.

Keller-Rudek, H., Moortgat, G. K., Sander, R., and Sörensen, R.: The MPI-Mainz UV/VIS Spectral Atlas of Gaseous Molecules of Atmospheric Interest, Earth Syst. Sci. Data, 5, 365–373, https://doi.org/10.5194/essd-5-365-2013, 2013.

Kerkweg, A., Buchholz, J., Ganzeveld, L., Pozzer, A., Tost, H., and Jöckel, P.: Technical Note: An implementation of the dry removal processes DRY DEPosition and SEDImentation in the Modular Earth Submodel System (MESSy), Atmos. Chem. Phys., 6, 4617–632, https://doi.org/10.5194/acp-6-4617-2006, 2006a.

Kerkweg, A., Sander, R., Tost, H., and Jöckel, P.: Technical note: Implementation of prescribed (OFFLEM), calculated (ONLEM), and pseudo-emissions (TNUDGE) of chemical species in the Modular Earth Submodel System (MESSy), Atmos. Chem. Phys., 6, 3603–3609, https://doi.org/10.5194/acp-6-3603-2006, 2006b.

Koss, A. R., Sekimoto, K., Gilman, J. B., Selimovic, V., Coggon, M. M., Zarzana, K. J., Yuan, B., Lerner, B. M., Brown, S. S., Jimenez, J. L., Krechmer, J., Roberts, J. M., Warneke, C., Yokelson, R. J., and de Gouw, J.: Non-methane organic gas emissions from biomass burning: identification, quantification, and emission factors from PTR-ToF during the FIREX 2016 laboratory experiment, Atmos. Chem. Phys., 18, 3299–3319, https://doi.org/10.5194/acp-18-3299-2018, 2018.

Kumar, V., Chandra, B. P., and Sinha, V.: Large unexplained suite of chemically reactive compounds present in ambient air due to biomass fires, Sci. Rep.-UK, 8, 626, https://doi.org/10.1038/s41598-017-19139-3, 2018.

Lee, C., Yang, W., and Parr, R. G.: Development of the Colle-Salvetti correlation-energy formula into a functional of the electron density, Phys. Rev. B, 37, 785–789, https://doi.org/10.1103/PhysRevB.37.785, 1988.

Le Picard, S. D., Tizniti, M., Canosa, A., Sims, I. R., and Smith, I. W. M.: The Thermodynamics of the Elusive HO_3 Radical, Science, 328, 1258–1262, https://doi.org/10.1126/science.1184459, 2010.

Leslie, M. D., Ridoli, M., Murphy, J. G., and Borduas-Dedekind, N.: Isocyanic acid (HNCO) and its fate in the atmosphere: a review, Environ. Sci.-Process. Impacts, 21, 793–808, https://doi.org/10.1039/c9em00003h, 2019.

Liebig, J. and Wöhler, F.: Untersuchungen über die Cyansäure, Ann. Phys., 96, 369–400, https://doi.org/10.1002/andp.18300961102, 1830.

Liggio, J., Stroud, C. A., Wentzell, J. J. B., Zhang, J. H., Sommers, J., Darlington, A., Liu, P. S. K., Moussa, S. G., Leithead, A., Hayden, K., Mittermeier, R. L., Staebler, R., Wolde, M., and Li, S. M.: Quantifying the Primary Emissions and Photochemical Formation of Isocyanic Acid Downwind of Oil Sands Operations, Environ. Sci. Technol., 51, 14462–14471, https://doi.org/10.1021/acs.est.7b04346, 2017.

Luo, Y.-R.: Comprehensive Handbook of Chemical Bond Energies, 1st edn., CRC Press, Boca Raton, 2007.

Manion, J. A., Huie, R. E., Levin, R. D., Burgess Jr., D. R., Orkin, V. L., Tsang, W., McGivern, W. S., Hudgens, J. W., Knyazev, V. D., Atkinson, D. B., Chai, E., Tereza, A. M., Lin, C.-Y., Allison, T. C., Mallard, W. G., Westley, F., Herron, J. T., Hampson, R. F., and Frizzell, D. H.: NIST Chemical Kinetics Database – Standard Reference Database 17, Version 7.0 (Web Version), Release 1.6.8, Data Version 2017.07, available at: http://kinetics.nist.gov/kinetics/, last access: 29 May 2020.

Marcelino, N., Agundez, M., Cernicharo, J., Roueff, E., and Tafalla, M.: Discovery of the elusive radical NCO and confirmation of H_2NCO^+ in space, Astron. Astrophys., 612, L10, https://doi.org/10.1051/0004-6361/201833074, 2018.

Martin, J. M. L.: Ab initio total atomization energies of small molecules – towards the basis set limit, Chem. Phys. Lett., 259, 669–678, https://doi.org/10.1016/0009-2614(96)00898-6, 1996.

Mertens, J. D., Chang, A. Y., Hanson, R. K., and Bowman, C. T.: A Shock-Tube Study of Reactions of Atomic Oxygen with Isocyanic Acid, Int. J. Chem. Kinet., 24, 279–295, https://doi.org/10.1002/kin.550240306, 1992.

Nielsen, C. J., Herrmann, H., and Weller, C.: Atmospheric chemistry and environmental impact of the use of amines in carbon capture and storage (CCS), Chem. Soc. Rev., 41, 6684–6704, https://doi.org/10.1039/c2cs35059a, 2012.

Okabe, H.: Photodissociation of HNCO in Vacuum Ultraviolet – Production of NCO $A^2\Sigma$ and NH($A^3\pi$, πc^1), J. Chem. Phys., 53, 3507–3515, https://doi.org/10.1063/1.1674525, 1970.

Papajak, E. and Truhlar, D. G.: What are the most efficient basis set strategies for correlated wave function calculations of reaction energies and barrier heights?, J. Chem. Phys., 137, 064110, https://doi.org/10.1063/1.4738980, 2012.

Parandaman, A., Tangtartharakul, C. B., Kumar, M., Francisco, J. S., and Sinha, A.: A Computational Study Investigating the Energetics and Kinetics of the HNCO + $(CH_3)_2NH$ Reaction Catalyzed by a Single Water Molecule, J. Phys. Chem. A, 121, 8465–8473, https://doi.org/10.1021/acs.jpca.7b08657, 2017.

Pumphrey, H. C., Glatthor, N., Bernath, P. F., Boone, C. D., Hannigan, J. W., Ortega, I., Livesey, N. J., and Read, W. G.: MLS measurements of stratospheric hydrogen cyanide during the 2015–2016 El Niño event, Atmos. Chem. Phys., 18, 691–703, https://doi.org/10.5194/acp-18-691-2018, 2018.

Purvis, G. D. and Bartlett, R. J.: A full coupled-cluster singles and doubles model: The inclusion of disconnected triples, J. Chem. Phys., 76, 1910, https://doi.org/10.1063/1.443164, 1982.

Roberts, J. M. and Liu, Y.: Solubility and solution-phase chemistry of isocyanic acid, methyl isocyanate, and cyanogen halides, Atmos. Chem. Phys., 19, 4419–4437, https://doi.org/10.5194/acp-19-4419-2019, 2019.

Roberts, J. M., Veres, P., Warneke, C., Neuman, J. A., Washenfelder, R. A., Brown, S. S., Baasandorj, M., Burkholder, J. B., Burling, I. R., Johnson, T. J., Yokelson, R. J., and de Gouw, J.: Measurement of HONO, HNCO, and other inorganic acids by negative-ion proton-transfer chemical-ionization mass spectrometry (NI-PT-CIMS): application to biomass burning emissions, Atmos. Meas. Tech., 3, 981–990, https://doi.org/10.5194/amt-3-981-2010, 2010.

Roberts, J. M., Veres, P. R., Cochran, A. K., Warneke, C., Burling, I. R., Yokelson, R. J., Lerner, B., Gilman, J. B., Kuster, W. C., Fall, R., and de Gouw, J.: Isocyanic acid in the atmosphere and its possible link to smoke-related health effects, P. Natl. Acad. Sci. USA, 108, 8966–8971, https://doi.org/10.1073/pnas.1103352108, 2011.

Roberts, J. M., Veres, P. R., VandenBoer, T. C., Warneke, C., Graus, M., Williams, E. J., Lefer, B., Brock, C. A., Bahreini, R., Ozturk, F., Middlebrook, A. M., Wagner, N. L., Dube, W. P., and de Gouw, J. A.: New insights into atmospheric sources and sinks of isocyanic acid, HNCO, from recent urban and regional observations, J. Geophys. Res.-Atmos., 119, 1060–1072, https://doi.org/10.1002/2013JD019931, 2014.

Roeckner, E., Brokopf, R., Esch, M., Giorgetta, M., Hagemann, S., Kornblueh, L., Manzini, E., Schlese, U., and Schulzweida, U.: Sensitivity of simulated climate to horizontal and vertical reso-

lution in the ECHAM5 atmosphere model, J. Climate, 19, 3771–3791, https://doi.org/10.1175/JCLI3824.1, 2006.

Ruscic, B.: Uncertainty quantification in thermochemistry, benchmarking electronic structure computations, and Active Thermochemical Tables, Int. J. Quantum Chem., 114, 1097–1101, https://doi.org/10.1002/qua.24605, 2014.

Ruscic, B. and Bross, D. H.: Active Thermochemical Tables (ATcT) values based on ver. 1.122g of the Thermochemical Network (2019), available at: http://atct.anl.gov/ (last access: 29 May 2020), Argonne Natl. Lab. Act. Thermochem, 2019.

Ruscic, B., Wagner, A. F., Harding, L. B., Asher, R. L., Feller, D., Dixon, D. A., Peterson, K. A., Song, Y., Qian, X. M., Ng, C. Y., Liu, J. B., and Chen, W. W.: On the enthalpy of formation of hydroxyl radical and gas-phase bond dissociation energies of water and hydroxyl, J. Phys. Chem. A, 106, 2727–2747, https://doi.org/10.1021/jp013909s, 2002.

Sander, R., Baumgaertner, A., Gromov, S., Harder, H., Jöckel, P., Kerkweg, A., Kubistin, D., Regelin, E., Riede, H., Sandu, A., Taraborrelli, D., Tost, H., and Xie, Z.-Q.: The atmospheric chemistry box model CAABA/MECCA-3.0, Geosci. Model Dev., 4, 373–380, https://doi.org/10.5194/gmd-4-373-2011, 2011.

Schacke, H., Schmatjko, K. J., and Wolfrum, J.: Reaktionen von CN-Radikalen im H-C-N-O-System, Arch. Proces. Spalania, 5, 363, 1974.

Sengupta, D. and Nguyen, M. T.: Mechanism of $NH_2 + CO_2$ formation in OH + HNCO reaction: Rate constant evaluation via ab initio calculations and statistical theory, J. Chem. Phys., 106, 9703–9707, https://doi.org/10.1063/1.474090, 1997.

Sharpe, S. W., Johnson, T. J., Sams, R. L., Chu, P. M., Rhoderick, G. C., and Johnson, P. A.: Gas-phase databases for quantitative infrared spectroscopy, Appl. Spectrosc., 58, 1452–1461, https://doi.org/10.1366/0003702042641281, 2004.

Spiglanin, T. A. and Chandler, D. W.: Rotational State Distributions of NH($a^1\Delta$) from HNCO Photodissociation, J. Chem. Phys., 87, 1577–1581, https://doi.org/10.1063/1.453216, 1987.

Spiglanin, T. A., Perry, R. A., and Chandler, D. W.: Internal State Distributions of CO from HNCO Photodissociation, J. Chem. Phys., 87, 1568–1576, https://doi.org/10.1063/1.453215, 1987.

Stanton, J. F.: On the vibronic level structure in the NO3 radical. I. The ground electronic state, J. Chem. Phys., 126, 134309, https://doi.org/10.1063/1.2715547, 2007.

Stanton, J. F.: On the vibronic level structure in the NO_3 radical: II. Adiabatic calculation of the infrared spectrum, Mol. Phys., 107, 1059–1075, https://doi.org/10.1080/00268970902740530, 2009.

Stanton, J. F. and Okumura, M.: On the vibronic level structure in the NO_3 radical?: Part III. Observation of intensity borrowing via ground state mixing, Phys. Chem. Chem. Phys., 11, 4742, https://doi.org/10.1039/b902252j, 2009.

Stone, D., Whalley, L. K., and Heard, D. E.: Tropospheric OH and HO_2 radicals: field measurements and model comparisons, Chem. Soc. Rev., 41, 6348–6404, https://doi.org/10.1039/c2cs35140d, 2012.

Suarez-Bertoa, R. and Astorga, C.: Isocyanic acid and ammonia in vehicle emissions, Transp. Res. Part-Transp. Environ., 49, 259–270, https://doi.org/10.1016/j.trd.2016.08.039, 2016.

SUVA: Grenzwerte am Arbeitsplatz 2016, available at: https://www.suva.ch/1903.d (last access: 29 May 2020), 2016.

SWEA: Occupational exposure limit values. Provision (AFS) 2011:18, Swedish Work Environment Authority, Stockholm, Sweden, ISBN 978-91-7930-559-8, 2011.

Taylor, W. D., Allston, T. D., Moscato, M. J., Fazekas, G. B., Kozlowski, R., and Takacs, G. A.: Atmospheric Photo-Dissociation Lifetimes for Nitromethane, Methyl Nitrite, and Methyl Nitrate, Int. J. Chem. Kinet., 12, 231–240, https://doi.org/10.1002/kin.550120404, 1980.

Tost, H., Jöckel, P., Kerkweg, A., Sander, R., and Lelieveld, J.: Technical note: A new comprehensive SCAVenging submodel for global atmospheric chemistry modelling, Atmos. Chem. Phys., 6, 565–574, https://doi.org/10.5194/acp-6-565-2006, 2006.

Truhlar, D. G., Garrett, B. C., and Klippenstein, S. J.: Current Status of Transition-State Theory, J. Phys. Chem., 100, 12771–12800, https://doi.org/10.1021/jp953748q, 1996.

Tsang, W.: Chemical Kinetic Data Base for Propellant Combustion. II. Reactions Involving CN, NCO, and HNCO, J. Phys. Chem. Ref. Data, 21, 753, https://doi.org/10.1063/1.555914, 1992.

Tully, F. P., Perry, R. A., Thorne, L. R., and Allendorf, M. D.: Free-radical oxidation of isocyanic acid, Symp. Int. Combust., 22, 1101–1106, https://doi.org/10.1016/S0082-0784(89)80120-1, 1989.

Uno, K., Hikida, T., Hiraya, A., and Shobatake, K.: Formation of NH($C^1\Pi$), NH($A^3\Pi$) and NCO($A^2\Sigma$) in the VUV Photolysis of HNCO, Chem. Phys. Lett., 166, 475–479, https://doi.org/10.1016/0009-2614(90)87136-F, 1990.

Varandas, A. J. C.: Odd-Hydrogen: An Account on Electronic Structure, Kinetics, and Role of Water in Mediating Reactions with Atmospheric Ozone. Just a Catalyst or Far Beyond?, Int. J. Quantum Chem., 114, 1327–1349, https://doi.org/10.1002/qua.24580, 2014.

Vatsa, R. K. and Volpp, H. R.: Absorption cross-sections for some atmospherically important molecules at the H atom Lyman-alpha wavelength (121.567 nm), Chem. Phys. Lett., 340, 289–295, https://doi.org/10.1016/S0009-2614(01)00373-6, 2001.

Vereecken, L. and Francisco, J. S.: Theoretical studies of atmospheric reaction mechanisms in the troposphere, Chem. Soc. Rev., 41, 6259–6293, https://doi.org/10.1039/c2cs35070j, 2012.

Vereecken, L., Glowacki, D. R., and Pilling, M. J.: Theoretical Chemical Kinetics in Tropospheric Chemistry: Methodologies and Applications, Chem. Rev., 115, 4063–4114, https://doi.org/10.1021/cr500488p, 2015.

Wang, Z., Nicholls, S. J., Rodriguez, E. R., Kummu, O., Horkko, S., Barnard, J., Reynolds, W. F., Topol, E. J., DiDonato, J. A., and Hazen, S. L.: Protein carbamylation links inflammation, smoking, uremia and atherogenesis, Nat. Med., 13, 1176–1184, https://doi.org/10.1038/nm1637, 2007.

Wentzell, J. J. B., Liggio, J., Li, S.-M., Vlasenko, A., Staebler, R., Lu, G., Poitras, M.-J., Chan, T., and Brook, J. R.: Measurements of Gas phase Acids in Diesel Exhaust: A Relevant Source of HNCO?, Environ. Sci. Technol., 47, 7663–7671, https://doi.org/10.1021/es401127j, 2013.

Wooldridge, M. S., Hanson, R. K., and Bowman, C. T.: A shock tube study of $CO + OH \rightarrow CO_2 + H$ and HNCO + OH → products via simultaneous laser adsorption measurements of OH and CO_2, Int. J. Chem. Kinet., 28, 361–372, https://doi.org/10.1002/(SICI)1097-4601(1996)28:5<361::AID-KIN5>3.0.CO;2-T, 1996.

Wren, S. N., Liggio, J., Han, Y., Hayden, K., Lu, G., Mihele, C. M., Mittermeier, R. L., Stroud, C., Wentzell, J. J. B., and Brook, J. R.: Elucidating real-world vehicle emission factors from mobile measurements over a large metropolitan region: a focus on isocyanic acid, hydrogen cyanide, and black carbon, Atmos. Chem. Phys., 18, 16979–17001, https://doi.org/10.5194/acp-18-16979-2018, 2018.

Young, P. J., Emmons, L. K., Roberts, J. M., Lamarque, J.-F., Wiedinmyer, C., Veres, P., and VandenBoer, T. C.: Isocyanic acid in a global chemistry transport model: Tropospheric distribution, budget, and identification of regions with potential health impacts, J. Geophys. Res.-Atmos., 117, D10308, https://doi.org/10.1029/2011JD017393, 2012.

Zabardasti, A. and Solimannejad, M.: Theoretical study and AIM analysis of hydrogen bonded clusters of water and isocyanic acid, J. Mol. Struct.-Theochem, 819, 52–59, https://doi.org/10.1016/j.theochem.2007.05.032, 2007.

Zabardasti, A., Amani, S., Solimannejad, M., and Salehnassaj, M.: Theoretical study and atoms in molecule analysis of hydrogen bonded clusters of ammonia and isocyanic acid, Struct. Chem., 20, 1087–1092, https://doi.org/10.1007/s11224-009-9513-1, 2009.

Zabardasti, A., Kakanejadifard, A., Kikhaei, M., and Solimannejad, M.: Theoretical studies and topological analysis of the electron density of clusters of O_3 with HNCO and HCNO, J. Mol. Struct.-Theochem., 961, 1–5, https://doi.org/10.1016/j.theochem.2010.08.015, 2010.

Zhao, Y. and Truhlar, D. G.: The M06 suite of density functionals for main group thermochemistry, thermochemical kinetics, noncovalent interactions, excited states, and transition elements: two new functionals and systematic testing of four M06-class functionals and 12 other functionals, Theor. Chem. Acc., 120, 215–241, https://doi.org/10.1007/s00214-007-0310-x, 2008.

Chapter 5

Oxidation of low-molecular-weight organic compounds in cloud droplets: development of the Jülich Aqueous-phase Mechanism of Organic Chemistry (JAMOC) in CAABA/MECCA (version 4.5.0)

Rosanka, S., Sander, R., Wahner, A., and Taraborrelli, D.: Oxidation of low-molecular-weight organic compounds in cloud droplets: development of the Jülich Aqueous-phase Mechanism of Organic Chemistry (JAMOC) in CAABA/MECCA (version 4.5.0), Geoscientific Model Development, 14, 4103–4115, https://doi.org/10.5194/gmd-14-4103-2021, 2021a.

General information:

Importance for this thesis and the author's contribution:
In this study, an explicit in-cloud OVOC oxidation mechanism is developed, which is suitable for global model simulations. It therefore contributes to the assessment of the representation of aqueous-phase OVOC chemistry in global models. This is further discussed in Sect. 8.3.

The idea for this study was developed together with Domenico Taraborrelli. I developed the chemical mechanism JAMOC and implemented the mechanism into MECCA. I discussed the results with all co-authors. I created all figures and wrote the manuscript. Further information and the contributions of all co-authors are available in the manuscript's 'Author contributions' section.

[1] `https://creativecommons.org/licenses/by/4.0/` (last access: 6 September 2020)

Geosci. Model Dev., 14, 4103–4115, 2021
https://doi.org/10.5194/gmd-14-4103-2021

Geoscientific Model Development
Open Access
EGU

Oxidation of low-molecular-weight organic compounds in cloud droplets: development of the Jülich Aqueous-phase Mechanism of Organic Chemistry (JAMOC) in CAABA/MECCA (version 4.5.0)

Simon Rosanka[1], **Rolf Sander**[2], **Andreas Wahner**[1], **and Domenico Taraborrelli**[1]

[1]Institute of Energy and Climate Research: Troposphere (IEK-8), Forschungszentrum Jülich GmbH, Jülich, Germany
[2]Atmospheric Chemistry Department, Max Planck Institute for Chemistry, Mainz, Germany

Correspondence: Simon Rosanka (s.rosanka@fz-juelich.de)

Received: 6 October 2020 – Discussion started: 29 October 2020
Revised: 2 April 2021 – Accepted: 8 April 2021 – Published: 1 July 2021

Abstract. The Jülich Aqueous-phase Mechanism of Organic Chemistry (JAMOC) is developed and implemented in the Module Efficiently Calculating the Chemistry of the Atmosphere (MECCA; version 4.5.0). JAMOC is an explicit in-cloud oxidation scheme for oxygenated volatile organic compounds (OVOCs), suitable for global model applications. It is based on a subset of the comprehensive Cloud Explicit Physico-chemical Scheme (CLEPS; version 1.0). The phase transfer of species containing up to 10 carbon atoms is included, and a selection of species containing up to 4 carbon atoms reacts in the aqueous phase. In addition, the following main advances are implemented: (1) simulating hydration and dehydration explicitly; (2) taking oligomerisation of formaldehyde, glyoxal, and methylglyoxal into account; (3) adding further photolysis reactions; and (4) considering gas-phase oxidation of new outgassed species. The implementation of JAMOC in MECCA makes a detailed in-cloud OVOC oxidation model readily available for box as well as for regional and global simulations that are affordable with modern supercomputing facilities. The new mechanism is tested inside the box model Chemistry As A Boxmodel Application (CAABA), yielding reduced gas-phase concentrations of most oxidants and OVOCs except for the nitrogen oxides.

1 Introduction

Aqueous-phase chemistry in cloud droplets differs significantly from gas-phase chemistry, mainly due to enhanced photolysis based on scattering effects within cloud droplets (Bott and Zdunkowski, 1987; Mayer and Madronich, 2004), faster reaction rates, and ion reactions that do not occur in the gas phase (Herrmann, 2003; Epstein and Nizkorodov, 2012). Moreover, conversion of nitrogen monoxide (NO) to nitrogen dioxide (NO_2) by peroxy radicals (RO_2) essentially does not take place in aqueous droplets because NO is insoluble. In the aqueous phase, oxygenated volatile organic compounds (OVOCs) are mainly oxidised during the daytime by the hydroxyl radical (OH) and by the nitrate radical (NO_3) during the nighttime (Herrmann et al., 2015). Even though ozone (O_3) is not very soluble, it can be taken up into cloud droplets where it is destroyed by

$$O_3 + O_2^- \rightarrow O_3^- + O_2, \quad \text{(R1)}$$

for which the superoxide anion (O_2^-) is in equilibrium with its conjugate acid, the hydroperoxyl radical (HO_2). This indicates that the in-cloud O_3 destruction is sensitive to in-cloud OVOC oxidation. Lelieveld and Crutzen (1990) have already proposed that clouds can influence HO_x ($HO_x = OH + HO_2$) and NO_x ($NO_x = NO + NO_x$), resulting in regional changes of up to 40 % in particular locations, being subject to cloud processing. At the tropics and mid-latitudes, Liang and Jacob (1997) suggest that clouds may reduce O_3 by 3 % in summer. By changing the gas-phase oxidant budgets, clouds can indirectly influence the formation of secondary organic

aerosols (SOAs). Within cloud droplets, OVOC oxidation additionally can lead to the formation and destruction of SOA precursors, and clouds can act as SOA sources (Blando and Turpin, 2000). Further modelling studies suggest that clouds may contribute to the SOA formation on a par with gas-phase sources (Ervens et al., 2011; Lin et al., 2012; Ervens, 2015). By scattering, SOAs are known to influence the aerosol optical depth (AOD), leading to a reduction in NO_2 photolysis (Tie et al., 2005). In addition, SOAs may act as cloud condensation nuclei (CCN) (Andreae and Rosenfeld, 2008), affecting cloud properties. An increased formation of SOAs would thus influence tropospheric HO_x and O_3 chemistry.

When performing global modelling studies, it is thus desirable to include the in-cloud oxidation of OVOCs. However, compared to gas-phase chemistry, knowledge of aqueous-phase chemistry still suffers from large uncertainties and most global models only include very limited representations. Most global models include only the uptake of a few soluble compounds, their acid–base equilibria, and the oxidation of sulfur dioxide (SO_2) by ozone (O_3) and hydrogen peroxide (H_2O_2) (Ervens, 2015, their Table 1). The explicit oxidation of OVOCs is currently not considered in any global model, with one exception – though limited to species containing one carbon atom (Tost et al., 2006). Mouchel-Vallon et al. (2017) recently presented the Cloud Explicit Physicochemical Scheme (CLEPS; version 1.0), a complex new oxidation scheme coupled to the gas-phase Master Chemical Mechanism (MCM; version 3.3.1; Jenkin et al., 2015). However, their comprehensive mechanism is targeted for box-model applications and is not suitable for global model applications due to its complexity.

In this study, the in-cloud OVOC oxidation scheme Jülich Aqueous-phase Mechanism of Organic Chemistry (JAMOC) is presented and implemented into the chemistry mechanism Module Efficiently Calculating the Chemistry of the Atmosphere (MECCA). Here, JAMOC's representation of organic chemistry is based on CLEPS and is thus an addition to MECCA's existing aqueous-phase chemical mechanism. Therefore, JAMOC needs to be selected by the user upon compilation of MECCA's chemical mechanism. A visualisation of this procedure can be found in MECCA's user manual available in the archived model code (caaba_mecca_manual.pdf). The modular structure of MECCA allows it to be connected to different base models, e.g. to the Chemistry As A Boxmodel Application (CAABA) by Sander et al. (2019) or to the global ECHAM/MESSy Atmospheric Chemistry Model (EMAC) by Jöckel et al. (2010). In this combination, the proposed mechanism closes the gap between box models and global model applications. In addition to the new aqueous-phase OVOC chemistry, MECCA also contains the gas-phase Mainz Organic Mechanism (MOM; Sander et al., 2019) with an extensive oxidation scheme for isoprene (Taraborrelli et al., 2009, 2012; Nölscher et al., 2014), monoterpenes (Hens et al., 2014), and aromatics (Cabrera-Perez et al., 2016). VOCs are oxidised by OH, O_3, and NO_3, whereas RO_2 reacts with HO_2, NO_x, and NO_3 and undergoes self- and cross-reactions (Sander et al., 2019).

The mechanism of JAMOC is described in Sect. 2, followed by a short description of its implications in the box model CAABA (Sect. 3). Global implications are analysed in our companion paper (Rosanka et al., 2021a), and the mechanism's importance for global models simulating extreme pollution events is addressed by Rosanka et al. (2020). Modelling uncertainties are discussed in Sect. 4 before drawing final conclusions in Sect. 5.

2 The Jülich Aqueous-phase Mechanism of Organic Chemistry (JAMOC)

The detailed mechanism CLEPS includes 850 aqueous-phase reactions, focusing on the oxidation of species containing up to four carbon atoms (Mouchel-Vallon et al., 2017). Since our target is to simulate OVOC chemistry inside the global model EMAC (Rosanka et al., 2021a), using such a large mechanism is not feasible. Therefore, we have developed the reduced mechanism JAMOC. Only a selection of species containing up to four carbon atoms is considered in the aqueous phase. The gas-phase oxidation of the most abundant hydrocarbons (e.g. methane, isoprene) leads to many highly soluble organic species with one or two carbon atoms (e.g. formaldehyde, methanol, glyoxal). In order to properly represent these degradation products, JAMOC includes the aqueous-phase oxidation of all species containing one and two carbon atoms treated in CLEPS. Even though isoprene (C_5H_8), the biogenic VOC emitted the most (Guenther et al., 2012), is not soluble, the representation of its oxidation products containing more than two carbon atoms (i.e. methylglyoxal, methacrolein, methyl vinyl ketone) is desirable for global model applications. Therefore, the oxidation of species containing three carbon atoms in JAMOC focuses on the representation of the aqueous-phase oxidation of methylglyoxal and its aqueous-phase oxidation products (e.g. pyruvic acid). Additionally, its aqueous-phase sources from acetone, hydroxy acetone, isopropanol, hydroperoxide, and isopropyl hydroperoxide are included. The aqueous-phase oxidation of species containing four carbon atoms in JAMOC is limited to methacrolein (MACR) and methyl vinyl ketone (MVK). The phase transfer of species containing up to 10 carbon atoms is included so that their wet deposition can be represented in global model applications (i.e. by using EMAC; see Rosanka et al., 2021a). In order to reduce the stiffness of the ordinary differential equation (ODE) system and the required computational demand, the representation of organic radicals (see Sect. 2.7) is simplified. It is assumed that the following reactions occur instantly and are not explicitly represented in the ODE system if they are the only fate of the respective radical: (1) the O_2 addition to alkyl radicals; (2) the HO_2 elimination of α-hydroxyperoxyl; and (3) the carbon bond scission or 1,2-

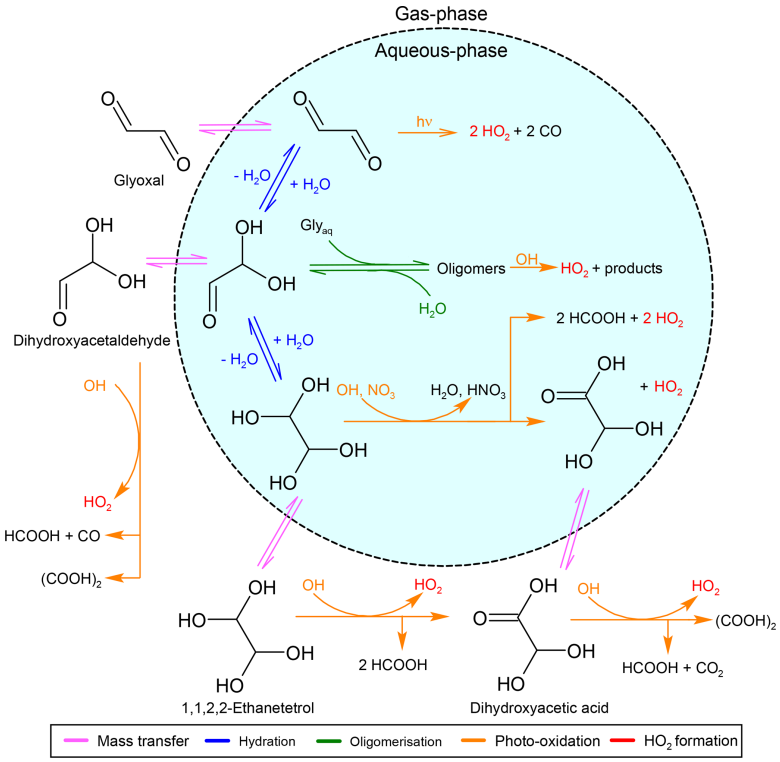

Figure 1. Oxidation of glyoxal (CHOCHO) by radicals in JAMOC. The oligomerisation of the glyoxal monohydrate occurs with glyoxal as well as with its hydrates (see Sect. 2.6). Here, Gly_{aq} denotes all three forms of glyoxal (glyoxal, its monohydrate, and its dihydrate), which is consistent with the kinetic data published by Ervens and Volkamer (2010). $(COOH)_2$ denotes oxalic acid whose representation in JAMOC is illustrated in Fig. 2. The following aspects are not explicitly represented: (1) the oxidation of the glyoxal dihydrate by the sulfate radical anion (SO_4^-), (2) the aqueous-phase sources of glyoxal and the glyoxal monohydrate from the oxidation of glycolaldehyde and the glycolaldehyde monohydrate, and (3) the aqueous-phase oxidation of dihydroxyacetic acid.

hydrogen shift of alkoxyl radicals. In addition to the chemistry from CLEPS, JAMOC includes (1) explicit hydration and dehydration; (2) oligomerisation of formaldehyde, glyoxal, and methylglyoxal as an in-cloud SOA source; (3) further aqueous-phase photolysis reactions; and (4) the gas-phase photo-oxidation of new outgassed species. The complete aqueous-phase mechanism represents the phase transfer of 368 species, 68 equilibria (acid–base and hydration–dehydration), 402 reactions, and 27 aqueous-phase photolysis reactions. In the gas phase, 1 photolysis and 18 OH oxidation reactions are added to MOM. A list detailing the complete mechanism is available in the archived model code.

This section provides a general overview of the developed mechanism. For completeness, short summaries of CLEPS are provided if no significant difference exists between both mechanisms. Figures 1 and 2 give a graphical representation of all parts of the developed mechanism, using glyoxal and oxalic acid as examples.

2.1 Inorganic chemistry

The inorganic chemistry for the proposed mechanism is very similar to the inorganic chemistry of the standard aqueous-phase mechanism used in EMAC (Tost et al., 2007; Jöckel et al., 2016). In this standard mechanism, the major aqueous-phase O_3 sink, the reaction with O_2^-, is represented as

$$O_3 + O_2^- \rightarrow OH + OH^- . \quad \text{(R2)}$$

In JAMOC, this aqueous-phase O_3 chemistry is updated to the mechanism proposed by Staehelin et al. (1984) with corrections from Staehelin and Hoigné (1985), in which the O_3 destruction by O_2^- is represented as given in Reaction (R1).

2.2 Uptake of gaseous species into cloud droplets

The mass transfer of species between the gas and the aqueous phase is described following Schwartz (1986) (see Sander, 1999; Tost et al., 2006). The explicit bidirectional phase

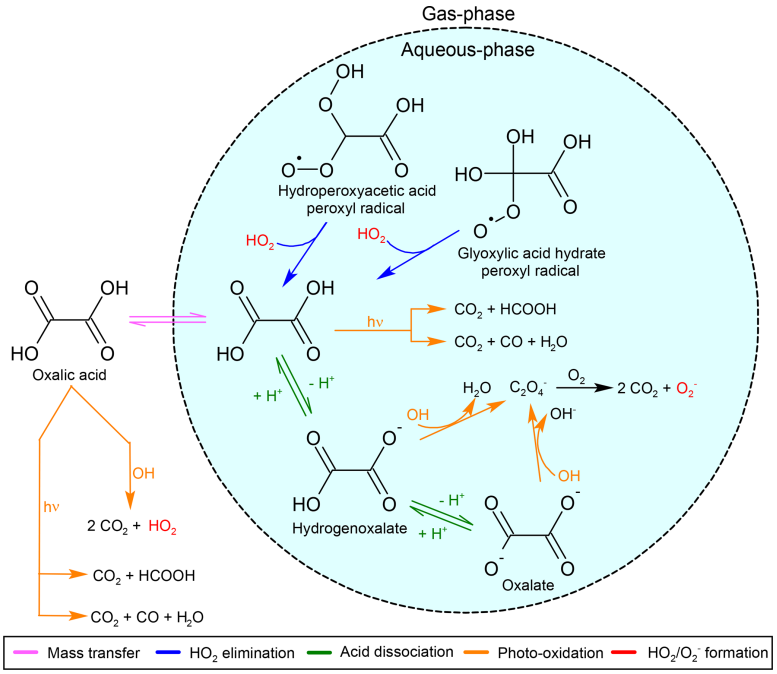

Figure 2. Formation and oxidation of oxalic acid ($(COOH)_2$) by radicals in JAMOC. The oxidation by the sulfate radical anion (SO_4^-) is not shown.

transfer of 45 carbon-containing species, which explicitly react in the aqueous phase, is considered (indicated in pink in Figs. 1 and 2). In this model framework, Henry's law constants are mainly taken from Sander (2015), Burkholder et al. (2015), and sources therein. In order to account for the hydration of aldehydes (for more details see Sect. 2.3), a distinction is made between the effective Henry's law constant (H^*) and the intrinsic Henry's law constant (H). The latter is calculated by

$$H = H^*/(1 + K_{hyd}), \quad (1)$$

where K_{hyd} is the ratio between the forward and reverse kinetic rate constant of the hydration equilibrium (see Reaction R3). Table 1 gives an overview of the hydration constants and the effective Henry's law constants, including the resulting intrinsic Henry's law constants, for all aldehydes. The temperature dependencies of the intrinsic Henry's law constants are assumed to be the same as for the effective constants. The accommodation constant (α) is known for a few species; if unknown, the standard EMAC estimate of 0.1 is used. In addition to the phase transfer of all species that explicitly react in the aqueous phase, the phase transfer of all soluble MOM species containing up to 10 carbon atoms is represented in order to allow their removal by wet deposition in global models (i.e. by using EMAC; see Rosanka et al., 2021a). A list summarising all Henry's law and accommodation constants is available in the archived model code.

Table 1. Hydration constants (K_{hyd}) and effective (H^*) and intrinsic (H) Henry's law constants for aldehydes (see Sect. 2.2 for details). If not stated otherwise, hydration constants are obtained from Doussin and Monod (2013) and sources therein. If not stated otherwise, effective Henry's law constants are taken from Burkholder et al. (2015).

Species	K_{hyd}	H^* [M atm^{-1}]	H [M atm^{-1}]
Formaldehyde	1278.0	3.23×10^3	2.53
Acetaldehyde	1.2	1.29×10^1	5.91
Glycolaldehyde	15.7	4.00×10^4	2.40×10^3
Glyoxal	350.0[a]	4.19×10^5	1.19×10^3
Glyoxylic acid	1100.0	1.09×10^4	9.90
Methylglyoxal	2000.0	3.50×10^3[,b]	1.75

[a] Ervens and Volkamer (2010). [b] Betterton and Hoffmann (1988).

2.3 Hydration of carbonyls

Gem-diols are formed when aldehydes (carbonyl compounds) hydrate:

$$R_2C{=}O + H_2O \rightleftharpoons R_2C(OH)(OH) \quad (R3)$$

Table 2. Estimated effective (H^*) Henry's law constants for all gem-diols represented in JAMOC. Estimates with the bond method (Meylan and Howard, 1991) are obtained from United States Environmental Protection Agency (US EPA) (2012).

Species	H^* [M atm^{-1}]
Methanediol	1.02×10^4
1,1-Ethanediol	7.63×10^3
Dihydroxyacetaldehyde	2.58×10^3
1,1,2,2-Ethanetetrol	5.71×10^6
2,2-Dihydroxyacetic acid	3.21×10^5
1,1,2-Ethanetriol	2.09×10^5
Hydroperoxyacetaldehyde hydrate	2.09×10^5
1,1-Dihydroxyacetone	3.53×10^3

In the new mechanism, 12 carbonyl species undergo hydration (indicated with blue arrows in Fig. 1). The monohydrate of glyoxal (dihydroxyacetaldehyde) undergoes additional hydration to form its dihydrate (1,1,2,2-ethanetetrol). Pseudo-first-order rate constants for the hydration and dehydration are mainly obtained from the literature (e.g. Doussin and Monod, 2013). In the case of formyldioxidanyl and hydroperoxyacetaldehyde, the pseudo-first-order rate constants are assumed to be the same as for formaldehyde and glycolaldehyde, respectively.

The typical lifetime of a warm cloud droplet can be several minutes, but their typical evaporation timescale is less than 100 s (Jarecka et al., 2013). Following the dehydration constants presented by Doussin and Monod (2013), the dehydration of some gem-diols can be slower than the typical cloud droplet evaporation timescale. Additionally, their rapid transfer across the phases is expected to affect the gas-phase concentration of gem-diols, for which no other significant source is known. This process could be an important removal of gem-diols from the aqueous phase, without yielding the original aldehyde. Therefore, their outgassing is considered for use with the models representing evaporating clouds like the EMAC model (following Sect. 2.2). However, their Henry's law constants are unknown. Thus, estimates are obtained at 25 °C using the bond method (Meylan and Howard, 1991) from the United States Environmental Protection Agency Estimation Programs Interface (EPI) Suite (United States Environmental Protection Agency (US EPA), 2012). An overview of all estimated effective Henry's law constants is given in Table 2.

In CLEPS, acyl peroxy radicals (RC(O)(OO)) are assumed to be in a hydration–dehydration equilibrium similarly to their parent aldehydes (Mouchel-Vallon et al., 2017). However, experimental results by Villalta et al. (1996) show that in the case of peroxyacetyl radicals ($CH_3C(O)(OO)$), no equilibrium exists. Instead, hydrolysis takes place, likely yielding acetic acid (CH_3CO_2H) and HO_2. It is thus assumed that all acyl peroxy radicals undergo hydrolysis following Reaction (R4), with a reaction rate constant of 7.0×10^5 M^{-1} s^{-1}, as proposed by Villalta et al. (1996).

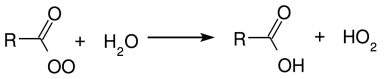

(R4)

2.4 Acid dissociation

The dissociation of acids is taken into account following

$$R_2CO(OH) \rightleftharpoons R_2CO(O^-) + H^+, \quad \text{(R5)}$$

which is indicated in green in Fig. 2. The acidity constants (K_a) for most of the one-carbon-, two-carbon-, and three-carbon-containing acids taken into account in JAMOC are known from the literature (Rumble, 2020). If unknown, the acidity constants are used as proposed by Mouchel-Vallon et al. (2017). The dissociation and association rate constants are selected such that the equilibrium between dissociation and association is reached quickly, while still avoiding numerical stiffness problems in the numerical integrator.

2.5 Oxidation by OH, NO_3, and other oxidants

In JAMOC, OH and NO_3 are the main oxidants taken into account. Reactions of OVOCs with oxidants are treated as proposed by Mouchel-Vallon et al. (2017). Organic compounds may react in three different ways with OH radicals (Herrmann et al., 2015), each indicated in orange in Figs. 1 and 2. They form an alkyl radical following H abstraction:

$$RH + OH \rightarrow R + H_2O. \quad \text{(R6)}$$

If the organic compound contains a double bond, OH addition is favoured.

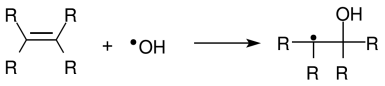

(R7)

With anions like carboxylates, electron transfer takes place.

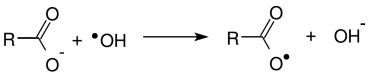

(R8)

When available, rate constants are obtained from the literature. If unavailable, the rate constant for the H abstraction is estimated based on the structure–activity relationship (SAR) by Doussin and Monod (2013), which for carboxylate compounds is extended to account for the electron transfer as described by Mouchel-Vallon et al. (2017). In all cases, branching ratios are obtained from the SAR with simplifications by Mouchel-Vallon et al. (2017).

During the nighttime, OH radical concentrations are low and, due to missing photolysis, NO_3 radicals are considered the main nighttime oxidant. Similar to CLEPS, JAMOC only

considers the H abstraction leading to alkyl radicals for NO_3 reactions (Herrmann et al., 2015):

$$RH + NO_3 \rightarrow R + NO_3^- + H^+. \quad \text{(R9)}$$

For most species containing one or two carbon atoms, rate constants are obtained from the literature. In contrast to OH, no SAR is available for the H abstraction by NO_3. Therefore, rate constants are obtained from the similar criteria described by Mouchel-Vallon et al. (2017). Due to missing branching ratios from the literature, branching ratios are assumed to be the same as for the H abstraction by OH.

In addition to reactions of organic compounds with OH and NO_3, reactions with other oxidants are implemented when available from the literature. The oxidants considered here are O_2^-, O_3, H_2O_2, CO_3^-, and sulfur-containing oxidants (SO_4^- and SO_5^-). For all oxidation reactions, reaction rates and branching ratios are either taken from the literature or as proposed by Mouchel-Vallon et al. (2017).

2.6 Oligomerisation

The formation of oligomers within the atmospheric aqueous phase is known to be a source of SOAs. Even though Tan et al. (2009) suggest that the formation of oligomers becomes increasingly important for aerosol water, where precursor concentrations are found to be higher, Lin et al. (2012) have demonstrated that SOA formation from cloud processing is globally important. Therefore, JAMOC includes self- and cross-reactions leading to oligomers for formaldehyde, glyoxal, and methylglyoxal. The oligomerisation of formaldehyde is implemented following Hahnenstein et al. (1995), in which the methanediol formed from hydrolysis (see Sect. 2.3) reacts with itself and the dimer formed from this self-reaction. Ervens and Volkamer (2010) studied the oligomerisation of glyoxal. Here, glyoxal and its hydrates react with the monohydrate to form three oligomers (indicated in green in Fig. 1). The oligomerisation of methylglyoxal is assumed to follow the same mechanisms as for glyoxal. However, only the monohydrate of methylglyoxal is taken into account in this mechanism, leading to only two oligomers. Each oligomer is assumed to react with OH, leading to HO_2, with reaction rate constants that are double for the corresponding (hydrated) monomer due to an increased number of abstractable H atoms.

2.7 Organic radicals

Organic radicals are generally treated following Mouchel-Vallon et al. (2017). Alkyl radicals can either form oligomers via self- and cross-reactions (e.g. Lim et al., 2013; Ervens et al., 2015) or undergo O_2 addition:

$$R + O_2 \rightarrow R(OO). \quad \text{(R10)}$$

As proposed by Mouchel-Vallon et al. (2017), it is assumed that O_2 addition is the fastest pathway, due to high O_2 concentrations following fast O_2 saturation in cloud droplets (Ervens, 2015). Thus, oligomers formed from the self- and cross-reactions of alkyl radicals are not considered in JAMOC.

Peroxyl radicals generally undergo self- or cross-reactions forming short-lived tetroxides that quickly decompose (von Sonntag and Schuchmann, 1997). Due to limited computation resources, only self-reactions are taken into account. Mouchel-Vallon et al. (2017) propose three similarity criteria for the decomposition of tetroxides depending on the peroxyl radical: (1) for β-peroxycarboxylic acids (RC(OO)C(=O)(OH)) experimental results from Schuchmann et al. (1985) are generalised, (2) β-hydroxyperoxyl radicals (> C(OH)C(OO) <) are represented according to Piesiak et al. (1984), and (3) β-oxoperoxyl radicals (−COC(OO) <) are treated based on Zegota et al. (1986) and Poulain et al. (2010). If some products are unknown, branching ratios of the known products are rescaled to 100 % in order to preserve mass. The peroxyl radicals undergo HO_2 elimination (von Sonntag, 1987) if the hydroxyl moiety is in the alpha position (α-hydroxyperoxyl).

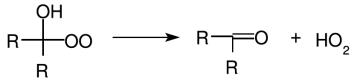

(R11)

The generalised corresponding rate constants are used as proposed by Mouchel-Vallon et al. (2017, Table 3), which are based on the work of von Sonntag (1987). In CLEPS, peroxyl radicals additionally undergo O_2^- elimination when reacting with OH^- (Zegota et al., 1986; Mouchel-Vallon et al., 2017).

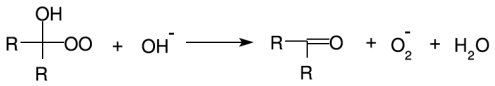

(R12)

In order to decrease the number of reactions and due to the fast HO_2 elimination, this O_2^- elimination is not considered explicitly in JAMOC.

Acyl peroxy radicals (RC(O)(OO)) are treated like peroxyl radicals, as described in Monod et al. (2007), but only form alkoxyl radicals. Peroxyl radicals that have not explicitly been discussed so far are treated following Monod et al. (2007) (Mouchel-Vallon et al., 2017).

Mouchel-Vallon et al. (2017) suggest that alkoxyl radicals (RO) undergo either a carbon bond scission (Hilborn and Pincock, 1991) if the neighbouring carbon atom is oxygenated (Reaction R13) or a 1,2-hydrogen shift (DeCosta and Pincock, 1989) if the neighbouring carbon atom is not oxygenated (Reaction R14).

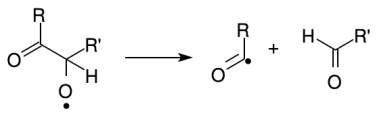

(R13)

(R14)

2.8 Photolysis

In general, the photolysis of some organic compounds (e.g. organic peroxides, pyruvic acid) competes with other oxidation pathways (see Sect. 2.5) and can be a source of OH. In Rosanka et al. (2021a), a global tropospheric in-cloud OH budget is presented. When using JAMOC, EMAC predicts that about 40 % of all in-cloud OH is produced from the photolysis of a selection of organic compounds. However, Fenton chemistry is not considered by Rosanka et al. (2021a), and the relative contribution is therefore expected to be overestimated. The photolysis of glyoxal and oxalic acid is indicated in orange in Figs. 1 and 2. The number of photolytic reactions known from the literature, of which some are implemented in CLEPS (Mouchel-Vallon et al., 2017), is limited. In JAMOC, the photolysis of additional compounds is taken into account. This includes the photolysis of oxalic acid ($(COOH)_2$), which is implemented following Yamamoto and Back (1985) using the ultraviolet absorption spectrum presented in Back (1984). If available, additional photolysis reactions are implemented following Sander et al. (2014). In order to account for scattering effects within cloud droplets (Ruggaber et al., 1997), an enhancement factor of 2.33, the same as that used in EMAC's standard aqueous-phase mechanism for the photolysis of H_2O_2 (Tost et al., 2007; Jöckel et al., 2016), is applied to each gas-phase photolysis rate.

2.9 Gas-phase oxidation of new species

Oxalic acid was not represented in the gas-phase mechanism (i.e. in MOM). The gas-phase oxidation of oxalic acid by OH and its photolysis are implemented in order to realistically represent oxalic acid in the gas phase. Similarly to the implementation in the aqueous phase, the photolysis of oxalic acid is implemented following Yamamoto and Back (1985) and Back (1984). All gem-diols (see Sect. 2.3) formed from hydration are transferred to the gas phase and oxidised by OH (indicated in orange in Figs. 1 and 2). All OH oxidation reaction rates are estimated following the description of Sander et al. (2019).

3 Influence of JAMOC on a single air parcel

The implications of the developed mechanism are tested by comparing it to the minimum in-cloud oxidation scheme available in CAABA/MECCA and EMAC. The minimum mechanism only includes the uptake of a few soluble compounds, their acid–base equilibria, and the oxidation of SO_2 by O_3 and H_2O_2 (Jöckel et al., 2006). This minimal mechanism is thus representative of most global models (Ervens, 2015). For both mechanisms, an air parcel is simulated in CAABA, taking the same conditions into account: the air parcel is simulated during summer at a mid-latitude with a constant temperature of 278 K and relative humidity of 100 %. Table 3 provides a selection of initial mixing ratios and emission fluxes of gas-phase species treated in MOM. The initial conditions are a modified version of the scenario used by Taraborrelli et al. (2009). Within the air parcel, a stable cloud droplet population is simulated with a radius of 20 µm and a liquid water content of $0.3\,g\,m^{-3}$. Both simulations are intended as a sensitivity study of JAMOC. Therefore, CAABA is initialised at 00:00 UTC and simulates the air parcel for 5 d in total. A realistic cloud event with a cloud droplet lifetime of 1 h using CAABA is presented in Rosanka et al. (2021a). In addition, Rosanka et al. (2021a) study the implications of JAMOC on a global scale using EMAC.

Table 3. Initial box-model (CAABA) mixing ratios and emission rates for selected gas-phase species. Initial mixing ratios are a modified version of the scenario used by Taraborrelli et al. (2012).

Gas-phase species	Initial mixing ratio [nmol mol^{-1}]	Emission [molec. cm^{-2} s^{-1}]
O_3	30	–
NO	0.01	3.3×10^{-9}
NO_2	0.1	–
HNO_3	5.0×10^{-3}	–
H_2O_2	7	–
CO	100	–
CO_2	3.5×10^5	–
CH_4	1.8×10^3	–
Formaldehyde	5	–
Methanol	0.5	–
Methyl peroxide	4	–
Formic acid	0.35	–
Acetic acid	2	–
Peroxy acetic acid	1.5	–
Hydroxy acetone	4	–
Methylglyoxal	0.5	–
Isoprene	0.1	–
Peroxyacetyl nitrate	0.1	–
Ethane	2	–

Figure 3 gives an overview of the temporal development of the total mixing ratios (gas + aqueous phase) for a selection of species during the simulated daily cycles of 5 d. Comparing the new and the minimum mechanisms, it becomes clear that the newly developed mechanism has a significant impact on most trace gases. With the explicit oxidation of many OVOCs in the aqueous phase, the mixing ratio of the sum of all OVOCs explicitly reacting in JAMOC ($\sum$OVOCs; see Eq. A1 in Appendix A) is significantly reduced. This reduction is a combined effect from (1) the in-cloud oxidation of these OVOCs and (2) their dampened gas-phase production. In the gas-phase, most OVOCs are formed by secondary production (e.g. oxidation of primarily emitted VOCs). The decrease in the main VOC oxidant (i.e. OH) leads to reduced oxidation of primarily emitted VOCs re-

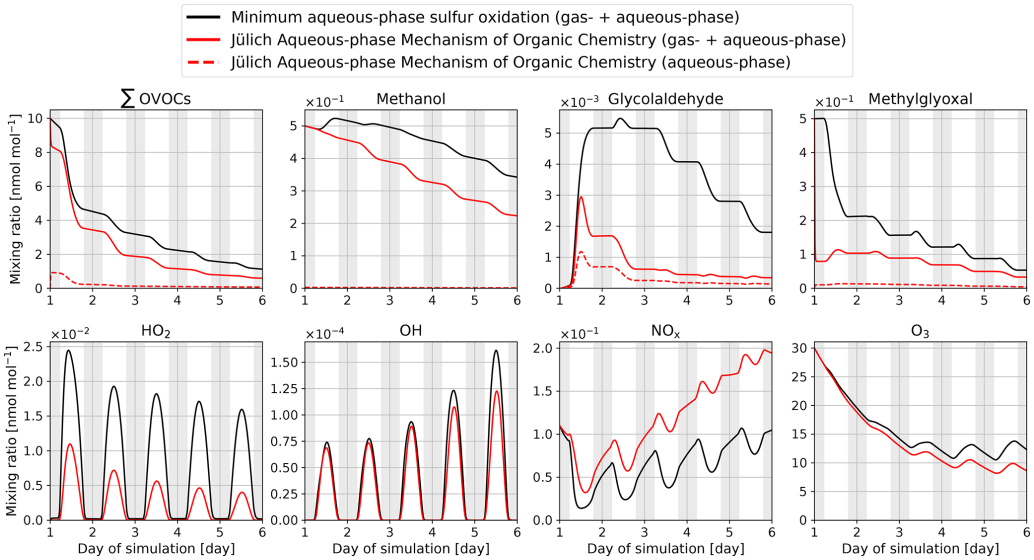

Figure 3. Time evolution for total mixing ratios (gas + aqueous phase) of the sum of all the OVOCs explicitly oxidised in the proposed mechanism (∑OVOCs; see Eq. A1 in Appendix A), methanol, glycolaldehyde, methylglyoxal, HO_2, OH, NO_x, and O_3 within the box model CAABA. Mixing ratios are provided for two cases, one using the minimum aqueous-phase mechanism in global models (sulfur oxidation only, black line) and the other using JAMOC (red line). In addition, aqueous-phase mixing ratios of ∑OVOCs, methanol, glycolaldehyde, and methylglyoxal are given for the simulation using JAMOC. The aqueous-phase mixing ratios include the gem-diols formed for the species listed in Table 1. Nighttime is indicated by grey background shading. Note that lines may overlap.

sulting in a reduced gas-phase OVOC formation. The calculated diurnal cycles of OH, HO_2, NO_x, and O_3 are similar for both mechanisms and differ mainly in the absolute mixing ratios calculated. When JAMOC is used, HO_2 partitions into the cloud droplets, whereas NO stays in the gas phase due to its low solubility (Jacob, 1986; Lelieveld and Crutzen, 1990). This results in substantial changes in the NO_x–HO_x relation, resulting in reduced OH formation from its second-most-important atmospheric gas-phase source:

$$NO + HO_2 \rightarrow NO_2 + OH. \quad \text{(R15)}$$

Overall, this results in reduced HO_x and elevated NO_x mixing ratios. In addition, lower HO_2 mixing ratios lead to a reduced removal of NO_x by the formation of nitric acid (HNO_3) and peroxynitric acid (HNO_4). Within the cloud droplet, O_2^- is in equilibrium with its conjugated base HO_2. Higher in-cloud HO_2 concentrations, caused by mass transfer and in-cloud OVOC oxidation, consequently lead to an increased destruction of O_3 via Reaction (R1). This results in an enhanced uptake of O_3 into the cloud droplet and an increased importance of cloud droplets as O_3 sinks.

The impact of the newly proposed mechanism is consistent with earlier box-model studies. The reduction in OVOCs is similar to the findings given in Mouchel-Vallon et al. (2017) when using CLEPS. In contrast, the reduction in methylglyoxal differs since, in CLEPS, gas-phase methylglyoxal mixing ratios first increase and later decrease during the modelled cloud event of Mouchel-Vallon et al. (2017). This difference is most likely linked to the usage of the intrinsic Henry's law constant and the explicit representation of the methylglyoxal hydration–dehydration in JAMOC. In contrast to Mouchel-Vallon et al. (2017), CAABA predicts a reduction in OH levels. However, this reduction in OH is in line with other modelling studies predicting a similar reduction in gas-phase OH during cloud events (Tilgner et al., 2013). It is important to keep in mind that in Mouchel-Vallon et al. (2017), a different cloud event is simulated, including different initial conditions and a different emission scenario. In their study, the cloud forms after a certain time period, whereas in CAABA the cloud is present the whole time.

4 Model uncertainties

The uncertainties associated with the present kinetic model are mainly attributed to (1) assumptions and simplifications in the aqueous-phase mechanism and (2) missing sinks of key oxidants. Each possible uncertainty is discussed in this section.

In general, aqueous-phase kinetics data suffer from many large uncertainties compared to the data available for the gas phase. In the development of the implemented in-cloud

oxidation scheme JAMOC, some assumptions are made that introduce modelling uncertainties. If rate constants are unknown, estimates are taken from Mouchel-Vallon et al. (2017). These are based on a structure–activity relationship (SAR) for the H abstraction by OH for dissolved carbonyls and carboxylic acids considered in this study (Doussin and Monod, 2013). However, it is expected that the uncertainty in the estimated rate constants is low since Doussin and Monod (2013) report that when evaluated using experimental data, their estimates were within ±20 % for 58 % of the calculated rate constants. Also the up-scaling of branching ratios to conserve mass further influences the predictions of VOC oxidation. The mechanism should be updated with rate constants and branching ratios as soon as experimental results become available. The increased concentration and burden of certain organic acids heavily depend on the chemistry and solubility of some gem-diols. For example, the gas-phase oxidation of the methylglyoxal monohydrate leads to the formation of pyruvic acid. The gas-phase production of pyruvic acid therefore depends on the mass transfer of this specific monohydrate. In the current implementation, the Henry's law constants for all gem-diols are estimated. For the methylglyoxal monohydrate, the estimated values range from 3.5×10^3 to $2.4 \times 10^4\,\mathrm{M\,atm^{-1}}$.

Phase transfer of soluble VOCs into cloud droplets is considered in JAMOC even when their oxidation is not explicitly represented (see Sect. 2.2). This allows their removal from the atmosphere by rain-out when JAMOC is connected to a global model (e.g. using EMAC; see Rosanka et al., 2021a). Arakaki et al. (2013) point out that by not taking the oxidation of all dissolved organic carbon (DOC) into account, aqueous-phase OH concentrations might be overestimated. Based on observational estimates, they suggest a general scavenging rate constant of $k_{C,OH} = (3.8 \pm 1.9) \times 10^8\,\mathrm{M^{-1}\,s^{-1}}$ for all DOC. If each DOC species reacts with OH, the gas-phase concentration would be reduced, further influencing gas-phase VOC concentrations and the overall oxidation capacity. Implementing the DOC oxidation, suggested by Arakaki et al. (2013), for every scavenged DOC species would increase the aqueous-phase mechanism by more than 280 reactions, which is almost a doubling of the proposed organic mechanism. Within the scope of this study, it is thus computationally not feasible to include this additional OH sink. Currently, the model runtime increases from 4.3 s for EMACs minimum in-cloud oxidation scheme to 6.5 s for the newly proposed mechanism JAMOC.

Reducing the model uncertainties introduced by estimates of Henry's law constants of gem-diols and missing in-cloud DOC oxidation is outside the scope of this study due to the uncertainties' complexity. Model representation of the latter is expected to influence the oxidation rate of VOCs in the cloud droplets and aerosols.

5 Conclusions

In this study, the new in-cloud oxidation scheme of soluble VOCs JAMOC is developed and implemented into MECCA. This mechanism is suitable for global model applications and based on the box-model mechanism CLEPS proposed by Mouchel-Vallon et al. (2017). The mechanism considers the phase transfer of OVOCs containing up to 10 carbon atoms. For a selection of OVOCs containing up to 4 carbon atoms, their acid–base and/or hydration–dehydration equilibria and their reactions with OH, NO_3, and other oxidants (if available) are explicitly represented. Additionally, the gas-phase photo-oxidation of gem-diols and oxalic acid is implemented into the gas-phase mechanism MOM. Finally, JAMOC is tested within the CAABA box model.

The proposed mechanism leads to a significant reduction in OVOCs and an overall reduction in important oxidants. These findings are in line with other box-model studies and demonstrate the importance of in-cloud chemistry in atmospheric chemistry. By not taking the in-cloud oxidation of OVOCs into account, global models will tend to overestimate the levels of OVOCs and atmospheric oxidants. A complete analysis on the importance of JAMOC at a global scale is presented in Rosanka et al. (2021a). In future studies, the modular implementation of JAMOC, with the necessary adjustments, will allow its application to aerosol water.

Appendix A: Definition of $\sum$OVOCs

In Fig. 3, the mixing ratios of the sum of all the OVOCs explicitly reacting in JAMOC ($\sum$OVOCs) are shown. In these cases, $\sum$ OVOCs is defined as follows:

$$\begin{aligned}\sum \text{OVOCs} = {} & \text{methanol} + \text{formaldehyde} \\ & + \text{methyl hydroperoxide} \\ & + \text{hydroxymethylhydroperoxide} + \text{ethanol} \\ & + \text{ethylene glycol} + \text{acetaldehyde} \\ & + \text{glycolaldehyde} + \text{glyoxal} \\ & + \text{1-hydroperoxyacetone} + \text{methylglyoxal} \\ & + \text{isopropanol} + \text{isopropyl hydroperoxide} \\ & + \text{methacrolein} + \text{methyl vinyl ketone}.\end{aligned} \tag{A1}$$

Code and data availability. The current version of the CAABA/MECCA model code is available as a community model in the code repository at https://gitlab.com/RolfSander/caaba-mecca (last access: 25 May 2021, Sander, 2021a), published under the GNU General Public License (http://www.gnu.org/copyleft/gpl.html, last access: 23 April 2021).

The exact version of the CAABA/MECCA model (version 4.5.0) developed in this paper and used in each simulation presented in this paper is archived at Zenodo (http://doi.org/10.5281/zenodo.4707938; Sander, 2021b). All future versions of CAABA/MECCA will be made available at https://doi.org/10.5281/zenodo.4707937.

The archived model code includes a list of all chemical reactions including rate constants and references (caaba/manual/meccanism.pdf), a list of all Henry's law and accommodation constants (caaba/tools/chemprop/chemprop.pdf), and a user manual (caaba/manual/caaba_manual_manual.pdf). For further information and updates, the CAABA/MECCA web page at http://www.mecca.messy-interface.org (last access: 23 April 2021) can be consulted.

The model output of all simulations presented in this paper is archived at Jülich DATA (https://doi.org/10.26165/JUELICH-DATA/SD9F6B; Rosanka et al., 2021b).

Author contributions. SR and DT developed the chemical mechanism. The chemical mechanism was reviewed by RS. SR, DT, and RS implemented the mechanism into MECCA. The results were discussed by all co-authors. The manuscript was prepared by SR with the help of all co-authors.

Competing interests. The authors declare that they have no competing interests.

Acknowledgements. The work described in this paper has received funding from the Initiative and Networking Fund of the Helmholtz Association through the project Advanced Earth System Modelling Capacity (ESM). The content of this paper is the sole responsibility of the authors, and it does not represent the opinion of the Helmholtz Association, and the Helmholtz Association is not responsible for any use that might be made of the information contained. The authors gratefully acknowledge the Earth System Modelling (ESM) project for funding this work by providing computing time on the ESM partition of the supercomputer JUWELS at the Jülich Supercomputing Centre (JSC).

Financial support. This research has been supported by the Initiative and Networking Fund of the Helmholtz Association through the project Advanced Earth System Modelling Capacity (ESM) (grant no. DB001549).

The article processing charges for this open-access publication were covered by the Forschungszentrum Jülich.

Review statement. This paper was edited by Christoph Knote and reviewed by two anonymous referees.

References

Andreae, M. and Rosenfeld, D.: Aerosol–cloud–precipitation interactions. Part 1. The nature and sources of cloud-active aerosols, Earth-Sci. Rev., 89, 13–41, https://doi.org/10.1016/j.earscirev.2008.03.001, 2008.

Arakaki, T., Anastasio, C., Kuroki, Y., Nakajima, H., Okada, K., Kotani, Y., Handa, D., Azechi, S., Kimura, T., Tsuhako, A., and Miyagi, Y.: A General Scavenging Rate Constant for Reaction of Hydroxyl Radical with Organic Carbon in Atmospheric Waters, Environ. Sci. Technol., 47, 8196–8203, https://doi.org/10.1021/es401927b, 2013.

Back, R. A.: The ultraviolet absorption spectrum of oxalic acid vapor, Canadian J. Chem., 62, 1414–1428, https://doi.org/10.1139/v84-241, 1984.

Betterton, E. A. and Hoffmann, M. R.: Henry's law constants of some environmentally important aldehydes, Environ. Sci. Technol., 22, 1415–1418, https://doi.org/10.1021/ES00177A004, 1988.

Blando, J. D. and Turpin, B. J.: Secondary organic aerosol formation in cloud and fog droplets: a literature evaluation of plausibility, Atmos. Environ., 34, 1623–1632, https://doi.org/10.1016/S1352-2310(99)00392-1, 2000.

Bott, A. and Zdunkowski, W.: Electromagnetic energy within dielectric spheres, J. Opt. Soc. Am. A, 4, 1361–1365, https://doi.org/10.1364/JOSAA.4.001361, 1987.

Burkholder, J. B., Sander, S. P., Abbatt, J., Barker, J. R., Huie, R. E., Kolb, C. E., Kurylo, M. J., Orkin, V. L., Wilmouth, D. M., and Wine, P. H.: Chemical Kinetics and Photochemical Data for Use in Atmospheric Studies, Evaluation No. 18, JPL Publication 15-10, Jet Propulsion Laboratory, Pasadena, available at: https://jpldataeval.jpl.nasa.gov/pdf/JPL_Publication_15-10.pdf (last access: 26 May 2021), 2015.

Cabrera-Perez, D., Taraborrelli, D., Sander, R., and Pozzer, A.: Global atmospheric budget of simple monocyclic aromatic compounds, Atmos. Chem. Phys., 16, 6931–6947, https://doi.org/10.5194/acp-16-6931-2016, 2016.

DeCosta, D. P. and Pincock, J. A.: Control of product distribution by Marcus type electron-transfer rates for the radical pair generated in benzylic ester photochemistry, J. Am. Chem. Soc., 111, 8948–8950, https://doi.org/10.1021/ja00206a045, 1989.

Doussin, J.-F. and Monod, A.: Structure–activity relationship for the estimation of OH-oxidation rate constants of carbonyl compounds in the aqueous phase, Atmos. Chem. Phys., 13, 11625–11641, https://doi.org/10.5194/acp-13-11625-2013, 2013.

Epstein, S. A. and Nizkorodov, S. A.: A comparison of the chemical sinks of atmospheric organics in the gas and aqueous phase, Atmos. Chem. Phys., 12, 8205–8222, https://doi.org/10.5194/acp-12-8205-2012, 2012.

Ervens, B.: Modeling the Processing of Aerosol and Trace Gases in Clouds and Fogs, Chem. Rev., 115, 4157–4198, https://doi.org/10.1021/cr5005887, 2015.

Ervens, B. and Volkamer, R.: Glyoxal processing by aerosol multiphase chemistry: towards a kinetic modeling framework of secondary organic aerosol formation in aqueous particles, Atmos. Chem. Phys., 10, 8219–8244, https://doi.org/10.5194/acp-10-8219-2010, 2010.

Ervens, B., Turpin, B. J., and Weber, R. J.: Secondary organic aerosol formation in cloud droplets and aqueous particles (aqSOA): a review of laboratory, field and model studies, Atmos.

Chem. Phys., 11, 11069–11102, https://doi.org/10.5194/acp-11-11069-2011, 2011.

Ervens, B., Renard, P., Tlili, S., Ravier, S., Clément, J.-L., and Monod, A.: Aqueous-phase oligomerization of methyl vinyl ketone through photooxidation – Part 2: Development of the chemical mechanism and atmospheric implications, Atmos. Chem. Phys., 15, 9109–9127, https://doi.org/10.5194/acp-15-9109-2015, 2015.

Guenther, A. B., Jiang, X., Heald, C. L., Sakulyanontvittaya, T., Duhl, T., Emmons, L. K., and Wang, X.: The Model of Emissions of Gases and Aerosols from Nature version 2.1 (MEGAN2.1): an extended and updated framework for modeling biogenic emissions, Geosci. Model Dev., 5, 1471–1492, https://doi.org/10.5194/gmd-5-1471-2012, 2012.

Hahnenstein, I., Albert, M., Hasse, H., Kreiter, C. G., and Maurer, G.: NMR Spectroscopic and Densimetric Study of Reaction Kinetics of Formaldehyde Polymer Formation in Water, Deuterium Oxide, and Methanol, Ind. Eng. Chem. Res., 34, 440–450, https://doi.org/10.1021/ie00041a003, 1995.

Hens, K., Novelli, A., Martinez, M., Auld, J., Axinte, R., Bohn, B., Fischer, H., Keronen, P., Kubistin, D., Nölscher, A. C., Oswald, R., Paasonen, P., Petäjä, T., Regelin, E., Sander, R., Sinha, V., Sipilä, M., Taraborrelli, D., Tatum Ernest, C., Williams, J., Lelieveld, J., and Harder, H.: Observation and modelling of HO_x radicals in a boreal forest, Atmos. Chem. Phys., 14, 8723–8747, https://doi.org/10.5194/acp-14-8723-2014, 2014.

Herrmann, H.: Kinetics of Aqueous Phase Reactions Relevant for Atmospheric Chemistry, Chem. Rev., 103, 4691–4716, https://doi.org/10.1021/cr020658q, 2003.

Herrmann, H., Schaefer, T., Tilgner, A., Styler, S. A., Weller, C., Teich, M., and Otto, T.: Tropospheric Aqueous-Phase Chemistry: Kinetics, Mechanisms, and Its Coupling to a Changing Gas Phase, Chem. Rev., 115, 4259–4334, https://doi.org/10.1021/cr500447k, 2015.

Hilborn, J. W. and Pincock, J. A.: Rates of decarboxylation of acyloxy radicals formed in the photocleavage of substituted 1-naphthylmethyl alkanoates, J. Am. Chem. Soc., 113, 2683–2686, https://doi.org/10.1021/ja00007a049, 1991.

Jacob, D. J.: Chemistry of OH in remote clouds and its role in the production of formic acid and peroxymonosulfate, J. Geophys. Res.-Atmos., 91, 9807–9826, https://doi.org/10.1029/JD091iD09p09807, 1986.

Jarecka, D., Grabowski, W. W., Morrison, H., and Pawlowska, H.: Homogeneity of the Subgrid-Scale Turbulent Mixing in Large-Eddy Simulation of Shallow Convection, J. Atmos. Sci., 70, 2751–2767, https://doi.org/10.1175/JAS-D-13-042.1, 2013.

Jenkin, M. E., Young, J. C., and Rickard, A. R.: The MCM v3.3.1 degradation scheme for isoprene, Atmos. Chem. Phys., 15, 11433–11459, https://doi.org/10.5194/acp-15-11433-2015, 2015.

Jöckel, P., Tost, H., Pozzer, A., Brühl, C., Buchholz, J., Ganzeveld, L., Hoor, P., Kerkweg, A., Lawrence, M. G., Sander, R., Steil, B., Stiller, G., Tanarhte, M., Taraborrelli, D., van Aardenne, J., and Lelieveld, J.: The atmospheric chemistry general circulation model ECHAM5/MESSy1: consistent simulation of ozone from the surface to the mesosphere, Atmos. Chem. Phys., 6, 5067–5104, https://doi.org/10.5194/acp-6-5067-2006, 2006.

Jöckel, P., Kerkweg, A., Pozzer, A., Sander, R., Tost, H., Riede, H., Baumgaertner, A., Gromov, S., and Kern, B.: Development cycle 2 of the Modular Earth Submodel System (MESSy2), Geosci. Model Dev., 3, 717–752, https://doi.org/10.5194/gmd-3-717-2010, 2010.

Jöckel, P., Tost, H., Pozzer, A., Kunze, M., Kirner, O., Brenninkmeijer, C. A. M., Brinkop, S., Cai, D. S., Dyroff, C., Eckstein, J., Frank, F., Garny, H., Gottschaldt, K.-D., Graf, P., Grewe, V., Kerkweg, A., Kern, B., Matthes, S., Mertens, M., Meul, S., Neumaier, M., Nützel, M., Oberländer-Hayn, S., Ruhnke, R., Runde, T., Sander, R., Scharffe, D., and Zahn, A.: Earth System Chemistry integrated Modelling (ESCiMo) with the Modular Earth Submodel System (MESSy) version 2.51, Geosci. Model Dev., 9, 1153–1200, https://doi.org/10.5194/gmd-9-1153-2016, 2016.

Jülich Supercomputing Centre: JUWELS: Modular Tier-0/1 Supercomputer at the Jülich Supercomputing Centre, J. Large-Scale Res. Fac., 5, A171, https://doi.org/10.17815/jlsrf-5-171, 2019.

Lelieveld, J. and Crutzen, P. J.: Influences of cloud photochemical processes on tropospheric ozone, Nature, 343, 227–233, https://doi.org/10.1038/343227a0, 1990.

Liang, J. and Jacob, D. J.: Effect of aqueous phase cloud chemistry on tropospheric ozone, J. Geophys. Res.-Atmos., 102, 5993–6001, https://doi.org/10.1029/96JD02957, 1997.

Lim, Y. B., Tan, Y., and Turpin, B. J.: Chemical insights, explicit chemistry, and yields of secondary organic aerosol from OH radical oxidation of methylglyoxal and glyoxal in the aqueous phase, Atmos. Chem. Phys., 13, 8651–8667, https://doi.org/10.5194/acp-13-8651-2013, 2013.

Lin, G., Penner, J. E., Sillman, S., Taraborrelli, D., and Lelieveld, J.: Global modeling of SOA formation from dicarbonyls, epoxides, organic nitrates and peroxides, Atmos. Chem. Phys., 12, 4743–4774, https://doi.org/10.5194/acp-12-4743-2012, 2012.

Mayer, B. and Madronich, S.: Actinic flux and photolysis in water droplets: Mie calculations and geometrical optics limit, Atmos. Chem. Phys., 4, 2241–2250, https://doi.org/10.5194/acp-4-2241-2004, 2004.

Meylan, W. M. and Howard, P. H.: Bond contribution method for estimating henry's law constants, Environ. Toxicol. Chem., 10, 1283–1293, https://doi.org/10.1002/etc.5620101007, 1991.

Monod, A., Chevallier, E., Jolibois, R. D., Doussin, J., Picquet-Varrault, B., and Carlier, P.: Photooxidation of methylhydroperoxide and ethylhydroperoxide in the aqueous phase under simulated cloud droplet conditions, Atmos. Environ., 41, 2412–2426, https://doi.org/10.1016/j.atmosenv.2006.10.006, 2007.

Mouchel-Vallon, C., Deguillaume, L., Monod, A., Perroux, H., Rose, C., Ghigo, G., Long, Y., Leriche, M., Aumont, B., Patryl, L., Armand, P., and Chaumerliac, N.: CLEPS 1.0: A new protocol for cloud aqueous phase oxidation of VOC mechanisms, Geosci. Model Dev., 10, 1339–1362, https://doi.org/10.5194/gmd-10-1339-2017, 2017.

Nölscher, A., Butler, T., Auld, J., Veres, P., Muñoz, A., Taraborrelli, D., Vereecken, L., Lelieveld, J., and Williams, J.: Using total OH reactivity to assess isoprene photooxidation via measurement and model, Atmos. Environ., 89, 453–463, https://doi.org/10.1016/j.atmosenv.2014.02.024, 2014.

Piesiak, A., Schuchmann, M. N., Zegota, H., and von Sonntag, C.: β-Hydroxyethylperoxyl radicals: a study of the γ-radiolysis and-pulse radiolysis of ethylene in oxygenated aqueous solutions, Z. Naturforsch., 39, 1262–1267, 1984.

Poulain, L., Katrib, Y., Isikli, E., Liu, Y., Wortham, H., Mirabel, P., Calvé, S. L., and Monod, A.: In-cloud multiphase behaviour of

acetone in the troposphere: Gas uptake, Henry's law equilibrium and aqueous phase photooxidation, Chemosphere, 81, 312–320, https://doi.org/10.1016/j.chemosphere.2010.07.032, 2010.

Rosanka, S., Franco, B., Clarisse, L., Coheur, P.-F., Wahner, A., and Taraborrelli, D.: Organic pollutants from tropical peatland fires: regional influences and its impact on lower stratospheric ozone, Atmos. Chem. Phys. Discuss. [preprint], https://doi.org/10.5194/acp-2020-1130, in review, 2020.

Rosanka, S., Sander, R., Franco, B., Wespes, C., Wahner, A., and Taraborrelli, D.: Oxidation of low-molecular-weight organic compounds in cloud droplets: global impact on tropospheric oxidants, Atmos. Chem. Phys., 21, 9909–9930, https://doi.org/10.5194/acp-21-9909-2021, 2021a.

Rosanka, S., Sander, R., Wahner, A., and Taraborrelli, D.: Model output from CAABA/MECCA obtained during the development of JAMOC [Data set], Jülich DATA, https://doi.org/10.26165/JUELICH-DATA/SD9F6B, 2021b.

Ruggaber, A., Dlugi, R., Bott, A., Forkel, R., Herrmann, H., and Jacobi, H.-W.: Modelling of radiation quantities and photolysis frequencies in the aqueous phase in the troposphere, Atmos. Environ., 31, 3137–3150, https://doi.org/10.1016/S1352-2310(97)00058-7,1997.

Rumble, J. R. (Ed.): CRC Handbook of Chemistry and Physics, 101st edn., CRC Press, Boca Raton, FL, 2020.

Sander, R.: Modeling Atmospheric Chemistry: Interactions between Gas-Phase Species and Liquid Cloud/Aerosol Particles, Surv. Geophys., 20, 1–31, https://doi.org/10.1023/A:1006501706704, 1999.

Sander, R.: Compilation of Henry's law constants (version 4.0) for water as solvent, Atmos. Chem. Phys., 15, 4399–4981, https://doi.org/10.5194/acp-15-4399-2015, 2015.

Sander, R.: Chemistry As A Boxmodel Application / Module Efficiently Calculating the Chemistry of the Atmosphere, available at: https://gitlab.com/RolfSander/caaba-mecca, last access: 25 May 2021a.

Sander, R.: The community atmospheric chemistry box model CAABA/MECCA [Data set], version 4.5.0, Zenodo, https://doi.org/10.5281/zenodo.4707938, 2021b.

Sander, R., Jöckel, P., Kirner, O., Kunert, A. T., Landgraf, J., and Pozzer, A.: The photolysis module JVAL-14, compatible with the MESSy standard, and the JVal PreProcessor (JVPP), Geosci. Model Dev., 7, 2653–2662, https://doi.org/10.5194/gmd-7-2653-2014, 2014.

Sander, R., Baumgaertner, A., Cabrera-Perez, D., Frank, F., Gromov, S., Grooß, J.-U., Harder, H., Huijnen, V., Jöckel, P., Karydis, V. A., Niemeyer, K. E., Pozzer, A., Riede, H., Schultz, M. G., Taraborrelli, D., and Tauer, S.: The community atmospheric chemistry box model CAABA/MECCA-4.0, Geosci. Model Dev., 12, 1365–1385, https://doi.org/10.5194/gmd-12-1365-2019, 2019.

Schuchmann, M. N., Zegota, H., and von Sonntag, C.: Acetateperoxyl radicals, $O_2CH_2CO_2^-$: a study on the γ-radiolysis andpulse radiolysis of acetate in oxygenated aqueous solutions, Z. Naturforsch. Pt. B, 40, 215–221, 1985.

Schwartz, S. E.: Mass-Transport Considerations Pertinent to Aqueous Phase Reactions of Gases in Liquid-Water Clouds, in: Chemistry of Multiphase Atmospheric Systems, edited by: Jaeschke, W., Springer Berlin Heidelberg, Berlin, Heidelberg, 415–471, 1986.

Staehelin, J. and Hoigné, J.: Decomposition of ozone in water in the presence of organic solutes acting as promoters and inhibitors of radical chain reactions, Environ. Sci. Technol., 19, 1206–1213, https://doi.org/10.1021/es00142a012, 1985.

Staehelin, J., Buehler, R. E., and Hoigné, J.: Ozone decomposition in water studied by pulse radiolysis. 2. Hydroxyl and hydrogen tetroxide (HO4) as chain intermediates, J. Phys. Chem., 88, 5999–6004, https://doi.org/10.1021/j150668a051, 1984.

Tan, Y., Perri, M. J., Seitzinger, S. P., and Turpin, B. J.: Effects of Precursor Concentration and Acidic Sulfate in Aqueous Glyoxal–OH Radical Oxidation and Implications for Secondary Organic Aerosol, Environ. Sci. Technol., 43, 8105–8112, https://doi.org/10.1021/es901742f, 2009.

Taraborrelli, D., Lawrence, M. G., Butler, T. M., Sander, R., and Lelieveld, J.: Mainz Isoprene Mechanism 2 (MIM2): an isoprene oxidation mechanism for regional and global atmospheric modelling, Atmos. Chem. Phys., 9, 2751–2777, https://doi.org/10.5194/acp-9-2751-2009, 2009.

Taraborrelli, D., Lawrence, M. G., Crowley, J. N., Dillon, T. J., Gromov, S., Groß, C. B. M., Vereecken, L., and Lelieveld, J.: Hydroxyl radical buffered by isoprene oxidation over tropical forests, Nat. Geosci., 5, 190–193, https://doi.org/10.1038/ngeo1405, 2012.

Tie, X., Madronich, S., Walters, S., Edwards, D. P., Ginoux, P., Mahowald, N., Zhang, R., Lou, C., and Brasseur, G.: Assessment of the global impact of aerosols on tropospheric oxidants, J. Geophys. Res.-Atmos., 110, D03204, https://doi.org/10.1029/2004JD005359, 2005.

Tilgner, A., Bräuer, P., Wolke, R., and Herrmann, H.: Modelling multiphase chemistry in deliquescent aerosols and clouds using CAPRAM3.0i, J. Atmos. Chem., 70, 221–256, https://doi.org/10.1007/s10874-013-9267-4, 2013.

Tost, H., Jöckel, P., Kerkweg, A., Sander, R., and Lelieveld, J.: Technical note: A new comprehensive SCAVenging submodel for global atmospheric chemistry modelling, Atmos. Chem. Phys., 6, 565–574, https://doi.org/10.5194/acp-6-565-2006, 2006.

Tost, H., Jöckel, P., Kerkweg, A., Pozzer, A., Sander, R., and Lelieveld, J.: Global cloud and precipitation chemistry and wet deposition: tropospheric model simulations with ECHAM5/MESSy1, Atmos. Chem. Phys., 7, 2733–2757, https://doi.org/10.5194/acp-7-2733-2007, 2007.

United States Environmental Protection Agency (US EPA): Estimation Programs Interface Suite™ for Microsoft® Windows, Washington, DC, USA, 2012.

Villalta, P. W., Lovejoy, E. R., and Hanson, D. R.: Reaction probability of peroxyacetyl radical on aqueous surfaces, Geophys. Res. Lett., 23, 1765–1768, https://doi.org/10.1029/96GL01286, 1996.

von Sonntag, C.: The chemical basis of radiation biology, Taylor & Francis London, 1987.

von Sonntag, C. and Schuchmann, H.-P.: Peroxyl Radicals in Aqueous Solutions, in: The Chemistry of Free Radicals: Peroxyl Radicals, Wiley, New York, 1997.

Yamamoto, S. and Back, R. A.: The gas-phase photochemistry of oxalic acid, J. Phys. Chem., 89, 622–625, https://doi.org/10.1021/j100250a014, 1985.

Zegota, H., Schuchmann, M. N., Schulz, D., and von Sonntag, C.: Acetonylperoxyl radicals, $CH_3COCH_2O_2$: A study on the γ-radiolysis and pulse radiolysis of acetone in oxygenated aqueoussolutions, Z. Naturforsch., 41, 1015–1022, 1986.

Chapter 6

Oxidation of low-molecular-weight organic compounds in cloud droplets: global impact on tropospheric oxidants

Rosanka, S., Sander, R., Franco, B., Wespes, C., Wahner, A., and Taraborrelli, D.: Oxidation of low-molecular-weight organic compounds in cloud droplets: global impact on tropospheric oxidants, Atmospheric Chemistry and Physics, 21, 9909–9930, https://doi.org/10.5194/acp-21-9909-2021, 2021b

General information:

Importance for this thesis and the author's contribution:
In this study, the importance of explicit in-cloud OVOC oxidation is addressed on a global scale. It contributes to the assessment of the representation of aqueous-phase OVOC chemistry and VOC emissions in global models. This is further discussed in Sect. 8.4.

The idea for this study was developed together with Domenico Taraborrelli. I implemented JAMOC into EMAC, performed the simulations, and analysed the data. I discussed the results with all co-authors. I created all figures and wrote the manuscript. Further information and the contributions of all co-authors are available in the manuscript's 'Author contributions' section.

[1] `https://creativecommons.org/licenses/by/4.0/` (last access: 6 September 2020)

Atmos. Chem. Phys., 21, 9909–9930, 2021
https://doi.org/10.5194/acp-21-9909-2021

Atmospheric Chemistry and Physics Open Access EGU

Oxidation of low-molecular-weight organic compounds in cloud droplets: global impact on tropospheric oxidants

Simon Rosanka[1], Rolf Sander[2], Bruno Franco[3], Catherine Wespes[3], Andreas Wahner[1], and Domenico Taraborrelli[1]

[1]Institute of Energy and Climate Research: Troposphere (IEK-8), Forschungszentrum Jülich GmbH, Jülich, Germany
[2]Atmospheric Chemistry Department, Max Planck Institute for Chemistry, Mainz, Germany
[3]Spectroscopy, Quantum Chemistry and Atmospheric Remote Sensing (SQUARES), Université libre de Bruxelles (ULB), Brussels, 1050, Belgium

Correspondence: Simon Rosanka (s.rosanka@fz-juelich.de)

Received: 6 October 2020 – Discussion started: 4 November 2020
Revised: 2 March 2021 – Accepted: 7 April 2021 – Published: 1 July 2021

Abstract. In liquid cloud droplets, superoxide anion ($O^-_{2(aq)}$) is known to quickly consume ozone ($O_{3(aq)}$), which is relatively insoluble. The significance of this reaction as a tropospheric O_3 sink is sensitive to the abundance of $O^-_{2(aq)}$ and therefore to the production of its main precursor, the hydroperoxyl radical ($HO_{2(aq)}$). The aqueous-phase oxidation of oxygenated volatile organic compounds (OVOCs) is the major source of $HO_{2(aq)}$ in cloud droplets. Hence, the lack of explicit aqueous-phase chemical kinetics in global atmospheric models leads to a general underestimation of clouds as O_3 sinks. In this study, the importance of in-cloud OVOC oxidation for tropospheric composition is assessed by using the Chemistry As A Boxmodel Application (CAABA) and the global ECHAM/MESSy Atmospheric Chemistry (EMAC) model, which are both capable of explicitly representing the relevant chemical transformations. For this analysis, three different in-cloud oxidation mechanisms are employed: (1) one including the basic oxidation of $SO_{2(aq)}$ by $O_{3(aq)}$ and $H_2O_{2(aq)}$, which thus represents the capabilities of most global models; (2) the more advanced standard EMAC mechanism, which includes inorganic chemistry and simplified degradation of methane oxidation products; and (3) the detailed in-cloud OVOC oxidation scheme Jülich Aqueous-phase Mechanism of Organic Chemistry (JAMOC). By using EMAC, the global impact of each mechanism is assessed focusing mainly on tropospheric volatile organic compounds (VOCs), HO_x ($HO_x = OH + HO_2$), and O_3. This is achieved by performing a detailed HO_x and O_3 budget analysis in the gas and aqueous phase. The resulting changes are evaluated against O_3 and methanol (CH_3OH) satellite observations from the Infrared Atmospheric Sounding Interferometer (IASI) for 2015. In general, the explicit in-cloud oxidation leads to an overall reduction in predicted OVOC levels and reduces EMAC's overestimation of some OVOCs in the tropics. The in-cloud OVOC oxidation shifts the HO_2 production from the gas to the aqueous phase. As a result, the O_3 budget is perturbed with scavenging being enhanced and the gas-phase chemical losses being reduced. With the simplified in-cloud chemistry, about 13 Tg yr^{-1} of O_3 is scavenged, which increases to 336 Tg yr^{-1} when JAMOC is used. The highest O_3 reduction of 12 % is predicted in the upper troposphere–lower stratosphere (UTLS). These changes in the free troposphere significantly reduce the modelled tropospheric ozone columns, which are known to be generally overestimated by EMAC and other global atmospheric models.

1 Introduction

Aqueous-phase chemistry in cloud droplets differs significantly from gas-phase chemistry, mainly due to photolysis enhanced by scattering effects within cloud droplets (Bott and Zdunkowski, 1987; Mayer and Madronich, 2004), faster reaction rates, and chemical reactions that do not occur in the gas phase (Herrmann, 2003; Epstein and Nizkorodov, 2012). Moreover, the conversion of nitrogen monoxide (NO) to nitrogen dioxide (NO_2) by peroxy radicals (RO_2) essentially does not take place in liquid droplets because NO is very insoluble (Lelieveld and Crutzen, 1990). Compared to gas-phase chemistry, models of aqueous-phase chemistry

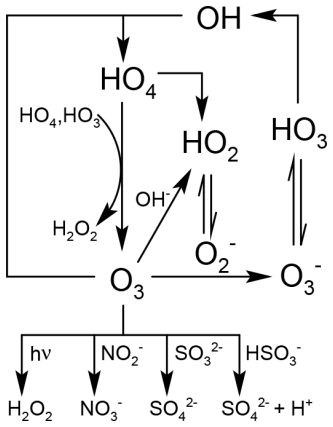

Figure 1. Graphical representation of inorganic aqueous-phase ozone chemistry based on Staehelin et al. (1984).

still suffer from large uncertainties, and most global models only include rudimentary implementations (Ervens, 2015). In general, warm (liquid) clouds can act as a sink for ozone (O_3) and its precursors in the troposphere. Figure 1 gives an overview of the inorganic aqueous-phase chemistry for $O_{3(aq)}$ according to the mechanism by Staehelin et al. (1984). When O_3 is taken up into cloud droplets, it is mainly destroyed via

$$O_{3(aq)} + O^-_{2(aq)} \rightarrow O^-_{3(aq)} + O_{2(aq)} \ . \quad \text{(R1)}$$

The superoxide anion ($O^-_{2(aq)}$) is in equilibrium with its conjugate acid, the hydroperoxyl radical ($HO_{2(aq)}$):

$$HO_{2(aq)} \rightleftharpoons O^-_{2(aq)} + H^+_{(aq)} \ . \quad \text{(R2)}$$

Here, $HO_{2(aq)}$ is either scavenged from the gas phase or produced by photo-oxidation inside the cloud droplet. The realistic representation of clouds as O_3 sinks is thus sensitive to a proper representation of $HO_{2(aq)}$ in cloud droplets.

The importance of aqueous-phase chemistry for tropospheric O_3 has already been the topic of many earlier studies. Lelieveld and Crutzen (1990) proposed that clouds strongly influence O_3, HO_x ($HO_x = HO_2 + OH$), and NO_x ($NO_x = NO + NO_2$). They concluded that under high-NO_x conditions, the net O_3 production is decreased by as much as 40 % at particular regions affected by clouds. However, Liang and Jacob (1997) suggested that Lelieveld and Crutzen (1990) grossly overestimated the impact of clouds on O_3 because they made the assumption that the methyl peroxy radical (CH_3O_2) could have the same solubility as HO_2. They predicted that clouds reduce tropospheric O_3 by less than 3 % in the tropics and at mid-latitudes during summer. A major aqueous-phase source of $HO_{2(aq)}$ is the oxidation of water-soluble oxygenated volatile organic compounds (OVOCs). However, by not considering additional in-cloud $HO_{2(aq)}$ sources, Liang and Jacob (1997) underestimated $O^-_{2(aq)}$ concentrations dampening the in-cloud destruction of $O_{3(aq)}$. Due to these changes in the gas-phase oxidation budgets, clouds indirectly impact the formation of secondary organic aerosols (SOAs). Further, the in-cloud oxidation of OVOC leads to the formation and destruction of SOA precursors. Therefore, clouds can act as SOA sources (Blando and Turpin, 2000), and modelling studies suggest that clouds may contribute on the same order of magnitude to the SOA formation as gas-phase sources (Ervens et al., 2011; Ervens, 2015; Lin et al., 2012).

It is thus desirable to properly represent aqueous-phase chemistry in global models. Unfortunately, the detailed representation of aqueous-phase chemistry comes at a high computational cost. Thus, compared to gas-phase chemistry, aqueous-phase chemistry is poorly represented in most regional and global models. Further, it is often limited to basic sulfur dioxide ($SO_{2(aq)}$) oxidation as the only in-cloud $O_{3(aq)}$ destruction pathway in the aqueous phase (Ervens, 2015). The reduced Chemical Aqueous Phase Radical Mechanism (CAPRAM-RED) is based on CAPRAM 3.0i (Tilgner and Herrmann, 2010) and represents about 200 reactions (Deguillaume et al., 2009). So far, it has been applied in 2-D applications using the regional chemistry transport model COSMO-MUSCAT (Deguillaume et al., 2009; Schrödner et al., 2014). On a global scale, Myriokefalitakis et al. (2011) studied the formation of oxalate using an explicit aqueous-phase mechanism using about 50 reactions in an offline 3-D model. When investigating present online global modelling capabilities, the global ECHAM/MESSy Atmospheric Chemistry (EMAC) model constitutes an exception. The technical advances implemented by Tost et al. (2006) allow an explicit representation of aqueous-phase processes. EMAC's standard aqueous-phase mechanism represents more than 150 reactions and even includes a simplified degradation scheme of methane oxidation products (Tost et al., 2007). However, an extensive and explicit in-cloud OVOC oxidation scheme suitable for EMAC and other global models in general has not been available. By neglecting in-cloud OVOC oxidation, aqueous-phase $HO_{2(aq)}$ concentrations are very likely underestimated. Thus, it is expected that global atmospheric models underestimate clouds as O_3 sinks. In order to make a detailed in-cloud OVOC oxidation scheme readily available for box as well as for regional and global simulations that is affordable with modern supercomputing facilities, we have developed the Jülich Aqueous-phase Mechanism of Organic Chemistry (JAMOC) and implemented it into the atmospheric chemistry mechanism Module Efficiently Calculating the Chemistry of the Atmosphere (MECCA) in our companion paper by Rosanka et al. (2021). In JAMOC, the phase transfer of species containing up to 10 carbon atoms is taken into account, and a selection of species containing up to 4 carbon atoms is considered to react in the aqueous phase, resulting in more than 1000 reactions. Isoprene (C_5H_8), the most abundantly emit-

ted volatile organic compound (VOC), is not explicitly dissolved but many of its oxidation products explicitly react inside cloud droplets. Here, OVOC reactions with hydroxyl radicals ($OH_{(aq)}$) are implemented as the main daytime oxidation pathway, whereas nitrate radicals ($NO_{3(aq)}$) represent the main nighttime oxidant.

In this study, JAMOC is implemented into the global model EMAC (Sect. 2) and its importance for tropospheric VOCs, HO_x, and O_3 is addressed. The performance of JAMOC is compared to the performance of an aqueous-phase mechanism including only minimal aqueous-phase chemistry and to that of the standard mechanism of EMAC (each presented in Sect. 2.1). In order to understand the mechanism behind the impact of in-cloud OVOC oxidation on a single air parcel, a box-model study is performed in Sect. 3. Afterwards, the impact on a global scale is analysed (Sect. 4). The analysis focuses on a selection of VOCs, HO_x, and O_3. The multiphase chemistry of JAMOC is expected to impact tropospheric organic acids, which will be the topic of a further study. When considering the global O_3 budget, odd oxygen (O_x) is analysed to account for rapid cycling between species of the O_x family. In the scope of this study, O_x is defined as

$$\begin{aligned} O_x \equiv\ & O + O_3 + NO_2 + 2 \times NO_3 + 3 \times N_2O_5 + HNO_3 \\ & + HNO_4 + ClO + HOCl + ClNO_2 + 2 \times ClNO_3 \\ & + BrO + HOBr + BrNO_2 + 2 \times BrNO_3 + PANs \\ & + PNs + ANs + NPs, \end{aligned} \quad (1)$$

where PANs are peroxyacyl nitrates, PNs are alkyl peroxy nitrates, ANs are alkyl nitrates, and NPs are nitrophenols. In Sect. 4, all EMAC simulations performed are evaluated against satellite observations of O_3 and methanol (CH_3OH) obtained from the Infrared Atmospheric Sounding Interferometer (IASI). Model uncertainties are discussed in Sect. 5, followed by a general conclusion (Sect. 6).

2 Modelling approach

The aqueous- and gas-phase mechanisms are presented in Sect. 2.1. They are used within two different modelling frameworks: a box model and a global atmospheric model. The box model, used to investigate the local impact on an air parcel, is presented in Sect. 2.2, and the global chemical atmospheric model is presented in Sect. 2.3. Section 2.4 provides an overview of all simulations performed in this study.

2.1 The chemical mechanisms

The study is based on the comparison of three different aqueous-phase mechanisms (Sect. 2.1.1). While they are characterised by different levels of complexity, especially in terms of the species and reactions taken into account, they are all coupled to the same gas-phase mechanism (Sect. 2.1.2).

2.1.1 Aqueous phase

The first aqueous-phase mechanism includes the uptake of a few soluble compounds, their acid–base equilibria, and the oxidation of $SO_{2(aq)}$ by $O_{3(aq)}$ and $H_2O_{2(aq)}$. This mechanism was applied by Jöckel et al. (2006) and is considered to represent the capabilities of most global models (Ervens, 2015). The second aqueous-phase mechanism includes an advanced scheme, representing more than 150 reactions (Tost et al., 2007; Jöckel et al., 2016). It includes in-cloud $HO_{x(aq)}$ chemistry and the destruction of $O_{3(aq)}$ by $O^-_{2(aq)}$, but it misses a detailed in-cloud OVOC oxidation scheme. This mechanism can be considered the current standard mechanism used in EMAC. The last aqueous-phase mechanism is the complex OVOC oxidation scheme JAMOC developed in our companion paper by Rosanka et al. (2021). This mechanism is based on the box-model mechanism Cloud Explicit Physico-chemical Scheme (CLEPS 1.0; Mouchel-Vallon et al., 2017). In order to make it applicable for global models, Rosanka et al. (2021) reduced the number of aqueous-phase species to a selection containing up to 4 carbon atoms. JAMOC represents the photo-oxidation of all species containing 1 and 2 carbon atoms represented in CLEPS but limits the photo-oxidation of species with 3 or 4 carbon atoms to the major products from C_5H_8 oxidation (i.e. methylglyoxal, methacrolein, and methyl vinyl ketone) and the in-cloud sources of methylglyoxal. Still, the phase transfer of soluble species containing up to 10 carbon atoms is represented in JAMOC. In addition to CLEPS, Rosanka et al. (2021) extended JAMOC by (1) simulating hydration and dehydration explicitly; (2) taking the oligomerisation of formaldehyde, glyoxal, and methylglyoxal into account; (3) adding further aqueous-phase photolysis reactions; and (4) considering the gas-phase photo-oxidation of new outgassed species. Overall, JAMOC represents the phase transfer of 350 species, 43 equilibria (acid–base and hydration), and more than 280 photo-oxidation reactions. A complete description of JAMOC, including a list of all reactions, is available in Rosanka et al. (2021). Even though Fenton's chemistry is an in-cloud source of $OH_{(aq)}$, this chemistry is not considered in this study (switched off in JAMOC) due to missing global iron (Fe) distributions and emissions in EMAC. The associated uncertainties for excluding this $OH_{(aq)}$ sources are discussed in Sect. 5.

2.1.2 Gas phase

The Mainz Organic Mechanism (MOM; Sander et al., 2019) is used to model gas-phase chemistry, containing an extensive oxidation scheme for isoprene (Taraborrelli et al., 2009, 2012; Nölscher et al., 2014), monoterpenes (Hens et al., 2014), and aromatics (Cabrera-Perez et al., 2016). In addition, comprehensive reaction schemes are considered for the modelling of the chemistry of NO_x, HO_x, CH_4, and anthropogenic linear hydrocarbons. VOCs are oxidised by

OH, O_3, and NO_3, whereas RO_2 reacts with HO_2, NO_x, and NO_3 and undergoes self- and cross-reactions (Sander et al., 2019). When the complex in-cloud OVOC oxidation scheme JAMOC is coupled to MOM, MOM is modified following the gas-phase additions as described in Rosanka et al. (2021).

2.2 Chemistry box model CAABA

Each of the three mechanisms is implemented in the Chemistry As A Boxmodel Application (CAABA; Sander et al., 2019) in order to investigate their implications for a single air parcel under predefined atmospheric conditions. The MECCA submodel in CAABA is capable of numerically integrating the multiphase chemical mechanism as one single system of ordinary differential equations (ODEs) with appropriate phase-transfer reactions (Sander, 1999; Kerkweg et al., 2007). The Kinetic PreProcessor (KPP version 2.2.3; Sandu and Sander, 2006) is used in MECCA to integrate these ODE systems. Further, photolysis, emissions and dry deposition of chemical species, and the exchange with other air masses outside the box (entrainment) are represented in a simplified manner.

In this study, an air parcel during summer is simulated at a mid-latitude with a constant temperature of 278 K and a relative humidity of 100 %. The same initial conditions are used as proposed in Rosanka et al. (2021, see their Table 3), but the NO emissions are neglected in this study. In order to represent a realistic atmospheric cloud event and investigate the impact of the newly developed aqueous-phase mechanism, three atmospheric conditions are modelled during the simulated day. First, CAABA is initialised at 00:00 UTC, and no cloud droplets are present until 12:00 UTC. At 12:00 UTC a cloud is formed with droplet radii of 20 µm and a liquid water content of 0.3 $g\,m^{-3}$. After 1 h, the cloud evaporates and all species outgas. The rest of the day is simulated using the same conditions as before the cloud event.

2.3 Global model EMAC

The ECHAM/MESSy Atmospheric Chemistry (EMAC) model is a numerical chemistry and climate simulation system that includes submodels describing tropospheric and middle atmospheric processes and their interaction with oceans, land, and human influences (Jöckel et al., 2010). It uses the second version of the Modular Earth Submodel System (MESSy2) to link multi-institutional computer codes. The core atmospheric model is the fifth-generation European Centre Hamburg general circulation model (ECHAM5; Roeckner et al., 2003). For the present study, EMAC (ECHAM5 version 5.3.02, MESSy version 2.54.0) is used at T63L90MA resolution, i.e. with a spherical truncation of T63 (corresponding to a quadratic Gaussian grid of approximately 1.875° by 1.875° in latitude and longitude) with 90 vertical hybrid pressure levels up to 0.01 hPa.

In contrast to CAABA, gas- and aqueous-phase chemistry are calculated separately. In order to model the gas-phase mechanism MOM in the troposphere and stratosphere, the submodel MECCA is used. The SCAVenging submodel (SCAV; Tost et al., 2006) is used to simulate the removal of trace gases and aerosol particles by clouds and precipitation. SCAV calculates the transfer of species into and out of rain and cloud droplets using the Henry's law equilibrium, acid dissociation equilibria, oxidation–reduction reactions, heterogeneous reactions on droplet surfaces, and aqueous-phase photolysis reactions (Tost et al., 2006). In this study, SCAV is used to calculate the three aqueous-phase mechanisms presented in Sect. 2.1.1. Like MECCA, SCAV treats the aqueous-phase mechanism as an ODE system and uses KPP (version 1) to solve it. This operator splitting is necessary because the ODE systems resulting from the combination of gas-phase and in-cloud aqueous-phase mechanisms would suffer from (1) a higher stiffness due to fast acid–base equilibria and phase-transfer reactions and (2) load imbalances on high-performance computing (HPC) systems due to the sparsity of clouds. In both MECCA and to some degree SCAV, tagging systems are used to calculate detailed gas- and aqueous-phase O_x and HO_x budgets. These systems allow the estimation of the full implications of the aqueous-phase mechanism for atmospheric chemistry. The tagging system of MECCA is more sophisticated and allows for obtaining reaction rates from multiple reactions and combining them into a single tracer (Gromov et al., 2010). For the tropospheric O_x budget, the gas-phase chemical production and loss and the scavenging and wet deposition are taken into account by using MECCA and SCAV, respectively. Additionally, the dry deposition of O_x and many MOM species is calculated by the submodel Dry DEPosition (DDEP; Kerkweg et al., 2006) using its default scheme.

The MESSy submodel Model of Emissions of Gases and Aerosols from Nature (MEGAN) is used to model biogenic VOC emissions (Guenther et al., 2006). Global isoprene emissions are scaled to the best estimate of Sindelarova et al. (2014), which is 595 $Tg\,yr^{-1}$. Biomass burning emission fluxes are calculated using the MESSy submodel BIOBURN, which calculates these fluxes based on biomass burning emission factors and dry matter combustion rates. For the latter, Global Fire Assimilation System (GFAS) data are used, which are based on satellite observations of fire radiative power from the Moderate Resolution Imaging Spectroradiometer (MODIS) satellite instruments (Kaiser et al., 2012). The biomass burning emission factors for VOCs are based on Akagi et al. (2011).

The submodel SORBIT (Jöckel et al., 2010) is used to sample the model state along sun-synchronous satellite orbits, at the time of the satellite overpass, and to compare the model outputs to satellite observations obtained from the Infrared Atmospheric Sounding Interferometer (IASI, Clerbaux et al., 2009) on board the Metop-A (IASI-A) and Metop-B (IASI-B) satellites. In particular, Fast Opti-

mal Retrievals on Layers for IASI Ozone (FORLI-O_3, version 20151001; see Hurtmans et al., 2012, for a description of the retrievals) is used for the comparison of tropospheric O_3 columns. In general, when analysing tropospheric burdens and budgets, the standard EMAC tropopause definition is used. Here, the tropopause is defined in the extratropics using potential vorticity, whereas temperature lapse rates are used in the tropics (Jöckel et al., 2006). However, when comparing modelled tropospheric O_3 columns to IASI-FORLI measurements, the troposphere is defined as ranging from the ground to 300 hPa in order to limit the influences of the stratospheric O_3 but to include the altitude of maximum sensitivity of IASI in the troposphere (Wespes et al., 2017). Moreover, this allows the avoiding of larger errors that affect the O_3 retrievals in the upper troposphere–lower stratosphere (UTLS) (Wespes et al., 2016) and that result in a positive column bias (Boynard et al., 2016). The evaluation of simulation results against global observational datasets of VOC abundance can be performed for only a few species. Daily global distributions of methanol total columns are available from IASI-A and IASI-B observations, using a neural-network-based retrieval approach (Franco et al., 2018). Due to the limited vertical information on methanol that is contained in the IASI spectra, only total columns have been retrieved. Since the neural-network-based retrievals do not rely on scene-dependent a priori information, no averaging kernels are produced and the retrieved total columns are meant to be compared at face value with model data (see Franco et al., 2018, and references therein). For this purpose, the IASI methanol measurements have been daily averaged on the EMAC T63 spatial grid. The comparisons with IASI O_3 and methanol data are associated with some observational uncertainties. IASI retrievals are obtained in the thermal infrared range, resulting in an especially high sensitivity to clouds. Appropriate filters are applied in order to account for cloud-contaminated IASI scene observations. These filters are based on defined cloud cover thresholds, using information from the EUMETCast operational processing system (August et al., 2012). The fractional cloud cover threshold depends on the species observed. For O_3 and methanol, all observations with a fractional cloud cover above 13 % (Wespes et al., 2017) and 25 % (Franco et al., 2018) have been excluded, respectively. The IASI methanol retrievals are less sensitive to the presence of residual clouds since no radiative transfer model is used, resulting in a higher threshold for methanol. Of course, it cannot be completely ruled out that individual IASI measurements are locally affected by residual clouds that passed the filtering. However, due to the huge dataset used for the seasonal averages, it is considered that such an effect is diluted and is globally negligible.

2.4 Simulations performed

In both modelling frameworks, multiple simulations are performed. In CAABA, the impact of each aqueous-phase mechanism on a single air parcel is investigated. For comparison, the same day is simulated in CAABA using the same initial conditions but excluding the specific cloud event at 12:00 UTC. The global impact is investigated by performing a reference and two sensitivity simulations with EMAC. Global simulations without any in-cloud aqueous-phase chemistry lead to unrealistic concentrations of O_3 and other chemical species (Tost et al., 2007). Therefore, the reference simulation includes the minimal scavenging mechanism (in the following called Scm). The two sensitivity simulations use the standard EMAC (in the following called ScSta) and the detailed OVOC oxidation aqueous-phase mechanism (in the following called ScJAMOC). For consistency, the same simulation names are used for the CAABA simulations. In EMAC, the years 2014 and 2015 are simulated, where 2014 is discarded as spin-up. A summary of the gas- and aqueous-phase mechanisms used in each CAABA and EMAC simulation performed in this study is given in Table 1. All simulations were performed at the Jülich Supercomputing Centre with the JURECA and JUWELS clusters (Jülich Supercomputing Centre, 2018, 2019).

3 Box-model results

Figure 2 shows the time evolution of selected gas-phase species for the different aqueous-phase mechanisms Scm, ScSta, and ScJAMOC for the cloud scenario of CAABA (see Sect. 2.2). For comparison, the results of the no-cloud scenario are also shown. Both Scm and ScSta have only little impact on most of the OVOCs explicitly treated in JAMOC. For some OVOCs, the phase transfer considered in Scm and ScSta leads to reduced gas-phase concentrations during the cloud event. After the cloud evaporates, gas-phase concentrations are slightly higher compared to the no-cloud scenario, since the OVOCs transferred into the cloud droplet generally do not oxidise. Within ScSta, a subset of these OVOCs (containing one carbon atom) are oxidised, leading to a slight reduction compared to Scm. In contrast, ScJAMOC efficiently removes OVOCs, leading to reduced OVOC concentrations overall. Glyoxal, one of the OVOC examples presented in Fig. 2, is completely removed from the gas phase and quickly hydrated within the cloud droplet. The irreversible oxidation of its hydrated forms and oligomers leads to a reduction in in-cloud glyoxal concentrations. In the gas-phase, glyoxal itself is produced by the oxidation of hydrocarbons. Due to low aqueous-phase HO_x concentrations during the cloud event, the oxidation of these hydrocarbons is reduced. After the cloud evaporates, the higher hydrocarbon concentrations lead to some glyoxal being produced.

Each mechanism leads to changes in most gas-phase radical concentrations. As soon as the cloud droplets form, gas-phase HO_x is reduced due to the uptake of radicals and radical precursors within the first few minutes. This becomes evident when inspecting the results of Scm: in this mecha-

Table 1. Characteristics of the gas- and aqueous-phase mechanism used for each simulation performed in this study using CAABA and EMAC.

Simulation	Gas-phase mechanism	Aqueous-phase mechanism				
		Phase transfer	Equilibria[a]	Oxidation	Photolysis	Original reference
Scm	MOM[b]	14	12	3	–	Jöckel et al. (2006) [c]
ScSta	MOM[b]	34	17	58	3	Tost et al. (2007)
ScJAMOC	MOM[b, d]	350	43	266	23	Rosanka et al. (2021)

[a] Acid–base and hydration equilibria. [b] Mainz Organic Mechanism (MOM; Sander et al., 2019). [c] Representative of most global models (see Table 1 in Ervens, 2015). [d] Modified to represent the gas-phase photo-oxidation of gem-diols and oxalic acid (see Sect. 2.1.2 and Rosanka et al., 2021).

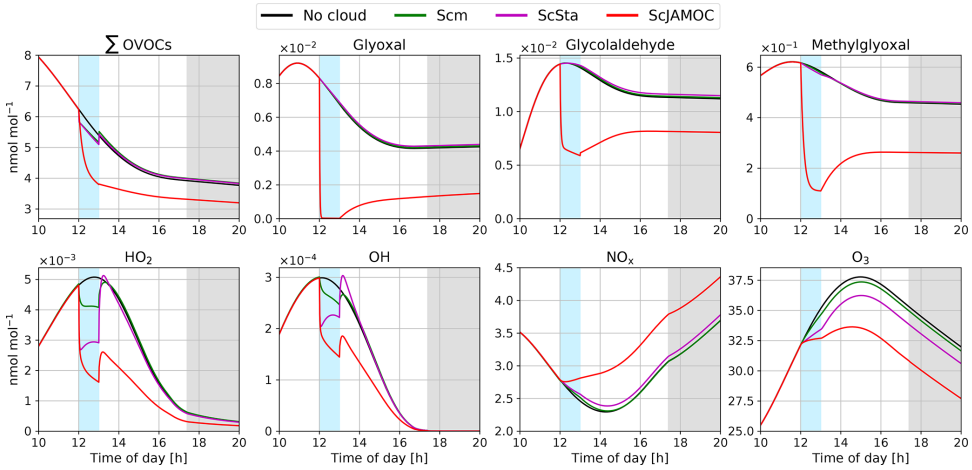

Figure 2. Time evolution for gas-phase mixing ratios of the sum of all the OVOCs explicitly reacting in JAMOC ($\sum$OVOCs; see Eq. A1 in Appendix A), glyoxal, glycolaldehyde, methylglyoxal, HO_2, OH, NO_x, and O_3 within the box model CAABA. The time when the cloud is present (between 12:00 and 13:00 UTC) is indicated by blue background shading. Nighttime is indicated by grey background shading. Mixing ratios are provided for no-cloud event (black line), Scm (green line), ScSta (purple line), and ScJAMOC (red line). The characteristics of each simulation are provided in Table 1. Note that lines may overlap.

nism, the uptake of HO_x is not taken into account. Here, the gas-phase HO_2 concentration is still reduced due to the uptake of a few HO_2 sources (e.g. formaldehyde). In the case of the other mechanisms, the uptake of HO_x is explicitly considered and leads to an additional reduction in gas-phase concentrations when the cloud forms. In the case of ScJAMOC and, to some extent, of ScSta, the additional partitioning of OVOCs into the cloud droplet leads to a further decrease in gas-phase HO_x concentrations. The reduction in OH is in line with other modelling studies for cloud events (Tilgner et al., 2013). When the cloud evaporates, radicals and radical sources are transferred to the gas phase. For ScJAMOC, the efficient in-cloud oxidation of radical sources induces significantly lower HO_x concentrations after the cloud evaporates. The photolysis of OVOCs and their oxidation within cloud droplets cause an increase in $HO_{x(aq)}$ of about 50 %. In ScJAMOC, CAABA predicts average in-cloud concentrations of 1.3×10^{-13} and 2.5×10^{-8} M for $OH_{(aq)}$ and $HO_{2(aq)}$, respectively. These predictions are of similar magnitude compared to the results of CLEPS (see Fig. 4 in Mouchel-Vallon et al., 2017) and observations and predictions by Tilgner et al. (2013) and Arakaki et al. (2013).

When the cloud forms, gas-phase O_3 is reduced in comparison to the no-cloud scenario because of its reactive uptake into the cloud droplet. Within Scm, $O_{3(aq)}$ only reacts with $SO_{2(aq)}$, leading to only a little reduction in gas-phase O_3. This reduction is more pronounced for ScSta and ScJAMOC due to additional aqueous-phase sinks and the uptake of HO_2 into the cloud droplet. For ScJAMOC, the reduction in O_3 is larger due to the additional aqueous-phase $HO_{2(aq)}$ sources from OVOC oxidation. In the gas phase, the significantly reduced HO_2 concentrations cause NO_x to increase (HO_2 being the major sink of NO_x). However, it mostly dampens the production of O_3 after the cloud event.

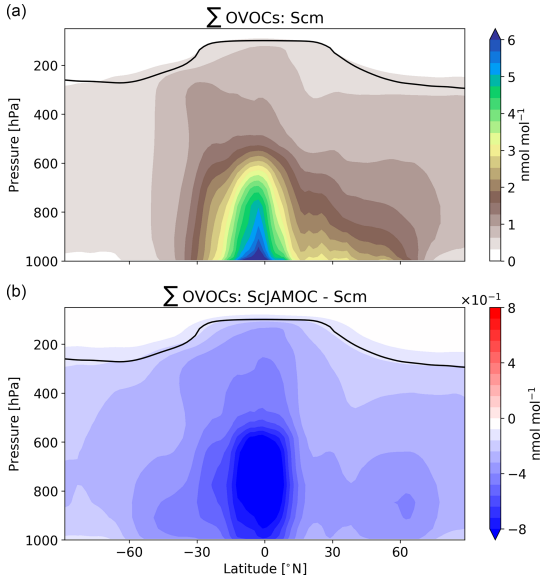

Figure 3. Yearly zonal mean mixing ratio of the sum of all the OVOCs explicitly reacting in JAMOC (∑OVOCs; see Eq. A1 in Appendix A) for Scm **(a)** and in comparison to ScJAMOC **(b)**. The characteristics of each simulation are provided in Table 1. The yearly mean tropopause is depicted by a black line.

4 Global impact on atmospheric composition

This section evaluates the importance of in-cloud OVOC oxidation on a global scale by focusing on VOCs (Sect. 4.1), and HO_x (Sect. 4.2). The importance for tropospheric O_3 is discussed in Sect. 4.3.

4.1 Impact on tropospheric VOCs

The extensive aqueous-phase OVOC oxidation scheme JAMOC considers many VOC sinks. These significantly influence the concentrations of tropospheric VOCs. In general, VOCs can be split into primarily emitted VOCs and OVOCs mostly formed from secondary production (e.g. oxidation of primarily emitted VOCs). The main global source of primarily emitted VOCs is biogenic processes. The largest biogenic emissions take place in the equatorial region (e.g. Amazon Basin, Central Africa) with additional emissions in the Northern Hemisphere (NH) and Southern Hemisphere (SH) extratropics. Isoprene, the most abundant biogenic VOC, is only slightly influenced by ScJAMOC. The yearly mean tropospheric burden increases from 204 (Scm) to 213 Gg (ScJAMOC). This increase is caused by changes in OH concentrations, the main isoprene oxidant (see Sect. 4.2). Primarily emitted VOCs are quickly oxidised in the lower troposphere, leading to low concentrations in the free troposphere. The top panel of Fig. 3 shows the zonal mean mixing ratio of the sum of all OVOCs that are explicitly treated in JAMOC (∑OVOCs; see Eq. A1 in Appendix A) for Scm. High OVOC concentrations are predicted in the lower troposphere and at lower latitudes, consistent with strong terrestrial biogenic emissions at the Earth surface. By the general upward transport in the equatorial region, OVOCs are transported into the free troposphere. Due to deep convection events in the same region, OVOCs are even transported into the dry tropical upper troposphere. The lower panel of Fig. 3 shows the changes in the sum of OVOCs explicitly treated in JAMOC (∑OVOCs; see Eq. A1 in Appendix A) obtained by comparing Scm and ScJAMOC. Overall, the tropospheric OVOC burden is reduced with the largest change in the tropical free troposphere. The frequent occurrence of clouds in this region and the high OVOC concentrations lead to an efficient removal of gas-phase OVOCs. The ubiquity of clouds in the NH extratropics allows for additional removal of OVOCs from the gas phase. These results are in line with the box-model results presented above (see Fig. 2). The efficient removal of OVOCs in warm clouds significantly affects the OVOC levels in the dry tropical upper troposphere. Here, these OVOCs act as an important HO_x source, potentially influencing the production of O_3 (Jaeglé et al., 2001).

Table 2. Mean gas-phase tropospheric burden in 2015 for a selection of VOCs for Scm and the changes induced by ScSta and ScJAMOC. The characteristics of each simulation are provided in Table 1. Burden values are given in gigagrams (Gg).

	Scm	ΔScSta	ΔScJAMOC
C_1 VOCs			
Formaldehyde	1212.3	−46.6	−204.2
Methanol	3279.3	−341.0	−998.8
Methyl hydroperoxide	1914.5	−32.9	−849.9
Hydroxymethyl hydroperoxide	67.8	+0.2	−16.0
C_2 VOCs			
Ethanol	110.9	+0.4	−16.6
Ethylene glycol	3.1	+0.1	−1.4
Acetaldehyde	147.1	+1.7	+12.1
Glycolaldehyde	278.8	−0.9	−101.2
Glyoxal	44.6	0.0	−12.7
Ethyl hydroperoxide	62.9	−0.9	−28.3
C_3 VOCs			
Methylglyoxal	181.8	−0.6	−35.3
Isopropyl hydroperoxide	13.0	−0.2	−4.6

Table 2 provides an overview of the annual tropospheric burden for a selection of VOCs explicitly treated in JAMOC. As shown in Fig. 3, the global burden of most VOCs is reduced due to the uptake and oxidation processes implemented in ScJAMOC. Because of the low number of VOCs containing one carbon atom treated in ScSta, changes between Scm and ScSta are only minor. The burden of some VOCs even increases in ScSta, which is caused by reduced

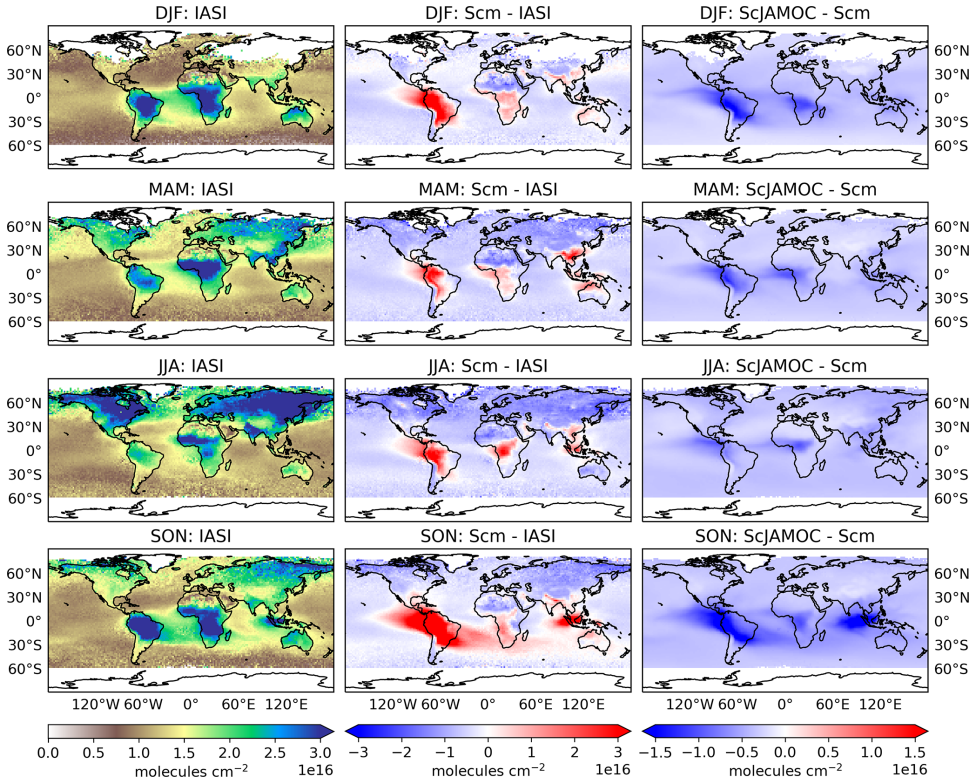

Figure 4. Seasonal-mean (seasons are December–February, DJF; March–May, MAM; June–August, JJA; September–November, SON) integrated methanol column obtained from IASI satellite observations (left), of the Scm simulation in comparison to IASI observations (centre), and of ScJAMOC in comparison to Scm (right). The characteristics of each simulation are provided in Table 1.

HO_x concentrations (see Sect. 4.2). The impact in ScJAMOC differs for each VOC, with some VOCs in terms of absolute changes being efficiently removed, whereas others are only slightly impacted. The varying efficiency of the VOCs removal by clouds is explained by differences in their Henry's law constants, accommodation coefficients, and aqueous-phase reactivities. The burden of methanol, the OVOC containing one carbon atom for which the highest absolute change is predicted, is reduced by about 1000 Gg. For methyl hydroperoxide the total change is lower but the relative reduction is higher, which is due to slightly higher solubility and overall higher reaction rate constants for the oxidation by $OH_{(aq)}$ and $NO_{3(aq)}$. Formaldehyde is reduced by about 16 %. Even though ethanol has a Henry's law constant similar to that of methanol, the relative reduction is still significantly smaller, due to slower aqueous-phase oxidation. Ethylene glycol has slow aqueous-phase oxidation but very high solubility, which results in a substantial reduction in its tropospheric burden. The opposite holds for ethyl hydroperoxide, which is 4 times less soluble but undergoes fast aqueous-phase oxidation. This leads to a relative change that is similar to the one of ethylene glycol. Acetaldehyde is the only OVOC for which an enhanced burden is predicted. This is partially due to newly implemented in-cloud sources but in particular to the aqueous-phase oxidation of methylglyoxal yielding pyruvic acid, which is a known source of acetaldehyde (Berges and Warneck, 1992).

Figure 4 shows the seasonal-mean methanol column for the IASI observations. In addition, the differences of Scm vs. IASI and ScJAMOC vs. Scm are shown. The highest methanol columns occur close to its major biogenic sources (e.g. Amazon Basin, boreal forests). When using Scm, EMAC underestimates methanol at mid-latitudes and overestimates it close to methanol's main tropical biogenic sources (see centre column, Fig. 4). Both these model inconsistencies are caused by an incorrect spatial distribution of biogenic emissions. The submodel MEGAN, used to simulate biogenic methanol emissions (see Sect. 2.3), estimates yearly biogenic methanol emissions of 104 Tg yr^{-1}, which is close to the 103 Tg yr^{-1} estimated by Millet et al.

(2008, their Table 2). However, the spatial distribution of biogenic emissions from MEGAN is different to their predictions. Compared to Millet et al. (2008), MEGAN significantly overestimates biogenic emissions in the Amazon Basin but underestimates emissions at middle and high latitudes. EMAC simulates the Amazon Basin as too dry in the dry season (September–November, SON) and consequently too hot (Hagemann and Stacke, 2015). The biogenic emissions in MEGAN are temperature-dependent, and generally higher temperatures induce higher emissions. Thus, the positive bias in surface temperatures in EMAC leads to an overestimation in the Amazon Basin. Additionally, uncertainties for all coefficients used in MEGAN, related to the emissions of methanol and primarily emitted VOCs (e.g. isoprene) further influence the incorrect emission distribution. EMAC also underestimates methanol over the oceans. In the current simulation setup, the ocean is represented to only act as a methanol sink but should be considered a source as well over certain oceans (e.g. over the Pacific; see Millet et al., 2008). However, EMAC models the ocean as a net sink with an uptake of about 2.1 Tg yr^{-1}, which is smaller than the predicted net sink from Millet et al. (2008) of 16 Tg yr^{-1}. It is thus expected that there is an additional deficiency in the representation of the gas-phase chemistry of methanol in MOM. Still, when using ScJAMOC, the model bias for methanol is partially resolved (see right column of Fig. 4). In areas where the sources are expected to be modelled correctly (i.e. Central Africa, East Asia), the additional in-cloud OVOC oxidation leads to a reduction in methanol partially resolving the model bias in these regions. However, ScJAMOC is not able to completely resolve the model bias over the Amazon Basin. The positive model bias away from its major sources (i.e. over oceans) is reduced and partially resolved. Especially during the NH autumn (SON), the strong model bias over the East Pacific and the South Atlantic Ocean is reduced. At the same time, a high overestimation for Scm is observed southeast of India over the Indian Ocean. The strong El Niño event in 2015/16 led to droughts, draining the already-dry Indonesian peatland. This drying, in combination with widespread deforestation, led to strong Indonesian fires, emitting large amounts of VOCs (Parker et al., 2016). This positive model bias is strongly reduced when in-cloud methanol oxidation is taken into account (ScJAMOC). A detailed analysis of the Indonesian peatland fires in 2015 and the importance of detailed in-cloud OVOC oxidation during such a pollution event is presented by Rosanka et al. (2020b).

To the best of our knowledge, glyoxal satellite retrievals from the Ozone Monitoring Instrument (OMI; Levelt et al., 2006) are only available up to 2014, while the TROPOspheric Monitoring Instrument (TROPOMI) started its operations in late 2017. Levelt et al. (2018) report that this is due to detector degradation and the challenging nature of glyoxal retrievals. A detailed analysis for the year 2007 is performed by Alvarado et al. (2014). Figure 5 gives the yearly mean integrated glyoxal column for Scm and the changes introduced

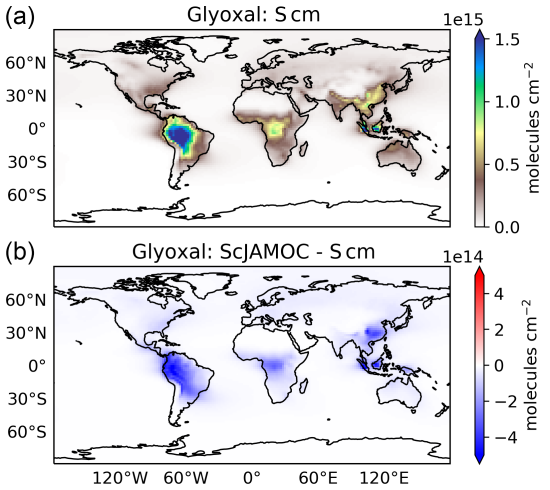

Figure 5. Mean integrated tropospheric glyoxal column for Scm **(a)** and in comparison to ScJAMOC **(b)**. The characteristics of each simulation are provided in Table 1.

by ScJAMOC. In the gas phase, glyoxal is an oxidation product of hydrocarbons. Therefore, high glyoxal concentrations are predicted by EMAC close to strong biogenic hydrocarbon sources (e.g. Amazon Basin). As found with the CAABA box model, atmospheric glyoxal levels are significantly reduced by the chemical loss in cloud droplets with ScJAMOC (see Table 2). When comparing these results to satellite retrievals from Alvarado et al. (2014, their Fig. 9), it can be concluded that the spatial distribution is reasonably well captured by Scm. However, glyoxal levels are generally overestimated in regions where biogenic emissions dominate. The additional sink introduced into ScJAMOC leads to a significant reduction in the model bias, especially in the Amazon Basin and over Central Africa. However, the model bias is not yet fully resolved in the Amazon Basin. Here, the too-high biogenic hydrocarbon emissions from MEGAN are the cause of an overestimated production of glyoxal. It is important to keep in mind that the comparability with these satellite retrievals is limited due to a different year simulated. It is still expected that the yearly mean spatial distributions of biogenic emissions are comparable for both years and mainly vary in their magnitudes. To conclude, when using JAMOC (ScJAMOC) the representation of methanol and glyoxal gas-phase concentrations is significantly improved within EMAC.

4.2 Impact on tropospheric HO_x

VOCs play an important role in the production and loss of OH and HO_2. Thus, the additional uptake of VOCs will influence the tropospheric OH budget. In the troposphere, OH is primarily produced by the reaction of $O(^1D)$ with H_2O. Here, the main source of $O(^1D)$ is the photolysis of O_3. Figure 6

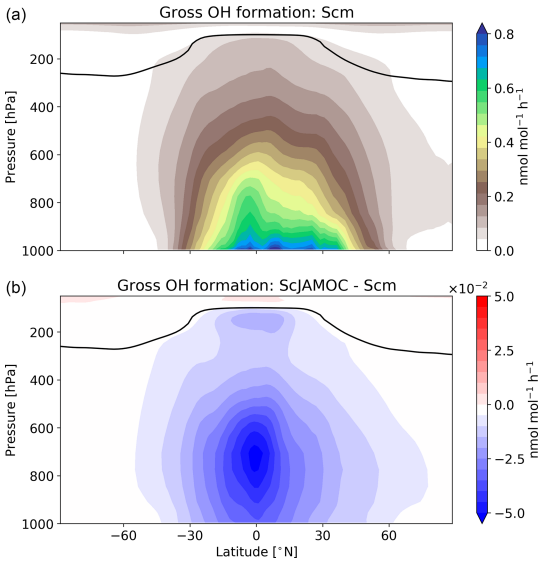

Figure 6. Zonal-mean gross OH formation for Scm **(a)** and in comparison to ScJAMOC **(b)**. The characteristics of each simulation are provided in Table 1. The yearly mean tropopause is depicted by a black line.

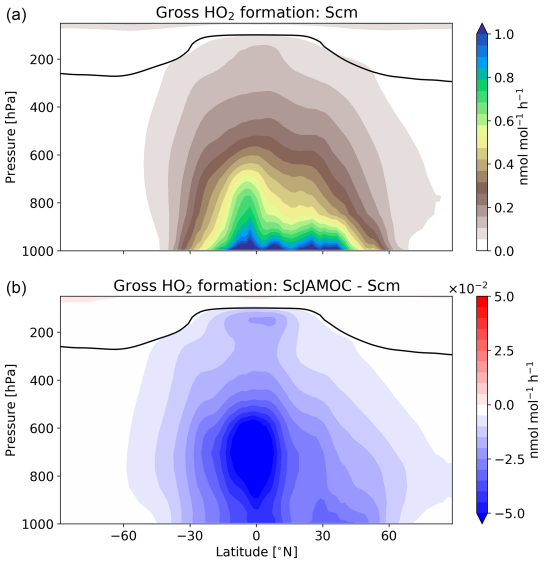

Figure 7. Zonal-mean gross HO_2 formation for Scm **(a)** and in comparison to ScJAMOC **(b)**. The characteristics of each simulation are provided in Table 1. The yearly mean tropopause is depicted by a black line.

gives the zonal mean of the total OH production of Scm and the changes predicted by ScJAMOC. OH is mainly produced in the lower troposphere by both its primary and its secondary sources, whereas in the upper troposphere secondary sources dominate. Table 3 gives an overview of the tropospheric gas-phase OH sources and sinks. With ScJAMOC, the gross OH formation decreases by about 7.3 % from 280.2 to 259.8 Tmol yr^{-1}. This finding is consistent with the box-model results (Fig. 2). The uptake and oxidation of VOCs in the aqueous phase reduce the contribution of VOCs to the OH production. However, the major reduction in the OH production is caused by overall reduced tropospheric O_3 concentrations. Specifically, the two largest O_3 sinks, namely the OH production induced by O_3 photolysis and the reaction of O_3 with HO_2, are reduced by 8.5 %. O_3 has a long atmospheric lifetime, leading to low spatial variability in the reduction in tropospheric O_3. However, the reduction in VOC concentrations has high spatial variability (see Fig. 3), largely determining the spatial distribution of the reduction in the total OH formation by ScJAMOC (Fig. 6b). The removal of VOCs containing one carbon atom presents the largest contribution to the reduction. The reduction in HO_x leads to an additional reduction in the destruction of OH from HO_x cross-reactions ($HO_2 + OH$ and $OH + OH$). The OH budget presented in this study compares well with earlier EMAC studies by Lelieveld et al. (2016), which used the standard in-cloud EMAC mechanism (ScSta). The relative contributions of each OH source and sink in ScSta are comparable with their reported budgets. However, the authors report a lower tropospheric gross OH formation of 251.2 Tmol yr^{-1} while using the same tropopause definition. This difference is mainly related to the different years simulated (leading to different emissions) and a lower model resolution used (T42L31, approximately 2.8 by 2.8° in latitude and longitude with 31 vertical layers). Specifically, the lower number of tropospheric levels is expected to influence tropospheric budgets.

Figure 7 shows the zonal HO_2 production for Scm and the changes predicted in ScJAMOC. Due to the fast interconversion within the HO_x family, the spatial distribution and magnitude of the HO_2 production are similar to the production of OH. Table 4 gives the gas-phase HO_2 budget for each simulation. The HO_2 production changes from about 315 to 290 Tmol yr^{-1} for Scm and ScJAMOC, respectively. Lower VOC concentrations lead to a reduction in the HO_2 production. Here, the influence of VOCs containing one carbon atom is the highest (see Table 2). Thus, VOCs become less important as an HO_2 sink. The highest reduction is caused by the reduced availability of HO_2, significantly reducing radical–radical reactions as an HO_2 sink.

Tables 3 and 4 also provide the in-cloud budgets for $OH_{(aq)}$ and $HO_{2(aq)}$. The representation of the aqueous-phase chemistry of $OH_{(aq)}$ in clouds strongly affects the $HO_{2(aq)}$ production. The aqueous-phase budget of $OH_{(aq)}$ differs significantly between ScSta and ScJAMOC, which explicitly treat in-cloud $HO_{x(aq)}$ kinetics. ScJAMOC has the highest total

Table 3. Global tropospheric mean gas- and aqueous-phase source and sink fluxes of OH for Scm and the changes induced by ScSta and ScJAMOC. The characteristics of each simulation are provided in Table 1. All values are given in Tmol yr^{-1}. The aqueous-phase budget is only based on cloud droplets. Rain droplets are not taken into account. For comparison, the tropospheric OH budget presented by Lelieveld et al. (2016) is shown in the last column. Please note that Lelieveld et al. (2016) simulated a different year and used EMAC at a lower model resolution.

	Scm	ΔScSta	ΔScJAMOC	Lelieveld et al. (2016)
Gas-phase sources				
$O(^1D) + H_2O$	96.67	−1.39	−7.11	84.0
$NO + HO_2$	84.53	−0.25	−2.10	76.6
$O_3 + HO_2$	32.36	−0.95	−3.93	34.4
$H_2O_2 + h\nu$	26.70	−0.85	−1.39	24.8
OVOCs	30.40	−0.30	−5.82	31.4
Other	9.54	+0.01	−0.02	–
Total	280.20	−3.73	−20.37	251.2
Gas-phase sinks				
$OH + HO_{y_g}$ [a]	49.88	+0.06	−1.90	46.2
$OH + NO_y$ [b]	4.73	+0.01	+0.11	4.1
$OH + CH_4$	32.85	−0.02	−0.35	29.8
$OH + C_1$ [c]	150.90	−2.73	−16.20	134.8
$OH + C_n$ VOCs	39.75	−0.15	−2.70	34.7
Other	2.09	0.00	0.00	1.6
Total	280.20	−3.73	−20.37	251.2
Aqueous-phase sources				
$O_3 + O_2^-$	–	+1.94	+6.30	–
$H_2O_2 + h\nu$	–	+0.95	+1.08	–
C_1 VOCs $+ h\nu$	–	–	+4.71	–
C_n VOCs $+ h\nu$	–	–	+0.32	–
Other	–	+0.02	+0.02	–
Total	–	+2.91	+12.43	–
Aqueous-phase sinks				
$OH + HO_{y_{aq}}$ [d]	–	+0.42	+2.20	–
C_1 VOCs	–	+2.40	+8.98	–
C_n VOCs	–	–	+0.91	–
Other	–	+0.09	+0.34	–
Total	–	+2.91	+12.43	–

[a] $HO_{y_g} \equiv H_2, O_3, H_2O_2$, radical–radical reactions. [b] $NO_y \equiv NO, NO_2, HNO_2. HNO_3, HNO_4, NH_3$, N-reaction products. [c] $C_1 \equiv CO$, VOCs with one C atom. [d] $HO_{y_{aq}} \equiv O_2^-, H_2O_2$, radical–radical reactions.

$OH_{(aq)}$ production with more than 12 Tmol yr^{-1}, which is about 4 times higher than in ScSta. The higher increase, compared to the box model (Sect. 3), is attributed to the specific box-model scenario (Sect. 2.2 and Rosanka et al., 2021, their Table 3). In both ScSta and ScJAMOC, most $OH_{(aq)}$ is formed by the destruction of $O_{3(aq)}$. In ScJAMOC, the photolysis of OVOCs leads to the second-highest formation of $OH_{(aq)}$. Here, OVOCs containing one carbon atom contribute the most, of which most $OH_{(aq)}$ is formed from methyl hydroperoxide. Due to higher radical concentrations, the reactions of $OH_{(aq)}$ with $O_{3(aq)}$ and radical–radical reactions in ScJAMOC contribute about 4 times as much to the loss of $HO_{x(aq)}$ compared to in ScSta. The oxidation of OVOCs is the major $OH_{(aq)}$ sink, with OVOCs containing one carbon atom contributing the most. This oxidation leads to the most significant production of $HO_{2(aq)}$, followed by OVOC photolysis. Due to increased aqueous-phase $OH_{(aq)}$ and $H_2O_{2(aq)}$ concentrations, the oxidation of $H_2O_{2(aq)}$ increases by a factor of 4 in ScJAMOC. The destruction of $O_{3(aq)}$ leads to a reduction in $O_{2(aq)}^-$. This equilibrium is therefore the dominant $HO_{2(aq)}$ sink for both ScSta and ScJAMOC, since $HO_{2(aq)}$ is in equilibrium with $O_{2(aq)}^-$ (Reaction R2). To the best of our knowledge, no in-cloud $HO_{x(aq)}$ budget has been presented so far in the literature on a global scale. The novel in-cloud aqueous-phase budgets can thus not be compared to earlier studies.

Table 4. Global tropospheric mean gas- and aqueous-phase source and sink fluxes of HO_2 for Scm and the changes induced by ScSta and ScJAMOC. The characteristics of each simulation are provided in Table 1. All values are given in $\mathrm{Tmol\,yr^{-1}}$. The aqueous-phase budget is only based on cloud droplets. Rain droplets are not taken into account.

	Scm	ΔScSta	ΔScJAMOC
Gas-phase sources			
$OH + O_3$	12.51	−0.18	−0.71
$H_2O_2 + OH$	13.86	−0.44	−0.56
HNO_4[a]	26.38	−0.52	−1.59
C_1 VOCs	214.71	−3.58	−17.76
C_n VOCs	22.33	+0.01	−0.64
Photolysis	24.64	−0.47	−3.88
Other	1.26	−0.01	−0.01
Total	315.69	−5.19	−25.15
Gas-phase sinks			
$HO_2 + O_3$	32.36	−0.95	−3.93
$HO_2 + OH$	12.86	−0.21	−0.69
$HO_2 + HO_2$	77.34	−2.33	−8.37
$HO_2 + NO$	84.53	−0.25	−2.10
$HO_2 + NO_2$ and NO_3	27.31	−0.44	−1.58
C_1 VOCs + HO_2	47.63	−1.34	−6.74
C_n VOCs + HO_2	26.85	−0.22	−2.08
Other	6.81	+0.55	+0.34
Total	315.69	−5.19	−25.15
Aqueous-phase sources			
Mass transfer	–	+0.60	+0.51
$H_2O_2 + OH$	–	+0.38	+1.61
C_1 VOCs	–	+2.39	+10.80
C_2 VOCs	–	–	+0.92
Other	–	+0.01	+0.09
Total	–	+3.38	+13.93
Aqueous-phase sinks			
$HO_2 \rightleftharpoons O_2^- + H^+$	–	+2.68	+8.69
$HO_2 + HO_{y_{aq}}$[b]	–	+0.69	+5.22
Other	–	+0.01	+0.02
Total	–	+3.38	+13.93

[a] $HNO_4 \rightarrow NO_2 + HO_2$. [b] $HO_{y_{aq}} \equiv O_2^-$, radical–radical reactions.

4.3 Impact on tropospheric O_3

The efficient oxidation of OVOCs by cloud droplets leads to elevated aqueous-phase $HO_{2(aq)}$ concentrations accelerating the in-cloud $O_{3(aq)}$ destruction. This has a significant impact on tropospheric O_3 levels predicted by EMAC. Table 5 gives the O_x budget for the three simulations. The chemical production increases for ScSta compared to Scm. Slightly elevated NO_x concentrations lead to an increased contribution of methylperoxy radicals and RO_2 reactions with NO, compensating for the reduced production from HO_2. For ScJAMOC, the chemical production decreases by about $150\,\mathrm{Tg\,yr^{-1}}$ (2.6 %), mainly caused by an overall reduction in HO_2 (see Sect. 4.2) and in RO_2 radicals due to the uptake and explicit oxidation of VOCs. The chemical loss on the other hand is reduced by about 90 (1.7 %) and about $420\,\mathrm{Tg\,yr^{-1}}$ (8.0 %) for ScSta and ScJAMOC, respectively. This reduction is mainly attributed to an overall reduction in tropospheric levels of O_3 and HO_x. The loss by dry deposition reduces by about $50\,\mathrm{Tg\,yr^{-1}}$ (5.6 %) for ScJAMOC, due to generally reduced surface O_3 concentrations. The largest change in the O_x budget is related to scavenging processes. O_x scavenging increases from about 150 (Scm) to about 260 (73.3 %) and $480\,\mathrm{Tg\,yr^{-1}}$ (220.0 %) for ScSta and ScJAMOC, respectively. Here, the biggest increase occurs for O_3 scavenging, due to the accelerated $O_{3(aq)}$ destruction by enhanced $HO_{2(aq)}$ (Reaction R1), which in turn enhances the O_3 uptake. These changes in the O_x budget terms lead to a reduced O_3 burden. Compared to the literature, the O_3 burden from ScJAMOC is closer to the observational estimate from satellite retrievals for the same time period of 287–311 Tg in the 60° S–60° N latitudinal band and closer to the global tropospheric burden of 324 Tg derived from the IASI-FORLI observations (Gaudel et al., 2018, their Table 5). However, it is important to take into account that different tropopause definitions are used in the extratropics. In Gaudel et al. (2018), the tropopause definition for IASI-FORLI is the WMO tropopause altitude definition, based on the temperature lapse rate (WMO, 1957). In this study, potential vorticity is used as the tropopause definition in the extratropics (see Sect. 2.3). All three O_x budgets (Table 5) compare well with a recent multi-model comparison of Young et al. (2018, see their Fig. 3). The chemical loss and chemical production get closer to the multi-model mean of 4442 and $4937\,\mathrm{Tg\,yr^{-1}}$, respectively. The tropospheric O_3 burden in ScJAMOC is now lower than the multi-model mean of 337 Tg but closer to the observational estimate from Ziemke et al. (2011). The increased stratospheric–tropospheric exchange (STE) is still lower than the multi-model mean ($535\,\mathrm{Tg\,yr^{-1}}$) and the observational estimate of $489\,\mathrm{Tg\,yr^{-1}}$ by Olsen et al. (2013). The tropospheric O_3 lifetime is reduced by 1 d, due to higher relative changes in the O_x loss than in the tropospheric O_3 burden.

Figure 8 gives the zonal net O_x production for Scm and the changes in ScJAMOC. In general, O_x is produced where NO_x concentrations are high (close to the surface and in the upper troposphere). In the free troposphere, above the planetary boundary layer (PBL), the increased destruction of O_3 over the ocean leads to an overall net O_x loss in the zonal mean. The changes in the chemical production and in the loss of O_x and the increase in scavenging lead to changes in the net O_x production in ScJAMOC. At the surface, the net O_x production increases. Here, the efficient uptake of O_3 sink precursors overcompensates for the reduction in the chemical production and leads to a reduced chemical loss. This increase mainly occurs over continental regions. In the free tro-

Table 5. Detailed tropospheric O_x budget for Scm and the changes induced by ScSta and ScJAMOC. The characteristics of each simulation are provided in Table 1. The gross terms as well as the relative contributions of the major contributors are given. For comparison, the range of O_x budgets in other models and the multi-model mean values from the Tropospheric Ozone Assessment Report (TOAR) are also shown. Please note that the models in the multi-model comparison and from TOAR differ in their resolution, tropopause definition, O_x definition, and chemical mechanism used.

	Scm	ΔScSta	ΔScJAMOC	Other models[a]	TOAR[b]
Sources [$Tg\,yr^{-1}$]					
Chemical production	5895.6	+7.1	−155.8	4751–5249	4937 ± 656
$HO_2 + NO$	4050.3	−12.8	−101.3	3185–3436	–
$CH_3O_2 + NO$	1084.8	+13.1	−22.9	1092–1288	–
$RO_2 + NO$	731.1	+6.7	−30.8	345–525	–
Other	29.4	+0.1	+0.1	–	–
STE[c]	355.2	+5.6	+15.3	325–391	535 ± 161
Sinks [$Tg\,yr^{-1}$]					
Chemical loss	5254.7	−91.2	−423.2	4193–4841	4442 ± 570
$O(^1D) + H_2O$	2317.3	−35.0	−167.3	1997–2224	–
$HO_2 + O_3$	1550.1	−42.4	−187.6	1061–1356	–
$OH + O_3$	599.0	−1.4	−0.6	518–654	–
$HOBr + h\nu$	341.6	−0.8	−54.6	174–285	–
$PhO + O_3$[d]	215.4	+1.5	−31.8	–	–
Other	231.3	−4.1	−81.5	–	–
Dry deposition	846.5	−9.1	−47.3	799–908	996 ± 203
O_3	801.6	−9.4	−47.1	–	–
Other	44.9	+0.3	−0.2	–	–
Scavenging	149.7	+112.9	+329.7	–	–
O_3	13.2	+104.4	+323.1	–	–
N_2O_5	25.0	−2.3	−2.7	–	–
HNO_3	111.5	−0.3	−1.0	–	–
Other	–	+11.2	+10.3	–	–
O_3 burden [Tg]	348.2	−5.0	−25.0	339–351	337 ± 23
O_3 lifetime [d]	20.3	−0.3	−1.0	22–24.2	22.5[e]

[a] Based on Sherwen et al. (2016), Hu et al. (2017), and Griffiths et al. (2020). [b] Values obtained from Young et al. (2018) and Gaudel et al. (2018). [c] Stratospheric–tropospheric exchange. [d] O_3 loss due to reaction with phenoxy radicals from oxidation of aromatics (Taraborrelli et al., 2021). [e] Calculated based on mean burden and the mean total production.

posphere above the PBL, the net O_x change is reduced, leading to increased O_x destruction. This is directly caused by the efficient uptake of HO_2, VOCs, and O_3 precursors in this cloud-dominated region in ScJAMOC. In the tropical UTLS, VOCs are an important HO_2 source. The efficient removal of VOCs in the lower troposphere reduces the total VOC mass transported into this region (see Fig. 3). The chemical production of O_x is therefore reduced in the tropical UTLS, due to limited availability of HO_2.

Figures 9 and 10 give the yearly mean surface mixing ratio and the zonal mean O_3 mixing ratios for Scm and the changes in ScJAMOC. In general, O_3 concentrations are higher in the NH with the highest values found over continental areas. Overall, surface O_3 slightly decreases for ScJAMOC with the maximum mean reduction of about $4\,nmol\,mol^{-1}$. The decrease in surface O_3 is very low where the net O_x production increases. The highest reduction in O_3 is predicted in the UTLS, where tropospheric O_3 concentrations are the highest. Here, O_3 is reduced by more than 12 % for ScJAMOC. Even though the total lower tropospheric change is similar in both hemispheres, the relative reduction is higher in the SH (NH, about 4 %; SH, about 10 %).

Figure 11 shows the seasonal, tropospheric integrated O_3 columns from IASI-FORLI O_3 retrievals. In addition, the differences in Scm with respect to IASI-FORLI and in ScJAMOC with respect to Scm are shown. As explained previously, the comparison is performed here by using the tropospheric O_3 column integrated between the Earth surface and 300 hPa (see Sect. 2.3). To meaningfully compare the model profile to the IASI observation, the non-uniform sensitivity of the IASI-FORLI retrievals to the O_3 vertical distribution was accounted for by applying the averaging kernels. They provide the model vertical distribution of O_3 as would be seen by IASI. For this purpose, the model profiles sampled at the place and time of the IASI overpasses (see Sect. 2.3) were first vertically interpolated to the IASI

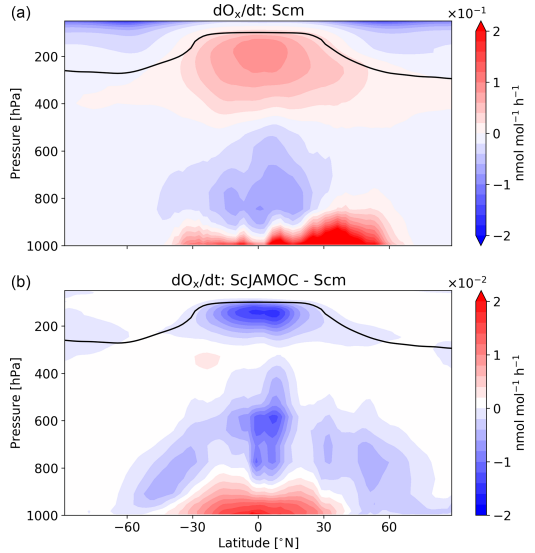

Figure 8. Mean zonal net O_x change for Scm **(a)** and in comparison to ScJAMOC **(b)**. The characteristics of each simulation are provided in Table 1. The yearly mean tropopause is depicted by a black line. Deposition in the lowest model layer is not taken into account.

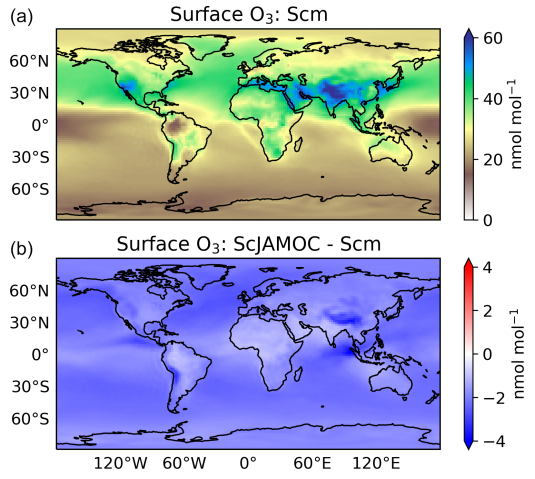

Figure 9. Mean surface O_3 mixing ratios for Scm **(a)** and in comparison to ScJAMOC **(b)**. The characteristics of each simulation are provided in Table 1.

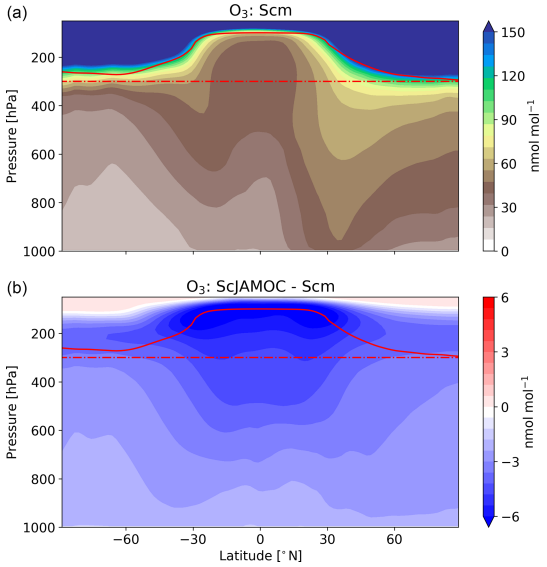

Figure 10. Mean zonal O_3 mixing ratios for Scm **(a)** and in comparison to ScJAMOC **(b)**. The characteristics of each simulation are provided in Table 1. The yearly mean tropopause is depicted by a solid red line. In addition, the 300 hPa tropopause layer used for the O_3 IASI-FORLI comparison (see Fig. 11) is depicted by a dash-dotted red line.

pressure levels. Then the smoothing of the model profiles to the lower vertical resolution of IASI was performed following Rodgers (2000). In order to take the specific scene of each IASI observation into account, the averaging kernels of the different observations contained in the model grid cell have all been considered to smooth the gridded model profile, similarly to previous model–FORLI-O_3 comparison studies (Wespes et al., 2012; Supplement in Wespes et al., 2016). The smoothed model profiles are finally averaged to derive the smoothed gridded model profile. In Scm, EMAC generally overestimates tropospheric O_3 in the tropics and at mid-latitudes regionally by more than 10 DU. This general overestimation is lower but consistent with an earlier EMAC study by Jöckel et al. (2016). They report an overestimation of up to 15 DU (see their Fig. 29), based on a comparison of a nudged simulation with OMI O_3 retrievals using EMAC's standard aqueous-phase mechanism (here ScSta). These differences can be attributed to a much simplified gas-phase chemical mechanism, a lower spatial resolution (inducing artificial dilution of NO_x point sources; Fiore et al., 2003), and different emission datasets. At higher latitudes, especially during the NH winter (December–February, DJF) and spring (March–May, MAM), EMAC slightly underestimates tropospheric O_3. In ScJAMOC, the overall modelled O_3 bias compared to IASI-FORLI is reduced by 1–2 DU, improving the representation of O_3 in EMAC. Here, due to the long lifetime of O_3, the reduction in tropospheric O_3 is not limited to the typical cloud-dominated and precipitation regions. This demonstrates the importance of a proper representation of in-cloud $O_{3(aq)}$ and OVOC oxidation chemistry in global models. By not taking these processes into account, as is the

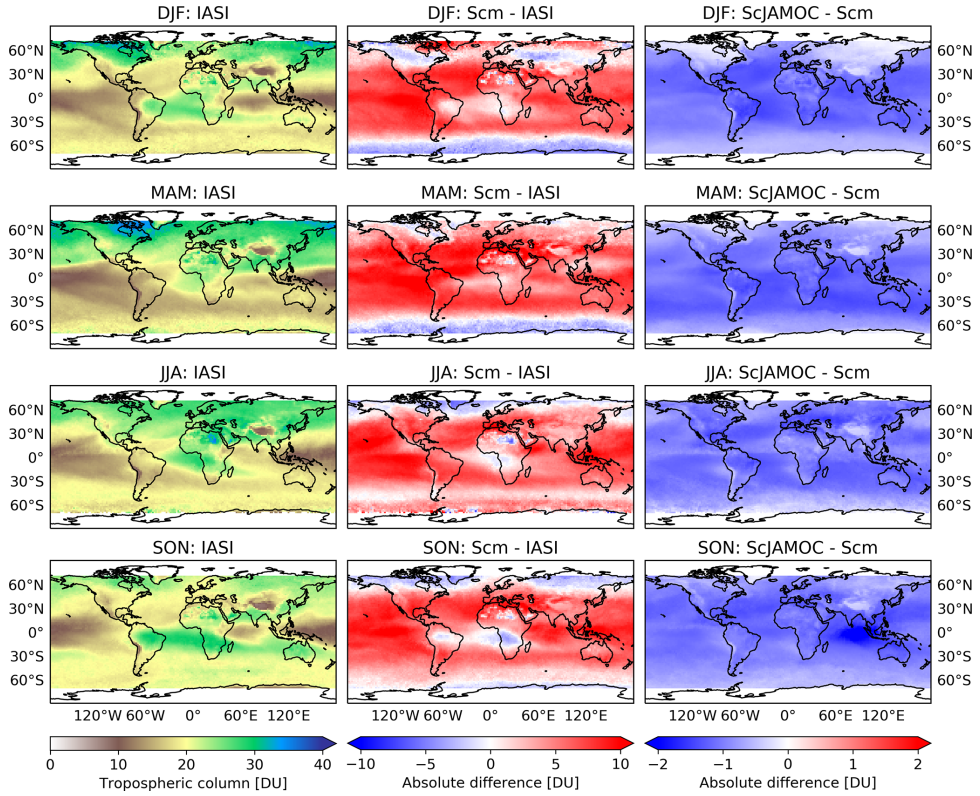

Figure 11. Seasonal (December–February, DJF; March–May, MAM; June–August, JJA; September–November, SON) tropospheric O_3 column comparison between IASI-FORLI satellite observations and EMAC: IASI-FORLI satellite observations (left), Scm simulation in comparison to IASI-FORLI observations (centre), and ScJAMOC in comparison to Scm (right). The characteristics of each simulation are provided in Table 1. For this comparison, the tropopause is defined at 300 hPa.

case in most global models (Ervens, 2015), tropospheric O_3 is overestimated. It is expected that the bias reduction is even more pronounced for the complete troposphere (when using the standard EMAC definition, see Sect. 2.3), since the highest relative reduction in O_3 is predicted in the UTLS above 300 hPa (Fig. 10). Similarly to methanol, Scm strongly overestimates the tropospheric O_3 column west of Indonesia over the Indian Ocean in the NH autumn. This overestimation is also linked to the strong Indonesian peatland fires (Parker et al., 2016). Due to the ongoing Asian monsoon, the emitted VOCs are quickly transported to higher altitudes, where they act as O_3 precursors. The efficient upward transport of the biomass burning tracers isocyanic acid (HNCO) and hydrogen cyanide (HCN) during the summer monsoon phase has already been investigated in earlier EMAC simulations by Rosanka et al. (2020a). In the same region, surface O_3 is also substantially reduced in ScJAMOC (Fig. 9). These results indicate that soluble OVOCs are efficiently removed by clouds. As a consequence, the reactive uptake of O_3 is enhanced and O_3 production dampens. This leads to a reduction in the modelled bias for this region and period when using JAMOC.

5 Model uncertainties

In our companion paper (Rosanka et al., 2021), uncertainties related to the kinetic data used in JAMOC are discussed. The global model simulations performed in this study suffer from additional uncertainties mainly attributed to (1) the representation of VOC emissions and (2) missing sources of key oxidants. Each uncertainty will be briefly discussed in this section.

As demonstrated for methanol (see Sect. 4.1), a satisfactory reproduction of tropospheric VOC concentrations strongly depends on the realistic representation of VOC emissions. As pointed out earlier, the highest uncertainty is introduced by the biogenic emission submodel MEGAN. For instance, isoprene emissions are very sensitive to temperature and light. These uncertainties are not well quanti-

fied. Drought stress also affects isoprene emissions, and it is estimated to reduce the emissions by 17 %–50 % globally (Jiang et al., 2018; Sindelarova et al., 2014). Additionally, biomass burning emissions in Indonesia are potentially underestimated. Parker et al. (2016) pointed out that in the monsoon period of 2015, a high fraction of the Indonesian fire emissions originates from peatland, which is known to produce significantly high VOC emissions (Akagi et al., 2011). In the GFAS retrievals used for biomass burning, the dominant fire type in Indonesia is assigned to tropical forest fires with the exceptions of a few grid points. The strength of VOC emissions for the Indonesian fire period in 2015 is therefore underestimated. It is thus expected that when using JAMOC and a realistic combination of peatland and tropical forest fire types, the overestimation of tropospheric O_3 in this region and time period will be further reduced (see Sect. 4.3 and Fig. 11).

Fenton chemistry is a major source of in-cloud $OH_{(aq)}$ (Deguillaume et al., 2004). Even though these reactions are available in JAMOC, Fenton chemistry is not taken into account in this study, due to missing global iron (Fe) distributions and emissions in EMAC. However, Scanza et al. (2018) present an approach to implementing these into a global model. Realising this approach in EMAC would make Fenton chemistry feasible in the future. From the literature, no global modelling study is known that couples this $OH_{(aq)}$ source to a detailed in-cloud OVOC oxidation scheme, making it difficult to estimate its impact on a global scale. In the highly idealised box-modelling study of Mouchel-Vallon et al. (2017), most $OH_{(aq)}$ (63 %) is produced from Fenton chemistry (see their supplemental material SM5). This indicates the importance of Fenton chemistry in areas with high iron concentrations. The major source of atmospheric iron is mineral dust. Fossil fuel and biomass burning also emit some iron. Thus, iron concentrations are high close to deserts with the highest concentrations in the Sahara, Lut Desert, Thar Desert, and Arabian Desert (Wang et al., 2015, their Fig. 6). Not considering this $OH_{(aq)}$ source catalysed by iron might lead to an underestimation of OVOC oxidation rates in the aqueous phase. In particular Central Africa, a region with high biogenic VOC emissions, might be influenced by Fe being transported from the Sahara. In addition, mineral dust will be transported over the tropical Atlantic to the Amazon Basin. Here, the missing $OH_{(aq)}$ source could be responsible for the underestimation of in-cloud OVOC oxidation and thus the destruction of $O_{3(aq)}$.

To conclude, the impact of the in-cloud OVOC chemistry on the tropospheric composition estimated in this study is influenced by some model and observational uncertainties. However, the findings of the simulations performed in this study are still consistent with earlier studies and improve the representation of a selection of OVOCs and the EMAC bias towards high O_3 concentrations. Due to their complexity, reducing the model uncertainties introduced by biogenic and biomass burning emissions and missing aqueous-phase Fenton chemistry is outside the scope of this study. Model representation of the latter is expected to substantially increase the oxidation rate of OVOCs in the cloud droplets and aerosols. Additional global modelling studies need to be performed to address these issues.

6 Conclusions

In this study, the influence of in-cloud oxidation of soluble OVOCs on the tropospheric gas-phase composition was studied. This was achieved by implementing the extensive aqueous-phase OVOC oxidation scheme JAMOC, initially presented by Rosanka et al. (2021), into the global model EMAC. The mechanism considers a selection of VOCs containing up to 4 carbon atoms; their acid–base and/or hydration–dehydration equilibria; and their reactions with $OH_{(aq)}$, $NO_{3(aq)}$, and other oxidants (if available). Additionally, the phase transfer of species containing up to 10 carbon atoms is taken into account. In addition to the EMAC simulations, a representative cloud droplet was simulated in the box model CAABA in order to understand all processes involved.

When in-cloud OVOC oxidation is taken into account, VOCs are efficiently removed from the gas phase, leading to generally reduced tropospheric VOC burdens. The reduction in modelled methanol and glyoxal concentrations is in line with satellite retrievals. The overall reduction in VOC concentrations leads to lower formation rates of HO_x in the gas phase. Higher in-cloud $HO_{2(aq)}$ concentrations, formed from OVOC oxidation, lead to accelerated destruction of $O_{3(aq)}$ in clouds. In addition, the chemical production and loss of O_3 in the gas phase are reduced due to lower VOC and HO_x concentrations. This results in a reduced O_3 burden and decreases EMAC's bias towards too-high O_3 concentrations. In ScJAMOC, many secondary organic aerosol (SOA) precursors are explicitly treated, impacting the formation of SOAs (Blando and Turpin, 2000; Ervens et al., 2011; Ervens, 2015). The potentially enhanced SOA formation will further influence tropospheric HO_x chemistry and NO_2 photolysis, resulting in a higher reduction in tropospheric O_3 and EMAC's O_3 bias. However, studying the influence of in-cloud OVOC oxidation on SOA formation is outside the scope of this study.

The findings in this study demonstrate the importance of in-cloud chemistry on tropospheric O_3. Most atmospheric global models do not take detailed aqueous-phase chemistry into account (Ervens, 2015). With the minimal oxidation of $SO_{2(aq)}$ by $O_{3(aq)}$, which is representative of most global models, only about 13 Tg yr^{-1} of O_3 is scavenged by clouds. With explicit in-cloud OVOC oxidation considered, O_3 scavenging increases to about 336 Tg yr^{-1}. This estimate neglects the O_3 sink in deliquescent aerosols, which might turn out to be significant as well. The predicted O_3 loss by clouds is significantly higher than the global estimates by Liang and Jacob (1997), and regional changes might be on the same order

of magnitude as predicted by Lelieveld and Crutzen (1990). To conclude, global models, which neglect explicit in-cloud OVOC oxidation, significantly underestimate clouds as O_3 sinks and show a general tendency to overestimate tropospheric O_3.

Appendix A: Definition of $\sum$OVOCs

In Figs. 2 and 3, the mixing ratios of the sum of all the OVOCs explicitly reacting in JAMOC ($\sum$OVOCs) are shown. In these cases, $\sum$OVOCs is defined as follows:

$$\begin{aligned}\sum \text{OVOCs} = {} & \text{methanol} + \text{formaldehyde} \\ & + \text{methyl hydroperoxide} \\ & + \text{hydroxymethylhydroperoxide} + \text{ethanol} \\ & + \text{ethylene glycol} + \text{acetaldehyde} \\ & + \text{glycolaldehyde} + \text{glyoxal} \\ & + \text{1-hydroperoxyacetone} + \text{methylglyoxal} \\ & + \text{isopropanol} + \text{isopropyl hydroperoxide} \\ & + \text{methacrolein} + \text{methyl vinyl ketone}. \quad \text{(A1)}\end{aligned}$$

Data availability. The simulation results are archived at the Jülich Supercomputing Centre (JSC) and are available on request. The IASI O_3 data processed with FORLI-O_3 v0151001 can be downloaded from the AERIS portal at http://iasi.aeris-data.fr/O3/ (last access: 2 August 2020) (IASI, 2020). The IASI methanol columns are archived at ULB and available on request.

Author contributions. SR and DT designed the study. SR performed the simulations and analysed the data with contributions from DT. BF and CW acted as IASI data providers and analysts. SR and DT discussed the results with contributions from RS, BF, and AW. The manuscript was prepared by SR with the help of all co-authors.

Competing interests. The authors declare that they have no competing interests.

Special issue statement. This article is part of the special issue "The Modular Earth Submodel System (MESSy) (ACP/GMD interjournal SI)". It is not associated with a conference.

Acknowledgements. The work described in this paper has received funding from the Initiative and Networking Fund of the Helmholtz Association through the project Advanced Earth System Modelling Capacity (ESM). The content of this paper is the sole responsibility of the authors, and it does not represent the opinion of the Helmholtz Association, and the Helmholtz Association is not responsible for any use that might be made of the information contained. The authors gratefully acknowledge the ESM project for funding this work by providing computing time on the ESM partition of the supercomputer JUWELS at the Jülich Supercomputing Centre (JSC). The authors gratefully acknowledge the computing time granted through JARA on the supercomputer JURECA at Forschungszentrum Jülich. IASI is a joint mission of EUMETSAT and the Centre National d'Etudes Spatiales (CNES, France). The authors acknowledge the AERIS data infrastructure for providing access to the IASI data in this study and ULB-LATMOS, in particular Daniel Hurtmans, for the development of the retrieval algorithms. The research in Belgium is funded by the Belgian Federal Science Policy Office (BELSPO) and the European Space Agency (ESA–BELSPO Prodex arrangement IASI.FLOW and Satellite Application Facility on Atmospheric Composition Monitoring (ACSAF)).

Financial support. This research has been supported by the Initiative and Networking Fund of the Helmholtz Association through the project Advanced Earth System Modelling Capacity (ESM) (grant no. DB001549).

The article processing charges for this open-access publication were covered by the Forschungszentrum Jülich.

Review statement. This paper was edited by John Orlando and reviewed by Hartmut Herrmann and one anonymous referee.

References

Akagi, S. K., Yokelson, R. J., Wiedinmyer, C., Alvarado, M. J., Reid, J. S., Karl, T., Crounse, J. D., and Wennberg, P. O.: Emission factors for open and domestic biomass burning for use in atmospheric models, Atmos. Chem. Phys., 11, 4039–4072, https://doi.org/10.5194/acp-11-4039-2011, 2011.

Alvarado, L. M. A., Richter, A., Vrekoussis, M., Wittrock, F., Hilboll, A., Schreier, S. F., and Burrows, J. P.: An improved glyoxal retrieval from OMI measurements, Atmos. Meas. Tech., 7, 4133–4150, https://doi.org/10.5194/amt-7-4133-2014, 2014.

Arakaki, T., Anastasio, C., Kuroki, Y., Nakajima, H., Okada, K., Kotani, Y., Handa, D., Azechi, S., Kimura, T., Tsuhako, A., and Miyagi, Y.: A General Scavenging Rate Constant for Reaction of Hydroxyl Radical with Organic Carbon in Atmospheric Waters, Environ. Sci. Technol., 47, 8196–8203, https://doi.org/10.1021/es401927b, 2013.

August, T., Klaes, D., Schlüssel, P., Hultberg, T., Crapeau, M., Arriaga, A., O'Carroll, A., Coppens, D., Munro, R., and Calbet, X.: IASI on Metop-A: Operational Level 2 retrievals after five years in orbit, three Leaders in Spectroscopy, J. Quant. Spectrosc. Ra., 113, 1340–1371, https://doi.org/10.1016/j.jqsrt.2012.02.028, 2012.

Berges, M. G. M. and Warneck, P.: Product Quantum Yields for the 350 nm Photodecomposition of Pyruvic Acid in Air, Berichte der Bunsengesellschaft für physikalische Chemie, 96, 413–416, https://doi.org/10.1002/bbpc.19920960334, 1992.

Blando, J. D. and Turpin, B. J.: Secondary organic aerosol formation in cloud and fog droplets: a literature evaluation of plausibility, Atmos. Environ., 34, 1623–1632, https://doi.org/10.1016/S1352-2310(99)00392-1, 2000.

Bott, A. and Zdunkowski, W.: Electromagnetic energy within dielectric spheres, J. Opt. Soc. Am. A, 4, 1361–1365, https://doi.org/10.1364/JOSAA.4.001361, 1987.

Boynard, A., Hurtmans, D., Koukouli, M. E., Goutail, F., Bureau, J., Safieddine, S., Lerot, C., Hadji-Lazaro, J., Wespes, C., Pommereau, J.-P., Pazmino, A., Zyrichidou, I., Balis, D., Barbe, A., Mikhailenko, S. N., Loyola, D., Valks, P., Van Roozendael, M., Coheur, P.-F., and Clerbaux, C.: Seven years of IASI ozone retrievals from FORLI: validation with independent total column and vertical profile measurements, Atmos. Meas. Tech., 9, 4327–4353, https://doi.org/10.5194/amt-9-4327-2016, 2016.

Cabrera-Perez, D., Taraborrelli, D., Sander, R., and Pozzer, A.: Global atmospheric budget of simple monocyclic aromatic compounds, Atmos. Chem. Phys., 16, 6931–6947, https://doi.org/10.5194/acp-16-6931-2016, 2016.

Clerbaux, C., Boynard, A., Clarisse, L., George, M., Hadji-Lazaro, J., Herbin, H., Hurtmans, D., Pommier, M., Razavi, A., Turquety, S., Wespes, C., and Coheur, P.-F.: Monitoring of atmospheric composition using the thermal infrared IASI/MetOp sounder, Atmos. Chem. Phys., 9, 6041–6054, https://doi.org/10.5194/acp-9-6041-2009, 2009.

Deguillaume, L., Leriche, M., Monod, A., and Chaumerliac, N.: The role of transition metal ions on HO_x radicals in clouds: a numerical evaluation of its impact on multiphase chemistry, Atmos.

Chem. Phys., 4, 95–110, https://doi.org/10.5194/acp-4-95-2004, 2004.

Deguillaume, L., Tilgner, A., Schrödner, R., Wolke, R., Chaumerliac, N., and Herrmann, H.: Towards an operational aqueous phase chemistry mechanism for regional chemistry-transport models: CAPRAM-RED and its application to the COSMO-MUSCAT model, J. Atmos. Chem., 64, 1–35, https://doi.org/10.1007/s10874-010-9168-8, 2009.

Epstein, S. A. and Nizkorodov, S. A.: A comparison of the chemical sinks of atmospheric organics in the gas and aqueous phase, Atmos. Chem. Phys., 12, 8205–8222, https://doi.org/10.5194/acp-12-8205-2012, 2012.

Ervens, B.: Modeling the Processing of Aerosol and Trace Gases in Clouds and Fogs, Chem. Rev., 115, 4157–4198, https://doi.org/10.1021/cr5005887, 2015.

Ervens, B., Turpin, B. J., and Weber, R. J.: Secondary organic aerosol formation in cloud droplets and aqueous particles (aqSOA): a review of laboratory, field and model studies, Atmos. Chem. Phys., 11, 11069–11102, https://doi.org/10.5194/acp-11-11069-2011, 2011.

Fiore, A. M., Jacob, D. J., Mathur, R., and Martin, R. V.: Application of empirical orthogonal functions to evaluate ozone simulations with regional and global models, J. Geophys. Res.-Atmos., 108, 4431, https://doi.org/10.1029/2002JD003151, 2003.

Franco, B., Clarisse, L., Stavrakou, T., Müller, J.-F., Van Damme, M., Whitburn, S., Hadji-Lazaro, J., Hurtmans, D., Taraborrelli, D., Clerbaux, C., and Coheur, P.-F.: A General Framework for Global Retrievals of Trace Gases From IASI: Application to Methanol, Formic Acid, and PAN, J. Geophys. Res.-Atmos., 123, 13963–13984, https://doi.org/10.1029/2018JD029633, 2018.

Gaudel, A., Cooper, O. R., Ancellet, G., Barret, B., Boynard, A., Burrows, J. P., Clerbaux, C., Coheur, P. F., Cuesta, J., Cuevas, E., Doniki, S., Dufour, G., Ebojie, F., Foret, G., Garcia, O., Granados Muños, M. J., Hannigan, J. W., Hase, F., Huang, G., Hassler, B., Hurtmans, D., Jaffe, D., Jones, N., Kalabokas, P., Kerridge, B., Kulawik, S. S., Latter, B., Leblanc, T., Le Flochmoën, E., Lin, W., Liu, J., Liu, X., Mahieu, E., McClure-Begley, A., Neu, J. L., Osman, M., Palm, M., Petetin, H., Petropavlovskikh, I., Querel, R., Rahpoe, N., Rozanov, A., Schultz, M. G., Schwab, J., Siddans, R., Smale, D., Steinbacher, M., Tanimoto, H., Tarasick, D. W., Thouret, V., Thompson, A. M., Trickl, T., Weatherhead, E., Wespes, C., Worden, H. M., Vigouroux, C., Xu, X., Zeng, G., and Ziemke, J.: Tropospheric Ozone Assessment Report: Present-day distribution and trends of tropospheric ozone relevant to climate and global atmospheric chemistry model evaluation, LK 01, Elementa, 6, 39, https://doi.org/10.1525/elementa.291, 2018.

Griffiths, P. T., Keeble, J., Shin, Y. M., Abraham, N. L., Archibald, A. T., and Pyle, J. A.: On the Changing Role of the Stratosphere on the Tropospheric Ozone Budget: 1979–2010, Geophys. Res. Lett., 47, e2019GL086 901, https://doi.org/10.1029/2019GL086901, 2020.

Gromov, S., Jöckel, P., Sander, R., and Brenninkmeijer, C. A. M.: A kinetic chemistry tagging technique and its application to modelling the stable isotopic composition of atmospheric trace gases, Geosci. Model Dev., 3, 337–364, https://doi.org/10.5194/gmd-3-337-2010, 2010.

Guenther, A., Karl, T., Harley, P., Wiedinmyer, C., Palmer, P. I., and Geron, C.: Estimates of global terrestrial isoprene emissions using MEGAN (Model of Emissions of Gases and Aerosols from Nature), Atmos. Chem. Phys., 6, 3181–3210, https://doi.org/10.5194/acp-6-3181-2006, 2006.

Hagemann, S. and Stacke, T.: Impact of the soil hydrology scheme on simulated soil moisture memory, Clim. Dynam., 44, 1731–1750, https://doi.org/10.1007/s00382-014-2221-6, 2015.

Hens, K., Novelli, A., Martinez, M., Auld, J., Axinte, R., Bohn, B., Fischer, H., Keronen, P., Kubistin, D., Nölscher, A. C., Oswald, R., Paasonen, P., Petäjä, T., Regelin, E., Sander, R., Sinha, V., Sipilä, M., Taraborrelli, D., Tatum Ernest, C., Williams, J., Lelieveld, J., and Harder, H.: Observation and modelling of HO_x radicals in a boreal forest, Atmos. Chem. Phys., 14, 8723–8747, https://doi.org/10.5194/acp-14-8723-2014, 2014.

Herrmann, H.: Kinetics of Aqueous Phase Reactions Relevant for Atmospheric Chemistry, Chem. Rev., 103, 4691–4716, https://doi.org/10.1021/cr020658q, 2003.

Hu, L., Jacob, D. J., Liu, X., Zhang, Y., Zhang, L., Kim, P. S., Sulprizio, M. P., and Yantosca, R. M.: Global budget of tropospheric ozone: Evaluating recent model advances with satellite (OMI), aircraft (IAGOS), and ozonesonde observations, Atmos. Environ., 167, 323–334, https://doi.org/10.1016/j.atmosenv.2017.08.036, 2017.

Hurtmans, D., Coheur, P.-F., Wespes, C., Clarisse, L., Scharf, O., Clerbaux, C., Hadji-Lazaro, J., George, M., and Turquety, S.: FORLI radiative transfer and retrieval code for IASI, three Leaders in Spectroscopy, J. Quant. Spectrosc. Ra., 113, 1391–1408, https://doi.org/10.1016/j.jqsrt.2012.02.036, 2012.

IASI: O_3 total column from IASI (Level 2), available at: http://iasi.aeris-data.fr/O3/, last access: 2 August 2020.

Jaeglé, L., Jacob, D. J., Brune, W. H., and Wennberg, P. O.: Chemistry of HO_x radicals in the upper troposphere, Atmos. Environ., 35, 469–489, https://doi.org/10.1016/S1352-2310(00)00376-9, 2001.

Jiang, X., Guenther, A., Potosnak, M., Geron, C., Seco, R., Karl, T., Kim, S., Gu, L., and Pallardy, S.: Isoprene emission response to drought and the impact on global atmospheric chemistry, Atmos. Environ., 183, 69–83, https://doi.org/10.1016/j.atmosenv.2018.01.026, 2018.

Jöckel, P., Tost, H., Pozzer, A., Brühl, C., Buchholz, J., Ganzeveld, L., Hoor, P., Kerkweg, A., Lawrence, M. G., Sander, R., Steil, B., Stiller, G., Tanarhte, M., Taraborrelli, D., van Aardenne, J., and Lelieveld, J.: The atmospheric chemistry general circulation model ECHAM5/MESSy1: consistent simulation of ozone from the surface to the mesosphere, Atmos. Chem. Phys., 6, 5067–5104, https://doi.org/10.5194/acp-6-5067-2006, 2006.

Jöckel, P., Kerkweg, A., Pozzer, A., Sander, R., Tost, H., Riede, H., Baumgaertner, A., Gromov, S., and Kern, B.: Development cycle 2 of the Modular Earth Submodel System (MESSy2), Geosci. Model Dev., 3, 717–752, https://doi.org/10.5194/gmd-3-717-2010, 2010.

Jöckel, P., Tost, H., Pozzer, A., Kunze, M., Kirner, O., Brenninkmeijer, C. A. M., Brinkop, S., Cai, D. S., Dyroff, C., Eckstein, J., Frank, F., Garny, H., Gottschaldt, K.-D., Graf, P., Grewe, V., Kerkweg, A., Kern, B., Matthes, S., Mertens, M., Meul, S., Neumaier, M., Nützel, M., Oberländer-Hayn, S., Ruhnke, R., Runde, T., Sander, R., Scharffe, D., and Zahn, A.: Earth System Chemistry integrated Modelling (ESCiMo) with the Modular Earth Submodel System (MESSy) version 2.51, Geosci. Model Dev., 9, 1153–1200, https://doi.org/10.5194/gmd-9-1153-2016, 2016.

Jülich Supercomputing Centre: JURECA: Modular supercomputer at Jülich Supercomputing Centre, J. Large-scale Res. Facil., 4, A132, https://doi.org/10.17815/jlsrf-4-121-1, 2018.

Jülich Supercomputing Centre: JUWELS: Modular Tier-0/1 Supercomputer at the Jülich Supercomputing Centre, J. Large-scale Res. Facil., 5, A135, https://doi.org/10.17815/jlsrf-5-171, 2019.

Kaiser, J. W., Heil, A., Andreae, M. O., Benedetti, A., Chubarova, N., Jones, L., Morcrette, J.-J., Razinger, M., Schultz, M. G., Suttie, M., and van der Werf, G. R.: Biomass burning emissions estimated with a global fire assimilation system based on observed fire radiative power, Biogeosciences, 9, 527–554, https://doi.org/10.5194/bg-9-527-2012, 2012.

Kerkweg, A., Buchholz, J., Ganzeveld, L., Pozzer, A., Tost, H., and Jöckel, P.: Technical Note: An implementation of the dry removal processes DRY DEPosition and SEDImentation in the Modular Earth Submodel System (MESSy), Atmos. Chem. Phys., 6, 4617–4632, https://doi.org/10.5194/acp-6-4617-2006, 2006.

Kerkweg, A., Sander, R., Tost, H., Jöckel, P., and Lelieveld, J.: Technical Note: Simulation of detailed aerosol chemistry on the global scale using MECCA-AERO, Atmos. Chem. Phys., 7, 2973–2985, https://doi.org/10.5194/acp-7-2973-2007, 2007.

Lelieveld, J. and Crutzen, P. J.: Influences of cloud photochemical processes on tropospheric ozone, Nature, 343, 227–233, https://doi.org/10.1038/343227a0, 1990.

Lelieveld, J., Gromov, S., Pozzer, A., and Taraborrelli, D.: Global tropospheric hydroxyl distribution, budget and reactivity, Atmos. Chem. Phys., 16, 12477–12493, https://doi.org/10.5194/acp-16-12477-2016, 2016.

Levelt, P. F., van den Oord, G. H. J., Dobber, M. R., Malkki, A., Huib Visser, Johan de Vries, Stammes, P., Lundell, J. O. V., and Saari, H.: The ozone monitoring instrument, IEEE T. Geosci. Remote, 44, 1093–1101, https://doi.org/10.1109/TGRS.2006.872333, 2006.

Levelt, P. F., Joiner, J., Tamminen, J., Veefkind, J. P., Bhartia, P. K., Stein Zweers, D. C., Duncan, B. N., Streets, D. G., Eskes, H., van der A, R., McLinden, C., Fioletov, V., Carn, S., de Laat, J., DeLand, M., Marchenko, S., McPeters, R., Ziemke, J., Fu, D., Liu, X., Pickering, K., Apituley, A., González Abad, G., Arola, A., Boersma, F., Chan Miller, C., Chance, K., de Graaf, M., Hakkarainen, J., Hassinen, S., Ialongo, I., Kleipool, Q., Krotkov, N., Li, C., Lamsal, L., Newman, P., Nowlan, C., Suleiman, R., Tilstra, L. G., Torres, O., Wang, H., and Wargan, K.: The Ozone Monitoring Instrument: overview of 14 years in space, Atmos. Chem. Phys., 18, 5699–5745, https://doi.org/10.5194/acp-18-5699-2018, 2018.

Liang, J. and Jacob, D. J.: Effect of aqueous phase cloud chemistry on tropospheric ozone, J. Geophys. Res.-Atmos., 102, 5993–6001, https://doi.org/10.1029/96JD02957, 1997.

Lin, G., Penner, J. E., Sillman, S., Taraborrelli, D., and Lelieveld, J.: Global modeling of SOA formation from dicarbonyls, epoxides, organic nitrates and peroxides, Atmos. Chem. Phys., 12, 4743–4774, https://doi.org/10.5194/acp-12-4743-2012, 2012.

Mayer, B. and Madronich, S.: Actinic flux and photolysis in water droplets: Mie calculations and geometrical optics limit, Atmos. Chem. Phys., 4, 2241–2250, https://doi.org/10.5194/acp-4-2241-2004, 2004.

Millet, D. B., Jacob, D. J., Custer, T. G., de Gouw, J. A., Goldstein, A. H., Karl, T., Singh, H. B., Sive, B. C., Talbot, R. W., Warneke, C., and Williams, J.: New constraints on terrestrial and oceanic sources of atmospheric methanol, Atmos. Chem. Phys., 8, 6887–6905, https://doi.org/10.5194/acp-8-6887-2008, 2008.

Mouchel-Vallon, C., Deguillaume, L., Monod, A., Perroux, H., Rose, C., Ghigo, G., Long, Y., Leriche, M., Aumont, B., Patryl, L., Armand, P., and Chaumerliac, N.: CLEPS 1.0: A new protocol for cloud aqueous phase oxidation of VOC mechanisms, Geosci. Model Dev., 10, 1339–1362, https://doi.org/10.5194/gmd-10-1339-2017, 2017.

Myriokefalitakis, S., Tsigaridis, K., Mihalopoulos, N., Sciare, J., Nenes, A., Kawamura, K., Segers, A., and Kanakidou, M.: In-cloud oxalate formation in the global troposphere: a 3-D modeling study, Atmos. Chem. Phys., 11, 5761–5782, https://doi.org/10.5194/acp-11-5761-2011, 2011.

Nölscher, A., Butler, T., Auld, J., Veres, P., Muñoz, A., Taraborrelli, D., Vereecken, L., Lelieveld, J., and Williams, J.: Using total OH reactivity to assess isoprene photooxidation via measurement and model, Atmos. Environ., 89, 453–463, https://doi.org/10.1016/j.atmosenv.2014.02.024, 2014.

Olsen, M. A., Douglass, A. R., and Kaplan, T. B.: Variability of extratropical ozone stratosphere–troposphere exchange using microwave limb sounder observations, J. Geophys. Res.-Atmos., 118, 1090–1099, https://doi.org/10.1029/2012JD018465, 2013.

Parker, R. J., Boesch, H., Wooster, M. J., Moore, D. P., Webb, A. J., Gaveau, D., and Murdiyarso, D.: Atmospheric CH_4 and CO_2 enhancements and biomass burning emission ratios derived from satellite observations of the 2015 Indonesian fire plumes, Atmos. Chem. Phys., 16, 10111–10131, https://doi.org/10.5194/acp-16-10111-2016, 2016.

Rodgers, C. D.: Inverse Methods for Atmospheric Sounding, World Scientific, Singapore, https://doi.org/10.1142/3171, 2000.

Roeckner, E., Bäuml, G., Bonaventura, L., Brokopf, R., Esch, M., Giorgetta, M., Hagemann, S., Kirchner, I., Kornblueh, L., Manzini, E., Rhodin, A., Schlese, U., Schulzweida, U., and Tompkins, A.: The atmospheric general circulation model ECHAM 5. Part I: Model description, Tech. Rep. 349, Max-Planck-Institute for Meteorology, Hamburg, 2003.

Rosanka, S., Vu, G. H. T., Nguyen, H. M. T., Pham, T. V., Javed, U., Taraborrelli, D., and Vereecken, L.: Atmospheric chemical loss processes of isocyanic acid (HNCO): a combined theoretical kinetic and global modelling study, Atmos. Chem. Phys., 20, 6671–6686, https://doi.org/10.5194/acp-20-6671-2020, 2020a.

Rosanka, S., Franco, B., Clarisse, L., Coheur, P.-F., Wahner, A., and Taraborrelli, D.: Organic pollutants from tropical peatland fires: regional influences and its impact on lower stratospheric ozone, Atmos. Chem. Phys. Discuss. [preprint], https://doi.org/10.5194/acp-2020-1130, in review, 2020b.

Rosanka, S., Sander, R., Wahner, A., and Taraborrelli, D.: Oxidation of low-molecular-weight organic compounds in cloud droplets: development of the Jülich Aqueous-phase Mechanism of Organic Chemistry (JAMOC) in CAABA/MECCA (version 4.5.0), Geosci. Model Dev., 14, 4103–4115, https://doi.org/10.5194/gmd-14-4103-2021, 2021.

Sander, R.: Modeling Atmospheric Chemistry: Interactions between Gas-Phase Species and Liquid Cloud/Aerosol Particles, Surv. Geophys., 20, 1–31, https://doi.org/10.1023/A:1006501706704, 1999.

Sander, R., Baumgaertner, A., Cabrera-Perez, D., Frank, F., Gromov, S., Grooß, J.-U., Harder, H., Huijnen, V., Jöckel, P., Karydis, V. A., Niemeyer, K. E., Pozzer, A., Riede, H., Schultz,

M. G., Taraborrelli, D., and Tauer, S.: The community atmospheric chemistry box model CAABA/MECCA-4.0, Geosci. Model Dev., 12, 1365–1385, https://doi.org/10.5194/gmd-12-1365-2019, 2019.

Sandu, A. and Sander, R.: Technical note: Simulating chemical systems in Fortran90 and Matlab with the Kinetic PreProcessor KPP-2.1, Atmos. Chem. Phys., 6, 187–195, https://doi.org/10.5194/acp-6-187-2006, 2006.

Scanza, R. A., Hamilton, D. S., Perez Garcia-Pando, C., Buck, C., Baker, A., and Mahowald, N. M.: Atmospheric processing of iron in mineral and combustion aerosols: development of an intermediate-complexity mechanism suitable for Earth system models, Atmos. Chem. Phys., 18, 14175–14196, https://doi.org/10.5194/acp-18-14175-2018, 2018.

Schrödner, R., Tilgner, A., Wolke, R., and Herrmann, H.: Modeling the multiphase processing of an urban and a rural air mass with COSMO–MUSCAT, source apportionment and modelling of urban air pollution, Urban Climate, 10, 720–731, https://doi.org/10.1016/j.uclim.2014.02.001, 2014.

Sherwen, T., Schmidt, J. A., Evans, M. J., Carpenter, L. J., Großmann, K., Eastham, S. D., Jacob, D. J., Dix, B., Koenig, T. K., Sinreich, R., Ortega, I., Volkamer, R., Saiz-Lopez, A., Prados-Roman, C., Mahajan, A. S., and Ordóñez, C.: Global impacts of tropospheric halogens (Cl, Br, I) on oxidants and composition in GEOS-Chem, Atmos. Chem. Phys., 16, 12239–12271, https://doi.org/10.5194/acp-16-12239-2016, 2016.

Sindelarova, K., Granier, C., Bouarar, I., Guenther, A., Tilmes, S., Stavrakou, T., Müller, J.-F., Kuhn, U., Stefani, P., and Knorr, W.: Global data set of biogenic VOC emissions calculated by the MEGAN model over the last 30 years, Atmos. Chem. Phys., 14, 9317–9341, https://doi.org/10.5194/acp-14-9317-2014, 2014.

Staehelin, J., Buehler, R. E., and Hoigné, J.: Ozone decomposition in water studied by pulse radiolysis. 2. Hydroxyl and hydrogen tetroxide (HO_4) as chain intermediates, J. Phys. Chem.-US, 88, 5999–6004, https://doi.org/10.1021/j150668a051, 1984.

Taraborrelli, D., Lawrence, M. G., Butler, T. M., Sander, R., and Lelieveld, J.: Mainz Isoprene Mechanism 2 (MIM2): an isoprene oxidation mechanism for regional and global atmospheric modelling, Atmos. Chem. Phys., 9, 2751–2777, https://doi.org/10.5194/acp-9-2751-2009, 2009.

Taraborrelli, D., Lawrence, M. G., Crowley, J. N., Dillon, T. J., Gromov, S., Groß, C. B. M., Vereecken, L., and Lelieveld, J.: Hydroxyl radical buffered by isoprene oxidation over tropical forests, Nat. Geosci., 5, 190–193, https://doi.org/10.1038/ngeo1405, 2012.

Taraborrelli, D., Cabrera-Perez, D., Bacer, S., Gromov, S., Lelieveld, J., Sander, R., and Pozzer, A.: Influence of aromatics on tropospheric gas-phase composition, Atmos. Chem. Phys., 21, 2615–2636, https://doi.org/10.5194/acp-21-2615-2021, 2021.

Tilgner, A. and Herrmann, H.: Radical-driven carbonyl-to-acid conversion and acid degradation in tropospheric aqueous systems studied by CAPRAM, atmospheric Chemical Mechanisms: Selected Papers from the 2008 Conference, Atmos. Environ., 44, 5415–5422, https://doi.org/10.1016/j.atmosenv.2010.07.050, 2010.

Tilgner, A., Bräuer, P., Wolke, R., and Herrmann, H.: Modelling multiphase chemistry in deliquescent aerosols and clouds using CAPRAM3.0i, J. Atmos. Chem., 70, 221–256, https://doi.org/10.1007/s10874-013-9267-4, 2013.

Tost, H., Jöckel, P., Kerkweg, A., Sander, R., and Lelieveld, J.: Technical note: A new comprehensive SCAVenging submodel for global atmospheric chemistry modelling, Atmos. Chem. Phys., 6, 565–574, https://doi.org/10.5194/acp-6-565-2006, 2006.

Tost, H., Jöckel, P., Kerkweg, A., Pozzer, A., Sander, R., and Lelieveld, J.: Global cloud and precipitation chemistry and wet deposition: tropospheric model simulations with ECHAM5/MESSy1, Atmos. Chem. Phys., 7, 2733–2757, https://doi.org/10.5194/acp-7-2733-2007, 2007.

Wang, R., Balkanski, Y., Boucher, O., Bopp, L., Chappell, A., Ciais, P., Hauglustaine, D., Peñuelas, J., and Tao, S.: Sources, transport and deposition of iron in the global atmosphere, Atmos. Chem. Phys., 15, 6247–6270, https://doi.org/10.5194/acp-15-6247-2015, 2015.

Wespes, C., Emmons, L., Edwards, D. P., Hannigan, J., Hurtmans, D., Saunois, M., Coheur, P.-F., Clerbaux, C., Coffey, M. T., Batchelor, R. L., Lindenmaier, R., Strong, K., Weinheimer, A. J., Nowak, J. B., Ryerson, T. B., Crounse, J. D., and Wennberg, P. O.: Analysis of ozone and nitric acid in spring and summer Arctic pollution using aircraft, ground-based, satellite observations and MOZART-4 model: source attribution and partitioning, Atmos. Chem. Phys., 12, 237–259, https://doi.org/10.5194/acp-12-237-2012, 2012.

Wespes, C., Hurtmans, D., Emmons, L. K., Safieddine, S., Clerbaux, C., Edwards, D. P., and Coheur, P.-F.: Ozone variability in the troposphere and the stratosphere from the first 6 years of IASI observations (2008–2013), Atmos. Chem. Phys., 16, 5721–5743, https://doi.org/10.5194/acp-16-5721-2016, 2016.

Wespes, C., Hurtmans, D., Clerbaux, C., and Coheur, P.-F.: O_3 variability in the troposphere as observed by IASI over 2008–2016: Contribution of atmospheric chemistry and dynamics, J. Geophys. Res.-Atmos., 122, 2429–2451, https://doi.org/10.1002/2016JD025875, 2017.

WMO: Meteorology-A three-dimensional science: Second sessionof the commission for aerology, WMO Bull., Geneva, 134–138, 1957.

Young, P. J., Naik, V., Fiore, A. M., Gaudel, A., Guo, J., Lin, M., Neu, J., Parrish, D., Rieder, H., Schnell, J. L., Tilmes, S., Wild, O., Zhang, L., Ziemke, J., Brandt, J., Delcloo, A., Doherty, R. M., Geels, C., Hegglin, M. I., Hu, L., Im, U., Kumar, R., Luhar, A., Murray, L., Plummer, D., Rodriguez, J., Saiz-Lopez, A., Schultz, M. G., Woodhouse, M. T., and Zeng, G.: Tropospheric Ozone Assessment Report: Assessment of global-scale model performance for global and regional ozone distributions, variability, and trends, Elementa, 6, 10, https://doi.org/10.1525/elementa.265, 2018.

Ziemke, J. R., Chandra, S., Labow, G. J., Bhartia, P. K., Froidevaux, L., and Witte, J. C.: A global climatology of tropospheric and stratospheric ozone derived from Aura OMI and MLS measurements, Atmos. Chem. Phys., 11, 9237–9251, https://doi.org/10.5194/acp-11-9237-2011, 2011.

Chapter 7

The impact of organic pollutants from Indonesian peatland fires on the tropospheric and lower stratospheric composition

Rosanka, S., Franco, B., Clarisse, L., Coheur, P.-F., Pozzer, A., Wahner, A., and Taraborrelli, D.: The impact of organic pollutants from Indonesian peatland fires on the tropospheric and lower stratospheric composition, Atmospheric Chemistry and Physics, 21, 11 257–11 288, https://doi.org/10.5194/acp-21-11257-2021, 2021c

General information:

Importance for this thesis and the author's contribution:
In this study, the importance of VOC biomass burning emissions on the atmospheric composition and the importance of in-cloud OVOC oxidation during such events are addressed. It contributes to the assessment of the representation of aqueous-phase OVOC chemistry and VOC emissions in global models. This is further discussed in Sect. 8.5.

The idea for this study was developed together with Domenico Taraborrelli. I performed all EMAC simulations, analysed the results, and discussed the results with all co-authors. I created all figures in the manuscript, except for the figures in the appendix, and I wrote the manuscript. Further information and the contributions of all co-authors are available in the manuscript's 'Author contributions' section.

[1] `https://creativecommons.org/licenses/by/4.0/` (last access: 6 September 2020)

Atmos. Chem. Phys., 21, 11257–11288, 2021
https://doi.org/10.5194/acp-21-11257-2021

Atmospheric Chemistry and Physics Open Access EGU

The impact of organic pollutants from Indonesian peatland fires on the tropospheric and lower stratospheric composition

Simon Rosanka[1], Bruno Franco[2], Lieven Clarisse[2], Pierre-François Coheur[2], Andrea Pozzer[3], Andreas Wahner[1], and Domenico Taraborrelli[1]

[1]Institute of Energy and Climate Research: Troposphere (IEK-8), Forschungszentrum Jülich GmbH, Jülich, Germany
[2]Spectroscopy, Quantum Chemistry and Atmospheric Remote Sensing (SQUARES), Université libre de Bruxelles (ULB), Brussels, Belgium
[3]Atmospheric Chemistry Department, Max-Planck-Institute for Chemistry, Mainz, Germany

Correspondence: Simon Rosanka (s.rosanka@fz-juelich.de)

Received: 28 October 2020 – Discussion started: 17 November 2020
Revised: 21 May 2021 – Accepted: 25 May 2021 – Published: 27 July 2021

Abstract. The particularly strong dry season in Indonesia in 2015, caused by an exceptionally strong El Niño, led to severe peatland fires resulting in high volatile organic compound (VOC) biomass burning emissions. At the same time, the developing Asian monsoon anticyclone (ASMA) and the general upward transport in the Intertropical Convergence Zone (ITCZ) efficiently transported the resulting primary and secondary pollutants to the upper troposphere and lower stratosphere (UTLS). In this study, we assess the importance of these VOC emissions for the composition of the lower troposphere and the UTLS and investigate the effect of in-cloud oxygenated VOC (OVOC) oxidation during such a strong pollution event. This is achieved by performing multiple chemistry simulations using the global atmospheric model ECHAM/MESSy (EMAC). By comparing modelled columns of the biomass burning marker hydrogen cyanide (HCN) and carbon monoxide (CO) to spaceborne measurements from the Infrared Atmospheric Sounding Interferometer (IASI), we find that EMAC properly captures the exceptional strength of the Indonesian fires.

In the lower troposphere, the increase in VOC levels is higher in Indonesia compared to other biomass burning regions. This has a direct impact on the oxidation capacity, resulting in the largest regional reduction in the hydroxyl radical (OH) and nitrogen oxides (NO_x). While an increase in ozone (O_3) is predicted close to the peatland fires, simulated O_3 decreases in eastern Indonesia due to particularly high phenol concentrations. In the ASMA and the ITCZ, the upward transport leads to elevated VOC concentrations in the lower stratosphere, which results in the reduction of OH and NO_x and the increase in the hydroperoxyl radical (HO_2). In addition, the degradation of VOC emissions from the Indonesian fires becomes a major source of lower stratospheric nitrate radicals (NO_3), which increase by up to 20 %. Enhanced phenol levels in the upper troposphere result in a 20 % increase in the contribution of phenoxy radicals to the chemical destruction of O_3, which is predicted to be as large as 40 % of the total chemical O_3 loss in the UTLS. In the months following the fires, this loss propagates into the lower stratosphere and potentially contributes to the variability of lower stratospheric O_3 observed by satellite retrievals. The Indonesian peatland fires regularly occur during El Niño years, and the largest perturbations of radical concentrations in the lower stratosphere are predicted for particularly strong El Niño years. By activating the detailed in-cloud OVOC oxidation scheme Jülich Aqueous-phase Mechanism of Organic Chemistry (JAMOC), we find that the predicted changes are dampened. Global models that neglect in-cloud OVOC oxidation tend to overestimate the impact of such extreme pollution events on the atmospheric composition.

Published by Copernicus Publications on behalf of the European Geosciences Union.

1 Introduction

Particularly strong Indonesian wildfires during the El Niño in 2015 led to severe air pollution and reduced visibility (Kim et al., 2015; Lee et al., 2017), resulting in increased morbidity and mortality (Marlier et al., 2013; Reddington et al., 2014; Crippa et al., 2016) in South East Asia (SEA). In general, El Niño is a large-scale climate anomaly, which is characterised by significantly warmer eastern equatorial Pacific Ocean sea surface temperatures (Trenberth, 1997), resulting in a dry season in SEA (Weng et al., 2007). The very strong El Niño phase in 2015–2016, which is the third strongest on record (after 1997–1998 and 1982–1983, NOAA, 2020), led to a particularly strong dry season in Indonesia (Jiménez-Muñoz et al., 2016), which started in mid-July and lasted until November (Field et al., 2016). In the past, much of the originally forested and moist peatland in Kalimantan and Sumatra has been drained and cleared during agricultural land management. In order to clear these forests, landscape fires are commonly used. Even small local fires in these regions during non-El Niño years may induce particularly strong biomass burning emissions. Gaveau et al. (2014) estimated that a local 1-week Indonesian biomass burning event in 2013 contributed to about 5 %–10 % of Indonesian's total greenhouse gas emissions in that year. The additional drying during El Niño years favours fires that burn deep down into the peat and can last for multiple weeks. Due to their long lifetimes, these fires spread and ignite new areas, which are not necessarily prone to biomass burning. Compared to non-El Niño years, this results in strong biomass burning emissions from Indonesia (van der Werf et al., 2017). The underground conditions inherently determine smouldering fires, which are characterised by low combustion temperatures. In combination with the high carbon content of peat, smouldering fires emit much larger amounts of non-CO_2 emissions from peatlands than from other fuels (Christian et al., 2003; Rein et al., 2009; Yu et al., 2010). A major fraction of these non-CO_2 emissions is volatile organic compounds (VOCs), which comprise a large variety of species and can influence atmospheric chemistry on a regional and global scale. In the atmosphere, VOCs mainly react with the hydroxyl radical (OH), ozone (O_3), and the nitrate radical (NO_3) or photodissociate. Their atmospheric lifetimes range from minutes to years. Figure 1 shows the dry matter burned (DMB) during the 2015 Indonesian fires along the distribution of the peatlands (indicated in blue). It becomes evident that most of the areas influenced by biomass burning (e.g. Sumatra, Kalimantan) are covered with peatland, indicating that the 2015 Indonesian fires are characterised by high VOC emissions.

During the Indonesian biomass burning season, usually the Asian monsoon is ongoing such that a large anticyclone spanning from tropical to temperate regions (from about 10 to 40° N) evolves. This semi-stationary large-scale meteorological pattern typically extends from the Middle East to Asia in the upper troposphere and lower stratosphere (UTLS) (Basha et al., 2020). As a convective system, the Asian monsoon anticyclone (ASMA) acts as a pollution pump facilitating a fast transport of surface emissions to the UTLS (Park et al., 2008; Randel et al., 2010; Lelieveld et al., 2018). Vogel et al. (2015) analysed the impact of different regions in Asia on the chemical composition of the 2012 ASMA by using a chemical Lagrangian model. They found that air masses from SEA contribute significantly to the composition of the anticyclone in the UTLS. In addition, the vertically convective transport in the Intertropical Convergence Zone (ITCZ) and in the south-eastern flank of the anticyclone carries air masses from SEA into the UTLS. Thus, even short-lived VOCs from Indonesian fires are transported into the UTLS and potentially affect the lower stratospheric composition.

The Asian monsoon is characterised by the frequent occurrence of clouds and precipitation, and it has been demonstrated that the ASMA has a higher water vapour content than other meteorological systems (Fu et al., 2006). At the same time, the Madden–Julian Oscillation (MJO) leads to enhanced water vapour concentrations and precipitation over the Indian Ocean and Indonesia (Zhang, 2013). Many oxygenated VOCs (OVOCs) have a high solubility and quickly partition and react in cloud droplets influencing radical concentrations and the atmospheric composition in general (Herrmann et al., 2015). Rosanka et al. (2021a) showed that the in-cloud OVOC oxidation has a significant impact on the predicted concentrations of VOCs, key oxidants, and O_3. In the past, global atmospheric chemistry models were not capable of representing this process explicitly or in its full complexity (Ervens, 2015). However, the recently developed Jülich Aqueous-phase Mechanism of Organic Chemistry (JAMOC, Rosanka et al., 2021a, b) comprises an advanced in-cloud OVOC oxidation scheme suitable to be used in the ECHAM/MESSy Atmospheric Chemistry (EMAC, Jöckel et al., 2010) model. This allows us to assess the importance of this in-cloud oxidation process during the VOC-dominated Indonesian peatland fires.

In this study, we therefore investigate the importance of biomass burning VOC emissions from the strong 2015 Indonesian peatland fires on (1) the lower tropospheric composition, (2) the UTLS, and (3) the importance of in-cloud OVOC oxidation in such an extreme pollution event. This is addressed by performing multiple global chemistry simulations using the ECHAM/MESSy Atmospheric Chemistry (EMAC, Sect. 2) model. In addition to the 2015 fires, strong peatland fires frequently occur in Indonesia. Especially during El Niño years (in 2002–2003, 2004–2005, 2006–2007, 2009–2010, and 2014–2016), high emissions have been observed (van der Werf et al., 2017). Therefore, the long-term impact of these periodically occurring events is additionally addressed. Globally, biomass burning is not limited to Indonesia, and many regions are frequently affected. In each region, biomass burning varies in strength, frequency, the characteristics of the biomass burned, and the chemical background conditions. In a first step, we therefore compare the

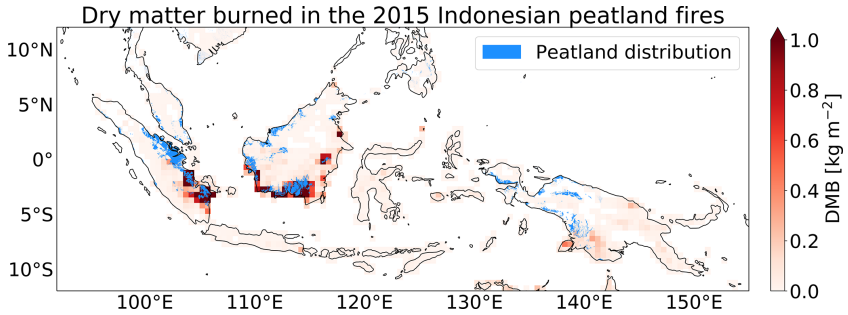

Figure 1. Accumulated dry matter burned (DMB) during the Indonesian peatland fires of 2015. The distribution of Indonesian peatland is indicated in blue. The data for the peatland distribution are obtained from Xu et al. (2017, 2018).

Indonesian peatland fires to other biomass burning regions, focusing on their specific emission footprint (Sect. 3). The ability of EMAC to represent biomass burning events is evaluated using hydrogen cyanide (HCN) and carbon monoxide (CO) satellite retrievals (Sect. 4). Afterwards the impact of the 2015 Indonesian peatland fires on the troposphere and the UTLS is analysed, focusing on hydrocarbons, oxygenated organics, nitrogen-containing compounds, key radicals, and O_3 in Sects. 5 and 6, respectively. In Sect. 7, the importance of in-cloud OVOC oxidation during this pollution event is addressed. Modelling uncertainties related to this study are discussed in Sect. 8 before drawing final conclusions (Sect. 9).

2 Modelling approach

This section provides an overview on the global model used in this study. The main focus is placed on the representation of atmospheric gas- and aqueous-phase chemistry, biogenic and biomass burning emissions, and the strategy to compare EMAC's simulated results with satellite retrievals (Sect. 2.1). Section 2.2 provides an overview of each simulation performed in this study.

2.1 EMAC

The ECHAM/MESSy Atmospheric Chemistry (EMAC) model is a numerical chemistry and climate simulation system that includes submodels describing tropospheric and middle-atmosphere processes and their interaction with oceans, land, and human influences (Jöckel et al., 2010). It uses the second version of the Modular Earth Submodel System (MESSy2) to link multi-institutional computer codes. The core atmospheric model is the fifth-generation European Centre Hamburg general circulation model (ECHAM5, Roeckner et al., 2006). Jöckel et al. (2010) provided an update on all modelling components used. For the present study, we applied EMAC (ECHAM5 version 5.3.02, MESSy version 2.54.0) in the T106L90MA and T42L90MA resolution, i.e. with a spherical truncation of T106 and T42 (corresponding to a quadratic Gaussian grid of approximately 1.1° by 1.1° and 2.8° by 2.8°, respectively). By using this horizontal resolution, addressing the short-term implications for 2015–2016 as well as the long-term impact (2001–2016) on a global scale is still feasible while at the same time the computational costs are affordable. For both resolutions, 90 (L90) vertical hybrid pressure levels up to 0.01 hPa are used focusing on the lower and middle atmosphere (MA), representing tropospheric and stratospheric transport processes reasonably well (Jöckel et al., 2010). Thus, the impact on the troposphere and the UTLS can be addressed. A detailed discussion on the comparability of both resolutions is performed in Sect. 8.

2.1.1 Atmospheric chemistry

For this study, the gas- and aqueous-phase chemical kinetics is integrated by two separate submodels. For the atmospheric gas-phase chemistry, the applied model setup comprised the submodel Module Efficiently Calculating the Chemistry of the Atmosphere (MECCA, Sander et al., 2019) using the gas-phase Mainz Organic Mechanism (MOM). MOM contains an extensive oxidation scheme for isoprene (Taraborrelli et al., 2009, 2012; Nölscher et al., 2014), monoterpenes (Hens et al., 2014), and aromatics (Cabrera-Perez et al., 2016) and is therefore capable of representing all the biomass burning VOCs considered in EMAC. In addition, comprehensive reactions schemes are considered for the modelling of the chemistry of NO_x ($NO + NO_2$), HO_x ($OH + HO_2$), CH_4, and anthropogenic aliphatic and aromatic hydrocarbons. VOCs are oxidised by OH, O_3, and NO_3, whereas peroxy radicals (RO_2) react with HO_2, NO_x, and NO_3 and undergo self- and cross-reactions (Sander et al., 2019). Isocyanic acid (HNCO) is a chemical constituent that is primarily emitted by biomass burning and potentially harmful to humans (Wang et al., 2007; Roberts et al., 2011; Leslie et al., 2019). In order to properly represent this toxic constituent within EMAC, MOM has been extended to represent the atmospheric chemistry of HNCO. For this, the mech-

anism proposed by Rosanka et al. (2020a) is implemented into MOM. Their mechanism includes formamide as an additional chemical source of HNCO and chemical mechanisms for nitromethane, methylamine, dimethylamine, and trimethylamine.

The atmospheric aqueous-phase chemistry is modelled using the SCAVenging submodel (SCAV, Tost et al., 2006). It simulates the removal of trace gases and aerosol particles by clouds and precipitation. SCAV calculates the transfer of species into and out of rain and cloud droplets using the Henry's law equilibrium, acid dissociation equilibria, oxidation–reduction reactions, heterogeneous reactions on droplet surfaces, and aqueous-phase photolysis reactions (Tost et al., 2006). As mentioned earlier and as demonstrated by Rosanka et al. (2021a), in-cloud OVOC oxidation significantly influences the atmospheric composition. However, the ordinary differential equations (ODE) systems resulting from the combination of gas-phase and in-cloud aqueous-phase suffer from (1) a higher stiffness due to fast acid–base equilibria and phase-transfer reactions and (2) load imbalance on high-performance computing (HPC) systems due to the sparsity of clouds. This leads to a significant increase in computational costs when using larger chemical mechanisms like the Jülich Aqueous-phase Mechanism of Organic Chemistry (JAMOC), i.e. larger ODE systems (Rosanka et al., 2021b). Using JAMOC in each simulation performed in this study is thus not feasible. As a trade-off, JAMOC is used in a simulation subset in order to address and estimate its implications on the other simulations. Thus, two different aqueous-phase mechanisms are used within this study: (1) the standard aqueous-phase mechanism of EMAC (in the following called ScSta), which includes a detailed oxidation scheme and represents more than 150 reactions (Jöckel et al., 2016), and (2) JAMOC (Rosanka et al., 2021b), which includes a complex in-cloud OVOC oxidation scheme. In JAMOC, the phase transfer of species containing up to 10 carbon atoms and the oxidation of species containing up to 4 carbon atoms are represented. Similar to MOM, both aqueous-phase mechanisms are modified to include the changes proposed by Rosanka et al. (2020a) to properly represent HNCO.

2.1.2 Biogenic and biomass burning VOC emissions

In the atmosphere, biogenic and biomass burning emissions are two major sources of VOCs. The largest biogenic emissions take place in the equatorial region (e.g. Amazon basin, central Africa) with additional emissions in the Northern Hemisphere (NH) and Southern Hemisphere (SH) extratropics. The MESSy submodel uses the Model of Emissions of Gases and Aerosols from Nature (MEGAN, Guenther et al., 2006) to calculate biogenic VOC emissions. The global emissions of isoprene, the most abundant biogenic VOC, are scaled to $595\,\mathrm{Tg\,a^{-1}}$, the best estimate of Sindelarova et al. (2014).

Biomass burning emission fluxes are calculated using the MESSy submodel BIOBURN, which determines these fluxes based on biomass burning emission factors and dry matter combustion rates. For the latter, data from the Global Fire Assimilation System (GFAS) that are based on satellite observations of the fire radiative power obtained from the Moderate Resolution Imaging Spectroradiometer (MODIS) satellite instruments are used (Kaiser et al., 2012). In BIOBURN, the emission strength depends on the dominant fuel type in the respective area. From the GFAS dataset used in EMAC, in 2015, the dominant fuel type over Indonesia is tropical forest fire. However, as discussed earlier, peatland fires contribute substantially to the Indonesian fires. The GFAS dataset of EMAC is changed such that the dominant fuel type over Indonesia is a combination of peat and tropical forest fires with equal contributions (following van der Werf et al., 2017). In general, biomass burning emission factors for VOCs are based on Akagi et al. (2011). Biomass burning emissions for HNCO, formamide, nitromethane, methylamine, dimethylamine, and trimethylamine are implemented following Rosanka et al. (2020a) using emission factors from Koss et al. (2018) for HNCO and formamide.

2.1.3 Observational comparison

The evaluation of model simulation results against global observational datasets of VOC abundance can be performed for only a few species, mainly because of the limited availability in spaceborne measurements of such compounds. Among them, several VOCs are retrieved globally from the observations made by the nadir-viewing hyperspectral Infrared Atmospheric Sounding Interferometer (IASI, Clerbaux et al., 2009). Embarked on the Metop platforms on sun-synchronous polar orbits, IASI crosses the Equator at 09:30 and 21:30 local solar time and achieves a global coverage twice daily with a fairly dense spatial sampling. Here, we make use of the HCN abundance retrieved from the IASI/Metop-A and B observations to assess the ability of EMAC to represent such an important biomass burning event. In addition, IASI methanol (CH_3OH) data are used to assess the impact of in-cloud OVOC oxidation in the model simulations (Sect. 7).

The retrieval method used to obtain the HCN measurements from the IASI observations follows closely the version 3 of the Artificial Neural Network for IASI (ANNI), which already allowed the retrieval of a suite of VOCs, including CH_3OH (Franco et al., 2018). ANNI is a general retrieval framework that consists in quantifying, for each IASI observation, the spectral signature of the target gas with a sensitive hyperspectral metric and in converting this metric into gas total column via an artificial feedforward neural network (NN). Details on the ANNI retrieval approach, the HCN retrieval specificities, and the HCN product itself are provided in Appendix A. We refer to Franco et al. (2018) for a description of the IASI methanol retrievals. The satel-

lite datasets exploited in this study consist of daily global distributions of HCN and CH_3OH total columns derived from the daytime observations (approximately 09:30 local time) of the IASI/Metop-A and B overpasses. These offer a better measurement sensitivity than the evening overpasses (Franco et al., 2018). Scenes affected by clouds or poor retrieval performance are removed from the final dataset by specific filters. Examples of daily regional distributions of HCN columns in the 2015 Indonesian fires as well as the seasonal global distributions of HCN as retrieved from IASI are presented in Appendix A. Those highlight the ability of IASI to capture the enhancements of HCN during biomass burning events as well as its downwind transport over long distances.

Significant enhancements of carbon monoxide (CO) have already been captured by IASI in the 2015 Indonesian fires (e.g. Whitburn et al., 2016b; Nechita-Banda et al., 2018). Therefore, we also evaluate the ability of EMAC to reproduce the CO columns observed from space during this event. The vertical profile and column abundance of CO are obtained in near real time from the IASI/Metop-A and B spectra with the Fast Optimal Retrievals on Layers for IASI (FORLI) algorithm (Hurtmans et al., 2012). Several quality flags ensure that IASI observations affected by clouds, unstable retrieval, and measurement sensitivity that is too weak are excluded from the final CO dataset. The FORLI algorithm, characterisation of the retrieved CO product, and validation against independent measurements are reported in Hurtmans et al. (2012) and George et al. (2015). Following the formalism of Rodgers (2000), the IASI averaging kernels are applied to the CO model profiles to account for the inhomogeneous vertical sensitivity of the IASI measurements and to compute modelled CO columns as would be seen by the satellite instrument (see e.g. Sect. 5.1 in Schultz et al., 2018).

2.2 Simulations performed

Within this study, seven simulations are performed, which can be summarised in three simulation sets. Each simulation differs either in the biomass burning emissions, the aqueous-phase mechanism used, or the modelled time period. Table 1 provides an overview of all simulations and their characteristics. For each simulation set, in one simulation all VOC emissions from biomass burning are switched off (named REF and REF_{LONG}). A second simulation includes biomass burning VOC emissions as described in Sect. 2.1.2 (named FIR and FIR_{LONG}). Performing high-resolution simulations with the highest complexity in the chemical mechanisms in EMAC comes with high computational costs. The strong Indonesian peatland fires of 2015 and the following year are selected as a specific case study (named REF and FIR). For both simulations, the year 2014 is simulated as spin-up, which is not considered for the analysis. For this case study, high-resolution simulations are performed at T106L90MA. In order to isolate the impact of the Indonesian peatland fires in 2015, an additional simulation (named FIR_{NOINDO}) is performed, for which all biomass burning VOC emissions from Indonesia are switched off. In order to address the impact of in-cloud OVOC oxidation on such a VOC-dominated pollution event, two simulations including JAMOC are performed (named REF_{JAMOC} and FIR_{JAMOC}). However, to reduce the computational demand (see Sect. 2.1.1), these simulations focus only on the second half of 2015 at a resolution of T106L90MA. The long-term effect of reoccurring Indonesian peatland fires are addressed by performing two long simulations for the time period of 2001–2016 (named REF_{LONG} and FIR_{LONG}). Here, the year 2000 is simulated for spin-up, which is not used for the analysis. Performing these simulations at T106L90MA and using JAMOC is computationally not feasible. Therefore, the EMAC's standard aqueous-phase mechanism is used and the resolution is reduced to T42L90MA. All simulations are performed using the quasi chemistry–transport model mode (QCTM mode, Deckert et al., 2011), meaning that chemistry and dynamics are decoupled; e.g. fixed tracer mixing rations are used as input for the radiation scheme instead of the prognostic chemical tracers. In this way, the meteorology is the same for all simulations, and all changes in the atmospheric chemical composition predicted by EMAC are due to either the additional VOC emissions from biomass burning (when comparing REF with FIR or REF_{LONG} with FIR_{LONG}) or the in-cloud OVOC oxidation (when comparing REF, FIR, REF_{JAMOC}, and FIR_{JAMOC}).

3 Peatland fires in Indonesia compared to biomass burning in other regions

Globally, biomass burning frequently occurs in seven regions for which Fig. 2 and Table 2 provide an overview. In each region, biomass burning varies in strength, frequency, the characteristics of the biomass burned, and the chemical background conditions. Only about 2.84 % of the Earth's land mass is covered by peatland (Xu et al., 2018), making equatorial Asia the region where the most of peatland is burned. Since non-peatland biomass burning fuels have lower VOC (and higher NO_x) emission factors (Akagi et al., 2011), Indonesia is characterised by a unique emission footprint. Figure 3 shows the total trace gas (VOC and non-VOC), the VOC, and the aromatic biomass burning emissions for each region in non-El Niño years, El Niño years, and in 2015 predicted by EMAC (based on FIR_{LONG}). In non-El Niño years, the highest total biomass burning emissions of about 1.38 and 1.76 $Pg\,a^{-1}$ originate from central Africa (CAF) and southern Africa (SAF), respectively, whereas the lowest biomass burning emissions of about 0.13 $Pg\,a^{-1}$ occur in Alaska (ALA). SEA contributes only 0.55 $Pg\,a^{-1}$ to the total biomass burning emissions, which is about one-third of the SAF biomass burning emissions. However, in El Niño years this almost doubles (1.05 $Pg\,a^{-1}$), and in the exception-

Table 1. List of EMAC simulations performed in this study. Here, ScSta indicates EMAC's standard aqueous-phase mechanism (Jöckel et al., 2016) and JAMOC indicates the complex in-cloud OVOC oxidation scheme by Rosanka et al. (2021b, a) (for further details see Sect. 2.1.1).

Name	Analysed period	VOC BIOBURN emissions	Aqueous-phase mechanism	Resolution
REF	2015–2016	no	ScSta	T106L90MA
FIR	2015–2016	yes	ScSta	T106L90MA
FIR_{NOINDO}	SOND[a] in 2015	yes[b]	ScSta	T106L90MA
REF_{LONG}	2001–2016	no	ScSta	T42L90MA
FIR_{LONG}	2001–2016	yes	ScSta	T42L90MA
REF_{JAMOC}	SOND[a] in 2015	no	JAMOC	T106L90MA
FIR_{JAMOC}	SOND[a] in 2015	yes	JAMOC	T106L90MA

[a] Focus on Indonesia in September, October, November, and December. [b] No VOC biomass burning emissions from Indonesian peatland fires.

ally strong year 2015 the biomass burning emissions from SEA of about $1.62\,\mathrm{Pg\,a^{-1}}$ are almost the same as the total biomass burning emissions from SAF. In CAF and SAF, mainly tropical forest and savanna are burned, resulting in low VOC emissions. In 2015, the VOC and aromatic emissions of both regions ranged between 11.32 to $14.34\,\mathrm{Tg\,a^{-1}}$ and 0.89 to $1.20\,\mathrm{Tg\,a^{-1}}$, respectively, which compared to SEA is significantly lower (VOCs: $23.61\,\mathrm{Tg\,a^{-1}}$; aromatics: $2.52\,\mathrm{Tg\,a^{-1}}$). The two northern regions ALA and northern Asia (NAS), which are characterised by extratropical forest with organic soil, add significantly to the global VOC emissions from biomass burning, even though their contribution to the total biomass burning emissions is low. The contribution of NAS to the total biomass burning is less than half of the contribution by SAF ($0.69\,\mathrm{Pg\,a^{-1}}$ compared to $1.76\,\mathrm{Pg\,a^{-1}}$), but its contribution to the aromatic biomass burning emissions is almost the same ($1.11\,\mathrm{Tg\,a^{-1}}$ compared to $1.20\,\mathrm{Tg\,a^{-1}}$). The contribution of ALA strongly depends on the El Niño. In non-El Niño years, the total biomass burning emissions are very low ($0.13\,\mathrm{Pg\,a^{-1}}$) but increase in El Niño years ($0.29\,\mathrm{Pg\,a^{-1}}$). In the exceptionally strong year 2015, the contribution of ALA to the aromatic biomass burning emissions is $0.82\,\mathrm{Tg\,a^{-1}}$, which is of similar strength as from CAF ($0.89\,\mathrm{Tg\,a^{-1}}$) even though its total contribution is only one-third when compared to CAF. The two regions dominated by savanna, central South America (CSA) and northern Australia (NAU) emit 7.72 and $3.30\,\mathrm{Tg\,a^{-1}}$ of VOCs from biomass burning, respectively.

4 The representation of the Indonesian peatland fires in EMAC

In order to analyse the ability of EMAC to represent the Indonesian peatland fires, we compare predicted EMAC total columns of HCN and CO to observations obtained from IASI retrievals.

4.1 Comparison to IASI HCN retrievals

HCN mainly originates from combustion processes and is therefore largely emitted by biomass burning (Shim et al., 2007). Other emission sources including industrial activities, automobile exhaust, and domestic biofuel are assumed to be very weak (Lobert et al., 1990; Li et al., 2009). Reactions involving acetonitrile (CH_3CN) are the only gas-phase source of HCN, but those are estimated to be a minor contribution to the atmospheric HCN burden (Li et al., 2009). The slow oxidation of HCN by OH and $O(^1D)$ is considered to be the most important atmospheric gas-phase sink, leading to long chemical lifetimes (Cicerone and Zellner, 1983). However, due to a strong ocean uptake, the overall atmospheric lifetime is reduced to a few months (Li et al., 2000, 2009). The almost exclusive biomass burning source, combined with a long atmospheric residence time that allows for long-range transport, makes HCN a widely used primary tracer of biomass burning emissions and fire plumes (Li et al., 2009). Moreover, substantial emissions of HCN are expected from strong peatland fires (e.g. Akagi et al., 2011; Andreae, 2019). Therefore, HCN satellite data from IASI are used here to evaluate the performance of EMAC in representing the 2015 Indonesian peatland fires.

At the beginning of the Indonesian fires, the emitted HCN is transported westward, leading to high HCN column values over the Indian Ocean (see Fig. A3). While the fires are ongoing throughout October, the strong westward transport of HCN results in the complete covering of the Indian Ocean. Some HCN is also transported eastward over Australia and the Pacific Ocean. In November, the air masses from Indonesia mix with emissions from Africa and the eastward-transported air masses reach South America. Figure 4 shows the comparison of modelled HCN total columns to IASI satellite retrievals for the 3-month mean with strong peatland emissions in Indonesia. In general, EMAC strongly underestimates HCN when its main source from biomass burning is not taken into account (simulation REF). Once the HCN biomass burning emissions are taken into account,

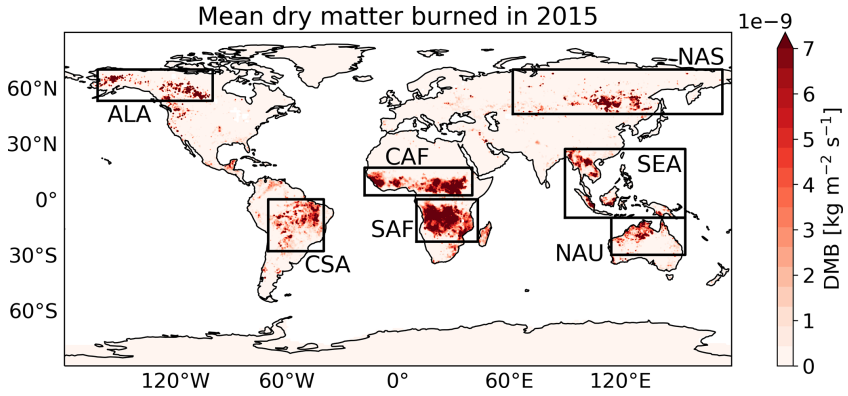

Figure 2. Mean dry matter burned (DMB) in 2015. The naming of each region is as follows: Alaska (ALA), central Africa (CAF), central South America (CSA), northern Asia (NAS), northern Australia (NAU), southern Africa (SAF), and South East Asia (SEA). Further details about each region are presented in Table 2.

Table 2. Characteristics of the different biomass burning regions focusing on the dominant fuel type, the main biomass burning season, and the dry matter burned (DMB). The global DMB by GFAS (Kaiser et al., 2012) for the year 2015 is 4985 Tg a^{-1}. The naming of each region is as follows: Alaska (ALA), central Africa (CAF), central South America (CSA), northern Asia (NAS), northern Australia (NAU), southern Africa (SAF), and South East Asia (SEA). Each region is graphically illustrated in Fig. 2.

Region	Dominant fuel type	Main biomass burning season	2015 DMB [Tg a^{-1}]
ALA	Extratropical forest with organic soil	JJA	295
CAF	Tropical forest and savanna	DJF	778
CSA	Savanna	SON	439
NAS	Extratropical forest with organic soil	MMA and JJA	363
NAU	Savanna	SON	260
SAF	Tropical forest and savanna	JJA	1036
SEA	Tropical forest[a]	SON	1237[b]

[a] In this study a combination of tropical forest (50 %) and peatland (50 %) is assumed in Indonesia (Sect. 2.1.2).
[b] Of which 949 Tg a^{-1} is from Indonesian peatland fires.

the overall underprediction in EMAC is mostly resolved, but EMAC partially overpredicts HCN in SEA. Figure 5 gives the frequency of the global HCN EMAC total column bias in relation to the IASI retrievals during the Indonesian peatland fires, once including biomass burning emissions in the simulations and once not. This comparison clearly shows that HCN is strongly underestimated when its main source is not represented in EMAC. With HCN from biomass burning, the mean column bias reduces from -5.32×10^{15} to -1.06×10^{15} molecules cm^{-2}, and its variance reduces from 1.75×10^{31} to 2.57×10^{30} molecules^2 cm^{-4}, significantly improving the representation of HCN in EMAC.

In general, EMAC's representation of HCN is associated with some uncertainties. Another important source of HCN is terrestrial vegetation, which may contribute to atmospheric concentrations by up to 18 % (Shim et al., 2007). In EMAC, the submodule MEGAN calculates that biogenic emissions contribute about 15 % to the total HCN emissions. Considering the particularly high atmospheric concentrations in 2015, this slightly lower contribution suggests that this source strength may be well represented in EMAC. Overall, it is expected that the HCN atmospheric lifetime is realistically modelled, since globally HCN columns are well reproduced. Moreover, the ocean uptake accounts for 1.2 Tg(N) a^{-1}, which is well in the range of 1.1 to 2.6 Tg(N) a^{-1} proposed by Li et al. (2000) and very close to the Singh et al. (2003) estimate of 1.0 Tg(N) a^{-1}. The representation of biomass burning within EMAC depends on satellite observations (Sect. 2.1.2), which retrieve the fire radiative power and are thus sensitive to clouds. This introduces some uncertainties in regions that are characterised by the frequent occurrence of clouds, like equatorial Asia. Focusing on Indonesia, Liu et al. (2020) compared five different global fire inventories and found that GFAS, the inventory used in this study, represents the strength of these fires best. Still, GFAS tends to slightly underestimate the strength, when

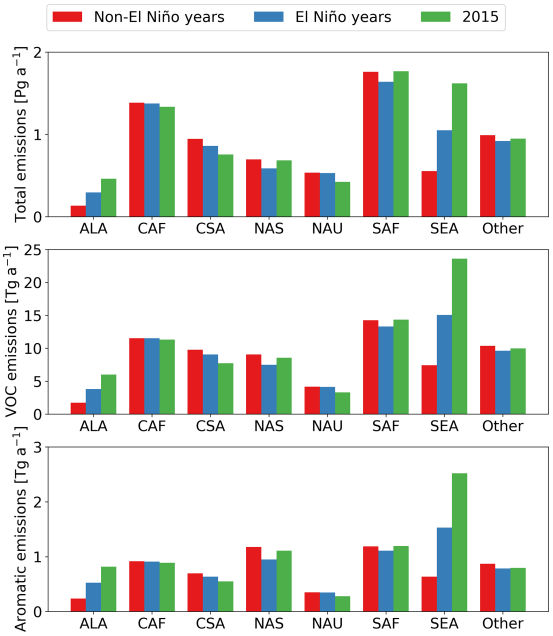

Figure 3. The total trace gas (VOC and non-VOC), the VOC, and the aromatic biomass emissions for each region in non-El Niño years, El Niño years, and in 2015 predicted by EMAC (based on REF_{LONG} and FIR_{LONG}). Further details about each region are presented in Table 2 and Fig. 2.

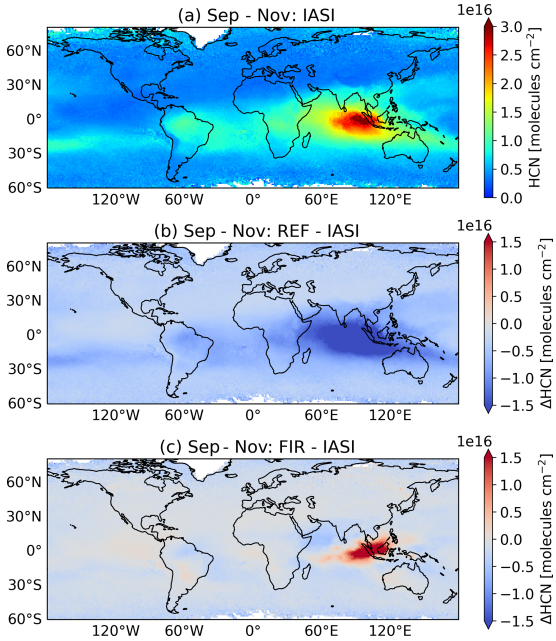

Figure 4. HCN comparison between IASI, REF, and FIR. **(a)** Mean global observed IASI HCN columns for September to November. **(b)** Mean global HCN column comparison between REF and IASI for September to November. **(c)** Mean global HCN column comparison between FIR and IASI for September to November.

compared to regional observations in Singapore, Malaysia, and Indonesia. This suggests that the magnitude of the Indonesian fires is well represented in EMAC. However, from the literature a high uncertainty in the emission factors for HCN is reported. Here, we use the emission factors optimised for atmospheric models by Akagi et al. (2011), which suggest 5.0 g kg^{-1} for HCN from peatland fires. From recent field measurements in Indonesia and Malaysia, Stockwell et al. (2016) and Smith et al. (2018) report values ranging from 0.34 to 8.21 g kg^{-1}, whereas lab measurements for Indonesian peatland by Stockwell et al. (2015) suggest values between 3.30 and 3.83 g kg^{-1}. Overall, this results in a mean emission factor of 4.40 g kg^{-1} across all studies (Andreae, 2019), suggesting that the HCN emission factor used in EMAC is slightly too high, influencing EMAC's overprediction of HCN columns. Lastly, EMAC's overprediction west of Indonesia suggests that some of the overprediction is caused by the deviation of horizontal transport (further discussed in Sect. 8).

4.2 Comparison to IASI CO retrievals

At the surface, CO is primarily emitted by natural and anthropogenic combustion processes like biomass and fossil fuel burning and to a lesser extent by biogenic and oceanic sources. The degradation of methane (CH_4) and non-methane hydrocarbons (NMHC) in the atmosphere accounts for almost half of the global CO sources (Zheng et al., 2019). In the atmosphere, CO mainly reacts with OH, and the EMAC estimates by Lelieveld et al. (2016) and more recently by Rosanka et al. (2021a) show that CO largely determines the atmospheric oxidation capacity. To a lesser extent, CO is deposited (Stein et al., 2014).

Figure 6a shows the total CO columns observed by IASI for the 3-month mean with strong peatland emissions in Indonesia. Similar to HCN, high CO columns up to about 6.0×10^{18} molecules cm^{-2} are observed over Indonesia. Additionally, high CO columns are also observed in Africa and South America. Compared to HCN, CO is characterised by a shorter lifetime. Therefore, less CO from Indonesia is transported towards Africa at the end of the peatland fire period. Figure 6b shows the comparison of modelled total CO columns for FIR to the IASI retrievals for the same period. Overall EMAC captures the spatial CO pattern with overprediction of 1.0×10^{18} molecules cm^{-2} in South America. Rosanka et al. (2021a) showed that EMAC predicts total methanol columns too high in this region, which is related to EMAC's tendency to simulate the Amazon basin too dry in

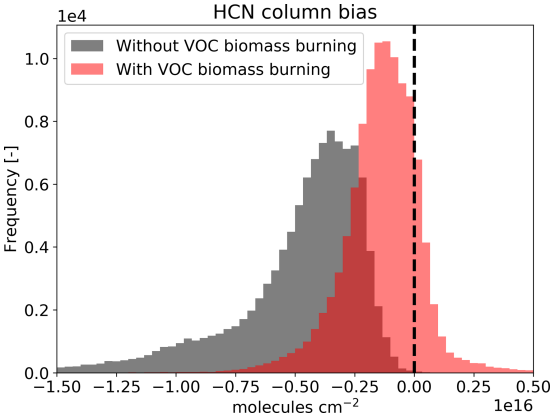

Figure 5. Global HCN column bias between EMAC simulations and IASI satellite data. The column bias is calculated based on monthly mean data during the Indonesian peatland fires in 2015.

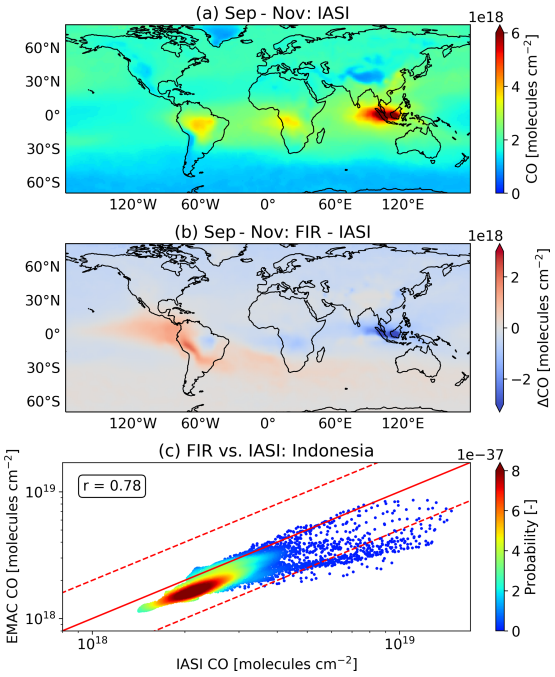

Figure 6. CO comparison between IASI and FIR. **(a)** Mean global observed IASI CO columns for September to November. **(b)** Mean global CO column comparison between FIR and IASI for September to November. **(c)** Scatter plot for direct comparison between FIR and IASI over Indonesia for September to November.

the dry season (September–November) and consequently too hot (Hagemann and Stacke, 2015). This results in an overestimation of biogenic VOC emissions in South America. Since VOC degradation is the main atmospheric CO source, their overprediction explains EMAC's high bias for CO total columns in this region and its outflows.

As seen in Fig. 6b and c, EMAC constantly underestimate total CO columns over Indonesia during the main peatland fire period. However, overall the model bias stays within a factor of 2 (dashed lines in Fig. 6c). This underprediction can be explained by the emission factors used by EMAC. Stockwell et al. (2016) and Smith et al. (2018) report CO emission factors ranging from 216 to 314 g kg^{-1} obtained from observation in Indonesia and Malaysia during the Indonesian peatland fires of 2015. In addition, in the recent assessment of Andreae (2019) a mean emission factor of 260 g kg^{-1} for peatland is reported across multiple studies, which is higher than the emission factor used by EMAC (182 g kg^{-1}, Akagi et al., 2011).

From this analysis we conclude that even though EMAC does not reproduce HCN and CO columns perfectly, the Indonesian fires are reasonably well represented, especially when considering the exceptional strength of the 2015 Indonesian fires (for further discussion see Appendix A and Fig. A3). This also holds true considering all global biomass burning emission events.

5 The impact of biomass burning on the troposphere

In the following subsections, the impact of the 2015 Indonesian peatland fires on the lower tropospheric composition is analysed. In addition, substantial differences compared to the other six biomass-burning-dominated regions are discussed. All results are based on the simulations REF and FIR. Figure 7 depicts how the Indonesian peatland fires affect the atmospheric gas-phase composition. Table 3 provides an overview on the global and regional changes (between simulation REF and FIR) in the tropospheric burden of each species discussed in the following subsections. The regional changes reported in Table 3 are calculated for the respective main biomass burning season defined in Table 2.

5.1 Hydrocarbons

Many VOCs are characterised by short lifetimes resulting in highly-location-dependent changes within the troposphere. Globally, biomass burning emissions of VOCs significantly increase the atmospheric concentration of many hydrocarbons. In general, hydrocarbons can be separated into the aliphatic hydrocarbons and aromatic hydrocarbons. For both, direct emissions are the only atmospheric source.

Aliphatic hydrocarbons are further grouped into alkanes (only single covalent bonds), alkenes (containing at least one C−C double bond), and alkynes (containing at least one C−C triple bond). Ethane (C_2H_6) is globally the most abundant alkane and is impacted the most by biomass burning.

https://doi.org/10.5194/acp-21-11257-2021

Table 3. Absolute (Abs.) and relative (Rel.) changes in the tropospheric burden for each region and each species discussed. Regional differences are calculated for the main biomass burning season (see Table 2), and the global changes are calculated for the complete year of 2015. The units for the absolute differences are explicitly given, whereas relative changes are always given in percent (%). Most radical burdens are presented in moles (mol). The differences are calculated between simulation REF and FIR.

Species	Unit*	Global		ALA		CAF		CSA		NAS		NAU		SAF		SEA	
		Abs.	Rel.	Abs.	Rel.	Abs.	Rel.	Abs.	Rel.	Abs.	Rel.	Abs.	Rel.	Abs.	Rel.	Abs.	Rel.
Aliphatic hydrocarbons																	
Ethane	Gg	422.9	32.6	20.4	140.1	18.4	43.6	23.9	144.9	31.8	47.3	16.7	128.3	26.5	123.8	47.6	48.2
Propane	Gg	19.4	6.3	2.3	290.8	1.5	12.8	1.7	51.9	3.1	18.7	0.7	79.8	2.4	84.3	2.8	18.1
n-Butane	Mg	3727.4	2.4	470.4	242.7	256.1	6.0	336.3	16.9	671.3	8.6	86.3	33.2	324.9	34.9	779.6	9.4
Ethylene	Gg	13.5	12.5	2.0	103.5	2.9	59.9	3.6	9.2	2.2	46.3	0.8	26.4	4.5	81.5	8.3	85.3
Propene	Mg	3283.5	11.3	590.7	116.2	1021.5	83.4	863.5	5.4	560.7	54.3	279.5	34.5	1420.7	100.9	2304.0	83.6
Isobutene	Mg	107.1	20.2	36.2	7299.4	21.7	103.8	41.0	379.8	29.3	293.8	4.1	380.5	27.0	161.0	53.8	70.9
Acetylene	Gg	45.7	20.5	1.4	119.8	4.4	56.0	6.0	305.0	2.5	20.8	2.8	258.8	6.6	184.5	13.2	64.2
Aromatic hydrocarbons																	
Benzene	Gg	38.8	27.3	4.4	1312.7	2.7	46.4	4.3	368.2	5.9	84.2	1.9	498.1	4.6	228.7	20.0	207.7
Toluene	Mg	6655.3	15.3	802.6	1308.7	595.5	62.8	1007.7	85.0	968.2	62.0	175.9	198.2	950.0	199.0	10169.8	366.8
Styrene	Mg	56.2	29.8	42.8	11375.3	8.0	270.4	10.2	151.1	31.7	627.7	2.1	181.9	13.2	582.3	10.0	35.6
Ethylbenzene	Mg	2431.9	65.9	774.2	27408.4	421.5	958.0	351.8	470.8	820.3	592.5	139.2	1377.7	731.0	3203.8	237.3	75.4
OVOCs																	
Formaldehyde	Gg	25.4	2.2	3.6	35.1	5.4	11.7	5.3	2.2	3.4	12.6	1.6	3.9	8.4	17.7	17.9	15.9
Acetaldehyde	Gg	15.5	11.4	1.0	79.0	2.6	47.7	4.2	6.9	1.3	31.2	0.9	22.5	3.7	74.3	8.8	80.7
Glycolaldehyde	Gg	21.3	8.0	1.7	65.6	3.7	27.8	6.9	5.1	2.4	36.5	1.2	9.5	5.8	34.7	17.2	67.1
Methanol	Gg	223.3	7.9	11.7	31.6	17.0	16.8	31.5	6.6	18.8	16.2	14.4	17.5	27.4	28.5	112.3	60.7
Glyoxal	Mg	3872.3	9.3	388.7	126.2	633.0	24.5	591.5	3.9	397.3	38.6	240.1	12.7	1048.3	36.7	3186.1	62.2
Methylglyoxal	Mg	2481.7	1.3	208.1	17.4	438.9	4.1	206.5	0.2	212.4	6.9	144.4	1.3	743.4	5.8	2195.8	10.2
2,3-Butanedione	Mg	487.1	205.5	0.4	180.5	125.7	812.6	319.7	8060.4	1.0	21.0	6.4	960.4	94.2	2588.8	304.2	807.0
Phenol	Mg	1167.8	105.7	171.8	4282.2	179.1	316.4	275.7	1305.1	155.7	323.5	63.9	1353.8	277.1	1339.7	1400.3	1226.3
Benzaldehyde	Mg	282.1	14.6	102.9	4472.0	76.1	196.9	48.6	92.4	83.2	221.3	19.4	284.9	108.2	574.7	125.2	49.9
CO	Gg	8341.1	2.4	153.3	3.9	253.4	2.4	446.4	2.8	307.5	2.6	503.2	6.2	273.4	3.4	1908.0	6.5
Acids																	
Formic acid	Gg	32.9	4.9	1.5	24.0	7.0	25.2	5.8	4.7	2.1	12.9	3.2	13.0	11.4	49.9	11.3	20.7
Acetic acid	Gg	119.3	23.3	8.7	441.7	29.0	124.3	34.1	15.3	9.8	128.5	10.4	45.3	48.7	238.9	37.7	117.4
Oxidants																	
O_3	Gg	1115.3	0.3	92.0	1.9	61.6	0.7	−28.3	−0.3	104.7	0.7	2.0	0.0	60.4	0.8	83.2	0.4
OH	kmol	−240.3	−1.7	−6.4	−4.9	−8.5	−2.4	−15.9	−4.7	−10.8	−3.4	−21.6	−6.8	−10.3	−3.5	−58.2	−4.5
HO_2	kmol	3537.2	0.4	354.6	3.7	410.0	1.7	367.6	0.8	409.6	1.8	157.7	0.7	533.4	2.8	945.4	1.3
NO	Mmol	−82.3	−2.8	−38.4	−52.7	−5.9	−6.5	−5.7	−6.6	−26.0	−26.6	−6.8	−10.6	−6.4	−7.5	−22.0	−7.7
NO_2	Mmol	−178.5	−2.2	−73.5	−36.7	−16.3	−4.7	−14.2	−4.1	−60.1	−19.3	−13.0	−6.5	−18.8	−5.5	−70.5	−8.3
NO_3	kmol	6926.5	5.3	151.3	35.5	385.0	6.0	193.8	6.6	407.2	15.2	497.8	16.9	432.3	9.3	2368.5	15.5

* Unit for absolute values only. Relative values given in percent (%).

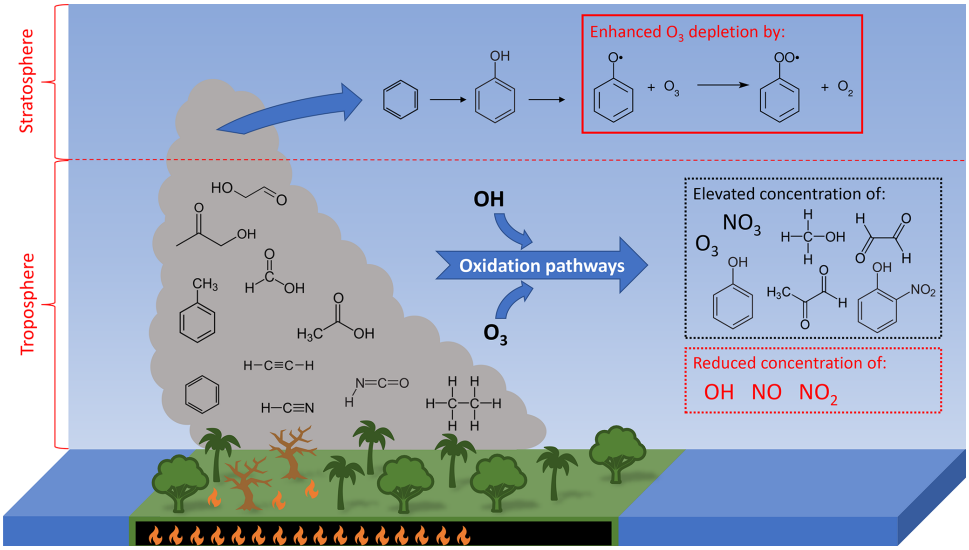

Figure 7. Illustration of the impact of VOC emissions from the Indonesian peatland fires on the atmospheric composition.

Its global burden is increased by 32.6 %, whereas the burden of less abundant alkanes like propane (C_3H_8) and *n*-butane (C_4H_{10}) only increases by 6.3 % and 2.4 %, respectively. Overall, the global change in the burden of alkenes is lower than that of alkanes. Here, ethylene (C_2H_4) has the highest absolute change of 13.5 Gg (12.5 %) followed by propene (C_3H_6) with 3.3 Gg (11.3 %). Even tough its abundance is the lowest, the highest global relative change of 20.2 % is predicted for isobutene (C_4H_8). In addition, EMAC predicts an increase of 20.5 % due to biomass burning emissions for the alkyne acetylene (C_2H_2). In general, the highest absolute change is predicted for SEA, except for propane since its burden increase is 0.3 Gg higher in NAS than in SEA. In both cases, the relative change is very similar. For many aliphatic hydrocarbons, the lowest absolute changes are predicted in ALA. However, due to the generally low background concentrations in this area, the relative changes are the highest, making biomass burning in this region the major source of these hydrocarbons.

The two most abundant aromatic hydrocarbons, benzene (C_6H_6) and toluene ($C_6H_5CH_3$), are strongly emitted by biomass burning events. In the FIR simulation, the tropospheric burden of benzene increases by 27.3 %. Toluene has a slightly lower increase of only 15.3 %. A higher relative impact is predicted for less abundant aromatics like ethylbenzene (C_8H_{10}) and styrene (C_8H_8). Here, the global burden changes by 65.9 % and 29.8 %, respectively. As it is for the aliphatic hydrocarbons, the highest absolute changes for benzene and toluene are predicted in SEA during the Indonesian peatland fires. Opposite to this, EMAC predicts the lowest change in SEA for ethylbenzene and styrene, which is related to the fact that EMAC uses significant lower emissions for both aromatic hydrocarbons for peatland when compared to the recent values reported by Andreae (2019).

5.2 Oxygenated organics

The degradation of aliphatic and aromatic hydrocarbons leads to the formation of oxygenated organic compounds. Additionally, they are emitted by biomass burning such as the Indonesian peatland fires. Globally, biomass burning has only a little impact on formaldehyde (HCHO), the simplest aldehyde (R−CHO). However, regional changes are predicted to be higher and range from 2.2 % to 35.1 %. The global and regional changes are higher for more complex aldehydes. The global burden of acetaldehyde (CH_3CHO) and glycolaldehyde ($HOCH_2CHO$) increases by 11.4 % and 8.0 %, respectively. In all cases, the highest absolute and relative change is predicted in SEA. The two α-dicarbonyls glyoxal (OCHCHO) and methylglyoxal ($CH_3C(O)CHO$) are primarily produced from VOC oxidation. Their global burden increases by 9.3 % and 1.3 %, respectively. Again, the highest absolute changes are predicted in SEA. However, the highest relative change occurs in ALA due to generally low background VOC concentrations. Globally, methanol (CH_3OH) increases by 7.9 % when biomass burning VOC emissions are taken into account. Here, the Indonesian peatland fires contribute by far the most. A significantly higher impact is predicted for 2,3-butanedione ($(CH_3CO)_2$). Its global burden is tripled due to biomass burning, and the absolute changes predicted regionally are the highest in NAS and SEA.

In the atmosphere, organic acids are mainly produced from the photo-oxidation of biogenic and anthropogenic VOCs but may also be emitted from biomass burning. Formic acid (HCOOH) is slightly impacted by biomass burning VOC emissions and globally increases by 4.9 % with the highest changes in SEA and Africa (CAF and SAF). The acid impacted the most by biomass burning is acetic acid (CH_3COOH), which globally gains 23.3 % with the highest changes in SEA, CAF, CSA, and SAF. Interestingly, the high increase predicted in CSA only leads to a low relative rise. This is due to generally high background concentrations in this region from high biogenic VOC emissions.

The largest change in oxygenated aromatics is predicted for phenol (C_6H_5OH), whose tropospheric burden is more than doubled and increases to 2.3 Gg. Even though phenol is directly emitted by biomass burning, the overall high aromatic emissions lead to an enhanced chemical production of phenol from benzene oxidation. The highest absolute change is observed in SEA. However, due to low aromatic background concentrations, the relative increase is higher in ALA, CSA, and NAU. The increase in benzaldehyde (C_6H_5CHO) is significantly lower (globally by 14.6 %) with similar absolute changes in ALA, CAF, NAS, SAF, and SEA.

The oxidation of VOCs leads to the formation of CO (see Sect. 4.2). Overall, the VOC emissions from biomass burning only result in a global CO increase of 2.4 %, with regional changes between 2.4 % and 6.5 %.

5.3 Nitrogen-containing compounds

Besides looking at HCN, we also analysed the impact of the Indonesian peatland fires on two nitrogen-bearing compounds that are toxic for humans (isocyanic acid) and for vegetation (nitrophenols). Isocyanic acid (HNCO) is known to be a toxic constituent of biomass burning emissions. It is linked to protein carbamylation, which causes adverse health effects such as rheumatoid arthritis, cardiovascular diseases, and cataracts (Wang et al., 2007; Roberts et al., 2011; Leslie et al., 2019). It is expected that the protein carbamylation potentially starts if humans are exposed to ambient concentrations above 1 ppb (Roberts et al., 2011). Rosanka et al. (2020a) already reported that HNCO concentrations are high in regions characterised by strong biomass burning events. Globally, similar high concentrations are predicted in this study. However, we predict higher concentrations in Indonesia than Rosanka et al. (2020a), who reported that ambient HNCO conditions of 1 ppb are exceeded for less than 30 d in Indonesia in 2011. The year 2011 is known to have low biomass burning emissions in this region (van der Werf et al., 2017). Figure 8 shows the number of days in which this threshold is exceeded during the 2015 Indonesian peatland fires between August and October. Here, 1 ppb of HNCO is regularly exceeded, and some regions are affected during the complete fire period. This causes potentially severe health effects for the population of Indonesia, which is the world's fourth highest (United Nations, 2019).

In the atmosphere, nitrophenols are mainly formed from the oxidation of the aromatic compounds benzene, toluene, phenols, and cresols (Nojima et al., 1975; Atkinson et al., 1980; Grosjean, 1984), of which the first three are emitted by biomass burning (see Sect. 5.1 and 5.2). Without biomass burning emissions of aromatics, the modelled nitrophenol concentrations are only high in regions with high anthropogenic activities (Fig. 9a). When biomass burning emissions of benzene, toluene, and phenols are included, nitrophenol concentrations significantly increase in areas affected by biomass burning. The strongest changes occur in SEA, CAF, and SAF (Fig. 9b). Many biomass burning regions frequently exceed nitrophenol thresholds that are determined for regions where anthropogenic aromatic emissions dominate. On a global scale, biomass burning becomes the main source of nitrophenols. Nitrophenols are known to have a high phytotoxic activity that is prolonged given their photochemical stability (Grosjean, 1991). Rippen et al. (1987) and Natangelo et al. (1999) suggested that nitrophenols could have contributed to the forest decline in northern and central Europe in the 1980s but also in other parts of the world. Therefore, the overall increase in nitrophenols in biomass burning areas is a potential danger for plants in these regions where plants are already under stressed conditions due to the biomass burning itself. At the same time, nitrophenols are known to absorb solar radiation (Hems and Abbatt, 2018) and therefore enhance hazy conditions in those areas (Lee et al., 2017), contributing to increased morbidity and mortality (Crippa et al., 2016).

5.4 Radicals

In general, organic molecules react with OH by either H abstraction or addition to double bonds, making OH the most important daytime VOC oxidant. Figure 10a gives the mean tropospheric surface OH concentration in 2015, and Fig. 10b presents the changes due to biomass burning VOC emissions. OH concentrations are significantly reduced in most regions with frequent biomass burning events. This reduction is caused by the direct reaction of OH with VOCs and the enhanced formation of CO from VOC degradation. The reduction in OH is not uniformly distributed and depends on the local chemical regime. In Indonesia, the high VOC emissions lead to the highest absolute and relative OH reduction. The enhanced oxidation of VOCs by OH leads to an overall increase in HO_2. In ALA and NAS, the most northern areas of interest, the absolute change in OH is low (see Table 3). Within the biomass burning plume, the enhanced HO_2 concentrations react with NO, producing OH and compensating for the OH reduction by VOC degradation, resulting in a regional surface OH increase. Still, outside the biomass burning plume, an overall decrease in OH is predicted in ALA and NAS. Here, VOCs from biomass burning become the highest

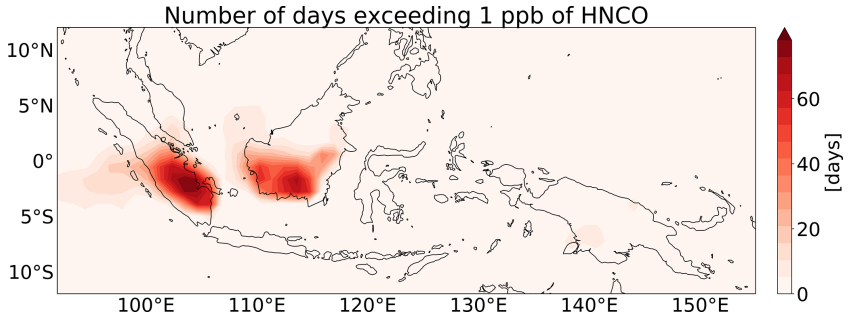

Figure 8. Number of days in which ambient concentrations of 1 ppb of HNCO are exceeded during the Indonesian peatland fires in 2015 between August and October.

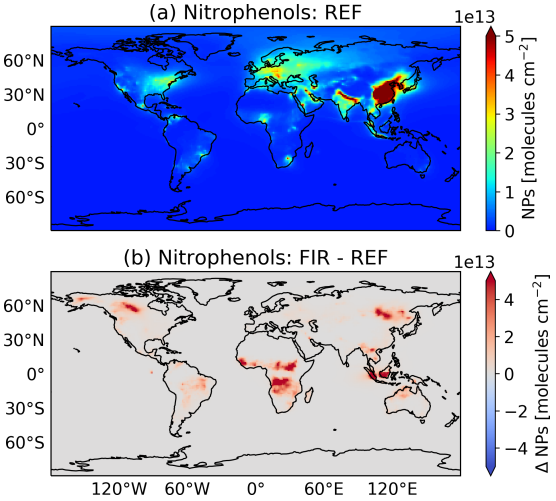

Figure 9. (a) Yearly mean tropospheric nitrophenol (NPs) column without biomass burning VOC emissions. **(b)** Changes in the yearly mean tropospheric nitrophenol (NPs) due to VOC biomass burning.

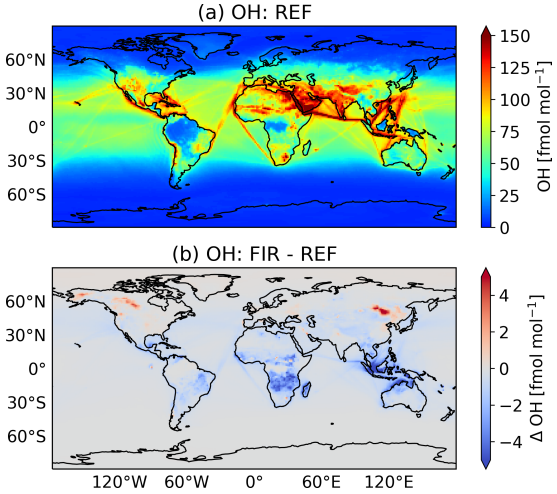

Figure 10. (a) Yearly mean surface OH concentration without biomass burning VOC emissions. **(b)** Changes in the yearly mean surface OH concentration due to VOC biomass burning.

OH sink, resulting in strong relative changes in OH reactivity. In general, OH reactivity is the highest in the Amazon basin ($100\,s^{-1}$) and the lowest in Antarctica ($0.5\,s^{-1}$). The additional VOC emissions in Indonesia result in a significant increase of about 50 % in the OH reactivity, which is similar to the increases predicted in ALA and NAS.

Figure 11a and b show the mean surface NO_x concentrations and the changes induced by the VOC biomass burning emissions, respectively. The additional VOC emissions significantly reduce the regional concentrations in tropospheric NO_x. In SEA, the absolute changes are large but small relatively (about 8 %), whereas the highest absolute and relative NO_x changes are predicted in ALA. These reductions are caused by enhanced reactions of RO_2 with NO_x, resulting in an increased formation of NO_x reservoir species (i.e. alkyl and acyl peroxy nitrates) and nitrogen-containing aromatics (e.g. nitrophenols).

NO_3 is the most important nighttime oxidant, which is globally increased by about 5 % when the biomass burning emissions of VOCs are included (see Table 3). On the one hand, the formation of NO_3 is enhanced by aromatic RO_2 reacting with NO_2, but on the other hand the loss of NO_3 by reactions with RO_2 and aldehydes is increased. In the two northern regions (ALA and NAS), the elevated O_3 and regionally increased NO_2 concentrations induce an enhanced formation from inorganic reactions, resulting in an additional rise of NO_3. The absolute increase in NO_3 is high in SEA, especially in Indonesia. Here, the particularly large increase in phenols results in enhanced concentrations of phenyl peroxy radicals ($C_6H_5O_2$), which form NO_3 when reacting with

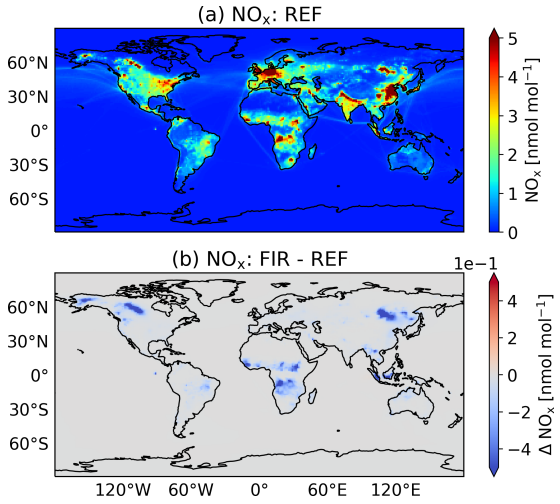

Figure 11. **(a)** Yearly mean surface NO_x concentration without biomass burning VOC emissions. **(b)** Changes in the yearly mean surface NO_x concentration due to VOC biomass burning.

NO_2 following Jagiella and Zabel (2007):

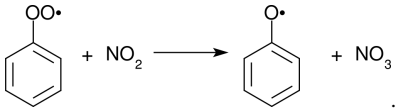

(R1)

Taraborrelli et al. (2021) recently studied the importance of aromatics on the atmospheric composition on a global scale. They also demonstrated the importance of this reaction but, in opposition to our findings, predicted a reduction of NO_3 in Indonesia. Taraborrelli et al. (2021) used a different resolution and analysed 2010, a year with little biomass burning emissions in Indonesia (van der Werf et al., 2017), reducing the importance of this production channel.

5.5 Ozone

The perturbed NO_x–HO_x relation consequently leads to changes in tropospheric O_3. Overall, EMAC predicts an enhanced formation of O_3 when the biomass burning emissions are included (see Table 3). The increase in HO_2 leads to an enhanced chemical O_3 production by reacting with NO. Due to high NO_x emissions from biomass burning, the O_3 production is to a large extent VOC-limited. In the two northern regions, the background VOC concentrations are low, resulting in the highest relative changes of more than 10 %. Based on the long-term simulations (REF_{LONG} and FIR_{LONG}) we find that the largest changes are predicted in the NH high latitudes in 2003, a year with intense biomass burning in boreal Asia (van der Werf et al., 2017). However, compared to the averaged tropospheric background O_3 concentrations, these changes are negligible on a global scale. As described in Sect. 4, most VOC emissions from Indonesia are transported towards the Indian Ocean. Therefore, O_3 is predicted to increase in Sumatra and west of it. Interestingly, away from biomass burning emissions in Kalimantan and in east Indonesia, O_3 concentrations are slightly reduced, even though the chemical O_3 production still increases in this area. The particularly strong emissions of aromatics lead to enhanced concentrations of phenoxy radicals (C_6H_5O), which directly destroy O_3 (Tao and Li, 1999) in lower NO_x regions:

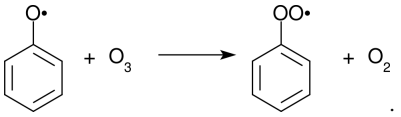

(R2)

This O_3 sink increases by 780 %, resulting in a net loss of O_3 in these areas. Globally, this O_3 destruction channel increases from 144.9 to 200.1 Tg a^{-1} in the troposphere. Also, Taraborrelli et al. (2021) reported a similar strength of this destruction channel of about 200 Tg a^{-1}. Therefore, biomass burning emissions regionally control the importance of this destruction channel.

6 The influence of Indonesian peatland fires on the UTLS

As illustrated in Fig. 7, some of the biomass burning VOC emissions from Indonesia are quickly transported by the ASMA and the general tropical updraught into the UTLS (see Sect. 1 and Vogel et al., 2015). In the following, we define the lower stratosphere between 147–32 hPa (about 13–24 km) above 30° in latitudinal direction and between 100–32 hPa (about 17–24 km) below 30° latitude. In Table 4, the lower stratospheric burden in November for each discussed species is presented, including the changes induced by biomass burning and the contribution from the Indonesian peatland fires.

6.1 Hydrocarbons

Even though their atmospheric lifetime is generally short, the upward transport in the tropics leads to an increase in hydrocarbons in the lower stratosphere due to biomass burning. Similar to the changes in the troposphere, the aliphatic hydrocarbon with the highest absolute change is ethane. The lower stratospheric burden in November increases by about 41 % to 43.56 Gg. The lower stratospheric burden of other aliphatic hydrocarbons like propane and *n*-butane changes by around 30 %. The lower stratospheric burden of benzene is tripled, whereas toluene is doubled, which is consistent with the difference between their chemical lifetimes. The contribution of the Indonesian peatland fires for most hydrocarbons ranges between 69 % and 87 %, except ethane. We expect that additional non-Indonesian fires from SEA contribute the rest,

Table 4. Stratospheric burden in November 2015 and changes induced by VOC biomass burning emissions. In addition, the relative difference (Rel.) and the Indonesian contribution (Indo. contr.) are shown. The latter is calculated based on the difference of FIR and FIR_{NOINDO}.

Species	Unit	REF	ΔFIR	Rel. [%]	Indo. contr. [%]
Ethane	Gg	30.8	43.6	41.6	24.1
Propane	Mg	666.3	855.9	28.5	69.1
n-Butane	Mg	116.2	152.2	31.0	80.0
Benzene	Mg	242.1	724.2	199.2	87.2
Methanol	Gg	17.1	22.9	34.0	76.0
Glyoxal	Mg	9.8	14.7	48.9	69.4
Phenol	kg	629.8	1685.6	167.7	85.8
Acetic acid	Mg	289.4	473.6	63.7	72.6
HCN	Gg	16.7	53.5	220.4	62.6
Nitrophenols	Mg	14.7	23.6	60.2	69.5
OH	Mmol	3.8	-0.1	-3.2	70.2
NO	Gmol	1.9	-0.1	-6.1	67.7
NO_2	Gmol	3.6	-0.2	-4.2	66.2
NO_3	Mmol	10.3	1.0	9.5	74.7
HO_2	Mmol	24.1	0.6	2.4	63.9

since the Indonesian peatland fires contribute about 76 % to the total biomass burning emissions from SEA in 2015. In the case of ethane, the contribution from the Indonesian peatland fires is only about 24 %. Compared to other hydrocarbons, ethane has an atmospheric lifetime of about 2 months (Hodnebrog et al., 2018). Thus, we expect that its long lifetime allows ethane emitted from other biomass burning regions to be transported into the lower stratosphere. At the same time, the recent biomass burning inventory by Andreae (2019) indicates that EMAC underestimates ethane emissions from the Indonesian peatland fires by a factor of 3.

6.2 Oxygenated organics

In addition to the upward transport of the directly emitted OVOCs, the elevated hydrocarbon concentrations also form OVOCs in the lower stratosphere. In the lower stratosphere, methanol is one of the most abundant OVOCs, and its burden increases by 34 %. EMAC predicts a higher relative increase for less abundant OVOCs like glyoxal (about 49 %) and acetic acid (about 64 %). The high increase in benzene, due to the strong aromatic emissions from the Indonesian peatland fires (see Sect. 3), results in the particularly large production of phenol. Here, the lower stratospheric burden increases by about 167 %. The contribution from the Indonesian peatland fires to the lower stratospheric burden of all OVOCs is in a similar range as for the hydrocarbons, namely from about 72 % to 86 %.

6.3 Nitrogen-containing compounds

The Indonesian peatland fires resulted in substantial HCN emissions, as seen in Fig. 4 and as discussed in Sect. 4.1, which results in a strong increase in HCN in the lower stratosphere. Here, EMAC predicts an increase of more than 36 Gg (about 220 %). Sheese et al. (2017) report that the highest increase on record in lower stratospheric HCN was observed by the Atmospheric Chemistry Experiment Fourier transform spectrometer (ACE-FTS) instrument on the SCISAT satellite following the 2015 Indonesian peatland fires. Therefore, based on the long-term simulations (simulation REF_{LONG} and FIR_{LONG}), EMAC reproduces their findings. The elevated lower stratospheric benzene and toluene concentrations lead to an increase in lower stratospheric nitrophenol concentrations of about 60 %.

6.4 Radicals

The oxidation of VOCs transported into the lower stratosphere influences the lower stratospheric oxidation capacity. Overall, the lower stratospheric OH burden is reduced by about 3 %, whereas the burden of HO_2 increases by 2.4 % (see Table 4). The enhanced formation of NO_x reservoir species results in a 6 % and 4.2 % reduction of NO and NO_2, respectively. At the same time, the enhanced reactions of NO_2 with aromatic RO_2 results in an increase in NO_3 of more than 9 %. Figure 12 provides the mean longitudinal relative change in lower stratospheric OH, HO_2, NO_x, and NO_3 between 2001 and 2016 based on the long-term simulations (simulation REF_{LONG} and FIR_{LONG}). After each Indonesian peatland fire period, the lower stratospheric oxidants are influenced. With decreasing lower stratospheric VOC concentrations over time, the influence on the oxidants vanishes in the second half of the following year. Particularly strong influences are observed during El Niño periods, caused by enhanced VOC emissions from peatland fires. For example, intense fires in 2006 and 2015 led to a significant change in lower stratospheric oxidants in early 2007 and 2016, respectively. In 2010, almost no fires occurred in Indonesia (van der Werf et al., 2017), resulting in only a little change in oxidant

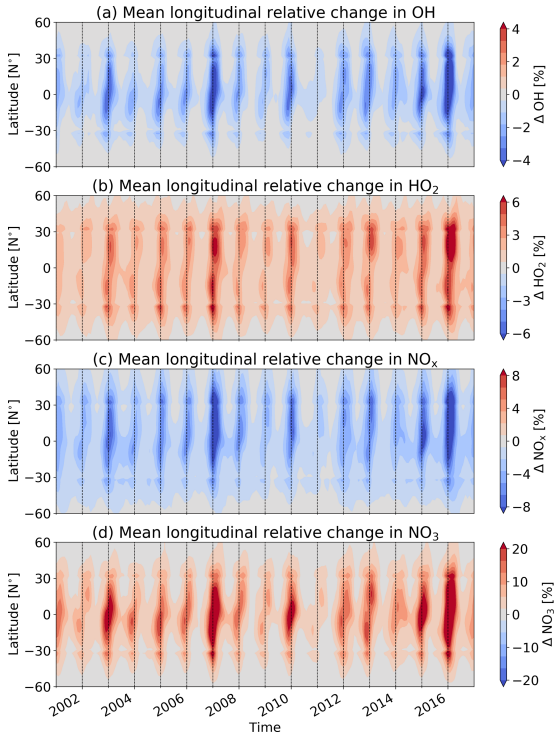

Figure 12. The mean longitudinal relative change in lower stratospheric **(a)** OH, **(b)** HO_2, **(c)** NO_x, and **(d)** NO_3 between 2001 and 2016. Results are based on both long-term simulations (simulation REF_{LONG} and FIR_{LONG}). The lower stratosphere is defined between 147–32 hPa (about 13–24 km) above 30° in latitudinal direction and between 100–32 hPa (about 17–24 km) below 30° latitude.

concentrations in 2011. Even in non-El Niño years, EMAC predicts changes in lower stratospheric radicals due to VOC biomass burning emissions. We expect that these originate from other biomass burning events in SEA (see Sect. 6.1). In each year, the highest influence is predicted for NO_3. Following the intense fires of 2002, 2006, 2009, 2014, and 2015 the zonal mean NO_3 concentration changes by more than 20 % in the tropical and subtropical lower stratosphere at the end of the same year and at the beginning of the next year. Thus, our findings indicate that VOC emissions from the Indonesian peatland fires quickly transported into the lower stratosphere become a major source of lower stratospheric NO_3.

6.5 Ozone

The elevated phenol and consequently phenoxy radicals in the UTLS influence the importance of the O_3 loss due to reaction with phenoxy radicals (Reaction R2). In the upper tropical troposphere this loss process contributes significantly to the total chemical O_3 loss. Figure 13a shows the zonal mean in the relative contribution of this O_3 loss pathway to the total chemical O_3 loss without VOC biomass burning emissions in November 2015. Especially in the upper northern tropical troposphere, this loss process contributes up to 40 % to the total chemical O_3 loss. Following the benzene emissions from biomass burning, elevated phenoxy radicals in the UTLS double the contribution of this O_3 loss processes in the upper southern tropical troposphere (i.e. an increase of more than 20 %) and increase the contribution in the upper northern tropical troposphere by about 10 % in November 2015 (see Fig. 13b). A similar impact can be observed following other intense Indonesian biomass burning seasons. Figure 13c shows the zonal mean change in the relative contribution of this O_3 loss pathway in the UTLS between 2001 and 2016. Here, we define the UTLS from 250 to 50 hPa above the tropopause calculated by EMAC. Especially after the intense Indonesian peatland fires during strong El Niño periods, a change in the upper southern tropical UTLS of more than 10 % is predicted at the end of each year. In all years, the increase in the upper northern tropical UTLS is lower. Figure 14 shows the zonal mean relative change in the phenoxy radical O_3 loss pathway due to VOC biomass burning in April 2016. Following the increase in benzene in the lower stratosphere (Sect. 6.1), EMAC predicts an increase in this O_3 loss process by more than 400 %, which propagates into the upper tropical lower stratosphere. These findings suggest that the frequent re-occurrence of strong Indonesian peatland fires could contribute to the variability in lower stratospheric O_3 which is observed by remote sensing measurements (Kyrölä et al., 2013; Nair et al., 2015; Vigouroux et al., 2015; Chipperfield et al., 2018).

In the UTLS, aviation is the only direct anthropogenic activity and contributes about 3.5 % to the total anthropogenic climate change (Lee et al., 2021). Here, aviation NO_x emissions lead to a formation of O_3 and a depletion of methane (CH_4). Recently, Rosanka et al. (2020b) showed that the enhancement in O_3 is limited by the background concentrations of NO_x and HO_x. If enough HO_x is available, a lower background NO_x concentration results in a higher O_3 gain. In general, low background HO_x concentrations limit the O_3 gain in winter. In our study, we find (not shown) that in the North Atlantic flight sector (between 400–100 hPa), the NO_x burden is reduced due to VOC emissions from SEA fires by about 6 %, with regional changes of more than 20 % in 2015. At the same time, HO_x increases regionally by 10 %. Even though NO_x emissions from the frequently occurring Indonesian peatland fires are expected to result in an increase in UTLS NO_x, substantial VOC emissions from the same fires potentially compensate for the impact of the NO_x increase and favour the formation of O_3 from aviation activities. In the simulation setup used, EMAC neglects VOC emissions reported from aviation activity (e.g. Wilkerson et al., 2010). Our findings indicate that the direct emissions of benzene, toluene, and phenol in the UTLS potentially enhance the loss

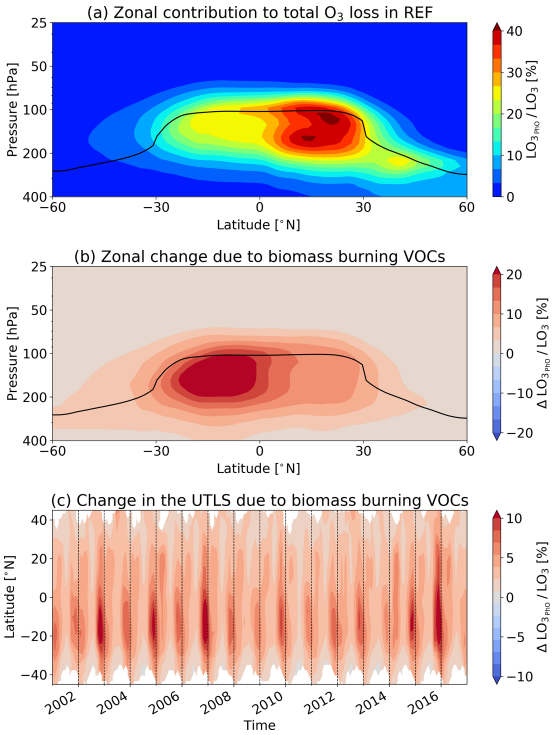

Figure 13. Zonal mean contribution of the destruction of O_3 by phenoxy radicals (Reaction R2) to the total chemical O_3 loss. **(a)** Relative contribution if no VOC biomass burning emissions are taken into account (REF) in November 2015. **(b)** Changes in the relative contribution due to VOC biomass burning emissions (FIR) in November 2015. **(c)** Changes in the relative contribution due to VOC biomass burning emissions in the UTLS. Here, we define the UTLS from 250 to 50 hPa above the tropopause calculated by EMAC. The tropopause pressure level in panels **(a)** and **(b)** is indicated in black.

of O_3 by phenoxy radicals and consequently affect the impact of aviation on O_3 in that region.

7 The influence of in-cloud OVOC oxidation

Recently, Rosanka et al. (2021a) showed that the in-cloud oxidation of OVOCs significantly influences tropospheric VOCs and oxidants. By using JAMOC (Rosanka et al., 2021b, a), we investigate the importance of in-cloud OVOC oxidation during the Indonesian peatland fires on the troposphere and lower stratosphere (simulations REF_{JAMOC} and FIR_{JAMOC}). In order to isolate the influence of the Indonesian peatland fires from the background changes induced by JAMOC, the changes from the Indonesian fires due to the

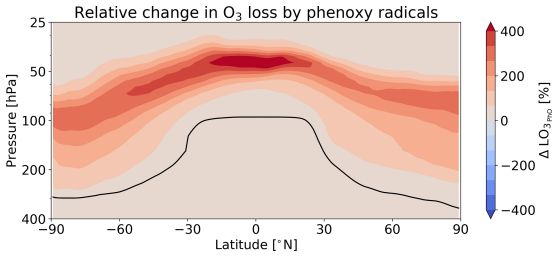

Figure 14. Zonal mean relative change in the destruction of O_3 by phenoxy radicals (Reaction R2) due to VOC biomass burning emissions (FIR vs. REF) in April 2016. The tropopause pressure level is indicated in black.

in-cloud OVOC oxidation are calculated following

$$\Delta JAMOC = (FIR_{JAMOC} - FIR) - (REF_{JAMOC} - REF). \quad (1)$$

7.1 On the lower troposphere

Figure 15 shows the changes in the zonal mean concentration over Indonesia and the Indian Ocean of all OVOCs explicitly reacting in JAMOC ($\sum$OVOCs; see Eq. B1 in Appendix B) for the simulations without JAMOC (Fig. 15a) and the predicted changes due to JAMOC (Fig. 15b; calculated using Eq. 1), focusing on the Indonesian fire period (SON). Due to the high solubility of many OVOCs and their in-cloud oxidation, their concentration is strongly reduced at altitudes that are characterised by frequent cloud events. Table 5 provides the SEA burden changes for a selection of species that are represented in JAMOC. Overall, the additional in-cloud sink results in a more limited increase in their predicted burden (e.g. only about 87.9 Gg instead of 112.3 Gg for methanol). However, their predicted burden in the reference simulation (REF_{JAMOC}) is also significantly lower, which results in a relative change which is of a similar order as if no in-cloud OVOC oxidation were taken into account.

Figure 16 shows the probability density function (PDF) for EMAC's methanol column bias when compared to IASI satellite retrievals (Franco et al., 2018) in SEA during the Indonesian peatland fires. Without VOC emissions from biomass burning, methanol is slightly underestimated by simulation REF. This underestimation is more pronounced when the in-cloud oxidation of OVOCs is taken into account (simulation REF_{JAMOC}). In both cases, EMAC tends to strongly underestimate methanol in some regions. When VOC biomass burning emissions are taken into account (simulation FIR), these underpredictions are resolved. However, now EMAC tends to strongly overestimate methanol mainly close to biomass burning sources (not shown). These overpredictions are reduced once in-cloud OVOC oxidation is implemented (simulation FIR_{JAMOC}). A high fraction of SEA is

Table 5. The SEA tropospheric burden during the Indonesian fire period with and without VOC biomass burning emissions of OVOCs explicitly reacting in JAMOC. The tropospheric burden is given in gigagrams (Gg).

Species	REF	ΔFIR	Rel. [%]	REF_{JAMOC}	$ΔFIR_{JAMOC}$	Rel. [%]
Methanol	185.2	112.3	60.7	133.8	87.9	65.7
Methyl hydroperoxide	140.8	10.7	7.6	71.7	4.0	5.6
Hydroxymethylhydroperoxide	5.0	1.0	20.2	3.4	0.6	17.0
Ethanol	9.1	1.0	10.5	7.1	0.8	11.5
Ethylene glycol	0.2	0.2	73.6	0.1	0.1	70.1
Glycolaldehyde	25.6	17.2	67.1	13.2	10.6	80.8
1-Hydroperoxyacetone	4.7	0.7	14.5	2.4	0.3	13.2
Methylglyoxal	21.5	2.2	10.2	15.5	1.7	10.9
Isopropyl hydroperoxide	0.8	0.1	18.1	0.4	0.1	17.3

covered by oceans. Millet et al. (2008) suggested that some regions of the Pacific and Indian Ocean are a net source of methanol. As discussed by Rosanka et al. (2021a), EMAC represents the ocean as a net methanol sink. Therefore, when comparing the predictions of methanol from EMAC to satellite observations, a certain underestimation is expected. Thus, simulation FIR_{JAMOC} compares the best with IASI retrievals, since it has overall the lowest relative biases.

Changes in hydrocarbons are minimal due to their low solubility, whereas strong changes are predicted for the relatively insoluble O_3. Due to in-cloud OVOC oxidation, the initially predicted increase in O_3 in western Indonesia and over the Indian Ocean (Sect. 5.4) is dampened by more than 60 % once JAMOC is implemented. This limited increase is caused by the importance of clouds as an O_3 sink. This process is globally analysed by Rosanka et al. (2021a) and is based on the enhanced HO_2 formation in cloud droplets by OVOC oxidation. Within clouds, HO_2 is in acid equilibrium with the superoxide anion (O_2^-), which actively destroys O_3.

7.2 On the lower stratosphere

As seen in Fig. 15b, the in-cloud OVOC oxidation leads to the reduction of their concentrations in the UTLS. Table 6 presents the lower stratospheric burden changes in November due to JAMOC. Overall, the in-cloud oxidation of the OVOCs leads to a more limited increase in their concentration in the lower stratospheric burden induced by the biomass burning emissions. For example, the increase in the methanol burden is limited to 2.6 Gg (instead of 5.8 Gg). In the case of ethylene glycol ($HOCH_2CH_2OH$), the lower stratospheric burden decreases even by about 85 % when JAMOC is used, with and without VOC biomass burning emissions taken into account. Similarly to the changes in the lower stratosphere, the relative change for the simulation using JAMOC is of a similar order as for the simulation without VOC biomass burning emissions but tends to be slightly lower for some OVOCs. This is especially the case for isopropyl hydroperoxide ($(CH_3)_2CHOOH$), which is lower by about 23 %. The increase in the lower stratospheric phenol concentrations is

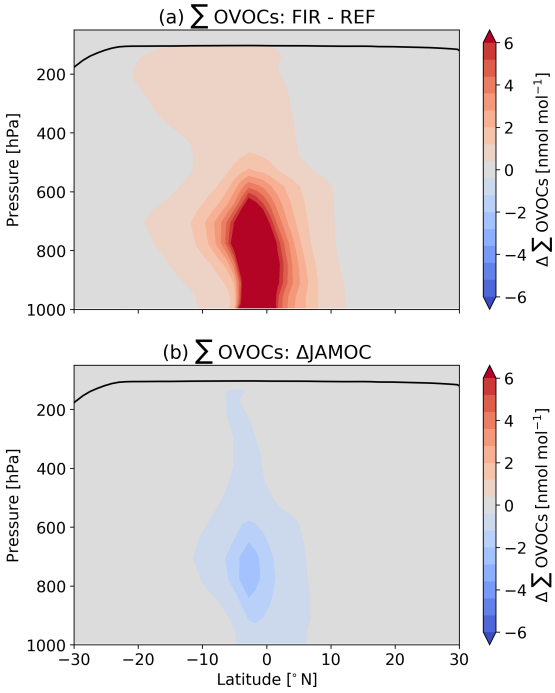

Figure 15. Mean zonal change in the sum of all OVOCs explicitly reacting in JAMOC (∑OVOCs; see Eq. B1 in Appendix B) over Indonesia and the Indian Ocean during the 2015 Indonesian fire period (SON). **(a)** Changes due to VOC biomass burning emissions (difference between simulation FIR and REF) and **(b)** changes due to JAMOC (ΔJAMOC).

only slightly impacted and decrease by about 13 % (from 167 % originally; see Table 4) and thus has only little impact on the destruction of O_3 by phenoxy radicals. This is consistent with the main source of phenol being the oxidation of benzene, which has a lifetime of the order of 1–2 weeks.

Table 6. The lower stratospheric burden in November with and without VOC biomass burning emissions of OVOCs explicitly reacting in JAMOC. The stratospheric burden is given in megagrams (Mg).

Species	REF	ΔFIR	Rel. [%]	REF_{JAMOC}	$ΔFIR_{JAMOC}$	Rel. [%]
Methanol	17 097.9	5821.0	34.1	10 102.3	2634.3	26.1
Methyl hydroperoxide	637.9	55.5	8.7	562.1	28.3	5.0
Hydroxy methyl hydroperoxide	60.6	12.1	20.0	49.2	6.2	12.6
Ethanol	45.4	15.5	34.2	24.2	5.5	22.6
Ethylene glycol	0.6	0.2	38.5	0.1	0.03	31.0
Glycolaldehyde	84.2	16.4	19.5	54.3	11.7	21.6
1-Hydroperoxyacetone	10.8	3.9	35.6	6.0	1.8	29.6
Methylglyoxal	6.6	0.3	5.1	3.5	0.2	5.6
Isopropyl hydroperoxide	2.6	1.9	72.5	2.1	1.0	49.1

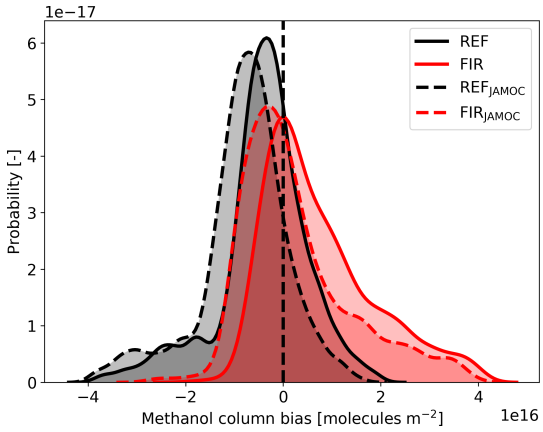

Figure 16. Probability density function of EMAC's methanol column bias compared to the IASI satellite measurements for simulation REF, FIR, REF_{JAMOC}, and FIR_{JAMOC} in SEA during the 2015 Indonesian peatland fires.

To conclude, in-cloud OVOC oxidation is important to properly represent the resulting impacts from strong pollution events especially during the monsoon season. Overall, the predicted impact on VOCs, radicals, and O_3 is dampened by the in-cloud oxidation and models neglecting this process probably tend to overestimate the impact of such an event. It is widely recognised that clouds may act as a source of secondary organic aerosols (SOAs) due to in-cloud oxidation processes (Blando and Turpin, 2000; Ervens et al., 2011; Ervens, 2015). Ervens et al. (2011) suggested that cloud processes might contribute to SOA formation on the same order as gas-phase processes. Within this study, SOA formation from cloud processes is not explicitly represented. However, it is expected that the enhanced VOC concentrations from biomass burning will lead to an increased SOA formation from aqueous-phase processes due to the enhanced formation of oligomers (e.g. from glyoxal and methylglyoxal) within clouds.

8 Model uncertainties

The most important aspects that influence our results are the representation of the transport processes, using different model resolutions, and the chemical kinetics. Each aspect is associated with some uncertainties, which are all shortly discussed in this section.

The magnitude of the changes in the lower stratospheric composition depends closely on the representation of the vertical transport that conveys the emitted VOCs into the UTLS. In order to evaluate the vertical transport processes of global models, ^{222}Radon (^{222}Rn, radioactive decay half-life of 3.8 d) is typically used (Mahowald et al., 1997; Zhang et al., 2008; Jöckel et al., 2010). Jöckel et al. (2010) and more recently Brinkop and Jöckel (2019) analysed the ability of EMAC to capture the ^{222}Rn surface concentrations and vertical profiles. Their findings indicate that the vertical transport is well represented in EMAC (using the T42L90MA resolution) and that they are comparable to the earlier analysis with ECHAM5 (the base model of EMAC) by Zhang et al. (2008). Figure 4 shows that the horizontal transport is also an important aspect that influences the distribution of the emitted VOCs from Indonesian peatland fires. Evaluating the horizontal transport using observations (like ^{222}Rn) is currently not possible. Recently however, Orbe et al. (2018) compared transport timescales of various global models, including EMAC. They found that the horizontal transport from NH mid-latitudes to the tropics differs by 30 %. Based on this comparison, it can be assumed that the horizontal transport is reasonably well represented in EMAC.

In this study, we transfer our process understanding from the fine-resolution (T106L90MA) to the coarse-resolution (T42L90MA) simulations. It is therefore important to understand how well transport processes agree between both resolutions. Currently, no direct analysis has been performed that focuses on the impact of different resolutions on transport processes in EMAC. However, Aghedo et al. (2010) analysed the influence of different horizontal and vertical resolutions in ECHAM5. Since EMAC uses the same horizontal and vertical transport scheme as ECHAM5, we assume that

their findings also apply to EMAC. They find that the vertical transport mainly depends on the number of levels used. By increasing the number of layers from 19 to 31 levels, the mass transported into the stratosphere reduces globally by about 36 %, whereas increasing the resolution from T42 to T106 only decreases the vertically transported mass globally by about 10 %. Here, the influence is the lowest (about 7 %) at high latitudes and the highest in the tropics (about 17 %). Aghedo et al. (2010) suggested that the higher impact in the tropics is probably related to tropical convection processes. Increasing the resolution changes the meridional transport in most regions by less than 2 % and is thus negligible. For our purposes, differences in the inter-hemispheric transport are also negligible. The mean transport time from the NH to SH decreases from 11.9 to 11.8 months and for the SH to NH transport from 11.4 to 11.5 months when increasing the horizontal resolution from T42 to T106. By using the same vertical resolution (90 levels), the highest uncertainty introduced by using different resolutions is eliminated. It is therefore expected that the important transport processes are comparable and properly represented in both resolutions.

We find that the reaction of phenoxy radicals with O_3 (Reaction R2) has a significant influence at the surface, in the troposphere, and in the lower stratosphere. As discussed by Taraborrelli et al. (2021), the chemical kinetics used in MOM to represent this O_3 loss is associated with some uncertainties. Currently, only the measured reaction rate constant for C_6H_5O is available, and this is used for all phenoxy radicals. Yet, no experimental evidence has been found for the formation of phenyl peroxy radical ($C_6H_5O_2$), which might influence the cycling nature of this O_3 loss by Reactions (R1) and (R2). However, this product is still to be expected. Even with different products, a significant depletion of O_3 is anticipated by Reaction (R2). At the same time, the reaction rate from Tao and Li (1999) is reported to be at the lower end, whereas a higher reaction rate would increase the depleted O_3. Additionally, Taraborrelli et al. (2021) report that MOM neglects the non-HONO formation channel from nitrophenol photolysis, which does not destroy the aromatic ring and reforms phenoxy radicals (Cheng et al., 2009; Vereecken et al., 2016). It is therefore expected that, due to increasing nitrophenol concentrations in the lower troposphere (Sect. 5.3) as well as in the UTLS, the importance of Reaction (R2) as an O_3 sink is potentially underestimated.

9 Conclusions

In this study, the influence of VOC emissions from reoccurring Indonesian peatland fires is analysed with the main focus on 2015, a particularly strong year. This is achieved by performing multiple global simulations using EMAC. By comparing EMAC's prediction of HCN and CO columns to IASI satellite retrievals, we show that EMAC properly represents the emissions from the Indonesian peatland fires and global biomass burning events.

Our results indicate that VOC emissions from biomass burning are important to reproduce hydrocarbons and secondary OVOCs in the atmosphere. Compared to other biomass burning regions, a particularly strong increase is modelled in the SEA region, due to the unique emission footprint from the Indonesian peatland fires. The enhanced formation of nitrophenols and strong HNCO emissions create toxic conditions in most parts of Indonesia, directly influencing its population. Regionally, significant changes in radical concentrations (HO_x and NO_x) are predicted. In general, O_3 increases in the lower troposphere with the highest changes in the NH high latitudes due to strong fires in boreal Asia. However, on a global scale, tropospheric changes in O_3 are negligible. High aromatic emissions from peatland fires lead to a depletion of O_3 in eastern Indonesia.

The ongoing ASMA and the general tropical upward transport during the Indonesian fires lift the emitted VOCs and their oxidation products quickly to the lower stratosphere. Here, especially large increases are predicted for levels of the aromatic compounds benzene and toluene. The oxidation of VOCs results in the reduction of OH and NO_x and the increase in HO_2. Additionally, the Indonesian fires becomes a major source of lower stratospheric NO_3. Indonesian fires enhance the O_3 destruction by phenoxy radicals by up to 20 % in the southern tropical UTLS. This chemical loss propagates into the lower stratosphere and potentially influences the variability of O_3 retrieved from satellite observations. Overall, the highest changes in lower stratospheric radicals during the period between 2001 to 2016 are predicted for particularly strong El Niño years, due to strong Indonesian peatland fires.

The overall impact of Indonesian fires on the composition of the troposphere and lower stratosphere is reduced when in-cloud OVOC oxidation is taken into account. In particular, the predicted O_3 increase in the troposphere is dampened due to enhanced destruction of O_3 within clouds. This suggests that models neglecting the in-cloud oxidation of OVOCs probably tend to overestimate the impact of such an event like the Indonesian peatland fires.

Appendix A: HCN retrievals from IASI observations

The spaceborne data of HCN columns used in this study are obtained from the IASI radiance spectra by applying the version 3 of the Artificial Neural Network for IASI (ANNI) retrieval framework. Initially developed for the retrieval of NH_3 and dust from the IASI observations (Whitburn et al., 2016a; Clarisse et al., 2019), ANNI v3 incorporates updates and modifications to allow the retrieval of a suite of VOCs. Until now, it has been used to retrieve methanol, formic acid, and PAN (Franco et al., 2018) and then acetone (Franco et al., 2019) and acetic acid (Franco et al., 2020). Here, we perform the HCN retrieval by applying the full ANNI v3 procedure. As this approach has already been described in detail (see Franco et al., 2018, and references therein), we limit ourselves here to a summary of the main retrieval steps and to the elements specific to the retrieval of HCN. Examples of HCN columns from IASI single overpasses in the 2015 Indonesian fire plumes and averaged distributions are also presented.

As mentioned in Sect. 2.1.3, the ANNI retrieval method proceeds in two major steps. First, in each individual IASI radiance spectrum, the target species is detected and the strength of its absorption is quantified by a metric called the hyperspectral range index (HRI). Then, the HRI is converted into a gas total column by means of an artificial feedforward neural network (NN), which also provides an uncertainty on the retrieved column.

The HRI is a dimensionless metric of the magnitude of the spectral signature of a target species in a given IASI spectrum, relative to the spectral variability of a "background" atmosphere in the absence of the target gas, i.e. a variability resulting from all other parameters that contribute to the spectral radiance, such as other atmospheric gases (see Walker et al., 2011). The HRI is calculated over the main spectral range, in which the target species absorbs. The HCN absorption band (ν_2 branch) included in the IASI spectrum is situated close to a strong Q branch of CO_2 near 720 cm^{-1}. Therefore, the whole 700–800 cm^{-1} spectral range covering many HCN features is used to calculate the HRI. The CO_2 line mixing in that range is accounted for as described by Duflot et al. (2013). A first HRI of HCN was already set up for the IASI observations by Duflot et al. (2015), but here we set up a new more sensitive one following the iterative procedure presented by Franco et al. (2018).

In contrast to Duflot et al. (2015), who used pre-calculated coefficients to link the HRI to the HCN total column, the ANNI v3 procedure implements an artificial feedforward NN for this purpose. Such a NN is set up to mimic in a comprehensive way the complex connections that exist between the HRI, the state of the atmosphere and Earth's surface, and the gas abundance. Setting up a NN requires a training phase in which the NN learns from the presentation of an extensive dataset including all the necessary input and output variables. In ANNI v3, the NN inputs are the HRI, a spectral baseline temperature, the H_2O columns, the temperature profile, the surface pressure and emissivity, and the IASI viewing angle, whereas the output is the HCN column. Here, we built this training set from over 250 000 synthetic IASI spectra simulated by a line-by-line radiative transfer model. The advantage of such a synthetic training set is that it is free of the noise and/or scarcity of real measurements and that the spectra can be generated in large amounts in order to make the training set – and hence the NN – representative of all possible conditions. For example, the NN set up for HCN is trained to retrieve gas column from 1×10^{14} to 15×10^{16} molecules cm^{-2}. Actually, two separate synthetic datasets are assembled per target species, one being representative of conditions close to emission sources and the other of mixing/transport conditions (see Whitburn et al., 2016a; Franco et al., 2018, for the rationale). Each training set leads to the setup of a specific NN that is used to globally retrieve the target species in emission or transport regimes, successively. The training performances are similar to those of the other VOCs retrieved with ANNI v3 and are reached with a NN made of two computational layers, with each layer deploying eight nodes.

In addition to the total column, the NN returns an associated error that is calculated via a perturbation method of the input variables (see Whitburn et al., 2016a). A pre-filter prevents the retrieval on cloudy scenes (cloud coverage > 10 %) or for observations with missing ancillary data. Consistent with the other ANNI VOCs products, a post-filter discards the individual retrievals affected by uncertainties that are too large or by poor measurement sensitivity to HCN, specifically when

$$\left|\text{column}_{(\text{HCN})} \Big/ \text{HRI}_{(\text{HCN})}\right| > 8 \times 10^{15} \text{ molecules cm}^{-2} \quad \text{(A1)}$$

or spectral baseline temperatures < 268 K. This post-filter is not (directly) driven by the gas abundance but rather by the thermal contrast (Franco et al., 2020). Finally, the constant climatological background of target gas abundance that is not accounted for by the HRI has been estimated as 1.85×10^{15} molecules cm^{-2} for HCN (see Franco et al., 2018); this offset is thus added to the individual retrieved columns. Once set up, the NN is fed for each individual IASI observation with the appropriate input data. Here, we chose to use the ERA-5 reanalysis dataset (Hersbach et al., 2020) for the meteorological input data in the network. In the framework of the evaluation of EMAC in the 2015 Indonesian fires (see Sect. 4), only the HCN product obtained with the NN in transport/mixing regime has been exploited. Indeed, the Cloud-Aerosol Lidar with Orthogonal Polarization (CALIOP) aboard CALIPSO indicates the fire plume located in the free troposphere during this massive biomass burning event.

Figure A1 presents the daily distributions of HCN total columns from IASI/Metop-A and B observations in South East Asia, for 6 successive days taken during the 2015 Indonesian fires. Whereas background ar-

eas are characterised by HCN total columns generally lower than 0.5×10^{16} molecules cm^{-2}, on the first day (29 September 2015), strong HCN enhancements ($> 4 \times 10^{16}$ molecules cm^{-2}) are detected by IASI in the vicinity of Sumatra, indicating a massive fire plume. After 6 d (4 October 2015), we can observe that the plume has grown progressively and that the bulk of HCN has been transported to the west across the Indian Ocean. The retrieved column uncertainties in the area generally fall in the range of 2–5×10^{15} molecules cm^{-2}. Note that these uncertainties are reduced significantly by averaging numerous IASI measurements to build monthly or seasonal mean distributions of HCN columns. The typical seasonal distributions of IASI/Metop-A HCN columns are presented in Fig. A2 for the 2011–2014 time period, i.e. for years without massive fire events, such as the 2010 Russian fires or the 2015 Indonesian fires. These distributions highlight the dominant contribution of biomass burning to the atmospheric HCN burden, with HCN enhancements detected in Africa throughout the year; in South East Asia in March–April–May; in India, eastern China, and the Northern Hemisphere mid- and high latitudes during the boreal summer; and within the tropics in September–October–November. Important outflows from these source regions are also noticeable, especially over the oceans. Figure A3 presents the monthly mean HCN columns during the 2015 Indonesian fires (from September–December) along with the corresponding distributions over the 2011–2014 time period. It illustrates the exceptional intensity of the 2015 fires compared to the previous years, with important HCN enhancements detected throughout the entire intertropical band.

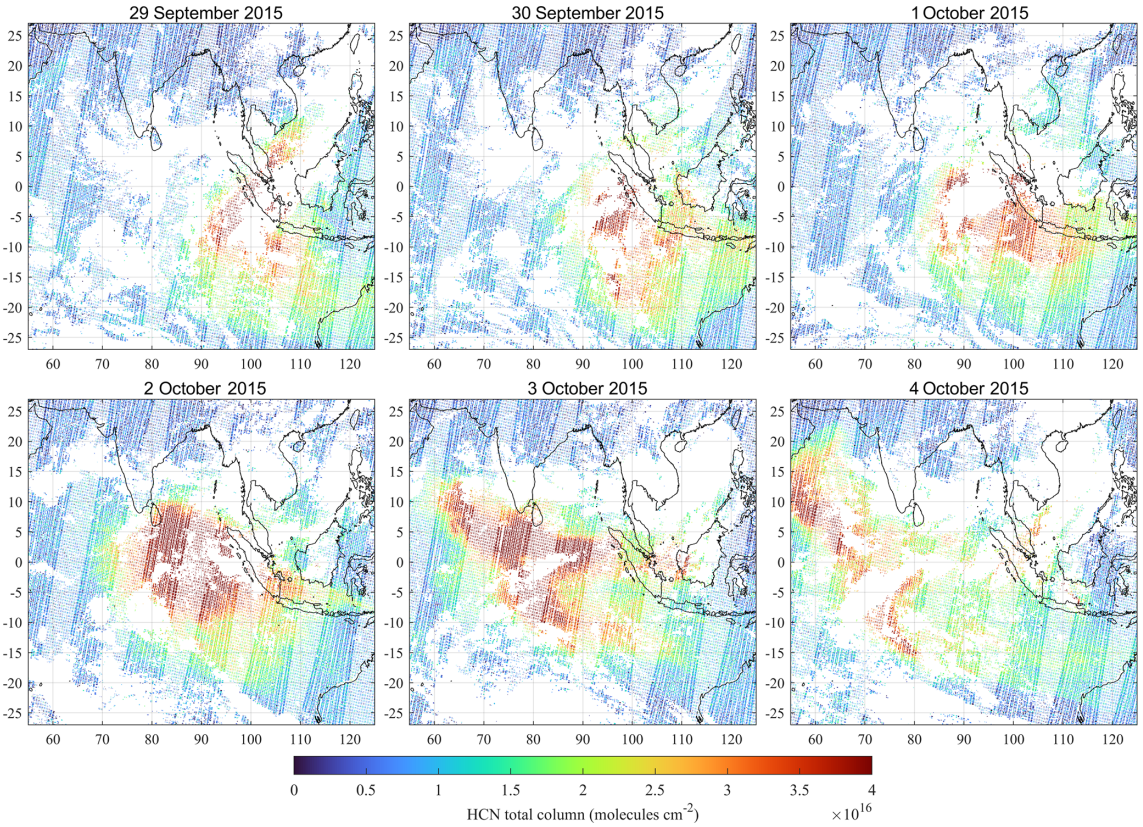

Figure A1. Daily regional distributions of HCN total column (in molecules cm^{-2}) derived from the IASI spectra recorded in the morning overpasses of Metop-A and B, for 6 successive days during the 2015 Indonesian fires. These distributions take into account the actual footprint on the Earth's surface of each individual IASI measurement, i.e. a small circle at nadir and an elongated ellipse at the limit of the across-track swath of the satellite. Note the complementarity of the IASI/Metop-A and B flight tracks that avoid gaps between the successive overpasses in the tropics. The white areas correspond to data filtered out because of unsatisfactory retrieval quality or the presence of clouds.

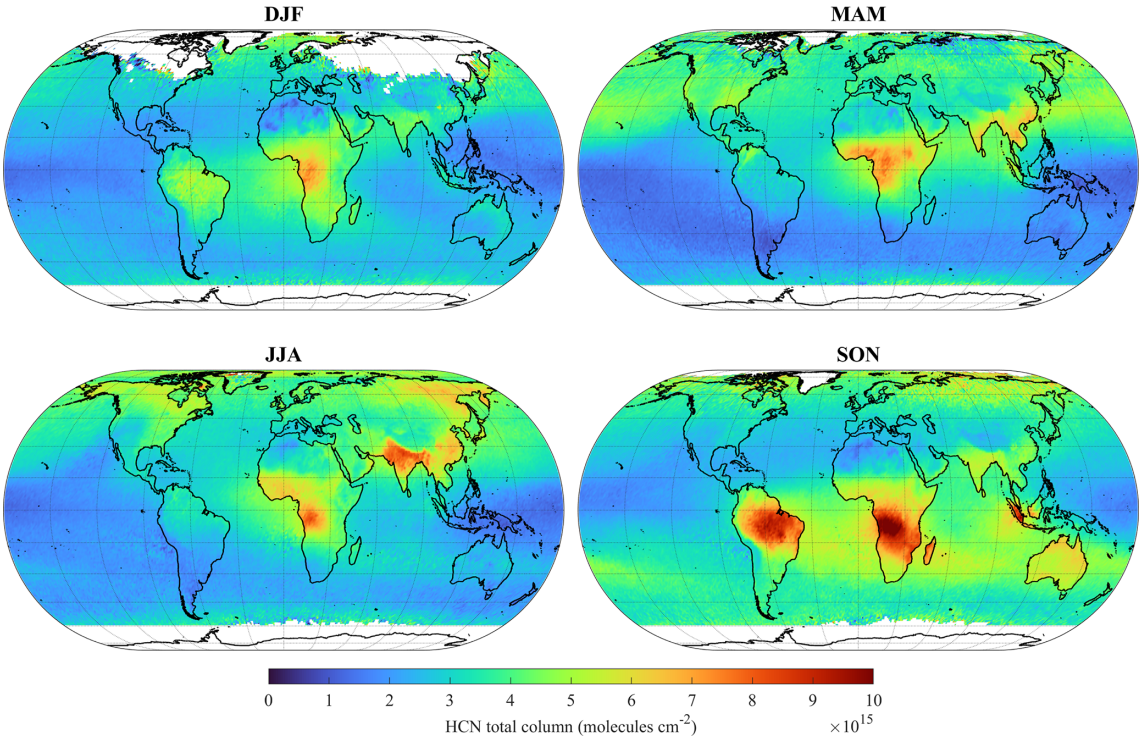

Figure A2. Seasonal means (on a $1 \times 1^{\circ}$ grid) of the HCN total columns (in molecules cm^{-2}) retrieved from the IASI/Metop-A measurements over the 2011–2014 time period. The HCN columns over the continents have been retrieved with the NN in emission regime, whereas the NN in transport/mixing regime has been used over the oceans.

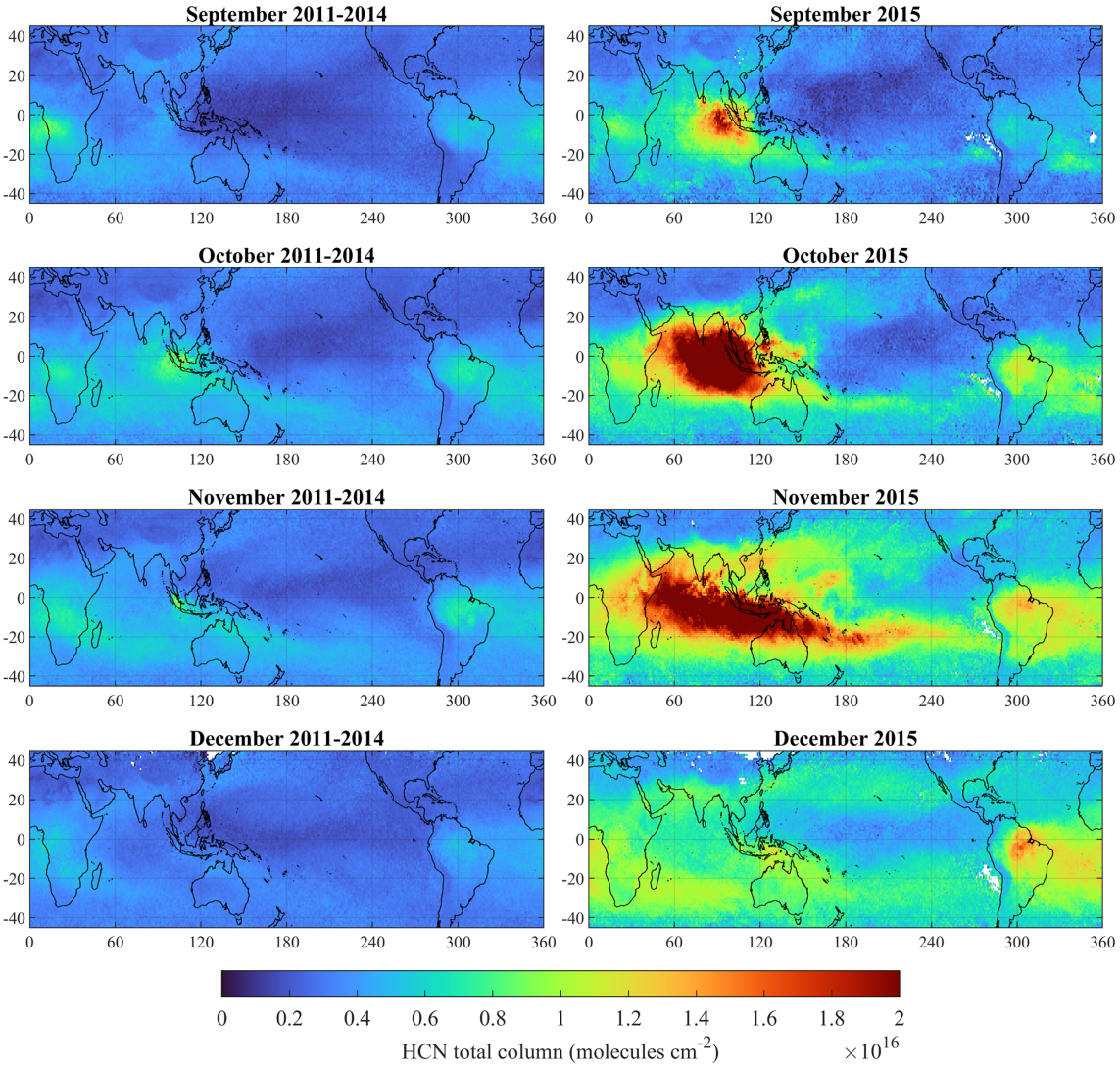

Figure A3. Monthly means (on a 1 × 1° grid) of the HCN total columns (in molecules cm^{-2}) retrieved from the IASI/Metop-A measurements over the 2011–2014 time period (left plots) and over the year 2015 (right plots).

Appendix B: Definition of $\sum$OVOCs

In Fig. 15, the mixing ratios of the sum of all the OVOCs explicitly reacting in JAMOC ($\sum$OVOCs) are shown. In this case, $\sum$ OVOCs is defined as

$$\begin{aligned}\sum \text{OVOCs} = {} & \text{methanol} + \text{formaldehyde} \\ & + \text{methyl hydroperoxide} \\ & + \text{hydroxymethylhydroperoxide} \\ & + \text{ethanol} + \text{ethylene glycol} \\ & + \text{acetaldehyde} + \text{glycolaldehyde} \\ & + \text{glyoxal} + \text{1-hydroperoxyacetone} \\ & + \text{methylglyoxal} + \text{isopropanol} \\ & + \text{isopropyl hydroperoxide} \\ & + \text{methacrolein} + \text{methyl vinyl ketone.} \end{aligned} \quad \text{(B1)}$$

Data availability. The simulation results are archived at the Jülich Supercomputing Centre (JSC) and are available upon request. The IASI VOC columns retrieved with the ANNI framework are available upon request. The IASI CO data processed with FORLI-CO v0151001 can be downloaded from the AERIS portal at http://iasi.aeris-data.fr/CO/ (last access: 6 July 2021). The peatland distribution data used in Fig. 1 are available from Xu et al. (2017).

Author contributions. The study was designed by SR and DT. AP implemented the algorithms for VOC emissions from biomass burning and terrestrial vegetation. SR adjusted the biomass burning emission factors. AP and DT implemented HCN deposition to the ocean. SR performed the simulations and analysed the data with contributions from DT. BF, LC, and PFC developed the IASI VOC products and contributed to the analyses. SR and DT discussed the results with contributions from BF and AW. The manuscript was prepared by SR with the help of all co-authors.

Competing interests. The authors declare that they have no conflict of interest.

Disclaimer. Publisher's note: Copernicus Publications remains neutral with regard to jurisdictional claims in published maps and institutional affiliations.

Special issue statement. This article is part of the special issue "The Modular Earth Submodel System (MESSy) (ACP/GMD inter-journal SI)". It is not associated with a conference.

Acknowledgements. The work described in this paper has received funding from the Initiative and Networking Fund of the Helmholtz Association through the project Advanced Earth System Modelling Capacity (ESM). The content of this paper is the sole responsibility of the author(s), and it does not represent the opinion of the Helmholtz Association, and the Helmholtz Association is not responsible for any use that might be made of the information contained. The authors gratefully acknowledge the Earth System Modelling project (ESM) for funding this work by providing computing time on the ESM partition of the supercomputer JUWELS at the Jülich Supercomputing Centre (JSC). IASI is a joint mission of EUMETSAT and the Centre National d'Etudes Spatiales (CNES, France). The authors acknowledge the AERIS data infrastructure for providing access to the IASI data, Daniel Hurtmans for the development of the CO retrievals, and EUMETSAT AC SAF for CO data production. The research at ULB has been supported by the project OCTAVE (Oxygenated Compounds in the Tropical Atmosphere: Variability and Exchanges, http://octave.aeronomie.be/, last access: 6 July 2021) of the Belgian Research Action through Interdisciplinary Networks (BRAIN-be; 2017–2021; research project BR/175/A2/OCTAVE) and by the IASI.Flow Prodex arrangement (ESA–BELSPO). Lieven Clarisse is a research associate supported by the F.R.S.–FNRS.

Financial support. This research has been supported by the Initiative and Networking Fund of the Helmholtz Association through the project Advanced Earth System Modelling Capacity (ESM) (grant no. DB001549).

The article processing charges for this open-access publication were covered by the Forschungszentrum Jülich.

Review statement. This paper was edited by Bryan N. Duncan and reviewed by two anonymous referees.

References

Aghedo, A. M., Rast, S., and Schultz, M. G.: Sensitivity of tracer transport to model resolution, prescribed meteorology and tracer lifetime in the general circulation model ECHAM5, Atmos. Chem. Phys., 10, 3385–3396, https://doi.org/10.5194/acp-10-3385-2010, 2010.

Akagi, S. K., Yokelson, R. J., Wiedinmyer, C., Alvarado, M. J., Reid, J. S., Karl, T., Crounse, J. D., and Wennberg, P. O.: Emission factors for open and domestic biomass burning for use in atmospheric models, Atmos. Chem. Phys., 11, 4039–4072, https://doi.org/10.5194/acp-11-4039-2011, 2011.

Andreae, M. O.: Emission of trace gases and aerosols from biomass burning – an updated assessment, Atmos. Chem. Phys., 19, 8523–8546, https://doi.org/10.5194/acp-19-8523-2019, 2019.

Atkinson, R., Carter, W. P. L., Darnall, K. R., Winer, A. M., and Pitts Jr., J. N.: A smog chamber and modeling study of the gas phase NO_x–air photooxidation of toluene and the cresols, Int. J. Chem. Kinet., 12, 779–836, https://doi.org/10.1002/kin.550121102, 1980.

Basha, G., Ratnam, M. V., and Kishore, P.: Asian summer monsoon anticyclone: trends and variability, Atmos. Chem. Phys., 20, 6789–6801, https://doi.org/10.5194/acp-20-6789-2020, 2020.

Blando, J. D. and Turpin, B. J.: Secondary organic aerosol formation in cloud and fog droplets: a literature evaluation of plausibility, Atmos. Environ., 34, 1623–1632, https://doi.org/10.1016/S1352-2310(99)00392-1, 2000.

Brinkop, S. and Jöckel, P.: ATTILA 4.0: Lagrangian advective and convective transport of passive tracers within the ECHAM5/MESSy (2.53.0) chemistry–climate model, Geosci. Model Dev., 12, 1991–2008, https://doi.org/10.5194/gmd-12-1991-2019, 2019.

Cabrera-Perez, D., Taraborrelli, D., Sander, R., and Pozzer, A.: Global atmospheric budget of simple monocyclic aromatic compounds, Atmos. Chem. Phys., 16, 6931–6947, https://doi.org/10.5194/acp-16-6931-2016, 2016.

Cheng, S.-B., Zhou, C.-H., Yin, H.-M., Sun, J.-L., and Han, K.-L.: OH produced from o-nitrophenol photolysis: A combined experimental and theoretical investigation, J. Chem. Phys., 130, 234311, https://doi.org/10.1063/1.3152635, 2009.

Chipperfield, M. P., Dhomse, S., Hossaini, R., Feng, W., Santee, M. L., Weber, M., Burrows, J. P., Wild, J. D., Loyola, D., and Coldewey-Egbers, M.: On the Cause of Recent Variations in Lower Stratospheric Ozone, Geophys. Res. Lett., 45, 5718–5726, https://doi.org/10.1029/2018GL078071, 2018.

Christian, T. J., Kleiss, B., Yokelson, R. J., Holzinger, R., Crutzen, P. J., Hao, W. M., Saharjo, B. H., and Ward, D. E.: Comprehensive laboratory measurements of biomass-burning emissions: 1. Emissions from Indonesian, African, and other fuels, J. Geophys. Res.-Atmos., 108, 4719, https://doi.org/10.1029/2003JD003704, 2003.

Cicerone, R. J. and Zellner, R.: The atmospheric chemistry of hydrogen cyanide (HCN), J. Geophys. Res.-Ocean., 88, 10689–10696, https://doi.org/10.1029/JC088iC15p10689, 1983.

Clarisse, L., Clerbaux, C., Franco, B., Hadji-Lazaro, J., Whitburn, S., Kopp, A. K., Hurtmans, D., and Coheur, P.-F.: A Decadal Data Set of Global Atmospheric Dust Retrieved From IASI Satellite Measurements, J. Geophys. Res.-Atmos., 124, 1618–1647, https://doi.org/10.1029/2018jd029701, 2019.

Clerbaux, C., Boynard, A., Clarisse, L., George, M., Hadji-Lazaro, J., Herbin, H., Hurtmans, D., Pommier, M., Razavi, A., Turquety, S., Wespes, C., and Coheur, P.-F.: Monitoring of atmospheric composition using the thermal infrared IASI/MetOp sounder, Atmos. Chem. Phys., 9, 6041–6054, https://doi.org/10.5194/acp-9-6041-2009, 2009.

Crippa, P., Castruccio, S., Archer-Nicholls, S., Lebron, G. B., Kuwata, M., Thota, A., Sumin, S., Butt, E., Wiedinmyer, C., and Spracklen, D. V.: Population exposure to hazardous air quality due to the 2015 fires in Equatorial Asia, Sci. Rep., 6, 37074, https://doi.org/10.1038/srep37074, 2016.

Deckert, R., Jöckel, P., Grewe, V., Gottschaldt, K.-D., and Hoor, P.: A quasi chemistry-transport model mode for EMAC, Geosci. Model Dev., 4, 195–206, https://doi.org/10.5194/gmd-4-195-2011, 2011.

Duflot, V., Hurtmans, D., Clarisse, L., R'honi, Y., Vigouroux, C., Mazière, M. D., Mahieu, E., Servais, C., Clerbaux, C., and Coheur, P.-F.: Measurements of hydrogen cyanide (HCN) and acetylene (C_2H_2) from the Infrared Atmospheric Sounding Interferometer (IASI), Atmos. Meas. Tech., 6, 917–925, https://doi.org/10.5194/amt-6-917-2013, 2013.

Duflot, V., Wespes, C., Clarisse, L., Hurtmans, D., Ngadi, Y., Jones, N., Paton-Walsh, C., Hadji-Lazaro, J., Vigouroux, C., Mazière, M. D., Metzger, J.-M., Mahieu, E., Servais, C., Hase, F., Schneider, M., Clerbaux, C., and Coheur, P.-F.: Acetylene (C_2H_2) and hydrogen cyanide (HCN) from IASI satellite observations: global distributions, validation, and comparison with model, Atmos. Chem. Phys., 15, 10509–10527, https://doi.org/10.5194/acp-15-10509-2015, 2015.

Ervens, B.: Modeling the Processing of Aerosol and Trace Gases in Clouds and Fogs, Chem. Rev., 115, 4157–4198, https://doi.org/10.1021/cr5005887, 2015.

Ervens, B., Turpin, B. J., and Weber, R. J.: Secondary organic aerosol formation in cloud droplets and aqueous particles (aqSOA): a review of laboratory, field and model studies, Atmos. Chem. Phys., 11, 11069–11102, https://doi.org/10.5194/acp-11-11069-2011, 2011.

Field, R. D., van der Werf, G. R., Fanin, T., Fetzer, E. J., Fuller, R., Jethva, H., Levy, R., Livesey, N. J., Luo, M., Torres, O., and Worden, H. M.: Indonesian fire activity and smoke pollution in 2015 show persistent nonlinear sensitivity to El Niño-induced drought, P. Natl. Acad. Sci. USA, 113, 9204–9209, https://doi.org/10.1073/pnas.1524888113, 2016.

Franco, B., Clarisse, L., Stavrakou, T., Müller, J.-F., Van Damme, M., Whitburn, S., Hadji-Lazaro, J., Hurtmans, D., Taraborrelli, D., Clerbaux, C., and Coheur, P.-F.: A General Framework for Global Retrievals of Trace Gases From IASI: Application to Methanol, Formic Acid, and PAN, J. Geophys. Res.-Atmos., 123, 13963–13984, https://doi.org/10.1029/2018JD029633, 2018.

Franco, B., Clarisse, L., Stavrakou, T., Müller, J.-F., Pozzer, A., Hadji-Lazaro, J., Hurtmans, D., Clerbaux, C., and Coheur, P.-F.: Acetone Atmospheric Distribution Retrieved From Space, Geophys. Res. Lett., 46, 2884–2893, https://doi.org/10.1029/2019gl082052, 2019.

Franco, B., Clarisse, L., Stavrakou, T., Müller, J.-F., Taraborrelli, D., Hadji-Lazaro, J., Hannigan, J. W., Hase, F., Hurtmans, D., Jones, N., Lutsch, E., Mahieu, E., Ortega, I., Schneider, M., Strong, K., Vigouroux, C., Clerbaux, C., and Coheur, P.-F.: Spaceborne Measurements of Formic and Acetic Acids: A Global View of the Regional Sources, Geophys. Res. Lett., 47, e2019GL086239, https://doi.org/10.1029/2019gl086239, 2020.

Fu, R., Hu, Y., Wright, J. S., Jiang, J. H., Dickinson, R. E., Chen, M., Filipiak, M., Read, W. G., Waters, J. W., and Wu, D. L.: Short circuit of water vapor and polluted air to the global stratosphere by convective transport over the Tibetan Plateau, P. Natl. Acad. Sci. USA, 103, 5664–5669, https://doi.org/10.1073/pnas.0601584103, 2006.

Gaveau, D. L. A., Salim, M. A., Hergoualc'h, K., Locatelli, B., Sloan, S., Wooster, M., Marlier, M. E., Molidena, E., Yaen, H., DeFries, R., Verchot, L., Murdiyarso, D., Nasi, R., Holmgren, P., and Sheil, D.: Major atmospheric emissions from peat fires in Southeast Asia during non-drought years: evidence from the 2013 Sumatran fires, Sci. Rep., 4, 6112, https://doi.org/10.1038/srep06112, 2014.

George, M., Clerbaux, C., Bouarar, I., Coheur, P.-F., Deeter, M. N., Edwards, D. P., Francis, G., Gille, J. C., Hadji-Lazaro, J., Hurtmans, D., Inness, A., Mao, D., and Worden, H. M.: An examination of the long-term CO records from MOPITT and IASI: comparison of retrieval methodology, Atmos. Meas. Tech., 8, 4313–4328, https://doi.org/10.5194/amt-8-4313-2015, 2015.

Grosjean, D.: Atmospheric reactions of ortho cresol: Gas phase and aerosol products, Atmos. Environ., 18, 1641–1652, https://doi.org/10.1016/0004-6981(84)90386-X, 1984.

Grosjean, D.: Atmospheric fate of toxic aromatic compounds, Sci. Total Environ., 100, 367–414, https://doi.org/10.1016/0048-9697(91)90386-S, 1991.

Guenther, A., Karl, T., Harley, P., Wiedinmyer, C., Palmer, P. I., and Geron, C.: Estimates of global terrestrial isoprene emissions using MEGAN (Model of Emissions of Gases and Aerosols from Nature), Atmos. Chem. Phys., 6, 3181–3210, https://doi.org/10.5194/acp-6-3181-2006, 2006.

Hagemann, S. and Stacke, T.: Impact of the soil hydrology scheme on simulated soil moisture memory, Clim. Dynam., 44, 1731–1750, https://doi.org/10.1007/s00382-014-2221-6, 2015.

Hems, R. F. and Abbatt, J. P. D.: Aqueous Phase Photo-oxidation of Brown Carbon Nitrophenols: Reaction Kinetics, Mechanism, and Evolution of Light Absorption, ACS Earth Space Chem., 2, 225–234, https://doi.org/10.1021/acsearthspacechem.7b00123, 2018.

Hens, K., Novelli, A., Martinez, M., Auld, J., Axinte, R., Bohn, B., Fischer, H., Keronen, P., Kubistin, D., Nölscher, A. C., Oswald, R., Paasonen, P., Petäjä, T., Regelin, E., Sander, R., Sinha, V., Sipilä, M., Taraborrelli, D., Tatum Ernest, C., Williams, J., Lelieveld, J., and Harder, H.: Observation and modelling of HO_x

radicals in a boreal forest, Atmos. Chem. Phys., 14, 8723–8747, https://doi.org/10.5194/ACP-14-8723-2014, 2014.

Herrmann, H., Schaefer, T., Tilgner, A., Styler, S. A., Weller, C., Teich, M., and Otto, T.: Tropospheric Aqueous-Phase Chemistry: Kinetics, Mechanisms, and Its Coupling to a Changing Gas Phase, Chem. Rev., 115, 4259–4334, https://doi.org/10.1021/cr500447k, pMID: 25950643, 2015.

Hersbach, H., Bell, B., Berrisford, P., Hirahara, S., Horányi, A., Muñoz-Sabater, J., Nicolas, J., Peubey, C., Radu, R., Schepers, D., Simmons, A., Soci, C., Abdalla, S., Abellan, X., Balsamo, G., Bechtold, P., Biavati, G., Bidlot, J., Bonavita, M., Chiara, G., Dahlgren, P., Dee, D., Diamantakis, M., Dragani, R., Flemming, J., Forbes, R., Fuentes, M., Geer, A., Haimberger, L., Healy, S., Hogan, R. J., Hólm, E., Janisková, M., Keeley, S., Laloyaux, P., Lopez, P., Lupu, C., Radnoti, G., Rosnay, P., Rozum, I., Vamborg, F., Villaume, S., and Thépaut, J.-N.: The ERA5 global reanalysis, Q. J. Roy. Meteorol. Soc., 146, 1999–2049, https://doi.org/10.1002/qj.3803, 2020.

Hodnebrog, Ø., Dalsøren, S. B., and Myhre, G.: Lifetimes, direct and indirect radiative forcing, and global warming potentials of ethane (C_2H_6), propane (C_3H_8), and butane (C_4H_{10}), Atmos. Sc. Lett., 19, e804, https://doi.org/10.1002/asl.804, 2018.

Hurtmans, D., Coheur, P.-F., Wespes, C., Clarisse, L., Scharf, O., Clerbaux, C., Hadji-Lazaro, J., George, M., and Turquety, S.: FORLI radiative transfer and retrieval code for IASI, J. Quant. Spectrosc. Ra., 113, 1391–1408, https://doi.org/10.1016/j.jqsrt.2012.02.036, 2012.

Jagiella, S. and Zabel, F.: Reaction of phenylperoxy radicals with NO_2 at 298 K, Phys. Chem. Chem. Phys., 9, 5036–5051, https://doi.org/10.1039/B705193J, 2007.

Jiménez-Muñoz, J. C., Mattar, C., Barichivich, J., Santamaría-Artigas, A., Takahashi, K., Malhi, Y., Sobrino, J. A., and Schrier, G. v. d.: Record-breaking warming and extreme drought in the Amazon rainforest during the course of El Niño 2015–2016, Sci. Rep., 6, 33130, https://doi.org/10.1038/srep33130, 2016.

Jöckel, P., Kerkweg, A., Pozzer, A., Sander, R., Tost, H., Riede, H., Baumgaertner, A., Gromov, S., and Kern, B.: Development cycle 2 of the Modular Earth Submodel System (MESSy2), Geosci. Model Dev., 3, 717–752, https://doi.org/10.5194/gmd-3-717-2010, 2010.

Jöckel, P., Tost, H., Pozzer, A., Kunze, M., Kirner, O., Brenninkmeijer, C. A. M., Brinkop, S., Cai, D. S., Dyroff, C., Eckstein, J., Frank, F., Garny, H., Gottschaldt, K.-D., Graf, P., Grewe, V., Kerkweg, A., Kern, B., Matthes, S., Mertens, M., Meul, S., Neumaier, M., Nützel, M., Oberländer-Hayn, S., Ruhnke, R., Runde, T., Sander, R., Scharffe, D., and Zahn, A.: Earth System Chemistry integrated Modelling (ESCiMo) with the Modular Earth Submodel System (MESSy) version 2.51, Geosci. Model Dev., 9, 1153–1200, https://doi.org/10.5194/gmd-9-1153-2016, 2016.

Kaiser, J. W., Heil, A., Andreae, M. O., Benedetti, A., Chubarova, N., Jones, L., Morcrette, J.-J., Razinger, M., Schultz, M. G., Suttie, M., and van der Werf, G. R.: Biomass burning emissions estimated with a global fire assimilation system based on observed fire radiative power, Biogeosciences, 9, 527–554, https://doi.org/10.5194/bg-9-527-2012, 2012.

Kim, P. S., Jacob, D. J., Mickley, L. J., Koplitz, S. N., Marlier, M. E., DeFries, R. S., Myers, S. S., Chew, B. N., and Mao, Y. H.: Sensitivity of population smoke exposure to fire locations in Equatorial Asia, Atmos. Environ., 102, 11–17, https://doi.org/10.1016/j.atmosenv.2014.09.045, 2015.

Koss, A. R., Sekimoto, K., Gilman, J. B., Selimovic, V., Coggon, M. M., Zarzana, K. J., Yuan, B., Lerner, B. M., Brown, S. S., Jimenez, J. L., Krechmer, J., Roberts, J. M., Warneke, C., Yokelson, R. J., and de Gouw, J.: Non-methane organic gas emissions from biomass burning: identification, quantification, and emission factors from PTR-ToF during the FIREX 2016 laboratory experiment, Atmos. Chem. Phys., 18, 3299–3319, https://doi.org/10.5194/acp-18-3299-2018, 2018.

Kyrölä, E., Laine, M., Sofieva, V., Tamminen, J., Päivärinta, S.-M., Tukiainen, S., Zawodny, J., and Thomason, L.: Combined SAGE II–GOMOS ozone profile data set for 1984–2011 and trend analysis of the vertical distribution of ozone, Atmos. Chem. Phys., 13, 10645–10658, https://doi.org/10.5194/acp-13-10645-2013, 2013.

Lee, D., Fahey, D., Skowron, A., Allen, M., Burkhardt, U., Chen, Q., Doherty, S., Freeman, S., Forster, P., Fuglestvedt, J., Gettelman, A., De León, R., Lim, L., Lund, M., Millar, R., Owen, B., Penner, J., Pitari, G., Prather, M., Sausen, R., and Wilcox, L.: The contribution of global aviation to anthropogenic climate forcing for 2000 to 2018, Atmos. Environ., 244, 117834, https://doi.org/10.1016/j.atmosenv.2020.117834, 2021.

Lee, H.-H., Bar-Or, R. Z., and Wang, C.: Biomass burning aerosols and the low-visibility events in Southeast Asia, Atmos. Chem. Phys., 17, 965–980, https://doi.org/10.5194/acp-17-965-2017, 2017.

Lelieveld, J., Gromov, S., Pozzer, A., and Taraborrelli, D.: Global tropospheric hydroxyl distribution, budget and reactivity, Atmos. Chem. Phys., 16, 12477–12493, https://doi.org/10.5194/acp-16-12477-2016, 2016.

Lelieveld, J., Bourtsoukidis, E., Brühl, C., Fischer, H., Fuchs, H., Harder, H., Hofzumahaus, A., Holland, F., Marno, D., Neumaier, M., Pozzer, A., Schlager, H., Williams, J., Zahn, A., and Ziereis, H.: The South Asian monsoon–pollution pump and purifier, Science, 361, 270–273, https://doi.org/10.1126/science.aar2501, 2018.

Leslie, M. D., Ridoli, M., Murphy, J. G., and Borduas-Dedekind, N.: Isocyanic acid (HNCO) and its fate in the atmosphere: a review, Environ. Sci., 21, 793–808, https://doi.org/10.1039/C9EM00003H, 2019.

Li, Q., Jacob, D. J., Bey, I., Yantosca, R. M., Zhao, Y., Kondo, Y., and Notholt, J.: Atmospheric hydrogen cyanide (HCN): Biomass burning source, ocean sink?, Geophys. Res. Lett., 27, 357–360, https://doi.org/10.1029/1999GL010935, 2000.

Li, Q., Palmer, P. I., Pumphrey, H. C., Bernath, P., and Mahieu, E.: What drives the observed variability of HCN in the troposphere and lower stratosphere?, Atmos. Chem. Phys., 9, 8531–8543, https://doi.org/10.5194/acp-9-8531-2009, 2009.

Liu, T., Mickley, L. J., Marlier, M. E., DeFries, R. S., Khan, M. F., Latif, M. T., and Karambelas, A.: Diagnosing spatial biases and uncertainties in global fire emissions inventories: Indonesia as regional case study, Remote Sens. Environ., 237, 111557, https://doi.org/10.1016/j.rse.2019.111557, 2020.

Lobert, J. M., Scharffe, D. H., Hao, W. M., and Crutzen, P. J.: Importance of biomass burning in the atmospheric budgets of nitrogen-containing gases, Nature, 346, 552–554, https://doi.org/10.1038/346552a0, 1990.

Mahowald, N. M., Rasch, P. J., Eaton, B. E., Whittlestone, S., and Prinn, R. G.: Transport of 222radon to the remote troposphere using the Model of Atmospheric Transport and Chemistry and assimilated winds from ECMWF and the National Center for Environmental Prediction/NCAR, J. Geophys. Res.-Atmos., 102, 28139–28151, https://doi.org/10.1029/97JD02084, 1997.

Marlier, M. E., DeFries, R. S., Voulgarakis, A., Kinney, P. L., Randerson, J. T., Shindell, D. T., Chen, Y., and Faluvegi, G.: El Niño and health risks from landscape fire emissions in southeast Asia, Nat. Clim. Change, 3, 131–136, https://doi.org/10.1038/nclimate1658, 2013.

Millet, D. B., Jacob, D. J., Custer, T. G., de Gouw, J. A., Goldstein, A. H., Karl, T., Singh, H. B., Sive, B. C., Talbot, R. W., Warneke, C., and Williams, J.: New constraints on terrestrial and oceanic sources of atmospheric methanol, Atmos. Chem. Phys., 8, 6887–6905, https://doi.org/10.5194/acp-8-6887-2008, 2008.

Nair, P. J., Froidevaux, L., Kuttippurath, J., Zawodny, J. M., Russell III, J. M., Steinbrecht, W., Claude, H., Leblanc, T., van Gijsel, J. A. E., Johnson, B., Swart, D. P. J., Thomas, A., Querel, R., Wang, R., and Anderson, J.: Subtropical and midlatitude ozone trends in the stratosphere: Implications for recovery, J. Geophys. Res.-Atmos., 120, 7247–7257, https://doi.org/10.1002/2014JD022371, 2015.

Natangelo, M., Mangiapan, S., Bagnati, R., Benfenati, E., and Fanelli, R.: Increased concentrations of nitrophenols in leaves from a damaged forestal site, Chemosphere, 38, 1495–1503, https://doi.org/10.1016/S0045-6535(98)00370-1, 1999.

Nechita-Banda, N., Krol, M., van der Werf, G. R., Kaiser, J. W., Pandey, S., Huijnen, V., Clerbaux, C., Coheur, P., Deeter, M. N., and Röckmann, T.: Monitoring emissions from the 2015 Indonesian fires using CO satellite data, Philos. T. R. Soc. B, 373, 20170307, https://doi.org/10.1098/rstb.2017.0307, 2018.

NOAA: Multivariate ENSO Index Version 2 (MEI.v2), available at: https://psl.noaa.gov/enso/mei/, last access: 19 September 2020.

Nojima, K., Fukaya, K., Fukui, S., and Kanno, S.: Studies on photochemistry of aromatic hydrocarbons II: The formation of nitrophenols and nitrobenzene by the photochemical reaction of benzene in the presence of nitrogen monoxide, Chemosphere, 4, 77–82, 1975.

Nölscher, A., Butler, T., Auld, J., Veres, P., Muñoz, A., Taraborrelli, D., Vereecken, L., Lelieveld, J., and Williams, J.: Using total OH reactivity to assess isoprene photooxidation via measurement and model, Atmos. Environ., 89, 453–463, https://doi.org/10.1016/j.atmosenv.2014.02.024, 2014.

Orbe, C., Yang, H., Waugh, D. W., Zeng, G., Morgenstern, O., Kinnison, D. E., Lamarque, J.-F., Tilmes, S., Plummer, D. A., Scinocca, J. F., Josse, B., Marecal, V., Jöckel, P., Oman, L. D., Strahan, S. E., Deushi, M., Tanaka, T. Y., Yoshida, K., Akiyoshi, H., Yamashita, Y., Stenke, A., Revell, L., Sukhodolov, T., Rozanov, E., Pitari, G., Visioni, D., Stone, K. A., Schofield, R., and Banerjee, A.: Large-scale tropospheric transport in the Chemistry–Climate Model Initiative (CCMI) simulations, Atmos. Chem. Phys., 18, 7217–7235, https://doi.org/10.5194/acp-18-7217-2018, 2018.

Park, M., Randel, W. J., Emmons, L. K., Bernath, P. F., Walker, K. A., and Boone, C. D.: Chemical isolation in the Asian monsoon anticyclone observed in Atmospheric Chemistry Experiment (ACE-FTS) data, Atmos. Chem. Phys., 8, 757–764, https://doi.org/10.5194/acp-8-757-2008, 2008.

Randel, W. J., Park, M., Emmons, L., Kinnison, D., Bernath, P., Walker, K. A., Boone, C., and Pumphrey, H.: Asian Monsoon Transport of Pollution to the Stratosphere, Science, 328, 611–613, https://doi.org/10.1126/science.1182274, 2010.

Reddington, C. L., Yoshioka, M., Balasubramanian, R., Ridley, D., Toh, Y. Y., Arnold, S. R., and Spracklen, D. V.: Contribution of vegetation and peat fires to particulate air pollution in Southeast Asia, Environ. Res. Lett., 9, 094006, https://doi.org/10.1088/1748-9326/9/9/094006, 2014.

Rein, G., Cohen, S., and Simeoni, A.: Carbon emissions from smouldering peat in shallow and strong fronts, P. Combust. Inst., 32, 2489–2496, https://doi.org/10.1016/j.proci.2008.07.008, 2009.

Rippen, G., Zietz, E., Frank, R., Knacker, T., and Klöpffer, W.: Do airborne nitrophenols contribute to forest decline?, Environ. Technol. Lett., 8, 475–482, https://doi.org/10.1080/09593338709384508, 1987.

Roberts, J. M., Veres, P. R., Cochran, A. K., Warneke, C., Burling, I. R., Yokelson, R. J., Lerner, B., Gilman, J. B., Kuster, W. C., Fall, R., and de Gouw, J.: Isocyanic acid in the atmosphere and its possible link to smoke-related health effects, P. Natl. Acad. Sci. USA, 108, 8966–8971, https://doi.org/10.1073/pnas.1103352108, 2011.

Rodgers, C. D.: Inverse Methods for Atmospheric Sounding, World Sci., 2, 256, https://doi.org/10.1142/3171, 2000.

Roeckner, E., Brokopf, R., Esch, M., Giorgetta, M., Hagemann, S., Kornblueh, L., Manzini, E., Schlese, U., and Schulzweida, U.: Sensitivity of Simulated Climate to Horizontal and Vertical Resolution in the ECHAM5 Atmosphere Model, J. Clim., 19, 3771–3791, https://doi.org/10.1175/JCLI3824.1, 2006.

Rosanka, S., Vu, G. H. T., Nguyen, H. M. T., Pham, T. V., Javed, U., Taraborrelli, D., and Vereecken, L.: Atmospheric chemical loss processes of isocyanic acid (HNCO): a combined theoretical kinetic and global modelling study, Atmos. Chem. Phys., 20, 6671–6686, https://doi.org/10.5194/acp-20-6671-2020, 2020a.

Rosanka, S., Frömming, C., and Grewe, V.: The impact of weather patterns and related transport processes on aviation's contribution to ozone and methane concentrations from NO_x emissions, Atmos. Chem. Phys., 20, 12347–12361, https://doi.org/10.5194/acp-20-12347-2020, 2020b.

Rosanka, S., Sander, R., Franco, B., Wespes, C., Wahner, A., and Taraborrelli, D.: Oxidation of low-molecular-weight organic compounds in cloud droplets: global impact on tropospheric oxidants, Atmos. Chem. Phys., 21, 9909–9930, https://doi.org/10.5194/acp-21-9909-2021, 2021a.

Rosanka, S., Sander, R., Wahner, A., and Taraborrelli, D.: Oxidation of low-molecular-weight organic compounds in cloud droplets: development of the Jülich Aqueous-phase Mechanism of Organic Chemistry (JAMOC) in CAABA/MECCA (version 4.5.0), Geosci. Model Dev., 14, 4103–4115, https://doi.org/10.5194/gmd-14-4103-2021, 2021b.

Sander, R., Baumgaertner, A., Cabrera-Perez, D., Frank, F., Gromov, S., Grooß, J.-U., Harder, H., Huijnen, V., Jöckel, P., Karydis, V. A., Niemeyer, K. E., Pozzer, A., Riede, H., Schultz, M. G., Taraborrelli, D., and Tauer, S.: The community atmospheric chemistry box model CAABA/MECCA-4.0, Geosci. Model Dev., 12, 1365–1385, https://doi.org/10.5194/gmd-12-1365-2019, 2019.

Schultz, M. G., Stadtler, S., Schröder, S., Taraborrelli, D., Franco, B., Krefting, J., Henrot, A., Ferrachat, S., Lohmann, U., Neubauer, D., Siegenthaler-Le Drian, C., Wahl, S., Kokkola, H., Kühn, T., Rast, S., Schmidt, H., Stier, P., Kinnison, D., Tyndall, G. S., Orlando, J. J., and Wespes, C.: The chemistry–climate model ECHAM6.3-HAM2.3-MOZ1.0, Geosci. Model Dev., 11, 1695–1723, https://doi.org/10.5194/gmd-11-1695-2018, 2018.

Sheese, P. E., Walker, K. A., and Boone, C. D.: A global enhancement of hydrogen cyanide in the lower stratosphere throughout 2016, Geophys. Res. Lett., 44, 5791–5797, https://doi.org/10.1002/2017GL073519, 2017.

Shim, C., Wang, Y., Singh, H. B., Blake, D. R., and Guenther, A. B.: Source characteristics of oxygenated volatile organic compounds and hydrogen cyanide, J. Geophys. Res.-Atmos., 112, D10305, https://doi.org/10.1029/2006JD007543, 2007.

Sindelarova, K., Granier, C., Bouarar, I., Guenther, A., Tilmes, S., Stavrakou, T., Müller, J.-F., Kuhn, U., Stefani, P., and Knorr, W.: Global data set of biogenic VOC emissions calculated by the MEGAN model over the last 30 years, Atmos. Chem. Phys., 14, 9317–9341, https://doi.org/10.5194/acp-14-9317-2014, 2014.

Singh, H. B., Salas, L., Herlth, D., Kolyer, R., Czech, E., Viezee, W., Li, Q., Jacob, D. J., Blake, D., Sachse, G., Harward, C. N., Fuelberg, H., Kiley, C. M., Zhao, Y., and Kondo, Y.: In situ measurements of HCN and CH_3CN over the Pacific Ocean: Sources, sinks, and budgets, J. Geophys. Res.-Atmos., 108, 8795, https://doi.org/10.1029/2002JD003006, 2003.

Smith, T. E. L., Evers, S., Yule, C. M., and Gan, J. Y.: In Situ Tropical Peatland Fire Emission Factors and Their Variability, as Determined by Field Measurements in Peninsula Malaysia, Global Biogeochem. Cy., 32, 18–31, https://doi.org/10.1002/2017GB005709, 2018.

Stein, O., Schultz, M. G., Bouarar, I., Clark, H., Huijnen, V., Gaudel, A., George, M., and Clerbaux, C.: On the wintertime low bias of Northern Hemisphere carbon monoxide found in global model simulations, Atmos. Chem. Phys., 14, 9295–9316, https://doi.org/10.5194/acp-14-9295-2014, 2014.

Stockwell, C. E., Veres, P. R., Williams, J., and Yokelson, R. J.: Characterization of biomass burning emissions from cooking fires, peat, crop residue, and other fuels with high-resolution proton-transfer-reaction time-of-flight mass spectrometry, Atmos. Chem. Phys., 15, 845–865, https://doi.org/10.5194/acp-15-845-2015, 2015.

Stockwell, C. E., Jayarathne, T., Cochrane, M. A., Ryan, K. C., Putra, E. I., Saharjo, B. H., Nurhayati, A. D., Albar, I., Blake, D. R., Simpson, I. J., Stone, E. A., and Yokelson, R. J.: Field measurements of trace gases and aerosols emitted by peat fires in Central Kalimantan, Indonesia, during the 2015 El Niño, Atmos. Chem. Phys., 16, 11711–11732, https://doi.org/10.5194/acp-16-11711-2016, 2016.

Tao, Z. and Li, Z.: A kinetics study on reactions of C_6H_5O with C_6H_5O and O_3 at 298 k, Int. J. Chem. Kinet., 31, 65–72, https://doi.org/10.1002/(SICI)1097-4601(1999)31:1<65::AID-KIN8>3.0.CO;2-J, 1999.

Taraborrelli, D., Lawrence, M. G., Butler, T. M., Sander, R., and Lelieveld, J.: Mainz Isoprene Mechanism 2 (MIM2): an isoprene oxidation mechanism for regional and global atmospheric modelling, Atmos. Chem. Phys., 9, 2751–2777, https://doi.org/10.5194/acp-9-2751-2009, 2009.

Taraborrelli, D., Lawrence, M. G., Crowley, J. N., Dillon, T. J., Gromov, S., Groß, C. B. M., Vereecken, L., and Lelieveld, J.: Hydroxyl radical buffered by isoprene oxidation over tropical forests, Nat. Geosci., 5, 190–193, https://doi.org/10.1038/ngeo1405, 2012.

Taraborrelli, D., Cabrera-Perez, D., Bacer, S., Gromov, S., Lelieveld, J., Sander, R., and Pozzer, A.: Influence of aromatics on tropospheric gas-phase composition, Atmos. Chem. Phys., 21, 2615–2636, https://doi.org/10.5194/acp-21-2615-2021, 2021.

Tost, H., Jöckel, P., Kerkweg, A., Sander, R., and Lelieveld, J.: Technical note: A new comprehensive SCAVenging submodel for global atmospheric chemistry modelling, Atmos. Chem. Phys., 6, 565–574, https://doi.org/10.5194/acp-6-565-2006, 2006.

Trenberth, K. E.: The Definition of El Niño, Bull.e Am.n Meteorol. Soc., 78, 2771–2778, https://doi.org/10.1175/1520-0477(1997)078<2771:TDOENO>2.0.CO;2, 1997.

United Nations: Department of Economic and Social Affairs, Population Division: World Population Prospects 2019: Data Booklet, available at: https://population.un.org/wpp/Publications/Files/WPP2019_DataBooklet.pdf (last access: 6 July 2021), 2019.

van der Werf, G. R., Randerson, J. T., Giglio, L., van Leeuwen, T. T., Chen, Y., Rogers, B. M., Mu, M., van Marle, M. J. E., Morton, D. C., Collatz, G. J., Yokelson, R. J., and Kasibhatla, P. S.: Global fire emissions estimates during 1997–2016, Earth Syst. Sci. Data, 9, 697–720, https://doi.org/10.5194/essd-9-697-2017, 2017.

Vereecken, L., Chakravarty, H. K., Bohn, B., and Lelieveld, J.: Theoretical Study on the Formation of H- and O-Atoms, HONO, OH, NO, and NO_2 from the Lowest Lying Singlet and Triplet States in Ortho-Nitrophenol Photolysis, Int. J. Chem. Kinet., 48, 785–795, https://doi.org/10.1002/kin.21033, 2016.

Vigouroux, C., Blumenstock, T., Coffey, M., Errera, Q., García, O., Jones, N. B., Hannigan, J. W., Hase, F., Liley, B., Mahieu, E., Mellqvist, J., Notholt, J., Palm, M., Persson, G., Schneider, M., Servais, C., Smale, D., Thölix, L., and De Mazière, M.: Trends of ozone total columns and vertical distribution from FTIR observations at eight NDACC stations around the globe, Atmos. Chem. Phys., 15, 2915–2933, https://doi.org/10.5194/acp-15-2915-2015, 2015.

Vogel, B., Günther, G., Müller, R., Grooß, J.-U., and Riese, M.: Impact of different Asian source regions on the composition of the Asian monsoon anticyclone and of the extratropical lowermost stratosphere, Atmos. Chem. Phys., 15, 13699–13716, https://doi.org/10.5194/acp-15-13699-2015, 2015.

Walker, J. C., Dudhia, A., and Carboni, E.: An effective method for the detection of trace species demonstrated using the MetOp Infrared Atmospheric Sounding Interferometer, Atmos. Meas. Tech., 4, 1567–1580, https://doi.org/10.5194/amt-4-1567-2011, 2011.

Wang, Z., Nicholls, S. J., Rodriguez, E. R., Kummu, O., Hörkkö, S., Barnard, J., Reynolds, W. F., Topol, E. J., DiDonato, J. A., and Hazen, S. L.: Protein carbamylation links inflammation, smoking, uremia and atherogenesis, Nat. Med., 13, 1176–1184, https://doi.org/10.1038/nm1637, 2007.

Weng, H., Ashok, K., Behera, S. K., Rao, S. A., and Yamagata, T.: Impacts of recent El Niño Modoki on dry/wet conditions in the Pacific rim during boreal summer, Clim. Dynam., 29, 113–129, https://doi.org/10.1007/s00382-007-0234-0, 2007.

Whitburn, S., Van Damme, M., Clarisse, L., Bauduin, S., Heald, C. L., Hadji-Lazaro, J., Hurtmans, D., Zondlo, M. A., Clerbaux,

C., and Coheur, P.-F.: A flexible and robust neural network IASI-NH3 retrieval algorithm, J. Geophys. Res.-Atmos., 121, 6581–6599, https://doi.org/10.1002/2016jd024828, 2016a.

Whitburn, S., Van Damme, M., Clarisse, L., Turquety, S., Clerbaux, C., and Coheur, P.-F.: Doubling of annual ammonia emissions from the peat fires in Indonesia during the 2015 El Niño, Geophys. Res. Lett., 43, 11007–11014, https://doi.org/10.1002/2016gl070620, 2016b.

Wilkerson, J. T., Jacobson, M. Z., Malwitz, A., Balasubramanian, S., Wayson, R., Fleming, G., Naiman, A. D., and Lele, S. K.: Analysis of emission data from global commercial aviation: 2004 and 2006, Atmos. Chem. Phys., 10, 6391–6408, https://doi.org/10.5194/acp-10-6391-2010, 2010.

Xu, J., Morris, P. J., Liu, J., and Holden, J.: PEATMAP: Refining estimates of global peatland distribution based on a meta-analysis, Research Data Leeds Repository [Dataset], https://doi.org/10.5518/252, 2017.

Xu, J., Morris, P. J., Liu, J., and Holden, J.: PEATMAP: Refining estimates of global peatland distribution based on a meta-analysis, CATENA, 160, 134–140, https://doi.org/10.1016/j.catena.2017.09.010, 2018.

Yu, Z., Loisel, J., Brosseau, D. P., Beilman, D. W., and Hunt, S. J.: Global peatland dynamics since the Last Glacial Maximum, Geophys. Res. Lett., 37, L13402, https://doi.org/10.1029/2010GL043584, 2010.

Zhang, C.: Madden–Julian Oscillation: Bridging Weather and Climate, Bull. Am. Meteorol. Soc., 94, 1849–1870, https://doi.org/10.1175/BAMS-D-12-00026.1, 2013.

Zhang, K., Wan, H., Zhang, M., and Wang, B.: Evaluation of the atmospheric transport in a GCM using radon measurements: sensitivity to cumulus convection parameterization, Atmos. Chem. Phys., 8, 2811–2832, https://doi.org/10.5194/acp-8-2811-2008, 2008.

Zheng, B., Chevallier, F., Yin, Y., Ciais, P., Fortems-Cheiney, A., Deeter, M. N., Parker, R. J., Wang, Y., Worden, H. M., and Zhao, Y.: Global atmospheric carbon monoxide budget 2000–2017 inferred from multi-species atmospheric inversions, Earth Syst. Sci. Data, 11, 1411–1436, https://doi.org/10.5194/essd-11-1411-2019, 2019.

Chapter 8

Summary and Discussion

This thesis aims to provide a comprehensive assessment on the influence of OVOCs on the atmospheric composition by focusing on their importance and associated uncertainties in their representation in global models. The five studies that form the core of this thesis are connected with each other by addressing different aspects concerning OVOCs. Those are the formation and degradation of OVOCs in the gas-phase, the impact and representation of in-cloud OVOC oxidation, and the impact of VOC emissions on OVOC concentrations. Table 8.1 provides an overview on each study's contribution to these three foci. In the following, each study is shortly summarised and discussed in the scope of this thesis.

Table 8.1: Contribution of each study in the context of this thesis and their respective chapter.

Study	Chapter	Gas-phase	Aqueous-phase	VOC emissions
Novelli et al. (2020)	3	√		
Rosanka et al. (2020)	4	√	√	√
Rosanka et al. (2021a)	5	√	√	
Rosanka et al. (2021b)	6	√	√	√
Rosanka et al. (2021c)	7	√	√	√

8.1 The importance of isoprene oxidation

Novelli et al. (2020) (here Chapter 3) study the importance of isomerization reactions of isoprene peroxy radicals. In a first step, the OH regeneration in isoprene oxidation is directly quantified by using data obtained from experiments in the Simulation of Atmospheric PHotochemistry In a large Reaction Chamber (SAPHIR) focusing on relevant NO levels in the atmosphere. These range from 0.15 ppb to 2 ppb, which is representative for areas with low NO concentrations like the Amazonian rain forest and remote areas partially influenced by anthropogenic NO emissions. It is found that the regeneration efficiency of OH is almost 1 in areas partially influenced by anthropogenic NO emissions and reduces to about 0.5 in areas with low NO concentrations. This high OH regeneration efficiency in the low NO regime exceeds

the explainable regeneration efficiency in the absence of unimolecular reactions by a factor of 2 to 3.

In a second step, these findings are compared to quantum chemical and theoretical kinetic calculations and box-model simulations using the MCM (v3.3.1). Results show that at low NO concentrations (below 0.2 ppb), at least 50 % of the total loss of isoprene peroxy radical conformers occur via isomerization reactions. At these levels, the 1,6-α-hydroxy-hydrogen shift of isoprene Z-δ-RO_2 radicals yields unsaturated hydroperoxy aldehydes (HPALDs) and di-hydroperoxy carbonyl peroxy radicals (di-HPCARP-RO_2). HPALDs photolize quickly and di-HPCARP-RO_2 undergo a fast aldehydic hydrogen shift. Together they regenerate up to 50 % of the OH radicals.

In order to study the global implication of the proposed changes, these are implemented into EMAC's gas-phase chemical mechanism MOM (Sect. 2.1.1) in a third step. Globally, it is found that the OH regeneration by HO_2 reacting with NO is suppressed. However, this reduction is compensated by the OH regeneration from RO_2 radical isomerization reactions. The latter have the largest impact in regions characterised by high isoprene concentrations and high temperatures (e.g. Amazon basin and tropics in general). It is predicted that the isomerization globally maintains an OH regeneration efficiency of at least 0.6 over vegetated land masses. In the Amazon basin, which is the area with the highest isoprene emissions, the OH radical concentrations are increased by a factor of up to 3. At the same time, the concentrations of important OVOCs like methanol, glyoxal, methylglyoxal, formaldehyde, formic acid, hydroxyacetone, and peroxy acetyl nitrate increase by up to 30 % close to the surface.

In the context of this thesis, this study shows the importance of isoprene degradation on OVOC formation. This demonstrates that even for isoprene (a well studied VOC), considerable uncertainties still remain on the distribution of oxygenated products. By neglecting the isomerization of isoprene peroxy radicals, global models will tend to underestimate OVOC concentrations and the OH regeneration efficiency in isoprene dominated regions. The study of Novelli et al. (2020) (here Chapter 3) additionally illustrates that gas-phase chemical mechanisms used in global models suffer, among other things, from the uncertainties of the original mechanism from which they are derived.

8.2 Atmospheric loss processes of isocyanic acid

Isocyanic acid (HNCO) is an atmospheric chemical constituent that is linked to protein carbamylation, which causes adverse health effects for humans such as rheumatoid arthritis, cardiovascular diseases, and cataracts (Wang et al., 2007; Roberts et al., 2011; Leslie et al., 2019) if ambient concentrations exceed 1 ppb. It is mainly emitted by combustion processes like biomass burning, but is also inadvertently released by NO_x mitigation measures in flue gas treatments. With increasing biomass burning and more widespread usage of catalytic converters in car engines, a good prediction of HNCO atmospheric levels with global models is desirable.

Rosanka et al. (2020) (here Chapter 4) therefore analyse the importance of atmospheric HNCO loss processes on a global scale. This is achieved by first studying the potential energy surfaces of HNCO reacting with OH and NO_3 radicals, Cl atoms, and O_3 using high-level quantum chemical methodologies. Afterwards, theoretical kinetic predictions of the rate coefficients at temperatures ranging from 200 to 3000 K are performed using Transition State Theory (TST). Finally, these findings are implemented into EMAC (Sect. 2.3) including the gas-phase mechanism for formamide as an additional chemical source of HNCO, following Bunkan et al. (2016). The gas-phase chemical mechanism for nitromethane is implemented based on Taylor et al. (1980) and Calvert et al. (2008), while the mechanisms of methylamine, dimethylamine, and trimethylamine are implemented corresponding to Nielsen et al. (2012). Additionally, EMAC's standard aqueous-phase mechanism is extended to include HNCO and formamide following Behar (1974), Barnes et al. (2010), and Borduas et al. (2016).

From the theoretical kinetics analysis, it can be concluded that the atmospheric reactions of HNCO are slow and the product formation occurs predominantly by H-abstraction. This is in good agreement with earlier experimental work by Tully et al. (1989), Mertens et al. (1992), and Wooldridge et al. (1996). EMAC's predictions confirm that the gas-phase chemical loss of HNCO is a negligible process, contributing less than 1 % to the total loss, leaving heterogeneous losses as the major sinks. The removal of HNCO by clouds and precipitation contributes about 10 % to the total loss, while globally, dry deposition is the main sink, accounting for 90 %. Daily-averaged mixing ratios of ground-level HNCO are found to regularly exceed 1 ppb in regions dominated by biomass burning events. Additionally, the global simulations show that due to its long chemical lifetime in the free troposphere, HNCO can be efficiently transported into the UTLS by deep convection events.

In the context of this thesis, this study highlights that representing aqueous-phase loss processes for some OVOCs in global models can be more important than gas-phase loss processes. For HNCO, the only gas-phase chemical loss reaction that needs to be considered in global models is the reaction with OH. These findings regarding the insignificance of gas-phase loss processes are robust against varying biomass burning emission factors by Koss et al. (2018) and Kumar et al. (2018). However, the two different biomass burning emission factors lead to varying contributions of direct HNCO emissions and the formation from formamide oxidation. When using the emission factors by Kumar et al. (2018), the secondary production from formamide oxidation becomes the primary source of HNCO, resulting in tropospheric burdens of 272 Gg, which is about 26 % higher than for the simulation applying the emission factors by Koss et al. (2018). This demonstrates that the strongest modelling uncertainty related to HNCO is introduced by the representation of HNCO sources and not by the representation of its chemical loss processes.

8.3 The Jülich Aqueous-phase Mechanism of Organic Chemistry

Rosanka et al. (2020) (here Chapter 4) clearly demonstrated the importance of OVOC in-cloud oxidation, which is currently not represented in most global models (Ervens, 2015). In order to include this process, Rosanka et al. (2021a) (here Chapter 5) develop the oxidation scheme Jülich Aqueous-phase Mechanism of Organic Chemistry (JAMOC), which is suitable for global model applications, and implement it into MECCA (Sect. 2.3.3).

JAMOC is based on the recently developed comprehensive CLoud Explicit Physicochemical Scheme (CLEPS, version 1.0, Mouchel-Vallon et al., 2017), which is targeted for box-model applications. Its high complexity is not feasible for global model applications. Therefore, JAMOC includes the phase transfer of species containing up to ten carbon atoms, and a selection of species containing up to four carbon atoms react in the aqueous-phase. Compared to CLEPS, JAMOC explicitly (1) simulates hydration and dehydration of aldehydes, (2) includes the oligomerisation of formaldehyde based on Hahnenstein et al. (1995), and of glyoxal and methylglyoxal following Ervens and Volkamer (2010), (3) includes further photolysis reactions, and (4) considers the gas-phase oxidation of new outgassed species. During daytime, the main in-cloud OVOC oxidant is OH, which reacts by either H-abstraction, OH-addition if the organic compound contains a double bond, or electron transfer if an anion is present (Herrmann et al., 2015). For reactions with the main in-cloud OVOC nighttime oxidant NO_3, only H-abstraction is taken into account. Organic radicals are treated as proposed by Mouchel-Vallon et al. (2017) with the difference that in JAMOC, α-hydroxyperoxyl radicals do not undergo O_2^- elimination. The inorganic aqueous-phase chemistry is mainly based on EMAC's standard aqueous-phase mechanism (Sect. 2.1.2). Here, the inorganic O_3 chemistry is updated to the mechanism of Staehelin et al. (1984) with modifications from Staehelin and Hoigné (1985).

Rosanka et al. (2021a) (here Chapter 5) compare JAMOC to a minimum aqueous-phase oxidation scheme using CAABA (Sect. 2.2). This minimum scheme is limited to the uptake of a few soluble compounds, their acid-base equilibria, and the oxidation of SO_2 via O_3 and H_2O_2 (Jöckel et al., 2006). In the comparison, JAMOC predicts significantly lower gas-phase OVOC concentrations. This is caused by their in-cloud oxidation and a dampened gas-phase production. The predicted diurnal cycles of HO_x, NO_x, and O_3 are similar for both mechanisms and differ mainly in the absolute concentrations. With the improved representation of in-cloud OVOC reactions within JAMOC, HO_x, and O_3 concentrations are reduced, whereas NO_x concentrations slightly increase. The enhanced in-cloud OVOC oxidation leads to increased aqueous-phase $HO_{2(aq)}$ and consequently enhanced $O_{2(aq)}^-$ concentrations, resulting in an increased in-cloud destruction of $O_{3(aq)}$. Overall, the predicted impact of JAMOC is in line with earlier box-model studies (Tilgner et al., 2013; Mouchel-Vallon et al., 2017).

Within this thesis, JAMOC provides a computationally affordable method to include in-cloud OVOC oxidation in box and global model applications. The performed analysis shows the importance of aqueous-phase chemistry on the atmospheric composition and suggests that global models, which ignore this process, will tend to overestimate OVOCs and oxidants (e.g. OH, HO_2, and O_3). JAMOC is therefore the first step towards estimating the global importance of in-cloud OVOC oxidation on atmospheric oxidants (see Rosanka et al., 2021b) and to assess its influence during extreme pollution events (see Rosanka et al., 2021c). At the same time, JAMOC is designed such that its application is not limited to cloud droplets and its kinetics can also be applied to aerosols.

8.4 The influence of in-cloud OVOC oxidation on tropospheric oxidants

In Rosanka et al. (2021b) (here Chapter 6), the developed in-cloud OVOC oxidation scheme JAMOC (Rosanka et al., 2021a) (here Chapter 5) is implemented into the global model EMAC, allowing to address its implication on tropospheric oxidants. Therefore, three simulations are performed, varying in the aqueous-phase mechanism used. These include the minimum in-cloud oxidation scheme representative for most global models (Ervens, 2015), EMAC's standard aqueous-phase mechanism (Sect. 2.1.2), and JAMOC.

When in-cloud OVOC oxidation is taken into account, lower OVOC concentrations are generally predicted with the highest reduction in the tropical free troposphere. The comparison of methanol and glyoxal total columns to satellite observations confirms that the additional in-cloud sink leads to an improved representation in EMAC. Following the reduced OVOC concentration, the free tropospheric HO_x formation decreases. The enhanced in-cloud oxidation of OVOCs leads to elevated $HO_{2(aq)}$ concentrations and to an enlarged $O_{3(aq)}$ destruction (via Reaction R 1.14) in clouds. The highest O_3 change of 12 % is predicted in the UTLS. Here, lower HO_x concentrations additionally lead to a reduced chemical production of O_3. Globally, the tropospheric O_3 column is reduced by 1-2 DU. The comparison of modelled tropospheric O_3 columns to IASI satellite retrievals reveals that the newly implemented mechanism JAMOC leads to a reduction of EMAC's bias towards too high tropospheric O_3 columns.

Setting these results in the framework of this thesis, the study demonstrates the importance of in-cloud OVOC oxidation for the tropospheric oxidation capacity. In particular, OVOC, HO_x, and O_3 concentrations are influenced. Changes in O_3, methanol, and glyoxal lead to their improved representation in EMAC. Since most global models have no explicit representation of in-cloud chemistry and certainly miss the representation of the complex in-cloud OVOC oxidation, these models tend to overpredict tropospheric oxidants and to underestimate the importance of clouds as O_3 sink. Additionally, in-cloud chemical processes are known to lead to the formation of secondary organic aerosol (SOA) (Blando and Turpin, 2000; Ervens

et al., 2011; Ervens, 2015). By explicitly treating these SOA sources in JAMOC (e.g. from the oligomerisation of formaldehyde, glyoxal, and methylglyoxal), their influence on tropospheric HO_x, NO_2 photolysis, and ultimately O_3 can be addressed. Finally, the infrastructure of EMAC allows to apply JAMOC's kinetics to aerosols. However, this is outside the scope of this thesis. Even though it is not the main intention of this study, insides on the representation of VOC sources in EMAC are obtained. The comparison of modelled methanol and glyoxal columns with satellite retrievals shows that biogenic VOC sources are overestimated in the tropics, leading to higher modelled than observed OVOC concentrations. Biogenic emissions are temperature-dependent and ECHAM5 tends to simulate the Amazon basin too dry and consequently too hot (Hagemann and Stacke, 2015). Therefore, these uncertainties in VOC emissions can ultimately be related to EMAC's dynamical core. Jiang et al. (2018) demonstrated that by representing drought stress for isoprene emissions, its global emission is reduced by 17 %. Especially in regions where EMAC currently overpredicts methanol columns (e.g. central South America), drought stresses would reduce isoprene emissions. This implies that the representation of methanol and glyoxal would be improved if the drought stress for isoprene emissions was included in EMAC.

8.5 VOC emissions from Indonesian peatland fires

Rosanka et al. (2021c) (here Chapter 7) address the importance of biomass burning attributed VOC emissions to the atmospheric composition. In particular, the exceptionally strong Indonesian peatland fire period in 2015 is analysed. It was characterised by the third strongest El Niño on record, leading to a particular dry season in Indonesia. In combination with the high carbon content of peat, these fires contribute with about 30 % to the total VOC biomass burning emissions in 2015, making it the ideal test case to investigate the wild fires' impact on the atmospheric composition.

When biomass burning VOC emissions are included, OH concentrations in Indonesia are significantly reduced. This is mainly caused by OH reacting with those emitted VOCs and an enhanced reaction with CO. The latter is enhanced by VOC degradation. The intensified formation of NO_x reservoir species leads to an overall NO_x reduction. Additionally, regional toxic conditions of HNCO and nitrophenols are regularly exceeded. Elevated VOC concentrations lead to a higher chemical O_3 formation but high aromatic emissions and the consequent increase in phenoxy radicals lead to a depletion of O_3 in eastern Indonesia. The upward transport within the Asian Monsoon Anticyclone (ASMA) and the Intertropical Convergence Zone (ITCZ) in general, leads to a quick transport of the emitted VOCs and their oxidation products into the UTLS. Due to the reoccurring nature of Indonesian pealtand fires, elevated phenol concentrations lead to an enhanced destruction of O_3, potentially contributing to the variability of O_3 observed in satellite retrievals.

Regarding the context of this thesis, the study shows that biomass burning VOC

emissions lead to significant regional changes of oxidants in the lower troposphere. In combination with deep convection events, these local surface emissions have a global importance for lower stratospheric O_3. With the increasing occurrence of biomass burning events, the representation of biomass burning VOC emissions and their chemistry within global models is of importance. The comparison of modelled hydrogen cyanide (HCN) columns with IASI satellite retrievals indicates that the Indonesian peatland fires and biomass burning in general are reasonably well represented within EMAC. Here, the correct representation of the dominant fire type is of special importance. Simulating the 2015 event using JAMOC in EMAC leads to a lower increase in OVOCs and O_3 in comparison to simulations without in-cloud OVOC oxidation. This demonstrates that global models ignoring this in-cloud process will overpredict the atmospheric influence of such an event.

Chapter 9

Conclusions and Outlook

A comprehensive assessment of the influence of OVOCs on the atmospheric composition and their representation in global models has been performed, focusing on OVOCs in the gas-phase, their relevance to aqueous-phase chemistry, and the importance of VOC emissions. This has been achieved by performing five individual studies, in which measurements in SAPHIR, quantum chemical and theoretical kinetic calculations, and literature findings have been implemented in box-models and the global atmospheric chemistry model EMAC.

With respect to gas-phase processes, it has been shown that isomerization reactions of isoprene peroxy radicals are an important loss under conditions characterised by low-NO_x concentrations and lead to higher OH concentrations than previously predicted for isoprene-rich regions. Consequently, the formation of OVOCs like methanol, glyoxal, and methylglyoxal is enhanced by about 30 % in these regions. It has been further demonstrated that the gas-phase oxidation of isocyanic acid is on a global scale negligible since it removes less than 1 % from the atmosphere and that heterogeneous losses (e.g. cloud scavenging) are the dominant sink. Once above warm clouds, isocyanic acid can be easily transported to the stratosphere similarly as HCN.

In order to address the importance of aqueous-phase OVOC oxidation on tropospheric oxidants like HO_x and O_3, the Jülich Aqueous-phase Mechanism of Organic Chemistry (JAMOC) has been developed. JAMOC includes a complex OVOC oxidation scheme, which is suitable for global model applications and includes the uptake and oxidation of species containing up to ten and four carbon atoms, respectively. The uptake and in-cloud oxidation of OVOCs lowers the overall OVOC burden, resulting in a reduced OH and HO_2 formation, which is in line with earlier box-model studies. Within cloud droplets, most $HO_{2(aq)}$ is formed by the oxidation of OVOCs containing one carbon atom. Elevated $HO_{2(aq)}$ concentrations lead to an increased destruction of $O_{3(aq)}$, resulting in an enhanced O_3 scavenging. The comparison of model results to satellite retrievals revealed that EMAC's tendency to overpredict methanol, glyoxal, and O_3 has been reduced. A similar conclusion has been drawn while studying the extreme pollution from the Indonesian peatland fires in 2015. This demonstrates that global models that do not include explicit in-cloud OVOC oxidation are expected to underestimate clouds as O_3 sink.

The major atmospheric OVOC source is VOC degradation, whereas VOCs are

mainly directly emitted. In this thesis, it has been shown that biomass burning VOC emissions significantly influence regional, and to some degree global concentrations of VOCs, acids, and oxidants. Further, an increase of toxic conditions for humans and plants from these emissions has been demonstrated. The upward transport in the ASMA and the prevailing tropical convective systems leads to a quick transport of the emitted VOCs and their oxidation products into the UTLS. Here, phenoxy radicals react with O_3, potentially contributing to the variability of O_3 observed in satellite retrievals. It has been shown that the uncertainties introduced by the biomass burning emission factors are higher for some OVOCs than uncertainties in gas-phase losses. Further, uncertainties are introduced by the incorrect attribution of the dominant fire type in some regions. Based on the comparison of simulation results with satellite retrievals, it is expected that the representation of biogenic VOC emissions needs further improvement.

Ultimately, this thesis significantly improves the understanding of the three aspects that define the representation of OVOCs in global models. For the first time, a complex in-cloud OVOC oxidation scheme has been applied in a global model, demonstrating that the representation of this process is of substantial importance for future applications. The further development and application of JAMOC offers a unique opportunity to study the influence of OVOC oxidation on the tropospheric composition beyond the investigations of this thesis. JAMOC has been implemented in a modular way that allows for future additional enhancements and expansions, which are desirable for further research.

The in-cloud HO_x budget by Rosanka et al. (2021b) (here Chapter 6) showed that the importance of clouds as OVOC and O_3 sinks strongly depends on the representation of in-cloud OH concentrations. Even though available in JAMOC, the influence of transition metal ions (Fenton's chemistry) is currently not used in EMAC, due to missing global iron (Fe) distributions and emissions. As pointed out by Deguillaume et al. (2004), transition metal ion chemistry has a significant impact on in-cloud H_xO_y ($H_xO_y = H_2O_2$, HO_2/O_2^-, and OH). For example, H_2O_2 oxidises Fe^{2+} leading to the formation of OH and Fe^{3+}, which reduces to Fe^{2+} by reaction with H_2O_2, forming HO_2:

$$\mathrm{Fe^{2+} + H_2O_2 \rightarrow Fe^{3+} + OH + OH^-} \quad \text{(R 9.1)}$$

$$\mathrm{Fe^{3+} + H_2O_2 \rightarrow Fe^{2+} + HO_2 + H^+} \quad \text{(R 9.2)}$$

$$\mathrm{2\,H_2O_2 \rightarrow OH + HO_2 + H^+ + OH^-} \quad \text{(R 9.3)}$$

resulting in a major in-cloud HO_x source. In CLEPS, Fenton's chemistry contributes with about 63 % to the in-cloud OH concentration (Mouchel-Vallon et al., 2017), suggesting that HO_x is currently underestimated when using JAMOC in EMAC. Scanza et al. (2018) recently presented an approach to represent Fe concentrations in global models. Implementing this approach into EMAC would therefore make it feasible to study the importance of transition metal iron chemistry on in-cloud OVOC oxidation. The major source of atmospheric iron is mineral dust, leading to high iron concentrations close to deserts (e.g. Sahara, Lut, Thar, and Arabian

desert, Wang et al., 2015, their Fig. 6). Thus, Fenton's chemistry will lead to elevated HO_x concentrations in regions in proximity to these deserts. Further, mineral dust will be transported over the tropical Atlantic to the Amazon basin also enhancing HO_x concentrations in this region. Here, Rosanka et al. (2021b) (here Chapter 6) predict the highest changes in OVOCs due to in-cloud oxidation. Overall, elevated HO_x concentrations will lead to a higher destruction of O_3, increasing the importance of clouds as O_3 sink. This also leads to an elevated production of OH via Reaction R 1.14 and R 1.15. The OH formation from Fenton's chemistry will lead to a reduced importance of OVOC photolysis as OH source, which in Rosanka et al. (2021b) (here Chapter 6) is the second most important. Further, the photolysis of H_2O_2 as OH source will become negligible.

One example for a future expansion of JAMOC is to include the oxidation of nitrophenols. Rosanka et al. (2021c) (here Chapter 7) clearly showed that the formation of nitrophenols from biomass burning VOC emissions is high. As they can explicitly be detected in rain droplets (Leuenberger et al., 1985; Schummer et al., 2009), they contribute to the in-cloud photo-oxidation (as proposed by Hems and Abbatt, 2018). However, currently JAMOC only includes the phase transfer of some nitrophenols. For future applications of JAMOC, this additional nitrophenol sink should be included. The main fragmentation products of nitrocatechol ($C_6H_5NO_4$) oxidation are glyoxylic acid, glycolic acid, oxalic acid, and HNCO. Hence, the consideration of nitrophenols in the oxidation mechanism will improve the representation of HNCO as discussed in Rosanka et al. (2020) (here Chapter 4).

The association of aqueous-phase oxidation with acid formation is not yet explored using JAMOC, but will be part of future research. Organic acids are mainly produced by the photo-oxidation of biogenic and anthropogenic VOCs. In JAMOC, many additional organic acid sources are introduced. During a cloud event, the efficient uptake and hydration of carbonyls lead to the formation of gem-diols, which quickly equilibrate with the gas-phase. The gas-phase oxidation of these gem-diols by OH leads to the formation of acids (i.e. pyruvic and oxalic acid). When the cloud evaporates, all aqueous-phase gem-diols outgas, leading to an additional enhancement of the gas-phase organic acid production. Moreover, oxalic acid has been newly introduced in EMAC by JAMOC. It is expected that during cloud events, oxalic acid is formed within cloud droplets and transferred into the gas-phase. The gas-phase oxidation of the glyoxalic acid gem-diol potentially leads to a continuous increase in oxalic acid during and after the cloud event. Thus, the enhanced in-cloud formation of organic acid and gem-diols is expected to alter atmospheric acid concentrations.

It is well known that organic acids can lower and buffer the pH of cloud droplets. In fact, their pKa, which describes the negative of the logarithm of the acid equilibrium constant K_a, is below the natural pH of about 5.6 determined by the current atmospheric levels of CO_2 (Pye et al., 2020). Thus, enhanced organic acid concentrations lower the cloud pH in areas characterised by high VOC emissions. When studying the impact of in-cloud OVOC oxidation on organic acids using JAMOC, this effect should be addressed, quantified, and validated by using observational datasets. However, the comparison of modelled cloud pH to observations is diffi-

cult. As pointed out by Pye et al. (2020), local cloud pH observations are scarce and global observations are non-existing. Accordingly, local observations are also limited in the Amazon Basin, the region in which the highest change in cloud pH is expected due to globally highest VOC emissions.

Additionally, the organic acids mentioned above are considered to influence the formation of cloud condensation nuclei and, therefore, affect cloud formation (Yu, 2000). This impact can be investigated within the MESSy modelling system by using JAMOC for aerosol kinetics in combination with a prognostic cloud droplet nucleation scheme (Pringle et al., 2010; Chang et al., 2017). A substantial impact is expected during haze events, which are characterised by high VOC emissions like the Indonesian peatland fires (see Rosanka et al., 2021c).

The coupling of JAMOC to an aerosol module will also allow to address the impact of aqueous-phase OVOC oxidation on SOA precursors. In addition to the potential SOA formation of formaldehde-, glyoxal-, and methylglyoxal-oligomers, the formation of heterooligomers will lead to a further enhancement of SOA precursors. Paulot et al. (2009) showed that the photo-oxidation of isoprene under low-NO_x conditions leads to the formation of epoxydiols. When these epoxydiols are taken up into aerosols, they undergo ring-opening reactions leading to the direct formation of SOA (Minerath and Elrod, 2009; Eddingsaas et al., 2010). The representation of these processes are thus desirable to be included in JAMOC in order to study the importance for SOA formation.

The assessment that has been performed in this thesis shows the impact of OVOCs on the atmospheric composition and the importance of explicitly representing OVOC processing in global models. In particular, the missing representation of detailed aqueous-phase OVOC chemistry is expected to be a significant factor why many global models overpredict oxidants and the GHG O_3. In a nutshell, the development of JAMOC provides many opportunities to improve our understanding of the impact of aqueous-phase chemistry on oxidant concentrations and SOA.

Code and data availability

Within each of the five studies that form the core of this thesis, primary data have been created and analysed. These data consist of datasets created by global model simulations, quantum chemical calculations, data obtained from spaceborne measurements, and data, which have been obtained during experimental measurements. A detailed description of the code and the data availability for each study is listed in the respective 'Data availability', 'Code availability', or 'Code and data availability' sections.

The global ECHAM/MESSy Atmospheric Chemistry model (EMAC) was utilised to perform all global model simulations. EMAC includes MESSy, which is continuously developed and applied by a consortium of institutions. The usage of MESSy and access to the source code are licensed to all affiliated institutions, which are members of the MESSy Consortium. More information on the model can be found on the MESSy Consortium website (`http://www.messy-interface.org`, last access: 28 October 2020). The CAABA/MECCA model code is available as a community model published under the GNU General Public License (`http://www.gnu.org/copyleft/gpl.html`, last access: 28 October 2020). The model code is publicly available in the code repository at `https://gitlab.com/RolfSander/caaba-mecca` (last access: 28 October 2020). The exact version of the CAABA/MECCA model (version 4.5.0) developed in Rosanka et al. (2021a) (here Chapter 5) is archived at Zenodo (`https://doi.org/10.5281/zenodo.4707938`; Sander, 2021). Please consult the CAABA/MECCA web page at `http://www.mecca.messy-interface.org` (last access: 28 October 2020) for further information and updates.

In general, all global model simulations have been performed at the Jülich Supercomputing Centre (JSC) using the two high-performance computing facilities Jülich Research on Exascale Cluster Architectures (JURECA, Jülich Supercomputing Centre, 2018) and the Jülich Wizard for European Leadership Science (JUWELS, Jülich Supercomputing Centre, 2019). These simulation results are all archived at the JSC and are available on request. The model output of all CAABA/MECCA simulations presented in Rosanka et al. (2021a) (here Chapter 5) is archived at Jülich DATA (`https://doi.org/10.26165/JUELICH-DATA/SD9F6B`; Rosanka et al., 2021d). The quantum chemical calculations have been performed using the JuKinet cluster located at the JSC, which is owned by the Institute of Energy and Climate Research, Troposphere (IEK-8) of the Forschungszentrum Jülich GmbH. The resulting data are included in the supplemental material of the respective studies (Appendix A and B). The IASI O_3 data processed with FORLI-O3 v0151001 can be downloaded from the Aeris portal at (`http://iasi.aeris-data.fr/O3/`, last access: 28 October 2020). The IASI VOC columns retrieved with the ANNI framework are avail-

able upon request. The experimental data have been obtained from experiments performed in SAPHIR. These data are available on the EUROCHAMP data home page (`https://data.eurochamp.org/`, last access: 28 October 2020).

General acknowledgements

The work described in this thesis has received funding from the Initiative and Networking Fund of the Helmholtz Association through the project "Advanced Earth System Modelling Capacity (ESM)". The content of this work is the sole responsibility of the author and it does not represent the opinion of the Helmholtz Association, and the Helmholtz Association is not responsible for any use that might be made of the information contained.

The author gratefully acknowledges the computing time granted through JARA-HPC on the supercomputer Jülich Research on Exascale Cluster Architectures (JURECA, Jülich Supercomputing Centre, 2018) at Forschungszentrum Jülich.

The author gratefully acknowledges the Earth System Modelling Project (ESM) for funding this work by providing computing time on the ESM partition of the supercomputer Jülich Wizard for European Leadership Science (JUWELS, Jülich Supercomputing Centre, 2019) at the Jülich Supercomputing Centre (JSC).

Appendix A

Supporting Information: Novelli et al. (2020)

In the following, the supplemental material of Novelli et al. (2020) (here Chapter 3) is presented.

Supplement of Atmos. Chem. Phys., 20, 3333–3355, 2020
https://doi.org/10.5194/acp-20-3333-2020-supplement

Atmospheric Chemistry and Physics Open Access

Supplement of

Importance of isomerization reactions for OH radical regeneration from the photo-oxidation of isoprene investigated in the atmospheric simulation chamber SAPHIR

Anna Novelli et al.

Correspondence to: Anna Novelli (a.novelli@fz-juelich.de)

- acp-20-3333-2020-supplement-title-page.pdf
- acp-2019-794_SI.pdf
- acp-2019-794_Theoretical_data.txt

Importance of isomerization reactions for the OH radical regeneration from the photo-oxidation of isoprene investigated in the atmospheric simulation chamber SAPHIR

Anna Novelli[1], Luc Vereecken[1], Birger Bohn[1], Hans-Peter Dorn[1], Georgios I. Gkatzelis[1,2,3], Andreas Hofzumahaus[1], Frank Holland[1], David Reimer[1], Franz Rohrer[1], Simon Rosanka[1], Domenico Taraborrelli[1], Ralf Tillmann[1], Robert Wegener[1], Zhujun Yu[1,2], Astrid Kiendler-Scharr[1], Andreas Wahner[1] and Hendrik Fuchs[1]

[1]Forschungszentrum Jülich, Institute for Energy and Climate Research: Troposphere (IEK-8), 52425 Jülich, Germany
[2]now at: NOAA Earth Systems Research Laboratory, Boulder, Colorado 80305, United States
[3]now at: Cooperative Institute for Research in Environmental Sciences, Boulder, Colorado 80309, United States
[4]now at: Institute of Mass Spectrometry and Atmospheric Environment, Jinan University, Guangzhou 510632, China

Correspondence to: Anna Novelli (a.novelli@fz-juelich.de)

Supporting information

Table of content

A Theoretical work

A.1 Isoprene di-HPCARP-RO_2-I

A 1.1 Methodology

The reactants, transition states and products in the studied mechanistic branches of the isoprene chemistry were characterized at the M06-2X and CCSD(T) levels of theory. A brute force search of the conformer space for each of these structures was performed at the M06-2X/cc-pVDZ level of theory,(Dunning, 1989; Zhao and Truhlar, 2008; Alecu et al., 2010; Bao et al., 2017) starting from a systematic series of starting geometries generated by orienting the internal rotors along a set of dihedral angles reasonable for the type of rotor, and optimizing the geometry. While there is no guarantee that this approach yields all stable conformers, it should provide a near-complete description of the rotameric space. For the case at hand, ~24000 distinguishable structures were located from ~60000 starting geometries. The most relevant conformers (~850 structures across all reactions examined) were then fully re-optimized at the M06-2X/aug-cc-pVTZ level of theory.(Dunning, 1989) The number of conformers re-optimized at this higher level of theory differs per structure (see Table S1), but enough were included to cover over ~80% of the thermal population at 300K. Intrinsic reaction coordinate (IRC) calculations were performed on the lowest transition states (TS) to verify the nature to the transition state; the end points of these trajectories were further optimized and the energies used for determining an Eckart energy barrier shape. Finally, single energy point calculations at the CCSD(T)/aug-cc-pVTZ level of theory (Purvis and Bartlett, 1982) were performed on the energetically lowest-lying geometries of each structure, to further refine the energy barrier estimates.

The rate coefficients are calculated using multi-conformer canonical transition state theory (MC-CTST), where each structure is described as the ensemble of each of its conformers in a rigid rotor, harmonic oscillator approximation (Vereecken and Peeters, 2003).

$$k(T) = \frac{kT}{h}\frac{\kappa \cdot Q^{\neq}(T)}{Q_{reactant}(T)} exp\left(\frac{-E_b}{kT}\right) \qquad \text{(eq. S1)}$$

The barrier height E_b is the ZPE-corrected energy difference between the lowest conformers of transition state and reactant. The partition functions for each critical point is obtained from a Boltzmann-weighted sum of the partition functions $Q_i(T)$ of the n_{conf} conformers constituting that critical point, with $E_i = 0$ for the lowest-energy conformer:

$$Q(T) = \sum_{i=1}^{n_{conf}} Q_i\,(T) \cdot exp\left(\frac{-E_i}{kT}\right) \qquad \text{(eq. S2)}$$

This relies on a (near-)Boltzmann equilibrium population across all conformers, e.g. by internal rotation being significantly faster than chemical transformation reactions, a condition easily fulfilled for the reaction examined, given the much higher energy barriers for chemical reaction. To improve the prediction of k(T) and its temperature dependence, the partition functions $Q(T)^{all}$ are estimated for the M06-2X/aug-cc-pVTZ level of theory by combining the high level M06-2X/aug-cc-pVTZ result, available for the dominant conformers, with the low-level M06-2X/cc-pVDZ rovibrational characteristics, available for all conformers, as follows:

$$Q(T)_{high}^{all} = Q(T)_{high}^{selected} \times \frac{Q(T)_{low}^{all}}{Q(T)_{low}^{selected}} \quad \text{(eq. S3)}$$

i.e. the full partition function at the M06-2X/aug-cc-pVTZ level of theory is estimated by scaling the partition function for the dominant conformers to the total population, using the M06-2X/cc-pVDZ information of the minor conformers scaled to higher-level M06-2X/aug-cc-pVTZ. This procedure mitigates most of the impact of omitting the higher-energy conformers at the more costly levels of theory, and provides an approach that can be systematically improved to the limit of full characterization at the higher level of theory. Alternative additive schemes for merging of the high- and low levels of theory, e.g. the following:

$$Q(T)^{all} = Q(T)_{high}^{selected} + Q(T)_{low}^{all} - Q(T)_{low}^{selected} \quad \text{(eq. S4)}$$

were not retained, as such additive schemes do not scale the low-level conformer partition functions to the high-level properties, and thus converge somewhat slower to the limit where all conformers are treated at the high level of theory. Tunneling, κ, is accounted for by asymmetric Eckart tunneling, where the conformer-specific reactant and product energies, and imaginary wavenumber, of the lowest-lying TS conformer are used in the calculation. As the modeling study shows that the chemistry is not overly sensitive to the exact rate coefficient, we saved some computational cost at this time by not implementing conformer-specific tunneling κ_i in $Q^{\neq}(T)$ (e.g. Ocana et al., 2019(Ocaña et al., 2019)) but applying the same tunneling correction κ to all conformers. Conformer-specific tunneling will be implemented later when merging the current data into a structure-activity relationship (SAR).

As shown below, the rates of fast H-scrambling exceed the rates of product formation by 3 to 4 orders of magnitude, instating a fast equilibrium between **di-HPCARP-RO$_2$-Ia**, **-Ib**, and **-Ic**. In the absence of other loss processes that approach the rate of H-scrambling (as would be the case in e.g. high concentrations of NO, HO_2 or RO_2 radicals), one can then calculate a bulk rate coefficient for aldehyde H-migration, forming the tri-hydroperoxy-acyl radical. Within the MC-TST paradigm, this involves calculating the partition functions in eq. S1 across all **di-HPCARP-RO$_2$-I** and all aldehyde-H-shift TS conformers, as follows:

$$Q_{reactant}(T) = \sum_{j=a,b,c} \sum_{i=1}^{n_{conf\,j}} Q_{\text{di-HPCARP-RO2-I}j,i}(T) \cdot exp\left(\frac{-E_{\text{di-HPCARP-RO2-I}j,i}}{kT}\right) \quad \text{(eq. S5)}$$

$$Q^{\neq}(T) = \sum_{j=1,4;1,5;1,6} \sum_{i=1}^{n_{conf\,j}} Q^{\neq}_{j\text{-aldehyde-H-shift},i}(T) \cdot exp\left(\frac{-E_{\text{TS}j,i}}{kT}\right) \quad \text{(eq. S6)}$$

where $E_{\text{diHPCARP\_I}j,i}$ is the energy of the i-th conformer of **di-HPCARP-RO$_2$-I*j*** (j=a,b,c) relative to the lowest **di-HPCARP-RO$_2$-I** conformer, and $E_{TSj,i}$ the energy of the i-th conformer of the 1,4-, 1,5-, and 1,6-aldehyde-H-shift relative to the lowest aldehyde-H-shift TS conformer, while $Q_{\text{di-HPCARP-RO2-I}\,j,i}(T)$ and $Q^{\neq}_{j\text{-aldehyde-H-shift},i}$ are the conformer-specific partition functions; $n_{conf\,j}$ signifies the number of conformers for structure j. The overall barrier E_b in eq. S1 is then the (ZPE-corrected) energy difference between the lowest **diHPCARP-RO$_2$-I** conformer and the lowest aldehyde-H-shift TS conformer (in this case, the lowest-energy **diHPCARP-RO$_2$-Ic** and 1,6-aldehyde-H-shift conformers). The rate coefficients calculated thus are included in Table 3. Note that H-scrambling does not alter the stereo-specificity, i.e. eq. S5 and S6 must be calculated for each stereo-specific pool of reactants/TS. In the current case, the

difference in reaction rate between the two isomeric pools is not overly large, and a generalized expression can be obtained by averaging the two stereo-specific rate coefficients (see Table S1).

A 1.2 Reaction mechanism for di-HPCARP peroxy radicals

Table S1 shows a summary of the quantum chemical analysis of the **di-HPCARP-RO_2-I** system. These molecules have 2 chiral carbon atoms, where (2R,3R) and (2S,3S) enantiomers have identical rovibrational data, with a second distinct set of data for the (2R,3S) and (2S,3R) enantiomers. For some reactions the energetic differences are slight, but barrier height differences of several kcal mol^{-1} exist for H-migration reactions spanning across both chiral atoms, owing to the impact on ring strain and substituent interaction in the cyclic TS.

Formation of acyl radicals by migration of the aldehyde H-atom is an accessible channel for all **di-HPCARP-RO_2-I** isomers; the barrier height depends strongly on the TS cycle size, and changes from over 20 kcal mol^{-1} for a 1,4-aldehyde-H-migration, to as low as 16.3 kcal mol^{-1} for a 1,6-aldehyde-H-migration. The energetically most favorable H-migrations, however, are those involving migration of H-atoms of the hydroperoxide groups to the peroxy radical site, which allows rapid scrambling of the H-atoms, thus allowing access to reaction channels inaccessible from **di-HPCARP-RO_2-Ia** formed initially from **Z-δ-RO_2-I** (see main paper). The reactions of the **di-HPCARP-RO_2-II** isomers can be expected to be similar, i.e. fast hydroperoxide H-scrambling with energy barriers several kcal mol^{-1} below the aldehyde-H-migration pathways. Our results are analogous to those of Møller et al. (2019) (see also below).

HO_2 elimination is found to have too high barriers to compete (see Table S1 and 2), and is not studied in great detail. HO_2 elimination with a $–CH_3$ H-atom is omitted as this is expected to be even less favorable than those with aldehyde- or α-OOH H-atoms owing to the stronger C–H bond. 1,4- and 1,5-migration of the H-atoms from an -OOH-substituted carbon in **di-HPCARP-RO_2-I** is found to be less favorable than shifting the aldehyde-H-atom; while the energy barrier for the α-OOH 1,5-H-shift is only slightly higher than for the 1,4-aldehyde-H-migration, the additional entropic disadvantage of losing an additional degree of internal rotation in the TS lowers the rate coefficient significantly (see Table S1). While HO_2 elimination and α-OOH H-migrations were only examined for **di-HPCARP-RO_2-Ia**, the H-scrambled forms -**Ib** and -**Ic** are not expected to present more favorable channels for these reaction classes, as no pathways exist with more weakly bonded H-atoms, nor allowing for a TS with a lower ring strain. Likewise, it is improbable that **di-HPCARP-RO_2-II** isomers, which differ only by the position of the $-CH_3$ group, show channels that are competitive against the aldehyde- and hydroperoxide-H-migrations discussed above.

Table S1: Relative energies (kcal mol^{-1}) of the reactants and transition states for the stereo-specific chemistry of di-HPCARP-RO$_2$-I (2-Me-3,4-diOOH-butanal-2-peroxyl), at the CCSD(T)/aug-cc-pVTZ//M06-2X/aug-cc-pVTZ level of theory. Also indicated are the number of distinguishable conformers characterized at the different levels of theory, and the fraction of the population covered by the data at the highest level of theory.

Reaction	E_{rel}	# Conformers [a]	Pop. fraction [b]
(*2R,3R*)-2-Me-3,4-diOOH-butanal-2-peroxyl (**A**)	0.0	64 / 1470	0.91
1,4-aldehyde-H-migration	21.4	24 / 251	0.88
1,4-α-OOH-H-migration	28.6	6 / 125	0.98
1,5-α-OOH-H-migration	22.6	22 / 212	0.96
1,6-OOH-H-migration to **B**	19.3	6 / 100	0.88
1,7-OOH-H-migration to **C**	12.3	14 / 35	0.99
Aldehyde-HO$_2$-elimination	29.4[c]	[d]	
α-OOH-HO$_2$-elimination	31.9[c]	[d]	
(*2R,3R*)-2-Me-2,4-diOOH-butanal-3-peroxyl (**B**)	0.6	47 / 1290	0.83
1,5-aldehyde-H-migration	18.5	18 / 146	0.95
1,6-OOH-H-migration to **C**	18.9	33 / 95	0.99
(*2R,3R*)-2-Me-2,3-diOOH-butanal-4-peroxyl (**C**)	-1.2	39 / 1234	0.96
1,6-aldehyde-H-migration	17.6	27 / 157	0.97
(*2R,3R*)-2-Me-2,3,4-diOOH-1-oxo-1-butyl (**D**)	3.4	82 / 2719	0.79
CO elimination	11.1	104 / 2335	0.83
(*2R,3S*)-2-Me-3,4-diOOH-butanal-2-peroxyl (**A'**)	0.0	26 / 1362	0.87
1,4-aldehyde-H-migration	20.6	25 / 253	0.96
1,4-α-OOH-H-migration	27.2	4 / 128	0.99
1,5-α-OOH-H-migration	23.0	27 / 215	0.98
1,6-OOH-H-migration to **B'**	16.4	9 / 74	0.99
1,7-OOH-H-migration to **C'**	14.2	14 / 60	0.99
Aldehyde-HO$_2$-elimination	29.3[c]	[d]	
α-OOH-HO$_2$-elimination	31.3[c]	[d]	
(*2R,3S*)-2-Me-2,4-diOOH-butanal-3-peroxyl (**B'**)	-1.5	40 / 1280	0.91
1,5-aldehyde-H-migration	19.4	24 / 157	0.93
1,6-OOH-H-migration to **C'**	18.9	17 / 99	0.96
(*2R,3S*)-2-Me-2,3-diOOH-butanal-4-peroxyl (**C'**)	-1.3	46 / 1172	0.94
1,6-aldehyde-H-migration	16.3	25 / 146	0.98
(*2R,3S*)-2-Me-2,3,4-diOOH-1-oxo-1-butyl (**D'**)	3.1	65 / 2904	0.83
CO elimination	10.8	68 / 2495	0.78
2,2,2-triMe-acetyl	0.00		
CO elimination	9.66		
O$_2$ addition	0.47		
2,2,2-triMe-acetylperoxy	-32.80		
2,2-diMe-2-OOH-acetyl	0.00		
CO elimination	7.83		
O$_2$ addition	0.63		
2,2-diMe-2-OOH-acetylperoxy	-31.31		

[a] Number of distinguishable conformers found, with the last number indicating all conformers characterized at the M06-2X/cc-pVDZ level of theory, and the number before the dividus the number of conformers re-optimized at the M06-2X/aug-cc-pVTZ level of theory. [b] Fraction of the population at 300K that is based on M06-2X/aug-cc-pVTZ rovibrational data. The remainder of the population is described by scaling the partition function at the M06-2X/cc-pVDZ level towards the aug-cc-pVTZ data (see methodology section). [c] Energy barrier at the M06-2X/aug-cc-pVTZ level of theory. [d] The conformational space is not examined in as much detail as the other structures; statistics are omitted.

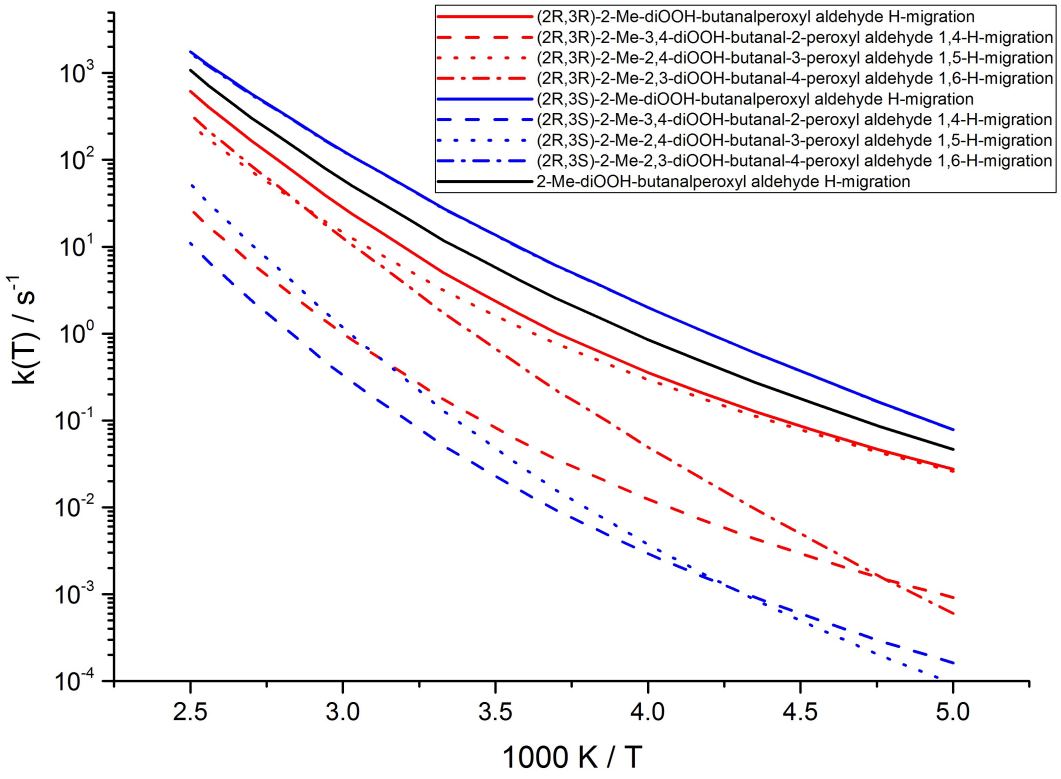

Figure S1: Temperature-dependent rate coefficients for the aldehyde H-shift in di-HPCARP-RO_2-I.

A 1.3 Comparison to literature theoretical data

There are two recent theoretical kinetic studies available examining the di-HPCARP-RO_2-I chemical system. A detailed comparison of the methodological differences is technical, and outside the scope of the current paper. To assess the uncertainties of the predictions, however, it is useful to give a short comparison of the results. We limit ourselves here to a discussion of the (R,R)-conformers, though the comparison can be generalized.

The first study by Wang et al. (2018) identified 9 conformers for di-HPCARP-RO_2-Ia, and 9 conformers for the transition state for 1,4-aldehyde-H-migration, from an examination of a subset of the conformational space with a selection of conformers based on semi-empirical methods. Despite the limited set of conformers, the rate coefficient at 298K, 0.86 s^{-1}, is only a factor 1.3 below our predicted rate of 1.15 s^{-1} based on all conformers. It is unclear whether this accuracy is due to fortuitous cancellation of error, or from judicious selection of the two (out of 8) degrees of freedom for internal rotation considered; note that the authors state that all 9 di-HPCARP-RO_2-Ia conformers can undergo the 1,4-aldehyde-H-migration directly, which indicates they include some less stable conformers, as our set of 9 energetically lowest conformers includes structures where the aldehyde H-atom and the radical oxygen

are not pointing towards each other. We optimized some of the provided conformers at the M06-2X/cc-pVDZ level of theory, finding them to be up to 8.7 kcal mol^{-1} above our most stable conformer, indicating that at least some of the 9 conformers have a negligible contribution to the thermal population. For the 1,5-α-OOH-H-migration, this study finds a rate coefficient 9.2×10^{-1} s^{-1}, over an order of magnitude higher than our value of 5×10^{-3} s^{-1}, mostly due to their reported barrier height being several kcal mol^{-1} below our value; these results are again likely distorted due to the strongly reduced conformer space missing low-energy conformers. Wang et al. (2018) do not examine any of the other aldehyde H-migration pathways to allow further comparison. The barrier for CO elimination after aldehyde H-migration, 8.5 kcal mol^{-1}, somewhat higher than our value which, combined with the limited set of conformers considered, results in a slower dissociation rate of 6.6×10^{6} s^{-1} compared to our value of 2×10^{8} s^{-1}. For such low values of CO elimination barrier heights, O_2 addition forming acylperoxy radicals would become competitive.

The methodology used by Møller et al. (2019) is more directly comparable to our methodology, and includes an extensive search of the conformer space, while the ROCCSD(T)-F12a/cc-pVDZ-F12//ωB97X-D/aug-cc-pVTZ level of theory used for the rovibrational and energetic parameters in the multi-conformer kinetics is of a comparable class of methods as the methodology used in our work. In most cases, we find strongly comparable barrier heights, with differences of a few tenths of a kcal mol^{-1} only, as expected from the levels of theory applied. Despite these resemblances, the predicted rate coefficients still differ by over an order of magnitude at room temperature. We surmise that these differences are caused by the low-level methodology used to discover and screen the conformers as outlined in Møller et al. (2016), which returns only a subset of the conformers. For example, Møller et al. (2019) report finding over 600 conformers for R,R-di-HPCARP-RO_2-Ia, whereas we have characterized almost 1500 conformers for this compound, over twice as many. Their semi-empirical screening might hope to find predominantly the most important, lowest-energy conformers, where the ~800 missed conformers would then be almost exclusively unstable, high-energy conformers with negligible contribution to the population. However, Møller et al. (2019) found 11 conformers below a 2 kcal mol^{-1} cutoff, whereas we found 27 conformers below 2 kcal mol^{-1} (M06-2X/aug-cc-pVTZ level of theory), indicating that low-energy conformers are missed in about equal proportion as for the total conformer pool. The 11 lowest conformers in our subset of 27 contribute less than 50 % of the thermal population at 300K, thus not describing the population all that well; it is unclear if the 11 conformers of Møller et al. (2019) actually correspond to our lowest 11. Furthermore, while the use of an energetic cut-off (typically 2 kcal mol^{-1} for work based on Møller et al. (2016)) is likely a reasonable choice for aliphatic compounds, it is less appropriate for work with oxygenated compounds. In particular, H-bonded conformers are energetically more favorable, but tend to be more rigid, while higher-energy conformers with less or no hydrogen bonds are more loose, i.e. more entropically favorable. Thus, as can be seen in the population analysis (shown in the supporting information), conformers with energies above 2 kcal mol^{-1} are still contributing strongly to the population. In our analysis, enough conformers are included in our high-level calculations to ascertain the bulk of the population, ≥80%, is covered, and all remaining conformers are still included in the kinetic analysis using the data at the lower level of theory. Another drawback of using an energetic cut-off in the population analysis is that, with hundreds to thousands of conformers, the high number of conformers can overcome a Boltzmann weight disadvantage of one or two orders of magnitude and still provide a non-negligible contribution to the population compared to the dozen lowest-energy conformers. The impact of this can't be assessed properly without a more complete population analysis; for the case at hand, we find that at 300K over 30% of the R,R-di-HPCARP-RO_2-Ia population is

contributed by conformers over the 2 kcal mol^{-1} energy cut-off (over 50% when referenced to the 11 lowest conformers). Having most of the conformer population represented in the kinetic analysis is especially important when the temperature-dependence is examined, e.g. the contribution of the 11 lowest conformers decreases to less than 35% of the population at 400K (though obviously Møller et al. (2019) would have used a higher energy cut-off value at this temperature). As described by Møller et al. (2019), using semi-empirical methods for screening of conformers is significantly more problematic for transition states than for reactants, spreading the conformer energy range (typically 10 to 20 kcal mol^{-1} for the multi-oxygenated compounds studied here) to over more than 1000 kcal mol^{-1}. It seems unlikely that the recovered fraction of the conformers, or fraction of the population, is always sufficiently similar for minima and TS to provide reliable cancellation of error, incurring a larger uncertainty on the rate coefficient predictions and their temperature dependence. In the following section, we shortly discuss technical aspects for further improvements in MC-TST methodologies building on the benefits of both our and Møller et al. approach.

A.2 Outlook for multi-conformer methodologies

Based on the comparison between our theoretical results and that of other authors, we find that using semi-empirical methods for screening the conformers relies more on cancellation of error than has been assumed so far, at least for more complex molecules such as studied here. To our knowledge, this is the first exploratory comparison for a complex reaction system between the Møller et al. (2016) methodology based on semi-empirical screening with a kinetic analysis of a subset of the conformers on the one hand, and the all-conformer MC-TST (Vereecken and Peeters, 2003) based on DFT screening as typically performed by our research group. Hence, it is too early to properly assess the relative performance of the two MC-TST approaches. An ineffective screening method can lead to larger *a priori* uncertainties of the kinetic predictions, probably exceeding an order of magnitude when using semi-empirical methods, though the statistical nature of the sampling prevents systematic under- or over-prediction across many reactions. It is important to stress that the search of the conformer space remains a heuristic process in practice, and all practical screening methods are likely to miss some conformer in complex cases, as well as return structures that are non-existing at higher levels of theory. Furthermore, due to the large number of structures involved, it becomes more likely that e.g. erroneous structures are not removed from the populations, or that other flaws are missed by the scientist, despite extensive use of software in generating, handling, and testing all structures. Our more rigorous screening is thus also likely both a subset and superset of the true conformer pool. The larger number of conformers found, and the inclusion of all conformers in the kinetic analysis, dampens the impact to a larger extend than in the methodology of Møller et al. (2016), but this increased robustness comes at a considerable additional computational cost. Note that applying higher levels of theory afterwards on the subset of conformers obtained can't rectify shortcomings in the conformer screening.

For the reactions classes studied here, i.e. H-migration in RO_2 intermediates leading to poly-functionalized species and HOMs, there is significant interest in the chemistry of larger terpenoids. The increased computational cost of characterizing these molecules could become overwhelming, so developing efficient and accurate screening methods are critical. Despite the challenges encountered when using semi-empirical methods, the computationally more affordable methodology implemented by Møller et al. (2016) has then many uses; in particular, it remains a cost-effective method for identifying which reactions might be important or can be neglected (e.g. the α-OOH H-shift reactions or HO_2

eliminations given in Table S1), providing an order-of-magnitude estimate of the rate coefficient, and of its temperature dependence over small temperature ranges. Future work should try to identify screening methods that are computationally less costly than used in our work, yet are more reliable than semi-empirical methods in returning most conformers, or returning all low-energy conformers. A detailed numerical comparison between this work and the data in Møller et al. (2019) is outside the scope of this paper, but would be an excellent starting point in the search for reliable yet affordable screening methods. This method development would need to include quantum chemical methods such as semi-empirical, molecular mechanics, DFT, and wavefunction-based methodologies, include sampling methods such as explicit iteration over all variables, nearest-neighbor search, random walks, or Monte-Carlo sampling, and include ensemble methods, asymptotic convergence, and other quality metrics to assess the completeness of the sampling. Superimposed on this sampling problem, the traditional improvements on the prediction of energetic and rovibrational characteristics of the molecules and on the theoretical kinetic analysis, remain an important factor facing its own challenges when dealing with exceedingly large sets of conformers.

A.3 Chemistry of enol-peroxy radicals

Earlier studies have shown that unsaturated peroxy radicals can have fast ring closure reactions (Vereecken and Peeters, 2004), and this reaction class has been invoked in atmospheric models such as the OH-initiated β-pinene oxidation to explain experimentally observed nopinone and acetone yields (Kaminski et al., 2017). Similarly, H-migrations accelerated by double bonds have been proposed (Peeters et al., 2014). In contrast, the enol peroxy radicals, formed in the isoprene mechanism from Z,E'-HOO-hydroxy-allyl radicals by O_2 addition (see figure S2), are thought by Müller et al. (2019) to have no viable reaction channels competing with redissociation to an alkyl radical + O_2, implying that H-migration and ring closure reactions are negligibly slow. In this section, we perform some exploratory calculations on template enol-peroxy radicals to examine at the impact of unsaturated bonds and of –OH substitution on these two reaction classes.

Figure S2 shows the barrier heights and rate coefficients obtained for 6-membered ring closure reactions in enols. In our earlier work we only examined isoprene-derived unsaturated peroxy radicals where the –OH substituent was not attached to the double-bonded carbons, finding ring closure rates of the order of 0.3 s^{-1} at 303 K (Vereecken and Peeters, 2004). In this work, we find that the formation of α-OH cyclic peroxides significantly lowers the barriers compared to aliphatic peroxide radicals with only a spectator –OH substituent, thus increasing the reaction rates significantly (to ~10 s^{-1}). We also observe strong stereo-specificity in the calculated rates, with the Z-enols reaction being slower than E-enols. The underlying reason is the H-bond in the Z-enol reactant, which needs to break when performing the ring closure, and thus leading to a higher effective reaction barrier. Still, the rate coefficient difference between Z- and E-enols is not as large as would be expected from the difference in barrier height, as the dominant H-bonded Z-enol conformer is also much more rigid then the E-enols, leading to a lower state density for the Z-enol reactant and hence a more favorable entropic factor in the rate coefficient calculations. Figure S2 also shows the impact of a methyl group on the double bond, where we find that formation of a tertiary product radical further lowers the ring closure barrier height by 2 kcal mol^{-1}, again enhancing the reaction rate. This result is expected, confirming a traditional Evans-Polanyi correlation. Combined, we find that ring closure is accelerated by several orders of magnitude compared to the ring closure rates found in our earlier work, with ring closure rate coefficients as high as 10^3 s^{-1}.

Similar enhancement was found for H-migration reactions (see figure S2), where formation of an hydroxy-allyl-resonance stabilized radical product leads to H-migration reactions several orders of magnitude faster ($k \sim 6\times10^{-2}$ s^{-1}) than traditional, aliphatic methyl-H-abstractions which have rather slow reaction rates ($k \sim 10^{-4}$ s^{-1}) as predicted by theory and observed by experiment (Nozière and Vereecken; Sharma et al., 2010; Miyoshi, 2011; Otkjær et al., 2018). In this particular case, the H-migration rate coefficients are too low to compete against the ring closure reaction. However, the enhancement of the H-migration rates could be important for formation of oxygenates and highly oxygenated molecules (HOMs) from other compounds, where experimental evidence on HOM formation shows very high oxygen to carbon ratios, which can only be explained if all carbons in the reactant molecule are activated for oxidation. Allyl-resonance stabilization of the product radical, possibly aided by stabilizing substituents on the second radical site, could thus prove an important mechanism to enable oxygenation of otherwise mostly unreactive methyl groups in terpenoids and other atmospherically relevant compounds.

At this time, it is unclear whether the current results are directly applicable to the isoprene-derived intermediates discussed elsewhere in this work. The enol-peroxy radicals of interest there have additional oxygenated substituents, which may either enhance or reduce the reaction rate, or affect alternative loss processes such as loss of O_2. Future work will examine reactions of a wider range of enol-peroxy radicals to investigate these effects.

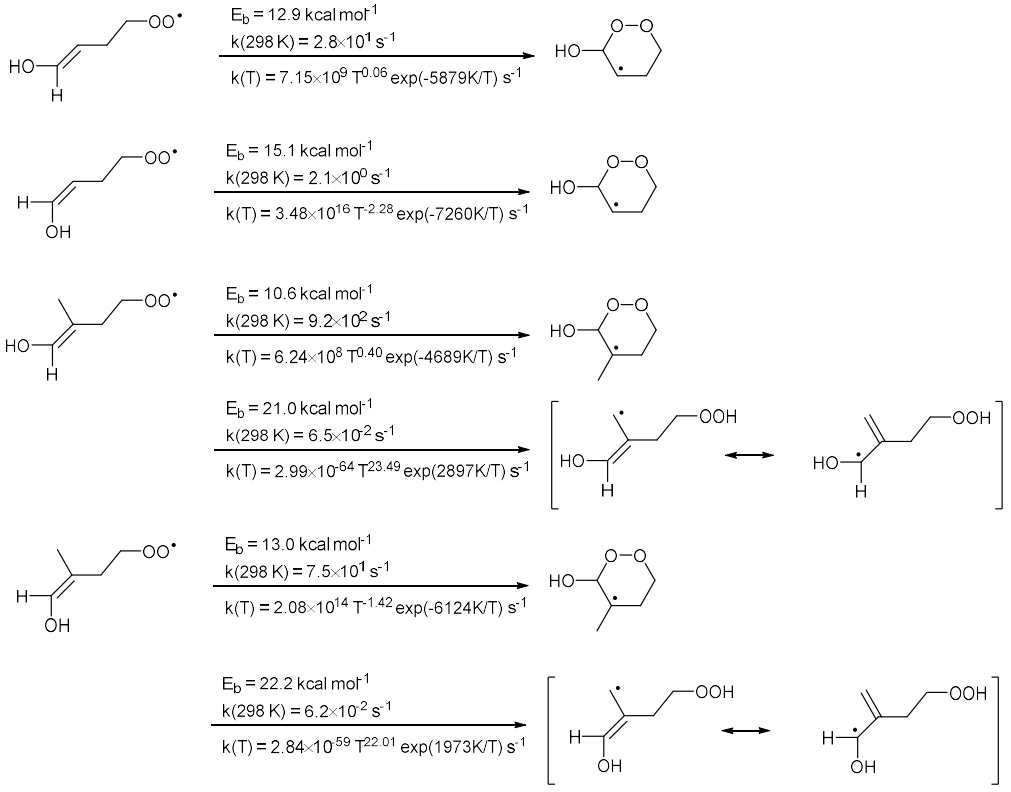

Figure S2: Barrier heights, room-temperature rate coefficients and temperature-dependent rate coefficients for ring closure and H-migration reactions in enol-peroxy radicals.

B. Kinetic models

B.1 M0 model

The M0 model is the same as the MCMv3.3.1 model but with H-shift isomerization reactions removed. To keep the number of changes as limited as possible, the removal of the isomerization reaction was implemented by removing the OH-isoprene adducts CISOPA, CISOPC, TISOPA, TISOPC that were introduced in the 2015 update to the MCM chemistry (Jenkin et al., 2015), and their equilibrium reactions. The reactions with formation of either CISOPCO2 or CISOPAO2 were likewise removed, as was the 1,5-H shift reaction as a loss path for ISOPBO2, ISOPDO2 and C524O2. To account for the resulting removal of two of the RO_2 isomers formed after reaction of isoprene with OH radicals, the yields for the remaining RO_2 radicals were scaled, accommodating the attack of the OH radicals on the isoprene carbons C2 and C3 introduced in MCMv3.3.1 (Jenkin et al., 2015). Table S2 lists all reactions affected.

Table S2 Reactions removed (in red), or modified (black) within the M0 model, compared to th MCMv3.3.1. The names of the compounds are as in the MCMv3.3.1.

Model	Reaction	Partial rate coefficient ($cm^3\ s^{-1}$)
M0	OH + C5H8 --> CISOPA	[removed]
	OH + C5H8 --> CISOPC	[removed]
	OH + C5H8 --> TISOPA	[removed]
	OH + C5H8 --> TISOPC	[removed]
	ISOPAO2 --> TISOPA	[removed]
	ISOPBO2 --> CISOPA	[removed]
	ISOPBO2 --> TISOPA	[removed]
	ISOPCO2 --> TISOPC	[removed]
	ISOPDO2 --> CISOPC	[removed]
	ISOPDO2 --> TISOPC	[removed]
	OH + C5H8 --> ISOPAO2	$2.7\times10^{-11}\times\exp(390/T)\times0.14$
	OH + C5H8 --> ISOPBO2	$2.7 \times 10^{-11}\times\exp(390/T)\times0.41$
	OH + C5H8 --> ISOPCO2	$2.7 \times 10^{-11}\times\exp(390/T)\times0.09$
	OH + C5H8 --> ISOPDO2	$2.7 \times 10^{-11}\times\exp(390/T)\times0.28$
	ISOPBO2 --> MVK + HCHO + OH	[removed]
	ISOPDO2 --> MACR + HCHO + OH	[removed]
	C524O2 --> HMACR + HCHO + OH	[removed]

B.2 M1 model

The M1 model is based on the MCMv3.3.1 model but contains:

1- The equilibrium reactions between OH-isoprene adducts and isoprene-RO_2 conformers as implemented in the Caltech mechanism (Wennberg et al., 2018).
2- A faster 1,6-H shift for the Z-δ-RO_2 combined with a higher yield of formation for di-HPCARP-RO_2 (0.6), as suggested by experimental and theoretical results (Peeters et al., 2014; Teng et al., 2017) and as described in the Caltech mechanism (Wennberg et al., 2018).
3- The rate coefficients for the aldehyde-H shift of di-HPCARP-RO_2 and product distribution as calculated from theory within this study.

Table S3 lists all reactions affected.

Table S3 Reactions modified within the M1 model, compared to th MCMv3.3.1. The names of the compounds are as in the MCMv3.3.1.

Model	Reaction	Partial rate coefficients ($cm^3\ s^{-1}$ or s^{-1})
M1	TISOPA-->ISOPAO2	0.4×10^{-12}
	TISOPA--> ISOPBO2	0.8×10^{-12}
	CISOPA-->ISOPBO2	0.8×10^{-12}
	CISOPA-->CISOPAO2	0.1×10^{-12}
	CISOPC-->CISOPCO2	0.2×10^{-12}
	CISOPC-->ISOPDO2	0.7×10^{-12}
	TISOPC-->ISOPDO2	0.7×10^{-12}
	TISOPC-->ISOPCO2	0.5×10^{-12}
	ISOPAO2-->TISOPA	$1.8\times10^{14}\times\exp(-8930/T)$
	ISOPBO2-->TISOPA	$2.2\times10^{15}\times\exp(-10355/T)$
	ISOPBO2-->CISOPA	$2.2\times10^{15}\times\exp(-10865/T)$
	CISOPAO2-->CISOPA	$1.8\times10^{14}\times\exp(-8830/T)$
	CISOPCO2-->CISOPC	$1.7\times10^{14}\times\exp(-9054/T)$
	ISOPDO2-->CISOPC	$2.5\times10^{15}\times\exp(-10890/T)$
	ISOPDO2-->TISOPC	$2.5\times10^{15}\times\exp(-11112/T)$
	ISOPCO2-->TISOPC	$2.1\times10^{14}\times\exp(-9400/T)$
	CISOPAO2-->C5HPALD1+HO2	$5.0\times10^{15}\times\exp(-12200/T)\times\exp(1\times10^{8}/T^{3})\times0.4$
	CISOPAO2-->C536O2	$5.0\times10^{15}\times\exp(-12200/T)\times\exp(1\times10^{8}/T^{3})\times0.6$
	CISOPCO2-->C5HPALD2+HO2	$2.2\times10^{9}\times\exp(-7160/T)\times\exp(1\times10^{8}/T^{3})\times0.4$
	CISOPCO2-->C537O2	$2.2\times10^{9}\times\exp(-7160/T)\times\exp(1\times10^{8}/T^{3})\times0.6$
	C536O2-->DHPMEK+CO+OH	$6.5\times10^{-53}\times T^{20.52}\times\exp(1669/T)$
	C537O2-->DHPMPAL+CO+OH	$6.5\times10^{-53}\times T^{20.52}\times\exp(1669/T)$

B.3 M2 model

The M2 model is based on the MCMv3.3.1 model but contains:

1- A faster 1,6-H shift for the Z-δ-RO_2 combined with a higher yield of formation for di-HPCARP-RO_2 (0.6), as suggested by experimental and theoretical results (Peeters et al., 2014; Teng et al., 2017) and as described in the Caltech mechanism (Wennberg et al., 2018).
2- The rate coefficients for the aldehyde-H shift of di-HPCARP-RO_2 and product distribution as calculated from theory within this study.

Table S4 lists all reactions affected.

Table S4 Reactions modified within the M2 model, compared to th MCMv3.3.1. The names of the compounds are as in the MCMv3.3.1.

Model	Reaction	Partial rate coefficients (s^{-1})
M2	CISOPAO2-->C5HPALD1+HO2	$5.0\times10^{15}\times\exp(-12200/T)\times\exp(1\times10^{8}/T^{3})\times0.4$
	CISOPAO2-->C536O2	$5.0\times10^{15}\times\exp(-12200/T)\times\exp(1\times10^{8}/T^{3})\times0.6$
	CISOPCO2-->C5HPALD2+HO2	$2.2\times10^{9}\times\exp(-7160/T)\times\exp(1\times10^{8}/T^{3})\times0.4$
	CISOPCO2-->C537O2	$2.2\times10^{9}\times\exp(-7160/T)\times\exp(1\times10^{8}/T^{3})\times0.6$
	C536O2-->DHPMEK+CO+OH	$6.5\times10^{-53}\times T^{20.52}\times\exp(1669/T)$
	C537O2-->DHPMPAL+CO+OH	$6.5\times10^{-53}\times T^{20.52}\times\exp(1669/T)$

B.4 M3 model

The M3 model is based on the MCMv3.3.1 model but contains:

1- A faster 1,6-H shift for the Z-δ-RO_2 as suggested by experimental and theoretical results (Peeters et al., 2014; Teng et al., 2017) and as described in the Caltech mechanism (Wennberg et al., 2018).
2- A larger yield for HPALD as described in the study by Berndt et al. (2019)
3- The rate coefficients for the aldehyde-H shift of di-HPCARP-RO_2 and product distribution as calculated from theory within this study.

Table S5 lists all reactions affected.

Table S5 Reactions modified within the M3 model, compared to th MCMv3.3.1. The names of the compounds are as in the MCMv3.3.1.

Model	Reaction	Partial rate coefficients (s^{-1})
M3	CISOPAO2-->C5HPALD1+HO2	$5.0\times10^{15}\times\exp(-12200/T)\times\exp(1\times10^{8}/T^{3})\times0.75$
	CISOPAO2-->C536O2	$5.0\times10^{15}\times\exp(-12200/T)\times\exp(1\times10^{8}/T^{3})\times0.25$
	CISOPCO2-->C5HPALD2+HO2	$2.2\times10^{9}\times\exp(-7160/T)\times\exp(1\times10^{8}/T^{3})\times0.75$
	CISOPCO2-->C537O2	$2.2\times10^{9}\times\exp(-7160/T)\times\exp(1\times10^{8}/T^{3})\times0.25$
	C536O2-->DHPMEK+CO+OH	$6.5\times10^{-53}\times T^{20.52}\times\exp(1669/T)$
	C537O2-->DHPMPAL+CO+OH	$6.5\times10^{-53}\times T^{20.52}\times\exp(1669/T)$

C. Modelled OH regeneration efficiency (RE)

The aldehyde-H shift includes the isomerization reaction of the di-HPCARP-RO_2 (C536O2 and C537O2) formed after the isomerization of the Z-*δ*-RO_2, combined with the OH radical which is directly recycled from the products of the aldehyde-H shift (dihydroperoxy carbonyl compounds, DHPMEK and DHPMPAL). In addition, the isomerization of the RO_2 which originates from OH reaction with MACR (MACRO2) is included (Table S6).

Table S6. Reaction paths forming OH radicals included in the modelled OH regeneration efficiency, with their label as used in figure 7. The names of the compounds are as in the MCMv3.3.1.

Reaction label	Reaction paths included
HONO + *hv*	HONO + *hv*
O_3 + *hv*	O_3 + *hv*
HO_2+ O_3	HO_2+ O_3
HO_2 + NO	HO_2 + NO
1,5-H shift	ISOPBO2 and ISOPDO2
HPALD + *hv*	C5HPALD1+ C5HPALD2+ C5PACALD1+ C5PACALD2 + *hv*
Aldehyde-H shift	C536O2, C537O2, DHPMEK, DHPMPAL, MACRO2

D. Global model

The ECHAM/MESSy Atmospheric Chemistry (EMAC) (Jöckel et al., 2010) model was used to investigate the global impact of changes in the isomerization of the isoprene chemistry. In this study, two simulations were performed using the Mainz Organic Mechanism (MOM) (Sander et al., 2019). The first simulation served as a reference and the second one included changes as discussed in this study. In the reference simulation, no 1,6-H shift and aldehyde-H shift isomerization in the isoprene chemistry were included (comparable to the no-H shift model). The second simulation is comparable to the M2 model and includes isomerization reactions (1,5-, 1,6- and aldehyde –H shift) using a 0.4 yield for HPALD and 0.6 yield for di-HPCARP-RO_2 from the 1,6-H shift. In addition, traditional RO_2 chemistry was included for HPALD and di-HPCARP as used in the MCMv3.3.1. For both simulations, the reaction rates adapted from LIM1 (Peeters et al., 2014) for the equilibrium reactions between OH-isoprene adducts and isoprene-RO_2 conformers were used. Finally, a third simulation was run where the yield of HPALD was set to 0.75, comparable to model M3. The relevant reactions are listed in table S7, while the impact on the OH concentrations is illustrated in figure S3.

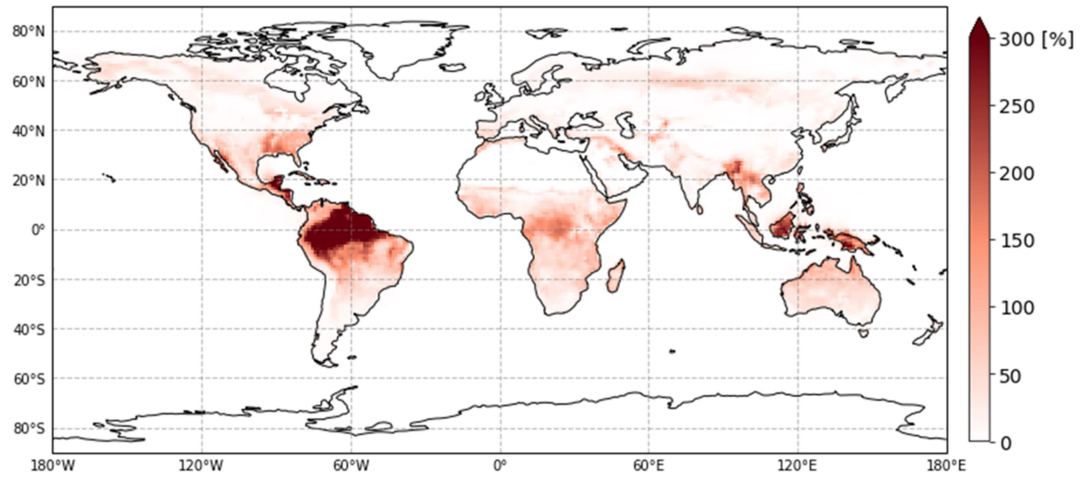

Figure S3. Relative increase of the global ground-level concentration of OH radicals. The implementation of a fast rate coefficient for the 1,6-H shift together with the inclusion of the aldehyde-H shift results in an increase of more than a factor of 3 for the OH radical concentrations in regions with large concentrations of isoprene and low NO, when compared to a model without isomerization reactions.

Table S7. Changes to the MOM mechanism used in this study to assess the global impact of isomerisation reaction in the isoprene chemistry. The names of the compounds are as in the original MOM mechanism, whereas newly added compounds are labeled as in the MCMv3.3.1.

Reaction	(Partial) Rate coefficients (cm^3 s^{-1} or s^{-1})
LISOPACO2-->C536O2	5.47 x 10^{15} x EXP(-12200/T) x EXP(1.D8/T^3) x 0.6
LISOPACO2-->ZCODC23DBCOOH+HO2	5.47 x 10^{15} x EXP(-12200/T) x EXP(1.D8/T^3))x 0.4
LDISOPACO2-->C537O2	5.47 x 10^{15} x EXP(-12200/T) x EXP(1.D8/T^3) x 0.6
LDISOPACO2-->ZCODC23DBCOOH+HO2	5.47 x 10^{15} x EXP(-12200/T) x EXP(1.D8/T^3) x 0.4
C536O2+HO2-->C536OOH+O2	2.91 x 10^{-13} x EXP(1300/T)*0.706
C536O2+NO-->C536O+NO2	2.54 x 10^{-12} x EXP(360./T)
C536O2+NO3-->C536O+NO2	2.50 x 10^{-12}
C536O2-->C536O	9.20 x 10^{-14} x RO2
C536O2-->DHPMEK+CO+OH	$6.52\times10^{-53}\times T^{20.52}\times\exp(1669/T)$
C537O2+HO2-->C537OOH+O2	2.91 x 10^{-13} x EXP(1300/T)*0.706
C537O2+NO-->C537O+NO2	2.54 x 10^{-12} x EXP(360./T)
C537O2+NO3-->C537O+NO2	2.50 x 10^{-12}
C537O2-->C537O	8.80 x 10^{-13} x RO2
C537O2-->DHPMPAL+CO+OH	$6.52\times10^{-53}\times T^{20.52}\times\exp(1669/T)$
C536OOH+OH-->DHPMEK+CO+OH	6.60 x 10^{-11}
C536O-->MGLYOX+HOOCH2CHO+OH	1.00 x 10^{6}
C537OOH+OH-->DHPMPAL+CO+OH	5.64 x 10^{-11}
C537O-->GLYOX+HYPERACET+OH	1.00 x 10^{6}
DHPMEK+OH-->BIACETOOH+OH+H2O	2.92 x 10^{-11} x 0.56
DHPMEK+OH-->C4CO2OOH+OH+H2O	2.92 x 10^{-11} x 0.44
DHPMPAL+OH-->C3MDIALOOH+OH+H2O	3.77 x 10^{-11} x 0.32
DHPMPAL+OH-->HYPERACET+CO+OH+ H2O	3.77 x 10^{-11} x 0.68
C3MDIALOOH+OH-->C3MDIALO2+H2O	1.35 x 10^{-10}
C4CO2OOH+OH-->CO23C3CHO+OH+H2O	7.83 x 10^{-11}
C4CO2O+O2-->GLYOX+CH3CO3	1.00 x 10^{6} x 0.5
C4CO2O+O2-->MGLYOX+HO2+CO	1.00 x 10^{6} x 0.5
C3MDIALO+O2-->MGLYOX+CO+HO2	1.00 x 10^{6}
C536OOH+hv-->C3MDIALOOH+HCHO+OH+OH	jx(ip_CH3OOH)
C536OOH+hv-->DHPMEK+CO+OH+HO2	jx(ip_IPRCHO2HCO)
C536OOH+hv-->MGLYOX+HOOCH2CHO+OH+OH	jx(ip_CH3OOH)*2
C537OOH+hv-->C4CO2OOH+HCHO+OH+OH	jx(ip_CH3OOH)
C537OOH+hv-->DHPMPAL+CO+OH+HO2	jx(ip_IPRCHO2HCO)
C537OOH+hv-->GLYOX+HYPERACET+OH+OH	jx(ip_CH3OOH)*2
DHPMEK+hv-->CH3CO3+HOOCH2CHO+OH	jx(ip_CH3OOH)+ jx(ip_CHOH)* 0.42
DHPMEK+hv-->MGLYOX+HCHO+OH+OH	jx(ip_CH3OOH)
DHPMPAL+hv-->C3MDIALOOH+OH	jx(ip_CH3OOH)
DHPMPAL+hv-->HYPERACET+OH+CO+HO2	jx(ip_C3H7CHO2HCO)
DHPMPAL+hv-->MGLYOX+OH+HCHO+OH	jx(ip_CH3OOH)
C3MDIALOOH+hv-->C3MDIALO+OH	jx(ip_CH3OOH)
C3MDIALOOH+hv-->MGLYOX+OH+HO2+CO	jx(ip_IPRCHO2HCO)*2
C4CO2OOH+hv-->C4CO2O+OH	jx(ip_CH3OOH)
C4CO2OOH+hv-->CH3CO3+GLYOX+OH	jx(ip_CHOH)* 0.42
C4CO2OOH+hv-->HO2+CO+MGLYOX+OH	jx(ip_IPRCHO2HCO)

D. Additional tables and figures

Table S8. Rate coefficients for the addition of O_2 to OH-isoprene adducts, and for re-dissociation of isoprene-RO_2 (Fig. 1). The rate coefficients for the oxygen additions (kf) are in cm^3 s^{-1} and are typically temperature independent. The rate coefficient for the re-dissociations (kr) are in s^{-1}.

	LIM1(Peeters et al., 2014)	MCMv3.3.1 (Jenkin et al., 2015)	Caltech (Wennberg et al., 2018)
kf1	$0.5\times10^{-12}\times\exp(-480/T)$ -	$2.5\times10^{-12}\times\exp(-480/T)$	0.4×10^{-12}
kf2	0.6×10^{-12}	3.0×10^{-12}	0.8×10^{-12}
kf3	0.6×10^{-12}	3.0×10^{-12}	0.8×10^{-12}
kf4	0.7×10^{-12}	3.5×10^{-12}	0.1×10^{-12}
kf5	0.4×10^{-12}	2.0×10^{-12}	0.2×10^{-12}
kf6	0.7×10^{-12}	3.5×10^{-12}	0.7×10^{-12}
kf7	0.7×10^{-12}	3.5×10^{-12}	0.7×10^{-12}
kf8	$0.5\times10^{-12}\times\exp(-480/T)$	$2.5\times10^{-12}\times\exp(-480/T)$	0.5×10^{-12}
kr1	$5.7\times10^{13}\times\exp(-9028/T)$	$2.9\times10^{14}\times\exp(-9028/T)$	$1.8\times10^{14}\times\exp(-8930/T)$
kr2	$1.7\times10^{15}\times\exp(-10743/T)$	$8.5\times10^{15}\times\exp(-10743/T)$	$2.2\times10^{15}\times\exp(-10355/T)$
kr3	$1.7\times10^{15}\times\exp(-11322/T)$	$8.6\times10^{15}\times\exp(-11322/T)$	$2.2\times10^{15}\times\exp(-10865/T)$
kr4	$1.0\times10^{15}\times\exp(-9838/T)$	$5.2\times10^{15}\times\exp(-9838/T)$	$1.8\times10^{14}\times\exp(-8830/T)$
kr5	$6.1\times10^{14}\times\exp(-10254/T)$	$3.1\times10^{15}\times\exp(-10254/T)$	$1.7\times10^{14}\times\exp(-9054/T)$
kr6	$2.1\times10^{15}\times\exp(-11705/T)$	$1.1\times10^{16}\times\exp(-11705/T)$	$2.5\times10^{15}\times\exp(-10890/T)$
kr7	$2.1\times10^{15}\times\exp(-11569/T)$	$1.1\times10^{16}\times\exp(-11569/T)$	$2.5\times10^{15}\times\exp(-11112/T)$
kr8	$4.2\times10^{13}\times\exp(-9984/T)$	$2.1\times10^{14}\times\exp(-9984/T)$	$2.1\times10^{14}\times\exp(-9400/T)$

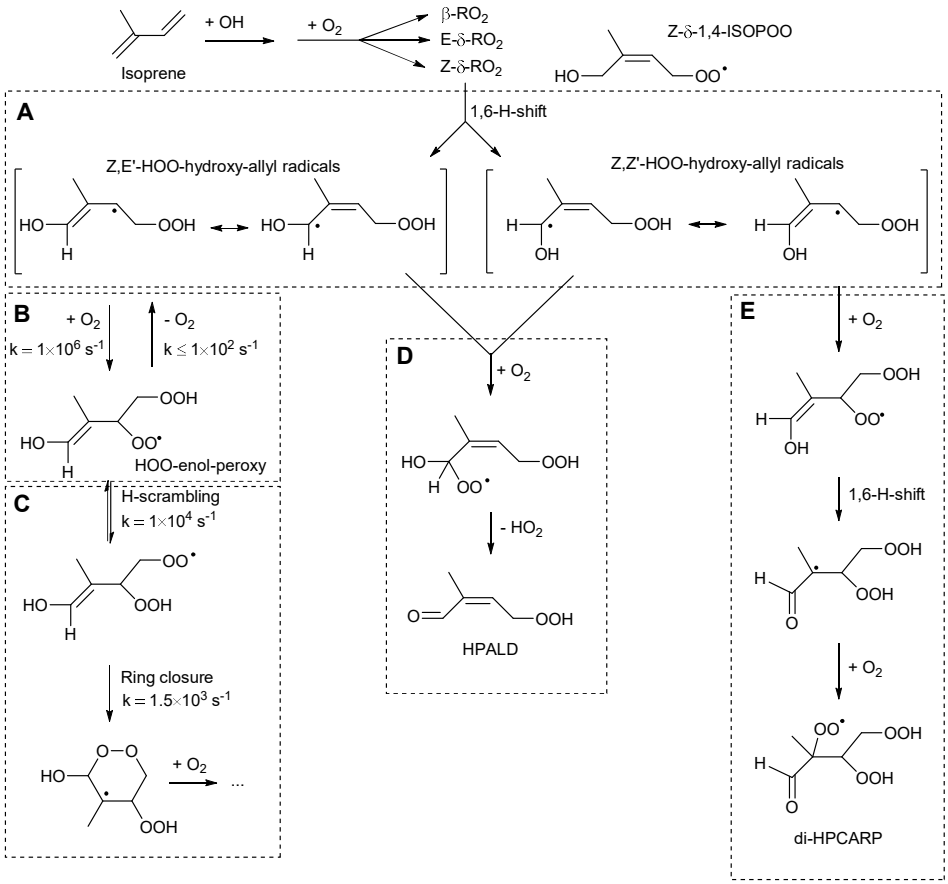

Figure S4: Reaction scheme detailing the reaction steps affecting the HPALD vrs. di-HPCARP yields. The submechanism in the labeled boxes A through E are discussed in the text.

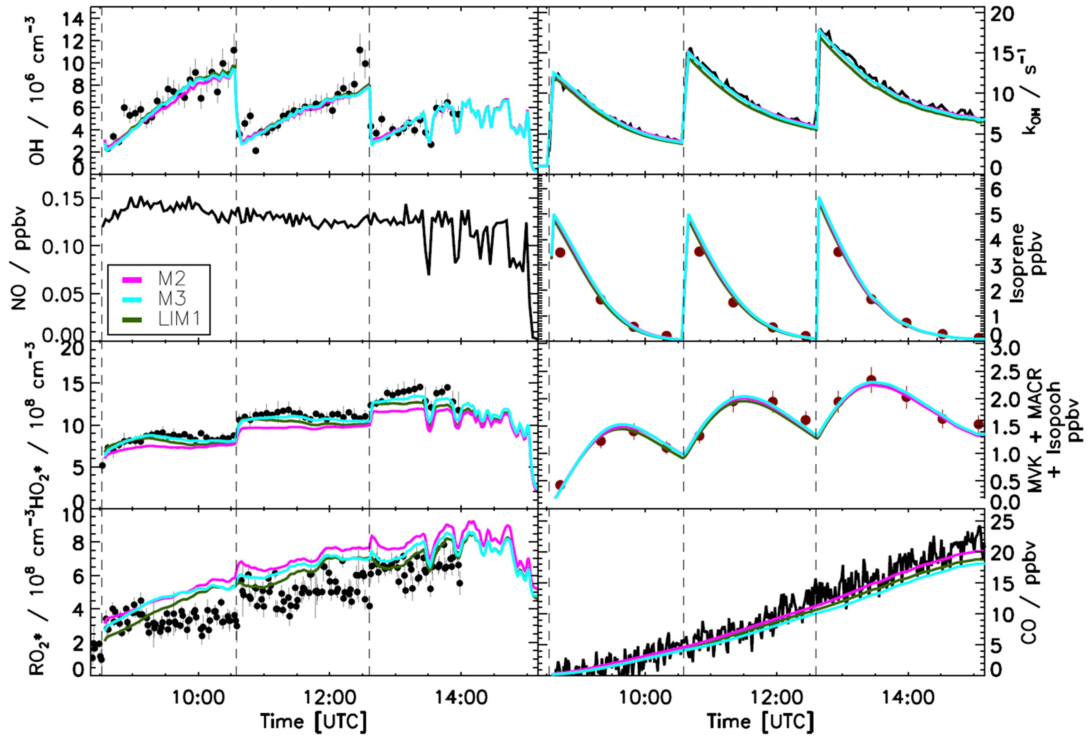

Figure S5. Comparison of modelled and measured trace gases for an experiment with NO < 0.2 ppbv. Measured time series of radicals and OH reactivity (LIF), isoprene and MVK+MACR+ISOPOOHs (GC) and CO (Picarro) are compared to model calculations. Vertical dashed lines indicate the times when isoprene was injected. Good agreement is observed when using M2, M3 or LIM1 (Table 2). Error bars represent 1 σ standard deviation.

References

Alecu, I. M., Zheng, J., Zhao, Y., and Truhlar, D. G.: Computational Thermochemistry: Scale Factor Databases and Scale Factors for Vibrational Frequencies Obtained from Electronic Model Chemistries, Journal of Chemical Theory and Computation, 6, 2872-2887, doi:10.1021/ct100326h, 2010.

Bao, J. L., Zheng, J., Alecu, I. M., Lynch, B. J., Zhao, Y., and Truhlar, D. G.: Database of Frequency Scale Factors for Electronic Model Chemistries (Version 3 Beta 2), 2017.

Berndt, T., Hyttinen, N., Herrmann, H., and Hansel, A.: First oxidation products from the reaction of hydroxyl radicals with isoprene for pristine environmental conditions, Comm. Chem., 2, 21, doi:10.1038/s42004-019-0120-9, 2019.

Dunning, T. H.: Gaussian basis sets for use in correlated molecular calculations. I. The atoms boron through neon and hydrogen, The Journal of Chemical Physics, 90, 1007-1023, doi:10.1063/1.456153, 1989.

Jenkin, M. E., Young, J. C., and Rickard, A. R.: The MCM v3.3.1 degradation scheme for isoprene, Atmos Chem Phys, 15, 11433-11459, doi:10.5194/acp-15-11433-2015, 2015.

Jöckel, P., Kerkweg, A., Pozzer, A., Sander, R., Tost, H., Riede, H., Baumgaertner, A., Gromov, S., and Kern, B.: Development cycle 2 of the Modular Earth Submodel System (MESSy2), Geosci. Model Dev., 3, 717-752, doi:10.5194/gmd-3-717-2010, 2010.

Kaminski, M., Fuchs, H., Acir, I. H., Bohn, B., Brauers, T., Dorn, H. P., Häseler, R., Hofzumahaus, A., Li, X., Lutz, A., Nehr, S., Rohrer, F., Tillmann, R., Vereecken, L., Wegener, R., and Wahner, A.: Investigation of the β-pinene photooxidation by OH in the atmosphere simulation chamber SAPHIR, Atmos. Chem. Phys., 17, 6631-6650, doi:10.5194/acp-17-6631-2017, 2017.

Miyoshi, A.: Systematic computational study on the unimolecular reactions of alkylperoxy (RO_2), hydroperoxyalkyl (QOOH), and hydroperoxyalkylperoxy (O_2QOOH) radicals, J. Phys. Chem. A, 115, 3301-3325, doi:10.1021/jp112152n, 2011.

Møller, K. H., Otkjær, R. V., Hyttinen, N., Kurtén, T., and Kjaergaard, H. G.: Cost-Effective Implementation of Multiconformer Transition State Theory for Peroxy Radical Hydrogen Shift Reactions, J Phys Chem A, 120, 10072-10087, doi:10.1021/acs.jpca.6b09370, 2016.

Møller, K. H., Bates, K. H., and Kjaergaard, H. G.: The importance of peroxy radical hydrogen-shift reactions in atmospheric isoprene oxidation, J. Phys. Chem. A, 123, 920-932, doi:10.1021/acs.jpca.8b10432, 2019.

Müller, J. F., Stavrakou, T., and Peeters, J.: Chemistry and deposition in the Model of Atmospheric composition at Global and Regional scales using Inversion Techniques for Trace gas Emissions (MAGRITTE v1.1) – Part 1: Chemical mechanism, Geosci. Model Dev., 12, 2307-2356, doi:10.5194/gmd-12-2307-2019, 2019.

Nozière, B., and Vereecken, L.: Direct Observation of Aliphatic Peroxy Radical Autoxidation and Water Effects: An Experimental and Theoretical Study, Angewandte Chemie International Edition, 0, doi:10.1002/anie.201907981.

Ocaña, A. J., Blázquez, S., Potapov, A., Ballesteros, B., Canosa, A., Antiñolo, M., Vereecken, L., Albaladejo, J., and Jiménez, E.: Gas-phase reactivity of CH₃OH toward OH at interstellar temperatures (11.7–177.5 K): experimental and theoretical study, Phys Chem Chem Phys, DOI:-10.1039/C1039CP00439D, doi:10.1039/C9CP00439D, 2019.

Otkjær, R. V., Jakobsen, H. H., Tram, C. M., and Kjaergaard, H. G.: Calculated Hydrogen Shift Rate Constants in Substituted Alkyl Peroxy Radicals, The Journal of Physical Chemistry A, 122, 8665-8673, doi:10.1021/acs.jpca.8b06223, 2018.

Peeters, J., Müller, J.-F., Stavrakou, T., and Nguyen, V. S.: Hydroxyl radical recycling in isoprene oxidation driven by hydrogen bonding and hydrogen tunneling: the upgraded LIM1 mechanism, J. Phys. Chem. A, doi:10.1021/jp5033146, 2014.

Purvis, G. D., and Bartlett, R. J.: A full coupled-cluster singles and doubles model: The inclusion of disconnected triples, The Journal of Chemical Physics, 76, 1910, doi:10.1063/1.443164, 1982.

Sander, R., Baumgaertner, A., Cabrera-Perez, D., Frank, F., Gromov, S., Grooß, J. U., Harder, H., Huijnen, V., Jöckel, P., Karydis, V. A., Niemeyer, K. E., Pozzer, A., Riede, H., Schultz, M. G., Taraborrelli, D., and Tauer, S.: The community atmospheric chemistry box model CAABA/MECCA-4.0, Geosci. Model Dev., 12, 1365-1385, doi:10.5194/gmd-12-1365-2019, 2019.

Sharma, S., Raman, S., and Green, W. H.: Intramolecular Hydrogen Migration in Alkylperoxy and Hydroperoxyalkylperoxy Radicals: Accurate Treatment of Hindered Rotors, The Journal of Physical Chemistry A, 114, 5689-5701, doi:10.1021/jp9098792, 2010.

Teng, A. P., Crounse, J. D., and Wennberg, P. O.: Isoprene peroxy radical dynamics, J Am Chem Soc, 139, 5367-5377, doi:10.1021/jacs.6b12838, 2017.

Vereecken, L., and Peeters, J.: The 1,5-H-shift in 1-butoxy: A case study in the rigorous implementation of transition state theory for a multirotamer system, J. Chem. Phys., 119, 5159-5170, doi:10.1063/1.1597479, 2003.

Vereecken, L., and Peeters, J.: Nontraditional (Per)oxy Ring-Closure Paths in the Atmospheric Oxidation of Isoprene and Monoterpenes, The Journal of Physical Chemistry A, 108, 5197-5204, doi:10.1021/jp049219g, 2004.

Wang, S., Riva, M., Yan, C., Ehn, M., and Wang, L.: Primary formation of highly oxidized multifunctional products in the OH-Initiated oxidation of Isoprene: a combined theoretical and experimental study, Environ Sci Technol, 52, 12255-12264, doi:10.1021/acs.est.8b02783, 2018.

Wennberg, P. O., Bates, K. H., Crounse, J. D., Dodson, L. G., McVay, R. C., Mertens, L. A., Nguyen, T. B., Praske, E., Schwantes, R. H., Smarte, M. D., St Clair, J. M., Teng, A. P., Zhang, X., and Seinfeld, J. H.: Gas-phase reactions of isoprene and its major oxidation products, Chem. Rev., doi:10.1021/acs.chemrev.7b00439, 2018.

Zhao, Y., and Truhlar, D. G.: The M06 suite of density functionals for main group thermochemistry, thermochemical kinetics, noncovalent interactions, excited states, and transition elements: two new functionals and systematic testing of four M06-class functionals and 12 other functionals, Theoretical Chemistry Accounts, 120, 215-241, doi:10.1007/s00214-007-0310-x, 2008.

Raw quantum chemical data:

```
################################################################################
E-HOCH=CHCH2CH2OO ring closure
################################################################################

HOCHCHCH2CH2OO.Ecpmc
~~~~~~~~~~~~~~~~~~~
E(UM062X/Aug-CC-pVTZ) (Hartree): -382.13875016
Electronic state : 2-A
Cartesian coordinates (Angs):
     C      -1.464605     -0.422977       0.119382
     C      -1.214437      0.847892      -0.164136
     C       0.132747      1.506700      -0.092726
     C       1.242428      0.655855       0.476854
     O       1.542377     -0.394003      -0.472187
     O       2.422013     -1.221736      -0.000305
     O      -2.679471     -1.027466       0.067432
     H      -0.700741     -1.127820       0.419328
     H      -2.038291      1.479660      -0.483204
     H       0.436862      1.853511      -1.084376
     H       0.067173      2.402931       0.529284
     H       2.158746      1.227493       0.615094
     H       0.967614      0.177698       1.416724
     H      -3.347513     -0.392658      -0.208613
Rotational constants (GHz):    4.5202800    1.4779300    1.1717900
Vibrational harmonic frequencies (cm-1):
       48.1026                 124.2428                 131.8012
      214.6629                 263.0421                 302.0468
      395.1256                 448.3625                 524.2222
      619.2420                 798.5684                 872.2430
      939.1204                 992.9402                1001.4340
     1064.1514                1112.3987                1161.7700
     1229.2525                1254.3525                1293.3706
     1297.0187                1350.5167                1387.6863
     1403.8246                1421.8062                1476.3599
     1506.1178                1767.7863                3052.5511
     3078.7936                3092.3963                3144.1966
     3156.9067                3222.3314                3857.5254
Zero-point correction (Hartree): 0.111644

HOCHCHCH2CH2OO.Ecpmt
~~~~~~~~~~~~~~~~~~~
E(UM062X/Aug-CC-pVTZ) (Hartree): -382.13755268
Electronic state : 2-A
Cartesian coordinates (Angs):
     C      -1.459720     -0.380138       0.100018
     C      -1.195673      0.890109      -0.161260
     C       0.160351      1.527147      -0.087119
     C       1.259783      0.656818       0.472133
     O       1.538632     -0.395509      -0.482336
     O       2.331305     -1.292747       0.015563
     O      -2.730887     -0.869703       0.027081
     H      -0.695940     -1.096969       0.379060
     H      -2.021999      1.524596      -0.459245
     H       0.465324      1.880214      -1.076448
     H       0.109175      2.419006       0.542606
     H       2.186733      1.212246       0.607498
     H       0.982718      0.178054       1.410801
     H      -2.726850     -1.817098       0.170634
Rotational constants (GHz):    4.4196600    1.5059900    1.1816000
Vibrational harmonic frequencies (cm-1):
       42.0257                 126.7007                 135.7249
      206.3338                 235.5286                 286.2958
      312.5589                 394.5795                 519.4377
      621.7216                 802.1858                 879.4116
      933.8539                 972.8706                 994.0134
     1062.5462                1111.2065                1185.9560
     1215.4124                1235.8830                1286.2828
     1299.1804                1353.5418                1387.9902
     1389.6808                1417.4445                1475.1009
     1504.8745                1790.0874                3052.1121
     3078.1940                3091.5871                3143.5744
     3188.7776                3190.6990                3917.2498
Zero-point correction (Hartree): 0.111267

HOCHCHCH2CH2OO.Ecppc
~~~~~~~~~~~~~~~~~~~
E(UM062X/Aug-CC-pVTZ) (Hartree): -382.13947030
Electronic state : 2-A
Cartesian coordinates (Angs):
     C      -1.529484     -0.302489       0.170987
     C      -1.034845      0.811980      -0.349991
     C       0.374698      1.300939      -0.188853
     C       1.232616      0.510313       0.773581
     O       1.481866     -0.830752       0.290517
     O       2.258116     -0.821903      -0.748450
     O      -2.804690     -0.750430       0.033491
     H      -0.945277     -0.991818       0.765712
     H      -1.686990      1.431986      -0.958476
     H       0.886349      1.319515      -1.154593
     H       0.364612      2.334302       0.167739
     H       2.203798      0.980548       0.914588
```

```
     H       0.745164      0.362278       1.736279
     H      -3.307907     -0.136598      -0.510058
Rotational constants (GHz):    4.9983100    1.4387300    1.2663800
Vibrational harmonic frequencies (cm-1):
       67.8308                117.8662                148.3515
      204.1084                269.3890                314.1250
      431.1025                446.1421                535.4174
      625.5700                811.4498                862.5680
      928.0912                984.7397                995.4913
     1037.2588               1118.6221               1160.2299
     1227.7424               1248.8181               1283.3823
     1316.4783               1350.1384               1390.1106
     1399.1873               1413.6909               1474.9318
     1494.2587               1766.1610               3055.8556
     3083.2992               3099.4234               3154.0351
     3155.0453               3223.1537               3859.8894
Zero-point correction (Hartree): 0.111753

HOCHCHCH2CH2OO.Ecppt
~~~~~~~~~~~~~~~~~~~~
E(UM062X/Aug-CC-pVTZ) (Hartree): -382.13802000
Electronic state : 2-A
Cartesian coordinates (Angs):
     C      -1.529449     -0.270471       0.138609
     C      -1.022385      0.847727      -0.355323
     C       0.393919      1.310374      -0.189437
     C       1.239116      0.507328       0.773733
     O       1.461834     -0.842237       0.299354
     O       2.237854     -0.857438      -0.739800
     O      -2.840301     -0.599535      -0.051762
     H      -0.944052     -0.982245       0.709316
     H      -1.680273      1.480772      -0.939231
     H       0.906484      1.324864      -1.154913
     H       0.399687      2.343160       0.169092
     H       2.219956      0.958170       0.911539
     H       0.749641      0.373436       1.737641
     H      -3.013743     -1.474224       0.298727
Rotational constants (GHz):    4.9691000    1.4437000    1.2654800
Vibrational harmonic frequencies (cm-1):
       67.3447                120.3136                150.1679
      197.9145                232.0141                293.8005
      317.3200                440.0979                534.0222
      625.9645                814.0036                865.5497
      925.5620                971.6286                985.4511
     1035.0411               1118.1520               1185.3130
     1218.1745               1229.5988               1278.3390
     1313.1957               1355.4120               1387.3704
     1392.6868               1407.0145               1473.1566
     1491.9981               1788.7664               3055.7378
     3082.3562               3098.1625               3153.7357
     3187.0484               3189.4940               3917.0116
Zero-point correction (Hartree): 0.111400

HOCHCHCH2CH2OO.Ectpc
~~~~~~~~~~~~~~~~~~~~
E(UM062X/Aug-CC-pVTZ) (Hartree): -382.13938546
Electronic state : 2-A
Cartesian coordinates (Angs):
     C       1.936312     -0.344147      -0.048058
     C       1.221437      0.766858       0.066513
     C      -0.268783      0.828034       0.220496
     C      -0.935101     -0.530449       0.227231
     O      -2.358621     -0.381508       0.409864
     O      -2.926371      0.085049      -0.659898
     O       3.285433     -0.418540      -0.190501
     H       1.502893     -1.335730      -0.039989
     H       1.740157      1.720866       0.048268
     H      -0.526798      1.344957       1.148427
     H      -0.706390      1.411545      -0.592537
     H      -0.780617     -1.069171      -0.707047
     H      -0.617071     -1.141356       1.070902
     H       3.661109      0.467113      -0.200841
Rotational constants (GHz):    9.8150100    0.9944200    0.9536900
Vibrational harmonic frequencies (cm-1):
       69.9008                110.5973                147.6182
      162.2996                271.1103                322.2673
      376.4266                438.7931                543.6010
      669.5200                774.6993                854.3725
      955.3967                987.5271                994.7808
     1101.3430               1108.4992               1158.9623
     1238.2333               1253.1820               1285.9201
     1320.6570               1340.1831               1350.9176
     1403.4472               1422.6524               1492.0627
     1503.2176               1766.7069               3055.1602
     3089.3721               3090.7007               3150.9597
     3159.3541               3214.6008               3858.0659
Zero-point correction (Hartree): 0.111728

HOCHCHCH2CH2OO.Ectpt
~~~~~~~~~~~~~~~~~~~~
E(UM062X/Aug-CC-pVTZ) (Hartree): -382.13741398
Electronic state : 2-A
Cartesian coordinates (Angs):
```

```
     C       1.939941     -0.306288      -0.043998
     C       1.212318      0.795109       0.054537
     C      -0.277420      0.841180       0.204218
     C      -0.931955     -0.522116       0.240755
     O      -2.357334     -0.384119       0.418383
     O      -2.929968      0.042776      -0.665264
     O       3.297206     -0.251505      -0.178406
     H       1.511880     -1.302568      -0.024448
     H       1.733897      1.744451       0.023800
     H      -0.541629      1.377099       1.119589
     H      -0.719151      1.403362      -0.621714
     H      -0.772293     -1.080333      -0.681255
     H      -0.609342     -1.110884       1.098530
     H       3.660101     -1.135645      -0.245271
Rotational constants (GHz):    9.8556000    0.9914600    0.9518100
Vibrational harmonic frequencies (cm-1):
       68.2076                106.6733                144.7125
      160.4354                191.3743                296.9736
      323.3690                370.0179                543.0483
      668.8520                773.9917                862.0336
      949.6565                970.6268                991.1841
     1100.9311               1106.9279               1182.2731
     1219.8489               1238.4636               1285.5997
     1318.8167               1339.1135               1355.0051
     1384.0531               1421.4667               1490.5967
     1501.8193               1787.9223               3055.0370
     3087.8865               3089.4569               3148.9799
     3179.5770               3191.1718               3919.9732
Zero-point correction (Hartree): 0.111234

HOCHCHCH2CH2OO.Ecttc
~~~~~~~~~~~~~~~~~~~
E(UM062X/Aug-CC-pVTZ) (Hartree): -382.13876938
Point group : CS
Electronic state : 2-A"
Cartesian coordinates (Angs):
     C      -0.771975     -1.802408       0.000000
     C       0.515982     -1.485695       0.000000
     C       1.065624     -0.090714       0.000000
     C      -0.000000      0.979201       0.000000
     O       0.681606      2.250581       0.000000
     O      -0.157836      3.238907       0.000000
     O      -1.288633     -3.057915       0.000000
     H      -1.565508     -1.066926       0.000000
     H       1.246994     -2.288398       0.000000
     H       1.705699      0.056392       0.873368
     H       1.705699      0.056392      -0.873368
     H      -0.628043      0.945712      -0.890070
     H      -0.628043      0.945712       0.890070
     H      -0.575674     -3.703771       0.000000
Rotational constants (GHz):    9.0291200    0.9776300    0.8918700
Vibrational harmonic frequencies (cm-1):
       73.9734 (  A")          103.8979 (  A")          122.8267 (  A')
      131.4241 (  A")          268.2891 (  A")          288.7826 (  A')
      369.1405 (  A')          428.2408 (  A")          526.8094 (  A')
      646.7481 (  A')          765.5339 (  A")          849.9082 (  A")
      979.3574 (  A')          985.2831 (  A")         1031.1827 (  A')
     1082.6697 (  A")         1125.1460 (  A')         1161.8411 (  A')
     1227.6135 (  A")         1258.5921 (  A')         1296.4638 (  A')
     1307.5496 (  A")         1331.8992 (  A')         1351.7050 (  A')
     1404.0158 (  A')         1431.0892 (  A')         1498.7546 (  A')
     1512.6102 (  A')         1765.5679 (  A')         3055.2827 (  A')
     3083.1958 (  A')         3084.1565 (  A")         3140.6048 (  A")
     3162.7702 (  A')         3218.6361 (  A')         3860.5767 (  A')
Zero-point correction (Hartree): 0.111476

HOCHCHCH2CH2OO.Ecttt
~~~~~~~~~~~~~~~~~~~
E(UM062X/Aug-CC-pVTZ) (Hartree): -382.13700871
Point group : CS
Electronic state : 2-A"
Cartesian coordinates (Angs):
     C      -0.730667     -1.816974       0.000000
     C       0.550123     -1.482173       0.000000
     C       1.078835     -0.080256       0.000000
     C      -0.000000      0.976032       0.000000
     O       0.661347      2.258959       0.000000
     O      -0.193057      3.234275       0.000000
     O      -1.122947     -3.123534       0.000000
     H      -1.532954     -1.087177       0.000000
     H       1.278914     -2.283852       0.000000
     H       1.717525      0.073764       0.873326
     H       1.717525      0.073764      -0.873326
     H      -0.627193      0.934602      -0.890543
     H      -0.627193      0.934602       0.890543
     H      -2.079119     -3.183081       0.000000
Rotational constants (GHz):    9.0451300    0.9756500    0.8903900
Vibrational harmonic frequencies (cm-1):
       78.1147 (  A")          105.6336 (  A")          123.3877 (  A')
      141.6512 (  A")          214.4010 (  A")          288.1418 (  A')
      304.9511 (  A")          364.9563 (  A')          524.9464 (  A')
      646.4276 (  A')          765.6786 (  A")          858.0770 (  A")
      969.0092 (  A")          971.9698 (  A')         1029.4277 (  A')
```

```
     1082.5480 (  A")          1124.5327 (  A')          1184.5187 (  A')
     1224.9998 (  A')          1228.0631 (  A")          1296.3103 (  A')
     1306.9655 (  A")          1329.6117 (  A')          1356.7021 (  A')
     1384.6632 (  A')          1429.1669 (  A')          1497.5473 (  A')
     1511.9850 (  A')          1787.3630 (  A')          3054.9617 (  A')
     3080.6423 (  A')          3083.6770 (  A")          3137.9846 (  A")
     3181.5268 (  A')          3193.1579 (  A')          3919.4957 (  A')
Zero-point correction (Hartree): 0.111136

HOCHCHCH2CH2OO.Egppc
~~~~~~~~~~~~~~~~~~~~
E(CCSD(T)/Aug-CC-pVTZ) (Hartree): -381.59741321
E(CCSD/Aug-CC-pVTZ) (Hartree): -381.53562656
     T1 diagnostic:  0.021635
E(MP2/Aug-CC-pVTZ) (Hartree): -381.49135115
E(MP3/Aug-CC-pVTZ) (Hartree): -381.52284012
E(PMP2/Aug-CC-pVTZ) (Hartree): -381.49450832
E(PMP3/Aug-CC-pVTZ) (Hartree): -381.52470252
E(PUHF/Aug-CC-pVTZ) (Hartree): -380.13366994
E(UHF/Aug-CC-pVTZ) (Hartree): -380.12852112
E(UM062X/Aug-CC-pVTZ) (Hartree): -382.14077322
Electronic state : 2-A
Cartesian coordinates (Angs):
     C       1.710511     -0.236631       0.326987
     C       0.944346      0.767676      -0.075868
     C      -0.364970      1.093381       0.572448
     C      -1.559565      0.810304      -0.322689
     O      -1.648835     -0.595790      -0.641420
     O      -1.913557     -1.302412       0.413399
     O       2.897580     -0.615656      -0.206873
     H       1.435802     -0.870144       1.161279
     H       1.254587      1.369726      -0.925861
     H      -0.486348      0.518270       1.490682
     H      -0.411223      2.150053       0.846885
     H      -2.497548      1.093650       0.152897
     H      -1.469744      1.294969      -1.293789
     H       3.111038     -0.054046      -0.958204
Rotational constants (GHz):    4.8942000    1.4051200    1.2198500
Vibrational harmonic frequencies (cm-1):
       48.4327                  73.9465                 138.6868
      203.0000                 282.0698                 338.0806
      432.5349                 464.7401                 534.2373
      576.6960                 817.7682                 871.9379
      917.7207                 978.5767                 989.2948
     1056.1982                1130.6006                1160.8082
     1215.2377                1261.8162                1278.7131
     1308.6740                1341.0988                1362.0063
     1399.2443                1409.4212                1476.6644
     1490.7193                1764.6782                3063.6467
     3091.5359                3117.6738                3151.0787
     3153.2238                3205.8634                3858.7646
Zero-point correction (Hartree): 0.111551

HOCHCHCH2CH2OO.Egppt
~~~~~~~~~~~~~~~~~~~~
E(UM062X/Aug-CC-pVTZ) (Hartree): -382.13943708
Electronic state : 2-A
Cartesian coordinates (Angs):
     C       1.687236     -0.201097       0.290896
     C       0.928303      0.817527      -0.079823
     C      -0.388725      1.111221       0.566132
     C      -1.573046      0.788725      -0.329917
     O      -1.625150     -0.623845      -0.632210
     O      -1.858347     -1.327385       0.431741
     O       2.875457     -0.478173      -0.312634
     H       1.391623     -0.864289       1.097960
     H       1.258737      1.441503      -0.902645
     H      -0.499833      0.540022       1.488258
     H      -0.463606      2.168069       0.832364
     H      -2.520100      1.052277       0.139199
     H      -1.491630      1.262981      -1.306601
     H       3.266520     -1.263601       0.072556
Rotational constants (GHz):    4.8400900    1.4303100    1.2324500
Vibrational harmonic frequencies (cm-1):
       47.9251                  75.1564                 145.3360
      199.4227                 255.2148                 299.2435
      337.1138                 454.6666                 532.7269
      576.7199                 824.7387                 880.4943
      914.9683                 965.1112                 979.4742
     1051.9435                1134.6384                1179.6874
     1207.3830                1246.9137                1270.9962
     1304.0541                1339.5274                1365.6406
     1395.8855                1399.3995                1477.7779
     1490.5910                1787.2229                3065.8359
     3092.1485                3116.9292                3153.6702
     3169.3150                3183.6903                3915.4862
Zero-point correction (Hartree): 0.111259

HOCHCHCH2CH2OO.Egptt
~~~~~~~~~~~~~~~~~~~~
E(UM062X/Aug-CC-pVTZ) (Hartree): -382.13810416
Electronic state : 2-A
Cartesian coordinates (Angs):
```

```
     C       1.871289     -0.153176       0.329989
     C       1.054218      0.635267      -0.348775
     C      -0.127526      1.310639       0.274269
     C      -1.450685      0.761239      -0.222213
     O      -1.582532     -0.580829       0.295585
     O      -2.656826     -1.158544      -0.143306
     O       2.936654     -0.767166      -0.254017
     H       1.728227     -0.344927       1.388712
     H       1.232642      0.780890      -1.408353
     H      -0.094393      1.210822       1.360925
     H      -0.117389      2.380612       0.054960
     H      -2.303019      1.331426       0.145625
     H      -1.494215      0.695959      -1.308917
     H       3.386003     -1.326284       0.381331
Rotational constants (GHz):    5.3088800    1.2317300    1.0613900
Vibrational harmonic frequencies (cm-1):
       44.1585                72.5962                110.5274
      188.9176                240.8283                278.9011
      332.8114                396.6938                537.4121
      566.3702                818.6533                871.5105
      917.0749                963.8968               1031.6287
     1067.3404               1123.0761               1179.5649
     1205.2590               1250.2644               1276.6812
     1299.0977               1337.7871               1364.5492
     1392.9945               1406.0468               1473.0211
     1500.3771               1790.1720               3062.0313
     3083.9850               3105.3708               3142.0309
     3170.7630               3183.3007               3917.6972
Zero-point correction (Hartree): 0.110954

HOCHCHCH2CH2OO.Elmmc
~~~~~~~~~~~~~~~~~~~~
E(CCSD(T)/Aug-CC-pVTZ) (Hartree): -381.59783370
E(CCSD/Aug-CC-pVTZ) (Hartree): -381.53613947
     T1 diagnostic:  0.021613
E(MP2/Aug-CC-pVTZ) (Hartree): -381.49167334
E(MP3/Aug-CC-pVTZ) (Hartree): -381.52332066
E(PMP2/Aug-CC-pVTZ) (Hartree): -381.49483364
E(PMP3/Aug-CC-pVTZ) (Hartree): -381.52518461
E(PUHF/Aug-CC-pVTZ) (Hartree): -380.13467350
E(UHF/Aug-CC-pVTZ) (Hartree): -380.12952628
E(UM062X/Aug-CC-pVTZ) (Hartree): -382.14119558
Electronic state : 2-A
Cartesian coordinates (Angs):
     C       2.124153      0.276916      -0.042485
     C       0.874173     -0.099991      -0.272337
     C      -0.241856      0.871925      -0.502115
     C      -1.331538      0.777029       0.551962
     O      -1.920688     -0.543726       0.557753
     O      -2.625917     -0.751207      -0.511793
     O       3.188259     -0.535457       0.177972
     H       2.419325      1.318728      -0.015007
     H       0.628268     -1.157591      -0.294153
     H       0.142333      1.893574      -0.495348
     H      -0.708634      0.706852      -1.475186
     H      -0.933191      0.894050       1.558058
     H      -2.137311      1.487177       0.372899
     H       2.906379     -1.454950       0.147128
Rotational constants (GHz):    7.1870100    1.0976100    1.0399700
Vibrational harmonic frequencies (cm-1):
       56.8155                83.9327                145.6926
      184.7958               282.8152                330.2073
      441.3317               475.5827                532.5543
      584.2154               819.8312                856.1046
      908.1255               989.8147                997.8385
     1093.6706              1120.4717               1158.1126
     1207.1273              1245.8661               1294.7724
     1306.4289              1340.7014               1365.5644
     1394.4322              1413.1006               1474.5714
     1489.2539              1763.9730               3068.0372
     3093.6743              3112.8341               3158.6898
     3163.9251              3203.8754               3858.7945
Zero-point correction (Hartree): 0.111670

HOCHCHCH2CH2OO.Elmmt
~~~~~~~~~~~~~~~~~~~~
E(UM062X/Aug-CC-pVTZ) (Hartree): -382.13870637
Electronic state : 2-A
Cartesian coordinates (Angs):
     C       2.125235      0.248322      -0.058651
     C       0.872717     -0.128232      -0.259321
     C      -0.238762      0.845137      -0.498006
     C      -1.328976      0.766348       0.557172
     O      -1.950491     -0.538911       0.551717
     O      -2.674554     -0.711942      -0.511242
     O       3.126265     -0.649485       0.162286
     H       2.416229      1.294412      -0.065456
     H       0.636743     -1.185922      -0.247669
     H       0.146936      1.866620      -0.504487
     H      -0.709261      0.670049      -1.467856
     H      -0.927013      0.865361       1.563809
     H      -2.117523      1.497240       0.384897
     H       3.962841     -0.194512       0.267517
```

```
Rotational constants (GHz):    7.4165000    1.0823000    1.0299300
Vibrational harmonic frequencies (cm-1):
       58.1094                 83.5004                145.1692
      179.0405                261.2688                283.6740
      343.9772                473.3522                529.3861
      579.8470                819.7825                865.7344
      908.1426                967.9874                997.4035
     1095.1717               1120.2871               1176.8371
     1197.1457               1237.6120               1272.9478
     1306.9577               1339.9534               1366.4940
     1393.0371               1401.3962               1474.2716
     1488.3671               1786.6412               3064.6038
     3092.0681               3109.0438               3157.2482
     3166.1291               3193.1663               3917.7310
Zero-point correction (Hartree): 0.111296

HOCHCHCH2CH2OO.Elmpc
--------------------
E(UM062X/Aug-CC-pVTZ) (Hartree): -382.14045498
Electronic state : 2-A
Cartesian coordinates (Angs):
     C       1.990995      0.290723       0.147957
     C       0.783071      0.146789      -0.378955
     C      -0.267488      1.210011      -0.300446
     C      -1.511384      0.771514       0.459024
     O      -2.173244     -0.296686      -0.251029
     O      -1.760532     -1.467795       0.130963
     O       2.994221     -0.622237       0.132025
     H       2.297937      1.195879       0.657647
     H       0.524123     -0.780504      -0.880382
     H       0.132568      2.092020       0.204050
     H      -0.576875      1.525457      -1.299715
     H      -1.276596      0.401779       1.454863
     H      -2.249624      1.570606       0.506442
     H       2.693745     -1.425720      -0.304047
Rotational constants (GHz):    5.3864800    1.3147700    1.1153500
Vibrational harmonic frequencies (cm-1):
       63.8294                 89.1137                132.6084
      185.0105                288.9820                340.3975
      444.6962                474.8875                529.9831
      562.1000                845.9667                860.7239
      884.3868                990.1286               1016.3122
     1084.0668               1116.5833               1160.1911
     1213.2703               1237.8761               1291.0053
     1322.3524               1344.0177               1370.2374
     1386.2854               1415.5074               1472.7173
     1485.0646               1763.5710               3057.6900
     3092.6181               3104.3023               3161.1612
     3167.6961               3201.1436               3857.5971
Zero-point correction (Hartree): 0.111662

HOCHCHCH2CH2OO.Elmpt
--------------------
E(UM062X/Aug-CC-pVTZ) (Hartree): -382.13752742
Electronic state : 2-A
Cartesian coordinates (Angs):
     C       1.989507      0.262297       0.130044
     C       0.777124      0.125563      -0.382394
     C      -0.261349      1.198630      -0.291182
     C      -1.508613      0.770590       0.468626
     O      -2.193658     -0.275300      -0.251268
     O      -1.812128     -1.459012       0.124798
     O       2.930095     -0.719142       0.038424
     H       2.295569      1.168905       0.643384
     H       0.522343     -0.800812      -0.883005
     H       0.147817      2.075144       0.216406
     H      -0.571089      1.522324      -1.287893
     H      -1.275494      0.383278       1.458211
     H      -2.231510      1.582752       0.531264
     H       3.737879     -0.446456       0.475440
Rotational constants (GHz):    5.4572000    1.2998800    1.1070100
Vibrational harmonic frequencies (cm-1):
       64.2559                 86.3268                130.5274
      178.1882                258.9797                287.9710
      353.5359                474.4244                526.6953
      558.9309                844.4467                871.0567
      882.9824                970.8423               1018.2529
     1084.6321               1117.4167               1179.0426
     1201.6086               1237.9409               1264.4799
     1319.0775               1345.9730               1370.6756
     1385.7920               1403.8346               1472.6167
     1484.7002               1785.9588               3055.0045
     3090.6026               3101.1149               3159.7897
     3162.9384               3196.9708               3918.7962
Zero-point correction (Hartree): 0.111280

HOCHCHCH2CH2OO.Elmtc
--------------------
E(UM062X/Aug-CC-pVTZ) (Hartree): -382.14044555
Electronic state : 2-A
Cartesian coordinates (Angs):
     C       2.175963      0.186009       0.179724
     C       0.978214      0.057207      -0.373761
```

```
     C      -0.069240      1.126498      -0.303036
     C      -1.324123      0.674537       0.417155
     O      -1.901820     -0.397832      -0.361864
     O      -2.954285     -0.892729       0.211247
     O       3.175990     -0.730064       0.170248
     H       2.475424      1.081714       0.710223
     H       0.723648     -0.859065      -0.897583
     H       0.322422      1.997960       0.224062
     H      -0.351103      1.458940      -1.304999
     H      -1.111008      0.276191       1.408134
     H      -2.073764      1.462124       0.484559
     H       2.890411     -1.518371      -0.301936
Rotational constants (GHz):    7.0870600    1.0463600    0.9597700
Vibrational harmonic frequencies (cm-1):
       49.5994                 90.3886                116.2541
      189.2059                270.1401                329.0272
      396.3809                452.8971                546.4457
      570.7131                812.1939                856.0773
      929.8350                991.5934               1033.3265
     1078.2671               1125.6248               1160.3652
     1217.0645               1246.0738               1296.9406
     1298.3373               1341.4574               1365.5075
     1398.7018               1414.1608               1472.0318
     1501.0744               1763.3001               3060.7044
     3085.6154               3109.2440               3146.6216
     3165.8735               3201.7740               3857.2177
Zero-point correction (Hartree): 0.111494

HOCHCHCH2CH2OO.Elmtt
~~~~~~~~~~~~~~~~~~~
E(UM062X/Aug-CC-pVTZ) (Hartree): -382.13798496
Electronic state : 2-A
Cartesian coordinates (Angs):
     C       2.173117      0.167424       0.157258
     C       0.970963      0.041464      -0.381228
     C      -0.072376      1.111851      -0.290724
     C      -1.324757      0.656602       0.432221
     O      -1.926112     -0.388564      -0.364734
     O      -2.984436     -0.874250       0.205234
     O       3.112428     -0.815310       0.071604
     H       2.470110      1.065938       0.689801
     H       0.724771     -0.874854      -0.904278
     H       0.322664      1.978532       0.242455
     H      -0.361053      1.454522      -1.287458
     H      -1.105852      0.232019       1.411023
     H      -2.063330      1.451864       0.527200
     H       3.915968     -0.547075       0.519265
Rotational constants (GHz):    7.2581100    1.0369700    0.9544000
Vibrational harmonic frequencies (cm-1):
       51.3622                 91.4555                114.8537
      180.4182                259.3054                273.7506
      340.7793                398.9651                541.7653
      570.7578                811.9286                867.1642
      927.9807                970.4569               1033.7417
     1079.4163               1128.4707               1178.0868
     1206.8534               1237.1343               1279.3676
     1297.4922               1339.9602               1367.0724
     1398.1003               1403.2247               1471.8138
     1500.6779               1786.2808               3058.6410
     3085.1347               3105.6017               3145.9876
     3164.0356               3195.5698               3917.2662
Zero-point correction (Hartree): 0.111131

HOCHCHCH2CH2OO.Elpmc
~~~~~~~~~~~~~~~~~~~
E(UM062X/Aug-CC-pVTZ) (Hartree): -382.14031527
Electronic state : 2-A
Cartesian coordinates (Angs):
     C      -1.716898      0.146092      -0.385021
     C      -0.768732      0.610804       0.416624
     C       0.428961      1.348511      -0.088900
     C       1.742575      0.638342       0.211557
     O       1.802244     -0.622303      -0.477781
     O       1.259329     -1.577483       0.218050
     O      -2.823031     -0.544588      -0.015065
     H      -1.686140      0.288376      -1.458048
     H      -0.834430      0.427859       1.485386
     H       0.348477      1.499505      -1.166609
     H       0.496962      2.339651       0.368448
     H       2.593005      1.204843      -0.164387
     H       1.864156      0.433781       1.274056
     H      -2.805809     -0.701510       0.933953
Rotational constants (GHz):    4.6279400    1.5523400    1.2629400
Vibrational harmonic frequencies (cm-1):
       62.2880                 96.0757                108.9101
      193.1536                290.6709                350.8344
      422.9886                466.9158                540.3184
      553.9728                824.1871                861.6162
      942.6393                983.8111                993.8037
     1040.3522               1132.5951               1164.1930
     1225.5704               1237.3195               1280.0041
     1318.0575               1343.4109               1360.5222
     1394.6357               1413.1371               1473.5582
```

```
     1485.7583                1764.5370                3051.7259
     3091.9388                3105.8278                3154.9038
     3159.3070                3207.7406                3860.3590
Zero-point correction (Hartree): 0.111534

HOCHCHCH2CH2OO.Elpmt
--------------------
E(UM062X/Aug-CC-pVTZ) (Hartree): -382.13829904
Electronic state : 2-A
Cartesian coordinates (Angs):
     C       1.679246      0.110683       0.354616
     C       0.765612      0.682938      -0.412719
     C      -0.448739      1.353033       0.142140
     C      -1.743553      0.626339      -0.199469
     O      -1.783544     -0.650949       0.461241
     O      -1.236397     -1.586352      -0.258257
     O       2.781777     -0.496873      -0.162806
     H       1.592392      0.106015       1.436620
     H       0.886845      0.636445      -1.488836
     H      -0.374506      1.436458       1.227989
     H      -0.541797      2.369393      -0.249760
     H      -2.611147      1.164789       0.178867
     H      -1.844907      0.444686      -1.267936
     H       3.283043     -0.922361       0.534221
Rotational constants (GHz):    4.5792500    1.5738300    1.2710500
Vibrational harmonic frequencies (cm-1):
       56.7528                  97.4223                 108.0751
      185.1658                 241.9628                 299.6491
      352.1428                 462.0451                 539.3009
      549.7923                 828.6190                 865.8652
      946.9980                 961.6997                 986.9639
     1038.2792                1136.0127                1180.7630
     1211.3605                1235.3846                1257.8402
     1313.9456                1340.3052                1361.4416
     1392.6747                1399.1790                1473.5968
     1484.3704                1787.1973                3054.9106
     3091.7525                3103.3339                3155.9447
     3170.1119                3189.6327                3917.6516
Zero-point correction (Hartree): 0.111125

HOCHCHCH2CH2OO.Elptc
--------------------
E(UM062X/Aug-CC-pVTZ) (Hartree): -382.13968393
Electronic state : 2-A
Cartesian coordinates (Angs):
     C      -1.897069     -0.144664      -0.371056
     C      -1.056654      0.583217       0.350585
     C       0.114627      1.304085      -0.242630
     C       1.447573      0.762783       0.234917
     O       1.597683     -0.567063      -0.306902
     O       2.675606     -1.139922       0.129742
     O      -2.970820     -0.834603       0.085399
     H      -1.789832     -0.253802      -1.443022
     H      -1.197984      0.654553       1.425816
     H       0.080097      1.244268      -1.331847
     H       0.085634      2.364985       0.016705
     H       2.288937      1.353669      -0.125466
     H       1.498795      0.678604       1.320216
     H      -3.036259     -0.742095       1.040786
Rotational constants (GHz):    5.3681500    1.2172800    1.0551600
Vibrational harmonic frequencies (cm-1):
       47.1882                  74.8600                 110.7871
      204.1682                 265.0175                 334.2196
      391.4892                 446.2482                 540.5382
      567.6268                 814.9271                 863.6201
      917.8374                 988.6263                1035.2476
     1069.2262                1122.3981                1159.4625
     1215.5601                1267.2054                1288.0298
     1298.6105                1341.6350                1362.4937
     1398.3535                1414.8400                1472.9430
     1500.9427                1766.3020                3062.0597
     3082.9820                3106.9162                3140.2931
     3153.5250                3208.4551                3860.2757
Zero-point correction (Hartree): 0.111391

HOCHCHCH2CH2OO.Eltmc
--------------------
E(CCSD(T)/Aug-CC-pVTZ) (Hartree): -381.59757712
E(CCSD/Aug-CC-pVTZ) (Hartree): -381.53594843
     T1 diagnostic:  0.021541
E(MP2/Aug-CC-pVTZ) (Hartree): -381.49136426
E(MP3/Aug-CC-pVTZ) (Hartree): -381.52330142
E(PMP2/Aug-CC-pVTZ) (Hartree): -381.49452390
E(PMP3/Aug-CC-pVTZ) (Hartree): -381.52516264
E(PUHF/Aug-CC-pVTZ) (Hartree): -380.13519483
E(UHF/Aug-CC-pVTZ) (Hartree): -380.13005206
E(UM062X/Aug-CC-pVTZ) (Hartree): -382.14085582
Electronic state : 2-A
Cartesian coordinates (Angs):
     C      -2.116996      0.458740       0.023049
     C      -1.201545     -0.458753       0.304944
     C       0.215959     -0.116171       0.646310
     C       1.167619     -0.590526      -0.439314
```

```
     O       2.539002     -0.357420      -0.056058
     O       2.828865      0.907518      -0.091009
     O      -3.413943      0.237036      -0.302756
     H      -1.893836      1.518356       0.037417
     H      -1.476744     -1.509855       0.279228
     H       0.330920      0.961839       0.759748
     H       0.510763     -0.579923       1.590163
     H       1.107798     -1.667516      -0.590321
     H       0.992433     -0.071408      -1.380229
     H      -3.592948     -0.708296      -0.307352
Rotational constants (GHz):   10.0368700    0.9316200    0.9000000
Vibrational harmonic frequencies (cm-1):
       62.6193                86.0716               114.6904
      178.5780               307.7151               321.7048
      372.5639               446.0057               522.6093
      624.6712               795.8463               850.8975
      958.7976               991.0461              1019.8069
     1068.2658              1129.2750              1160.1231
     1220.7535              1266.9190              1283.4531
     1312.2745              1329.5215              1347.5466
     1395.5665              1412.2663              1485.2413
     1499.6656              1761.8549              3064.9628
     3093.7449              3118.4546              3151.9409
     3157.1601              3205.8173              3858.7043
Zero-point correction (Hartree): 0.111578

HOCHCHCH2CH2OO.Eltmt
~~~~~~~~~~~~~~~~~~~
E(UM062X/Aug-CC-pVTZ) (Hartree): -382.13929131
Electronic state : 2-A
Cartesian coordinates (Angs):
     C      -2.116572      0.416829       0.046261
     C      -1.191134     -0.498223       0.288145
     C       0.220217     -0.150112       0.644152
     C       1.178600     -0.580618      -0.453727
     O       2.546494     -0.334731      -0.064552
     O       2.817275      0.934757      -0.071963
     O      -3.393009      0.084359      -0.290855
     H      -1.898587      1.478277       0.110791
     H      -1.466099     -1.544455       0.212146
     H       0.326348      0.924914       0.792302
     H       0.517839     -0.642064       1.572851
     H       1.135422     -1.653914      -0.632830
     H       0.995182     -0.039785      -1.380697
     H      -3.922847      0.874692      -0.404589
Rotational constants (GHz):   10.0574900    0.9318000    0.9003200
Vibrational harmonic frequencies (cm-1):
       62.7043                88.0215               115.2441
      181.9248               265.8166               316.5343
      323.3749               385.1449               520.7013
      621.7596               796.6855               865.7763
      956.6579               970.6860              1017.8475
     1067.6172              1133.8664              1179.0186
     1212.3615              1246.3360              1283.4095
     1299.5434              1330.5167              1356.9055
     1382.7914              1407.6503              1484.8791
     1499.8352              1785.0922              3063.0106
     3094.1621              3115.4457              3156.4935
     3171.1139              3181.9716              3915.6844
Zero-point correction (Hartree): 0.111303

HOCHCHCH2CH2OO.Eltpc
~~~~~~~~~~~~~~~~~~~
E(CCSD(T)/Aug-CC-pVTZ) (Hartree): -381.59774833
E(CCSD/Aug-CC-pVTZ) (Hartree): -381.53608544
     T1 diagnostic:  0.021615
E(MP2/Aug-CC-pVTZ) (Hartree): -381.49148884
E(MP3/Aug-CC-pVTZ) (Hartree): -381.52339626
E(PMP2/Aug-CC-pVTZ) (Hartree): -381.49466624
E(PMP3/Aug-CC-pVTZ) (Hartree): -381.52527544
E(PUHF/Aug-CC-pVTZ) (Hartree): -380.13522254
E(UHF/Aug-CC-pVTZ) (Hartree): -380.13007016
E(UM062X/Aug-CC-pVTZ) (Hartree): -382.14108463
Electronic state : 2-A
Cartesian coordinates (Angs):
     C       2.234338      0.135592      -0.357583
     C       1.152266     -0.409745       0.181764
     C      -0.208548     -0.304048      -0.433368
     C      -1.139220      0.517425       0.443306
     O      -2.467277      0.557499      -0.118814
     O      -3.071055     -0.583770       0.015422
     O       3.496844      0.090426       0.134221
     H       2.198969      0.685380      -1.290008
     H       1.240777     -0.954326       1.118051
     H      -0.143183      0.158791      -1.418965
     H      -0.656921     -1.291129      -0.560283
     H      -1.221690      0.101001       1.446713
     H      -0.828505      1.559128       0.495662
     H       3.509436     -0.407433       0.957481
Rotational constants (GHz):   13.1446600    0.8826300    0.8713100
Vibrational harmonic frequencies (cm-1):
       67.8392                71.8809               132.1719
      170.9503               293.7329               332.8483
```

```
      372.3254                440.9682                536.2726
      616.7591                789.1311                849.8083
      973.1622                989.9596               1014.5884
     1068.2345               1126.4066               1158.0426
     1225.3138               1255.7702               1293.0913
     1309.0186               1331.2088               1346.1744
     1393.1945               1412.4869               1483.8683
     1498.2063               1764.3313               3068.2706
     3092.7231               3113.9544               3151.3558
     3158.2694               3205.3995               3859.9303
Zero-point correction (Hartree): 0.111557

HOCHCHCH2CH2OO.Eltpt
~~~~~~~~~~~~~~~~~~~~
E(UM062X/Aug-CC-pVTZ) (Hartree): -382.13930049
Electronic state : 2-A
Cartesian coordinates (Angs):
     C      -2.230972      0.064200       0.344730
     C      -1.142923     -0.387317      -0.259035
     C       0.211479     -0.361046       0.375652
     C       1.147173      0.565479      -0.382958
     O       2.467725      0.545511       0.198395
     O       3.082314     -0.567691      -0.062484
     O      -3.453504      0.041539      -0.254464
     H      -2.198295      0.469898       1.351149
     H      -1.236164     -0.785712      -1.263260
     H       0.141500     -0.028243       1.412508
     H       0.660147     -1.356295       0.376634
     H       1.244648      0.273692      -1.427997
     H       0.830008      1.604246      -0.313275
     H      -4.122658      0.379656       0.342337
Rotational constants (GHz):   13.3164800    0.8817100    0.8703500
Vibrational harmonic frequencies (cm-1):
       68.0919                 72.1152                131.6989
      167.9317                240.6208                305.5826
      330.2599                384.9810                534.3830
      612.6315                793.2149                862.2344
      970.0369                973.8711               1011.7579
     1068.5068               1129.8299               1178.0602
     1214.5548               1242.4344               1280.3932
     1305.1409               1331.0117               1354.6634
     1382.6060               1408.1982               1484.8761
     1499.3454               1785.4662               3065.4744
     3093.5087               3110.7624               3157.8435
     3168.6656               3184.8947               3916.5030
Zero-point correction (Hartree): 0.111225

HOCHCHCH2CH2OO.Elttc
~~~~~~~~~~~~~~~~~~~~
E(UM062X/Aug-CC-pVTZ) (Hartree): -382.14004222
Electronic state : 2-A
Cartesian coordinates (Angs):
     C      -2.275809      0.148690      -0.367891
     C      -1.260724      0.112279       0.484643
     C       0.071423      0.733498       0.193929
     C       1.150763     -0.325924       0.094412
     O       2.412869      0.349900      -0.093776
     O       3.395681     -0.491871      -0.180792
     O      -3.506287     -0.390315      -0.187617
     H      -2.204780      0.644611      -1.328060
     H      -1.382734     -0.396042       1.437314
     H       0.028218      1.293552      -0.740915
     H       0.348530      1.438096       0.981051
     H       1.231526     -0.919900       1.004892
     H       0.998327     -0.988116      -0.756826
     H      -3.551102     -0.825174       0.669474
Rotational constants (GHz):   13.6874400    0.8329600    0.8191700
Vibrational harmonic frequencies (cm-1):
       60.8092                 90.3699                 93.3198
      165.2775                280.7597                313.8347
      355.1919                453.9746                528.9095
      593.7630                785.7557                851.2485
      989.6390                993.0427               1029.7627
     1104.1590               1122.0018               1159.0048
     1206.0828               1269.0806               1294.2590
     1309.3283               1318.2802               1346.6675
     1397.3583               1419.6101               1490.8330
     1507.2386               1765.0976               3063.5670
     3084.8968               3108.9567               3144.2032
     3154.2420               3207.2976               3859.5147
Zero-point correction (Hartree): 0.111442

HOCHCHCH2CH2OO.Elttt
~~~~~~~~~~~~~~~~~~~~
E(UM062X/Aug-CC-pVTZ) (Hartree): -382.13833875
Electronic state : 2-A
Cartesian coordinates (Angs):
     C      -2.273429      0.105513      -0.345910
     C      -1.250519      0.154109       0.492492
     C       0.075477      0.744656       0.126087
     C       1.158404     -0.315660       0.135892
     O       2.416046      0.340116      -0.137218
     O       3.400500     -0.503981      -0.153931
```

```
     O      -3.469088     -0.443689      0.003341
     H      -2.206311      0.507793     -1.351936
     H      -1.375714     -0.260890      1.486384
     H       0.027645      1.201252     -0.863577
     H       0.354735      1.529938      0.832104
     H       1.248309     -0.804624      1.105828
     H       1.003251     -1.068940     -0.635313
     H      -4.091178     -0.375805     -0.722381
Rotational constants (GHz):   13.8484500    0.8326000    0.8185100
Vibrational harmonic frequencies (cm-1):
       57.7469                90.3574               103.0039
      158.1623               229.2563               299.1034
      314.3737               359.8705               526.9658
      590.0482               784.7093               863.0777
      967.4995               986.9136              1029.3380
     1103.2365              1124.1121              1179.2551
     1199.0412              1244.0592              1293.4717
     1302.6613              1312.7888              1355.5095
     1382.0788              1415.5474              1491.3168
     1507.2022              1788.3995              3061.7607
     3086.0660              3106.1688              3145.2990
     3169.8118              3184.8758              3916.9350
Zero-point correction (Hartree): 0.111015


TS.HOCHCHCH2CH2OO.cycHOCHCHCH2CH2OO.Ec.b
~~~~~~~~~~~~~~~~~~~~~~~~~~~~~~~~~~~~~~~
E(UM062X/Aug-CC-pVTZ) (Hartree): -382.10724016
Electronic state : 2-A
Cartesian coordinates (Angs):
     C       1.217486      0.279742      0.364305
     C       0.341773      1.097742     -0.320596
     C      -1.027092      1.246613      0.229747
     C      -1.844235     -0.064593     -0.045476
     O      -0.992753     -1.095210     -0.485394
     O       0.005605     -1.255843      0.439528
     O       2.391428     -0.139894     -0.136307
     H       1.213890      0.247341      1.445253
     H       0.518331      1.286381     -1.373712
     H      -0.974047      1.394725      1.307886
     H      -1.549034      2.096788     -0.204608
     H      -2.361650     -0.370132      0.865237
     H      -2.563582      0.066706     -0.852405
     H       2.354263     -0.151259     -1.098142
Rotational constants (GHz):    4.7724200    2.2768000    1.7445200
Vibrational harmonic frequencies (cm-1):
     i685.0331                79.5739               248.9258
      266.7727               368.0530               402.7393
      421.1075               441.7393               542.8748
      651.4000               781.5885               819.2272
      891.5753               903.7398               977.2995
     1039.4828              1100.8839              1133.4693
     1159.3361              1225.4296              1268.0599
     1279.5097              1296.2485              1321.3174
     1371.2509              1405.3781              1487.8162
     1504.3742              1563.6009              3068.4393
     3087.8182              3127.3766              3146.3952
     3173.8162              3211.4429              3854.2426
Zero-point correction (Hartree): 0.110770

TS.HOCHCHCH2CH2OO.cycHOCHCHCH2CH2OO.Ec
~~~~~~~~~~~~~~~~~~~~~~~~~~~~~~~~~~~~~
E(CCSD(T)/Aug-CC-pVTZ) (Hartree): -381.57644612
E(CCSD/Aug-CC-pVTZ) (Hartree): -381.50999223
     T1 diagnostic:  0.028421
E(MP2/Aug-CC-pVTZ) (Hartree): -381.46077651
E(MP3/Aug-CC-pVTZ) (Hartree): -381.49072084
E(PMP2/Aug-CC-pVTZ) (Hartree): -381.47834524
E(PMP3/Aug-CC-pVTZ) (Hartree): -381.50387730
E(PUHF/Aug-CC-pVTZ) (Hartree): -380.10921509
E(UHF/Aug-CC-pVTZ) (Hartree): -380.08883155
E(UM062X/Aug-CC-pVTZ) (Hartree): -382.11687402
Electronic state : 2-A
Cartesian coordinates (Angs):
     C       1.155879      0.174702      0.396882
     C       0.378016      1.143937     -0.200909
     C      -1.050426      1.263609      0.187134
     C      -1.791931     -0.024462     -0.246750
     O      -1.122666     -1.127408      0.316294
     O       0.084327     -1.281446     -0.319510
     O       2.404324     -0.122337      0.004603
     H       0.959046     -0.158255      1.406366
     H       0.705464      1.550892     -1.151471
     H      -1.160467      1.353572      1.268525
     H      -1.521335      2.128324     -0.278811
     H      -2.806017     -0.050121      0.151243
     H      -1.807149     -0.117482     -1.333491
     H       2.553350      0.195881     -0.891592
Rotational constants (GHz):    4.8099700    2.3018300    1.7081900
Vibrational harmonic frequencies (cm-1):
     i612.2148               155.8931               259.5245
      308.9601               339.9696               400.6085
      432.1901               440.3496               541.4172
```

```
      590.7723                747.5627                862.9943
      933.5439                972.9901                987.3404
     1024.8407               1090.4612               1128.1823
     1165.3542               1214.9112               1262.3010
     1277.6477               1318.6330               1327.6199
     1367.9829               1403.7461               1484.0993
     1488.6522               1571.1142               3073.6098
     3076.3357               3128.1857               3139.6010
     3172.6958               3222.8911               3853.6386
Zero-point correction (Hartree): 0.111099

TS.HOCHCHCH2CH2OO.cycHOCHCHCH2CH2OO.Et.b
----------------------------------------
E(UM062X/Aug-CC-pVTZ) (Hartree): -382.10677807
Electronic state : 2-A
Cartesian coordinates (Angs):
     C       1.214263      0.289700       0.332681
     C       0.326195      1.114648      -0.316324
     C      -1.033088      1.235463       0.261697
     C      -1.845033     -0.070021      -0.053565
     O      -0.991057     -1.100931      -0.491333
     O       0.004584     -1.260867       0.433509
     O       2.353683     -0.063418      -0.294347
     H       1.212212      0.218401       1.414086
     H       0.498114      1.324250      -1.363766
     H      -0.967915      1.341177       1.344097
     H      -1.571161      2.095330      -0.132183
     H      -2.385987     -0.385297       0.840440
     H      -2.544451      0.076333      -0.875285
     H       2.847487     -0.687210       0.243044
Rotational constants (GHz):    4.7508600    2.2809700    1.7416400
Vibrational harmonic frequencies (cm-1):
     i672.3229                91.4225                 248.4742
      275.6830                318.7083                368.7678
      416.8751                431.7870                540.0841
      655.4871                795.1183                823.1929
      885.9184                903.5206                972.9894
     1036.2457               1094.7108               1133.0696
     1177.5571               1217.2911               1251.4219
     1276.5256               1297.2793               1318.4758
     1357.5098               1390.8892               1487.3773
     1503.7334               1588.4282               3065.0986
     3087.2872               3126.5789               3145.9153
     3174.3288               3205.5509               3893.7939
Zero-point correction (Hartree): 0.110621

TS.HOCHCHCH2CH2OO.cycHOCHCHCH2CH2OO.Et
--------------------------------------
E(CCSD(T)/Aug-CC-pVTZ) (Hartree): -381.57685956
E(CCSD/Aug-CC-pVTZ) (Hartree): -381.51053770
     T1 diagnostic:  0.028927
E(MP2/Aug-CC-pVTZ) (Hartree): -381.46051972
E(MP3/Aug-CC-pVTZ) (Hartree): -381.49081210
E(PMP2/Aug-CC-pVTZ) (Hartree): -381.47833678
E(PMP3/Aug-CC-pVTZ) (Hartree): -381.50423593
E(PUHF/Aug-CC-pVTZ) (Hartree): -380.11048561
E(UHF/Aug-CC-pVTZ) (Hartree): -380.08990202
E(UM062X/Aug-CC-pVTZ) (Hartree): -382.11743003
Electronic state : 2-A
Cartesian coordinates (Angs):
     C       1.147043      0.214569       0.362170
     C       0.350660      1.166516      -0.223427
     C      -1.071962      1.255057       0.192903
     C      -1.791056     -0.052670      -0.223763
     O      -1.091404     -1.144407       0.327652
     O       0.098491     -1.285160      -0.343113
     O       2.388067      0.005591      -0.115672
     H       0.939296     -0.138660       1.365124
     H       0.673943      1.583833      -1.167781
     H      -1.167356      1.347532       1.275518
     H      -1.573728      2.104419      -0.268728
     H      -2.797301     -0.098079       0.192044
     H      -1.822870     -0.148961      -1.309517
     H       2.778671     -0.759101       0.315106
Rotational constants (GHz):    4.7651800    2.3156100    1.7036200
Vibrational harmonic frequencies (cm-1):
     i590.6847                159.4186                269.6552
      294.5891                342.8123                374.2063
      399.9901                435.6672                538.4892
      595.4815                773.5039                860.5234
      934.0770                971.0382                982.5272
     1020.8763               1084.1233               1128.2875
     1182.8838               1208.9500               1256.2854
     1265.7570               1319.9350               1332.9792
     1358.1819               1384.0530               1483.8822
     1488.5767               1600.3175               3075.6803
     3076.1514               3129.3890               3140.5615
     3185.3172               3208.4006               3884.7204
Zero-point correction (Hartree): 0.111054


################################################################################
Z-HOCH=CHCH2CH2OO ring closure
```

```
################################################################################

HOCHCHCH2CH2OO.Zcptt
~~~~~~~~~~~~~~~~~~~
E(UM062X/Aug-CC-pVTZ) (Hartree): -382.13711336
Electronic state : 2-A
Cartesian coordinates (Angs):
     C      -1.776794     -0.554659      -0.256263
     C      -1.493800      0.732244      -0.393931
     C      -0.341202      1.507229       0.179422
     C       0.865022      0.702094       0.611509
     O       1.362636      0.001504      -0.550034
     O       2.306136     -0.829333      -0.236274
     O      -1.045956     -1.415474       0.509502
     H      -2.641959     -0.983117      -0.748092
     H      -2.189973      1.293835      -1.001782
     H      -0.017457      2.242074      -0.560669
     H      -0.672659      2.085016       1.047217
     H       1.667247      1.352616       0.959066
     H       0.637097     -0.043564       1.366069
     H      -1.284185     -2.321888       0.308221
Rotational constants (GHz):    3.9278800    2.0404800    1.5310900
Vibrational harmonic frequencies (cm-1):
       45.9236                   64.9179                  135.0800
      247.0910                  265.4998                  269.3807
      385.3755                  449.8302                  535.0364
      742.0012                  759.3706                  851.3365
      877.4570                  975.0962                 1014.7206
     1055.0647                 1080.1995                 1130.9052
     1232.4978                 1259.8112                 1284.3392
     1303.6282                 1317.0023                 1385.4671
     1420.2666                 1446.4422                 1472.3424
     1505.9929                 1788.8382                 3052.2248
     3086.2696                 3096.1607                 3178.5278
     3182.7917                 3214.4693                 3910.7664
Zero-point correction (Hartree): 0.111681

HOCHCHCH2CH2OO.Zctpt
~~~~~~~~~~~~~~~~~~~
E(UM062X/Aug-CC-pVTZ) (Hartree): -382.13858979
Electronic state : 2-A
Cartesian coordinates (Angs):
     C       2.258555      0.186620      -0.159502
     C       1.324382      1.115087      -0.020896
     C      -0.138910      0.947789       0.264829
     C      -0.670348     -0.470054       0.176316
     O      -2.097451     -0.455162       0.413555
     O      -2.742614      0.049252      -0.592871
     O       2.019007     -1.155385      -0.046563
     H       3.284895      0.462810      -0.367898
     H       1.671553      2.134578      -0.122294
     H      -0.365199      1.344959       1.258467
     H      -0.708414      1.553057      -0.443552
     H      -0.503577     -0.913031      -0.802703
     H      -0.273150     -1.120533       0.949555
     H       2.820279     -1.648133      -0.229019
Rotational constants (GHz):    6.2539000    1.3314300    1.1658700
Vibrational harmonic frequencies (cm-1):
       21.5428                   88.9392                  136.3872
      180.6831                  222.3307                  282.7500
      372.7885                  454.7840                  567.1876
      745.0536                  765.6149                  806.7722
      929.2624                  975.1060                  977.1411
     1054.0019                 1098.4514                 1128.5862
     1236.7695                 1247.2451                 1290.1310
     1310.8892                 1328.5947                 1348.8740
     1422.8371                 1441.6560                 1484.8573
     1496.2722                 1791.5757                 3050.7558
     3091.2172                 3117.6643                 3185.2642
     3187.6863                 3213.3065                 3917.4230
Zero-point correction (Hartree): 0.111563

HOCHCHCH2CH2OO.Zcttc
~~~~~~~~~~~~~~~~~~~
E(UM062X/Aug-CC-pVTZ) (Hartree): -382.13442233
Point group : CS
Electronic state : 2-A"
Cartesian coordinates (Angs):
     C      -0.377205     -2.307271       0.000000
     C       0.796415     -1.684238       0.000000
     C       1.154718     -0.224566       0.000000
     C      -0.000000      0.750786       0.000000
     O       0.571304      2.076013       0.000000
     O      -0.349166      2.989418       0.000000
     O      -1.641430     -1.809192       0.000000
     H      -0.408505     -3.388123       0.000000
     H       1.648626     -2.350758       0.000000
     H       1.777089     -0.010247       0.872495
     H       1.777089     -0.010247      -0.872495
     H      -0.617134      0.675760      -0.897332
     H      -0.617134      0.675760       0.897332
     H      -1.649264     -0.850327       0.000000
Rotational constants (GHz):    5.8449000    1.2754700    1.0608800
```

```
Vibrational harmonic frequencies (cm-1):
       43.1149 (  A")            81.4073 (  A")           129.0539 (  A')
      149.1265 (  A")           268.3374 (  A')           311.4776 (  A")
      379.5594 (  A')           482.1220 (  A")           508.2954 (  A')
      751.1183 (  A")           767.0594 (  A')           814.7686 (  A")
      913.8562 (  A')          1003.6698 (  A")          1031.8930 (  A')
     1073.4671 (  A')          1088.9370 (  A")          1145.5511 (  A')
     1230.7542 (  A')          1253.1947 (  A")          1290.3416 (  A')
     1317.5934 (  A")          1342.4242 (  A')          1362.1290 (  A')
     1427.3542 (  A')          1444.3698 (  A')          1497.6006 (  A')
     1532.5811 (  A')          1767.2677 (  A')          3052.1786 (  A')
     3061.3874 (  A')          3082.0577 (  A")          3121.4614 (  A")
     3196.9164 (  A')          3224.9995 (  A')          3910.9139 (  A')
Zero-point correction (Hartree): 0.111763

HOCHCHCH2CH2OO.Zcttt
~~~~~~~~~~~~~~~~~~~~
E(UM062X/Aug-CC-pVTZ) (Hartree): -382.13769930
Point group : CS
Electronic state : 2-A"
Cartesian coordinates (Angs):
     C      -0.410643     -2.264632       0.000000
     C       0.790060     -1.705198       0.000000
     C       1.158136     -0.250913       0.000000
     C       0.000000      0.723795       0.000000
     O       0.595745      2.042813       0.000000
     O      -0.306243      2.973965       0.000000
     O      -1.579759     -1.557348       0.000000
     H      -0.514846     -3.342783       0.000000
     H       1.619897     -2.399009       0.000000
     H       1.783976     -0.042358       0.871782
     H       1.783976     -0.042358      -0.871782
     H      -0.624334      0.644558      -0.886550
     H      -0.624334      0.644558       0.886550
     H      -2.327588     -2.156356       0.000000
Rotational constants (GHz):    5.8453500    1.3275400    1.0964700
Vibrational harmonic frequencies (cm-1):
       17.2363 (  A")            78.2270 (  A")           128.1975 (  A")
      138.3477 (  A')           253.4598 (  A')           270.7581 (  A")
      380.3751 (  A')           456.1568 (  A")           510.4761 (  A')
      745.6136 (  A")           770.0082 (  A')           803.5707 (  A")
      930.3358 (  A')           978.1798 (  A")          1016.3361 (  A')
     1069.1464 (  A')          1076.6634 (  A")          1144.0290 (  A')
     1221.3629 (  A")          1252.0845 (  A')          1299.7341 (  A')
     1314.2764 (  A')          1315.9130 (  A")          1340.0882 (  A')
     1428.7474 (  A')          1443.9492 (  A')          1493.9967 (  A')
     1503.7163 (  A')          1792.5665 (  A')          3051.8416 (  A')
     3079.8236 (  A")          3111.9295 (  A')          3171.9629 (  A")
     3187.6752 (  A')          3213.1564 (  A')          3916.7245 (  A')
Zero-point correction (Hartree): 0.111418

HOCHCHCH2CH2OO.Zgpmc
~~~~~~~~~~~~~~~~~~~~
E(UM062X/Aug-CC-pVTZ) (Hartree): -382.14139996
Electronic state : 2-A
Cartesian coordinates (Angs):
     C      -1.737468     -0.146900       0.370704
     C      -0.997116      0.936025       0.587248
     C       0.077260      1.427802      -0.337557
     C       1.434514      0.783067      -0.094846
     O       1.333949     -0.627424      -0.393721
     O       1.297258     -1.365867       0.677108
     O      -1.644538     -0.999462      -0.676321
     H      -2.531448     -0.435613       1.045857
     H      -1.192722      1.491430       1.493099
     H      -0.201334      1.255270      -1.380993
     H       0.200699      2.505915      -0.228546
     H       2.192512      1.171852      -0.773936
     H       1.761229      0.867044       0.938717
     H      -0.785432     -0.913843      -1.104020
Rotational constants (GHz):    3.6140200    2.2889700    1.7079300
Vibrational harmonic frequencies (cm-1):
       58.2574                  93.1132                 123.1605
      232.3401                 265.0035                 361.0549
      456.4881                 524.6469                 582.7744
      657.9690                 761.3718                 837.5371
      919.5851                 981.6888                 992.3137
     1035.9988                1083.2694                1141.7043
     1223.1119                1228.6007                1276.7832
     1312.6929                1350.0219                1370.6682
     1383.0603                1438.3066                1483.6831
     1488.0368                1742.8540                3054.4239
     3091.7480                3110.0397                3163.6564
     3210.9156                3231.1092                3838.7502
Zero-point correction (Hartree): 0.111873

HOCHCHCH2CH2OO.Zgppt
~~~~~~~~~~~~~~~~~~~~
E(UM062X/Aug-CC-pVTZ) (Hartree): -382.13954204
Electronic state : 2-A
Cartesian coordinates (Angs):
     C       1.914859      0.090571      -0.431387
     C       0.985666      1.025018      -0.298066
```

```
     C      -0.116046      0.973688       0.714388
     C      -1.485281      0.843125       0.071006
     O      -1.596557     -0.397079      -0.661614
     O      -1.635879     -1.415766       0.141001
     O       1.969504     -0.998001       0.385586
     H       2.684108      0.156570      -1.191408
     H       1.022074      1.860050      -0.985306
     H       0.028552      0.133836       1.392152
     H      -0.126916      1.885411       1.316826
     H      -2.284305      0.853205       0.810695
     H      -1.659541      1.610620      -0.682013
     H       2.644287     -1.607334       0.083620
Rotational constants (GHz):    4.1422700    1.8180600    1.4550000
Vibrational harmonic frequencies (cm-1):
       28.3230                59.2797                144.7891
      214.5535                252.6226               295.0937
      378.7974                519.7864               568.4510
      668.2856                766.4669               861.6718
      890.9170                973.7082               995.9278
     1047.5808               1076.0585              1148.4667
     1215.0584               1257.7825              1277.3019
     1296.0053               1313.5432              1357.1520
     1398.7465               1444.7125              1481.0926
     1490.7725               1785.2217              3064.5679
     3089.8000               3132.9715              3151.1366
     3184.5111               3210.8037              3919.8909
Zero-point correction (Hartree): 0.111543

HOCHCHCH2CH2OO.Zgptc
~~~~~~~~~~~~~~~~~~~
E(UM062X/Aug-CC-pVTZ) (Hartree): -382.14241976
Electronic state : 2-A
Cartesian coordinates (Angs):
     C       1.897914     -0.385648      -0.365766
     C       1.383603      0.840262      -0.401496
     C       0.264452      1.332044       0.474141
     C      -1.122747      0.977069      -0.024651
     O      -1.262451     -0.455486       0.137606
     O      -2.386318     -0.899974      -0.330991
     O       1.496806     -1.417339       0.410545
     H       2.743478     -0.659416      -0.982587
     H       1.826601      1.532954      -1.102642
     H       0.369226      0.941970       1.491084
     H       0.315083      2.417337       0.557387
     H      -1.913850      1.441070       0.563359
     H      -1.261010      1.196692      -1.081776
     H       0.596840     -1.270578       0.724538
Rotational constants (GHz):    4.0906500    1.8775300    1.4146100
Vibrational harmonic frequencies (cm-1):
       68.9838                87.6903                136.6126
      229.9296                265.9066               335.7055
      440.9411                503.4870               609.9387
      656.8277                765.8418               844.7707
      899.0257                994.9890              1024.7678
     1053.7330               1087.6190              1138.3086
     1222.6732               1254.0154              1290.0043
     1295.5010               1353.6839              1378.2692
     1396.6054               1439.7699              1481.4740
     1500.2293               1746.2514              3053.1188
     3087.8198               3118.3686              3150.7968
     3205.2596               3225.7012              3823.1965
Zero-point correction (Hartree): 0.112013

HOCHCHCH2CH2OO.Zgtmt
~~~~~~~~~~~~~~~~~~~
E(UM062X/Aug-CC-pVTZ) (Hartree): -382.14019926
Electronic state : 2-A
Cartesian coordinates (Angs):
     C       2.270326     -0.081809       0.116109
     C       1.368345     -1.008545      -0.173754
     C      -0.033049     -0.679805      -0.596835
     C      -0.912228     -0.443690       0.621475
     O      -2.280375     -0.204704       0.228308
     O      -2.418909      0.964599      -0.318224
     O       1.972686      1.245837       0.034722
     H       3.276542     -0.331255       0.429921
     H       1.665202     -2.041996      -0.067885
     H      -0.047455      0.226657      -1.201609
     H      -0.455768     -1.491488      -1.188285
     H      -0.964202     -1.321549       1.263055
     H      -0.572122      0.420624       1.189408
     H       2.750225      1.776249       0.214973
Rotational constants (GHz):    5.5989900    1.3520200    1.1808600
Vibrational harmonic frequencies (cm-1):
       43.3704                65.7348                120.2632
      202.9634                257.3635               286.3124
      355.0370                527.0481               572.4761
      679.5690                764.8308               817.1081
      959.4980                972.6762               985.8933
     1066.5337               1079.6370              1137.5424
     1223.2900               1259.5267              1290.9339
     1294.5599               1306.4462              1335.8659
     1399.4687               1434.0395              1485.8825
```

```
     1502.2942                1772.3973                3082.3660
     3098.7856                3130.6060                3162.4014
     3191.4227                3226.1186                3915.6145
Zero-point correction (Hartree): 0.111644

HOCHCHCH2CH2OO.Zgtpc
--------------------
E(UM062X/Aug-CC-pVTZ) (Hartree): -382.14075752
Electronic state : 2-A
Cartesian coordinates (Angs):
     C      -2.374942      0.337594       0.155917
     C      -1.213663      0.969303       0.026282
     C       0.051787      0.353347      -0.491740
     C       0.940906     -0.095044       0.658214
     O       2.162758     -0.680760       0.162951
     O       2.948064      0.222433      -0.339989
     O      -2.645564     -0.950933      -0.168538
     H      -3.253375      0.830196       0.548466
     H      -1.180539      2.000982       0.346920
     H      -0.142237     -0.503852      -1.142065
     H       0.609705      1.072998      -1.090594
     H       1.211162      0.739468       1.303249
     H       0.474510     -0.883184       1.247021
     H      -1.865818     -1.373723      -0.540433
Rotational constants (GHz):    7.9091100    1.1060900    1.0406700
Vibrational harmonic frequencies (cm-1):
       27.6412                  67.0647                 124.0091
      202.9161                 276.6980                 353.9663
      400.0936                 544.5398                 578.0624
      659.8564                 773.9056                 803.7664
      971.0301                 980.5378                 995.6468
     1062.8364                1078.2751                1139.3897
     1219.6081                1248.4100                1274.1562
     1303.1465                1327.5545                1348.3426
     1397.1146                1436.2636                1488.9787
     1512.6791                1754.1465                3055.7317
     3094.2064                3114.3684                3156.7534
     3212.0556                3233.4812                3862.2667
Zero-point correction (Hartree): 0.111811

HOCHCHCH2CH2OO.Zgtpt
--------------------
E(UM062X/Aug-CC-pVTZ) (Hartree): -382.14074793
Electronic state : 2-A
Cartesian coordinates (Angs):
     C      -2.324227      0.311436       0.177412
     C      -1.219788      1.035274       0.068940
     C       0.059043      0.494489      -0.498552
     C       0.866340     -0.199202       0.587154
     O       2.103565     -0.717299       0.053086
     O       2.945104      0.237649      -0.200539
     O      -2.363701     -0.988806      -0.234841
     H      -3.239998      0.710018       0.596257
     H      -1.251137      2.050569       0.437250
     H      -0.153083     -0.226551      -1.288160
     H       0.664985      1.295553      -0.919357
     H       1.120232      0.478128       1.401064
     H       0.342422     -1.072435       0.970777
     H      -3.251384     -1.339617      -0.149199
Rotational constants (GHz):    7.5430100    1.1750500    1.0826100
Vibrational harmonic frequencies (cm-1):
       24.4640                  68.1809                 125.1362
      203.0655                 252.2195                 270.6904
      363.9977                 526.6943                 578.7486
      676.4526                 766.1211                 809.5074
      966.7978                 974.4646                 988.3892
     1065.2591                1078.1403                1135.2163
     1225.4347                1262.0164                1288.1527
     1294.5643                1310.5307                1334.8408
     1397.7532                1434.8279                1485.8232
     1501.1418                1774.3630                3082.8514
     3097.4074                3132.3512                3162.7554
     3193.8803                3228.2664                3916.4641
Zero-point correction (Hartree): 0.111623

HOCHCHCH2CH2OO.Zgttc
--------------------
E(UM062X/Aug-CC-pVTZ) (Hartree): -382.13967776
Electronic state : 2-A
Cartesian coordinates (Angs):
     C       2.398795      0.120656      -0.319230
     C       1.388901      0.958388      -0.113563
     C       0.123169      0.616565       0.617809
     C      -0.960737      0.190896      -0.354749
     O      -2.151912     -0.090414       0.411191
     O      -3.129570     -0.472234      -0.351222
     O       2.490714     -1.166102       0.096813
     H       3.285422      0.415956      -0.862452
     H       1.484300      1.951272      -0.529376
     H       0.277657     -0.180984       1.349411
     H      -0.228776      1.479200       1.183930
     H      -1.203033      0.978332      -1.067333
     H      -0.693941     -0.714815      -0.898969
```

```
     H       1.703757     -1.418004       0.588932
Rotational constants (GHz):    7.1967100    1.0749200    1.0053600
Vibrational harmonic frequencies (cm-1):
       27.6140                 75.3062                103.2976
      164.6930                279.9752                327.4172
      409.5551                486.7181                584.7638
      659.6895                772.5865                798.5818
      963.9454                998.3189               1023.3267
     1066.5952               1102.6237               1135.4684
     1203.3977               1251.5210               1290.0301
     1301.4801               1310.1920               1349.7321
     1403.9103               1437.3067               1501.7698
     1515.9947               1754.9348               3056.6056
     3086.3611               3107.6039               3144.8072
     3213.9386               3234.4311               3863.8149
Zero-point correction (Hartree): 0.111649

HOCHCHCH2CH2OO.Zgttt
~~~~~~~~~~~~~~~~~~~
E(UM062X/Aug-CC-pVTZ) (Hartree): -382.13973051
Electronic state : 2-A
Cartesian coordinates (Angs):
     C       2.351439      0.076127      -0.312571
     C       1.403691      0.990183      -0.166351
     C       0.127070      0.732235       0.579489
     C      -0.917596      0.150776      -0.353388
     O      -2.130330     -0.040952       0.408884
     O      -3.082366     -0.527365      -0.325056
     O       2.223606     -1.171407       0.223381
     H       3.264418      0.272205      -0.861180
     H       1.560642      1.950948      -0.635060
     H       0.303140      0.027431       1.391986
     H      -0.254728      1.656223       1.013054
     H      -1.154796      0.818428      -1.180964
     H      -0.613335     -0.819983      -0.742173
     H       3.019754     -1.683391       0.073604
Rotational constants (GHz):    6.8219700    1.1327600    1.0449100
Vibrational harmonic frequencies (cm-1):
       17.7531                 75.6068                100.6331
      163.6008                251.6023                256.2517
      357.1504                470.8270                578.0969
      671.1409                764.7380                804.8320
      967.3141                972.8733               1022.0913
     1068.3820               1103.5542               1130.0493
     1208.6234               1269.6215               1292.2993
     1293.7736               1312.5331               1316.4638
     1403.7061               1435.9979               1494.8269
     1505.7502               1776.5340               3080.9903
     3090.6090               3125.2729               3151.1963
     3192.8048               3228.0659               3916.2471
Zero-point correction (Hartree): 0.111338

HOCHCHCH2CH2OO.Zlmmc
~~~~~~~~~~~~~~~~~~~
E(UM062X/Aug-CC-pVTZ) (Hartree): -382.13994056
Electronic state : 2-A
Cartesian coordinates (Angs):
     C       2.143768     -0.664679       0.139343
     C       0.823500     -0.626813       0.007766
     C       0.009027      0.560010      -0.410802
     C      -1.165145      0.807557       0.521676
     O      -2.073223     -0.316307       0.501905
     O      -2.704934     -0.391193      -0.629406
     O       3.028093      0.339703      -0.091022
     H       2.655945     -1.560534       0.461000
     H       0.286885     -1.541015       0.221674
     H       0.598678      1.479894      -0.427379
     H      -0.393321      0.426727      -1.417786
     H      -0.850580      0.878497       1.561091
     H      -1.737194      1.687549       0.232840
     H       2.573202      1.114817      -0.431159
Rotational constants (GHz):    8.3236200    1.1198900    1.0759200
Vibrational harmonic frequencies (cm-1):
       17.6350                 67.8239                141.9868
      214.7837                252.1685                318.5315
      428.7667                524.9213                588.2432
      647.9435                778.0323                823.9482
      899.4037                997.0807               1004.6641
     1043.3525               1106.6705               1128.8582
     1219.1224               1238.5768               1279.6884
     1305.2664               1337.6068               1369.0230
     1397.5003               1441.7449               1472.6402
     1491.9527               1760.7025               3057.5479
     3090.4578               3101.2578               3159.9774
     3209.5933               3231.4405               3876.0568
Zero-point correction (Hartree): 0.111687

HOCHCHCH2CH2OO.Zlmmt
~~~~~~~~~~~~~~~~~~~
E(UM062X/Aug-CC-pVTZ) (Hartree): -382.14069596
Electronic state : 2-A
Cartesian coordinates (Angs):
     C      -2.088309     -0.661230      -0.159614
```

```
     C      -0.799558     -0.727793       0.137412
     C       0.004714      0.427704       0.647944
     C       1.058514      0.886017      -0.344729
     O       1.993842     -0.180062      -0.630865
     O       2.748805     -0.433773       0.393502
     O      -2.807425      0.491902      -0.019341
     H      -2.635411     -1.519816      -0.529306
     H      -0.303212     -1.676494      -0.011978
     H      -0.647327      1.274451       0.860453
     H       0.514923      0.159490       1.574692
     H       0.624742      1.125067      -1.313747
     H       1.637611      1.726756       0.033916
     H      -3.725278      0.337827      -0.246486
Rotational constants (GHz):    8.0364600    1.1756500    1.1218800
Vibrational harmonic frequencies (cm-1):
       23.9377                  62.4069                 135.4223
      205.8432                 253.4339                 279.2227
      389.6089                 524.3234                 602.4719
      656.0122                 778.7954                 827.2330
      890.9544                 976.7741                1004.8483
     1048.0315                1099.1372                1132.7352
     1211.3681                1247.2811                1294.7766
     1300.3257                1305.2226                1357.3751
     1392.5991                1444.6908                1480.8993
     1489.5894                1781.4930                3077.5404
     3094.8937                3130.4073                3159.1728
     3191.1439                3224.0324                3920.0462
Zero-point correction (Hartree): 0.111617

HOCHCHCH2CH2OO.Zlmpc
~~~~~~~~~~~~~~~~~~~~
E(UM062X/Aug-CC-pVTZ) (Hartree): -382.13868808
Electronic state : 2-A
Cartesian coordinates (Angs):
     C      -1.989705     -0.744530       0.029943
     C      -0.720256     -0.485431       0.318009
     C      -0.087986      0.872455       0.366130
     C       1.236003      0.929434      -0.382633
     O       2.209234      0.096137       0.280618
     O       2.301386     -1.081886      -0.259005
     O      -2.973361      0.146858      -0.259003
     H      -2.368788     -1.756248       0.000843
     H      -0.087874     -1.335139       0.534889
     H      -0.728776      1.638039      -0.079650
     H       0.094512      1.182833       1.398414
     H       1.147655      0.572355      -1.406187
     H       1.661348      1.931503      -0.357447
     H      -2.644486      1.046223      -0.180442
Rotational constants (GHz):    6.7689600    1.2445200    1.1083900
Vibrational harmonic frequencies (cm-1):
       18.0344                  91.5867                 105.7143
      226.4445                 232.0717                 322.9611
      433.7305                 515.3716                 568.8543
      651.4993                 779.4896                 844.9060
      878.1583                 999.1262                1017.5783
     1051.9170                1093.4299                1129.7210
     1230.1992                1236.6756                1271.0215
     1318.5707                1345.2177                1372.6220
     1390.8427                1445.6145                1469.7737
     1485.7653                1760.8773                3047.9076
     3082.0069                3098.8408                3163.8554
     3211.9308                3234.1030                3877.2726
Zero-point correction (Hartree): 0.111639

HOCHCHCH2CH2OO.Zlmpt
~~~~~~~~~~~~~~~~~~~~
E(UM062X/Aug-CC-pVTZ) (Hartree): -382.13978773
Electronic state : 2-A
Cartesian coordinates (Angs):
     C      -1.922704     -0.708652       0.104527
     C      -0.703461     -0.461169       0.557734
     C      -0.057498      0.888661       0.521306
     C       1.167248      0.936171      -0.379521
     O       2.204704      0.079601       0.144661
     O       2.144685     -1.121019      -0.347727
     O      -2.709907      0.267767      -0.438055
     H      -2.355496     -1.700688       0.142598
     H      -0.144789     -1.293540       0.961654
     H      -0.767207      1.631260       0.156524
     H       0.247172      1.192543       1.525260
     H       0.948198      0.597554      -1.389685
     H       1.610516      1.930687      -0.392956
     H      -3.555761     -0.098666      -0.698706
Rotational constants (GHz):    6.1146800    1.3366200    1.2016300
Vibrational harmonic frequencies (cm-1):
       27.3716                  88.2057                 114.5263
      221.3444                 238.6604                 267.6976
      403.9375                 513.5193                 587.8196
      654.3555                 781.7969                 849.4386
      877.1053                 977.9788                1013.9296
     1054.9938                1090.2377                1130.0488
     1216.4038                1236.8401                1291.6605
     1297.7336                1321.4059                1361.5667
```

```
     1385.6273                1446.8172                1479.1669
     1485.9362                1781.7754                3066.5438
     3096.1160                3123.3747                3162.6365
     3192.2612                3226.0934                3921.1846
Zero-point correction (Hartree): 0.111599

HOCHCHCH2CH2OO.Zlmtc
~~~~~~~~~~~~~~~~~~~
E(UM062X/Aug-CC-pVTZ) (Hartree): -382.13905289
Electronic state : 2-A
Cartesian coordinates (Angs):
     C      -2.192234     -0.718371      -0.080291
     C      -0.903735     -0.591983       0.212102
     C      -0.170168      0.700361       0.418640
     C       1.165032      0.721580      -0.299271
     O       1.997363     -0.285070       0.318060
     O       3.143934     -0.386438      -0.278970
     O      -3.107001      0.273427      -0.230218
     H      -2.647185     -1.686944      -0.232436
     H      -0.333417     -1.505117       0.311545
     H      -0.739251      1.555554       0.046180
     H       0.009899      0.884330       1.481313
     H       1.071934      0.464778      -1.353488
     H       1.680731      1.674843      -0.191820
     H      -2.710451      1.127670      -0.039355
Rotational constants (GHz):    9.7604000    1.0288300    0.9728300
Vibrational harmonic frequencies (cm-1):
       19.6535                  66.5428                 120.1996
      217.3154                 241.8543                 313.8582
      388.7097                 501.0476                 578.1024
      661.9453                 779.6506                 823.0225
      908.1268                 998.9615                1044.1810
     1051.8555                1090.0733                1136.9804
     1229.3177                1236.2048                1287.8689
     1296.4890                1335.1353                1372.6237
     1400.6148                1444.0866                1469.3469
     1501.9053                1759.4537                3050.8456
     3083.3175                3094.3059                3148.6704
     3211.1193                3233.2802                3875.4610
Zero-point correction (Hartree): 0.111567

HOCHCHCH2CH2OO.Zlmtt
~~~~~~~~~~~~~~~~~~~
E(UM062X/Aug-CC-pVTZ) (Hartree): -382.14001114
Electronic state : 2-A
Cartesian coordinates (Angs):
     C      -2.129890     -0.693101      -0.078516
     C      -0.912971     -0.635025       0.440602
     C      -0.162846      0.640650       0.675647
     C       1.084324      0.746825      -0.178450
     O       1.976008     -0.318638       0.223395
     O       3.051639     -0.340873      -0.499865
     O      -2.819622      0.428371      -0.441076
     H      -2.637773     -1.636103      -0.239607
     H      -0.434511     -1.570323       0.694454
     H      -0.799649      1.494655       0.448190
     H       0.129922      0.721365       1.724899
     H       0.872470      0.609029      -1.237642
     H       1.616475      1.684755      -0.024412
     H      -3.682831      0.189645      -0.781210
Rotational constants (GHz):    8.1761600    1.0884600    1.0485000
Vibrational harmonic frequencies (cm-1):
       23.2548                  68.7763                 118.9651
      204.1627                 245.2082                 274.0911
      350.5013                 480.3196                 602.0876
      655.5972                 780.3875                 824.4920
      907.0490                 976.6682                1041.0311
     1052.1215                1085.7309                1138.5377
     1217.7992                1245.1212                1293.7441
     1300.0195                1304.5116                1356.4493
     1395.4060                1446.1590                1480.4572
     1500.4784                1781.5388                3067.6293
     3086.9684                3129.9267                3147.0592
     3191.7444                3226.1869                3920.6148
Zero-point correction (Hartree): 0.111450

HOCHCHCH2CH2OO.Zlpmt
~~~~~~~~~~~~~~~~~~~
E(UM062X/Aug-CC-pVTZ) (Hartree): -382.13945018
Electronic state : 2-A
Cartesian coordinates (Angs):
     C      -1.792042     -0.245705       0.497000
     C      -0.763719      0.514753       0.840462
     C       0.080855      1.269692      -0.135131
     C       1.532826      0.812047      -0.131362
     O       1.629254     -0.554384      -0.573924
     O       1.511557     -1.390915       0.414204
     O      -2.197243     -0.376930      -0.798829
     H      -2.365981     -0.794326       1.233637
     H      -0.507953      0.557576       1.890440
     H      -0.322875      1.165542      -1.141313
     H       0.084996      2.336127       0.106554
     H       2.127656      1.380476      -0.844490
```

```
     H       1.979199      0.862095       0.860435
     H      -2.891109     -1.034385      -0.862684
Rotational constants (GHz):    4.2484800    1.7298900    1.5147800
Vibrational harmonic frequencies (cm-1):
       17.9802                  96.2996                 108.0144
      219.1300                 246.6748                 290.6683
      387.2275                 523.5856                 545.1065
      672.0064                 766.3136                 846.1595
      923.9577                 971.3979                 991.2150
     1047.3391                1068.3295                1149.5674
     1225.9786                1235.6111                1284.1883
     1297.3051                1318.1810                1360.7644
     1393.2404                1446.2410                1477.8737
     1486.1508                1782.0974                3058.1557
     3092.6592                3127.6936                3155.3540
     3189.6091                3217.7380                3919.5797
Zero-point correction (Hartree): 0.111492

HOCHCHCH2CH2OO.Zlptt
~~~~~~~~~~~~~~~~~~~
E(UM062X/Aug-CC-pVTZ) (Hartree): -382.13906481
Electronic state : 2-A
Cartesian coordinates (Angs):
     C      -2.005846     -0.189901       0.557402
     C      -1.055449      0.728700       0.636447
     C      -0.149303      1.104773      -0.494933
     C       1.307147      0.824153      -0.185709
     O       1.465252     -0.607883      -0.080592
     O       2.673323     -0.927575       0.263857
     O      -2.267356     -0.865206      -0.597161
     H      -2.627361     -0.440774       1.408355
     H      -0.920009      1.219966       1.591008
     H      -0.434299      0.569448      -1.399886
     H      -0.232266      2.172840      -0.710148
     H       1.972741      1.163634      -0.978403
     H       1.622660      1.253347       0.765125
     H      -2.930518     -1.539498      -0.444117
Rotational constants (GHz):    5.0261900    1.3870900    1.2335400
Vibrational harmonic frequencies (cm-1):
       21.3258                  66.7347                 117.6948
      209.2188                 235.3191                 293.1693
      337.7011                 470.2339                 570.4101
      675.2776                 764.1390                 852.0397
      890.5305                 971.6337                1039.7919
     1062.8667                1072.7564                1140.2453
     1216.0551                1265.2629                1288.7033
     1296.4313                1299.1031                1356.4039
     1399.5920                1448.0565                1478.8844
     1502.9722                1786.2420                3066.2634
     3082.7260                3125.5137                3141.4267
     3187.1186                3213.1129                3920.4763
Zero-point correction (Hartree): 0.111324

HOCHCHCH2CH2OO.Zpmmc
~~~~~~~~~~~~~~~~~~~
E(CCSD(T)/Aug-CC-pVTZ) (Hartree): -381.60037010
E(CCSD/Aug-CC-pVTZ) (Hartree): -381.53772838
     T1 diagnostic:  0.022191
E(MP2/Aug-CC-pVTZ) (Hartree): -381.49448818
E(MP3/Aug-CC-pVTZ) (Hartree): -381.52479655
E(PMP2/Aug-CC-pVTZ) (Hartree): -381.49774632
E(PMP3/Aug-CC-pVTZ) (Hartree): -381.52669599
E(PUHF/Aug-CC-pVTZ) (Hartree): -380.13149271
E(UHF/Aug-CC-pVTZ) (Hartree): -380.12616632
E(UM062X/Aug-CC-pVTZ) (Hartree): -382.14414641
Electronic state : 2-A
Cartesian coordinates (Angs):
     C       1.838020      0.079555       0.342809
     C       1.016432      1.117681       0.218070
     C      -0.200990      1.144807      -0.658951
     C      -1.489617      0.807122       0.068881
     O      -1.451380     -0.522535       0.649006
     O      -1.199537     -1.432397      -0.236220
     O       1.729213     -1.129048      -0.251044
     H       2.725321      0.135368       0.959152
     H       1.258623      2.004009       0.787568
     H      -0.332366      2.141817      -1.082837
     H      -0.092628      0.466424      -1.506073
     H      -1.657397      1.451712       0.929058
     H      -2.353180      0.834791      -0.595467
     H       0.842185     -1.257284      -0.610196
Rotational constants (GHz):    3.8427200    2.2415600    1.6192300
Vibrational harmonic frequencies (cm-1):
       53.1930                 131.5021                 148.7968
      214.3796                 291.8812                 357.7868
      466.1477                 541.8760                 599.5496
      667.3210                 761.4688                 849.8795
      886.5390                 981.9506                 996.2389
     1037.1786                1088.8224                1148.0690
     1222.6972                1260.3105                1275.4686
     1306.3988                1351.2209                1373.7689
     1404.3696                1442.6719                1490.4872
     1495.2118                1747.8273                3075.1083
```

```
     3090.8924                3114.1355                3157.0129
     3205.6803                3226.0874                3797.6382
Zero-point correction (Hartree): 0.112222

HOCHCHCH2CH2OO.Zptpc
~~~~~~~~~~~~~~~~~~~
E(UM062X/Aug-CC-pVTZ) (Hartree): -382.14299943
Electronic state : 2-A
Cartesian coordinates (Angs):
     C       1.990719     -0.256495       0.149012
     C       1.485695      0.947781      -0.106531
     C       0.056334      1.134753      -0.529354
     C      -0.937822      0.806510       0.595548
     O      -2.050788      0.022964       0.099607
     O      -1.651134     -1.141169      -0.305940
     O       1.331854     -1.432158       0.068728
     H       3.017806     -0.397564       0.456449
     H       2.133420      1.803863       0.003447
     H      -0.110610      2.147300      -0.887896
     H      -0.173160      0.466885      -1.364114
     H      -0.471153      0.216023       1.382390
     H      -1.404024      1.688816       1.026043
     H       0.398713     -1.317709      -0.167528
Rotational constants (GHz):    4.3235600    1.9772300    1.4811700
Vibrational harmonic frequencies (cm-1):
       86.7356                 102.9580                 196.4536
      219.3773                 324.4331                 366.9969
      522.0243                 568.6202                 624.7459
      707.6098                 753.2826                 813.2521
      954.6509                 992.7960                1003.1022
     1032.6939                1079.1186                1135.4807
     1230.2006                1263.6910                1287.2719
     1308.1613                1339.8173                1375.1774
     1399.4617                1431.3431                1493.5697
     1509.4091                1733.6295                3059.1022
     3101.0760                3136.5884                3168.4579
     3216.8284                3242.0571                3721.9528
Zero-point correction (Hartree): 0.112774


TS.HOCHCHCH2CH2OO.cycHOCHCHCH2CH2OO.Zp
~~~~~~~~~~~~~~~~~~~~~~~~~~~~~~~~~~~~~
E(CCSD(T)/Aug-CC-pVTZ) (Hartree): -381.57530128
E(CCSD/Aug-CC-pVTZ) (Hartree): -381.50813416
     T1 diagnostic:  0.028163
E(MP2/Aug-CC-pVTZ) (Hartree): -381.46065809
E(MP3/Aug-CC-pVTZ) (Hartree): -381.48930848
E(PMP2/Aug-CC-pVTZ) (Hartree): -381.47781124
E(PMP3/Aug-CC-pVTZ) (Hartree): -381.50213210
E(PUHF/Aug-CC-pVTZ) (Hartree): -380.10312287
E(UHF/Aug-CC-pVTZ) (Hartree): -380.08321231
E(UM062X/Aug-CC-pVTZ) (Hartree): -382.11528532
Electronic state : 2-A
Cartesian coordinates (Angs):
     C      -1.313651      0.291233       0.341855
     C      -0.290224      1.192205       0.597926
     C       0.894511      1.228012      -0.296765
     C       1.630403     -0.125664      -0.144674
     O       0.687093     -1.170389      -0.292135
     O      -0.130432     -1.179717       0.824619
     O      -1.677701     -0.116515      -0.885788
     H      -2.107594      0.163169       1.065677
     H      -0.202646      1.551906       1.612946
     H       0.601424      1.347293      -1.342140
     H       1.571932      2.041338      -0.041842
     H       2.372267     -0.273285      -0.929519
     H       2.096557     -0.203814       0.837668
     H      -0.889856     -0.408346      -1.366413
Rotational constants (GHz):    3.8895600    2.8846500    2.2593700
Vibrational harmonic frequencies (cm-1):
     i623.4638                 177.6328                 248.3701
      280.9721                 391.9599                 432.6138
      452.0873                 500.3075                 587.6845
      663.9523                 737.8072                 875.1450
      919.1406                 932.5186                 979.4588
     1017.9830                1061.3809                1077.5628
     1148.8220                1210.9937                1256.2309
     1268.3454                1318.6422                1340.3793
     1369.6287                1434.1885                1484.4078
     1497.9549                1538.4045                3065.6462
     3076.6998                3128.7866                3140.1905
     3209.6855                3225.6704                3759.1579
Zero-point correction (Hartree): 0.111198

TS.HOCHCHCH2CH2OO.cycHOCHCHCH2CH2OO.Zt
~~~~~~~~~~~~~~~~~~~~~~~~~~~~~~~~~~~~~
E(UM062X/Aug-CC-pVTZ) (Hartree): -382.11419635
Electronic state : 2-A
Cartesian coordinates (Angs):
     C      -1.287511      0.259883       0.386557
     C      -0.294591      1.181154       0.633815
     C       0.851787      1.247950      -0.305377
     C       1.636262     -0.084230      -0.149982
```

```
     O       0.753486     -1.169180      -0.328771
     O      -0.090769     -1.241275       0.751995
     O      -1.630822     -0.007392      -0.891770
     H      -2.019276      0.015380       1.147963
     H      -0.171789      1.509338       1.655646
     H       0.518979      1.326247      -1.338814
     H       1.519237      2.078630      -0.080707
     H       2.397095     -0.186422      -0.923444
     H       2.090673     -0.145555       0.840312
     H      -2.025769     -0.883393      -0.942661
Rotational constants (GHz):    3.8492700    2.8899600    2.2304200
Vibrational harmonic frequencies (cm-1):
     i636.9546                172.7885                237.3710
      258.3095                345.3806                425.8914
      446.6402                470.7412                581.9767
      665.6133                750.0642                868.5386
      930.9654                944.1562                984.0003
     1021.3281               1065.7209               1080.7316
     1155.5223               1207.5550               1260.3485
     1273.2681               1283.4913               1320.2074
     1368.5899               1434.2763               1481.3443
     1490.0791               1559.9629               3068.6534
     3091.3822               3132.4485               3147.5517
     3178.7540               3223.6184               3862.1701
Zero-point correction (Hartree): 0.111151


################################################################################
E-HOCH=C(CH3)CH2CH2OO ring closure and H-shift
################################################################################

HOCHCCH3CH2CH2OO.Ecppc
----------------------
E(UM062X/Aug-CC-pVTZ) (Hartree): -421.45033361
Electronic state : 2-A
Cartesian coordinates (Angs):
     C      -1.103065     -0.871471       0.191141
     C      -0.923169      0.437989       0.049117
     C       0.395924      1.105234       0.334463
     C       1.491277      0.242106       0.917800
     O       1.954620     -0.751298      -0.027162
     O       2.592063     -0.202878      -1.014324
     O      -2.250252     -1.571520      -0.021246
     H      -0.307885     -1.538884       0.491128
     C      -1.996493      1.381879      -0.412544
     H       0.784451      1.565845      -0.579038
     H       0.231319      1.930178       1.035728
     H       2.356948      0.841506       1.192988
     H       1.153244     -0.338338       1.774789
     H      -2.959546     -0.976412      -0.277049
     H      -2.282302      2.070261       0.386228
     H      -2.903590      0.887905      -0.759677
     H      -1.630930      1.989086      -1.243099
Rotational constants (GHz):    3.2229900    1.1959300    1.0071900
Vibrational harmonic frequencies (cm-1):
       51.8982                 69.8197                 73.8428
      147.1759                217.6721                261.0593
      300.7799                325.5790                340.9710
      477.0424                492.8291                545.1056
      613.4975                792.7749                844.9085
      922.6439                972.1016                990.6421
     1022.9268               1055.5205               1118.1250
     1179.2911               1217.1855               1231.9348
     1277.5549               1296.8105               1317.5123
     1396.5873               1402.2311               1423.3292
     1438.1956               1472.3417               1478.9286
     1496.0521               1505.6938               1781.0266
     3038.5655               3048.2013               3068.5338
     3098.9307               3100.1948               3124.0822
     3154.6785               3232.9326               3881.6709
Zero-point correction (Hartree): 0.139650

HOCHCCH3CH2CH2OO.Ecppt
----------------------
E(UM062X/Aug-CC-pVTZ) (Hartree): -421.45049488
Electronic state : 2-A
Cartesian coordinates (Angs):
     C      -1.104756     -0.841832       0.194140
     C      -0.917761      0.462519       0.041328
     C       0.404086      1.129509       0.303331
     C       1.497118      0.278838       0.908852
     O       1.943860     -0.756505       0.000620
     O       2.585868     -0.256450      -1.009129
     O      -2.321172     -1.428384      -0.034035
     H      -0.313292     -1.514921       0.498488
     C      -2.014262      1.373580      -0.423936
     H       0.789235      1.563549      -0.624469
     H       0.244566      1.974288       0.981369
     H       2.371537      0.878173       1.155111
     H       1.158947     -0.265689       1.789342
     H      -2.238138     -2.380469       0.030156
     H      -2.237775      2.126436       0.335668
     H      -2.924844      0.823720      -0.643640
```

```
     H      -1.705234      1.909941      -1.323966
Rotational constants (GHz):    3.2608800    1.1933500    1.0065700
Vibrational harmonic frequencies (cm-1):
       64.2134                69.7592                128.4212
      147.9245               202.7073                220.2890
      280.1259               304.5266                309.7661
      459.1385               476.7862                545.6244
      617.3729               804.5104                838.1869
      894.5427               972.8820                987.6513
     1020.9739              1061.4689               1119.3137
     1187.0261              1200.6626               1231.1333
     1279.8442              1304.1932               1315.6101
     1387.4788              1398.6469               1409.4114
     1438.5514              1469.9868               1491.9479
     1493.7130              1495.7324               1800.1772
     3041.0298              3049.1693               3070.3455
     3095.7183              3097.7090               3153.4042
     3168.7181              3202.3506               3921.7865
Zero-point correction (Hartree): 0.139493

HOCHCCH3CH2CH2OO.Ecptc
~~~~~~~~~~~~~~~~~~~~~~
E(UM062X/Aug-CC-pVTZ) (Hartree): -421.44964409
Electronic state : 2-A
Cartesian coordinates (Angs):
     C       0.958460      0.920769       0.176224
     C       1.056457     -0.394701       0.011636
     C      -0.134754     -1.309029       0.129860
     C      -1.439234     -0.683554       0.559397
     O      -1.928124      0.141653      -0.523660
     O      -3.012965      0.767980      -0.188622
     O       1.964580      1.833701       0.114548
     H       0.017272      1.414141       0.372494
     C       2.341567     -1.103477      -0.306493
     H      -0.295534     -1.825626      -0.822258
     H       0.096126     -2.096372       0.854757
     H      -2.201540     -1.437712       0.748404
     H      -1.336795     -0.046262       1.437080
     H       2.803597      1.393954      -0.044874
     H       2.649076     -1.746589       0.521495
     H       3.173599     -0.436166      -0.529254
     H       2.211299     -1.746085      -1.179711
Rotational constants (GHz):    3.3065000    1.1620200    0.9115700
Vibrational harmonic frequencies (cm-1):
       39.4128                52.5256                 72.1304
      128.7292               228.7058                257.5636
      290.8939               323.7623                338.1896
      394.0621               493.4623                563.6174
      607.2767               795.5039                831.6187
      933.5204               977.2514               1009.9132
     1030.1231              1074.5935               1109.3652
     1180.0895              1216.7749               1236.2106
     1283.9118              1295.7526               1302.1399
     1391.7808              1407.0620               1424.9217
     1441.9287              1471.4976               1479.7302
     1505.3723              1508.0329               1781.5179
     3035.6387              3047.6372               3061.6866
     3090.1179              3098.7149               3125.4747
     3142.3662              3234.4097               3881.7042
Zero-point correction (Hartree): 0.139416

HOCHCCH3CH2CH2OO.Ecptt
~~~~~~~~~~~~~~~~~~~~~~
E(UM062X/Aug-CC-pVTZ) (Hartree): -421.45008565
Electronic state : 2-A
Cartesian coordinates (Angs):
     C       0.949245      0.896312       0.173511
     C       1.049244     -0.416643       0.012924
     C      -0.135912     -1.337351       0.118120
     C      -1.445615     -0.719812       0.542801
     O      -1.925296      0.123323      -0.531726
     O      -2.955198      0.820810      -0.165589
     O       2.041054      1.717938       0.093176
     H       0.007111      1.392579       0.368978
     C       2.355536     -1.083852      -0.297378
     H      -0.284575     -1.849886      -0.838045
     H       0.095114     -2.126970       0.840052
     H      -2.210711     -1.475964       0.713060
     H      -1.351997     -0.094804       1.430111
     H       1.762803      2.632521       0.154340
     H       2.621025     -1.794855       0.488654
     H       3.160225     -0.360887      -0.395257
     H       2.281535     -1.650231      -1.228646
Rotational constants (GHz):    3.3040500    1.1760800    0.9184100
Vibrational harmonic frequencies (cm-1):
       39.1216                64.6219                128.1937
      134.5810               219.8758                237.7368
      275.3857               299.8364                306.6485
      395.6929               461.5607                564.4930
      611.0092               806.0451                825.4997
      902.5628               978.5088               1008.2744
     1030.0588              1075.5645               1111.3507
     1188.2078              1201.5821               1235.4196
```

```
     1286.3389                1298.9974                1305.7658
     1387.2775                1395.9645                1413.2556
     1443.2880                1469.1613                1493.2110
     1494.0080                1506.8397                1800.8022
     3038.4796                3048.6987                3064.8658
     3089.6645                3094.9998                3142.0858
     3168.8376                3203.8529                3920.8200
Zero-point correction (Hartree): 0.139353

HOCHCCH3CH2CH2OO.Ectpc
~~~~~~~~~~~~~~~~~~~~~~
E(UM062X/Aug-CC-pVTZ) (Hartree): -421.45041178
Electronic state : 2-A
Cartesian coordinates (Angs):
     C       1.572068     -0.848306      -0.035840
     C       1.048365      0.370431       0.058022
     C      -0.430853      0.592940       0.216823
     C      -1.275230     -0.662205       0.231476
     O      -2.664912     -0.314663       0.411511
     O      -3.163533      0.215424      -0.662995
     O       2.883973     -1.174345      -0.191749
     H       0.970192     -1.745366       0.005025
     C       1.858942      1.633757       0.008171
     H      -0.617029      1.146169       1.142711
     H      -0.792868      1.228042      -0.596810
     H      -1.198296     -1.223420      -0.698772
     H      -1.047709     -1.305710       1.079830
     H       3.418857     -0.378750      -0.252772
     H       2.936081      1.471320      -0.013281
     H       1.647700      2.253607       0.881680
     H       1.599093      2.223085      -0.873668
Rotational constants (GHz):    4.4348700    0.9033900    0.7892900
Vibrational harmonic frequencies (cm-1):
       53.6282                  69.9208                  88.4423
      135.7319                 170.3219                 257.5520
      290.1776                 336.9574                 353.7257
      404.0617                 491.8700                 547.3106
      647.4542                 792.2281                 844.8403
      918.2831                 977.5671                1004.5079
     1035.6693                1091.3277                1117.8562
     1178.3510                1218.5345                1240.8101
     1279.3550                1293.0455                1329.7371
     1349.0943                1410.2839                1426.3496
     1442.5403                1479.1171                1490.3443
     1503.1670                1506.4381                1778.2516
     3040.4836                3052.2854                3075.5687
     3093.2477                3105.0726                3127.5160
     3154.5866                3227.0072                3881.4336
Zero-point correction (Hartree): 0.139679

HOCHCCH3CH2CH2OO.Ectpt
~~~~~~~~~~~~~~~~~~~~~~
E(UM062X/Aug-CC-pVTZ) (Hartree): -421.45000645
Electronic state : 2-A
Cartesian coordinates (Angs):
     C       1.577852     -0.819250      -0.040591
     C       1.039649      0.390526       0.048849
     C      -0.439288      0.606583       0.202344
     C      -1.275694     -0.652926       0.243520
     O      -2.668115     -0.314816       0.420538
     O      -3.177044      0.179949      -0.665932
     O       2.928480     -1.001619      -0.177833
     H       0.988561     -1.727576      -0.009288
     C       1.873460      1.636055       0.003073
     H      -0.626141      1.177823       1.116948
     H      -0.803352      1.224427      -0.623312
     H      -1.197913     -1.231149      -0.676395
     H      -1.040261     -1.278141       1.103607
     H       3.126312     -1.936141      -0.247113
     H       2.928756      1.407436      -0.114273
     H       1.742175      2.216290       0.919033
     H       1.559429      2.272992      -0.826568
Rotational constants (GHz):    4.5430900    0.8957900    0.7869900
Vibrational harmonic frequencies (cm-1):
       66.1054                  81.8442                 118.2333
      133.7300                 168.4497                 211.6414
      270.5425                 300.3762                 340.0182
      401.4638                 463.2389                 548.0668
      655.0680                 787.2887                 856.5622
      882.6100                 976.6554                1004.0975
     1038.8936                1090.5760                1119.9076
     1183.3872                1200.1907                1240.4372
     1284.8237                1297.3005                1328.9850
     1344.8630                1391.9456                1417.1383
     1441.1149                1486.2883                1493.8206
     1495.3588                1502.2354                1796.0394
     3042.9124                3052.9699                3078.1945
     3090.6331                3100.8132                3151.6730
     3170.4785                3193.7375                3923.0461
Zero-point correction (Hartree): 0.139478

HOCHCCH3CH2CH2OO.Ecttc
~~~~~~~~~~~~~~~~~~~~~~
```

```
E(UM062X/Aug-CC-pVTZ) (Hartree): -421.44977810
Electronic state : 2-A
Cartesian coordinates (Angs):
     C       1.488099     -0.916064      -0.005446
     C       1.157250      0.372000      -0.004153
     C      -0.277382      0.825472      -0.006417
     C      -1.301472     -0.284018       0.000130
     O      -2.599710      0.348790       0.000616
     O      -3.555657     -0.527145       0.004487
     O       2.740169     -1.447403       0.002084
     H       0.750225     -1.706120      -0.013362
     C       2.156681      1.492604       0.004339
     H      -0.453841      1.465276       0.863764
     H      -0.454740      1.456607      -0.882589
     H      -1.248142     -0.912948      -0.888009
     H      -1.243594     -0.906166       0.892763
     H       3.398381     -0.748000       0.022418
     H       3.194147      1.164942      -0.051675
     H       2.053967      2.092384       0.911142
     H       1.986132      2.160124      -0.842661
Rotational constants (GHz):    4.5196000    0.8584100    0.7311900
Vibrational harmonic frequencies (cm-1):
       39.9873                66.4798                104.0525
      118.0175               126.4742                258.2234
      277.4712               336.0857                345.7019
      356.7540               491.5233                552.7374
      628.5252               781.4722                838.9029
      916.1860              1004.7024               1027.4762
     1032.3684              1102.6472               1113.7519
     1180.2951              1219.2221               1231.7335
     1285.5998              1297.2377               1310.4639
     1346.4920              1411.7788               1429.2141
     1447.0180              1479.5478               1495.7512
     1506.2214              1512.9631               1778.6707
     3041.0038              3052.2032               3069.5630
     3084.7357              3103.9782               3128.5020
     3142.6828              3227.4756               3881.6338
Zero-point correction (Hartree): 0.139386

HOCHCCH3CH2CH2OO.Ecttt
~~~~~~~~~~~~~~~~~~~~~~
E(UM062X/Aug-CC-pVTZ) (Hartree): -421.44960190
Electronic state : 2-A
Cartesian coordinates (Angs):
     C       1.497402     -0.887783       0.000047
     C       1.149149      0.392873      -0.000195
     C      -0.286555      0.836909      -0.000243
     C      -1.302947     -0.279254       0.000509
     O      -2.608087      0.338922       0.000809
     O      -3.554154     -0.547667      -0.000566
     O       2.808980     -1.279956       0.000127
     H       0.772529     -1.692773       0.000239
     C       2.167038      1.493856      -0.000459
     H      -0.464979      1.472336       0.872425
     H      -0.465223      1.471424      -0.873521
     H      -1.242267     -0.904675      -0.889847
     H      -1.241502     -0.903978       0.891323
     H       2.863827     -2.236095       0.000007
     H       3.180058      1.102198      -0.000860
     H       2.039886      2.130695       0.877666
     H       2.039237      2.130865      -0.878364
Rotational constants (GHz):    4.6297500    0.8525500    0.7297200
Vibrational harmonic frequencies (cm-1):
       61.1190                98.7035                106.0269
      120.7515               124.9046                216.6812
      263.0903               301.9858                333.7557
      352.6867               461.9462                551.4865
      637.3932               777.7230                851.1881
      881.7542              1005.5986               1027.6191
     1032.6477              1105.6258               1112.9235
     1188.1821              1201.6842               1231.4127
     1295.4491              1297.7054               1308.7258
     1343.6335              1393.4035               1420.2363
     1446.5771              1489.3928               1494.3233
     1498.0086              1512.2925               1796.4653
     3043.6363              3052.7079               3072.4169
     3082.2130              3100.2050               3139.7630
     3170.4924              3194.7409               3923.5816
Zero-point correction (Hartree): 0.139248

HOCHCCH3CH2CH2OO.Egmpc
~~~~~~~~~~~~~~~~~~~~~~
E(UM062X/Aug-CC-pVTZ) (Hartree): -421.45079312
Electronic state : 2-A
Cartesian coordinates (Angs):
     C      -1.828722      0.593462      -0.318153
     C      -0.749123      0.228923       0.366273
     C       0.356813      1.221157       0.592489
     C       1.588782      1.000573      -0.274274
     O       2.226603     -0.254941       0.045546
     O       1.867639     -1.208950      -0.758884
     O      -2.888998     -0.203964      -0.611804
     H      -1.967069      1.592998      -0.708991
```

```
     C      -0.625813     -1.165153       0.928019
     H       0.001192      2.230566       0.374814
     H       0.665992      1.211051       1.640907
     H       1.340216      0.972306      -1.333044
     H       2.348091      1.756234      -0.075769
     H      -2.717138     -1.099473      -0.304838
     H      -0.474526     -1.911017       0.144251
     H      -1.516950     -1.442277       1.497998
     H       0.226614     -1.241311       1.599681
Rotational constants (GHz):    3.5834100    1.2111900    1.0713800
Vibrational harmonic frequencies (cm-1):
       39.9458                73.1485                128.2640
      167.4782               175.8704                263.8396
      308.0215               339.6564                396.1107
      471.1996               520.2774                540.9332
      609.5298               795.0616                861.5924
      923.9655               937.1037               1016.3156
     1031.4899              1050.5768               1093.6730
     1179.3530              1227.8926               1241.8213
     1251.0525              1320.3644               1328.3232
     1378.4174              1391.6522               1405.0569
     1421.3944              1470.4582               1481.4939
     1496.5170              1502.0666               1765.0900
     3040.3305              3053.9698               3088.4239
     3093.0150              3102.2243               3146.0031
     3158.5547              3212.6987               3861.4501
Zero-point correction (Hartree): 0.139792

HOCHCCH3CH2CH2OO.Elmmc
----------------------
E(UM062X/Aug-CC-pVTZ) (Hartree): -421.45242156
Electronic state : 2-A
Cartesian coordinates (Angs):
     C       2.013050     -0.583300       0.048600
     C       0.822405     -0.037761       0.280218
     C      -0.330897     -0.920787       0.665404
     C      -1.401168     -1.046745      -0.407538
     O      -2.022990      0.228051      -0.691483
     O      -2.717012      0.653555       0.318701
     O       3.144830      0.064818      -0.333535
     H       2.192013     -1.644901       0.158839
     C       0.576416      1.443144       0.170143
     H       0.025312     -1.930256       0.878572
     H      -0.813437     -0.547858       1.572093
     H      -0.979016     -1.352464      -1.363281
     H      -2.195381     -1.728309      -0.105657
     H       2.954627      0.995628      -0.481461
     H       0.217636      1.728786      -0.820826
     H       1.471402      2.028463       0.390908
     H      -0.190622      1.752218       0.880397
Rotational constants (GHz):    4.6129000    1.0605600    0.9487100
Vibrational harmonic frequencies (cm-1):
       38.6505                77.3705                130.5209
      169.8811               176.6163                264.7294
      311.8036               328.6012                402.1490
      459.2398               517.9373                551.3201
      617.6214               797.0893                847.4594
      928.4938               943.3898                996.1643
     1036.3604              1052.8646               1106.3434
     1176.3255              1219.7146               1234.3742
     1269.0028              1305.5852               1318.0439
     1378.3035              1395.9793               1409.7986
     1426.5379              1469.6655               1485.0410
     1489.3419              1505.1048               1769.2464
     3047.6348              3061.1003               3088.9961
     3104.5789              3110.0293               3124.2378
     3153.5715              3211.4230               3868.8059
Zero-point correction (Hartree): 0.139827

HOCHCCH3CH2CH2OO.Elmmt
----------------------
E(UM062X/Aug-CC-pVTZ) (Hartree): -421.45107126
Electronic state : 2-A
Cartesian coordinates (Angs):
     C      -2.045545     -0.556310      -0.080610
     C      -0.840502     -0.020493      -0.231501
     C       0.320886     -0.905756      -0.581414
     C       1.398805     -0.977272       0.489546
     O       2.113025      0.274231       0.616461
     O       2.827360      0.521781      -0.437538
     O      -3.140708      0.192148       0.252576
     H      -2.218904     -1.618909      -0.211558
     C      -0.596830      1.451270      -0.071279
     H      -0.024704     -1.925997      -0.758613
     H       0.802291     -0.563348      -1.501394
     H       0.977864     -1.144065       1.479792
     H       2.140528     -1.740460       0.258152
     H      -3.929223     -0.350927       0.223254
     H      -0.062021      1.665449       0.855983
     H      -1.533593      2.002421      -0.061156
     H       0.029452      1.821923      -0.884911
Rotational constants (GHz):    4.9357000    1.0140300    0.9163200
Vibrational harmonic frequencies (cm-1):
```

```
       36.7960                  71.9341                 147.3537
      166.4145                 200.7384                 220.6476
      267.5188                 297.9678                 374.2763
      433.4844                 506.7578                 553.2612
      611.9254                 806.4659                 851.1981
      888.6263                 946.0686                 989.6621
     1041.5967                1058.7229                1110.1534
     1180.1000                1210.4322                1229.0814
     1272.1106                1305.5993                1308.5329
     1380.5998                1394.8994                1397.4725
     1430.8916                1468.7159                1487.8996
     1493.0969                1493.7255                1791.2177
     3056.7129                3057.7261                3087.8331
     3106.6378                3107.8842                3152.1624
     3161.8569                3175.6031                3920.5807
Zero-point correction (Hartree): 0.139544

HOCHCCH3CH2CH2OO.Elmtc
~~~~~~~~~~~~~~~~~~~~~~
E(UM062X/Aug-CC-pVTZ) (Hartree): -421.45103902
Electronic state : 2-A
Cartesian coordinates (Angs):
     C       2.057130     -0.569428      -0.201725
     C       0.932723     -0.082448       0.315439
     C      -0.172671     -1.032065       0.687609
     C      -1.412079     -0.918236      -0.180575
     O      -2.063491      0.337284       0.123070
     O      -3.099629      0.531724      -0.632015
     O       3.138556      0.138524      -0.620488
     H       2.215710     -1.631877      -0.333222
     C       0.710421      1.388304       0.540609
     H       0.181427     -2.060750       0.604398
     H      -0.471987     -0.880858       1.728956
     H      -1.171835     -0.910268      -1.243110
     H      -2.133812     -1.706963       0.029789
     H       2.960188      1.080858      -0.554230
     H       0.152950      1.849424      -0.276981
     H       1.646002      1.936518       0.665775
     H       0.124727      1.546901       1.445953
Rotational constants (GHz):    4.5600900    0.9613500    0.8826200
Vibrational harmonic frequencies (cm-1):
       33.2861                  60.1466                  98.9528
      149.4043                 179.0129                 256.2755
      302.3820                 334.3240                 390.1704
      410.9641                 501.4042                 575.1685
      600.9007                 797.4821                 840.6084
      925.9919                 961.2699                1025.1453
     1044.0113                1059.1274                1093.6388
     1180.0190                1218.9880                1237.1159
     1276.0249                1295.5166                1318.5902
     1380.5161                1398.0782                1412.0442
     1428.2151                1467.6952                1485.1955
     1498.0731                1503.1657                1769.5168
     3049.7919                3050.6693                3082.3847
     3107.0257                3108.5436                3125.5393
     3142.4746                3209.4681                3871.6575
Zero-point correction (Hartree): 0.139551

HOCHCCH3CH2CH2OO.Elmtt
~~~~~~~~~~~~~~~~~~~~~~
E(UM062X/Aug-CC-pVTZ) (Hartree): -421.44993064
Electronic state : 2-A
Cartesian coordinates (Angs):
     C      -2.102942      0.538206      -0.143436
     C      -0.937721      0.060986       0.276054
     C       0.166425      1.019365       0.624421
     C       1.406567      0.886346      -0.241243
     O       2.135432     -0.287980       0.187571
     O       3.181418     -0.493893      -0.550088
     O      -3.144905     -0.277302      -0.488645
     H      -2.283931      1.603643      -0.234672
     C      -0.681508     -1.410118       0.417318
     H      -0.189171      2.046483       0.528509
     H       0.472598      0.885162       1.666565
     H       1.166525      0.752649      -1.295559
     H       2.081468      1.733116      -0.121316
     H      -3.916446      0.249339      -0.700408
     H       0.027256     -1.761330      -0.335032
     H      -1.602277     -1.977775       0.312444
     H      -0.236502     -1.626603       1.390083
Rotational constants (GHz):    4.9541800    0.9345000    0.8533500
Vibrational harmonic frequencies (cm-1):
       38.2223                  60.7487                 118.7998
      167.5998                 208.7623                 239.9630
      253.9018                 295.9806                 369.6034
      380.9865                 471.5233                 579.6108
      597.9815                 807.2849                 841.7321
      891.1782                 958.9019                1021.9535
     1049.8199                1064.5119                1098.2331
     1185.8944                1209.9780                1231.6886
     1279.2776                1296.1262                1305.4640
     1382.0083                1397.4037                1398.7941
     1432.0567                1465.6511                1490.4287
```

```
     1496.2937                1500.0287                1794.8727
     3047.2310                3058.8339                3081.9629
     3106.0061                3109.1757                3141.2796
     3163.4507                3177.9344                3921.3390
Zero-point correction (Hartree): 0.139402

HOCHCCH3CH2CH2OO.Elpmc
~~~~~~~~~~~~~~~~~~~~~~
E(CCSD(T)/Aug-CC-pVTZ) (Hartree): -420.84408640
E(CCSD/Aug-CC-pVTZ) (Hartree): -420.77348661
     T1 diagnostic:  0.020724
E(MP2/Aug-CC-pVTZ) (Hartree): -420.72102249
E(MP3/Aug-CC-pVTZ) (Hartree): -420.76040125
E(PMP2/Aug-CC-pVTZ) (Hartree): -420.72446597
E(PMP3/Aug-CC-pVTZ) (Hartree): -420.76254263
E(PUHF/Aug-CC-pVTZ) (Hartree): -419.18070042
E(UHF/Aug-CC-pVTZ) (Hartree): -419.17544253
E(UM062X/Aug-CC-pVTZ) (Hartree): -421.45265451
Electronic state : 2-A
Cartesian coordinates (Angs):
     C      -1.517607     -0.283437      -0.753321
     C      -0.688102      0.550324      -0.133217
     C       0.538745      1.038517      -0.843823
     C       1.838957      0.611526      -0.173038
     O       1.985009     -0.818500      -0.218460
     O       1.354129     -1.396059       0.761167
     O      -2.645530     -0.839962      -0.241593
     H      -1.353689     -0.601333      -1.774347
     C      -0.894450      1.005527       1.283658
     H       0.547096      0.688579      -1.876849
     H       0.549588      2.133239      -0.871075
     H       2.704278      0.996970      -0.709256
     H       1.882456      0.910749       0.873250
     H      -2.716026     -0.636878       0.695306
     H      -0.360153      0.364472       1.988530
     H      -1.947769      1.023448       1.568417
     H      -0.519904      2.022190       1.415556
Rotational constants (GHz):    3.0806800    1.3277200    1.2131600
Vibrational harmonic frequencies (cm-1):
       63.9862                  104.7020                 108.6729
      122.1413                  201.4260                 273.4201
      300.7804                  361.7789                 395.4514
      458.0915                  513.3197                 555.9277
      598.5636                  800.0066                 863.5417
      918.9867                  962.5085                1003.3209
     1035.1931                 1053.7956                1078.6200
     1184.2846                 1224.9307                1237.2872
     1246.1949                 1314.7995                1323.2196
     1372.5476                 1393.5532                1406.8474
     1425.4227                 1469.2816                1484.0931
     1495.6961                 1505.2614                1772.5644
     3040.6819                 3046.7273                3093.4939
     3107.1019                 3108.7996                3113.8965
     3154.7250                 3216.3431                3873.0163
Zero-point correction (Hartree): 0.139845

HOCHCCH3CH2CH2OO.Elpmt
~~~~~~~~~~~~~~~~~~~~~~
E(UM062X/Aug-CC-pVTZ) (Hartree): -421.45177275
Electronic state : 2-A
Cartesian coordinates (Angs):
     C      -1.510210     -0.336826      -0.690902
     C      -0.683259      0.546226      -0.145920
     C       0.539959      0.977063      -0.898706
     C       1.847651      0.597746      -0.214740
     O       2.000095     -0.831905      -0.179810
     O       1.380285     -1.354796       0.837605
     O      -2.640887     -0.764850      -0.055396
     H      -1.323918     -0.761340      -1.671016
     C      -0.911633      1.122466       1.218494
     H       0.541037      0.556366      -1.905497
     H       0.548957      2.066978      -1.003651
     H       2.705532      0.954743      -0.781869
     H       1.899584      0.958318       0.811076
     H      -3.092511     -1.415167      -0.594411
     H      -0.205936      0.698501       1.936264
     H      -1.917224      0.908862       1.570994
     H      -0.766517      2.205095       1.209553
Rotational constants (GHz):    3.1009500    1.3187700    1.1980700
Vibrational harmonic frequencies (cm-1):
       57.1189                   93.4475                 104.6185
      131.9094                  219.1160                 232.0021
      276.1121                  311.2246                 387.5974
      438.8327                  494.0006                 557.1893
      600.1569                  807.2122                 858.7543
      894.0112                  961.8466                 999.8902
     1036.6439                 1062.5751                1080.2574
     1193.8357                 1210.0610                1235.1229
     1248.8211                 1303.8493                1319.1174
     1375.2739                 1390.0143                1398.2793
     1430.4524                 1469.6591                1486.2454
     1489.9780                 1504.9210                1796.2725
     3041.9251                 3050.8094                3095.6879
```

```
     3102.2293                3104.9275                3157.8622
     3162.0273                3180.0152                3922.6773
Zero-point correction (Hartree): 0.139594

HOCHCCH3CH2CH2OO.Elppc
~~~~~~~~~~~~~~~~~~~~~~
E(UM062X/Aug-CC-pVTZ) (Hartree): -421.45195093
Electronic state : 2-A
Cartesian coordinates (Angs):
     C       1.459781     -0.776614       0.420568
     C       0.809440      0.376741       0.306445
     C      -0.482178      0.573410       1.045944
     C      -1.666117      0.819506       0.124995
     O      -1.850534     -0.277332      -0.795413
     O      -2.187652     -1.364440      -0.172854
     O       2.617064     -1.127776      -0.198308
     H       1.098108     -1.575173       1.054509
     C       1.280687      1.502085      -0.571500
     H      -0.703645     -0.293698       1.667310
     H      -0.414759      1.443134       1.707674
     H      -2.593160      0.935477       0.684486
     H      -1.513927      1.681988      -0.522449
     H       2.881434     -0.442781      -0.818407
     H       0.815043      1.470810      -1.560068
     H       2.362349      1.500720      -0.714819
     H       1.027859      2.465136      -0.124337
Rotational constants (GHz):    3.1403500    1.2648500    1.0636500
Vibrational harmonic frequencies (cm-1):
       36.8765                  52.5879                 118.8400
      127.2007                 205.7481                 263.7766
      302.9698                 348.2542                 391.2698
      454.1732                 509.8571                 554.3828
      615.8995                 799.6879                 843.0226
      929.9481                 956.6517                 993.0827
     1035.7560                1052.2483                1089.8522
     1182.5724                1223.8758                1230.1082
     1265.2094                1299.6920                1317.9795
     1377.4525                1396.8678                1410.5049
     1426.5641                1472.3962                1486.1949
     1496.9209                1505.0832                1778.0527
     3041.6380                3043.2119                3093.3491
     3098.9139                3114.6308                3121.5831
     3151.6504                3215.2843                3874.0553
Zero-point correction (Hartree): 0.139665

HOCHCCH3CH2CH2OO.Elppt
~~~~~~~~~~~~~~~~~~~~~~
E(CCSD(T)/Aug-CC-pVTZ) (Hartree): -420.84385432
E(CCSD/Aug-CC-pVTZ) (Hartree): -420.77372382
     T1 diagnostic:  0.020573
E(MP2/Aug-CC-pVTZ) (Hartree): -420.72095663
E(MP3/Aug-CC-pVTZ) (Hartree): -420.76066693
E(PMP2/Aug-CC-pVTZ) (Hartree): -420.72411407
E(PMP3/Aug-CC-pVTZ) (Hartree): -420.76253098
E(PUHF/Aug-CC-pVTZ) (Hartree): -419.18205719
E(UHF/Aug-CC-pVTZ) (Hartree): -419.17690718
E(UM062X/Aug-CC-pVTZ) (Hartree): -421.45188619
Electronic state : 2-A
Cartesian coordinates (Angs):
     C       1.428909     -0.761649       0.387917
     C       0.808286      0.406145       0.287379
     C      -0.489208      0.617197       1.011743
     C      -1.672006      0.827860       0.080720
     O      -1.862434     -0.311367      -0.786966
     O      -2.193385     -1.369017      -0.113317
     O       2.607110     -1.019542      -0.254484
     H       1.022622     -1.570406       0.984909
     C       1.341535      1.528230      -0.552156
     H      -0.712932     -0.230656       1.658873
     H      -0.426996      1.506181       1.647335
     H      -2.598217      0.971458       0.635324
     H      -1.517559      1.658184      -0.605961
     H       2.895243     -1.912333      -0.060989
     H       0.735260      1.673752      -1.449666
     H       2.361263      1.329288      -0.871014
     H       1.325889      2.467235       0.005707
Rotational constants (GHz):    3.1486200    1.2674200    1.0540300
Vibrational harmonic frequencies (cm-1):
       26.7941                  45.7261                 108.2875
      130.5170                 215.3615                 233.3374
      275.5859                 299.0623                 385.1109
      433.3619                 493.0776                 557.0090
      615.4538                 807.4477                 840.0362
      902.1129                 957.7869                 984.3953
     1035.1859                1063.0966                1089.2179
     1192.4548                1208.3106                1233.7179
     1266.7916                1301.9615                1305.5584
     1381.0377                1389.3788                1401.8280
     1430.7164                1471.4674                1487.7331
     1490.5883                1502.7339                1800.3064
     3046.1368                3048.2779                3093.5697
     3097.0945                3117.7039                3155.1559
     3161.9043                3180.8921                3921.9245
```

```
Zero-point correction (Hartree): 0.139390

HOCHCCH3CH2CH2OO.Elptc
----------------------
E(UM062X/Aug-CC-pVTZ) (Hartree): -421.45093535
Electronic state : 2-A
Cartesian coordinates (Angs):
     C      -1.721411     -0.587870      -0.547802
     C      -0.916644      0.407847      -0.192202
     C       0.248419      0.773116      -1.068863
     C       1.585035      0.661313      -0.362510
     O       1.784646     -0.724568      -0.010541
     O       2.857524     -0.884493       0.700195
     O      -2.797669     -1.055815       0.136247
     H      -1.576378     -1.138501      -1.467638
     C      -1.090617      1.192064       1.078120
     H       0.263101      0.147565      -1.962174
     H       0.157778      1.811407      -1.403676
     H       2.415615      0.956359      -1.002489
     H       1.620835      1.237491       0.561719
     H      -2.868588     -0.611774       0.985637
     H      -0.462934      0.806120       1.885350
     H      -2.122091      1.195651       1.433353
     H      -0.812046      2.235865       0.922256
Rotational constants (GHz):    3.4451300    1.0522800    0.9883000
Vibrational harmonic frequencies (cm-1):
       41.6818                55.6782                95.2414
      122.1272               225.6290               255.4193
      298.1443               341.1793               386.6297
      405.9443               500.7129               568.1586
      599.1119               800.1281               838.2699
      929.8089               959.6360              1024.2254
     1049.3828              1067.1277              1077.5407
     1181.2537              1223.4907              1231.4619
     1276.1074              1297.0730              1318.4225
     1380.2345              1394.1162              1412.8135
     1428.6500              1470.7367              1488.4428
     1503.7162              1508.9518              1777.2567
     3043.4882              3044.8136              3085.8243
     3100.1926              3108.8349              3116.2341
     3140.7489              3215.3730              3874.7341
Zero-point correction (Hartree): 0.139571

HOCHCCH3CH2CH2OO.Elptt
----------------------
E(UM062X/Aug-CC-pVTZ) (Hartree): -421.45062207
Electronic state : 2-A
Cartesian coordinates (Angs):
     C       1.687998     -0.618795       0.492881
     C       0.915542      0.416456       0.192925
     C      -0.259700      0.749108       1.067999
     C      -1.591353      0.659142       0.349459
     O      -1.802077     -0.723348      -0.011109
     O      -2.887151     -0.874508      -0.704725
     O       2.769767     -0.965716      -0.266504
     H       1.492458     -1.242616       1.357736
     C       1.163201      1.278087      -1.009050
     H      -0.285528      0.095656       1.941473
     H      -0.170140      1.775429       1.437329
     H      -2.423692      0.956840       0.985921
     H      -1.613993      1.241844      -0.570464
     H       3.198522     -1.736052       0.107991
     H       2.139415      1.075352      -1.441349
     H       1.111298      2.335820      -0.741319
     H       0.413215      1.102318      -1.783897
Rotational constants (GHz):    3.4577100    1.0502500    0.9739700
Vibrational harmonic frequencies (cm-1):
       27.8590                56.3095                95.1152
      130.4504               229.9982               233.0775
      279.8611               281.8680               379.0604
      390.0224               473.3075               569.5506
      599.1604               808.7278               835.2397
      901.7905               959.8911              1022.4905
     1052.1236              1073.0370              1076.6099
     1189.3981              1207.2794              1234.9150
     1275.3578              1297.3689              1306.2990
     1383.6717              1387.5146              1402.9185
     1432.2372              1469.4858              1490.7696
     1493.0623              1509.5911              1800.9719
     3046.6909              3049.0555              3088.0839
     3097.1853              3103.7458              3144.0555
     3161.8549              3181.6663              3920.9978
Zero-point correction (Hartree): 0.139309

HOCHCCH3CH2CH2OO.Eltmc
----------------------
E(UM062X/Aug-CC-pVTZ) (Hartree): -421.45164869
Electronic state : 2-A
Cartesian coordinates (Angs):
     C       1.811935     -0.907621       0.071422
     C       1.027333      0.151265       0.247118
     C      -0.414545     -0.040563       0.622740
     C      -1.339242      0.420047      -0.492300
```

```
     O      -2.719465      0.331750      -0.081247
     O      -3.113306     -0.903396      -0.014655
     O       3.119974     -0.898855      -0.294994
     H       1.454965     -1.917711       0.221781
     C       1.516665      1.562881       0.063181
     H      -0.625008     -1.089135       0.831386
     H      -0.651596      0.533489       1.523087
     H      -1.198815      1.472892      -0.733562
     H      -1.219188     -0.188641      -1.387452
     H       3.407718      0.001017      -0.472667
     H       1.385050      1.918785      -0.961790
     H       2.571892      1.675366       0.319359
     H       0.964490      2.241889       0.714062
Rotational constants (GHz):    4.7964600    0.8767900    0.7807500
Vibrational harmonic frequencies (cm-1):
       53.7285                  71.7147                  89.4977
      116.3588                 155.1504                 271.1468
      307.8924                 327.9762                 383.8881
      406.1160                 510.9140                 539.2368
      656.5248                 795.4961                 837.0464
      933.8506                 968.3074                1016.5065
     1043.4275                1069.7756                1081.4272
     1183.6477                1220.7490                1236.2731
     1280.1390                1307.8771                1322.0944
     1335.7953                1400.0742                1409.7012
     1425.2233                1482.0790                1491.9171
     1499.1111                1505.3858                1772.0821
     3043.5621                3050.7344                3091.7159
     3098.1917                3117.5938                3121.3765
     3154.5905                3218.4321                3871.8645
Zero-point correction (Hartree): 0.139597

HOCHCCH3CH2CH2OO.Eltmt
~~~~~~~~~~~~~~~~~~~~~~
E(UM062X/Aug-CC-pVTZ) (Hartree): -421.45146190
Electronic state : 2-A
Cartesian coordinates (Angs):
     C       1.808449     -0.870946       0.073997
     C       1.022126      0.185896       0.234148
     C      -0.415721     -0.007658       0.623098
     C      -1.359154      0.443369      -0.480086
     O      -2.733501      0.297045      -0.063681
     O      -3.085753     -0.951642      -0.027514
     O       3.119356     -0.754994      -0.294526
     H       1.443150     -1.880050       0.228246
     C       1.518328      1.587994       0.035525
     H      -0.622997     -1.056074       0.837927
     H      -0.642754      0.569183       1.524220
     H      -1.258428      1.504409      -0.700972
     H      -1.223508     -0.143918      -1.387232
     H       3.537838     -1.616751      -0.290378
     H       1.112418      2.031524      -0.876723
     H       2.602370      1.614041      -0.037457
     H       1.206935      2.222439       0.868047
Rotational constants (GHz):    4.7876600    0.8777500    0.7801800
Vibrational harmonic frequencies (cm-1):
       56.3337                  61.5398                 111.1569
      118.4974                 170.4625                 240.0409
      267.4307                 321.2406                 359.2031
      385.4776                 485.3416                 538.0905
      660.2330                 793.0924                 844.5286
      900.1542                 966.8000                1014.9355
     1050.6590                1070.5620                1086.7521
     1194.8091                1209.8170                1236.0224
     1283.4324                1293.5699                1325.9942
     1339.2963                1393.4718                1406.7887
     1430.5021                1480.0410                1492.3605
     1497.0516                1499.6333                1795.6914
     3049.6415                3051.3162                3094.9246
     3099.0336                3116.9742                3159.8308
     3162.0614                3183.4444                3918.9380
Zero-point correction (Hartree): 0.139463

HOCHCCH3CH2CH2OO.Eltpc
~~~~~~~~~~~~~~~~~~~~~~
E(UM062X/Aug-CC-pVTZ) (Hartree): -421.45201182
Electronic state : 2-A
Cartesian coordinates (Angs):
     C      -2.007490     -0.766543      -0.158771
     C      -1.003670      0.103506      -0.211088
     C       0.386922     -0.368660      -0.524399
     C       1.307083     -0.192810       0.672840
     O       2.663592     -0.544892       0.329885
     O       3.209099      0.359872      -0.424121
     O      -3.304263     -0.488022       0.135709
     H      -1.870260     -1.819530      -0.365650
     C      -1.199234      1.573372       0.052831
     H       0.380775     -1.418458      -0.818898
     H       0.807641      0.209533      -1.351093
     H       1.321144      0.836694       1.029090
     H       1.041753     -0.866617       1.485571
     H      -3.399346      0.442897       0.356862
     H      -1.153800      1.815574       1.117656
```

```
     H      -2.155303      1.937117      -0.329843
     H      -0.421692      2.153930      -0.443958
Rotational constants (GHz):    5.5881300    0.8426200    0.7822800
Vibrational harmonic frequencies (cm-1):
       53.0781                   68.9128                   92.6832
      134.5309                  153.8551                  269.6361
      308.6222                  336.0594                  387.3273
      408.3134                  514.1855                  543.1282
      658.1054                  792.9716                  836.2138
      926.7746                  973.8020                 1018.9343
     1043.2789                 1062.5763                 1082.5295
     1183.7005                 1225.6114                 1233.7287
     1283.3615                 1305.6221                 1327.7582
     1335.9956                 1398.4848                 1407.9966
     1424.1372                 1481.3396                 1492.3829
     1498.2498                 1507.0122                 1770.7074
     3041.9336                 3058.3081                 3092.2916
     3095.3268                 3114.2838                 3122.0515
     3156.0048                 3216.5067                 3868.2763
Zero-point correction (Hartree): 0.139667

HOCHCCH3CH2CH2OO.Eltpt
~~~~~~~~~~~~~~~~~~~~~~
E(UM062X/Aug-CC-pVTZ) (Hartree): -421.45145415
Electronic state : 2-A
Cartesian coordinates (Angs):
     C      -2.001604     -0.742327      -0.143488
     C      -1.003878      0.131352      -0.193096
     C       0.388943     -0.341258      -0.495733
     C       1.325429     -0.112698       0.679639
     O       2.660431     -0.553504       0.354349
     O       3.240376      0.263637      -0.470784
     O      -3.284177     -0.367272       0.143806
     H      -1.843266     -1.799209      -0.327038
     C      -1.215763      1.598121       0.043935
     H       0.390938     -1.403170      -0.745496
     H       0.796207      0.204117      -1.351080
     H       1.390356      0.938782       0.954426
     H       1.039528     -0.710211       1.543648
     H      -3.874869     -1.114517       0.041352
     H      -0.835668      1.906024       1.020700
     H      -2.271803      1.852258       0.004772
     H      -0.683224      2.183896      -0.707787
Rotational constants (GHz):    5.6476000    0.8348200    0.7774800
Vibrational harmonic frequencies (cm-1):
       49.7688                   62.1260                  111.8830
      127.3880                  172.9634                  210.4648
      261.2065                  320.6001                  362.4027
      382.3184                  485.9407                  542.2492
      657.6454                  793.1815                  842.6844
      892.9237                  971.7160                 1015.6927
     1050.5671                 1064.3973                 1088.9214
     1195.4017                 1206.0764                 1235.3924
     1278.4451                 1296.7273                 1326.6436
     1338.9397                 1392.0899                 1404.1120
     1429.8617                 1479.4113                 1492.5962
     1497.1967                 1499.5171                 1794.2645
     3052.0717                 3056.5095                 3095.4248
     3101.9954                 3108.8201                 3158.4228
     3161.4501                 3179.2350                 3920.3404
Zero-point correction (Hartree): 0.139351

HOCHCCH3CH2CH2OO.Elttc
~~~~~~~~~~~~~~~~~~~~~~
E(UM062X/Aug-CC-pVTZ) (Hartree): -421.45091885
Electronic state : 2-A
Cartesian coordinates (Angs):
     C       2.019457     -0.817672       0.008327
     C       1.098313      0.106194       0.263784
     C      -0.265828     -0.308594       0.739631
     C      -1.331637      0.046086      -0.278635
     O      -2.612365     -0.306310       0.287546
     O      -3.586183     -0.017001      -0.518699
     O       3.280374     -0.604705      -0.449534
     H       1.832634     -1.872400       0.160319
     C       1.352064      1.578443       0.081059
     H      -0.294439     -1.382104       0.927499
     H      -0.506575      0.195948       1.679682
     H      -1.359513      1.112952      -0.500090
     H      -1.213321     -0.513727      -1.205893
     H       3.413792      0.330153      -0.629580
     H       1.084613      1.925417      -0.920047
     H       2.395599      1.846085       0.257166
     H       0.758393      2.155065       0.791451
Rotational constants (GHz):    5.6123100    0.7832700    0.7367300
Vibrational harmonic frequencies (cm-1):
       53.8263                   72.5390                   95.9165
      114.0774                  128.2612                  270.0024
      279.2909                  331.3963                  381.0101
      385.4593                  495.6250                  548.1192
      637.7717                  787.1260                  832.2222
      931.2207                 1006.1629                 1023.5025
     1047.5933                 1065.7010                 1104.9684
```

```
     1179.5446                1217.2770                1228.0802
     1292.8911                1306.1027                1310.3396
     1333.4085                1402.8581                1413.8348
     1426.4010                1485.5788                1492.6064
     1504.5213                1508.5126                1772.3846
     3044.6967                3051.5936                3084.0365
     3099.7247                3110.5957                3118.4691
     3143.5100                3214.7052                3871.4970
Zero-point correction (Hartree): 0.139435

HOCHCCH3CH2CH2OO.Elttt
~~~~~~~~~~~~~~~~~~~~~~
E(UM062X/Aug-CC-pVTZ) (Hartree): -421.45055503
Electronic state : 2-A
Cartesian coordinates (Angs):
     C       2.019747     -0.786239       0.012765
     C       1.092870      0.133198       0.249446
     C      -0.268522     -0.285052       0.729399
     C      -1.347484      0.078620      -0.271565
     O      -2.613552     -0.338726       0.285451
     O      -3.600278     -0.055760      -0.507019
     O       3.268503     -0.461379      -0.437772
     H       1.826796     -1.842387       0.164177
     C       1.353458      1.598099       0.055223
     H      -0.298640     -1.360915       0.906120
     H      -0.498650      0.209545       1.677373
     H      -1.411543      1.151424      -0.448613
     H      -1.217059     -0.439965      -1.220983
     H       3.818674     -1.244931      -0.472194
     H       0.843713      1.981548      -0.831597
     H       2.415948      1.794482      -0.062124
     H       0.982964      2.166359       0.910953
Rotational constants (GHz):    5.7031700    0.7796800    0.7330400
Vibrational harmonic frequencies (cm-1):
       49.4497                  85.7927                  94.1556
      109.3073                 155.9037                 223.1140
      264.6973                 296.5680                 353.0401
      371.2835                 465.2999                 545.6444
      640.9286                 785.9895                 840.5879
      895.2056                1002.6418                1021.9917
     1055.0963                1069.6735                1106.7878
     1189.2775                1208.1309                1226.7501
     1292.2113                1296.0405                1310.2441
     1338.0122                1392.7459                1413.1792
     1430.7267                1482.9877                1493.2188
     1498.6237                1508.4037                1795.6003
     3050.3658                3052.0386                3087.7339
     3100.1541                3106.2284                3147.3929
     3162.0558                3180.1953                3919.4495
Zero-point correction (Hartree): 0.139230


TS.HOCHCCH3CH2CH2OO.cycHOCHCCH3CH2CH2OO.Ec
~~~~~~~~~~~~~~~~~~~~~~~~~~~~~~~~~~~~~~~~~~
E(CCSD(T)/Aug-CC-pVTZ) (Hartree): -420.82495066
E(CCSD/Aug-CC-pVTZ) (Hartree): -420.74993036
     T1 diagnostic:  0.027178
E(MP2/Aug-CC-pVTZ) (Hartree): -420.69194733
E(MP3/Aug-CC-pVTZ) (Hartree): -420.73018644
E(PMP2/Aug-CC-pVTZ) (Hartree): -420.70966304
E(PMP3/Aug-CC-pVTZ) (Hartree): -420.74344876
E(PUHF/Aug-CC-pVTZ) (Hartree): -419.15893222
E(UHF/Aug-CC-pVTZ) (Hartree): -419.13843132
E(UM062X/Aug-CC-pVTZ) (Hartree): -421.43069294
Electronic state : 2-A
Cartesian coordinates (Angs):
     C       0.897061     -0.546190       0.623516
     C       0.499806      0.751999       0.364265
     C      -0.899828      1.100331       0.734933
     C      -1.862983      0.349260      -0.214481
     O      -1.608941     -1.029261      -0.103469
     O      -0.379546     -1.295814      -0.660220
     O       2.063821     -1.066021       0.210856
     H       0.465226     -1.110783       1.437486
     C       1.222207      1.567402      -0.659583
     H      -1.133763      0.784748       1.752116
     H      -1.076472      2.173656       0.656888
     H      -2.901957      0.490788       0.082090
     H      -1.719342      0.671026      -1.248151
     H       2.398259     -0.574510      -0.546052
     H       1.015811      1.199817      -1.672535
     H       2.304179      1.548632      -0.511108
     H       0.907815      2.608579      -0.619976
Rotational constants (GHz):    2.9232700    1.9578100    1.4160100
Vibrational harmonic frequencies (cm-1):
     i584.5270                 104.0146                 131.1446
      152.9753                 280.3153                 301.1201
      328.3390                 384.9481                 405.1223
      438.5013                 509.0466                 585.3565
      622.4213                 804.3175                 876.8799
      933.8620                 966.4459                 987.6532
     1013.3413                1029.7845                1074.4238
     1089.5739                1180.5453                1223.0220
```

```
     1246.1206                 1264.0096                 1324.3687
     1343.1694                 1375.3321                 1386.2243
     1413.1340                 1480.3285                 1482.9774
     1490.9019                 1502.0566                 1565.9389
     3013.5153                 3063.7344                 3073.1651
     3083.0540                 3122.8568                 3133.5583
     3139.1511                 3225.4811                 3857.2312
Zero-point correction (Hartree): 0.138990

TS.HOCHCCH3CH2CH2OO.cycHOCHCCH3CH2CH2OO.Et
------------------------------------------
E(CCSD(T)/Aug-CC-pVTZ) (Hartree): -420.82644110
E(CCSD/Aug-CC-pVTZ) (Hartree): -420.75168260
     T1 diagnostic:  0.027377
E(MP2/Aug-CC-pVTZ) (Hartree): -420.69320422
E(MP3/Aug-CC-pVTZ) (Hartree): -420.73169845
E(PMP2/Aug-CC-pVTZ) (Hartree): -420.71075959
E(PMP3/Aug-CC-pVTZ) (Hartree): -420.74484390
E(PUHF/Aug-CC-pVTZ) (Hartree): -419.16124987
E(UHF/Aug-CC-pVTZ) (Hartree): -419.14094997
E(UM062X/Aug-CC-pVTZ) (Hartree): -421.43224778
Electronic state : 2-A
Cartesian coordinates (Angs):
     C       0.901440     -0.521479       0.586849
     C       0.502829      0.769096       0.333071
     C      -0.894366      1.109763       0.725147
     C      -1.864531      0.326386      -0.190794
     O      -1.591884     -1.049777      -0.073455
     O      -0.384427     -1.307941      -0.683039
     O       2.095071     -0.960328       0.136906
     H       0.439773     -1.087856       1.386068
     C       1.212414      1.628625      -0.655606
     H      -1.109120      0.822969       1.754911
     H      -1.083272      2.178781       0.618222
     H      -2.898699      0.457600       0.126698
     H      -1.748306      0.635648      -1.231358
     H       2.156168     -1.910354       0.265310
     H       1.301757      2.650040      -0.281367
     H       0.641760      1.676875      -1.589447
     H       2.203139      1.246316      -0.884335
Rotational constants (GHz):    2.8787500    1.9716900    1.3999900
Vibrational harmonic frequencies (cm-1):
     i553.2027                  109.9272                  129.4570
      161.2925                  272.9190                  293.9918
      335.0045                  356.8991                  383.6058
      430.7677                  499.5686                  584.3038
      625.0749                  816.1024                  874.9959
      937.0347                  964.9763                  987.8429
     1010.4461                 1035.3106                 1075.9675
     1087.1538                 1189.3977                 1224.8218
     1245.0144                 1264.3001                 1303.5546
     1334.5962                 1374.3540                 1390.3968
     1422.9022                 1477.8849                 1482.0055
     1488.2023                 1492.0330                 1602.7358
     3031.4077                 3066.6412                 3072.5900
     3092.3654                 3121.7575                 3134.3623
     3168.0763                 3189.7552                 3887.1174
Zero-point correction (Hartree): 0.139034


TS.HOCHCCH3CH2CH2OO.1-6Hshift.a.Ec
----------------------------------
E(CCSD(T)/Aug-CC-pVTZ) (Hartree): -420.80543099
E(CCSD/Aug-CC-pVTZ) (Hartree): -420.73000039
     T1 diagnostic:  0.024966
E(MP2/Aug-CC-pVTZ) (Hartree): -420.67733307
E(MP3/Aug-CC-pVTZ) (Hartree): -420.71333383
E(PMP2/Aug-CC-pVTZ) (Hartree): -420.69231131
E(PMP3/Aug-CC-pVTZ) (Hartree): -420.72403263
E(PUHF/Aug-CC-pVTZ) (Hartree): -419.12957042
E(UHF/Aug-CC-pVTZ) (Hartree): -419.11164555
E(UM062X/Aug-CC-pVTZ) (Hartree): -421.41459562
Electronic state : 2-A
Cartesian coordinates (Angs):
     O       1.611663     -1.284114      -0.619711
     H       0.570609     -1.436504       0.047100
     C      -0.397947     -1.100677       0.836472
     O       2.231586     -0.228477       0.005948
     C      -0.728993      0.240864       0.373594
     C       1.585033      0.992460      -0.352959
     C       0.358900      1.279457       0.506288
     H       0.156254     -1.138816       1.772511
     H      -1.154259     -1.878237       0.771877
     C      -1.881294      0.561876      -0.234616
     O      -2.930091     -0.252592      -0.482316
     H      -2.076507      1.567403      -0.583044
     H       2.343442      1.759914      -0.195592
     H       1.326531      0.944954      -1.412172
     H      -0.024832      2.261609       0.223290
     H       0.680104      1.342327       1.549750
     H      -2.740806     -1.145064      -0.177763
Rotational constants (GHz):    3.7713900    1.2756300    1.0917400
Vibrational harmonic frequencies (cm-1):
```

```
    i2187.2165                 79.1229                145.5697
      202.8478                290.9588                295.2709
      344.0117                403.4398                455.9409
      495.2855                550.5102                563.2053
      629.2395                656.4428                815.4285
      873.4114                917.9509                956.2470
      990.7497               1016.8466               1060.0645
     1081.7357               1118.5491               1190.0307
     1204.8801               1238.1535               1253.3422
     1299.2440               1329.1686               1375.6154
     1396.7598               1416.0353               1465.7503
     1478.7994               1485.3532               1530.7273
     1702.6711               3050.4029               3069.6122
     3098.1448               3102.9731               3128.3971
     3176.8308               3215.6662               3865.5866
Zero-point correction (Hartree): 0.134451

TS.HOCHCCH3CH2CH2OO.1-6Hshift.a.Et
~~~~~~~~~~~~~~~~~~~~~~~~~~~~~~~~~
E(UM062X/Aug-CC-pVTZ) (Hartree): -421.41378992
Electronic state : 2-A
Cartesian coordinates (Angs):
     O       1.601501     -1.290271      -0.618535
     H       0.561291     -1.438259       0.056889
     C      -0.401768     -1.097574       0.847814
     O       2.232270     -0.235626       0.001025
     C      -0.713173      0.247279       0.381248
     C       1.594707      0.986734      -0.362118
     C       0.371862      1.287446       0.498634
     H       0.154954     -1.145404       1.781839
     H      -1.189898     -1.835589       0.756039
     C      -1.868947      0.544929      -0.223165
     O      -2.847699     -0.382535      -0.401426
     H      -2.078130      1.543523      -0.589924
     H       2.358378      1.750500      -0.211240
     H       1.332110      0.935967      -1.420313
     H      -0.010168      2.268012       0.206377
     H       0.697337      1.359552       1.540003
     H      -3.610527      0.016269      -0.822647
Rotational constants (GHz):    3.7784100    1.2856200    1.0982000
Vibrational harmonic frequencies (cm-1):
    i2126.1464                 82.8438                145.7752
      213.6238                269.8116                277.2568
      325.9406                373.3494                448.8572
      472.1455                554.2206                568.7976
      633.4221                661.9724                823.5970
      875.3510                878.8346                957.0137
     1001.7419               1015.9198               1062.1319
     1082.5804               1119.0508               1198.9166
     1199.9316               1231.2216               1252.2669
     1295.3559               1318.6255               1377.5621
     1397.1068               1404.6352               1462.3339
     1478.6047               1479.7281               1516.7170
     1730.1079               3050.1858               3067.5503
     3099.5063               3107.3536               3126.1656
     3182.5087               3211.7110               3914.6619
Zero-point correction (Hartree): 0.134291

TS.HOCHCCH3CH2CH2OO.1-6Hshift.b.Ec
~~~~~~~~~~~~~~~~~~~~~~~~~~~~~~~~~
E(UM062X/Aug-CC-pVTZ) (Hartree): -421.41342897
Electronic state : 2-A
Cartesian coordinates (Angs):
     O      -1.809153      1.189157      -0.280637
     H      -0.693200      1.491482       0.191782
     C       0.459690      1.311138       0.776573
     O      -1.506597      0.067604      -1.009623
     C       0.653638     -0.107794       0.532762
     C      -1.543084     -1.075315      -0.157669
     C      -0.494299     -0.994585       0.960701
     H       0.164990      1.569807       1.791662
     H       1.170044      2.019741       0.358664
     C       1.682250     -0.631587      -0.156204
     O       2.736439      0.031551      -0.672135
     H       1.754807     -1.694854      -0.345186
     H      -2.553466     -1.197939       0.236613
     H      -1.317258     -1.896094      -0.838222
     H      -0.152773     -2.001917       1.198934
     H      -0.942200     -0.582073       1.864560
     H       2.654362      0.974213      -0.496627
Rotational constants (GHz):    3.3187200    1.4055600    1.2662400
Vibrational harmonic frequencies (cm-1):
    i2094.4757                 79.0026                123.8287
      232.6307                277.1059                301.8495
      371.7860                378.3727                434.8235
      486.2273                537.4493                568.2219
      625.1325                708.2326                807.3081
      858.3569                921.8416                954.5784
     1018.9063               1030.5444               1058.5716
     1082.5619               1126.5080               1200.3832
     1219.9226               1253.2084               1266.0461
     1287.5495               1327.3345               1364.0460
     1396.2710               1414.5928               1482.8872
```

```
     1488.3685                 1498.0181                 1501.1903
     1689.9085                 3068.2305                 3082.1468
     3098.4667                 3116.4651                 3135.8086
     3174.3543                 3212.3579                 3857.4644
Zero-point correction (Hartree): 0.134683

TS.HOCHCCH3CH2CH2OO.1-6Hshift.b.Et
~~~~~~~~~~~~~~~~~~~~~~~~~~~~~~~~~
E(UM062X/Aug-CC-pVTZ) (Hartree): -421.41202505
Electronic state : 2-A
Cartesian coordinates (Angs):
     O      -1.801016      1.194880      -0.292037
     H      -0.680972      1.494659       0.182105
     C       0.458122      1.309432       0.788425
     O      -1.505795      0.067479      -1.018020
     C       0.640213     -0.110418       0.546060
     C      -1.555137     -1.071067      -0.163841
     C      -0.505830     -1.004294       0.957098
     H       0.137967      1.569895       1.795354
     H       1.204489      1.976818       0.373802
     C       1.677405     -0.607886      -0.141367
     O       2.680110      0.183750      -0.600182
     H       1.766000     -1.668997      -0.347278
     H      -2.566519     -1.181391       0.231818
     H      -1.340686     -1.896938      -0.842239
     H      -0.165710     -2.015214       1.183006
     H      -0.955428     -0.603189       1.865159
     H       3.325829     -0.339119      -1.078065
Rotational constants (GHz):    3.3264600    1.4097200    1.2706800
Vibrational harmonic frequencies (cm-1):
    i2051.6284                  80.8964                 118.0649
      234.7208                 253.7706                 296.7965
      327.8990                 367.3283                 412.4711
      463.3578                 542.0591                 565.4153
      629.6163                 708.5276                 808.9682
      856.5643                 886.7265                 954.9900
     1018.2313                1030.5736                1064.8990
     1082.5759                1127.6163                1207.4368
     1210.8433                1252.4923                1264.9906
     1289.6721                1309.7406                1357.9237
     1397.5991                1405.8849                1478.3326
     1482.6085                1488.6295                1499.8821
     1716.0912                3066.0063                3080.8514
     3108.1941                3113.8368                3133.5914
     3180.4327                3210.1388                3913.5482
Zero-point correction (Hartree): 0.134414


################################################################################
Z-HOCH=C(CH3)CH2CH2OO ring closure and H-shift
################################################################################

HOCHCCH3CH2CH2OO.Zcpmm
~~~~~~~~~~~~~~~~~~~~~~
E(UM062X/Aug-CC-pVTZ) (Hartree): -421.44926728
Electronic state : 2-A
Cartesian coordinates (Angs):
     C       1.130828      1.189643       0.118372
     C       1.238603     -0.132009      -0.010035
     C       0.223458     -1.204350       0.298823
     C      -1.174937     -0.855596       0.776147
     O      -2.076071     -0.621963      -0.337399
     O      -1.939195      0.550472      -0.866455
     O       0.048799      1.933320       0.470619
     H       2.005167      1.806843      -0.055894
     C       2.555327     -0.707592      -0.455973
     H       0.121413     -1.869420      -0.565394
     H       0.663012     -1.830250       1.083227
     H      -1.627782     -1.712607       1.269338
     H      -1.213156      0.009725       1.433576
     H      -0.745437      1.559668       0.057560
     H       3.299289      0.071191      -0.610861
     H       2.443891     -1.258622      -1.393007
     H       2.945669     -1.411728       0.283331
Rotational constants (GHz):    2.8902200    1.5369100    1.1689500
Vibrational harmonic frequencies (cm-1):
       24.0365                  77.6570                 189.7251
      198.5005                 212.4232                 301.1457
      319.7088                 342.3071                 426.8330
      433.3245                 555.5785                 612.1342
      683.9066                 774.3618                 863.0769
      915.0358                 972.8046                1009.5127
     1050.9749                1071.7262                1096.5676
     1181.8355                1220.7331                1247.8945
     1277.4254                1332.8511                1356.0380
     1407.6980                1409.2349                1419.2418
     1438.9876                1461.5529                1484.0105
     1501.8632                1507.0806                1769.4280
     3030.3042                3041.7617                3055.8862
     3088.3897                3111.8810                3143.4802
     3168.9225                3179.4980                3648.0915
Zero-point correction (Hartree): 0.140370
```

```
HOCHCCH3CH2CH2OO.Zcppc
~~~~~~~~~~~~~~~~~~~~~~
E(UM062X/Aug-CC-pVTZ) (Hartree): -421.44991842
Electronic state : 2-A
Cartesian coordinates (Angs):
     C       1.302368      1.134243      -0.052999
     C       1.292066     -0.197500      -0.038492
     C       0.113401     -1.112402       0.187562
     C      -1.101218     -0.564118       0.907252
     O      -1.906118      0.273034       0.035929
     O      -2.522093     -0.422441      -0.870935
     O       0.278841      2.017500       0.086638
     H       2.242014      1.657752      -0.178460
     C       2.581383     -0.932962      -0.282837
     H      -0.224491     -1.555842      -0.754835
     H       0.469624     -1.953295       0.789785
     H      -1.753771     -1.364950       1.247106
     H      -0.836395      0.090558       1.735721
     H      -0.571467      1.619975      -0.129949
     H       3.407289     -0.247262      -0.461502
     H       2.495186     -1.588545      -1.153039
     H       2.838972     -1.566692       0.569206
Rotational constants (GHz):    3.0876200    1.3938000    1.0892800
Vibrational harmonic frequencies (cm-1):
       41.4157                88.8959               158.4002
      203.7030               214.9268               267.4457
      306.5270               349.4743               426.3144
      468.9643               540.3332               555.0457
      616.7284               783.5881               848.6957
      920.2684               977.4469              1010.4465
     1023.8451              1070.5587              1118.5778
     1177.7980              1205.3420              1226.1172
     1285.3179              1308.7509              1328.8084
     1396.5434              1402.0385              1419.5250
     1434.5639              1466.7983              1484.7455
     1489.9621              1503.0773              1770.8431
     3041.0376              3043.7765              3071.5466
     3088.6966              3103.7687              3142.8778
     3164.1479              3197.6601              3816.3222
Zero-point correction (Hartree): 0.140248

HOCHCCH3CH2CH2OO.Zcptt
~~~~~~~~~~~~~~~~~~~~~~
E(UM062X/Aug-CC-pVTZ) (Hartree): -421.44798473
Electronic state : 2-A
Cartesian coordinates (Angs):
     C       1.111782      1.202708      -0.048985
     C       1.321607     -0.106468       0.000181
     C       0.372817     -1.143483       0.544186
     C      -1.082610     -0.764033       0.699462
     O      -1.584852     -0.416972      -0.610449
     O      -2.785048      0.066786      -0.547755
     O      -0.001108      1.821837       0.451410
     H       1.860828      1.861847      -0.473951
     C       2.623586     -0.662260      -0.501470
     H       0.429102     -2.020392      -0.107435
     H       0.730553     -1.483099       1.521683
     H      -1.670436     -1.612639       1.049149
     H      -1.242637      0.091413       1.346309
     H      -0.106376      2.684059       0.045726
     H       3.140249     -1.213026       0.288487
     H       3.289287      0.123328      -0.854380
     H       2.454407     -1.363486      -1.321472
Rotational constants (GHz):    3.1846200    1.3743500    1.1036000
Vibrational harmonic frequencies (cm-1):
       41.7350                54.6761               136.9906
      196.3076               224.8723               256.5599
      272.2639               309.1968               342.1811
      389.1014               449.4868               541.9392
      634.2976               783.3691               838.9369
      888.2290              1005.2984              1008.2993
     1044.5282              1077.3965              1102.6649
     1177.8265              1204.1175              1242.1809
     1276.9776              1294.3337              1304.8379
     1384.4248              1413.3817              1421.5673
     1433.4271              1466.7757              1483.4140
     1500.1768              1504.6908              1800.8913
     3040.9819              3045.7174              3070.2552
     3094.2460              3095.3060              3140.4667
     3175.4861              3184.9905              3907.3554
Zero-point correction (Hartree): 0.139565

HOCHCCH3CH2CH2OO.Zctpc
~~~~~~~~~~~~~~~~~~~~~~
E(UM062X/Aug-CC-pVTZ) (Hartree): -421.44515262
Electronic state : 2-A
Cartesian coordinates (Angs):
     C      -1.954737      0.702111      -0.066637
     C      -1.292319     -0.449834      -0.007600
     C       0.197765     -0.675928       0.038772
     C       1.099300      0.522071       0.262716
     O       2.448422      0.069257       0.503280
     O       3.004518     -0.353378      -0.590800
```

```
     O      -1.493168      1.984059      -0.122603
     H      -3.036633      0.701284      -0.068602
     C      -2.079754     -1.732002       0.012289
     H       0.399791     -1.381335       0.850752
     H       0.521164     -1.176700      -0.878264
     H       1.155607      1.183685      -0.603865
     H       0.836007      1.076985       1.162625
     H      -0.546872      2.014117      -0.268205
     H      -3.150674     -1.546910      -0.040197
     H      -1.874075     -2.301120       0.921577
     H      -1.804015     -2.368020      -0.832066
Rotational constants (GHz):    3.2170000    1.1150700    0.8728000
Vibrational harmonic frequencies (cm-1):
       25.4172                 78.3647                123.7774
      170.7876                196.9246                227.9818
      287.8662                320.1712                343.9952
      406.9443                474.0316                574.1455
      604.6082                791.2435                883.9768
      921.8576                975.5759               1005.4773
     1051.2166               1083.7976               1123.9663
     1173.5548               1183.5992               1246.7477
     1278.9744               1303.1522               1346.0534
     1355.9993               1411.8816               1419.2780
     1434.4271               1483.0102               1487.6386
     1504.0531               1515.7753               1779.0413
     3042.4192               3047.0036               3065.3448
     3076.6750               3095.3128               3140.2386
     3146.0393               3213.1117               3925.5280
Zero-point correction (Hartree): 0.139759

HOCHCCH3CH2CH2OO.Zctpt
----------------------
E(UM062X/Aug-CC-pVTZ) (Hartree): -421.44961874
Electronic state : 2-A
Cartesian coordinates (Angs):
     C      -1.910461      0.687968      -0.132568
     C      -1.279218     -0.468402       0.020212
     C       0.193008     -0.658194       0.265105
     C       1.080153      0.569106       0.189292
     O       2.452055      0.165698       0.416055
     O       2.935128     -0.475134      -0.603425
     O      -1.293149      1.911294      -0.076811
     H      -2.980286      0.712591      -0.304352
     C      -2.063894     -1.748177      -0.033569
     H       0.327699     -1.125570       1.246155
     H       0.572150     -1.379256      -0.464639
     H       1.037631      1.055505      -0.781581
     H       0.876641      1.290249       0.974713
     H      -1.926284      2.602984      -0.272360
     H      -3.124880     -1.566021      -0.195353
     H      -1.952764     -2.308170       0.897707
     H      -1.699699     -2.390990      -0.837673
Rotational constants (GHz):    3.1892200    1.1588400    0.8959600
Vibrational harmonic frequencies (cm-1):
       34.7291                 89.3545                133.3168
      169.8388                185.6689                216.9190
      265.2060                311.7155                345.4390
      397.6089                456.9792                567.6594
      604.5898                790.8203                878.8482
      888.6487                966.6599               1004.5028
     1046.3952               1088.0718               1117.8057
     1174.1608               1201.1280               1238.9297
     1268.2535               1294.4717               1332.8919
     1353.3483               1407.4306               1422.2608
     1431.8591               1481.9638               1483.7375
     1493.8845               1504.6745               1803.5656
     3037.9988               3048.1738               3074.2592
     3098.3665               3123.7778               3140.1703
     3183.9106               3189.7624               3920.7129
Zero-point correction (Hartree): 0.139584

HOCHCCH3CH2CH2OO.Zgmmc
----------------------
E(UM062X/Aug-CC-pVTZ) (Hartree): -421.45072057
Electronic state : 2-A
Cartesian coordinates (Angs):
     C       1.989804      0.208706      -0.313793
     C       0.826097      0.596713       0.196926
     C      -0.065618     -0.359934       0.947609
     C      -0.945036     -1.198469       0.032037
     O      -1.823393     -0.354934      -0.746128
     O      -2.718326      0.210818       0.003761
     O       2.543784     -1.034946      -0.234980
     H       2.629282      0.883352      -0.866545
     C       0.339780      2.005975       0.026131
     H       0.509180     -1.048789       1.575217
     H      -0.716760      0.191344       1.626975
     H      -0.361834     -1.730557      -0.718451
     H      -1.574360     -1.891379       0.589167
     H       2.003592     -1.606928       0.316729
     H      -0.624440      2.029662      -0.484220
     H       1.047187      2.600169      -0.550200
     H       0.201475      2.487689       0.996649
```

```
Rotational constants (GHz):    3.3559600    1.2984200    1.0556100
Vibrational harmonic frequencies (cm-1):
       40.9393                66.7204                142.3623
      169.4739               193.3883                289.2887
      302.5363               332.5190                387.9733
      421.2621               534.2735                570.9138
      613.4048               790.2132                848.8792
      917.2383               948.1353               1009.7677
     1031.0112              1071.8344               1097.2237
     1177.1280              1189.8680               1239.8074
     1266.6471              1299.3519               1313.3219
     1364.8695              1399.9540               1410.5359
     1423.9707              1481.6530               1488.0521
     1493.7835              1504.0293               1772.4866
     3041.5945              3051.1800               3087.2260
     3106.0248              3108.3076               3140.4678
     3149.7913              3219.9452               3871.8849
Zero-point correction (Hartree): 0.139837

HOCHCCH3CH2CH2OO.Zgmmt
~~~~~~~~~~~~~~~~~~~~~~
E(UM062X/Aug-CC-pVTZ) (Hartree): -421.45252662
Electronic state : 2-A
Cartesian coordinates (Angs):
     C       1.937512     -0.188903      -0.323205
     C       0.805674     -0.633427       0.203909
     C      -0.070602      0.296764       1.002205
     C      -0.912154      1.199539       0.117663
     O      -1.770587      0.420154      -0.748972
     O      -2.692514     -0.194761      -0.074327
     O       2.332130      1.115667      -0.158502
     H       2.592745     -0.818658      -0.913257
     C       0.345735     -2.044789       0.001752
     H      -0.736259     -0.273491       1.650451
     H       0.540127      0.946490       1.631171
     H      -1.556161      1.858637       0.698149
     H      -0.290957      1.773311      -0.566664
     H       3.207424      1.243071      -0.526465
     H       0.236027     -2.554879       0.961179
     H       1.048398     -2.611123      -0.608111
     H      -0.630563     -2.066941      -0.485989
Rotational constants (GHz):    3.2226000    1.3598600    1.0889800
Vibrational harmonic frequencies (cm-1):
       42.8964                65.6193                142.7389
      167.1418               189.3145                227.3757
      288.6729               320.2290                354.3743
      391.2909               531.7092                574.5252
      617.5566               798.6739                848.1971
      878.3959               950.0970               1009.2751
     1028.4883              1072.7596               1100.3847
     1182.1118              1197.7530               1226.2701
     1262.8379              1299.1358               1318.7714
     1362.3503              1390.7542               1407.4201
     1423.0941              1474.4708               1481.9141
     1491.8754              1503.0181               1794.6668
     3050.6164              3075.4455               3095.1329
     3105.4278              3124.1288               3136.8179
     3163.0238              3188.8317               3919.8657
Zero-point correction (Hartree): 0.139596

HOCHCCH3CH2CH2OO.Zgmpc
~~~~~~~~~~~~~~~~~~~~~~
E(UM062X/Aug-CC-pVTZ) (Hartree): -421.44933493
Electronic state : 2-A
Cartesian coordinates (Angs):
     C       1.782933      0.110969      -0.461481
     C       0.787914      0.564110       0.293452
     C      -0.004858     -0.353506       1.188551
     C      -1.119576     -1.100004       0.464262
     O      -2.097280     -0.166343      -0.034011
     O      -1.863617      0.176104      -1.265665
     O       2.230116     -1.173930      -0.541764
     H       2.351128      0.759979      -1.113582
     C       0.402348      2.013945       0.272419
     H       0.633315     -1.104711       1.666413
     H      -0.447622      0.220846       2.003959
     H      -0.752162     -1.663208      -0.392318
     H      -1.670244     -1.749300       1.143820
     H       1.742706     -1.737215       0.064959
     H       1.019339      2.575114      -0.427427
     H       0.518723      2.460585       1.262732
     H      -0.641492      2.138175      -0.020258
Rotational constants (GHz):    2.7294700    1.4523500    1.2564800
Vibrational harmonic frequencies (cm-1):
       48.7034                88.8848                105.7465
      169.7326               194.4482                263.3324
      294.1944               342.2144                378.2690
      420.1903               528.8116                569.2579
      604.0069               779.9811                872.6524
      918.2761               938.0512               1019.9914
     1036.1814              1069.0318               1087.0051
     1177.5739              1191.8773               1236.3051
     1258.3935              1300.3856               1329.8438
```

```
     1370.3998                1391.7892                1410.7006
     1423.2240                1481.1253                1483.1346
     1491.9566                1502.5607                1774.5235
     3036.0261                3048.8346                3086.6194
     3098.1440                3104.4574                3141.0885
     3151.2493                3221.7205                3877.9113
Zero-point correction (Hartree): 0.139695

HOCHCCH3CH2CH2OO.Zgmpt
----------------------
E(UM062X/Aug-CC-pVTZ) (Hartree): -421.45143242
Electronic state : 2-A
Cartesian coordinates (Angs):
     C       1.737121      0.063987      -0.456171
     C       0.779185      0.601911       0.284741
     C      -0.011417     -0.262962       1.230502
     C      -1.095726     -1.067273       0.528296
     O      -2.080353     -0.182475      -0.047689
     O      -1.816170      0.105465      -1.286838
     O       2.025882     -1.274731      -0.377320
     H       2.322426      0.642226      -1.160931
     C       0.431283      2.055253       0.184803
     H       0.645789     -0.982963       1.721704
     H      -0.471362      0.351282       2.006168
     H      -0.687958     -1.672298      -0.278096
     H      -1.653186     -1.683368       1.232423
     H       2.762741     -1.485878      -0.951833
     H       1.056551      2.565317      -0.546653
     H       0.559200      2.551269       1.149607
     H      -0.611754      2.182851      -0.110643
Rotational constants (GHz):    2.6594900    1.5166600    1.2947300
Vibrational harmonic frequencies (cm-1):
       45.6868                  87.5472                 103.4694
      176.4799                 193.2789                 234.0679
      281.1618                 330.6672                 348.3348
      397.9300                 526.6332                 570.6983
      607.3737                 787.0443                 870.6459
      876.5100                 939.9320                1016.1217
     1035.2074                1070.4997                1088.9494
     1183.0382                1198.2857                1234.1057
     1242.8935                1310.5007                1325.2313
     1366.3777                1382.6238                1408.4118
     1421.3718                1472.8623                1481.4155
     1485.9827                1501.6823                1796.0196
     3048.6422                3067.6456                3095.2545
     3103.2459                3114.5449                3137.1026
     3164.9746                3192.3371                3920.0508
Zero-point correction (Hartree): 0.139521

HOCHCCH3CH2CH2OO.Zgmtc
----------------------
E(UM062X/Aug-CC-pVTZ) (Hartree): -421.44965828
Electronic state : 2-A
Cartesian coordinates (Angs):
     C       1.939070     -0.129593      -0.510460
     C       1.011908      0.552033       0.154141
     C       0.089828     -0.124896       1.137626
     C      -1.102311     -0.796531       0.478876
     O      -1.901160      0.241346      -0.129589
     O      -2.928763     -0.251629      -0.747865
     O       2.204870     -1.462661      -0.411107
     H       2.596994      0.343679      -1.226528
     C       0.832012      2.025207      -0.065783
     H       0.613282     -0.886342       1.724394
     H      -0.277367      0.604850       1.861275
     H      -0.805748     -1.479880      -0.317169
     H      -1.739491     -1.315071       1.194778
     H       1.645233     -1.868477       0.256231
     H      -0.181116      2.248067      -0.403871
     H       1.532750      2.401156      -0.809499
     H       0.992846      2.578250       0.862484
Rotational constants (GHz):    3.0103600    1.2180800    1.0238900
Vibrational harmonic frequencies (cm-1):
       41.4082                  75.5142                 119.9922
      173.6373                 195.7565                 273.3382
      284.5693                 314.9211                 381.6568
      392.4674                 489.2844                 577.5848
      622.5919                 786.1280                 841.5853
      921.7769                 977.9475                1025.9881
     1049.6434                1070.3287                1087.9050
     1176.7408                1196.4185                1244.8787
     1276.7479                1294.6012                1306.7742
     1367.8364                1402.7677                1410.5180
     1422.6055                1481.9338                1491.9293
     1499.3863                1505.2994                1775.1273
     3043.9052                3050.1255                3078.3368
     3098.5812                3105.7877                3137.3926
     3141.1266                3219.1818                3876.0556
Zero-point correction (Hartree): 0.139670

HOCHCCH3CH2CH2OO.Zgmtt
----------------------
E(UM062X/Aug-CC-pVTZ) (Hartree): -421.45153725
```

```
Electronic state : 2-A
Cartesian coordinates (Angs):
     C       1.880460     -0.188728      -0.506354
     C       1.011983      0.572220       0.144584
     C       0.096187     -0.044062       1.170887
     C      -1.088956     -0.750130       0.542855
     O      -1.874325      0.247915      -0.150741
     O      -2.889016     -0.281038      -0.759924
     O       1.966358     -1.535761      -0.260800
     H       2.549319      0.206647      -1.261521
     C       0.889736      2.038765      -0.135028
     H       0.635776     -0.789604       1.756667
     H      -0.265876      0.721474       1.859021
     H      -0.775125     -1.488032      -0.193238
     H      -1.741217     -1.213280       1.282420
     H       2.681224     -1.918254      -0.771152
     H      -0.121915      2.284581      -0.462218
     H       1.588769      2.357583      -0.907021
     H       1.088445      2.621573       0.767096
Rotational constants (GHz):    2.9146800    1.2701200    1.0549900
Vibrational harmonic frequencies (cm-1):
       42.7504                  72.7486                 117.7732
      178.3161                 198.3964                 245.1979
      285.7025                 300.6185                 347.4777
      375.8057                 479.9849                 582.0684
      623.8398                 794.2295                 840.9293
      877.0195                 983.2028                1025.2759
     1042.4252                1075.1355                1088.8214
     1181.7763                1199.4183                1228.8308
     1269.4839                1298.6573                1317.1769
     1362.1365                1396.8202                1406.5667
     1421.5974                1473.6656                1482.2938
     1502.4534                1505.0698                1794.8735
     3050.0418                3071.5608                3089.2414
     3105.2245                3118.0648                3137.4365
     3152.1171                3190.2015                3919.1491
Zero-point correction (Hartree): 0.139541

HOCHCCH3CH2CH2OO.Zgpmc
~~~~~~~~~~~~~~~~~~~~~~
E(UM062X/Aug-CC-pVTZ) (Hartree): -421.45240759
Electronic state : 2-A
Cartesian coordinates (Angs):
     C       1.224405      1.071636       0.115225
     C       1.093779     -0.235051      -0.098039
     C       0.100153     -0.780139      -1.085588
     C      -1.252678     -1.100586      -0.463721
     O      -1.846708      0.122595       0.018775
     O      -1.626316      0.305916       1.289588
     O       0.501693      2.068096      -0.462038
     H       1.972419      1.462813       0.792974
     C       1.914167     -1.228647       0.668231
     H      -0.054263     -0.084383      -1.913673
     H       0.486521     -1.704024      -1.522661
     H      -1.953299     -1.490637      -1.200553
     H      -1.174329     -1.775711       0.385619
     H      -0.359671      1.738532      -0.737933
     H       1.276658     -1.891783       1.259108
     H       2.597727     -0.732283       1.354866
     H       2.499926     -1.858654      -0.004990
Rotational constants (GHz):    2.4124700    1.7738900    1.3808600
Vibrational harmonic frequencies (cm-1):
       53.2250                  92.8312                 110.8594
      190.7603                 202.6129                 259.5484
      307.3685                 344.1491                 378.7662
      437.9692                 526.9002                 582.3746
      602.7792                 774.7668                 862.8993
      918.0243                 979.9982                 993.6932
     1030.2699                1066.0743                1084.6708
     1184.8261                1199.6995                1224.5053
     1269.9523                1306.9516                1323.5696
     1366.7961                1384.1554                1411.7458
     1422.4428                1479.2083                1487.6470
     1488.9137                1500.8396                1764.8020
     3040.9682                3056.5544                3088.9997
     3091.9236                3100.8731                3138.8295
     3159.6501                3206.2195                3848.4104
Zero-point correction (Hartree): 0.139763

HOCHCCH3CH2CH2OO.Zgppc
~~~~~~~~~~~~~~~~~~~~~~
E(CCSD(T)/Aug-CC-pVTZ) (Hartree): -420.84631979
E(CCSD/Aug-CC-pVTZ) (Hartree): -420.77536686
     T1 diagnostic:  0.021002
E(MP2/Aug-CC-pVTZ) (Hartree): -420.72348730
E(MP3/Aug-CC-pVTZ) (Hartree): -420.76218978
E(PMP2/Aug-CC-pVTZ) (Hartree): -420.72673939
E(PMP3/Aug-CC-pVTZ) (Hartree): -420.76408756
E(PUHF/Aug-CC-pVTZ) (Hartree): -419.18016550
E(UHF/Aug-CC-pVTZ) (Hartree): -419.17484935
E(UM062X/Aug-CC-pVTZ) (Hartree): -421.45480404
Electronic state : 2-A
Cartesian coordinates (Angs):
```

```
     C      -1.212494      1.178878      -0.172259
     C      -1.161420     -0.120390       0.111263
     C      -0.063202     -0.717029       0.948967
     C       1.038780     -1.369346       0.134278
     O       1.696511     -0.421967      -0.746504
     O       2.167644      0.596960      -0.102567
     O      -0.325313      2.138965       0.186655
     H      -2.036973      1.595904      -0.737046
     C      -2.216824     -1.058983      -0.394807
     H       0.382627      0.021461       1.615150
     H      -0.480267     -1.497923       1.590496
     H       1.813810     -1.800446       0.767521
     H       0.656562     -2.124151      -0.549973
     H       0.523487      1.748654       0.428011
     H      -2.961550     -0.533786      -0.990435
     H      -2.729056     -1.555064       0.433194
     H      -1.788407     -1.845085      -1.022259
Rotational constants (GHz):    2.6040800    1.7509900    1.2063500
Vibrational harmonic frequencies (cm-1):
       44.7648                126.1924                134.7356
      191.5450                199.3966                275.1822
      313.8253                352.8731                395.9432
      453.1138                531.0890                580.7217
      633.5081                769.4751                848.0543
      928.5450                971.3108                982.7232
     1032.1058               1072.3501               1091.7482
     1189.0619               1205.0560               1249.2238
     1274.8693               1304.4794               1327.1191
     1372.8944               1403.2116               1416.6370
     1424.7850               1480.5896               1492.7890
     1495.1440               1502.5296               1770.9465
     3040.2241               3062.2873               3085.6176
     3092.1114               3115.3914               3138.1233
     3155.0114               3201.6968               3806.0569
Zero-point correction (Hartree): 0.140187

HOCHCCH3CH2CH2OO.Zgppt
~~~~~~~~~~~~~~~~~~~~~~
E(UM062X/Aug-CC-pVTZ) (Hartree): -421.45053934
Electronic state : 2-A
Cartesian coordinates (Angs):
     C      -1.451259      0.979163      -0.222332
     C      -1.140884     -0.268690       0.103488
     C       0.033012     -0.571021       0.992191
     C       1.204235     -1.175474       0.235921
     O       1.720483     -0.246319      -0.742162
     O       2.350518      0.735054      -0.172919
     O      -0.750905      2.051340       0.251475
     H      -2.292076      1.204611      -0.869038
     C      -1.948873     -1.422287      -0.410435
     H       0.381536      0.331125       1.491996
     H      -0.260136     -1.289196       1.763415
     H       2.025859     -1.431021       0.902989
     H       0.917013     -2.045772      -0.351916
     H      -1.030789      2.852096      -0.193360
     H      -2.767359     -1.083959      -1.044064
     H      -2.374184     -1.998170       0.415019
     H      -1.338005     -2.110464      -0.999191
Rotational constants (GHz):    2.5793500    1.6307200    1.1579300
Vibrational harmonic frequencies (cm-1):
       23.6969                 58.4108                132.3345
      164.5839                199.0826                216.6921
      280.8366                320.5261                381.6193
      386.6381                528.8669                572.3737
      614.8579                776.2974                854.9305
      893.9685                973.2870                992.2028
     1030.1971               1072.2597               1095.1143
     1184.1722               1200.4864               1231.9331
     1262.4902               1303.4023               1328.5719
     1356.8879               1397.4897               1415.4413
     1423.4672               1472.9296               1483.7819
     1495.5237               1502.2582               1800.5278
     3044.4417               3056.4649               3090.8389
     3096.1945               3134.4264               3134.7851
     3154.8935               3177.6820               3922.3740
Zero-point correction (Hartree): 0.139516

HOCHCCH3CH2CH2OO.Zgptc
~~~~~~~~~~~~~~~~~~~~~~
E(UM062X/Aug-CC-pVTZ) (Hartree): -421.45306200
Electronic state : 2-A
Cartesian coordinates (Angs):
     C      -1.371459      1.110287      -0.212460
     C      -1.279054     -0.192751       0.039897
     C      -0.238619     -0.760398       0.970525
     C       1.076458     -1.083310       0.289359
     O       1.692400      0.187561      -0.031864
     O       2.794303      0.047624      -0.699848
     O      -0.565969      2.095075       0.262908
     H      -2.159874      1.507199      -0.839848
     C      -2.218373     -1.170693      -0.601847
     H      -0.038244     -0.078086       1.801032
     H      -0.616913     -1.684079       1.412400
```

```
     H       1.770432     -1.617850       0.936960
     H       0.946632     -1.624807      -0.646736
     H       0.302756      1.738926       0.479120
     H      -2.920348     -0.670727      -1.267018
     H      -2.789432     -1.717126       0.152526
     H      -1.674596     -1.914337      -1.190851
Rotational constants (GHz):    2.8029500    1.4171900    1.0897600
Vibrational harmonic frequencies (cm-1):
       57.3231                80.2590                130.1165
      196.3217               214.8427                249.4889
      312.0548               331.1202                379.1148
      419.9506               492.9681                589.0586
      621.0146               776.7252                853.3318
      924.1319               978.4966               1023.9317
     1044.5439              1072.3649               1089.5633
     1187.7336              1201.8755               1242.6615
     1288.0289              1295.5147               1324.7652
     1375.5354              1395.8599               1414.3787
     1424.0857              1480.8590               1485.3804
     1499.6902              1502.5269               1768.9913
     3039.1369              3057.5259               3085.6433
     3086.1935              3104.6398               3138.6926
     3146.6525              3200.4163               3835.2996
Zero-point correction (Hartree): 0.139922

HOCHCCH3CH2CH2OO.Zgtmt
~~~~~~~~~~~~~~~~~~~~~~
E(UM062X/Aug-CC-pVTZ) (Hartree): -421.45141848
Electronic state : 2-A
Cartesian coordinates (Angs):
     C       1.910795      0.759196       0.121764
     C       1.289882     -0.377677      -0.163657
     C      -0.151579     -0.373830      -0.595839
     C      -1.058966     -0.353502       0.623931
     O      -2.443031     -0.497986       0.240163
     O      -2.891044      0.578278      -0.330829
     O       1.269773      1.963812       0.025290
     H       2.943778      0.787010       0.449125
     C       1.978439     -1.700807      -0.021869
     H      -0.376871      0.502971      -1.201488
     H      -0.368963     -1.266471      -1.184824
     H      -0.873423     -1.199722       1.283912
     H      -0.959773      0.582450       1.170849
     H       1.885295      2.681120       0.181772
     H       2.995821     -1.587669       0.349828
     H       2.019433     -2.220512      -0.981357
     H       1.437702     -2.352289       0.669216
Rotational constants (GHz):    3.1249400    1.1802200    0.9183300
Vibrational harmonic frequencies (cm-1):
       43.1009                58.2287                115.8739
      165.0305               197.0364                238.2868
      252.7400               310.3572                332.7529
      401.3085               536.1713                573.7785
      594.5100               790.6777                875.4494
      885.5576               963.3209               1008.2226
     1055.7709              1071.9139               1084.4082
     1192.6253              1201.1349               1234.1893
     1271.0156              1303.6814               1323.4556
     1342.5573              1394.4848               1404.8444
     1422.0094              1481.0544               1484.2054
     1496.6169              1504.6700               1794.8701
     3045.1051              3073.9297               3094.3677
     3096.8570              3130.5898               3137.3229
     3160.9014              3185.7677               3918.9888
Zero-point correction (Hartree): 0.139537

HOCHCCH3CH2CH2OO.Zgtpc
~~~~~~~~~~~~~~~~~~~~~~
E(UM062X/Aug-CC-pVTZ) (Hartree): -421.45153269
Electronic state : 2-A
Cartesian coordinates (Angs):
     C      -2.172461     -0.321246       0.095284
     C      -1.165908      0.518131      -0.127722
     C       0.187291      0.041686      -0.584998
     C       1.068171     -0.279022       0.612972
     O       2.385520     -0.687902       0.189328
     O       3.064743      0.317159      -0.272783
     O      -2.164945     -1.672241      -0.066668
     H      -3.137976      0.022345       0.441649
     C      -1.322705      1.991198       0.109069
     H       0.126622     -0.838889      -1.230495
     H       0.680113      0.819819      -1.169329
     H       1.185360      0.584699       1.265590
     H       0.686718     -1.124351       1.183673
     H      -1.320539     -1.962562      -0.423113
     H      -2.308195      2.227326       0.506967
     H      -1.184559      2.550868      -0.818376
     H      -0.576415      2.360131       0.816786
Rotational constants (GHz):    3.3818200    1.0889300    0.8774500
Vibrational harmonic frequencies (cm-1):
       47.0904                59.3591                123.6889
      170.7596               199.3611                262.7582
      289.7434               348.5679                378.5753
```

```
      401.8149                542.5799                582.9100
      584.9880                790.7431                859.8135
      922.9408                969.4043               1012.0313
     1055.9308               1070.7385               1080.7951
     1181.8975               1203.1236               1241.7774
     1275.1277               1291.2127               1326.6449
     1338.6892               1396.8576               1407.5070
     1424.5132               1482.0798               1488.2826
     1500.1410               1517.0705               1774.5180
     3046.0285               3051.1932               3094.0154
     3095.2825               3107.2019               3139.8687
     3155.7517               3215.6197               3868.0294
Zero-point correction (Hartree): 0.139827

HOCHCCH3CH2CH2OO.Zgtpt
----------------------
E(UM062X/Aug-CC-pVTZ) (Hartree): -421.45212613
Electronic state : 2-A
Cartesian coordinates (Angs):
     C       2.127603     -0.341528      -0.095140
     C       1.165326      0.542943       0.129471
     C      -0.187364      0.093080       0.611583
     C      -1.043209     -0.328801      -0.571457
     O      -2.372897     -0.693155      -0.141944
     O      -3.062456      0.351967       0.198994
     O       1.924794     -1.681023       0.107142
     H       3.108102     -0.051935      -0.454980
     C       1.367680      2.004129      -0.131708
     H      -0.093737     -0.750153       1.295365
     H      -0.694026      0.907621       1.130262
     H      -1.146821      0.470655      -1.304120
     H      -0.647740     -1.226149      -1.042759
     H       2.747212     -2.160115      -0.002551
     H       2.358161      2.207788      -0.536103
     H       1.245541      2.581101       0.787141
     H       0.627563      2.379937      -0.842295
Rotational constants (GHz):    3.3237100    1.1223700    0.8913600
Vibrational harmonic frequencies (cm-1):
       44.5717                 62.7876                124.9787
      165.7322                198.6336                247.3023
      251.3303                323.5266                341.8888
      388.0639                534.2879                585.8553
      590.3510                792.7493                869.2410
      883.3122                966.9106               1011.3992
     1053.3917               1076.6941               1081.4453
     1191.2637               1199.1809               1233.0549
     1281.3985               1292.1512               1332.3943
     1337.5528               1393.4216               1403.6697
     1422.3264               1480.7076               1484.0234
     1495.7953               1503.7741               1794.3768
     3046.1018               3078.2855               3095.8321
     3096.8492               3128.8474               3136.0435
     3162.9429               3187.1175               3917.9089
Zero-point correction (Hartree): 0.139628

HOCHCCH3CH2CH2OO.Zgttc
----------------------
E(UM062X/Aug-CC-pVTZ) (Hartree): -421.45042784
Electronic state : 2-A
Cartesian coordinates (Angs):
     C       2.104641     -0.568463      -0.240010
     C       1.312290      0.440597       0.107703
     C      -0.027993      0.218210       0.760028
     C      -1.112626      0.082160      -0.291915
     O      -2.377396     -0.051830       0.392218
     O      -3.360089     -0.181256      -0.444657
     O       1.870417     -1.896168      -0.060880
     H       3.059988     -0.404822      -0.720364
     C       1.705336      1.861328      -0.170639
     H      -0.036159     -0.666473       1.402354
     H      -0.266928      1.063845       1.407142
     H      -1.175497      0.961918      -0.931327
     H      -0.976950     -0.802550      -0.913781
     H       1.034099     -2.032532       0.393316
     H       2.655471      1.914321      -0.699395
     H       1.798883      2.428605       0.757942
     H       0.953749      2.368736      -0.780328
Rotational constants (GHz):    3.3294000    1.0160900    0.8374500
Vibrational harmonic frequencies (cm-1):
       38.7932                 77.6442                 94.8878
      139.8178                200.9508                250.4780
      290.2145                327.8353                372.3155
      417.0661                482.9092                583.9397
      592.0907                785.2912                855.9910
      925.0215               1001.1203               1021.6723
     1060.4102               1069.2113               1106.8713
     1179.7885               1189.0477               1240.3022
     1286.7704               1294.3287               1310.4366
     1338.5068               1401.1275               1410.1341
     1425.0838               1483.4063               1498.2418
     1503.4465               1519.3107               1774.2744
     3045.0797               3053.4774               3085.9181
     3093.3019               3098.8228               3140.5612
```

```
     3143.5995                3217.9271                3868.9362
Zero-point correction (Hartree): 0.139643

HOCHCCH3CH2CH2OO.Zgttt
~~~~~~~~~~~~~~~~~~~~~~
E(UM062X/Aug-CC-pVTZ) (Hartree): -421.45104760
Electronic state : 2-A
Cartesian coordinates (Angs):
     C      -2.053189      0.599099      -0.225343
     C      -1.317933     -0.453371       0.106343
     C       0.021659     -0.269816       0.769411
     C       1.093315     -0.063957      -0.283016
     O       2.369121      0.010541       0.392306
     O       3.344002      0.172234      -0.447333
     O      -1.626086      1.874716       0.028101
     H      -3.014937      0.501082      -0.715376
     C      -1.764448     -1.849604      -0.202493
     H       0.006837      0.594417       1.432625
     H       0.267704     -1.151374       1.363568
     H       1.148329     -0.892628      -0.988741
     H       0.949566      0.869895      -0.824176
     H      -2.309986      2.504765      -0.202678
     H      -2.716664     -1.859774      -0.730790
     H      -1.874359     -2.432432       0.714363
     H      -1.029221     -2.367983      -0.822790
Rotational constants (GHz):    3.3026200    1.0414100    0.8528300
Vibrational harmonic frequencies (cm-1):
       35.2380                  76.3247                  96.6421
      134.4576                 191.2049                 232.7439
      239.3380                 307.2442                 337.3690
      392.6337                 476.7409                 587.3282
      593.6222                 784.7065                 865.6428
      884.6411                1000.0943                1019.4168
     1061.7149                1066.9938                1109.0101
     1185.1855                1197.6959                1224.3470
     1291.9015                1296.4355                1313.5955
     1338.5135                1394.3958                1409.3311
     1422.4374                1481.1256                1490.5724
     1501.6101                1505.9176                1795.8774
     3045.8563                3073.8538                3087.7664
     3095.3978                3123.9218                3137.3848
     3150.5048                3187.7628                3918.4496
Zero-point correction (Hartree): 0.139339

HOCHCCH3CH2CH2OO.Zlpmt
~~~~~~~~~~~~~~~~~~~~~~
E(UM062X/Aug-CC-pVTZ) (Hartree): -421.45151641
Electronic state : 2-A
Cartesian coordinates (Angs):
     C       1.709130     -0.226743      -0.323255
     C       0.795301      0.611124       0.149026
     C      -0.135776      0.198069       1.251049
     C      -1.593007      0.117408       0.813127
     O      -1.758911     -0.884811      -0.205799
     O      -1.500924     -0.409033      -1.388435
     O       1.864615     -1.493909       0.166624
     H       2.384572      0.062005      -1.120454
     C       0.651378      1.990819      -0.417397
     H       0.163263     -0.765875       1.658631
     H      -0.093554      0.929779       2.064129
     H      -2.229950     -0.209878       1.632958
     H      -1.960679      1.057390       0.405589
     H       2.506297     -1.971295      -0.360311
     H      -0.318260      2.112806      -0.904269
     H       1.422064      2.196291      -1.158778
     H       0.725858      2.746742       0.368080
Rotational constants (GHz):    2.4927700    1.5844300    1.3619900
Vibrational harmonic frequencies (cm-1):
       38.5354                  95.0414                 105.8187
      171.9951                 201.3511                 235.2032
      277.7503                 319.9738                 379.0078
      387.2898                 530.7926                 560.7205
      611.0331                 778.5857                 863.2415
      888.8703                 973.1139                 999.1345
     1033.8970                1072.5724                1078.9874
     1185.7482                1204.4895                1233.3178
     1243.8367                1315.2524                1326.5390
     1359.1635                1393.7535                1416.5175
     1419.5859                1471.0735                1483.8980
     1491.5533                1505.6461                1794.0954
     3046.5267                3048.6438                3096.0378
     3101.3892                3132.5287                3136.3074
     3157.4578                3183.7466                3922.8972
Zero-point correction (Hartree): 0.139590

HOCHCCH3CH2CH2OO.Zlppt
~~~~~~~~~~~~~~~~~~~~~~
E(UM062X/Aug-CC-pVTZ) (Hartree): -421.45063142
Electronic state : 2-A
Cartesian coordinates (Angs):
     C       1.819552     -0.330908      -0.295792
     C       0.907450      0.556593       0.077349
     C      -0.151373      0.204237       1.084539
```

```
     C      -1.554601      0.556428       0.624112
     O      -1.857585     -0.056339      -0.648478
     O      -1.921103     -1.348537      -0.548453
     O       1.866143     -1.596525       0.219269
     H       2.588540     -0.082635      -1.018835
     C       0.908945      1.941423      -0.497872
     H      -0.110448     -0.857348       1.317768
     H       0.020190      0.753581       2.016356
     H      -2.305341      0.217826       1.336218
     H      -1.677583      1.621621       0.436252
     H       2.486993     -2.129793      -0.278425
     H       1.785546      2.109178      -1.121442
     H       0.908141      2.695031       0.293948
     H       0.024480      2.117110      -1.114549
Rotational constants (GHz):    2.5875400    1.5287200    1.1667400
Vibrational harmonic frequencies (cm-1):
       25.7644                  49.2800                 143.5286
      167.0971                 194.1854                 236.4249
      278.4320                 313.8739                 362.1245
      405.1788                 512.5127                 567.3335
      624.1476                 775.2516                 848.2362
      891.7903                 976.0122                 984.2137
     1030.8415                1070.1423                1099.5314
     1187.0526                1205.5319                1235.7481
     1259.3822                1295.7444                1330.1128
     1357.1006                1401.9563                1418.2209
     1421.4405                1472.1631                1484.9152
     1492.4410                1509.2736                1800.8498
     3041.9735                3043.3968                3091.0038
     3098.1414                3136.7252                3141.4738
     3157.9596                3179.4653                3920.8526
Zero-point correction (Hartree): 0.139512

HOCHCCH3CH2CH2OO.Zlptt
~~~~~~~~~~~~~~~~~~~~~~
E(UM062X/Aug-CC-pVTZ) (Hartree): -421.45028605
Electronic state : 2-A
Cartesian coordinates (Angs):
     C      -1.999039      0.048185      -0.452034
     C      -0.949007     -0.534742       0.109762
     C      -0.098358      0.197613       1.112093
     C       1.387094      0.049875       0.860514
     O       1.669237      0.580826      -0.453851
     O       2.902767      0.373239      -0.795236
     O      -2.371765      1.330853      -0.154412
     H      -2.623033     -0.474901      -1.167680
     C      -0.587990     -1.950106      -0.229491
     H      -0.365097      1.252916       1.129000
     H      -0.285842     -0.197648       2.115933
     H       1.981323      0.618614       1.574282
     H       1.718042     -0.987696       0.863734
     H      -3.072826      1.612212      -0.743375
     H      -1.339358     -2.404120      -0.873313
     H      -0.502860     -2.560579       0.673214
     H       0.371533     -2.003091      -0.748869
Rotational constants (GHz):    3.1424900    1.1632600    1.0333300
Vibrational harmonic frequencies (cm-1):
       31.1387                  57.4874                 108.7861
      193.6568                 213.3292                 241.8764
      280.4807                 312.9197                 337.6982
      395.8865                 470.8439                 561.6418
      628.8962                 777.3126                 841.8577
      886.3631                 973.2580                1014.9300
     1045.7805                1075.9053                1095.4822
     1182.3439                1204.6011                1236.3738
     1270.4945                1298.6339                1322.9877
     1356.8018                1401.3671                1418.2395
     1424.0884                1470.8202                1485.0320
     1497.3576                1514.2876                1801.0893
     3043.5390                3045.9127                3091.0014
     3095.0292                3129.7364                3138.1720
     3148.3095                3183.1646                3920.9824
Zero-point correction (Hartree): 0.139483

HOCHCCH3CH2CH2OO.Zpmtc
~~~~~~~~~~~~~~~~~~~~~~
E(UM062X/Aug-CC-pVTZ) (Hartree): -421.44892315
Electronic state : 2-A
Cartesian coordinates (Angs):
     C       1.225893      1.208723       0.077346
     C       1.410632     -0.105668      -0.028430
     C       0.343809     -1.167296      -0.161927
     C      -1.005756     -0.923354       0.481733
     O      -1.808500     -0.110126      -0.414995
     O      -3.030709      0.014428       0.005569
     O       0.073591      1.925072       0.060217
     H       2.079423      1.862132       0.207285
     C       2.814589     -0.644409      -0.047855
     H       0.183558     -1.430688      -1.213029
     H       0.736846     -2.074807       0.302965
     H      -1.558074     -1.849666       0.622762
     H      -0.932562     -0.385217       1.426376
     H      -0.657800      1.417526      -0.308304
```

```
     H       3.551357      0.153489       0.021877
     H       3.006202     -1.197355      -0.971065
     H       2.980993     -1.338376       0.779600
Rotational constants (GHz):    3.6361300    1.2623400    0.9796100
Vibrational harmonic frequencies (cm-1):
       19.6519                  76.2984                 145.2685
      207.5452                 220.5482                 267.3857
      294.9970                 345.4938                 349.8160
      448.9702                 518.0648                 563.8675
      624.1732                 787.7658                 832.0384
      925.1017                1004.3463                1016.8289
     1036.8728                1075.0445                1108.9520
     1184.7616                1207.4077                1234.1039
     1280.7706                1305.7384                1323.5230
     1391.9311                1412.2769                1419.7006
     1431.2856                1463.8643                1485.3120
     1500.8632                1503.7261                1772.1061
     3039.4061                3041.9396                3077.8754
     3087.7320                3096.2801                3142.7642
     3155.4912                3200.5034                3814.3305
Zero-point correction (Hartree): 0.139977

HOCHCCH3CH2CH2OO.Zptpc
~~~~~~~~~~~~~~~~~~~~~~
E(UM062X/Aug-CC-pVTZ) (Hartree): -421.45311898
Electronic state : 2-A
Cartesian coordinates (Angs):
     C      -1.337776      1.167113       0.144008
     C      -1.356078     -0.137348      -0.121298
     C      -0.086233     -0.827402      -0.549217
     C       0.933326     -0.932568       0.592911
     O       2.279812     -0.698882       0.113257
     O       2.414009      0.523274      -0.297511
     O      -0.265061      1.992419       0.069056
     H      -2.225219      1.700550       0.458868
     C      -2.610523     -0.947993       0.004703
     H      -0.305186     -1.817407      -0.945692
     H       0.390244     -0.264818      -1.356330
     H       0.747120     -0.187308       1.364677
     H       0.975110     -1.922479       1.039906
     H       0.546981      1.524914      -0.173442
     H      -2.881161     -1.403777      -0.950454
     H      -3.446566     -0.332927       0.334061
     H      -2.487689     -1.762045       0.723351
Rotational constants (GHz):    3.2290800    1.3886100    1.0409300
Vibrational harmonic frequencies (cm-1):
       70.9878                  75.4034                 181.5667
      196.5113                 214.0703                 295.3972
      296.6820                 349.5854                 401.9228
      527.4069                 567.3644                 592.9057
      606.8148                 804.7100                 871.8093
      930.0972                 964.8976                1014.9382
     1033.8493                1073.4721                1075.2889
     1200.6918                1213.1969                1246.7772
     1288.4881                1302.6108                1325.8487
     1368.4561                1398.8044                1406.8098
     1423.7255                1482.5153                1494.0460
     1503.4373                1508.8030                1762.0564
     3042.6950                3059.0856                3090.0887
     3100.2097                3121.8062                3137.0446
     3166.2918                3210.1517                3747.9121
Zero-point correction (Hartree): 0.140671


TS.HOCHCCH3CH2CH2OO.cycHOCHCCH3CH2CH2OO.Zh
~~~~~~~~~~~~~~~~~~~~~~~~~~~~~~~~~~~~~~~~~~
E(CCSD(T)/Aug-CC-pVTZ) (Hartree): -420.82290136
E(CCSD/Aug-CC-pVTZ) (Hartree): -420.74780200
     T1 diagnostic:  0.027632
E(MP2/Aug-CC-pVTZ) (Hartree): -420.68959699
E(MP3/Aug-CC-pVTZ) (Hartree): -420.72757334
E(PMP2/Aug-CC-pVTZ) (Hartree): -420.70732238
E(PMP3/Aug-CC-pVTZ) (Hartree): -420.74089315
E(PUHF/Aug-CC-pVTZ) (Hartree): -419.15569713
E(UHF/Aug-CC-pVTZ) (Hartree): -419.13522923
E(UM062X/Aug-CC-pVTZ) (Hartree): -421.42867123
Electronic state : 2-A
Cartesian coordinates (Angs):
     C      -0.225486      1.261185      -0.046634
     C      -1.014997      0.183361       0.288575
     C      -0.363531     -0.892676       1.084760
     C       0.671914     -1.572693       0.150479
     O       1.553838     -0.605444      -0.371589
     O       0.868505      0.186239      -1.267089
     O       0.726247      1.683063       0.817033
     H      -0.561307      1.977356      -0.789752
     C      -2.230068     -0.138468      -0.510283
     H       0.163980     -0.494518       1.949035
     H      -1.084801     -1.640822       1.415571
     H       1.293669     -2.278879       0.700038
     H       0.165493     -2.081734      -0.672729
     H       1.456220      2.067705       0.320778
     H      -2.071248     -1.044599      -1.103181
```

```
     H      -2.493173      0.669297      -1.190938
     H      -3.084554     -0.328926       0.142964
Rotational constants (GHz):    2.5274700    2.1855300    1.6981700
Vibrational harmonic frequencies (cm-1):
     i607.7865                138.5662                 158.4735
      173.2502                238.6210                 275.5832
      323.6091                378.7176                 434.5920
      442.6917                493.6161                 596.9295
      629.7035                804.2215                 874.7583
      916.7996                979.4077                 996.0024
     1008.2363               1035.3478                1071.6900
     1083.2220               1187.9358                1218.4413
     1238.7452               1263.3048                1313.8985
     1321.9079               1364.1076                1396.5419
     1416.4615               1474.0568                1476.2740
     1485.8078               1494.4816                1580.6759
     3035.2683               3061.8629                3082.5547
     3086.4816               3128.0387                3140.5013
     3146.2336               3165.6929                3852.5523
Zero-point correction (Hartree): 0.138936

TS.HOCHCCH3CH2CH2OO.cycHOCHCCH3CH2CH2OO.Zp
------------------------------------------
E(CCSD(T)/Aug-CC-pVTZ) (Hartree): -420.82459295
E(CCSD/Aug-CC-pVTZ) (Hartree): -420.74901814
     T1 diagnostic:  0.026545
E(MP2/Aug-CC-pVTZ) (Hartree): -420.69314458
E(MP3/Aug-CC-pVTZ) (Hartree): -420.73006351
E(PMP2/Aug-CC-pVTZ) (Hartree): -420.71010883
E(PMP3/Aug-CC-pVTZ) (Hartree): -420.74269577
E(PUHF/Aug-CC-pVTZ) (Hartree): -419.15379424
E(UHF/Aug-CC-pVTZ) (Hartree): -419.13410207
E(UM062X/Aug-CC-pVTZ) (Hartree): -421.42980062
Electronic state : 2-A
Cartesian coordinates (Angs):
     C       0.264881      1.272855      -0.006594
     C       1.007221      0.142348      -0.318909
     C       0.312532     -0.947264      -1.060958
     C      -0.752520     -1.543270      -0.111180
     O      -1.543094     -0.494526       0.416411
     O      -0.761392      0.238666       1.298738
     O      -0.752451      1.742482      -0.753384
     H       0.698749      2.032966       0.632045
     C       2.234549     -0.182764       0.460105
     H      -0.185913     -0.568288      -1.954860
     H       1.007489     -1.731098      -1.362977
     H      -1.439278     -2.204613      -0.639172
     H      -0.278491     -2.076997       0.713862
     H      -1.414245      1.040369      -0.847075
     H       2.049751     -1.019782       1.140764
     H       2.570915      0.664760       1.054642
     H       3.046541     -0.481714      -0.206128
Rotational constants (GHz):    2.5474400    2.2040800    1.7088700
Vibrational harmonic frequencies (cm-1):
     i589.2412                148.4698                 166.7360
      186.3656                244.1548                 319.1700
      376.0619                425.6069                 442.8246
      467.7017                500.0235                 595.2845
      636.0796                795.4367                 881.5022
      903.5941                973.4984                 995.5179
     1005.8630               1031.3427                1069.6499
     1073.5617               1184.2861                1214.3732
     1262.1894               1269.6616                1312.8932
     1340.3680               1369.4256                1395.9655
     1416.7420               1475.8834                1481.4894
     1487.0234               1499.0715                1554.8259
     3035.0817               3069.2795                3071.9588
     3088.6041               3120.4220                3135.5229
     3141.8760               3197.3187                3731.1289
Zero-point correction (Hartree): 0.139182


TS.HOCHCCH3CH2CH2OO.1-6Hshift.a.Zc
----------------------------------
E(UM062X/Aug-CC-pVTZ) (Hartree): -421.41388538
Electronic state : 2-A
Cartesian coordinates (Angs):
     O      -1.953200      0.709729      -0.843874
     H      -1.081665      1.382104      -0.240421
     C      -0.088042      1.598713       0.548536
     O      -2.176009     -0.349107       0.009137
     C       0.726041      0.401034       0.371658
     C      -1.110227     -1.286587      -0.097239
     C       0.083660     -0.903718       0.775320
     H      -0.639485      1.655303       1.485836
     H       0.370484      2.537415       0.253653
     C       1.930202      0.489202      -0.211689
     O       2.779922     -0.520931      -0.504577
     H       2.344672      1.445286      -0.502068
     H      -1.537182     -2.229748       0.245099
     H      -0.827718     -1.372330      -1.147986
     H       0.790085     -1.738092       0.760909
     H      -0.266085     -0.821483       1.807747
```

```
     H       2.391381     -1.367842      -0.267779
Rotational constants (GHz):    3.5653900    1.3311700    1.1269500
Vibrational harmonic frequencies (cm-1):
    i2089.6467                  73.3864                 144.2458
      252.2848                 254.3888                 295.2603
      348.6658                 402.9211                 446.4342
      498.5905                 580.1781                 589.5122
      631.7255                 644.0132                 781.6250
      877.4454                 914.9174                 957.1782
     1014.4730                1019.6854                1050.7670
     1089.1779                1119.6484                1187.5560
     1205.4486                1238.3923                1283.2037
     1302.1902                1329.7816                1360.7501
     1395.0488                1421.0353                1461.2732
     1480.4697                1489.5087                1522.7000
     1708.9601                3049.8736                3067.4395
     3089.7423                3096.8584                3127.0348
     3191.0539                3217.8402                3869.7027
Zero-point correction (Hartree): 0.134600

TS.HOCHCCH3CH2CH2OO.1-6Hshift.a.Zt
~~~~~~~~~~~~~~~~~~~~~~~~~~~~~~~~~
E(CCSD(T)/Aug-CC-pVTZ) (Hartree): -420.80534605
E(CCSD/Aug-CC-pVTZ) (Hartree): -420.73022356
     T1 diagnostic:  0.025215
E(MP2/Aug-CC-pVTZ) (Hartree): -420.67701734
E(MP3/Aug-CC-pVTZ) (Hartree): -420.71328940
E(PMP2/Aug-CC-pVTZ) (Hartree): -420.69250327
E(PMP3/Aug-CC-pVTZ) (Hartree): -420.72444558
E(PUHF/Aug-CC-pVTZ) (Hartree): -419.13115853
E(UHF/Aug-CC-pVTZ) (Hartree): -419.11271414
E(UM062X/Aug-CC-pVTZ) (Hartree): -421.41444056
Electronic state : 2-A
Cartesian coordinates (Angs):
     O      -1.958174      0.689970      -0.852131
     H      -1.100700      1.371563      -0.255314
     C      -0.107906      1.612556       0.537761
     O      -2.173687     -0.365790       0.004806
     C       0.708535      0.416080       0.378459
     C      -1.093869     -1.293638      -0.088837
     C       0.092307     -0.898487       0.784797
     H      -0.666306      1.675348       1.470149
     H       0.342921      2.551728       0.231718
     C       1.910845      0.483199      -0.203602
     O       2.663257     -0.627244      -0.435099
     H       2.336862      1.429326      -0.517010
     H      -1.514879     -2.238742       0.254936
     H      -0.805100     -1.382272      -1.137196
     H       0.835255     -1.693932       0.735464
     H      -0.255891     -0.826943       1.818525
     H       3.517194     -0.379830      -0.793344
Rotational constants (GHz):    3.5570000    1.3494100    1.1376500
Vibrational harmonic frequencies (cm-1):
    i2125.9030                  73.8258                 144.8234
      242.5021                 249.7489                 277.2143
      327.3942                 345.9792                 434.1601
      488.7135                 585.1494                 591.6852
      631.5893                 647.1744                 787.8479
      874.9232                 885.4648                 959.9891
     1010.0703                1018.8154                1048.2654
     1086.5471                1119.0282                1196.7306
     1207.3084                1240.5505                1248.2845
     1297.1116                1342.5440                1356.1230
     1389.9385                1421.1517                1460.2205
     1479.4794                1483.1757                1522.4986
     1730.6236                3059.4946                3072.5546
     3098.4729                3125.9796                3131.2908
     3185.5875                3190.1089                3913.8734
Zero-point correction (Hartree): 0.134375

TS.HOCHCCH3CH2CH2OO.1-6Hshift.b.Zc
~~~~~~~~~~~~~~~~~~~~~~~~~~~~~~~~~
E(UM062X/Aug-CC-pVTZ) (Hartree): -421.41379943
Electronic state : 2-A
Cartesian coordinates (Angs):
     O      -2.172289      0.392037      -0.380920
     H      -1.317307      1.295368      -0.178889
     C      -0.206735      1.814036       0.262017
     O      -1.391242     -0.629704      -0.865925
     C       0.611405      0.617457       0.350430
     C      -0.866227     -1.382095       0.221721
     C       0.006509     -0.517110       1.144415
     H      -0.575528      2.200157       1.210717
     H       0.132768      2.587840      -0.419221
     C       1.731349      0.477639      -0.376591
     O       2.518254     -0.619024      -0.430998
     H       2.115330      1.275673      -0.997117
     H      -1.684337     -1.853060       0.769799
     H      -0.276027     -2.153903      -0.274322
     H       0.755735     -1.145670       1.632699
     H      -0.605105     -0.096046       1.941020
     H       2.158878     -1.316387       0.126103
Rotational constants (GHz):    3.1329900    1.5781800    1.3050800
```

```
Vibrational harmonic frequencies (cm-1):
    i2020.1929                84.2323               122.3046
      255.4016               284.1316               331.6035
      358.5807               390.2188               436.0733
      500.3482               540.9057               592.0663
      625.1512               680.8618               806.0707
      858.9725               915.1989               955.7221
     1018.3961              1026.9489              1073.6031
     1080.3392              1124.4093              1184.5750
     1219.6511              1273.1274              1280.3392
     1294.0000              1322.8966              1362.4060
     1385.3673              1413.3022              1475.8292
     1489.2252              1497.7021              1511.2492
     1696.0246              3056.3752              3066.6361
     3098.0780              3108.6079              3127.2132
     3190.4441              3221.2841              3857.8356
Zero-point correction (Hartree): 0.134853

TS.HOCHCCH3CH2CH2OO.1-6Hshift.b.Zt
~~~~~~~~~~~~~~~~~~~~~~~~~~~~~~~~~
E(UM062X/Aug-CC-pVTZ) (Hartree): -421.41432079
Electronic state : 2-A
Cartesian coordinates (Angs):
     O      -2.168964      0.339083      -0.413326
     H      -1.346566      1.264500      -0.213022
     C      -0.251609      1.827108       0.230581
     O      -1.354748     -0.671518      -0.861320
     C       0.581625      0.646906       0.357829
     C      -0.820534     -1.388581       0.250952
     C       0.004495     -0.482768       1.174198
     H      -0.642849      2.226174       1.164337
     H       0.078148      2.591364      -0.466420
     C       1.697711      0.483597      -0.364566
     O       2.402750     -0.677734      -0.310386
     H       2.081282      1.259780      -1.015882
     H      -1.633378     -1.880493       0.788119
     H      -0.184189     -2.137160      -0.219485
     H       0.785654     -1.075760       1.647731
     H      -0.630097     -0.067457       1.955818
     H       3.189563     -0.617176      -0.854909
Rotational constants (GHz):    3.1095600    1.6159400    1.3292500
Vibrational harmonic frequencies (cm-1):
    i2067.2203                80.7269               124.9799
      250.6726               266.1617               300.6704
      356.4600               362.9145               392.0901
      485.5641               539.6044               596.8966
      623.0864               686.1959               811.2804
      863.2249               869.4587               959.7051
     1018.4655              1026.5592              1065.5672
     1082.7047              1121.8113              1197.6638
     1225.5901              1247.1964              1275.1394
     1282.8936              1324.1650              1362.3878
     1380.6641              1412.3404              1475.0907
     1485.7310              1494.0201              1503.3449
     1716.2163              3068.8958              3089.5693
     3101.5952              3126.8974              3144.1488
     3189.2682              3192.6181              3910.7707
Zero-point correction (Hartree): 0.134619


################################################################################
E-HOCH=CHCH2CH2OO ring closure
################################################################################

HOCHCHCH2CH2OO.Ecpmc
~~~~~~~~~~~~~~~~~~~
E(UM062X/Aug-CC-pVTZ) (Hartree): -382.13875016
Electronic state : 2-A
Cartesian coordinates (Angs):
     C      -1.464605     -0.422977       0.119382
     C      -1.214437      0.847892      -0.164136
     C       0.132747      1.506700      -0.092726
     C       1.242428      0.655855       0.476854
     O       1.542377     -0.394003      -0.472187
     O       2.422013     -1.221736      -0.000305
     O      -2.679471     -1.027466       0.067432
     H      -0.700741     -1.127820       0.419328
     H      -2.038291      1.479660      -0.483204
     H       0.436862      1.853511      -1.084376
     H       0.067173      2.402931       0.529284
     H       2.158746      1.227493       0.615094
     H       0.967614      0.177698       1.416724
     H      -3.347513     -0.392658      -0.208613
Rotational constants (GHz):    4.5202800    1.4779300    1.1717900
Vibrational harmonic frequencies (cm-1):
       48.1026               124.2428               131.8012
      214.6629               263.0421               302.0468
      395.1256               448.3625               524.2222
      619.2420               798.5684               872.2430
      939.1204               992.9402              1001.4340
     1064.1514              1112.3987              1161.7700
     1229.2525              1254.3525              1293.3706
     1297.0187              1350.5167              1387.6863
```

```
     1403.8246                1421.8062                1476.3599
     1506.1178                1767.7863                3052.5511
     3078.7936                3092.3963                3144.1966
     3156.9067                3222.3314                3857.5254
Zero-point correction (Hartree): 0.111644

HOCHCHCH2CH2OO.Ecpmt
~~~~~~~~~~~~~~~~~~~
E(UM062X/Aug-CC-pVTZ) (Hartree): -382.13755268
Electronic state : 2-A
Cartesian coordinates (Angs):
     C      -1.459720     -0.380138       0.100018
     C      -1.195673      0.890109      -0.161260
     C       0.160351      1.527147      -0.087119
     C       1.259783      0.656818       0.472133
     O       1.538632     -0.395509      -0.482336
     O       2.331305     -1.292747       0.015563
     O      -2.730887     -0.869703       0.027081
     H      -0.695940     -1.096969       0.379060
     H      -2.021999      1.524596      -0.459245
     H       0.465324      1.880214      -1.076448
     H       0.109175      2.419006       0.542606
     H       2.186733      1.212246       0.607498
     H       0.982718      0.178054       1.410801
     H      -2.726850     -1.817098       0.170634
Rotational constants (GHz):    4.4196600    1.5059900    1.1816000
Vibrational harmonic frequencies (cm-1):
       42.0257                  126.7007                  135.7249
      206.3338                  235.5286                  286.2958
      312.5589                  394.5795                  519.4377
      621.7216                  802.1858                  879.4116
      933.8539                  972.8706                  994.0134
     1062.5462                 1111.2065                 1185.9560
     1215.4124                 1235.8830                 1286.2828
     1299.1804                 1353.5418                 1387.9902
     1389.6808                 1417.4445                 1475.1009
     1504.8745                 1790.0874                 3052.1121
     3078.1940                 3091.5871                 3143.5744
     3188.7776                 3190.6990                 3917.2498
Zero-point correction (Hartree): 0.111267

HOCHCHCH2CH2OO.Ecppc
~~~~~~~~~~~~~~~~~~~
E(UM062X/Aug-CC-pVTZ) (Hartree): -382.13947030
Electronic state : 2-A
Cartesian coordinates (Angs):
     C      -1.529484     -0.302489       0.170987
     C      -1.034845      0.811980      -0.349991
     C       0.374698      1.300939      -0.188853
     C       1.232616      0.510313       0.773581
     O       1.481866     -0.830752       0.290517
     O       2.258116     -0.821903      -0.748450
     O      -2.804690     -0.750430       0.033491
     H      -0.945277     -0.991818       0.765712
     H      -1.686990      1.431986      -0.958476
     H       0.886349      1.319515      -1.154593
     H       0.364612      2.334302       0.167739
     H       2.203798      0.980548       0.914588
     H       0.745164      0.362278       1.736279
     H      -3.307907     -0.136598      -0.510058
Rotational constants (GHz):    4.9983100    1.4387300    1.2663800
Vibrational harmonic frequencies (cm-1):
       67.8308                  117.8662                  148.3515
      204.1084                  269.3890                  314.1250
      431.1025                  446.1421                  535.4174
      625.5700                  811.4498                  862.5680
      928.0912                  984.7397                  995.4913
     1037.2588                 1118.6221                 1160.2299
     1227.7424                 1248.8181                 1283.3823
     1316.4783                 1350.1384                 1390.1106
     1399.1873                 1413.6909                 1474.9318
     1494.2587                 1766.1610                 3055.8556
     3083.2992                 3099.4234                 3154.0351
     3155.0453                 3223.1537                 3859.8894
Zero-point correction (Hartree): 0.111753

HOCHCHCH2CH2OO.Ecppt
~~~~~~~~~~~~~~~~~~~
E(UM062X/Aug-CC-pVTZ) (Hartree): -382.13802000
Electronic state : 2-A
Cartesian coordinates (Angs):
     C      -1.529449     -0.270471       0.138609
     C      -1.022385      0.847727      -0.355323
     C       0.393919      1.310374      -0.189437
     C       1.239116      0.507328       0.773733
     O       1.461834     -0.842237       0.299354
     O       2.237854     -0.857438      -0.739800
     O      -2.840301     -0.599535      -0.051762
     H      -0.944052     -0.982245       0.709316
     H      -1.680273      1.480772      -0.939231
     H       0.906484      1.324864      -1.154913
     H       0.399687      2.343160       0.169092
     H       2.219956      0.958170       0.911539
```

```
     H       0.749641      0.373436       1.737641
     H      -3.013743     -1.474224       0.298727
Rotational constants (GHz):    4.9691000    1.4437000    1.2654800
Vibrational harmonic frequencies (cm-1):
       67.3447                120.3136                150.1679
      197.9145                232.0141                293.8005
      317.3200                440.0979                534.0222
      625.9645                814.0036                865.5497
      925.5620                971.6286                985.4511
     1035.0411               1118.1520               1185.3130
     1218.1745               1229.5988               1278.3390
     1313.1957               1355.4120               1387.3704
     1392.6868               1407.0145               1473.1566
     1491.9981               1788.7664               3055.7378
     3082.3562               3098.1625               3153.7357
     3187.0484               3189.4940               3917.0116
Zero-point correction (Hartree): 0.111400

HOCHCHCH2CH2OO.Ectpc
~~~~~~~~~~~~~~~~~~~~
E(UM062X/Aug-CC-pVTZ) (Hartree): -382.13938546
Electronic state : 2-A
Cartesian coordinates (Angs):
     C       1.936312     -0.344147      -0.048058
     C       1.221437      0.766858       0.066513
     C      -0.268783      0.828034       0.220496
     C      -0.935101     -0.530449       0.227231
     O      -2.358621     -0.381508       0.409864
     O      -2.926371      0.085049      -0.659898
     O       3.285433     -0.418540      -0.190501
     H       1.502893     -1.335730      -0.039989
     H       1.740157      1.720866       0.048268
     H      -0.526798      1.344957       1.148427
     H      -0.706390      1.411545      -0.592537
     H      -0.780617     -1.069171      -0.707047
     H      -0.617071     -1.141356       1.070902
     H       3.661109      0.467113      -0.200841
Rotational constants (GHz):    9.8150100    0.9944200    0.9536900
Vibrational harmonic frequencies (cm-1):
       69.9008                110.5973                147.6182
      162.2996                271.1103                322.2673
      376.4266                438.7931                543.6010
      669.5200                774.6993                854.3725
      955.3967                987.5271                994.7808
     1101.3430               1108.4992               1158.9623
     1238.2333               1253.1820               1285.9201
     1320.6570               1340.1831               1350.9176
     1403.4472               1422.6524               1492.0627
     1503.2176               1766.7069               3055.1602
     3089.3721               3090.7007               3150.9597
     3159.3541               3214.6008               3858.0659
Zero-point correction (Hartree): 0.111728

HOCHCHCH2CH2OO.Ectpt
~~~~~~~~~~~~~~~~~~~~
E(UM062X/Aug-CC-pVTZ) (Hartree): -382.13741398
Electronic state : 2-A
Cartesian coordinates (Angs):
     C       1.939941     -0.306288      -0.043998
     C       1.212318      0.795109       0.054537
     C      -0.277420      0.841180       0.204218
     C      -0.931955     -0.522116       0.240755
     O      -2.357334     -0.384119       0.418383
     O      -2.929968      0.042776      -0.665264
     O       3.297206     -0.251505      -0.178406
     H       1.511880     -1.302568      -0.024448
     H       1.733897      1.744451       0.023800
     H      -0.541629      1.377099       1.119589
     H      -0.719151      1.403362      -0.621714
     H      -0.772293     -1.080333      -0.681255
     H      -0.609342     -1.110884       1.098530
     H       3.660101     -1.135645      -0.245271
Rotational constants (GHz):    9.8556000    0.9914600    0.9518100
Vibrational harmonic frequencies (cm-1):
       68.2076                106.6733                144.7125
      160.4354                191.3743                296.9736
      323.3690                370.0179                543.0483
      668.8520                773.9917                862.0336
      949.6565                970.6268                991.1841
     1100.9311               1106.9279               1182.2731
     1219.8489               1238.4636               1285.5997
     1318.8167               1339.1135               1355.0051
     1384.0531               1421.4667               1490.5967
     1501.8193               1787.9223               3055.0370
     3087.8865               3089.4569               3148.9799
     3179.5770               3191.1718               3919.9732
Zero-point correction (Hartree): 0.111234

HOCHCHCH2CH2OO.Ecttc
~~~~~~~~~~~~~~~~~~~~
E(UM062X/Aug-CC-pVTZ) (Hartree): -382.13876938
Point group : CS
Electronic state : 2-A"
```

```
Cartesian coordinates (Angs):
     C      -0.771975     -1.802408       0.000000
     C       0.515982     -1.485695       0.000000
     C       1.065624     -0.090714       0.000000
     C      -0.000000      0.979201       0.000000
     O       0.681606      2.250581       0.000000
     O      -0.157836      3.238907       0.000000
     O      -1.288633     -3.057915       0.000000
     H      -1.565508     -1.066926       0.000000
     H       1.246994     -2.288398       0.000000
     H       1.705699      0.056392       0.873368
     H       1.705699      0.056392      -0.873368
     H      -0.628043      0.945712      -0.890070
     H      -0.628043      0.945712       0.890070
     H      -0.575674     -3.703771       0.000000
Rotational constants (GHz):    9.0291200    0.9776300    0.8918700
Vibrational harmonic frequencies (cm-1):
       73.9734 (  A")          103.8979 (  A")          122.8267 (  A')
      131.4241 (  A")          268.2891 (  A")          288.7826 (  A')
      369.1405 (  A')          428.2408 (  A")          526.8094 (  A')
      646.7481 (  A')          765.5339 (  A")          849.9082 (  A")
      979.3574 (  A')          985.2831 (  A")         1031.1827 (  A')
     1082.6697 (  A")         1125.1460 (  A')         1161.8411 (  A')
     1227.6135 (  A")         1258.5921 (  A')         1296.4638 (  A')
     1307.5496 (  A")         1331.8992 (  A')         1351.7050 (  A')
     1404.0158 (  A')         1431.0892 (  A')         1498.7546 (  A')
     1512.6102 (  A')         1765.5679 (  A')         3055.2827 (  A')
     3083.1958 (  A')         3084.1565 (  A")         3140.6048 (  A")
     3162.7702 (  A')         3218.6361 (  A')         3860.5767 (  A')
Zero-point correction (Hartree): 0.111476

HOCHCHCH2CH2OO.Ecttt
~~~~~~~~~~~~~~~~~~~
E(UM062X/Aug-CC-pVTZ) (Hartree): -382.13700871
Point group : CS
Electronic state : 2-A"
Cartesian coordinates (Angs):
     C      -0.730667     -1.816974       0.000000
     C       0.550123     -1.482173       0.000000
     C       1.078835     -0.080256       0.000000
     C      -0.000000      0.976032       0.000000
     O       0.661347      2.258959       0.000000
     O      -0.193057      3.234275       0.000000
     O      -1.122947     -3.123534       0.000000
     H      -1.532954     -1.087177       0.000000
     H       1.278914     -2.283852       0.000000
     H       1.717525      0.073764       0.873326
     H       1.717525      0.073764      -0.873326
     H      -0.627193      0.934602      -0.890543
     H      -0.627193      0.934602       0.890543
     H      -2.079119     -3.183081       0.000000
Rotational constants (GHz):    9.0451300    0.9756500    0.8903900
Vibrational harmonic frequencies (cm-1):
       78.1147 (  A")          105.6336 (  A")          123.3877 (  A')
      141.6512 (  A")          214.4010 (  A")          288.1418 (  A')
      304.9511 (  A")          364.9563 (  A')          524.9464 (  A')
      646.4276 (  A')          765.6786 (  A")          858.0770 (  A")
      969.0092 (  A")          971.9698 (  A')         1029.4277 (  A')
     1082.5480 (  A")         1124.5327 (  A')         1184.5187 (  A')
     1224.9998 (  A')         1228.0631 (  A")         1296.3103 (  A')
     1306.9655 (  A")         1329.6117 (  A')         1356.7021 (  A')
     1384.6632 (  A')         1429.1669 (  A')         1497.5473 (  A')
     1511.9850 (  A')         1787.3630 (  A')         3054.9617 (  A')
     3080.6423 (  A')         3083.6770 (  A")         3137.9846 (  A")
     3181.5268 (  A')         3193.1579 (  A')         3919.4957 (  A')
Zero-point correction (Hartree): 0.111136

HOCHCHCH2CH2OO.Egppc
~~~~~~~~~~~~~~~~~~~
E(CCSD(T)/Aug-CC-pVTZ) (Hartree): -381.59741321
E(CCSD/Aug-CC-pVTZ) (Hartree): -381.53562656
     T1 diagnostic:  0.021635
E(MP2/Aug-CC-pVTZ) (Hartree): -381.49135115
E(MP3/Aug-CC-pVTZ) (Hartree): -381.52284012
E(PMP2/Aug-CC-pVTZ) (Hartree): -381.49450832
E(PMP3/Aug-CC-pVTZ) (Hartree): -381.52470252
E(PUHF/Aug-CC-pVTZ) (Hartree): -380.13366994
E(UHF/Aug-CC-pVTZ) (Hartree): -380.12852112
E(UM062X/Aug-CC-pVTZ) (Hartree): -382.14077322
Electronic state : 2-A
Cartesian coordinates (Angs):
     C       1.710511     -0.236631       0.326987
     C       0.944346      0.767676      -0.075868
     C      -0.364970      1.093381       0.572448
     C      -1.559565      0.810304      -0.322689
     O      -1.648835     -0.595790      -0.641420
     O      -1.913557     -1.302412       0.413399
     O       2.897580     -0.615656      -0.206873
     H       1.435802     -0.870144       1.161279
     H       1.254587      1.369726      -0.925861
     H      -0.486348      0.518270       1.490682
     H      -0.411223      2.150053       0.846885
     H      -2.497548      1.093650       0.152897
```

```
     H      -1.469744      1.294969      -1.293789
     H       3.111038     -0.054046      -0.958204
Rotational constants (GHz):    4.8942000    1.4051200    1.2198500
Vibrational harmonic frequencies (cm-1):
       48.4327                  73.9465                 138.6868
      203.0000                 282.0698                 338.0806
      432.5349                 464.7401                 534.2373
      576.6960                 817.7682                 871.9379
      917.7207                 978.5767                 989.2948
     1056.1982                1130.6006                1160.8082
     1215.2377                1261.8162                1278.7131
     1308.6740                1341.0988                1362.0063
     1399.2443                1409.4212                1476.6644
     1490.7193                1764.6782                3063.6467
     3091.5359                3117.6738                3151.0787
     3153.2238                3205.8634                3858.7646
Zero-point correction (Hartree): 0.111551

HOCHCHCH2CH2OO.Egppt
~~~~~~~~~~~~~~~~~~~~
E(UM062X/Aug-CC-pVTZ) (Hartree): -382.13943708
Electronic state : 2-A
Cartesian coordinates (Angs):
     C       1.687236     -0.201097       0.290896
     C       0.928303      0.817527      -0.079823
     C      -0.388725      1.111221       0.566132
     C      -1.573046      0.788725      -0.329917
     O      -1.625150     -0.623845      -0.632210
     O      -1.858347     -1.327385       0.431741
     O       2.875457     -0.478173      -0.312634
     H       1.391623     -0.864289       1.097960
     H       1.258737      1.441503      -0.902645
     H      -0.499833      0.540022       1.488258
     H      -0.463606      2.168069       0.832364
     H      -2.520100      1.052277       0.139199
     H      -1.491630      1.262981      -1.306601
     H       3.266520     -1.263601       0.072556
Rotational constants (GHz):    4.8400900    1.4303100    1.2324500
Vibrational harmonic frequencies (cm-1):
       47.9251                  75.1564                 145.3360
      199.4227                 255.2148                 299.2435
      337.1138                 454.6666                 532.7269
      576.7199                 824.7387                 880.4943
      914.9683                 965.1112                 979.4742
     1051.9435                1134.6384                1179.6874
     1207.3830                1246.9137                1270.9962
     1304.0541                1339.5274                1365.6406
     1395.8855                1399.3995                1477.7779
     1490.5910                1787.2229                3065.8359
     3092.1485                3116.9292                3153.6702
     3169.3150                3183.6903                3915.4862
Zero-point correction (Hartree): 0.111259

HOCHCHCH2CH2OO.Egptt
~~~~~~~~~~~~~~~~~~~~
E(UM062X/Aug-CC-pVTZ) (Hartree): -382.13810416
Electronic state : 2-A
Cartesian coordinates (Angs):
     C       1.871289     -0.153176       0.329989
     C       1.054218      0.635267      -0.348775
     C      -0.127526      1.310639       0.274269
     C      -1.450685      0.761239      -0.222213
     O      -1.582532     -0.580829       0.295585
     O      -2.656826     -1.158544      -0.143306
     O       2.936654     -0.767166      -0.254017
     H       1.728227     -0.344927       1.388712
     H       1.232642      0.780890      -1.408353
     H      -0.094393      1.210822       1.360925
     H      -0.117389      2.380612       0.054960
     H      -2.303019      1.331426       0.145625
     H      -1.494215      0.695959      -1.308917
     H       3.386003     -1.326284       0.381331
Rotational constants (GHz):    5.3088800    1.2317300    1.0613900
Vibrational harmonic frequencies (cm-1):
       44.1585                  72.5962                 110.5274
      188.9176                 240.8283                 278.9011
      332.8114                 396.6938                 537.4121
      566.3702                 818.6533                 871.5105
      917.0749                 963.8968                1031.6287
     1067.3404                1123.0761                1179.5649
     1205.2590                1250.2644                1276.6812
     1299.0977                1337.7871                1364.5492
     1392.9945                1406.0468                1473.0211
     1500.3771                1790.1720                3062.0313
     3083.9850                3105.3708                3142.0309
     3170.7630                3183.3007                3917.6972
Zero-point correction (Hartree): 0.110954

HOCHCHCH2CH2OO.Elmmc
~~~~~~~~~~~~~~~~~~~~
E(CCSD(T)/Aug-CC-pVTZ) (Hartree): -381.59783370
E(CCSD/Aug-CC-pVTZ) (Hartree): -381.53613947
     T1 diagnostic:  0.021613
```

```
E(MP2/Aug-CC-pVTZ) (Hartree): -381.49167334
E(MP3/Aug-CC-pVTZ) (Hartree): -381.52332066
E(PMP2/Aug-CC-pVTZ) (Hartree): -381.49483364
E(PMP3/Aug-CC-pVTZ) (Hartree): -381.52518461
E(PUHF/Aug-CC-pVTZ) (Hartree): -380.13467350
E(UHF/Aug-CC-pVTZ) (Hartree): -380.12952628
E(UM062X/Aug-CC-pVTZ) (Hartree): -382.14119558
Electronic state : 2-A
Cartesian coordinates (Angs):
     C       2.124153      0.276916      -0.042485
     C       0.874173     -0.099991      -0.272337
     C      -0.241856      0.871925      -0.502115
     C      -1.331538      0.777029       0.551962
     O      -1.920688     -0.543726       0.557753
     O      -2.625917     -0.751207      -0.511793
     O       3.188259     -0.535457       0.177972
     H       2.419325      1.318728      -0.015007
     H       0.628268     -1.157591      -0.294153
     H       0.142333      1.893574      -0.495348
     H      -0.708634      0.706852      -1.475186
     H      -0.933191      0.894050       1.558058
     H      -2.137311      1.487177       0.372899
     H       2.906379     -1.454950       0.147128
Rotational constants (GHz):    7.1870100    1.0976100    1.0399700
Vibrational harmonic frequencies (cm-1):
      56.8155                  83.9327                 145.6926
     184.7958                 282.8152                 330.2073
     441.3317                 475.5827                 532.5543
     584.2154                 819.8312                 856.1046
     908.1255                 989.8147                 997.8385
    1093.6706                1120.4717                1158.1126
    1207.1273                1245.8661                1294.7724
    1306.4289                1340.7014                1365.5644
    1394.4322                1413.1006                1474.5714
    1489.2539                1763.9730                3068.0372
    3093.6743                3112.8341                3158.6898
    3163.9251                3203.8754                3858.7945
Zero-point correction (Hartree): 0.111670

HOCHCHCH2CH2OO.Elmmt
~~~~~~~~~~~~~~~~~~~
E(UM062X/Aug-CC-pVTZ) (Hartree): -382.13870637
Electronic state : 2-A
Cartesian coordinates (Angs):
     C       2.125235      0.248322      -0.058651
     C       0.872717     -0.128232      -0.259321
     C      -0.238762      0.845137      -0.498006
     C      -1.328976      0.766348       0.557172
     O      -1.950491     -0.538911       0.551717
     O      -2.674554     -0.711942      -0.511242
     O       3.126265     -0.649485       0.162286
     H       2.416229      1.294412      -0.065456
     H       0.636743     -1.185922      -0.247669
     H       0.146936      1.866620      -0.504487
     H      -0.709261      0.670049      -1.467856
     H      -0.927013      0.865361       1.563809
     H      -2.117523      1.497240       0.384897
     H       3.962841     -0.194512       0.267517
Rotational constants (GHz):    7.4165000    1.0823000    1.0299300
Vibrational harmonic frequencies (cm-1):
      58.1094                  83.5004                 145.1692
     179.0405                 261.2688                 283.6740
     343.9772                 473.3522                 529.3861
     579.8470                 819.7825                 865.7344
     908.1426                 967.9874                 997.4035
    1095.1717                1120.2871                1176.8371
    1197.1457                1237.6120                1272.9478
    1306.9577                1339.9534                1366.4940
    1393.0371                1401.3962                1474.2716
    1488.3671                1786.6412                3064.6038
    3092.0681                3109.0438                3157.2482
    3166.1291                3193.1663                3917.7310
Zero-point correction (Hartree): 0.111296

HOCHCHCH2CH2OO.Elmpc
~~~~~~~~~~~~~~~~~~~
E(UM062X/Aug-CC-pVTZ) (Hartree): -382.14045498
Electronic state : 2-A
Cartesian coordinates (Angs):
     C       1.990995      0.290723       0.147957
     C       0.783071      0.146789      -0.378955
     C      -0.267488      1.210011      -0.300446
     C      -1.511384      0.771514       0.459024
     O      -2.173244     -0.296686      -0.251029
     O      -1.760532     -1.467795       0.130963
     O       2.994221     -0.622237       0.132025
     H       2.297937      1.195879       0.657647
     H       0.524123     -0.780504      -0.880382
     H       0.132568      2.092020       0.204050
     H      -0.576875      1.525457      -1.299715
     H      -1.276596      0.401779       1.454863
     H      -2.249624      1.570606       0.506442
     H       2.693745     -1.425720      -0.304047
```

```
Rotational constants (GHz):    5.3864800    1.3147700    1.1153500
Vibrational harmonic frequencies (cm-1):
       63.8294                89.1137                132.6084
      185.0105                288.9820                340.3975
      444.6962                474.8875                529.9831
      562.1000                845.9667                860.7239
      884.3868                990.1286               1016.3122
     1084.0668               1116.5833               1160.1911
     1213.2703               1237.8761               1291.0053
     1322.3524               1344.0177               1370.2374
     1386.2854               1415.5074               1472.7173
     1485.0646               1763.5710               3057.6900
     3092.6181               3104.3023               3161.1612
     3167.6961               3201.1436               3857.5971
Zero-point correction (Hartree): 0.111662

HOCHCHCH2CH2OO.Elmpt
--------------------
E(UM062X/Aug-CC-pVTZ) (Hartree): -382.13752742
Electronic state : 2-A
Cartesian coordinates (Angs):
     C       1.989507      0.262297       0.130044
     C       0.777124      0.125563      -0.382394
     C      -0.261349      1.198630      -0.291182
     C      -1.508613      0.770590       0.468626
     O      -2.193658     -0.275300      -0.251268
     O      -1.812128     -1.459012       0.124798
     O       2.930095     -0.719142       0.038424
     H       2.295569      1.168905       0.643384
     H       0.522343     -0.800812      -0.883005
     H       0.147817      2.075144       0.216406
     H      -0.571089      1.522324      -1.287893
     H      -1.275494      0.383278       1.458211
     H      -2.231510      1.582752       0.531264
     H       3.737879     -0.446456       0.475440
Rotational constants (GHz):    5.4572000    1.2998800    1.1070100
Vibrational harmonic frequencies (cm-1):
       64.2559                86.3268                130.5274
      178.1882               258.9797                287.9710
      353.5359               474.4244                526.6953
      558.9309               844.4467                871.0567
      882.9824               970.8423               1018.2529
     1084.6321              1117.4167               1179.0426
     1201.6086              1237.9409               1264.4799
     1319.0775              1345.9730               1370.6756
     1385.7920              1403.8346               1472.6167
     1484.7002              1785.9588               3055.0045
     3090.6026              3101.1149               3159.7897
     3162.9384              3196.9708               3918.7962
Zero-point correction (Hartree): 0.111280

HOCHCHCH2CH2OO.Elmtc
--------------------
E(UM062X/Aug-CC-pVTZ) (Hartree): -382.14044555
Electronic state : 2-A
Cartesian coordinates (Angs):
     C       2.175963      0.186009       0.179724
     C       0.978214      0.057207      -0.373761
     C      -0.069240      1.126498      -0.303036
     C      -1.324123      0.674537       0.417155
     O      -1.901820     -0.397832      -0.361864
     O      -2.954285     -0.892729       0.211247
     O       3.175990     -0.730064       0.170248
     H       2.475424      1.081714       0.710223
     H       0.723648     -0.859065      -0.897583
     H       0.322422      1.997960       0.224062
     H      -0.351103      1.458940      -1.304999
     H      -1.111008      0.276191       1.408134
     H      -2.073764      1.462124       0.484559
     H       2.890411     -1.518371      -0.301936
Rotational constants (GHz):    7.0870600    1.0463600    0.9597700
Vibrational harmonic frequencies (cm-1):
       49.5994                90.3886                116.2541
      189.2059               270.1401                329.0272
      396.3809               452.8971                546.4457
      570.7131               812.1939                856.0773
      929.8350               991.5934               1033.3265
     1078.2671              1125.6248               1160.3652
     1217.0645              1246.0738               1296.9406
     1298.3373              1341.4574               1365.5075
     1398.7018              1414.1608               1472.0318
     1501.0744              1763.3001               3060.7044
     3085.6154              3109.2440               3146.6216
     3165.8735              3201.7740               3857.2177
Zero-point correction (Hartree): 0.111494

HOCHCHCH2CH2OO.Elmtt
--------------------
E(UM062X/Aug-CC-pVTZ) (Hartree): -382.13798496
Electronic state : 2-A
Cartesian coordinates (Angs):
     C       2.173117      0.167424       0.157258
     C       0.970963      0.041464      -0.381228
```

```
     C      -0.072376      1.111851      -0.290724
     C      -1.324757      0.656602       0.432221
     O      -1.926112     -0.388564      -0.364734
     O      -2.984436     -0.874250       0.205234
     O       3.112428     -0.815310       0.071604
     H       2.470110      1.065938       0.689801
     H       0.724771     -0.874854      -0.904278
     H       0.322664      1.978532       0.242455
     H      -0.361053      1.454522      -1.287458
     H      -1.105852      0.232019       1.411023
     H      -2.063330      1.451864       0.527200
     H       3.915968     -0.547075       0.519265
Rotational constants (GHz):    7.2581100    1.0369700    0.9544000
Vibrational harmonic frequencies (cm-1):
       51.3622                91.4555                114.8537
      180.4182               259.3054                273.7506
      340.7793               398.9651                541.7653
      570.7578               811.9286                867.1642
      927.9807               970.4569               1033.7417
     1079.4163              1128.4707               1178.0868
     1206.8534              1237.1343               1279.3676
     1297.4922              1339.9602               1367.0724
     1398.1003              1403.2247               1471.8138
     1500.6779              1786.2808               3058.6410
     3085.1347              3105.6017               3145.9876
     3164.0356              3195.5698               3917.2662
Zero-point correction (Hartree): 0.111131

HOCHCHCH2CH2OO.Elpmc
~~~~~~~~~~~~~~~~~~~
E(UM062X/Aug-CC-pVTZ) (Hartree): -382.14031527
Electronic state : 2-A
Cartesian coordinates (Angs):
     C      -1.716898      0.146092      -0.385021
     C      -0.768732      0.610804       0.416624
     C       0.428961      1.348511      -0.088900
     C       1.742575      0.638342       0.211557
     O       1.802244     -0.622303      -0.477781
     O       1.259329     -1.577483       0.218050
     O      -2.823031     -0.544588      -0.015065
     H      -1.686140      0.288376      -1.458048
     H      -0.834430      0.427859       1.485386
     H       0.348477      1.499505      -1.166609
     H       0.496962      2.339651       0.368448
     H       2.593005      1.204843      -0.164387
     H       1.864156      0.433781       1.274056
     H      -2.805809     -0.701510       0.933953
Rotational constants (GHz):    4.6279400    1.5523400    1.2629400
Vibrational harmonic frequencies (cm-1):
       62.2880                96.0757                108.9101
      193.1536               290.6709                350.8344
      422.9886               466.9158                540.3184
      553.9728               824.1871                861.6162
      942.6393               983.8111                993.8037
     1040.3522              1132.5951               1164.1930
     1225.5704              1237.3195               1280.0041
     1318.0575              1343.4109               1360.5222
     1394.6357              1413.1371               1473.5582
     1485.7583              1764.5370               3051.7259
     3091.9388              3105.8278               3154.9038
     3159.3070              3207.7406               3860.3590
Zero-point correction (Hartree): 0.111534

HOCHCHCH2CH2OO.Elpmt
~~~~~~~~~~~~~~~~~~~
E(UM062X/Aug-CC-pVTZ) (Hartree): -382.13829904
Electronic state : 2-A
Cartesian coordinates (Angs):
     C       1.679246      0.110683       0.354616
     C       0.765612      0.682938      -0.412719
     C      -0.448739      1.353033       0.142140
     C      -1.743553      0.626339      -0.199469
     O      -1.783544     -0.650949       0.461241
     O      -1.236397     -1.586352      -0.258257
     O       2.781777     -0.496873      -0.162806
     H       1.592392      0.106015       1.436620
     H       0.886845      0.636445      -1.488836
     H      -0.374506      1.436458       1.227989
     H      -0.541797      2.369393      -0.249760
     H      -2.611147      1.164789       0.178867
     H      -1.844907      0.444686      -1.267936
     H       3.283043     -0.922361       0.534221
Rotational constants (GHz):    4.5792500    1.5738300    1.2710500
Vibrational harmonic frequencies (cm-1):
       56.7528                97.4223                108.0751
      185.1658               241.9628                299.6491
      352.1428               462.0451                539.3009
      549.7923               828.6190                865.8652
      946.9980               961.6997                986.9639
     1038.2792              1136.0127               1180.7630
     1211.3605              1235.3846               1257.8402
     1313.9456              1340.3052               1361.4416
     1392.6747              1399.1790               1473.5968
```

```
     1484.3704                1787.1973                3054.9106
     3091.7525                3103.3339                3155.9447
     3170.1119                3189.6327                3917.6516
Zero-point correction (Hartree): 0.111125

HOCHCHCH2CH2OO.Elptc
--------------------
E(UM062X/Aug-CC-pVTZ) (Hartree): -382.13968393
Electronic state : 2-A
Cartesian coordinates (Angs):
     C      -1.897069     -0.144664      -0.371056
     C      -1.056654      0.583217       0.350585
     C       0.114627      1.304085      -0.242630
     C       1.447573      0.762783       0.234917
     O       1.597683     -0.567063      -0.306902
     O       2.675606     -1.139922       0.129742
     O      -2.970820     -0.834603       0.085399
     H      -1.789832     -0.253802      -1.443022
     H      -1.197984      0.654553       1.425816
     H       0.080097      1.244268      -1.331847
     H       0.085634      2.364985       0.016705
     H       2.288937      1.353669      -0.125466
     H       1.498795      0.678604       1.320216
     H      -3.036259     -0.742095       1.040786
Rotational constants (GHz):    5.3681500    1.2172800    1.0551600
Vibrational harmonic frequencies (cm-1):
       47.1882                  74.8600                 110.7871
      204.1682                 265.0175                 334.2196
      391.4892                 446.2482                 540.5382
      567.6268                 814.9271                 863.6201
      917.8374                 988.6263                1035.2476
     1069.2262                1122.3981                1159.4625
     1215.5601                1267.2054                1288.0298
     1298.6105                1341.6350                1362.4937
     1398.3535                1414.8400                1472.9430
     1500.9427                1766.3020                3062.0597
     3082.9820                3106.9162                3140.2931
     3153.5250                3208.4551                3860.2757
Zero-point correction (Hartree): 0.111391

HOCHCHCH2CH2OO.Eltmc
--------------------
E(CCSD(T)/Aug-CC-pVTZ) (Hartree): -381.59757712
E(CCSD/Aug-CC-pVTZ) (Hartree): -381.53594843
     T1 diagnostic:  0.021541
E(MP2/Aug-CC-pVTZ) (Hartree): -381.49136426
E(MP3/Aug-CC-pVTZ) (Hartree): -381.52330142
E(PMP2/Aug-CC-pVTZ) (Hartree): -381.49452390
E(PMP3/Aug-CC-pVTZ) (Hartree): -381.52516264
E(PUHF/Aug-CC-pVTZ) (Hartree): -380.13519483
E(UHF/Aug-CC-pVTZ) (Hartree): -380.13005206
E(UM062X/Aug-CC-pVTZ) (Hartree): -382.14085582
Electronic state : 2-A
Cartesian coordinates (Angs):
     C      -2.116996      0.458740       0.023049
     C      -1.201545     -0.458753       0.304944
     C       0.215959     -0.116171       0.646310
     C       1.167619     -0.590526      -0.439314
     O       2.539002     -0.357420      -0.056058
     O       2.828865      0.907518      -0.091009
     O      -3.413943      0.237036      -0.302756
     H      -1.893836      1.518356       0.037417
     H      -1.476744     -1.509855       0.279228
     H       0.330920      0.961839       0.759748
     H       0.510763     -0.579923       1.590163
     H       1.107798     -1.667516      -0.590321
     H       0.992433     -0.071408      -1.380229
     H      -3.592948     -0.708296      -0.307352
Rotational constants (GHz):   10.0368700    0.9316200    0.9000000
Vibrational harmonic frequencies (cm-1):
       62.6193                  86.0716                 114.6904
      178.5780                 307.7151                 321.7048
      372.5639                 446.0057                 522.6093
      624.6712                 795.8463                 850.8975
      958.7976                 991.0461                1019.8069
     1068.2658                1129.2750                1160.1231
     1220.7535                1266.9190                1283.4531
     1312.2745                1329.5215                1347.5466
     1395.5665                1412.2663                1485.2413
     1499.6656                1761.8549                3064.9628
     3093.7449                3118.4546                3151.9409
     3157.1601                3205.8173                3858.7043
Zero-point correction (Hartree): 0.111578

HOCHCHCH2CH2OO.Eltmt
--------------------
E(UM062X/Aug-CC-pVTZ) (Hartree): -382.13929131
Electronic state : 2-A
Cartesian coordinates (Angs):
     C      -2.116572      0.416829       0.046261
     C      -1.191134     -0.498223       0.288145
     C       0.220217     -0.150112       0.644152
     C       1.178600     -0.580618      -0.453727
```

```
     O       2.546494     -0.334731      -0.064552
     O       2.817275      0.934757      -0.071963
     O      -3.393009      0.084359      -0.290855
     H      -1.898587      1.478277       0.110791
     H      -1.466099     -1.544455       0.212146
     H       0.326348      0.924914       0.792302
     H       0.517839     -0.642064       1.572851
     H       1.135422     -1.653914      -0.632830
     H       0.995182     -0.039785      -1.380697
     H      -3.922847      0.874692      -0.404589
Rotational constants (GHz):   10.0574900    0.9318000    0.9003200
Vibrational harmonic frequencies (cm-1):
       62.7043                88.0215                115.2441
      181.9248               265.8166                316.5343
      323.3749               385.1449                520.7013
      621.7596               796.6855                865.7763
      956.6579               970.6860               1017.8475
     1067.6172              1133.8664               1179.0186
     1212.3615              1246.3360               1283.4095
     1299.5434              1330.5167               1356.9055
     1382.7914              1407.6503               1484.8791
     1499.8352              1785.0922               3063.0106
     3094.1621              3115.4457               3156.4935
     3171.1139              3181.9716               3915.6844
Zero-point correction (Hartree): 0.111303

HOCHCHCH2CH2OO.Eltpc
~~~~~~~~~~~~~~~~~~~
E(CCSD(T)/Aug-CC-pVTZ) (Hartree): -381.59774833
E(CCSD/Aug-CC-pVTZ) (Hartree): -381.53608544
     T1 diagnostic:  0.021615
E(MP2/Aug-CC-pVTZ) (Hartree): -381.49148884
E(MP3/Aug-CC-pVTZ) (Hartree): -381.52339626
E(PMP2/Aug-CC-pVTZ) (Hartree): -381.49466624
E(PMP3/Aug-CC-pVTZ) (Hartree): -381.52527544
E(PUHF/Aug-CC-pVTZ) (Hartree): -380.13522254
E(UHF/Aug-CC-pVTZ) (Hartree): -380.13007016
E(UM062X/Aug-CC-pVTZ) (Hartree): -382.14108463
Electronic state : 2-A
Cartesian coordinates (Angs):
     C       2.234338      0.135592      -0.357583
     C       1.152266     -0.409745       0.181764
     C      -0.208548     -0.304048      -0.433368
     C      -1.139220      0.517425       0.443306
     O      -2.467277      0.557499      -0.118814
     O      -3.071055     -0.583770       0.015422
     O       3.496844      0.090426       0.134221
     H       2.198969      0.685380      -1.290008
     H       1.240777     -0.954326       1.118051
     H      -0.143183      0.158791      -1.418965
     H      -0.656921     -1.291129      -0.560283
     H      -1.221690      0.101001       1.446713
     H      -0.828505      1.559128       0.495662
     H       3.509436     -0.407433       0.957481
Rotational constants (GHz):   13.1446600    0.8826300    0.8713100
Vibrational harmonic frequencies (cm-1):
       67.8392                71.8809                132.1719
      170.9503               293.7329                332.8483
      372.3254               440.9682                536.2726
      616.7591               789.1311                849.8083
      973.1622               989.9596               1014.5884
     1068.2345              1126.4066               1158.0426
     1225.3138              1255.7702               1293.0913
     1309.0186              1331.2088               1346.1744
     1393.1945              1412.4869               1483.8683
     1498.2063              1764.3313               3068.2706
     3092.7231              3113.9544               3151.3558
     3158.2694              3205.3995               3859.9303
Zero-point correction (Hartree): 0.111557

HOCHCHCH2CH2OO.Eltpt
~~~~~~~~~~~~~~~~~~~
E(UM062X/Aug-CC-pVTZ) (Hartree): -382.13930049
Electronic state : 2-A
Cartesian coordinates (Angs):
     C      -2.230972      0.064200       0.344730
     C      -1.142923     -0.387317      -0.259035
     C       0.211479     -0.361046       0.375652
     C       1.147173      0.565479      -0.382958
     O       2.467725      0.545511       0.198395
     O       3.082314     -0.567691      -0.062484
     O      -3.453504      0.041539      -0.254464
     H      -2.198295      0.469898       1.351149
     H      -1.236164     -0.785712      -1.263260
     H       0.141500     -0.028243       1.412508
     H       0.660147     -1.356295       0.376634
     H       1.244648      0.273692      -1.427997
     H       0.830008      1.604246      -0.313275
     H      -4.122658      0.379656       0.342337
Rotational constants (GHz):   13.3164800    0.8817100    0.8703500
Vibrational harmonic frequencies (cm-1):
       68.0919                72.1152                131.6989
      167.9317               240.6208                305.5826
```

```
      330.2599                384.9810                534.3830
      612.6315                793.2149                862.2344
      970.0369                973.8711               1011.7579
     1068.5068               1129.8299               1178.0602
     1214.5548               1242.4344               1280.3932
     1305.1409               1331.0117               1354.6634
     1382.6060               1408.1982               1484.8761
     1499.3454               1785.4662               3065.4744
     3093.5087               3110.7624               3157.8435
     3168.6656               3184.8947               3916.5030
Zero-point correction (Hartree): 0.111225

HOCHCHCH2CH2OO.Elttc
~~~~~~~~~~~~~~~~~~~~
E(UM062X/Aug-CC-pVTZ) (Hartree): -382.14004222
Electronic state : 2-A
Cartesian coordinates (Angs):
     C      -2.275809      0.148690      -0.367891
     C      -1.260724      0.112279       0.484643
     C       0.071423      0.733498       0.193929
     C       1.150763     -0.325924       0.094412
     O       2.412869      0.349900      -0.093776
     O       3.395681     -0.491871      -0.180792
     O      -3.506287     -0.390315      -0.187617
     H      -2.204780      0.644611      -1.328060
     H      -1.382734     -0.396042       1.437314
     H       0.028218      1.293552      -0.740915
     H       0.348530      1.438096       0.981051
     H       1.231526     -0.919900       1.004892
     H       0.998327     -0.988116      -0.756826
     H      -3.551102     -0.825174       0.669474
Rotational constants (GHz):   13.6874400    0.8329600    0.8191700
Vibrational harmonic frequencies (cm-1):
      60.8092                 90.3699                 93.3198
     165.2775                280.7597                313.8347
     355.1919                453.9746                528.9095
     593.7630                785.7557                851.2485
     989.6390                993.0427               1029.7627
    1104.1590               1122.0018               1159.0048
    1206.0828               1269.0806               1294.2590
    1309.3283               1318.2802               1346.6675
    1397.3583               1419.6101               1490.8330
    1507.2386               1765.0976               3063.5670
    3084.8968               3108.9567               3144.2032
    3154.2420               3207.2976               3859.5147
Zero-point correction (Hartree): 0.111442

HOCHCHCH2CH2OO.Elttt
~~~~~~~~~~~~~~~~~~~~
E(UM062X/Aug-CC-pVTZ) (Hartree): -382.13833875
Electronic state : 2-A
Cartesian coordinates (Angs):
     C      -2.273429      0.105513      -0.345910
     C      -1.250519      0.154109       0.492492
     C       0.075477      0.744656       0.126087
     C       1.158404     -0.315660       0.135892
     O       2.416046      0.340116      -0.137218
     O       3.400500     -0.503981      -0.153931
     O      -3.469088     -0.443689       0.003341
     H      -2.206311      0.507793      -1.351936
     H      -1.375714     -0.260890       1.486384
     H       0.027645      1.201252      -0.863577
     H       0.354735      1.529938       0.832104
     H       1.248309     -0.804624       1.105828
     H       1.003251     -1.068940      -0.635313
     H      -4.091178     -0.375805      -0.722381
Rotational constants (GHz):   13.8484500    0.8326000    0.8185100
Vibrational harmonic frequencies (cm-1):
      57.7469                 90.3574                103.0039
     158.1623                229.2563                299.1034
     314.3737                359.8705                526.9658
     590.0482                784.7093                863.0777
     967.4995                986.9136               1029.3380
    1103.2365               1124.1121               1179.2551
    1199.0412               1244.0592               1293.4717
    1302.6613               1312.7888               1355.5095
    1382.0788               1415.5474               1491.3168
    1507.2022               1788.3995               3061.7607
    3086.0660               3106.1688               3145.2990
    3169.8118               3184.8758               3916.9350
Zero-point correction (Hartree): 0.111015


TS.HOCHCHCH2CH2OO.cycHOCHCHCH2CH2OO.Ec.b
~~~~~~~~~~~~~~~~~~~~~~~~~~~~~~~~~~~~~~~
E(UM062X/Aug-CC-pVTZ) (Hartree): -382.10724016
Electronic state : 2-A
Cartesian coordinates (Angs):
     C       1.217486      0.279742       0.364305
     C       0.341773      1.097742      -0.320596
     C      -1.027092      1.246613       0.229747
     C      -1.844235     -0.064593      -0.045476
     O      -0.992753     -1.095210      -0.485394
```

```
     O       0.005605     -1.255843       0.439528
     O       2.391428     -0.139894      -0.136307
     H       1.213890      0.247341       1.445253
     H       0.518331      1.286381      -1.373712
     H      -0.974047      1.394725       1.307886
     H      -1.549034      2.096788      -0.204608
     H      -2.361650     -0.370132       0.865237
     H      -2.563582      0.066706      -0.852405
     H       2.354263     -0.151259      -1.098142
Rotational constants (GHz):    4.7724200    2.2768000    1.7445200
Vibrational harmonic frequencies (cm-1):
     i685.0331                79.5739                248.9258
      266.7727               368.0530                402.7393
      421.1075               441.7393                542.8748
      651.4000               781.5885                819.2272
      891.5753               903.7398                977.2995
     1039.4828              1100.8839               1133.4693
     1159.3361              1225.4296               1268.0599
     1279.5097              1296.2485               1321.3174
     1371.2509              1405.3781               1487.8162
     1504.3742              1563.6009               3068.4393
     3087.8182              3127.3766               3146.3952
     3173.8162              3211.4429               3854.2426
Zero-point correction (Hartree): 0.110770

TS.HOCHCHCH2CH2OO.cycHOCHCHCH2CH2OO.Ec
~~~~~~~~~~~~~~~~~~~~~~~~~~~~~~~~~~~~~
E(CCSD(T)/Aug-CC-pVTZ) (Hartree): -381.57644612
E(CCSD/Aug-CC-pVTZ) (Hartree): -381.50999223
     T1 diagnostic:  0.028421
E(MP2/Aug-CC-pVTZ) (Hartree): -381.46077651
E(MP3/Aug-CC-pVTZ) (Hartree): -381.49072084
E(PMP2/Aug-CC-pVTZ) (Hartree): -381.47834524
E(PMP3/Aug-CC-pVTZ) (Hartree): -381.50387730
E(PUHF/Aug-CC-pVTZ) (Hartree): -380.10921509
E(UHF/Aug-CC-pVTZ) (Hartree): -380.08883155
E(UM062X/Aug-CC-pVTZ) (Hartree): -382.11687402
Electronic state : 2-A
Cartesian coordinates (Angs):
     C       1.155879      0.174702       0.396882
     C       0.378016      1.143937      -0.200909
     C      -1.050426      1.263609       0.187134
     C      -1.791931     -0.024462      -0.246750
     O      -1.122666     -1.127408       0.316294
     O       0.084327     -1.281446      -0.319510
     O       2.404324     -0.122337       0.004603
     H       0.959046     -0.158255       1.406366
     H       0.705464      1.550892      -1.151471
     H      -1.160467      1.353572       1.268525
     H      -1.521335      2.128324      -0.278811
     H      -2.806017     -0.050121       0.151243
     H      -1.807149     -0.117482      -1.333491
     H       2.553350      0.195881      -0.891592
Rotational constants (GHz):    4.8099700    2.3018300    1.7081900
Vibrational harmonic frequencies (cm-1):
     i612.2148              155.8931                259.5245
      308.9601              339.9696                400.6085
      432.1901              440.3496                541.4172
      590.7723              747.5627                862.9943
      933.5439              972.9901                987.3404
     1024.8407             1090.4612               1128.1823
     1165.3542             1214.9112               1262.3010
     1277.6477             1318.6330               1327.6199
     1367.9829             1403.7461               1484.0993
     1488.6522             1571.1142               3073.6098
     3076.3357             3128.1857               3139.6010
     3172.6958             3222.8911               3853.6386
Zero-point correction (Hartree): 0.111099

TS.HOCHCHCH2CH2OO.cycHOCHCHCH2CH2OO.Et.b
~~~~~~~~~~~~~~~~~~~~~~~~~~~~~~~~~~~~~~~
E(UM062X/Aug-CC-pVTZ) (Hartree): -382.10677807
Electronic state : 2-A
Cartesian coordinates (Angs):
     C       1.214263      0.289700       0.332681
     C       0.326195      1.114648      -0.316324
     C      -1.033088      1.235463       0.261697
     C      -1.845033     -0.070021      -0.053565
     O      -0.991057     -1.100931      -0.491333
     O       0.004584     -1.260867       0.433509
     O       2.353683     -0.063418      -0.294347
     H       1.212212      0.218401       1.414086
     H       0.498114      1.324250      -1.363766
     H      -0.967915      1.341177       1.344097
     H      -1.571161      2.095330      -0.132183
     H      -2.385987     -0.385297       0.840440
     H      -2.544451      0.076333      -0.875285
     H       2.847487     -0.687210       0.243044
Rotational constants (GHz):    4.7508600    2.2809700    1.7416400
Vibrational harmonic frequencies (cm-1):
     i672.3229               91.4225                248.4742
      275.6830              318.7083                368.7678
      416.8751              431.7870                540.0841
```

```
      655.4871                  795.1183                  823.1929
      885.9184                  903.5206                  972.9894
     1036.2457                 1094.7108                 1133.0696
     1177.5571                 1217.2911                 1251.4219
     1276.5256                 1297.2793                 1318.4758
     1357.5098                 1390.8892                 1487.3773
     1503.7334                 1588.4282                 3065.0986
     3087.2872                 3126.5789                 3145.9153
     3174.3288                 3205.5509                 3893.7939
Zero-point correction (Hartree): 0.110621

TS.HOCHCHCH2CH2OO.cycHOCHCHCH2CH2OO.Et
--------------------------------------
E(CCSD(T)/Aug-CC-pVTZ) (Hartree): -381.57685956
E(CCSD/Aug-CC-pVTZ) (Hartree): -381.51053770
     T1 diagnostic:  0.028927
E(MP2/Aug-CC-pVTZ) (Hartree): -381.46051972
E(MP3/Aug-CC-pVTZ) (Hartree): -381.49081210
E(PMP2/Aug-CC-pVTZ) (Hartree): -381.47833678
E(PMP3/Aug-CC-pVTZ) (Hartree): -381.50423593
E(PUHF/Aug-CC-pVTZ) (Hartree): -380.11048561
E(UHF/Aug-CC-pVTZ) (Hartree): -380.08990202
E(UM062X/Aug-CC-pVTZ) (Hartree): -382.11743003
Electronic state : 2-A
Cartesian coordinates (Angs):
     C       1.147043      0.214569       0.362170
     C       0.350660      1.166516      -0.223427
     C      -1.071962      1.255057       0.192903
     C      -1.791056     -0.052670      -0.223763
     O      -1.091404     -1.144407       0.327652
     O       0.098491     -1.285160      -0.343113
     O       2.388067      0.005591      -0.115672
     H       0.939296     -0.138660       1.365124
     H       0.673943      1.583833      -1.167781
     H      -1.167356      1.347532       1.275518
     H      -1.573728      2.104419      -0.268728
     H      -2.797301     -0.098079       0.192044
     H      -1.822870     -0.148961      -1.309517
     H       2.778671     -0.759101       0.315106
Rotational constants (GHz):    4.7651800    2.3156100    1.7036200
Vibrational harmonic frequencies (cm-1):
     i590.6847                  159.4186                  269.6552
      294.5891                  342.8123                  374.2063
      399.9901                  435.6672                  538.4892
      595.4815                  773.5039                  860.5234
      934.0770                  971.0382                  982.5272
     1020.8763                 1084.1233                 1128.2875
     1182.8838                 1208.9500                 1256.2854
     1265.7570                 1319.9350                 1332.9792
     1358.1819                 1384.0530                 1483.8822
     1488.5767                 1600.3175                 3075.6803
     3076.1514                 3129.3890                 3140.5615
     3185.3172                 3208.4006                 3884.7204
Zero-point correction (Hartree): 0.111054


################################################################################
Z-HOCH=CHCH2CH2OO ring closure
################################################################################

HOCHCHCH2CH2OO.Zcptt
--------------------
E(UM062X/Aug-CC-pVTZ) (Hartree): -382.13711336
Electronic state : 2-A
Cartesian coordinates (Angs):
     C      -1.776794     -0.554659      -0.256263
     C      -1.493800      0.732244      -0.393931
     C      -0.341202      1.507229       0.179422
     C       0.865022      0.702094       0.611509
     O       1.362636      0.001504      -0.550034
     O       2.306136     -0.829333      -0.236274
     O      -1.045956     -1.415474       0.509502
     H      -2.641959     -0.983117      -0.748092
     H      -2.189973      1.293835      -1.001782
     H      -0.017457      2.242074      -0.560669
     H      -0.672659      2.085016       1.047217
     H       1.667247      1.352616       0.959066
     H       0.637097     -0.043564       1.366069
     H      -1.284185     -2.321888       0.308221
Rotational constants (GHz):    3.9278800    2.0404800    1.5310900
Vibrational harmonic frequencies (cm-1):
       45.9236                   64.9179                  135.0800
      247.0910                  265.4998                  269.3807
      385.3755                  449.8302                  535.0364
      742.0012                  759.3706                  851.3365
      877.4570                  975.0962                 1014.7206
     1055.0647                 1080.1995                 1130.9052
     1232.4978                 1259.8112                 1284.3392
     1303.6282                 1317.0023                 1385.4671
     1420.2666                 1446.4422                 1472.3424
     1505.9929                 1788.8382                 3052.2248
     3086.2696                 3096.1607                 3178.5278
     3182.7917                 3214.4693                 3910.7664
```

```
Zero-point correction (Hartree): 0.111681

HOCHCHCH2CH2OO.Zctpt
~~~~~~~~~~~~~~~~~~~
E(UM062X/Aug-CC-pVTZ) (Hartree): -382.13858979
Electronic state : 2-A
Cartesian coordinates (Angs):
     C       2.258555      0.186620      -0.159502
     C       1.324382      1.115087      -0.020896
     C      -0.138910      0.947789       0.264829
     C      -0.670348     -0.470054       0.176316
     O      -2.097451     -0.455162       0.413555
     O      -2.742614      0.049252      -0.592871
     O       2.019007     -1.155385      -0.046563
     H       3.284895      0.462810      -0.367898
     H       1.671553      2.134578      -0.122294
     H      -0.365199      1.344959       1.258467
     H      -0.708414      1.553057      -0.443552
     H      -0.503577     -0.913031      -0.802703
     H      -0.273150     -1.120533       0.949555
     H       2.820279     -1.648133      -0.229019
Rotational constants (GHz):    6.2539000    1.3314300    1.1658700
Vibrational harmonic frequencies (cm-1):
       21.5428                88.9392                136.3872
      180.6831               222.3307                282.7500
      372.7885               454.7840                567.1876
      745.0536               765.6149                806.7722
      929.2624               975.1060                977.1411
     1054.0019              1098.4514               1128.5862
     1236.7695              1247.2451               1290.1310
     1310.8892              1328.5947               1348.8740
     1422.8371              1441.6560               1484.8573
     1496.2722              1791.5757               3050.7558
     3091.2172              3117.6643               3185.2642
     3187.6863              3213.3065               3917.4230
Zero-point correction (Hartree): 0.111563

HOCHCHCH2CH2OO.Zcttc
~~~~~~~~~~~~~~~~~~~
E(UM062X/Aug-CC-pVTZ) (Hartree): -382.13442233
Point group : CS
Electronic state : 2-A"
Cartesian coordinates (Angs):
     C      -0.377205     -2.307271       0.000000
     C       0.796415     -1.684238       0.000000
     C       1.154718     -0.224566       0.000000
     C      -0.000000      0.750786       0.000000
     O       0.571304      2.076013       0.000000
     O      -0.349166      2.989418       0.000000
     O      -1.641430     -1.809192       0.000000
     H      -0.408505     -3.388123       0.000000
     H       1.648626     -2.350758       0.000000
     H       1.777089     -0.010247       0.872495
     H       1.777089     -0.010247      -0.872495
     H      -0.617134      0.675760      -0.897332
     H      -0.617134      0.675760       0.897332
     H      -1.649264     -0.850327       0.000000
Rotational constants (GHz):    5.8449000    1.2754700    1.0608800
Vibrational harmonic frequencies (cm-1):
       43.1149 (  A")            81.4073 (  A")          129.0539 (  A')
      149.1265 (  A")           268.3374 (  A')          311.4776 (  A")
      379.5594 (  A')           482.1220 (  A")          508.2954 (  A')
      751.1183 (  A")           767.0594 (  A')          814.7686 (  A")
      913.8562 (  A')          1003.6698 (  A")         1031.8930 (  A')
     1073.4671 (  A')          1088.9370 (  A")         1145.5511 (  A')
     1230.7542 (  A')          1253.1947 (  A")         1290.3416 (  A')
     1317.5934 (  A")          1342.4242 (  A')         1362.1290 (  A')
     1427.3542 (  A')          1444.3698 (  A')         1497.6006 (  A')
     1532.5811 (  A')          1767.2677 (  A')         3052.1786 (  A')
     3061.3874 (  A')          3082.0577 (  A")         3121.4614 (  A")
     3196.9164 (  A')          3224.9995 (  A')         3910.9139 (  A')
Zero-point correction (Hartree): 0.111763

HOCHCHCH2CH2OO.Zcttt
~~~~~~~~~~~~~~~~~~~
E(UM062X/Aug-CC-pVTZ) (Hartree): -382.13769930
Point group : CS
Electronic state : 2-A"
Cartesian coordinates (Angs):
     C      -0.410643     -2.264632       0.000000
     C       0.790060     -1.705198       0.000000
     C       1.158136     -0.250913       0.000000
     C       0.000000      0.723795       0.000000
     O       0.595745      2.042813       0.000000
     O      -0.306243      2.973965       0.000000
     O      -1.579759     -1.557348       0.000000
     H      -0.514846     -3.342783       0.000000
     H       1.619897     -2.399009       0.000000
     H       1.783976     -0.042358       0.871782
     H       1.783976     -0.042358      -0.871782
     H      -0.624334      0.644558      -0.886550
     H      -0.624334      0.644558       0.886550
     H      -2.327588     -2.156356       0.000000
```

```
Rotational constants (GHz):    5.8453500    1.3275400    1.0964700
Vibrational harmonic frequencies (cm-1):
       17.2363 (  A")            78.2270 (  A")           128.1975 (  A")
      138.3477 (  A')           253.4598 (  A')           270.7581 (  A")
      380.3751 (  A')           456.1568 (  A")           510.4761 (  A')
      745.6136 (  A")           770.0082 (  A')           803.5707 (  A")
      930.3358 (  A')           978.1798 (  A")          1016.3361 (  A')
     1069.1464 (  A')          1076.6634 (  A")          1144.0290 (  A')
     1221.3629 (  A")          1252.0845 (  A')          1299.7341 (  A')
     1314.2764 (  A')          1315.9130 (  A")          1340.0882 (  A')
     1428.7474 (  A')          1443.9492 (  A')          1493.9967 (  A')
     1503.7163 (  A')          1792.5665 (  A')          3051.8416 (  A')
     3079.8236 (  A")          3111.9295 (  A')          3171.9629 (  A")
     3187.6752 (  A')          3213.1564 (  A')          3916.7245 (  A')
Zero-point correction (Hartree): 0.111418

HOCHCHCH2CH2OO.Zgpmc
--------------------
E(UM062X/Aug-CC-pVTZ) (Hartree): -382.14139996
Electronic state : 2-A
Cartesian coordinates (Angs):
     C      -1.737468     -0.146900       0.370704
     C      -0.997116      0.936025       0.587248
     C       0.077260      1.427802      -0.337557
     C       1.434514      0.783067      -0.094846
     O       1.333949     -0.627424      -0.393721
     O       1.297258     -1.365867       0.677108
     O      -1.644538     -0.999462      -0.676321
     H      -2.531448     -0.435613       1.045857
     H      -1.192722      1.491430       1.493099
     H      -0.201334      1.255270      -1.380993
     H       0.200699      2.505915      -0.228546
     H       2.192512      1.171852      -0.773936
     H       1.761229      0.867044       0.938717
     H      -0.785432     -0.913843      -1.104020
Rotational constants (GHz):    3.6140200    2.2889700    1.7079300
Vibrational harmonic frequencies (cm-1):
       58.2574                93.1132                123.1605
      232.3401               265.0035                361.0549
      456.4881               524.6469                582.7744
      657.9690               761.3718                837.5371
      919.5851               981.6888                992.3137
     1035.9988              1083.2694               1141.7043
     1223.1119              1228.6007               1276.7832
     1312.6929              1350.0219               1370.6682
     1383.0603              1438.3066               1483.6831
     1488.0368              1742.8540               3054.4239
     3091.7480              3110.0397               3163.6564
     3210.9156              3231.1092               3838.7502
Zero-point correction (Hartree): 0.111873

HOCHCHCH2CH2OO.Zgppt
--------------------
E(UM062X/Aug-CC-pVTZ) (Hartree): -382.13954204
Electronic state : 2-A
Cartesian coordinates (Angs):
     C       1.914859      0.090571      -0.431387
     C       0.985666      1.025018      -0.298066
     C      -0.116046      0.973688       0.714388
     C      -1.485281      0.843125       0.071006
     O      -1.596557     -0.397079      -0.661614
     O      -1.635879     -1.415766       0.141001
     O       1.969504     -0.998001       0.385586
     H       2.684108      0.156570      -1.191408
     H       1.022074      1.860050      -0.985306
     H       0.028552      0.133836       1.392152
     H      -0.126916      1.885411       1.316826
     H      -2.284305      0.853205       0.810695
     H      -1.659541      1.610620      -0.682013
     H       2.644287     -1.607334       0.083620
Rotational constants (GHz):    4.1422700    1.8180600    1.4550000
Vibrational harmonic frequencies (cm-1):
       28.3230                59.2797                144.7891
      214.5535               252.6226                295.0937
      378.7974               519.7864                568.4510
      668.2856               766.4669                861.6718
      890.9170               973.7082                995.9278
     1047.5808              1076.0585               1148.4667
     1215.0584              1257.7825               1277.3019
     1296.0053              1313.5432               1357.1520
     1398.7465              1444.7125               1481.0926
     1490.7725              1785.2217               3064.5679
     3089.8000              3132.9715               3151.1366
     3184.5111              3210.8037               3919.8909
Zero-point correction (Hartree): 0.111543

HOCHCHCH2CH2OO.Zgptc
--------------------
E(UM062X/Aug-CC-pVTZ) (Hartree): -382.14241976
Electronic state : 2-A
Cartesian coordinates (Angs):
     C       1.897914     -0.385648      -0.365766
     C       1.383603      0.840262      -0.401496
```

```
     C       0.264452      1.332044       0.474141
     C      -1.122747      0.977069      -0.024651
     O      -1.262451     -0.455486       0.137606
     O      -2.386318     -0.899974      -0.330991
     O       1.496806     -1.417339       0.410545
     H       2.743478     -0.659416      -0.982587
     H       1.826601      1.532954      -1.102642
     H       0.369226      0.941970       1.491084
     H       0.315083      2.417337       0.557387
     H      -1.913850      1.441070       0.563359
     H      -1.261010      1.196692      -1.081776
     H       0.596840     -1.270578       0.724538
Rotational constants (GHz):    4.0906500    1.8775300    1.4146100
Vibrational harmonic frequencies (cm-1):
       68.9838                87.6903               136.6126
      229.9296               265.9066               335.7055
      440.9411               503.4870               609.9387
      656.8277               765.8418               844.7707
      899.0257               994.9890              1024.7678
     1053.7330              1087.6190              1138.3086
     1222.6732              1254.0154              1290.0043
     1295.5010              1353.6839              1378.2692
     1396.6054              1439.7699              1481.4740
     1500.2293              1746.2514              3053.1188
     3087.8198              3118.3686              3150.7968
     3205.2596              3225.7012              3823.1965
Zero-point correction (Hartree): 0.112013

HOCHCHCH2CH2OO.Zgtmt
~~~~~~~~~~~~~~~~~~~
E(UM062X/Aug-CC-pVTZ) (Hartree): -382.14019926
Electronic state : 2-A
Cartesian coordinates (Angs):
     C       2.270326     -0.081809       0.116109
     C       1.368345     -1.008545      -0.173754
     C      -0.033049     -0.679805      -0.596835
     C      -0.912228     -0.443690       0.621475
     O      -2.280375     -0.204704       0.228308
     O      -2.418909      0.964599      -0.318224
     O       1.972686      1.245837       0.034722
     H       3.276542     -0.331255       0.429921
     H       1.665202     -2.041996      -0.067885
     H      -0.047455      0.226657      -1.201609
     H      -0.455768     -1.491488      -1.188285
     H      -0.964202     -1.321549       1.263055
     H      -0.572122      0.420624       1.189408
     H       2.750225      1.776249       0.214973
Rotational constants (GHz):    5.5989900    1.3520200    1.1808600
Vibrational harmonic frequencies (cm-1):
       43.3704                65.7348               120.2632
      202.9634               257.3635               286.3124
      355.0370               527.0481               572.4761
      679.5690               764.8308               817.1081
      959.4980               972.6762               985.8933
     1066.5337              1079.6370              1137.5424
     1223.2900              1259.5267              1290.9339
     1294.5599              1306.4462              1335.8659
     1399.4687              1434.0395              1485.8825
     1502.2942              1772.3973              3082.3660
     3098.7856              3130.6060              3162.4014
     3191.4227              3226.1186              3915.6145
Zero-point correction (Hartree): 0.111644

HOCHCHCH2CH2OO.Zgtpc
~~~~~~~~~~~~~~~~~~~
E(UM062X/Aug-CC-pVTZ) (Hartree): -382.14075752
Electronic state : 2-A
Cartesian coordinates (Angs):
     C      -2.374942      0.337594       0.155917
     C      -1.213663      0.969303       0.026282
     C       0.051787      0.353347      -0.491740
     C       0.940906     -0.095044       0.658214
     O       2.162758     -0.680760       0.162951
     O       2.948064      0.222433      -0.339989
     O      -2.645564     -0.950933      -0.168538
     H      -3.253375      0.830196       0.548466
     H      -1.180539      2.000982       0.346920
     H      -0.142237     -0.503852      -1.142065
     H       0.609705      1.072998      -1.090594
     H       1.211162      0.739468       1.303249
     H       0.474510     -0.883184       1.247021
     H      -1.865818     -1.373723      -0.540433
Rotational constants (GHz):    7.9091100    1.1060900    1.0406700
Vibrational harmonic frequencies (cm-1):
       27.6412                67.0647               124.0091
      202.9161               276.6980               353.9663
      400.0936               544.5398               578.0624
      659.8564               773.9056               803.7664
      971.0301               980.5378               995.6468
     1062.8364              1078.2751              1139.3897
     1219.6081              1248.4100              1274.1562
     1303.1465              1327.5545              1348.3426
     1397.1146              1436.2636              1488.9787
```

```
     1512.6791                1754.1465                3055.7317
     3094.2064                3114.3684                3156.7534
     3212.0556                3233.4812                3862.2667
Zero-point correction (Hartree): 0.111811

HOCHCHCH2CH2OO.Zgtpt
--------------------
E(UM062X/Aug-CC-pVTZ) (Hartree): -382.14074793
Electronic state : 2-A
Cartesian coordinates (Angs):
     C      -2.324227      0.311436       0.177412
     C      -1.219788      1.035274       0.068940
     C       0.059043      0.494489      -0.498552
     C       0.866340     -0.199202       0.587154
     O       2.103565     -0.717299       0.053086
     O       2.945104      0.237649      -0.200539
     O      -2.363701     -0.988806      -0.234841
     H      -3.239998      0.710018       0.596257
     H      -1.251137      2.050569       0.437250
     H      -0.153083     -0.226551      -1.288160
     H       0.664985      1.295553      -0.919357
     H       1.120232      0.478128       1.401064
     H       0.342422     -1.072435       0.970777
     H      -3.251384     -1.339617      -0.149199
Rotational constants (GHz):    7.5430100    1.1750500    1.0826100
Vibrational harmonic frequencies (cm-1):
       24.4640                  68.1809                 125.1362
      203.0655                 252.2195                 270.6904
      363.9977                 526.6943                 578.7486
      676.4526                 766.1211                 809.5074
      966.7978                 974.4646                 988.3892
     1065.2591                1078.1403                1135.2163
     1225.4347                1262.0164                1288.1527
     1294.5643                1310.5307                1334.8408
     1397.7532                1434.8279                1485.8232
     1501.1418                1774.3630                3082.8514
     3097.4074                3132.3512                3162.7554
     3193.8803                3228.2664                3916.4641
Zero-point correction (Hartree): 0.111623

HOCHCHCH2CH2OO.Zgttc
--------------------
E(UM062X/Aug-CC-pVTZ) (Hartree): -382.13967776
Electronic state : 2-A
Cartesian coordinates (Angs):
     C       2.398795      0.120656      -0.319230
     C       1.388901      0.958388      -0.113563
     C       0.123169      0.616565       0.617809
     C      -0.960737      0.190896      -0.354749
     O      -2.151912     -0.090414       0.411191
     O      -3.129570     -0.472234      -0.351222
     O       2.490714     -1.166102       0.096813
     H       3.285422      0.415956      -0.862452
     H       1.484300      1.951272      -0.529376
     H       0.277657     -0.180984       1.349411
     H      -0.228776      1.479200       1.183930
     H      -1.203033      0.978332      -1.067333
     H      -0.693941     -0.714815      -0.898969
     H       1.703757     -1.418004       0.588932
Rotational constants (GHz):    7.1967100    1.0749200    1.0053600
Vibrational harmonic frequencies (cm-1):
       27.6140                  75.3062                 103.2976
      164.6930                 279.9752                 327.4172
      409.5551                 486.7181                 584.7638
      659.6895                 772.5865                 798.5818
      963.9454                 998.3189                1023.3267
     1066.5952                1102.6237                1135.4684
     1203.3977                1251.5210                1290.0301
     1301.4801                1310.1920                1349.7321
     1403.9103                1437.3067                1501.7698
     1515.9947                1754.9348                3056.6056
     3086.3611                3107.6039                3144.8072
     3213.9386                3234.4311                3863.8149
Zero-point correction (Hartree): 0.111649

HOCHCHCH2CH2OO.Zgttt
--------------------
E(UM062X/Aug-CC-pVTZ) (Hartree): -382.13973051
Electronic state : 2-A
Cartesian coordinates (Angs):
     C       2.351439      0.076127      -0.312571
     C       1.403691      0.990183      -0.166351
     C       0.127070      0.732235       0.579489
     C      -0.917596      0.150776      -0.353388
     O      -2.130330     -0.040952       0.408884
     O      -3.082366     -0.527365      -0.325056
     O       2.223606     -1.171407       0.223381
     H       3.264418      0.272205      -0.861180
     H       1.560642      1.950948      -0.635060
     H       0.303140      0.027431       1.391986
     H      -0.254728      1.656223       1.013054
     H      -1.154796      0.818428      -1.180964
     H      -0.613335     -0.819983      -0.742173
```

```
     H       3.019754     -1.683391       0.073604
Rotational constants (GHz):    6.8219700    1.1327600    1.0449100
Vibrational harmonic frequencies (cm-1):
       17.7531                  75.6068                 100.6331
      163.6008                 251.6023                 256.2517
      357.1504                 470.8270                 578.0969
      671.1409                 764.7380                 804.8320
      967.3141                 972.8733                1022.0913
     1068.3820                1103.5542                1130.0493
     1208.6234                1269.6215                1292.2993
     1293.7736                1312.5331                1316.4638
     1403.7061                1435.9979                1494.8269
     1505.7502                1776.5340                3080.9903
     3090.6090                3125.2729                3151.1963
     3192.8048                3228.0659                3916.2471
Zero-point correction (Hartree): 0.111338

HOCHCHCH2CH2OO.Zlmmc
~~~~~~~~~~~~~~~~~~~
E(UM062X/Aug-CC-pVTZ) (Hartree): -382.13994056
Electronic state : 2-A
Cartesian coordinates (Angs):
     C       2.143768     -0.664679       0.139343
     C       0.823500     -0.626813       0.007766
     C       0.009027      0.560010      -0.410802
     C      -1.165145      0.807557       0.521676
     O      -2.073223     -0.316307       0.501905
     O      -2.704934     -0.391193      -0.629406
     O       3.028093      0.339703      -0.091022
     H       2.655945     -1.560534       0.461000
     H       0.286885     -1.541015       0.221674
     H       0.598678      1.479894      -0.427379
     H      -0.393321      0.426727      -1.417786
     H      -0.850580      0.878497       1.561091
     H      -1.737194      1.687549       0.232840
     H       2.573202      1.114817      -0.431159
Rotational constants (GHz):    8.3236200    1.1198900    1.0759200
Vibrational harmonic frequencies (cm-1):
       17.6350                  67.8239                 141.9868
      214.7837                 252.1685                 318.5315
      428.7667                 524.9213                 588.2432
      647.9435                 778.0323                 823.9482
      899.4037                 997.0807                1004.6641
     1043.3525                1106.6705                1128.8582
     1219.1224                1238.5768                1279.6884
     1305.2664                1337.6068                1369.0230
     1397.5003                1441.7449                1472.6402
     1491.9527                1760.7025                3057.5479
     3090.4578                3101.2578                3159.9774
     3209.5933                3231.4405                3876.0568
Zero-point correction (Hartree): 0.111687

HOCHCHCH2CH2OO.Zlmmt
~~~~~~~~~~~~~~~~~~~
E(UM062X/Aug-CC-pVTZ) (Hartree): -382.14069596
Electronic state : 2-A
Cartesian coordinates (Angs):
     C      -2.088309     -0.661230      -0.159614
     C      -0.799558     -0.727793       0.137412
     C       0.004714      0.427704       0.647944
     C       1.058514      0.886017      -0.344729
     O       1.993842     -0.180062      -0.630865
     O       2.748805     -0.433773       0.393502
     O      -2.807425      0.491902      -0.019341
     H      -2.635411     -1.519816      -0.529306
     H      -0.303212     -1.676494      -0.011978
     H      -0.647327      1.274451       0.860453
     H       0.514923      0.159490       1.574692
     H       0.624742      1.125067      -1.313747
     H       1.637611      1.726756       0.033916
     H      -3.725278      0.337827      -0.246486
Rotational constants (GHz):    8.0364600    1.1756500    1.1218800
Vibrational harmonic frequencies (cm-1):
       23.9377                  62.4069                 135.4223
      205.8432                 253.4339                 279.2227
      389.6089                 524.3234                 602.4719
      656.0122                 778.7954                 827.2330
      890.9544                 976.7741                1004.8483
     1048.0315                1099.1372                1132.7352
     1211.3681                1247.2811                1294.7766
     1300.3257                1305.2226                1357.3751
     1392.5991                1444.6908                1480.8993
     1489.5894                1781.4930                3077.5404
     3094.8937                3130.4073                3159.1728
     3191.1439                3224.0324                3920.0462
Zero-point correction (Hartree): 0.111617

HOCHCHCH2CH2OO.Zlmpc
~~~~~~~~~~~~~~~~~~~
E(UM062X/Aug-CC-pVTZ) (Hartree): -382.13868808
Electronic state : 2-A
Cartesian coordinates (Angs):
     C      -1.989705     -0.744530       0.029943
```

```
     C      -0.720256     -0.485431       0.318009
     C      -0.087986      0.872455       0.366130
     C       1.236003      0.929434      -0.382633
     O       2.209234      0.096137       0.280618
     O       2.301386     -1.081886      -0.259005
     O      -2.973361      0.146858      -0.259003
     H      -2.368788     -1.756248       0.000843
     H      -0.087874     -1.335139       0.534889
     H      -0.728776      1.638039      -0.079650
     H       0.094512      1.182833       1.398414
     H       1.147655      0.572355      -1.406187
     H       1.661348      1.931503      -0.357447
     H      -2.644486      1.046223      -0.180442
Rotational constants (GHz):    6.7689600    1.2445200    1.1083900
Vibrational harmonic frequencies (cm-1):
       18.0344                  91.5867                 105.7143
      226.4445                 232.0717                 322.9611
      433.7305                 515.3716                 568.8543
      651.4993                 779.4896                 844.9060
      878.1583                 999.1262                1017.5783
     1051.9170                1093.4299                1129.7210
     1230.1992                1236.6756                1271.0215
     1318.5707                1345.2177                1372.6220
     1390.8427                1445.6145                1469.7737
     1485.7653                1760.8773                3047.9076
     3082.0069                3098.8408                3163.8554
     3211.9308                3234.1030                3877.2726
Zero-point correction (Hartree): 0.111639

HOCHCHCH2CH2OO.Zlmpt
--------------------
E(UM062X/Aug-CC-pVTZ) (Hartree): -382.13978773
Electronic state : 2-A
Cartesian coordinates (Angs):
     C      -1.922704     -0.708652       0.104527
     C      -0.703461     -0.461169       0.557734
     C      -0.057498      0.888661       0.521306
     C       1.167248      0.936171      -0.379521
     O       2.204704      0.079601       0.144661
     O       2.144685     -1.121019      -0.347727
     O      -2.709907      0.267767      -0.438055
     H      -2.355496     -1.700688       0.142598
     H      -0.144789     -1.293540       0.961654
     H      -0.767207      1.631260       0.156524
     H       0.247172      1.192543       1.525260
     H       0.948198      0.597554      -1.389685
     H       1.610516      1.930687      -0.392956
     H      -3.555761     -0.098666      -0.698706
Rotational constants (GHz):    6.1146800    1.3366200    1.2016300
Vibrational harmonic frequencies (cm-1):
       27.3716                  88.2057                 114.5263
      221.3444                 238.6604                 267.6976
      403.9375                 513.5193                 587.8196
      654.3555                 781.7969                 849.4386
      877.1053                 977.9788                1013.9296
     1054.9938                1090.2377                1130.0488
     1216.4038                1236.8401                1291.6605
     1297.7336                1321.4059                1361.5667
     1385.6273                1446.8172                1479.1669
     1485.9362                1781.7754                3066.5438
     3096.1160                3123.3747                3162.6365
     3192.2612                3226.0934                3921.1846
Zero-point correction (Hartree): 0.111599

HOCHCHCH2CH2OO.Zlmtc
--------------------
E(UM062X/Aug-CC-pVTZ) (Hartree): -382.13905289
Electronic state : 2-A
Cartesian coordinates (Angs):
     C      -2.192234     -0.718371      -0.080291
     C      -0.903735     -0.591983       0.212102
     C      -0.170168      0.700361       0.418640
     C       1.165032      0.721580      -0.299271
     O       1.997363     -0.285070       0.318060
     O       3.143934     -0.386438      -0.278970
     O      -3.107001      0.273427      -0.230218
     H      -2.647185     -1.686944      -0.232436
     H      -0.333417     -1.505117       0.311545
     H      -0.739251      1.555554       0.046180
     H       0.009899      0.884330       1.481313
     H       1.071934      0.464778      -1.353488
     H       1.680731      1.674843      -0.191820
     H      -2.710451      1.127670      -0.039355
Rotational constants (GHz):    9.7604000    1.0288300    0.9728300
Vibrational harmonic frequencies (cm-1):
       19.6535                  66.5428                 120.1996
      217.3154                 241.8543                 313.8582
      388.7097                 501.0476                 578.1024
      661.9453                 779.6506                 823.0225
      908.1268                 998.9615                1044.1810
     1051.8555                1090.0733                1136.9804
     1229.3177                1236.2048                1287.8689
     1296.4890                1335.1353                1372.6237
```

```
     1400.6148                1444.0866                1469.3469
     1501.9053                1759.4537                3050.8456
     3083.3175                3094.3059                3148.6704
     3211.1193                3233.2802                3875.4610
Zero-point correction (Hartree): 0.111567

HOCHCHCH2CH2OO.Zlmtt
~~~~~~~~~~~~~~~~~~~
E(UM062X/Aug-CC-pVTZ) (Hartree): -382.14001114
Electronic state : 2-A
Cartesian coordinates (Angs):
     C      -2.129890     -0.693101      -0.078516
     C      -0.912971     -0.635025       0.440602
     C      -0.162846      0.640650       0.675647
     C       1.084324      0.746825      -0.178450
     O       1.976008     -0.318638       0.223395
     O       3.051639     -0.340873      -0.499865
     O      -2.819622      0.428371      -0.441076
     H      -2.637773     -1.636103      -0.239607
     H      -0.434511     -1.570323       0.694454
     H      -0.799649      1.494655       0.448190
     H       0.129922      0.721365       1.724899
     H       0.872470      0.609029      -1.237642
     H       1.616475      1.684755      -0.024412
     H      -3.682831      0.189645      -0.781210
Rotational constants (GHz):    8.1761600    1.0884600    1.0485000
Vibrational harmonic frequencies (cm-1):
       23.2548                  68.7763                 118.9651
      204.1627                 245.2082                 274.0911
      350.5013                 480.3196                 602.0876
      655.5972                 780.3875                 824.4920
      907.0490                 976.6682                1041.0311
     1052.1215                1085.7309                1138.5377
     1217.7992                1245.1212                1293.7441
     1300.0195                1304.5116                1356.4493
     1395.4060                1446.1590                1480.4572
     1500.4784                1781.5388                3067.6293
     3086.9684                3129.9267                3147.0592
     3191.7444                3226.1869                3920.6148
Zero-point correction (Hartree): 0.111450

HOCHCHCH2CH2OO.Zlpmt
~~~~~~~~~~~~~~~~~~~
E(UM062X/Aug-CC-pVTZ) (Hartree): -382.13945018
Electronic state : 2-A
Cartesian coordinates (Angs):
     C      -1.792042     -0.245705       0.497000
     C      -0.763719      0.514753       0.840462
     C       0.080855      1.269692      -0.135131
     C       1.532826      0.812047      -0.131362
     O       1.629254     -0.554384      -0.573924
     O       1.511557     -1.390915       0.414204
     O      -2.197243     -0.376930      -0.798829
     H      -2.365981     -0.794326       1.233637
     H      -0.507953      0.557576       1.890440
     H      -0.322875      1.165542      -1.141313
     H       0.084996      2.336127       0.106554
     H       2.127656      1.380476      -0.844490
     H       1.979199      0.862095       0.860435
     H      -2.891109     -1.034385      -0.862684
Rotational constants (GHz):    4.2484800    1.7298900    1.5147800
Vibrational harmonic frequencies (cm-1):
       17.9802                  96.2996                 108.0144
      219.1300                 246.6748                 290.6683
      387.2275                 523.5856                 545.1065
      672.0064                 766.3136                 846.1595
      923.9577                 971.3979                 991.2150
     1047.3391                1068.3295                1149.5674
     1225.9786                1235.6111                1284.1883
     1297.3051                1318.1810                1360.7644
     1393.2404                1446.2410                1477.8737
     1486.1508                1782.0974                3058.1557
     3092.6592                3127.6936                3155.3540
     3189.6091                3217.7380                3919.5797
Zero-point correction (Hartree): 0.111492

HOCHCHCH2CH2OO.Zlptt
~~~~~~~~~~~~~~~~~~~
E(UM062X/Aug-CC-pVTZ) (Hartree): -382.13906481
Electronic state : 2-A
Cartesian coordinates (Angs):
     C      -2.005846     -0.189901       0.557402
     C      -1.055449      0.728700       0.636447
     C      -0.149303      1.104773      -0.494933
     C       1.307147      0.824153      -0.185709
     O       1.465252     -0.607883      -0.080592
     O       2.673323     -0.927575       0.263857
     O      -2.267356     -0.865206      -0.597161
     H      -2.627361     -0.440774       1.408355
     H      -0.920009      1.219966       1.591008
     H      -0.434299      0.569448      -1.399886
     H      -0.232266      2.172840      -0.710148
     H       1.972741      1.163634      -0.978403
```

```
     H       1.622660      1.253347       0.765125
     H      -2.930518     -1.539498      -0.444117
Rotational constants (GHz):    5.0261900    1.3870900    1.2335400
Vibrational harmonic frequencies (cm-1):
       21.3258                  66.7347                 117.6948
      209.2188                 235.3191                 293.1693
      337.7011                 470.2339                 570.4101
      675.2776                 764.1390                 852.0397
      890.5305                 971.6337                1039.7919
     1062.8667                1072.7564                1140.2453
     1216.0551                1265.2629                1288.7033
     1296.4313                1299.1031                1356.4039
     1399.5920                1448.0565                1478.8844
     1502.9722                1786.2420                3066.2634
     3082.7260                3125.5137                3141.4267
     3187.1186                3213.1129                3920.4763
Zero-point correction (Hartree): 0.111324

HOCHCHCH2CH2OO.Zpmmc
~~~~~~~~~~~~~~~~~~~
E(CCSD(T)/Aug-CC-pVTZ) (Hartree): -381.60037010
E(CCSD/Aug-CC-pVTZ) (Hartree): -381.53772838
     T1 diagnostic:  0.022191
E(MP2/Aug-CC-pVTZ) (Hartree): -381.49448818
E(MP3/Aug-CC-pVTZ) (Hartree): -381.52479655
E(PMP2/Aug-CC-pVTZ) (Hartree): -381.49774632
E(PMP3/Aug-CC-pVTZ) (Hartree): -381.52669599
E(PUHF/Aug-CC-pVTZ) (Hartree): -380.13149271
E(UHF/Aug-CC-pVTZ) (Hartree): -380.12616632
E(UM062X/Aug-CC-pVTZ) (Hartree): -382.14414641
Electronic state : 2-A
Cartesian coordinates (Angs):
     C       1.838020      0.079555       0.342809
     C       1.016432      1.117681       0.218070
     C      -0.200990      1.144807      -0.658951
     C      -1.489617      0.807122       0.068881
     O      -1.451380     -0.522535       0.649006
     O      -1.199537     -1.432397      -0.236220
     O       1.729213     -1.129048      -0.251044
     H       2.725321      0.135368       0.959152
     H       1.258623      2.004009       0.787568
     H      -0.332366      2.141817      -1.082837
     H      -0.092628      0.466424      -1.506073
     H      -1.657397      1.451712       0.929058
     H      -2.353180      0.834791      -0.595467
     H       0.842185     -1.257284      -0.610196
Rotational constants (GHz):    3.8427200    2.2415600    1.6192300
Vibrational harmonic frequencies (cm-1):
       53.1930                 131.5021                 148.7968
      214.3796                 291.8812                 357.7868
      466.1477                 541.8760                 599.5496
      667.3210                 761.4688                 849.8795
      886.5390                 981.9506                 996.2389
     1037.1786                1088.8224                1148.0690
     1222.6972                1260.3105                1275.4686
     1306.3988                1351.2209                1373.7689
     1404.3696                1442.6719                1490.4872
     1495.2118                1747.8273                3075.1083
     3090.8924                3114.1355                3157.0129
     3205.6803                3226.0874                3797.6382
Zero-point correction (Hartree): 0.112222

HOCHCHCH2CH2OO.Zptpc
~~~~~~~~~~~~~~~~~~~
E(UM062X/Aug-CC-pVTZ) (Hartree): -382.14299943
Electronic state : 2-A
Cartesian coordinates (Angs):
     C       1.990719     -0.256495       0.149012
     C       1.485695      0.947781      -0.106531
     C       0.056334      1.134753      -0.529354
     C      -0.937822      0.806510       0.595548
     O      -2.050788      0.022964       0.099607
     O      -1.651134     -1.141169      -0.305940
     O       1.331854     -1.432158       0.068728
     H       3.017806     -0.397564       0.456449
     H       2.133420      1.803863       0.003447
     H      -0.110610      2.147300      -0.887896
     H      -0.173160      0.466885      -1.364114
     H      -0.471153      0.216023       1.382390
     H      -1.404024      1.688816       1.026043
     H       0.398713     -1.317709      -0.167528
Rotational constants (GHz):    4.3235600    1.9772300    1.4811700
Vibrational harmonic frequencies (cm-1):
       86.7356                 102.9580                 196.4536
      219.3773                 324.4331                 366.9969
      522.0243                 568.6202                 624.7459
      707.6098                 753.2826                 813.2521
      954.6509                 992.7960                1003.1022
     1032.6939                1079.1186                1135.4807
     1230.2006                1263.6910                1287.2719
     1308.1613                1339.8173                1375.1774
     1399.4617                1431.3431                1493.5697
     1509.4091                1733.6295                3059.1022
```

```
     3101.0760                3136.5884                3168.4579
     3216.8284                3242.0571                3721.9528
Zero-point correction (Hartree): 0.112774


TS.HOCHCHCH2CH2OO.cycHOCHCHCH2CH2OO.Zp
~~~~~~~~~~~~~~~~~~~~~~~~~~~~~~~~~~~~~
E(CCSD(T)/Aug-CC-pVTZ) (Hartree): -381.57530128
E(CCSD/Aug-CC-pVTZ) (Hartree): -381.50813416
     T1 diagnostic:  0.028163
E(MP2/Aug-CC-pVTZ) (Hartree): -381.46065809
E(MP3/Aug-CC-pVTZ) (Hartree): -381.48930848
E(PMP2/Aug-CC-pVTZ) (Hartree): -381.47781124
E(PMP3/Aug-CC-pVTZ) (Hartree): -381.50213210
E(PUHF/Aug-CC-pVTZ) (Hartree): -380.10312287
E(UHF/Aug-CC-pVTZ) (Hartree): -380.08321231
E(UM062X/Aug-CC-pVTZ) (Hartree): -382.11528532
Electronic state : 2-A
Cartesian coordinates (Angs):
     C      -1.313651      0.291233       0.341855
     C      -0.290224      1.192205       0.597926
     C       0.894511      1.228012      -0.296765
     C       1.630403     -0.125664      -0.144674
     O       0.687093     -1.170389      -0.292135
     O      -0.130432     -1.179717       0.824619
     O      -1.677701     -0.116515      -0.885788
     H      -2.107594      0.163169       1.065677
     H      -0.202646      1.551906       1.612946
     H       0.601424      1.347293      -1.342140
     H       1.571932      2.041338      -0.041842
     H       2.372267     -0.273285      -0.929519
     H       2.096557     -0.203814       0.837668
     H      -0.889856     -0.408346      -1.366413
Rotational constants (GHz):    3.8895600    2.8846500    2.2593700
Vibrational harmonic frequencies (cm-1):
     i623.4638                 177.6328                  248.3701
      280.9721                 391.9599                  432.6138
      452.0873                 500.3075                  587.6845
      663.9523                 737.8072                  875.1450
      919.1406                 932.5186                  979.4588
     1017.9830                1061.3809                 1077.5628
     1148.8220                1210.9937                 1256.2309
     1268.3454                1318.6422                 1340.3793
     1369.6287                1434.1885                 1484.4078
     1497.9549                1538.4045                 3065.6462
     3076.6998                3128.7866                 3140.1905
     3209.6855                3225.6704                 3759.1579
Zero-point correction (Hartree): 0.111198

TS.HOCHCHCH2CH2OO.cycHOCHCHCH2CH2OO.Zt
~~~~~~~~~~~~~~~~~~~~~~~~~~~~~~~~~~~~~
E(UM062X/Aug-CC-pVTZ) (Hartree): -382.11419635
Electronic state : 2-A
Cartesian coordinates (Angs):
     C      -1.287511      0.259883       0.386557
     C      -0.294591      1.181154       0.633815
     C       0.851787      1.247950      -0.305377
     C       1.636262     -0.084230      -0.149982
     O       0.753486     -1.169180      -0.328771
     O      -0.090769     -1.241275       0.751995
     O      -1.630822     -0.007392      -0.891770
     H      -2.019276      0.015380       1.147963
     H      -0.171789      1.509338       1.655646
     H       0.518979      1.326247      -1.338814
     H       1.519237      2.078630      -0.080707
     H       2.397095     -0.186422      -0.923444
     H       2.090673     -0.145555       0.840312
     H      -2.025769     -0.883393      -0.942661
Rotational constants (GHz):    3.8492700    2.8899600    2.2304200
Vibrational harmonic frequencies (cm-1):
     i636.9546                 172.7885                  237.3710
      258.3095                 345.3806                  425.8914
      446.6402                 470.7412                  581.9767
      665.6133                 750.0642                  868.5386
      930.9654                 944.1562                  984.0003
     1021.3281                1065.7209                 1080.7316
     1155.5223                1207.5550                 1260.3485
     1273.2681                1283.4913                 1320.2074
     1368.5899                1434.2763                 1481.3443
     1490.0791                1559.9629                 3068.6534
     3091.3822                3132.4485                 3147.5517
     3178.7540                3223.6184                 3862.1701
Zero-point correction (Hartree): 0.111151


################################################################################
E-HOCH=C(CH3)CH2CH2OO ring closure and H-shift
################################################################################

HOCHCCH3CH2CH2OO.Ecppc
~~~~~~~~~~~~~~~~~~~~~~
E(UM062X/Aug-CC-pVTZ) (Hartree): -421.45033361
Electronic state : 2-A
```

```
Cartesian coordinates (Angs):
     C      -1.103065     -0.871471       0.191141
     C      -0.923169      0.437989       0.049117
     C       0.395924      1.105234       0.334463
     C       1.491277      0.242106       0.917800
     O       1.954620     -0.751298      -0.027162
     O       2.592063     -0.202878      -1.014324
     O      -2.250252     -1.571520      -0.021246
     H      -0.307885     -1.538884       0.491128
     C      -1.996493      1.381879      -0.412544
     H       0.784451      1.565845      -0.579038
     H       0.231319      1.930178       1.035728
     H       2.356948      0.841506       1.192988
     H       1.153244     -0.338338       1.774789
     H      -2.959546     -0.976412      -0.277049
     H      -2.282302      2.070261       0.386228
     H      -2.903590      0.887905      -0.759677
     H      -1.630930      1.989086      -1.243099
Rotational constants (GHz):    3.2229900    1.1959300    1.0071900
Vibrational harmonic frequencies (cm-1):
       51.8982                69.8197                73.8428
      147.1759               217.6721               261.0593
      300.7799               325.5790               340.9710
      477.0424               492.8291               545.1056
      613.4975               792.7749               844.9085
      922.6439               972.1016               990.6421
     1022.9268              1055.5205              1118.1250
     1179.2911              1217.1855              1231.9348
     1277.5549              1296.8105              1317.5123
     1396.5873              1402.2311              1423.3292
     1438.1956              1472.3417              1478.9286
     1496.0521              1505.6938              1781.0266
     3038.5655              3048.2013              3068.5338
     3098.9307              3100.1948              3124.0822
     3154.6785              3232.9326              3881.6709
Zero-point correction (Hartree): 0.139650

HOCHCCH3CH2CH2OO.Ecppt
----------------------
E(UM062X/Aug-CC-pVTZ) (Hartree): -421.45049488
Electronic state : 2-A
Cartesian coordinates (Angs):
     C      -1.104756     -0.841832       0.194140
     C      -0.917761      0.462519       0.041328
     C       0.404086      1.129509       0.303331
     C       1.497118      0.278838       0.908852
     O       1.943860     -0.756505       0.000620
     O       2.585868     -0.256450      -1.009129
     O      -2.321172     -1.428384      -0.034035
     H      -0.313292     -1.514921       0.498488
     C      -2.014262      1.373580      -0.423936
     H       0.789235      1.563549      -0.624469
     H       0.244566      1.974288       0.981369
     H       2.371537      0.878173       1.155111
     H       1.158947     -0.265689       1.789342
     H      -2.238138     -2.380469       0.030156
     H      -2.237775      2.126436       0.335668
     H      -2.924844      0.823720      -0.643640
     H      -1.705234      1.909941      -1.323966
Rotational constants (GHz):    3.2608800    1.1933500    1.0065700
Vibrational harmonic frequencies (cm-1):
       64.2134                69.7592               128.4212
      147.9245               202.7073               220.2890
      280.1259               304.5266               309.7661
      459.1385               476.7862               545.6244
      617.3729               804.5104               838.1869
      894.5427               972.8820               987.6513
     1020.9739              1061.4689              1119.3137
     1187.0261              1200.6626              1231.1333
     1279.8442              1304.1932              1315.6101
     1387.4788              1398.6469              1409.4114
     1438.5514              1469.9868              1491.9479
     1493.7130              1495.7324              1800.1772
     3041.0298              3049.1693              3070.3455
     3095.7183              3097.7090              3153.4042
     3168.7181              3202.3506              3921.7865
Zero-point correction (Hartree): 0.139493

HOCHCCH3CH2CH2OO.Ecptc
----------------------
E(UM062X/Aug-CC-pVTZ) (Hartree): -421.44964409
Electronic state : 2-A
Cartesian coordinates (Angs):
     C       0.958460      0.920769       0.176224
     C       1.056457     -0.394701       0.011636
     C      -0.134754     -1.309029       0.129860
     C      -1.439234     -0.683554       0.559397
     O      -1.928124      0.141653      -0.523660
     O      -3.012965      0.767980      -0.188622
     O       1.964580      1.833701       0.114548
     H       0.017272      1.414141       0.372494
     C       2.341567     -1.103477      -0.306493
     H      -0.295534     -1.825626      -0.822258
```

```
     H       0.096126     -2.096372       0.854757
     H      -2.201540     -1.437712       0.748404
     H      -1.336795     -0.046262       1.437080
     H       2.803597      1.393954      -0.044874
     H       2.649076     -1.746589       0.521495
     H       3.173599     -0.436166      -0.529254
     H       2.211299     -1.746085      -1.179711
Rotational constants (GHz):    3.3065000    1.1620200    0.9115700
Vibrational harmonic frequencies (cm-1):
       39.4128                52.5256                72.1304
      128.7292               228.7058               257.5636
      290.8939               323.7623               338.1896
      394.0621               493.4623               563.6174
      607.2767               795.5039               831.6187
      933.5204               977.2514              1009.9132
     1030.1231              1074.5935              1109.3652
     1180.0895              1216.7749              1236.2106
     1283.9118              1295.7526              1302.1399
     1391.7808              1407.0620              1424.9217
     1441.9287              1471.4976              1479.7302
     1505.3723              1508.0329              1781.5179
     3035.6387              3047.6372              3061.6866
     3090.1179              3098.7149              3125.4747
     3142.3662              3234.4097              3881.7042
Zero-point correction (Hartree): 0.139416

HOCHCCH3CH2CH2OO.Ecptt
~~~~~~~~~~~~~~~~~~~~~~
E(UM062X/Aug-CC-pVTZ) (Hartree): -421.45008565
Electronic state : 2-A
Cartesian coordinates (Angs):
     C       0.949245      0.896312       0.173511
     C       1.049244     -0.416643       0.012924
     C      -0.135912     -1.337351       0.118120
     C      -1.445615     -0.719812       0.542801
     O      -1.925296      0.123323      -0.531726
     O      -2.955198      0.820810      -0.165589
     O       2.041054      1.717938       0.093176
     H       0.007111      1.392579       0.368978
     C       2.355536     -1.083852      -0.297378
     H      -0.284575     -1.849886      -0.838045
     H       0.095114     -2.126970       0.840052
     H      -2.210711     -1.475964       0.713060
     H      -1.351997     -0.094804       1.430111
     H       1.762803      2.632521       0.154340
     H       2.621025     -1.794855       0.488654
     H       3.160225     -0.360887      -0.395257
     H       2.281535     -1.650231      -1.228646
Rotational constants (GHz):    3.3040500    1.1760800    0.9184100
Vibrational harmonic frequencies (cm-1):
       39.1216                64.6219               128.1937
      134.5810               219.8758               237.7368
      275.3857               299.8364               306.6485
      395.6929               461.5607               564.4930
      611.0092               806.0451               825.4997
      902.5628               978.5088              1008.2744
     1030.0588              1075.5645              1111.3507
     1188.2078              1201.5821              1235.4196
     1286.3389              1298.9974              1305.7658
     1387.2775              1395.9645              1413.2556
     1443.2880              1469.1613              1493.2110
     1494.0080              1506.8397              1800.8022
     3038.4796              3048.6987              3064.8658
     3089.6645              3094.9998              3142.0858
     3168.8376              3203.8529              3920.8200
Zero-point correction (Hartree): 0.139353

HOCHCCH3CH2CH2OO.Ectpc
~~~~~~~~~~~~~~~~~~~~~~
E(UM062X/Aug-CC-pVTZ) (Hartree): -421.45041178
Electronic state : 2-A
Cartesian coordinates (Angs):
     C       1.572068     -0.848306      -0.035840
     C       1.048365      0.370431       0.058022
     C      -0.430853      0.592940       0.216823
     C      -1.275230     -0.662205       0.231476
     O      -2.664912     -0.314663       0.411511
     O      -3.163533      0.215424      -0.662995
     O       2.883973     -1.174345      -0.191749
     H       0.970192     -1.745366       0.005025
     C       1.858942      1.633757       0.008171
     H      -0.617029      1.146169       1.142711
     H      -0.792868      1.228042      -0.596810
     H      -1.198296     -1.223420      -0.698772
     H      -1.047709     -1.305710       1.079830
     H       3.418857     -0.378750      -0.252772
     H       2.936081      1.471320      -0.013281
     H       1.647700      2.253607       0.881680
     H       1.599093      2.223085      -0.873668
Rotational constants (GHz):    4.4348700    0.9033900    0.7892900
Vibrational harmonic frequencies (cm-1):
       53.6282                69.9208                88.4423
      135.7319               170.3219               257.5520
```

```
      290.1776                336.9574                353.7257
      404.0617                491.8700                547.3106
      647.4542                792.2281                844.8403
      918.2831                977.5671               1004.5079
     1035.6693               1091.3277               1117.8562
     1178.3510               1218.5345               1240.8101
     1279.3550               1293.0455               1329.7371
     1349.0943               1410.2839               1426.3496
     1442.5403               1479.1171               1490.3443
     1503.1670               1506.4381               1778.2516
     3040.4836               3052.2854               3075.5687
     3093.2477               3105.0726               3127.5160
     3154.5866               3227.0072               3881.4336
Zero-point correction (Hartree): 0.139679

HOCHCCH3CH2CH2OO.Ectpt
~~~~~~~~~~~~~~~~~~~~~~
E(UM062X/Aug-CC-pVTZ) (Hartree): -421.45000645
Electronic state : 2-A
Cartesian coordinates (Angs):
     C       1.577852     -0.819250      -0.040591
     C       1.039649      0.390526       0.048849
     C      -0.439288      0.606583       0.202344
     C      -1.275694     -0.652926       0.243520
     O      -2.668115     -0.314816       0.420538
     O      -3.177044      0.179949      -0.665932
     O       2.928480     -1.001619      -0.177833
     H       0.988561     -1.727576      -0.009288
     C       1.873460      1.636055       0.003073
     H      -0.626141      1.177823       1.116948
     H      -0.803352      1.224427      -0.623312
     H      -1.197913     -1.231149      -0.676395
     H      -1.040261     -1.278141       1.103607
     H       3.126312     -1.936141      -0.247113
     H       2.928756      1.407436      -0.114273
     H       1.742175      2.216290       0.919033
     H       1.559429      2.272992      -0.826568
Rotational constants (GHz):    4.5430900    0.8957900    0.7869900
Vibrational harmonic frequencies (cm-1):
       66.1054                 81.8442                118.2333
      133.7300                168.4497                211.6414
      270.5425                300.3762                340.0182
      401.4638                463.2389                548.0668
      655.0680                787.2887                856.5622
      882.6100                976.6554               1004.0975
     1038.8936               1090.5760               1119.9076
     1183.3872               1200.1907               1240.4372
     1284.8237               1297.3005               1328.9850
     1344.8630               1391.9456               1417.1383
     1441.1149               1486.2883               1493.8206
     1495.3588               1502.2354               1796.0394
     3042.9124               3052.9699               3078.1945
     3090.6331               3100.8132               3151.6730
     3170.4785               3193.7375               3923.0461
Zero-point correction (Hartree): 0.139478

HOCHCCH3CH2CH2OO.Ecttc
~~~~~~~~~~~~~~~~~~~~~~
E(UM062X/Aug-CC-pVTZ) (Hartree): -421.44977810
Electronic state : 2-A
Cartesian coordinates (Angs):
     C       1.488099     -0.916064      -0.005446
     C       1.157250      0.372000      -0.004153
     C      -0.277382      0.825472      -0.006417
     C      -1.301472     -0.284018       0.000130
     O      -2.599710      0.348790       0.000616
     O      -3.555657     -0.527145       0.004487
     O       2.740169     -1.447403       0.002084
     H       0.750225     -1.706120      -0.013362
     C       2.156681      1.492604       0.004339
     H      -0.453841      1.465276       0.863764
     H      -0.454740      1.456607      -0.882589
     H      -1.248142     -0.912948      -0.888009
     H      -1.243594     -0.906166       0.892763
     H       3.398381     -0.748000       0.022418
     H       3.194147      1.164942      -0.051675
     H       2.053967      2.092384       0.911142
     H       1.986132      2.160124      -0.842661
Rotational constants (GHz):    4.5196000    0.8584100    0.7311900
Vibrational harmonic frequencies (cm-1):
       39.9873                 66.4798                104.0525
      118.0175                126.4742                258.2234
      277.4712                336.0857                345.7019
      356.7540                491.5233                552.7374
      628.5252                781.4722                838.9029
      916.1860               1004.7024               1027.4762
     1032.3684               1102.6472               1113.7519
     1180.2951               1219.2221               1231.7335
     1285.5998               1297.2377               1310.4639
     1346.4920               1411.7788               1429.2141
     1447.0180               1479.5478               1495.7512
     1506.2214               1512.9631               1778.6707
     3041.0038               3052.2032               3069.5630
```

```
     3084.7357                3103.9782                3128.5020
     3142.6828                3227.4756                3881.6338
Zero-point correction (Hartree): 0.139386

HOCHCCH3CH2CH2OO.Ecttt
~~~~~~~~~~~~~~~~~~~~~~
E(UM062X/Aug-CC-pVTZ) (Hartree): -421.44960190
Electronic state : 2-A
Cartesian coordinates (Angs):
     C       1.497402     -0.887783       0.000047
     C       1.149149      0.392873      -0.000195
     C      -0.286555      0.836909      -0.000243
     C      -1.302947     -0.279254       0.000509
     O      -2.608087      0.338922       0.000809
     O      -3.554154     -0.547667      -0.000566
     O       2.808980     -1.279956       0.000127
     H       0.772529     -1.692773       0.000239
     C       2.167038      1.493856      -0.000459
     H      -0.464979      1.472336       0.872425
     H      -0.465223      1.471424      -0.873521
     H      -1.242267     -0.904675      -0.889847
     H      -1.241502     -0.903978       0.891323
     H       2.863827     -2.236095       0.000007
     H       3.180058      1.102198      -0.000860
     H       2.039886      2.130695       0.877666
     H       2.039237      2.130865      -0.878364
Rotational constants (GHz):    4.6297500    0.8525500    0.7297200
Vibrational harmonic frequencies (cm-1):
       61.1190                  98.7035                 106.0269
      120.7515                 124.9046                 216.6812
      263.0903                 301.9858                 333.7557
      352.6867                 461.9462                 551.4865
      637.3932                 777.7230                 851.1881
      881.7542                1005.5986                1027.6191
     1032.6477                1105.6258                1112.9235
     1188.1821                1201.6842                1231.4127
     1295.4491                1297.7054                1308.7258
     1343.6335                1393.4035                1420.2363
     1446.5771                1489.3928                1494.3233
     1498.0086                1512.2925                1796.4653
     3043.6363                3052.7079                3072.4169
     3082.2130                3100.2050                3139.7630
     3170.4924                3194.7409                3923.5816
Zero-point correction (Hartree): 0.139248

HOCHCCH3CH2CH2OO.Egmpc
~~~~~~~~~~~~~~~~~~~~~~
E(UM062X/Aug-CC-pVTZ) (Hartree): -421.45079312
Electronic state : 2-A
Cartesian coordinates (Angs):
     C      -1.828722      0.593462      -0.318153
     C      -0.749123      0.228923       0.366273
     C       0.356813      1.221157       0.592489
     C       1.588782      1.000573      -0.274274
     O       2.226603     -0.254941       0.045546
     O       1.867639     -1.208950      -0.758884
     O      -2.888998     -0.203964      -0.611804
     H      -1.967069      1.592998      -0.708991
     C      -0.625813     -1.165153       0.928019
     H       0.001192      2.230566       0.374814
     H       0.665992      1.211051       1.640907
     H       1.340216      0.972306      -1.333044
     H       2.348091      1.756234      -0.075769
     H      -2.717138     -1.099473      -0.304838
     H      -0.474526     -1.911017       0.144251
     H      -1.516950     -1.442277       1.497998
     H       0.226614     -1.241311       1.599681
Rotational constants (GHz):    3.5834100    1.2111900    1.0713800
Vibrational harmonic frequencies (cm-1):
       39.9458                  73.1485                 128.2640
      167.4782                 175.8704                 263.8396
      308.0215                 339.6564                 396.1107
      471.1996                 520.2774                 540.9332
      609.5298                 795.0616                 861.5924
      923.9655                 937.1037                1016.3156
     1031.4899                1050.5768                1093.6730
     1179.3530                1227.8926                1241.8213
     1251.0525                1320.3644                1328.3232
     1378.4174                1391.6522                1405.0569
     1421.3944                1470.4582                1481.4939
     1496.5170                1502.0666                1765.0900
     3040.3305                3053.9698                3088.4239
     3093.0150                3102.2243                3146.0031
     3158.5547                3212.6987                3861.4501
Zero-point correction (Hartree): 0.139792

HOCHCCH3CH2CH2OO.Elmmc
~~~~~~~~~~~~~~~~~~~~~~
E(UM062X/Aug-CC-pVTZ) (Hartree): -421.45242156
Electronic state : 2-A
Cartesian coordinates (Angs):
     C       2.013050     -0.583300       0.048600
     C       0.822405     -0.037761       0.280218
```

```
     C      -0.330897     -0.920787       0.665404
     C      -1.401168     -1.046745      -0.407538
     O      -2.022990      0.228051      -0.691483
     O      -2.717012      0.653555       0.318701
     O       3.144830      0.064818      -0.333535
     H       2.192013     -1.644901       0.158839
     C       0.576416      1.443144       0.170143
     H       0.025312     -1.930256       0.878572
     H      -0.813437     -0.547858       1.572093
     H      -0.979016     -1.352464      -1.363281
     H      -2.195381     -1.728309      -0.105657
     H       2.954627      0.995628      -0.481461
     H       0.217636      1.728786      -0.820826
     H       1.471402      2.028463       0.390908
     H      -0.190622      1.752218       0.880397
Rotational constants (GHz):    4.6129000    1.0605600    0.9487100
Vibrational harmonic frequencies (cm-1):
       38.6505                77.3705                130.5209
      169.8811               176.6163                264.7294
      311.8036               328.6012                402.1490
      459.2398               517.9373                551.3201
      617.6214               797.0893                847.4594
      928.4938               943.3898                996.1643
     1036.3604              1052.8646               1106.3434
     1176.3255              1219.7146               1234.3742
     1269.0028              1305.5852               1318.0439
     1378.3035              1395.9793               1409.7986
     1426.5379              1469.6655               1485.0410
     1489.3419              1505.1048               1769.2464
     3047.6348              3061.1003               3088.9961
     3104.5789              3110.0293               3124.2378
     3153.5715              3211.4230               3868.8059
Zero-point correction (Hartree): 0.139827

HOCHCCH3CH2CH2OO.Elmmt
----------------------
E(UM062X/Aug-CC-pVTZ) (Hartree): -421.45107126
Electronic state : 2-A
Cartesian coordinates (Angs):
     C      -2.045545     -0.556310      -0.080610
     C      -0.840502     -0.020493      -0.231501
     C       0.320886     -0.905756      -0.581414
     C       1.398805     -0.977272       0.489546
     O       2.113025      0.274231       0.616461
     O       2.827360      0.521781      -0.437538
     O      -3.140708      0.192148       0.252576
     H      -2.218904     -1.618909      -0.211558
     C      -0.596830      1.451270      -0.071279
     H      -0.024704     -1.925997      -0.758613
     H       0.802291     -0.563348      -1.501394
     H       0.977864     -1.144065       1.479792
     H       2.140528     -1.740460       0.258152
     H      -3.929223     -0.350927       0.223254
     H      -0.062021      1.665449       0.855983
     H      -1.533593      2.002421      -0.061156
     H       0.029452      1.821923      -0.884911
Rotational constants (GHz):    4.9357000    1.0140300    0.9163200
Vibrational harmonic frequencies (cm-1):
       36.7960                71.9341                147.3537
      166.4145               200.7384                220.6476
      267.5188               297.9678                374.2763
      433.4844               506.7578                553.2612
      611.9254               806.4659                851.1981
      888.6263               946.0686                989.6621
     1041.5967              1058.7229               1110.1534
     1180.1000              1210.4322               1229.0814
     1272.1106              1305.5993               1308.5329
     1380.5998              1394.8994               1397.4725
     1430.8916              1468.7159               1487.8996
     1493.0969              1493.7255               1791.2177
     3056.7129              3057.7261               3087.8331
     3106.6378              3107.8842               3152.1624
     3161.8569              3175.6031               3920.5807
Zero-point correction (Hartree): 0.139544

HOCHCCH3CH2CH2OO.Elmtc
----------------------
E(UM062X/Aug-CC-pVTZ) (Hartree): -421.45103902
Electronic state : 2-A
Cartesian coordinates (Angs):
     C       2.057130     -0.569428      -0.201725
     C       0.932723     -0.082448       0.315439
     C      -0.172671     -1.032065       0.687609
     C      -1.412079     -0.918236      -0.180575
     O      -2.063491      0.337284       0.123070
     O      -3.099629      0.531724      -0.632015
     O       3.138556      0.138524      -0.620488
     H       2.215710     -1.631877      -0.333222
     C       0.710421      1.388304       0.540609
     H       0.181427     -2.060750       0.604398
     H      -0.471987     -0.880858       1.728956
     H      -1.171835     -0.910268      -1.243110
     H      -2.133812     -1.706963       0.029789
```

```
     H       2.960188      1.080858      -0.554230
     H       0.152950      1.849424      -0.276981
     H       1.646002      1.936518       0.665775
     H       0.124727      1.546901       1.445953
Rotational constants (GHz):    4.5600900    0.9613500    0.8826200
Vibrational harmonic frequencies (cm-1):
       33.2861                  60.1466                  98.9528
      149.4043                 179.0129                 256.2755
      302.3820                 334.3240                 390.1704
      410.9641                 501.4042                 575.1685
      600.9007                 797.4821                 840.6084
      925.9919                 961.2699                1025.1453
     1044.0113                1059.1274                1093.6388
     1180.0190                1218.9880                1237.1159
     1276.0249                1295.5166                1318.5902
     1380.5161                1398.0782                1412.0442
     1428.2151                1467.6952                1485.1955
     1498.0731                1503.1657                1769.5168
     3049.7919                3050.6693                3082.3847
     3107.0257                3108.5436                3125.5393
     3142.4746                3209.4681                3871.6575
Zero-point correction (Hartree): 0.139551

HOCHCCH3CH2CH2OO.Elmtt
~~~~~~~~~~~~~~~~~~~~~
E(UM062X/Aug-CC-pVTZ) (Hartree): -421.44993064
Electronic state : 2-A
Cartesian coordinates (Angs):
     C      -2.102942      0.538206      -0.143436
     C      -0.937721      0.060986       0.276054
     C       0.166425      1.019365       0.624421
     C       1.406567      0.886346      -0.241243
     O       2.135432     -0.287980       0.187571
     O       3.181418     -0.493893      -0.550088
     O      -3.144905     -0.277302      -0.488645
     H      -2.283931      1.603643      -0.234672
     C      -0.681508     -1.410118       0.417318
     H      -0.189171      2.046483       0.528509
     H       0.472598      0.885162       1.666565
     H       1.166525      0.752649      -1.295559
     H       2.081468      1.733116      -0.121316
     H      -3.916446      0.249339      -0.700408
     H       0.027256     -1.761330      -0.335032
     H      -1.602277     -1.977775       0.312444
     H      -0.236502     -1.626603       1.390083
Rotational constants (GHz):    4.9541800    0.9345000    0.8533500
Vibrational harmonic frequencies (cm-1):
       38.2223                  60.7487                 118.7998
      167.5998                 208.7623                 239.9630
      253.9018                 295.9806                 369.6034
      380.9865                 471.5233                 579.6108
      597.9815                 807.2849                 841.7321
      891.1782                 958.9019                1021.9535
     1049.8199                1064.5119                1098.2331
     1185.8944                1209.9780                1231.6886
     1279.2776                1296.1262                1305.4640
     1382.0083                1397.4037                1398.7941
     1432.0567                1465.6511                1490.4287
     1496.2937                1500.0287                1794.8727
     3047.2310                3058.8339                3081.9629
     3106.0061                3109.1757                3141.2796
     3163.4507                3177.9344                3921.3390
Zero-point correction (Hartree): 0.139402

HOCHCCH3CH2CH2OO.Elpmc
~~~~~~~~~~~~~~~~~~~~~
E(CCSD(T)/Aug-CC-pVTZ) (Hartree): -420.84408640
E(CCSD/Aug-CC-pVTZ) (Hartree): -420.77348661
     T1 diagnostic:  0.020724
E(MP2/Aug-CC-pVTZ) (Hartree): -420.72102249
E(MP3/Aug-CC-pVTZ) (Hartree): -420.76040125
E(PMP2/Aug-CC-pVTZ) (Hartree): -420.72446597
E(PMP3/Aug-CC-pVTZ) (Hartree): -420.76254263
E(PUHF/Aug-CC-pVTZ) (Hartree): -419.18070042
E(UHF/Aug-CC-pVTZ) (Hartree): -419.17544253
E(UM062X/Aug-CC-pVTZ) (Hartree): -421.45265451
Electronic state : 2-A
Cartesian coordinates (Angs):
     C      -1.517607     -0.283437      -0.753321
     C      -0.688102      0.550324      -0.133217
     C       0.538745      1.038517      -0.843823
     C       1.838957      0.611526      -0.173038
     O       1.985009     -0.818500      -0.218460
     O       1.354129     -1.396059       0.761167
     O      -2.645530     -0.839962      -0.241593
     H      -1.353689     -0.601333      -1.774347
     C      -0.894450      1.005527       1.283658
     H       0.547096      0.688579      -1.876849
     H       0.549588      2.133239      -0.871075
     H       2.704278      0.996970      -0.709256
     H       1.882456      0.910749       0.873250
     H      -2.716026     -0.636878       0.695306
     H      -0.360153      0.364472       1.988530
```

```
     H      -1.947769      1.023448       1.568417
     H      -0.519904      2.022190       1.415556
Rotational constants (GHz):    3.0806800    1.3277200    1.2131600
Vibrational harmonic frequencies (cm-1):
       63.9862                104.7020                108.6729
      122.1413                201.4260                273.4201
      300.7804                361.7789                395.4514
      458.0915                513.3197                555.9277
      598.5636                800.0066                863.5417
      918.9867                962.5085               1003.3209
     1035.1931               1053.7956               1078.6200
     1184.2846               1224.9307               1237.2872
     1246.1949               1314.7995               1323.2196
     1372.5476               1393.5532               1406.8474
     1425.4227               1469.2816               1484.0931
     1495.6961               1505.2614               1772.5644
     3040.6819               3046.7273               3093.4939
     3107.1019               3108.7996               3113.8965
     3154.7250               3216.3431               3873.0163
Zero-point correction (Hartree): 0.139845

HOCHCCH3CH2CH2OO.Elpmt
~~~~~~~~~~~~~~~~~~~~~~
E(UM062X/Aug-CC-pVTZ) (Hartree): -421.45177275
Electronic state : 2-A
Cartesian coordinates (Angs):
     C      -1.510210     -0.336826      -0.690902
     C      -0.683259      0.546226      -0.145920
     C       0.539959      0.977063      -0.898706
     C       1.847651      0.597746      -0.214740
     O       2.000095     -0.831905      -0.179810
     O       1.380285     -1.354796       0.837605
     O      -2.640887     -0.764850      -0.055396
     H      -1.323918     -0.761340      -1.671016
     C      -0.911633      1.122466       1.218494
     H       0.541037      0.556366      -1.905497
     H       0.548957      2.066978      -1.003651
     H       2.705532      0.954743      -0.781869
     H       1.899584      0.958318       0.811076
     H      -3.092511     -1.415167      -0.594411
     H      -0.205936      0.698501       1.936264
     H      -1.917224      0.908862       1.570994
     H      -0.766517      2.205095       1.209553
Rotational constants (GHz):    3.1009500    1.3187700    1.1980700
Vibrational harmonic frequencies (cm-1):
       57.1189                 93.4475                104.6185
      131.9094                219.1160                232.0021
      276.1121                311.2246                387.5974
      438.8327                494.0006                557.1893
      600.1569                807.2122                858.7543
      894.0112                961.8466                999.8902
     1036.6439               1062.5751               1080.2574
     1193.8357               1210.0610               1235.1229
     1248.8211               1303.8493               1319.1174
     1375.2739               1390.0143               1398.2793
     1430.4524               1469.6591               1486.2454
     1489.9780               1504.9210               1796.2725
     3041.9251               3050.8094               3095.6879
     3102.2293               3104.9275               3157.8622
     3162.0273               3180.0152               3922.6773
Zero-point correction (Hartree): 0.139594

HOCHCCH3CH2CH2OO.Elppc
~~~~~~~~~~~~~~~~~~~~~~
E(UM062X/Aug-CC-pVTZ) (Hartree): -421.45195093
Electronic state : 2-A
Cartesian coordinates (Angs):
     C       1.459781     -0.776614       0.420568
     C       0.809440      0.376741       0.306445
     C      -0.482178      0.573410       1.045944
     C      -1.666117      0.819506       0.124995
     O      -1.850534     -0.277332      -0.795413
     O      -2.187652     -1.364440      -0.172854
     O       2.617064     -1.127776      -0.198308
     H       1.098108     -1.575173       1.054509
     C       1.280687      1.502085      -0.571500
     H      -0.703645     -0.293698       1.667310
     H      -0.414759      1.443134       1.707674
     H      -2.593160      0.935477       0.684486
     H      -1.513927      1.681988      -0.522449
     H       2.881434     -0.442781      -0.818407
     H       0.815043      1.470810      -1.560068
     H       2.362349      1.500720      -0.714819
     H       1.027859      2.465136      -0.124337
Rotational constants (GHz):    3.1403500    1.2648500    1.0636500
Vibrational harmonic frequencies (cm-1):
       36.8765                 52.5879                118.8400
      127.2007                205.7481                263.7766
      302.9698                348.2542                391.2698
      454.1732                509.8571                554.3828
      615.8995                799.6879                843.0226
      929.9481                956.6517                993.0827
     1035.7560               1052.2483               1089.8522
```

```
     1182.5724                1223.8758                1230.1082
     1265.2094                1299.6920                1317.9795
     1377.4525                1396.8678                1410.5049
     1426.5641                1472.3962                1486.1949
     1496.9209                1505.0832                1778.0527
     3041.6380                3043.2119                3093.3491
     3098.9139                3114.6308                3121.5831
     3151.6504                3215.2843                3874.0553
Zero-point correction (Hartree): 0.139665

HOCHCCH3CH2CH2OO.Elppt
~~~~~~~~~~~~~~~~~~~~~~
E(CCSD(T)/Aug-CC-pVTZ) (Hartree): -420.84385432
E(CCSD/Aug-CC-pVTZ) (Hartree): -420.77372382
     T1 diagnostic:  0.020573
E(MP2/Aug-CC-pVTZ) (Hartree): -420.72095663
E(MP3/Aug-CC-pVTZ) (Hartree): -420.76066693
E(PMP2/Aug-CC-pVTZ) (Hartree): -420.72411407
E(PMP3/Aug-CC-pVTZ) (Hartree): -420.76253098
E(PUHF/Aug-CC-pVTZ) (Hartree): -419.18205719
E(UHF/Aug-CC-pVTZ) (Hartree): -419.17690718
E(UM062X/Aug-CC-pVTZ) (Hartree): -421.45188619
Electronic state : 2-A
Cartesian coordinates (Angs):
     C       1.428909     -0.761649       0.387917
     C       0.808286      0.406145       0.287379
     C      -0.489208      0.617197       1.011743
     C      -1.672006      0.827860       0.080720
     O      -1.862434     -0.311367      -0.786966
     O      -2.193385     -1.369017      -0.113317
     O       2.607110     -1.019542      -0.254484
     H       1.022622     -1.570406       0.984909
     C       1.341535      1.528230      -0.552156
     H      -0.712932     -0.230656       1.658873
     H      -0.426996      1.506181       1.647335
     H      -2.598217      0.971458       0.635324
     H      -1.517559      1.658184      -0.605961
     H       2.895243     -1.912333      -0.060989
     H       0.735260      1.673752      -1.449666
     H       2.361263      1.329288      -0.871014
     H       1.325889      2.467235       0.005707
Rotational constants (GHz):    3.1486200    1.2674200    1.0540300
Vibrational harmonic frequencies (cm-1):
       26.7941                  45.7261                 108.2875
      130.5170                 215.3615                 233.3374
      275.5859                 299.0623                 385.1109
      433.3619                 493.0776                 557.0090
      615.4538                 807.4477                 840.0362
      902.1129                 957.7869                 984.3953
     1035.1859                1063.0966                1089.2179
     1192.4548                1208.3106                1233.7179
     1266.7916                1301.9615                1305.5584
     1381.0377                1389.3788                1401.8280
     1430.7164                1471.4674                1487.7331
     1490.5883                1502.7339                1800.3064
     3046.1368                3048.2779                3093.5697
     3097.0945                3117.7039                3155.1559
     3161.9043                3180.8921                3921.9245
Zero-point correction (Hartree): 0.139390

HOCHCCH3CH2CH2OO.Elptc
~~~~~~~~~~~~~~~~~~~~~~
E(UM062X/Aug-CC-pVTZ) (Hartree): -421.45093535
Electronic state : 2-A
Cartesian coordinates (Angs):
     C      -1.721411     -0.587870      -0.547802
     C      -0.916644      0.407847      -0.192202
     C       0.248419      0.773116      -1.068863
     C       1.585035      0.661313      -0.362510
     O       1.784646     -0.724568      -0.010541
     O       2.857524     -0.884493       0.700195
     O      -2.797669     -1.055815       0.136247
     H      -1.576378     -1.138501      -1.467638
     C      -1.090617      1.192064       1.078120
     H       0.263101      0.147565      -1.962174
     H       0.157778      1.811407      -1.403676
     H       2.415615      0.956359      -1.002489
     H       1.620835      1.237491       0.561719
     H      -2.868588     -0.611774       0.985637
     H      -0.462934      0.806120       1.885350
     H      -2.122091      1.195651       1.433353
     H      -0.812046      2.235865       0.922256
Rotational constants (GHz):    3.4451300    1.0522800    0.9883000
Vibrational harmonic frequencies (cm-1):
       41.6818                  55.6782                  95.2414
      122.1272                 225.6290                 255.4193
      298.1443                 341.1793                 386.6297
      405.9443                 500.7129                 568.1586
      599.1119                 800.1281                 838.2699
      929.8089                 959.6360                1024.2254
     1049.3828                1067.1277                1077.5407
     1181.2537                1223.4907                1231.4619
     1276.1074                1297.0730                1318.4225
```

```
     1380.2345                1394.1162                1412.8135
     1428.6500                1470.7367                1488.4428
     1503.7162                1508.9518                1777.2567
     3043.4882                3044.8136                3085.8243
     3100.1926                3108.8349                3116.2341
     3140.7489                3215.3730                3874.7341
Zero-point correction (Hartree): 0.139571

HOCHCCH3CH2CH2OO.Elptt
----------------------
E(UM062X/Aug-CC-pVTZ) (Hartree): -421.45062207
Electronic state : 2-A
Cartesian coordinates (Angs):
     C       1.687998     -0.618795       0.492881
     C       0.915542      0.416456       0.192925
     C      -0.259700      0.749108       1.067999
     C      -1.591353      0.659142       0.349459
     O      -1.802077     -0.723348      -0.011109
     O      -2.887151     -0.874508      -0.704725
     O       2.769767     -0.965716      -0.266504
     H       1.492458     -1.242616       1.357736
     C       1.163201      1.278087      -1.009050
     H      -0.285528      0.095656       1.941473
     H      -0.170140      1.775429       1.437329
     H      -2.423692      0.956840       0.985921
     H      -1.613993      1.241844      -0.570464
     H       3.198522     -1.736052       0.107991
     H       2.139415      1.075352      -1.441349
     H       1.111298      2.335820      -0.741319
     H       0.413215      1.102318      -1.783897
Rotational constants (GHz):    3.4577100    1.0502500    0.9739700
Vibrational harmonic frequencies (cm-1):
       27.8590                  56.3095                  95.1152
      130.4504                 229.9982                 233.0775
      279.8611                 281.8680                 379.0604
      390.0224                 473.3075                 569.5506
      599.1604                 808.7278                 835.2397
      901.7905                 959.8911                1022.4905
     1052.1236                1073.0370                1076.6099
     1189.3981                1207.2794                1234.9150
     1275.3578                1297.3689                1306.2990
     1383.6717                1387.5146                1402.9185
     1432.2372                1469.4858                1490.7696
     1493.0623                1509.5911                1800.9719
     3046.6909                3049.0555                3088.0839
     3097.1853                3103.7458                3144.0555
     3161.8549                3181.6663                3920.9978
Zero-point correction (Hartree): 0.139309

HOCHCCH3CH2CH2OO.Eltmc
----------------------
E(UM062X/Aug-CC-pVTZ) (Hartree): -421.45164869
Electronic state : 2-A
Cartesian coordinates (Angs):
     C       1.811935     -0.907621       0.071422
     C       1.027333      0.151265       0.247118
     C      -0.414545     -0.040563       0.622740
     C      -1.339242      0.420047      -0.492300
     O      -2.719465      0.331750      -0.081247
     O      -3.113306     -0.903396      -0.014655
     O       3.119974     -0.898855      -0.294994
     H       1.454965     -1.917711       0.221781
     C       1.516665      1.562881       0.063181
     H      -0.625008     -1.089135       0.831386
     H      -0.651596      0.533489       1.523087
     H      -1.198815      1.472892      -0.733562
     H      -1.219188     -0.188641      -1.387452
     H       3.407718      0.001017      -0.472667
     H       1.385050      1.918785      -0.961790
     H       2.571892      1.675366       0.319359
     H       0.964490      2.241889       0.714062
Rotational constants (GHz):    4.7964600    0.8767900    0.7807500
Vibrational harmonic frequencies (cm-1):
       53.7285                  71.7147                  89.4977
      116.3588                 155.1504                 271.1468
      307.8924                 327.9762                 383.8881
      406.1160                 510.9140                 539.2368
      656.5248                 795.4961                 837.0464
      933.8506                 968.3074                1016.5065
     1043.4275                1069.7756                1081.4272
     1183.6477                1220.7490                1236.2731
     1280.1390                1307.8771                1322.0944
     1335.7953                1400.0742                1409.7012
     1425.2233                1482.0790                1491.9171
     1499.1111                1505.3858                1772.0821
     3043.5621                3050.7344                3091.7159
     3098.1917                3117.5938                3121.3765
     3154.5905                3218.4321                3871.8645
Zero-point correction (Hartree): 0.139597

HOCHCCH3CH2CH2OO.Eltmt
----------------------
E(UM062X/Aug-CC-pVTZ) (Hartree): -421.45146190
```

```
Electronic state : 2-A
Cartesian coordinates (Angs):
     C       1.808449     -0.870946       0.073997
     C       1.022126      0.185896       0.234148
     C      -0.415721     -0.007658       0.623098
     C      -1.359154      0.443369      -0.480086
     O      -2.733501      0.297045      -0.063681
     O      -3.085753     -0.951642      -0.027514
     O       3.119356     -0.754994      -0.294526
     H       1.443150     -1.880050       0.228246
     C       1.518328      1.587994       0.035525
     H      -0.622997     -1.056074       0.837927
     H      -0.642754      0.569183       1.524220
     H      -1.258428      1.504409      -0.700972
     H      -1.223508     -0.143918      -1.387232
     H       3.537838     -1.616751      -0.290378
     H       1.112418      2.031524      -0.876723
     H       2.602370      1.614041      -0.037457
     H       1.206935      2.222439       0.868047
Rotational constants (GHz):    4.7876600    0.8777500    0.7801800
Vibrational harmonic frequencies (cm-1):
       56.3337                61.5398                111.1569
      118.4974               170.4625                240.0409
      267.4307               321.2406                359.2031
      385.4776               485.3416                538.0905
      660.2330               793.0924                844.5286
      900.1542               966.8000               1014.9355
     1050.6590              1070.5620               1086.7521
     1194.8091              1209.8170               1236.0224
     1283.4324              1293.5699               1325.9942
     1339.2963              1393.4718               1406.7887
     1430.5021              1480.0410               1492.3605
     1497.0516              1499.6333               1795.6914
     3049.6415              3051.3162               3094.9246
     3099.0336              3116.9742               3159.8308
     3162.0614              3183.4444               3918.9380
Zero-point correction (Hartree): 0.139463

HOCHCCH3CH2CH2OO.Eltpc
~~~~~~~~~~~~~~~~~~~~~~
E(UM062X/Aug-CC-pVTZ) (Hartree): -421.45201182
Electronic state : 2-A
Cartesian coordinates (Angs):
     C      -2.007490     -0.766543      -0.158771
     C      -1.003670      0.103506      -0.211088
     C       0.386922     -0.368660      -0.524399
     C       1.307083     -0.192810       0.672840
     O       2.663592     -0.544892       0.329885
     O       3.209099      0.359872      -0.424121
     O      -3.304263     -0.488022       0.135709
     H      -1.870260     -1.819530      -0.365650
     C      -1.199234      1.573372       0.052831
     H       0.380775     -1.418458      -0.818898
     H       0.807641      0.209533      -1.351093
     H       1.321144      0.836694       1.029090
     H       1.041753     -0.866617       1.485571
     H      -3.399346      0.442897       0.356862
     H      -1.153800      1.815574       1.117656
     H      -2.155303      1.937117      -0.329843
     H      -0.421692      2.153930      -0.443958
Rotational constants (GHz):    5.5881300    0.8426200    0.7822800
Vibrational harmonic frequencies (cm-1):
       53.0781                68.9128                 92.6832
      134.5309               153.8551                269.6361
      308.6222               336.0594                387.3273
      408.3134               514.1855                543.1282
      658.1054               792.9716                836.2138
      926.7746               973.8020               1018.9343
     1043.2789              1062.5763               1082.5295
     1183.7005              1225.6114               1233.7287
     1283.3615              1305.6221               1327.7582
     1335.9956              1398.4848               1407.9966
     1424.1372              1481.3396               1492.3829
     1498.2498              1507.0122               1770.7074
     3041.9336              3058.3081               3092.2916
     3095.3268              3114.2838               3122.0515
     3156.0048              3216.5067               3868.2763
Zero-point correction (Hartree): 0.139667

HOCHCCH3CH2CH2OO.Eltpt
~~~~~~~~~~~~~~~~~~~~~~
E(UM062X/Aug-CC-pVTZ) (Hartree): -421.45145415
Electronic state : 2-A
Cartesian coordinates (Angs):
     C      -2.001604     -0.742327      -0.143488
     C      -1.003878      0.131352      -0.193096
     C       0.388943     -0.341258      -0.495733
     C       1.325429     -0.112698       0.679639
     O       2.660431     -0.553504       0.354349
     O       3.240376      0.263637      -0.470784
     O      -3.284177     -0.367272       0.143806
     H      -1.843266     -1.799209      -0.327038
     C      -1.215763      1.598121       0.043935
```

```
     H       0.390938     -1.403170      -0.745496
     H       0.796207      0.204117      -1.351080
     H       1.390356      0.938782       0.954426
     H       1.039528     -0.710211       1.543648
     H      -3.874869     -1.114517       0.041352
     H      -0.835668      1.906024       1.020700
     H      -2.271803      1.852258       0.004772
     H      -0.683224      2.183896      -0.707787
Rotational constants (GHz):    5.6476000    0.8348200    0.7774800
Vibrational harmonic frequencies (cm-1):
       49.7688                  62.1260                 111.8830
      127.3880                 172.9634                 210.4648
      261.2065                 320.6001                 362.4027
      382.3184                 485.9407                 542.2492
      657.6454                 793.1815                 842.6844
      892.9237                 971.7160                1015.6927
     1050.5671                1064.3973                1088.9214
     1195.4017                1206.0764                1235.3924
     1278.4451                1296.7273                1326.6436
     1338.9397                1392.0899                1404.1120
     1429.8617                1479.4113                1492.5962
     1497.1967                1499.5171                1794.2645
     3052.0717                3056.5095                3095.4248
     3101.9954                3108.8201                3158.4228
     3161.4501                3179.2350                3920.3404
Zero-point correction (Hartree): 0.139351

HOCHCCH3CH2CH2OO.Elttc
~~~~~~~~~~~~~~~~~~~~~~
E(UM062X/Aug-CC-pVTZ) (Hartree): -421.45091885
Electronic state : 2-A
Cartesian coordinates (Angs):
     C       2.019457     -0.817672       0.008327
     C       1.098313      0.106194       0.263784
     C      -0.265828     -0.308594       0.739631
     C      -1.331637      0.046086      -0.278635
     O      -2.612365     -0.306310       0.287546
     O      -3.586183     -0.017001      -0.518699
     O       3.280374     -0.604705      -0.449534
     H       1.832634     -1.872400       0.160319
     C       1.352064      1.578443       0.081059
     H      -0.294439     -1.382104       0.927499
     H      -0.506575      0.195948       1.679682
     H      -1.359513      1.112952      -0.500090
     H      -1.213321     -0.513727      -1.205893
     H       3.413792      0.330153      -0.629580
     H       1.084613      1.925417      -0.920047
     H       2.395599      1.846085       0.257166
     H       0.758393      2.155065       0.791451
Rotational constants (GHz):    5.6123100    0.7832700    0.7367300
Vibrational harmonic frequencies (cm-1):
       53.8263                  72.5390                  95.9165
      114.0774                 128.2612                 270.0024
      279.2909                 331.3963                 381.0101
      385.4593                 495.6250                 548.1192
      637.7717                 787.1260                 832.2222
      931.2207                1006.1629                1023.5025
     1047.5933                1065.7010                1104.9684
     1179.5446                1217.2770                1228.0802
     1292.8911                1306.1027                1310.3396
     1333.4085                1402.8581                1413.8348
     1426.4010                1485.5788                1492.6064
     1504.5213                1508.5126                1772.3846
     3044.6967                3051.5936                3084.0365
     3099.7247                3110.5957                3118.4691
     3143.5100                3214.7052                3871.4970
Zero-point correction (Hartree): 0.139435

HOCHCCH3CH2CH2OO.Elttt
~~~~~~~~~~~~~~~~~~~~~~
E(UM062X/Aug-CC-pVTZ) (Hartree): -421.45055503
Electronic state : 2-A
Cartesian coordinates (Angs):
     C       2.019747     -0.786239       0.012765
     C       1.092870      0.133198       0.249446
     C      -0.268522     -0.285052       0.729399
     C      -1.347484      0.078620      -0.271565
     O      -2.613552     -0.338726       0.285451
     O      -3.600278     -0.055760      -0.507019
     O       3.268503     -0.461379      -0.437772
     H       1.826796     -1.842387       0.164177
     C       1.353458      1.598099       0.055223
     H      -0.298640     -1.360915       0.906120
     H      -0.498650      0.209545       1.677373
     H      -1.411543      1.151424      -0.448613
     H      -1.217059     -0.439965      -1.220983
     H       3.818674     -1.244931      -0.472194
     H       0.843713      1.981548      -0.831597
     H       2.415948      1.794482      -0.062124
     H       0.982964      2.166359       0.910953
Rotational constants (GHz):    5.7031700    0.7796800    0.7330400
Vibrational harmonic frequencies (cm-1):
       49.4497                  85.7927                  94.1556
```

```
      109.3073                155.9037                223.1140
      264.6973                296.5680                353.0401
      371.2835                465.2999                545.6444
      640.9286                785.9895                840.5879
      895.2056               1002.6418               1021.9917
     1055.0963               1069.6735               1106.7878
     1189.2775               1208.1309               1226.7501
     1292.2113               1296.0405               1310.2441
     1338.0122               1392.7459               1413.1792
     1430.7267               1482.9877               1493.2188
     1498.6237               1508.4037               1795.6003
     3050.3658               3052.0386               3087.7339
     3100.1541               3106.2284               3147.3929
     3162.0558               3180.1953               3919.4495
Zero-point correction (Hartree): 0.139230


TS.HOCHCCH3CH2CH2OO.cycHOCHCCH3CH2CH2OO.Ec
~~~~~~~~~~~~~~~~~~~~~~~~~~~~~~~~~~~~~~~~~~
E(CCSD(T)/Aug-CC-pVTZ) (Hartree): -420.82495066
E(CCSD/Aug-CC-pVTZ) (Hartree): -420.74993036
     T1 diagnostic:  0.027178
E(MP2/Aug-CC-pVTZ) (Hartree): -420.69194733
E(MP3/Aug-CC-pVTZ) (Hartree): -420.73018644
E(PMP2/Aug-CC-pVTZ) (Hartree): -420.70966304
E(PMP3/Aug-CC-pVTZ) (Hartree): -420.74344876
E(PUHF/Aug-CC-pVTZ) (Hartree): -419.15893222
E(UHF/Aug-CC-pVTZ) (Hartree): -419.13843132
E(UM062X/Aug-CC-pVTZ) (Hartree): -421.43069294
Electronic state : 2-A
Cartesian coordinates (Angs):
     C       0.897061     -0.546190       0.623516
     C       0.499806      0.751999       0.364265
     C      -0.899828      1.100331       0.734933
     C      -1.862983      0.349260      -0.214481
     O      -1.608941     -1.029261      -0.103469
     O      -0.379546     -1.295814      -0.660220
     O       2.063821     -1.066021       0.210856
     H       0.465226     -1.110783       1.437486
     C       1.222207      1.567402      -0.659583
     H      -1.133763      0.784748       1.752116
     H      -1.076472      2.173656       0.656888
     H      -2.901957      0.490788       0.082090
     H      -1.719342      0.671026      -1.248151
     H       2.398259     -0.574510      -0.546052
     H       1.015811      1.199817      -1.672535
     H       2.304179      1.548632      -0.511108
     H       0.907815      2.608579      -0.619976
Rotational constants (GHz):    2.9232700    1.9578100    1.4160100
Vibrational harmonic frequencies (cm-1):
     i584.5270                104.0146                 131.1446
      152.9753                280.3153                 301.1201
      328.3390                384.9481                 405.1223
      438.5013                509.0466                 585.3565
      622.4213                804.3175                 876.8799
      933.8620                966.4459                 987.6532
     1013.3413               1029.7845                1074.4238
     1089.5739               1180.5453                1223.0220
     1246.1206               1264.0096                1324.3687
     1343.1694               1375.3321                1386.2243
     1413.1340               1480.3285                1482.9774
     1490.9019               1502.0566                1565.9389
     3013.5153               3063.7344                3073.1651
     3083.0540               3122.8568                3133.5583
     3139.1511               3225.4811                3857.2312
Zero-point correction (Hartree): 0.138990

TS.HOCHCCH3CH2CH2OO.cycHOCHCCH3CH2CH2OO.Et
~~~~~~~~~~~~~~~~~~~~~~~~~~~~~~~~~~~~~~~~~~
E(CCSD(T)/Aug-CC-pVTZ) (Hartree): -420.82644110
E(CCSD/Aug-CC-pVTZ) (Hartree): -420.75168260
     T1 diagnostic:  0.027377
E(MP2/Aug-CC-pVTZ) (Hartree): -420.69320422
E(MP3/Aug-CC-pVTZ) (Hartree): -420.73169845
E(PMP2/Aug-CC-pVTZ) (Hartree): -420.71075959
E(PMP3/Aug-CC-pVTZ) (Hartree): -420.74484390
E(PUHF/Aug-CC-pVTZ) (Hartree): -419.16124987
E(UHF/Aug-CC-pVTZ) (Hartree): -419.14094997
E(UM062X/Aug-CC-pVTZ) (Hartree): -421.43224778
Electronic state : 2-A
Cartesian coordinates (Angs):
     C       0.901440     -0.521479       0.586849
     C       0.502829      0.769096       0.333071
     C      -0.894366      1.109763       0.725147
     C      -1.864531      0.326386      -0.190794
     O      -1.591884     -1.049777      -0.073455
     O      -0.384427     -1.307941      -0.683039
     O       2.095071     -0.960328       0.136906
     H       0.439773     -1.087856       1.386068
     C       1.212414      1.628625      -0.655606
     H      -1.109120      0.822969       1.754911
     H      -1.083272      2.178781       0.618222
     H      -2.898699      0.457600       0.126698
```

```
     H      -1.748306      0.635648      -1.231358
     H       2.156168     -1.910354       0.265310
     H       1.301757      2.650040      -0.281367
     H       0.641760      1.676875      -1.589447
     H       2.203139      1.246316      -0.884335
Rotational constants (GHz):    2.8787500    1.9716900    1.3999900
Vibrational harmonic frequencies (cm-1):
     i553.2027                109.9272                129.4570
      161.2925                272.9190                293.9918
      335.0045                356.8991                383.6058
      430.7677                499.5686                584.3038
      625.0749                816.1024                874.9959
      937.0347                964.9763                987.8429
     1010.4461               1035.3106               1075.9675
     1087.1538               1189.3977               1224.8218
     1245.0144               1264.3001               1303.5546
     1334.5962               1374.3540               1390.3968
     1422.9022               1477.8849               1482.0055
     1488.2023               1492.0330               1602.7358
     3031.4077               3066.6412               3072.5900
     3092.3654               3121.7575               3134.3623
     3168.0763               3189.7552               3887.1174
Zero-point correction (Hartree): 0.139034


TS.HOCHCCH3CH2CH2OO.1-6Hshift.a.Ec
----------------------------------
E(CCSD(T)/Aug-CC-pVTZ) (Hartree): -420.80543099
E(CCSD/Aug-CC-pVTZ) (Hartree): -420.73000039
     T1 diagnostic:  0.024966
E(MP2/Aug-CC-pVTZ) (Hartree): -420.67733307
E(MP3/Aug-CC-pVTZ) (Hartree): -420.71333383
E(PMP2/Aug-CC-pVTZ) (Hartree): -420.69231131
E(PMP3/Aug-CC-pVTZ) (Hartree): -420.72403263
E(PUHF/Aug-CC-pVTZ) (Hartree): -419.12957042
E(UHF/Aug-CC-pVTZ) (Hartree): -419.11164555
E(UM062X/Aug-CC-pVTZ) (Hartree): -421.41459562
Electronic state : 2-A
Cartesian coordinates (Angs):
     O       1.611663     -1.284114      -0.619711
     H       0.570609     -1.436504       0.047100
     C      -0.397947     -1.100677       0.836472
     O       2.231586     -0.228477       0.005948
     C      -0.728993      0.240864       0.373594
     C       1.585033      0.992460      -0.352959
     C       0.358900      1.279457       0.506288
     H       0.156254     -1.138816       1.772511
     H      -1.154259     -1.878237       0.771877
     C      -1.881294      0.561876      -0.234616
     O      -2.930091     -0.252592      -0.482316
     H      -2.076507      1.567403      -0.583044
     H       2.343442      1.759914      -0.195592
     H       1.326531      0.944954      -1.412172
     H      -0.024832      2.261609       0.223290
     H       0.680104      1.342327       1.549750
     H      -2.740806     -1.145064      -0.177763
Rotational constants (GHz):    3.7713900    1.2756300    1.0917400
Vibrational harmonic frequencies (cm-1):
    i2187.2165                79.1229                145.5697
      202.8478               290.9588                295.2709
      344.0117               403.4398                455.9409
      495.2855               550.5102                563.2053
      629.2395               656.4428                815.4285
      873.4114               917.9509                956.2470
      990.7497              1016.8466               1060.0645
     1081.7357              1118.5491               1190.0307
     1204.8801              1238.1535               1253.3422
     1299.2440              1329.1686               1375.6154
     1396.7598              1416.0353               1465.7503
     1478.7994              1485.3532               1530.7273
     1702.6711              3050.4029               3069.6122
     3098.1448              3102.9731               3128.3971
     3176.8308              3215.6662               3865.5866
Zero-point correction (Hartree): 0.134451

TS.HOCHCCH3CH2CH2OO.1-6Hshift.a.Et
----------------------------------
E(UM062X/Aug-CC-pVTZ) (Hartree): -421.41378992
Electronic state : 2-A
Cartesian coordinates (Angs):
     O       1.601501     -1.290271      -0.618535
     H       0.561291     -1.438259       0.056889
     C      -0.401768     -1.097574       0.847814
     O       2.232270     -0.235626       0.001025
     C      -0.713173      0.247279       0.381248
     C       1.594707      0.986734      -0.362118
     C       0.371862      1.287446       0.498634
     H       0.154954     -1.145404       1.781839
     H      -1.189898     -1.835589       0.756039
     C      -1.868947      0.544929      -0.223165
     O      -2.847699     -0.382535      -0.401426
     H      -2.078130      1.543523      -0.589924
     H       2.358378      1.750500      -0.211240
```

```
     H       1.332110      0.935967      -1.420313
     H      -0.010168      2.268012       0.206377
     H       0.697337      1.359552       1.540003
     H      -3.610527      0.016269      -0.822647
Rotational constants (GHz):    3.7784100    1.2856200    1.0982000
Vibrational harmonic frequencies (cm-1):
    i2126.1464                  82.8438                 145.7752
      213.6238                 269.8116                 277.2568
      325.9406                 373.3494                 448.8572
      472.1455                 554.2206                 568.7976
      633.4221                 661.9724                 823.5970
      875.3510                 878.8346                 957.0137
     1001.7419                1015.9198                1062.1319
     1082.5804                1119.0508                1198.9166
     1199.9316                1231.2216                1252.2669
     1295.3559                1318.6255                1377.5621
     1397.1068                1404.6352                1462.3339
     1478.6047                1479.7281                1516.7170
     1730.1079                3050.1858                3067.5503
     3099.5063                3107.3536                3126.1656
     3182.5087                3211.7110                3914.6619
Zero-point correction (Hartree): 0.134291

TS.HOCHCCH3CH2CH2OO.1-6Hshift.b.Ec
----------------------------------
E(UM062X/Aug-CC-pVTZ) (Hartree): -421.41342897
Electronic state : 2-A
Cartesian coordinates (Angs):
     O      -1.809153      1.189157      -0.280637
     H      -0.693200      1.491482       0.191782
     C       0.459690      1.311138       0.776573
     O      -1.506597      0.067604      -1.009623
     C       0.653638     -0.107794       0.532762
     C      -1.543084     -1.075315      -0.157669
     C      -0.494299     -0.994585       0.960701
     H       0.164990      1.569807       1.791662
     H       1.170044      2.019741       0.358664
     C       1.682250     -0.631587      -0.156204
     O       2.736439      0.031551      -0.672135
     H       1.754807     -1.694854      -0.345186
     H      -2.553466     -1.197939       0.236613
     H      -1.317258     -1.896094      -0.838222
     H      -0.152773     -2.001917       1.198934
     H      -0.942200     -0.582073       1.864560
     H       2.654362      0.974213      -0.496627
Rotational constants (GHz):    3.3187200    1.4055600    1.2662400
Vibrational harmonic frequencies (cm-1):
    i2094.4757                  79.0026                 123.8287
      232.6307                 277.1059                 301.8495
      371.7860                 378.3727                 434.8235
      486.2273                 537.4493                 568.2219
      625.1325                 708.2326                 807.3081
      858.3569                 921.8416                 954.5784
     1018.9063                1030.5444                1058.5716
     1082.5619                1126.5080                1200.3832
     1219.9226                1253.2084                1266.0461
     1287.5495                1327.3345                1364.0460
     1396.2710                1414.5928                1482.8872
     1488.3685                1498.0181                1501.1903
     1689.9085                3068.2305                3082.1468
     3098.4667                3116.4651                3135.8086
     3174.3543                3212.3579                3857.4644
Zero-point correction (Hartree): 0.134683

TS.HOCHCCH3CH2CH2OO.1-6Hshift.b.Et
----------------------------------
E(UM062X/Aug-CC-pVTZ) (Hartree): -421.41202505
Electronic state : 2-A
Cartesian coordinates (Angs):
     O      -1.801016      1.194880      -0.292037
     H      -0.680972      1.494659       0.182105
     C       0.458122      1.309432       0.788425
     O      -1.505795      0.067479      -1.018020
     C       0.640213     -0.110418       0.546060
     C      -1.555137     -1.071067      -0.163841
     C      -0.505830     -1.004294       0.957098
     H       0.137967      1.569895       1.795354
     H       1.204489      1.976818       0.373802
     C       1.677405     -0.607886      -0.141367
     O       2.680110      0.183750      -0.600182
     H       1.766000     -1.668997      -0.347278
     H      -2.566519     -1.181391       0.231818
     H      -1.340686     -1.896938      -0.842239
     H      -0.165710     -2.015214       1.183006
     H      -0.955428     -0.603189       1.865159
     H       3.325829     -0.339119      -1.078065
Rotational constants (GHz):    3.3264600    1.4097200    1.2706800
Vibrational harmonic frequencies (cm-1):
    i2051.6284                  80.8964                 118.0649
      234.7208                 253.7706                 296.7965
      327.8990                 367.3283                 412.4711
      463.3578                 542.0591                 565.4153
      629.6163                 708.5276                 808.9682
```

```
      856.5643                886.7265                954.9900
     1018.2313               1030.5736               1064.8990
     1082.5759               1127.6163               1207.4368
     1210.8433               1252.4923               1264.9906
     1289.6721               1309.7406               1357.9237
     1397.5991               1405.8849               1478.3326
     1482.6085               1488.6295               1499.8821
     1716.0912               3066.0063               3080.8514
     3108.1941               3113.8368               3133.5914
     3180.4327               3210.1388               3913.5482
Zero-point correction (Hartree): 0.134414


################################################################################
Z-HOCH=C(CH3)CH2CH2OO ring closure and H-shift
################################################################################

HOCHCCH3CH2CH2OO.Zcpmm
----------------------
E(UM062X/Aug-CC-pVTZ) (Hartree): -421.44926728
Electronic state : 2-A
Cartesian coordinates (Angs):
     C       1.130828      1.189643       0.118372
     C       1.238603     -0.132009      -0.010035
     C       0.223458     -1.204350       0.298823
     C      -1.174937     -0.855596       0.776147
     O      -2.076071     -0.621963      -0.337399
     O      -1.939195      0.550472      -0.866455
     O       0.048799      1.933320       0.470619
     H       2.005167      1.806843      -0.055894
     C       2.555327     -0.707592      -0.455973
     H       0.121413     -1.869420      -0.565394
     H       0.663012     -1.830250       1.083227
     H      -1.627782     -1.712607       1.269338
     H      -1.213156      0.009725       1.433576
     H      -0.745437      1.559668       0.057560
     H       3.299289      0.071191      -0.610861
     H       2.443891     -1.258622      -1.393007
     H       2.945669     -1.411728       0.283331
Rotational constants (GHz):    2.8902200    1.5369100    1.1689500
Vibrational harmonic frequencies (cm-1):
       24.0365                 77.6570                189.7251
      198.5005                212.4232                301.1457
      319.7088                342.3071                426.8330
      433.3245                555.5785                612.1342
      683.9066                774.3618                863.0769
      915.0358                972.8046               1009.5127
     1050.9749               1071.7262               1096.5676
     1181.8355               1220.7331               1247.8945
     1277.4254               1332.8511               1356.0380
     1407.6980               1409.2349               1419.2418
     1438.9876               1461.5529               1484.0105
     1501.8632               1507.0806               1769.4280
     3030.3042               3041.7617               3055.8862
     3088.3897               3111.8810               3143.4802
     3168.9225               3179.4980               3648.0915
Zero-point correction (Hartree): 0.140370

HOCHCCH3CH2CH2OO.Zcppc
----------------------
E(UM062X/Aug-CC-pVTZ) (Hartree): -421.44991842
Electronic state : 2-A
Cartesian coordinates (Angs):
     C       1.302368      1.134243      -0.052999
     C       1.292066     -0.197500      -0.038492
     C       0.113401     -1.112402       0.187562
     C      -1.101218     -0.564118       0.907252
     O      -1.906118      0.273034       0.035929
     O      -2.522093     -0.422441      -0.870935
     O       0.278841      2.017500       0.086638
     H       2.242014      1.657752      -0.178460
     C       2.581383     -0.932962      -0.282837
     H      -0.224491     -1.555842      -0.754835
     H       0.469624     -1.953295       0.789785
     H      -1.753771     -1.364950       1.247106
     H      -0.836395      0.090558       1.735721
     H      -0.571467      1.619975      -0.129949
     H       3.407289     -0.247262      -0.461502
     H       2.495186     -1.588545      -1.153039
     H       2.838972     -1.566692       0.569206
Rotational constants (GHz):    3.0876200    1.3938000    1.0892800
Vibrational harmonic frequencies (cm-1):
       41.4157                 88.8959                158.4002
      203.7030                214.9268                267.4457
      306.5270                349.4743                426.3144
      468.9643                540.3332                555.0457
      616.7284                783.5881                848.6957
      920.2684                977.4469               1010.4465
     1023.8451               1070.5587               1118.5778
     1177.7980               1205.3420               1226.1172
     1285.3179               1308.7509               1328.8084
     1396.5434               1402.0385               1419.5250
     1434.5639               1466.7983               1484.7455
```

```
     1489.9621                1503.0773                1770.8431
     3041.0376                3043.7765                3071.5466
     3088.6966                3103.7687                3142.8778
     3164.1479                3197.6601                3816.3222
Zero-point correction (Hartree): 0.140248

HOCHCCH3CH2CH2OO.Zcptt
~~~~~~~~~~~~~~~~~~~~~~
E(UM062X/Aug-CC-pVTZ) (Hartree): -421.44798473
Electronic state : 2-A
Cartesian coordinates (Angs):
     C       1.111782      1.202708      -0.048985
     C       1.321607     -0.106468       0.000181
     C       0.372817     -1.143483       0.544186
     C      -1.082610     -0.764033       0.699462
     O      -1.584852     -0.416972      -0.610449
     O      -2.785048      0.066786      -0.547755
     O      -0.001108      1.821837       0.451410
     H       1.860828      1.861847      -0.473951
     C       2.623586     -0.662260      -0.501470
     H       0.429102     -2.020392      -0.107435
     H       0.730553     -1.483099       1.521683
     H      -1.670436     -1.612639       1.049149
     H      -1.242637      0.091413       1.346309
     H      -0.106376      2.684059       0.045726
     H       3.140249     -1.213026       0.288487
     H       3.289287      0.123328      -0.854380
     H       2.454407     -1.363486      -1.321472
Rotational constants (GHz):    3.1846200    1.3743500    1.1036000
Vibrational harmonic frequencies (cm-1):
       41.7350                  54.6761                 136.9906
      196.3076                 224.8723                 256.5599
      272.2639                 309.1968                 342.1811
      389.1014                 449.4868                 541.9392
      634.2976                 783.3691                 838.9369
      888.2290                1005.2984                1008.2993
     1044.5282                1077.3965                1102.6649
     1177.8265                1204.1175                1242.1809
     1276.9776                1294.3337                1304.8379
     1384.4248                1413.3817                1421.5673
     1433.4271                1466.7757                1483.4140
     1500.1768                1504.6908                1800.8913
     3040.9819                3045.7174                3070.2552
     3094.2460                3095.3060                3140.4667
     3175.4861                3184.9905                3907.3554
Zero-point correction (Hartree): 0.139565

HOCHCCH3CH2CH2OO.Zctpc
~~~~~~~~~~~~~~~~~~~~~~
E(UM062X/Aug-CC-pVTZ) (Hartree): -421.44515262
Electronic state : 2-A
Cartesian coordinates (Angs):
     C      -1.954737      0.702111      -0.066637
     C      -1.292319     -0.449834      -0.007600
     C       0.197765     -0.675928       0.038772
     C       1.099300      0.522071       0.262716
     O       2.448422      0.069257       0.503280
     O       3.004518     -0.353378      -0.590800
     O      -1.493168      1.984059      -0.122603
     H      -3.036633      0.701284      -0.068602
     C      -2.079754     -1.732002       0.012289
     H       0.399791     -1.381335       0.850752
     H       0.521164     -1.176700      -0.878264
     H       1.155607      1.183685      -0.603865
     H       0.836007      1.076985       1.162625
     H      -0.546872      2.014117      -0.268205
     H      -3.150674     -1.546910      -0.040197
     H      -1.874075     -2.301120       0.921577
     H      -1.804015     -2.368020      -0.832066
Rotational constants (GHz):    3.2170000    1.1150700    0.8728000
Vibrational harmonic frequencies (cm-1):
       25.4172                  78.3647                 123.7774
      170.7876                 196.9246                 227.9818
      287.8662                 320.1712                 343.9952
      406.9443                 474.0316                 574.1455
      604.6082                 791.2435                 883.9768
      921.8576                 975.5759                1005.4773
     1051.2166                1083.7976                1123.9663
     1173.5548                1183.5992                1246.7477
     1278.9744                1303.1522                1346.0534
     1355.9993                1411.8816                1419.2780
     1434.4271                1483.0102                1487.6386
     1504.0531                1515.7753                1779.0413
     3042.4192                3047.0036                3065.3448
     3076.6750                3095.3128                3140.2386
     3146.0393                3213.1117                3925.5280
Zero-point correction (Hartree): 0.139759

HOCHCCH3CH2CH2OO.Zctpt
~~~~~~~~~~~~~~~~~~~~~~
E(UM062X/Aug-CC-pVTZ) (Hartree): -421.44961874
Electronic state : 2-A
Cartesian coordinates (Angs):
```

```
     C      -1.910461      0.687968      -0.132568
     C      -1.279218     -0.468402       0.020212
     C       0.193008     -0.658194       0.265105
     C       1.080153      0.569106       0.189292
     O       2.452055      0.165698       0.416055
     O       2.935128     -0.475134      -0.603425
     O      -1.293149      1.911294      -0.076811
     H      -2.980286      0.712591      -0.304352
     C      -2.063894     -1.748177      -0.033569
     H       0.327699     -1.125570       1.246155
     H       0.572150     -1.379256      -0.464639
     H       1.037631      1.055505      -0.781581
     H       0.876641      1.290249       0.974713
     H      -1.926284      2.602984      -0.272360
     H      -3.124880     -1.566021      -0.195353
     H      -1.952764     -2.308170       0.897707
     H      -1.699699     -2.390990      -0.837673
Rotational constants (GHz):    3.1892200    1.1588400    0.8959600
Vibrational harmonic frequencies (cm-1):
       34.7291                  89.3545                 133.3168
      169.8388                 185.6689                 216.9190
      265.2060                 311.7155                 345.4390
      397.6089                 456.9792                 567.6594
      604.5898                 790.8203                 878.8482
      888.6487                 966.6599                1004.5028
     1046.3952                1088.0718                1117.8057
     1174.1608                1201.1280                1238.9297
     1268.2535                1294.4717                1332.8919
     1353.3483                1407.4306                1422.2608
     1431.8591                1481.9638                1483.7375
     1493.8845                1504.6745                1803.5656
     3037.9988                3048.1738                3074.2592
     3098.3665                3123.7778                3140.1703
     3183.9106                3189.7624                3920.7129
Zero-point correction (Hartree): 0.139584

HOCHCCH3CH2CH2OO.Zgmmc
~~~~~~~~~~~~~~~~~~~~~~
E(UM062X/Aug-CC-pVTZ) (Hartree): -421.45072057
Electronic state : 2-A
Cartesian coordinates (Angs):
     C       1.989804      0.208706      -0.313793
     C       0.826097      0.596713       0.196926
     C      -0.065618     -0.359934       0.947609
     C      -0.945036     -1.198469       0.032037
     O      -1.823393     -0.354934      -0.746128
     O      -2.718326      0.210818       0.003761
     O       2.543784     -1.034946      -0.234980
     H       2.629282      0.883352      -0.866545
     C       0.339780      2.005975       0.026131
     H       0.509180     -1.048789       1.575217
     H      -0.716760      0.191344       1.626975
     H      -0.361834     -1.730557      -0.718451
     H      -1.574360     -1.891379       0.589167
     H       2.003592     -1.606928       0.316729
     H      -0.624440      2.029662      -0.484220
     H       1.047187      2.600169      -0.550200
     H       0.201475      2.487689       0.996649
Rotational constants (GHz):    3.3559600    1.2984200    1.0556100
Vibrational harmonic frequencies (cm-1):
       40.9393                  66.7204                 142.3623
      169.4739                 193.3883                 289.2887
      302.5363                 332.5190                 387.9733
      421.2621                 534.2735                 570.9138
      613.4048                 790.2132                 848.8792
      917.2383                 948.1353                1009.7677
     1031.0112                1071.8344                1097.2237
     1177.1280                1189.8680                1239.8074
     1266.6471                1299.3519                1313.3219
     1364.8695                1399.9540                1410.5359
     1423.9707                1481.6530                1488.0521
     1493.7835                1504.0293                1772.4866
     3041.5945                3051.1800                3087.2260
     3106.0248                3108.3076                3140.4678
     3149.7913                3219.9452                3871.8849
Zero-point correction (Hartree): 0.139837

HOCHCCH3CH2CH2OO.Zgmmt
~~~~~~~~~~~~~~~~~~~~~~
E(UM062X/Aug-CC-pVTZ) (Hartree): -421.45252662
Electronic state : 2-A
Cartesian coordinates (Angs):
     C       1.937512     -0.188903      -0.323205
     C       0.805674     -0.633427       0.203909
     C      -0.070602      0.296764       1.002205
     C      -0.912154      1.199539       0.117663
     O      -1.770587      0.420154      -0.748972
     O      -2.692514     -0.194761      -0.074327
     O       2.332130      1.115667      -0.158502
     H       2.592745     -0.818658      -0.913257
     C       0.345735     -2.044789       0.001752
     H      -0.736259     -0.273491       1.650451
     H       0.540127      0.946490       1.631171
```

```
     H      -1.556161      1.858637       0.698149
     H      -0.290957      1.773311      -0.566664
     H       3.207424      1.243071      -0.526465
     H       0.236027     -2.554879       0.961179
     H       1.048398     -2.611123      -0.608111
     H      -0.630563     -2.066941      -0.485989
Rotational constants (GHz):    3.2226000    1.3598600    1.0889800
Vibrational harmonic frequencies (cm-1):
       42.8964                65.6193                142.7389
      167.1418               189.3145                227.3757
      288.6729               320.2290                354.3743
      391.2909               531.7092                574.5252
      617.5566               798.6739                848.1971
      878.3959               950.0970               1009.2751
     1028.4883              1072.7596               1100.3847
     1182.1118              1197.7530               1226.2701
     1262.8379              1299.1358               1318.7714
     1362.3503              1390.7542               1407.4201
     1423.0941              1474.4708               1481.9141
     1491.8754              1503.0181               1794.6668
     3050.6164              3075.4455               3095.1329
     3105.4278              3124.1288               3136.8179
     3163.0238              3188.8317               3919.8657
Zero-point correction (Hartree): 0.139596

HOCHCCH3CH2CH2OO.Zgmpc
~~~~~~~~~~~~~~~~~~~~~~
E(UM062X/Aug-CC-pVTZ) (Hartree): -421.44933493
Electronic state : 2-A
Cartesian coordinates (Angs):
     C       1.782933      0.110969      -0.461481
     C       0.787914      0.564110       0.293452
     C      -0.004858     -0.353506       1.188551
     C      -1.119576     -1.100004       0.464262
     O      -2.097280     -0.166343      -0.034011
     O      -1.863617      0.176104      -1.265665
     O       2.230116     -1.173930      -0.541764
     H       2.351128      0.759979      -1.113582
     C       0.402348      2.013945       0.272419
     H       0.633315     -1.104711       1.666413
     H      -0.447622      0.220846       2.003959
     H      -0.752162     -1.663208      -0.392318
     H      -1.670244     -1.749300       1.143820
     H       1.742706     -1.737215       0.064959
     H       1.019339      2.575114      -0.427427
     H       0.518723      2.460585       1.262732
     H      -0.641492      2.138175      -0.020258
Rotational constants (GHz):    2.7294700    1.4523500    1.2564800
Vibrational harmonic frequencies (cm-1):
       48.7034                88.8848                105.7465
      169.7326               194.4482                263.3324
      294.1944               342.2144                378.2690
      420.1903               528.8116                569.2579
      604.0069               779.9811                872.6524
      918.2761               938.0512               1019.9914
     1036.1814              1069.0318               1087.0051
     1177.5739              1191.8773               1236.3051
     1258.3935              1300.3856               1329.8438
     1370.3998              1391.7892               1410.7006
     1423.2240              1481.1253               1483.1346
     1491.9566              1502.5607               1774.5235
     3036.0261              3048.8346               3086.6194
     3098.1440              3104.4574               3141.0885
     3151.2493              3221.7205               3877.9113
Zero-point correction (Hartree): 0.139695

HOCHCCH3CH2CH2OO.Zgmpt
~~~~~~~~~~~~~~~~~~~~~~
E(UM062X/Aug-CC-pVTZ) (Hartree): -421.45143242
Electronic state : 2-A
Cartesian coordinates (Angs):
     C       1.737121      0.063987      -0.456171
     C       0.779185      0.601911       0.284741
     C      -0.011417     -0.262962       1.230502
     C      -1.095726     -1.067273       0.528296
     O      -2.080353     -0.182475      -0.047689
     O      -1.816170      0.105465      -1.286838
     O       2.025882     -1.274731      -0.377320
     H       2.322426      0.642226      -1.160931
     C       0.431283      2.055253       0.184803
     H       0.645789     -0.982963       1.721704
     H      -0.471362      0.351282       2.006168
     H      -0.687958     -1.672298      -0.278096
     H      -1.653186     -1.683368       1.232423
     H       2.762741     -1.485878      -0.951833
     H       1.056551      2.565317      -0.546653
     H       0.559200      2.551269       1.149607
     H      -0.611754      2.182851      -0.110643
Rotational constants (GHz):    2.6594900    1.5166600    1.2947300
Vibrational harmonic frequencies (cm-1):
       45.6868                87.5472                103.4694
      176.4799               193.2789                234.0679
      281.1618               330.6672                348.3348
```

```
      397.9300                 526.6332                 570.6983
      607.3737                 787.0443                 870.6459
      876.5100                 939.9320                1016.1217
     1035.2074                1070.4997                1088.9494
     1183.0382                1198.2857                1234.1057
     1242.8935                1310.5007                1325.2313
     1366.3777                1382.6238                1408.4118
     1421.3718                1472.8623                1481.4155
     1485.9827                1501.6823                1796.0196
     3048.6422                3067.6456                3095.2545
     3103.2459                3114.5449                3137.1026
     3164.9746                3192.3371                3920.0508
Zero-point correction (Hartree): 0.139521

HOCHCCH3CH2CH2OO.Zgmtc
----------------------
E(UM062X/Aug-CC-pVTZ) (Hartree): -421.44965828
Electronic state : 2-A
Cartesian coordinates (Angs):
     C       1.939070     -0.129593      -0.510460
     C       1.011908      0.552033       0.154141
     C       0.089828     -0.124896       1.137626
     C      -1.102311     -0.796531       0.478876
     O      -1.901160      0.241346      -0.129589
     O      -2.928763     -0.251629      -0.747865
     O       2.204870     -1.462661      -0.411107
     H       2.596994      0.343679      -1.226528
     C       0.832012      2.025207      -0.065783
     H       0.613282     -0.886342       1.724394
     H      -0.277367      0.604850       1.861275
     H      -0.805748     -1.479880      -0.317169
     H      -1.739491     -1.315071       1.194778
     H       1.645233     -1.868477       0.256231
     H      -0.181116      2.248067      -0.403871
     H       1.532750      2.401156      -0.809499
     H       0.992846      2.578250       0.862484
Rotational constants (GHz):    3.0103600    1.2180800    1.0238900
Vibrational harmonic frequencies (cm-1):
       41.4082                  75.5142                 119.9922
      173.6373                 195.7565                 273.3382
      284.5693                 314.9211                 381.6568
      392.4674                 489.2844                 577.5848
      622.5919                 786.1280                 841.5853
      921.7769                 977.9475                1025.9881
     1049.6434                1070.3287                1087.9050
     1176.7408                1196.4185                1244.8787
     1276.7479                1294.6012                1306.7742
     1367.8364                1402.7677                1410.5180
     1422.6055                1481.9338                1491.9293
     1499.3863                1505.2994                1775.1273
     3043.9052                3050.1255                3078.3368
     3098.5812                3105.7877                3137.3926
     3141.1266                3219.1818                3876.0556
Zero-point correction (Hartree): 0.139670

HOCHCCH3CH2CH2OO.Zgmtt
----------------------
E(UM062X/Aug-CC-pVTZ) (Hartree): -421.45153725
Electronic state : 2-A
Cartesian coordinates (Angs):
     C       1.880460     -0.188728      -0.506354
     C       1.011983      0.572220       0.144584
     C       0.096187     -0.044062       1.170887
     C      -1.088956     -0.750130       0.542855
     O      -1.874325      0.247915      -0.150741
     O      -2.889016     -0.281038      -0.759924
     O       1.966358     -1.535761      -0.260800
     H       2.549319      0.206647      -1.261521
     C       0.889736      2.038765      -0.135028
     H       0.635776     -0.789604       1.756667
     H      -0.265876      0.721474       1.859021
     H      -0.775125     -1.488032      -0.193238
     H      -1.741217     -1.213280       1.282420
     H       2.681224     -1.918254      -0.771152
     H      -0.121915      2.284581      -0.462218
     H       1.588769      2.357583      -0.907021
     H       1.088445      2.621573       0.767096
Rotational constants (GHz):    2.9146800    1.2701200    1.0549900
Vibrational harmonic frequencies (cm-1):
       42.7504                  72.7486                 117.7732
      178.3161                 198.3964                 245.1979
      285.7025                 300.6185                 347.4777
      375.8057                 479.9849                 582.0684
      623.8398                 794.2295                 840.9293
      877.0195                 983.2028                1025.2759
     1042.4252                1075.1355                1088.8214
     1181.7763                1199.4183                1228.8308
     1269.4839                1298.6573                1317.1769
     1362.1365                1396.8202                1406.5667
     1421.5974                1473.6656                1482.2938
     1502.4534                1505.0698                1794.8735
     3050.0418                3071.5608                3089.2414
     3105.2245                3118.0648                3137.4365
```

```
     3152.1171                3190.2015                3919.1491
Zero-point correction (Hartree): 0.139541

HOCHCCH3CH2CH2OO.Zgpmc
~~~~~~~~~~~~~~~~~~~~~~
E(UM062X/Aug-CC-pVTZ) (Hartree): -421.45240759
Electronic state : 2-A
Cartesian coordinates (Angs):
     C       1.224405      1.071636       0.115225
     C       1.093779     -0.235051      -0.098039
     C       0.100153     -0.780139      -1.085588
     C      -1.252678     -1.100586      -0.463721
     O      -1.846708      0.122595       0.018775
     O      -1.626316      0.305916       1.289588
     O       0.501693      2.068096      -0.462038
     H       1.972419      1.462813       0.792974
     C       1.914167     -1.228647       0.668231
     H      -0.054263     -0.084383      -1.913673
     H       0.486521     -1.704024      -1.522661
     H      -1.953299     -1.490637      -1.200553
     H      -1.174329     -1.775711       0.385619
     H      -0.359671      1.738532      -0.737933
     H       1.276658     -1.891783       1.259108
     H       2.597727     -0.732283       1.354866
     H       2.499926     -1.858654      -0.004990
Rotational constants (GHz):    2.4124700    1.7738900    1.3808600
Vibrational harmonic frequencies (cm-1):
       53.2250                  92.8312                 110.8594
      190.7603                 202.6129                 259.5484
      307.3685                 344.1491                 378.7662
      437.9692                 526.9002                 582.3746
      602.7792                 774.7668                 862.8993
      918.0243                 979.9982                 993.6932
     1030.2699                1066.0743                1084.6708
     1184.8261                1199.6995                1224.5053
     1269.9523                1306.9516                1323.5696
     1366.7961                1384.1554                1411.7458
     1422.4428                1479.2083                1487.6470
     1488.9137                1500.8396                1764.8020
     3040.9682                3056.5544                3088.9997
     3091.9236                3100.8731                3138.8295
     3159.6501                3206.2195                3848.4104
Zero-point correction (Hartree): 0.139763

HOCHCCH3CH2CH2OO.Zgppc
~~~~~~~~~~~~~~~~~~~~~~
E(CCSD(T)/Aug-CC-pVTZ) (Hartree): -420.84631979
E(CCSD/Aug-CC-pVTZ) (Hartree): -420.77536686
     T1 diagnostic:  0.021002
E(MP2/Aug-CC-pVTZ) (Hartree): -420.72348730
E(MP3/Aug-CC-pVTZ) (Hartree): -420.76218978
E(PMP2/Aug-CC-pVTZ) (Hartree): -420.72673939
E(PMP3/Aug-CC-pVTZ) (Hartree): -420.76408756
E(PUHF/Aug-CC-pVTZ) (Hartree): -419.18016550
E(UHF/Aug-CC-pVTZ) (Hartree): -419.17484935
E(UM062X/Aug-CC-pVTZ) (Hartree): -421.45480404
Electronic state : 2-A
Cartesian coordinates (Angs):
     C      -1.212494      1.178878      -0.172259
     C      -1.161420     -0.120390       0.111263
     C      -0.063202     -0.717029       0.948967
     C       1.038780     -1.369346       0.134278
     O       1.696511     -0.421967      -0.746504
     O       2.167644      0.596960      -0.102567
     O      -0.325313      2.138965       0.186655
     H      -2.036973      1.595904      -0.737046
     C      -2.216824     -1.058983      -0.394807
     H       0.382627      0.021461       1.615150
     H      -0.480267     -1.497923       1.590496
     H       1.813810     -1.800446       0.767521
     H       0.656562     -2.124151      -0.549973
     H       0.523487      1.748654       0.428011
     H      -2.961550     -0.533786      -0.990435
     H      -2.729056     -1.555064       0.433194
     H      -1.788407     -1.845085      -1.022259
Rotational constants (GHz):    2.6040800    1.7509900    1.2063500
Vibrational harmonic frequencies (cm-1):
       44.7648                 126.1924                 134.7356
      191.5450                 199.3966                 275.1822
      313.8253                 352.8731                 395.9432
      453.1138                 531.0890                 580.7217
      633.5081                 769.4751                 848.0543
      928.5450                 971.3108                 982.7232
     1032.1058                1072.3501                1091.7482
     1189.0619                1205.0560                1249.2238
     1274.8693                1304.4794                1327.1191
     1372.8944                1403.2116                1416.6370
     1424.7850                1480.5896                1492.7890
     1495.1440                1502.5296                1770.9465
     3040.2241                3062.2873                3085.6176
     3092.1114                3115.3914                3138.1233
     3155.0114                3201.6968                3806.0569
Zero-point correction (Hartree): 0.140187
```

```
HOCHCCH3CH2CH2OO.Zgppt
~~~~~~~~~~~~~~~~~~~~~~
E(UM062X/Aug-CC-pVTZ) (Hartree): -421.45053934
Electronic state : 2-A
Cartesian coordinates (Angs):
     C      -1.451259      0.979163      -0.222332
     C      -1.140884     -0.268690       0.103488
     C       0.033012     -0.571021       0.992191
     C       1.204235     -1.175474       0.235921
     O       1.720483     -0.246319      -0.742162
     O       2.350518      0.735054      -0.172919
     O      -0.750905      2.051340       0.251475
     H      -2.292076      1.204611      -0.869038
     C      -1.948873     -1.422287      -0.410435
     H       0.381536      0.331125       1.491996
     H      -0.260136     -1.289196       1.763415
     H       2.025859     -1.431021       0.902989
     H       0.917013     -2.045772      -0.351916
     H      -1.030789      2.852096      -0.193360
     H      -2.767359     -1.083959      -1.044064
     H      -2.374184     -1.998170       0.415019
     H      -1.338005     -2.110464      -0.999191
Rotational constants (GHz):    2.5793500    1.6307200    1.1579300
Vibrational harmonic frequencies (cm-1):
       23.6969                58.4108               132.3345
      164.5839               199.0826               216.6921
      280.8366               320.5261               381.6193
      386.6381               528.8669               572.3737
      614.8579               776.2974               854.9305
      893.9685               973.2870               992.2028
     1030.1971              1072.2597              1095.1143
     1184.1722              1200.4864              1231.9331
     1262.4902              1303.4023              1328.5719
     1356.8879              1397.4897              1415.4413
     1423.4672              1472.9296              1483.7819
     1495.5237              1502.2582              1800.5278
     3044.4417              3056.4649              3090.8389
     3096.1945              3134.4264              3134.7851
     3154.8935              3177.6820              3922.3740
Zero-point correction (Hartree): 0.139516

HOCHCCH3CH2CH2OO.Zgptc
~~~~~~~~~~~~~~~~~~~~~~
E(UM062X/Aug-CC-pVTZ) (Hartree): -421.45306200
Electronic state : 2-A
Cartesian coordinates (Angs):
     C      -1.371459      1.110287      -0.212460
     C      -1.279054     -0.192751       0.039897
     C      -0.238619     -0.760398       0.970525
     C       1.076458     -1.083310       0.289359
     O       1.692400      0.187561      -0.031864
     O       2.794303      0.047624      -0.699848
     O      -0.565969      2.095075       0.262908
     H      -2.159874      1.507199      -0.839848
     C      -2.218373     -1.170693      -0.601847
     H      -0.038244     -0.078086       1.801032
     H      -0.616913     -1.684079       1.412400
     H       1.770432     -1.617850       0.936960
     H       0.946632     -1.624807      -0.646736
     H       0.302756      1.738926       0.479120
     H      -2.920348     -0.670727      -1.267018
     H      -2.789432     -1.717126       0.152526
     H      -1.674596     -1.914337      -1.190851
Rotational constants (GHz):    2.8029500    1.4171900    1.0897600
Vibrational harmonic frequencies (cm-1):
       57.3231                80.2590               130.1165
      196.3217               214.8427               249.4889
      312.0548               331.1202               379.1148
      419.9506               492.9681               589.0586
      621.0146               776.7252               853.3318
      924.1319               978.4966              1023.9317
     1044.5439              1072.3649              1089.5633
     1187.7336              1201.8755              1242.6615
     1288.0289              1295.5147              1324.7652
     1375.5354              1395.8599              1414.3787
     1424.0857              1480.8590              1485.3804
     1499.6902              1502.5269              1768.9913
     3039.1369              3057.5259              3085.6433
     3086.1935              3104.6398              3138.6926
     3146.6525              3200.4163              3835.2996
Zero-point correction (Hartree): 0.139922

HOCHCCH3CH2CH2OO.Zgtmt
~~~~~~~~~~~~~~~~~~~~~~
E(UM062X/Aug-CC-pVTZ) (Hartree): -421.45141848
Electronic state : 2-A
Cartesian coordinates (Angs):
     C       1.910795      0.759196       0.121764
     C       1.289882     -0.377677      -0.163657
     C      -0.151579     -0.373830      -0.595839
     C      -1.058966     -0.353502       0.623931
     O      -2.443031     -0.497986       0.240163
```

```
     O      -2.891044      0.578278      -0.330829
     O       1.269773      1.963812       0.025290
     H       2.943778      0.787010       0.449125
     C       1.978439     -1.700807      -0.021869
     H      -0.376871      0.502971      -1.201488
     H      -0.368963     -1.266471      -1.184824
     H      -0.873423     -1.199722       1.283912
     H      -0.959773      0.582450       1.170849
     H       1.885295      2.681120       0.181772
     H       2.995821     -1.587669       0.349828
     H       2.019433     -2.220512      -0.981357
     H       1.437702     -2.352289       0.669216
Rotational constants (GHz):    3.1249400    1.1802200    0.9183300
Vibrational harmonic frequencies (cm-1):
       43.1009                58.2287                115.8739
      165.0305               197.0364                238.2868
      252.7400               310.3572                332.7529
      401.3085               536.1713                573.7785
      594.5100               790.6777                875.4494
      885.5576               963.3209               1008.2226
     1055.7709              1071.9139               1084.4082
     1192.6253              1201.1349               1234.1893
     1271.0156              1303.6814               1323.4556
     1342.5573              1394.4848               1404.8444
     1422.0094              1481.0544               1484.2054
     1496.6169              1504.6700               1794.8701
     3045.1051              3073.9297               3094.3677
     3096.8570              3130.5898               3137.3229
     3160.9014              3185.7677               3918.9888
Zero-point correction (Hartree): 0.139537

HOCHCCH3CH2CH2OO.Zgtpc
~~~~~~~~~~~~~~~~~~~~~~
E(UM062X/Aug-CC-pVTZ) (Hartree): -421.45153269
Electronic state : 2-A
Cartesian coordinates (Angs):
     C      -2.172461     -0.321246       0.095284
     C      -1.165908      0.518131      -0.127722
     C       0.187291      0.041686      -0.584998
     C       1.068171     -0.279022       0.612972
     O       2.385520     -0.687902       0.189328
     O       3.064743      0.317159      -0.272783
     O      -2.164945     -1.672241      -0.066668
     H      -3.137976      0.022345       0.441649
     C      -1.322705      1.991198       0.109069
     H       0.126622     -0.838889      -1.230495
     H       0.680113      0.819819      -1.169329
     H       1.185360      0.584699       1.265590
     H       0.686718     -1.124351       1.183673
     H      -1.320539     -1.962562      -0.423113
     H      -2.308195      2.227326       0.506967
     H      -1.184559      2.550868      -0.818376
     H      -0.576415      2.360131       0.816786
Rotational constants (GHz):    3.3818200    1.0889300    0.8774500
Vibrational harmonic frequencies (cm-1):
       47.0904                59.3591                123.6889
      170.7596               199.3611                262.7582
      289.7434               348.5679                378.5753
      401.8149               542.5799                582.9100
      584.9880               790.7431                859.8135
      922.9408               969.4043               1012.0313
     1055.9308              1070.7385               1080.7951
     1181.8975              1203.1236               1241.7774
     1275.1277              1291.2127               1326.6449
     1338.6892              1396.8576               1407.5070
     1424.5132              1482.0798               1488.2826
     1500.1410              1517.0705               1774.5180
     3046.0285              3051.1932               3094.0154
     3095.2825              3107.2019               3139.8687
     3155.7517              3215.6197               3868.0294
Zero-point correction (Hartree): 0.139827

HOCHCCH3CH2CH2OO.Zgtpt
~~~~~~~~~~~~~~~~~~~~~~
E(UM062X/Aug-CC-pVTZ) (Hartree): -421.45212613
Electronic state : 2-A
Cartesian coordinates (Angs):
     C       2.127603     -0.341528      -0.095140
     C       1.165326      0.542943       0.129471
     C      -0.187364      0.093080       0.611583
     C      -1.043209     -0.328801      -0.571457
     O      -2.372897     -0.693155      -0.141944
     O      -3.062456      0.351967       0.198994
     O       1.924794     -1.681023       0.107142
     H       3.108102     -0.051935      -0.454980
     C       1.367680      2.004129      -0.131708
     H      -0.093737     -0.750153       1.295365
     H      -0.694026      0.907621       1.130262
     H      -1.146821      0.470655      -1.304120
     H      -0.647740     -1.226149      -1.042759
     H       2.747212     -2.160115      -0.002551
     H       2.358161      2.207788      -0.536103
     H       1.245541      2.581101       0.787141
```

```
     H       0.627563      2.379937      -0.842295
Rotational constants (GHz):    3.3237100    1.1223700    0.8913600
Vibrational harmonic frequencies (cm-1):
       44.5717                  62.7876                 124.9787
      165.7322                 198.6336                 247.3023
      251.3303                 323.5266                 341.8888
      388.0639                 534.2879                 585.8553
      590.3510                 792.7493                 869.2410
      883.3122                 966.9106                1011.3992
     1053.3917                1076.6941                1081.4453
     1191.2637                1199.1809                1233.0549
     1281.3985                1292.1512                1332.3943
     1337.5528                1393.4216                1403.6697
     1422.3264                1480.7076                1484.0234
     1495.7953                1503.7741                1794.3768
     3046.1018                3078.2855                3095.8321
     3096.8492                3128.8474                3136.0435
     3162.9429                3187.1175                3917.9089
Zero-point correction (Hartree): 0.139628

HOCHCCH3CH2CH2OO.Zgttc
----------------------
E(UM062X/Aug-CC-pVTZ) (Hartree): -421.45042784
Electronic state : 2-A
Cartesian coordinates (Angs):
     C       2.104641     -0.568463      -0.240010
     C       1.312290      0.440597       0.107703
     C      -0.027993      0.218210       0.760028
     C      -1.112626      0.082160      -0.291915
     O      -2.377396     -0.051830       0.392218
     O      -3.360089     -0.181256      -0.444657
     O       1.870417     -1.896168      -0.060880
     H       3.059988     -0.404822      -0.720364
     C       1.705336      1.861328      -0.170639
     H      -0.036159     -0.666473       1.402354
     H      -0.266928      1.063845       1.407142
     H      -1.175497      0.961918      -0.931327
     H      -0.976950     -0.802550      -0.913781
     H       1.034099     -2.032532       0.393316
     H       2.655471      1.914321      -0.699395
     H       1.798883      2.428605       0.757942
     H       0.953749      2.368736      -0.780328
Rotational constants (GHz):    3.3294000    1.0160900    0.8374500
Vibrational harmonic frequencies (cm-1):
       38.7932                  77.6442                  94.8878
      139.8178                 200.9508                 250.4780
      290.2145                 327.8353                 372.3155
      417.0661                 482.9092                 583.9397
      592.0907                 785.2912                 855.9910
      925.0215                1001.1203                1021.6723
     1060.4102                1069.2113                1106.8713
     1179.7885                1189.0477                1240.3022
     1286.7704                1294.3287                1310.4366
     1338.5068                1401.1275                1410.1341
     1425.0838                1483.4063                1498.2418
     1503.4465                1519.3107                1774.2744
     3045.0797                3053.4774                3085.9181
     3093.3019                3098.8228                3140.5612
     3143.5995                3217.9271                3868.9362
Zero-point correction (Hartree): 0.139643

HOCHCCH3CH2CH2OO.Zgttt
----------------------
E(UM062X/Aug-CC-pVTZ) (Hartree): -421.45104760
Electronic state : 2-A
Cartesian coordinates (Angs):
     C      -2.053189      0.599099      -0.225343
     C      -1.317933     -0.453371       0.106343
     C       0.021659     -0.269816       0.769411
     C       1.093315     -0.063957      -0.283016
     O       2.369121      0.010541       0.392306
     O       3.344002      0.172234      -0.447333
     O      -1.626086      1.874716       0.028101
     H      -3.014937      0.501082      -0.715376
     C      -1.764448     -1.849604      -0.202493
     H       0.006837      0.594417       1.432625
     H       0.267704     -1.151374       1.363568
     H       1.148329     -0.892628      -0.988741
     H       0.949566      0.869895      -0.824176
     H      -2.309986      2.504765      -0.202678
     H      -2.716664     -1.859774      -0.730790
     H      -1.874359     -2.432432       0.714363
     H      -1.029221     -2.367983      -0.822790
Rotational constants (GHz):    3.3026200    1.0414100    0.8528300
Vibrational harmonic frequencies (cm-1):
       35.2380                  76.3247                  96.6421
      134.4576                 191.2049                 232.7439
      239.3380                 307.2442                 337.3690
      392.6337                 476.7409                 587.3282
      593.6222                 784.7065                 865.6428
      884.6411                1000.0943                1019.4168
     1061.7149                1066.9938                1109.0101
     1185.1855                1197.6959                1224.3470
```

```
     1291.9015                1296.4355                1313.5955
     1338.5135                1394.3958                1409.3311
     1422.4374                1481.1256                1490.5724
     1501.6101                1505.9176                1795.8774
     3045.8563                3073.8538                3087.7664
     3095.3978                3123.9218                3137.3848
     3150.5048                3187.7628                3918.4496
Zero-point correction (Hartree): 0.139339

HOCHCCH3CH2CH2OO.Z1pmt
~~~~~~~~~~~~~~~~~~~~~~
E(UM062X/Aug-CC-pVTZ) (Hartree): -421.45151641
Electronic state : 2-A
Cartesian coordinates (Angs):
     C       1.709130     -0.226743      -0.323255
     C       0.795301      0.611124       0.149026
     C      -0.135776      0.198069       1.251049
     C      -1.593007      0.117408       0.813127
     O      -1.758911     -0.884811      -0.205799
     O      -1.500924     -0.409033      -1.388435
     O       1.864615     -1.493909       0.166624
     H       2.384572      0.062005      -1.120454
     C       0.651378      1.990819      -0.417397
     H       0.163263     -0.765875       1.658631
     H      -0.093554      0.929779       2.064129
     H      -2.229950     -0.209878       1.632958
     H      -1.960679      1.057390       0.405589
     H       2.506297     -1.971295      -0.360311
     H      -0.318260      2.112806      -0.904269
     H       1.422064      2.196291      -1.158778
     H       0.725858      2.746742       0.368080
Rotational constants (GHz):    2.4927700    1.5844300    1.3619900
Vibrational harmonic frequencies (cm-1):
       38.5354                  95.0414                 105.8187
      171.9951                 201.3511                 235.2032
      277.7503                 319.9738                 379.0078
      387.2898                 530.7926                 560.7205
      611.0331                 778.5857                 863.2415
      888.8703                 973.1139                 999.1345
     1033.8970                1072.5724                1078.9874
     1185.7482                1204.4895                1233.3178
     1243.8367                1315.2524                1326.5390
     1359.1635                1393.7535                1416.5175
     1419.5859                1471.0735                1483.8980
     1491.5533                1505.6461                1794.0954
     3046.5267                3048.6438                3096.0378
     3101.3892                3132.5287                3136.3074
     3157.4578                3183.7466                3922.8972
Zero-point correction (Hartree): 0.139590

HOCHCCH3CH2CH2OO.Z1ppt
~~~~~~~~~~~~~~~~~~~~~~
E(UM062X/Aug-CC-pVTZ) (Hartree): -421.45063142
Electronic state : 2-A
Cartesian coordinates (Angs):
     C       1.819552     -0.330908      -0.295792
     C       0.907450      0.556593       0.077349
     C      -0.151373      0.204237       1.084539
     C      -1.554601      0.556428       0.624112
     O      -1.857585     -0.056339      -0.648478
     O      -1.921103     -1.348537      -0.548453
     O       1.866143     -1.596525       0.219269
     H       2.588540     -0.082635      -1.018835
     C       0.908945      1.941423      -0.497872
     H      -0.110448     -0.857348       1.317768
     H       0.020190      0.753581       2.016356
     H      -2.305341      0.217826       1.336218
     H      -1.677583      1.621621       0.436252
     H       2.486993     -2.129793      -0.278425
     H       1.785546      2.109178      -1.121442
     H       0.908141      2.695031       0.293948
     H       0.024480      2.117110      -1.114549
Rotational constants (GHz):    2.5875400    1.5287200    1.1667400
Vibrational harmonic frequencies (cm-1):
       25.7644                  49.2800                 143.5286
      167.0971                 194.1854                 236.4249
      278.4320                 313.8739                 362.1245
      405.1788                 512.5127                 567.3335
      624.1476                 775.2516                 848.2362
      891.7903                 976.0122                 984.2137
     1030.8415                1070.1423                1099.5314
     1187.0526                1205.5319                1235.7481
     1259.3822                1295.7444                1330.1128
     1357.1006                1401.9563                1418.2209
     1421.4405                1472.1631                1484.9152
     1492.4410                1509.2736                1800.8498
     3041.9735                3043.3968                3091.0038
     3098.1414                3136.7252                3141.4738
     3157.9596                3179.4653                3920.8526
Zero-point correction (Hartree): 0.139512

HOCHCCH3CH2CH2OO.Z1ptt
~~~~~~~~~~~~~~~~~~~~~~
```

```
E(UM062X/Aug-CC-pVTZ) (Hartree): -421.45028605
Electronic state : 2-A
Cartesian coordinates (Angs):
     C      -1.999039      0.048185      -0.452034
     C      -0.949007     -0.534742       0.109762
     C      -0.098358      0.197613       1.112093
     C       1.387094      0.049875       0.860514
     O       1.669237      0.580826      -0.453851
     O       2.902767      0.373239      -0.795236
     O      -2.371765      1.330853      -0.154412
     H      -2.623033     -0.474901      -1.167680
     C      -0.587990     -1.950106      -0.229491
     H      -0.365097      1.252916       1.129000
     H      -0.285842     -0.197648       2.115933
     H       1.981323      0.618614       1.574282
     H       1.718042     -0.987696       0.863734
     H      -3.072826      1.612212      -0.743375
     H      -1.339358     -2.404120      -0.873313
     H      -0.502860     -2.560579       0.673214
     H       0.371533     -2.003091      -0.748869
Rotational constants (GHz):    3.1424900    1.1632600    1.0333300
Vibrational harmonic frequencies (cm-1):
       31.1387                57.4874                108.7861
      193.6568                213.3292               241.8764
      280.4807                312.9197               337.6982
      395.8865                470.8439               561.6418
      628.8962                777.3126               841.8577
      886.3631                973.2580              1014.9300
     1045.7805               1075.9053              1095.4822
     1182.3439               1204.6011              1236.3738
     1270.4945               1298.6339              1322.9877
     1356.8018               1401.3671              1418.2395
     1424.0884               1470.8202              1485.0320
     1497.3576               1514.2876              1801.0893
     3043.5390               3045.9127              3091.0014
     3095.0292               3129.7364              3138.1720
     3148.3095               3183.1646              3920.9824
Zero-point correction (Hartree): 0.139483

HOCHCCH3CH2CH2OO.Zpmtc
~~~~~~~~~~~~~~~~~~~~~~
E(UM062X/Aug-CC-pVTZ) (Hartree): -421.44892315
Electronic state : 2-A
Cartesian coordinates (Angs):
     C       1.225893      1.208723       0.077346
     C       1.410632     -0.105668      -0.028430
     C       0.343809     -1.167296      -0.161927
     C      -1.005756     -0.923354       0.481733
     O      -1.808500     -0.110126      -0.414995
     O      -3.030709      0.014428       0.005569
     O       0.073591      1.925072       0.060217
     H       2.079423      1.862132       0.207285
     C       2.814589     -0.644409      -0.047855
     H       0.183558     -1.430688      -1.213029
     H       0.736846     -2.074807       0.302965
     H      -1.558074     -1.849666       0.622762
     H      -0.932562     -0.385217       1.426376
     H      -0.657800      1.417526      -0.308304
     H       3.551357      0.153489       0.021877
     H       3.006202     -1.197355      -0.971065
     H       2.980993     -1.338376       0.779600
Rotational constants (GHz):    3.6361300    1.2623400    0.9796100
Vibrational harmonic frequencies (cm-1):
       19.6519                76.2984                145.2685
      207.5452                220.5482               267.3857
      294.9970                345.4938               349.8160
      448.9702                518.0648               563.8675
      624.1732                787.7658               832.0384
      925.1017               1004.3463              1016.8289
     1036.8728               1075.0445              1108.9520
     1184.7616               1207.4077              1234.1039
     1280.7706               1305.7384              1323.5230
     1391.9311               1412.2769              1419.7006
     1431.2856               1463.8643              1485.3120
     1500.8632               1503.7261              1772.1061
     3039.4061               3041.9396              3077.8754
     3087.7320               3096.2801              3142.7642
     3155.4912               3200.5034              3814.3305
Zero-point correction (Hartree): 0.139977

HOCHCCH3CH2CH2OO.Zptpc
~~~~~~~~~~~~~~~~~~~~~~
E(UM062X/Aug-CC-pVTZ) (Hartree): -421.45311898
Electronic state : 2-A
Cartesian coordinates (Angs):
     C      -1.337776      1.167113       0.144008
     C      -1.356078     -0.137348      -0.121298
     C      -0.086233     -0.827402      -0.549217
     C       0.933326     -0.932568       0.592911
     O       2.279812     -0.698882       0.113257
     O       2.414009      0.523274      -0.297511
     O      -0.265061      1.992419       0.069056
     H      -2.225219      1.700550       0.458868
```

```
     C      -2.610523     -0.947993       0.004703
     H      -0.305186     -1.817407      -0.945692
     H       0.390244     -0.264818      -1.356330
     H       0.747120     -0.187308       1.364677
     H       0.975110     -1.922479       1.039906
     H       0.546981      1.524914      -0.173442
     H      -2.881161     -1.403777      -0.950454
     H      -3.446566     -0.332927       0.334061
     H      -2.487689     -1.762045       0.723351
Rotational constants (GHz):    3.2290800    1.3886100    1.0409300
Vibrational harmonic frequencies (cm-1):
       70.9878                 75.4034                181.5667
      196.5113                214.0703                295.3972
      296.6820                349.5854                401.9228
      527.4069                567.3644                592.9057
      606.8148                804.7100                871.8093
      930.0972                964.8976               1014.9382
     1033.8493               1073.4721               1075.2889
     1200.6918               1213.1969               1246.7772
     1288.4881               1302.6108               1325.8487
     1368.4561               1398.8044               1406.8098
     1423.7255               1482.5153               1494.0460
     1503.4373               1508.8030               1762.0564
     3042.6950               3059.0856               3090.0887
     3100.2097               3121.8062               3137.0446
     3166.2918               3210.1517               3747.9121
Zero-point correction (Hartree): 0.140671


TS.HOCHCCH3CH2CH2OO.cycHOCHCCH3CH2CH2OO.Zh
~~~~~~~~~~~~~~~~~~~~~~~~~~~~~~~~~~~~~~~~~~
E(CCSD(T)/Aug-CC-pVTZ) (Hartree): -420.82290136
E(CCSD/Aug-CC-pVTZ) (Hartree): -420.74780200
     T1 diagnostic:  0.027632
E(MP2/Aug-CC-pVTZ) (Hartree): -420.68959699
E(MP3/Aug-CC-pVTZ) (Hartree): -420.72757334
E(PMP2/Aug-CC-pVTZ) (Hartree): -420.70732238
E(PMP3/Aug-CC-pVTZ) (Hartree): -420.74089315
E(PUHF/Aug-CC-pVTZ) (Hartree): -419.15569713
E(UHF/Aug-CC-pVTZ) (Hartree): -419.13522923
E(UM062X/Aug-CC-pVTZ) (Hartree): -421.42867123
Electronic state : 2-A
Cartesian coordinates (Angs):
     C      -0.225486      1.261185      -0.046634
     C      -1.014997      0.183361       0.288575
     C      -0.363531     -0.892676       1.084760
     C       0.671914     -1.572693       0.150479
     O       1.553838     -0.605444      -0.371589
     O       0.868505      0.186239      -1.267089
     O       0.726247      1.683063       0.817033
     H      -0.561307      1.977356      -0.789752
     C      -2.230068     -0.138468      -0.510283
     H       0.163980     -0.494518       1.949035
     H      -1.084801     -1.640822       1.415571
     H       1.293669     -2.278879       0.700038
     H       0.165493     -2.081734      -0.672729
     H       1.456220      2.067705       0.320778
     H      -2.071248     -1.044599      -1.103181
     H      -2.493173      0.669297      -1.190938
     H      -3.084554     -0.328926       0.142964
Rotational constants (GHz):    2.5274700    2.1855300    1.6981700
Vibrational harmonic frequencies (cm-1):
     i607.7865                138.5662                158.4735
      173.2502                238.6210                275.5832
      323.6091                378.7176                434.5920
      442.6917                493.6161                596.9295
      629.7035                804.2215                874.7583
      916.7996                979.4077                996.0024
     1008.2363               1035.3478               1071.6900
     1083.2220               1187.9358               1218.4413
     1238.7452               1263.3048               1313.8985
     1321.9079               1364.1076               1396.5419
     1416.4615               1474.0568               1476.2740
     1485.8078               1494.4816               1580.6759
     3035.2683               3061.8629               3082.5547
     3086.4816               3128.0387               3140.5013
     3146.2336               3165.6929               3852.5523
Zero-point correction (Hartree): 0.138936

TS.HOCHCCH3CH2CH2OO.cycHOCHCCH3CH2CH2OO.Zp
~~~~~~~~~~~~~~~~~~~~~~~~~~~~~~~~~~~~~~~~~~
E(CCSD(T)/Aug-CC-pVTZ) (Hartree): -420.82459295
E(CCSD/Aug-CC-pVTZ) (Hartree): -420.74901814
     T1 diagnostic:  0.026545
E(MP2/Aug-CC-pVTZ) (Hartree): -420.69314458
E(MP3/Aug-CC-pVTZ) (Hartree): -420.73006351
E(PMP2/Aug-CC-pVTZ) (Hartree): -420.71010883
E(PMP3/Aug-CC-pVTZ) (Hartree): -420.74269577
E(PUHF/Aug-CC-pVTZ) (Hartree): -419.15379424
E(UHF/Aug-CC-pVTZ) (Hartree): -419.13410207
E(UM062X/Aug-CC-pVTZ) (Hartree): -421.42980062
Electronic state : 2-A
Cartesian coordinates (Angs):
```

```
     C       0.264881      1.272855      -0.006594
     C       1.007221      0.142348      -0.318909
     C       0.312532     -0.947264      -1.060958
     C      -0.752520     -1.543270      -0.111180
     O      -1.543094     -0.494526       0.416411
     O      -0.761392      0.238666       1.298738
     O      -0.752451      1.742482      -0.753384
     H       0.698749      2.032966       0.632045
     C       2.234549     -0.182764       0.460105
     H      -0.185913     -0.568288      -1.954860
     H       1.007489     -1.731098      -1.362977
     H      -1.439278     -2.204613      -0.639172
     H      -0.278491     -2.076997       0.713862
     H      -1.414245      1.040369      -0.847075
     H       2.049751     -1.019782       1.140764
     H       2.570915      0.664760       1.054642
     H       3.046541     -0.481714      -0.206128
Rotational constants (GHz):    2.5474400    2.2040800    1.7088700
Vibrational harmonic frequencies (cm-1):
     i589.2412                148.4698                166.7360
      186.3656                244.1548                319.1700
      376.0619                425.6069                442.8246
      467.7017                500.0235                595.2845
      636.0796                795.4367                881.5022
      903.5941                973.4984                995.5179
     1005.8630               1031.3427               1069.6499
     1073.5617               1184.2861               1214.3732
     1262.1894               1269.6616               1312.8932
     1340.3680               1369.4256               1395.9655
     1416.7420               1475.8834               1481.4894
     1487.0234               1499.0715               1554.8259
     3035.0817               3069.2795               3071.9588
     3088.6041               3120.4220               3135.5229
     3141.8760               3197.3187               3731.1289
Zero-point correction (Hartree): 0.139182


TS.HOCHCCH3CH2CH2OO.1-6Hshift.a.Zc
----------------------------------
E(UM062X/Aug-CC-pVTZ) (Hartree): -421.41388538
Electronic state : 2-A
Cartesian coordinates (Angs):
     O      -1.953200      0.709729      -0.843874
     H      -1.081665      1.382104      -0.240421
     C      -0.088042      1.598713       0.548536
     O      -2.176009     -0.349107       0.009137
     C       0.726041      0.401034       0.371658
     C      -1.110227     -1.286587      -0.097239
     C       0.083660     -0.903718       0.775320
     H      -0.639485      1.655303       1.485836
     H       0.370484      2.537415       0.253653
     C       1.930202      0.489202      -0.211689
     O       2.779922     -0.520931      -0.504577
     H       2.344672      1.445286      -0.502068
     H      -1.537182     -2.229748       0.245099
     H      -0.827718     -1.372330      -1.147986
     H       0.790085     -1.738092       0.760909
     H      -0.266085     -0.821483       1.807747
     H       2.391381     -1.367842      -0.267779
Rotational constants (GHz):    3.5653900    1.3311700    1.1269500
Vibrational harmonic frequencies (cm-1):
    i2089.6467                73.3864                144.2458
      252.2848                254.3888                295.2603
      348.6658                402.9211                446.4342
      498.5905                580.1781                589.5122
      631.7255                644.0132                781.6250
      877.4454                914.9174                957.1782
     1014.4730               1019.6854               1050.7670
     1089.1779               1119.6484               1187.5560
     1205.4486               1238.3923               1283.2037
     1302.1902               1329.7816               1360.7501
     1395.0488               1421.0353               1461.2732
     1480.4697               1489.5087               1522.7000
     1708.9601               3049.8736               3067.4395
     3089.7423               3096.8584               3127.0348
     3191.0539               3217.8402               3869.7027
Zero-point correction (Hartree): 0.134600

TS.HOCHCCH3CH2CH2OO.1-6Hshift.a.Zt
----------------------------------
E(CCSD(T)/Aug-CC-pVTZ) (Hartree): -420.80534605
E(CCSD/Aug-CC-pVTZ) (Hartree): -420.73022356
     T1 diagnostic:  0.025215
E(MP2/Aug-CC-pVTZ) (Hartree): -420.67701734
E(MP3/Aug-CC-pVTZ) (Hartree): -420.71328940
E(PMP2/Aug-CC-pVTZ) (Hartree): -420.69250327
E(PMP3/Aug-CC-pVTZ) (Hartree): -420.72444558
E(PUHF/Aug-CC-pVTZ) (Hartree): -419.13115853
E(UHF/Aug-CC-pVTZ) (Hartree): -419.11271414
E(UM062X/Aug-CC-pVTZ) (Hartree): -421.41444056
Electronic state : 2-A
Cartesian coordinates (Angs):
     O      -1.958174      0.689970      -0.852131
```

```
     H      -1.100700      1.371563      -0.255314
     C      -0.107906      1.612556       0.537761
     O      -2.173687     -0.365790       0.004806
     C       0.708535      0.416080       0.378459
     C      -1.093869     -1.293638      -0.088837
     C       0.092307     -0.898487       0.784797
     H      -0.666306      1.675348       1.470149
     H       0.342921      2.551728       0.231718
     C       1.910845      0.483199      -0.203602
     O       2.663257     -0.627244      -0.435099
     H       2.336862      1.429326      -0.517010
     H      -1.514879     -2.238742       0.254936
     H      -0.805100     -1.382272      -1.137196
     H       0.835255     -1.693932       0.735464
     H      -0.255891     -0.826943       1.818525
     H       3.517194     -0.379830      -0.793344
Rotational constants (GHz):    3.5570000    1.3494100    1.1376500
Vibrational harmonic frequencies (cm-1):
    i2125.9030                   73.8258                  144.8234
      242.5021                  249.7489                  277.2143
      327.3942                  345.9792                  434.1601
      488.7135                  585.1494                  591.6852
      631.5893                  647.1744                  787.8479
      874.9232                  885.4648                  959.9891
     1010.0703                 1018.8154                 1048.2654
     1086.5471                 1119.0282                 1196.7306
     1207.3084                 1240.5505                 1248.2845
     1297.1116                 1342.5440                 1356.1230
     1389.9385                 1421.1517                 1460.2205
     1479.4794                 1483.1757                 1522.4986
     1730.6236                 3059.4946                 3072.5546
     3098.4729                 3125.9796                 3131.2908
     3185.5875                 3190.1089                 3913.8734
Zero-point correction (Hartree): 0.134375

TS.HOCHCCH3CH2CH2OO.1-6Hshift.b.Zc
~~~~~~~~~~~~~~~~~~~~~~~~~~~~~~~~~
E(UM062X/Aug-CC-pVTZ) (Hartree): -421.41379943
Electronic state : 2-A
Cartesian coordinates (Angs):
     O      -2.172289      0.392037      -0.380920
     H      -1.317307      1.295368      -0.178889
     C      -0.206735      1.814036       0.262017
     O      -1.391242     -0.629704      -0.865925
     C       0.611405      0.617457       0.350430
     C      -0.866227     -1.382095       0.221721
     C       0.006509     -0.517110       1.144415
     H      -0.575528      2.200157       1.210717
     H       0.132768      2.587840      -0.419221
     C       1.731349      0.477639      -0.376591
     O       2.518254     -0.619024      -0.430998
     H       2.115330      1.275673      -0.997117
     H      -1.684337     -1.853060       0.769799
     H      -0.276027     -2.153903      -0.274322
     H       0.755735     -1.145670       1.632699
     H      -0.605105     -0.096046       1.941020
     H       2.158878     -1.316387       0.126103
Rotational constants (GHz):    3.1329900    1.5781800    1.3050800
Vibrational harmonic frequencies (cm-1):
    i2020.1929                   84.2323                  122.3046
      255.4016                  284.1316                  331.6035
      358.5807                  390.2188                  436.0733
      500.3482                  540.9057                  592.0663
      625.1512                  680.8618                  806.0707
      858.9725                  915.1989                  955.7221
     1018.3961                 1026.9489                 1073.6031
     1080.3392                 1124.4093                 1184.5750
     1219.6511                 1273.1274                 1280.3392
     1294.0000                 1322.8966                 1362.4060
     1385.3673                 1413.3022                 1475.8292
     1489.2252                 1497.7021                 1511.2492
     1696.0246                 3056.3752                 3066.6361
     3098.0780                 3108.6079                 3127.2132
     3190.4441                 3221.2841                 3857.8356
Zero-point correction (Hartree): 0.134853

TS.HOCHCCH3CH2CH2OO.1-6Hshift.b.Zt
~~~~~~~~~~~~~~~~~~~~~~~~~~~~~~~~~
E(UM062X/Aug-CC-pVTZ) (Hartree): -421.41432079
Electronic state : 2-A
Cartesian coordinates (Angs):
     O      -2.168964      0.339083      -0.413326
     H      -1.346566      1.264500      -0.213022
     C      -0.251609      1.827108       0.230581
     O      -1.354748     -0.671518      -0.861320
     C       0.581625      0.646906       0.357829
     C      -0.820534     -1.388581       0.250952
     C       0.004495     -0.482768       1.174198
     H      -0.642849      2.226174       1.164337
     H       0.078148      2.591364      -0.466420
     C       1.697711      0.483597      -0.364566
     O       2.402750     -0.677734      -0.310386
     H       2.081282      1.259780      -1.015882
```

```
     H      -1.633378     -1.880493       0.788119
     H      -0.184189     -2.137160      -0.219485
     H       0.785654     -1.075760       1.647731
     H      -0.630097     -0.067457       1.955818
     H       3.189563     -0.617176      -0.854909
Rotational constants (GHz):    3.1095600    1.6159400    1.3292500
Vibrational harmonic frequencies (cm-1):
    i2067.2203                  80.7269                 124.9799
      250.6726                 266.1617                 300.6704
      356.4600                 362.9145                 392.0901
      485.5641                 539.6044                 596.8966
      623.0864                 686.1959                 811.2804
      863.2249                 869.4587                 959.7051
     1018.4655                1026.5592                1065.5672
     1082.7047                1121.8113                1197.6638
     1225.5901                1247.1964                1275.1394
     1282.8936                1324.1650                1362.3878
     1380.6641                1412.3404                1475.0907
     1485.7310                1494.0201                1503.3449
     1716.2163                3068.8958                3089.5693
     3101.5952                3126.8974                3144.1488
     3189.2682                3192.6181                3910.7707
Zero-point correction (Hartree): 0.134619
```

Appendix B

Supporting Information: Rosanka et al. (2020)

In the following, the supplemental material of Rosanka et al. (2020) (here Chapter 4) is presented.

Supplement of Atmos. Chem. Phys., 20, 6671–6686, 2020
https://doi.org/10.5194/acp-20-6671-2020-supplement

Atmospheric Chemistry and Physics Open Access

Supplement of

Atmospheric chemical loss processes of isocyanic acid (HNCO): a combined theoretical kinetic and global modelling study

Simon Rosanka et al.

Correspondence to: Hue M. T. Nguyen (hue.nguyen@hnue.edu.vn) and Domenico Taraborrelli (d.taraborrelli@fz-juelich.de)

Contents

Additional modifications to chemical mechanism in EMAC

a. Gas phase

Table 1: Reactions added to MOM supplementing reactions presented in main text

Reaction	Rate coefficient and branching ratio	Reference
$NH_2CHO + OH \rightarrow HNCO + HO_2 + H_2O$	4.47×10^{-12}	Bunkan et al., 2016
$CH_3NO_2 + OH \rightarrow HCHO + NO_2 + H_2O$	$5.8\times10^{-13}\times\exp(-1102/T)$	Calvert et al., 2008
$CH_3NO_2 + hv \rightarrow CH_3 + NO_2$	-	Taylor et al., 1980
$CH_3NH_2 + OH \rightarrow CH_2NH + H_2O + HO_2$	1.97×10^{-11}	Nielsen et al., 2012
$(CH_3)_2NH + OH \rightarrow CH_2NCH_3 + HO_2$	$0.42\times6.71\times10^{-11}$	Nielsen et al., 2012
$(CH_3)_2NH + OH \rightarrow CH_3NHCH_2 + H_2O$	$0.58\times6.71\times10^{-11}$	Nielsen et al., 2012
$CH_3NHCH_2 \rightarrow CH_2NCH_3 + HO_2$	$0.55\times1.0\times10^{6}$	Nielsen et al., 2012
$CH_3NHCH_2 \rightarrow CH_3NHCH_2O_2$	$0.45\times1.0\times10^{6}$	Nielsen et al., 2012
$CH_3NHCH_2O_2 + NO \rightarrow CH_3NHCHO + NO_2 + HO_2$	$0.5\times2.54\times10^{12}\times\exp(360/T)$	Nielsen et al., 2012
$CH_3NHCH_2O_2 + NO \rightarrow CH_2NH + HCHO + NO_2+HO_2$	$0.5\times2.54\times10^{12}\times\exp(360/T)$	Nielsen et al., 2012
$(CH_3)_3N + OH \rightarrow (CH_3)_2NCH_2O_2 + H_2O$	4.50×10^{-11}	Nielsen et al., 2012
$(CH_3)_2NCH_2O_2 + NO \rightarrow (CH_3)_2NCHO + NO_2 + HO_2$	$0.4\times2.54\times10^{12}\times\exp(360/T)$	Nielsen et al., 2012
$(CH_3)_2NCH_2O_2 + NO \rightarrow CH_2NCH_3 + HCHO + NO_2 + HO_2$	$0.6\times2.54\times10^{12}\times\exp(360/T)$	Nielsen et al., 2012

b. Aqueous phase

Table 2: Reactions added to aqueous phase mechanism in the submodel SCAV of EMAC

Reaction	Rate coefficient	Reference
$HNCO + H^+ \rightarrow NH_3 + CO_2 + H^+$	$4.4\times10^{7}\times\exp(-6000/T)$	Borduas et al., 2016b
$HNCO \rightarrow NH_3 + CO2$	$8.9\times10^{6}\times\exp(-6770/T)$	Borduas et al., 2016b
$NCO^- \rightarrow NH_3 + HCO_3^-$	$7.2\times10^{8}\times\exp(-10900/T)$	Borduas et al., 2016b
$NH_2CHO + OH \rightarrow HNCO + H_2O + HO_2$	5.0×10^{8}	Barnes et al., 2010
$CN^- + OH \rightarrow HNCO + HO_2$	7.35×10^{9}	Behar 1974
$HCN + OH \rightarrow H_2O + product$	6.00×10^{7}	Buechler et al., 1976

HNCO + OH potential energy surface

a. M06-2X/aug-cc-pVTZ PES and reaction diagram

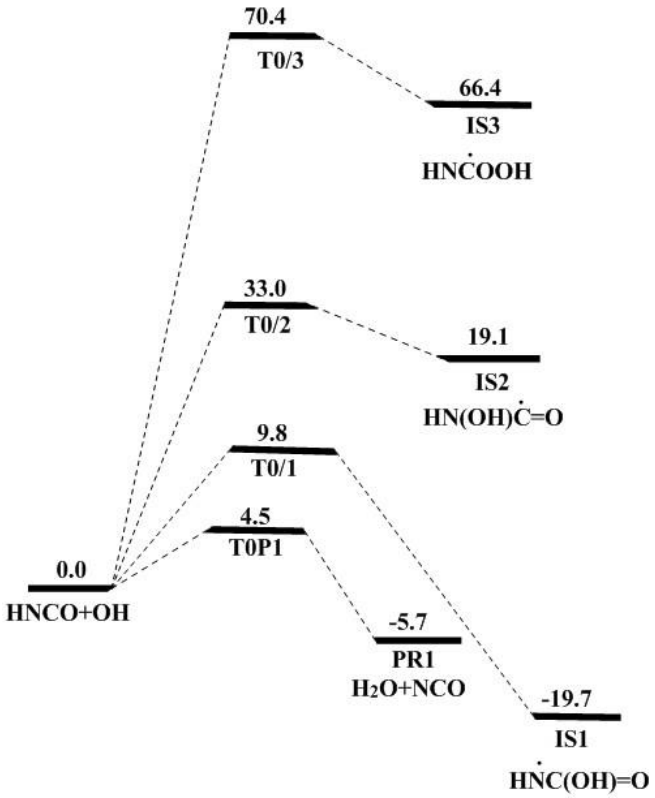

Figure 1: OH addition and hydrogen abstraction pathways of the HNCO + OH reaction calculated at the M06-2X/ aug-cc-pVTZ level of theory

Figure 2: Diagram of the HNCO + OH reaction

b. Geometries obtained using M06-2X/aug-cc-pVTZ

Bond lengths in Ångstrom, angles in degrees

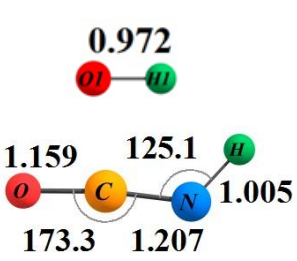

RA

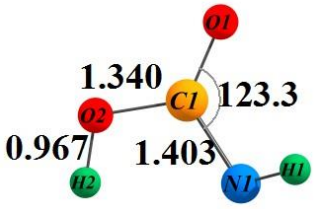

IS1

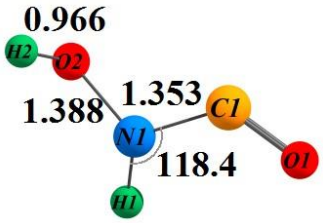

IS2

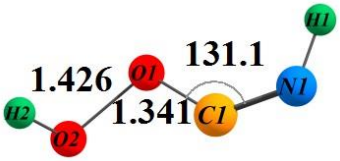

IS3

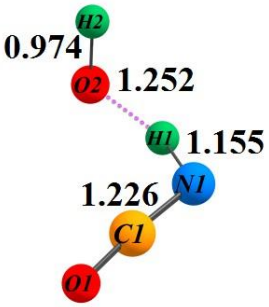

T0P1

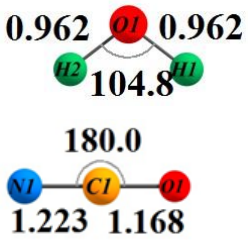

PR1

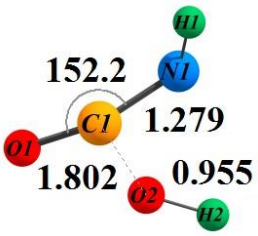

T0/1

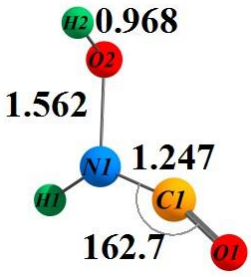

T0/2

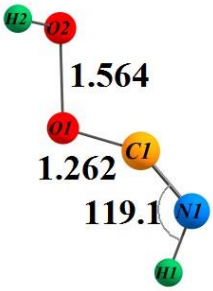

T0/3

HNCO + Cl potential energy surface

a. CCSD(T)/aVTZ//B3LYP/aVTZ extended PES and reaction diagram

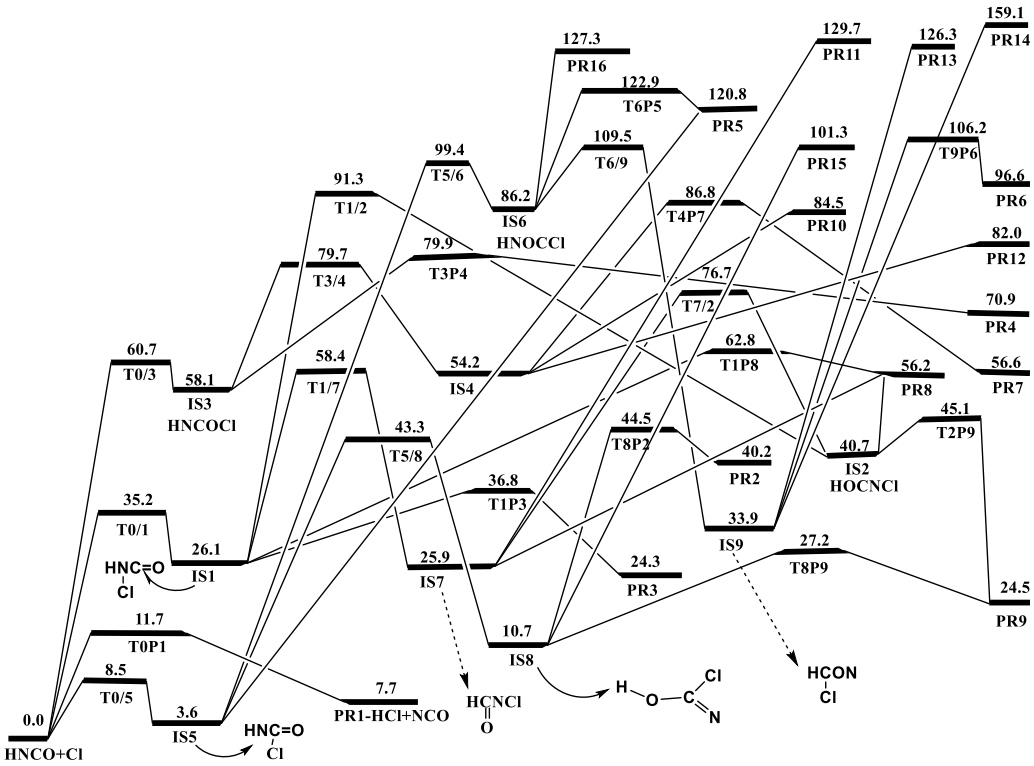

Figure 3: Detailed potential energy surface of the HNCO + Cl reaction based on ZPE-corrected CCSD(T)/aug-cc-pVTZ//B3LYP/aug-cc-pVTZ energies. The intermediates are depicted below.

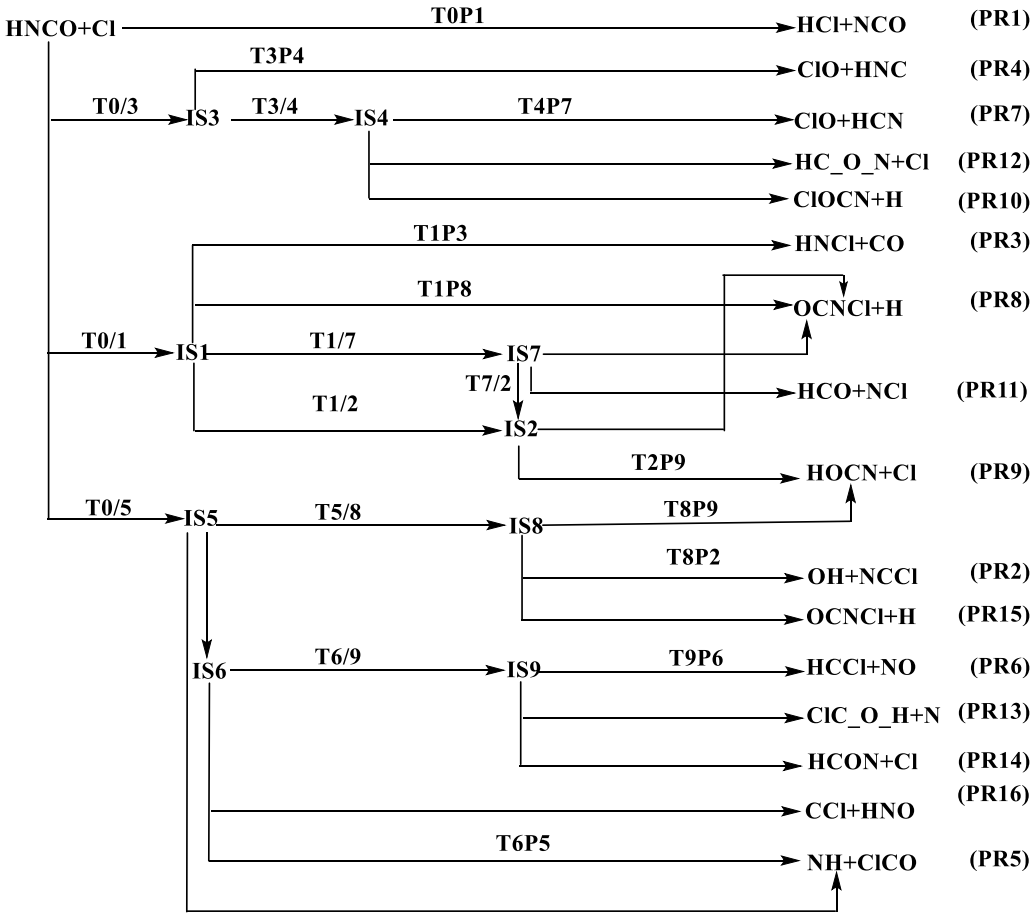

Figure 4: Diagram of the HNCO + Cl reaction

b. Geometries obtained using B3LYP/aug-cc-pVTZ

Bond lengths in Ångstrom, angles in degrees

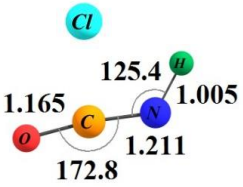

RA

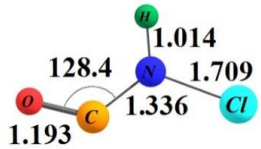

IS1

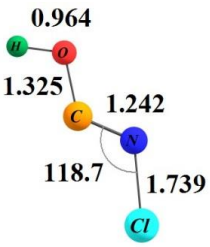

IS2

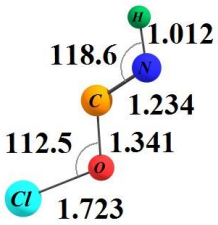

IS3

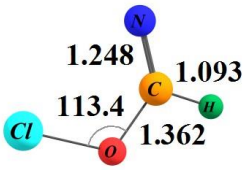

IS4

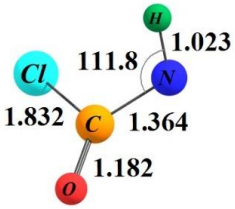

IS5

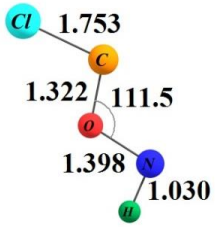

IS6

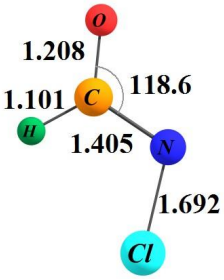

IS7

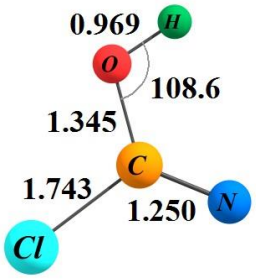

IS8

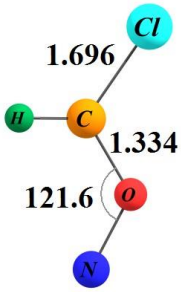

IS9

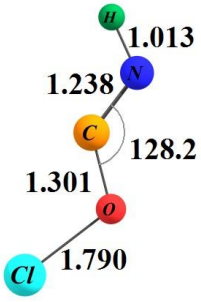

T0/3

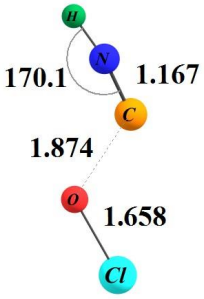

T3P4

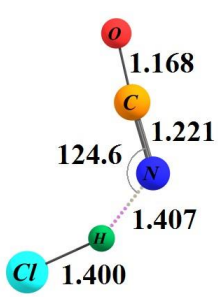

T0P1

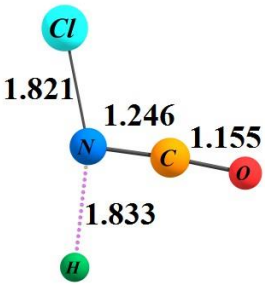

T1P8

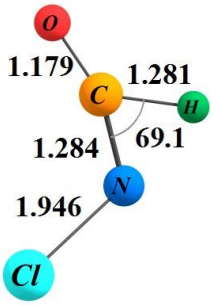

T1/7

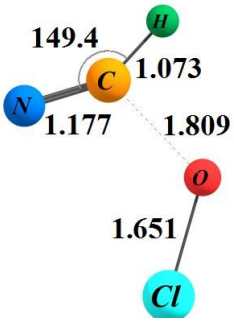

T4P7

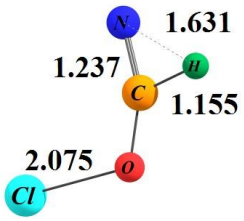

T3P4

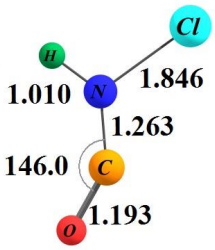

T0/1

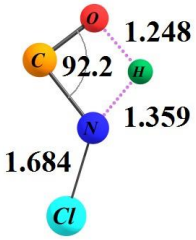

T1/2

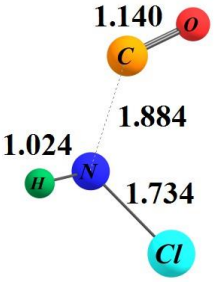

T1P3

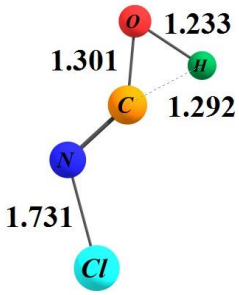

T7/2

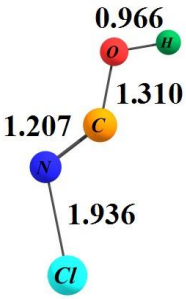

T2P9

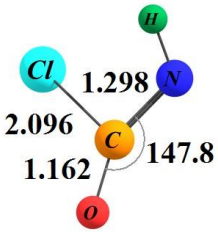

T0/5

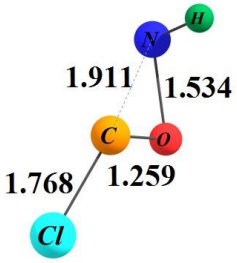

T5/6

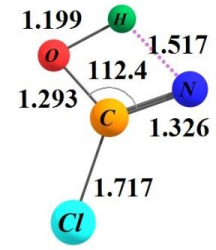

T5/8

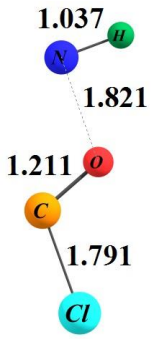

T6P5

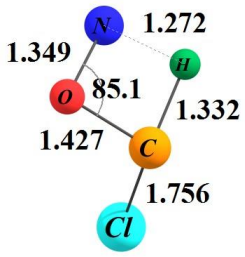

T6/9

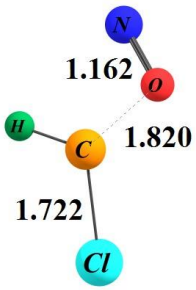

T9P6

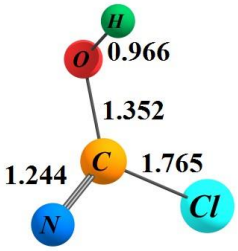

T8P9

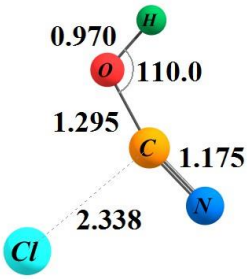

T8P2

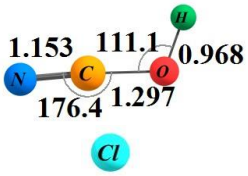

PR9

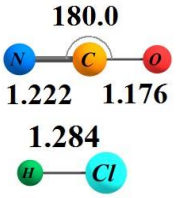

PR1

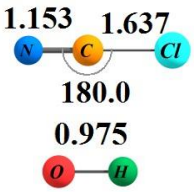

PR2

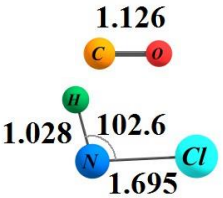

PR3

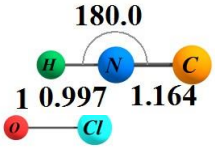

PR4

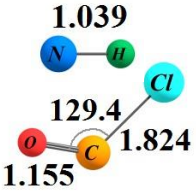

PR5

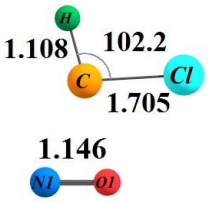

PR6

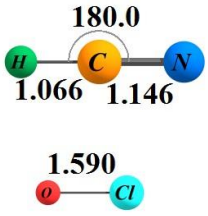

PR7

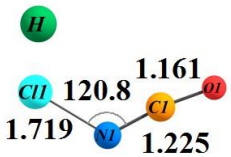

PR8

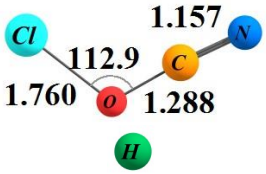

PR10

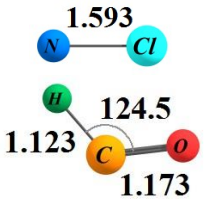

PR11

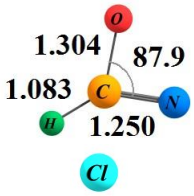

PR12

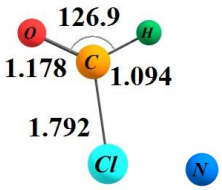

PR13

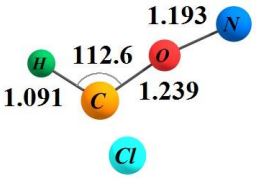

PR14

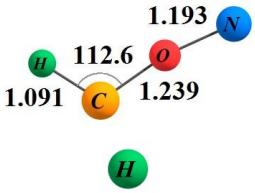

PR15

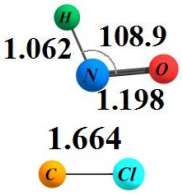

PR16

c. Geometries obtained using M06-2X/aug-cc-pVTZ

Bond lengths in Ångstrom, angles in degrees

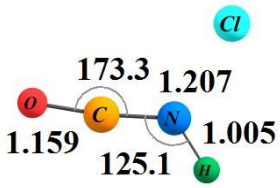

RA

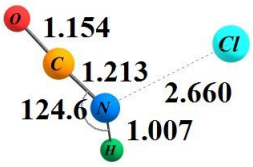

COM

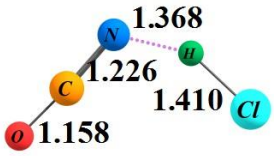

T0P1

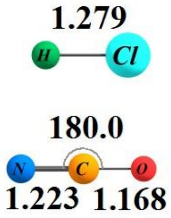

PR1

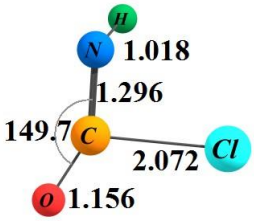

T0/5

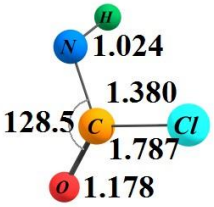

IS5

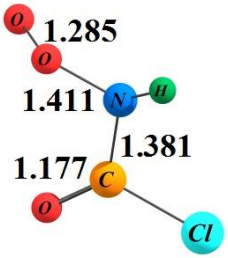

ClC(=O)NHOO

d. Energetic and entropic data

Table 3: Gibbs free energies (ΔG^0) and entropies (ΔS^0) for the Cl + HNCO reaction products at the CCSD(T)//B3LYP/aug-cc-pVTZ level of theory

Species	**(ΔG^0) (298.15 K) (kcal mol^{-1})**	**(ΔS^0) (298.15 K) (cal mol^{-1} K^{-1})**
PR1 (HCl + NCO)	6.9	3.7
PR2 (OH + NCCl)	39.6	3.9
PR3 (HNCl + CO)	21.9	10.0
PR4 (OCl + HNC)	69.2	7.0
PR5 (NH + ClCO)	118.7	9.3
PR6 (HCCl + NO)	94.1	10.2
PR7 (HCN + OCl)	92.6	-0.5
PR8 (OCNCl + H)	56.8	-0.7
PR9 (HOCN + Cl)	24.3	0.7
PR10 (ClOCN + H)	92.6	-0.5
PR11 (HCO + NCl)	118.3	9.8
PR12 (HC(O)N + Cl)	88.7	1.7
PR13 (HC(O)Cl + NCl)	125.62	2.2
PR14 (HCON + Cl)	158.9	0.6
PR15 (ClC(O)N + H)	102.0	-1.1
PR16 (CCl + HNO)	124.7	10.1

Table 4: Comparison of calculated heats of reaction (kcal mol^{-1}) of the products of the HNCO + Cl reaction, against available literature data at 298.15 K. Levels of theory used are B3LYP/aug-cc-pVTZ (designated as B3LYP) and CCSD(T)/aug-cc-pVTZ (CCSD(T). Literature data is from NIST (webbook.nist.gov).

Species	B3LYP	CCSD(T)	Literature
PR1 (HCl + NCO)	7.6	8.01	8.7
PR2 (OH + NCCl)	49.6	39.6	
PR3 (HNCl + CO)	26.3	24.7	
PR4 (OCl + HNC)	70.0	84.5	
PR5 (NH + ClCO)	127.3	121.4	123.4
PR6 (HCCl + NO)	129.2	127.6	
PR7 (ClO+HCN)	56.6	52.4	
PR8 (OCNCl + H)	58.2	56.8	
PR9 (HOCN + Cl)	28.4	24.3	21.4
PR10 (ClOCN + H)	96.7	92.4	
PR11 (HCO + NCl)	120.4	118.3	
PR12 (HC(O)N + Cl)	95.1	84.5	
PR13 (HC(O)Cl + NCl)	136.9	126.3	
PR14 (HCON + Cl)	165.5	159.0	
PR15 (ClC(O)N + H)	109.9	101.9	
PR16 (CCl + HNO)	129.2	127.6	

Table 5: Theoretical predication of relative energies ΔE (kcal/mol) for reactants, intermediates, transition states and products of the Cl + HNCO reaction. Levels of theory used are B3LYP/aug-cc-pVTZ (designated as B3LYP) and CCSD(T)/aug-cc-pVTZ//B3LYP (CCSD(T))

Species	**B3LYP**	**CCSD(T)**
RA(HNCO+Cl)	0.0	0.0
IS1	26.1	26.1
IS2	41.3	40.7
IS3	58.8	58.1
IS4	55.6	54.2
IS5	3.9	3.6
IS6	70.7	86.2
IS7	26.5	25.9
IS8	12.5	10.7
IS9	87.3	33.9
T0P1	6.7	11.7
T0/1	30.6	35.2
T1P3	39.0	36.8
T1/2	93.3	91.3
T1/7	55.2	56.4
T2P9	43.6	45.1
T1P8	62.1	62.8
T2/7	76.3	76.7
T0/3	58.6	60.7
T3/4	75.3	79.7
T3P4	78.4	79.9
T0/5	5.7	8.5
T5/8	65.6	43.3
T5/6	99.9	99.4
T6P5	104.2	122.9
T6/9	114.8	109.5
T9P6	105.4	106.2
T8P2	47.9	44.5
T8P9	28.3	28.4
PR1 (HCl + NCO)	7.2	7.7
PR2 (OH + NCCl)	45.3	40.2
PR3 (HNCl + CO)	28.7	24.3
PR4 (Ocl + HNC)	71.7	70.9
PR5 (NH + ClCO)	129.3	120.8
PR6 (HCCl + NO)	101.0	96.6
PR7 (ClO + HCl)	96.1	82.0
PR8 (OCNCl + H)	57.6	56.2
PR9 (HOCN + Cl)	28.5	24.5
PR10 (ClOCN+H)	96.1	82.0
PR11 (HCO+NCl)	122.8	120.7
PR12 (HC(O)N+Cl)	90.9	84.5
PR13 (HC(O)Cl+N)	137.6	126.3
PR14 (HCON+Cl)	165.6	159.1
PR15 (ClC(O)N+H)	109.2	101.3
PR16 (CCl+HNO)	131.7	127.3

HNCO + NO_3 potential energy surface

a. M06-2X/aug-cc-pVTZ PES and reaction diagram

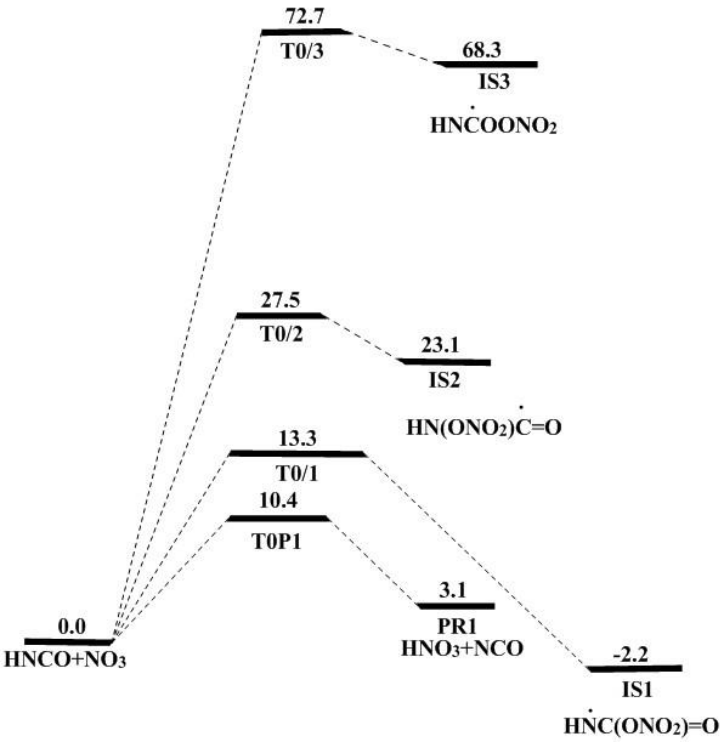

Figure 5: NO_3 addition and hydrogen abstraction pathways of the HNCO + NO_3 reaction calculated at the M06-2X/ aug-cc-pVTZ level of theory

Figure 6: Diagram of the HNCO + NO_3 reaction

b. Geometries obtained using M06-2X/aug-cc-pVTZ

Bond lengths in Ångstrom, angles in degrees

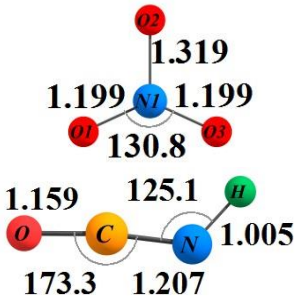

RA

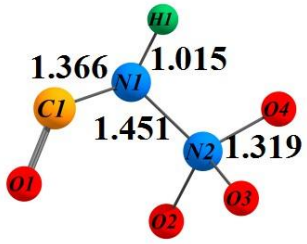

IS1

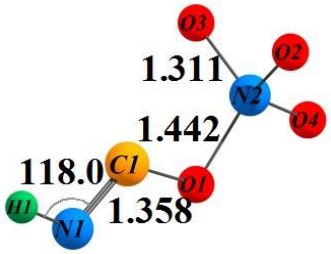

IS2

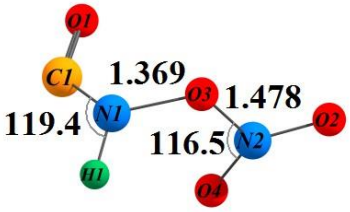

IS3

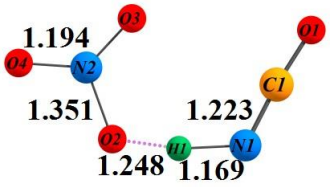

T0P1

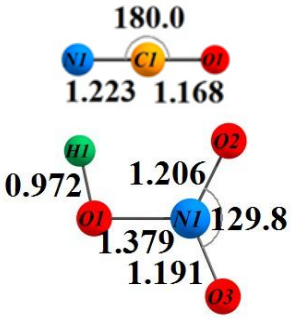

PR1

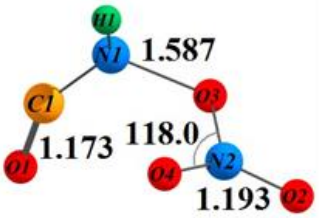

T0/3

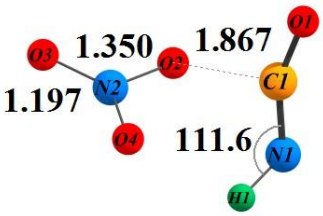

T0/4

$HNCO + O_3$ potential energy surface

a. CCSD(T)/aVTZ//M06-2X/aVTZ extended PES and reaction diagram

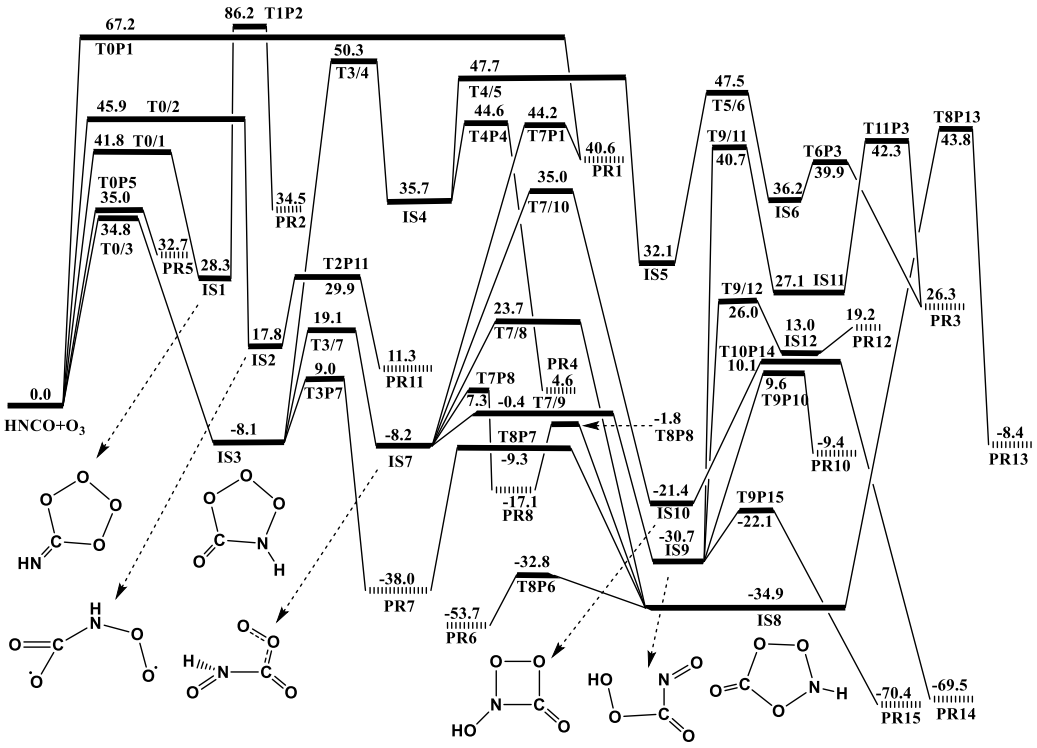

Figure 7: Detailed potential energy surface of the HNCO + O_3 reaction based on ZPE-corrected CCSD(T)/aug-cc-pVTZ//M06-2X/aug-cc-pVTZ energies. The intermediates are depicted below.

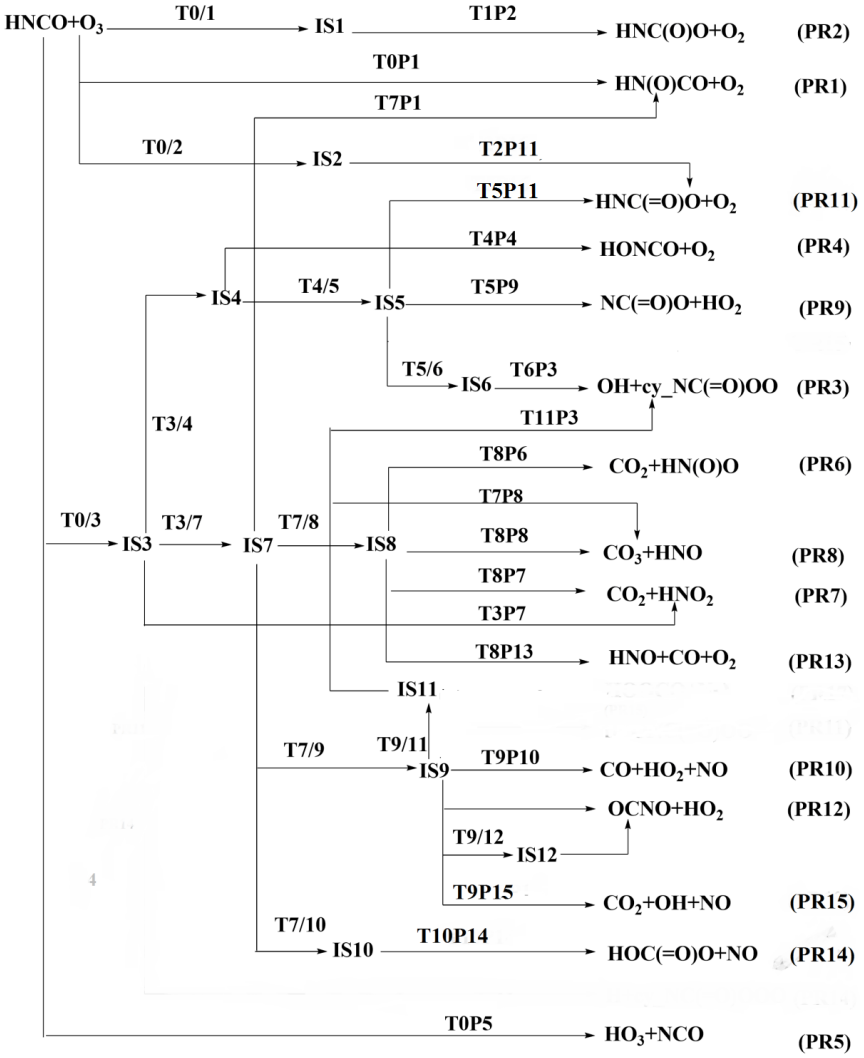

Figure 8: Diagram of the HNCO + O_3 reaction

b. Geometries obtained using M06-2X/aug-cc-pVTZ

Bond lengths in Ångstrom, angles in degrees

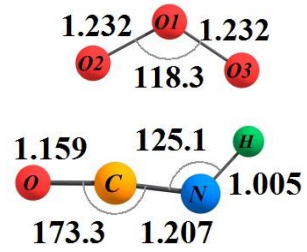

RA

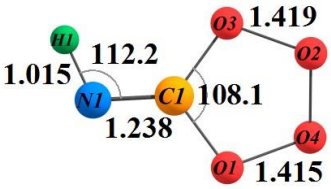

IS1

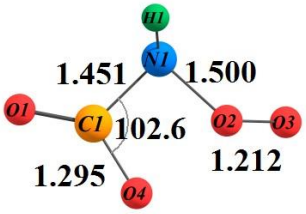

IS2

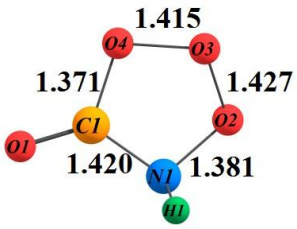

IS3

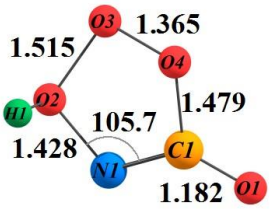

IS4

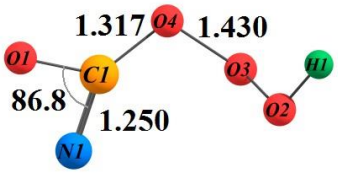

IS5

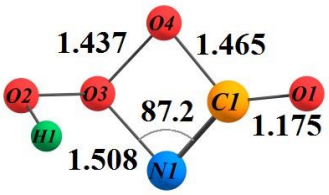

IS6

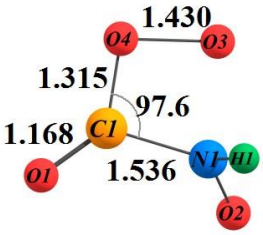

IS7

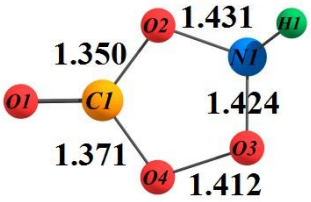

IS8

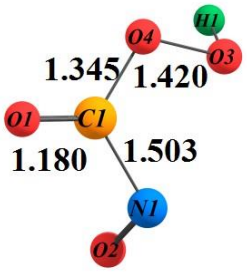

IS9

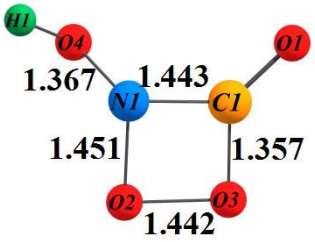

IS10

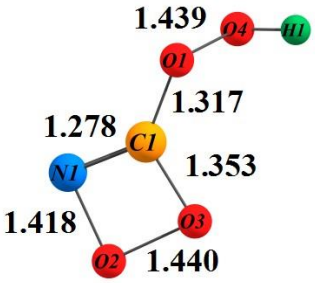

IS11

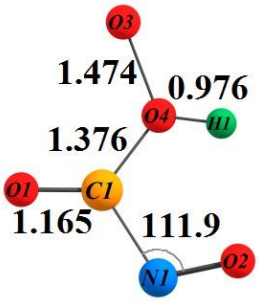

IS12

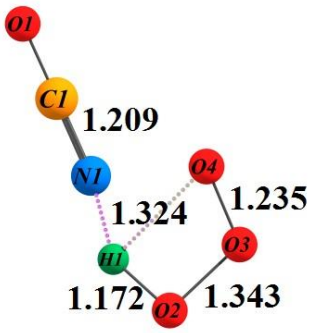

T0P5

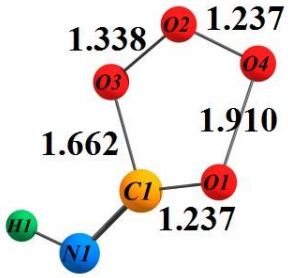

T0/1

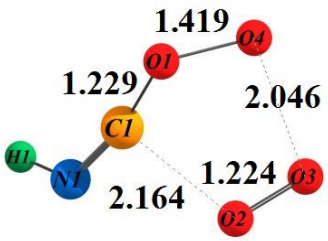

T1P2

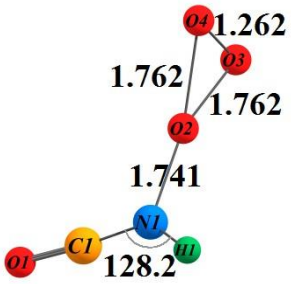

T0P1

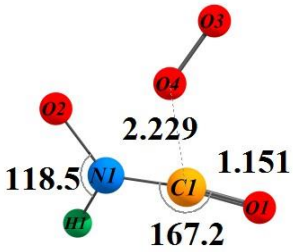

T7P1

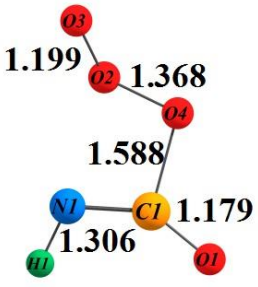

T0/2

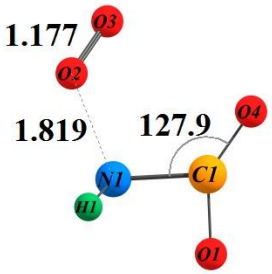

T2P11

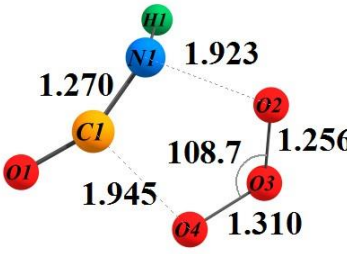

T0/3

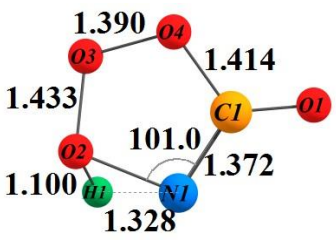

T3/4

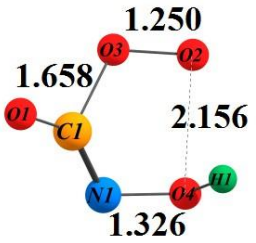

T4P4

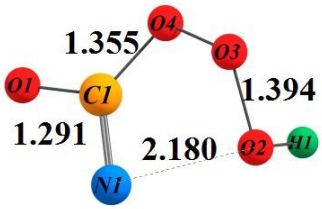

T4/5

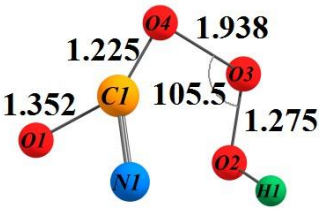

T5P9

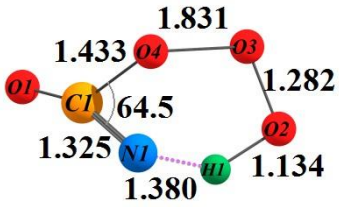

T5P11

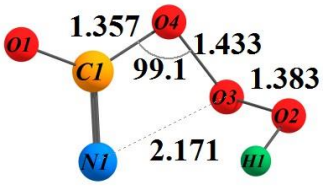

T5/6

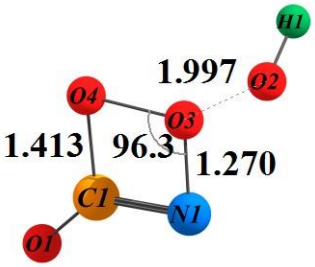

T6P3

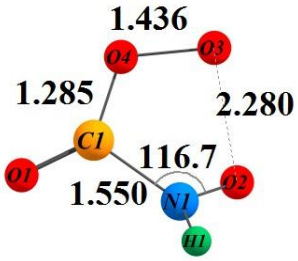

T3/7

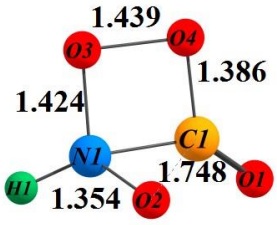

T7/8

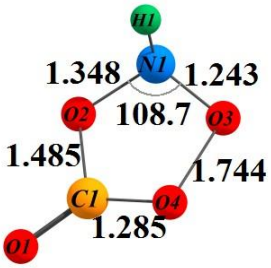

T8P6

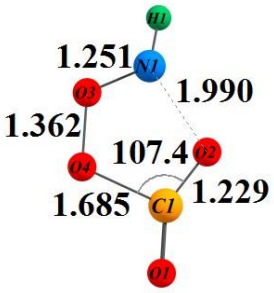

T8P7

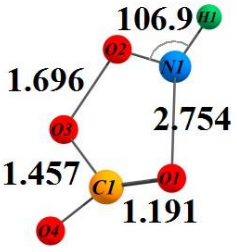

T8P8

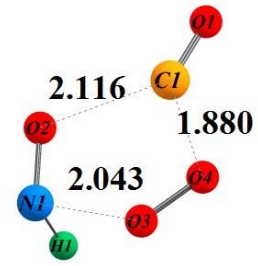

T8P13

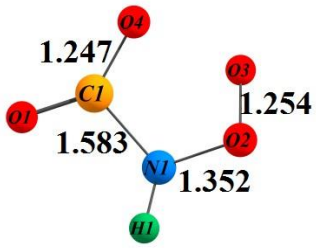

T3P7

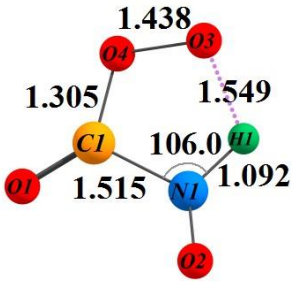

T7/9

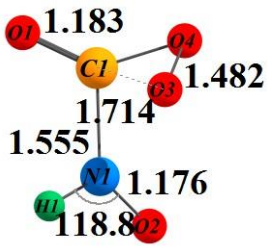

T7P8

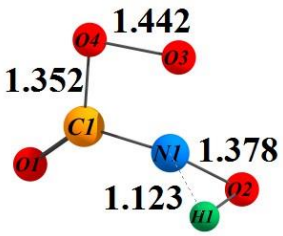

T7/10

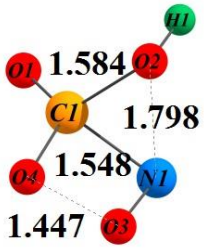

T10P14

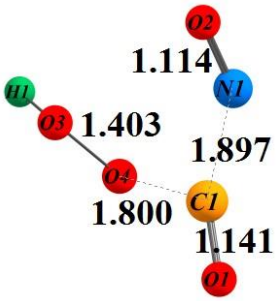

T9P10

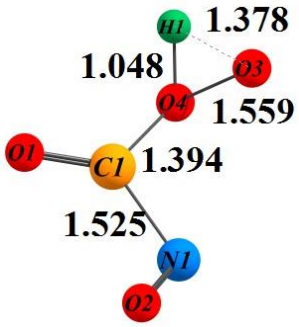

T9/12

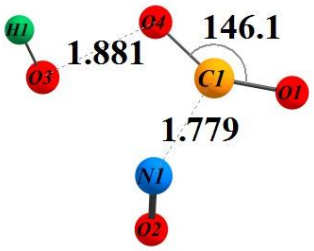

T9P15

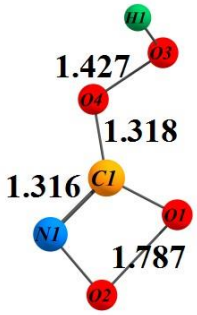

T9/11

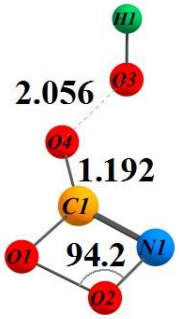

T11P3

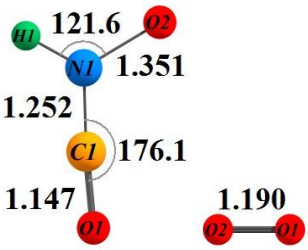

PR1

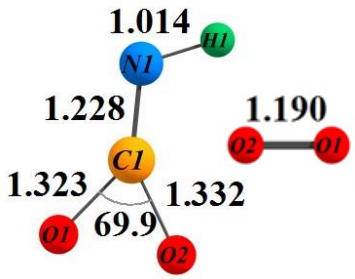

PR2

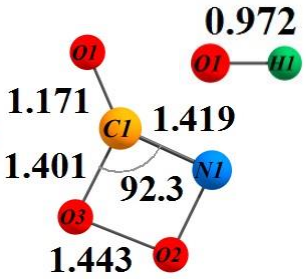

PR3

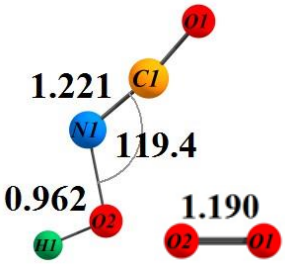

PR4

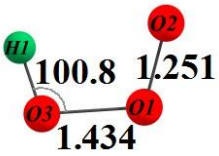

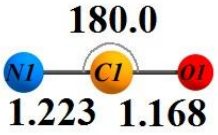

PR5

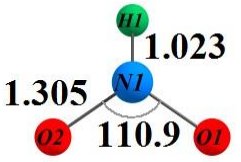

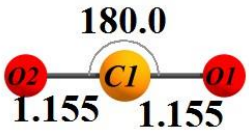

PR6

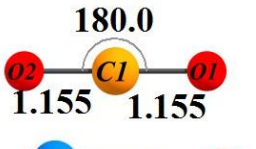

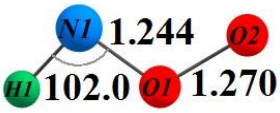

PR7

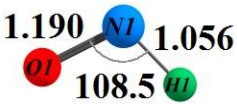

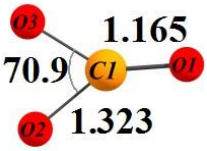

PR8

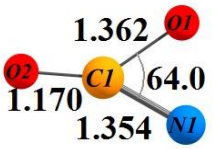

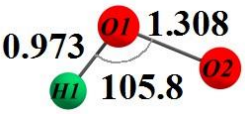

PR9

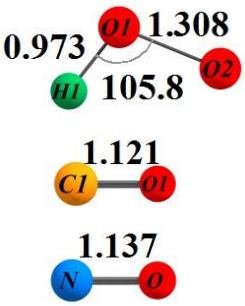

PR10

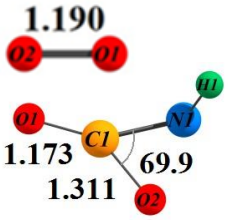

PR11

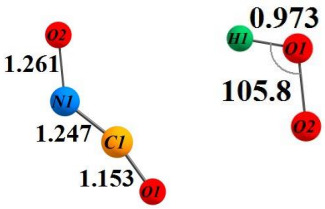

PR12

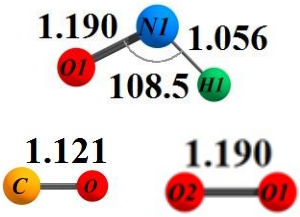

PR13

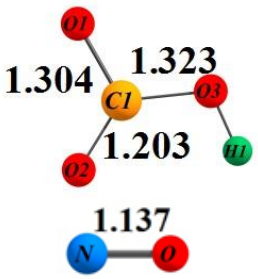

PR14

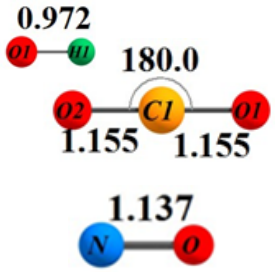

PR15

c. Energetic and entropic data

Table 6: Gibbs free energies (ΔG_0) and entropies (ΔS_0) for the O_3 + HNCO reaction products at the CCSD(T)//M06-2X /aug-cc-pVTZ level of theory

Species	(ΔG^o) (298.15 K) (kcal mol^{-1})	(ΔS^o) (298.15 K) (cal mol^{-1}K^{-1})
PR1 (HN(O)CO + O_2)	41.7	-3.1
PR2 (HNC(=O)O + O_2)	34.5	-5.5
PR3 (cy_NC(=O)OO + OH)	22.8	-5.2
PR4 (HONCO + O_2)	5.6	-2.4
PR5 (HO3 + NCO)	29.5	1.8
PR6 (HN(O)O + CO_2)	-60.3	-2.3
PR7 (HNOO + CO_2)	-41.7	-5.4
PR8 (HNO + CO_3)	-21.7	-1.6
PR9 (NC(=O)O + HO_2)	15.7	2.9
PR10 (HO_2 + CO + NO)	-23.3	34.7
PR11 (HNC(=O)O + O_2)	12.7	-5.8
PR12 (HO_2 + ONCO)	13.2	4.2
PR13 (HNO + O_2 + CO)	-21.8	32.8
PR14 (HOC(=O)O + NO)	-74.4	-0.4
PR15 (HO_2 + CO + NO)	-82.1	26.7

Table 7: Comparison of calculated heats of reaction (kcal mol^{-1}) of the products of the O_3 + HNCO reaction, against available literature data at 298.15 K. Levels of theory used are M06-2X/aug-cc-pVTZ (designated as M06-2X) and CCSD(T)/aug-cc-pVTZ (CCSD(T)

Species	M06-2X	CCSD(T)	Reference[a,b,c]
PR1 (HN(O)CO + O_2)	34.4	40.8	
PR2 (HNC(=O)O + O_2)	37.1	41.0	
PR3 (cy_NC(=O)OO + OH)	14.0	21.2	
PR4 (HONCO + O_2)	-2.1	4.9	
PR5 (HO_3 + NCO)	29.5	30.1	30.4
PR6 (HN(O)O + CO_2)	-61.0	-56.1	
PR7 (HNOO + CO_2)	-45.6	-43.3	
PR8 (HNO + CO_3)	-27.9	-22.2	
PR9 (NC(=O)O + HO_2)	5.9	16.6	
PR10 (HO_2 + CO + NO)	-19.8	-13.0	-11.3
PR11 (HNC(=O)O + O_2)	6.4	11.0	
PR12 (HO_2 + ONCO)	1.3	14.5	
PR13 (HNO + O_2 + CO)	-18.5	-12.0	-10.4
PR14 (HOC(=O)O + NO)	-84.5	-74.5	
PR15 (HO_2 + CO + NO)	-82.0	-74.1	-72.9

[a] Ruscic, B. and Bross, D. H.: Active Thermochemical Tables (ATcT) values based on ver. 1.122g of the Thermochemical Network (2019); available at ATcT.anl.gov, Argonne National Laboratory Active Thermochemical Tables [online] Available from: http://atct.anl.gov/, 2019.

[b] Ruscic, B., Pinzon, R. E., von Laszewski, G., Kodeboyina, D., Burcat, A., Leahy, D., Montoya, D. and Wagner, A. F.: Active Thermochemical Tables: thermochemistry for the 21st century, in SciDAC 2005: Scientific Discovery Through Advanced Computing, vol. 16, edited by A. Mezzacappa, pp. 561–570, Iop Publishing Ltd, Bristol., 2005.

Table 8: Theoretical predication of relative energies ΔE (kcal/mol) for reactants, intermediates, transition states and products of the O_3 + HNCO reaction. Levels of theory used are M06-2X/aug-cc-pVTZ (designated as M06-2X) and CCSD(T)/aug-cc-pVTZ (CCSD(T)

Species	***M06-2X***	**CCSD(T)**
RA(HNCO+O_3)	0.0	0.0
IS1	13.0	28.3
IS2	20.7	17.8
IS3	-23.8	-8.1
IS4	21.8	35.7
IS5	31.4	32.1
IS6	25.7	36.2
IS7	-18.7	-8.2
IS8	-44.9	-34.9
IS9	-45.3	-30.7
IS10	-36.5	-21.4
IS11	13.6	27.1
IS12	9.5	13.0
T0P5	27.6	35.0
T0/1	37.9	41.8
T1P2	75.4	86.2
T0/2	43.2	45.9
T2P11	25.9	29.9
T0P1	62.4	67.2
T7P1	31.7	44.2
T0/3	29.4	34.8
T3/4	37.1	50.3
T4P4	15.4	44.6
T4/5	39.2	47.7
T5P9	50.1	46.7
T5P11	30.1	37.1
T5/6	40.1	47.5
T6P3	50.3	39.9
T3P7	-1.5	9.0
T3/7	10.6	19.1
T7P8	-4.0	7.25
T7/8	8.7	23.7
T8P6	-44.4	-32.8
T8P7	-20.4	-9.3
T8P8	-7.1	-1.8
T7/9	-10.4	-0.4
T7/10	21.1	35.0
T8P13	37.4	43.8
T9/11	35.3	40.7
T9/12	14.3	26.0
T9P10	1.3	9.6
T9P15	-8.3	-22.1
T11P3	57.1	42.3

T10P14	-0.5	10.1
PR1 (HN(O)CO + O_2)	34.3	40.6
PR2 (HNC(=O)O + O_2)	28.3	34.5
PR3 (cy_NC(=O)OO + OH)	14.0	26.3
PR4 (HONCO + O_2)	-2.4	4.6
PR5 (HO_3 + NCO)	29.6	32.7
PR6 (HN(O)O + CO_2)	-60.8	-53.7
PR7 (HNOO + CO_2)	-45.3	-38.0
PR8 (HNO + CO_3)	-27.9	-17.1
PR9 (NC(=O)O + HO_2)	5.9	21.6
PR10 (HO_2 + CO + NO)	-21.2	-9.4
PR11 (HNC(=O)O + O_2)	6.7	11.3
PR12 (HO_2 + ONCO)	1.0	19.2
PR13 (HNO + O_2 + CO)	-19.9	-8.4
PR14 (HOC(=O)O + NO)	-84.4	-69.5
PR15 (HO_2 + CO + NO)	-83.3	-70.4

Raw quantum chemical data

```
################################################################################
HNCO + OH : M06-2X/aug-cc-pVTZ geometry
################################################################################

Fragments
=========

H2O
---
E(CCSD(T)/Aug-CC-pVDZ) (Hartree):  -76.27379178
E(CCSD/Aug-CC-pVDZ) (Hartree):  -76.26857150
     T1 diagnostic:  0.012291
E(MP2/Aug-CC-pVDZ) (Hartree):  -76.26080866
E(MP3/Aug-CC-pVDZ) (Hartree):  -76.26554049
E(RHF/Aug-CC-pVDZ) (Hartree):  -76.04130375
E(CCSD(T)/Aug-CC-pVTZ) (Hartree):  -76.34229785
E(CCSD/Aug-CC-pVTZ) (Hartree):  -76.33365392
     T1 diagnostic:  0.010020
E(MP2/Aug-CC-pVTZ) (Hartree):  -76.32896290
E(MP3/Aug-CC-pVTZ) (Hartree):  -76.33161488
E(RHF/Aug-CC-pVTZ) (Hartree):  -76.06047622
E(CCSD(T)/Aug-CC-pVQZ) (Hartree):  -76.36356927
E(CCSD/Aug-CC-pVQZ) (Hartree):  -76.35418141
     T1 diagnostic:  0.009322
E(MP2/Aug-CC-pVQZ) (Hartree):  -76.35189638
E(MP3/Aug-CC-pVQZ) (Hartree):  -76.35263788
E(RHF/Aug-CC-pVQZ) (Hartree):  -76.06585061
E(RM062X/Aug-CC-pVTZ) (Hartree):  -76.43010625
Point group : C2V
Electronic state : 1-A1
Cartesian coordinates (Angs):
     H       0.000000      0.762173      -0.466394
     H      -0.000000     -0.762173      -0.466394
     O       0.000000     -0.000000       0.116598
Rotational constants (GHz):  830.6570700  431.6138700  284.0302400
Vibrational harmonic frequencies (cm-1):
     1621.7919                3864.9482                3966.9566
Zero-point correction (Hartree): 0.021537

HNCO
----
E(CCSD(T)/Aug-CC-pVDZ) (Hartree): -168.30258465
E(CCSD/Aug-CC-pVDZ) (Hartree): -168.28124890
     T1 diagnostic:  0.018038
E(MP2/Aug-CC-pVDZ) (Hartree): -168.27834689
E(MP3/Aug-CC-pVDZ) (Hartree): -168.27384035
E(RHF/Aug-CC-pVDZ) (Hartree): -167.79177923
E(CCSD(T)/Aug-CC-pVTZ) (Hartree): -168.44532616
E(CCSD/Aug-CC-pVTZ) (Hartree): -168.41561675
     T1 diagnostic:  0.017532
E(MP2/Aug-CC-pVTZ) (Hartree): -168.41955710
E(MP3/Aug-CC-pVTZ) (Hartree): -168.41062749
E(RHF/Aug-CC-pVTZ) (Hartree): -167.83284283
E(CCSD(T)/Aug-CC-pVQZ) (Hartree): -168.48867842
E(CCSD/Aug-CC-pVQZ) (Hartree): -168.45707212
     T1 diagnostic:  0.017338
E(MP2/Aug-CC-pVQZ) (Hartree): -168.46658212
E(MP3/Aug-CC-pVQZ) (Hartree): -168.45326510
E(RHF/Aug-CC-pVQZ) (Hartree): -167.84366530
E(RM062X/Aug-CC-pVTZ) (Hartree): -168.68730418
Electronic state : 1-A
Cartesian coordinates (Angs):
     N       1.154202     -0.122224       0.000000
     C      -0.045116      0.016799       0.000000
     O      -1.204025      0.015866      -0.000000
     H       1.823480      0.627848       0.000002
Rotational constants (GHz):  879.6416200   11.1877300   11.0472300
Vibrational harmonic frequencies (cm-1):
      565.6997                 656.9786                 786.0660
     1369.4348                2362.7298                3698.6854
Zero-point correction (Hartree): 0.021505

NCO
---
E(CCSD(T)/Aug-CC-pVDZ) (Hartree): -167.62691510
E(CCSD/Aug-CC-pVDZ) (Hartree): -167.60765916
     T1 diagnostic:  0.026290
E(MP2/Aug-CC-pVDZ) (Hartree): -167.58945819
E(MP3/Aug-CC-pVDZ) (Hartree): -167.59640402
E(PMP2/Aug-CC-pVDZ) (Hartree): -167.59849852
```

```
E(PMP3/Aug-CC-pVDZ) (Hartree): -167.60212188
E(PUHF/Aug-CC-pVDZ) (Hartree): -167.16611850
E(UHF/Aug-CC-pVDZ) (Hartree): -167.15459686
E(CCSD(T)/Aug-CC-pVTZ) (Hartree): -167.76182535
E(CCSD/Aug-CC-pVTZ) (Hartree): -167.73450406
     T1 diagnostic:  0.025897
E(MP2/Aug-CC-pVTZ) (Hartree): -167.72247683
E(MP3/Aug-CC-pVTZ) (Hartree): -167.72587006
E(PMP2/Aug-CC-pVTZ) (Hartree): -167.73164060
E(PMP3/Aug-CC-pVTZ) (Hartree): -167.73164486
E(PUHF/Aug-CC-pVTZ) (Hartree): -167.20496466
E(UHF/Aug-CC-pVTZ) (Hartree): -167.19327287
E(CCSD(T)/Aug-CC-pVQZ) (Hartree): -167.80302538
E(CCSD/Aug-CC-pVQZ) (Hartree): -167.77384889
     T1 diagnostic:  0.025899
E(MP2/Aug-CC-pVQZ) (Hartree): -167.76694762
E(MP3/Aug-CC-pVQZ) (Hartree): -167.76640616
E(PMP2/Aug-CC-pVQZ) (Hartree): -167.77617939
E(PMP3/Aug-CC-pVQZ) (Hartree): -167.77220396
E(PUHF/Aug-CC-pVQZ) (Hartree): -167.21556437
E(UHF/Aug-CC-pVQZ) (Hartree): -167.20379254
E(UM062X/Aug-CC-pVTZ) (Hartree): -168.00175758
Point group : C*V
Cartesian coordinates (Angs):
     N       0.000000      0.000000      -1.259810
     C       0.000000      0.000000      -0.037198
     O       0.000000      0.000000       1.130232
Rotational constants (GHz):    0.0000000   11.8429381   11.8429381
Vibrational harmonic frequencies (cm-1):
      533.0069 (  PI)           614.6584 (  PI)          1326.9293 (  SG)
     2040.1488 (  SG)
Zero-point correction (Hartree): 0.010285

OH
--
E(CCSD(T)/Aug-CC-pVDZ) (Hartree):  -75.58402897
E(CCSD/Aug-CC-pVDZ) (Hartree):  -75.58066382
     T1 diagnostic:  0.012130
E(MP2/Aug-CC-pVDZ) (Hartree):  -75.56556301
E(MP3/Aug-CC-pVDZ) (Hartree):  -75.57786050
E(PMP2/Aug-CC-pVDZ) (Hartree):  -75.56732488
E(PMP3/Aug-CC-pVDZ) (Hartree):  -75.57892297
E(PUHF/Aug-CC-pVDZ) (Hartree):  -75.40650834
E(UHF/Aug-CC-pVDZ) (Hartree):  -75.40358239
E(CCSD(T)/Aug-CC-pVTZ) (Hartree):  -75.64558463
E(CCSD/Aug-CC-pVTZ) (Hartree):  -75.63969553
     T1 diagnostic:  0.010033
E(MP2/Aug-CC-pVTZ) (Hartree):  -75.62633093
E(MP3/Aug-CC-pVTZ) (Hartree):  -75.63789591
E(PMP2/Aug-CC-pVTZ) (Hartree):  -75.62832174
E(PMP3/Aug-CC-pVTZ) (Hartree):  -75.63903909
E(PUHF/Aug-CC-pVTZ) (Hartree):  -75.42490811
E(UHF/Aug-CC-pVTZ) (Hartree):  -75.42155521
E(CCSD(T)/Aug-CC-pVQZ) (Hartree):  -75.66449303
E(CCSD/Aug-CC-pVQZ) (Hartree):  -75.65800936
     T1 diagnostic:  0.009515
E(MP2/Aug-CC-pVQZ) (Hartree):  -75.64661096
E(MP3/Aug-CC-pVQZ) (Hartree):  -75.65671803
E(PMP2/Aug-CC-pVQZ) (Hartree):  -75.64862588
E(PMP3/Aug-CC-pVQZ) (Hartree):  -75.65786011
E(PUHF/Aug-CC-pVQZ) (Hartree):  -75.42993312
E(UHF/Aug-CC-pVQZ) (Hartree):  -75.42654255
E(UM062X/Aug-CC-pVTZ) (Hartree):  -75.73381015
Point group : C*V
Cartesian coordinates (Angs):
     O       0.000000      0.000000       0.108007
     H       0.000000      0.000000      -0.864057
Rotational constants (GHz):    0.0000000  564.1304540  564.1304540
Vibrational harmonic frequencies (cm-1):
     3767.8625 (  SG)
Zero-point correction (Hartree): 0.008584

Adducts
=======

HNC_OH_O (HNC(OH)O)
-------------------
E(CCSD(T)/Aug-CC-pVDZ) (Hartree): -243.92382876
E(CCSD/Aug-CC-pVDZ) (Hartree): -243.89930153
     T1 diagnostic:  0.024293
E(MP2/Aug-CC-pVDZ) (Hartree): -243.87662636
E(MP3/Aug-CC-pVDZ) (Hartree): -243.88756468
E(PMP2/Aug-CC-pVDZ) (Hartree): -243.88095809
E(PMP3/Aug-CC-pVDZ) (Hartree): -243.89045477
E(PUHF/Aug-CC-pVDZ) (Hartree): -243.22614352
E(UHF/Aug-CC-pVDZ) (Hartree): -243.22051292
E(CCSD(T)/Aug-CC-pVTZ) (Hartree): -244.12846223
E(CCSD/Aug-CC-pVTZ) (Hartree): -244.09269439
```

```
     T1 diagnostic:  0.022869
E(MP2/Aug-CC-pVTZ) (Hartree): -244.07895732
E(MP3/Aug-CC-pVTZ) (Hartree): -244.08473400
E(PMP2/Aug-CC-pVTZ) (Hartree): -244.08346168
E(PMP3/Aug-CC-pVTZ) (Hartree): -244.08772099
E(PUHF/Aug-CC-pVTZ) (Hartree): -243.28345339
E(UHF/Aug-CC-pVTZ) (Hartree): -243.27757772
E(CCSD(T)/Aug-CC-pVQZ) (Hartree): -244.19131662
E(CCSD/Aug-CC-pVQZ) (Hartree): -244.15292312
     T1 diagnostic:  0.022449
E(MP2/Aug-CC-pVQZ) (Hartree): -244.14672930
E(MP3/Aug-CC-pVQZ) (Hartree): -244.14678585
E(PMP2/Aug-CC-pVQZ) (Hartree): -244.15127448
E(PMP3/Aug-CC-pVQZ) (Hartree): -244.14978746
E(PUHF/Aug-CC-pVQZ) (Hartree): -243.29922308
E(UHF/Aug-CC-pVQZ) (Hartree): -243.29329855
E(UM062X/Aug-CC-pVTZ) (Hartree): -244.45951097
Electronic state : 2-A
Cartesian coordinates (Angs):
     N       0.743463     -1.106842      -0.077404
     C       0.046336      0.104153       0.008487
     O       0.584355      1.174896      -0.020002
     H       1.608817     -1.002616       0.455638
     O      -1.282325     -0.037661       0.030718
     H      -1.507315     -0.972286      -0.050459
Rotational constants (GHz):   12.1530700   11.2949100    5.8946200
Vibrational harmonic frequencies (cm-1):
      300.4381                467.4051                532.8139
      596.1793                710.4215                942.0890
     1108.7750               1237.2313               1383.4561
     1796.0740               3481.9335               3838.1229
Zero-point correction (Hartree): 0.037350

HNCOOH
------
E(CCSD(T)/Aug-CC-pVDZ) (Hartree): -243.78233506
E(CCSD/Aug-CC-pVDZ) (Hartree): -243.75491909
     T1 diagnostic:  0.026100
E(MP2/Aug-CC-pVDZ) (Hartree): -243.73146131
E(MP3/Aug-CC-pVDZ) (Hartree): -243.74087503
E(PMP2/Aug-CC-pVDZ) (Hartree): -243.73530097
E(PMP3/Aug-CC-pVDZ) (Hartree): -243.74364239
E(PUHF/Aug-CC-pVDZ) (Hartree): -243.06089368
E(UHF/Aug-CC-pVDZ) (Hartree): -243.05626195
E(CCSD(T)/Aug-CC-pVTZ) (Hartree): -243.98861061
E(CCSD/Aug-CC-pVTZ) (Hartree): -243.94932749
     T1 diagnostic:  0.025325
E(MP2/Aug-CC-pVTZ) (Hartree): -243.93572757
E(MP3/Aug-CC-pVTZ) (Hartree): -243.93923855
E(PMP2/Aug-CC-pVTZ) (Hartree): -243.93964602
E(PMP3/Aug-CC-pVTZ) (Hartree): -243.94204334
E(PUHF/Aug-CC-pVTZ) (Hartree): -243.11981582
E(UHF/Aug-CC-pVTZ) (Hartree): -243.11508675
E(CCSD(T)/Aug-CC-pVQZ) (Hartree): -244.05073026
E(CCSD/Aug-CC-pVQZ) (Hartree): -244.00869547
     T1 diagnostic:  0.025161
E(MP2/Aug-CC-pVQZ) (Hartree): -244.00290066
E(MP3/Aug-CC-pVQZ) (Hartree): -244.00047998
E(PMP2/Aug-CC-pVQZ) (Hartree): -244.00685193
E(PMP3/Aug-CC-pVQZ) (Hartree): -244.00329641
E(PUHF/Aug-CC-pVQZ) (Hartree): -243.13527996
E(UHF/Aug-CC-pVQZ) (Hartree): -243.13051368
E(UM062X/Aug-CC-pVTZ) (Hartree): -244.32029053
Electronic state : 2-A
Cartesian coordinates (Angs):
     N       1.813840     -0.146658       0.011359
     C       0.608771     -0.337989       0.012316
     O      -0.421905      0.511006      -0.001847
     H       2.186714      0.801214      -0.040014
     O      -1.646548     -0.211644      -0.111112
     H      -1.988594     -0.141571       0.790283
Rotational constants (GHz):   63.3231200    4.7501100    4.4807800
Vibrational harmonic frequencies (cm-1):
      150.3017                198.5905                334.4188
      568.7742                641.7866                822.9540
     1026.4883               1087.9781               1427.1535
     1908.5495               3461.5976               3811.7931
Zero-point correction (Hartree): 0.035176

HN_OH_CO (HN(OH)CO)
-------------------
E(CCSD(T)/Aug-CC-pVDZ) (Hartree): -243.85940138
E(CCSD/Aug-CC-pVDZ) (Hartree): -243.83350296
     T1 diagnostic:  0.020302
E(MP2/Aug-CC-pVDZ) (Hartree): -243.81648757
E(MP3/Aug-CC-pVDZ) (Hartree): -243.82183243
E(PMP2/Aug-CC-pVDZ) (Hartree): -243.81865224
E(PMP3/Aug-CC-pVDZ) (Hartree): -243.82300490
```

```
E(PUHF/Aug-CC-pVDZ) (Hartree): -243.14380357
E(UHF/Aug-CC-pVDZ) (Hartree): -243.14024635
E(CCSD(T)/Aug-CC-pVTZ) (Hartree): -244.06455049
E(CCSD/Aug-CC-pVTZ) (Hartree): -244.02691558
     T1 diagnostic:  0.019122
E(MP2/Aug-CC-pVTZ) (Hartree): -244.01957063
E(MP3/Aug-CC-pVTZ) (Hartree): -244.01903430
E(PMP2/Aug-CC-pVTZ) (Hartree): -244.02183232
E(PMP3/Aug-CC-pVTZ) (Hartree): -244.02023660
E(PUHF/Aug-CC-pVTZ) (Hartree): -243.20150770
E(UHF/Aug-CC-pVTZ) (Hartree): -243.19780057
E(CCSD(T)/Aug-CC-pVQZ) (Hartree): -244.12770089
E(CCSD/Aug-CC-pVQZ) (Hartree): -244.08736004
     T1 diagnostic:  0.018637
E(MP2/Aug-CC-pVQZ) (Hartree): -244.08779258
E(MP3/Aug-CC-pVQZ) (Hartree): -244.08137288
E(PMP2/Aug-CC-pVQZ) (Hartree): -244.09007903
E(PMP3/Aug-CC-pVQZ) (Hartree): -244.08257494
E(PUHF/Aug-CC-pVQZ) (Hartree): -243.21743084
E(UHF/Aug-CC-pVQZ) (Hartree): -243.21368737
E(UM062X/Aug-CC-pVTZ) (Hartree): -244.39804484
Electronic state : 2-A
Cartesian coordinates (Angs):
     N       0.424721      0.402442       0.106287
     C      -0.680317     -0.356372       0.010537
     O      -1.813431     -0.010756      -0.018064
     H       0.399400      1.365332      -0.210956
     O       1.645538     -0.204754      -0.146319
     H       2.052605     -0.320112       0.718790
Rotational constants (GHz):   67.5754300    4.6229100    4.4025200
Vibrational harmonic frequencies (cm-1):
      223.6267                340.4888                385.1750
      511.6656                623.8900               1116.2621
     1243.7149               1415.2825               1440.5571
     1901.1431               3529.1986               3838.4925
Zero-point correction (Hartree): 0.037748

Transition states
=================

TS.HNCO+OH.H2O+NCO
------------------
E(CCSD(T)/Aug-CC-pVDZ) (Hartree): -243.87640877
E(CCSD/Aug-CC-pVDZ) (Hartree): -243.84637161
     T1 diagnostic:  0.041435
E(MP2/Aug-CC-pVDZ) (Hartree): -243.82696477
E(MP3/Aug-CC-pVDZ) (Hartree): -243.82907020
E(PMP2/Aug-CC-pVDZ) (Hartree): -243.83016369
E(PMP3/Aug-CC-pVDZ) (Hartree): -243.83107480
E(PUHF/Aug-CC-pVDZ) (Hartree): -243.15841045
E(UHF/Aug-CC-pVDZ) (Hartree): -243.15345576
E(CCSD(T)/Aug-CC-pVTZ) (Hartree): -244.08081628
E(CCSD/Aug-CC-pVTZ) (Hartree): -244.03918090
     T1 diagnostic:  0.039727
E(MP2/Aug-CC-pVTZ) (Hartree): -244.02932519
E(MP3/Aug-CC-pVTZ) (Hartree): -244.02604766
E(PMP2/Aug-CC-pVTZ) (Hartree): -244.03269815
E(PMP3/Aug-CC-pVTZ) (Hartree): -244.02812029
E(PUHF/Aug-CC-pVTZ) (Hartree): -243.21704552
E(UHF/Aug-CC-pVTZ) (Hartree): -243.21179389
E(CCSD(T)/Aug-CC-pVQZ) (Hartree): -244.14280122
E(CCSD/Aug-CC-pVQZ) (Hartree): -244.09850032
     T1 diagnostic:  0.039304
E(MP2/Aug-CC-pVQZ) (Hartree): -244.09648655
E(MP3/Aug-CC-pVQZ) (Hartree): -244.08722632
E(PMP2/Aug-CC-pVQZ) (Hartree): -244.09988037
E(PMP3/Aug-CC-pVQZ) (Hartree): -244.08929603
E(PUHF/Aug-CC-pVQZ) (Hartree): -243.23263004
E(UHF/Aug-CC-pVQZ) (Hartree): -243.22734742
E(UM062X/Aug-CC-pVTZ) (Hartree): -244.41296055
Electronic state : 2-A
Cartesian coordinates (Angs):
     N      -0.094447      0.925704       0.027832
     H      -1.165667      0.532358      -0.191323
     C       0.846001      0.151877       0.000427
     O       1.803466     -0.501425      -0.003313
     O      -1.948555     -0.423785      -0.103876
     H      -2.088502     -0.521868       0.851450
Rotational constants (GHz):   24.4700100    3.9486100    3.4420400
Vibrational harmonic frequencies (cm-1):
    i1687.0870                111.8064                 199.5012
      421.0194                616.6612                 643.1380
      739.1833               1086.3718                1324.9759
     1545.1352               2262.3379                3789.7463
Zero-point correction (Hartree): 0.029024

TS.HNCO+OH.HNC_OH_.O (TS.HNCO+OH.HNC(OH)O)
------------------------------------------
```

```
E(CCSD(T)/Aug-CC-pVDZ) (Hartree): -243.87677763
E(CCSD/Aug-CC-pVDZ) (Hartree): -243.84725316
     T1 diagnostic:  0.029780
E(MP2/Aug-CC-pVDZ) (Hartree): -243.82584727
E(MP3/Aug-CC-pVDZ) (Hartree): -243.83068568
E(PMP2/Aug-CC-pVDZ) (Hartree): -243.83432126
E(PMP3/Aug-CC-pVDZ) (Hartree): -243.83622672
E(PUHF/Aug-CC-pVDZ) (Hartree): -243.16450794
E(UHF/Aug-CC-pVDZ) (Hartree): -243.15356505
E(CCSD(T)/Aug-CC-pVTZ) (Hartree): -244.08076434
E(CCSD/Aug-CC-pVTZ) (Hartree): -244.03965645
     T1 diagnostic:  0.028672
E(MP2/Aug-CC-pVTZ) (Hartree): -244.02776550
E(MP3/Aug-CC-pVTZ) (Hartree): -244.02715647
E(PMP2/Aug-CC-pVTZ) (Hartree): -244.03640530
E(PMP3/Aug-CC-pVTZ) (Hartree): -244.03280683
E(PUHF/Aug-CC-pVTZ) (Hartree): -243.22231964
E(UHF/Aug-CC-pVTZ) (Hartree): -243.21115223
E(CCSD(T)/Aug-CC-pVQZ) (Hartree): -244.14299039
E(CCSD/Aug-CC-pVQZ) (Hartree): -244.09916704
     T1 diagnostic:  0.028459
E(MP2/Aug-CC-pVQZ) (Hartree): -244.09500706
E(MP3/Aug-CC-pVQZ) (Hartree): -244.08848149
E(PMP2/Aug-CC-pVQZ) (Hartree): -244.10369237
E(PMP3/Aug-CC-pVQZ) (Hartree): -244.09414998
E(PUHF/Aug-CC-pVQZ) (Hartree): -243.23796533
E(UHF/Aug-CC-pVQZ) (Hartree): -243.22674277
E(UM062X/Aug-CC-pVTZ) (Hartree): -244.40918730
Electronic state : 2-A
Cartesian coordinates (Angs):
     N      -0.247355      1.225121       0.108835
     C       0.432564      0.170639      -0.020970
     O       1.369730     -0.504604      -0.002494
     H      -0.895532      1.447530      -0.637603
     O      -1.176170     -0.781380      -0.098383
     H      -1.516845     -0.759339       0.808596
Rotational constants (GHz):   12.8674800    8.4791500    5.2517000
Vibrational harmonic frequencies (cm-1):
     i592.4667                258.4603                 368.8116
      480.6795                541.8280                 609.1365
      837.0991                936.0857                1233.2469
     2194.2622               3598.6215                3804.3947
Zero-point correction (Hartree): 0.033860

TS.HNCO+OH.HNCOOH
-----------------
E(CCSD(T)/Aug-CC-pVDZ) (Hartree): -243.77589344
E(CCSD/Aug-CC-pVDZ) (Hartree): -243.74600542
     T1 diagnostic:  0.044717
E(MP2/Aug-CC-pVDZ) (Hartree): -243.70055619
E(MP3/Aug-CC-pVDZ) (Hartree): -243.71559663
E(PMP2/Aug-CC-pVDZ) (Hartree): -243.72239276
E(PMP3/Aug-CC-pVDZ) (Hartree): -243.73245491
E(PUHF/Aug-CC-pVDZ) (Hartree): -243.06984628
E(UHF/Aug-CC-pVDZ) (Hartree): -243.04523126
E(CCSD(T)/Aug-CC-pVTZ) (Hartree): -243.98133797
E(CCSD/Aug-CC-pVTZ) (Hartree): -243.93945759
     T1 diagnostic:  0.043971
E(MP2/Aug-CC-pVTZ) (Hartree): -243.90342200
E(MP3/Aug-CC-pVTZ) (Hartree): -243.91345485
E(PMP2/Aug-CC-pVTZ) (Hartree): -243.92578064
E(PMP3/Aug-CC-pVTZ) (Hartree): -243.93073760
E(PUHF/Aug-CC-pVTZ) (Hartree): -243.12918491
E(UHF/Aug-CC-pVTZ) (Hartree): -243.10400968
E(CCSD(T)/Aug-CC-pVQZ) (Hartree): -244.04311992
E(CCSD/Aug-CC-pVQZ) (Hartree): -243.99841112
     T1 diagnostic:  0.043940
E(MP2/Aug-CC-pVQZ) (Hartree): -243.96997477
E(MP3/Aug-CC-pVQZ) (Hartree): -243.97422933
E(PMP2/Aug-CC-pVQZ) (Hartree): -243.99244577
E(PMP3/Aug-CC-pVQZ) (Hartree): -243.99158068
E(PUHF/Aug-CC-pVQZ) (Hartree): -243.14467688
E(UHF/Aug-CC-pVQZ) (Hartree): -243.11938158
E(UM062X/Aug-CC-pVTZ) (Hartree): -244.31155642
Electronic state : 2-A
Cartesian coordinates (Angs):
     N      -1.827379     -0.239308       0.027687
     C      -0.607169     -0.174829       0.001920
     O       0.403230      0.572612      -0.045794
     H      -2.385121      0.616043       0.017677
     O       1.677342     -0.327151      -0.060064
     H       2.175214      0.144395       0.623854
Rotational constants (GHz):   56.2899800    4.6032400    4.2892900
Vibrational harmonic frequencies (cm-1):
    i1173.0904                135.4402                 272.2672
      327.4267                606.7060                 685.8963
      908.7694                994.1114                1260.8447
     1987.5535               3421.4460                3801.0214
```

```
Zero-point correction (Hartree): 0.032809

TS.HNCO+OH.HN_OH_CO (TS.HNCO+OH.HN(OH)CO)
-----------------------------------------
E(CCSD(T)/Aug-CC-pVDZ) (Hartree): -243.83209726
E(CCSD/Aug-CC-pVDZ) (Hartree): -243.80301942
     T1 diagnostic:  0.028702
E(MP2/Aug-CC-pVDZ) (Hartree): -243.78291892
E(MP3/Aug-CC-pVDZ) (Hartree): -243.78606807
E(PMP2/Aug-CC-pVDZ) (Hartree): -243.79152814
E(PMP3/Aug-CC-pVDZ) (Hartree): -243.79156463
E(PUHF/Aug-CC-pVDZ) (Hartree): -243.10557871
E(UHF/Aug-CC-pVDZ) (Hartree): -243.09470552
E(CCSD(T)/Aug-CC-pVTZ) (Hartree): -244.03837288
E(CCSD/Aug-CC-pVTZ) (Hartree): -243.99718277
     T1 diagnostic:  0.027961
E(MP2/Aug-CC-pVTZ) (Hartree): -243.98704695
E(MP3/Aug-CC-pVTZ) (Hartree): -243.98420639
E(PMP2/Aug-CC-pVTZ) (Hartree): -243.99593536
E(PMP3/Aug-CC-pVTZ) (Hartree): -243.98987896
E(PUHF/Aug-CC-pVTZ) (Hartree): -243.16430656
E(UHF/Aug-CC-pVTZ) (Hartree): -243.15309912
E(CCSD(T)/Aug-CC-pVQZ) (Hartree): -244.10111173
E(CCSD/Aug-CC-pVQZ) (Hartree): -244.05713802
     T1 diagnostic:  0.027825
E(MP2/Aug-CC-pVQZ) (Hartree): -244.05482845
E(MP3/Aug-CC-pVQZ) (Hartree): -244.04600301
E(PMP2/Aug-CC-pVQZ) (Hartree): -244.06377796
E(PMP3/Aug-CC-pVQZ) (Hartree): -244.05169759
E(PUHF/Aug-CC-pVQZ) (Hartree): -243.17992715
E(UHF/Aug-CC-pVQZ) (Hartree): -243.16864636
E(UM062X/Aug-CC-pVTZ) (Hartree): -244.37283905
Electronic state : 2-A
Cartesian coordinates (Angs):
     N       0.413433      0.524216       0.077387
     C      -0.694245     -0.025343      -0.003000
     O      -1.862626     -0.206939      -0.015009
     H       0.720615      1.468582      -0.107214
     O       1.699234     -0.333478      -0.132226
     H       1.857954     -0.662708       0.761388
Rotational constants (GHz):   51.2302800    4.4080000    4.1174500
Vibrational harmonic frequencies (cm-1):
     i882.6904                194.5410                 310.3632
      352.8994                522.7920                 669.5841
     1125.8480               1183.7050                1250.7705
     2177.7008               3552.7436                3826.8909
Zero-point correction (Hartree): 0.034555


################################################################################
HNCO + Cl : M06-2X/aug-cc-pVTZ geometry
################################################################################

Fragments
=========

Cl
--
E(CCSD(T)/Aug-CC-pVDZ) (Hartree): -459.61222148
E(CCSD/Aug-CC-pVDZ) (Hartree): -459.60993098
     T1 diagnostic:  0.006428
E(MP2/Aug-CC-pVDZ) (Hartree): -459.59214974
E(MP3/Aug-CC-pVDZ) (Hartree): -459.60854055
E(PMP2/Aug-CC-pVDZ) (Hartree): -459.59352697
E(PMP3/Aug-CC-pVDZ) (Hartree): -459.60915212
E(PUHF/Aug-CC-pVDZ) (Hartree): -459.47549404
E(UHF/Aug-CC-pVDZ) (Hartree): -459.47278114
E(CCSD(T)/Aug-CC-pVTZ) (Hartree): -459.67621572
E(CCSD/Aug-CC-pVTZ) (Hartree): -459.67005135
     T1 diagnostic:  0.006592
E(MP2/Aug-CC-pVTZ) (Hartree): -459.64733174
E(MP3/Aug-CC-pVTZ) (Hartree): -459.66892113
E(PMP2/Aug-CC-pVTZ) (Hartree): -459.64932188
E(PMP3/Aug-CC-pVTZ) (Hartree): -459.66984266
E(PUHF/Aug-CC-pVTZ) (Hartree): -459.48966776
E(UHF/Aug-CC-pVTZ) (Hartree): -459.48596887
E(CCSD(T)/Aug-CC-pVQZ) (Hartree): -459.69474301
E(CCSD/Aug-CC-pVQZ) (Hartree): -459.68742578
     T1 diagnostic:  0.007068
E(MP2/Aug-CC-pVQZ) (Hartree): -459.66563967
E(MP3/Aug-CC-pVQZ) (Hartree): -459.68684405
E(PMP2/Aug-CC-pVQZ) (Hartree): -459.66768698
E(PMP3/Aug-CC-pVQZ) (Hartree): -459.68779580
E(PUHF/Aug-CC-pVQZ) (Hartree): -459.49294399
E(UHF/Aug-CC-pVQZ) (Hartree): -459.48917948
E(UM062X/Aug-CC-pVTZ) (Hartree): -460.14120758
Point group : OH
Cartesian coordinates (Angs):
```

```
    Cl       0.000000      0.000000       0.000000
Zero-point correction (Hartree): 0.000000

HCl
---
E(CCSD(T)/Aug-CC-pVDZ) (Hartree): -460.27219722
E(CCSD/Aug-CC-pVDZ) (Hartree): -460.26823945
     T1 diagnostic:  0.006710
E(MP2/Aug-CC-pVDZ) (Hartree): -460.25177347
E(MP3/Aug-CC-pVDZ) (Hartree): -460.26801920
E(RHF/Aug-CC-pVDZ) (Hartree): -460.09261749
E(CCSD(T)/Aug-CC-pVTZ) (Hartree): -460.34324107
E(CCSD/Aug-CC-pVTZ) (Hartree): -460.33472154
     T1 diagnostic:  0.006078
E(MP2/Aug-CC-pVTZ) (Hartree): -460.31511908
E(MP3/Aug-CC-pVTZ) (Hartree): -460.33545761
E(RHF/Aug-CC-pVTZ) (Hartree): -460.10754718
E(CCSD(T)/Aug-CC-pVQZ) (Hartree): -460.36416565
E(CCSD/Aug-CC-pVQZ) (Hartree): -460.35437945
     T1 diagnostic:  0.006303
E(MP2/Aug-CC-pVQZ) (Hartree): -460.33607995
E(MP3/Aug-CC-pVQZ) (Hartree): -460.35570430
E(RHF/Aug-CC-pVQZ) (Hartree): -460.11133250
E(RM062X/Aug-CC-pVTZ) (Hartree): -460.80750704
Point group : C*V
Electronic state : 1-SG
Cartesian coordinates (Angs):
     H       0.000000      0.000000      -1.207931
    Cl       0.000000      0.000000       0.071055
Rotational constants (GHz):    0.0000000  315.3843834  315.3843834
Vibrational harmonic frequencies (cm-1):
     2988.5153 (  SG)
Zero-point correction (Hartree): 0.006808

HNCO
----
E(CCSD(T)/Aug-CC-pVDZ) (Hartree): -168.30258139
E(CCSD/Aug-CC-pVDZ) (Hartree): -168.28124581
     T1 diagnostic:  0.018038
E(MP2/Aug-CC-pVDZ) (Hartree): -168.27834469
E(MP3/Aug-CC-pVDZ) (Hartree): -168.27383710
E(RHF/Aug-CC-pVDZ) (Hartree): -167.79177692
E(CCSD(T)/Aug-CC-pVTZ) (Hartree): -168.44532500
E(CCSD/Aug-CC-pVTZ) (Hartree): -168.41561572
     T1 diagnostic:  0.017532
E(MP2/Aug-CC-pVTZ) (Hartree): -168.41955688
E(MP3/Aug-CC-pVTZ) (Hartree): -168.41062627
E(RHF/Aug-CC-pVTZ) (Hartree): -167.83284184
E(CCSD(T)/Aug-CC-pVQZ) (Hartree): -168.48867748
E(CCSD/Aug-CC-pVQZ) (Hartree): -168.45707130
     T1 diagnostic:  0.017338
E(MP2/Aug-CC-pVQZ) (Hartree): -168.46658210
E(MP3/Aug-CC-pVQZ) (Hartree): -168.45326411
E(RHF/Aug-CC-pVQZ) (Hartree): -167.84366420
E(RM062X/Aug-CC-pVTZ) (Hartree): -168.68730197
Point group : CS
Electronic state : 1-A'
Cartesian coordinates (Angs):
     H       1.224195     -1.490249      -0.000000
     N       0.287949     -1.124328      -0.000000
     C      -0.000000      0.048088       0.000000
     O      -0.404979      1.134003       0.000000
Rotational constants (GHz):  880.1178000   11.1877600   11.0473300
Vibrational harmonic frequencies (cm-1):
      560.3477 (  A')           656.2172 (  A")           783.0612 (  A')
     1369.4169 (  A')          2362.5435 (  A')          3698.8989 (  A')
Zero-point correction (Hartree): 0.021484

NCO
---
E(CCSD(T)/Aug-CC-pVDZ) (Hartree): -167.62690657
E(CCSD/Aug-CC-pVDZ) (Hartree): -167.60765264
     T1 diagnostic:  0.026292
E(MP2/Aug-CC-pVDZ) (Hartree): -167.58944503
E(MP3/Aug-CC-pVDZ) (Hartree): -167.59639592
E(PMP2/Aug-CC-pVDZ) (Hartree): -167.59848982
E(PMP3/Aug-CC-pVDZ) (Hartree): -167.60211632
E(PUHF/Aug-CC-pVDZ) (Hartree): -167.16612650
E(UHF/Aug-CC-pVDZ) (Hartree): -167.15459901
E(CCSD(T)/Aug-CC-pVTZ) (Hartree): -167.76182169
E(CCSD/Aug-CC-pVTZ) (Hartree): -167.73450254
     T1 diagnostic:  0.025900
E(MP2/Aug-CC-pVTZ) (Hartree): -167.72246818
E(MP3/Aug-CC-pVTZ) (Hartree): -167.72586701
E(PMP2/Aug-CC-pVTZ) (Hartree): -167.73163653
E(PMP3/Aug-CC-pVTZ) (Hartree): -167.73164444
E(PUHF/Aug-CC-pVTZ) (Hartree): -167.20497544
E(UHF/Aug-CC-pVTZ) (Hartree): -167.19327769
```

```
E(CCSD(T)/Aug-CC-pVQZ) (Hartree): -167.80302270
E(CCSD/Aug-CC-pVQZ) (Hartree): -167.77384835
     T1 diagnostic:  0.025902
E(MP2/Aug-CC-pVQZ) (Hartree): -167.76693975
E(MP3/Aug-CC-pVQZ) (Hartree): -167.76640405
E(PMP2/Aug-CC-pVQZ) (Hartree): -167.77617611
E(PMP3/Aug-CC-pVQZ) (Hartree): -167.77220449
E(PUHF/Aug-CC-pVQZ) (Hartree): -167.21557545
E(UHF/Aug-CC-pVQZ) (Hartree): -167.20379764
E(UM062X/Aug-CC-pVTZ) (Hartree): -168.00175757
Point group : C*V
Cartesian coordinates (Angs):
     N       0.000000      0.000000      -1.259735
     C       0.000000      0.000000      -0.037247
     O       0.000000      0.000000       1.130203
Rotational constants (GHz):    0.0000000   11.8439475   11.8439475
Vibrational harmonic frequencies (cm-1):
      532.8259 (  PI)           614.5324 (  PI)          1327.2296 (  SG)
     2040.2979 (  SG)
Zero-point correction (Hartree): 0.010286

Adducts
=======

HNCClO
------
E(CCSD(T)/Aug-CC-pVDZ) (Hartree): -627.91079551
E(CCSD/Aug-CC-pVDZ) (Hartree): -627.88596678
     T1 diagnostic:  0.020530
E(MP2/Aug-CC-pVDZ) (Hartree): -627.86017243
E(MP3/Aug-CC-pVDZ) (Hartree): -627.87734760
E(PMP2/Aug-CC-pVDZ) (Hartree): -627.86242980
E(PMP3/Aug-CC-pVDZ) (Hartree): -627.87875690
E(PUHF/Aug-CC-pVDZ) (Hartree): -627.25504247
E(UHF/Aug-CC-pVDZ) (Hartree): -627.25151538
E(CCSD(T)/Aug-CC-pVTZ) (Hartree): -628.11725074
E(CCSD/Aug-CC-pVTZ) (Hartree): -628.07962712
     T1 diagnostic:  0.019532
E(MP2/Aug-CC-pVTZ) (Hartree): -628.05736701
E(MP3/Aug-CC-pVTZ) (Hartree): -628.07491336
E(PMP2/Aug-CC-pVTZ) (Hartree): -628.05979335
E(PMP3/Aug-CC-pVTZ) (Hartree): -628.07639035
E(PUHF/Aug-CC-pVTZ) (Hartree): -627.30784514
E(UHF/Aug-CC-pVTZ) (Hartree): -627.30403301
E(CCSD(T)/Aug-CC-pVQZ) (Hartree): -628.18028414
E(CCSD/Aug-CC-pVQZ) (Hartree): -628.13940542
     T1 diagnostic:  0.019233
E(MP2/Aug-CC-pVQZ) (Hartree): -628.12386077
E(MP3/Aug-CC-pVQZ) (Hartree): -628.13673622
E(PMP2/Aug-CC-pVQZ) (Hartree): -628.12630958
E(PMP3/Aug-CC-pVQZ) (Hartree): -628.13821508
E(PUHF/Aug-CC-pVQZ) (Hartree): -627.32219808
E(UHF/Aug-CC-pVQZ) (Hartree): -627.31835427
E(UM062X/Aug-CC-pVTZ) (Hartree): -628.82407848
Electronic state : 2-A
Cartesian coordinates (Angs):
     O       1.148609     -1.122831       0.023782
     N       1.057393      1.176217      -0.127494
     C       0.558457     -0.103751      -0.001324
    Cl      -1.227290     -0.018981      -0.002037
     H       0.922561      1.694309       0.744767
Rotational constants (GHz):   11.6787100    5.3326900    3.7009200
Vibrational harmonic frequencies (cm-1):
      276.3917                346.4679                457.8337
      604.5605                658.2736               1037.3322
     1115.1290               1903.9291               3462.7109
Zero-point correction (Hartree): 0.022469

HNClCO
------
E(CCSD(T)/Aug-CC-pVDZ) (Hartree): -627.87076054
E(CCSD/Aug-CC-pVDZ) (Hartree): -627.84567500
     T1 diagnostic:  0.019731
E(MP2/Aug-CC-pVDZ) (Hartree): -627.82355213
E(MP3/Aug-CC-pVDZ) (Hartree): -627.83579822
E(PMP2/Aug-CC-pVDZ) (Hartree): -627.82575898
E(PMP3/Aug-CC-pVDZ) (Hartree): -627.83699785
E(PUHF/Aug-CC-pVDZ) (Hartree): -627.20484593
E(UHF/Aug-CC-pVDZ) (Hartree): -627.20124831
E(CCSD(T)/Aug-CC-pVTZ) (Hartree): -628.08156646
E(CCSD/Aug-CC-pVTZ) (Hartree): -628.04345225
     T1 diagnostic:  0.018870
E(MP2/Aug-CC-pVTZ) (Hartree): -628.02512472
E(MP3/Aug-CC-pVTZ) (Hartree): -628.03734726
E(PMP2/Aug-CC-pVTZ) (Hartree): -628.02742052
E(PMP3/Aug-CC-pVTZ) (Hartree): -628.03857493
E(PUHF/Aug-CC-pVTZ) (Hartree): -627.26123357
E(UHF/Aug-CC-pVTZ) (Hartree): -627.25749827
```

```
E(CCSD(T)/Aug-CC-pVQZ) (Hartree): -628.14526549
E(CCSD/Aug-CC-pVQZ) (Hartree): -628.10387436
     T1 diagnostic:  0.018467
E(MP2/Aug-CC-pVQZ) (Hartree): -628.09241495
E(MP3/Aug-CC-pVQZ) (Hartree): -628.09983458
E(PMP2/Aug-CC-pVQZ) (Hartree): -628.09473433
E(PMP3/Aug-CC-pVQZ) (Hartree): -628.10106225
E(PUHF/Aug-CC-pVQZ) (Hartree): -627.27622735
E(UHF/Aug-CC-pVQZ) (Hartree): -627.27245768
E(UM062X/Aug-CC-pVTZ) (Hartree): -628.79192110
Electronic state : 2-A
Cartesian coordinates (Angs):
     N       0.070682      0.471152      -0.025534
     C       1.126466     -0.350678      -0.011114
     H       0.159634      1.476968       0.053741
     O       2.278003     -0.070216       0.012158
    Cl      -1.508072     -0.124073       0.005554
Rotational constants (GHz):   68.4372500    2.8418200    2.7290000
Vibrational harmonic frequencies (cm-1):
       79.6325                286.5276                437.3775
      507.8972                906.1193               1229.6722
     1341.8952               1884.4775               3545.6281
Zero-point correction (Hartree): 0.023281

HNCOCl
------
E(CCSD(T)/Aug-CC-pVDZ) (Hartree): -627.81925657
E(CCSD/Aug-CC-pVDZ) (Hartree): -627.79293620
     T1 diagnostic:  0.024842
E(MP2/Aug-CC-pVDZ) (Hartree): -627.76533217
E(MP3/Aug-CC-pVDZ) (Hartree): -627.78110515
E(PMP2/Aug-CC-pVDZ) (Hartree): -627.76896903
E(PMP3/Aug-CC-pVDZ) (Hartree): -627.78369047
E(PUHF/Aug-CC-pVDZ) (Hartree): -627.14697118
E(UHF/Aug-CC-pVDZ) (Hartree): -627.14251767
E(CCSD(T)/Aug-CC-pVTZ) (Hartree): -628.02945748
E(CCSD/Aug-CC-pVTZ) (Hartree): -627.99004904
     T1 diagnostic:  0.024486
E(MP2/Aug-CC-pVTZ) (Hartree): -627.96644218
E(MP3/Aug-CC-pVTZ) (Hartree): -627.98193546
E(PMP2/Aug-CC-pVTZ) (Hartree): -627.97022208
E(PMP3/Aug-CC-pVTZ) (Hartree): -627.98460763
E(PUHF/Aug-CC-pVTZ) (Hartree): -627.20310242
E(UHF/Aug-CC-pVTZ) (Hartree): -627.19847540
E(CCSD(T)/Aug-CC-pVQZ) (Hartree): -628.09234067
E(CCSD/Aug-CC-pVQZ) (Hartree): -628.04960159
     T1 diagnostic:  0.024391
E(MP2/Aug-CC-pVQZ) (Hartree): -628.03288502
E(MP3/Aug-CC-pVQZ) (Hartree): -628.04349862
E(PMP2/Aug-CC-pVQZ) (Hartree): -628.03670425
E(PMP3/Aug-CC-pVQZ) (Hartree): -628.04618843
E(PUHF/Aug-CC-pVQZ) (Hartree): -627.21781166
E(UHF/Aug-CC-pVQZ) (Hartree): -627.21314037
E(UM062X/Aug-CC-pVTZ) (Hartree): -628.73800888
Electronic state : 2-A
Cartesian coordinates (Angs):
     N       2.230960      0.016153       0.000075
     H       2.912786     -0.732335       0.000017
     C       1.042338     -0.293556       0.000008
     O       0.039600      0.596248       0.000083
    Cl      -1.476490     -0.140552      -0.000074
Rotational constants (GHz):   63.8396400    3.0201100    2.8836800
Vibrational harmonic frequencies (cm-1):
      115.1707                283.2697                509.9345
      651.8376                792.2196                957.8781
     1161.5138               1822.4680               3592.7023
Zero-point correction (Hartree): 0.022524

Transition states
=================

TS.HNCO+Cl.HCl+NCO
------------------
E(CCSD(T)/Aug-CC-pVDZ) (Hartree): -627.89122699
E(CCSD/Aug-CC-pVDZ) (Hartree): -627.86447772
     T1 diagnostic:  0.027862
E(MP2/Aug-CC-pVDZ) (Hartree): -627.83565345
E(MP3/Aug-CC-pVDZ) (Hartree): -627.85215352
E(PMP2/Aug-CC-pVDZ) (Hartree): -627.84439346
E(PMP3/Aug-CC-pVDZ) (Hartree): -627.85766445
E(PUHF/Aug-CC-pVDZ) (Hartree): -627.23064752
E(UHF/Aug-CC-pVDZ) (Hartree): -627.21937647
E(CCSD(T)/Aug-CC-pVTZ) (Hartree): -628.09755192
E(CCSD/Aug-CC-pVTZ) (Hartree): -628.05756114
     T1 diagnostic:  0.027168
E(MP2/Aug-CC-pVTZ) (Hartree): -628.03250374
E(MP3/Aug-CC-pVTZ) (Hartree): -628.04917496
E(PMP2/Aug-CC-pVTZ) (Hartree): -628.04136194
```

```
E(PMP3/Aug-CC-pVTZ) (Hartree): -628.05474096
E(PUHF/Aug-CC-pVTZ) (Hartree): -627.28338540
E(UHF/Aug-CC-pVTZ) (Hartree): -627.27194483
E(CCSD(T)/Aug-CC-pVQZ) (Hartree): -628.15968091
E(CCSD/Aug-CC-pVQZ) (Hartree): -628.11644606
     T1 diagnostic:  0.026792
E(MP2/Aug-CC-pVQZ) (Hartree): -628.09812154
E(MP3/Aug-CC-pVQZ) (Hartree): -628.11005328
E(PMP2/Aug-CC-pVQZ) (Hartree): -628.10704285
E(PMP3/Aug-CC-pVQZ) (Hartree): -628.11563944
E(PUHF/Aug-CC-pVQZ) (Hartree): -627.29741195
E(UHF/Aug-CC-pVQZ) (Hartree): -627.28589721
E(UM062X/Aug-CC-pVTZ) (Hartree): -628.80562943
Electronic state : 2-A
Cartesian coordinates (Angs):
     N      -0.598765      1.068778       0.000040
     C      -1.411294      0.150445      -0.000019
     O      -2.233770     -0.665122      -0.000072
     H       0.728758      0.744631       0.000059
    Cl       1.752972     -0.223987       0.000021
Rotational constants (GHz):   19.7103300    2.3320000    2.0852800
Vibrational harmonic frequencies (cm-1):
    i1200.1648                89.9257                385.7978
      422.5687               619.3701                645.0230
     1234.8766              1348.7962               2137.3940
Zero-point correction (Hartree): 0.015682

TS.HNCO+Cl.HNCClO
-----------------
E(CCSD(T)/Aug-CC-pVDZ) (Hartree): -627.90145327
E(CCSD/Aug-CC-pVDZ) (Hartree): -627.87371363
     T1 diagnostic:  0.027968
E(MP2/Aug-CC-pVDZ) (Hartree): -627.84856911
E(MP3/Aug-CC-pVDZ) (Hartree): -627.86209735
E(PMP2/Aug-CC-pVDZ) (Hartree): -627.85508783
E(PMP3/Aug-CC-pVDZ) (Hartree): -627.86640122
E(PUHF/Aug-CC-pVDZ) (Hartree): -627.23844719
E(UHF/Aug-CC-pVDZ) (Hartree): -627.22990453
E(CCSD(T)/Aug-CC-pVTZ) (Hartree): -628.10871220
E(CCSD/Aug-CC-pVTZ) (Hartree): -628.06770704
     T1 diagnostic:  0.027260
E(MP2/Aug-CC-pVTZ) (Hartree): -628.04611547
E(MP3/Aug-CC-pVTZ) (Hartree): -628.05995852
E(PMP2/Aug-CC-pVTZ) (Hartree): -628.05316565
E(PMP3/Aug-CC-pVTZ) (Hartree): -628.06463020
E(PUHF/Aug-CC-pVTZ) (Hartree): -627.29178549
E(UHF/Aug-CC-pVTZ) (Hartree): -627.28259331
E(CCSD(T)/Aug-CC-pVQZ) (Hartree): -628.17141825
E(CCSD/Aug-CC-pVQZ) (Hartree): -628.12709127
     T1 diagnostic:  0.026797
E(MP2/Aug-CC-pVQZ) (Hartree): -628.11227108
E(MP3/Aug-CC-pVQZ) (Hartree): -628.12146359
E(PMP2/Aug-CC-pVQZ) (Hartree): -628.11940350
E(PMP3/Aug-CC-pVQZ) (Hartree): -628.12617315
E(PUHF/Aug-CC-pVQZ) (Hartree): -627.30580219
E(UHF/Aug-CC-pVQZ) (Hartree): -627.29651268
E(UM062X/Aug-CC-pVTZ) (Hartree): -628.81589008
Electronic state : 2-A
Cartesian coordinates (Angs):
     N       0.734479      1.287760      -0.121418
     C       0.795582      0.000933       0.021703
     O       1.413462     -0.975980       0.016133
     H       0.341536      1.784654       0.675425
    Cl      -1.268475     -0.176278      -0.004987
Rotational constants (GHz):   11.6517300    4.8549300    3.4568000
Vibrational harmonic frequencies (cm-1):
     i506.0835               351.7867                416.7688
      457.4830               604.2081                951.3182
     1137.7169              2119.0894               3540.9621
Zero-point correction (Hartree): 0.021823

TS.HNCO+Cl.HNClCO
-----------------
E(CCSD(T)/Aug-CC-pVDZ) (Hartree): -627.85424253
E(CCSD/Aug-CC-pVDZ) (Hartree): -627.82737184
     T1 diagnostic:  0.028762
E(MP2/Aug-CC-pVDZ) (Hartree): -627.80306103
E(MP3/Aug-CC-pVDZ) (Hartree): -627.81570831
E(PMP2/Aug-CC-pVDZ) (Hartree): -627.80667665
E(PMP3/Aug-CC-pVDZ) (Hartree): -627.81790532
E(PUHF/Aug-CC-pVDZ) (Hartree): -627.18017620
E(UHF/Aug-CC-pVDZ) (Hartree): -627.17510707
E(CCSD(T)/Aug-CC-pVTZ) (Hartree): -628.06431547
E(CCSD/Aug-CC-pVTZ) (Hartree): -628.02414402
     T1 diagnostic:  0.028110
E(MP2/Aug-CC-pVTZ) (Hartree): -628.00384687
E(MP3/Aug-CC-pVTZ) (Hartree): -628.01641242
E(PMP2/Aug-CC-pVTZ) (Hartree): -628.00754998
```

```
E(PMP3/Aug-CC-pVTZ) (Hartree): -628.01864920
E(PUHF/Aug-CC-pVTZ) (Hartree): -627.23559239
E(UHF/Aug-CC-pVTZ) (Hartree): -627.23039303
E(CCSD(T)/Aug-CC-pVQZ) (Hartree): -628.12739577
E(CCSD/Aug-CC-pVQZ) (Hartree): -628.08386200
     T1 diagnostic:  0.028439
E(MP2/Aug-CC-pVQZ) (Hartree): -628.07041661
E(MP3/Aug-CC-pVQZ) (Hartree): -628.07809640
E(PMP2/Aug-CC-pVQZ) (Hartree): -628.07413253
E(PMP3/Aug-CC-pVQZ) (Hartree): -628.08032758
E(PUHF/Aug-CC-pVQZ) (Hartree): -627.25001152
E(UHF/Aug-CC-pVQZ) (Hartree): -627.24478905
E(UM062X/Aug-CC-pVTZ) (Hartree): -628.77757623
Electronic state : 2-A
Cartesian coordinates (Angs):
     N       0.119302      0.584078      -0.003340
     H      -0.005870      1.586415       0.010454
     C       1.150096     -0.130437      -0.000612
     O       2.330955     -0.230820       0.001057
    Cl      -1.551615     -0.179164       0.000479
Rotational constants (GHz):   53.4607900    2.7005800    2.5707300
Vibrational harmonic frequencies (cm-1):
    i1019.5189                 114.5305                 269.4452
      463.6429                 725.6795                 997.8335
     1214.9774                2066.3541                3548.4561
Zero-point correction (Hartree): 0.021417

TS.HNCO+Cl.HNCOCl
-----------------
E(CCSD(T)/Aug-CC-pVDZ) (Hartree): -627.81525783
E(CCSD/Aug-CC-pVDZ) (Hartree): -627.78722485
     T1 diagnostic:  0.036320
E(MP2/Aug-CC-pVDZ) (Hartree): -627.75025656
E(MP3/Aug-CC-pVDZ) (Hartree): -627.76884155
E(PMP2/Aug-CC-pVDZ) (Hartree): -627.76169245
E(PMP3/Aug-CC-pVDZ) (Hartree): -627.77728087
E(PUHF/Aug-CC-pVDZ) (Hartree): -627.14636933
E(UHF/Aug-CC-pVDZ) (Hartree): -627.13318093
E(CCSD(T)/Aug-CC-pVTZ) (Hartree): -628.02313037
E(CCSD/Aug-CC-pVTZ) (Hartree): -627.98187847
     T1 diagnostic:  0.035675
E(MP2/Aug-CC-pVTZ) (Hartree): -627.94881603
E(MP3/Aug-CC-pVTZ) (Hartree): -627.96748882
E(PMP2/Aug-CC-pVTZ) (Hartree): -627.96052811
E(PMP3/Aug-CC-pVTZ) (Hartree): -627.97613574
E(PUHF/Aug-CC-pVTZ) (Hartree): -627.20079411
E(UHF/Aug-CC-pVTZ) (Hartree): -627.18730280
E(CCSD(T)/Aug-CC-pVQZ) (Hartree): -628.08546760
E(CCSD/Aug-CC-pVQZ) (Hartree): -628.04082319
     T1 diagnostic:  0.035697
E(MP2/Aug-CC-pVQZ) (Hartree): -628.01477985
E(MP3/Aug-CC-pVQZ) (Hartree): -628.02853381
E(PMP2/Aug-CC-pVQZ) (Hartree): -628.02640123
E(PMP3/Aug-CC-pVQZ) (Hartree): -628.03709087
E(PUHF/Aug-CC-pVQZ) (Hartree): -627.21499731
E(UHF/Aug-CC-pVQZ) (Hartree): -627.20160703
E(UM062X/Aug-CC-pVTZ) (Hartree): -628.73214784
Electronic state : 2-A
Cartesian coordinates (Angs):
     N       2.282495     -0.058189       0.000092
     H       2.836872     -0.906779       0.000007
     C       1.056965     -0.183169       0.000024
     O       0.090294      0.646267       0.000091
    Cl      -1.522263     -0.162178      -0.000089
Rotational constants (GHz):   57.2747400    2.8805400    2.7426000
Vibrational harmonic frequencies (cm-1):
    i1240.3388                 218.9565                 270.9608
      650.4230                 714.8489                 852.1748
     1016.2749                1851.1572                3560.1427
Zero-point correction (Hartree): 0.020811



################################################################################
HNCO + NO3 : M06-2X/aug-cc-pVTZ geometry
################################################################################

Fragments
=========

HNCO
----
E(CCSD(T)/Aug-CC-pVDZ) (Hartree): -168.30258465
E(CCSD/Aug-CC-pVDZ) (Hartree): -168.28124890
     T1 diagnostic:  0.018038
E(MP2/Aug-CC-pVDZ) (Hartree): -168.27834689
E(MP3/Aug-CC-pVDZ) (Hartree): -168.27384035
```

```
E(RHF/Aug-CC-pVDZ) (Hartree): -167.79177923
E(CCSD(T)/Aug-CC-pVTZ) (Hartree): -168.44532616
E(CCSD/Aug-CC-pVTZ) (Hartree): -168.41561675
     T1 diagnostic:  0.017532
E(MP2/Aug-CC-pVTZ) (Hartree): -168.41955710
E(MP3/Aug-CC-pVTZ) (Hartree): -168.41062749
E(RHF/Aug-CC-pVTZ) (Hartree): -167.83284283
E(CCSD(T)/Aug-CC-pVQZ) (Hartree): -168.48867842
E(CCSD/Aug-CC-pVQZ) (Hartree): -168.45707212
     T1 diagnostic:  0.017338
E(MP2/Aug-CC-pVQZ) (Hartree): -168.46658212
E(MP3/Aug-CC-pVQZ) (Hartree): -168.45326510
E(RHF/Aug-CC-pVQZ) (Hartree): -167.84366530
E(RM062X/Aug-CC-pVTZ) (Hartree): -168.68730418
Electronic state : 1-A
Cartesian coordinates (Angs):
     N       1.154202     -0.122224       0.000000
     C      -0.045116      0.016799       0.000000
     O      -1.204025      0.015866      -0.000000
     H       1.823480      0.627848       0.000002
Rotational constants (GHz):  879.6416200   11.1877300   11.0472300
Vibrational harmonic frequencies (cm-1):
      565.6997                  656.9786                  786.0660
     1369.4348                 2362.7298                 3698.6854
Zero-point correction (Hartree): 0.021505

HNO3
----
E(CCSD(T)/Aug-CC-pVDZ) (Hartree): -280.30992814
E(CCSD/Aug-CC-pVDZ) (Hartree): -280.27671910
     T1 diagnostic:  0.018872
E(MP2/Aug-CC-pVDZ) (Hartree): -280.28216767
E(MP3/Aug-CC-pVDZ) (Hartree): -280.26419787
E(RHF/Aug-CC-pVDZ) (Hartree): -279.50039771
E(CCSD(T)/Aug-CC-pVTZ) (Hartree): -280.54402187
E(CCSD/Aug-CC-pVTZ) (Hartree): -280.49739612
     T1 diagnostic:  0.018110
E(MP2/Aug-CC-pVTZ) (Hartree): -280.51317150
E(MP3/Aug-CC-pVTZ) (Hartree): -280.48824374
E(RHF/Aug-CC-pVTZ) (Hartree): -279.56681902
E(CCSD(T)/Aug-CC-pVQZ) (Hartree): -280.61798362
E(CCSD/Aug-CC-pVQZ) (Hartree): -280.56824782
     T1 diagnostic:  0.017859
E(MP2/Aug-CC-pVQZ) (Hartree): -280.59216705
E(MP3/Aug-CC-pVQZ) (Hartree): -280.56115931
E(RHF/Aug-CC-pVQZ) (Hartree): -279.58592174
E(RM062X/Aug-CC-pVTZ) (Hartree): -280.89733052
Electronic state : 1-A
Cartesian coordinates (Angs):
     H       1.716795      0.178522       0.000001
     O       1.098616     -0.568576       0.000001
     N      -0.140829      0.035612       0.000000
     O      -0.136825      1.236669      -0.000000
     O      -1.053165     -0.721569      -0.000001
Rotational constants (GHz):   13.3089300   12.4524700    6.4332300
Vibrational harmonic frequencies (cm-1):
      505.5130                  621.6476                  706.5789
      825.2542                  983.4229                 1358.6868
     1416.0974                 1808.8840                 3782.0136
Zero-point correction (Hartree): 0.027356

NCO
---
E(CCSD(T)/Aug-CC-pVDZ) (Hartree): -167.62797128
E(CCSD/Aug-CC-pVDZ) (Hartree): -167.60844012
     T1 diagnostic:  0.026892
E(MP2/Aug-CC-pVDZ) (Hartree): -167.59017232
E(MP3/Aug-CC-pVDZ) (Hartree): -167.59683207
E(PMP2/Aug-CC-pVDZ) (Hartree): -167.59948361
E(PMP3/Aug-CC-pVDZ) (Hartree): -167.60276840
E(PUHF/Aug-CC-pVDZ) (Hartree): -167.16572546
E(UHF/Aug-CC-pVDZ) (Hartree): -167.15393031
E(CCSD(T)/Aug-CC-pVTZ) (Hartree): -167.76225014
E(CCSD/Aug-CC-pVTZ) (Hartree): -167.73461730
     T1 diagnostic:  0.026506
E(MP2/Aug-CC-pVTZ) (Hartree): -167.72258397
E(MP3/Aug-CC-pVTZ) (Hartree): -167.72563789
E(PMP2/Aug-CC-pVTZ) (Hartree): -167.73202135
E(PMP3/Aug-CC-pVTZ) (Hartree): -167.73163223
E(PUHF/Aug-CC-pVTZ) (Hartree): -167.20420545
E(UHF/Aug-CC-pVTZ) (Hartree): -167.19223761
E(CCSD(T)/Aug-CC-pVQZ) (Hartree): -167.80328045
E(CCSD/Aug-CC-pVQZ) (Hartree): -167.77378740
     T1 diagnostic:  0.026521
E(MP2/Aug-CC-pVQZ) (Hartree): -167.76689329
E(MP3/Aug-CC-pVQZ) (Hartree): -167.76599684
E(PMP2/Aug-CC-pVQZ) (Hartree): -167.77640225
E(PMP3/Aug-CC-pVQZ) (Hartree): -167.77201636
```

```
E(PUHF/Aug-CC-pVQZ) (Hartree): -167.21474443
E(UHF/Aug-CC-pVQZ) (Hartree): -167.20269276
E(UM062X/Aug-CC-pVTZ) (Hartree): -168.00175758
Point group : C*V
Cartesian coordinates (Angs):
     N       0.000000      0.000000      -1.259810
     C       0.000000      0.000000      -0.037198
     O       0.000000      0.000000       1.130232
Rotational constants (GHz):    0.0000000   11.8429381   11.8429381
Vibrational harmonic frequencies (cm-1):
      533.0069 (  PI)           614.6584 (  PI)          1326.9293 (  SG)
     2040.1488 (  SG)
Zero-point correction (Hartree): 0.010285

NO3
---
E(CCSD(T)/Aug-CC-pVDZ) (Hartree): -279.63880313
E(CCSD/Aug-CC-pVDZ) (Hartree): -279.60369390
     T1 diagnostic:  0.040113
E(MP2/Aug-CC-pVDZ) (Hartree): -279.59508373
E(MP3/Aug-CC-pVDZ) (Hartree): -279.58333011
E(PMP2/Aug-CC-pVDZ) (Hartree): -279.59729565
E(PMP3/Aug-CC-pVDZ) (Hartree): -279.58485291
E(PUHF/Aug-CC-pVDZ) (Hartree): -278.87110190
E(UHF/Aug-CC-pVDZ) (Hartree): -278.86753216
E(CCSD(T)/Aug-CC-pVTZ) (Hartree): -279.86543977
E(CCSD/Aug-CC-pVTZ) (Hartree): -279.81759238
     T1 diagnostic:  0.039912
E(MP2/Aug-CC-pVTZ) (Hartree): -279.81685032
E(MP3/Aug-CC-pVTZ) (Hartree): -279.80057579
E(PMP2/Aug-CC-pVTZ) (Hartree): -279.82105102
E(PMP3/Aug-CC-pVTZ) (Hartree): -279.80355269
E(PUHF/Aug-CC-pVTZ) (Hartree): -278.93836722
E(UHF/Aug-CC-pVTZ) (Hartree): -278.93320112
E(CCSD(T)/Aug-CC-pVQZ) (Hartree): -279.93748312
E(CCSD/Aug-CC-pVQZ) (Hartree): -279.88655503
     T1 diagnostic:  0.037108
E(MP2/Aug-CC-pVQZ) (Hartree): -279.89561241
E(MP3/Aug-CC-pVQZ) (Hartree): -279.87267534
E(PMP2/Aug-CC-pVQZ) (Hartree): -279.89804323
E(PMP3/Aug-CC-pVQZ) (Hartree): -279.87427648
E(PUHF/Aug-CC-pVQZ) (Hartree): -278.95617416
E(UHF/Aug-CC-pVQZ) (Hartree): -278.95221601
E(UM062X/Aug-CC-pVTZ) (Hartree): -280.21367243
Electronic state : 2-A
Cartesian coordinates (Angs):
     N      -0.000003      0.087298       0.000018
     O      -1.085665      0.581007      -0.000006
     O       0.000028     -1.238446      -0.000004
     O       1.085639      0.581053      -0.000006
Rotational constants (GHz):   14.2607200   13.4036900    6.9094600
Vibrational harmonic frequencies (cm-1):
      330.1049                 677.6175                 816.5198
      862.2603                1378.4575                1670.6793
Zero-point correction (Hartree): 0.013067

Adducts
=======

HNCONO2
-------
E(CCSD(T)/Aug-CC-pVDZ) (Hartree): -447.83468679
E(CCSD/Aug-CC-pVDZ) (Hartree): -447.77549766
     T1 diagnostic:  0.025098
E(MP2/Aug-CC-pVDZ) (Hartree): -447.77207128
E(MP3/Aug-CC-pVDZ) (Hartree): -447.75075071
E(PMP2/Aug-CC-pVDZ) (Hartree): -447.77572976
E(PMP3/Aug-CC-pVDZ) (Hartree): -447.75333899
E(PUHF/Aug-CC-pVDZ) (Hartree): -446.51667265
E(UHF/Aug-CC-pVDZ) (Hartree): -446.51216620
E(CCSD(T)/Aug-CC-pVTZ) (Hartree): -448.20395521
E(CCSD/Aug-CC-pVTZ) (Hartree): -448.12308628
     T1 diagnostic:  0.032066
E(MP2/Aug-CC-pVTZ) (Hartree): -448.12639062
E(MP3/Aug-CC-pVTZ) (Hartree): -448.09954983
E(PMP2/Aug-CC-pVTZ) (Hartree): -448.13648150
E(PMP3/Aug-CC-pVTZ) (Hartree): -448.10702951
E(PUHF/Aug-CC-pVTZ) (Hartree): -446.62930714
E(UHF/Aug-CC-pVTZ) (Hartree): -446.61786079
E(CCSD(T)/Aug-CC-pVQZ) (Hartree): -448.31799009
E(CCSD/Aug-CC-pVQZ) (Hartree): -448.23194010
     T1 diagnostic:  0.032119
E(MP2/Aug-CC-pVQZ) (Hartree): -448.24856992
E(MP3/Aug-CC-pVQZ) (Hartree): -448.21166999
E(PMP2/Aug-CC-pVQZ) (Hartree): -448.25890139
E(PMP3/Aug-CC-pVQZ) (Hartree): -448.21932756
E(PUHF/Aug-CC-pVQZ) (Hartree): -446.65854174
E(UHF/Aug-CC-pVQZ) (Hartree): -446.64683372
```

```
E(UM062X/Aug-CC-pVTZ) (Hartree): -448.79629090
Electronic state : 2-A
Cartesian coordinates (Angs):
     N      -2.757495      0.298347      -0.145477
     C      -1.602251     -0.042522      -0.359750
     O      -0.798307     -0.575633       0.587582
     H      -3.299825      0.710171      -0.894335
     N       1.319140      0.180919      -0.014666
     O       0.410265     -0.959951       0.013442
     O       2.380458     -0.163579      -0.401242
     O       0.880311      1.222925       0.321948
Rotational constants (GHz):    8.5695600    1.6797800    1.5081300
Vibrational harmonic frequencies (cm-1):
       82.9604                  96.5466                 186.9753
      363.3217                 377.1206                 469.2427
      636.1642                 656.5788                 750.6646
      784.8460                 856.6373                 892.3273
     1064.6767                1138.2196                1402.3818
     1846.0096                1851.0918                3596.2795
Zero-point correction (Hartree): 0.038847

HN_CO_NO3
---------
E(CCSD(T)/Aug-CC-pVDZ) (Hartree): -447.76835173
E(CCSD/Aug-CC-pVDZ) (Hartree): -447.71304249
     T1 diagnostic:  0.047193
E(MP2/Aug-CC-pVDZ) (Hartree): -447.66653071
E(MP3/Aug-CC-pVDZ) (Hartree): -447.67274132
E(PMP2/Aug-CC-pVDZ) (Hartree): -447.67249384
E(PMP3/Aug-CC-pVDZ) (Hartree): -447.67646134
E(PUHF/Aug-CC-pVDZ) (Hartree): -446.50570535
E(UHF/Aug-CC-pVDZ) (Hartree): -446.49656152
E(CCSD(T)/Aug-CC-pVTZ) (Hartree): -448.13053096
E(CCSD/Aug-CC-pVTZ) (Hartree): -448.05382276
     T1 diagnostic:  0.045372
E(MP2/Aug-CC-pVTZ) (Hartree): -448.02384648
E(MP3/Aug-CC-pVTZ) (Hartree): -448.02125753
E(PMP2/Aug-CC-pVTZ) (Hartree): -448.03007606
E(PMP3/Aug-CC-pVTZ) (Hartree): -448.02510184
E(PUHF/Aug-CC-pVTZ) (Hartree): -446.60759149
E(UHF/Aug-CC-pVTZ) (Hartree): -446.59803703
E(CCSD(T)/Aug-CC-pVQZ) (Hartree): -448.24286886
E(CCSD/Aug-CC-pVQZ) (Hartree): -448.16105421
     T1 diagnostic:  0.044852
E(MP2/Aug-CC-pVQZ) (Hartree): -448.14455877
E(MP3/Aug-CC-pVQZ) (Hartree): -448.13223172
E(PMP2/Aug-CC-pVQZ) (Hartree): -448.15083931
E(PMP3/Aug-CC-pVQZ) (Hartree): -448.13608043
E(PUHF/Aug-CC-pVQZ) (Hartree): -446.63651358
E(UHF/Aug-CC-pVQZ) (Hartree): -446.62688475
E(UM062X/Aug-CC-pVTZ) (Hartree): -448.71962621
Electronic state : 4-A
Cartesian coordinates (Angs):
     N      -0.384171      0.961601      -0.202182
     C      -1.671425      0.598486       0.025383
     O      -2.173123     -0.460608       0.109653
     H      -0.054355      1.873792       0.082741
     N       0.691783     -0.004732      -0.073050
     O       0.516326     -1.026977      -0.911695
     O       0.792143     -0.638502       1.093561
     O       1.855856      0.605737      -0.080070
Rotational constants (GHz):    5.8233600    2.2909400    2.1002500
Vibrational harmonic frequencies (cm-1):
       75.2213                 171.2716                 284.2731
      315.6095                 422.3125                 448.5183
      523.9130                 538.7488                 601.2211
      740.0396                 834.2998                 911.2036
     1002.4201                1073.6435                1148.7603
     1412.2611                1949.9249                3615.5994
Zero-point correction (Hartree): 0.036608

HNCONO3
-------
E(CCSD(T)/Aug-CC-pVDZ) (Hartree): -447.71948766
E(CCSD/Aug-CC-pVDZ) (Hartree): -447.66302906
     T1 diagnostic:  0.048308
E(MP2/Aug-CC-pVDZ) (Hartree): -447.61083942
E(MP3/Aug-CC-pVDZ) (Hartree): -447.62118579
E(PMP2/Aug-CC-pVDZ) (Hartree): -447.61774234
E(PMP3/Aug-CC-pVDZ) (Hartree): -447.62600374
E(PUHF/Aug-CC-pVDZ) (Hartree): -446.45484460
E(UHF/Aug-CC-pVDZ) (Hartree): -446.44569926
E(CCSD(T)/Aug-CC-pVTZ) (Hartree): -448.08253458
E(CCSD/Aug-CC-pVTZ) (Hartree): -448.00488096
     T1 diagnostic:  0.046578
E(MP2/Aug-CC-pVTZ) (Hartree): -447.96946120
E(MP3/Aug-CC-pVTZ) (Hartree): -447.97097428
E(PMP2/Aug-CC-pVTZ) (Hartree): -447.97670530
```

```
E(PMP3/Aug-CC-pVTZ) (Hartree): -447.97599035
E(PUHF/Aug-CC-pVTZ) (Hartree): -446.55823885
E(UHF/Aug-CC-pVTZ) (Hartree): -446.54864135
E(CCSD(T)/Aug-CC-pVQZ) (Hartree): -448.19416759
E(CCSD/Aug-CC-pVQZ) (Hartree): -448.11141030
     T1 diagnostic:  0.046141
E(MP2/Aug-CC-pVQZ) (Hartree): -448.08945257
E(MP3/Aug-CC-pVQZ) (Hartree): -448.08119131
E(PMP2/Aug-CC-pVQZ) (Hartree): -448.09676384
E(PMP3/Aug-CC-pVQZ) (Hartree): -448.08623184
E(PUHF/Aug-CC-pVQZ) (Hartree): -446.58686172
E(UHF/Aug-CC-pVQZ) (Hartree): -446.57718416
E(UM062X/Aug-CC-pVTZ) (Hartree): -448.67121076
Electronic state : 4-A
Cartesian coordinates (Angs):
     N       2.667881     -0.132886       0.011696
     C       1.487555      0.181169       0.067340
     O       0.473604     -0.688004      -0.146387
     H       3.369909      0.572135       0.202021
     N      -0.794964     -0.010742      -0.053140
     O      -0.874473      1.024623      -0.844577
     O      -1.050496      0.534385       1.108466
     O      -1.724342     -0.952723      -0.156996
Rotational constants (GHz):    6.6207900    1.9483000    1.8589500
Vibrational harmonic frequencies (cm-1):
       96.4498                173.0601                211.8487
      294.7894                411.7617                431.5474
      517.5092                573.0284                670.2045
      674.5736                808.0994                907.9057
      924.7908                966.8306               1055.2107
     1176.4688               1865.6046               3586.7681
Zero-point correction (Hartree): 0.034962

HNC_O_ONO2
----------
E(CCSD(T)/Aug-CC-pVDZ) (Hartree): -447.94832392
E(CCSD/Aug-CC-pVDZ) (Hartree): -447.89290147
     T1 diagnostic:  0.022259
E(MP2/Aug-CC-pVDZ) (Hartree): -447.88988692
E(MP3/Aug-CC-pVDZ) (Hartree): -447.87073151
E(PMP2/Aug-CC-pVDZ) (Hartree): -447.89263145
E(PMP3/Aug-CC-pVDZ) (Hartree): -447.87252243
E(PUHF/Aug-CC-pVDZ) (Hartree): -446.65738325
E(UHF/Aug-CC-pVDZ) (Hartree): -446.65347647
E(CCSD(T)/Aug-CC-pVTZ) (Hartree): -448.31706238
E(CCSD/Aug-CC-pVTZ) (Hartree): -448.24040623
     T1 diagnostic:  0.021370
E(MP2/Aug-CC-pVTZ) (Hartree): -448.25402507
E(MP3/Aug-CC-pVTZ) (Hartree): -448.22437808
E(PMP2/Aug-CC-pVTZ) (Hartree): -448.25692364
E(PMP3/Aug-CC-pVTZ) (Hartree): -448.22623760
E(PUHF/Aug-CC-pVTZ) (Hartree): -446.76209278
E(UHF/Aug-CC-pVTZ) (Hartree): -446.75793113
E(CCSD(T)/Aug-CC-pVQZ) (Hartree): -448.42953025
E(CCSD/Aug-CC-pVQZ) (Hartree): -448.34864327
     T1 diagnostic:  0.038117
E(MP2/Aug-CC-pVQZ) (Hartree): -448.35002173
E(MP3/Aug-CC-pVQZ) (Hartree): -448.32397019
E(PMP2/Aug-CC-pVQZ) (Hartree): -448.36764194
E(PMP3/Aug-CC-pVQZ) (Hartree): -448.33776349
E(PUHF/Aug-CC-pVQZ) (Hartree): -446.80913087
E(UHF/Aug-CC-pVQZ) (Hartree): -446.78966266
E(UM062X/Aug-CC-pVTZ) (Hartree): -448.90882469
Electronic state : 2-A
Cartesian coordinates (Angs):
     N      -2.333561     -0.545724      -0.124297
     C      -1.110459      0.101049      -0.000263
     O      -0.948077      1.281000       0.057406
     H      -2.938819     -0.248089       0.644571
     N       1.197157     -0.145941      -0.002173
     O      -0.105784     -0.818213      -0.056135
     O       1.630512      0.123252      -1.063727
     O       1.617899     -0.025608       1.092744
Rotational constants (GHz):    6.3354100    1.9693700    1.9394400
Vibrational harmonic frequencies (cm-1):
       56.2533                104.8318                185.0609
      211.4836                381.0355                571.1414
      593.2440                695.0646                702.8288
      823.8631                853.2956                994.6111
     1087.1537               1285.2453               1429.9387
     1829.4751               1850.6685               3471.4383
Zero-point correction (Hartree): 0.039017

OCN_H_ONO2
----------
E(CCSD(T)/Aug-CC-pVDZ) (Hartree): -447.90744407
E(CCSD/Aug-CC-pVDZ) (Hartree): -447.84962528
     T1 diagnostic:  0.021784
```

```
E(MP2/Aug-CC-pVDZ) (Hartree): -447.85265821
E(MP3/Aug-CC-pVDZ) (Hartree): -447.82659963
E(PMP2/Aug-CC-pVDZ) (Hartree): -447.85509292
E(PMP3/Aug-CC-pVDZ) (Hartree): -447.82790131
E(PUHF/Aug-CC-pVDZ) (Hartree): -446.59663831
E(UHF/Aug-CC-pVDZ) (Hartree): -446.59271211
E(CCSD(T)/Aug-CC-pVTZ) (Hartree): -448.27566368
E(CCSD/Aug-CC-pVTZ) (Hartree): -448.19626493
     T1 diagnostic:  0.028753
E(MP2/Aug-CC-pVTZ) (Hartree): -448.20675557
E(MP3/Aug-CC-pVTZ) (Hartree): -448.17476340
E(PMP2/Aug-CC-pVTZ) (Hartree): -448.21563389
E(PMP3/Aug-CC-pVTZ) (Hartree): -448.18118264
E(PUHF/Aug-CC-pVTZ) (Hartree): -446.70733666
E(UHF/Aug-CC-pVTZ) (Hartree): -446.69710149
E(CCSD(T)/Aug-CC-pVQZ) (Hartree): -448.39062739
E(CCSD/Aug-CC-pVQZ) (Hartree): -448.30609762
     T1 diagnostic:  0.028749
E(MP2/Aug-CC-pVQZ) (Hartree): -448.32981074
E(MP3/Aug-CC-pVQZ) (Hartree): -448.28785958
E(PMP2/Aug-CC-pVQZ) (Hartree): -448.33892683
E(PMP3/Aug-CC-pVQZ) (Hartree): -448.29445417
E(PUHF/Aug-CC-pVQZ) (Hartree): -446.73695388
E(UHF/Aug-CC-pVQZ) (Hartree): -446.72645958
E(UM062X/Aug-CC-pVTZ) (Hartree): -448.86994197
Electronic state : 2-A
Cartesian coordinates (Angs):
     N      -0.925881      0.949977       0.300677
     C      -1.841371     -0.037257       0.189420
     O      -1.902514     -0.926618      -0.580818
     H      -0.840380      1.461634       1.165351
     N       1.163888     -0.114496       0.061872
     O       2.109801     -0.191725      -0.636093
     O       0.220434      0.901700      -0.446897
     O       0.850099     -0.669164       1.058843
Rotational constants (GHz):    5.9077000    2.0240300    1.9181300
Vibrational harmonic frequencies (cm-1):
       83.9815                 87.7485                242.4385
      304.6657                434.4910                510.6740
      526.2356                686.7446                789.2816
      840.9261                848.8429               1051.4098
     1118.2884               1400.9113               1467.2479
     1846.8035               1934.4903               3630.6724
Zero-point correction (Hartree): 0.040565

Transition states
=================

TS.HN_CO_NO3.HNCONO3
--------------------
IRC pathway available
E(CCSD(T)/Aug-CC-pVDZ) (Hartree): -447.71626493
E(CCSD/Aug-CC-pVDZ) (Hartree): -447.65699461
     T1 diagnostic:  0.047928
E(MP2/Aug-CC-pVDZ) (Hartree): -447.60658475
E(MP3/Aug-CC-pVDZ) (Hartree): -447.61367308
E(PMP2/Aug-CC-pVDZ) (Hartree): -447.62003564
E(PMP3/Aug-CC-pVDZ) (Hartree): -447.62383390
E(PUHF/Aug-CC-pVDZ) (Hartree): -446.44995473
E(UHF/Aug-CC-pVDZ) (Hartree): -446.43415028
E(CCSD(T)/Aug-CC-pVTZ) (Hartree): -448.07887058
E(CCSD/Aug-CC-pVTZ) (Hartree): -447.99840413
     T1 diagnostic:  0.046298
E(MP2/Aug-CC-pVTZ) (Hartree): -447.96496710
E(MP3/Aug-CC-pVTZ) (Hartree): -447.96299287
E(PMP2/Aug-CC-pVTZ) (Hartree): -447.97827284
E(PMP3/Aug-CC-pVTZ) (Hartree): -447.97300892
E(PUHF/Aug-CC-pVTZ) (Hartree): -446.55294012
E(UHF/Aug-CC-pVTZ) (Hartree): -446.53722591
E(CCSD(T)/Aug-CC-pVQZ) (Hartree): -448.19024300
E(CCSD/Aug-CC-pVQZ) (Hartree): -448.10467088
     T1 diagnostic:  0.045976
E(MP2/Aug-CC-pVQZ) (Hartree): -448.08460211
E(MP3/Aug-CC-pVQZ) (Hartree): -448.07283676
E(PMP2/Aug-CC-pVQZ) (Hartree): -448.09802275
E(PMP3/Aug-CC-pVQZ) (Hartree): -448.08292476
E(PUHF/Aug-CC-pVQZ) (Hartree): -446.58153865
E(UHF/Aug-CC-pVQZ) (Hartree): -446.56569512
E(UM062X/Aug-CC-pVTZ) (Hartree): -448.66809056
Electronic state : 4-A
Cartesian coordinates (Angs):
     N      -2.721579      0.061092       0.025259
     C      -1.500662     -0.081773       0.022743
     O      -0.533874      0.765421      -0.061156
     H      -3.295926     -0.768552       0.119737
     N       0.859402     -0.029047      -0.032234
     O       0.865638     -0.983479      -0.890029
     O       1.083737     -0.614337       1.083480
```

```
     O       1.751391      0.961755      -0.158215
Rotational constants (GHz):    6.4524000    1.8835500    1.7874600
Vibrational harmonic frequencies (cm-1):
     i638.6682                  76.9447                 192.9219
      230.8149                 327.9030                 373.4452
      469.0494                 546.8272                 621.8592
      661.2569                 710.5062                 872.8815
      933.5951                1001.6425                1074.9399
     1173.7211                1872.7839                3567.9279
Zero-point correction (Hartree): 0.033510

TS.HNCO+NO3.HN_CO_NO3
---------------------
IRC pathway available
E(CCSD(T)/Aug-CC-pVDZ) (Hartree): -447.76324348
E(CCSD/Aug-CC-pVDZ) (Hartree): -447.70497742
     T1 diagnostic:  0.048993
E(MP2/Aug-CC-pVDZ) (Hartree): -447.65994248
E(MP3/Aug-CC-pVDZ) (Hartree): -447.66251019
E(PMP2/Aug-CC-pVDZ) (Hartree): -447.66881732
E(PMP3/Aug-CC-pVDZ) (Hartree): -447.66842366
E(PUHF/Aug-CC-pVDZ) (Hartree): -446.49337479
E(UHF/Aug-CC-pVDZ) (Hartree): -446.48142843
E(CCSD(T)/Aug-CC-pVTZ) (Hartree): -448.12572772
E(CCSD/Aug-CC-pVTZ) (Hartree): -448.04598262
     T1 diagnostic:  0.047413
E(MP2/Aug-CC-pVTZ) (Hartree): -448.01748858
E(MP3/Aug-CC-pVTZ) (Hartree): -448.01123102
E(PMP2/Aug-CC-pVTZ) (Hartree): -448.02674129
E(PMP3/Aug-CC-pVTZ) (Hartree): -448.01736901
E(PUHF/Aug-CC-pVTZ) (Hartree): -446.59627183
E(UHF/Aug-CC-pVTZ) (Hartree): -446.58382402
E(CCSD(T)/Aug-CC-pVQZ) (Hartree): -448.23779972
E(CCSD/Aug-CC-pVQZ) (Hartree): -448.15293674
     T1 diagnostic:  0.046977
E(MP2/Aug-CC-pVQZ) (Hartree): -448.13792598
E(MP3/Aug-CC-pVQZ) (Hartree): -448.12187813
E(PMP2/Aug-CC-pVQZ) (Hartree): -448.14724641
E(PMP3/Aug-CC-pVQZ) (Hartree): -448.12803783
E(PUHF/Aug-CC-pVQZ) (Hartree): -446.62503474
E(UHF/Aug-CC-pVQZ) (Hartree): -446.61250016
E(UM062X/Aug-CC-pVTZ) (Hartree): -448.71493483
Electronic state : 4-A
Cartesian coordinates (Angs):
     N      -0.529247      0.925686      -0.118820
     C      -1.745074      0.510892       0.021737
     O      -2.408703     -0.454413       0.085945
     H      -0.220318      1.861990       0.103323
     N       0.793681     -0.029074      -0.053147
     O       0.577435     -1.112890      -0.800707
     O       1.081322     -0.526621       1.122279
     O       1.854912      0.693471      -0.286264
Rotational constants (GHz):    5.8814300    1.9952900    1.8374000
Vibrational harmonic frequencies (cm-1):
     i666.3535                  42.5926                 142.5663
      240.8409                 292.7199                 355.1398
      391.2660                 507.6311                 536.5005
      607.5437                 704.5381                 904.8785
      934.3876                1081.1172                1171.2339
     1243.7209                2033.9099                3623.1896
Zero-point correction (Hartree): 0.033748

TS.HNCO+NO3.HNC_O_ONO2
----------------------
E(CCSD(T)/Aug-CC-pVDZ) (Hartree): -447.92324708
E(CCSD/Aug-CC-pVDZ) (Hartree): -447.86355987
     T1 diagnostic:  0.029199
E(MP2/Aug-CC-pVDZ) (Hartree): -447.85997336
E(MP3/Aug-CC-pVDZ) (Hartree): -447.83640850
E(PMP2/Aug-CC-pVDZ) (Hartree): -447.86712231
E(PMP3/Aug-CC-pVDZ) (Hartree): -447.84118406
E(PUHF/Aug-CC-pVDZ) (Hartree): -446.62200765
E(UHF/Aug-CC-pVDZ) (Hartree): -446.61270241
E(CCSD(T)/Aug-CC-pVTZ) (Hartree): -448.29074922
E(CCSD/Aug-CC-pVTZ) (Hartree): -448.20931431
     T1 diagnostic:  0.028168
E(MP2/Aug-CC-pVTZ) (Hartree): -448.22276651
E(MP3/Aug-CC-pVTZ) (Hartree): -448.18846245
E(PMP2/Aug-CC-pVTZ) (Hartree): -448.23037490
E(PMP3/Aug-CC-pVTZ) (Hartree): -448.19353743
E(PUHF/Aug-CC-pVTZ) (Hartree): -446.72553910
E(UHF/Aug-CC-pVTZ) (Hartree): -446.71568752
E(CCSD(T)/Aug-CC-pVQZ) (Hartree): -448.40533058
E(CCSD/Aug-CC-pVQZ) (Hartree): -448.31882795
     T1 diagnostic:  0.027763
E(MP2/Aug-CC-pVQZ) (Hartree): -448.34583160
E(MP3/Aug-CC-pVQZ) (Hartree): -448.30145743
E(PMP2/Aug-CC-pVQZ) (Hartree): -448.35352362
```

```
E(PMP3/Aug-CC-pVQZ) (Hartree): -448.30657471
E(PUHF/Aug-CC-pVQZ) (Hartree): -446.75486771
E(UHF/Aug-CC-pVQZ) (Hartree): -446.74492411
E(UM062X/Aug-CC-pVTZ) (Hartree): -448.88247734
Electronic state : 2-A
Cartesian coordinates (Angs):
     N      -1.526240      1.045070      -0.570242
     C      -1.453230     -0.096502       0.012972
     O      -1.851016     -1.018372       0.569351
     H      -0.883559      1.733458      -0.172599
     N       1.186958      0.015407       0.032640
     O       0.190168     -0.401018      -0.779455
     O       2.239437     -0.501039      -0.177380
     O       0.918650      0.848205       0.869730
Rotational constants (GHz):    5.9327800    1.9461700    1.8006700
Vibrational harmonic frequencies (cm-1):
     i654.3013                 61.8303                 80.6348
      218.8012                351.0109                415.1662
      544.4675                608.7446                689.5620
      724.5802                828.0938                949.2871
      991.1491               1167.0884               1357.2151
     1706.5101               2183.2506               3483.8702
Zero-point correction (Hartree): 0.037274

TS.HNCO+NO3.HNCOONO2
--------------------
E(CCSD(T)/Aug-CC-pVDZ) (Hartree): -447.82771064
E(CCSD/Aug-CC-pVDZ) (Hartree): -447.76594976
     T1 diagnostic:  0.038074
E(MP2/Aug-CC-pVDZ) (Hartree): -447.73981763
E(MP3/Aug-CC-pVDZ) (Hartree): -447.72532444
E(PMP2/Aug-CC-pVDZ) (Hartree): -447.76014779
E(PMP3/Aug-CC-pVDZ) (Hartree): -447.74073410
E(PUHF/Aug-CC-pVDZ) (Hartree): -446.52299449
E(UHF/Aug-CC-pVDZ) (Hartree): -446.50001310
E(CCSD(T)/Aug-CC-pVTZ) (Hartree): -448.19634354
E(CCSD/Aug-CC-pVTZ) (Hartree): -448.11273690
     T1 diagnostic:  0.042515
E(MP2/Aug-CC-pVTZ) (Hartree): -448.09375724
E(MP3/Aug-CC-pVTZ) (Hartree): -448.07410674
E(PMP2/Aug-CC-pVTZ) (Hartree): -448.12155087
E(PMP3/Aug-CC-pVTZ) (Hartree): -448.09583193
E(PUHF/Aug-CC-pVTZ) (Hartree): -446.63647192
E(UHF/Aug-CC-pVTZ) (Hartree): -446.60562779
E(CCSD(T)/Aug-CC-pVQZ) (Hartree): -448.30992974
E(CCSD/Aug-CC-pVQZ) (Hartree): -448.22113198
     T1 diagnostic:  0.043740
E(MP2/Aug-CC-pVQZ) (Hartree): -448.21270023
E(MP3/Aug-CC-pVQZ) (Hartree): -448.18453917
E(PMP2/Aug-CC-pVQZ) (Hartree): -448.24301501
E(PMP3/Aug-CC-pVQZ) (Hartree): -448.20847499
E(PUHF/Aug-CC-pVQZ) (Hartree): -446.66844358
E(UHF/Aug-CC-pVQZ) (Hartree): -446.63495559
E(UM062X/Aug-CC-pVTZ) (Hartree): -448.78719036
Electronic state : 2-A
Cartesian coordinates (Angs):
     N       2.773889      0.349330      -0.244432
     C       1.622629     -0.069751      -0.229917
     O       0.864174     -0.613513       0.633305
     H       3.141205      0.751528      -1.099107
     N      -1.323335      0.171797      -0.015485
     O      -0.471550     -0.965974      -0.043033
     O      -0.878948      1.191833       0.391312
     O      -2.392534     -0.109960      -0.444331
Rotational constants (GHz):    8.2482700    1.6415600    1.4872700
Vibrational harmonic frequencies (cm-1):
    i1276.1019                 74.1346                 81.0958
      253.7342                319.1771                361.5089
      558.2201                634.4485                701.7712
      719.0916                792.0341                899.9476
      988.9351               1056.5823               1390.0042
     1804.1552               1904.3414               3562.9273
Zero-point correction (Hartree): 0.036683

TS.HNCO+NO3.HNO3+NCO
--------------------
E(CCSD(T)/Aug-CC-pVDZ) (Hartree): -447.92365964
E(CCSD/Aug-CC-pVDZ) (Hartree): -447.85365836
     T1 diagnostic:  0.120771
E(MP2/Aug-CC-pVDZ) (Hartree): -447.83549404
E(MP3/Aug-CC-pVDZ) (Hartree): -447.82060313
E(PMP2/Aug-CC-pVDZ) (Hartree): -447.84619369
E(PMP3/Aug-CC-pVDZ) (Hartree): -447.82741244
E(PUHF/Aug-CC-pVDZ) (Hartree): -446.62136780
E(UHF/Aug-CC-pVDZ) (Hartree): -446.60784032
E(CCSD(T)/Aug-CC-pVTZ) (Hartree): -448.29164641
E(CCSD/Aug-CC-pVTZ) (Hartree): -448.20001143
     T1 diagnostic:  0.108144
```

```
E(MP2/Aug-CC-pVTZ) (Hartree): -448.19962777
E(MP3/Aug-CC-pVTZ) (Hartree): -448.17429081
E(PMP2/Aug-CC-pVTZ) (Hartree): -448.21052750
E(PMP3/Aug-CC-pVTZ) (Hartree): -448.18121597
E(PUHF/Aug-CC-pVTZ) (Hartree): -446.72569306
E(UHF/Aug-CC-pVTZ) (Hartree): -446.71191794
E(CCSD(T)/Aug-CC-pVQZ) (Hartree): -448.40533852
E(CCSD/Aug-CC-pVQZ) (Hartree): -448.30933524
     T1 diagnostic:  0.103260
E(MP2/Aug-CC-pVQZ) (Hartree): -448.32270412
E(MP3/Aug-CC-pVQZ) (Hartree): -448.28734611
E(PMP2/Aug-CC-pVQZ) (Hartree): -448.33368324
E(PMP3/Aug-CC-pVQZ) (Hartree): -448.29430092
E(PUHF/Aug-CC-pVQZ) (Hartree): -446.75504145
E(UHF/Aug-CC-pVQZ) (Hartree): -446.74117411
E(UM062X/Aug-CC-pVTZ) (Hartree): -448.88170942
Electronic state : 2-A
Cartesian coordinates (Angs):
     N      -1.407432      1.169833       0.260627
     C      -1.956590      0.108300       0.000399
     O      -2.567458     -0.846103      -0.224116
     H      -0.241296      1.224465       0.198501
     N       1.384187     -0.187370       0.011315
     O       0.922966      1.061707      -0.217704
     O       0.590669     -1.049432       0.262667
     O       2.571767     -0.260110      -0.083908
Rotational constants (GHz):    6.9002700    1.5096500    1.2619700
Vibrational harmonic frequencies (cm-1):
    i1946.8251                45.3896                72.4187
       96.0041               204.2822               377.7978
      588.9523               622.5818               672.1903
      721.7630               813.9969               915.3122
      945.5214              1255.0150              1362.1822
     1400.5051              1698.6268              2171.7913
Zero-point correction (Hartree): 0.031813

TS.HNCO+NO3.OCN_H_ONO2
----------------------
E(CCSD(T)/Aug-CC-pVDZ) (Hartree): -447.89950221
E(CCSD/Aug-CC-pVDZ) (Hartree): -447.83959913
     T1 diagnostic:  0.026509
E(MP2/Aug-CC-pVDZ) (Hartree): -447.83631380
E(MP3/Aug-CC-pVDZ) (Hartree): -447.81128996
E(PMP2/Aug-CC-pVDZ) (Hartree): -447.84584321
E(PMP3/Aug-CC-pVDZ) (Hartree): -447.81725656
E(PUHF/Aug-CC-pVDZ) (Hartree): -446.58848884
E(UHF/Aug-CC-pVDZ) (Hartree): -446.57639678
E(CCSD(T)/Aug-CC-pVTZ) (Hartree): -448.26829089
E(CCSD/Aug-CC-pVTZ) (Hartree): -448.18634090
     T1 diagnostic:  0.025967
E(MP2/Aug-CC-pVTZ) (Hartree): -448.20026303
E(MP3/Aug-CC-pVTZ) (Hartree): -448.16420237
E(PMP2/Aug-CC-pVTZ) (Hartree): -448.21010983
E(PMP3/Aug-CC-pVTZ) (Hartree): -448.17035903
E(PUHF/Aug-CC-pVTZ) (Hartree): -446.69305243
E(UHF/Aug-CC-pVTZ) (Hartree): -446.68056857
E(CCSD(T)/Aug-CC-pVQZ) (Hartree): -448.38294999
E(CCSD/Aug-CC-pVQZ) (Hartree): -448.29584621
     T1 diagnostic:  0.025809
E(MP2/Aug-CC-pVQZ) (Hartree): -448.32334721
E(MP3/Aug-CC-pVQZ) (Hartree): -448.27708364
E(PMP2/Aug-CC-pVQZ) (Hartree): -448.33324380
E(PMP3/Aug-CC-pVQZ) (Hartree): -448.28325237
E(PUHF/Aug-CC-pVQZ) (Hartree): -446.72223346
E(UHF/Aug-CC-pVQZ) (Hartree): -446.70968788
E(UM062X/Aug-CC-pVTZ) (Hartree): -448.86066721
Electronic state : 2-A
Cartesian coordinates (Angs):
     N      -0.973736      0.926014       0.396251
     C      -1.854685      0.031639       0.132271
     O      -2.204819     -0.809361      -0.598411
     H      -0.796890      1.232188       1.340981
     N       1.224962     -0.128510       0.031841
     O       2.238771     -0.166526      -0.585161
     O       0.403353      0.934154      -0.371532
     O       0.833497     -0.833836       0.913698
Rotational constants (GHz):    6.2592400    1.8134600    1.6972900
Vibrational harmonic frequencies (cm-1):
     i813.3798                 49.4042                73.7675
      214.0136                302.5979               464.2818
      542.7230                572.4193               693.8503
      779.8991                811.6935               913.0002
     1154.2011               1257.5356              1392.5106
     1770.0088               2091.3030              3650.1056
Zero-point correction (Hartree): 0.038121
```

```
################################################################################
HNCO + O3 : M06-2X/aug-cc-pVTZ geometry
################################################################################

Fragments
=========

HNCO
----
E(CCSD(T)/Aug-CC-pVDZ) (Hartree): -168.30258903
E(CCSD/Aug-CC-pVDZ) (Hartree): -168.28125135
     T1 diagnostic:  0.018041
E(MP2/Aug-CC-pVDZ) (Hartree): -168.27835301
E(MP3/Aug-CC-pVDZ) (Hartree): -168.27384099
E(RHF/Aug-CC-pVDZ) (Hartree): -167.79177355
E(CCSD(T)/Aug-CC-pVTZ) (Hartree): -168.44533015
E(CCSD/Aug-CC-pVTZ) (Hartree): -168.41561850
E(MP2/Aug-CC-pVTZ) (Hartree): -168.41956259
E(MP3/Aug-CC-pVTZ) (Hartree): -168.41062722
E(RHF/6-31G(d,p)) (Hartree): -167.76545219
E(RHF/Aug-CC-pVTZ) (Hartree): -167.83283656
E(CCSD(T)/Aug-CC-pVQZ) (Hartree): -168.48868126
E(CCSD/Aug-CC-pVQZ) (Hartree): -168.45707276
     T1 diagnostic:  0.017340
E(MP2/Aug-CC-pVQZ) (Hartree): -168.46658688
E(MP3/Aug-CC-pVQZ) (Hartree): -168.45326396
E(RHF/Aug-CC-pVQZ) (Hartree): -167.84365842
E(RM062X/Aug-CC-pVTZ) (Hartree): -168.68730523
Point group : CS
Electronic state : 1-A'
Cartesian coordinates (Angs):
     N       0.289904     -1.123860       0.000000
     H       1.226714     -1.488086       0.000000
     C       0.000000      0.048082       0.000000
     O      -0.407005      1.133327       0.000000
Rotational constants (GHz):  880.1140600   11.1871200   11.0467000
Vibrational harmonic frequencies (cm-1):
      563.8698 (  A')           657.1801 (  A")           782.7913 (  A')
     1369.4249 (  A')          2366.0466 (  A')          3706.3649 (  A')
Zero-point correction (Hartree): 0.021519

HN_O_CO
-------
E(CCSD(T)/Aug-CC-pVDZ) (Hartree): -243.23568465
E(CCSD/Aug-CC-pVDZ) (Hartree): -243.20564724
     T1 diagnostic:  0.024289
E(MP2/Aug-CC-pVDZ) (Hartree): -243.19909173
E(MP3/Aug-CC-pVDZ) (Hartree): -243.19254550
E(RHF/Aug-CC-pVDZ) (Hartree): -242.51533725
E(CCSD(T)/Aug-CC-pVTZ) (Hartree): -243.43870340
E(CCSD/Aug-CC-pVTZ) (Hartree): -243.39658695
E(MP2/Aug-CC-pVTZ) (Hartree): -243.40004390
E(MP3/Aug-CC-pVTZ) (Hartree): -243.38724333
E(RHF/6-31G(d,p)) (Hartree): -242.46936665
E(RHF/Aug-CC-pVTZ) (Hartree): -242.57275756
E(CCSD(T)/Aug-CC-pVQZ) (Hartree): -243.50138267
E(CCSD/Aug-CC-pVQZ) (Hartree): -243.45650850
     T1 diagnostic:  0.022614
E(MP2/Aug-CC-pVQZ) (Hartree): -243.46773727
E(MP3/Aug-CC-pVQZ) (Hartree): -243.44907503
E(RHF/Aug-CC-pVQZ) (Hartree): -242.58839770
E(RM062X/Aug-CC-pVTZ) (Hartree): -243.77249424
Point group : CS
Electronic state : 1-A'
Cartesian coordinates (Angs):
     N       0.616198     -0.460388       0.000000
     C       0.000000      0.629903       0.000000
     O      -0.630978      1.587739       0.000000
     H       1.634338     -0.478560       0.000000
     O      -0.112488     -1.597506       0.000000
Rotational constants (GHz):   48.3078300    5.4242000    4.8766300
Vibrational harmonic frequencies (cm-1):
      206.3218 (  A')           424.8644 (  A")           551.2151 (  A")
      671.7966 (  A')           971.9498 (  A')          1222.3629 (  A')
     1402.2747 (  A')          2345.0872 (  A')          3444.4356 (  A')
Zero-point correction (Hartree): 0.025607

NCO
---
E(CCSD(T)/Aug-CC-pVDZ) (Hartree): -167.62693028
E(CCSD/Aug-CC-pVDZ) (Hartree): -167.60767126
     T1 diagnostic:  0.026310
E(MP2/Aug-CC-pVDZ) (Hartree): -167.58945443
E(MP3/Aug-CC-pVDZ) (Hartree): -167.59640341
E(PMP2/Aug-CC-pVDZ) (Hartree): -167.59851147
E(PMP3/Aug-CC-pVDZ) (Hartree): -167.60213246
E(PUHF/Aug-CC-pVDZ) (Hartree): -167.16612982
```

```
E(UHF/Aug-CC-pVDZ) (Hartree): -167.15458842
E(CCSD(T)/Aug-CC-pVTZ) (Hartree): -167.76183039
E(CCSD/Aug-CC-pVTZ) (Hartree): -167.73450689
E(MP2/Aug-CC-pVTZ) (Hartree): -167.72246615
E(MP3/Aug-CC-pVTZ) (Hartree): -167.72586224
E(PMP2/Aug-CC-pVTZ) (Hartree): -167.73164695
E(PMP3/Aug-CC-pVTZ) (Hartree): -167.73164844
E(PUHF/Aug-CC-pVTZ) (Hartree): -167.20497190
E(UHF/6-31G(d,p)) (Hartree): -167.12855965
E(UHF/Aug-CC-pVTZ) (Hartree): -167.19326003
E(CCSD(T)/Aug-CC-pVQZ) (Hartree): -167.80303120
E(CCSD/Aug-CC-pVQZ) (Hartree): -167.77385078
     T1 diagnostic:  0.025921
E(MP2/Aug-CC-pVQZ) (Hartree): -167.76693421
E(MP3/Aug-CC-pVQZ) (Hartree): -167.76639553
E(PMP2/Aug-CC-pVQZ) (Hartree): -167.77618313
E(PMP3/Aug-CC-pVQZ) (Hartree): -167.77220480
E(PUHF/Aug-CC-pVQZ) (Hartree): -167.21557056
E(UHF/Aug-CC-pVQZ) (Hartree): -167.20377852
E(UM062X/Aug-CC-pVTZ) (Hartree): -168.00176764
Point group : C*V
Cartesian coordinates (Angs):
     O       0.000000      0.000000       1.130345
     C       0.000000      0.000000      -0.037292
     N       0.000000      0.000000      -1.259859
Rotational constants (GHz):    0.0000000   11.8412931   11.8412931
Vibrational harmonic frequencies (cm-1):
      545.5037 (  PI)           619.5696 (  PI)          1329.1219 (  SG)
     2052.4724 (  SG)
Zero-point correction (Hartree): 0.010358

O2 (triplet)
------------
E(CCSD(T)/Aug-CC-pVDZ) (Hartree): -150.01974519
E(CCSD/Aug-CC-pVDZ) (Hartree): -150.00798962
     T1 diagnostic:  0.017239
E(MP2/Aug-CC-pVDZ) (Hartree): -150.00188564
E(MP3/Aug-CC-pVDZ) (Hartree): -149.99996195
E(PMP2/Aug-CC-pVDZ) (Hartree): -150.00861128
E(PMP3/Aug-CC-pVDZ) (Hartree): -150.00309471
E(PUHF/Aug-CC-pVDZ) (Hartree): -149.65562305
E(UHF/Aug-CC-pVDZ) (Hartree): -149.64482099
E(CCSD(T)/Aug-CC-pVTZ) (Hartree): -150.14024980
E(CCSD/Aug-CC-pVTZ) (Hartree): -150.12182279
E(MP2/Aug-CC-pVTZ) (Hartree): -150.11944130
E(MP3/Aug-CC-pVTZ) (Hartree): -150.11498987
E(PMP2/Aug-CC-pVTZ) (Hartree): -150.12652379
E(PMP3/Aug-CC-pVTZ) (Hartree): -150.11821008
E(PUHF/Aug-CC-pVTZ) (Hartree): -149.69197969
E(UHF/6-31G(d,p)) (Hartree): -149.61689809
E(UHF/Aug-CC-pVTZ) (Hartree): -149.68069574
E(CCSD(T)/Aug-CC-pVQZ) (Hartree): -150.17820201
E(CCSD/Aug-CC-pVQZ) (Hartree): -150.15821114
     T1 diagnostic:  0.017206
E(MP2/Aug-CC-pVQZ) (Hartree): -150.15935385
E(MP3/Aug-CC-pVQZ) (Hartree): -150.15234763
E(PMP2/Aug-CC-pVQZ) (Hartree): -150.16652801
E(PMP3/Aug-CC-pVQZ) (Hartree): -150.15557503
E(PUHF/Aug-CC-pVQZ) (Hartree): -149.70247961
E(UHF/Aug-CC-pVQZ) (Hartree): -149.69108999
E(UM062X/Aug-CC-pVTZ) (Hartree): -150.32481496
Point group : D*H
Electronic state : 3-SGG
Cartesian coordinates (Angs):
     O       0.000000      0.000000       0.594953
     O       0.000000      0.000000      -0.594953
Rotational constants (GHz):    0.0000000   44.6313876   44.6313876
Vibrational harmonic frequencies (cm-1):
     1757.6183 ( SGG)
Zero-point correction (Hartree): 0.004004

O2 (singlet)
------------

E(CCSD(T)/Aug-CC-pVDZ) (Hartree): -149.96951201
E(CCSD/Aug-CC-pVDZ) (Hartree): -149.95369083
     T1 diagnostic:  0.015546
E(MP2/Aug-CC-pVDZ) (Hartree): -149.95020430
E(MP3/Aug-CC-pVDZ) (Hartree): -149.94364960
E(RHF/Aug-CC-pVDZ) (Hartree): -149.55943179
E(CCSD(T)/Aug-CC-pVTZ) (Hartree): -150.09177700
E(CCSD/Aug-CC-pVTZ) (Hartree): -150.06904109
     T1 diagnostic:  0.014672
E(MP2/Aug-CC-pVTZ) (Hartree): -150.07077477
E(MP3/Aug-CC-pVTZ) (Hartree): -150.06086175
E(RHF/Aug-CC-pVTZ) (Hartree): -149.59507488
E(CCSD(T)/Aug-CC-pVQZ) (Hartree): -150.13032570
E(CCSD/Aug-CC-pVQZ) (Hartree): -150.10602219
```

```
     T1 diagnostic:  0.014546
E(MP2/Aug-CC-pVQZ) (Hartree): -150.11192750
E(MP3/Aug-CC-pVQZ) (Hartree): -150.09907027
E(RHF/Aug-CC-pVQZ) (Hartree): -149.60535832
E(RM062X/Aug-CC-pVTZ) (Hartree): -150.26570483
Point group : D*H
Cartesian coordinates (Angs):
     O       0.000000      0.000000       0.593979
     O       0.000000      0.000000      -0.593979
Rotational constants (GHz):    0.0000000   44.7778544   44.7778544
Vibrational harmonic frequencies (cm-1):
     1749.4267 ( SGG)
Zero-point correction (Hartree): 0.003985


O3
--
E(CCSD(T)/Aug-CC-pVDZ) (Hartree): -224.96402704
E(CCSD/Aug-CC-pVDZ) (Hartree): -224.93019226
     T1 diagnostic:  0.025459
E(MP2/Aug-CC-pVDZ) (Hartree): -224.95076976
E(MP3/Aug-CC-pVDZ) (Hartree): -224.91583494
E(RHF/Aug-CC-pVDZ) (Hartree): -224.30230914
E(CCSD(T)/Aug-CC-pVTZ) (Hartree): -225.14987055
E(CCSD/Aug-CC-pVTZ) (Hartree): -225.10453547
E(MP2/Aug-CC-pVTZ) (Hartree): -225.13397192
E(MP3/Aug-CC-pVTZ) (Hartree): -225.09297033
E(RHF/6-31G(d,p)) (Hartree): -224.25916614
E(RHF/Aug-CC-pVTZ) (Hartree): -224.35728323
E(CCSD(T)/Aug-CC-pVQZ) (Hartree): -225.20810633
E(CCSD/Aug-CC-pVQZ) (Hartree): -225.16016260
     T1 diagnostic:  0.024377
E(MP2/Aug-CC-pVQZ) (Hartree): -225.19606922
E(MP3/Aug-CC-pVQZ) (Hartree): -225.15039623
E(RHF/Aug-CC-pVQZ) (Hartree): -224.37274046
E(RM062X/Aug-CC-pVTZ) (Hartree): -225.40547093
Point group : CS
Electronic state : 1-A'
Cartesian coordinates (Angs):
     O       0.000000      0.421186       0.000000
     O       1.057275     -0.210593       0.000000
     O      -1.057275     -0.210593       0.000000
Rotational constants (GHz):  118.7400400   14.1328300   12.6296200
Vibrational harmonic frequencies (cm-1):
      792.9313 (  A')          1363.1357 (  A')          1363.5294 (  A')
Zero-point correction (Hartree): 0.008018

Adducts
=======

cy_C_NH_OOOO
------------
E(CCSD(T)/Aug-CC-pVDZ) (Hartree): -393.23257589
E(CCSD/Aug-CC-pVDZ) (Hartree): -393.18514800
     T1 diagnostic:  0.019538
E(MP2/Aug-CC-pVDZ) (Hartree): -393.16993467
E(MP3/Aug-CC-pVDZ) (Hartree): -393.16982322
E(RHF/Aug-CC-pVDZ) (Hartree): -392.08454011
E(CCSD(T)/Aug-CC-pVTZ) (Hartree): -393.56421032
E(CCSD/Aug-CC-pVTZ) (Hartree): -393.49769124
E(MP2/Aug-CC-pVTZ) (Hartree): -393.49839338
E(MP3/Aug-CC-pVTZ) (Hartree): -393.48846082
E(RHF/6-31G(d,p)) (Hartree): -392.02093361
E(RHF/Aug-CC-pVTZ) (Hartree): -392.18068073
E(CCSD(T)/Aug-CC-pVQZ) (Hartree): -393.66421183
E(CCSD/Aug-CC-pVQZ) (Hartree): -393.59317121
     T1 diagnostic:  0.018153
E(MP2/Aug-CC-pVQZ) (Hartree): -393.60599534
E(MP3/Aug-CC-pVQZ) (Hartree): -393.58718362
E(RHF/Aug-CC-pVQZ) (Hartree): -392.20527405
E(RM062X/Aug-CC-pVTZ) (Hartree): -394.07807221
Electronic state : 1-A
Cartesian coordinates (Angs):
     N       2.009276     -0.131572       0.002917
     H       2.464916      0.774423       0.036954
     C       0.775058     -0.034441      -0.003242
     O      -0.060921     -1.103550      -0.167808
     O      -1.283738      0.665231      -0.268091
     O       0.004223      1.090601       0.148365
     O      -1.307088     -0.608128       0.282794
Rotational constants (GHz):    9.1005400    3.9846800    2.8731400
Vibrational harmonic frequencies (cm-1):
      173.3041                451.9977                465.0206
      694.4502                726.9493                797.1010
      802.0077                912.6836                942.0971
      980.4905               1025.4069               1043.3074
     1272.3421               1862.0364               3559.9118
Zero-point correction (Hartree): 0.035788
```

```
cy_N_H_C_O_OOO
--------------
E(CCSD(T)/Aug-CC-pVDZ) (Hartree): -393.29336201
E(CCSD/Aug-CC-pVDZ) (Hartree): -393.24730186
     T1 diagnostic:  0.019248
E(MP2/Aug-CC-pVDZ) (Hartree): -393.23472686
E(MP3/Aug-CC-pVDZ) (Hartree): -393.23124254
E(RHF/Aug-CC-pVDZ) (Hartree): -392.15347405
E(CCSD(T)/Aug-CC-pVTZ) (Hartree): -393.62318191
E(CCSD/Aug-CC-pVTZ) (Hartree): -393.55818073
E(MP2/Aug-CC-pVTZ) (Hartree): -393.56113073
E(MP3/Aug-CC-pVTZ) (Hartree): -393.54809819
E(RHF/6-31G(d,p)) (Hartree): -392.08933928
E(RHF/Aug-CC-pVTZ) (Hartree): -392.24768499
E(CCSD(T)/Aug-CC-pVQZ) (Hartree): -393.72378873
E(CCSD/Aug-CC-pVQZ) (Hartree): -393.65431251
     T1 diagnostic:  0.017762
E(MP2/Aug-CC-pVQZ) (Hartree): -393.66923453
E(MP3/Aug-CC-pVQZ) (Hartree): -393.64745748
E(RHF/Aug-CC-pVQZ) (Hartree): -392.27252394
E(RM062X/Aug-CC-pVTZ) (Hartree): -394.13765090
Electronic state : 1-A
Cartesian coordinates (Angs):
     N      -0.070709      1.128511       0.031724
     C       0.811905      0.016759      -0.021234
     O       1.990015      0.016242       0.004440
     H      -0.086374      1.532911       0.969066
     O      -1.311579      0.607948      -0.279911
     O      -1.253486     -0.705461       0.275587
     O       0.038788     -1.110360      -0.133082
Rotational constants (GHz):    8.7917500    3.9586600    2.8420600
Vibrational harmonic frequencies (cm-1):
      187.5161                392.8537                513.3355
      646.3573                722.7067                786.8801
      863.6550                878.6671                952.1559
     1029.4235               1099.5336               1200.9928
     1408.3970               1977.3872               3439.9504
Zero-point correction (Hartree): 0.036678

OC_O_N_H_OO
-----------
E(CCSD(T)/Aug-CC-pVDZ) (Hartree): -393.25629555
E(CCSD/Aug-CC-pVDZ) (Hartree): -393.18873036
     T1 diagnostic:  0.035006
E(MP2/Aug-CC-pVDZ) (Hartree): -393.20425933
E(MP3/Aug-CC-pVDZ) (Hartree): -393.16099520
E(RHF/Aug-CC-pVDZ) (Hartree): -392.04555991
E(CCSD(T)/Aug-CC-pVTZ) (Hartree): -393.58035675
E(CCSD/Aug-CC-pVTZ) (Hartree): -393.49291826
E(MP2/Aug-CC-pVTZ) (Hartree): -393.52564973
E(MP3/Aug-CC-pVTZ) (Hartree): -393.47125663
E(RHF/6-31G(d,p)) (Hartree): -391.97753686
E(RHF/Aug-CC-pVTZ) (Hartree): -392.13686092
E(CCSD(T)/Aug-CC-pVQZ) (Hartree): -393.68021968
E(CCSD/Aug-CC-pVQZ) (Hartree): -393.58823743
     T1 diagnostic:  0.033554
E(MP2/Aug-CC-pVQZ) (Hartree): -393.63347143
E(MP3/Aug-CC-pVQZ) (Hartree): -393.56991710
E(RHF/Aug-CC-pVQZ) (Hartree): -392.16203706
E(RM062X/Aug-CC-pVTZ) (Hartree): -394.06519495
Electronic state : 1-A
Cartesian coordinates (Angs):
     C       0.987419      0.051038      -0.034199
     N      -0.047579     -0.965433      -0.049990
     H       0.010912     -1.645191       0.710555
     O       2.150525     -0.164691      -0.143843
     O      -1.112674     -0.012041       0.404086
     O      -2.045010      0.042428      -0.368664
     O       0.306863      1.146428       0.088991
Rotational constants (GHz):   11.7353900    2.8130200    2.3927000
Vibrational harmonic frequencies (cm-1):
      135.5822                256.7675                458.8756
      507.1398                601.0420                642.0171
      719.9268                824.4984                884.9283
     1009.1998               1232.3274               1335.4959
     1452.6617               1924.3081               3455.9903
Zero-point correction (Hartree): 0.035177

Transition states
=================

TS.HNCO+O3.cy_C_NH_OOOO
-----------------------
E(CCSD(T)/Aug-CC-pVDZ) (Hartree): -393.21425434
E(CCSD/Aug-CC-pVDZ) (Hartree): -393.15060335
     T1 diagnostic:  0.038429
E(MP2/Aug-CC-pVDZ) (Hartree): -393.15547870
```

```
E(MP3/Aug-CC-pVDZ) (Hartree): -393.12359387
E(RHF/Aug-CC-pVDZ) (Hartree): -392.01073158
E(CCSD(T)/Aug-CC-pVTZ) (Hartree): -393.53998104
E(CCSD/Aug-CC-pVTZ) (Hartree): -393.45626749
E(MP2/Aug-CC-pVTZ) (Hartree): -393.47810321
E(MP3/Aug-CC-pVTZ) (Hartree): -393.43547331
E(RHF/6-31G(d,p)) (Hartree): -391.94343984
E(RHF/Aug-CC-pVTZ) (Hartree): -392.10325578
E(CCSD(T)/Aug-CC-pVQZ) (Hartree): -393.64005897
E(CCSD/Aug-CC-pVQZ) (Hartree): -393.55168392
     T1 diagnostic:  0.037145
E(MP2/Aug-CC-pVQZ) (Hartree): -393.58592336
E(MP3/Aug-CC-pVQZ) (Hartree): -393.53419946
E(RHF/Aug-CC-pVQZ) (Hartree): -392.12850051
E(RM062X/Aug-CC-pVTZ) (Hartree): -394.03578149
Electronic state : 1-A
Cartesian coordinates (Angs):
     N      -2.068268     -0.128887       0.107236
     H      -2.188556     -1.132308       0.187122
     C      -0.883750      0.214754      -0.032124
     O      -0.194667      1.225384      -0.218626
     O       1.329088     -0.538218      -0.290278
     O       0.150511     -1.084198       0.030757
     O       1.461184      0.490281       0.385019
Rotational constants (GHz):    8.7143200    3.5539500    2.6489200
Vibrational harmonic frequencies (cm-1):
     i641.4321                137.7413                 333.7787
      481.1350                527.5903                 681.6602
      683.5741                733.9279                 826.6644
     1015.7604               1084.3039                1214.5230
     1306.8747               1875.3845                3572.2633
Zero-point correction (Hartree): 0.032977

TS.HNCO+O3.cy_N_H_C_O_OOO
-------------------------
E(CCSD(T)/Aug-CC-pVDZ) (Hartree): -393.22437247
E(CCSD/Aug-CC-pVDZ) (Hartree): -393.16215473
     T1 diagnostic:  0.037450
E(MP2/Aug-CC-pVDZ) (Hartree): -393.17527172
E(MP3/Aug-CC-pVDZ) (Hartree): -393.13731545
E(RHF/Aug-CC-pVDZ) (Hartree): -392.02240764
E(CCSD(T)/Aug-CC-pVTZ) (Hartree): -393.55036463
E(CCSD/Aug-CC-pVTZ) (Hartree): -393.46786571
E(MP2/Aug-CC-pVTZ) (Hartree): -393.49810008
E(MP3/Aug-CC-pVTZ) (Hartree): -393.44904786
E(RHF/6-31G(d,p)) (Hartree): -391.95560007
E(RHF/Aug-CC-pVTZ) (Hartree): -392.11467745
E(CCSD(T)/Aug-CC-pVQZ) (Hartree): -393.65053184
E(CCSD/Aug-CC-pVQZ) (Hartree): -393.56334578
     T1 diagnostic:  0.036147
E(MP2/Aug-CC-pVQZ) (Hartree): -393.60598779
E(MP3/Aug-CC-pVQZ) (Hartree): -393.54778370
E(RHF/Aug-CC-pVQZ) (Hartree): -392.13992146
E(RM062X/Aug-CC-pVTZ) (Hartree): -394.04850529
Electronic state : 1-A
Cartesian coordinates (Angs):
     N       0.314593      1.241803      -0.011267
     H       0.196104      1.795062       0.826679
     C       1.045997      0.204167       0.017336
     O       2.054624     -0.370033      -0.020763
     O      -1.466176      0.573237      -0.295167
     O      -1.346726     -0.500825       0.345430
     O      -0.326003     -1.166465      -0.135978
Rotational constants (GHz):    8.0451000    3.3375700    2.4564200
Vibrational harmonic frequencies (cm-1):
     i643.5327                119.5269                 271.6102
      393.1549                463.2466                 546.7089
      641.8543                657.1761                 809.7450
      910.5677               1087.3114                1214.0559
     1272.3605               2142.7675                3600.1179
Zero-point correction (Hartree): 0.032191

TS.HNCO+O3.HN_O_CO+O2
---------------------
E(CCSD(T)/Aug-CC-pVDZ) (Hartree): -393.16933291
E(CCSD/Aug-CC-pVDZ) (Hartree): -393.11130194
     T1 diagnostic:  0.030142
E(MP2/Aug-CC-pVDZ) (Hartree): -393.10696261
E(MP3/Aug-CC-pVDZ) (Hartree): -393.08271719
E(RHF/Aug-CC-pVDZ) (Hartree): -391.99696427
E(CCSD(T)/Aug-CC-pVTZ) (Hartree): -393.49562738
E(CCSD/Aug-CC-pVTZ) (Hartree): -393.41807532
E(MP2/Aug-CC-pVTZ) (Hartree): -393.43045920
E(MP3/Aug-CC-pVTZ) (Hartree): -393.39601167
E(RHF/6-31G(d,p)) (Hartree): -391.93435226
E(RHF/Aug-CC-pVTZ) (Hartree): -392.09173481
E(CCSD(T)/Aug-CC-pVQZ) (Hartree): -393.59493902
E(CCSD/Aug-CC-pVQZ) (Hartree): -393.51284851
```

```
     T1 diagnostic:  0.028433
E(MP2/Aug-CC-pVQZ) (Hartree): -393.53756286
E(MP3/Aug-CC-pVQZ) (Hartree): -393.49413683
E(RHF/Aug-CC-pVQZ) (Hartree): -392.11652776
E(RM062X/Aug-CC-pVTZ) (Hartree): -393.99287981
Electronic state : 1-A
Cartesian coordinates (Angs):
     N      -0.992644      0.923071      -0.000157
     C      -1.853225      0.056515      -0.000003
     O      -2.578412     -0.831640       0.000258
     H      -1.115518      1.921663      -0.001329
     O       0.624660      0.279333      -0.000050
     O       2.175961     -0.268432       0.631090
     O       2.175714     -0.269543      -0.630992
Rotational constants (GHz):   11.7530100    1.5175000    1.4416500
Vibrational harmonic frequencies (cm-1):
     i816.7682                 60.8409                  85.2170
      115.8623                154.6666                 313.1689
      405.4050                610.2117                 639.0544
      642.9089                930.9578                1357.0847
     1402.7476               2371.7850                3680.7108
Zero-point correction (Hartree): 0.029094

TS.HNCO+O3.HO3+NCO
------------------
E(CCSD(T)/Aug-CC-pVDZ) (Hartree): -393.21947422
E(CCSD/Aug-CC-pVDZ) (Hartree): -393.15650943
     T1 diagnostic:  0.037799
E(MP2/Aug-CC-pVDZ) (Hartree): -393.16888505
E(MP3/Aug-CC-pVDZ) (Hartree): -393.13055999
E(RHF/Aug-CC-pVDZ) (Hartree): -392.02019818
E(CCSD(T)/Aug-CC-pVTZ) (Hartree): -393.54687307
E(CCSD/Aug-CC-pVTZ) (Hartree): -393.46379739
E(MP2/Aug-CC-pVTZ) (Hartree): -393.49295827
E(MP3/Aug-CC-pVTZ) (Hartree): -393.44394106
E(RHF/6-31G(d,p)) (Hartree): -391.95401143
E(RHF/Aug-CC-pVTZ) (Hartree): -392.11451023
E(CCSD(T)/Aug-CC-pVQZ) (Hartree): -393.64691612
E(CCSD/Aug-CC-pVQZ) (Hartree): -393.55922155
     T1 diagnostic:  0.036144
E(MP2/Aug-CC-pVQZ) (Hartree): -393.60079263
E(MP3/Aug-CC-pVQZ) (Hartree): -393.54259894
E(RHF/Aug-CC-pVQZ) (Hartree): -392.13978898
E(RM062X/Aug-CC-pVTZ) (Hartree): -394.04818822
Electronic state : 1-A
Cartesian coordinates (Angs):
     C       1.575555     -0.219476       0.062467
     N       0.498562     -0.684926       0.356175
     H      -0.690004     -1.009522      -0.129684
     O       2.634664      0.199420      -0.169607
     O      -1.816945     -0.749291      -0.316422
     O      -1.700933      0.457972       0.261511
     O      -0.648444      0.982006      -0.117776
Rotational constants (GHz):   12.0979700    1.9757100    1.7600700
Vibrational harmonic frequencies (cm-1):
    i1353.1295                54.7923                 100.8968
      334.2962               478.8113                 556.3274
      646.5053               673.3756                 811.5787
     1037.2417              1117.5813                1303.6615
     1422.4970              1861.9079                2301.5000
Zero-point correction (Hartree): 0.028935

TS.HNCO+O3.OC_O_N_H_OO
----------------------
E(CCSD(T)/Aug-CC-pVDZ) (Hartree): -393.20755552
E(CCSD/Aug-CC-pVDZ) (Hartree): -393.14157943
     T1 diagnostic:  0.043962
E(MP2/Aug-CC-pVDZ) (Hartree): -393.14492233
E(MP3/Aug-CC-pVDZ) (Hartree): -393.11171907
E(RHF/Aug-CC-pVDZ) (Hartree): -392.00473865
E(CCSD(T)/Aug-CC-pVTZ) (Hartree): -393.53298073
E(CCSD/Aug-CC-pVTZ) (Hartree): -393.44737647
E(MP2/Aug-CC-pVTZ) (Hartree): -393.46716648
E(MP3/Aug-CC-pVTZ) (Hartree): -393.42366756
E(RHF/6-31G(d,p)) (Hartree): -391.93659793
E(RHF/Aug-CC-pVTZ) (Hartree): -392.09852017
E(CCSD(T)/Aug-CC-pVQZ) (Hartree): -393.63305004
E(CCSD/Aug-CC-pVQZ) (Hartree): -393.54284944
     T1 diagnostic:  0.042860
E(MP2/Aug-CC-pVQZ) (Hartree): -393.57493448
E(MP3/Aug-CC-pVQZ) (Hartree): -393.52236092
E(RHF/Aug-CC-pVQZ) (Hartree): -392.12401976
E(RM062X/Aug-CC-pVTZ) (Hartree): -394.02679946
Electronic state : 1-A
Cartesian coordinates (Angs):
     N       0.504538      1.246251      -0.077161
     C       1.064212      0.066844      -0.034212
     O       2.099559     -0.496818      -0.021080
```

```
     H       1.171844      1.978391       0.154970
     O      -1.150520     -0.034262       0.423369
     O      -2.132367      0.032856      -0.260892
     O      -0.202783     -0.889677      -0.067594
Rotational constants (GHz):   10.8757300    2.6912800    2.2367500
Vibrational harmonic frequencies (cm-1):
     i572.5421                114.1327                 217.5569
      346.5962                499.6931                 615.8756
      695.1183                709.0945                 768.5036
      975.3033               1145.3223                1217.5113
     1471.5528               1973.7783                3514.2273
Zero-point correction (Hartree): 0.032496
```

Appendix C

Supporting Information: Rosanka et al. (2021a)

The supplemental material of Rosanka et al. (2021a) (here Chapter 5) consists of the CAABA/MECCA model code and model output. However, listing the complete code and listing all model data in this thesis is not feasible. Thus only the non code and non data supplemental material is listed here. The model code developed and used in each simulation presented in Rosanka et al. (2021a) (here Chapter 5) is archived at Zenodo (`https://doi.org/10.5281/zenodo.4707938`; Sander, 2021). The model output of all simulations presented in Rosanka et al. (2021a) (here Chapter 5) is archived at Jülich DATA (`https://doi.org/10.26165/JUELICH-DATA/SD9F6B`; Rosanka et al., 2021d).

In the following, Tables 1 to 6 provide a summary of the chemical mechanism and are presented as published in caaba/manual/meccanism.pdf in the archived model code (`https://doi.org/10.5281/zenodo.4707938`; Sander, 2021). Tables 7 and 8 provide the chemical properties (Henry's law and accommodation coefficients) of each species used within CAABA/MECCA. For improved readability, all species for which no values are defined are excluded. The original tables including further species properties are published in caaba/tools/chemprop/chemprop.pdf in the archived model code (`https://doi.org/10.5281/zenodo.4707938`; Sander, 2021).

The Chemical Mechanism of MECCA

KPP version: `2.2.3_rs3`

MECCA version: `4.5.0`

Date: April 21, 2021

Batch file: `latex`

Integrator: `rosenbrock_posdef`

Gas equation file: `gas.eqn`

Replacement file:

Selected reactions:
"`1`"

Number of aerosol phases: 1

Number of species in selected mechanism:

Gas phase:	708
Aqueous phase:	481
All species:	1189

Number of reactions in selected mechanism:

Gas phase (Gnnn):	1815
Aqueous phase (Annn):	402
Henry (Hnnn):	735
Photolysis (Jnnn):	385
Aqueous phase photolysis (PHnnn):	27
Heterogeneous (HETnnn):	21
Equilibria (EQnn):	138
Isotope exchange (IEXnnn):	0
Tagging equations (TAGnnn):	0
Dummy (Dnn):	1
All equations:	3524

Table 1: Gas phase reactions

#	labels	reaction	rate coefficient	reference
G1000	UpStTrG	$O_2 + O(^1D) \rightarrow O(^3P) + O_2$	3.3E-11*EXP(55./temp)	Burkholder et al. (2015)
G1001	UpStTrG	$O_2 + O(^3P) \rightarrow O_3$	6.0E-34*((temp/300.)**(-2.4)) *cair	Burkholder et al. (2015)
G1002a	UpStG	$O_3 + O(^1D) \rightarrow 2\ O_2$	1.2E-10	Burkholder et al. (2015)*
G1002b	UpG	$O_3 + O(^1D) \rightarrow O_2 + 2\ O(^3P)$	1.2E-10	Burkholder et al. (2015)
G1003	UpStG	$O_3 + O(^3P) \rightarrow 2\ O_2$	8.0E-12*EXP(-2060./temp)	Burkholder et al. (2015)
G1004	UpG	$O_2 + O^+ \rightarrow O_2^+ + O(^3P)$	k_Op_O2(temp,temp_ion)	Fuller-Rowell (1993)
G1101	UpG	$O_2^+ + e^- \rightarrow 2\ O(^3P)$	2.7E-7*(300./temp_elec)**(.7)	Fuller-Rowell (1993)
G2100	UpStTrG	$H + O_2 \rightarrow HO_2$	k_3rd(temp,cair,4.4E-32,1.3, 7.5E-11,-0.2,0.6)	Burkholder et al. (2015)
G2101	UpStG	$H + O_3 \rightarrow OH + O_2$	1.4E-10*EXP(-470./temp)	Burkholder et al. (2015)
G2102	UpStG	$H_2 + O(^1D) \rightarrow H + OH$	1.2E-10	Burkholder et al. (2015)
G2103	UpStG	$OH + O(^3P) \rightarrow H + O_2$	1.8E-11*EXP(180./temp)	Burkholder et al. (2015)
G2104	UpStTrG	$OH + O_3 \rightarrow HO_2 + O_2$	1.7E-12*EXP(-940./temp)	Burkholder et al. (2015)
G2105	UpStTrG	$OH + H_2 \rightarrow H_2O + H$	2.8E-12*EXP(-1800./temp)	Burkholder et al. (2015)
G2106	UpStG	$HO_2 + O(^3P) \rightarrow OH + O_2$	3.E-11*EXP(200./temp)	Burkholder et al. (2015)
G2107	UpStTrG	$HO_2 + O_3 \rightarrow OH + 2\ O_2$	1.E-14*EXP(-490./temp)	Burkholder et al. (2015)
G2108a	UpStG	$HO_2 + H \rightarrow 2\ OH$	7.2E-11	Burkholder et al. (2015)
G2108b	UpStG	$HO_2 + H \rightarrow H_2 + O_2$	6.9E-12	Burkholder et al. (2015)
G2108c	UpStG	$HO_2 + H \rightarrow O(^3P) + H_2O$	1.6E-12	Burkholder et al. (2015)
G2109	UpStTrG	$HO_2 + OH \rightarrow H_2O + O_2$	4.8E-11*EXP(250./temp)	Burkholder et al. (2015)
G2110	UpStTrG	$HO_2 + HO_2 \rightarrow H_2O_2 + O_2$	k_HO2_HO2	Burkholder et al. (2015)*
G2111	UpStTrG	$H_2O + O(^1D) \rightarrow 2\ OH$	1.63E-10*EXP(60./temp)	Burkholder et al. (2015)
G2112	UpStTrG	$H_2O_2 + OH \rightarrow H_2O + HO_2$	1.8E-12	Burkholder et al. (2015)
G2113	UpG	$H_2 + O(^3P) \rightarrow H + OH$	1.60E-11*EXP(-4570./temp)	Roble (1995)
G2114a	UpG	$OH + OH \rightarrow H_2O + O(^3P)$	4.20E-12*EXP(-240./temp)	Sander et al. (2003)
G2114b	UpG	$OH + OH \rightarrow H_2O_2$	k_3rd(temp,cair,6.9E-31,1.0, 2.6E-11,0.,0.6)	Burkholder et al. (2015)
G2115	UpG	$H + H \rightarrow H_2$	5.7E-32*(300./temp)**(1.6)*cair	Roble (1995)
G2116	UpG	$H_2O_2 + O(^3P) \rightarrow OH + HO_2$	1.40E-12*EXP(-2000./temp)	Sander et al. (2003)
G2117	UpStTrG	$H_2O + H_2O \rightarrow (H_2O)_2$	6.521E-26*temp*EXP(1851.09/temp) *EXP(-5.10485E-3*temp)	Scribano et al. (2006)*
G2118	UpStTrG	$(H_2O)_2 \rightarrow H_2O + H_2O$	1.E0	see note*
G3001	UpGN	$NO^+ + e^- \rightarrow .15\ N + .85\ N(^2D) + O(^3P)$	4.2E-7*(300./temp_elec)**(0.85)	Bailey et al. (2002)

Table 1: Gas phase reactions (... continued)

#	labels	reaction	rate coefficient	reference
G3002	UpGN	$N_2^+ + e^- \rightarrow .88\ N + 1.12\ N(^2D)$	1.8E-7*(temp_elec/300.)**(-0.39)	Swaminathan et al. (1998)
G3003	UpGN	$N(^2D) + e^- \rightarrow N + e^-$	3.8E-12*(temp_elec)**(.81)	Swaminathan et al. (1998)
G3100	UpStGN	$N + O_2 \rightarrow NO + O(^3P)$	1.5E-11*EXP(-3600./temp)	Burkholder et al. (2015)
G3101	UpStTrGN	$N_2 + O(^1D) \rightarrow O(^3P) + N_2$	2.15E-11*EXP(110./temp)	Burkholder et al. (2015)
G3102a	UpStGN	$N_2O + O(^1D) \rightarrow 2\ NO$	7.259E-11*EXP(20./temp)	Burkholder et al. (2015)
G3102b	StGN	$N_2O + O(^1D) \rightarrow N_2 + O_2$	4.641E-11*EXP(20./temp)	Burkholder et al. (2015)
G3103	UpStTrGN	$NO + O_3 \rightarrow NO_2 + O_2$	3.0E-12*EXP(-1500./temp)	Burkholder et al. (2015)
G3104	UpStGN	$NO + N \rightarrow O(^3P) + N_2$	2.1E-11*EXP(100./temp)	Burkholder et al. (2015)
G3105	UpStGN	$NO_2 + O(^3P) \rightarrow NO + O_2$	5.1E-12*EXP(210./temp)	Burkholder et al. (2015)
G3106	StTrGN	$NO_2 + O_3 \rightarrow NO_3 + O_2$	1.2E-13*EXP(-2450./temp)	Burkholder et al. (2015)
G3107	UpStGN	$NO_2 + N \rightarrow N_2O + O(^3P)$	5.8E-12*EXP(220./temp)	Burkholder et al. (2015)
G3108	StTrGN	$NO_3 + NO \rightarrow 2\ NO_2$	1.5E-11*EXP(170./temp)	Burkholder et al. (2015)
G3109	UpStTrGN	$NO_3 + NO_2 \rightarrow N_2O_5$	k_NO3_NO2	Burkholder et al. (2015)*
G3110	StTrGN	$N_2O_5 \rightarrow NO_2 + NO_3$	k_NO3_NO2/(5.8E-27*EXP(10840./temp))	Burkholder et al. (2015)*
G3111	UpGN	$N(^2D) + NO \rightarrow N_2 + O(^3P)$	6.70E-11	Fuller-Rowell (1993)
G3112	UpGN	$N(^2D) + O_2 \rightarrow NO + O(^3P)$	6.20E-12*(temp/300.)	Duff et al. (2003)
G3113	UpGN	$N(^2D) + O(^3P) \rightarrow N + O(^3P)$	6.90E-13	Fell et al. (1990)
G3114	UpGN	$N(^2D) + O_3 \rightarrow NO + O_2$	0.80E-16	Sander et al. (2003)
G3115	UpGN	$NO + O(^3P) \rightarrow NO_2$	k_3rd(temp,cair,9.0E-32,1.5,3.0E-11,0.0,0.6)	Burkholder et al. (2015)
G3116	UpGN	$NO_2 + O(^3P) \rightarrow NO_3$	k_3rd(temp,cair,2.5E-31,1.8,2.2E-11,0.7,0.6)	Burkholder et al. (2015)
G3117	UpGN	$N(^2D) \rightarrow N$	10.6	Fuller-Rowell (1993)
G3118	UpGN	$N^+ + O_2 \rightarrow NO + O^+$	3.66E-11	Barth (1992)
G3119	UpGN	$N_2^+ + O(^3P) \rightarrow NO^+ + N(^2D)$	k_N2_O(temp,temp_ion)	Fuller-Rowell (1993)
G3120a	UpGN	$N^+ + O_2 \rightarrow NO^+ + O(^3P)$	2.60E-10	Fuller-Rowell (1993)
G3120b	UpGN	$N^+ + O_2 \rightarrow O_2^+ + N$	3.10E-10	Swaminathan et al. (1998)
G3121	UpGN	$N^+ + O(^3P) \rightarrow O^+ + N$	1.00E-12	Fuller-Rowell (1993)
G3122	UpGN	$O_2^+ + N \rightarrow NO^+ + O(^3P)$	1.20E-10	Fuller-Rowell (1993)
G3123	UpGN	$O_2^+ + NO \rightarrow NO^+ + O_2$	4.40E-10	Fuller-Rowell (1993)
G3124	UpGN	$O^+ + N_2 \rightarrow NO^+ + N$	k_Op_N2(temp,temp_ion)	Fuller-Rowell (1993)
G3125	UpGN	$N_2^+ + O_2 \rightarrow N_2 + O_2^+$	5.10E-11*(temp/300.)**(-0.8)	Fuller-Rowell (1993)
G3200	TrGN	$NO + OH \rightarrow HONO$	k_3rd(temp,cair,7.0E-31,2.6,3.6E-11,0.1,0.6)	Burkholder et al. (2015)

Table 1: Gas phase reactions (... continued)

#	labels	reaction	rate coefficient	reference
G3201	UpStTrGN	$NO + HO_2 \rightarrow NO_2 + OH$	3.3E-12*EXP(270./temp)	Burkholder et al. (2015)
G3202a	UpStTrGN	$NO_2 + OH \rightarrow HNO_3$	(1.-alpha_HOONO) * k_NO2_OH	Amedro et al. (2020)
G3202b	UpStTrGN	$NO_2 + OH \rightarrow HOONO$	alpha_HOONO * k_NO2_OH	Amedro et al. (2020)
G3203	StTrGN	$NO_2 + HO_2 \rightarrow HNO_4$	k_NO2_HO2	Burkholder et al. (2015)*
G3204	TrGN	$NO_3 + HO_2 \rightarrow NO_2 + OH + O_2$	3.5E-12	Burkholder et al. (2015)
G3205	TrGN	$HONO + OH \rightarrow NO_2 + H_2O$	1.8E-11*EXP(-390./temp)	Burkholder et al. (2015)
G3206	StTrGN	$HNO_3 + OH \rightarrow H_2O + NO_3$	k_HNO3_OH	Dulitz et al. (2018)*
G3207	StTrGN	$HNO_4 \rightarrow NO_2 + HO_2$	k_NO2_HO2/(2.1E-27*EXP(10900./temp))	Burkholder et al. (2015)*
G3208	StTrGN	$HNO_4 + OH \rightarrow NO_2 + H_2O$	1.3E-12*EXP(380./temp)	Burkholder et al. (2015)
G3209	TrGN	$NH_3 + OH \rightarrow NH_2 + H_2O$	1.7E-12*EXP(-710./temp)	Kohlmann and Poppe (1999)
G3210	TrGN	$NH_2 + O_3 \rightarrow NH_2O + O_2$	4.3E-12*EXP(-930./temp)	Kohlmann and Poppe (1999)
G3211	TrGN	$NH_2 + HO_2 \rightarrow NH_2O + OH$	4.8E-07*EXP(-628./temp)*(temp)**(-1.32)	Kohlmann and Poppe (1999)
G3212	TrGN	$NH_2 + HO_2 \rightarrow HNO + H_2O$	9.4E-09*EXP(-356./temp)*(temp)**(-1.12)	Kohlmann and Poppe (1999)
G3213	TrGN	$NH_2 + NO \rightarrow HO_2 + OH + N_2$	1.92E-12*((temp/298.)**(-1.5))	Kohlmann and Poppe (1999)
G3214	TrGN	$NH_2 + NO \rightarrow N_2 + H_2O$	1.41E-11*((temp/298.)**(-1.5))	Kohlmann and Poppe (1999)
G3215	TrGN	$NH_2 + NO_2 \rightarrow N_2O + H_2O$	1.2E-11*((temp/298.)**(-2.0))	Kohlmann and Poppe (1999)
G3216	TrGN	$NH_2 + NO_2 \rightarrow NH_2O + NO$	0.8E-11*((temp/298.)**(-2.0))	Kohlmann and Poppe (1999)
G3217	TrGN	$NH_2O + O_3 \rightarrow NH_2 + O_2$	1.2E-14	Kohlmann and Poppe (1999)
G3218	TrGN	$NH_2O \rightarrow NHOH$	1.3E3	Kohlmann and Poppe (1999)
G3219	TrGN	$HNO + OH \rightarrow NO + H_2O$	8.0E-11*EXP(-500./temp)	Kohlmann and Poppe (1999)
G3220	TrGN	$HNO + NHOH \rightarrow NH_2OH + NO$	1.66E-12*EXP(-1500./temp)	Kohlmann and Poppe (1999)
G3221	TrGN	$HNO + NO_2 \rightarrow HONO + NO$	1.0E-12*EXP(-1000./temp)	Kohlmann and Poppe (1999)
G3222	TrGN	$NHOH + OH \rightarrow HNO + H_2O$	1.66E-12	Kohlmann and Poppe (1999)
G3223	TrGN	$NH_2OH + OH \rightarrow NHOH + H_2O$	4.13E-11*EXP(-2138./temp)	Kohlmann and Poppe (1999)
G3224	TrGN	$HNO + O_2 \rightarrow HO_2 + NO$	3.65E-14*EXP(-4600./temp)	Kohlmann and Poppe (1999)
G3225	UpGN	$N + OH \rightarrow NO + H$	5.00E-11	Roble (1995)
G3226	UpGN	$NO_2 + H \rightarrow NO + OH$	4.00E-10*EXP(-340./temp)	Sander et al. (2003)
G3227	UpStTrGN	$HOONO \rightarrow NO_2 + OH$	(alpha_HOONO*k_NO2_OH)/(3.5E-27*EXP(10135./temp))	see note*
G3228	UpStTrGN	$HOONO + OH \rightarrow H_2O + NO_3$	1.3E-12*EXP(380./temp)	Burkholder et al. (2015)*
G4100	UpStG	$CH_4 + O(^1D) \rightarrow .75\ CH_3 + .75\ OH + .25\ HCHO + .4\ H + .05\ H_2$	1.75E-10	Burkholder et al. (2015)

Table 1: Gas phase reactions (... continued)

#	labels	reaction	rate coefficient	reference
G4101	StTrG	$CH_4 + OH \rightarrow CH_3 + H_2O$	1.85E-20*EXP(2.82*LOG(temp) -987./temp)	Atkinson (2003)
G4102	TrG	$CH_3OH + OH \rightarrow .85\ HCHO + .85\ HO_2 + .15\ CH_3O + H_2O$	6.38E-18*((temp)**2)*EXP(144./ temp)	Atkinson et al. (2006)
G4103a	StTrG	$CH_3O_2 + HO_2 \rightarrow CH_3OOH + O_2$	3.8E-13*EXP(780./temp)/(1.+1./ 498.*EXP(1160./temp))	Atkinson et al. (2006)
G4103b	StTrG	$CH_3O_2 + HO_2 \rightarrow HCHO + H_2O + O_2$	3.8E-13*EXP(780./temp)/(1.+ 498.*EXP(-1160./temp))	Atkinson et al. (2006)
G4104a	StTrGN	$CH_3O_2 + NO \rightarrow CH_3O + NO_2$	2.3E-12*EXP(360./temp)*(1.-beta_ CH3NO3)	Atkinson et al. (2006), Butkovskaya et al. (2012), Flocke et al. (1998)
G4104b	StTrGN	$CH_3O_2 + NO \rightarrow CH_3ONO_2$	2.3E-12*EXP(360./temp)*beta_ CH3NO3	Atkinson et al. (2006), Butkovskaya et al. (2012), Flocke et al. (1998)*
G4105	TrGN	$CH_3O_2 + NO_3 \rightarrow CH_3O + NO_2 + O_2$	1.2E-12	Atkinson et al. (2006)
G4106a	StTrG	$CH_3O_2 \rightarrow CH_3O + .5\ O_2$	7.4E-13*EXP(-520./temp)*RO2*2.	Atkinson et al. (2006)
G4106b	StTrG	$CH_3O_2 \rightarrow .5\ HCHO + .5\ CH_3OH + .5\ O_2$	(k_CH3O2-7.4E-13*EXP(-520./temp)) *RO2*2.	Atkinson et al. (2006)
G4107	StTrG	$CH_3OOH + OH \rightarrow .6\ CH_3O_2 + .4\ HCHO + .4\ OH + H_2O$	k_CH3OOH_OH	Wallington et al. (2018)
G4108	StTrG	$HCHO + OH \rightarrow CO + H_2O + HO_2$	9.52E-18*EXP(2.03*LOG(temp) +636./temp)	Sivakumaran et al. (2003)
G4109	TrGN	$HCHO + NO_3 \rightarrow HNO_3 + CO + HO_2$	3.4E-13*EXP(-1900./temp)	Burkholder et al. (2015)*
G4110	UpStTrG	$CO + OH \rightarrow H + CO_2$	(1.57E-13+cair*3.54E-33)	McCabe et al. (2001)
G4111	TrG	$HCOOH + OH \rightarrow CO_2 + HO_2 + H_2O$	2.94E-14*exp(786./temp) +9.85E-13*EXP(-1036./temp)	Paulot et al. (2011)
G4112	UpStG	$CO + O(^3P) \rightarrow CO_2$	6.60E-33*EXP(-1103./temp)	Roble (1995)
G4113	UpStG	$CH_4 + O(^3P) \rightarrow .51\ CH_3 + .51\ OH + .49\ CH_3O + .49\ H$	6.03E-18*(temp)**(2.17) *EXP(-3619./temp)	Roble (1995), Garton et al. (2003), Espinosa-Garcia and Garcia-Bernáldez (2000)
G4114	StTrGN	$CH_3O_2 + NO_2 \rightarrow CH_3O_2NO_2$	k_NO2_CH3O2	Burkholder et al. (2015)
G4115	StTrGN	$CH_3O_2NO_2 \rightarrow CH_3O_2 + NO_2$	k_NO2_CH3O2/(9.5E-29*EXP(11234./ temp))	Burkholder et al. (2015)*
G4116	StTrGN	$CH_3O_2NO_2 + OH \rightarrow HCHO + NO_3 + H_2O$	3.00E-14	see note*
G4117	StTrGN	$CH_3ONO_2 + OH \rightarrow H_2O + HCHO + NO_2$	4.0E-13*EXP(-845./temp)	Atkinson et al. (2006)
G4118	StTrG	$CH_3O \rightarrow HO_2 + HCHO$	1.3E-14*exp(-663./temp)*c(ind_O2)	Chai et al. (2014)

Table 1: Gas phase reactions (... continued)

#	labels	reaction	rate coefficient	reference
G4119a	StTrGN	$CH_3O + NO_2 \rightarrow CH_3ONO_2$	k_3rd_iupac(temp,cair,8.1E-29, 4.5,2.1E-11,0.,0.44)	Atkinson et al. (2006)
G4119b	StTrGN	$CH_3O + NO_2 \rightarrow HCHO + HONO$	9.6E-12*EXP(-1150./temp)	Atkinson et al. (2006)
G4120a	StTrGN	$CH_3O + NO \rightarrow CH_3ONO$	k_3rd_iupac(temp,cair,2.6E-29, 2.8,3.3E-11,0.6,REAL(EXP(-temp/ 900.),SP))	Atkinson et al. (2006)
G4120b	StTrGN	$CH_3O + NO \rightarrow HCHO + HNO$	2.3E-12*(temp/300.)**(0.7)	Atkinson et al. (2006)
G4121	StTrG	$CH_3O_2 + O_3 \rightarrow CH_3O + 2\ O_2$	2.9E-16*exp(-1000./temp)	Burkholder et al. (2015)
G4122	StTrGN	$CH_3ONO + OH \rightarrow H_2O + HCHO + NO$	1.E-10*exp(-1764./temp)	Nielsen et al. (1991)
G4123	StTrG	$HCHO + HO_2 \rightarrow HOCH_2O_2$	9.7E-15*EXP(625./temp)	Atkinson et al. (2006)
G4124	StTrG	$HOCH_2O_2 \rightarrow HCHO + HO_2$	2.4E12*EXP(-7000./temp)	Atkinson et al. (2006)
G4125	StTrG	$HOCH_2O_2 + HO_2 \rightarrow .5\ HOCH_2OOH + .5\ HCOOH + .2\ OH + .2\ HO_2 + .3\ H_2O + .8\ O_2$	5.6E-15*EXP(2300./temp)	Atkinson et al. (2006)
G4126	StTrGN	$HOCH_2O_2 + NO \rightarrow NO_2 + HO_2 + HCOOH$	0.7275*2.3E-12*EXP(360./temp)	Atkinson et al. (2006)*
G4127	StTrGN	$HOCH_2O_2 + NO_3 \rightarrow NO_2 + HO_2 + HCOOH$	1.2E-12	see note*
G4129a	StTrG	$HOCH_2O_2 \rightarrow HCOOH + HO_2$	(k_CH3O2*5.5E-12)**(0.5)*RO2*2.	Atkinson et al. (2006)
G4129b	StTrG	$HOCH_2O_2 \rightarrow .5\ HCOOH + .5\ HOCH_2OH + .5\ O_2$	(k_CH3O2*5.7E-14*EXP(750./temp)) **(0.5)*RO2*2.	Atkinson et al. (2006)
G4130a	StTrG	$HOCH_2OOH + OH \rightarrow HOCH_2O_2 + H_2O$	k_ROOHRO	Taraborrelli (2010)*
G4130b	StTrG	$HOCH_2OOH + OH \rightarrow HCOOH + H_2O + OH$	k_ROHRO + k_s*f_sOOH*f_sOH	Taraborrelli (2010)*
G4132	StTrG	$HOCH_2OH + OH \rightarrow HO_2 + HCOOH + H_2O$	2.*k_ROHRO + k_s*f_sOH*f_sOH	Taraborrelli (2010)*
G4133	StTrG	$CH_3O_2 + OH \rightarrow CH_3O + HO_2$	1.4E-10	Bossolasco et al. (2014)*
G4134	StTrG	$CH_2OO \rightarrow CO + HO_2 + OH$	1.124E+14*EXP(-10000./temp)	see note*
G4135	StTrG	$CH_2OO + H_2O \rightarrow HOCH_2OOH$	k_CH2OO_NO2*3.6E-6	Ouyang et al. (2013)*
G4136	StTrG	$CH_2OO + (H_2O)_2 \rightarrow HOCH_2OOH + H_2O$	5.2E-12	Chao et al. (2015), Lewis et al. (2015)*
G4137	StTrGN	$CH_2OO + NO \rightarrow HCHO + NO_2$	6.E-14	Welz et al. (2012)*
G4138	StTrGN	$CH_2OO + NO_2 \rightarrow HCHO + NO_3$	k_CH2OO_NO2	Welz et al. (2012), Stone et al. (2014)*
G4140	StTrG	$CH_2OO + CO \rightarrow HCHO + CO_2$	3.6E-14	Vereecken et al. (2012)
G4141	StTrG	$CH_2OO + HCOOH \rightarrow 2\ HCOOH$	1.E-10	Welz et al. (2014)*
G4142	StTrG	$CH_2OO + HCHO \rightarrow 2\ LCARBON$	1.7E-12	Stone et al. (2014)*
G4143	StTrG	$CH_2OO + CH_3OH \rightarrow 2\ LCARBON$	5.E-12	Vereecken et al. (2012)*
G4144	StTrG	$CH_2OO + CH_3O_2 \rightarrow 2\ LCARBON$	5.E-12	Vereecken et al. (2012)*
G4145	StTrG	$CH_2OO + HO_2 \rightarrow LCARBON$	5.E-12	Vereecken et al. (2012)

Table 1: Gas phase reactions (... continued)

#	labels	reaction	rate coefficient	reference
G4146	StTrG	$CH_2OO + O_3 \rightarrow HCHO + 2\ O_2$	1.E-12	Vereecken et al. (2014)
G4147	StTrG	$CH_2OO + CH_2OO \rightarrow 2\ HCHO + O_2$	6.E-11	Buras et al. (2014)
G4148	StTrGN	$HOCH_2O_2 + NO_2 \rightarrow HOCH_2O_2NO_2$	k_NO2_CH3O2	see note*
G4149	StTrGN	$HOCH_2O_2NO_2 \rightarrow HOCH_2O_2 + NO_2$	k_NO2_CH3O2/(9.5E-29*EXP(11234./temp))	Barnes et al. (1985)*
G4150	StTrGN	$HOCH_2O_2NO_2 + OH \rightarrow HCOOH + NO_3 + H_2O$	9.50E-13*EXP(-650./temp)*f_sOH	see note*
G4151	StTrG	$CH_3 + O_2 \rightarrow CH_3O_2$	k_3rd_iupac(temp,cair,7.0E-31,3.,1.8E-12,-1.1,0.33)	Atkinson et al. (2006)
G4152	StTrG	$CH_3 + O_3 \rightarrow .956\ HCHO + .956\ H + .044\ CH_3O + O_2$	5.1E-12*exp(-210./temp)	Albaladejo et al. (2002), Ogryzlo et al. (1981)
G4153	StTrG	$CH_3 + O(^3P) \rightarrow .83\ HCHO + .83\ H + .17\ CO + .17\ H_2 + .17\ H$	1.3E-10	Atkinson et al. (2006)
G4154	StTrG	$CH_3O + O_3 \rightarrow CH_3O_2 + O_2$	2.53E-14	Albaladejo et al. (2002)*
G4155	StTrG	$CH_3O + O(^3P) \rightarrow .75\ CH_3 + .75\ O_2 + .25\ HCHO + .25\ OH$	2.5E-11	Baulch et al. (2005)
G4156	StTrG	$CH_3O_2 + O(^3P) \rightarrow CH_3O + O_2$	4.3E-11	Zellner et al. (1988)
G4157	StTrG	$HCHO + O(^3P) \rightarrow .7\ OH + .7\ CO + .3\ H + .3\ CO_2 + HO_2$	3.4E-11*EXP(-1600./temp)	Burkholder et al. (2015)
G4158	TrG	$CH_2OO^* \rightarrow .37\ CH_2OO + .47\ CO + .47\ H_2O + .16\ HO_2 + .16\ CO + .16\ OH$	KDEC	Atkinson et al. (2006)
G4159	TrGN	$HCN + OH \rightarrow H_2O + CN$	k_3rd(temp,cair,4.28E-33,1.0,REAL(4.25E-13*EXP(-1150./temp),SP),1.0,0.8)	Kleinböhl et al. (2006)
G4160a	TrGN	$HCN + O(^1D) \rightarrow O(^3P) + HCN$	1.08E-10*EXP(105./temp)*0.15*EXP(200./temp)	Strekowski et al. (2010)
G4160b	TrGN	$HCN + O(^1D) \rightarrow H + NCO$	1.08E-10*EXP(105./temp)*0.68/2.	Strekowski et al. (2010)*
G4160c	TrGN	$HCN + O(^1D) \rightarrow OH + CN$	1.08E-10*EXP(105./temp)*(1.-(0.68/2.+0.15*EXP(200./temp)))	Strekowski et al. (2010)*
G4161	TrGN	$HCN + O(^3P) \rightarrow H + NCO$	1.0E-11*EXP(-4000./temp)	Burkholder et al. (2015)*
G4162	TrGN	$CN + O_2 \rightarrow NCO + O(^3P)$	1.2E-11*EXP(210./temp)*0.75	Baulch et al. (2005)
G4163	TrGN	$CN + O_2 \rightarrow CO + NO$	1.2E-11*EXP(210./temp)*0.25	Baulch et al. (2005)
G4164	TrGN	$NCO + O_2 \rightarrow CO_2 + NO$	7.E-15	Becker et al. (2000)*
G42000	TrGC	$C_2H_6 + OH \rightarrow C_2H_5O_2 + H_2O$	1.49E-17*temp*temp*EXP(-499./temp)	Atkinson et al. (2006)
G42001	TrGC	$C_2H_4 + O_3 \rightarrow HCHO + CH_2OO^*$	9.1E-15*EXP(-2580./temp)	Atkinson et al. (2006)*

Table 1: Gas phase reactions (... continued)

#	labels	reaction	rate coefficient	reference
G42002	TrGC	$C_2H_4 + OH \rightarrow HOCH_2CH_2O_2$	k_3rd_iupac(temp,cair,8.6E-29, 3.1,9.E-12,0.85,0.48)	Atkinson et al. (2006), Rickard and Pascoe (2009)
G42003	TrGC	$C_2H_5O_2 + HO_2 \rightarrow C_2H_5OOH$	7.5E-13*EXP(700./temp)	Burkholder et al. (2015)
G42004a	TrGCN	$C_2H_5O_2 + NO \rightarrow CH_3CHO + HO_2 + NO_2$	2.55E-12*EXP(380./temp)*(1.-beta_C2H5NO3)	Atkinson et al. (2006), Butkovskaya et al. (2010)
G42004b	TrGCN	$C_2H_5O_2 + NO \rightarrow C_2H_5ONO_2$	2.55E-12*EXP(380./temp)*beta_C2H5NO3	Atkinson et al. (2006), Butkovskaya et al. (2010)
G42005	TrGCN	$C_2H_5O_2 + NO_3 \rightarrow CH_3CHO + HO_2 + NO_2$	2.3E-12	Wallington et al. (2018)
G42006	TrGC	$C_2H_5O_2 \rightarrow .8\ CH_3CHO + .6\ HO_2 + .2\ C_2H_5OH$	2.*(7.6E-14*k_CH3O2)**(.5)*RO2	Sander et al. (2019), Atkinson et al. (2006)
G42007a	TrGC	$C_2H_5OOH + OH \rightarrow C_2H_5O_2 + H_2O$	k_ROOHRO	Sander et al. (2019)
G42007b	TrGC	$C_2H_5OOH + OH \rightarrow CH_3CHO + OH$	k_s*f_sOOH	Sander et al. (2019)
G42008a	TrGC	$CH_3CHO + OH \rightarrow CH_3C(O) + H_2O$	4.4E-12*EXP(365./temp)*0.95	Atkinson et al. (2006)
G42008b	TrGC	$CH_3CHO + OH \rightarrow HCOCH_2O_2 + H_2O$	4.4E-12*EXP(365./temp)*0.05	Atkinson et al. (2006)
G42009	TrGCN	$CH_3CHO + NO_3 \rightarrow CH_3C(O) + HNO_3$	KNO3AL	Rickard and Pascoe (2009)
G42010	TrGC	$CH_3COOH + OH \rightarrow CH_3 + CO_2 + H_2O$	k_CH3CO2H_OH	Atkinson et al. (2006)*
G42011a	TrGC	$CH_3C(O)OO + HO_2 \rightarrow OH + CH_3 + CO_2$	5.20E-13*EXP(980./temp)*1.507*0.61	Groß et al. (2014)
G42011b	TrGC	$CH_3C(O)OO + HO_2 \rightarrow CH_3C(O)OOH$	5.20E-13*EXP(980./temp)*1.507*0.23	Groß et al. (2014)
G42011c	TrGC	$CH_3C(O)OO + HO_2 \rightarrow CH_3COOH + O_3$	5.20E-13*EXP(980./temp)*1.507*0.16	Groß et al. (2014)
G42012	TrGCN	$CH_3C(O)OO + NO \rightarrow CH_3 + CO_2 + NO_2$	8.1E-12*EXP(270./temp)	Tyndall et al. (2001a)
G42013	TrGCN	$CH_3C(O)OO + NO_2 \rightarrow PAN$	k_CH3CO3_NO2	Burkholder et al. (2015)*
G42014	TrGCN	$CH_3C(O)OO + NO_3 \rightarrow CH_3 + NO_2 + CO_2$	4.E-12	Canosa-Mas et al. (1996)
G42017a	TrGC	$CH_3C(O)OO \rightarrow CH_3 + CO_2$	k1_RO2RCO3*0.9	Sander et al. (2019)
G42017b	TrGC	$CH_3C(O)OO \rightarrow CH_3COOH$	k1_RO2RCO3*0.1	Sander et al. (2019)
G42018	TrGC	$CH_3C(O)OOH + OH \rightarrow CH_3C(O)OO + H_2O$	k_ROOHRO	Rickard and Pascoe (2009)*
G42020	TrGCN	$PAN + OH \rightarrow HCHO + CO + NO_2 + H_2O$	3.00E-14	Rickard and Pascoe (2009)
G42021	TrGCN	$PAN \rightarrow CH_3C(O)OO + NO_2$	k_PAN_M	Burkholder et al. (2015)*
G42022a	TrGC	$C_2H_2 + OH \rightarrow GLYOX + OH$	k_3rd(temp,cair,5.5e-30,0.0, 8.3e-13,-2.,0.6)*0.71	Burkholder et al. (2015)*
G42022b	TrGC	$C_2H_2 + OH \rightarrow HCOOH + CO + HO_2$	k_3rd(temp,cair,5.5e-30,0.0, 8.3e-13,-2.,0.6)*0.29	Burkholder et al. (2015)*
G42023a	TrGC	$HOCH_2CHO + OH \rightarrow HOCH2CO + H_2O$	8.00E-12*0.80	Atkinson et al. (2006)
G42023b	TrGC	$HOCH_2CHO + OH \rightarrow HOCHCHO + H_2O$	8.00E-12*0.20	Atkinson et al. (2006)
G42024a	TrGC	$HOCH2CO + O_2 \rightarrow HOCH_2CO_3$	5.1E-12*(1.-1./(1+1.85E-18*cair))	Atkinson et al. (2006), Beyersdorf et al. (2010)*

Table 1: Gas phase reactions (... continued)

#	labels	reaction	rate coefficient	reference
G42024b	TrGC	$HOCH2CO + O_2 \rightarrow OH + HCHO + CO_2$	5.1E-12*1./(1+1.85E-18*cair)	Atkinson et al. (2006), Beyersdorf et al. (2010)*
G42025	TrGC	$HOCHCHO \rightarrow GLYOX + HO_2$	KDEC	Sander et al. (2019)
G42026	TrGCN	$HOCH_2CHO + NO_3 \rightarrow HOCH2CO + HNO_3$	KNO3AL	Rickard and Pascoe (2009)
G42027a	TrGC	$HOCH_2CO_3 \rightarrow HCHO + CO_2 + HO_2$	k1_RO2RCO3*0.9	Sander et al. (2019)
G42027b	TrGC	$HOCH_2CO_3 \rightarrow HOCH_2CO_2H$	k1_RO2RCO3*0.1	Sander et al. (2019)
G42028a	TrGC	$HOCH_2CO_3 + HO_2 \rightarrow HCHO + HO_2 + OH + CO_2$	KAPHO2*r_CO3_OH	Sander et al. (2019), Groß et al. (2014)
G42028b	TrGC	$HOCH_2CO_3 + HO_2 \rightarrow HOCH_2CO_3H$	KAPHO2*r_CO3_OOH	Sander et al. (2019), Groß et al. (2014)
G42028c	TrGC	$HOCH_2CO_3 + HO_2 \rightarrow HOCH_2CO_2H + O_3$	KAPHO2*r_CO3_O3	Sander et al. (2019), Groß et al. (2014)
G42029	TrGCN	$HOCH_2CO_3 + NO \rightarrow NO_2 + HO_2 + HCHO + CO_2$	KAPNO	Rickard and Pascoe (2009)
G42030	TrGCN	$HOCH_2CO_3 + NO_2 \rightarrow PHAN$	k_CH3CO3_NO2	Rickard and Pascoe (2009)
G42031	TrGCN	$HOCH_2CO_3 + NO_3 \rightarrow NO_2 + HO_2 + HCHO + CO_2$	KRO2NO3*1.74	Rickard and Pascoe (2009)
G42032	TrGC	$HOCH_2CO_2H + OH \rightarrow .09\ HCHO + .09\ CO_2 + .91\ HCOCO_2H + HO_2 + H_2O$	k_CO2H+k_s*f_sOH*f_CO2H	Sander et al. (2019)
G42033a	TrGC	$HOCH_2CO_3H + OH \rightarrow HOCH_2CO_3 + H_2O$	k_ROOHRO	Sander et al. (2019)
G42033b	TrGC	$HOCH_2CO_3H + OH \rightarrow HCOCO_3H + HO_2$	k_s*f_sOH*f_CO2H	Sander et al. (2019)
G42034	TrGCN	$PHAN \rightarrow HOCH_2CO_3 + NO_2$	k_PAN_M	Rickard and Pascoe (2009)
G42035	TrGCN	$PHAN + OH \rightarrow HCHO + CO + NO_2 + H_2O$	k_s*f_sOH*f_cpan+k_ROHRO	Sander et al. (2019)
G42036	TrGC	$GLYOX + OH \rightarrow HCOCO + H_2O$	3.1E-12*EXP(340./temp)	Atkinson et al. (2006), Orlando and Tyndall (2001), Lockhart et al. (2013)
G42037	TrGCN	$GLYOX + NO_3 \rightarrow HCOCO + HNO_3$	KNO3AL	Rickard and Pascoe (2009)
G42038a	TrGC	$HCOCO \rightarrow CO + CO + HO_2$	7.E11*EXP(-3160./temp) +5.E-12*c(ind_O2)	Orlando and Tyndall (2001), Lockhart et al. (2013), Rickard and Pascoe (2009)
G42037b	TrGC	$HCOCO \rightarrow HCOCO_3$	5.E-12*c(ind_O2)*3.2*exp(-550./temp)	Lockhart et al. (2013), Rickard and Pascoe (2009)
G42037c	TrGC	$HCOCO \rightarrow OH + CO + CO_2$	5.E-12*c(ind_O2) *(1.-3.2*exp(-550./temp))	Lockhart et al. (2013), Rickard and Pascoe (2009)
G42039a	TrGC	$HCOCO_3 \rightarrow CO + HO_2 + CO_2$	k1_RO2RCO3*0.9	Sander et al. (2019)
G42039b	TrGC	$HCOCO_3 \rightarrow HCOCO_2H$	k1_RO2RCO3*0.1	Sander et al. (2019)

Table 1: Gas phase reactions (... continued)

#	labels	reaction	rate coefficient	reference
G42040	TrGC	$HCOCO_3 + HO_2 \rightarrow HO_2 + CO + CO_2 + OH$	KAPHO2	Feierabend et al. (2008), Sander et al. (2019)
G42041	TrGCN	$HCOCO_3 + NO \rightarrow HO_2 + CO + NO_2 + CO_2$	KAPNO	Rickard and Pascoe (2009)
G42042	TrGCN	$HCOCO_3 + NO_3 \rightarrow HO_2 + CO + NO_2 + CO_2$	KRO2NO3*1.74	Rickard and Pascoe (2009)
G42043	TrGCN	$HCOCO_3 + NO_2 \rightarrow HO_2 + CO + NO_3 + CO_2$	k_CH3CO3_NO2	Orlando and Tyndall (2001), Sander et al. (2019)
G42044	TrGC	$HCOCO_2H + OH \rightarrow CO + HO_2 + CO_2 + H_2O$	k_CO2H+k_t*f_O*f_CO2H	Sander et al. (2019)
G42045a	TrGC	$HCOCO_3H + OH \rightarrow HCOCO_3 + H_2O$	k_ROOHRO	Sander et al. (2019)
G42045b	TrGC	$HCOCO_3H + OH \rightarrow CO + CO_2 + H_2O + OH$	k_t*f_O*f_CO2H	Sander et al. (2019)
G42046	TrGC	$HOCH_2CH_2O_2 \rightarrow .6\ HOCH_2CH_2O + .2\ HOCH_2CHO + .2$ ETHGLY	2.*(7.8E-14*EXP(1000./temp) *k_CH3O2)**(.5)*RO2	Atkinson et al. (2006), Rickard and Pascoe (2009)
G42047	TrGCN	$HOCH_2CH_2O_2 + NO \rightarrow .25\ HO_2 + .5\ HCHO + .75\ HOCH_2CH_2O + NO_2$	KRO2NO*(1.-alpha_AN(3,1,0,0,0, temp,cair))	Rickard and Pascoe (2009)*
G42048	TrGCN	$HOCH_2CH_2O_2 + NO \rightarrow$ ETHOHNO3	KRO2NO*alpha_AN(3,1,0,0,0,temp, cair)	Sander et al. (2019)
G42049a	TrGC	$HOCH_2CH_2O_2 + HO_2 \rightarrow$ HYETHO2H	1.53E-13*EXP(1300./temp) *(1.-r_CHOHCH2O2_OH)	Rickard and Pascoe (2009)
G42049b	TrGC	$HOCH_2CH_2O_2 + HO_2 \rightarrow HOCH_2CH_2O + OH$	1.53E-13*EXP(1300./temp) *r_CHOHCH2O2_OH	Rickard and Pascoe (2009)
G42050	TrGCN	ETHOHNO3 + OH $\rightarrow .93\ NO_3CH2CHO + .93\ HO_2 + .07\ HOCH_2CHO + .07\ NO_2 + H_2O$	k_s*(f_sOH*f_CH2ONO2+f_ONO2*f_ pCH2OH)+k_ROHRO	Sander et al. (2019)
G42051a	TrGC	$HYETHO2H + OH \rightarrow HOCH_2CH_2O_2 + H_2O$	k_ROOHRO	Rickard and Pascoe (2009)*
G42051b	TrGC	$HYETHO2H + OH \rightarrow HOCH_2CHO + OH + H_2O$	k_s*f_sOOH*f_pCH2OH	Sander et al. (2019)
G42051c	TrGC	$HYETHO2H + OH \rightarrow HOOCH2CHO + HO_2 + H_2O$	k_s*f_sOH*f_pCH2OH+k_ROHRO	Sander et al. (2019)
G42052a	TrGC	$HOCH_2CH_2O \rightarrow HO_2 + HOCH_2CHO$	6.00E-14*EXP(-550./temp) *C(ind_O2)	Rickard and Pascoe (2009)
G42052b	TrGC	$HOCH_2CH_2O \rightarrow HO_2 + HCHO + HCHO$	9.50E13*EXP(-5988./temp)	Rickard and Pascoe (2009)
G42053	TrGC	ETHGLY + OH $\rightarrow HOCH_2CHO + HO_2 + H_2O$	2.*k_s*f_sOH*f_pCH2OH+2.*k_ROHRO	Sander et al. (2019)
G42054	TrGC	$HCOCH_2O_2 \rightarrow .6\ HCHO + .6\ CO + .6\ HO_2 + .2$ GLYOX $+ .2\ HOCH_2CHO$	k1_RO2pORO2	Sander et al. (2019)
G42055a	TrGC	$HCOCH_2O_2 + HO_2 \rightarrow$ HOOCH2CHO	k_RO2_HO2(temp,2)*r_COCH2O2_OOH	Sander et al. (2019)
G42055b	TrGC	$HCOCH_2O_2 + HO_2 \rightarrow HCHO + CO + HO_2 + OH$	k_RO2_HO2(temp,2)*r_COCH2O2_OH	Sander et al. (2019)
G42056a	TrGCN	$HCOCH_2O_2 + NO \rightarrow NO_2 + HCHO + CO + HO_2$	KRO2NO*(1.-alpha_AN(3,1,1,0,0, temp,cair))	Sander et al. (2019)

Table 1: Gas phase reactions (... continued)

#	labels	reaction	rate coefficient	reference
G42056b	TrGCN	$HCOCH_2O_2 + NO \rightarrow NO_3CH2CHO$	KRO2NO*alpha_AN(3,1,1,0,0,temp, cair)	Sander et al. (2019)
G42057	TrGCN	$HCOCH_2O_2 + NO_3 \rightarrow HCHO + CO + HO_2 + NO_2$	KRO2NO3	Sander et al. (2019)
G42058a	TrGC	$HOOCH2CHO + OH \rightarrow HCOCH_2O_2$	k_ROOHRO	Sander et al. (2019)
G42058b	TrGC	$HOOCH2CHO + OH \rightarrow HCHO + CO + OH$	0.8*8.E-12	Sander et al. (2019)*
G42058c	TrGC	$HOOCH2CHO + OH \rightarrow GLYOX + OH$	k_s*f_sOOH*f_CHO	Sander et al. (2019)
G42059	TrGCN	$HOOCH2CHO + NO_3 \rightarrow OH + HCHO + CO + HNO_3$	KNO3AL	Rickard and Pascoe (2009)
G42060	TrGCN	$HOOCH_2CO_3 + NO \rightarrow NO_2 + OH + HCHO + CO_2$	KAPNO	Sander et al. (2019)
G42061	TrGCN	$HOOCH_2CO_3 + NO_3 \rightarrow NO_2 + OH + HCHO + CO_2$	KRO2NO3*1.74	Sander et al. (2019)
G42062a	TrGC	$HOOCH_2CO_3 + HO_2 \rightarrow 2\ OH + HCHO + CO_2$	KAPHO2*r_CO3_OH	Sander et al. (2019)
G42062b	TrGC	$HOOCH_2CO_3 + HO_2 \rightarrow HOOCH2CO3H$	KAPHO2*r_CO3_OOH	Sander et al. (2019)
G42062c	TrGC	$HOOCH_2CO_3 + HO_2 \rightarrow HOOCH2CO2H + O_3$	KAPHO2*r_CO3_O3	Sander et al. (2019)
G42063a	TrGC	$HOOCH_2CO_3 \rightarrow OH + HCHO + CO_2$	k1_RO2RCO3*0.9	Sander et al. (2019)
G42063b	TrGC	$HOOCH_2CO_3 \rightarrow HOOCH2CO2H$	k1_RO2RCO3*0.1	Sander et al. (2019)
G42064a	TrGC	$HOOCH2CO3H + OH \rightarrow HOOCH_2CO_3 + H_2O$	2.*k_ROOHRO	Sander et al. (2019)
G42064b	TrGC	$HOOCH2CO3H + OH \rightarrow HCOCO_3H + OH + H_2O$	k_s*f_sOOH*f_CO2H	Sander et al. (2019)
G42065	TrGC	$HOOCH2CO2H + OH \rightarrow HCOCO_2H + OH + H_2O$	k_s*f_sOOH*f_CO2H+k_CO2H	Sander et al. (2019)
G42066	TrGC	$CH2CO + OH \rightarrow .6\ HCHO + .6\ HO_2 + .6\ CO + .4$ HOOCH2CO2H	2.8E-12*exp(510./temp)	Baulch et al. (2005), Sander et al. (2019)
G42067a	TrGC	$CH3CHOHOOH + OH \rightarrow CH_3COOH + OH$	(k_t*f_tOOH*f_tOH + k_ROHRO)	Sander et al. (2019)
G42067b	TrGC	$CH3CHOHOOH + OH \rightarrow CH3CHOHO2$	k_ROOHRO	Sander et al. (2019)
G42068	TrGC	$CH3CHOHO2 \rightarrow CH_3CHO + HO_2$	3.46E12*EXP(-12500./(1.98*temp))	Hermans et al. (2005), Sander et al. (2019)
G42069	TrGC	$CH_3CHO + HO_2 \rightarrow CH3CHOHO2$	3.46E12*EXP(-12500./(1.98*temp)) /(6.34E26*EXP(-14700./ (1.98*temp)))	Hermans et al. (2005), Sander et al. (2019)
G42070	TrGC	$CH3CHOHO2 + HO_2 \rightarrow .5\ CH3CHOHOOH + .3$ $CH_3COOH + .2\ CH_3 + .2\ HCOOH + .2\ OH$	5.6E-15*EXP(2300./temp)	Sander et al. (2019)
G42071	TrGC	$CH3CHOHO2 \rightarrow CH_3 + HCOOH + OH$	k1_RO2sORO2	Sander et al. (2019)
G42072	TrGCN	$CH3CHOHO2 + NO \rightarrow CH_3 + HCOOH + OH + NO_2$	KRO2NO	Sander et al. (2019)
G42073	TrGCN	$C_2H_5ONO_2 + OH \rightarrow CH_3CHO + H_2O + NO_2$	6.7E-13*EXP(-395./temp)	Atkinson et al. (2006)
G42074a	TrGCN	$NO_3CH2CHO + OH \rightarrow GLYOX + NO_2 + H_2O$	k_s*f_CH2ONO2*f_CHO	Paulot et al. (2009a), Sander et al. (2019)*
G42074b	TrGCN	$NO_3CH2CHO + OH \rightarrow NO_3CH2CO_3 + H_2O$	k_t*f_O*f_CH2ONO2*3.	Paulot et al. (2009a), Sander et al. (2019)*

Table 1: Gas phase reactions (... continued)

#	labels	reaction	rate coefficient	reference
G42075	TrGCN	$NO_3CH2CO_3 + HO_2 \rightarrow HCHO + NO_2 + CO_2 + OH$	KAPHO2	Rickard and Pascoe (2009)*
G42076	TrGCN	$NO_3CH2CO_3 + NO \rightarrow HCHO + NO_2 + CO_2 + NO_2$	KAPNO	Rickard and Pascoe (2009)
G42077	TrGCN	$NO_3CH2CO_3 + NO_2 \rightarrow NO_3CH2CHO$	k_CH3CO3_NO2	Rickard and Pascoe (2009)
G42078	TrGCN	$NO_3CH2CO_3 \rightarrow HCHO + NO_2 + CO_2$	k1_RO2RCO3	Rickard and Pascoe (2009)*
G42079	TrGCN	$NO_3CH2CHO \rightarrow NO_3CH2CO_3 + NO_2$	k_PAN_M	Rickard and Pascoe (2009)
G42080	StTrGCN	$C_2H_5O_2 + NO_2 \rightarrow C_2H_5O_2NO_2$	k_3rd_iupac(temp,cair,1.3E-29, 6.2,8.8E-12,0.0,0.31)	Atkinson et al. (2006)
G42081	StTrGCN	$C_2H_5O_2NO_2 \rightarrow C_2H_5O_2 + NO_2$	k_3rd_iupac(temp,cair, REAL(4.8E-4*EXP(-9285./temp) ,SP),0.0,REAL(8.8E15*EXP(-10440./ temp),SP),0.0,0.31)	Atkinson et al. (2006)
G42082	StTrGCN	$C_2H_5O_2NO_2 + OH \rightarrow CH_3CHO + NO_3 + H_2O$	9.50E-13*EXP(-650./temp)	Sander et al. (2019)*
G42083a	TrGC	$CH_3C(O) + O_2 \rightarrow CH_3C(O)OO$	5.1E-12*(1. - 1./(1.+ 9.4E-18*cair))	Atkinson et al. (2006), Beyersdorf et al. (2010)*
G42083b	TrGC	$CH_3C(O) + O_2 \rightarrow OH + HCHO + CO$	5.1E-12*1./(1.+9.4E-18*cair)	Atkinson et al. (2006), Beyersdorf et al. (2010)*
G42084	TrGC	$C_2H_5OH + OH \rightarrow .95\ C_2H_5O_2 + .95\ HO_2 + .05\ HOCH_2CH_2O_2 + H_2O$	3.0E-12*EXP(20./temp)	Sander et al. (2019), Atkinson et al. (2006)
G42085a	TrGCN	$CH_3CN + OH \rightarrow NCCH_2O_2 + H_2O$	8.1E-13*EXP(-1080./temp)*0.40	Atkinson et al. (2006), Tyndall et al. (2001b)*
G42085b	TrGCN	$CH_3CN + OH \rightarrow OH + CH_3C(O) + NO$	8.1E-13*EXP(-1080./temp)*(1.-0.40)	Atkinson et al. (2006), Tyndall et al. (2001b)*
G42086a	TrGCN	$CH_3CN + O(^1D) \rightarrow O(^3P) + CH_3CN$	2.54E-10*EXP(-24./temp) *0.0269*EXP(137./temp)	Strekowski et al. (2010)
G42086b	TrGCN	$CH_3CN + O(^1D) \rightarrow 2\ H + CO + HCN$	2.54E-10*EXP(-24./temp)*0.16	Strekowski et al. (2010)*
G42086c	TrGCN	$CH_3CN + O(^1D) \rightarrow .5\ CH_3 + .5\ NCO + .5\ NCCH_2O_2 + .5\ OH$	2.54E-10*EXP(-24./temp)*(1.-(0.16+ 0.0269*EXP(137./temp)))	Strekowski et al. (2010)*
G42087	TrGCN	$NCCH_2O_2 + NO \rightarrow HCN + CO_2 + HO_2 + NO_2$	KRO2NO	see note*
G42088	TrGCN	$NCCH_2O_2 + HO_2 \rightarrow HCN + CO_2 + HO_2$	k_RO2_HO2(temp,2)	see note*
G42089a	TrGC	$CH_2CHOH + OH \rightarrow HCOOH + OH + HCHO$	k_CH2CHOH_OH_HCOOH	Sander et al. (2019), So et al. (2014)*
G42089b	TrGC	$CH_2CHOH + OH \rightarrow HOCH_2CHO + HO_2$	k_CH2CHOH_OH_ALD	Sander et al. (2019), So et al. (2014)
G42090	TrGC	$CH_2CHOH + HCOOH \rightarrow CH_3CHO + HCOOH$	k_CH2CHOH_HCOOH	Sander et al. (2019), da Silva (2010)*

Table 1: Gas phase reactions (... continued)

#	labels	reaction	rate coefficient	reference
G42091	TrGC	$CH_3CHO + HCOOH \rightarrow CH_2CHOH + HCOOH$	k_ALD_HCOOH	Sander et al. (2019), da Silva (2010)*
G42092	TrGC	$HOOCCOOH + OH \rightarrow 2\ CO_2 + HO_2 + H_2O$	2.0 *k_co2h	see note*
G42093a	TrGC	$HOCH_2CHOHOH + OH \rightarrow HOCH_2CO_2H + HO_2 + H_2O$	k_t*f_toh*f_toh	see note*
G42093b	TrGC	$HOCH_2CHOHOH + OH \rightarrow CHOCHOHOH + HO_2 + H_2O$	k_s*f_soh*f_pch2oh	see note*
G42093c	TrGC	$HOCH_2CHOHOH + OH \rightarrow HCOOH + HOCH_2O_2 + H_2O$	2.0 * k_rohro	see note*
G42093d	TrGC	$HOCH_2CHOHOH + OH \rightarrow HCHO + HCOOH + HO_2 + H_2O$	k_rohro	see note*
G42094a	TrGC	$CH_3CHOHOH + OH \rightarrow CH_3COOH + HO_2 + H_2O$	k_t*f_toh*f_toh	see note*
G42094b	TrGC	$CH_3CHOHOH + OH \rightarrow CH_3 + HCOOH + H_2O$	2.0 * k_rohro	see note*
G42095a	TrGC	$CHOHOHCOOH + OH \rightarrow HOOCCOOH + HO_2 + H_2O$	k_t*f_toh*f_toh*f_co2h	see note*
G42095b	TrGC	$CHOHOHCOOH + OH \rightarrow HCOOH + CO_2 + HO_2 + H_2O$	2.0 * k_rohro + k_co2h	see note*
G42096a	TrGC	$CHOHOHCHOHOH + OH \rightarrow 2\ HCOOH + HO_2 + H_2O$	4.0 * k_rohro	see note*
G42096b	TrGC	$CHOHOHCHOHOH + OH \rightarrow CHOHOHCOOH + HO_2 + H_2O$	2.0 * k_t*f_toh*f_toh*f_pch2oh	see note*
G42097a	TrGC	$CHOCHOHOH + OH \rightarrow HCOOH + CO + HO_2 + H_2O$	2.0 * k_rohro + k_t*f_o*f_pch2oh	see note*
G42097b	TrGC	$CHOCHOHOH + OH \rightarrow HCOCO_2H + HO_2 + H_2O$	k_t*f_toh*f_toh*f_cho	see note*
G42098a	TrGC	$HOOCH_2CHOHOH + OH \rightarrow HOOCH2CO2H + HO_2 + H_2O$	k_t*f_toh*f_toh*f_pch2oh	see note*
G42098b	TrGC	$HOOCH_2CHOHOH + OH \rightarrow HCOOH + HCHO + OH + H_2O$	2.0 * k_rohro	see note*
G42098c	TrGC	$HOOCH_2CHOHOH + OH \rightarrow CHOCHOHOH + OH + H_2O$	k_s*f_pch2oh*f_sooh	see note*
G43000a	TrGC	$C_3H_8 + OH \rightarrow iC_3H_7O_2 + H_2O$	k_s	Sander et al. (2019)
G43000b	TrGC	$C_3H_8 + OH \rightarrow C_3H_7O_2 + H_2O$	2.*k_p	Sander et al. (2019)
G43001a	TrGC	$C_3H_6 + O_3 \rightarrow HCHO + .16\ CH3CHOHOOH + .50\ OH + .50\ HCOCH_2O_2 + .05\ CH2CO + .09\ CH_3OH + .09\ CO + .2\ CH_4 + .2\ CO_2$	5.5E-15*EXP(-1880./temp)*.57	Atkinson et al. (2006)*
G43001b	TrGC	$C_3H_6 + O_3 \rightarrow CH_3CHO + CH_2OO^*$	5.5E-15*EXP(-1880./temp)*.43	Atkinson et al. (2006)*
G43002	TrGC	$C_3H_6 + OH \rightarrow HYPROPO2$	k_3rd_iupac(temp,cair,8.6E-27, 3.5,3.E-11,1.,0.5)	Atkinson et al. (2006), Rickard and Pascoe (2009)
G43003	TrGCN	$C_3H_6 + NO_3 \rightarrow PRONO3BO2$	4.6E-13*EXP(-1155./temp)	Wallington et al. (2018)
G43004	TrGC	$iC_3H_7O_2 + HO_2 \rightarrow iC_3H_7OOH$	1.9E-13*EXP(1300./temp)	Atkinson (1997)*
G43005a	TrGCN	$iC_3H_7O_2 + NO \rightarrow CH_3COCH_3 + HO_2 + NO_2$	2.7E-12*EXP(360./temp)*(1.-alpha_ AN(3,2,0,0,0,temp,cair))	Wallington et al. (2018)

Table 1: Gas phase reactions (... continued)

#	labels	reaction	rate coefficient	reference
G43005b	TrGCN	$iC_3H_7O_2$ + NO → $iC_3H_7ONO_2$	2.7E-12*EXP(360./temp)*alpha_AN(3,2,0,0,0,temp,cair)	Wallington et al. (2018)
G43006	TrGC	$iC_3H_7O_2$ → .8 CH_3COCH_3 + .2 IPROPOL + .6 HO_2	2.*(1.6E-12*EXP(-2200./temp)*k_CH3O2)**(.5)*RO2	Rickard and Pascoe (2009), Atkinson et al. (2006)
G43007a	TrGC	iC_3H_7OOH + OH → $iC_3H_7O_2$ + H_2O	k_ROOHRO	Sander et al. (2019)
G43007b	TrGC	iC_3H_7OOH + OH → CH_3COCH_3 + H_2O + OH	k_t*f_tOOH	Sander et al. (2019)
G43008	TrGC	$C_3H_7O_2$ + HO_2 → C_3H_7OOH	1.9E-13*EXP(1300./temp)	Atkinson (1997)*
G43009a	TrGCN	$C_3H_7O_2$ + NO → C_2H_5CHO + HO_2 + NO_2	2.7E-12*EXP(360./temp)*(1.-alpha_AN(3,1,0,0,0,temp,cair))	Wallington et al. (2018)
G43009b	TrGCN	$C_3H_7O_2$ + NO → $C_3H_7ONO_2$	2.7E-12*EXP(360./temp)*alpha_AN(3,1,0,0,0,temp,cair)	Wallington et al. (2018)
G43010	TrGC	$C_3H_7O_2$ → .8 CH_3COCH_3 + .2 NPROPOL + .6 HO_2	2.*(k_CH3O2*3.E-13)**(.5)*RO2	Rickard and Pascoe (2009), Atkinson et al. (2006)
G43011	TrGC	CH_3COCH_3 + OH → $CH_3COCH_2O_2$ + H_2O	(8.8E-12*EXP(-1320./temp)+1.7E-14*EXP(423./temp))	Atkinson et al. (2006)*
G43012a	TrGC	$CH_3COCH_2O_2$ + HO_2 → $CH_3COCH_2O_2H$	8.6E-13*EXP(700./temp)*r_COCH2O2_OOH	Tyndall et al. (2001a), Sander et al. (2019)
G43012b	TrGC	$CH_3COCH_2O_2$ + HO_2 → OH + $CH_3C(O)$ + HCHO	8.6E-13*EXP(700./temp)*r_COCH2O2_OH	Tyndall et al. (2001a), Sander et al. (2019)
G43013a	TrGCN	$CH_3COCH_2O_2$ + NO → $CH_3C(O)$ + HCHO + NO_2	2.9E-12*EXP(300./temp)*(1.-alpha_AN(4,1,1,0,0,temp,cair))	Burkholder et al. (2015)
G43013b	TrGCN	$CH_3COCH_2O_2$ + NO → NOA	2.9E-12*EXP(300./temp)*alpha_AN(4,1,1,0,0,temp,cair)	Burkholder et al. (2015)
G43014	TrGC	$CH_3COCH_2O_2$ → .3 $CH_3C(O)$ + .3 HCHO + .5 MGLYOX + .2 CH_3COCH_2OH	k1_RO2pORO2	Orlando and Tyndall (2012)
G43015a	TrGC	$CH_3COCH_2O_2H$ + OH → $CH_3COCH_2O_2$ + H_2O	k_ROOHRO	see note*
G43015b	TrGC	$CH_3COCH_2O_2H$ + OH → MGLYOX + OH + H_2O	k_s*f_sOOH*f_CO	Sander et al. (2019)
G43016	TrGC	CH_3COCH_2OH + OH → MGLYOX + HO_2 + H_2O	1.6E-12*EXP(305./temp)	Atkinson et al. (2006)
G43017	TrGC	MGLYOX + OH → .4 CH_3 + .6 $CH_3C(O)$ + 1.4 CO + H_2O	1.9E-12*EXP(575./temp)	Baeza-Romero et al. (2007), Atkinson et al. (2006)
G43020	TrGCN	$iC_3H_7ONO_2$ + OH → CH_3COCH_3 + NO_2	6.2E-13*EXP(-230./temp)	Wallington et al. (2018)
G43021	TrGCN	$CH_3COCH_2O_2$ + NO_3 → $CH_3C(O)$ + HCHO + NO_2	KRO2NO3	Rickard and Pascoe (2009)
G43022	TrGC	HYPROPO2 → CH_3CHO + HCHO + HO_2	k1_RO2sORO2	Rickard and Pascoe (2009)
G43023a	TrGC	HYPROPO2 + HO_2 → HYPROPO2H	k_RO2_HO2(temp,3)*(1.-r_CHOHCH2O2_OH)	Rickard and Pascoe (2009)

Table 1: Gas phase reactions (... continued)

#	labels	reaction	rate coefficient	reference
G43023b	TrGC	HYPROPO2 + HO_2 → CH_3CHO + HCHO + HO_2 + OH	k_RO2_HO2(temp,3)*r_CHOHCH2O2_OH	Rickard and Pascoe (2009)
G43024a	TrGCN	HYPROPO2 + NO → CH_3CHO + HCHO + HO_2 + NO_2	KRO2NO*(1.-alpha_AN(4,1,0,0,0, temp,cair))	Rickard and Pascoe (2009)
G43024b	TrGCN	HYPROPO2 + NO → PROPOLNO3	KRO2NO*alpha_AN(4,1,0,0,0,temp, cair)	Rickard and Pascoe (2009)
G43025	TrGCN	HYPROPO2 + NO_3 → CH_3CHO + HCHO + HO_2 + NO_2	KRO2NO3	Rickard and Pascoe (2009)
G43026a	TrGC	HYPROPO2H + OH → HYPROPO2	k_ROOHRO	Rickard and Pascoe (2009)
G43026b	TrGC	HYPROPO2H + OH → CH_3COCH_2OH + OH	(k_s*f_sOH*f_pCH2OH+k_t*f_ tOOH*f_pCH2OH)	Sander et al. (2019)
G43027	TrGCN	PRONO3BO2 + HO_2 → PR2O2HNO3	k_RO2_HO2(temp,3)	Rickard and Pascoe (2009)
G43028	TrGCN	PRONO3BO2 + NO → NOA + HO_2 + NO_2	KRO2NO	Rickard and Pascoe (2009)*
G43029	TrGCN	PRONO3BO2 + NO_3 → NOA + HO_2 + NO_2	KRO2NO3	Rickard and Pascoe (2009)
G43030a	TrGCN	PR2O2HNO3 + OH → PRONO3BO2	k_ROOHRO	Rickard and Pascoe (2009)
G43030b	TrGCN	PR2O2HNO3 + OH → NOA + OH	k_t*f_tOOH*f_CH2ONO2	Sander et al. (2019)
G43031	TrGCN	MGLYOX + NO_3 → $CH_3C(O)$ + CO + HNO_3	KNO3AL*2.4	Rickard and Pascoe (2009)
G43032	TrGCN	NOA + OH → MGLYOX + NO_2	(k_s*f_CO*f_ONO2+k_p*f_CO)	Sander et al. (2019)
G43033	TrGC	HOCH2COCHO + OH → .8609 HOCH2CO + .8609 CO + .1391 HCOCOCHO + .1391 HO_2	(1.9E-12*EXP(575./temp)+k_s*f_ sOH*f_CO)	Sander et al. (2019)
G43034	TrGCN	HOCH2COCHO + NO_3 → HOCH2CO + CO + HNO_3	KNO3AL*2.4	Sander et al. (2019)
G43035	TrGC	CH_3COCO_2H + OH → $CH_3C(O)$ + H_2O + CO_2	4.9E-14*EXP(276./temp)	Mellouki and Mu (2003), Sander et al. (2019)
G43036	TrGC	$HCOCOCH_2O_2$ → .6 HCOCO + .6 HCHO + .2 HCOCOCHO + .2 HOCH2COCHO	k1_RO2pORO2	Sander et al. (2019)
G43037	TrGCN	$HCOCOCH_2O_2$ + NO → HCOCO + HCHO + NO_2	KRO2NO	Sander et al. (2019)*
G43038a	TrGC	$HCOCOCH_2O_2$ + HO_2 → $HCOCOCH_2OOH$	k_RO2_HO2(temp,3)*r_COCH2O2_OOH	Sander et al. (2019)
G43038b	TrGC	$HCOCOCH_2O_2$ + HO_2 → HCOCO + HCHO + OH	k_RO2_HO2(temp,3)*r_COCH2O2_OH	Sander et al. (2019)
G43039	TrGCN	$HCOCOCH_2O_2$ + NO_3 → HCOCO + HCHO + NO_2	KRO2NO3	Sander et al. (2019)
G43040a	TrGC	$HCOCOCH_2OOH$ + OH → $HOOCH_2CO_3$ + CO + H_2O	k_t*f_CO*f_O	Sander et al. (2019)*
G43040b	TrGC	$HCOCOCH_2OOH$ + OH → HCOCOCHO + H_2O + OH	k_s*f_sOOH*f_CO	Sander et al. (2019)*
G43040c	TrGC	$HCOCOCH_2OOH$ + OH → $HCOCOCH_2O_2$ + H_2O	k_ROOHRO	Sander et al. (2019)
G43041	TrGCN	$HCOCOCH_2OOH$ + NO_3 → $HOOCH_2CO_3$ + CO + HNO_3	KNO3AL*2.4	Sander et al. (2019)
G43042	TrGC	HOCH2COCH2O2 → HCHO + HOCH2CO	k1_RO2pORO2	Sander et al. (2019)
G43043a	TrGC	HOCH2COCH2O2 + HO_2 → HOCH2COCH2OOH	k_RO2_HO2(temp,3)*r_COCH2O2_OOH	Sander et al. (2019)
G43043b	TrGC	HOCH2COCH2O2 + HO_2 → HCHO + HOCH2CO + OH	k_RO2_HO2(temp,3)*r_COCH2O2_OH	Sander et al. (2019)
G43044	TrGCN	HOCH2COCH2O2 + NO → HCHO + HOCH2CO + NO_2	KRO2NO	Sander et al. (2019)*

Table 1: Gas phase reactions (... continued)

#	labels	reaction	rate coefficient	reference
G43045a	TrGC	HOCH2COCH2OOH + OH → HOCH2COCHO + OH	k_s*f_sOOH*f_CO	Sander et al. (2019)
G43045b	TrGC	HOCH2COCH2OOH + OH → HOCH2COCH2O2	k_ROOHRO	Sander et al. (2019)
G43045c	TrGC	HOCH2COCH2OOH + OH → $HCOCOCH_2OOH$ + HO_2	1.60E-12*EXP(305./temp)	Sander et al. (2019)*
G43046	TrGC	CH3CHCO + OH → .72 CO + .72 CH_3CHO + .72 HO_2 + .21 CH_3COCO_2H + .07 CH_3CHO + .07 HO_2 + .07 CO_2	7.6E-11	Hatakeyama et al. (1985), Sander et al. (2019)
G43047	TrGCN	PROPOLNO3 + OH → CH_3COCH_2OH + NO_2	k_t*f_ONO2*f_pCH2OH+k_s*f_sOH*f_CH2ONO2	Sander et al. (2019)
G43048	TrGCN	$CH_3COCH_2O_2$ + NO_2 → $CH_3COCH_2OONO_2$	2.3E-12*EXP(300./temp)	Tyndall et al. (2001a)*
G43049	TrGCN	$CH_3COCH_2OONO_2$ → $CH_3COCH_2O_2$ + NO_2	1.9E16*EXP(-10830./temp)	Sehested et al. (1998)*
G43050	TrGCN	$CH_3COCH_2OONO_2$ + OH → MGLYOX + NO_3 + H_2O	9.50E-13*EXP(-650./temp)*f_CO	Sander et al. (2019)*
G43051a	TrGC	C_3H_7OOH + OH → $C_3H_7O_2$ + H_2O	k_ROOHRO	Sander et al. (2019)
G43051b	TrGC	C_3H_7OOH + OH → C_2H_5CHO + H_2O + OH	k_s*f_sOOH	Sander et al. (2019)
G43051c	TrGC	C_3H_7OOH + OH → C_2H_5CHO + HO_2 + H_2O	k_s*f_pCH2OH	Sander et al. (2019)*
G43052	TrGC	C_2H_5CHO + OH → $C_2H_5CO_3$ + H_2O	4.9E-12*EXP(405./temp)	Atkinson et al. (2006)*
G43053	TrGCN	C_2H_5CHO + NO_3 → $C_2H_5CO_3$ + HNO_3	6.3E-15	Atkinson et al. (2006)
G43054a	TrGC	$C_2H_5CO_3$ → $C_2H_5O_2$ + CO_2	k1_RO2RCO3*0.9	Sander et al. (2019)
G43054b	TrGC	$C_2H_5CO_3$ → $C_2H_5CO_2H$	k1_RO2RCO3*0.1	Sander et al. (2019)
G43055a	TrGC	$C_2H_5CO_3$ + HO_2 → $C_2H_5O_2$ + CO_2 + OH	KAPHO2*r_CO3_OH	Sander et al. (2019), Groß et al. (2014)
G43055b	TrGC	$C_2H_5CO_3$ + HO_2 → $C_2H_5CO_3H$	KAPHO2*r_CO3_OOH	Sander et al. (2019), Groß et al. (2014)
G43055c	TrGC	$C_2H_5CO_3$ + HO_2 → $C_2H_5CO_2H$ + O_3	KAPHO2*r_CO3_O3	Sander et al. (2019), Groß et al. (2014)
G43056	TrGCN	$C_2H_5CO_3$ + NO → NO_2 + $C_2H_5O_2$ + CO_2	KAPNO	Rickard and Pascoe (2009)
G43057	TrGCN	$C_2H_5CO_3$ + NO_2 → PPN	k_CH3CO3_NO2	Rickard and Pascoe (2009)
G43058	TrGCN	PPN → $C_2H_5CO_3$ + NO_2	k_PAN_M	Rickard and Pascoe (2009)
G43059	TrGC	$C_2H_5CO_2H$ + OH → CH_3CHO + CO_2 + H_2O	k_CO2H+k_p+k_s*f_CO2H	Sander et al. (2019)*
G43060a	TrGC	$C_2H_5CO_3H$ + OH → $C_2H_5CO_3$ + H_2O	k_ROOHRO	Sander et al. (2019)
G43060b	TrGC	$C_2H_5CO_3H$ + OH → CH_3CHO + CO_2 + H_2O	k_s*f_CO2H+k_p	Sander et al. (2019)*
G43061	TrGCN	PPN + OH → CH_3CHO + CO_2 + NO_2 + H_2O	k_s*f_cpan+k_p	Sander et al. (2019)*
G43062	TrGC	CH_3COCO_3H + OH → CH_3COCO_3 + H_2O	k_ROOHRO	Sander et al. (2019)
G43063a	TrGC	CH_3COCO_3 + HO_2 → $CH_3C(O)$ + CO_2 + OH	KAPHO2*r_CO3_OH	Sander et al. (2019)
G43063b	TrGC	CH_3COCO_3 + HO_2 → CH_3COCO_3H	KAPHO2*(r_CO3_OOH+r_CO3_O3)	Sander et al. (2019)
G43064	TrGCN	CH_3COCO_3 + NO → $CH_3C(O)$ + CO_2 + NO_2	KAPNO	Sander et al. (2019)
G43065	TrGCN	CH_3COCO_3 + NO_2 → $CH_3C(O)$ + CO_2 + NO_3	k_CH3CO3_NO2	Sander et al. (2019)*

Table 1: Gas phase reactions (... continued)

#	labels	reaction	rate coefficient	reference
G43066	TrGCN	$CH_3COCO_3 + NO_3 \rightarrow CH_3C(O)OO + CO_2 + NO_2$	KRO2NO3*1.74	Sander et al. (2019)
G43067	TrGC	$CH_3COCO_3 \rightarrow CH_3C(O)OO + CO_2$	k1_RO2RCO3	Sander et al. (2019)
G43068	TrGC	$HCOCOCHO + OH \rightarrow 3\ CO + HO_2$	2.*k_t*f_CO*f_O	Sander et al. (2019)
G43069	TrGC	$IPROPOL + OH \rightarrow CH_3COCH_3 + HO_2 + H_2O$	2.6E-12*EXP(200./temp)	Atkinson et al. (2006)
G43070a	TrGC	$NPROPOL + OH \rightarrow C_2H_5CHO + HO_2 + H_2O$	4.6E-12*EXP(70./temp)*(k_s*f_sOH/(k_p+k_s*f_pCH2OH+k_s*f_sOH))	Atkinson et al. (2006), Sander et al. (2019)*
G43070b	TrGC	$NPROPOL + OH \rightarrow HYPROPO2 + H_2O$	4.6E-12*EXP(70./temp)*((k_p+k_s*f_pCH2OH)/(k_p+k_s*f_pCH2OH+k_s*f_sOH))	Atkinson et al. (2006), Sander et al. (2019)*
G43071a	TrGC	$CH_2CHCH_2OH + OH \rightarrow HCOOH + OH + CH_3CHO$	k_CH2CHOH_OH_HCOOH	Sander et al. (2019), So et al. (2014)*
G43072	TrGC	$CH_2CHCH_2OH + HCOOH \rightarrow C_2H_5CHO + HCOOH$	k_CH2CHOH_HCOOH	Sander et al. (2019), da Silva (2010)*
G43073	TrGC	$C_2H_5CHO + HCOOH \rightarrow CH_2CHCH_2OH + HCOOH$	k_ALD_HCOOH	Sander et al. (2019), da Silva (2010)*
G43074	TrGC	$HCOCOCH_2OOH + OH \rightarrow HCOCO + CO + HO_2 + OH$	k_s*f_sOOH*f_CO+k_ROOHRO	Sander et al. (2019)*
G43075a	TrGC	$CH_3COCHOHOH + OH \rightarrow CH_3C(O) + HCOOH + H_2O$	2.0 * k_rohro	see note*
G43075b	TrGC	$CH_3COCHOHOH + OH \rightarrow CH_3COCO_2H + H_2O$	k_t*f_toh*f_toh*f_co	see note*
G43202	TrGTerC	HCOCH2CHO + OH → HCOCH2CO3	4.29E-11	Rickard and Pascoe (2009)
G43203	TrGTerCN	HCOCH2CHO + NO3 → HCOCH2CO3 + HNO3	2.*KNO3AL*2.4	Rickard and Pascoe (2009)
G43204a	TrGTerC	HCOCH2CO3 → $HCOCH_2O_2 + CO_2$	k1_RO2RCO3*0.9	Sander et al. (2019)
G43204b	TrGTerC	HCOCH2CO3 → HCOCH2CO2H	k1_RO2RCO3*0.1	Sander et al. (2019)
G43205	TrGTerCN	HCOCH2CO3 + NO → $HCOCH_2O_2 + CO_2 + NO_2$	KAPNO	Rickard and Pascoe (2009)
G43206	TrGTerCN	HCOCH2CO3 + NO2 → C3PAN2	k_CH3CO3_NO2	Rickard and Pascoe (2009)
G43207a	TrGTerC	HCOCH2CO3 + HO2 → HCOCH2CO3H	KAPHO2*r_CO3_OOH	Rickard and Pascoe (2009)
G43207b	TrGTerC	HCOCH2CO3 + HO2 → HCOCH2CO2H + O3	KAPHO2*r_CO3_O3	Rickard and Pascoe (2009)
G43207c	TrGTerC	HCOCH2CO3 + HO2 → $HCOCH_2O_2 + CO_2 + OH$	KAPHO2*r_CO3_OH	Rickard and Pascoe (2009)
G43210	TrGTerCN	C3PAN2 → HCOCH2CO3 + NO2	k_PAN_M	Rickard and Pascoe (2009)
G43211	TrGTerCN	C3PAN2 + OH → GLYOX + CO + NO2	2.10E-11	Rickard and Pascoe (2009)
G43212	TrGTerC	HCOCH2CO2H + OH → $HCOCH_2O_2 + CO_2$	2.14E-11	Rickard and Pascoe (2009)
G43213a	TrGTerC	$HOC_2H_4CO_3 \rightarrow HOCH_2CH_2O_2 + CO_2$	k1_RO2RCO3*0.9	Sander et al. (2019)
G43213b	TrGTerC	$HOC_2H_4CO_3 \rightarrow$ HOC2H4CO2H	k1_RO2RCO3*0.1	Sander et al. (2019)
G43214	TrGTerCN	$HOC_2H_4CO_3 + NO \rightarrow HOCH_2CH_2O_2 + CO_2 + NO_2$	KAPNO	Rickard and Pascoe (2009)
G43215a	TrGTerC	$HOC_2H_4CO_3 + HO_2 \rightarrow$ HOC2H4CO3H	KAPHO2*r_CO3_OOH	Rickard and Pascoe (2009)
G43215b	TrGTerC	$HOC_2H_4CO_3 + HO_2 \rightarrow HOCH_2CH_2O_2 + CO_2 + OH$	KAPHO2*r_CO3_OH	Rickard and Pascoe (2009)

Table 1: Gas phase reactions (... continued)

#	labels	reaction	rate coefficient	reference
G43215c	TrGTerC	$HOC_2H_4CO_3 + HO_2 \rightarrow$ HOC2H4CO2H + O_3	KAPHO2*r_CO3_O3	Rickard and Pascoe (2009)
G43218	TrGTerCN	$HOC_2H_4CO_3 + NO_2 \rightarrow C_3$PAN1	k_CH3CO3_NO2	Rickard and Pascoe (2009)
G43219	TrGTerC	HOC2H4CO2H + OH $\rightarrow HOCH_2CH_2O_2 + CO_2$	1.39E-11	Rickard and Pascoe (2009)
G43220	TrGTerC	HOC2H4CO3H + OH $\rightarrow HOC_2H_4CO_3$	1.73E-11	Rickard and Pascoe (2009)
G43221	TrGTerCN	C_3PAN1 $\rightarrow HOC_2H_4CO_3 + NO_2$	k_PAN_M	Rickard and Pascoe (2009)
G43222	TrGTerCN	C_3PAN1 + OH $\rightarrow HOCH_2CHO + CO + NO_2$	4.51E-12	Rickard and Pascoe (2009)
G43223	TrGTerC	HCOCH2CO3H + OH $\rightarrow HCOCH_2O_2 + CO_2 + H_2O$	2.49E-11	Rickard and Pascoe (2009)*
G43415	TrGAroC	C3DIALOOH + OH $\rightarrow$ HCOCOCHO + OH	1.44E-10	Rickard and Pascoe (2009)
G43418a	TrGAroC	C3DIALO2 + $HO_2 \rightarrow$ C3DIALOOH	k_RO2_HO2(temp,3)*(r_CO3_OOH+r_CO3_O3)	Rickard and Pascoe (2009)
G43418b	TrGAroC	C3DIALO2 + $HO_2 \rightarrow$ GLYOX + CO + HO_2 + OH	k_RO2_HO2(temp,3)*r_CO3_OH	Rickard and Pascoe (2009)
G43419	TrGAroCN	C3DIALO2 + NO $\rightarrow$ GLYOX + CO + $HO_2 + NO_2$	KRO2NO	Rickard and Pascoe (2009)*
G43420	TrGAroCN	C3DIALO2 + $NO_3 \rightarrow$ GLYOX + CO + $HO_2 + NO_2$	KRO2NO3	Rickard and Pascoe (2009)*
G43421	TrGAroC	C3DIALO2 $\rightarrow$ GLYOX + CO + HO_2	k1_RO2sORO2	Rickard and Pascoe (2009)*
G43422a	TrGAroC	HCOCOHCO3 + $HO_2 \rightarrow$ GLYOX + $CO_2 + HO_2$ + OH	KAPHO2*r_CO3_OH	Rickard and Pascoe (2009)
G43422b	TrGAroC	HCOCOHCO3 + $HO_2 \rightarrow$ HCOCOHCO3H	KAPHO2*(r_CO3_OOH+r_CO3_O3)	Rickard and Pascoe (2009)
G43424	TrGAroCN	HCOCOHCO3 + NO $\rightarrow$ GLYOX + $CO_2 + HO_2 + NO_2$	KAPNO	Rickard and Pascoe (2009)
G43425	TrGAroCN	HCOCOHCO3 + $NO_2 \rightarrow$ HCOCOHPAN	k_CH3CO3_NO2	Rickard and Pascoe (2009)
G43426	TrGAroCN	HCOCOHCO3 + $NO_3 \rightarrow$ GLYOX + $CO_2 + HO_2 + NO_2$	KRO2NO3*1.74	Rickard and Pascoe (2009)
G43427	TrGAroC	HCOCOHCO3 $\rightarrow$ GLYOX + $CO_2 + HO_2$	k1_RO2RCO3	Rickard and Pascoe (2009)
G43428	TrGAroC	METACETHO + OH $\rightarrow CH_3C(O) + CO_2$	9.82E-11	Rickard and Pascoe (2009)
G43442	TrGAroCN	HCOCOHPAN + OH $\rightarrow$ GLYOX + CO + NO_2	6.97E-11	Rickard and Pascoe (2009)
G43443	TrGAroCN	HCOCOHPAN $\rightarrow$ HCOCOHCO3 + NO_2	k_PAN_M	Rickard and Pascoe (2009)
G43444	TrGAroC	C32OH13CO + OH $\rightarrow$ HCOCOHCO3	1.36E-10	Rickard and Pascoe (2009)
G43446	TrGAroC	HCOCOHCO3H + OH $\rightarrow$ HCOCOHCO3	7.33E-11	Rickard and Pascoe (2009)
G44000	TrGC	C_4H_{10} + OH $\rightarrow LC_4H_9O_2 + H_2O$	2.03E-17*temp*temp*EXP(78./temp)	Atkinson et al. (2006)*
G44001a	TrGC	$LC_4H_9O_2 \rightarrow C_3H_7CHO + HO_2$	(k1_RO2pRO2*0.1273+k1_RO2sRO2*0.8727)*0.1273	Rickard and Pascoe (2009), Sander et al. (2019)
G44001b	TrGC	$LC_4H_9O_2 \rightarrow$ .636 MEK + .636 HO_2 + .364 CH_3CHO + .364 $C_2H_5O_2$	(k1_RO2pRO2*0.1273+k1_RO2sRO2*0.8727)*0.8727	Rickard and Pascoe (2009), Sander et al. (2019)*
G44002	TrGC	$LC_4H_9O_2 + HO_2 \rightarrow LC_4H_9OOH$	k_RO2_HO2(temp,4)	Rickard and Pascoe (2009)
G44003a	TrGCN	$LC_4H_9O_2$ + NO $\rightarrow NO_2 + C_3H_7CHO + HO_2$	KRO2NO*(1.-(0.1273*alpha_AN(4,1,0,0,0,temp,cair)+0.8727*alpha_AN(4,2,0,0,0,temp,cair)))*0.1273	Rickard and Pascoe (2009), Sander et al. (2019)

Table 1: Gas phase reactions (... continued)

#	labels	reaction	rate coefficient	reference
G44003b	TrGCN	$LC_4H_9O_2 + NO \rightarrow NO_2 + .636\ MEK + .636\ HO_2 + .364\ CH_3CHO + .364\ C_2H_5O_2$	KRO2NO*(1.-(0.1273*alpha_AN(4,1,0,0,0,temp,cair)+0.8727*alpha_AN(4,2,0,0,0,temp,cair)))*0.8727	Rickard and Pascoe (2009), Sander et al. (2019)
G44003c	TrGCN	$LC_4H_9O_2 + NO \rightarrow$ LC4H9NO3	KRO2NO*(0.1273*alpha_AN(4,1,0,0,0,temp,cair)+0.8727*alpha_AN(4,2,0,0,0,temp,cair))	Rickard and Pascoe (2009)*
G44004a	TrGCN	$LC_4H_9O_2 + NO_3 \rightarrow NO_2 + C_3H_7CHO + HO_2$	KRO2NO3*0.1273	Rickard and Pascoe (2009), Sander et al. (2019)
G44004b	TrGCN	$LC_4H_9O_2 + NO_3 \rightarrow NO_2 + .636\ MEK + .636\ HO_2 + .364\ CH_3CHO + .364\ C_2H_5O_2$	KRO2NO3*0.8727	Rickard and Pascoe (2009), Sander et al. (2019)
G44005a	TrGC	$LC_4H_9OOH + OH \rightarrow LC_4H_9O_2 + H_2O$	k_ROOHRO	Sander et al. (2019)
G44005b	TrGC	$LC_4H_9OOH + OH \rightarrow C_3H_7CHO + H_2O + OH$	k_s*f_tOOH*f_alk*(k_p/(k_p+k_s))	Sander et al. (2019)
G44005c	TrGC	$LC_4H_9OOH + OH \rightarrow MEK + H_2O + OH$	k_t*f_tOOH*f_alk*(k_s/(k_p+k_s))	Sander et al. (2019)
G44006a	TrGC	$iC_4H_{10} + OH \rightarrow TC_4H_9O_2 + H_2O$	1.17E-17*temp*temp*EXP(213./temp)*k_t/(3.*k_p+k_t)	Atkinson (2003)
G44006b	TrGC	$iC_4H_{10} + OH \rightarrow IC_4H_9O_2 + H_2O$	1.17E-17*temp*temp*EXP(213./temp)*3.*k_p/(3.*k_p+k_t)	Atkinson (2003)
G44007	TrGC	$TC_4H_9O_2 \rightarrow CH_3COCH_3 + CH_3$	k1_RO2tRO2	Rickard and Pascoe (2009), Sander et al. (2019)
G44008	TrGC	$TC_4H_9O_2 + HO_2 \rightarrow TC_4H_9OOH$	k_RO2_HO2(temp,4)	Rickard and Pascoe (2009)
G44009a	TrGCN	$TC_4H_9O_2 + NO \rightarrow NO_2 + CH_3COCH_3 + CH_3$	KRO2NO*(1.-alpha_AN(4,3,0,0,0,temp,cair))	Rickard and Pascoe (2009), Sander et al. (2019)
G44009b	TrGCN	$TC_4H_9O_2 + NO \rightarrow$ TC4H9NO3	KRO2NO*alpha_AN(4,3,0,0,0,temp,cair)	Rickard and Pascoe (2009)
G44010a	TrGC	$TC_4H_9OOH + OH \rightarrow TC_4H_9O_2 + H_2O$	k_ROOHRO	Sander et al. (2019)
G44010b	TrGC	$TC_4H_9OOH + OH \rightarrow CH_3COCH_3 + HCHO + OH + H_2O$	3.*k_p*f_tCH2OH	Sander et al. (2019)*
G44011	TrGCN	$TC4H9NO3 + OH \rightarrow CH_3COCH_3 + HCHO + NO_2 + H_2O$	3.*k_p*f_CH2ONO2	Sander et al. (2019)*
G44012	TrGC	$IC_4H_9O_2 \rightarrow$ IPRCHO	k1_RO2sRO2	Rickard and Pascoe (2009), Sander et al. (2019)
G44013	TrGC	$IC_4H_9O_2 + HO_2 \rightarrow IC_4H_9OOH$	k_RO2_HO2(temp,4)	Rickard and Pascoe (2009)
G44014a	TrGCN	$IC_4H_9O_2 + NO \rightarrow NO_2 + IPRCHO$	KRO2NO*(1.-alpha_AN(4,2,0,0,0,temp,cair))	Rickard and Pascoe (2009), Sander et al. (2019)
G44014b	TrGCN	$IC_4H_9O_2 + NO \rightarrow$ IC4H9NO3	KRO2NO*alpha_AN(4,2,0,0,0,temp,cair)	Rickard and Pascoe (2009)
G44015a	TrGC	$IC_4H_9OOH + OH \rightarrow IC_4H_9O_2 + H_2O$	k_ROOHRO	Sander et al. (2019)

Table 1: Gas phase reactions (... continued)

#	labels	reaction	rate coefficient	reference
G44015b	TrGC	$IC_4H_9OOH + OH \rightarrow IPRCHO + OH + H_2O$	k_s*f_sOOH+2.*k_s+k_t*f_pCH2OH	Sander et al. (2019)*
G44016	TrGCN	$IC4H9NO3 + OH \rightarrow IPRCHO + NO_2 + H_2O$	k_s*f_ONO2+2.*k_p+k_t*f_CH2ONO2	Sander et al. (2019)*
G44017	TrGC	$MVK + O_3 \rightarrow .87\ MGLYOX + .5481\ CO + .1392\ HO_2 + .1392\ OH + .3219\ CH_2OO + .13\ HCHO + .04680\ OH + .04680\ CO + .07280\ CH_3C(O) + .026\ CH_3CHO + .026\ CO_2 + .026\ HCHO + .026\ HO_2 + .02402\ MGLYOX + .02402\ H_2O_2 + .00718\ CH_3COCO_2H$	8.5E-16*EXP(-1520./temp)	Sander et al. (2019)
G44018	TrGC	$MVK + OH \rightarrow LHMVKABO2$	2.6E-12*EXP(610./temp)	Sander et al. (2019), Atkinson et al. (2006)*
G44019	TrGC	$MEK + OH \rightarrow LMEKO2 + H_2O$	1.5E-12*EXP(-90./temp)	Atkinson et al. (2006), Sander et al. (2019)*
G44020	TrGC	$LMEKO2 + HO_2 \rightarrow LMEKOOH$	k_RO2_HO2(temp,4)	Sander et al. (2019)
G44021a	TrGCN	$LMEKO2 + NO \rightarrow .62\ CH_3CHO + .62\ CH_3C(O) + .38\ HCHO + .38\ CO_2 + .38\ HOCH_2CH_2O_2 + NO_2$	KRO2NO*(1.-(.62*alpha_AN(4,2,1,0,0,temp,cair)+.38*alpha_AN(4,1,0,1,0,temp,cair)))	Sander et al. (2019)*
G44021b	TrGCN	$LMEKO2 + NO \rightarrow LMEKNO3$	KRO2NO*(.62*alpha_AN(4,2,1,0,0,temp,cair)+.38*alpha_AN(4,1,0,1,0,temp,cair))	Sander et al. (2019)
G44022a	TrGC	$LMEKOOH + OH \rightarrow LMEKO2 + H_2O$	k_ROOHRO	Sander et al. (2019)
G44022b	TrGC	$LMEKOOH + OH \rightarrow .62\ BIACET + .38\ HCHO + .38\ CO_2 + .38\ HOCH_2CH_2O_2 + H_2O + OH$	(.62*k_t*f_tOOH*f_CO+.38*k_s*f_sOOH)	Sander et al. (2019)
G44023a	TrGCN	$LC4H9NO3 + OH \rightarrow MEK + NO_2 + H_2O$	(k_t*f_ONO2*f_alk+k_p*f_alk+k_s*f_CH2ONO2+k_p)*(k_s/(k_p+k_s))	Sander et al. (2019)*
G44023b	TrGCN	$LC4H9NO3 + OH \rightarrow C_3H_7CHO + NO_2 + H_2O$	(k_p+k_s*(1.+f_CH2ONO2+f_ONO2)*f_alk)*(k_p/(k_p+k_s))	Sander et al. (2019)*
G44024	TrGCN	$MPAN + OH \rightarrow CH_3COCH_2OH + CO + NO_2$	3.2E-11	Orlando et al. (2002)
G44025	TrGCN	$MPAN \rightarrow MACO3 + NO_2$	k_PAN_M	see note*
G44026	TrGC	$LMEKO2 \rightarrow .538\ HCHO + .538\ CO_2 + .459\ HOCH_2CH_2O_2 + .079\ C_2H_5O_2 + .462\ CH_3C(O) + .462\ CH_3CHO$	(.62*k1_RO2sORO2+.38*k1_RO2pORO2)	Rickard and Pascoe (2009)*
G44027	TrGC	$MACR + OH \rightarrow .45\ MACO3 + .55\ MACRO2$	8.E-12*EXP(380./temp)	Orlando et al. (1999b), Sander et al. (2019)
G44028	TrGC	$MACR + O_3 \rightarrow .5481\ CO + .1392\ HO_2 + .1392\ OH + .3219\ CH_2OO + .87\ MGLYOX + .13\ HCHO + .13\ OH + .065\ HCOCOCH_2O_2 + .065\ CO + .065\ CH_3C(O)$	1.36E-15*EXP(-2112./temp)	Sander et al. (2019)

Table 1: Gas phase reactions (... continued)

#	labels	reaction	rate coefficient	reference
G44029	TrGCN	MACR + NO_3 → MACO3 + HNO_3	KNO3AL*2.0	Rickard and Pascoe (2009)
G44030a	TrGC	MACO3 → $CH_3C(O)$ + HCHO + CO_2	k1_RO2RCO3*0.9	Sander et al. (2019)
G44030b	TrGC	MACO3 → MACO2H	k1_RO2RCO3*0.1	Sander et al. (2019)
G44031a	TrGC	MACO3 + HO_2 → MACO2 + OH	KAPHO2*r_CO3_OH	Sander et al. (2019)
G44031b	TrGC	MACO3 + HO_2 → MACO3H	KAPHO2*r_CO3_OOH	Sander et al. (2019)
G44031c	TrGC	MACO3 + HO_2 → MACO2H + O_3	KAPHO2*r_CO3_O3	Sander et al. (2019)
G44032	TrGCN	MACO3 + NO → MACO2 + NO_2	8.70E-12*EXP(290./temp)	Sander et al. (2019)
G44033	TrGCN	MACO3 + NO_2 → MPAN	k_CH3CO3_NO2	Rickard and Pascoe (2009)
G44034	TrGCN	MACO3 + NO_3 → MACO2 + NO_2	KRO2NO3*1.74	Sander et al. (2019)
G44035	TrGC	MACRO2 → .7 CH_3COCH_2OH + .7 HCHO + .7 HO_2 + .3 MACROH	k1_RO2tORO2	Rickard and Pascoe (2009)*
G44036a	TrGC	MACRO2 + HO_2 → MACRO + OH	k_RO2_HO2(temp,4)*r_COCH2O2_OH	Sander et al. (2019)
G44036b	TrGC	MACRO2 + HO_2 → MACROOH	k_RO2_HO2(temp,4)*r_COCH2O2_OOH	Sander et al. (2019)
G44037a	TrGCN	MACRO2 + NO → MACRO + NO_2	KRO2NO*(1.-alpha_AN(6,3,1,0,0, temp,cair))	Sander et al. (2019)
G44037b	TrGCN	MACRO2 + NO → MACRNO3	KRO2NO*alpha_AN(6,3,1,0,0,temp, cair)	Sander et al. (2019)
G44038	TrGCN	MACRO2 + NO_3 → MACRO + NO_2	KRO2NO3	Sander et al. (2019)
G44039a	TrGC	MACROOH + OH → MACRO2	k_ROOHRO	Sander et al. (2019)
G44039b	TrGC	MACROOH + OH → CO + CH_3COCH_2OH + OH	k_t*f_O*f_tCH2OH*f_alk	Sander et al. (2019)
G44039c	TrGC	MACROOH + OH → CO + MGLYOX + HO_2	(k_s*f_sOH*f_pCH2OH + k_ROHRO)	Sander et al. (2019)
G44040	TrGC	MACROH + OH → CH_3COCH_2OH + CO + HO_2	k_t*f_O*f_tCH2OH*f_alk	Sander et al. (2019)
G44041	TrGC	MACRO → .885 CH_3COCH_2OH + .885 CO + .115 MGLYOX + .115 HCHO + HO_2	KDEC	Sander et al. (2019)
G44042	TrGC	MACO2H + OH → CH_3COCH_2OH + HO_2 + CO_2	((k_adt+k_adp)*a_CO2H+k_CO2H)	Sander et al. (2019)
G44043a	TrGC	MACO3H + OH → CH_3COCH_2OH + CO_2 + OH	(k_adt+k_adp)*a_CO2H	Sander et al. (2019)
G44043b	TrGC	MACO3H + OH → MACO3	k_ROOHRO	Sander et al. (2019)
G44044	TrGC	LHMVKABO2 → .024 CO2H3CHO + .072 MGLYOX + .072 HO_2 + .072 HCHO + .5280 $CH_3C(O)$ + .5280 $HOCH_2CHO$ + .176 BIACETOH + .2 HO12CO3C4	(.12*k1_RO2pORO2+.88*k1_RO2sORO2)	Sander et al. (2019)
G44045a	TrGC	LHMVKABO2 + HO_2 → OH + $HOCH_2CHO$ + $CH_3C(O)$	k_RO2_HO2(temp,4)*.88*r_COCH2O2_ OH	Sander et al. (2019)
G44045b	TrGC	LHMVKABO2 + HO_2 → LHMVKABOOH	k_RO2_HO2(temp,4)*(.12+.88*r_ COCH2O2_OOH)	Sander et al. (2019)

Table 1: Gas phase reactions (... continued)

#	labels	reaction	rate coefficient	reference
G44046a	TrGCN	LHMVKABO2 + NO → .12 MGLYOX + .12 HO_2 + .88 $HOCH_2CHO$ + .88 $CH_3C(O)$ + .12 HCHO + NO_2	KRO2NO*(1.-(.12*alpha_AN(6,1,0,1,0,temp,cair)+.88*alpha_AN(6,2,1,0,0,temp,cair)))	Sander et al. (2019)
G44046b	TrGCN	LHMVKABO2 + NO → MVKNO3	KRO2NO*(.12*alpha_AN(6,1,0,1,0,temp,cair)+.88*alpha_AN(6,2,1,0,0,temp,cair))	Sander et al. (2019)*
G44047	TrGCN	LHMVKABO2 + NO_3 → .12 MGLYOX + .12 HO_2 + .88 $HOCH_2CHO$ + .88 $CH_3C(O)$ + .12 HCHO + .12 HO_2 + NO_2	KRO2NO3	Sander et al. (2019)
G44048a	TrGC	LHMVKABOOH + OH → LHMVKABO2	k_ROOHRO	Sander et al. (2019)
G44048b	TrGC	LHMVKABOOH + OH → .12 CO2H3CHO + .88 BIACETOH + OH	(.12*k_s*f_sOOH*f_pCH2OH+.88*k_t*f_tOOH*f_pCH2OH*f_CO)	Sander et al. (2019)
G44049a	TrGC	CO2H3CHO + OH → CO2H3CO3	k_t*f_O*f_alk	Sander et al. (2019)
G44049b	TrGC	CO2H3CHO + OH → $CH_3COCOCHO$ + HO_2 + H_2O	k_t*f_CO*f_tOH*f_CHO	Sander et al. (2019)
G44050	TrGCN	CO2H3CHO + NO_3 → CO2H3CO3 + HNO_3	KNO3AL*4.0	Rickard and Pascoe (2009)
G44051	TrGC	CO2H3CO3 → MGLYOX + HO_2 + CO_2	k1_RO2RCO3	Sander et al. (2019)
G44052a	TrGC	CO2H3CO3 + HO_2 → OH + MGLYOX + HO_2 + CO_2	KAPHO2*r_CO3_OH	Sander et al. (2019)
G44052b	TrGC	CO2H3CO3 + HO_2 → CO2H3CO2H + O_3	KAPHO2*r_CO3_O3	Sander et al. (2019)
G44052c	TrGC	CO2H3CO3 + HO_2 → CO2H3CO3H	KAPHO2*r_CO3_OOH	Sander et al. (2019)
G44053	TrGCN	CO2H3CO3 + NO → MGLYOX + HO_2 + NO_2 + CO_2	KAPNO	Sander et al. (2019)
G44054	TrGCN	CO2H3CO3 + NO_3 → MGLYOX + HO_2 + NO_2 + CO_2	KRO2NO3*1.74	Sander et al. (2019)
G44055a	TrGC	CO2H3CO3H + OH → CO2H3CO3	k_ROOHRO	Sander et al. (2019)
G44055b	TrGC	CO2H3CO3H + OH → $CH_3C(O)$ + CO + CO_2 + OH	(k_t*f_CO2H*f_CO*f_tOH)	Sander et al. (2019)
G44056	TrGC	CO2H3CO2H + OH → CH3COCOCO2H + HO_2	k_t*f_CO2H*f_CO*f_tOH+k_CO2H	Sander et al. (2019)
G44057a	TrGC	HO12CO3C4 + OH → BIACETOH + HO_2	k_t*f_tOH*f_alk*f_CO	Sander et al. (2019)
G44057b	TrGC	HO12CO3C4 + OH → CO2H3CHO + HO_2	k_s*f_sOH*f_alk	Sander et al. (2019)
G44058	TrGC	MACO2 → .65 CH_3 + .65 CO + .65 HCHO + .35 OH + .35 $CH_3COCH_2O_2$ + CO_2	KDEC	Sander et al. (2019)
G44059	TrGC	LHMVKABO2 → .88 MGLYOX + .88 HCHO + .12 HOOCH2CHO + .12 $CH_3C(O)$ + OH	k_hsd	Sander et al. (2019)
G44060	TrGC	MACRO2 → MGLYOX + HCHO + OH	k_hsb	Sander et al. (2019)
G44061a	TrGCN	MVKNO3 + OH → MGLYOX + CO_2 + HO_2 + NO_2 + H_2O	k_s*f_sOOH*f_CH2ONO2+k_ROHRO	Sander et al. (2019)*
G44061b	TrGCN	MVKNO3 + OH → BIACETOH + NO_2 + H_2O	k_t*f_ONO2*f_CO*f_pCH2OH	Sander et al. (2019)*

Table 1: Gas phase reactions (... continued)

#	labels	reaction	rate coefficient	reference
G44062a	TrGCN	MACRNO3 + OH → CH_3COCH_2OH + CO_2 + NO_2 + H_2O	k_t*f_O*f_CH2ONO2	Sander et al. (2019)*
G44062b	TrGCN	MACRNO3 + OH → MGLYOX + CO + NO_2 + H_2O	k_ROHRO+k_s*f_sOOH*f_CH2ONO2	Sander et al. (2019)*
G44063	TrGC	MACRO2 → CH_3COCH_2OH + OH + CO	k_14hsal	Sander et al. (2019)
G44064	TrGC	EZCH3CO2CHCHO → .9 $CH_3COCHCO$ + .1 $CH_3C(O)$ + .01 GLYOX + .18 CO + .09 HO_2 + OH	k_15hs24vynal	Sander et al. (2019)
G44065	TrGC	EZCH3CO2CHCHO + HO_2→ $CH_3COOHCHCHO$	k_RO2_HO2(temp,4)	Sander et al. (2019)
G44066	TrGCN	EZCH3CO2CHCHO + NO → CH_3COCHO_2CHO + NO_2	KRO2NO	Sander et al. (2019)*
G44067	TrGCN	EZCH3CO2CHCHO + NO_3→ CH_3COCHO_2CHO + NO_2	KRO2NO3	Sander et al. (2019)
G44068	TrGC	EZCH3CO2CHCHO → CH_3COCHO_2CHO	k1_RO2sORO2	Sander et al. (2019)
G44069	TrGC	EZCHOCCH3CHO2 → $HCOCCH_3CO$ + OH	k_15hs24vynal	Sander et al. (2019)
G44070	TrGCN	EZCHOCCH3CHO2 + NO → $HCOCO_2CH_3CHO$ + NO_2	KRO2NO	Sander et al. (2019)*
G44071	TrGC	EZCHOCCH3CHO2 + HO_2→ $HCOCCH_3CHOOH$	k_RO2_HO2(temp,4)	Sander et al. (2019)
G44072	TrGCN	EZCHOCCH3CHO2 + NO_3→ $HCOCO_2CH_3CHO$ + NO_2	KRO2NO3	Sander et al. (2019)
G44073	TrGC	EZCHOCCH3CHO2 → $HCOCO_2CH_3CHO$	k1_RO2pORO2	Sander et al. (2019)
G44074	TrGC	$CH_3COOHCHCHO$ → CH_3COCHO_2CHO + OH	k_hydec	Sander et al. (2019)
G44075	TrGC	$HCOCCH_3CHOOH$ → $HCOCO_2CH_3CHO$ + OH	k_hydec	Sander et al. (2019)
G44076	TrGCN	CH_3COCHO_2CHO + NO → $CH_3C(O)$ + GLYOX + NO_2	KRO2NO	Sander et al. (2019)*
G44077	TrGCN	CH_3COCHO_2CHO + NO_3 → $CH_3C(O)$ + GLYOX + NO_2	KRO2NO3	Sander et al. (2019)
G44078	TrGC	CH_3COCHO_2CHO + HO_2 → $CH_3C(O)$ + GLYOX + OH	k_RO2_HO2(temp,4)	Sander et al. (2019)*
G44079	TrGC	CH_3COCHO_2CHO → $CH_3C(O)$ + GLYOX	k1_RO2sORO2	Sander et al. (2019)
G44080	TrGC	$HCOCO_2CH_3CHO$ → MGLYOX + CO + HO_2	k1_RO2tORO2	Sander et al. (2019)
G44081	TrGCN	$HCOCO_2CH_3CHO$ + NO → MGLYOX + CO + HO_2 + NO_2	KRO2NO	Sander et al. (2019)*
G44082	TrGC	$HCOCO_2CH_3CHO$ + HO_2 → MGLYOX + CO + HO_2 + OH	k_RO2_HO2(temp,4)	Sander et al. (2019)*
G44083	TrGCN	$HCOCO_2CH_3CHO$ + NO_3 → MGLYOX + CO + HO_2 + NO_2	KRO2NO3	Sander et al. (2019)
G44084	TrGC	$HCOCCH_3CO$ + OH → CO + MGLYOX + HO_2	1E-10*a_CHO	Hatakeyama et al. (1985), Sander et al. (2019)
G44085	TrGC	$CH_3COCHCO$ + OH → CO + MGLYOX + HO_2	7.6E-11*a_COCH3	Hatakeyama et al. (1985), Sander et al. (2019)*
G44086	TrGCN	LMEKNO3 + OH → .62 MGLYOX + .62 HCHO + .62 HO_2 + .62 NO_2 + .38 $CH_3C(O)$ + .38 $NO_3CH2CHO$	.62*(k_p*(f_CO+f_CH2ONO2)) +.38*(k_s*f_CH2ONO2*f_CO)	Sander et al. (2019)*
G44087	TrGC	MEPROPENE + OH → IBUTOLBO2	9.4E-12*EXP(505./temp)	Atkinson et al. (2006)

Table 1: Gas phase reactions (... continued)

#	labels	reaction	rate coefficient	reference
G44088a	TrGC	MEPROPENE + O_3 → CH_3COCH_3 + CH_2OO^*	2.7E-15*EXP(-1630./temp)*0.33	Atkinson et al. (2006), Sander et al. (2019)
G44088b	TrGC	MEPROPENE + O_3 → $CH_3COCH_2O_2$ + OH + HCHO	2.7E-15*EXP(-1630./temp)*0.67	Atkinson et al. (2006), Sander et al. (2019)
G44089	TrGCN	MEPROPENE + NO_3 → CH_3COCH_3 + HCHO + NO_2	3.4E-13	Atkinson et al. (2006), Sander et al. (2019)*
G44090	TrGC	IBUTOLBO2 → CH_3COCH_3 + HCHO + HO_2	k1_RO2tORO2	Sander et al. (2019)
G44091a	TrGC	IBUTOLBO2 + HO_2 → IBUTOLBOOH	k_RO2_HO2(temp,4)*r_COCH2O2_OOH	Sander et al. (2019)
G44091b	TrGC	IBUTOLBO2 + HO_2 → CH_3COCH_3 + HCHO + HO_2 + OH	k_RO2_HO2(temp,4)*r_COCH2O2_OH	Sander et al. (2019)
G44092a	TrGCN	IBUTOLBO2 + NO → CH_3COCH_3 + HCHO + HO_2 + NO_2	KRO2NO*(1.-alpha_AN(5,3,0,0,0,temp,cair))	Sander et al. (2019)
G44092b	TrGCN	IBUTOLBO2 + NO → IBUTOLBNO3	KRO2NO*alpha_AN(5,3,0,0,0,temp,cair)	Sander et al. (2019)
G44093	TrGCN	IBUTOLBO2 + NO_3 → CH_3COCH_3 + HCHO + HO_2 + NO_2	KRO2NO3	Sander et al. (2019)
G44094a	TrGC	IBUTOLBOOH + OH → IBUTOLBO2	k_ROOHRO	Sander et al. (2019)
G44094b	TrGC	IBUTOLBOOH + OH → CH_3COCH_3 + HCHO + HO_2	k_s*f_sOOH*f_pCH2OH	Sander et al. (2019)
G44095	TrGCN	IBUTOLBNO3 + OH → CH_3COCH_3 + HCHO + HO_2 + NO_2	3.*k_p	Sander et al. (2019)
G44096	TrGC	BUT1ENE + OH → LBUT1ENO2	6.6E-12*EXP(465./temp)	Atkinson et al. (2006)*
G44097a	TrGC	BUT1ENE + O_3 → HCHO + .5 C_2H_5CHO + .5 H_2O_2 + .5 CH_3CHO + .5 CO + .5 HO_2	3.35E-15*EXP(-1745./temp)*.57	Atkinson et al. (2006), Sander et al. (2019)*
G44097b	TrGC	BUT1ENE + O_3 → C_2H_5CHO + CH_2OO^*	3.35E-15*EXP(-1745./temp)*.43	Atkinson et al. (2006), Sander et al. (2019)*
G44098	TrGCN	BUT1ENE + NO_3 → C_2H_5CHO + HCHO + NO_2	3.2E-13*EXP(-950./temp)	Atkinson et al. (2006), Sander et al. (2019)*
G44099	TrGC	LBUT1ENO2 → C_2H_5CHO + HCHO + HO_2	k1_RO2sORO2	Sander et al. (2019)
G44100a	TrGC	LBUT1ENO2 + HO_2 → LBUT1ENOOH	k_RO2_HO2(temp,4)*r_COCH2O2_OOH	Sander et al. (2019)
G44100b	TrGC	LBUT1ENO2 + HO_2 → C_2H_5CHO + HCHO + HO_2 + OH	k_RO2_HO2(temp,4)*r_COCH2O2_OH	Sander et al. (2019)
G44101a	TrGCN	LBUT1ENO2 + NO → C_2H_5CHO + HCHO + HO_2 + NO_2	KRO2NO*(1.-alpha_AN(5,2,0,0,0,temp,cair))	Sander et al. (2019)
G44101b	TrGCN	LBUT1ENO2 + NO → LBUT1ENNO3	KRO2NO*alpha_AN(5,2,0,0,0,temp,cair)	Sander et al. (2019)

Table 1: Gas phase reactions (... continued)

#	labels	reaction	rate coefficient	reference
G44102	TrGCN	LBUT1ENO2 + NO_3 → C_2H_5CHO + HCHO + HO_2 + NO_2	KRO2NO3	Sander et al. (2019)
G44103a	TrGC	LBUT1ENOOH + OH → LBUT1ENO2	k_ROOHRO	Sander et al. (2019)
G44103b	TrGC	LBUT1ENOOH + OH → $C_2H_5CO_3$ + HCHO + HO_2	k_t*f_tOOH*f_pCH2OH	Sander et al. (2019)*
G44104	TrGCN	LBUT1ENNO3 + OH → C_2H_5CHO + CO + HO_2 + NO_2	k_s*f_sOH*f_CH2ONO2	Sander et al. (2019)*
G44105	TrGC	CBUT2ENE + OH → BUT2OLO2	1.1E-11*EXP(485./temp)	Atkinson et al. (2006)
G44106	TrGC	CBUT2ENE + O_3 → CH_3CHO + .16 CH3CHOHOOH + .50 OH + .50 $HCOCH_2O_2$ + .05 CH2CO + .09 CH_3OH + .09 CO + .2 CH_4 + .2 CO_2	3.2E-15*EXP(-965./temp)	Atkinson et al. (2006), Sander et al. (2019)*
G44107	TrGCN	CBUT2ENE + NO_3 → 2 CH_3CHO + NO_2	3.5E-13	Atkinson et al. (2006), Sander et al. (2019)*
G44108	TrGC	TBUT2ENE + OH → BUT2OLO2	1.0E-11*EXP(553./temp)	Atkinson et al. (2006)
G44109	TrGC	TBUT2ENE + O_3 → CH_3CHO + .16 CH3CHOHOOH + .50 OH + .50 $HCOCH_2O_2$ + .05 CH2CO + .09 CH_3OH + .09 CO + .2 CH_4 + .2 CO_2	6.6E-15*EXP(-1060./temp)	Atkinson et al. (2006), Sander et al. (2019)
G44110	TrGCN	TBUT2ENE + NO_3 → 2 CH_3CHO + NO_2	1.78E-12*EXP(-530./temp) +1.28E-14*EXP(570./temp)	Atkinson et al. (2006), Sander et al. (2019)*
G44111	TrGC	BUT2OLO2 → C_2H_5CHO + HCHO + HO_2	k1_RO2sORO2	Sander et al. (2019)
G44112a	TrGC	BUT2OLO2 + HO_2 → BUT2OLOOH	k_RO2_HO2(temp,4)*r_COCH2O2_OOH	Sander et al. (2019)
G44112b	TrGC	BUT2OLO2 + HO_2 → 2 CH_3CHO + HO_2 + OH	k_RO2_HO2(temp,4)*r_COCH2O2_OH	Sander et al. (2019)
G44113a	TrGCN	BUT2OLO2 + NO → 2 CH_3CHO + HO_2 + NO_2	KRO2NO*(1.-alpha_AN(5,2,0,0,0, temp,cair))	Sander et al. (2019)
G44113b	TrGCN	BUT2OLO2 + NO → BUT2OLNO3	KRO2NO*alpha_AN(5,2,0,0,0,temp, cair)	Sander et al. (2019)
G44114	TrGCN	BUT2OLO2 + NO_3 → 2 CH_3CHO + HO_2 + NO_2	KRO2NO3	Sander et al. (2019)
G44115a	TrGC	BUT2OLOOH + OH → BUT2OLO2	k_ROOHRO	Sander et al. (2019)
G44115b	TrGC	BUT2OLOOH + OH → LMEKOOH + HO_2	k_t*f_tOH*f_pCH2OH	Sander et al. (2019)
G44115c	TrGC	BUT2OLOOH + OH → BUT2OLO + OH	k_t*f_tOOH*f_pCH2OH	Sander et al. (2019)
G44116	TrGCN	BUT2OLNO3 + OH → LMEKNO3 + HO_2	k_t*f_tOH*f_CH2ONO2	Sander et al. (2019)
G44117	TrGC	BUT2OLO + OH → BIACET + HO_2	k_t*f_tOH*f_CO	Sander et al. (2019)
G44118	TrGC	IPRCHO + OH → IPRCO3 + H_2O	6.8E-12*EXP(410./temp)	Atkinson et al. (2006)
G44119	TrGCN	IPRCHO + NO_3 → IPRCO3 + HNO_3	1.67E-12*EXP(-1460./temp)	Atkinson et al. (2006)
G44120	TrGC	IPRCO3 → $iC_3H_7O_2$ + CO_2	k1_RO2RCO3	Rickard and Pascoe (2009)
G44121a	TrGC	IPRCO3 + HO_2 → PERIBUACID	KAPHO2*r_CO3_OOH	Rickard and Pascoe (2009), Sander et al. (2019)

Table 1: Gas phase reactions (... continued)

#	labels	reaction	rate coefficient	reference
G44121b	TrGC	IPRCO3 + HO_2 → $iC_3H_7O_2$ + CO_2 + OH	KAPHO2*(1.-r_CO3_OOH)	Rickard and Pascoe (2009), Sander et al. (2019)
G44122	TrGCN	IPRCO3 + NO_2 → PIPN	k_CH3CO3_NO2	Rickard and Pascoe (2009)
G44123	TrGCN	IPRCO3 + NO → $iC_3H_7O_2$ + CO_2 + NO_2	KAPNO	Rickard and Pascoe (2009)
G44124a	TrGC	PERIBUACID + OH → IPRCO3 + H_2O	k_ROOHRO	Rickard and Pascoe (2009)
G44124b	TrGC	PERIBUACID + OH → CH_3COCH_3 + H_2O + CO_2	k_s*f_CO2H	Sander et al. (2019)*
G44125	TrGCN	PIPN → IPRCO3 + NO_2	k_PAN_M	Rickard and Pascoe (2009)
G44126	TrGCN	PIPN + OH → CH_3COCH_3 + CO_2 + NO_2	k_s*f_cpan	Sander et al. (2019)*
G44127	TrGC	MPROPENOL + OH → HCOOH + OH + CH_3COCH_3	k_CH2CHOH_OH_HCOOH	Sander et al. (2019), So et al. (2014)*
G44128	TrGC	MPROPENOL + HCOOH → IPRCHO + HCOOH	k_CH2CHOH_HCOOH	Sander et al. (2019), da Silva (2010)*
G44129	TrGC	IPRCHO + HCOOH → MPROPENOL + HCOOH	k_ALD_HCOOH	Sander et al. (2019), da Silva (2010)*
G44130	TrGC	BUTENOL + OH → HCOOH + OH + C_2H_5CHO	k_CH2CHOH_OH_HCOOH	Sander et al. (2019), So et al. (2014)*
G44131	TrGC	BUTENOL + HCOOH → C_3H_7CHO + HCOOH	k_CH2CHOH_HCOOH	Sander et al. (2019), da Silva (2010)*
G44132	TrGC	C_3H_7CHO + HCOOH → BUTENOL + HCOOH	k_ALD_HCOOH	Sander et al. (2019), da Silva (2010)*
G44133	TrGC	HVMK + OH → HCOOH + OH + MGLYOX	8.8E-11	Sander et al. (2019), So et al. (2014), Messaadia et al. (2015)*
G44134	TrGC	HVMK + HCOOH → CO2C3CHO + HCOOH	k_CH2CHOH_HCOOH	Sander et al. (2019), da Silva (2010)*
G44135	TrGC	CO2C3CHO + HCOOH → HVMK + HCOOH	k_ALD_HCOOH	Sander et al. (2019), da Silva (2010)*
G44136	TrGC	HMAC + OH → HCOOH + OH + MGLYOX	8.8E-11	Sander et al. (2019), So et al. (2014), Messaadia et al. (2015)*
G44137	TrGC	HMAC + HCOOH → IBUTDIAL + HCOOH	k_CH2CHOH_HCOOH	Sander et al. (2019), da Silva (2010)*
G44138	TrGC	IBUTDIAL + HCOOH → HMAC + HCOOH	k_ALD_HCOOH	Sander et al. (2019), da Silva (2010)*
G44139	TrGC	CO2C3CHO + OH → $CH_3COCH_2O_2$ + CO_2 + H_2O	k_t*f_O*f_alk+k_s*f_CHO*f_CO	Sander et al. (2019)*
G44140	TrGCN	CO2C3CHO + NO_3 → $CH_3COCH_2O_2$ + CO_2 + HNO_3	KNO3AL*4.0	Sander et al. (2019)*

Table 1: Gas phase reactions (... continued)

#	labels	reaction	rate coefficient	reference
G44141	TrGC	IBUTDIAL + OH → CH_3CHO + CO + HO_2 + CO_2 + H_2O	2.*k_t*f_O*f_alk+k_t*f_CHO*f_CHO	Sander et al. (2019)*
G44142	TrGCN	IBUTDIAL + NO_3 → CH_3CHO + CO + HO_2 + CO_2 + HNO_3	2.*KNO3AL*4.0	Sander et al. (2019)*
G44200	TrGTerC	$CH_3COCOCH_2O_2$ → $CH_3C(O)$ + HCHO + CO	k1_RO2pORO2	Rickard and Pascoe (2009)
G44201	TrGTerC	$CH_3COCOCH_2O_2$ + HO_2 → $CH_3COCOCH_2OOH$	k_RO2_HO2(temp,4)	Rickard and Pascoe (2009)
G44202	TrGTerCN	$CH_3COCOCH_2O_2$ + NO → $CH_3C(O)$ + HCHO + CO + NO_2	KRO2NO	Rickard and Pascoe (2009)*
G44203a	TrGTerC	$CH_3COCOCH_2OOH$ + OH → $CH_3COCOCHO$ + OH	k_s*f_CO*f_sOOH	Rickard and Pascoe (2009)*
G44203b	TrGTerC	$CH_3COCOCH_2OOH$ + OH → $CH_3COCOCH_2O_2$	k_ROOHRO	Rickard and Pascoe (2009)
G44204	TrGTerC	C44O2 + HO_2 → C44OOH	k_RO2_HO2(temp,4)	Rickard and Pascoe (2009)
G44205	TrGTerCN	C44O2 + NO → HCOCH2CHO + CO_2 + HO_2 + NO_2	KRO2NO	Rickard and Pascoe (2009)*
G44206	TrGTerC	C44O2 → HCOCH2CHO + CO_2 + HO_2	k1_RO2sORO2	Rickard and Pascoe (2009)
G44207	TrGTerC	C44OOH + OH → C44O2	7.46E-11	Rickard and Pascoe (2009)
G44208	TrGTerC	CHOC3COO2 → HCOCH2CO3 + HCHO	k1_RO2pORO2	Rickard and Pascoe (2009)
G44209	TrGTerC	CHOC3COO2 + HO_2 → C413COOOH	k_RO2_HO2(temp,4)	Rickard and Pascoe (2009)
G44210	TrGTerCN	CHOC3COO2 + NO → HCOCH2CO3 + HCHO + NO_2	KRO2NO	Rickard and Pascoe (2009)*
G44211	TrGTerC	C413COOOH + OH → CHOC3COO2	8.33E-11	Rickard and Pascoe (2009)
G44212	TrGTerC	C4CODIAL + OH → C312COCO3	3.39E-11	Rickard and Pascoe (2009)
G44213	TrGTerCN	C4CODIAL + NO_3 → C312COCO3 + HNO_3	2.*KNO3AL*4.0	Rickard and Pascoe (2009)
G44214	TrGTerC	C312COCO3 → $HCOCOCH_2O_2$ + CO_2	k1_RO2RCO3	Rickard and Pascoe (2009)
G44215a	TrGTerC	C312COCO3 + HO_2 → C312COCO3H	KAPHO2*r_CO3_OOH	Rickard and Pascoe (2009)
G44215b	TrGTerC	C312COCO3 + HO_2 → $HCOCOCH_2O_2$ + CO_2 + OH	KAPHO2*(1.-r_CO3_OOH)	Rickard and Pascoe (2009)
G44216	TrGTerCN	C312COCO3 + NO_2 → C312COPAN	k_CH3CO3_NO2	Rickard and Pascoe (2009)
G44217	TrGTerCN	C312COCO3 + NO → $HCOCOCH_2O_2$ + CO_2 + NO_2	KAPNO	Rickard and Pascoe (2009)
G44218	TrGTerC	C312COCO3H + OH → C312COCO3	1.63E-11	Rickard and Pascoe (2009)
G44219	TrGTerCN	C312COPAN → C312COCO3 + NO_2	k_PAN_M	Rickard and Pascoe (2009)
G44220	TrGTerCN	C312COPAN + OH → HCOCOCHO + CO + NO_2	1.27E-11	Rickard and Pascoe (2009)
G44221	TrGTerC	$CH_3COCOCHO$ + OH → $CH_3C(O)$ + 2 CO	8.4E-13*EXP(830./temp)	Sander et al. (2019)*
G44222	TrGTerCN	$CH_3COCOCHO$ + NO_3 → $CH_3C(O)$ + 2 CO + HNO_3	KNO3AL*4.0	Rickard and Pascoe (2009)
G44223	TrGTerC	IBUTALOH + OH → IPRHOCO3	1.4E-11	Rickard and Pascoe (2009)
G44224a	TrGTerC	IPRHOCO3 + HO_2 → CH_3COCH_3 + CO_2 + HO_2 + OH	KAPHO2*r_CO3_OH	Rickard and Pascoe (2009), Sander et al. (2019)
G44224b	TrGTerC	IPRHOCO3 + HO_2 → IPRHOCO2H + O_3	KAPHO2*r_CO3_O3	Rickard and Pascoe (2009), Sander et al. (2019)

Table 1: Gas phase reactions (... continued)

#	labels	reaction	rate coefficient	reference
G44224c	TrGTerC	IPRHOCO3 + HO_2 → IPRHOCO3H	KAPHO2*r_CO3_OOH	Rickard and Pascoe (2009), Sander et al. (2019)
G44225	TrGTerCN	IPRHOCO3 + NO → CH_3COCH_3 + CO_2 + HO_2 + NO_2	KAPNO	Rickard and Pascoe (2009)
G44226	TrGTerCN	IPRHOCO3 + NO_2 → C4PAN5	k_CH3CO3_NO2	Rickard and Pascoe (2009)
G44227	TrGTerCN	IPRHOCO3 + NO_3 → CH_3COCH_3 + CO_2 + HO_2 + NO_2	KRO2NO3*1.74	Rickard and Pascoe (2009)
G44228a	TrGTerC	IPRHOCO3 → CH_3COCH_3 + CO_2 + HO_2	k1_RO2RCO3*0.7	Rickard and Pascoe (2009)
G44228b	TrGTerC	IPRHOCO3 → IPRHOCO2H	k1_RO2RCO3*0.3	Rickard and Pascoe (2009)
G44229	TrGTerC	IPRHOCO2H + OH → CH_3COCH_3 + CO_2 + HO_2 + H_2O	1.72E-12	Rickard and Pascoe (2009)
G44230	TrGTerC	OH + IPRHOCO3H → IPRHOCO3	4.80E-12	Rickard and Pascoe (2009)
G44231	TrGTerCN	C4PAN5 → IPRHOCO3 + NO_2	k_PAN_M	Rickard and Pascoe (2009)
G44232	TrGTerCN	C4PAN5 + OH → CH_3COCH_3 + CO + NO_2	4.75E-13	Rickard and Pascoe (2009)
G44233a	TrGTerC	MBOOO → IPRHOCO2H	1.60E-17*C(ind_H2O)*(0.08+0.15)	Rickard and Pascoe (2009), Sander et al. (2019)
G44233b	TrGTerC	MBOOO → IBUTALOH + H_2O_2	1.60E-17*C(ind_H2O)*0.77	Rickard and Pascoe (2009), Sander et al. (2019)
G44234	TrGTerC	MBOOO + CO → IBUTALOH + CO_2	1.20E-15	Rickard and Pascoe (2009)
G44235	TrGTerCN	MBOOO + NO → IBUTALOH + NO_2	1.00E-14	Rickard and Pascoe (2009)
G44236	TrGTerCN	MBOOO + NO_2 → IBUTALOH + NO_3	1.00E-15	Rickard and Pascoe (2009)
G44400	TrGAroC	MALANHY + OH → MALANHYO2	1.4E-12	Rickard and Pascoe (2009)
G44401a	TrGAroC	MALDIALOOH + OH → HOCOC4DIAL + OH	1.22E-10	Rickard and Pascoe (2009)
G44401b	TrGAroC	MALDIALOOH + OH → MALDIALO2	k_ROOHRO	Rickard and Pascoe (2009)
G44402	TrGAroCN	NC4DCO2H + OH → MALANHY + NO_2	k_ROOHRO	Rickard and Pascoe (2009)*
G44403	TrGAroC	CO14O3CO2H + OH → $HCOCH_2O_2$ + 2 CO_2	2.19E-11	Rickard and Pascoe (2009)
G44404	TrGAroC	BZFUOOH + OH → BZFUO2	3.68E-11	Rickard and Pascoe (2009)
G44405	TrGAroC	HOCOC4DIAL + OH → CO2C4DIAL + HO_2	3.67E-11	Rickard and Pascoe (2009)
G44406a	TrGAroC	MALDIALCO3 + HO_2 → MALDALCO2H + O_3	KAPHO2*r_CO3_O3	Rickard and Pascoe (2009)
G44406b	TrGAroC	MALDIALCO3 + HO_2 → MALDALCO3H	KAPHO2*r_CO3_OOH	Rickard and Pascoe (2009)
G44406c	TrGAroC	MALDIALCO3 + HO_2 → .6 MALANHY + HO_2 + .4 GLYOX + .4 CO + .4 CO_2 + OH	KAPHO2*r_CO3_OH	Rickard and Pascoe (2009)*
G44407	TrGAroCN	MALDIALCO3 + NO → .6 MALANHY + HO_2 + .4 GLYOX + .4 CO + .4 CO_2 + NO_2	KAPNO	Rickard and Pascoe (2009)*
G44408	TrGAroCN	MALDIALCO3 + NO_2 → MALDIALPAN	k_CH3CO3_NO2	Rickard and Pascoe (2009)
G44409	TrGAroCN	MALDIALCO3 + NO_3 → .6 MALANHY + HO_2 + .4 GLYOX + .4 CO + .4 CO_2 + NO_2	KRO2NO3*1.74	Rickard and Pascoe (2009)*

Table 1: Gas phase reactions (... continued)

#	labels	reaction	rate coefficient	reference
G44410	TrGAroC	MALDIALCO3 → .6 MALANHY + HO_2 + .4 GLYOX + .4 CO + .4 CO_2	k1_RO2RCO3	Rickard and Pascoe (2009)*
G44411	TrGAroCN	BZFUONE + NO_3 → NBZFUO2	3.00E-13	Rickard and Pascoe (2009)
G44412	TrGAroC	BZFUONE + O_3 → .3125 CO14O3CO2H + .1875 CO14O3CHO + .1875 H_2O_2 + .5 CO + .5 CO_2 + .5 $HCOCH_2O_2$ + .5 OH	2.20E-19	see note*
G44413	TrGAroC	BZFUONE + OH → BZFUO2	4.45E-11	Rickard and Pascoe (2009)
G44414	TrGAroCN	NBZFUOOH + OH → NBZFUO2	6.18E-12	Rickard and Pascoe (2009)
G44415	TrGAroC	MALDALCO3H + OH → MALDIALCO3	4.00E-11	Rickard and Pascoe (2009)
G44416	TrGAroC	EPXDLCO2H + OH → C3DIALO2 + CO_2	2.31E-11	Rickard and Pascoe (2009)
G44417a	TrGAroC	EPXDLCO3 + HO_2 → C3DIALO2 + CO_2 + OH	KAPHO2*r_CO3_OH	Rickard and Pascoe (2009)
G44417b	TrGAroC	EPXDLCO3 + HO_2 → EPXDLCO2H + O_3	KAPHO2*r_CO3_O3	Rickard and Pascoe (2009)
G44417c	TrGAroC	EPXDLCO3 + HO_2 → EPXDLCO3H	KAPHO2*r_CO3_OOH	Rickard and Pascoe (2009)
G44418	TrGAroCN	EPXDLCO3 + NO → C3DIALO2 + CO_2 + NO_2	KAPNO	Rickard and Pascoe (2009)
G44419	TrGAroCN	EPXDLCO3 + NO_2 → EPXDLPAN	k_CH3CO3_NO2	Rickard and Pascoe (2009)
G44420	TrGAroCN	EPXDLCO3 + NO_3 → C3DIALO2 + CO_2 + NO_2	KRO2NO3*1.74	Rickard and Pascoe (2009)
G44421	TrGAroC	EPXDLCO3 → C3DIALO2 + CO_2	k1_RO2RCO3	Rickard and Pascoe (2009)*
G44422	TrGAroC	MALNHYOHCO + OH → CO + CO + CO + CO_2 + HO_2	5.68E-12	Rickard and Pascoe (2009)
G44423	TrGAroCN	MALDIAL + NO_3 → MALDIALCO3 + HNO_3	2.*KNO3AL*2.0	Rickard and Pascoe (2009)
G44424	TrGAroC	MALDIAL + O_3 → 1.0675 GLYOX + .125 HCHO + .1125 $HCOCO_2H$ + .0675 H_2O_2 + .82 HO_2 + .57 OH + 1.265 CO + .25 CO_2	2.00E-18	Rickard and Pascoe (2009)*
G44425	TrGAroC	MALDIAL + OH → .83 MALDIALCO3 + .17 MALDIALO2	5.20E-11	Rickard and Pascoe (2009)*
G44426	TrGAroC	MALANHYOOH + OH → MALNHYOHCO + OH	4.66E-11	Rickard and Pascoe (2009)
G44427	TrGAroCN	MALDIALPAN + OH → GLYOX + CO + CO + NO_2	3.70E-11	Rickard and Pascoe (2009)
G44428	TrGAroCN	MALDIALPAN → MALDIALCO3 + NO_2	k_PAN_M	Rickard and Pascoe (2009)
G44429a	TrGAroC	MALANHYO2 + HO_2 → MALANHYOOH	k_RO2_HO2(temp,4)*(1.-r_COCH2O2_OH-r_CHOHCH2O2_OH)	Rickard and Pascoe (2009), Sander et al. (2019)
G44429b	TrGAroC	MALANHYO2 + HO_2 → HCOCOHCO3 + CO_2 + OH	k_RO2_HO2(temp,4)*(r_COCH2O2_OH+r_CHOHCH2O2_OH)	Rickard and Pascoe (2009), Sander et al. (2019)
G44430	TrGAroCN	MALANHYO2 + NO → HCOCOHCO3 + CO_2 + NO_2	KRO2NO	Rickard and Pascoe (2009)*
G44431	TrGAroCN	MALANHYO2 + NO_3 → HCOCOHCO3 + CO_2 + NO_2	KRO2NO3	Rickard and Pascoe (2009)*
G44432	TrGAroC	MALANHYO2 → HCOCOHCO3 + CO_2	k1_RO2sORO2	Rickard and Pascoe (2009)*
G44433	TrGAroC	EPXDLCO3H + OH → EPXDLCO3	2.62E-11	Rickard and Pascoe (2009)

Table 1: Gas phase reactions (... continued)

#	labels	reaction	rate coefficient	reference
G44434	TrGAroC	CO2C4DIAL + OH → CO + CO + CO + CO + HO_2	2.45E-11	Rickard and Pascoe (2009)
G44435a	TrGAroCN	NBZFUO2 + HO_2 → NBZFUOOH	k_RO2_HO2(temp,4)*(1.-r_COCH2O2_OH)	Rickard and Pascoe (2009), Sander et al. (2019)
G44435b	TrGAroCN	NBZFUO2 + HO_2 → .5 CO14O3CHO + .5 NO_2 + .5 NBZFUONE + .5 HO_2 + OH	k_RO2_HO2(temp,4)*r_COCH2O2_OH	Rickard and Pascoe (2009), Sander et al. (2019)
G44436	TrGAroCN	NBZFUO2 + NO → .5 CO14O3CHO + .5 NO_2 + .5 NBZFUONE + .5 HO_2 + NO_2	KRO2NO	Rickard and Pascoe (2009)*
G44437	TrGAroCN	NBZFUO2 + NO_3 → .5 CO14O3CHO + .5 NO_2 + .5 NBZFUONE + .5 HO_2 + NO_2	KRO2NO3	Rickard and Pascoe (2009)*
G44438	TrGAroCN	NBZFUO2 → .5 CO14O3CHO + .5 NO_2 + .5 NBZFUONE + .5 HO_2	k1_RO2sORO2	Rickard and Pascoe (2009)*
G44439	TrGAroC	MALDALCO2H + OH → .6 MALANHY + HO_2 + .4 GLYOX + .4 CO + .4 CO_2	3.70E-11	Rickard and Pascoe (2009)*
G44440	TrGAroCN	EPXC4DIAL + NO_3 → EPXDLCO3 + HNO_3	2.*KNO3AL*4.0	Rickard and Pascoe (2009)
G44441	TrGAroC	EPXC4DIAL + OH → EPXDLCO3	4.32E-11	Rickard and Pascoe (2009)
G44442a	TrGAroC	MECOACETO2 + HO_2 → MECOACEOOH	k_RO2_HO2(temp,4)*(1.-r_COCH2O2_OH)	Rickard and Pascoe (2009), Sander et al. (2019)
G44442b	TrGAroC	MECOACETO2 + HO_2 → $CH_3C(O)OO$ + HCHO + CO_2 + OH	k_RO2_HO2(temp,4)*r_COCH2O2_OH	Rickard and Pascoe (2009), Sander et al. (2019)
G44443	TrGAroCN	MECOACETO2 + NO → $CH_3C(O)OO$ + HCHO + CO_2 + NO_2	KRO2NO	Rickard and Pascoe (2009)*
G44444	TrGAroCN	MECOACETO2 + NO_3 → $CH_3C(O)OO$ + HCHO + CO_2 + NO_2	KRO2NO3	Rickard and Pascoe (2009)*
G44445	TrGAroC	MECOACETO2 → $CH_3C(O)OO$ + HCHO + CO_2	k1_RO2pORO2	Rickard and Pascoe (2009)*
G44446	TrGAroCN	CO14O3CHO + NO_3 → CO + $HCOCH_2O_2$ + CO_2 + HNO_3	KNO3AL*8.0	Rickard and Pascoe (2009)
G44447	TrGAroC	CO14O3CHO + OH → CO + $HCOCH_2O_2$ + CO_2	3.44E-11	Rickard and Pascoe (2009)
G44448	TrGAroCN	NBZFUONE + OH → BZFUCO + NO_2	1.16E-12	Rickard and Pascoe (2009)
G44449a	TrGAroC	BZFUO2 + HO_2 → BZFUOOH	k_RO2_HO2(temp,4)*(1.-r_COCH2O2_OH-r_CHOHCH2O2_OH)	Rickard and Pascoe (2009), Sander et al. (2019)
G44449b	TrGAroC	BZFUO2 + HO_2 → CO14O3CHO + HO_2 + OH	k_RO2_HO2(temp,4)*(r_COCH2O2_OH+r_CHOHCH2O2_OH)	Rickard and Pascoe (2009), Sander et al. (2019)
G44450	TrGAroCN	BZFUO2 + NO → CO14O3CHO + HO_2 + NO_2	KRO2NO	Rickard and Pascoe (2009)*
G44451	TrGAroCN	BZFUO2 + NO_3 → CO14O3CHO + HO_2 + NO_2	KRO2NO3	Rickard and Pascoe (2009)*
G44452	TrGAroC	BZFUO2 → CO14O3CHO + HO_2	k1_RO2sORO2	Rickard and Pascoe (2009)*

Table 1: Gas phase reactions (... continued)

#	labels	reaction	rate coefficient	reference
G44453	TrGAroC	BZFUCO + OH → CO14O3CHO + HO_2	1.78E-11	Rickard and Pascoe (2009)
G44456a	TrGAroC	MALDIALO2 + HO_2 → MALDIALOOH	k_RO2_HO2(temp,4)*(1.-r_COCH2O2_OH-r_CHOHCH2O2_OH)	Rickard and Pascoe (2009)
G44456b	TrGAroC	MALDIALO2 + HO_2 → GLYOX + GLYOX + HO_2 + OH	k_RO2_HO2(temp,4)*(r_COCH2O2_OH+r_CHOHCH2O2_OH)	Rickard and Pascoe (2009)
G44457	TrGAroCN	MALDIALO2 + NO → GLYOX + GLYOX + HO_2 + NO_2	KRO2NO	Rickard and Pascoe (2009)*
G44458	TrGAroCN	MALDIALO2 + NO_3 → GLYOX + GLYOX + HO_2 + NO_2	KRO2NO3	Rickard and Pascoe (2009)*
G44459	TrGAroC	MALDIALO2 → GLYOX + GLYOX + HO_2	k1_RO2sORO2	Rickard and Pascoe (2009)*
G44460	TrGAroCN	EPXDLPAN + OH → HCOCOCHO + CO + NO_2	2.29E-11	Rickard and Pascoe (2009)
G44461	TrGAroCN	EPXDLPAN → EPXDLCO3 + NO_2	k_PAN_M	Rickard and Pascoe (2009)*
G44462	TrGAroC	MECOACEOOH + OH → MECOACETO2	3.59E-12	Rickard and Pascoe (2009)
G45000	TrGC	C_5H_8 + O_3 → .3508 MACR + .01518 MACO2H + .2440 MVK + .7085 HCHO + .11 CH_2OO + .1275 C_3H_6 + .1575 $CH_3C(O)$ + .0510 CH_3 + .2625 HO_2 + .27 OH + .09482 H_2O_2 + .255 CO_2 + .522 CO + .07182 HCHO + .03618 $HCOCH_2O_2$ + .01782 CO + 0.05408 LCARBON	1.03E-14*EXP(-1995./temp)	Atkinson et al. (2006), Sander et al. (2019)
G45001	TrGC	C_5H_8 + OH → .63 LISOPAB + .30 LISOPCD + .07 LISOPEFO2	2.7E-11*EXP(390./temp)	Atkinson et al. (2006), Sander et al. (2019)
G45002	TrGCN	C_5H_8 + NO_3 → NISOPO2	3.0E-12*EXP(-450./temp)	Atkinson et al. (2006)
G45003a	TrGC	LISOPAB + O_2 → LISOPACO2	5.530E-13	Sander et al. (2019)
G45003b	TrGC	LISOPAB + O_2 → ISOPBO2	3.E-12	Sander et al. (2019)
G45004a	TrGC	LISOPCD + O_2 → LDISOPACO2	6.780E-13	Sander et al. (2019)
G45004b	TrGC	LISOPCD + O_2 → ISOPDO2	3.E-12	Sander et al. (2019)
G45005	TrGC	LISOPACO2 → LISOPAB + O_2	3.1E12*exp(-7900./temp)*.6+7.8E13*exp(-8600./temp)*.4	Sander et al. (2019)
G45006	TrGC	ISOPBO2 → LISOPAB + O_2	3.7E14*exp(-9570./temp)+4.2E14*exp(-9970./temp)	Sander et al. (2019)
G45007	TrGC	LDISOPACO2 → LISOPCD + O_2	5.65E12*exp(-8410./temp)*.42+1.4E14*exp(-9110./temp)*.58	Sander et al. (2019)
G45008	TrGC	ISOPDO2 → LISOPCD + O_2	5.0E14*exp(-10120./temp)+8.25E14*exp(-10220./temp)	Sander et al. (2019)
G45009a	TrGC	LISOPACO2 → C1ODC2O2C4OOH	k_16hsz14 * 2./3.*(1.-f_HPAL)	Sander et al. (2019)
G45009b	TrGC	LISOPACO2 → LZCODC23DBCOOH + HO_2	k_16hsz14 * (2./3.*f_HPAL + 1./3.)	Sander et al. (2019)
G45010a	TrGC	LDISOPACO2 → C1OOHC3O2C4OD	k_16hsz41 * 2./3.*(1.-f_HPAL)	Sander et al. (2019)

Table 1: Gas phase reactions (... continued)

#	labels	reaction	rate coefficient	reference
G45010b	TrGC	LDISOPACO2 → LZCODC23DBCOOH + HO_2	k_16hsz41 * (2./3.*f_HPAL + 1./3.)	Sander et al. (2019)
G45011	TrGC	LISOPACO2 → .9 LISOPACO + .1 ISOPAOH	k1_RO2LISOPACO2	Rickard and Pascoe (2009), Sander et al. (2019)
G45012	TrGC	LISOPACO2 + HO_2 → LISOPACOOH	k_RO2_HO2(temp,5)	Rickard and Pascoe (2009)
G45013a	TrGCN	LISOPACO2 + NO → LISOPACO + NO_2	KRO2NO*(1.-alpha_AN(6,1,0,0,0,temp,cair))	Lockwood et al. (2010), Paulot et al. (2009a), Sander et al. (2019)
G45013b	TrGCN	LISOPACO2 + NO → LISOPACNO3	KRO2NO*alpha_AN(6,1,0,0,0,temp,cair)	Lockwood et al. (2010), Paulot et al. (2009a), Sander et al. (2019)
G45014	TrGCN	LISOPACO2 + NO_3 → LISOPACO + NO_2	KRO2NO3	Rickard and Pascoe (2009)
G45015	TrGC	LDISOPACO2 → .9 LISOPACO + .1 ISOPAOH	k1_RO2LISOPACO2	Rickard and Pascoe (2009), Sander et al. (2019)
G45016	TrGC	LDISOPACO2 + HO_2 → LISOPACOOH	k_RO2_HO2(temp,5)	Rickard and Pascoe (2009)
G45017a	TrGCN	LDISOPACO2 + NO → LISOPACO + NO_2	KRO2NO*(1.-alpha_AN(6,1,0,0,0,temp,cair))	Lockwood et al. (2010), Paulot et al. (2009a), Sander et al. (2019)
G45017b	TrGCN	LDISOPACO2 + NO → LISOPACNO3	KRO2NO*alpha_AN(6,1,0,0,0,temp,cair)	Lockwood et al. (2010), Paulot et al. (2009a), Sander et al. (2019)
G45018	TrGCN	LDISOPACO2 + NO_3 → LISOPACO + NO_2	KRO2NO3	Rickard and Pascoe (2009)
G45019a	TrGC	LISOPACOOH + OH → LISOPACO2	k_ROOHRO	Sander et al. (2019)
G45019b	TrGC	LISOPACOOH + OH → LZCODC23DBCOOH + HO_2	k_s*f_allyl*f_sOH	Sander et al. (2019)
G45019c	TrGC	LISOPACOOH + OH → LHC4ACCHO + OH	(k_s*f_sOOH*f_allyl+ k_ROHRO)	Sander et al. (2019)
G45019d	TrGC	LISOPACOOH + OH → LIEPOX + OH	(k_adt+k_ads)*a_CH2OH*a_CH2OOH	Sander et al. (2019)*
G45020	TrGC	ISOPAOH + OH → LHC4ACCHO + HO_2	(k_adt+k_ads)*a_CH2OH*a_CH2OH+k_s*f_sOH*f_allyl+k_ROHRO	Sander et al. (2019)
G45021	TrGCN	LISOPACNO3 + OH → LISOPACNO3O2	(k_adt+k_ads)*a_CH2ONO2*a_CH2OH	Sander et al. (2019)*
G45022	TrGC	ISOPBO2 → .8 MVK + .8 HCHO + .8 HO_2 + .2 ISOPBOH	k1_RO2ISOPBO2	Rickard and Pascoe (2009)
G45023a	TrGC	ISOPBO2 + HO_2 → ISOPBOOH	k_RO2_HO2(temp,5)*(1.-r_CHOHCH2O2_OH)	Sander et al. (2019)
G45023b	TrGC	ISOPBO2 + HO_2 → MVK + HCHO + HO_2 + OH	k_RO2_HO2(temp,5)*r_CHOHCH2O2_OH	Sander et al. (2019)
G45024a	TrGCN	ISOPBO2 + NO → MVK + HCHO + HO_2 + NO_2	KRO2NO*(1.-alpha_AN(6,3,0,0,0,temp,cair))	Lockwood et al. (2010), Sander et al. (2019)

Table 1: Gas phase reactions (... continued)

#	labels	reaction	rate coefficient	reference
G45024b	TrGCN	ISOPBO2 + NO → ISOPBNO3	KRO2NO*alpha_AN(6,3,0,0,0,temp, cair)	Lockwood et al. (2010), Sander et al. (2019)
G45025	TrGCN	ISOPBO2 + NO_3 → MVK + .75 HCHO + .75 HO_2 + .25 CH_3 + NO_2	KRO2NO3	Rickard and Pascoe (2009)
G45026a	TrGC	ISOPBOOH + OH → LIEPOX + OH	(k_ads+k_adp)*a_CH2OOH	Paulot et al. (2009b), Sander et al. (2019)
G45026b	TrGC	ISOPBOOH + OH → ISOPBO2	k_ROOHRO	Sander et al. (2019)
G45026c	TrGC	ISOPBOOH + OH → MGLYOX + $HOCH_2CHO$	k_ROHRO+k_s*f_alk*f_sOH	Sander et al. (2019)
G45027	TrGC	ISOPBOOH + O_3 → .1368 MACROOH + .1368 H_2O_2 + .2280 HO_2 + .4332 CH_3COCH_2OH + .2280 CO_2 + .6384 OH + .2052 CO + .57 HCHO + .43 MACROOH + .06880 HO_2 + .06880 OH + .2709 CO + .1591 CH_2OO	1.E-17	Sander et al. (2019)
G45028	TrGC	ISOPBOH + OH → MVK + .75 HCHO + .75 HO_2 + .25 CH_3	k_s*f_alk*f_sOH+(k_adp+k_ads) *a_CH2OH	Sander et al. (2019)
G45029	TrGCN	ISOPBNO3 + OH → ISOPBDNO3O2	(k_adt+k_adp)*f_CH2ONO2	Sander et al. (2019)
G45030	TrGC	ISOPDO2 → .8 MACR + .8 HCHO + .8 HO_2 + .1 HCOC5 + .1 ISOPDOH	k1_RO2ISOPDO2	Rickard and Pascoe (2009)
G45031a	TrGC	ISOPDO2 + HO_2 → ISOPDOOH	k_RO2_HO2(temp,5)*(1.-r_ CHOHCH2O2_OH)	Sander et al. (2019)
G45031b	TrGC	ISOPDO2 + HO_2 → MACR + HCHO + HO_2 + OH	k_RO2_HO2(temp,5)*r_CHOHCH2O2_OH	Sander et al. (2019)
G45032a	TrGCN	ISOPDO2 + NO → MACR + HCHO + HO_2 + NO_2	KRO2NO*(1.-alpha_AN(6,2,0,0,0, temp,cair))	Lockwood et al. (2010), Sander et al. (2019)
G45032b	TrGCN	ISOPDO2 + NO → ISOPDNO3	KRO2NO*alpha_AN(6,2,0,0,0,temp, cair)	Lockwood et al. (2010), Sander et al. (2019)
G45033	TrGCN	ISOPDO2 + NO_3 → MACR + HCHO + HO_2 + NO_2	KRO2NO3	Rickard and Pascoe (2009)
G45034a	TrGC	ISOPDOOH + OH → LIEPOX + OH	(k_adt+k_adp)*a_CH2OOH	Paulot et al. (2009b), Sander et al. (2019)
G45034b	TrGC	ISOPDOOH + OH → ISOPDO2	k_ROOHRO	Sander et al. (2019)
G45034c	TrGC	ISOPDOOH + OH → HCOC5 + OH	k_t*f_tOOH*f_allyl*f_pCH2OH	Sander et al. (2019)
G45034d	TrGC	ISOPDOOH + OH → CH_3COCH_2OH + GLYOX + OH	k_s*f_pCH2OH*f_sOH	Sander et al. (2019)
G45035	TrGC	ISOPDOOH + O_3 → 1.393 OH + BIACETOH + .67 HCHO + .05280 HO_2 + .2079 CO + .1221 CH_2OO	1.E-17	Sander et al. (2019)
G45036	TrGC	ISOPDOH + OH → HCOC5 + HO_2	2.*k_ROHRO+(k_t*f_tOH*f_allyl+k_ s*f_sOH)*f_pCH2OH+(k_adt+k_adp) *a_CH2OH	Sander et al. (2019)

Table 1: Gas phase reactions (... continued)

#	labels	reaction	rate coefficient	reference
G45037	TrGCN	ISOPDNO3 + OH → ISOPBDNO3O2	(k_adp+k_ads)*a_CH2ONO2	Sander et al. (2019)*
G45038	TrGCN	NISOPO2 → .8 NC4CHO + .6 HO_2 + .2 LISOPACNO3	k1_RO2LISOPACO2	Rickard and Pascoe (2009)
G45039	TrGCN	NISOPO2 + HO_2 → NISOPOOH	k_RO2_HO2(temp,5)	Rickard and Pascoe (2009)
G45040	TrGCN	NISOPO2 + NO → NC4CHO + HO_2 + NO_2	KRO2NO	Rickard and Pascoe (2009)*
G45041	TrGCN	NISOPO2 + NO_3 → NC4CHO + HO_2 + NO_2	KRO2NO3	Rickard and Pascoe (2009)
G45042	TrGCN	NISOPOOH + OH → NC4CHO + OH	1.03E-10	Rickard and Pascoe (2009)
G45043	TrGCN	NC4CHO + OH → LNISO3	(k_adt+k_ads)*a_CHO*a_CH2ONO2	Sander et al. (2019)*
G45044	TrGCN	NC4CHO + O_3 → .27 NOA + .027 $HCOCO_2H$ + .0162 GLYOX + .0162 H_2O_2 + .1458 HCOCO + .0405 HCOOH + .0405 CO + .8758 OH + .365 MGLYOX + .73 NO_2 + 0.7705 HCHO + .4055 CO_2 + .73 GLYOX	2.40E-17	Sander et al. (2019)
G45045	TrGCN	NC4CHO + NO_3 → LNISO3 + HNO_3	KNO3AL*4.25	Rickard and Pascoe (2009)
G45046	TrGCN	LNISO3 + HO_2 → LNISOOH	0.5*k_RO2_HO2(temp,5)+0.5*KAPHO2	Rickard and Pascoe (2009)
G45047	TrGCN	LNISO3 + NO → NOA + .5 HOCHCHO + .5 CO + .5 HO_2 + NO_2 + .5 CO_2	0.5*KAPNO+0.5*KRO2NO	Rickard and Pascoe (2009)*
G45048	TrGCN	LNISO3 + NO_3 → NOA + .5 HOCHCHO + .5 CO + .5 HO_2 + NO_2 + .5 CO_2	KRO2NO3*1.37	Rickard and Pascoe (2009)
G45049	TrGCN	LNISOOH + OH → LNISO3	2.65E-11	Rickard and Pascoe (2009)
G45050a	TrGC	LHC4ACCHO + OH → LC578O2	(k_adtertprim+k_ads)*a_CHO*a_CH2OH	Sander et al. (2019)
G45050b	TrGC	LHC4ACCHO + OH → LHC4ACCO3	k_t*f_O	Sander et al. (2019)
G45050c	TrGC	LHC4ACCHO + OH → C4MDIAL + HO_2	k_s*f_sOH*f_allyl	Sander et al. (2019)
G45051	TrGC	LHC4ACCHO + O_3 → .2225 $CH_3C(O)$ + .89 CO + .0171875 $HOCH_2CO_2H$ + .075625 H_2O_2 + .0171875 $HCOCO_2H$ + .2775 CH_3COCH_2OH + .6675 HO_2 + .2603125 GLYOX + .2225 HCHO + .89 OH + .2603125 $HOCH_2CHO$ + .5 MGLYOX	2.40E-17	Rickard and Pascoe (2009)
G45052	TrGCN	LHC4ACCHO + NO_3 → LHC4ACCO3 + HNO_3	KNO3AL*4.25	Rickard and Pascoe (2009)
G45053	TrGC	LC578O2 → .25 CH_3COCH_2OH + .75 MGLYOX + .25 HOCHCHO + .75 $HOCH_2CHO$ + .75 HO_2	k1_RO2tORO2	Rickard and Pascoe (2009)
G45054a	TrGC	LC578O2 + HO_2 → MGLYOX + $HOCH_2CHO$ + OH	k_RO2_HO2(temp,5)*r_COCH2O2_OH	Rickard and Pascoe (2009)
G45054b	TrGC	LC578O2 + HO_2 → LC578OOH	k_RO2_HO2(temp,5)*r_COCH2O2_OOH	Rickard and Pascoe (2009)
G45055	TrGCN	LC578O2 + NO → .25 CH_3COCH_2OH + .75 MGLYOX + .25 HOCHCHO + .75 $HOCH_2CHO$ + .75 HO_2 + NO_2	KRO2NO	Rickard and Pascoe (2009)*

Table 1: Gas phase reactions (... continued)

#	labels	reaction	rate coefficient	reference
G45056	TrGCN	LC578O2 + NO_3 → .25 CH_3COCH_2OH + .75 MGLYOX + .25 HOCHCHO + .75 $HOCH_2CHO$ + .75 HO_2 + NO_2	KRO2NO3	Rickard and Pascoe (2009)
G45057	TrGC	LC578O2 → .25 CH_3COCH_2OH + .75 MGLYOX + .25 $HOCH_2CHO$ + .75 $HOCH_2CHO$ + HO_2 + OH	k_hsb	Sander et al. (2019)
G45058a	TrGC	LC578OOH + OH → LC578O2	k_ROOHRO	Sander et al. (2019)
G45058b	TrGC	LC578OOH + OH → C1ODC2OOHC4OD + HO_2	k_t*f_O*f_tCH2OH*f_alk+k_t*f_tOH*f_pCH2OH*f_pCH2OH+k_s*f_sOH*f_pCH2OH	Sander et al. (2019)
G45059a	TrGC	LHC4ACCO3 → OH + .5 MACRO2 + .5 LHMVKABO2 + CO_2	k1_RO2RCO3*0.9	Sander et al. (2019)
G45059b	TrGC	LHC4ACCO3 → LHC4ACCO2H	k1_RO2RCO3*0.1	Sander et al. (2019)
G45060a	TrGC	LHC4ACCO3 + HO_2 → 2 OH + .5 MACRO2 + .5 LHMVKABO2 + CO_2	KAPHO2*r_CO3_OH	Sander et al. (2019)
G45060b	TrGC	LHC4ACCO3 + HO_2 → LHC4ACCO3H	KAPHO2*r_CO3_OOH	Sander et al. (2019)
G45060c	TrGC	LHC4ACCO3 + HO_2 → LHC4ACCO2H + O_3	KAPHO2*r_CO3_O3	Sander et al. (2019)
G45061	TrGCN	LHC4ACCO3 + NO → .5 MACRO2 + .5 LHMVKABO2 + NO_2 + CO_2	KAPNO	Sander et al. (2019)
G45062	TrGCN	LHC4ACCO3 + NO_2 → LC5PAN1719	k_CH3CO3_NO2	Rickard and Pascoe (2009)
G45063	TrGCN	LHC4ACCO3 + NO_3 → .5 MACRO2 + .5 LHMVKABO2 + NO_2 + CO_2	KRO2NO3*1.74	Sander et al. (2019)
G45064a	TrGC	LHC4ACCO2H + OH → OH + .5 MACRO2 + .5 LHMVKABO2 + CO_2	2.52E-11	Sander et al. (2019)
G45064b	TrGC	LHC4ACCO3H + OH → LHC4ACCO3	2.88E-11	Rickard and Pascoe (2009)
G45065	TrGCN	LC5PAN1719 → LHC4ACCO3 + NO_2	k_PAN_M	Rickard and Pascoe (2009)
G45066	TrGCN	LC5PAN1719 + OH → .5 MACROH + .5 HO12CO3C4 + CO + NO_2	2.52E-11	Rickard and Pascoe (2009)
G45067	TrGC	HCOC5 + OH → C59O2	3.81E-11	Rickard and Pascoe (2009)
G45068	TrGC	HCOC5 + O_3 → BIACETOH + .335 H_2O_2 + .67 HCHO + .2079 CO + .1221 CH_2OO + .05280 OH	7.51E-16*EXP(-1521./temp)	Sander et al. (2019)
G45069	TrGC	C59O2 → CH_3COCH_2OH + HOCH2CO	k1_RO2tORO2	Sander et al. (2019)
G45070a	TrGC	C59O2 + HO_2 → OH + CH_3COCH_2OH + HOCH2CO	k_RO2_HO2(temp,5)*r_COCH2O2_OH	Sander et al. (2019)
G45070b	TrGC	C59O2 + HO_2 → C59OOH	k_RO2_HO2(temp,5)*r_COCH2O2_OOH	Sander et al. (2019)
G45071	TrGCN	C59O2 + NO → CH_3COCH_2OH + HOCH2CO + NO_2	KRO2NO	Sander et al. (2019)*
G45072	TrGCN	C59O2 + NO_3 → CH_3COCH_2OH + HOCH2CO + NO_2	KRO2NO3	Sander et al. (2019)
G45073	TrGC	C59OOH + OH → C59O2	9.7E-12	Rickard and Pascoe (2009)

Table 1: Gas phase reactions (... continued)

#	labels	reaction	rate coefficient	reference
G45074	TrGC	LIEPOX + OH → DB1O2 + H_2O	5.78E-11*EXP(-400./temp) *(1.52/3.+0.98*2./3.)/1.51	Paulot et al. (2009b), Bates et al. (2014), Sander et al. (2019)*
G45075	TrGC	ISOPBO2 → MVK + HCHO + OH	k_hsb	Sander et al. (2019)
G45076	TrGC	ISOPDO2 → MACR + HCHO + OH	k_hsd	Sander et al. (2019)
G45077a	TrGC	LZCODC23DBCOOH + OH → .6 C1ODC2O2C4OOH + .4 C1OOHC2O2C4OD	k_adt*a_CHO*a_CH2OOH	Sander et al. (2019)
G45077b	TrGC	LZCODC23DBCOOH + OH → .6 C1ODC3O2C4OOH + .4 C1OOHC3O2C4OD	k_ads*a_CHO*a_CH2OOH	Sander et al. (2019)
G45077c	TrGC	LZCODC23DBCOOH + OH → LZCO3HC23DBCOD	k_t*f_O*f_alk+k_ROOHRO	Sander et al. (2019)
G45077d	TrGC	LZCODC23DBCOOH + OH → C4MDIAL + OH	k_s*f_sOOH*f_allyl	Sander et al. (2019)
G45078	TrGC	LZCODC23DBCOOH + O_3 → .4672 OH + .2336 $HCOCOCH_2O_2$ + .2336 CO + .2336 $CH_3C(O)$ + .4672 HOOCH2CHO + .1728 MGLYOX + .1901 OH + .0864 GLYOX + .02765 HOOCH2CHO + .02765 H_2O_2 + .02592 CH_3OOH + .02592 CO_2 + .01037 HCOCO + .01555 CH_2OO + .01555 CO + .006908 $HOOCH_2CO_3$ + .2628 OH + .1314 MGLYOX + .1314 OH + .1314 $HCOCOCH_2OOH$ + .2628 GLYOX + .0972 $CH_3COCH_2O_2H$ + .00972 $HCOCO_2H$ + .005832 GLYOX + .005832 H_2O_2 + .05249 OH + .05249 HCOCO + .01458 HCHO + .01458 CO_2 + .01458 HCOOH + .01458 CO	2.4E-17	Sander et al. (2019)
G45079	TrGC	C1OOHC2O2C4OD → .78 $CH_3COCH_2O_2H$ + .78 HOCHCHO + .22 CO2H3CHO + .22 HCHO + .22 OH	k1_RO2tORO2	Sander et al. (2019)
G45080	TrGCN	C1OOHC2O2C4OD + NO → .78 $CH_3COCH_2O_2H$ + .78 HOCHCHO + .22 CO2H3CHO + .22 HCHO + .22 OH + NO_2	KRO2NO	Sander et al. (2019)*
G45081a	TrGC	C1OOHC2O2C4OD + HO_2 → C1OOHC2OOHC4OD	k_RO2_HO2(temp,5)*r_COCH2O2_OOH	Sander et al. (2019)
G45081b	TrGC	C1OOHC2O2C4OD + HO_2 → .78 $CH_3COCH_2O_2H$ + .78 HOCHCHO + .22 CO2H3CHO + .22 HCHO + 1.22 OH	k_RO2_HO2(temp,5)*r_COCH2O2_OH	Sander et al. (2019)
G45082	TrGC	C1OOHC2O2C4OD → $CH_3COCH_2O_2H$ + GLYOX + OH	k_hsb	Sander et al. (2019)
G45083	TrGC	C1ODC2O2C4OOH → OH + C1ODC2OOHC4OD	k_15hsdhb	Sander et al. (2019)
G45084a	TrGC	C1OOHC2OOHC4OD + OH → C1ODC2OOHC4OD + OH	2.*k_s*f_sOOH*f_tCH2OH	Sander et al. (2019)
G45084b	TrGC	C1OOHC2OOHC4OD + OH → $CH_3COCH_2O_2H$ + 2 CO + 2 HO_2 + OH	k_t*f_tOH*f_pCH2OH*f_pCH2OH	Sander et al. (2019)

Table 1: Gas phase reactions (... continued)

#	labels	reaction	rate coefficient	reference
G45084c	TrGC	C1OOHC2OOHC4OD + OH → C1OOHC2O2C4OD	k_ROOHRO	Sander et al. (2019)
G45085	TrGC	C1ODC2OOHC4OD + OH → CO2H3CHO + CO + H_2O + OH	k_t*f_O*f_tCH2OH+k_t*f_tOH*f_tOH*f_CHO	Sander et al. (2019)
G45086	TrGC	C1ODC3O2C4OOH → MGLYOX + HOOCH2CHO + HO_2	k1_RO2sORO2	Sander et al. (2019)
G45087	TrGCN	C1ODC3O2C4OOH + NO → MGLYOX + HOOCH2CHO + HO_2 + NO_2	KRO2NO	Sander et al. (2019)
G45088	TrGC	C1ODC3O2C4OOH + HO_2 → .5 $CH_3C(O)$ + .5 CO + .5 MGLYOX + .5 HO_2 + $HOOCH_2CO_3$	k_RO2_HO2(temp,5)	Sander et al. (2019)
G45089	TrGC	C1ODC3O2C4OOH → MGLYOX + OH + HOOCH2CHO	k_hsd	Sander et al. (2019)
G45090	TrGC	C1OOHC3O2C4OD → .625 MGLYOX + 2 CO + 1.625 HO_2 + .375 $CH_3C(O)$ + .375 CO_2 + OH	k_15hsdhb	Sander et al. (2019)
G45091	TrGC	LHC4ACCO3 → LZCO3HC23DBCOD + HO_2	k_16hs	Sander et al. (2019)
G45092a	TrGC	C4MDIAL + OH → C1ODC2O2C4OD	(k_adt+k_ads)*a_CHO*a_CHO	Sander et al. (2019)*
G45092b	TrGC	C4MDIAL + OH → LZCO3C23DBCOD	2.*k_t*f_O*f_alk	Sander et al. (2019)*
G45093	TrGCN	C4MDIAL + NO_3 → LZCO3C23DBCOD + HNO_3	KNO3AL*4.25*2.	Sander et al. (2019)*
G45094a	TrGC	C1ODC2O2C4OD + HO_2 → OH + MGLYOX + HOCHCHO	k_RO2_HO2(temp,5)*r_COCH2O2_OH	Sander et al. (2019)
G45094b	TrGC	C1ODC2O2C4OD + HO_2 → C1ODC2OOHC4OD	k_RO2_HO2(temp,5)*r_COCH2O2_OOH	Sander et al. (2019)
G45095	TrGCN	C1ODC2O2C4OD + NO → NO_2 + MGLYOX + HOCHCHO	KRO2NO	Sander et al. (2019)*
G45096	TrGC	C1ODC2O2C4OD → MGLYOX + HOCHCHO	k1_RO2tORO2	Sander et al. (2019)
G45097a	TrGC	C1ODC2OOHC4OD + OH → MGLYOX + 2 CO	(2.*k_t*f_O*f_tCH2OH*f_alk+k_t*f_tOH*f_CHO*f_pCH2OH)*.5	Sander et al. (2019)
G45097b	TrGC	C1ODC2OOHC4OD + OH → MGLYOX + 2 CO + OH	(2.*k_t*f_O*f_tCH2OH*f_alk+k_t*f_tOH*f_CHO*f_pCH2OH)*.5	Sander et al. (2019)
G45098	TrGCN	LISOPACNO3O2 + NO → .21 NOA + .21 $HOCH_2CHO$ + .21 HO_2 + .49 HO12CO3C4 + .49 HCHO + .49 NO_2 + .045 MVKNO3 + .045 HCHO + .255 CH_3COCH_2OH + .255 $NO_3CH2CHO$ + .225 H_2O_2 + NO_2	KRO2NO	Sander et al. (2019)*
G45099	TrGCN	LISOPACNO3O2 → .21 NOA + .21 $HOCH_2CHO$ + .21 HO_2 + .49 HO12CO3C4 + .49 HCHO + .49 NO_2 + .045 MVKNO3 + .045 HCHO + .255 CH_3COCH_2OH + .255 $NO_3CH2CHO$ + .225 H_2O_2	k1_RO2tORO2+k_RO2_HO2(temp,5)*c(ind_HO2)	Sander et al. (2019)

Table 1: Gas phase reactions (... continued)

#	labels	reaction	rate coefficient	reference
G45100	TrGCN	ISOPBDNO3O2 + NO → .6 CH_3COCH_2OH + .6 $HOCH_2CHO$ + .26 MACRNO3 + .14 MVKNO3 + .4 HCHO + .4 HO_2 + 1.6 NO_2	KRO2NO	Sander et al. (2019)*
G45101	TrGCN	ISOPBDNO3O2 → .6 CH_3COCH_2OH + .6 $HOCH_2CHO$ + .26 MACRNO3 + .14 MVKNO3 + .4 HCHO + .4 HO_2 + .6 NO_2	k1_RO2sORO2+k_RO2_HO2(temp,5) *c(ind_HO2)	Sander et al. (2019)
G45102	TrGCN	LISOPACNO3 + O_3 → .8704 OH + .365 HO_2 + .73 MGLYOX + .4325 $NO_3CH2CHO$ + .135 CH_3COCH_2OH + .0675 GLYOX + .4325 NO_2 + .0891 H_2O_2 + .135 NOA + .0675 HOCHCHO + .3866 $HOCH_2CHO$ + .0405 CH_3OH + .0405 CO + .0054 HOCH2CO	2.8E-17	Feierabend et al. (2008), Sander et al. (2019)
G45103	TrGC	DB1O2 → DB1O2	k1_RO2sORO2	Sander et al. (2019)
G45104a	TrGC	DB1O2 + HO_2 → DB1OOH	k_RO2_HO2(temp,5)*(1.-r_ CHOHCH2O2_OH)	Sander et al. (2019)*
G45104b	TrGC	DB1O2 + HO_2 → DB1O2 + OH	k_RO2_HO2(temp,5)*r_CHOHCH2O2_OH	Sander et al. (2019)
G45105a	TrGCN	DB1O2 + NO → DB1O2 + NO_2	KRO2NO*(1.-alpha_AN(7,2,0,0,0, temp,cair))	Sander et al. (2019)
G45105b	TrGCN	DB1O2 + NO → DB1NO3	KRO2NO*alpha_AN(7,2,0,0,0,temp, cair)	Sander et al. (2019)
G45106	TrGCN	DB1O2 + NO_3 → DB1O2 + NO_2	KRO2NO3	Sander et al. (2019)
G45107	TrGC	DB1O2 → DB1O2 + OH	1.E4	Peeters and Nguyen (2012)*
G45108a	TrGC	DB1O2 → DB1O2	KDEC*0.72	see note*
G45108b	TrGC	DB1O2 → .5 HVMK + .5 HMAC + HCHO + HO_2	KDEC*0.28	see note*
G45109	TrGC	DB1O2 → .48 CH_3COCH_2OH + .52 $HOCH_2CHO$ + .52 MGLYOX + .48 GLYOX + HO_2	k1_RO2sORO2	Sander et al. (2019)
G45110a	TrGC	DB1O2 + HO_2 → DB2OOH	k_RO2_HO2(temp,5)*(1.-r_ CHOHCH2O2_OH)	Sander et al. (2019)
G45110b	TrGC	DB1O2 + HO_2 → .48 CH_3COCH_2OH + .52 $HOCH_2CHO$ + .52 MGLYOX + .48 GLYOX + HO_2 + OH	k_RO2_HO2(temp,5)*r_CHOHCH2O2_OH	Sander et al. (2019)
G45111	TrGCN	DB1O2 + NO → .48 CH_3COCH_2OH + .52 $HOCH_2CHO$ + .52 MGLYOX + .48 GLYOX + HO_2 + NO_2	KRO2NO	see note*
G45112	TrGCN	DB1O2 + NO_3 → .48 CH_3COCH_2OH + .52 $HOCH_2CHO$ + .52 MGLYOX + .48 GLYOX + HO_2 + NO_2	KRO2NO3	Sander et al. (2019)
G45113	TrGC	DB1O2 → .48 MACROOH + .52 LHMVKABOOH + CO + OH	k_14hsal	Sander et al. (2019)

Table 1: Gas phase reactions (... continued)

#	labels	reaction	rate coefficient	reference
G45114a	TrGC	DB1OOH + OH → DB1O2	k_ROOHRO	Sander et al. (2019)
G45114b	TrGC	DB1OOH + OH → HCOOH + HO_2 + CH_3COCHO_2CHO	k_adt	Sander et al. (2019)*
G45115	TrGC	DB1OOH + HCOOH → C1ODC2OOHC4OD + HCOOH	4.67E-26*(temp)**(3.286) *EXP(4509./(1.987*temp))	Sander et al. (2019), da Silva (2010)*
G45116	TrGCN	DB1NO3 + OH → HCOOH + NO_2 + CH_3COCHO_2CHO	k_adt	Sander et al. (2019)*
G45117	TrGC	DB2OOH + OH → DB1O2	k_ROOHRO	Sander et al. (2019)*
G45118	TrGC	LISOPACOOH + O_3 → 1.3272 OH + .36986 HO_2 + .0432 H_2O_2 + .08422 CO + .2025 CH_3OOH + .01215 CH_2OO + .3704 HCHO + .00405 CH_3OH + .0405 CO_2 + .1825 HOCH2COCH2O2 + .365 MGLYOX + .3866 HOOCH2CHO + .135 CH_3COCH_2OH + .0675 GLYOX + .00324 HCOCO + .3866 $HOCH_2CHO$ + .135 $CH_3COCH_2O_2H$ + .0675 HOCHCHO + .0054 HOCH2CO	4.829E-16	Sander et al. (2019)
G45119a	TrGC	LZCO3HC23DBCOD + OH → .62 CO2H3CHO + .62 OH + .62 CO_2 + .38 MGLYOX + .38 $HCOCO_3H$ + .38 HO_2	k_adt*a_CHO*a_CO2H	Sander et al. (2019)
G45119b	TrGC	LZCO3HC23DBCOD + OH → .62 CH_3COCO_3H + 1.24 CO + 1.24 HO_2 + .38 MGLYOX + .38 HO_2 + .38 CO + .38 HO_2 + .38 OH + .38 CO_2	k_ads*a_CHO*a_CO2H	Sander et al. (2019)
G45120	TrGC	LISOPEFO2 → LISOPEFO	k1_RO2pORO2	Sander et al. (2019)
G45121a	TrGCN	LISOPEFO2 + NO → LISOPEFO + NO_2	KRO2NO*(1.-alpha_AN(6,1,0,0,0, temp,cair))	Sander et al. (2019)
G45121b	TrGCN	LISOPEFO2 + NO → ISOPDNO3	KRO2NO*alpha_AN(6,1,0,0,0,temp, cair)	Sander et al. (2019)*
G45122a	TrGC	LISOPEFO2 + HO_2 → .7143 ISOPDOOH + .2857 ISOPBOOH	k_RO2_HO2(temp,5)*(1.-r_ CHOHCH2O2_OH)	Sander et al. (2019)
G45122b	TrGC	LISOPEFO2 + HO_2 → LISOPEFO + OH	k_RO2_HO2(temp,5)*r_CHOHCH2O2_OH	Sander et al. (2019)
G45123	TrGCN	LISOPEFO2 + NO_3 → LISOPEFO + NO_2	KRO2NO3	Sander et al. (2019)
G45124	TrGC	LISOPEFO2 → .7143 MACR + .2857 MVK + HCHO + OH	0.7143*k_hsd+.2857*k_hsb	Sander et al. (2019)
G45125	TrGC	LISOPEFO → .7143 MACR + .2857 MVK + HCHO + HO_2	KDEC	Sander et al. (2019)
G45126a	TrGC	LISOPACO → 3METHYLFURAN + HO_2	KDEC*0.37	Sander et al. (2019), Paulot et al. (2009a), Francisco-Marquez et al. (2003)

Table 1: Gas phase reactions (... continued)

#	labels	reaction	rate coefficient	reference
G45126b	TrGC	LISOPACO → .65 LHC4ACCHO + .65 HO_2 + .35 DB1O2	KDEC*(1.-0.37)	Sander et al. (2019), Paulot et al. (2009a), Francisco-Marquez et al. (2003)
G45127a	TrGC	LISOPACO → 3METHYLFURAN + HO_2	KDEC*0.37	Sander et al. (2019), Paulot et al. (2009a), Francisco-Marquez et al. (2003)
G45127b	TrGC	LISOPACO → .65 LHC4ACCHO + .65 HO_2 + .35 DB1O2	KDEC*(1.-0.37)	Sander et al. (2019), Paulot et al. (2009a), Francisco-Marquez et al. (2003)
G45128	TrGC	3METHYLFURAN + OH → L3METHYLFURANO2	3.2E-11*EXP(310./temp)	Sander et al. (2019)*
G45129	TrGCN	3METHYLFURAN + NO_3 → L3METHYLFURANO2 + NO_2	1.9E-11	Sander et al. (2019), Atkinson et al. (2006)*
G45130	TrGC	L3METHYLFURANO2 → C4MDIAL + HO_2	k1_RO2sORO2	Sander et al. (2019)
G45131	TrGCN	L3METHYLFURANO2 + NO → C4MDIAL + HO_2 + NO_2	KRO2NO	Sander et al. (2019)*
G45132	TrGC	L3METHYLFURANO2 + HO_2 → C4MDIAL + HO_2	k_RO2_HO2(temp,5)	Sander et al. (2019)*
G45133	TrGC	LZCO3C23DBCOD → .62 EZCH3CO2CHCHO + .38 EZCHOCCH3CHO2 + CO_2	k1_RO2RCO3	Sander et al. (2019)
G45134a	TrGC	LZCO3C23DBCOD + HO_2 → .62 EZCH3CO2CHCHO + .38 EZCHOCCH3CHO2 + CO_2 + OH	KAPHO2*r_CO3_OH	Sander et al. (2019)
G45134b	TrGC	LZCO3C23DBCOD + HO_2 → LZCO3HC23DBCOD	KAPHO2*(r_CO3_OOH+r_CO3_O3)	Sander et al. (2019)*
G45135	TrGCN	LZCO3C23DBCOD + NO → .62 EZCH3CO2CHCHO + .38 EZCHOCCH3CHO2 + CO_2 + NO_2	KAPNO	Sander et al. (2019)
G45136	TrGCN	LZCO3C23DBCOD + NO_2 → LZCPANC23DBCOD	k_CH3CO3_NO2	Rickard and Pascoe (2009)
G45137	TrGCN	LZCO3C23DBCOD + NO_3 → .62 EZCH3CO2CHCHO + .38 EZCHOCCH3CHO2 + CO_2 + NO_2	KRO2NO3*1.74	Sander et al. (2019)
G45138	TrGCN	LZCPANC23DBCOD → LZCO3C23DBCOD + NO_2	k_PAN_M	Rickard and Pascoe (2009)
G45139	TrGCN	LZCPANC23DBCOD + OH → .62 EZCH3CO2CHCHO + .38 EZCHOCCH3CHO2 + CO_2 + NO_2	2.52E-11	Sander et al. (2019)*
G45200	TrGTerC	C511O2 → $CH_3C(O)$ + HCOCH2CHO	k1_RO2sORO2	Rickard and Pascoe (2009)
G45201	TrGTerCN	C511O2 + NO → $CH_3C(O)$ + HCOCH2CHO + NO_2	KRO2NO	Rickard and Pascoe (2009)*
G45202a	TrGTerC	C511O2 + HO_2 → C511OOH	k_RO2_HO2(temp,5)*r_COCH2O2_OOH	Rickard and Pascoe (2009), Sander et al. (2019)
G45202b	TrGTerC	C511O2 + HO_2 → $CH_3C(O)$ + HCOCH2CHO + OH	k_RO2_HO2(temp,5)*r_COCH2O2_OH	Rickard and Pascoe (2009), Sander et al. (2019)

Table 1: Gas phase reactions (... continued)

#	labels	reaction	rate coefficient	reference
G45203	TrGTerC	C511OOH + OH → C511O2	7.49E-11	Rickard and Pascoe (2009)
G45204	TrGTerC	CO23C4CHO + OH → CO23C4CO3	6.65E-11	Rickard and Pascoe (2009)
G45205	TrGTerCN	CO23C4CHO + NO_3 → CO23C4CO3 + HNO_3	KNO3AL*5.5	Rickard and Pascoe (2009)
G45206	TrGTerC	CO23C4CO3 → $CH_3COCOCH_2O_2$ + CO_2	k1_RO2RCO3	Rickard and Pascoe (2009)
G45207	TrGTerCN	CO23C4CO3 + NO → $CH_3COCOCH_2O_2$ + CO_2 + NO_2	KAPNO	Rickard and Pascoe (2009)*
G45208	TrGTerCN	CO23C4CO3 + NO_2 → C5PAN9	k_CH3CO3_NO2	Rickard and Pascoe (2009)
G45209a	TrGTerC	CO23C4CO3 + HO_2 → CO23C4CO3H	KAPHO2*(r_CO3_OOH+r_CO3_O3)	Rickard and Pascoe (2009)
G45209b	TrGTerC	CO23C4CO3 + HO_2 → $CH_3COCOCH_2O_2$ + CO_2 + OH	KAPHO2*r_CO3_OH	Rickard and Pascoe (2009)
G45210	TrGTerCN	C5PAN9 → CO23C4CO3 + NO_2	k_PAN_M	Rickard and Pascoe (2009)
G45211	TrGTerCN	C5PAN9 + OH → $CH_3COCOCHO$ + CO + NO_2	3.12E-13	Rickard and Pascoe (2009)
G45212	TrGTerC	C512O2 → C513O2	k1_RO2pRO2	Rickard and Pascoe (2009)
G45213	TrGTerC	C512O2 + HO_2 → C512OOH	k_RO2_HO2(temp,5)	Rickard and Pascoe (2009)
G45214	TrGTerCN	C512O2 + NO → C513O2 + NO_2	KRO2NO	Rickard and Pascoe (2009)*
G45215	TrGTerC	C512OOH + OH → CO13C4CHO + OH	1.01E-10	Rickard and Pascoe (2009)
G45216	TrGTerC	C513O2 → GLYOX + $HOC_2H_4CO_3$	k1_RO2sORO2	Rickard and Pascoe (2009)
G45217	TrGTerCN	C513O2 + NO → GLYOX + $HOC_2H_4CO_3$ + NO_2	KRO2NO	Rickard and Pascoe (2009)*
G45218a	TrGTerC	C513O2 + HO_2 → C513OOH	k_RO2_HO2(temp,5)*r_COCH2O2_OOH	Rickard and Pascoe (2009), Sander et al. (2019)
G45218b	TrGTerC	C513O2 + HO_2 → GLYOX + $HOC_2H_4CO_3$ + OH	k_RO2_HO2(temp,5)*r_COCH2O2_OH	Rickard and Pascoe (2009), Sander et al. (2019)
G45219	TrGTerC	CO13C4CHO + OH → CHOC3COCO3	1.33E-10	Rickard and Pascoe (2009)
G45220	TrGTerCN	CO13C4CHO + NO_3 → CHOC3COCO3 + HNO_3	2.*KNO3AL*5.5	Rickard and Pascoe (2009)
G45221	TrGTerC	C513OOH + OH → C513CO + OH	9.23E-11	Rickard and Pascoe (2009)
G45222	TrGTerC	CHOC3COCO3 → CHOC3COO2 + CO_2	k1_RO2RCO3	Rickard and Pascoe (2009)
G45223	TrGTerC	CHOC3COCO3 + HO_2 → CHOC3COOOH	KAPHO2	Rickard and Pascoe (2009)
G45224	TrGTerCN	CHOC3COCO3 + NO_2 → CHOC3COPAN	k_CH3CO3_NO2	Rickard and Pascoe (2009)
G45225	TrGTerCN	CHOC3COCO3 + NO → CHOC3COO2 + CO_2 + NO_2	KAPNO	Rickard and Pascoe (2009)*
G45226	TrGTerC	C513CO + OH → $HOC_2H_4CO_3$ + CO + CO	2.64E-11	Rickard and Pascoe (2009)
G45227	TrGTerC	C514O2 + HO_2 → C514OOH	k_RO2_HO2(temp,5)	Rickard and Pascoe (2009)
G45228a	TrGTerCN	C514O2 + NO → CO13C4CHO + HO_2 + NO_2	KRO2NO*(1.-alpha_AN(7,2,0,1,0,temp,cair))	Rickard and Pascoe (2009), Sander et al. (2019)
G45228b	TrGTerCN	C514O2 + NO → C514NO3	KRO2NO*alpha_AN(7,2,0,1,0,temp,cair)	Rickard and Pascoe (2009), Sander et al. (2019)
G45229	TrGTerCN	C514O2 + NO_3 → CO13C4CHO + HO_2 + NO_2	KRO2NO3	Rickard and Pascoe (2009)
G45230	TrGTerC	C514O2 → CO13C4CHO + HO_2	k1_RO2sRO2	Rickard and Pascoe (2009)

Table 1: Gas phase reactions (... continued)

#	labels	reaction	rate coefficient	reference
G45231	TrGTerC	C514OOH + OH → CO13C4CHO + OH	1.10E-10	Rickard and Pascoe (2009)
G45232	TrGTerCN	C514NO3 + OH → CO13C4CHO + NO_2	4.33E-11	Rickard and Pascoe (2009)
G45233	TrGTerC	CHOC3COOOH + OH → CHOC3COCO3	7.55E-11	Rickard and Pascoe (2009)
G45234	TrGTerCN	CHOC3COPAN → CHOC3COCO3 + NO_2	k_PAN_M	Rickard and Pascoe (2009)
G45235	TrGTerCN	CHOC3COPAN + OH → C4CODIAL + CO + NO_2	7.19E-11	Rickard and Pascoe (2009)
G45236	TrGTerC	MBO + OH → LMBOABO2	8.1E-12*EXP(610./temp)	Rickard and Pascoe (2009), Sander et al. (2019)*
G45237a	TrGTerC	MBO + O_3 → HCHO + .16 CH_3COCH_3 + .16 HO_2 + .16 CO + .16 OH + .84 MBOOO	1.0E-17*0.57	Rickard and Pascoe (2009), Sander et al. (2019)
G45237b	TrGTerC	MBO + O_3 → IBUTALOH + .63 CO + .37 $HOCH_2OOH$ + .16 OH + .16 HO_2	1.0E-17*0.43	Rickard and Pascoe (2009), Sander et al. (2019)
G45238	TrGTerCN	MBO + NO_3 → LNMBOABO2	4.6E-14*EXP(-400./temp)	Rickard and Pascoe (2009), Sander et al. (2019)
G45239	TrGTerC	LMBOABO2 + HO_2 → LMBOABOOH	k_RO2_HO2(temp,5)	Rickard and Pascoe (2009), Sander et al. (2019)
G45240a	TrGTerCN	LMBOABO2 + NO → LMBOABNO3	KRO2NO*(.67*alpha_AN(7,2,0,0,0, temp,cair)+.33*alpha_AN(7,1,0,0, 0,temp,cair))	Rickard and Pascoe (2009), Sander et al. (2019)
G45240b	TrGTerCN	LMBOABO2 + NO → $HOCH_2CHO$ + CH_3COCH_3 + HO_2 + NO_2	KRO2NO*(1.-(.67*alpha_AN(7,2,0, 0,0,temp,cair)+.33*alpha_AN(7,1, 0,0,0,temp,cair)))*.67	Rickard and Pascoe (2009), Sander et al. (2019)
G45240c	TrGTerCN	LMBOABO2 + NO → IBUTALOH + HCHO + HO_2 + NO_2	KRO2NO*(1.-(.67*alpha_AN(7,2,0, 0,0,temp,cair)+.33*alpha_AN(7,1, 0,0,0,temp,cair)))*.33	Rickard and Pascoe (2009), Sander et al. (2019)
G45241a	TrGTerC	LMBOABO2 → $HOCH_2CHO$ + CH_3COCH_3 + HO_2	k1_RO2sORO2*.67	Rickard and Pascoe (2009), Sander et al. (2019)
G45241b	TrGTerC	LMBOABO2 → IBUTALOH + HCHO + HO_2	k1_RO2pORO2*.33	Rickard and Pascoe (2009), Sander et al. (2019)
G45242a	TrGTerC	LMBOABOOH + OH → MBOACO	0.67*2.93E-11+.33*2.05E-12	Rickard and Pascoe (2009), Sander et al. (2019)
G45242b	TrGTerC	LMBOABOOH + OH → LMBOABO2	k_ROOHRO	Rickard and Pascoe (2009), Sander et al. (2019)
G45243	TrGTerCN	LMBOABNO3 + OH → MBOACO + NO_2	0.67*1.75E-12+.33*2.69E-12	Rickard and Pascoe (2009), Sander et al. (2019)
G45244	TrGTerC	MBOACO + OH → MBOCOCO + HO_2	3.79E-12	Rickard and Pascoe (2009)

Table 1: Gas phase reactions (... continued)

#	labels	reaction	rate coefficient	reference
G45245	TrGTerC	MBOCOCO + OH → CO + IPRHOCO3	1.38E-11	Rickard and Pascoe (2009)
G45246	TrGTerCN	LNMBOABO2 + HO_2 → LNMBOABOOH	k_RO2_HO2(temp,5)	Rickard and Pascoe (2009), Sander et al. (2019)
G45247	TrGTerCN	LNMBOABO2 + NO → .65 $NO_3CH2CHO$ + .65 CH_3COCH_3 + .65 HO_2 + .35 IBUTALOH + .35 HCHO + .35 NO_2 + NO_2	KRO2NO	Rickard and Pascoe (2009), Sander et al. (2019)*
G45248	TrGTerCN	LNMBOABO2 + NO_3 → .65 $NO_3CH2CHO$ + .65 CH_3COCH_3 + .65 HO_2 + .35 IBUTALOH + .35 HCHO + .35 NO_2 + NO_2	KRO2NO3	Rickard and Pascoe (2009), Sander et al. (2019)
G45249	TrGTerCN	LNMBOABO2 → .65 $NO_3CH2CHO$ + .65 CH_3COCH_3 + .65 HO_2 + .35 IBUTALOH + .35 HCHO + .35 NO_2	k1_RO2sORO2	Rickard and Pascoe (2009), Sander et al. (2019)
G45250a	TrGTerCN	LNMBOABOOH + OH → .65 C4MCONO3OH + .35 NMBOBCO	0.65*4.89E-12+.35*2.52E-12	Rickard and Pascoe (2009), Sander et al. (2019)
G45250b	TrGTerCN	LNMBOABOOH + OH → LNMBOABO2	k_ROOHRO	Rickard and Pascoe (2009), Sander et al. (2019)
G45251	TrGTerCN	NMBOBCO + OH → NC4OHCO3	4.26E-12	Rickard and Pascoe (2009)
G45252a	TrGTerCN	NC4OHCO3 + HO_2 → IBUTALOH + CO_2 + NO_2 + OH	KAPHO2*r_CO3_OH	Rickard and Pascoe (2009), Sander et al. (2019)
G45252b	TrGTerCN	NC4OHCO3 + HO_2 → NC4OHCO3H	KAPHO2*(r_CO3_O3+r_CO3_OOH)	Rickard and Pascoe (2009), Sander et al. (2019)
G45253	TrGTerCN	NC4OHCO3 + NO → IBUTALOH + CO_2 + NO_2 + NO_2	KAPNO	Rickard and Pascoe (2009)
G45254	TrGTerCN	NC4OHCO3 + NO_2 → NC4OHCPAN	k_CH3CO3_NO2	Rickard and Pascoe (2009)
G45255	TrGTerCN	NC4OHCO3 + NO_3 → IBUTALOH + CO_2 + NO_2 + NO_2	KRO2NO3*1.74	Rickard and Pascoe (2009)
G45256	TrGTerCN	NC4OHCO3 → IBUTALOH + CO_2 + NO_2	k1_RO2RCO3	Rickard and Pascoe (2009)
G45257	TrGTerCN	NC4OHCO3H + OH → NC4OHCO3	4.50E-12	Rickard and Pascoe (2009)
G45258	TrGTerCN	NC4OHCPAN + OH → IBUTALOH + CO + NO_2 + NO_2	1.27E-12	Rickard and Pascoe (2009)
G45259	TrGTerCN	NC4OHCPAN → NC4OHCO3 + NO_2	k_PAN_M	Rickard and Pascoe (2009)
G45260	TrGTerCN	C4MCONO3OH + OH → CH_3COCH_3 + HCHO + CO_2 + NO_2	1.23E-12	Rickard and Pascoe (2009), Sander et al. (2019)
G45400	TrGAroCN	NC4MDCO2HN + OH → MMALANHY + NO_2	k_ROOHRO	Rickard and Pascoe (2009)*
G45401	TrGAroCN	C54CO + NO_3 → 3 CO + $CH_3C(O)OO$ + HNO_3	KNO3AL*5.5	Rickard and Pascoe (2009)
G45402	TrGAroC	C54CO + OH → 3 CO + $CH_3C(O)OO$	1.72E-11	Rickard and Pascoe (2009)
G45403a	TrGAroCN	NTLFUO2 + HO_2 → NTLFUOOH	k_RO2_HO2(temp,5)*(1.-r_COCH2O2_OH)	Rickard and Pascoe (2009)
G45403b	TrGAroCN	NTLFUO2 + HO_2 → ACCOMECHO + NO_2 + OH	k_RO2_HO2(temp,5)*r_COCH2O2_OH	Rickard and Pascoe (2009)

Table 1: Gas phase reactions (... continued)

#	labels	reaction	rate coefficient	reference
G45404	TrGAroCN	NTLFUO2 + NO → ACCOMECHO + NO_2 + NO_2	KRO2NO	Rickard and Pascoe (2009)*
G45405	TrGAroCN	NTLFUO2 + NO_3 → ACCOMECHO + NO_2 + NO_2	KRO2NO3	Rickard and Pascoe (2009)*
G45406	TrGAroCN	NTLFUO2 → ACCOMECHO + NO_2	k1_RO2tORO2	Rickard and Pascoe (2009)*
G45407	TrGAroC	C5134CO2OH + OH → C54CO + HO_2	7.48E-11	Rickard and Pascoe (2009)
G45408	TrGAroCN	C5COO2NO2 + OH → MGLYOX + CO + CO + NO_2	5.43E-11	Rickard and Pascoe (2009)
G45409	TrGAroCN	C5COO2NO2 → C5CO14O2 + NO_2	k_PAN_M	Rickard and Pascoe (2009)*
G45410	TrGAroC	C5DIALOOH + OH → C5DIALCO + OH	7.52E-11	Rickard and Pascoe (2009)
G45411a	TrGAroC	C4CO2DBCO3 + HO_2 → C4CO2DCO3H	KAPHO2*(r_CO3_OOH+r_CO3_O3)	Rickard and Pascoe (2009)
G45411b	TrGAroC	C4CO2DBCO3 + HO_2 → HO_2 + CO + HCOCOCHO + CO_2 + OH	KAPHO2*r_CO3_OH	Rickard and Pascoe (2009), Sander et al. (2019)
G45412	TrGAroCN	C4CO2DBCO3 + NO → HO_2 + CO + HCOCOCHO + CO_2 + NO_2	KAPNO	Rickard and Pascoe (2009)
G45413	TrGAroCN	C4CO2DBCO3 + NO_2 → C4CO2DBPAN	k_CH3CO3_NO2	Rickard and Pascoe (2009)*
G45414	TrGAroCN	C4CO2DBCO3 + NO_3 → HO_2 + CO + HCOCOCHO + CO_2 + NO_2	KRO2NO3*1.74	Rickard and Pascoe (2009)
G45415	TrGAroC	C4CO2DBCO3 → HO_2 + CO + HCOCOCHO + CO_2	k1_RO2RCO3	Rickard and Pascoe (2009)
G45416	TrGAroC	MMALANHY + OH → MMALANHYO2	1.50E-12	Rickard and Pascoe (2009)
G45421a	TrGAroC	MMALANHYO2 + HO_2 → MMALNHYOOH	k_RO2_HO2(temp,5)*(1.-r_COCH2O2_OH-r_CHOHCH2O2_OH)	Rickard and Pascoe (2009), Sander et al. (2019)
G45421b	TrGAroC	MMALANHYO2 + HO_2 → CO2H3CO3 + CO_2 + OH	k_RO2_HO2(temp,5)*(r_COCH2O2_OH+r_CHOHCH2O2_OH)	Rickard and Pascoe (2009), Sander et al. (2019)
G45422	TrGAroCN	MMALANHYO2 + NO → CO2H3CO3 + CO_2 + NO_2	KRO2NO	Rickard and Pascoe (2009)*
G45423	TrGAroCN	MMALANHYO2 + NO_3 → CO2H3CO3 + CO_2 + NO_2	KRO2NO3	Rickard and Pascoe (2009)*
G45424	TrGAroC	MMALANHYO2 → CO2H3CO3 + CO_2	k1_RO2tORO2	Rickard and Pascoe (2009)*
G45428	TrGAroCN	C4CO2DBPAN + OH → HCOCOCHO + CO_2 + CO + NO_2	2.74E-11	Rickard and Pascoe (2009)
G45429	TrGAroCN	C4CO2DBPAN → C4CO2DBCO3 + NO_2	k_PAN_M	Rickard and Pascoe (2009)*
G45430a	TrGAroC	C5CO14O2 + HO_2 → .83 MALANHY + .83 CH_3 + .17 MGLYOX + .17 HO_2 + .17 CO + .17 CO_2 + OH	KAPHO2*r_CO3_OH	Rickard and Pascoe (2009)*
G45430b	TrGAroC	C5CO14O2 + HO_2 → C5CO14OH + O_3	KAPHO2*r_CO3_O3	Rickard and Pascoe (2009)
G45430c	TrGAroC	C5CO14O2 + HO_2 → C5CO14OOH	KAPHO2*r_CO3_OOH	Rickard and Pascoe (2009)
G45431	TrGAroCN	C5CO14O2 + NO → .83 MALANHY + .83 CH_3 + .17 MGLYOX + .17 HO_2 + .17 CO + .17 CO_2 + NO_2	KAPNO	Rickard and Pascoe (2009)*
G45432	TrGAroCN	C5CO14O2 + NO_2 → C5COO2NO2	k_CH3CO3_NO2	Rickard and Pascoe (2009)*

Table 1: Gas phase reactions (... continued)

#	labels	reaction	rate coefficient	reference
G45433	TrGAroCN	C5CO14O2 + NO_3 → .83 MALANHY + .83 CH_3 + .17 MGLYOX + .17 HO_2 + .17 CO + .17 CO_2 + NO_2	KRO2NO3*1.74	Rickard and Pascoe (2009)*
G45434	TrGAroC	C5CO14O2 → .83 MALANHY + .83 CH_3 + .17 MGLYOX + .17 HO_2 + .17 CO + .17 CO_2	k1_RO2RCO3	Rickard and Pascoe (2009)*
G45436	TrGAroC	C5CO14OH + OH → .83 MALANHY + .83 CH_3 + .17 MGLYOX + .17 HO_2 + .17 CO + .17 CO_2	5.44E-11	Rickard and Pascoe (2009)*
G45441	TrGAroCN	C5DICARB + NO_3 → C5CO14O2 + HNO_3	KNO3AL*2.75	Rickard and Pascoe (2009)
G45442	TrGAroC	C5DICARB + O_3 → .5338 GLYOX + .063 CH_3CHO + .348 $CH_3C(O)OO$ + .918 CO + .57 OH + .473 HO_2 + .0563 CH_3COCO_2H + .5338 MGLYOX + .676 H_2O_2 + .063 HCHO + .0563 $HCOCO_2H$ + .2465 CO_2	2.00E-18	Rickard and Pascoe (2009)
G45443	TrGAroC	C5DICARB + OH → .48 C5CO14O2 + .52 C5DICARBO2	6.2E-11	Rickard and Pascoe (2009)
G45444	TrGAroC	MC3ODBCO2H + OH → .35 GLYOX + .35 CH_3 + .35 CO + .35 CO_2 + .65 MMALANHY + .65 HO_2	4.38E-11	Rickard and Pascoe (2009)*
G45451	TrGAroCN	TLFUONE + NO_3 → NTLFUO2	1.00E-12	Rickard and Pascoe (2009)
G45452	TrGAroC	TLFUONE + O_3 → .5 CO + .5 OH + .5 MECOACETO2 + .3125 C24O3CCO2H + .1875 ACCOMECHO + .1875 H_2O_2	8.00E-19	see note*
G45453	TrGAroC	TLFUONE + OH → TLFUO2	6.90E-11	Rickard and Pascoe (2009)
G45454a	TrGAroC	ACCOMECO3 + HO_2 → ACCOMECO3H	KAPHO2*(r_CO3_OOH+r_CO3_O3)	Rickard and Pascoe (2009)
G45454b	TrGAroC	ACCOMECO3 + HO_2 → MECOACETO2 + CO_2 + OH	KAPHO2*r_CO3_OH	Rickard and Pascoe (2009)
G45455	TrGAroCN	ACCOMECO3 + NO → MECOACETO2 + CO_2 + NO_2	KAPNO	Rickard and Pascoe (2009)
G45456	TrGAroCN	ACCOMECO3 + NO_2 → ACCOMEPAN	k_CH3CO3_NO2	Rickard and Pascoe (2009)*
G45457	TrGAroCN	ACCOMECO3 + NO_3 → MECOACETO2 + CO_2 + NO_2	KRO2NO3*1.74	Rickard and Pascoe (2009)
G45458	TrGAroC	ACCOMECO3 → MECOACETO2 + CO_2	k1_RO2RCO3	Rickard and Pascoe (2009)
G45459	TrGAroC	C4CO2DCO3H + OH → C4CO2DBCO3	3.06E-11	Rickard and Pascoe (2009)
G45464	TrGAroCN	ACCOMECHO + NO_3 → ACCOMECO3 + HNO_3	KNO3AL*5.5	Rickard and Pascoe (2009)
G45465	TrGAroC	ACCOMECHO + OH → ACCOMECO3	7.09E-11	Rickard and Pascoe (2009)
G45466	TrGAroC	MMALNHYOOH + OH → MMALANHYO2	1.69E-11	Rickard and Pascoe (2009)
G45467a	TrGAroC	C5DICAROOH + OH → C5134CO2OH + OH	1.21E-10	Rickard and Pascoe (2009)
G45467b	TrGAroC	C5DICAROOH + OH → C5DICARBO2	k_ROOHRO	Rickard and Pascoe (2009)
G45468	TrGAroC	C24O3CCO2H + OH → MECOACETO2 + CO_2	8.76E-13	Rickard and Pascoe (2009)
G45469	TrGAroCN	NTLFUOOH + OH → NTLFUO2	4.44E-12	Rickard and Pascoe (2009)
G45470	TrGAroCN	ACCOMEPAN + OH → METACETHO + CO + CO + NO_2	1.00E-14	Rickard and Pascoe (2009)

Table 1: Gas phase reactions (... continued)

#	labels	reaction	rate coefficient	reference
G45471	TrGAroCN	ACCOMEPAN → ACCOMECO3 + NO_2	k_PAN_M	Rickard and Pascoe (2009)
G45476a	TrGAroC	TLFUO2 + HO_2 → TLFUOOH	k_RO2_HO2(temp,5)*(1.-r_COCH2O2_OH-r_CHOHCH2O2_OH)	Rickard and Pascoe (2009)
G45476b	TrGAroC	TLFUO2 + HO_2 → ACCOMECHO + HO_2 + OH	k_RO2_HO2(temp,5)*(r_COCH2O2_OH+r_CHOHCH2O2_OH)	Rickard and Pascoe (2009)*
G45477	TrGAroCN	TLFUO2 + NO → ACCOMECHO + HO_2 + NO_2	KRO2NO	Rickard and Pascoe (2009)*
G45478	TrGAroCN	TLFUO2 + NO_3 → ACCOMECHO + HO_2 + NO_2	KRO2NO3	Rickard and Pascoe (2009)*
G45479	TrGAroC	TLFUO2 → ACCOMECHO + HO_2	k1_RO2tORO2	Rickard and Pascoe (2009)*
G45480	TrGAroC	C5CO14OOH + OH → C5CO14O2	3.59E-12	Rickard and Pascoe (2009)
G45483	TrGAroC	TLFUOOH + OH → TLFUO2	2.53E-11	Rickard and Pascoe (2009)
G45485	TrGAroC	ACCOMECO3H + OH → ACCOMECO3	3.59E-12	Rickard and Pascoe (2009)
G45486a	TrGAroC	C5DIALO2 + HO_2 → C5DIALOOH	k_RO2_HO2(temp,5)*(1.-r_COCH2O2_OH)	Rickard and Pascoe (2009)
G45486b	TrGAroC	C5DIALO2 + HO_2 → MALDIAL + CO + HO_2 + OH	k_RO2_HO2(temp,5)*r_COCH2O2_OH	Rickard and Pascoe (2009)*
G45487	TrGAroCN	C5DIALO2 + NO → MALDIAL + CO + HO_2 + NO_2	KRO2NO	Rickard and Pascoe (2009)*
G45488	TrGAroCN	C5DIALO2 + NO_3 → MALDIAL + CO + HO_2 + NO_2	KRO2NO3	Rickard and Pascoe (2009)*
G45489	TrGAroC	C5DIALO2 → MALDIAL + CO + HO_2	k1_RO2sORO2	Rickard and Pascoe (2009)*
G45490a	TrGAroC	C5DICARBO2 + HO_2 → C5DICAROOH	k_RO2_HO2(temp,5)*(r_CO3_OOH+r_CO3_O3)	Rickard and Pascoe (2009)
G45491b	TrGAroC	C5DICARBO2 + HO_2 → MGLYOX + GLYOX + HO_2 + OH	k_RO2_HO2(temp,5)*r_CO3_OH	Rickard and Pascoe (2009)*
G45492	TrGAroCN	C5DICARBO2 + NO → MGLYOX + GLYOX + HO_2 + NO_2	KRO2NO	Rickard and Pascoe (2009)*
G45493	TrGAroCN	C5DICARBO2 + NO_3 → MGLYOX + GLYOX + HO_2 + NO_2	KRO2NO3	Rickard and Pascoe (2009)*
G45494	TrGAroC	C5DICARBO2 → MGLYOX + GLYOX + HO_2	k1_RO2sORO2	Rickard and Pascoe (2009)*
G46200a	TrGTerC	CO235C6O2 + HO_2 → CO235C6OOH	k_RO2_HO2(temp,6)*r_COCH2O2_OOH	Rickard and Pascoe (2009), Sander et al. (2019)
G46200b	TrGTerC	CO235C6O2 + HO_2 → CO23C4CO3 + HCHO + OH	k_RO2_HO2(temp,6)*r_COCH2O2_OH	Rickard and Pascoe (2009), Sander et al. (2019)
G46201	TrGTerCN	CO235C6O2 + NO → CO23C4CO3 + HCHO + NO_2	KRO2NO	Rickard and Pascoe (2009)*
G46202	TrGTerC	CO235C6O2 → CO23C4CO3 + HCHO	k1_RO2pORO2	Rickard and Pascoe (2009)
G46203	TrGTerC	CO235C6OOH + OH → CO235C6O2	1.01E-11	Rickard and Pascoe (2009)
G46204	TrGTerC	C614O2 → CO23C4CHO + HCHO + HO_2	k1_RO2sORO2	Rickard and Pascoe (2009)

Table 1: Gas phase reactions (... continued)

#	labels	reaction	rate coefficient	reference
G46205a	TrGTerCN	C614O2 + NO → CO23C4CHO + HCHO + HO_2 + NO_2	KRO2NO*(1.-alpha_AN(9,2,0,1,0,temp,cair))	Rickard and Pascoe (2009)
G46205b	TrGTerCN	C614O2 + NO → C614NO3	KRO2NO*alpha_AN(9,2,0,1,0,temp,cair)	Rickard and Pascoe (2009)
G46206a	TrGTerC	C614O2 + HO_2 → C614OOH	k_RO2_HO2(temp,6)*(1.-r_CHOHCH2O2_OH)	Rickard and Pascoe (2009), Sander et al. (2019)
G46206b	TrGTerC	C614O2 + HO_2 → CO23C4CHO + HCHO + HO_2 + OH	k_RO2_HO2(temp,6)*r_CHOHCH2O2_OH	Rickard and Pascoe (2009), Sander et al. (2019)
G46207	TrGTerCN	C614NO3 + OH → C614CO + NO_2	7.11E-12	Rickard and Pascoe (2009)
G46208	TrGTerC	C614OOH + OH → C614CO + OH	8.69E-11	Rickard and Pascoe (2009)
G46209	TrGTerC	C614CO + OH → CO235C5CHO + HO_2	3.22E-12	Rickard and Pascoe (2009)
G46210	TrGTerC	CO235C5CHO + OH → CO23C4CO3 + CO	1.33E-11	Rickard and Pascoe (2009)
G46211	TrGTerCN	CO235C5CHO + NO_3 → CO23C4CO3 + CO + HNO_3	KNO3AL*5.5	Rickard and Pascoe (2009)
G46400	TrGAroC	PHENOOH + OH → PHENO2	1.16E-10	Rickard and Pascoe (2009)
G46401	TrGAroC	C6CO4DB + OH → CO + CO + HO_2 + CO + HCOCOCHO	7.70E-11	Rickard and Pascoe (2009)
G46402	TrGAroC	C5CO2DCO3H + OH → C5CO2DBCO3	3.60E-11	Rickard and Pascoe (2009)
G46403	TrGAroCN	NDNPHENOOH + OH → NDNPHENO2	k_ROOHRO	Rickard and Pascoe (2009)
G46404a	TrGAroC	C615CO2O2 + HO_2 → C615CO2OOH	k_RO2_HO2(temp,6)*(1.-r_COCH2O2_OH)	Rickard and Pascoe (2009)
G46404b	TrGAroC	C615CO2O2 + HO_2 → C5DICARB + CO + HO_2 + OH	k_RO2_HO2(temp,6)*r_COCH2O2_OH	Rickard and Pascoe (2009)*
G46405	TrGAroCN	C615CO2O2 + NO → C5DICARB + CO + HO_2 + NO_2	KRO2NO	Rickard and Pascoe (2009)*
G46406	TrGAroCN	C615CO2O2 + NO_3 → C5DICARB + CO + HO_2 + NO_2	KRO2NO3	Rickard and Pascoe (2009)*
G46407	TrGAroC	C615CO2O2 → C5DICARB + CO + HO_2	k1_RO2sORO2	Rickard and Pascoe (2009)*
G46408	TrGAroCN	BZEMUCPAN + OH → MALDIAL + CO + CO_2 + NO_2	4.05E-11	Rickard and Pascoe (2009)
G46409	TrGAroCN	BZEMUCPAN → BZEMUCCO3 + NO_2	k_PAN_M	Rickard and Pascoe (2009)
G46410	TrGAroCN	BZBIPERNO3 + OH → BZOBIPEROH + NO_2	7.30E-11	Rickard and Pascoe (2009)
G46411	TrGAroCN	HOC6H4NO2 + NO_3 → NPHEN1O + HNO_3	9.00E-14	Rickard and Pascoe (2009)
G46412	TrGAroCN	HOC6H4NO2 + OH → NPHEN1O	9.00E-13	Rickard and Pascoe (2009)
G46413a	TrGAroCN	NDNPHENO2 + HO_2 → NDNPHENOOH	k_RO2_HO2(temp,6)*(1.-r_CHOHCH2O2_OH)	Rickard and Pascoe (2009)
G46413b	TrGAroCN	NDNPHENO2 + HO_2 → NC4DCO2H + HNO_3 + CO + CO + NO_2 + OH	k_RO2_HO2(temp,6)*r_CHOHCH2O2_OH	Rickard and Pascoe (2009)*
G46414	TrGAroCN	NDNPHENO2 + NO → NC4DCO2H + HNO_3 + CO + CO + NO_2 + NO_2	KRO2NO	Rickard and Pascoe (2009)*

Table 1: Gas phase reactions (... continued)

#	labels	reaction	rate coefficient	reference
G46415	TrGAroCN	NDNPHENO2 + NO_3 → NC4DCO2H + HNO_3 + CO + CO + NO_2 + NO_2	KRO2NO3	Rickard and Pascoe (2009)*
G46416	TrGAroCN	NDNPHENO2 → NC4DCO2H + HNO_3 + CO + CO + NO_2	k1_RO2ISOPDO2	Rickard and Pascoe (2009)*
G46417	TrGAroC	PBZQCO + OH → C5CO2OHCO3	6.07E-11	Rickard and Pascoe (2009)
G46418	TrGAroCN	CATECHOL + NO_3 → CATEC1O + HNO_3	9.9E-11	Rickard and Pascoe (2009)*
G46419	TrGAroC	CATECHOL + O_3 → MALDALCO2H + $HCOCO_2H$ + HO_2 + OH	9.2E-18	Rickard and Pascoe (2009)
G46420	TrGAroC	CATECHOL + OH → CATEC1O	1.0E-10	Rickard and Pascoe (2009)
G46421	TrGAroC	C5COOHCO3H + OH → C5CO2OHCO3	8.01E-11	Rickard and Pascoe (2009)
G46422	TrGAroCN	NCATECHOL + NO_3 → NNCATECO2	2.60E-12	Rickard and Pascoe (2009)
G46423	TrGAroCN	NCATECHOL + OH → NCATECO2	3.47E-12	Rickard and Pascoe (2009)
G46424a	TrGAroC	C5CO2OHCO3 + HO_2 → C5COOHCO3H	KAPHO2*(r_CO3_OOH+r_CO3_O3)	Rickard and Pascoe (2009)
G46424b	TrGAroC	C5CO2OHCO3 + HO_2 → HOCOC4DIAL + HO_2 + CO + CO_2 + OH	KAPHO2*r_CO3_OH	Rickard and Pascoe (2009)
G46425	TrGAroCN	C5CO2OHCO3 + NO → HOCOC4DIAL + HO_2 + CO + CO_2 + NO_2	KAPNO	Rickard and Pascoe (2009)
G46426	TrGAroCN	C5CO2OHCO3 + NO_2 → C5CO2OHPAN	k_CH3CO3_NO2	Rickard and Pascoe (2009)*
G46427	TrGAroCN	C5CO2OHCO3 + NO_3 → HOCOC4DIAL + HO_2 + CO + CO_2 + NO_2	KRO2NO3*1.74	Rickard and Pascoe (2009)
G46428	TrGAroC	C5CO2OHCO3 → HOCOC4DIAL + HO_2 + CO + CO_2	k1_RO2RCO3	Rickard and Pascoe (2009)
G46429	TrGAroCN	BZEPOXMUC + NO_3 → BZEMUCCO3 + HNO_3	2.*KNO3AL*2.75	Rickard and Pascoe (2009)
G46430	TrGAroC	BZEPOXMUC + O_3 → EPXC4DIAL + .125 HCHO + .1125 $HCOCO_2H$ + .0675 GLYOX + .0675 H_2O_2 + .82 HO_2 + .57 OH + 1.265 CO + .25 CO_2	2.00E-18	Rickard and Pascoe (2009)*
G46431	TrGAroC	BZEPOXMUC + OH → .31 BZEMUCCO3 + .69 BZEMUCO2	6.08E-11	Rickard and Pascoe (2009)
G46432a	TrGAroCN	NCATECO2 + HO_2 → NCATECOOH	k_RO2_HO2(temp,6)*(1.-r_CHOHCH2O2_OH)	Rickard and Pascoe (2009)
G46432b	TrGAroCN	NCATECO2 + HO_2 → NC4DCO2H + $HCOCO_2H$ + HO_2 + OH	k_RO2_HO2(temp,6)*r_CHOHCH2O2_OH	Rickard and Pascoe (2009)*
G46433	TrGAroCN	NCATECO2 + NO → NC4DCO2H + $HCOCO_2H$ + HO_2 + NO_2	KRO2NO	Rickard and Pascoe (2009)*
G46434	TrGAroCN	NCATECO2 + NO_3 → NC4DCO2H + $HCOCO_2H$ + HO_2 + NO_2	KRO2NO3	Rickard and Pascoe (2009)*

Table 1: Gas phase reactions (... continued)

#	labels	reaction	rate coefficient	reference
G46435	TrGAroCN	NCATECO2 → NC4DCO2H + $HCOCO_2H$ + HO_2	k1_RO2ISOPDO2	Rickard and Pascoe (2009)*
G46436	TrGAroCN	NPHEN1OOH + OH → NPHEN1O2	9.00E-13	Rickard and Pascoe (2009)
G46437a	TrGAroCN	NPHENO2 + HO_2 → NPHENOOH	k_RO2_HO2(temp,6)*(1.-r_CHOHCH2O2_OH)	Rickard and Pascoe (2009)
G46437b	TrGAroCN	NPHENO2 + HO_2 → MALDALCO2H + GLYOX + NO_2 + OH	k_RO2_HO2(temp,6)*r_CHOHCH2O2_OH	Rickard and Pascoe (2009)*
G46438	TrGAroCN	NPHENO2 + NO → MALDALCO2H + GLYOX + NO_2 + NO_2	KRO2NO	Rickard and Pascoe (2009)*
G46439	TrGAroCN	NPHENO2 + NO_3 → MALDALCO2H + GLYOX + NO_2 + NO_2	KRO2NO3	Rickard and Pascoe (2009)*
G46440	TrGAroCN	NPHENO2 → MALDALCO2H + GLYOX + NO_2	k1_RO2ISOPDO2	Rickard and Pascoe (2009)*
G46441	TrGAroC	BENZENE + OH → .352 BZBIPERO2 + .118 BZEPOXMUC + .118 HO_2 + .53 PHENOL + .53 HO_2	2.3E-12*EXP(-190./temp)	Rickard and Pascoe (2009)*
G46442	TrGAroCN	C5CO2OHPAN + OH → HOCOC4DIAL + CO + CO + NO_2	7.66E-11	Rickard and Pascoe (2009)
G46443	TrGAroCN	C5CO2OHPAN → C5CO2OHCO3 + NO_2	k_PAN_M	Rickard and Pascoe (2009)
G46444	TrGAroCN	CATEC1O + NO_2 → NCATECHOL	k_C6H5O_NO2	Rickard and Pascoe (2009), Platz et al. (1998)
G46445	TrGAroC	CATEC1O + O_3 → CATEC1O2	k_C6H5O_O3	Rickard and Pascoe (2009), Tao and Li (1999)
G46446	TrGAroC	BZEMUCCO + OH → EPXDLCO3 + GLYOX	9.20E-11	Rickard and Pascoe (2009)
G46447a	TrGAroCN	NNCATECO2 + HO_2 → NNCATECOOH	k_RO2_HO2(temp,6)*(1.-r_CHOHCH2O2_OH)	Rickard and Pascoe (2009)
G46447b	TrGAroCN	NNCATECO2 + HO_2 → NC4DCO2H + $HCOCO_2H$ + NO_2 + OH	k_RO2_HO2(temp,6)*r_CHOHCH2O2_OH	Rickard and Pascoe (2009)*
G46448	TrGAroCN	NNCATECO2 + NO → NC4DCO2H + $HCOCO_2H$ + NO_2 + NO_2	KRO2NO	Rickard and Pascoe (2009)*
G46449	TrGAroCN	NNCATECO2 + NO_3 → NC4DCO2H + $HCOCO_2H$ + NO_2 + NO_2	KRO2NO3	Rickard and Pascoe (2009)*
G46450	TrGAroCN	NNCATECO2 → NC4DCO2H + $HCOCO_2H$ + NO_2	k1_RO2ISOPDO2	Rickard and Pascoe (2009)*
G46451	TrGAroC	BZEMUCCO2H + OH → C5DIALO2 + CO_2	4.06E-11	Rickard and Pascoe (2009)
G46452	TrGAroCN	NNCATECOOH + OH → NNCATECO2	k_ROOHRO	Rickard and Pascoe (2009)
G46453	TrGAroCN	NPHEN1O + NO_2 → DNPHEN	k_C6H5O_NO2	Rickard and Pascoe (2009), Platz et al. (1998)

Table 1: Gas phase reactions (... continued)

#	labels	reaction	rate coefficient	reference
G46454	TrGAroCN	NPHEN1O + O_3 → NPHEN1O2	k_C6H5O_O3	Rickard and Pascoe (2009), Tao and Li (1999)
G46455	TrGAroCN	DNPHEN + NO_3 → NDNPHENO2	2.25E-15	Rickard and Pascoe (2009)
G46456	TrGAroCN	DNPHEN + OH → DNPHENO2	3.00E-14	Rickard and Pascoe (2009)
G46457	TrGAroCN	PHENOL + NO_3 → .742 C6H5O + .742 HNO_3 + .258 NPHENO2	3.8E-12	Rickard and Pascoe (2009)*
G46458	TrGAroC	PHENOL + OH → .06 C6H5O + .8 CATECHOL + .8 HO_2 + .14 PHENO2	4.7E-13*EXP(1220./temp)	Rickard and Pascoe (2009)*
G46459	TrGAroCN	PBZQONE + NO_3 → NBZQO2	3.00E-13	Rickard and Pascoe (2009)
G46460	TrGAroC	PBZQONE + OH → PBZQO2	4.6E-12	Rickard and Pascoe (2009)
G46461a	TrGAroC	PHENO2 + HO_2 → PHENOOH	k_RO2_HO2(temp,6)*(1.-r_CHOHCH2O2_OH)	Rickard and Pascoe (2009)
G46461b	TrGAroC	PHENO2 + HO_2 → .71 MALDALCO2H + .71 GLYOX + .29 PBZQONE + HO_2 + OH	k_RO2_HO2(temp,6)*r_CHOHCH2O2_OH	Rickard and Pascoe (2009)*
G46462	TrGAroCN	PHENO2 + NO → .71 MALDALCO2H + .71 GLYOX + .29 PBZQONE + HO_2 + NO_2	KRO2NO	Rickard and Pascoe (2009)*
G46463	TrGAroCN	PHENO2 + NO_3 → .71 MALDALCO2H + .71 GLYOX + .29 PBZQONE + HO_2 + NO_2	KRO2NO3	Rickard and Pascoe (2009)*
G46464	TrGAroC	PHENO2 → .71 MALDALCO2H + .71 GLYOX + .29 PBZQONE + HO_2	k1_RO2ISOPDO2	Rickard and Pascoe (2009)*
G46465	TrGAroC	C615CO2OOH + OH → C6125CO + OH	9.42E-11	Rickard and Pascoe (2009)
G46466a	TrGAroC	C5CO2DBCO3 + HO_2 → C5CO2DCO3H	KAPHO2*(r_CO3_OOH+r_CO3_O3)	Rickard and Pascoe (2009)
G46466b	TrGAroC	C5CO2DBCO3 + HO_2 → $CH_3C(O)$ + HCOCOCHO + CO_2 + OH	KAPHO2*r_CO3_OH	Rickard and Pascoe (2009)
G46467	TrGAroCN	C5CO2DBCO3 + NO → $CH_3C(O)$ + HCOCOCHO + CO_2 + NO_2	KAPNO	Rickard and Pascoe (2009)
G46468	TrGAroCN	C5CO2DBCO3 + NO_2 → C5CO2DBPAN	k_CH3CO3_NO2	Rickard and Pascoe (2009)*
G46469	TrGAroCN	C5CO2DBCO3 + NO_3 → $CH_3C(O)$ + HCOCOCHO + CO_2 + NO_2	KRO2NO3*1.74	Rickard and Pascoe (2009)
G46470	TrGAroC	C5CO2DBCO3 → $CH_3C(O)$ + HCOCOCHO + CO_2	k1_RO2RCO3	Rickard and Pascoe (2009)
G46471	TrGAroCN	NPHEN1O2 + HO_2 → NPHEN1OOH	k_RO2_HO2(temp,6)	Rickard and Pascoe (2009)
G46472a	TrGAroCN	NPHEN1O2 + NO → NPHEN1O + NO_2	KRO2NO	Rickard and Pascoe (2009)
G46472b	TrGAroCN	NPHEN1O2 + NO_2 → NPHEN1O + NO_3	k_C6H5O2_NO2	Jagiella and Zabel (2007)*
G46473	TrGAroCN	NPHEN1O2 + NO_3 → NPHEN1O + NO_2	KRO2NO3	Rickard and Pascoe (2009)
G46474	TrGAroCN	NPHEN1O2 → NPHEN1O	k1_RO2sRO2	Rickard and Pascoe (2009)

Table 1: Gas phase reactions (... continued)

#	labels	reaction	rate coefficient	reference
G46475	TrGAroCN	NPHENOOH + OH → NPHENO2	1.07E-10	Rickard and Pascoe (2009)
G46476	TrGAroCN	C6H5O + NO_2 → HOC6H4NO2	k_C6H5O_NO2	Rickard and Pascoe (2009), Platz et al. (1998)*
G46477	TrGAroC	C6H5O + O_3 → C6H5O2	k_C6H5O_O3	Rickard and Pascoe (2009), Tao and Li (1999)
G46478	TrGAroCN	NCATECOOH + OH → NCATECO2	k_ROOHRO	Rickard and Pascoe (2009)
G46479	TrGAroC	PBZQOOH + OH → PBZQCO + OH	1.23E-10	Rickard and Pascoe (2009)
G46480a	TrGAroC	PBZQO2 + HO_2 → PBZQOOH	k_RO2_HO2(temp,6)*(1.-r_CHOHCH2O2_OH-r_COCH2O2_OH)	Rickard and Pascoe (2009)
G46480b	TrGAroC	PBZQO2 + HO_2 → C5CO2OHCO3 + OH	k_RO2_HO2(temp,6)*(r_CHOHCH2O2_OH+r_COCH2O2_OH)	Rickard and Pascoe (2009)*
G46481	TrGAroCN	PBZQO2 + NO → C5CO2OHCO3 + NO_2	KRO2NO	Rickard and Pascoe (2009)*
G46482	TrGAroCN	PBZQO2 + NO_3 → C5CO2OHCO3 + NO_2	KRO2NO3	Rickard and Pascoe (2009)*
G46483	TrGAroC	PBZQO2 → C5CO2OHCO3	k1_RO2sORO2	Rickard and Pascoe (2009)*
G46484	TrGAroC	BZOBIPEROH + OH → MALDIALCO3 + GLYOX	8.16E-11	Rickard and Pascoe (2009)
G46485a	TrGAroCN	DNPHENO2 + HO_2 → DNPHENOOH	k_RO2_HO2(temp,6)*(1.-r_CHOHCH2O2_OH)	Rickard and Pascoe (2009)
G46485b	TrGAroCN	DNPHENO2 + HO_2 → NC4DCO2H + $HCOCO_2H$ + NO_2 + OH	k_RO2_HO2(temp,6)*r_CHOHCH2O2_OH	Rickard and Pascoe (2009)*
G46486	TrGAroCN	DNPHENO2 + NO → NC4DCO2H + $HCOCO_2H$ + NO_2 + NO_2	KRO2NO	Rickard and Pascoe (2009)*
G46487	TrGAroCN	DNPHENO2 + NO_3 → NC4DCO2H + $HCOCO_2H$ + NO_2 + NO_2	KRO2NO3	Rickard and Pascoe (2009)*
G46488	TrGAroCN	DNPHENO2 → NC4DCO2H + $HCOCO_2H$ + NO_2	k1_RO2ISOPDO2	Rickard and Pascoe (2009)*
G46489	TrGAroC	BZBIPEROOH + OH → BZOBIPEROH + OH	9.77E-11	Rickard and Pascoe (2009)
G46490a	TrGAroC	BZEMUCO2 + HO_2 → BZEMUCOOH	k_RO2_HO2(temp,6)	Rickard and Pascoe (2009)
G46490b	TrGAroC	BZEMUCO2 + HO_2 → .5 EPXC4DIAL + .5 GLYOX + .5 HO_2 + .5 C3DIALO2 + .5 C32OH13CO + OH	k_RO2_HO2(temp,6)	Rickard and Pascoe (2009)*
G46491a	TrGAroCN	BZEMUCO2 + NO → BZEMUCNO3	KRO2NO*alpha_AN(10,2,0,1,0,temp,cair)	Rickard and Pascoe (2009)
G46491b	TrGAroCN	BZEMUCO2 + NO → .5 EPXC4DIAL + .5 GLYOX + .5 HO_2 + .5 C3DIALO2 + .5 C32OH13CO + NO_2	KRO2NO*(1.-alpha_AN(10,2,0,1,0,temp,cair))	Rickard and Pascoe (2009)*
G46492	TrGAroCN	BZEMUCO2 + NO_3 → .5 EPXC4DIAL + .5 GLYOX + .5 HO_2 + .5 C3DIALO2 + .5 C32OH13CO + NO_2	KRO2NO3	Rickard and Pascoe (2009)*

Table 1: Gas phase reactions (... continued)

#	labels	reaction	rate coefficient	reference
G46493	TrGAroC	BZEMUCO2 → .5 EPXC4DIAL + .5 GLYOX + .5 HO_2 + .5 C3DIALO2 + .5 C32OH13CO	k1_RO2sORO2	Rickard and Pascoe (2009)*
G46494	TrGAroCN	C5CO2DBPAN + OH → HCOCOCHO + CH_3CHO + CO_2 + NO_2	3.28E-11	Rickard and Pascoe (2009)
G46495	TrGAroCN	C5CO2DBPAN → C5CO2DBCO3 + NO_2	k_PAN_M	Rickard and Pascoe (2009)
G46496	TrGAroCN	NBZQOOH + OH → NBZQO2	6.68E-11	Rickard and Pascoe (2009)
G46497	TrGAroC	CATEC1OOH + OH → CATEC1O2	k_ROOHRO	Rickard and Pascoe (2009)
G46498	TrGAroC	C6125CO + OH → C5CO14O2 + CO	6.45E-11	Rickard and Pascoe (2009)
G46499a	TrGAroCN	NBZQO2 + HO_2 → NBZQOOH	k_RO2_HO2(temp,6)*(1.-r_COCH2O2_OH)	Rickard and Pascoe (2009)
G46499b	TrGAroCN	NBZQO2 + HO_2 → C6CO4DB + NO_2 + OH	k_RO2_HO2(temp,6)*r_COCH2O2_OH	Rickard and Pascoe (2009)*
G46500	TrGAroCN	NBZQO2 + NO → C6CO4DB + NO_2 + NO_2	KRO2NO	Rickard and Pascoe (2009)*
G46501	TrGAroCN	NBZQO2 + NO_3 → C6CO4DB + NO_2 + NO_2	KRO2NO3	Rickard and Pascoe (2009)*
G46502	TrGAroCN	NBZQO2 → C6CO4DB + NO_2	k1_RO2sORO2	Rickard and Pascoe (2009)*
G46503	TrGAroCN	DNPHENOOH + OH → DNPHENO2	k_ROOHRO	Rickard and Pascoe (2009)
G46504	TrGAroC	CATEC1O2 + HO_2 → CATEC1OOH	k_RO2_HO2(temp,6)	Rickard and Pascoe (2009)
G46505a	TrGAroCN	CATEC1O2 + NO → CATEC1O + NO_2	KRO2NO	Rickard and Pascoe (2009)
G46505b	TrGAroCN	CATEC1O2 + NO_2 → CATEC1O + NO_3	k_C6H5O2_NO2	Jagiella and Zabel (2007)*
G46506	TrGAroCN	CATEC1O2 + NO_3 → CATEC1O + NO_2	KRO2NO3	Rickard and Pascoe (2009)
G46507	TrGAroC	CATEC1O2 → CATEC1O	k1_RO2sORO2	Rickard and Pascoe (2009)
G46508	TrGAroC	BZEMUCCO3H + OH → BZEMUCCO3	4.37E-11	Rickard and Pascoe (2009)
G46509	TrGAroC	C6H5OOH + OH → C6H5O2	3.60E-12	Rickard and Pascoe (2009)
G46510	TrGAroC	BZEMUCOOH + OH → BZEMUCCO + OH	1.31E-10	Rickard and Pascoe (2009)
G46511a	TrGAroC	BZEMUCCO3 + HO_2 → BZEMUCCO2H + O_3	KAPHO2*r_CO3_O3	Rickard and Pascoe (2009)
G46511b	TrGAroC	BZEMUCCO3 + HO_2 → BZEMUCCO3H	KAPHO2*r_CO3_OOH	Rickard and Pascoe (2009)
G46511c	TrGAroC	BZEMUCCO3 + HO_2 → C5DIALO2 + CO_2 + OH	KAPHO2*r_CO3_OH	Rickard and Pascoe (2009)
G46512	TrGAroCN	BZEMUCCO3 + NO → C5DIALO2 + CO_2 + NO_2	KAPNO	Rickard and Pascoe (2009)
G46513	TrGAroCN	BZEMUCCO3 + NO_2 → BZEMUCPAN	k_CH3CO3_NO2	Rickard and Pascoe (2009)
G46514	TrGAroCN	BZEMUCCO3 + NO_3 → C5DIALO2 + CO_2 + NO_2	KRO2NO3*1.74	Rickard and Pascoe (2009)
G46515	TrGAroC	BZEMUCCO3 → C5DIALO2 + CO_2	k1_RO2RCO3	Rickard and Pascoe (2009)*
G46516	TrGAroC	C6H5O2 + HO_2 → C6H5OOH	k_RO2_HO2(temp,6)	Rickard and Pascoe (2009)
G46517	TrGAroCN	C6H5O2 + NO → C6H5O + NO_2	KRO2NO	Rickard and Pascoe (2009)
G46518	TrGAroCN	C6H5O2 + NO_3 → C6H5O + NO_2	KRO2NO3	Rickard and Pascoe (2009)
G46519	TrGAroC	C6H5O2 → C6H5O	k1_RO2sRO2	Rickard and Pascoe (2009)
G46520	TrGAroCN	C6H5O2 + NO_2 → C6H5O + NO_3	k_C6H5O2_NO2	Jagiella and Zabel (2007)

Table 1: Gas phase reactions (... continued)

#	labels	reaction	rate coefficient	reference
G46521	TrGAroCN	BZEMUCNO3 + OH → BZEMUCCO + NO_2	4.38E-11	Rickard and Pascoe (2009)
G46522a	TrGAroC	BZBIPERO2 + HO_2 → BZBIPEROOH	k_RO2_HO2(temp,6)*(1.-r_BIPERO2_OH)	Rickard and Pascoe (2009)
G46522b	TrGAroC	BZBIPERO2 + HO_2 → OH + GLYOX + HO_2 + .5 BZFUONE + .5 BZFUONE	k_RO2_HO2(temp,6)*r_BIPERO2_OH	Rickard and Pascoe (2009), Birdsall et al. (2010)*
G46523a	TrGAroCN	BZBIPERO2 + NO → BZBIPERNO3	KRO2NO*alpha_AN(9,2,0,0,1,temp,cair)	Rickard and Pascoe (2009)
G46523b	TrGAroCN	BZBIPERO2 + NO → NO_2 + GLYOX + HO_2 + .5 BZFUONE + .5 BZFUONE	KRO2NO*(1.-alpha_AN(9,2,0,0,1,temp,cair))	Rickard and Pascoe (2009)*
G46524	TrGAroCN	BZBIPERO2 + NO_3 → NO_2 + GLYOX + HO_2 + .5 BZFUONE + .5 BZFUONE	KRO2NO3	Rickard and Pascoe (2009)*
G46525	TrGAroC	BZBIPERO2 → GLYOX + HO_2 + BZFUONE	k1_RO2sORO2	Rickard and Pascoe (2009)*
G47200	TrGTerCN	CO235C6CHO + NO_3 → CO235C6CO3 + HNO_3	KNO3AL*5.5	Rickard and Pascoe (2009)
G47201	TrGTerC	CO235C6CHO + OH → CO235C6CO3	6.70E-11	Rickard and Pascoe (2009)
G47202a	TrGTerC	CO235C6CO3 + HO_2 → C235C6CO3H	KAPHO2*(r_CO3_OOH+r_CO3_O3)	Rickard and Pascoe (2009)
G47202b	TrGTerC	CO235C6CO3 + HO_2 → CO235C6O2 + CO_2 + OH	KAPHO2*r_CO3_OH	Rickard and Pascoe (2009)
G47203	TrGTerCN	CO235C6CO3 + NO → CO235C6O2 + CO_2 + NO_2	KAPNO	Rickard and Pascoe (2009)
G47204	TrGTerCN	CO235C6CO3 + NO_2 → C7PAN3	k_CH3CO3_NO2	Rickard and Pascoe (2009)
G47205	TrGTerC	CO235C6CO3 → CO235C6O2 + CO_2	k1_RO2RCO3	Rickard and Pascoe (2009)
G47206	TrGTerC	C235C6CO3H + OH → CO235C6CO3	4.75E-12	Rickard and Pascoe (2009)
G47207	TrGTerCN	C7PAN3 + OH → CO235C5CHO + CO + NO_2	8.83E-13	Rickard and Pascoe (2009)
G47208	TrGTerCN	C7PAN3 → CO235C6CO3 + NO_2	k_PAN_M	Rickard and Pascoe (2009)
G47209a	TrGTerC	C716O2 + HO_2 → C716OOH	k_RO2_HO2(temp,7)*r_COCH2O2_OOH	Rickard and Pascoe (2009), Sander et al. (2019)
G47209b	TrGTerC	C716O2 + HO_2 → CO13C4CHO + $CH_3C(O)$ + OH	k_RO2_HO2(temp,7)*r_COCH2O2_OH	Rickard and Pascoe (2009), Sander et al. (2019)
G47210	TrGTerCN	C716O2 + NO → CO13C4CHO + $CH_3C(O)$ + NO_2	KRO2NO	Rickard and Pascoe (2009)*
G47211	TrGTerC	C716O2 → CO13C4CHO + $CH_3C(O)$	k1_RO2sORO2	Rickard and Pascoe (2009)
G47212	TrGTerC	C716OOH + OH → CO235C6CHO + OH	1.20E-10	Rickard and Pascoe (2009)
G47213	TrGTerC	C721O2 + HO_2 → C721OOH	k_RO2_HO2(temp,7)	Rickard and Pascoe (2009)
G47214	TrGTerCN	C721O2 + NO → C722O2 + NO_2	KRO2NO	Rickard and Pascoe (2009)*
G47215	TrGTerC	C721O2 → C722O2	k1_RO2pRO2	Rickard and Pascoe (2009)
G47216	TrGTerC	C721OOH + OH → C721O2	1.27E-11	Rickard and Pascoe (2009)
G47217	TrGTerC	C722O2 + HO_2 → C722OOH	k_RO2_HO2(temp,7)	Rickard and Pascoe (2009)
G47218	TrGTerCN	C722O2 + NO → CH_3COCH_3 + C44O2 + NO_2	KRO2NO	Rickard and Pascoe (2009)*

Table 1: Gas phase reactions (... continued)

#	labels	reaction	rate coefficient	reference
G47219	TrGTerC	C722O2 → CH_3COCH_3 + C44O2	k1_RO2tRO2	Rickard and Pascoe (2009)
G47220	TrGTerC	C722OOH + OH → C722O2	3.31E-11	Rickard and Pascoe (2009)
G47221	TrGTerC	ROO6R3O2 → ROO6R5O2	5.68E10*EXP(-8745./temp)	Vereecken and Peeters (2012)
G47222	TrGTerCN	ROO6R3O2 + NO → ROO6R3O + NO_2	KRO2NO	Vereecken and Peeters (2012)*
G47223	TrGTerC	ROO6R3O2 + HO_2 → 7 LCARBON	k_RO2_HO2(temp,7)	Vereecken and Peeters (2012)*
G47224	TrGTerC	ROO6R3O2 → ROO6R3O	k1_RO2sRO2	Vereecken and Peeters (2012)
G47225	TrGTerC	ROO6R3O → 7 LCARBON + HO_2	5.7E10*EXP(-2949./temp)	Vereecken and Peeters (2012)*
G47226	TrGTerC	ROO6R5O2 → 7 LCARBON + OH	9.17E10*EXP(-8706./temp)	Vereecken and Peeters (2012)*
G47400	TrGAroC	TOLUENE + OH → .07 C6H5CH2O2 + .18 CRESOL + .18 HO_2 + .65 TLBIPERO2 + .10 TLEPOXMUC + .10 HO_2	1.8E-12*EXP(340./temp)	Rickard and Pascoe (2009)*
G47401	TrGAroC	C6H5CH2O2 + HO_2 → C6H5CH2OOH	1.5E-13*EXP(1310./temp)	Rickard and Pascoe (2009)
G47402a	TrGAroCN	C6H5CH2O2 + NO → C6H5CH2NO3	KRO2NO*alpha_AN(7,1,0,0,0,temp,cair)	Rickard and Pascoe (2009)*
G47402b	TrGAroCN	C6H5CH2O2 + NO → BENZAL + HO_2 + NO_2	KRO2NO*(1.-alpha_AN(7,1,0,0,0,temp,cair))	Rickard and Pascoe (2009)*
G47403	TrGAroCN	C6H5CH2O2 + NO_3 → BENZAL + HO_2 + NO_2	KRO2NO3	Rickard and Pascoe (2009)*
G47404	TrGAroC	C6H5CH2O2 → BENZAL + HO_2	2.*(k_CH3O2*2.4E-14*EXP(1620./temp))**(0.5)*RO2	Rickard and Pascoe (2009)*
G47405	TrGAroCN	CRESOL + NO_3 → .103 CRESO2 + .103 HNO_3 + .506 NCRESO2 + .391 TOL1O + .391 HNO_3	1.4E-11	Rickard and Pascoe (2009)*
G47406	TrGAroC	CRESOL + OH → .2 CRESO2 + .727 MCATECHOL + .727 HO_2 + .073 TOL1O	4.65E-11	Rickard and Pascoe (2009)*
G47407a	TrGAroC	TLBIPERO2 + HO_2 → TLBIPEROOH	k_RO2_HO2(temp,7)*(1.-r_BIPERO2_OH)	Rickard and Pascoe (2009)
G47407b	TrGAroC	TLBIPERO2 + HO_2 → OH + .6 GLYOX + .4 MGLYOX + HO_2 + .2 C4MDIAL + .2 C5DICARB + .2 TLFUONE + .2 BZFUONE + .2 MALDIAL	k_RO2_HO2(temp,7)*r_BIPERO2_OH	Rickard and Pascoe (2009), Birdsall et al. (2010)*
G47408a	TrGAroCN	TLBIPERO2 + NO → NO_2 + .6 GLYOX + .4 MGLYOX + HO_2 + .2 C4MDIAL + .2 C5DICARB + .2 TLFUONE + .2 BZFUONE + .2 MALDIAL	KRO2NO*(1.-alpha_AN(11,2,0,0,1,temp,cair))	Rickard and Pascoe (2009)*
G47408b	TrGAroCN	TLBIPERO2 + NO → TLBIPERNO3	KRO2NO*alpha_AN(11,2,0,0,1,temp,cair)	Rickard and Pascoe (2009)*

Table 1: Gas phase reactions (... continued)

#	labels	reaction	rate coefficient	reference
G47409	TrGAroCN	TLBIPERO2 + NO_3 → NO_2 + .6 GLYOX + .4 MGLYOX + HO_2 + .2 C4MDIAL + .2 C5DICARB + .2 TLFUONE + .2 BZFUONE + .2 MALDIAL	KRO2NO3	Rickard and Pascoe (2009)*
G47410	TrGAroC	TLBIPERO2 → .6 GLYOX + .4 MGLYOX + HO_2 + .2 C4MDIAL + .2 C5DICARB + .2 TLFUONE + .2 BZFUONE + .2 MALDIAL	k1_RO2sORO2	Rickard and Pascoe (2009)*
G47411	TrGAroCN	TLEPOXMUC + NO_3 → TLEMUCCO3 + HNO_3	KNO3AL*2.75	Rickard and Pascoe (2009)
G47412	TrGAroC	TLEPOXMUC + O_3 → EPXC4DIAL + .125 CH_3CHO + .695 $CH_3C(O)$ + .57 CO + .57 OH + .125 HO_2 + .1125 CH_3COCO_2H + .0675 MGLYOX + .0675 H_2O_2 + .25 CO_2	5.00E-18	Rickard and Pascoe (2009)*
G47413	TrGAroC	TLEPOXMUC + OH → .31 TLEMUCCO3 + .69 TLEMUCO2	7.99E-11	Rickard and Pascoe (2009)*
G47414	TrGAroC	C6H5CH2OOH + OH → BENZAL + OH	2.05E-11	Rickard and Pascoe (2009)
G47415	TrGAroCN	C6H5CH2NO3 + OH → BENZAL + NO_2	6.03E-12	Rickard and Pascoe (2009)
G47416	TrGAroCN	BENZAL + NO_3 → C6H5CO3 + HNO_3	2.40E-15	Rickard and Pascoe (2009)
G47417	TrGAroC	BENZAL + OH → C6H5CO3	5.9E-12*EXP(225./temp)	Rickard and Pascoe (2009)
G47418a	TrGAroC	CRESO2 + HO_2 → CRESOOH	k_RO2_HO2(temp,7)*(1.-r_CHOHCH2O2_OH)	Rickard and Pascoe (2009)
G47418b	TrGAroC	CRESO2 + HO_2 → .68 C5CO14OH + .68 GLYOX + HO_2 + .32 PTLQONE + OH	k_RO2_HO2(temp,7)*r_CHOHCH2O2_OH	Rickard and Pascoe (2009)*
G47419	TrGAroCN	CRESO2 + NO → .68 C5CO14OH + .68 GLYOX + HO_2 + .32 PTLQONE + NO_2	KRO2NO	Rickard and Pascoe (2009)*
G47420	TrGAroCN	CRESO2 + NO_3 → .68 C5CO14OH + .68 GLYOX + HO_2 + .32 PTLQONE + NO_2	KRO2NO3	Rickard and Pascoe (2009)*
G47421	TrGAroC	CRESO2 → .68 C5CO14OH + .68 GLYOX + HO_2 + .32 PTLQONE	k1_RO2ISOPDO2	Rickard and Pascoe (2009)*
G47422a	TrGAroCN	NCRESO2 + HO_2 → NCRESOOH	k_RO2_HO2(temp,7)*(1.-r_CHOHCH2O2_OH)	Rickard and Pascoe (2009)
G47422b	TrGAroCN	NCRESO2 + HO_2 → C5CO14OH + GLYOX + NO_2 + OH	k_RO2_HO2(temp,7)*r_CHOHCH2O2_OH	Rickard and Pascoe (2009)*
G47423	TrGAroCN	NCRESO2 + NO → C5CO14OH + GLYOX + NO_2 + NO_2	KRO2NO	Rickard and Pascoe (2009)*
G47424	TrGAroCN	NCRESO2 + NO_3 → C5CO14OH + GLYOX + NO_2 + NO_2	KRO2NO3	Rickard and Pascoe (2009)*
G47425	TrGAroCN	NCRESO2 → C5CO14OH + GLYOX + NO_2	k1_RO2ISOPDO2	Rickard and Pascoe (2009)*

Table 1: Gas phase reactions (... continued)

#	labels	reaction	rate coefficient	reference
G47426	TrGAroCN	TOL1O + NO_2 → TOL1OHNO2	k_C6H5O_NO2	Rickard and Pascoe (2009), Platz et al. (1998)*
G47427	TrGAroC	TOL1O + O_3 → OXYL1O2	k_C6H5O_O3	Rickard and Pascoe (2009), Tao and Li (1999)
G47428	TrGAroCN	MCATECHOL + NO_3 → MCATEC1O + HNO_3	1.7E-10*1.0	Rickard and Pascoe (2009)
G47429	TrGAroC	MCATECHOL + O_3 → MC3ODBCO2H + $HCOCO_2H$ + HO_2 + OH	2.8E-17	Rickard and Pascoe (2009)*
G47430	TrGAroC	MCATECHOL + OH → MCATEC1O	2.0E-10*1.0	Rickard and Pascoe (2009)
G47431	TrGAroC	TLBIPEROOH + OH → TLOBIPEROH + OH	9.64E-11	Rickard and Pascoe (2009)
G47432	TrGAroCN	TLBIPERNO3 + OH → TLOBIPEROH + NO_2	7.16E-11	Rickard and Pascoe (2009)
G47433	TrGAroC	TLOBIPEROH + OH → C5CO14O2 + GLYOX	7.99E-11	Rickard and Pascoe (2009)
G47434a	TrGAroC	TLEMUCCO3 + HO_2 → C615CO2O2 + CO_2 + OH	KAPHO2*r_CO3_OH	Rickard and Pascoe (2009)
G47434b	TrGAroC	TLEMUCCO3 + HO_2 → TLEMUCCO2H + O_3	KAPHO2*r_CO3_O3	Rickard and Pascoe (2009)
G47434c	TrGAroC	TLEMUCCO3 + HO_2 → TLEMUCCO3H	KAPHO2*r_CO3_OOH	Rickard and Pascoe (2009)
G47435	TrGAroCN	TLEMUCCO3 + NO → C615CO2O2 + CO_2 + NO_2	KAPNO	Rickard and Pascoe (2009)
G47436	TrGAroCN	TLEMUCCO3 + NO_2 → TLEMUCPAN	k_CH3CO3_NO2	Rickard and Pascoe (2009)*
G47437	TrGAroCN	TLEMUCCO3 + NO_3 → C615CO2O2 + CO_2 + NO_2	KRO2NO3*1.74	Rickard and Pascoe (2009)
G47438	TrGAroC	TLEMUCCO3 → C615CO2O2 + CO_2	k1_RO2RCO3	Rickard and Pascoe (2009)*
G47439a	TrGAroC	TLEMUCO2 + HO_2 → TLEMUCOOH	k_RO2_HO2(temp,7)*(1.-r_CHOHCH2O2_OH-r_COCH2O2_OH)	Rickard and Pascoe (2009)
G47439b	TrGAroC	TLEMUCO2 + HO_2 → .5 C3DIALO2 + .5 CO2H3CHO + .5 EPXC4DIAL + .5 MGLYOX + .5 HO_2 + OH	k_RO2_HO2(temp,7)*(r_CHOHCH2O2_OH+r_COCH2O2_OH)	Rickard and Pascoe (2009)*
G47440a	TrGAroCN	TLEMUCO2 + NO → TLEMUCNO3	KRO2NO*alpha_AN(11,2,1,0,0,temp,cair)	Rickard and Pascoe (2009)
G47440b	TrGAroCN	TLEMUCO2 + NO → .5 C3DIALO2 + .5 CO2H3CHO + .5 EPXC4DIAL + .5 MGLYOX + .5 HO_2 + NO_2	KRO2NO*(1.-alpha_AN(11,2,1,0,0,temp,cair))	Rickard and Pascoe (2009)*
G47441	TrGAroCN	TLEMUCO2 + NO_3 → .5 C3DIALO2 + .5 CO2H3CHO + .5 EPXC4DIAL + .5 MGLYOX + .5 HO_2 + NO_2	KRO2NO3	Rickard and Pascoe (2009)*
G47442	TrGAroC	TLEMUCO2 → .5 C3DIALO2 + .5 CO2H3CHO + .5 EPXC4DIAL + .5 MGLYOX + .5 HO_2	k1_RO2sORO2	Rickard and Pascoe (2009)*
G47443a	TrGAroC	C6H5CO3 + HO_2 → C6H5CO3H	1.1E-11*EXP(364./temp)*0.65	Roth et al. (2010)
G47443b	TrGAroC	C6H5CO3 + HO_2 → C6H5O2 + CO_2 + OH	1.1E-11*EXP(364./temp)*0.20	Roth et al. (2010)
G47443c	TrGAroC	C6H5CO3 + HO_2 → PHCOOH + O_3	1.1E-11*EXP(364./temp)*0.15	Roth et al. (2010)
G47444	TrGAroCN	C6H5CO3 + NO → C6H5O2 + CO_2 + NO_2	KAPNO	Rickard and Pascoe (2009)
G47445	TrGAroCN	C6H5CO3 + NO_2 → PBZN	k_CH3CO3_NO2	Rickard and Pascoe (2009)*

Table 1: Gas phase reactions (... continued)

#	labels	reaction	rate coefficient	reference
G47446	TrGAroCN	C6H5CO3 + NO_3 → C6H5O2 + CO_2 + NO_2	KRO2NO3*1.74	Rickard and Pascoe (2009)
G47447	TrGAroC	C6H5CO3 → C6H5O2 + CO_2	k1_RO2RCO3	Rickard and Pascoe (2009)*
G47448	TrGAroC	CRESOOH + OH → CRESO2	1.15E-10	Rickard and Pascoe (2009)
G47449	TrGAroCN	NCRESOOH + OH → NCRESO2	1.07E-10	Rickard and Pascoe (2009)
G47450	TrGAroCN	TOL1OHNO2 + NO_3 → NCRES1O + HNO_3	3.13E-13*1.0	Rickard and Pascoe (2009)
G47451	TrGAroCN	TOL1OHNO2 + OH → NCRES1O	2.8E-12	Rickard and Pascoe (2009)
G47452	TrGAroC	OXYL1O2 + HO_2 → OXYL1OOH	k_RO2_HO2(temp,7)	Rickard and Pascoe (2009)
G47453	TrGAroCN	OXYL1O2 + NO → TOL1O + NO_2	KRO2NO	Rickard and Pascoe (2009)
G47454	TrGAroCN	OXYL1O2 + NO_2 → TOL1O + NO_3	k_C6H5O2_NO2	Jagiella and Zabel (2007)*
G47455	TrGAroCN	OXYL1O2 + NO_3 → TOL1O + NO_2	KRO2NO3	Rickard and Pascoe (2009)
G47456	TrGAroC	OXYL1O2 → TOL1O	k1_RO2sRO2	Rickard and Pascoe (2009)
G47457	TrGAroCN	MCATEC1O + NO_2 → MNCATECH	k_C6H5O_NO2	Rickard and Pascoe (2009), Platz et al. (1998)
G47458	TrGAroC	MCATEC1O + O_3 → MCATEC1O2	k_C6H5O_O3	Rickard and Pascoe (2009), Tao and Li (1999)
G47459	TrGAroC	TLEMUCCO2H + OH → C615CO2O2 + CO_2	5.98E-11	Rickard and Pascoe (2009)
G47460	TrGAroC	TLEMUCCO3H + OH → TLEMUCCO3	6.29E-11	Rickard and Pascoe (2009)
G47461	TrGAroCN	TLEMUCPAN + OH → C5DICARB + CO + CO_2 + NO_2	5.96E-11	Rickard and Pascoe (2009)
G47462	TrGAroCN	TLEMUCPAN → TLEMUCCO3 + NO_2	k_PAN_M	Rickard and Pascoe (2009)
G47463	TrGAroC	TLEMUCOOH + OH → TLEMUCCO + OH	7.04E-11	Rickard and Pascoe (2009)
G47464	TrGAroCN	TLEMUCNO3 + OH → TLEMUCCO + NO_2	3.06E-11	Rickard and Pascoe (2009)
G47465	TrGAroC	TLEMUCCO + OH → $CH_3C(O)$ + EPXC4DIAL + CO	4.06E-11	Rickard and Pascoe (2009)
G47466	TrGAroC	C6H5CO3H + OH → C6H5CO3	4.66E-12	Rickard and Pascoe (2009)
G47467	TrGAroC	PHCOOH + OH → C6H5O2 + CO_2	1.10E-12	Rickard and Pascoe (2009)
G47468	TrGAroCN	PBZN + OH → C6H5OOH + CO + NO_2	1.06E-12	Rickard and Pascoe (2009)
G47469	TrGAroCN	PBZN → C6H5CO3 + NO_2	k_PAN_M*0.67	Rickard and Pascoe (2009)
G47470	TrGAroCN	PTLQONE + NO_3 → NPTLQO2	1.00E-12	Rickard and Pascoe (2009)
G47471	TrGAroC	PTLQONE + OH → PTLQO2	2.3E-11	Rickard and Pascoe (2009)
G47472	TrGAroCN	NCRES1O + NO_2 → DNCRES	k_C6H5O_NO2	Rickard and Pascoe (2009), Platz et al. (1998)
G47473	TrGAroCN	NCRES1O + O_3 → NCRES1O2	k_C6H5O_O3	Rickard and Pascoe (2009), Tao and Li (1999)
G47474	TrGAroC	OXYL1OOH + OH → OXYL1O2	4.65E-11	Rickard and Pascoe (2009)
G47475	TrGAroCN	MNCATECH + NO_3 → MNNCATECO2	5.03E-12	Rickard and Pascoe (2009)
G47476	TrGAroCN	MNCATECH + OH → MNCATECO2	6.83E-12	Rickard and Pascoe (2009)

Table 1: Gas phase reactions (... continued)

#	labels	reaction	rate coefficient	reference
G47477	TrGAroC	MCATEC1O2 + HO_2 → MCATEC1OOH	k_RO2_HO2(temp,7)	Rickard and Pascoe (2009)
G47478	TrGAroCN	MCATEC1O2 + NO → MCATEC1O + NO_2	KRO2NO	Rickard and Pascoe (2009)
G47479	TrGAroCN	MCATEC1O2 + NO_2 → MCATEC1O + NO_3	k_C6H5O2_NO2	Jagiella and Zabel (2007)*
G47480	TrGAroCN	MCATEC1O2 + NO_3 → MCATEC1O + NO_2	KRO2NO3	Rickard and Pascoe (2009)
G47481	TrGAroC	MCATEC1O2 → MCATEC1O	k1_RO2sORO2	Rickard and Pascoe (2009)
G47482a	TrGAroCN	NPTLQO2 + HO_2 → NPTLQOOH	k_RO2_HO2(temp,7)*(1.-r_COCH2O2_OH)	Rickard and Pascoe (2009)
G47482b	TrGAroCN	NPTLQO2 + HO_2 → C7CO4DB + NO_2 + OH	k_RO2_HO2(temp,7)*r_COCH2O2_OH	Rickard and Pascoe (2009)*
G47483	TrGAroCN	NPTLQO2 + NO → C7CO4DB + NO_2 + NO_2	KRO2NO	Rickard and Pascoe (2009)*
G47484	TrGAroCN	NPTLQO2 + NO_3 → C7CO4DB + NO_2 + NO_2	KRO2NO3	Rickard and Pascoe (2009)*
G47485	TrGAroCN	NPTLQO2 → C7CO4DB + NO_2	k1_RO2sORO2	Rickard and Pascoe (2009)*
G47486a	TrGAroC	PTLQO2 + HO_2 → PTLQOOH	k_RO2_HO2(temp,7)*(1.-r_CHOHCH2O2_OH-r_COCH2O2_OH)	Rickard and Pascoe (2009)
G47486b	TrGAroC	PTLQO2 + HO_2 → C6CO2OHCO3 + OH	k_RO2_HO2(temp,7)*(r_CHOHCH2O2_OH+r_COCH2O2_OH)	Rickard and Pascoe (2009)*
G47487	TrGAroCN	PTLQO2 + NO → C6CO2OHCO3 + NO_2	KRO2NO	Rickard and Pascoe (2009)*
G47488	TrGAroCN	PTLQO2 + NO_3 → C6CO2OHCO3 + NO_2	KRO2NO3	Rickard and Pascoe (2009)*
G47489	TrGAroC	PTLQO2 → C6CO2OHCO3	k1_RO2sORO2	Rickard and Pascoe (2009)*
G47490	TrGAroCN	DNCRES + NO_3 → NDNCRESO2	7.83E-15	Rickard and Pascoe (2009)
G47491	TrGAroCN	DNCRES + OH → DNCRESO2	5.10E-14	Rickard and Pascoe (2009)
G47492	TrGAroCN	NCRES1O2 + HO_2 → NCRES1OOH	k_RO2_HO2(temp,7)	Rickard and Pascoe (2009)
G47493	TrGAroCN	NCRES1O2 + NO → NCRES1O + NO_2	KRO2NO	Rickard and Pascoe (2009)
G47494	TrGAroCN	NCRES1O2 + NO_2 → NCRES1O + NO_3	k_C6H5O2_NO2	Jagiella and Zabel (2007)*
G47495	TrGAroCN	NCRES1O2 + NO_3 → NCRES1O + NO_2	KRO2NO3	Rickard and Pascoe (2009)
G47496	TrGAroCN	NCRES1O2 → NCRES1O	k1_RO2sRO2	Rickard and Pascoe (2009)
G47497a	TrGAroCN	MNNCATECO2 + HO_2 → MNNCATCOOH	k_RO2_HO2(temp,7)*(1.-r_CHOHCH2O2_OH)	Rickard and Pascoe (2009)
G47497b	TrGAroCN	MNNCATECO2 + HO_2 → NC4MDCO2HN + $HCOCO_2H$ + NO_2 + OH	k_RO2_HO2(temp,7)*r_CHOHCH2O2_OH	Rickard and Pascoe (2009)*
G47498	TrGAroCN	MNNCATECO2 + NO → NC4MDCO2HN + $HCOCO_2H$ + NO_2 + NO_2	KRO2NO	Rickard and Pascoe (2009)*
G47499	TrGAroCN	MNNCATECO2 + NO_3 → NC4MDCO2HN + $HCOCO_2H$ + NO_2 + NO_2	KRO2NO3	Rickard and Pascoe (2009)*
G47500	TrGAroCN	MNNCATECO2 → NC4MDCO2HN + $HCOCO_2H$ + NO_2	k1_RO2ISOPDO2	Rickard and Pascoe (2009)

Table 1: Gas phase reactions (... continued)

#	labels	reaction	rate coefficient	reference
G47501a	TrGAroCN	MNCATECO2 + HO_2 → MNCATECOOH	k_RO2_HO2(temp,7)*(1.-r_CHOHCH2O2_OH)	Rickard and Pascoe (2009)
G47501b	TrGAroCN	MNCATECO2 + HO_2 → NC4MDCO2HN + $HCOCO_2H$ + HO_2 + OH	k_RO2_HO2(temp,7)*r_CHOHCH2O2_OH	Rickard and Pascoe (2009)*
G47502	TrGAroCN	MNCATECO2 + NO → NC4MDCO2HN + $HCOCO_2H$ + HO_2 + NO_2	KRO2NO	Rickard and Pascoe (2009)*
G47503	TrGAroCN	MNCATECO2 + NO_3 → NC4MDCO2HN + $HCOCO_2H$ + HO_2 + NO_2	KRO2NO3	Rickard and Pascoe (2009)*
G47504	TrGAroCN	MNCATECO2 → NC4MDCO2HN + $HCOCO_2H$ + HO_2	k1_RO2ISOPDO2	Rickard and Pascoe (2009)*
G47505	TrGAroC	MCATEC1OOH + OH → MCATEC1O2	2.05E-10	Rickard and Pascoe (2009)
G47506	TrGAroCN	NPTLQOOH + OH → NPTLQO2	8.56E-11	Rickard and Pascoe (2009)
G47507	TrGAroC	PTLQOOH + OH → PTLQCO + OH	1.42E-10	Rickard and Pascoe (2009)
G47508	TrGAroC	PTLQCO + OH → C6CO2OHCO3	7.95E-11	Rickard and Pascoe (2009)
G47509a	TrGAroCN	NDNCRESO2 + HO_2 → NDNCRESOOH	k_RO2_HO2(temp,7)*(1.-r_CHOHCH2O2_OH)	Rickard and Pascoe (2009)
G47509b	TrGAroCN	NDNCRESO2 + HO_2 → NC4MDCO2HN + HNO_3 + 2 CO + NO_2 + OH	k_RO2_HO2(temp,7)*r_CHOHCH2O2_OH	Rickard and Pascoe (2009)*
G47510	TrGAroCN	NDNCRESO2 + NO → NC4MDCO2HN + HNO_3 + 2 CO + NO_2 + NO_2	KRO2NO	Rickard and Pascoe (2009)*
G47511	TrGAroCN	NDNCRESO2 + NO_3 → NC4MDCO2HN + HNO_3 + 2 CO + NO_2 + NO_2	KRO2NO3	Rickard and Pascoe (2009)*
G47512	TrGAroCN	NDNCRESO2 → NC4MDCO2HN + HNO_3 + 2 CO + NO_2	k1_RO2ISOPDO2	Rickard and Pascoe (2009)*
G47513a	TrGAroCN	DNCRESO2 + HO_2 → DNCRESOOH	k_RO2_HO2(temp,7)*(1.-r_CHOHCH2O2_OH)	Rickard and Pascoe (2009)
G47513b	TrGAroCN	DNCRESO2 + HO_2 → NC4MDCO2HN + $HCOCO_2H$ + NO_2 + OH	k_RO2_HO2(temp,7)*r_CHOHCH2O2_OH	Rickard and Pascoe (2009)*
G47514	TrGAroCN	DNCRESO2 + NO → NC4MDCO2HN + $HCOCO_2H$ + NO_2 + NO_2	KRO2NO	Rickard and Pascoe (2009)*
G47515	TrGAroCN	DNCRESO2 + NO_3 → NC4MDCO2HN + $HCOCO_2H$ + NO_2 + NO_2	KRO2NO3	Rickard and Pascoe (2009)*
G47516	TrGAroCN	DNCRESO2 → NC4MDCO2HN + $HCOCO_2H$ + NO_2	k1_RO2ISOPDO2	Rickard and Pascoe (2009)*
G47517	TrGAroCN	NCRES1OOH + OH → NCRES1O2	1.53E-12	Rickard and Pascoe (2009)
G47518	TrGAroCN	MNNCATCOOH + OH → MNNCATECO2	k_ROOHRO	Rickard and Pascoe (2009)
G47519	TrGAroCN	MNCATECOOH + OH → MNCATECO2	k_ROOHRO	Rickard and Pascoe (2009)

Table 1: Gas phase reactions (... continued)

#	labels	reaction	rate coefficient	reference
G47520	TrGAroC	C7CO4DB + OH → CO + CO + $CH_3C(O)$ + HCOCOCHO	9.58E-11	Rickard and Pascoe (2009)
G47521a	TrGAroC	C6CO2OHCO3 + HO_2 → C5134CO2OH + HO_2 + CO + CO_2 + OH	KAPHO2*r_CO3_OH	Rickard and Pascoe (2009)
G47521b	TrGAroC	C6CO2OHCO3 + HO_2 → C6COOHCO3H	KAPHO2*(r_CO3_OOH+r_CO3_O3)	Rickard and Pascoe (2009)
G47522	TrGAroCN	C6CO2OHCO3 + NO → C5134CO2OH + HO_2 + CO + CO_2 + NO_2	KAPNO	Rickard and Pascoe (2009)
G47523	TrGAroCN	C6CO2OHCO3 + NO_2 → C6CO2OHPAN	k_CH3CO3_NO2	Rickard and Pascoe (2009)
G47524	TrGAroCN	C6CO2OHCO3 + NO_3 → C5134CO2OH + HO_2 + CO + CO_2 + NO_2	KRO2NO3*1.74	Rickard and Pascoe (2009)
G47525	TrGAroC	C6CO2OHCO3 → C5134CO2OH + HO_2 + CO + CO_2	k1_RO2RCO3	Rickard and Pascoe (2009)
G47526	TrGAroCN	NDNCRESOOH + OH → NDNCRESO2	k_ROOHRO	Rickard and Pascoe (2009)
G47527	TrGAroCN	DNCRESOOH + OH → DNCRESO2	k_ROOHRO	Rickard and Pascoe (2009)
G47528	TrGAroC	C6COOHCO3H + OH → C6CO2OHCO3	9.29E-11	Rickard and Pascoe (2009)
G47529	TrGAroCN	C6CO2OHPAN + OH → C5134CO2OH + CO + CO + NO_2	8.96E-11	Rickard and Pascoe (2009)
G47530	TrGAroCN	C6CO2OHPAN → C6CO2OHCO3 + NO_2	k_PAN_M	Rickard and Pascoe (2009)
G48200	TrGTerC	C85O2 → C86O2	k1_RO2tRO2	Rickard and Pascoe (2009)
G48201	TrGTerC	C85O2 + HO_2 → C85OOH	k_RO2_HO2(temp,8)	Rickard and Pascoe (2009)
G48202	TrGTerCN	C85O2 + NO → C86O2 + NO_2	KRO2NO	Rickard and Pascoe (2009)*
G48203	TrGTerC	C85OOH + OH → C85O2	1.29E-11	Rickard and Pascoe (2009)
G48204	TrGTerC	C86O2 → C511O2 + CH_3COCH_3	k1_RO2tRO2	Rickard and Pascoe (2009)
G48205	TrGTerCN	C86O2 + NO → C511O2 + CH_3COCH_3 + NO_2	KRO2NO	Rickard and Pascoe (2009)*
G48206	TrGTerC	C86O2 + HO_2 → C86OOH	k_RO2_HO2(temp,8)	Rickard and Pascoe (2009)
G48207	TrGTerC	C86OOH + OH → C86O2	3.45E-11	Rickard and Pascoe (2009)
G48208	TrGTerC	C811O2 → C812O2	k1_RO2pRO2	Rickard and Pascoe (2009)
G48209	TrGTerC	C811O2 + HO_2 → 8 LCARBON	k_RO2_HO2(temp,8)	Rickard and Pascoe (2009)
G48210	TrGTerCN	C811O2 + NO → C812O2 + NO_2	KRO2NO	Rickard and Pascoe (2009)*
G48211	TrGTerC	C812O2 → C813O2	k1_RO2tORO2	Rickard and Pascoe (2009)
G48212	TrGTerCN	C812O2 + NO → C813O2 + NO_2	KRO2NO	Rickard and Pascoe (2009)*
G48213	TrGTerC	C812O2 + HO_2 → C812OOH	k_RO2_HO2(temp,8)	Rickard and Pascoe (2009)
G48214	TrGTerC	C812OOH + OH → C812O2	1.09E-11	Rickard and Pascoe (2009)
G48215	TrGTerC	C813O2 → CH_3COCH_3 + C512O2	k1_RO2tRO2	Rickard and Pascoe (2009)
G48216	TrGTerCN	C813O2 + NO → CH_3COCH_3 + C512O2 + NO_2	KRO2NO	Rickard and Pascoe (2009)*
G48217	TrGTerC	C813O2 + HO_2 → C813OOH	k_RO2_HO2(temp,8)	Rickard and Pascoe (2009)

Table 1: Gas phase reactions (... continued)

#	labels	reaction	rate coefficient	reference
G48218	TrGTerC	C813OOH + OH → C813O2	1.86E-11	Rickard and Pascoe (2009)
G48219	TrGTerCN	C721CHO + NO_3 → C721CO3 + HNO_3	KNO3AL*8.5	Rickard and Pascoe (2009)
G48220	TrGTerC	C721CHO + OH → C721CO3	2.63E-11	Rickard and Pascoe (2009)
G48221a	TrGTerC	C721CO3 + HO_2 → C721CO3H	KAPHO2*r_CO3_OOH	Rickard and Pascoe (2009)
G48221b	TrGTerC	C721CO3 + HO_2 → C721O2 + CO_2 + OH	KAPHO2*r_CO3_OH	Rickard and Pascoe (2009)
G48221c	TrGTerC	C721CO3 + HO_2 → NORPINIC + O_3	KAPHO2*r_CO3_O3	Rickard and Pascoe (2009)
G48222	TrGTerCN	C721CO3 + NO → C721O2 + CO_2 + NO_2	KAPNO	Rickard and Pascoe (2009)*
G48223	TrGTerCN	C721CO3 + NO_2 → C721PAN	k_CH3CO3_NO2	Rickard and Pascoe (2009)
G48224	TrGTerCN	C721CO3 + NO_3 → C721O2 + CO_2 + NO_2	KRO2NO3*1.74	Rickard and Pascoe (2009)
G48225	TrGTerC	C721CO3 → C721O2 + CO_2	k1_RO2RCO3*0.9	Sander et al. (2019)
G48226	TrGTerC	C721CO3 → NORPINIC	k1_RO2RCO3*0.1	Sander et al. (2019)
G48227	TrGTerC	C721CO3H + OH → C721CO3	9.65E-12	Rickard and Pascoe (2009)
G48228	TrGTerC	NORPINIC + OH → C721O2 + CO_2	6.57E-12	Rickard and Pascoe (2009)
G48229	TrGTerCN	C721PAN + OH → C721OOH + CO + NO_2	2.96E-12	Rickard and Pascoe (2009)
G48230	TrGTerCN	C721PAN → C721CO3 + NO_2	k_PAN_M	Rickard and Pascoe (2009)
G48231	TrGTerC	C8BC + OH → C8BCO2	3.04E-12	Rickard and Pascoe (2009)
G48232	TrGTerC	C8BCO2 + HO_2 → C8BCOOH	k_RO2_HO2(temp,8)	Rickard and Pascoe (2009)
G48233a	TrGTerCN	C8BCO2 + NO → C89O2 + NO_2	KRO2NO*(1.-alpha_AN(8,2,0,0,0,temp,cair))	Rickard and Pascoe (2009)
G48233b	TrGTerCN	C8BCO2 + NO → C8BCNO3	KRO2NO*alpha_AN(8,2,0,0,0,temp,cair)	Rickard and Pascoe (2009)
G48234	TrGTerC	C8BCO2 → C89O2	k1_RO2sRO2	Rickard and Pascoe (2009)
G48235	TrGTerC	C8BCOOH + OH → C8BCCO + OH	1.62E-11	Rickard and Pascoe (2009)
G48236	TrGTerCN	C8BCNO3 + OH → C8BCCO + NO_2	1.84E-12	Rickard and Pascoe (2009)
G48237	TrGTerC	C8BCCO + OH → C89O2	3.94E-12	Rickard and Pascoe (2009)
G48238	TrGTerC	C89O2 + HO_2 → C89OOH	k_RO2_HO2(temp,8)	Rickard and Pascoe (2009)
G48239a	TrGTerCN	C89O2 + NO → C810O2 + NO_2	KRO2NO*(1.-alpha_AN(7,2,0,0,0,temp,cair))	Rickard and Pascoe (2009)
G48239b	TrGTerCN	C89O2 + NO → C89NO3	KRO2NO*alpha_AN(7,2,0,0,0,temp,cair)	Rickard and Pascoe (2009)
G48240	TrGTerCN	C89O2 + NO_3 → C810O2 + NO_2	KRO2NO3	Rickard and Pascoe (2009)
G48241	TrGTerC	C89O2 → C810O2	k1_RO2tRO2	Rickard and Pascoe (2009)
G48242	TrGTerC	C89OOH + OH → C89O2	3.61E-11	Rickard and Pascoe (2009)
G48243	TrGTerCN	C89NO3 + OH → CH_3COCH_3 + CO13C4CHO + NO_2	2.56E-11	Rickard and Pascoe (2009)
G48244	TrGTerC	C810O2 + HO_2 → C810OOH	k_RO2_HO2(temp,8)	Rickard and Pascoe (2009)

Table 1: Gas phase reactions (... continued)

#	labels	reaction	rate coefficient	reference
G48245a	TrGTerCN	C810O2 + NO → CH_3COCH_3 + C514O2 + NO_2	KRO2NO*(1.-alpha_AN(10,3,0,0,0, temp,cair))	Rickard and Pascoe (2009)
G48245b	TrGTerCN	C810O2 + NO → C810NO3	KRO2NO*alpha_AN(10,3,0,0,0, temp,cair)	Rickard and Pascoe (2009)
G48246	TrGTerCN	C810O2 + NO_3 → CH_3COCH_3 + C514O2 + NO_2	KRO2NO3	Rickard and Pascoe (2009)
G48247	TrGTerC	C810O2 → CH_3COCH_3 + C514O2	k1_RO2tRO2	Rickard and Pascoe (2009)
G48248	TrGTerC	C810OOH + OH → C810O2	8.35E-11	Rickard and Pascoe (2009)
G48249	TrGTerCN	C810NO3 + OH → CH_3COCH_3 + CO13C4CHO + NO_2	4.96E-11	Rickard and Pascoe (2009)
G48400a	TrGAroC	LXYL + OH → TLEPOXMUC + HO_2 + LCARBON	0.401E-11	Rickard and Pascoe (2009)*
G48400b	TrGAroC	LXYL + OH → C6H5CH2O2 + LCARBON	0.101E-11	Rickard and Pascoe (2009)*
G48400c	TrGAroC	LXYL + OH → CRESOL + LCARBON	0.261E-11	Rickard and Pascoe (2009)*
G48400d	TrGAroC	LXYL + OH → TLBIPERO2 + HO_2 + LCARBON	0.932E-11	Rickard and Pascoe (2009)*
G48401	TrGAroCN	LXYL + NO_3 → C6H5CH2O2 + HNO_3 + LCARBON	3.9E-16	Rickard and Pascoe (2009)*
G48402	TrGAroC	EBENZ + OH → .10 TLEPOXMUC + .07 C6H5CH2O2 + .18 CRESOL + .65 TLBIPERO2 + .28 HO_2 + LCARBON	7.00E-12	Rickard and Pascoe (2009)*
G48403	TrGAroCN	EBENZ + NO_3 → C6H5CH2O2 + HNO_3 + LCARBON	1.20E-16	Rickard and Pascoe (2009)*
G48404	TrGAroCN	STYRENE + NO_3 → NSTYRENO2	1.50E-12	Rickard and Pascoe (2009)
G48405	TrGAroC	STYRENE + O_3 → .545 HCHO + .1 BENZENE + .28 C6H5O2 + .56 CO + .36 OH + .28 HO_2 + .075 PHCOOH + .545 BENZAL + .09 H_2O_2 + .075 HCOOH + .2 CO_2	1.70E-17	Rickard and Pascoe (2009)*
G48406	TrGAroC	STYRENE + OH → STYRENO2	5.80E-11	Rickard and Pascoe (2009)
G48407	TrGAroCN	NSTYRENO2 + HO_2 → NSTYRENOOH	k_RO2_HO2(temp,8)	Rickard and Pascoe (2009)
G48408	TrGAroCN	NSTYRENO2 + NO → NO_2 + NO_2 + HCHO + BENZAL	KRO2NO	Rickard and Pascoe (2009)*
G48409	TrGAroCN	NSTYRENO2 + NO_3 → NO_2 + NO_2 + HCHO + BENZAL	KRO2NO3	Rickard and Pascoe (2009)*
G48410	TrGAroCN	NSTYRENO2 → NO_2 + HCHO + BENZAL	k1_RO2sRO2	Rickard and Pascoe (2009)*
G48411	TrGAroCN	NSTYRENOOH + OH → NSTYRENO2	6.16E-11	Rickard and Pascoe (2009)
G48412a	TrGAroC	STYRENO2 + HO_2 → STYRENOOH	k_RO2_HO2(temp,8)*(1.-r_CHOHCH2O2_OH)	Rickard and Pascoe (2009)
G48412b	TrGAroC	STYRENO2 + HO_2 → HO_2 + OH + HCHO + BENZAL	k_RO2_HO2(temp,8)*r_CHOHCH2O2_OH	Rickard and Pascoe (2009)*
G48413	TrGAroCN	STYRENO2 + NO → NO_2 + HO_2 + HCHO + BENZAL	KRO2NO	Rickard and Pascoe (2009)*
G48414	TrGAroCN	STYRENO2 + NO_3 → NO_2 + HO_2 + HCHO + BENZAL	KRO2NO3	Rickard and Pascoe (2009)*
G48415	TrGAroC	STYRENO2 → HO_2 + HCHO + BENZAL	k1_RO2sRO2	Rickard and Pascoe (2009)*
G48416	TrGAroC	STYRENOOH + OH → STYRENO2	6.16E-11	Rickard and Pascoe (2009)
G49200	TrGTerC	C96O2 → C97O2	k1_RO2pRO2	Rickard and Pascoe (2009)

Table 1: Gas phase reactions (... continued)

#	labels	reaction	rate coefficient	reference
G49201	TrGTerC	C96O2 + HO_2 → C96OOH	k_RO2_HO2(temp,9)	Rickard and Pascoe (2009)
G49202a	TrGTerCN	C96O2 + NO → C97O2 + NO_2	KRO2NO*(1.-alpha_AN(10,1,0,0,0, temp,cair))	Rickard and Pascoe (2009)
G49202b	TrGTerCN	C96O2 + NO → C96NO3	KRO2NO*alpha_AN(10,1,0,0,0, temp,cair)	Rickard and Pascoe (2009)
G49203	TrGTerCN	C96NO3 + OH → NORPINAL + NO_2	2.88E-12	Rickard and Pascoe (2009)
G49204a	TrGTerC	C96OOH + OH → C96O2	k_ROOHRO	Rickard and Pascoe (2009)
G49205b	TrGTerC	C96OOH + OH → NORPINAL + OH	1.30E-11	Rickard and Pascoe (2009)
G49206	TrGTerC	C97O2 → C98O2	k1_RO2tRO2	Rickard and Pascoe (2009)
G49207	TrGTerCN	C97O2 + NO → C98O2 + NO_2	KRO2NO	Rickard and Pascoe (2009)*
G49208a	TrGTerC	C97O2 + HO_2 → C97OOH	k_RO2_HO2(temp,9)*r_COCH2O2_OOH	Rickard and Pascoe (2009), Sander et al. (2019)
G49208b	TrGTerC	C97O2 + HO_2 → C98O2 + OH	k_RO2_HO2(temp,9)*r_COCH2O2_OH	Rickard and Pascoe (2009), Sander et al. (2019)
G49209	TrGTerC	C97OOH + OH → C97O2	1.05E-11	Rickard and Pascoe (2009)
G49210	TrGTerC	C98O2 → C614O2 + CH_3COCH_3	k1_RO2tRO2	Rickard and Pascoe (2009)
G49211a	TrGTerCN	C98O2 + NO → C614O2 + CH_3COCH_3 + NO_2	KRO2NO*(1.-alpha_AN(12,3,0,0,0, temp,cair))	Rickard and Pascoe (2009)
G49211b	TrGTerCN	C98O2 + NO → 9 LCARBON + LNITROGEN	KRO2NO*alpha_AN(12,3,0,0,0, temp,cair)	Rickard and Pascoe (2009)
G49212	TrGTerC	C98O2 + HO_2 → C98OOH	k_RO2_HO2(temp,9)	Rickard and Pascoe (2009)
G49213	TrGTerC	C98OOH + OH → C98O2	2.05E-11	Rickard and Pascoe (2009)
G49214	TrGTerC	NORPINAL + OH → C85CO3	2.64E-11	Rickard and Pascoe (2009)
G49215	TrGTerCN	NORPINAL + NO_3 → C85CO3 + HNO_3	KNO3AL*8.5	Rickard and Pascoe (2009)
G49216	TrGTerC	C85CO3 → C85O2 + CO_2	k1_RO2RCO3	Rickard and Pascoe (2009)
G49217	TrGTerCN	C85CO3 + NO → C85O2 + CO_2 + NO_2	KAPNO	Rickard and Pascoe (2009)
G49218	TrGTerCN	C85CO3 + NO_2 → C9PAN2	k_CH3CO3_NO2	Rickard and Pascoe (2009)
G49219a	TrGTerC	C85CO3 + HO_2 → C85CO3H	KAPHO2*(r_CO3_OOH+r_CO3_O3)	Rickard and Pascoe (2009)
G49219b	TrGTerC	C85CO3 + HO_2 → C85O2 + CO_2 + OH	KAPHO2*r_CO3_OH	Rickard and Pascoe (2009)
G49220	TrGTerCN	C9PAN2 → C85CO3 + NO_2	k_PAN_M	Rickard and Pascoe (2009)
G49221	TrGTerCN	C9PAN2 + OH → C85OOH + CO + NO_2	6.60E-12	Rickard and Pascoe (2009)
G49222	TrGTerC	C85CO3H + OH → C85CO3	1.02E-11	Rickard and Pascoe (2009)
G49223a	TrGTerC	C89CO3 → .8 C811CO3 + .2 C89O2 + .2 CO_2	k1_RO2RCO3*0.9	Sander et al. (2019)
G49223b	TrGTerC	C89CO3 → C89CO2H	k1_RO2RCO3*0.1	Sander et al. (2019)
G49224a	TrGTerC	C89CO3 + HO_2 → C89CO3H	KAPHO2*r_CO3_OOH	Rickard and Pascoe (2009)

Table 1: Gas phase reactions (... continued)

#	labels	reaction	rate coefficient	reference
G49224b	TrGTerC	C89CO3 + HO_2 → C89CO2H + O_3	KAPHO2*r_CO3_O3	Rickard and Pascoe (2009)
G49224c	TrGTerC	C89CO3 + HO_2 → .80 C811CO3 + .20 C89O2 + .2 CO_2 + OH	KAPHO2*r_CO3_OH	Rickard and Pascoe (2009)
G49225	TrGTerCN	C89CO3 + NO_2 → C89PAN	k_CH3CO3_NO2	Rickard and Pascoe (2009)
G49226	TrGTerCN	C89CO3 + NO → .8 C811CO3 + .2 C89O2 + .2 CO_2 + NO_2	KAPNO	Rickard and Pascoe (2009)
G49227	TrGTerC	C89CO2H + OH → .8 C811CO3 + .2 C89O2 + .2 CO_2	2.69E-11	Rickard and Pascoe (2009)
G49228	TrGTerC	C89CO3H + OH → C89CO3	3.00E-11	Rickard and Pascoe (2009)
G49229	TrGTerCN	C89PAN → C89CO3 + NO_2	k_PAN_M	Rickard and Pascoe (2009)
G49230	TrGTerCN	C89PAN + OH → CH_3COCH_3 + CO13C4CHO + CO + NO_2	2.52E-11	Rickard and Pascoe (2009)
G49231a	TrGTerC	C811CO3 → C811O2 + CO_2	k1_RO2RCO3*0.9	Sander et al. (2019)
G49231b	TrGTerC	C811CO3 → PINIC	k1_RO2RCO3*0.1	Sander et al. (2019)
G49232a	TrGTerC	C811CO3 + HO_2 → C811CO3H	KAPHO2*r_CO3_OOH	Rickard and Pascoe (2009)
G49232b	TrGTerC	C811CO3 + HO_2 → PINIC + O_3	KAPHO2*r_CO3_O3	Rickard and Pascoe (2009)
G49232c	TrGTerC	C811CO3 + HO_2 → C811O2 + CO_2 + OH	KAPHO2*r_CO3_OH	Rickard and Pascoe (2009)
G49233	TrGTerCN	C811CO3 + NO → C811O2 + CO_2 + NO_2	KAPNO	Rickard and Pascoe (2009)
G49234	TrGTerCN	C811CO3 + NO_2 → C811PAN	k_CH3CO3_NO2	Rickard and Pascoe (2009)
G49235	TrGTerC	PINIC + OH → C811O2 + CO_2	7.29E-12	Rickard and Pascoe (2009)
G49236	TrGTerC	NOPINONE + OH → NOPINDO2	1.55E-11	Capouet et al. (2008), Rickard and Pascoe (2009)
G49237a	TrGTerC	NOPINDO2 + HO_2 → NOPINDOOH	k_RO2_HO2(temp,9)*r_COCH2O2_OOH	Rickard and Pascoe (2009), Sander et al. (2019)
G49237b	TrGTerC	NOPINDO2 + HO_2 → C89CO3 + OH	k_RO2_HO2(temp,9)*r_COCH2O2_OH	Rickard and Pascoe (2009), Sander et al. (2019)
G49238	TrGTerCN	NOPINDO2 + NO → C89CO3 + NO_2	KRO2NO	Rickard and Pascoe (2009)*
G49239	TrGTerC	NOPINDO2 → C89CO3	k1_RO2pORO2	Rickard and Pascoe (2009)
G49240	TrGTerC	NOPINDOOH → NOPINDCO	2.63E-11	Rickard and Pascoe (2009)
G49241	TrGTerC	NOPINDCO + OH → C89CO3	3.07E-12	Rickard and Pascoe (2009)
G49242	TrGTerC	NOPINOO → NOPINONE + H_2O_2	6.00E-18*c(ind_H2O)	Rickard and Pascoe (2009)
G49243	TrGTerC	NOPINOO + CO → NOPINONE + CO_2	1.2E-15	Rickard and Pascoe (2009)
G49244	TrGTerCN	NOPINOO + NO → NOPINONE + NO_2	1.E-14	Rickard and Pascoe (2009)
G49245	TrGTerCN	NOPINOO + NO_2 → NOPINONE + NO_3	1.E-15	Rickard and Pascoe (2009)
G49246	TrGTerC	NORPINENOL + OH → HCOOH + OH + C86O2	k_CH2CHOH_OH_HCOOH	Sander et al. (2019), So et al. (2014)*

Table 1: Gas phase reactions (... continued)

#	labels	reaction	rate coefficient	reference
G49247	TrGTerC	NORPINENOL + HCOOH → NORPINAL + HCOOH	k_CH2CHOH_HCOOH	Sander et al. (2019), da Silva (2010)*
G49248	TrGTerC	NORPINAL + HCOOH → NORPINENOL + HCOOH	k_ALD_HCOOH	Sander et al. (2019), da Silva (2010)*
G49249	TrGTerC	C811CO3H + OH → C811CO3	1.04E-11	Rickard and Pascoe (2009)
G49250	TrGTerCN	C811PAN → C811CO3 + NO_2	k_PAN_M	Rickard and Pascoe (2009)
G49251	TrGTerCN	C811PAN + OH → C721CHO + CO + NO_2	6.77E-12	Rickard and Pascoe (2009)
G49400a	TrGAroC	LTMB + OH → TLEPOXMUC + HO_2 + 2 LCARBON	0.827E-11	Rickard and Pascoe (2009)*
G49400b	TrGAroC	LTMB + OH → C6H5CH2O2 + 2 LCARBON	0.189E-11	Rickard and Pascoe (2009)*
G49400c	TrGAroC	LTMB + OH → CRESOL + 2 LCARBON	0.141E-11	Rickard and Pascoe (2009)*
G49400d	TrGAroC	LTMB + OH → TLBIPERO2 + HO_2 + 2 LCARBON	2.917E-11	Rickard and Pascoe (2009)*
G49401	TrGAroCN	LTMB + NO_3 → C6H5CH2O2 + HNO_3 + 2 LCARBON	1.52E-15	Rickard and Pascoe (2009)*
G40200	TrGTerC	APINENE + OH → .75 LAPINABO2 + .15 MENTHEN6ONE + .15 HO_2 + .10 ROO6R1O2	1.2E-11*EXP(440./temp)	Atkinson et al. (2006)*
G40201a	TrGTerCN	LAPINABO2 + NO → PINAL + HO_2 + NO_2	KRO2NO*(1.-(.65*alpha_AN(11,3,0,0,0,temp,cair)+.35*alpha_AN(11,2,0,0,0,temp,cair)))	Rickard and Pascoe (2009), Sander et al. (2019)
G40201b	TrGTerCN	LAPINABO2 + NO → LAPINABNO3	KRO2NO*(.65*alpha_AN(11,3,0,0,0,temp,cair)+.35*alpha_AN(11,2,0,0,0,temp,cair))	Rickard and Pascoe (2009), Sander et al. (2019)
G40202a	TrGTerC	LAPINABO2 + HO_2 → LAPINABOOH	k_RO2_HO2(temp,10)*(1.-r_CHOHCH2O2_OH)	Rickard and Pascoe (2009), Sander et al. (2019)
G40202b	TrGTerC	LAPINABO2 + HO_2 → PINAL + HO_2 + OH	k_RO2_HO2(temp,10)*r_CHOHCH2O2_OH	Rickard and Pascoe (2009), Sander et al. (2019)
G40203	TrGTerC	LAPINABO2 → PINAL + HO_2	RO2*(0.65*k1_RO2tORO2+.35*k1_RO2sORO2)	Rickard and Pascoe (2009)*
G40204	TrGTerC	LAPINABOOH + OH → .35 LAPINABO2 + .65 C96CO3	2.77E-11	Rickard and Pascoe (2009)*
G40205	TrGTerCN	LAPINABNO3 + OH → .35 PINAL + .65 C96CO3 + NO_2	4.29E-12	Rickard and Pascoe (2009)*
G40206	TrGTerC	MENTHEN6ONE + OH → OHMENTHEN6ONEO2	6.46E-11	Vereecken et al. (2007)*
G40207	TrGTerCN	OHMENTHEN6ONEO2 + NO → 2OHMENTHEN6ONE + HO_2 + NO_2	KRO2NO	Vereecken et al. (2007)*
G40208	TrGTerC	OHMENTHEN6ONEO2 + HO_2 → 2OHMENTHEN6ONE	k_RO2_HO2(temp,10)	Vereecken et al. (2007)
G40209	TrGTerC	OHMENTHEN6ONEO2 → 2OHMENTHEN6ONE + HO_2	k1_RO2tORO2	Vereecken et al. (2007)
G40210	TrGTerC	2OHMENTHEN6ONE + OH → 10 LCARBON	1E-11	Vereecken et al. (2007)
G40211	TrGTerC	PINAL + OH → .772 C96CO3 + .228 PINALO2	5.2E-12*EXP(600./temp)	Wallington et al. (2018)*

Table 1: Gas phase reactions (... continued)

#	labels	reaction	rate coefficient	reference
G40212	TrGTerCN	PINAL + NO_3 → C96CO3 + HNO_3	2.0E-14	Wallington et al. (2018)*
G40213a	TrGTerC	C96CO3 → C96O2 + CO_2	k1_RO2RCO3*0.9	Rickard and Pascoe (2009)
G40213b	TrGTerC	C96CO3 → PINONIC	k1_RO2RCO3*0.1	Rickard and Pascoe (2009)
G40214a	TrGTerC	C96CO3 + HO_2 → PERPINONIC	KAPHO2*r_CO3_OOH	Rickard and Pascoe (2009)
G40214b	TrGTerC	C96CO3 + HO_2 → PINONIC + O_3	KAPHO2*r_CO3_O3	Rickard and Pascoe (2009)
G40214c	TrGTerC	C96CO3 + HO_2 → C96O2 + OH + CO_2	KAPHO2*r_CO3_OH	Rickard and Pascoe (2009)
G40215	TrGTerCN	C96CO3 + NO_2 → C10PAN2	k_CH3CO3_NO2	Rickard and Pascoe (2009)
G40216	TrGTerCN	C96CO3 + NO → C96O2 + NO_2 + CO_2	KAPNO	Rickard and Pascoe (2009)
G40217	TrGTerCN	C96CO3 + NO_3 → C96O2 + NO_2 + CO_2	KRO2NO3*1.74	Rickard and Pascoe (2009)
G40218	TrGTerCN	C10PAN2 → C96CO3 + NO_2	k_PAN_M	Rickard and Pascoe (2009)
G40219	TrGTerCN	C10PAN2 + OH → NORPINAL + CO + NO_2	3.66E-12	Rickard and Pascoe (2009)
G40220	TrGTerC	PINONIC + OH → C96O2 + CO_2	6.65E-12	Rickard and Pascoe (2009)
G40221	TrGTerC	PERPINONIC + OH → C96CO3	9.73E-12	Rickard and Pascoe (2009)
G40222	TrGTerC	PINALO2 + HO_2 → PINALOOH	k_RO2_HO2(temp,10)	Rickard and Pascoe (2009)
G40223a	TrGTerCN	PINALO2 + NO → C106O2 + NO_2	KRO2NO*(1.-alpha_AN(12,3,0,1,0, temp,cair))	Rickard and Pascoe (2009), Sander et al. (2019)
G40223b	TrGTerCN	PINALO2 + NO → PINALNO3	KRO2NO*alpha_AN(12,3,0,1,0, temp,cair)	Rickard and Pascoe (2009), Sander et al. (2019)
G40224	TrGTerC	PINALO2 → C106O2	k1_RO2tRO2	Rickard and Pascoe (2009)
G40225	TrGTerC	PINALOOH + OH → PINALO2	2.75E-11	Rickard and Pascoe (2009)
G40226	TrGTerCN	PINALNO3 + OH → CO235C6CHO + CH_3COCH_3 + NO_2	2.25E-11	Rickard and Pascoe (2009)
G40227	TrGTerC	C106O2 + HO_2 → C106OOH	k_RO2_HO2(temp,10)	Rickard and Pascoe (2009)
G40228a	TrGTerCN	C106O2 + NO → C716O2 + CH_3COCH_3 + NO_2	KRO2NO*0.875*(1.-alpha_AN(13,3,0, 0,0,temp,cair))	Rickard and Pascoe (2009), Sander et al. (2019)
G40228b	TrGTerCN	C106O2 + NO → C106NO3	KRO2NO*0.875*alpha_AN(13,3,0,0, 0,temp,cair)	Rickard and Pascoe (2009), Sander et al. (2019)
G40229	TrGTerC	C106O2 → C716O2 + CH_3COCH_3	k1_RO2tRO2	Rickard and Pascoe (2009)
G40230	TrGTerC	C106OOH + OH → C106O2	8.01E-11	Rickard and Pascoe (2009)
G40231	TrGTerCN	C106NO3 + OH → CO235C6CHO + CH_3COCH_3 + NO_2	7.03E-11	Rickard and Pascoe (2009)
G40232	TrGTerC	APINENE + O_3 → .09 APINBOO + .08 PINONIC + .77 OH + .33 NORPINAL + .33 CO + .33 HO_2 + .06 APINAOO + .44 C109O2	8.05E-16*EXP(-640./temp)	Wallington et al. (2018)*
G40233	TrGTerC	APINAOO → PINAL + H_2O_2	1.00E-17*c(ind_H2O)	Rickard and Pascoe (2009)
G40234	TrGTerC	APINAOO + CO → PINAL + CO_2	1.20E-15	Rickard and Pascoe (2009)

Table 1: Gas phase reactions (... continued)

#	labels	reaction	rate coefficient	reference
G40235	TrGTerCN	APINAOO + NO → PINAL + NO_2	1.00E-14	Rickard and Pascoe (2009)
G40236	TrGTerCN	APINAOO + NO_2 → PINAL + NO_3	1.00E-15	Rickard and Pascoe (2009)
G40237a	TrGTerC	APINBOO → PINONIC	1.00E-17*c(ind_H2O)*(0.08+0.15)	Rickard and Pascoe (2009)
G40237b	TrGTerC	APINBOO → PINAL + H_2O_2	1.00E-17*c(ind_H2O)*0.77	Rickard and Pascoe (2009)
G40238	TrGTerC	APINBOO + CO → PINAL + CO_2	1.20E-15	Rickard and Pascoe (2009)
G40239	TrGTerCN	APINBOO + NO → PINAL + NO_2	1.00E-14	Rickard and Pascoe (2009)
G40240	TrGTerCN	APINBOO + NO_2 → PINAL + NO_3	1.00E-15	Rickard and Pascoe (2009)
G40241	TrGTerC	C109O2 → C89CO3 + HCHO	k1_RO2pORO2	Rickard and Pascoe (2009)
G40242	TrGTerCN	C109O2 + NO → C89CO3 + HCHO + NO_2	KRO2NO	Rickard and Pascoe (2009)*
G40243a	TrGTerC	C109O2 + HO_2 → C109OOH	k_RO2_HO2(temp,10)*r_COCH2O2_OOH	Rickard and Pascoe (2009), Sander et al. (2019)
G40243b	TrGTerC	C109O2 + HO_2 → C89CO3 + HCHO + OH	k_RO2_HO2(temp,10)*r_COCH2O2_OH	Rickard and Pascoe (2009), Sander et al. (2019)
G40244	TrGTerC	C109OOH + OH → C109CO + OH	5.47E-11	Rickard and Pascoe (2009)
G40245	TrGTerC	C109CO + OH → C89CO3 + CO	5.47E-11	Rickard and Pascoe (2009)
G40246	TrGTerCN	APINENE + NO_3 → LNAPINABO2	1.2E-12*EXP(490./temp)	Wallington et al. (2018)*
G40247	TrGTerCN	LNAPINABO2 → PINAL + NO_2	(0.65*k1_RO2tRO2 + 0.35*k1_RO2sRO2)	Rickard and Pascoe (2009)
G40248	TrGTerCN	LNAPINABO2 + NO → PINAL + NO_2 + NO_2	KRO2NO	Rickard and Pascoe (2009)*
G40249	TrGTerCN	LNAPINABO2 + HO_2 → LNAPINABOOH	k_RO2_HO2(temp,10)	Rickard and Pascoe (2009)
G40250	TrGTerCN	LNAPINABO2 + NO_3 → PINAL + NO_2 + NO_2	KRO2NO3	Rickard and Pascoe (2009)
G40251	TrGTerCN	LNAPINABOOH + OH → LNAPINABO2	(.65*6.87E-12+.35*1.23E-11)	Rickard and Pascoe (2009)
G40252a	TrGTerC	BPINENE + OH → BPINAO2	1.47E-11*EXP(467./temp) *(0.8326*0.3+0.068)/(0.8326+0.068)	Gill and Hites (2002)*
G40252b	TrGTerC	BPINENE + OH → ROO6R1O2	1.47E-11*EXP(467./temp) *0.8326*0.7/(0.8326+0.068)	Gill and Hites (2002)*
G40253a	TrGTerC	BPINAO2 + HO_2 → BPINAOOH	k_RO2_HO2(temp,10)*r_COCH2O2_OOH	Rickard and Pascoe (2009), Sander et al. (2019)
G40253b	TrGTerC	BPINAO2 + HO_2 → NOPINONE + HCHO + HO_2 + OH	k_RO2_HO2(temp,10)*r_COCH2O2_OH	Rickard and Pascoe (2009), Sander et al. (2019)
G40254a	TrGTerCN	BPINAO2 + NO → NOPINONE + HCHO + HO_2 + NO_2	KRO2NO*(1.-alpha_AN(11,3,0,0,0, temp,cair))	Rickard and Pascoe (2009), Sander et al. (2019)
G40254b	TrGTerCN	BPINAO2 + NO → BPINANO3	KRO2NO*alpha_AN(11,3,0,0,0, temp,cair)	Rickard and Pascoe (2009), Sander et al. (2019)
G40255	TrGTerC	BPINAO2 → NOPINONE + HCHO + HO_2	k1_RO2tORO2	Rickard and Pascoe (2009)

Table 1: Gas phase reactions (... continued)

#	labels	reaction	rate coefficient	reference
G40256	TrGTerC	BPINAOOH + OH → BPINAO2	1.33E-11	Rickard and Pascoe (2009)
G40257	TrGTerCN	BPINANO3 + OH → NOPINONE + HCHO + NO_2	4.70E-12	Rickard and Pascoe (2009)
G40258a	TrGTerCN	ROO6R1O2 + NO → ROO6R3O2 + CH_3COCH_3 + NO_2	KRO2NO*(1.-alpha_AN(13,3,0,0,0, temp,cair))	Vereecken and Peeters (2012)
G40258b	TrGTerCN	ROO6R1O2 + NO → ROO6R1NO3	KRO2NO*alpha_AN(13,3,0,0,0, temp,cair)	Vereecken and Peeters (2012)
G40259	TrGTerC	ROO6R1O2 + HO_2 → 10 LCARBON	k_RO2_HO2(temp,10)	Vereecken and Peeters (2012)*
G40260	TrGTerC	ROO6R1O2 → ROO6R3O2 + CH_3COCH_3	k1_RO2tORO2	Vereecken and Peeters (2012)
G40261a	TrGTerCN	RO6R1O2 + NO → RO6R3O2 + NO_2	KRO2NO*(1.-alpha_AN(12,3,0,0,0, temp,cair))	Vereecken and Peeters (2012)
G40261b	TrGTerCN	RO6R1O2 + NO → RO6R1NO3	KRO2NO*alpha_AN(12,3,0,0,0, temp,cair)	Vereecken and Peeters (2012)
G40262	TrGTerC	RO6R1O2 + HO_2 → 10 LCARBON	k_RO2_HO2(temp,10)	Vereecken and Peeters (2012)*
G40263	TrGTerC	RO6R1O2 → RO6R3O2	k1_RO2sORO2	Vereecken and Peeters (2012)
G40264a	TrGTerCN	RO6R3O2 + NO → 9 LCARBON + HCHO + HO_2 + NO_2	KRO2NO*(1.-alpha_AN(12,3,0,0,0, temp,cair))	Vereecken and Peeters (2012)
G40264b	TrGTerCN	RO6R3O2 + NO → 10 LCARBON + LNITROGEN	KRO2NO*alpha_AN(12,3,0,0,0, temp,cair)	Vereecken and Peeters (2012)
G40265	TrGTerC	RO6R3O2 + HO_2 → 10 LCARBON	k_RO2_HO2(temp,10)	Vereecken and Peeters (2012)
G40266	TrGTerC	RO6R3O2 → 9 LCARBON + HCHO + HO_2	k1_RO2sRO2	Vereecken and Peeters (2012)*
G40267a	TrGTerC	BPINENE + O_3 → NOPINONE + .63 CO + .37 CH_2OO + .16 OH + .16 HO_2	1.35E-15*EXP(-1270./temp) *.051/(1.-.027)	Wallington et al. (2018)*
G40267b	TrGTerC	BPINENE + O_3 → NOPINOO + CO_2	1.35E-15*EXP(-1270./temp) *.368/(1.-.027)	Nguyen et al. (2009), Wallington et al. (2018)
G40267c	TrGTerC	BPINENE + O_3 → NOPINDO2 + CO_2 + OH	1.35E-15*EXP(-1270./temp) *.283/(1.-.027)	Nguyen et al. (2009), Wallington et al. (2018)
G40267d	TrGTerC	BPINENE + O_3 → C8BC + 2 CO_2	1.35E-15*EXP(-1270./temp) *(.104+.167)/(1.-.027)	Nguyen et al. (2009), Wallington et al. (2018)
G40268	TrGTerCN	BPINENE + NO_3 → LNBPINABO2	2.51E-12	Wallington et al. (2018)*
G40269	TrGTerCN	LNBPINABO2 + HO_2 → LNBPINABOOH	k_RO2_HO2(temp,10)	Rickard and Pascoe (2009)
G40270	TrGTerCN	LNBPINABO2 + NO → NOPINONE + HCHO + NO_2 + NO_2	KRO2NO	Rickard and Pascoe (2009)*
G40271	TrGTerCN	LNBPINABO2 + NO_3 → NOPINONE + HCHO + NO_2 + NO_2	KRO2NO3	Rickard and Pascoe (2009)
G40272a	TrGTerCN	LNBPINABO2 → NOPINONE + HCHO + NO_2	k1_RO2tRO2*0.7	Rickard and Pascoe (2009)

Table 1: Gas phase reactions (... continued)

#	labels	reaction	rate coefficient	reference
G40272b	TrGTerCN	LNBPINABO2 → BPINANO3	k1_RO2tRO2*0.3	Rickard and Pascoe (2009)
G40273	TrGTerCN	LNBPINABOOH + OH → LNBPINABO2	9.58E-12	Rickard and Pascoe (2009)
G40274	TrGTerCN	ROO6R1NO3 + OH → ROO6R3O2 + CH_3COCH_3 + NO_2	9.16E-13	Vereecken and Peeters (2012), Gill and Hites (2002)*
G40275	TrGTerCN	RO6R1NO3 + OH → 9 LCARBON + HCHO + HO_2 + NO_2	9.16E-13	Vereecken and Peeters (2012), Gill and Hites (2002)
G40276	TrGTerC	PINEOL + OH → HCOOH + OH + NORPINAL	k_CH2CHOH_OH_HCOOH	Sander et al. (2019), So et al. (2014)*
G40277	TrGTerC	PINEOL + HCOOH → PINAL + HCOOH	k_CH2CHOH_HCOOH	Sander et al. (2019), da Silva (2010)*
G40278	TrGTerC	PINAL + HCOOH → PINEOL + HCOOH	k_ALD_HCOOH	Sander et al. (2019), da Silva (2010)*
G40279a	TrGC	CARENE + OH → LAPINABO2	8.8E-11*(.50+.25)	Atkinson and Arey (2003)
G40279b	TrGC	CARENE + OH → MENTHEN6ONE + HO_2	8.8E-11*.25*.60	Atkinson and Arey (2003)
G40279c	TrGC	CARENE + OH → ROO6R1O2	8.8E-11*.25*.40	Atkinson and Arey (2003)
G40280a	TrGC	CARENE + O_3 → APINBOO	3.7E-17*.50*.18	Atkinson and Arey (2003)
G40280b	TrGC	CARENE + O_3 → PINONIC	3.7E-17*.50*.16	Atkinson and Arey (2003)
G40280c	TrGC	CARENE + O_3 → OH + NORPINAL + CO + HO_2	3.7E-17*.50*.66	Atkinson and Arey (2003)
G40280d	TrGC	CARENE + O_3 → APINAOO	3.7E-17*.50*.12	Atkinson and Arey (2003)
G40280e	TrGC	CARENE + O_3 → OH + C109O2	3.7E-17*.50*(.22+.66)	Atkinson and Arey (2003)
G40281	TrGCN	CARENE + NO_3 → LNAPINABO2	9.1E-12	Atkinson and Arey (2003)
G40282a	TrGTerC	SABINENE + OH → BPINAO2	1.47E-11*EXP(467./temp) *(0.8326*0.3+0.068)/(0.8326+0.068)	Gill and Hites (2002)*
G40282b	TrGTerC	SABINENE + OH → ROO6R1O2	1.47E-11*EXP(467./temp) *0.8326*0.7/(0.8326+0.068)	Vereecken and Peeters (2012), Gill and Hites (2002)*
G40283a	TrGTerC	SABINENE + O_3 → NOPINONE + .63 CO + .37 $HOCH_2OOH$ + .16 OH + .16 HO_2	1.35E-15*EXP(-1270./temp) *.051/(1.-.027)	Wallington et al. (2018)*
G40283b	TrGTerC	SABINENE + O_3 → NOPINOO + CO_2	1.35E-15*EXP(-1270./temp) *.368/(1.-.027)	Nguyen et al. (2009), Wallington et al. (2018)
G40283c	TrGTerC	SABINENE + O_3 → NOPINDO2 + CO_2 + OH	1.35E-15*EXP(-1270./temp) *.283/(1.-.027)	Nguyen et al. (2009), Wallington et al. (2018)
G40283d	TrGTerC	SABINENE + O_3 → C8BC + 2 CO_2	1.35E-15*EXP(-1270./temp) *(.104+.167)/(1.-.027)	Nguyen et al. (2009), Wallington et al. (2018)
G40284	TrGTerCN	SABINENE + NO_3 → LNBPINABO2	2.51E-12	Wallington et al. (2018)*

Table 1: Gas phase reactions (... continued)

#	labels	reaction	rate coefficient	reference
G40285a	TrGTerC	CAMPHENE + OH → BPINAO2	1.47E-11*EXP(467./temp) *(0.8326*0.3+0.068)/(0.8326+0.068)	Gill and Hites (2002)*
G40285b	TrGTerC	CAMPHENE + OH → ROO6R1O2	1.47E-11*EXP(467./temp) *0.8326*0.7/(0.8326+0.068)	Vereecken and Peeters (2012), Gill and Hites (2002)*
G40286a	TrGTerC	CAMPHENE + O_3 → NOPINONE + .63 CO + .37 $HOCH_2OOH$ + .16 OH + .16 HO_2	1.35E-15*EXP(-1270./temp) *.051/(1.-.027)	Wallington et al. (2018)*
G40286b	TrGTerC	CAMPHENE + O_3 → NOPINOO + CO_2	1.35E-15*EXP(-1270./temp) *.368/(1.-.027)	Nguyen et al. (2009), Wallington et al. (2018)
G40286c	TrGTerC	CAMPHENE + O_3 → NOPINDO2 + CO_2 + OH	1.35E-15*EXP(-1270./temp) *.283/(1.-.027)	Nguyen et al. (2009), Wallington et al. (2018)
G40286d	TrGTerC	CAMPHENE + O_3 → C8BC + 2 CO_2	1.35E-15*EXP(-1270./temp) *(.104+.167)/(1.-.027)	Nguyen et al. (2009), Wallington et al. (2018)
G40287	TrGTerCN	CAMPHENE + NO_3 → LNBPINABO2	2.51E-12	Wallington et al. (2018)*
G40400	TrGAroC	LHAROM + OH → .14 TLEPOXMUC + .03 C6H5CH2O2 + .04 CRESOL + .79 TLBIPERO2 + .18 HO_2 + 4 LCARBON	5.67E-11	Rickard and Pascoe (2009)*
G40401	TrGAroCN	LHAROM + NO_3 → C6H5CH2O2 + HNO_3 + 4 LCARBON	2.60E-15	Rickard and Pascoe (2009)*
G6100	UpStTrGCl	Cl + O_3 → ClO + O_2	2.8E-11*EXP(-250./temp)	Atkinson et al. (2007)
G6101	UpStGCl	ClO + $O(^3P)$ → Cl + O_2	2.5E-11*EXP(110./temp)	Atkinson et al. (2007)
G6102a	StTrGCl	ClO + ClO → Cl_2 + O_2	1.0E-12*EXP(-1590./temp)	Atkinson et al. (2007)
G6102b	StTrGCl	ClO + ClO → 2 Cl + O_2	3.0E-11*EXP(-2450./temp)	Atkinson et al. (2007)
G6102c	StTrGCl	ClO + ClO → Cl + OClO	3.5E-13*EXP(-1370./temp)	Atkinson et al. (2007)
G6102d	StTrGCl	ClO + ClO → Cl_2O_2	k_ClO_ClO	Burkholder et al. (2015)
G6103	StTrGCl	Cl_2O_2 → ClO + ClO	k_ClO_ClO/(2.16E-27*EXP(8537./ temp))	Burkholder et al. (2015)*
G6200	StGCl	Cl + H_2 → HCl + H	3.9E-11*EXP(-2310./temp)	Atkinson et al. (2007)
G6201a	StGCl	Cl + HO_2 → HCl + O_2	4.4E-11-7.5E-11*EXP(-620./temp)	Atkinson et al. (2007)
G6201b	StGCl	Cl + HO_2 → ClO + OH	7.5E-11*EXP(-620./temp)	Atkinson et al. (2007)
G6202	StTrGCl	Cl + H_2O_2 → HCl + HO_2	1.1E-11*EXP(-980./temp)	Atkinson et al. (2007)
G6203	StGCl	ClO + OH → .94 Cl + .94 HO_2 + .06 HCl + .06 O_2	7.3E-12*EXP(300./temp)	Atkinson et al. (2007)
G6204	StTrGCl	ClO + HO_2 → HOCl + O_2	2.2E-12*EXP(340./temp)	Atkinson et al. (2007)*
G6205	StTrGCl	HCl + OH → Cl + H_2O	1.7E-12*EXP(-230./temp)	Atkinson et al. (2007)
G6206	StGCl	HOCl + OH → ClO + H_2O	3.0E-12*EXP(-500./temp)	Burkholder et al. (2015)
G6300	UpStTrGClN	ClO + NO → NO_2 + Cl	6.2E-12*EXP(295./temp)	Atkinson et al. (2007)

Table 1: Gas phase reactions (... continued)

#	labels	reaction	rate coefficient	reference
G6301	StTrGClN	$ClO + NO_2 \rightarrow ClNO_3$	k_3rd_iupac(temp,cair,1.6E-31, 3.4,7.E-11,0.,0.4)	Atkinson et al. (2007)
G6302	TrGClN	$ClNO_3 \rightarrow ClO + NO_2$	6.918E-7*EXP(-10909./temp)*cair	Anderson and Fahey (1990)
G6303	StGClN	$ClNO_3 + O(^3P) \rightarrow ClO + NO_3$	4.5E-12*EXP(-900./temp)	Atkinson et al. (2007)
G6304	StTrGClN	$ClNO_3 + Cl \rightarrow Cl_2 + NO_3$	6.2E-12*EXP(145./temp)	Atkinson et al. (2007)
G6400	StTrGCl	$Cl + CH_4 \rightarrow HCl + CH_3$	6.6E-12*EXP(-1240./temp)	Atkinson et al. (2006)
G6401	StTrGCl	$Cl + HCHO \rightarrow HCl + CO + HO_2$	8.1E-11*EXP(-34./temp)	Atkinson et al. (2006)
G6402	StTrGCl	$Cl + CH_3OOH \rightarrow HCHO + HCl + OH$	5.9E-11	Atkinson et al. (2006)*
G6403	StTrGCl	$ClO + CH_3O_2 \rightarrow HO_2 + Cl + HCHO$	1.8E-12*EXP(-600./temp)	Burkholder et al. (2015)
G6404	StGCl	$CCl_4 + O(^1D) \rightarrow$ LCARBON + ClO + 3 Cl	3.3E-10	Burkholder et al. (2015)
G6405	StGCl	$CH_3Cl + O(^1D) \rightarrow 0.1\ CH_3Cl + 0.1\ O(^3P) + 0.46$ ClO + 0.35 Cl + 0.09 H + 0.9 LCARBON + 0.09 LCHLORINE	1.65E-10	Burkholder et al. (2015)
G6406	StGCl	$CH_3Cl + OH \rightarrow$ LCARBON + H_2O + Cl	1.96E-12*EXP(-1200./temp)	Burkholder et al. (2015)
G6407	StGCCl	$CH_3CCl_3 + O(^1D) \rightarrow 2$ LCARBON + OH + 3 Cl	3.25E-10	Burkholder et al. (2015)
G6408	StTrGCCl	$CH_3CCl_3 + OH \rightarrow 2$ LCARBON + H_2O + 3 Cl	1.64E-12*EXP(-1520./temp)	Burkholder et al. (2015)
G6409	TrGCCl	$Cl + C_2H_4 \rightarrow HOCH_2CH_2O_2 + HCl$	k_3rd_iupac(temp,cair,1.85E-29, 3.3,6.0E-10,0.0,0.4)	Atkinson et al. (2006)*
G6410	TrGCCl	$Cl + CH_3CHO \rightarrow HCl + CH_3C(O)$	8.0e-11	Atkinson et al. (2006)
G6411	TrGCCl	$C_2H_2 + Cl \rightarrow$ LCARBON + CH_3 + HCl	k_3rd_iupac(temp,cair,6.1e-30, 3.0,2.0e-10,0.,0.6)	Atkinson et al. (2006)
G6412	TrGCCl	$C_2H_6 + Cl \rightarrow C_2H_5O_2 + HCl$	8.3E-11*EXP(-100./temp)	Atkinson et al. (2006)
G6413	StTrGClN	$Cl + CH_3ONO_2 \rightarrow HCl + HCHO + NO_2$	1.3E-11*EXP(-1200./temp)	Burkholder et al. (2015)
G6414	StTrGClN	$Cl + CH_3ONO \rightarrow HCl + HCHO + NO$	2.1E-12	Sokolov et al. (1999)
G6415	StTrGCl	$Cl + CH_3O_2 \rightarrow .5$ ClO + .5 CH_3O + .5 HCl + .5 CH_2OO	1.6E-10	Burkholder et al. (2015)
G6416	TrGCClN	$Cl + CH_3CN \rightarrow NCCH_2O_2 + HCl$	1.6E-11*EXP(-2104./temp)	Tyndall et al. (1996), Tyndall et al. (2001b), Sander et al. (2019)
G6500	StGClF	$CF_2Cl_2 + O(^1D) \rightarrow$ LCARBON + 2 LFLUORINE + ClO + Cl	1.4E-10	Burkholder et al. (2015)
G6501	StGClF	$CFCl_3 + O(^1D) \rightarrow$ LCARBON + LFLUORINE + ClO + 2 Cl	2.3E-10	Burkholder et al. (2015)
G7100	StTrGBr	$Br + O_3 \rightarrow BrO + O_2$	1.7E-11*EXP(-800./temp)	Atkinson et al. (2007)
G7101	StGBr	$BrO + O(^3P) \rightarrow Br + O_2$	1.9E-11*EXP(230./temp)	Atkinson et al. (2007)
G7102a	StTrGBr	$BrO + BrO \rightarrow 2\ Br + O_2$	2.7E-12	Atkinson et al. (2007)
G7102b	StTrGBr	$BrO + BrO \rightarrow Br_2 + O_2$	2.9E-14*EXP(840./temp)	Atkinson et al. (2007)

Table 1: Gas phase reactions (... continued)

#	labels	reaction	rate coefficient	reference
G7200	StTrGBr	$Br + HO_2 \rightarrow HBr + O_2$	7.7E-12*EXP(-450./temp)	Atkinson et al. (2007)
G7201	StTrGBr	$BrO + HO_2 \rightarrow HOBr + O_2$	4.5E-12*EXP(500./temp)	Atkinson et al. (2007)
G7202	StTrGBr	$HBr + OH \rightarrow Br + H_2O$	6.7E-12*EXP(155./temp)	Atkinson et al. (2007)
G7203	StGBr	$HOBr + O(^3P) \rightarrow OH + BrO$	1.2E-10*EXP(-430./temp)	Atkinson et al. (2007)
G7204	StTrGBr	$Br_2 + OH \rightarrow HOBr + Br$	2.0E-11*EXP(240./temp)	Atkinson et al. (2007)
G7300	TrGBrN	$Br + BrNO_3 \rightarrow Br_2 + NO_3$	4.9E-11	Orlando and Tyndall (1996)
G7301	StTrGBrN	$BrO + NO \rightarrow Br + NO_2$	8.7E-12*EXP(260./temp)	Atkinson et al. (2007)
G7302	StTrGBrN	$BrO + NO_2 \rightarrow BrNO_3$	k_BrO_NO2	Atkinson et al. (2007)*
G7303	TrGBrN	$BrNO_3 \rightarrow BrO + NO_2$	k_BrO_NO2/(5.44E-9*EXP(14192./temp)*1.E6*R_gas*temp/(atm2Pa*N_A))	Orlando and Tyndall (1996), Atkinson et al. (2007)*
G7400	StTrGBr	$Br + HCHO \rightarrow HBr + CO + HO_2$	7.7E-12*EXP(-580./temp)	Atkinson et al. (2006)
G7401	TrGBr	$Br + CH_3OOH \rightarrow CH_3O_2 + HBr$	2.6E-12*EXP(-1600./temp)	Kondo and Benson (1984)
G7402	TrGBr	$BrO + CH_3O_2 \rightarrow HOBr + CH_2OO$	2.42E-14*EXP(1617./temp)	Shallcross et al. (2015)
G7403	StTrGBr	$CH_3Br + OH \rightarrow LCARBON + H_2O + Br$	1.42E-12*EXP(-1150./temp)	Burkholder et al. (2015)
G7404	TrGBrC	$Br + C_2H_4 \rightarrow HOCH_2CH_2O_2 + HBr$	2.8E-13*EXP(224./temp)/(1.+1.13E24*EXP(-3200./temp)/C(ind_O2))	Atkinson et al. (2006)*
G7405	TrGBrC	$Br + CH_3CHO \rightarrow HBr + CH_3C(O)$	1.8e-11*EXP(-460./temp)	Atkinson et al. (2006)
G7406	TrGBrC	$Br + C_2H_2 \rightarrow LCARBON + CH_3O_2 + HBr$	6.35e-15*EXP(440./temp)	Atkinson et al. (2006)
G7407	TrGBr	$CHBr_3 + OH \rightarrow LCARBON + H_2O + 3\ Br$	9.0E-13*EXP(-360./temp)	Burkholder et al. (2015)*
G7408	TrGBr	$CH_2Br_2 + OH \rightarrow LCARBON + H_2O + 2\ Br$	2.0E-12*EXP(-840./temp)	Burkholder et al. (2015)*
G7600	TrGBrCl	$Br + BrCl \rightarrow Br_2 + Cl$	3.32E-15	Manion et al. (2015)
G7601	TrGBrCl	$Br + Cl_2 \rightarrow BrCl + Cl$	1.10E-15	Dolson and Leone (1987)
G7602	TrGBrCl	$Br_2 + Cl \rightarrow BrCl + Br$	2.3E-10*EXP(135./temp)	Bedjanian et al. (1998)
G7603a	StTrGBrCl	$BrO + ClO \rightarrow Br + OClO$	1.6E-12*EXP(430./temp)	Atkinson et al. (2007)
G7603b	StTrGBrCl	$BrO + ClO \rightarrow Br + Cl + O_2$	2.9E-12*EXP(220./temp)	Atkinson et al. (2007)
G7603c	StTrGBrCl	$BrO + ClO \rightarrow BrCl + O_2$	5.8E-13*EXP(170./temp)	Atkinson et al. (2007)
G7604	TrGBrCl	$BrCl + Cl \rightarrow Br + Cl_2$	1.45E-11	Clyne and Cruse (1972)
G7605	TrGBrCl	$CHCl_2Br + OH \rightarrow LCARBON + 2\ Cl + H_2O + Br$	2.0E-12*EXP(-840./temp)	see note*
G7606	TrGBrCl	$CHClBr_2 + OH \rightarrow LCARBON + Cl + H_2O + 2\ Br$	2.0E-12*EXP(-840./temp)	see note*
G7607	TrGBrCl	$CH_2ClBr + OH \rightarrow LCARBON + Cl + H_2O + Br$	2.1E-12*EXP(-880./temp)	Burkholder et al. (2015)*
G8100	TrGI	$I + O_3 \rightarrow IO + O_2$	2.1E-11*EXP(-830./temp)	Atkinson et al. (2007)
G8102	TrGI	$OIO + OIO \rightarrow I(part)$	5.E-11	von Glasow et al. (2002)*
G8103	TrGI	$IO + IO \rightarrow .38\ OIO + 1.62\ I + .62\ O_2$	5.4E-11*EXP(180./temp)	Atkinson et al. (2007)*

Table 1: Gas phase reactions (... continued)

#	labels	reaction	rate coefficient	reference
G8200	TrGI	$I + HO_2 \rightarrow HI + O_2$	1.5E-11*EXP(-1090./temp)	Atkinson et al. (2007)
G8201	TrGI	$IO + HO_2 \rightarrow HOI + O_2$	1.4E-11*EXP(540./temp)	Atkinson et al. (2007)
G8202	TrGI	$HI + OH \rightarrow I + H_2O$	1.6E-11*EXP(440./temp)	Atkinson et al. (2007)
G8203	TrGI	$OIO + OH \rightarrow HIO_3$	2.2E-10*EXP(243./temp)	Plane et al. (2006)
G8204	TrGI	$I_2 + OH \rightarrow HOI + I$	2.1E-10	Atkinson et al. (2007)
G8205	TrGI	$HOI + OH \rightarrow IO + H_2O$	5.0E-12	Riffault et al. (2005)
G8300	TrGIN	$I + NO_2 \rightarrow INO_2$	k_I_NO2	Atkinson et al. (2007)*
G8301	TrGIN	$I + NO_3 \rightarrow IO + NO_2$	1.E-10	Dillon et al. (2008)
G8302	TrGIN	$IO + NO \rightarrow I + NO_2$	7.15E-12*EXP(300./temp)	Atkinson et al. (2007)
G8303	TrGIN	$IO + NO_2 \rightarrow INO_3$	k_3rd_iupac(temp,cair,7.7E-31, 5.,1.6E-11,0.,0.4)	Atkinson et al. (2007)
G8304	TrGIN	$OIO + NO \rightarrow NO_2 + IO$	1.1E-12*EXP(542./temp)	Atkinson et al. (2007)
G8305	TrGIN	$INO_2 \rightarrow I + NO_2$	k_I_NO2/(3.7E-7*EXP(9568./temp) *1.E6*R_gas*temp/(atm2Pa*N_A))	van den Bergh and Troe (1976), Atkinson et al. (2007)*
G8306	TrGIN	$INO_3 \rightarrow IO + NO_2$	2.1e15*EXP(-13670./temp)	Kaltsoyannis and Plane (2008)
G8307	TrGIN	$I_2 + NO_3 \rightarrow I + INO_3$	1.5E-12	Atkinson et al. (2007)
G8308	TrGIN	$IO + NO_3 \rightarrow OIO + NO_2$	9.E-12	Dillon et al. (2008)
G8309	TrGIN	$I + INO_3 \rightarrow I_2 + NO_3$	9.1E-11*EXP(-146./temp)	Kaltsoyannis and Plane (2008)
G8400	TrGCI	$CH_3CHICH_3 + OH \rightarrow 2\ LCARBON + CH_3O_2 + I$	1.22E-12	Carl and Crowley (2001)
G8401	TrGI	$CH_3O_2 + IO \rightarrow .4\ I + .6\ OIO + HCHO + HO_2$	2.E-12	Dillon et al. (2006b), Bale et al. (2005)*
G8402	TrGIN	$CH_3I + NO_3 \rightarrow HNO_3 + HCHO + IO$	3.4E-17	Wayne et al. (1991)*
G8600	TrGClI	$IO + ClO \rightarrow .2\ ICl + .25\ Cl + .55\ OClO + .8\ I + .45\ O_2$	4.7E-12*EXP(280./temp)	Atkinson et al. (2007)
G8700	TrGBrI	$I + BrO \rightarrow IO + Br$	1.2E-11	Burkholder et al. (2015)
G8701	TrGBrI	$IO + BrO \rightarrow Br + .8\ OIO + .2\ I + .2\ O_2$	1.5E-11*EXP(510./temp)	Atkinson et al. (2007)*
G8702	TrGBrI	$IBr + OH \rightarrow .84\ HOI + .84\ Br + .16\ HOBr + .16\ I$	1.4E-10	Riffault et al. (2005)
G8703	TrGBrI	$IO + Br \rightarrow I + BrO$	2.3E-11	Bedjanian et al. (1997)
G8704	TrGBrI	$I_2 + Br \rightarrow IBr + I$	1.2E-10	Bedjanian et al. (1997)
G9200	StTrGS	$SO_2 + OH \rightarrow H_2SO_4 + HO_2$	k_3rd(temp,cair,3.3E-31,4.3, 1.6E-12,0.,0.6)	Burkholder et al. (2015)
G9400a	TrGCS	$DMS + OH \rightarrow CH_3SO_2 + HCHO$	1.13E-11*EXP(-253./temp)	Atkinson et al. (2004)*
G9400b	TrGCS	$DMS + OH \rightarrow DMSO + HO_2$	k_DMS_OH	Atkinson et al. (2004)*
G9401	TrGCNS	$DMS + NO_3 \rightarrow CH_3SO_2 + HNO_3 + HCHO$	1.9E-13*EXP(520./temp)	Atkinson et al. (2004)
G9402	TrGCS	$DMSO + OH \rightarrow .6\ SO_2 + HCHO + .6\ CH_3 + .4\ HO_2 + .4\ CH_3SO_3H$	1.E-10	Hynes and Wine (1996)*

Table 1: Gas phase reactions (... continued)

#	labels	reaction	rate coefficient	reference
G9403	TrGS	$CH_3SO_2 \rightarrow SO_2 + CH_3$	1.8E13*EXP(-8661./temp)	Barone et al. (1995)
G9404	TrGS	$CH_3SO_2 + O_3 \rightarrow CH_3SO_3$	3.E-13	Barone et al. (1995)
G9405	TrGS	$CH_3SO_3 + HO_2 \rightarrow CH_3SO_3H$	5.E-11	Barone et al. (1995)
G9408	StTrGS	$CH_2OO + SO_2 \rightarrow H_2SO_4 + HCHO$	k_CH2OO_SO2	Welz et al. (2012), Stone et al. (2014)*
G9409	TrGTerCS	$NOPINOO + SO_2 \rightarrow NOPINONE + H_2SO_4$	7.E-14	Rickard and Pascoe (2009)
G9410	TrGTerCS	$APINAOO + SO_2 \rightarrow PINAL + H_2SO_4$	7.00E-14	Rickard and Pascoe (2009)
G9411	TrGTerCS	$APINBOO + SO_2 \rightarrow PINAL + H_2SO_4$	7.00E-14	Rickard and Pascoe (2009)
G9412	TrGTerCS	$MBOOO + SO_2 \rightarrow IBUTALOH + H_2SO_4$	7.00E-14	Rickard and Pascoe (2009)
G9600	TrGCClS	$DMS + Cl \rightarrow CH_3SO_2 + HCl + HCHO$	3.3E-10	Atkinson et al. (2004)
G9700	TrGBrCS	$DMS + Br \rightarrow CH_3SO_2 + HBr + HCHO$	9.E-11*EXP(-2386./temp)	Jefferson et al. (1994)
G9701	TrGBrCS	$DMS + BrO \rightarrow DMSO + Br$	4.4E-13	Ingham et al. (1999)
G9800	TrGCIS	$DMS + IO \rightarrow DMSO + I$	3.2E-13*EXP(-925./temp)	Dillon et al. (2006a)
G10100	TrGHg	$Hg + O_3 \rightarrow HgO + O_2$	3.0E-20	Hall (1995)
G10200	TrGHg	$Hg + OH \rightarrow HgO + H$	3.55E-14*EXP(294./temp)	Pal and Ariya (2004)
G10201	TrGHg	$Hg + H_2O_2 \rightarrow HgO + H_2O$	8.5E-19	Tokos et al. (1998)*
G10600	TrGClHg	$Hg + Cl \rightarrow HgCl$	1.0E-11	Ariya et al. (2002)
G10601	TrGClHg	$Hg + Cl_2 \rightarrow HgCl_2$	2.6E-18	Ariya et al. (2002)
G10700	TrGBrHg	$Hg + Br \rightarrow HgBr$	3.0E-13	Donohoue et al. (2006)
G10701	TrGBrHg	$HgBr + Br \rightarrow HgBr_2$	2.5E-10*(temp/298.)**(-0.57)	Goodsite et al. (2004)
G10702	TrGBrHg	$Hg + Br_2 \rightarrow HgBr_2$	9.0E-17	Ariya et al. (2002)
G10703	TrGBrHg	$Hg + BrO \rightarrow HgO + Br$	1.0E-15	Raofie and Ariya (2003)
G10704	TrGBrHg	$HgBr + BrO \rightarrow BrHgOBr$	3.0E-12	Calvert and Lindberg (2003)
G10705	TrGBrClHg	$HgCl + BrO \rightarrow ClHgOBr$	3.0E-12	Calvert and Lindberg (2003)
G10706	TrGBrClHg	$HgBr + Cl \rightarrow ClHgBr$	3.0E-12	Calvert and Lindberg (2003)
G10707	TrGBrClHg	$HgCl + Br \rightarrow ClHgBr$	3.0E-12	Calvert and Lindberg (2003)

General notes

Three-body reactions

Rate coefficients for three-body reactions are defined via the function `k_3rd`(T, M, k_0^{300}, n, k_{inf}^{300}, m, f_c). In the code, the temperature T is called `temp` and the concentration of "air molecules" M is called `cair`. Using the auxiliary variables $k_0(T)$, $k_{\mathrm{inf}}(T)$, and k_{ratio}, `k_3rd` is defined as:

$$k_0(T) = k_0^{300} \times \left(\frac{300\mathrm{K}}{T}\right)^n \quad (1)$$

$$k_{\mathrm{inf}}(T) = k_{\mathrm{inf}}^{300} \times \left(\frac{300\mathrm{K}}{T}\right)^m \quad (2)$$

$$k_{\mathrm{ratio}} = \frac{k_0(T)M}{k_{\mathrm{inf}}(T)} \quad (3)$$

$$\texttt{k\_3rd} = \frac{k_0(T)M}{1+k_{\mathrm{ratio}}} \times f_\mathrm{c}^{\left(\frac{1}{1+(\log_{10}(k_{\mathrm{ratio}}))^2}\right)} \quad (4)$$

A similar function, called `k_3rd_iupac` here, is used by Wallington et al. (2018) for three-body reactions. It has the same function parameters as `k_3rd` and it is defined as:

$$k_0(T) = k_0^{300} \times \left(\frac{300\mathrm{K}}{T}\right)^n \quad (5)$$

$$k_{\mathrm{inf}}(T) = k_{\mathrm{inf}}^{300} \times \left(\frac{300\mathrm{K}}{T}\right)^m \quad (6)$$

$$k_{\mathrm{ratio}} = \frac{k_0(T)M}{k_{\mathrm{inf}}(T)} \quad (7)$$

$$N = 0.75 - 1.27 \times \log_{10}(f_\mathrm{c}) \quad (8)$$

$$\texttt{k\_3rd\_iupac} = \frac{k_0(T)M}{1+k_{\mathrm{ratio}}} \times f_\mathrm{c}^{\left(\frac{1}{1+(\log_{10}(k_{\mathrm{ratio}})/N)^2}\right)} \quad (9)$$

Structure-Activity Relationships (SAR)

Some unmeasured rate coefficients are estimated with structure-activity relationships, using the following parameters and substituent factors:

k for H-abstraction by OH in $\mathrm{cm^{-3}s^{-1}}$	
`k_p`	$4.49 \times 10^{-18} \times (T/\mathrm{K})^2 \exp(-320\,\mathrm{K}/T)$
`k_s`	$4.50 \times 10^{-18} \times (T/\mathrm{K})^2 \exp(253\,\mathrm{K}/T)$
`k_t`	$2.12 \times 10^{-18} \times (T/\mathrm{K})^2 \exp(696\,\mathrm{K}/T)$
`k_ROHRO`	$2.1 \times 10^{-18} \times (T/\mathrm{K})^2 \exp(-85\,\mathrm{K}/T)$
`k_CO2H`	$0.7 \times k_{\mathrm{CH_3CO_2H+OH}}$
`k_ROOHRO`	$0.6 \times k_{\mathrm{CH_3OOH+OH}}$
`f_alk`	1.23
`f_sOH`	3.44
`f_tOH`	2.68
`f_sOOH`	8.
`f_tOOH`	8.
`f_ONO2`	0.04
`f_CH2ONO2`	0.20
`f_cpan`	0.25
`f_allyl`	3.6
`f_CHO`	0.55
`f_CO2H`	1.67
`f_CO`	0.73
`f_O`	8.15
`f_pCH2OH`	1.29
`f_tCH2OH`	0.53

k for OH-addition to double bonds in $\mathrm{cm^{-3}s^{-1}}$	
`k_adp`	$4.5 \times 10^{-12} \times (T/300\,\mathrm{K})^{-0.85}$
`k_ads`	$1/4 \times (1.1 \times 10^{-11} \times \exp(485\,\mathrm{K}/T) + 1.0 \times 10^{-11} \times \exp(553\,\mathrm{K}/T))$
`k_adt`	$1.922 \times 10^{-11} \times \exp(450\,\mathrm{K}/T) - k_{\mathrm{ads}}$
`k_adsecprim`	3.0×10^{-11}
`k_adtertprim`	5.7×10^{-11}
`a_PAN`	0.56
`a_CHO`	0.31
`a_COCH3`	0.76
`a_CH2OH`	1.7
`a_CH2OOH`	1.7
`a_COH`	2.2
`a_COOH`	2.2
`a_CO2H`	0.25
`a_CH2ONO2`	0.64

RO_2 self and cross reactions

The self and cross reactions of organic peroxy radicals are treated according to the permutation reaction formalism as implemented in the MCM (Rickard and Pascoe, 2009), as decribed by Jenkin et al. (1997). Every organic peroxy radical reacts in a pseudo-first-order reaction with a rate constant that is expressed as $k^{1\mathrm{st}} = 2 \times \sqrt{k_{\mathrm{self}} \times \texttt{k\_CH3O2}} \times [\mathrm{RO_2}]$ where k_{self} = second-order rate coefficient of the self reaction of the organic peroxy radical, `k_CH3O2` = second-order rate coefficient of the self reaction of CH_3O_2, and $[\mathrm{RO_2}]$ = sum of the concentrations of all organic peroxy radicals.

Specific notes

G1002a: The path leading to 2 $O(^3P)$ + O_2 results in a null cycle regarding odd oxygen and is neglected.

G2110: The rate coefficient is: `k_HO2_HO2 = (3.0E-13*EXP(460./temp)+2.1E-33*EXP(920./temp) *cair)*(1.+1.4E-21*EXP(2200./temp)*C(ind_H2O))`.

G2117: Converted to Kc [molec-1 cm3]= Kp*R*T/NA, where R is 82.05736 [cm3atmK1mol1].

G2118: Assuming fast equilibrium.

G3109: The rate coefficient is: `k_NO3_NO2 = k_3rd(temp,cair,2.4E-30,3.0,1.6E-12,-0.1,0.6)`.

G3110: The rate coefficient is defined as backward reaction divided by equilibrium constant.

G3203: The rate coefficient is: `k_NO2_HO2 = k_3rd(temp,cair,1.9E-31,3.4,4.0E-12,0.3,0.6)`.

G3206: The rate coefficient is: `k_HNO3_OH = 1.32E-14 * EXP(527/temp) + 1 / ( 1 / (7.39E-32 * EXP(453/temp)*cair) + 1 / (9.73E-17 * EXP(1910/temp)) )`

G3207: The rate coefficient is defined as backward reaction divided by equilibrium constant.

G3227: Backward reaction divided by equilibrium constant from Burkholder et al. (2015).

G3228: Same as for OH + HNO_4.

G4104b: Methyl nitrate yield according to Banic et al. (2003) but reduced by a factor of 10 according to the upper limit derived from measurements by Munger et al. (1999).

G4109: Same temperature dependence as for CH_3CHO+NO_3 assumed.

G4115: The rate coefficient is defined as backward reaction divided by equilibrium constant.

G4116: Same value as for PAN + OH.

G4126: Same as for G4104 but scaled to match the recommeded value at 298K.

G4127: Same as for CH3O2 + NO3 in G4105.

G4130a: SAR for H-abstraction by OH.

G4130b: SAR for H-abstraction by OH.

G4132: SAR for H-abstraction by OH.

G4133: Lower limit of the rate constant. Products uncertain but CH_3OH can be excluded because of a likely high energy barrier (L. Vereecken, pers. comm.). CH_2OO production cannot be excluded.

G4134: Estimate based on the decomposition lifetime of 3 s (Olzmann et al., 1997) and a 20 kcal/mol energy barrier (Vereecken and Francisco, 2012).

G4135: Rate constant for $CH_2OO + NO_2$ (G4138) multiplied by the factor from Ouyang et al. (2013).

G4136: Average of two measurements.

G4137: Upper limit.

G4138: Average of 7.E-12 and 1.5E-12.

G4141: $HOOCH_2OCHO$ forms and then decomposes to formic anhydride (Gruzdev et al., 1993) which hydrolyses in the humid atmosphere (Conn et al., 1942).

G4142: High-pressure limit.

G4143: Generic estimate for reaction with alcohols.

G4144: Generic estimate for reaction with RO_2.

G4148: Same value as for NO_2+CH_3O_2.

G4149: Barnes et al. (1985) estimated a decomposition rate equal to that of $CH_3O_2NO_2$.

G4150: Value for $CH_3O_2NO_2$ + OH, H-abstraction enhanced by the HO-group by f_sOH.

G4154: Products assumed to be $CH_3O_2 + O_2$ (could also be $HCHO + O_2 + OH$).

G4160b: Half of the H-yield is attributed to fast secondary chemistry.

G4160c: The NH + CO channel is also significant but neglected here.

G4161: No studies below 450 K and only the major channel is considered.

G4164: Upper limit. Dominant pathway under atmospheric conditions.

G42001: The product distribution is from Rickard and Pascoe (2009), after substitution of the energized Criegee intermediate, CH_2OO, by its decomposition products and reaction of the stabilized CI with the water dimer.

G42010: Only major channel considered as the end products are essentially the same.

G42013: The rate coefficient is: `k_CH3CO3_NO2 = k_3rd(temp,cair,9.7E-29,5.6,9.3E-12,1.5,0.6)`.

G42018: The rate coefficient is the same as for the CH_3 channel in G4107 (CH_3OOH+OH).

G42021: The rate coefficient is `k_PAN_M = k_CH3CO3_NO2/9.0E-29*EXP(-14000./temp)`, i.e. the rate coefficient is defined as backward reaction divided by equilibrium constant.

G42022a: Quantum yields and products are from Glowacki et al. (2012).

G42022b: Quantum yields and products are from Glowacki et al. (2012).

G42024a: Rate constant is the high-pressure limit as recommended by Atkinson et al. (2006).

G42024b: Rate constant is the high-pressure limit as recommended by Atkinson et al. (2006).

G42047: Orlando et al. (1998) estimated that about 25% of the $HOCH_2CH_2O$ in this reaction is produced with sufficient excess energy that it decomposes

promptly. The decomposition products are 2 HCHO + HO_2.

G42051a: Same as for the CH_3O_2 channel in G4107: CH_3OOH+OH.

G42058b: The aldehydic H is assumed to be like the analogous H of $HOCH_2CHO$.

G42074a: Factor of 3 to match the estimate of k = 1.E-11 molec/cm3/s by Paulot et al. (2009a).

G42074b: Factor of 3 to match the estimate of k = 1.E-11 molec/cm3/s by Paulot et al. (2009a).

G42075: $NO_3CH_2CO_2H$ and $NO_3CH_2CO_3H$ neglected.

G42078: $NO_3CH_2CO_2H$ neglected.

G42082: Same rate constant as for PAN + OH.

G42083a: Rate constant is the high-pressure limit as recommended by Atkinson et al. (2006).

G42083b: Rate constant is the high-pressure limit as recommended by Atkinson et al. (2006).

G42085a: Uncertainties on the kinetics at pressures < 0.1 bar.

G42085b: Channel proposed by Hynes and Wine 1991, OH + HCHO + HOCN, could not be confirmed by Tyndall et al. (2001b). There is no alternative mechanism at the moment. Products assumed to be OH + CH3CO3 + NO

G42086b: Assuming HCN is from channel 2h, HCO + H + HCN. HCO is replaced by H + CO.

G42086c: Assuming exothermic channels 2b and 2d are equally important.

G42087: HCOCN is produced but replaced here by its likely oxidation products (HCN + CO_2) as studied by Tyndall et al. (2001b). The rate constant for a typical RO_2 + NO reaction is used.

G42088: $NCCH_2OOH$ is produced but replaced here by its likely oxidation products (HCN + CO_2) as studied by Tyndall et al. (2001b). The rate constant for a typical RO_2 + HO_2 reaction is used.

G42089a: The minor channel with k=5.2E-12 is combined with the major one producing HCOOH.

G42090: Theoretical keto-enol tautomerization catalyzed by formic acid (Grenfell et al., 2006).

G42091: Theoretical keto-enol tautomerization catalyzed by formic acid (Grenfell et al., 2006).

G42092: approximated OH reaction for oxalic acid

G42093a: SAR for H-abstraction by OH

G42093b: SAR for H-abstraction by OH, assuming that -CHOHOH has an effect like -CH2OH

G42093c: SAR for H-abstraction by OH

G42093d: SAR for H-abstraction by OH

G42094a: SAR for H-abstraction by OH

G42094b: SAR for H-abstraction by OH

G42095a: SAR for H-abstraction by OH

G42095b: SAR for H-abstraction by OH

G42096a: SAR for H-abstraction by OH

G42096b: SAR for H-abstraction by OH

G42097a: SAR for H-abstraction by OH

G42097b: SAR for H-abstraction by OH

G42098a: SAR for H-abstraction by OH, assuming that -CH2OOH has the same effect as -CH2OH

G42098b: SAR for H-abstraction by OH

G42098c: SAR for H-abstraction by OH

G43001a: Branching ratios according to Rickard et al. (1999).

G43001b: Branching ratios according to Rickard et al. (1999).

G43004: The value for the generic RO_2 + HO_2 reaction from Atkinson (1997) is used here.

G43008: The value for the generic RO_2 + HO_2 reaction from Atkinson (1997) is used here.

G43011: Strong positive deviation of k below 240 K compared to the expression recommended by JPL (Burkholder et al., 2015).

G43015a: The same value as for G4107 (CH_3OOH + OH) is used, multiplied by the branching ratio of the CH_3O_2 channel.

G43028: Alkyl nitrate formation neglected. (also not considered in MCM).

G43037: Alkyl nitrate formation neglected. (also not considered in MCM).

G43040a: Rate coefficient estimated with SAR (Taraborrelli, 2010).

G43040b: Rate coefficient estimated with SAR (Taraborrelli, 2010).

G43044: Alkyl nitrate formation neglected.

G43045c: Rate coefficient assumed to equal to the one of hydroxyacetone (ACETOL) for this channel.

G43048: Using the high-pressure limit.

G43049: The pressure fall-off between 1000 and 100 mbar is only 3% (Kirchner et al., 1999).

G43050: Value for $CH_3O_2NO_2$ + OH, H-abstraction enhanced by the CH_3CO-group by f_CO.

G43051c: Products approximated with C_2H_5CHO + HO_2.

G43052: Only major H-abstraction channel considered.

G43059: Products approximated with the major end-product CH_3CHO.

G43060b: Products approximated with the major end-product CH_3CHO.

G43061: Products approximated with the likely end-product CH_3CHO.

G43065: As for $HCOCO_3$.

G43070a: Branching ratios estimated with SAR for H-abstraction rate constants by OH.

G43070b: Branching ratios estimated with SAR for H-abstraction rate constants by OH.

G43071a: Only this channel considered as the intermediate radical is likely more stable than $CHCH(OH)_2$.

G43072: Theoretical keto-enol tautomerization catalyzed by formic acid (Grenfell et al., 2006).

G43073: Theoretical keto-enol tautomerization catalyzed by formic acid (Grenfell et al., 2006).

G43074: HCOCOCHO would be produced but undergoes fast photolysis (faster than MGLYOX) and is substituted with its products.

G43075a: Same value as for methanediol.

G43075b: Same value as for methanediol.

G43223: Products simplified

G43419: KDEC C3DIALO → GLYOX + CO + HO2

G43420: KDEC C3DIALO → GLYOX + CO + HO2

G43421: Permutation reaction (minor channels removed).

G44000: The $LC_4H_9O_2$ composition ($nC_4H_9O_2$:$sC_4H_9O_2$ ratio) is assumed to be equal to the ratio of the production rates at 298K: k_p/(k_p+k_s) = 0.1273 and k_s/(k_p+k_s) = 0.8727.

G44001b: $sC_4H_9O_2$ products are substituted with 0.636 MEK + HO_2 and 0.364 CH_3CHO + $C_2H_5O_2$ at 1 bar and 298 K.

G44003c: The alkyl nitrate yield is the weighted average yield for the two isomers forming from $nC_4H_9O_2$ and $sC_4H_9O_2$.

G44010b: H-abstraction from primary C and substitution of the resulting peroxy radical with its products from the reaction with NO.

G44011: H-abstraction from primary C and substitution of the resulting peroxy radical with its products from the reaction with NO.

G44015b: Products assumed to be only from H-abstraction from a secondary C bearing the -OOH group.

G44016: Products assumed to be only from H-abstraction from a secondary C bearing the -ONO_2 group.

G44018: LHMVKABO2 is 0.12 HMVKAO2 + 0.88 HMVKBO2.

G44019: LMEKO2 represents 0.62 MEKBO2 + 0.38 MEKAO2.

G44021a: The products of MEKAO are substituted with HCHO + CO_2 + $HOCH_2CH_2O_2$.

G44023a: Products from H-abstraction from the tertiary carbon bearing the ONO_2 group.

G44023b: Products from H-abstraction from the secondary carbon bearing the ONO_2 group.

G44025: Same value as for PAN.

G44026: Products as in G4415. Only the main channels for each isomer are considered. Weighted average for the isomers.

G44035: Rate constant replaced with the one of beta hydroxy RO_2.

G44046b: Using value for secondary nitrate (88% of total).

G44061a: Using value for secondary nitrate (88% of total).

G44061b: Using value for secondary nitrate (88% of total).

G44062a: Simplified products.

G44062b: Simplified products.

G44066: Alkyl nitrate formation neglected.

G44070: Alkyl nitrate formation neglected.

G44076: Alkyl nitrate formation neglected.

G44078: Other channel neglected.

G44081: Alkyl nitrate formation neglected.

G44082: Other channel neglected.

G44085: k for CH_3CHCO from Hatakeyama et al. (1985) adjusted.

G44086: Simplified product distribution.

G44089: The nitrated RO_2 is replaced by its products upon reaction with NO.

G44096: Both LBUT1ENO2 isomers mostly C_2H_5CHO.

G44097a: Branching ratios according to Rickard et al. (1999). CH_3CHO_2CHO is replaced with its major products CH_3CHO + CO + HO_2.

G44097b: Branching ratios according to Rickard et al. (1999).

G44098: The nitrated RO_2 is replaced by its products upon reaction with NO.

G44103b: MEKCOH replaced by its major oxidation products.

G44104: Carbonyl nitrate replaced by its major oxidation products.

G44106: CH3CHOOA products as from C_3H_6 + O_3 reaction.

G44107: The nitrated RO_2 is replaced by its products upon reaction with NO.

G44110: The nitrated RO_2 is replaced by its products upon reaction with NO.

G44124b: Skipping intermediate steps mostly leading to acetone.

G44126: Skipping intermediate steps mostly leading to acetone.

G44127: Only this channel considered as the intermediate radical is likely more stable than $CHCH(OH)_2$.

G44128: Theoretical keto-enol tautomerization catalyzed by formic acid (Grenfell et al., 2006).

G44129: Theoretical keto-enol tautomerization catalyzed by formic acid (Grenfell et al., 2006).

G44130: Only this channel considered as the intermediate radical is likely more stable than $CHCH(OH)_2$.

G44131: Theoretical keto-enol tautomerization catalyzed by formic acid (Grenfell et al., 2006).

G44132: Theoretical keto-enol tautomerization catalyzed by formic acid (Grenfell et al., 2006).

G44133: Only this channel considered as the intermediate radical is likely more stable than $CHCH(OH)_2$.

G44134: Theoretical keto-enol tautomerization catalyzed by formic acid (Grenfell et al., 2006).

G44135: Theoretical keto-enol tautomerization catalyzed by formic acid (Grenfell et al., 2006).

G44136: Only this channel considered as the intermediate radical is likely more stable than $CHCH(OH)_2$.

G44137: Theoretical keto-enol tautomerization catalyzed by formic acid (Grenfell et al., 2006).

G44138: Theoretical keto-enol tautomerization catalyzed by formic acid (Grenfell et al., 2006).

G44139: Simplified oxidation.

G44140: Simplified oxidation.

G44141: Simplified oxidation.

G44142: Simplified oxidation.

G44202: Alkyl nitrate formation neglected.

G44203a: Rate coefficient estimated with SAR (Taraborrelli, 2010).

G44205: Alkyl nitrate formation neglected.

G44210: Alkyl nitrate formation neglected.

G44221: Same k as for MGLYOX + OH (Tyndall et al., 1995).

G44402: KDEC NC4DCO2→ MALANHY + NO2

G44406c: KDEC MALDIALCO2 → 0.6 MALANHY + HO2 + 0.4 GLYOX + 0.4 CO + 0.4 CO2

G44407: KDEC MALDIALCO2 → 0.6 MALANHY + HO2 + 0.4 GLYOX + 0.4 CO + 0.4 CO2

G44409: KDEC MALDIALCO2 → 0.6 MALANHY + HO2 + 0.4 GLYOX + 0.4 CO + 0.4 CO2

G44410: KDEC MALDIALCO2 → 0.6 MALANHY + HO2 + 0.4 GLYOX + 0.4 CO + 0.4 CO2

G44412: KDEC BZFUONOOA → 0.5 BZFUONOO + 0.5 CO + 0.5 CO2 + 0.5 HCOCH2O2 + 0.5 OH and BZFUONOO → 0.625 CO14O3CO2H + 0.375 CO14O3CHO + 0.375 H2O2

G44421: Only major channel.

G44424: KDEC: GLYOOA → 0.125 HCHO + 0.18 GLYOO + 0.82 HO2 + 0.57 OH + 1.265 CO + 0.25 CO2 and H2O substitution GLYOO → 0.625 HCOCO2H + 0.375 GLYOX + 0.375 H2O2

G44425: Merged equations.

G44430: KDEC MALANHYO → HCOCOHCO3

G44431: KDEC MALANHYO → HCOCOHCO3

G44432: Only major channel. KDEC MALANHYO → HCOCOHCO3

G44436: KDEC NBZFUO → 0.5 CO14O3CHO + 0.5 NO2 + 0.5 NBZFUONE + 0.5 HO2

G44437: KDEC NBZFUO → 0.5 CO14O3CHO + 0.5 NO2 + 0.5 NBZFUONE + 0.5 HO2

G44438: KDEC NBZFUO → 0.5 CO14O3CHO + 0.5 NO2 + 0.5 NBZFUONE + 0.5 HO2 and RO2 Only major channel.

G44439: KDEC MALDIALCO2 → 0.6 MALANHY + HO2 + 0.4 GLYOX + 0.4 CO + 0.4 CO2

G44443: KDEC MECOACETO → CH3CO3 + HCHO

G44444: KDEC MECOACETO → CH3CO3 + HCHO

G44445: KDEC MECOACETO → CH3CO3 + HCHO

G44450: KDEC BZFUO → CO14O3CHO + HO2

G44451: KDEC BZFUO → CO14O3CHO + HO2

G44452: KDEC BZFUO → CO14O3CHO + HO2. Only major channel.

G44457: KDEC MALDIALO → GLYOX + GLYOX + HO2

G44458: KDEC MALDIALO → GLYOX + GLYOX + HO2

G44459: KDEC MALDIALO → GLYOX + GLYOX + HO2. Only major channel.

G44461: KBPAN → k_PAN_M

G45019d: Delta-1 and delta-2 LIEPOX are not considered and replaced by beta-LIEPOX formed by ISOPBOOH and ISOPDOOH.

G45021: SAR estimate within uncertainty range of the experimentally determined rate constant by Solberg et al. (1997), 1.1E-11.

G45037: SAR estimate within uncertainty range of the experimentally determined rate constant by Solberg et al. (1997), 4.2E-11.

G45040: Alkyl nitrate formation neglected.

G45043: Old MCM rate constant 4.16E-11.

G45047: Alkyl nitrate formation neglected.

G45055: Alkyl nitrate formation neglected.

G45071: Alkyl nitrate formation neglected.

G45074: Formic acid production consistent with results of Bates et al. (2014). Here, the high yields of formic acid and hydroxycarbonyls at low NO from oxidation of cis-beta-LIEPOX (the most abundant isomer) are approximated with the production of DB1O which undergo both the Dibble double H-transfer to DB2O2 and HOCH2 elimination yielding HVMK and HMAC (keto-vinyl alcohol potentially arising from decomposition of the alkoxy radical resulting from the ring opening after H-abstraction). The rate constant is from Paulot et al. (2009b) and adjusted based on Bates et al. (2014) that determined the single rate constants for the cis- and trans- beta isomer.

G45080: Alkyl nitrate formation neglected.

G45092a: C4MDIAL = CM4DIAL in MCM only from aromatics.

G45092b: Only one acyl peroxy radical considered.

G45093: Two aldehydic sites reacting with NO_3 but only one isomer product considered.

G45095: Alkyl nitrate formation neglected.

G45098: Alkyl nitrate formation neglected.

G45100: Alkyl nitrate formation neglected.

G45104a: DB1OOH is a hydroperoxide bearing a vinyl alcohol moiety that upon reaction with OH yields HCOOH (Davis et al., 1998).

G45107: OH production here is to take into account the hydroperoxidic function formed by the shift of the enolic hydrogen and not present in DB2O2. This approximation leads to spurious HO_2 production.

G45108a: Consistent with the results of Bates et al. (2014).

G45108b: Consistent with the results of Bates et al. (2014). Assuming that the enol alkoxy radical partly decomposes yielding a substitute vinyl alcohol.

G45111: Alkyl nitrate formation neglected.

G45114b: Here, formic acid is mechanistically produced by the OH-addition to the vinyl alcohol which, upon RO_2-to-RO conversion (skipped here), yields the HOCHOH fragment which in turn reacts with O_2 forming $HCOOH + HO_2$. Along $CH_3COCHOOHCHO$ should be produced but not in the mechanism. Only CH_3COCHO_2CHO. The rate constant is consistent with predictions by Ganzeveld et al. (2006) for ENOL. OH-addition to the OH-bearing carbon is considered the dominant channel as it is already for the ENOL (Ganzeveld et al., 2006).

G45115: Theoretical keto-enol tautomerization catalyzed by formic acid (Grenfell et al., 2006). The product should be C1ODC3OOHC4OD but it is neglected in the mechanism.

G45116: As for DB1OOH + OH.

G45117: Additional sinks for DB2OOH are neglected.

G45121b: Nitrate assumed to be major isomer that is mostly similar to products of ISOPDO2-chemistry.

G45128: Rate constant by Liljegren and Stevens (2013). A lumped RO_2 that upon conversion to RO yields 100% 2-methyl-butenedial (C4MDIAL) although Aschmann et al. (2014) quantified a 38% yield of the Z/E mixture.

G45129: As for 3METHYLFURAN + OH but with additional NO_2 production for mass conservation.

G45131: Alkyl nitrate formation neglected.

G45132: Hydroperoxide formation neglected.

G45134b: ZCO2HC23DBCOD formation is neglected. However, it is produced in MCM and in aromatic-related reactions under the name of MC3ODBCO2H.

G45139: LZCPANC23DBCOD is assumed to react like LC5PAN1719.

G45201: Alkyl nitrate formation neglected.

G45207: Alkyl nitrate formation neglected.

G45214: Alkyl nitrate formation neglected.

G45217: Alkyl nitrate formation neglected.

G45225: Alkyl nitrate formation neglected.

G45236: LMBOABO2 = 0.67 MBOAO2 + 0.33 MBOBO2

G45247: Alkyl nitrate formation neglected.

G45400: KDEC NC4MDCO2 → MMALANHY + NO2

G45404: KDEC NTLFUO → ACCOMECHO + NO2

G45405: KDEC NTLFUO → ACCOMECHO + NO2

G45406: KDEC NTLFUO → ACCOMECHO

G45409: KBPAN → k_PAN_M(renaming)

G45413: KFPAN → k_CH3CO3_NO2 (renaming)

G45422: KDEC MMALANHYO→CO2H3CO3

G45423: KDEC MMALANHYO→CO2H3CO3

G45424: KDEC MMALANHYO→CO2H3CO3 and Only major channel.

G45429: KBPAN → k_PAN_M (renamed)

G45430a: KDEC C5CO14CO2 → 0.83 MALANHY + 0.83 CH3 + 0.17 MGLYOX + 0.17 HO2 + 0.17 CO + 0.17 CO2

G45431: KDEC C5CO14CO2 → 0.83 MALANHY + 0.83 CH3 + 0.17 MGLYOX + 0.17 HO2 + 0.17 CO + 0.17 CO2

G45432: KFPAN →k_CH3CO3_NO2 (renaming)

G45433: KDEC C5CO14CO2 → 0.83 MALANHY + 0.83 CH3 + 0.17 MGLYOX + 0.17 HO2 + 0.17 CO + 0.17 CO2

G45434: KDEC C5CO14CO2 → 0.83 MALANHY + 0.83 CH3 + 0.17 MGLYOX + 0.17 HO2 + 0.17 CO + 0.17 CO2 and only major channel.

G45436: KDEC C5CO14CO2 → 0.83 MALANHY + 0.83 CH3 + 0.17 MGLYOX + 0.17 HO2 + 0.17 CO + 0.17 CO2

G45444: KDEC MC3CODBCO2 → 0.35 GLYOX + 0.35 CH3 + 0.35 CO + 0.35 CO2 + 0.65 MMALANHY + 0.65 HO2

G45452: KDEC TLFUONOOA → 0.5 CO + 0.5 OH + 0.5 MECOACETO2 + 0.5 TLFUONOO and H2O subs TLFUONOO → 0.625 C24O3CCO2H + 0.375 ACCOMECHO + 0.375 H2O2

G45456: KFPAN →k_CH3CO3_NO2 (renaming)

G45476b: KDEC NTLFUO → ACCOMECHO + NO2 and reactions with KRO2HO2.

G45477: KDEC NTLFUO → ACCOMECHO + NO2

G45478: KDEC NTLFUO → ACCOMECHO + NO2

G45479: KDEC NTLFUO → ACCOMECHO + NO2

G45486b: KDEC C5DIALO →MALDIAL + CO + HO2 and reactions with KRO2HO2.

G45487: KDEC C5DIALO →MALDIAL

G45488: KDEC C5DIALO →MALDIAL

G45489: KDEC C5DIALO →MALDIAL

G45491b: Reactions with KRO2HO2.

G45492: MGLYOX + GLYOX + HO2 from KDEC substitution

G45493: MGLYOX + GLYOX + HO2 from KDEC substitution

G45494: Permutation reaction (minor channels removed).

G46201: Alkyl nitrate formation neglected.

G46404b: Reactions with KRO2HO2 and KDEC C615CO2O → C5DICARB + CO + HO2.

G46405: KDEC C615CO2O → C5DICARB + CO + HO2

G46406: KDEC C615CO2O → C5DICARB + CO + HO2

G46407: Only major channel.

G46413b: Reactions with KRO2HO2 and KDEC NDNPHENO → NC4DCO2H + HNO3 + CO + CO + NO2.

G46414: KDEC NDNPHENO → NC4DCO2H + HNO3 + CO + CO + NO2

G46415: KDEC NDNPHENO → NC4DCO2H + HNO3 + CO + CO + NO2

G46416: KDEC NDNPHENO → NC4DCO2H + HNO3 + CO + CO + NO2

G46418: KDEC CATECOOA → MALDALCO2H + HCOCO2H + HO2 + OH

G46426: KFPAN →k_CH3CO3_NO2

G46430: KDEC GLYOOA → .125 HCHO + .18 GLYOO + .82 HO2 + .57 OH + 1.265 CO

G46432b: Reactions with KRO2HO2 and KDEC NCATECO → NC4DCO2H + HCOCO2H + HO2

G46433: KDEC NCATECO → NC4DCO2H + HCOCO2H + HO2

G46434: KDEC NCATECO → NC4DCO2H + HCOCO2H + HO2

G46435: KDEC NCATECO → NC4DCO2H + HCOCO2H + HO2

G46437b: Reactions with KRO2HO2 and KDEC NPHENO → MALDALCO2H + GLYOX + NO2

G46438: KDEC NPHENO → MALDALCO2H + GLYOX + NO2

G46439: KDEC NPHENO → MALDALCO2H + GLYOX + NO2

G46440: KDEC NPHENO → MALDALCO2H + GLYOX + NO2

G46441: Merged equations.

G46447b: reactions with KRO2HO2 and KDEC NNCATECO → NC4DCO2H + HCOCO2H + NO2

G46448: KDEC NNCATECO → NC4DCO2H + HCOCO2H + NO2

G46449: KDEC NNCATECO → NC4DCO2H + HCOCO2H + NO2

G46450: KDEC NNCATECO → NC4DCO2H + HCOCO2H + NO2

G46457: Merged equations.

G46458: Merged equations.

G46461b: Reactions with KRO2HO2 and KDEC PHENO → 0.71 MALDALCO2H + 0.71 GLYOX + 0.29 PBZQONE + HO2

G46462: KDEC PHENO → 0.71 MALDALCO2H + 0.71 GLYOX + 0.29 PBZQONE + HO2

G46463: KDEC PHENO → 0.71 MALDALCO2H + 0.71 GLYOX + 0.29 PBZQONE + HO2

G46464: KDEC PHENO → 0.71 MALDALCO2H + 0.71 GLYOX + 0.29 PBZQONE + HO2 and Only major channel.

G46468: KFPAN →k_CH3CO3_NO2

G46472b: new channel

G46476: HOC6H4NO2 is a nitro-phenol

G46480b: Reactions with KRO2HO2 and KDEC PBZQO →C5CO2OHCO3

G46481: KDEC PBZQO →C5CO2OHCO3

G46482: KDEC PBZQO →C5CO2OHCO3

G46483: KDEC PBZQO →C5CO2OHCO3 and Only major channel.

G46485b: Reactions with KRO2HO2 and KDEC DNPHENO → NC4DCO2H + HCOCO2H + NO2

G46486: KDEC DNPHENO → NC4DCO2H + HCOCO2H + NO2

G46487: KDEC DNPHENO → NC4DCO2H + HCOCO2H + NO2

G46488: KDEC DNPHENO → NC4DCO2H + HCOCO2H + NO2

G46490b: Reactions with KRO2HO2 and KDEC BZEMUCO → 0.5 EPXC4DIAL + 0.5 GLYOX + 0.5 HO2 + 0.5 C3DIALO2 + 0.5 C32OH13CO.

G46491b: KDEC BZEMUCO → 0.5 EPXC4DIAL + 0.5 GLYOX + 0.5 HO2 + 0.5 C3DIALO2 + 0.5 C32OH13CO.

G46492: KDEC BZEMUCO → 0.5 EPXC4DIAL + 0.5 GLYOX + 0.5 HO2 + 0.5 C3DIALO2 + 0.5 C32OH13CO

G46493: KDEC BZEMUCO → 0.5 EPXC4DIAL + 0.5 GLYOX + 0.5 HO2 + 0.5 C3DIALO2 + 0.5 C32OH13CO and Only major channel.

G46499b: Reactions with KRO2HO2 and KDEC NBZQO → C6CO4DB + NO2.

G46500: KDEC NBZQO → C6CO4DB + NO2

G46501: KDEC NBZQO → C6CO4DB + NO2

G46502: KDEC NBZQO → C6CO4DB + NO2

G46505b: New channel.

G46515: Only major channel.

G46522b: In analogy to TLBIPERO2 from toluene (Birdsall et al., 2010).

G46523b: KDEC BZBIPERO → GLYOX + HO2 + 0.5 BZFUONE + 0.5 BZFUONE

G46524: KDEC BZBIPERO → GLYOX + HO2 + 0.5 BZFUONE + 0.5 BZFUONE

G46525: KDEC BZBIPERO → GLYOX + HO2 + 0.5 BZFUONE + 0.5 BZFUONE and Only major channel.

G47210: Alkyl nitrate formation neglected.

G47214: Alkyl nitrate formation neglected.

G47218: Alkyl nitrate formation neglected.

G47222: Alkyl nitrate formation neglected.

G47223: ROO6R3OOH produced but no sink for it.

G47225: ROO6R4P produced but no sink for it.

G47226: ROO6R5P produced but no sink for it

G47400: Merged.

G47402a: KROPRIM*O2 fast reaction C6H5CH2O = BENZAL + HO2.

G47402b: KROPRIM*O2 fast reaction C6H5CH2O = BENZAL + HO2.

G47403: KROPRIM*O2 fast reaction C6H5CH2O = BENZAL + HO2.

G47404: KROPRIM*O2 fast reaction C6H5CH2O = BENZAL + HO2. C6H5CH2OH replaced by its oxidation product BENZAL.

G47405: Merged.

G47406: Merged.

G47407b: According to Birdsall et al. (2010), the branching ratio rbipero2_oh is set to 0.4 in order to take into account the OH-recycling and summed yield of butendial and methylbutendial.

G47408a: KDEC TLBIPERO → 0.6 GLYOX + 0.4 MGLYOX + HO2 + 0.2 C4MDIAL + 0.2 C5DICARB + 0.2 TLFUONE + 0.2 BZFUONE + 0.2 MALDIAL

G47408b: KDEC TLBIPERO → 0.6 GLYOX + 0.4 MGLYOX + HO2 + 0.2 ZCODC23DB COD + 0.2 C5DICARB + 0.2 TLFUONE + 0.2 BZFUONE + 0.2 MALDIAL

G47409: KDEC TLBIPERO → 0.6 GLYOX + 0.4 MGLYOX + HO2 + 0.2 ZCODC23DB COD + 0.2 C5DICARB + 0.2 TLFUONE + 0.2 BZFUONE + 0.2 MALDIAL

G47410: Only major channel and KDEC TLBIPERO → 0.6 GLYOX + 0.4 MGLYOX + HO2 + 0.2 ZCODC23DB COD + 0.2 C5DICARB + 0.2 TLFUONE + 0.2 BZFUONE + 0.2 MALDIAL

G47412: KDEC MGLOOB → 0.125 CH3CHO + 0.695 CH3CO + 0.57 CO + 0.57 OH + 0.125 HO2 + 0.18 MGLOO + 0.25 CO2

G47413: Merged.

G47418b: Reactions with KRO2HO2 and KDEC CRESO → 0.68 C5CO14OH + 0.68 GLYOX + HO2 + 0.32 PTLQONE.

G47419: KDEC CRESO → 0.68 C5CO14OH + 0.68 GLYOX + HO2 + 0.32 PTLQONE

G47420: KDEC CRESO → 0.68 C5CO14OH + 0.68 GLYOX + HO2 + 0.32 PTLQONE

G47421: KDEC CRESO → 0.68 C5CO14OH + 0.68 GLYOX + HO2 + 0.32 PTLQONE and Only major channel.

G47422b: Reactions with KRO2HO2 and KDEC NCRESO → C5CO14OH + GLYOX + NO2

G47423: KDEC NCRESO → C5CO14OH + GLYOX + NO2

G47424: KDEC NCRESO → C5CO14OH + GLYOX + NO2

G47425: KDEC NCRESO → C5CO14OH + GLYOX + NO2 and Only major channel.

G47426: TOL1OHNO2 is a nitro-phenol

G47429: KDEC MCATECOOA → MC3ODBCO2H + HCOCO2H + HO2 + OH

G47436: KFPAN →k_CH3CO3_NO2

G47438: Only major channel.

G47439b: Reactions with KRO2HO2 and KDEC TLEMUCO→ 0.5 C3DIALO2 + 0.5 CO2H3CHO + 0.5 EPXC4DIAL + 0.5 MGLYOX + 0.5 HO2

G47440b: KDEC TLEMUCO→ 0.5 C3DIALO2 + 0.5 CO2H3CHO + 0.5 EPXC4DIAL + 0.5 MGLYOX + 0.5 HO2

G47441: KDEC TLEMUCO→ 0.5 C3DIALO2 + 0.5 CO2H3CHO + 0.5 EPXC4DIAL + 0.5 MGLYOX + 0.5 HO2

G47442: KDEC TLEMUCO→ 0.5 C3DIALO2 + 0.5 CO2H3CHO + 0.5 EPXC4DIAL + 0.5 MGLYOX + 0.5 HO2 and Only major channel.

G47445: KFPAN →k_CH3CO3_NO2

G47447: Only major channel.

G47454: New channel.

G47479: New channel.

G47482b: Reactions with KRO2HO2 and KDEC NPTLQO → C7CO4DB + NO2

G47483: KDEC NPTLQO → C7CO4DB + NO2

G47484: KDEC NPTLQO → C7CO4DB + NO2

G47485: KDEC NPTLQO → C7CO4DB + NO2

G47486b: Reactions with KRO2HO2 and KDEC PTLQO → C6CO2OHCO3

G47487: KDEC PTLQO → C6CO2OHCO3

G47488: KDEC PTLQO → C6CO2OHCO3

G47489: Only major channel. KDEC PTLQO → C6CO2OHCO3.

G47494: New channel.

G47497b: Reactions with KRO2HO2 and KDEC MNNCATECO → NC4MDCO2H + HCOCO2H + NO2

G47498: KDEC MNNCATECO → NC4MDCO2H + HCOCO2H + NO2

G47499: KDEC MNNCATECO → NC4MDCO2H + HCOCO2H + NO2

G47501b: Reactions with KRO2HO2 and KDEC MNCATECO → NC4MDCO2H + HCOCO2H + HO2

G47502: KDEC MNCATECO → NC4MDCO2H + HCOCO2H + HO2

G47503: KDEC MNCATECO → NC4MDCO2H + HCOCO2H + HO2

G47504: KDEC MNCATECO → NC4MDCO2H + HCOCO2H + HO2

G47509b: Reactions with KRO2HO2 and KDEC NDNCRESO → NC4MDCO2H + HNO3 + CO + CO + NO2

G47510: KDEC NDNCRESO → NC4MDCO2H + HNO3 + CO + CO + NO2

G47511: KDEC NDNCRESO → NC4MDCO2H + HNO3 + CO + CO + NO2

G47512: KDEC NDNCRESO → NC4MDCO2H + HNO3 + CO + CO + NO2

G47513b: Reactions with KRO2HO2 and KDEC DNCRESO → NC4MDCO2H + HCOCO2H + NO2

G47514: KDEC DNCRESO → NC4MDCO2H + HCOCO2H + NO2

G47515: KDEC DNCRESO → NC4MDCO2H + HCOCO2H + NO2

G47516: KDEC DNCRESO → NC4MDCO2H + HCOCO2H + NO2

G48202: Alkyl nitrate formation neglected.

G48205: Alkyl nitrate formation neglected.

G48210: Alkyl nitrate formation neglected.

G48212: Alkyl nitrate formation neglected.

G48216: Alkyl nitrate formation neglected.

G48222: Alkyl nitrate formation neglected.

G48400a: Same products as for toluene. Assuming a 1:1:1 proportion in xylenes emissions the analogous toluene product is produced with a rate constant equal to (1.36E-11*0.24 + 2.31E-11*0.29 + 1.43E-11*0.155)/3, where k and coefficients are for the single isomers ortho, meta and para from MCM.

G48400b: Same products as for toluene. Assuming a 1:1:1 proportion in xylenes emissions the analogous toluene product is produced with a rate constant equal to (1.36E-11*0.05 + 2.31E-11*0.04 + 1.43E-11*0.10)/3, where k and coefficients are for the single isomers ortho, meta and para from MCM.

G48400c: Same products as for toluene. Assuming a 1:1:1 proportion in xylenes emissions the analogous toluene product is produced with a rate constant equal to (1.36E-11*0.16 + 2.31E-11*0.17 + 1.43E-11*0.12)/3, where k and coefficients are for the single isomers ortho, meta and para from MCM.

G48400d: Same products as for toluene. Assuming a 1:1:1 proportion in xylenes emissions the analogous toluene product is produced with a rate constant equal to (1.36E-11*0.55 + 2.31E-11*0.50 + 1.43E-11*0.625)/3, where k and coefficients are for the single isomers ortho, meta and para from MCM.

G48401: Same products as for toluene. The rate constant is the average of m, p, o k=(4.10E-16+2.60E-16+5.00E-16)/3 = 3.9E-16.

G48402: merged under same rate constant

G48403: Same products as for toluene

G48405: KDEC CH2OOB → 0.24 CH2OO + 0.40 CO + 0.36 HO2 + 0.36 CO + 0.36 OH and H2O + PHCHOO → 0.625 PHCOOH + 0.375 BENZAL + 0.375 H2O2 + 0.2 CO2

G48408: KDEC NSTYRENEO → NO2 + HCHO + BENZAL

G48409: KDEC NSTYRENEO → NO2 + HCHO + BENZAL

G48410: KDEC NSTYRENEO → NO2 + HCHO + BENZAL

G48412b: KDEC STYRENO → HO2 + HCHO + BENZAL and reactions with KRO2HO2.

G48413: KDEC STYRENO → HO2 + HCHO + BENZAL

G48414: KDEC STYRENO → HO2 + HCHO + BENZAL

G48415: KDEC STYRENO → HO2 + HCHO + BENZAL

G49207: Alkyl nitrate formation neglected.

G49238: Alkyl nitrate formation neglected.

G49246: Only this channel considered as the intermediate radical is likely more stable than $CHCH(OH)_2$.Instead of the (lacking) carbonyl a product of further degradation is assumed.

G49247: Theoretical keto-enol tautomerization catalyzed by formic acid (Grenfell et al., 2006).

G49248: Theoretical keto-enol tautomerization catalyzed by formic acid (Grenfell et al., 2006).

G49400a: Same products as for toluene. Assuming a 1:1:1 proportion in xylenes emissions the analogous toluene product is produced with a rate constant equal to (3.27E-11*0.21 + 3.25E-11*0.30 + 5.67E-11*0.14)/3, where k and coefficients are for the single isomers 1,2,3-, 1,3,4- and 1,3,5- from MCM.

G49400b: Same products as for toluene. Assuming a 1:1:1 proportion in xylenes emissions the analogous toluene product is produced with a rate constant equal to (3.27E-11*0.06 + 3.25E-11*0.06 + 5.67E-11*0.03)/3, where k and coefficients are for the single isomers 1,2,3-, 1,3,4- and 1,3,5- from MCM.

G49400c: Same products as for toluene. Assuming a 1:1:1 proportion in xylenes emissions the analogous toluene product is produced with a rate constant equal to (3.27E-11*0.03 + 3.25E-11*0.03 + 5.67E-11*.04)/3, where k and coefficients are for the single isomers 1,2,3-, 1,3,4- and 1,3,5- from MCM.

G49400d: Same products as for toluene. Assuming a 1:1:1 proportion in xylenes emissions the analogous toluene product is produced with a rate constant equal to (3.27E-11*0.70 + 3.25E-11*0.61 + 5.67E-11*0.79)/3, where k and coefficients are for the single isomers 1,2,3-, 1,3,4- and 1,3,5- from MCM.

G49401: Same products as for toluene. The rate constant is the average of m, p, o k=(1.90+1.80+0.88)E-15/3=1.52E-15.

G40200: Products from Vereecken et al. (2007). LAPINABO2 = 0.65 APINAO2 + 0.35 APINBO2

G40203: Weighted average for isomers A and B, `k = 0.33*9.20E-14+0.67*8.80E-13`.

G40204: Weighted average for isomers A and B, `k = 0.35*1.83E-11+0.65*3.28E-11`.

G40205: Weighted average for isomers A and B, `k = 0.35*5.50E-12+0.65*3.64E-12`.

G40206: SAR-estimated rate constant, `(kads+kadt)*acoch3 = 6.46E-11` where `kads = 3.0E-11`, `kadt = 5.5E-11`, `acoch3 = 0.76`

G40207: Alkyl nitrate formation neglected.

G40211: Products from Rickard and Pascoe (2009).

G40212: Products from Rickard and Pascoe (2009).

G40232: Products from Capouet et al. (2008).

G40242: Alkyl nitrate formation neglected.

G40246: Products from Rickard and Pascoe (2009).

G40248: Alkyl nitrate formation neglected.

G40252a: Products from Vereecken and Peeters (2012).

G40252b: Products from Vereecken and Peeters (2012).

G40259: ROO6R1OOH is produced but no sink for it.

G40262: RO6R1OOH is produced but no sink for it.

G40266: Rate constant modified according to MCM protocol.

G40267a: Products from Nguyen et al. (2009).

G40268: Products from Rickard and Pascoe (2009).

G40270: Alkyl nitrate neglected.

G40274: As for RO6R1NO3 in G4085.

G40276: Only this channel considered as the intermediate radical is likely more stable than $CHCH(OH)_2$.

G40277: Theoretical keto-enol tautomerization catalyzed by formic acid (Grenfell et al., 2006).

G40278: Theoretical keto-enol tautomerization catalyzed by formic acid (Grenfell et al., 2006).

G40282a: Products from Vereecken and Peeters (2012).

G40282b: Products from Vereecken and Peeters (2012).

G40283a: Products from Nguyen et al. (2009).

G40284: Products from Rickard and Pascoe (2009).

G40285a: Products from Vereecken and Peeters (2012).

G40285b: Products from Vereecken and Peeters (2012).

G40286a: Products from Nguyen et al. (2009).

G40287: Products from Rickard and Pascoe (2009).

G40400: DIET35TOL(from MCM) as representative of higher aromatics

G40401: Same products as for toluene.

G6103: The rate coefficient is defined as backward reaction divided by equilibrium constant.

G6204: At low temperatures, there may be a minor reaction channel leading to O_3+HCl. See Finkbeiner et al. (1995) for details. It is neglected here.

G6402: The initial products are probably HCl and CH_2OOH (Atkinson et al., 2006). It is assumed that CH_2OOH dissociates into HCHO and OH.

G6409: It is assumed that the reaction liberates all Cl atoms in the form of HCl.

G7302: The rate coefficient is: `k_BrO_NO2 = k_3rd(temp,cair,5.2E-31,3.2,6.9E-12,2.9,0.6)`.

G7303: The rate coefficient is defined as backward reaction (Atkinson et al., 2007) divided by equilibrium constant (Orlando and Tyndall, 1996).

G7404: It is assumed that the reaction liberates all Br atoms in the form of HBr.

G7407: It is assumed that the reaction liberates all Br atoms. The fate of the carbon atom is currently not considered.

G7408: It is assumed that the reaction liberates all Br atoms. The fate of the carbon atom is currently not considered.

G7605: Same value as for G7408: CH_2Br_2+OH assumed. It is assumed that the reaction liberates all Br and Cl atoms. The fate of the carbon atom is currently not considered.

G7606: Same value as for G7408: CH_2Br_2+OH assumed. It is assumed that the reaction liberates all Br and Cl atoms. The fate of the carbon atom is currently not considered.

G7607: It is assumed that the reaction liberates all Br and Cl atoms. The fate of the carbon atom is currently not considered.

G8102: Consistent with O'Dowd and Hoffmann (2005), it is assumed that the reaction produces new particles.

G8103: The yield of 38 % OIO is from Atkinson et al. (2007). It is assumed here that the remaining 62 % produce 2 I + O_2.

G8300: The rate coefficient is: `k_I_NO2 = k_3rd_iupac(temp,cair,3.E-31,1.,6.6E-11,0.,0.63)`.

G8305: The rate coefficient is defined as backward reaction (Atkinson et al., 2007) divided by equilibrium constant (van den Bergh and Troe, 1976).

G8401: The rate coefficient is from Dillon et al. (2006b), the yield of I atoms is a lower limit given on page 2170 of Bale et al. (2005).

G8402: The products are from Nakano et al. (2005).

G8701: 80% Br + OIO production is from Atkinson et al. (2007). The remaining channels are assumed to produce Br + I + O_2.

G9400a: For the abstraction path, the assumed reaction sequence (omitting H_2O and O_2 as products) according to Yin et al. (1990) is:

$$\begin{aligned}
\mathrm{DMS + OH} &\rightarrow \mathrm{CH_3SCH_2}\\
\mathrm{CH_3SCH_2 + O_2} &\rightarrow \mathrm{CH_3SCH_2OO}\\
\mathrm{CH_3SCH_2OO + NO} &\rightarrow \mathrm{CH_3SCH_2O + NO_2}\\
\mathrm{CH_3SCH_2O} &\rightarrow \mathrm{CH_3S + HCHO}\\
\mathrm{CH_3S + O_3} &\rightarrow \mathrm{CH_3SO}\\
\mathrm{CH_3SO + O_3} &\rightarrow \mathrm{CH_3SO_2}\\
\hline
\mathrm{DMS + OH + NO + 2O_3} &\rightarrow \mathrm{CH_3SO_2 + HCHO + NO_2}
\end{aligned}$$

Neglecting the effect on O_3 and NO_x, the remaining reaction is:

$$\mathrm{DMS + OH + O_3 \rightarrow CH_3SO_2 + HCHO}$$

.

G9400b: For the addition path, the rate coefficient is: `k_DMS_OH = 1.0E-39*EXP(5820./temp)*C(ind_O2) / (1.+5.0E-30*EXP(6280./temp)*C(ind_O2))`.

G9402: Products and yields are not from Hynes and Wine (1996).

G9408: Average of 3.9E-11 and 3.42E-11.

G10201: Upper limit.

Table 2: Photolysis reactions

#	labels	reaction	rate coefficient	reference
J (gas)				
J0001	UpGJ	$O(^3P) \rightarrow O^+ + e^-$	jx(ip_Op_em) +jx(ip_se_Op_em)	Fuller-Rowell (1993)
J0002a	UpGJ	$O_2 \rightarrow O_2^+ + e^-$	jx(ip_O2p_em) +jx(ip_se_O2_b1)	Fuller-Rowell (1993)
J0002b	UpGJ	$O_2 \rightarrow O^+ + O(^3P) + e^-$	jx(ip_Op_O_em) +jx(ip_se_O2_b2)	Fuller-Rowell (1993)
J0003a	UpGJN	$N_2 \rightarrow N_2^+ + e^-$	jx(ip_N2p_em) +jx(ip_se_N2_b1)	Fuller-Rowell (1993)
J0003b	UpGJN	$N_2 \rightarrow N^+ + N + e^-$	jx(ip_Np_N_em) +jx(ip_se_N2_b2)	Fuller-Rowell (1993)
J0003c	UpGJN	$N_2 \rightarrow N^+ + N(^2D) + e^-$	jx(ip_Np_N2D_em)+jx(ip_se_N2_b3)	Fuller-Rowell (1993)
J0003d	UpGJN	$N_2 \rightarrow N + N(^2D)$	jx(ip_N_N2D_em) +jx(ip_se_N2_b4)	Fuller-Rowell (1993)
J1000a	UpStTrGJ	$O_2 + h\nu \rightarrow O(^3P) + O(^3P)$	jx(ip_O2)	Sander et al. (2014)
J1000b	UpGJ	$O_2 + h\nu \rightarrow O(^3P) + O(^1D)$	jx(ip_O3PO1D)	Sander et al. (2014)
J1000c	UpGJ	$O_2 + h\nu \rightarrow O_2^+ + e^-$	jx(ip_O2_b1)	Sander et al. (2014)
J1000d	UpGJ	$O_2 + h\nu \rightarrow O^+ + O(^3P) + e^-$	jx(ip_O2_b2)	Sander et al. (2014)
J1001a	UpStTrGJ	$O_3 + h\nu \rightarrow O(^1D) + O_2$	jx(ip_O1D)	Sander et al. (2014)
J1001b	UpStTrGJ	$O_3 + h\nu \rightarrow O(^3P) + O_2$	jx(ip_O3P)	Sander et al. (2014)
J1002	UpGJ	$O(^3P) + h\nu \rightarrow O^+ + e^-$	jx(ip_O3Pp)	Sander et al. (2014)
J2100a	UpStGJ	$H_2O + h\nu \rightarrow H + OH$	jx(ip_H2O)	Sander et al. (2014)
J2100b	UpGJ	$H_2O + h\nu \rightarrow H_2 + O(^1D)$	jx(ip_H2O1D)	Sander et al. (2014)
J2101	UpStTrGJ	$H_2O_2 + h\nu \rightarrow 2\ OH$	jx(ip_H2O2)	Sander et al. (2014)
J3000a	UpGJN	$N_2 + h\nu \rightarrow N_2^+ + e^-$	jx(ip_N2_b1)	Sander et al. (2014)
J3000b	UpGJN	$N_2 + h\nu \rightarrow N^+ + N + e^-$	jx(ip_N2_b2)	Sander et al. (2014)
J3000c	UpGJN	$N_2 + h\nu \rightarrow N^+ + N(^2D) + e^-$	jx(ip_N2_b3)	Sander et al. (2014)
J3000d	UpGJN	$N_2 + h\nu \rightarrow N + N(^2D)$	jx(ip_NN2D)	Sander et al. (2014)
J3100	UpStGJN	$N_2O + h\nu \rightarrow O(^1D) + N_2$	jx(ip_N2O)	Sander et al. (2014)
J3101	UpStTrGJN	$NO_2 + h\nu \rightarrow NO + O(^3P)$	jx(ip_NO2)	Sander et al. (2014)
J3102a	UpStGJN	$NO + h\nu \rightarrow N + O(^3P)$	jx(ip_NO)	Sander et al. (2014)
J3102b	UpGJN	$NO + h\nu \rightarrow NO^+ + e^-$	jx(ip_NOp)	Sander et al. (2014)
J3103a	UpStTrGJN	$NO_3 + h\nu \rightarrow NO_2 + O(^3P)$	jx(ip_NO2O)	Sander et al. (2014)
J3103b	UpStTrGJN	$NO_3 + h\nu \rightarrow NO + O_2$	jx(ip_NOO2)	Sander et al. (2014)
J3104	StTrGJN	$N_2O_5 + h\nu \rightarrow NO_2 + NO_3$	jx(ip_N2O5)	Sander et al. (2014)
J3200	TrGJN	$HONO + h\nu \rightarrow NO + OH$	jx(ip_HONO)	Sander et al. (2014)
J3201	StTrGJN	$HNO_3 + h\nu \rightarrow NO_2 + OH$	jx(ip_HNO3)	Sander et al. (2014)
J3202	StTrGJN	$HNO_4 + h\nu \rightarrow .667\ NO_2 + .667\ HO_2 + .333\ NO_3 + .333\ OH$	jx(ip_HNO4)	Sander et al. (2014)
J41000	StTrGJ	$CH_3OOH + h\nu \rightarrow CH_3O + OH$	jx(ip_CH3OOH)	Sander et al. (2014)
J41001a	StTrGJ	$HCHO + h\nu \rightarrow H_2 + CO$	jx(ip_COH2)	Sander et al. (2014)

Table 2: Photolysis reactions (... continued)

#	labels	reaction	rate coefficient	reference
J41001b	StTrGJ	$HCHO + h\nu \rightarrow H + CO + HO_2$	jx(ip_CHOH)	Sander et al. (2014)
J41002	StGJ	$CO_2 + h\nu \rightarrow CO + O(^3P)$	jx(ip_CO2)	Sander et al. (2014)
J41003	StGJ	$CH_4 + h\nu \rightarrow .42\ CH_3 + .42\ H + .6912\ H_2 + .0864\ HCHO + .0864\ O(^3P) + .1584\ OH + .1584\ HO_2 + .2112\ CO_2 + .1824\ CO + .024\ H_2O + .10$ LCARBON	jx(ip_CH4)	Sander et al. (2014)*
J41004	StTrGJN	$CH_3ONO + h\nu \rightarrow CH_3O + NO$	jx(ip_CH3ONO)	Sander et al. (2014)
J41005	StTrGJN	$CH_3ONO_2 + h\nu \rightarrow CH_3O + NO_2$	jx(ip_CH3NO3)	Sander et al. (2014)
J41006	StTrGJN	$CH_3O_2NO_2 + h\nu \rightarrow .667\ NO_2 + .667\ CH_3O_2 + .333\ NO_3 + .333\ CH_3O$	jx(ip_CH3O2NO2)	Sander et al. (2014)*
J41007	StTrGJ	$HOCH_2OOH + h\nu \rightarrow HCOOH + OH + HO_2$	jx(ip_CH3OOH)	Sander et al. (2014)
J41008	StTrGJ	$CH_3O_2 + h\nu \rightarrow HCHO + OH$	jx(ip_CH3O2)	Sander et al. (2014)
J41009	StTrGJ	$HCOOH + h\nu \rightarrow CO + HO_2 + OH$	jx(ip_HCOOH)	Sander et al. (2014)
J41010	StTrGJN	$HOCH_2O_2NO_2 + h\nu \rightarrow .667\ NO_2 + .667\ HOCH_2O_2 + .333\ NO_3 + .333\ HCOOH + .333\ HO_2$	jx(ip_CH3O2NO2)	Sander et al. (2014)
J42000	TrGJC	$C_2H_5OOH + h\nu \rightarrow CH_3CHO + HO_2 + OH$	jx(ip_CH3OOH)	von Kuhlmann (2001)
J42001a	TrGJC	$CH_3CHO + h\nu \rightarrow CH_3 + HO_2 + CO$	jx(ip_CH3CHO)	Sander et al. (2014)
J42001b	TrGJC	$CH_3CHO + h\nu \rightarrow CH_2CHOH$	jx(ip_CH3CHO2VINY)	Clubb et al. (2012)
J42002	TrGJC	$CH_3C(O)OOH + h\nu \rightarrow CH_3 + OH + CO_2$	jx(ip_CH3CO3H)	Sander et al. (2014)
J42004	TrGJCN	$PAN + h\nu \rightarrow .7\ CH_3C(O) + .7\ NO_2 + .3\ CH_3 + .3\ CO_2 + .3\ NO_3$	jx(ip_PAN)	Sander et al. (2014)*
J42005a	TrGJC	$HOCH_2CHO + h\nu \rightarrow HCHO + 2\ HO_2 + CO$	jx(ip_HOCH2CHO)*0.83	Sander et al. (2014)*
J42005b	TrGJC	$HOCH_2CHO + h\nu \rightarrow OH + HCOCH_2O_2$	jx(ip_HOCH2CHO)*0.07	Sander et al. (2014)*
J42005c	TrGJC	$HOCH_2CHO + h\nu \rightarrow CH_3OH + CO$	jx(ip_HOCH2CHO)*0.10	Sander et al. (2014)*
J42006	TrGJC	$HOCH_2CO_3H + h\nu \rightarrow HCHO + HO_2 + OH + CO_2$	jx(ip_CH3OOH)	Rickard and Pascoe (2009)
J42007	TrGJCN	$PHAN + h\nu \rightarrow .7$ HOCH2CO $+ .7\ NO_2 + .3\ HCHO + .3\ HO_2 + .3\ CO_2 + .3\ NO_3$	jx(ip_PAN)	see note*
J42008	TrGJC	$GLYOX + h\nu \rightarrow 2\ CO + 2\ HO_2$	jx(ip_GLYOX)	Sander et al. (2014)
J42009	TrGJC	$HCOCO_2H + h\nu \rightarrow 2\ HO_2 + CO + CO_2$	jx(ip_MGLYOX)	Rickard and Pascoe (2009)
J42010	TrGJC	$HCOCO_3H + h\nu \rightarrow HO_2 + CO + OH + CO_2$	jx(ip_CH3OOH)+jx(ip_HOCH2CHO)	Rickard and Pascoe (2009)
J42011	TrGJC	HYETHO2H $+ h\nu \rightarrow HOCH_2CH_2O + OH$	jx(ip_CH3OOH)	Rickard and Pascoe (2009)
J42012	TrGJCN	ETHOHNO3 $+ h\nu \rightarrow HO_2 + 2$ HCHO $+ NO_2$	j_IC3H7NO3	Rickard and Pascoe (2009)
J42013	TrGJC	HOOCH2CO3H $+ h\nu \rightarrow OH +$ HCHO $+ CO_2 + OH$	2.*jx(ip_CH3OOH)	Sander et al. (2019)
J42014	TrGC	HOOCH2CO2H $+ h\nu \rightarrow OH +$ HCHO $+ HO_2 + CO_2$	jx(ip_CH3OOH)	Sander et al. (2019)
J42015	TrGC	CH2CO $+ h\nu \rightarrow .4\ CO_2 + .8\ H + .34\ CO + .34\ OH + .34\ HO_2 + .16$ HCHO $+ .16\ O(^3P) + .1$ HCOOH $+$ CO	j_ketene*0.36	Sander et al. (2019)

Table 2: Photolysis reactions (... continued)

#	labels	reaction	rate coefficient	reference
J42016	TrGC	CH3CHOHOOH + hν → CH_3 + HCOOH + OH	jx(ip_CH3OOH)	Sander et al. (2019)
J42017	TrGJCN	$NO_3CH2CHO$ + hν → HO_2 + CO + HCHO + NO_2	(jx(ip_C2H5NO3)+jx(ip_CH3CHO)) *(jx(ip_NOA)+1E-10)/(0.59*j_ IC3H7NO3+jx(ip_CH3COCH3)+1E-10)	Sander et al. (2019)*
J42018	TrGJC	HOOCH2CHO + hν → OH + HCHO + CO + HO_2	jx(ip_CH3OOH)+jx(ip_HOCH2CHO)	Sander et al. (2019)
J42019	TrGJCN	$C_2H_5ONO_2$ + hν → CH_3CHO + HO_2 + NO_2	jx(ip_C2H5NO3)	Sander et al. (2019)
J42020	TrGJCN	$NO_3CH2CHO$ + hν → .7 NO_3CH2CO_3 + .7 NO_2 + .3 HCHO + .3 NO_2 + .3 CO_2 + .3 NO_3	jx(ip_PAN)	Sander et al. (2019)*
J42021	StTrGJCN	$C_2H_5O_2NO_2$ + hν → .667 NO_2 + .667 $C_2H_5O_2$ + .333 NO_3 + .333 CH_3CHO + .333 HO_2	jx(ip_CH3O2NO2)	Sander et al. (2019)*
J42022	TrGJC	HOOCCOOH + hν → CO_2 + .72 HCOOH + .28 CO + .28 H_2O	jx(ip_HOOCCOOH)	Yamamoto and Back (1985)
J43000	TrGJC	iC_3H_7OOH + hν → CH_3COCH_3 + HO_2 + OH	jx(ip_CH3OOH)	von Kuhlmann (2001)
J43001	TrGJC	CH_3COCH_3 + hν → $CH_3C(O)$ + CH_3	jx(ip_CH3COCH3)	Sander et al. (2014)
J43002	TrGJC	CH_3COCH_2OH + hν → .5 $CH_3C(O)$ + .5 HCHO + .5 HO_2 + .5 HOCH2CO + .5 CH_3	j_ACETOL	Sander et al. (2014)*
J43003	TrGJC	MGLYOX + hν → $CH_3C(O)$ + CO + HO_2	jx(ip_MGLYOX)	Sander et al. (2014)
J43004	TrGJC	$CH_3COCH_2O_2H$ + hν → $CH_3C(O)$ + HCHO + OH	jx(ip_CH3OOH)+j_ACETOL	Rickard and Pascoe (2009)
J43005	TrGJC	HOCH2COCH2OOH + hν → HOCH2CO + HCHO + OH	jx(ip_CH3OOH)+j_ACETOL	Sander et al. (2019)
J43006	TrGJCN	$iC_3H_7ONO_2$ + hν → CH_3COCH_3 + NO_2 + HO_2	j_IC3H7NO3	von Kuhlmann et al. (2003)*
J43007	TrGJCN	NOA + hν → $CH_3C(O)$ + HCHO + NO_2	jx(ip_NOA)	Barnes et al. (1993)
J43009	TrGJC	HYPROPO2H + hν → CH_3CHO + HCHO + HO_2 + OH	jx(ip_CH3OOH)	Rickard and Pascoe (2009)
J43010	TrGJCN	PR2O2HNO3 + hν → NOA + HO_2 + OH	jx(ip_CH3OOH)	Rickard and Pascoe (2009)
J43011	TrGJC	HOCH2COCHO + hν → HOCH2CO + CO + HO_2	jx(ip_MGLYOX)	Rickard and Pascoe (2009)
J43012	TrGJC	$HCOCOCH_2OOH$ + hν → HCOCO + HCHO + OH	jx(ip_CH3OOH)+j_ACETOL	Sander et al. (2019)
J43013	TrGJC	$HCOCOCH_2OOH$ + hν → $HOOCH_2CO_3$ + CO + HO_2	jx(ip_MGLYOX)	Sander et al. (2019)
J43014	TrGJTerC	HCOCH2CHO + hν → $HCOCH_2O_2$ + HO_2 + CO	jx(ip_HOCH2CHO)*2.	Rickard and Pascoe (2009)
J43015	TrGJTerC	HCOCH2CO2H + hν → $HCOCH_2O_2$ + CO_2 + HO_2	jx(ip_HOCH2CHO)	Rickard and Pascoe (2009)
J43016	TrGJTerC	HOC2H4CO3H + hν → $HOCH_2CH_2O_2$ + CO_2 + OH	jx(ip_CH3OOH)	Rickard and Pascoe (2009)
J43017	TrGJC	HCOCOCHO + hν → HCOCO + HO_2 + CO	2.*jx(ip_MGLYOX)	Sander et al. (2019)
J43018	TrGJC	CH_3COCO_2H + hν → .32 CH_3CHO + .16 CH_2CHOH + .54 CO_2 + .38 $CH_3C(O)$ + .38 HO_2 + .38 CO_2 + .07 CH_3COOH + .07 CO + .05 $CH_3C(O)$ + .05 CO + .05 OH	jx(ip_CH3COCO2H)	Sander et al. (2019)*
J43019	TrGC	CH_3COCO_3H + hν → $CH_3C(O)$ + OH + CO_2	jx(ip_MGLYOX)+jx(ip_CH3OOH)	Sander et al. (2019)

Table 2: Photolysis reactions (... continued)

#	labels	reaction	rate coefficient	reference
J43020	TrGC	CH3CHCO + hν → C_2H_4 + CO	j_ketene*0.36*2.	Sander et al. (2019)
J43021	TrGCN	PROPOLNO3 + hν → $HOCH_2CHO$ + HCHO + HO_2 + NO_2	j_IC3H7NO3	Sander et al. (2019)
J43022	TrGCN	$CH_3COCH_2OONO_2$ + hν → $CH_3C(O)$ + HCHO + NO_3	jx(ip_CH3O2NO2)+jx(ip_CH3COCH3)	Sander et al. (2019)
J43023	TrGJC	C_3H_7OOH + hν → C_2H_5CHO + HO_2 + OH	jx(ip_CH3OOH)	von Kuhlmann (2001)
J43024	TrGJCN	$C_3H_7ONO_2$ + hν → C_2H_5CHO + NO_2 + HO_2	0.59*j_IC3H7NO3	see note*
J43025a	TrGJC	C_2H_5CHO + hν → $C_2H_5O_2$ + HO_2 + CO	jx(ip_C2H5CHO2HCO)	see note*
J43025b	TrGJC	C_2H_5CHO + hν → CH_2CHCH_2OH	jx(ip_C2H5CHO2ENOL)	Andrews et al. (2012), Sander et al. (2019)*
J43026	TrGJCN	PPN + hν → .7 $C_2H_5CO_3$ + .7 NO_2 + .3 $C_2H_5O_2$ + .3 CO_2 + .3 NO_3	jx(ip_PAN)	Sander et al. (2014)
J43027	TrGJC	$C_2H_5CO_3H$ + hν → $C_2H_5O_2$ + CO_2 + OH	jx(ip_CH3OOH)	von Kuhlmann (2001)
J43028a	TrGJC	$HCOCOCH_2OOH$ + hν → $HOOCH_2CO_3$ + CO + HO_2	jx(ip_MGLYOX)	Sander et al. (2019)
J43028b	TrGJC	$HCOCOCH_2OOH$ + hν → HCOCO + HCHO + OH	jx(ip_HOCH2CHO)+jx(ip_CH3OOH)	Sander et al. (2019)
J43200	TrGJTerC	HCOCH2CO3H + hν → $HCOCH_2O_2$ + CO_2 + OH	jx(ip_HOCH2CHO)+jx(ip_CH3OOH)	Rickard and Pascoe (2009)
J43400	TrGJAroC	C3DIALOOH + hν → GLYOX + CO + HO_2 + OH	jx(ip_HOCH2CHO)*2.+jx(ip_CH3OOH)	Rickard and Pascoe (2009)*
J43401	TrGJAroC	C32OH13CO + hν → GLYOX + HO_2 + HO_2 + CO	jx(ip_HOCH2CHO)*2.	Rickard and Pascoe (2009)
J43402	TrGJAroC	HCOCOHCO3H + hν → GLYOX + HO_2 + CO_2 + OH	jx(ip_CH3OOH)	Rickard and Pascoe (2009)
J44000a	TrGJC	LC_4H_9OOH + hν → OH + C_3H_7CHO + HO_2	jx(ip_CH3OOH)*(k_p/(k_p+k_s))	Rickard and Pascoe (2009), Sander et al. (2019)
J44000b	TrGJC	LC_4H_9OOH + hν → OH + .636 MEK + .636 HO_2 + .364 CH_3CHO + .364 $C_2H_5O_2$	jx(ip_CH3OOH)*(k_s/(k_p+k_s))	Rickard and Pascoe (2009), Sander et al. (2019)
J44001	TrGJC	MVK + hν → .5 C_3H_6 + .5 $CH_3C(O)$ + .5 HCHO + CO + .5 HO_2	jx(ip_MVK)	Sander et al. (2014)
J44002	TrGJC	MEK + hν → $CH_3C(O)$ + $C_2H_5O_2$	0.42*jx(ip_CHOH)	von Kuhlmann et al. (2003)
J44003	TrGJC	LMEKOOH + hν → .62 $CH_3C(O)$ + .62 CH_3CHO + .38 HCHO + .38 CO_2 + .38 $HOCH_2CH_2O_2$ + OH	jx(ip_CH3OOH)+0.42*jx(ip_CHOH)	Sander et al. (2019)
J44004	TrGJC	BIACET + hν → 2 $CH_3C(O)$	2.15*jx(ip_MGLYOX)	see note*
J44005a	TrGJCN	LC4H9NO3 + hν → NO_2 + C_3H_7CHO + HO_2	j_IC3H7NO3*(k_p/(k_p+k_s))	see note*
J44005b	TrGJCN	LC4H9NO3 + hν → NO_2 + MEK + HO_2	j_IC3H7NO3*(k_s/(k_p+k_s))	see note*
J44006	TrGJCN	MPAN + hν → .7 MACO3 + .7 NO_2 + .3 MACO2 + .3 NO_3	jx(ip_PAN)	see note*
J44007a	TrGJC	CO2H3CO3H + hν → MGLYOX + HO_2 + OH + CO_2	jx(ip_CH3OOH)	Rickard and Pascoe (2009)

Table 2: Photolysis reactions (... continued)

#	labels	reaction	rate coefficient	reference
J44007b	TrGJC	CO2H3CO3H + hν → $CH_3C(O)$ + HO_2 + $HCOCO_3H$	j_ACETOL	Rickard and Pascoe (2009)
J44008	TrGJC	MACR + hν → .5 MACO3 + .5 $CH_3C(O)$ + .5 HCHO + .5 CO + HO_2	jx(ip_MACR)	Sander et al. (2014)
J44009	TrGJC	MACROOH + hν → MACRO + OH	jx(ip_CH3OOH)+2.77*jx(ip_HOCH2CHO)	Sander et al. (2019)*
J44010	TrGJC	MACROH + hν → CH_3COCH_2OH + CO + HO_2 + HO_2	2.77*jx(ip_HOCH2CHO)	see note*
J44011	TrGJC	MACO3H + hν → MACO2 + OH	jx(ip_CH3OOH)	Sander et al. (2019)
J44012	TrGJC	LHMVKABOOH + hν → .12 MGLYOX + .12 HO_2 + .88 $CH_3C(O)$ + .88 $HOCH_2CHO$ + .12 HCHO + OH	jx(ip_CH3OOH)+j_ACETOL	Sander et al. (2019)
J44013	TrGJC	CO2H3CHO + hν → MGLYOX + CO + HO_2 + HO_2	jx(ip_HOCH2CHO)+j_ACETOL	Sander et al. (2019)
J44014	TrGJC	HO12CO3C4 + hν → $CH_3C(O)$ + $HOCH_2CHO$ + HO_2	j_ACETOL	Rickard and Pascoe (2009)
J44015	TrGJC	BIACETOH + hν → $CH_3C(O)$ + HOCH2CO	2.15*jx(ip_MGLYOX)	see note*
J44016	TrGC	$HCOCCH_3CO$ + hν → .5 OH + .5 CH_3CHO + CO + .5 CH3CHCO + .5 CO	j_ketene	Sander et al. (2019)
J44017a	TrGC	$CH_3COCHCO$ + hν → .0192 CH_3COCO_2H + .1848 H_2O_2 + .2208 MGLYOX + .36 OH + .36 CO + .56 $CH_3C(O)$ + .2 CH_3CHO + .2 CO_2 + .2 HCHO + .2 HO_2 + CO	j_ketene*0.5	Sander et al. (2019),Rickard and Pascoe (2009)*
J44017b	TrGC	$CH_3COCHCO$ + hν → CH3CHCO + CO	j_ketene*0.5	Sander et al. (2019)
J44018a	TrGJC	$CH_3COCOCHO$ + hν → $CH_3C(O)$ + 2 CO + HO_2	jx(ip_MGLYOX)	Sander et al. (2019)
J44018b	TrGJC	$CH_3COCOCHO$ + hν → HCOCO + $CH_3C(O)$	2.15*jx(ip_MGLYOX)	Sander et al. (2019)
J44019	TrGJC	CH3COCOCO2H + hν → $CH_3C(O)$ + CO + CO_2 + HO_2	3.15*jx(ip_MGLYOX)	Sander et al. (2019)
J44020a	TrGJTerC	$CH_3COCOCH_2OOH$ + hν → $CH_3C(O)$ + OH + HCHO + CO	jx(ip_CH3OOH)+j_ACETOL	Rickard and Pascoe (2009)
J44020b	TrGJTerC	$CH_3COCOCH_2OOH$ + hν → $CH_3C(O)$ + HCOCO	2.15*jx(ip_MGLYOX)	Rickard and Pascoe (2009)
J44021	TrGJTerC	C44OOH + hν → HCOCH2CHO + CO_2 + HO_2 + OH	jx(ip_CH3OOH)	Rickard and Pascoe (2009)
J44022	TrGJTerC	C413COOOH + hν → HCOCH2CO3 + HCHO + OH	jx(ip_CH3OOH)+jx(ip_HOCH2CHO)+j_ACETOL	Rickard and Pascoe (2009)
J44023a	TrGJTerC	C4CODIAL + hν → $HCOCOCH_2O_2$ + HO_2 + CO	jx(ip_HOCH2CHO)	Rickard and Pascoe (2009)
J44023b	TrGJTerC	C4CODIAL + hν → HCOCH2CO3 + HO_2 + CO	jx(ip_MGLYOX)	Rickard and Pascoe (2009)
J44024	TrGJTerC	C312COCO3H + hν → $HCOCOCH_2O_2$ + CO_2 + OH	jx(ip_CH3OOH)+jx(ip_MGLYOX)	Rickard and Pascoe (2009)
J44025	TrGJCN	LMEKNO3 + hν → .62 $CH_3C(O)$ + .62 CH_3CHO + .38 HCHO + .38 CO_2 + .38 $HOCH_2CH_2O_2$ + NO_2	jx(ip_MEKNO3)	Barnes et al. (1993), Sander et al. (2019)*
J44026	TrGJCN	MVKNO3 + hν → $CH_3C(O)$ + $HOCH_2CHO$ + NO_2	jx(ip_MEKNO3)	Barnes et al. (1993), Sander et al. (2019)*

Table 2: Photolysis reactions (... continued)

#	labels	reaction	rate coefficient	reference
J44027	TrGJCN	MACRNO3 + hν → CH_3COCH_2OH + CO + HO_2 + NO_2	(2.84*j_IC3H7NO3+jx(ip_CH3CHO)) *(jx(ip_MEKNO3)+1E-10)/(j_ IC3H7NO3+0.42*jx(ip_CHOH)+1E-10)	Müller et al. (2014), Sander et al. (2019)*
J44028	TrGJCN	TC4H9NO3 + hν → CH_3COCH_3 + CH_3 + NO_2	2.84*j_IC3H7NO3	Sander et al. (2019)
J44029	TrGJC	TC_4H_9OOH + hν → CH_3COCH_3 + CH_3 + OH	jx(ip_CH3OOH)	Sander et al. (2019)
J44030	TrGJCN	IBUTOLBNO3 + hν → CH_3COCH_3 + HCHO + HO_2 + NO_2	2.84*j_IC3H7NO3	Sander et al. (2019)
J44031	TrGJC	IBUTOLBOOH + hν → CH_3COCH_3 + HCHO + HO_2 + OH	jx(ip_CH3OOH)	Sander et al. (2019)
J44032	TrGJC	LBUT1ENOOH + hν → C_2H_5CHO + HCHO + HO_2 + OH	jx(ip_CH3OOH)	Sander et al. (2019)
J44033	TrGJCN	LBUT1ENNO3 + hν → C_2H_5CHO + HCHO + HO_2 + NO_2	j_IC3H7NO3	Sander et al. (2019)
J44034	TrGJC	BUT2OLOOH + hν → 2 CH_3CHO + HO_2 + OH	jx(ip_CH3OOH)	Sander et al. (2019)
J44035	TrGJCN	BUT2OLNO3 + hν → 2 CH_3CHO + HO_2 + NO_2	j_IC3H7NO3	Sander et al. (2019)
J44036	TrGJC	BUT2OLO + hν → $CH_3C(O)$ + HOCH2CO	j_ACETOL	Sander et al. (2019)
J44037a	TrGJC	C_3H_7CHO + hν → $C_3H_7O_2$ + CO + HO_2	jx(ip_C3H7CHO2HCO)	Sander et al. (2019)
J44037b	TrGJC	C_3H_7CHO + hν → C_2H_4 + CH_2CHOH	jx(ip_C3H7CHO2VINY)	Sander et al. (2019)*
J44038	TrGJC	IPRCHO + hν → $iC_3H_7O_2$ + CO + HO_2	jx(ip_IPRCHO2HCO)	Sander et al. (2019)
J44039	TrGJCN	IC4H9NO3 + hν → IPRCHO + NO_2	j_IC3H7NO3	Sander et al. (2019)
J44040	TrGJC	IC_4H_9OOH + hν → IPRCHO + HO_2 + OH	jx(ip_CH3OOH)	Sander et al. (2019)
J44041	TrGJC	PERIBUACID + hν → $iC_3H_7O_2$ + CO_2 + OH	jx(ip_CH3OOH)	Sander et al. (2019)
J44042	TrGJCN	PIPN + hν → .7 IPRCO3 + .7 NO_2 + .3 $iC_3H_7O_2$ + .3 CO_2 + .3 NO_3	jx(ip_PAN)	Sander et al. (2019), Sander et al. (2014)
J44043	TrGJC	HVMK + hν → MGLYOX + CO + 2 OH	jx(ip_PeDIONE24)	Sander et al. (2019), Nakanishi et al. (1977), Messaadia et al. (2015), Yoon et al. (1999)*
J44044	TrGJC	HMAC + hν → $HCOCCH_3CO$ + 2 OH	jx(ip_PeDIONE24)	Sander et al. (2019), Nakanishi et al. (1977), Messaadia et al. (2015), Yoon et al. (1999)*
J44045a	TrGJC	CO2C3CHO + hν → $CH_3COCH_2O_2$ + HO_2 + CO	jx(ip_C2H5CHO2HCO)	Rickard and Pascoe (2009)
J44045b	TrGJC	CO2C3CHO + hν → HVMK	jx(ip_C2H5CHO2ENOL)	Andrews et al. (2012), Sander et al. (2019)
J44046a	TrGJC	IBUTDIAL + hν → CH_3CHO + CO + HO_2 + CO_2 + H_2O	jx(ip_C2H5CHO2HCO)*2.	see note*
J44046b	TrGJC	IBUTDIAL + hν → HMAC	jx(ip_C2H5CHO2ENOL)*2.	Andrews et al. (2012), Sander et al. (2019)
J44200	TrGJTerC	IBUTALOH + hν → CH_3COCH_3 + HO_2 + HO_2 + CO	j_ACETOL	Rickard and Pascoe (2009)

Table 2: Photolysis reactions (... continued)

#	labels	reaction	rate coefficient	reference
J44201	TrGJTerC	IPRHOCO3H + hν → CH_3COCH_3 + HO_2 + CO_2 + OH	jx(ip_CH3OOH)	Rickard and Pascoe (2009)
J44400a	TrGJAroC	MALDIALOOH + hν → C32OH13CO + CO + OH + HO_2	jx(ip_HOCH2CHO)*2.	Rickard and Pascoe (2009)
J44400b	TrGJAroC	MALDIALOOH + hν → GLYOX + GLYOX + HO_2 + OH	jx(ip_CH3OOH)	Rickard and Pascoe (2009)*
J44401	TrGJAroC	BZFUOOH + hν → CO14O3CHO + HO_2 + OH	jx(ip_CH3OOH)	Rickard and Pascoe (2009)*
J44402	TrGJAroC	HOCOC4DIAL + hν → HCOCOHCO3 + HO_2 + CO	jx(ip_MGLYOX)+jx(ip_HOCH2CHO)	Rickard and Pascoe (2009)
J44403	TrGJAroCN	NBZFUOOH + hν → .5 CO14O3CHO + .5 NO_2 + .5 NBZFUONE + .5 HO_2 + OH	jx(ip_CH3OOH)	Rickard and Pascoe (2009)*
J44404a	TrGJAroC	MALDALCO3H + hν → $HCOCO_3H$ + HO_2 + CO + HO_2 + CO	jx(ip_MACR)	Rickard and Pascoe (2009)
J44404b	TrGJAroC	MALDALCO3H + hν → .6 MALANHY + HO_2 + .4 GLYOX + .4 CO + .4 CO_2 + OH	jx(ip_CH3OOH)	Rickard and Pascoe (2009)*
J44405	TrGJAroC	EPXDLCO2H + hν → C3DIALO2 + CO_2 + HO_2	2.77*jx(ip_HOCH2CHO)	Rickard and Pascoe (2009)
J44406	TrGJAroC	MALDIAL + hν → .4 BZFUONE + .6 MALDIALCO3 + .6 HO_2	jx(ip_NO2)*0.14	Rickard and Pascoe (2009)
J44407	TrGJAroC	MALANHYOOH + hν → HCOCOHCO3 + CO_2 + OH	jx(ip_CH3OOH)	Rickard and Pascoe (2009)*
J44408	TrGJAroC	EPXDLCO3H + hν → C3DIALO2 + OH + CO_2	jx(ip_CH3OOH)+2.77*jx(ip_HOCH2CHO)	Rickard and Pascoe (2009)
J44409	TrGJAroC	CO2C4DIAL + hν → CO + CO + HO_2 + HO_2 + CO + CO	jx(ip_MGLYOX)*2.	Rickard and Pascoe (2009)
J44410	TrGJAroC	MALDALCO2H + hν → $HCOCO_2H$ + HO_2 + CO + HO_2 + CO	jx(ip_MACR)	Rickard and Pascoe (2009)
J44411	TrGJAroC	EPXC4DIAL + hν → C3DIALO2 + CO + HO_2	2.77*jx(ip_HOCH2CHO)*2.	Rickard and Pascoe (2009)
J44412	TrGJAroC	CO14O3CHO + hν → HO_2 + CO + $HCOCH_2O_2$ + CO_2	jx(ip_MGLYOX)	Rickard and Pascoe (2009)
J44414	TrGJAroC	MECOACEOOH + hν → $CH_3C(O)$ + HCHO + CO_2 + OH	jx(ip_CH3OOH)	Rickard and Pascoe (2009)*
J45002	TrGJC	LISOPACOOH + hν → LISOPACO + OH	jx(ip_CH3OOH)	Rickard and Pascoe (2009)
J45003	TrGJCN	LISOPACNO3 + hν → LISOPACO + NO_2	0.59*j_IC3H7NO3	see note*
J45004	TrGJC	ISOPBOOH + hν → MVK + HCHO + HO_2 + OH	jx(ip_CH3OOH)	Rickard and Pascoe (2009)
J45005	TrGJCN	ISOPBNO3 + hν → MVK + HCHO + HO_2 + NO_2	2.84*j_IC3H7NO3	see note*
J45006	TrGJC	ISOPDOOH + hν → MACR + HCHO + HO_2 + OH	jx(ip_CH3OOH)	Rickard and Pascoe (2009)
J45007	TrGJCN	ISOPDNO3 + hν → MACR + HCHO + HO_2 + NO_2	j_IC3H7NO3	see note*
J45008	TrGJCN	NISOPOOH + hν → NC4CHO + HO_2 + OH	jx(ip_CH3OOH)	Rickard and Pascoe (2009)
J45009	TrGJCN	NC4CHO + hν → LHC4ACCO3 + NO_2	(.59*j_IC3H7NO3+jx(ip_MACR))*(jx(ip_MEKNO3)+1E-10)/(j_IC3H7NO3+0.42*jx(ip_CHOH)+1E-10)	Müller et al. (2014), Sander et al. (2019)*

Table 2: Photolysis reactions (... continued)

#	labels	reaction	rate coefficient	reference
J45010	TrGJCN	LNISOOH + hν → NOA + OH + .5 HOCHCHO + .5 CO + .5 HO_2 + .5 CO_2	jx(ip_CH3OOH)	Taraborrelli et al. (2009), Sander et al. (2019)
J45011	TrGJC	LHC4ACCHO + hν → .5 LHC4ACCO3 + .5 HO_2 + .5 CO + .5 OH + .25 MACRO2 + .25 LHMVKABO2	jx(ip_MACR)	Sander et al. (2019)
J45012	TrGJC	LC578OOH + hν → .25 CH_3COCH_2OH + .75 MGLYOX + .25 HOCHCHO + .75 $HOCH_2CHO$ + .75 HO_2 + OH	jx(ip_CH3OOH)+ 2.77*jx(ip_HOCH2CHO)	Sander et al. (2019)
J45013	TrGJC	LHC4ACCO3H + hν → OH + .5 MACRO2 + .5 LHMVKABO2 + OH + CO_2	j_HPALD	Sander et al. (2019)
J45014	TrGJCN	LC5PAN1719 + hν → .7 LHC4ACCO3 + .7 NO_2 + .15 MACRO2 + .15 LHMVKABO2 + .3 CO_2 + .3 NO_3	jx(ip_PAN)	Sander et al. (2019)
J45015	TrGJC	HCOC5 + hν → .65 CH_3 + .65 CO + .65 HCHO + .35 OH + .35 $CH_3COCH_2O_2$ + HOCH2CO	0.5*jx(ip_MVK)	Sander et al. (2019)*
J45016	TrGJC	C59OOH + hν → CH_3COCH_2OH + HOCH2CO + OH	j_ACETOL+jx(ip_CH3OOH)	Sander et al. (2019)
J45017	TrGJTerC	C511OOH + hν → $CH_3C(O)$ + HCOCH2CHO + OH	jx(ip_CH3OOH)+jx(ip_HOCH2CHO)	Rickard and Pascoe (2009)
J45018a	TrGJTerC	CO23C4CHO + hν → $CH_3COCOCH_2O_2$ + HO_2 + CO	jx(ip_HOCH2CHO)	Rickard and Pascoe (2009)
J45018b	TrGJTerC	CO23C4CHO + hν → $CH_3C(O)$ + HCOCH2CO3	2.15*jx(ip_MGLYOX)	Rickard and Pascoe (2009)
J45019	TrGJTerC	CO23C4CO3H + hν → $CH_3COCOCH_2O_2$ + CO_2 + OH	jx(ip_CH3OOH)+jx(ip_HOCH2CHO)	Rickard and Pascoe (2009)
J45020	TrGJTerC	C512OOH + hν → C513O2 + OH	jx(ip_CH3OOH)+jx(ip_HOCH2CHO)	Rickard and Pascoe (2009)
J45021	TrGJTerC	CO13C4CHO + hν → CHOC3COO2 + CO + HO_2	jx(ip_HOCH2CHO)*2.	Rickard and Pascoe (2009)
J45022	TrGJTerC	C513OOH + hν → GLYOX + $HOC_2H_4CO_3$ + OH	jx(ip_CH3OOH)+jx(ip_HOCH2CHO)	Rickard and Pascoe (2009)
J45023	TrGJTerC	C513CO + hν → $HOC_2H_4CO_3$ + HO_2 + CO + CO	jx(ip_MGLYOX)+2.15*jx(ip_MGLYOX)	Rickard and Pascoe (2009)
J45024	TrGJTerC	C514OOH + hν → CO13C4CHO + HO_2 + OH	jx(ip_CH3OOH)+jx(ip_HOCH2CHO)*2.	Rickard and Pascoe (2009)
J45025	TrGJTerCN	C514NO3 + hν → CO13C4CHO + HO_2 + NO_2	j_IC3H7NO3+jx(ip_HOCH2CHO)*2.	Rickard and Pascoe (2009)
J45026a	TrGJC	LZCODC23DBCOOH + hν → OH + CO + HVMK + OH	j_HPALD*0.6*0.5	Sander et al. (2019), Jenkin et al. (2015), Peeters et al. (2014)
J45026b	TrGJC	LZCODC23DBCOOH + hν → OH + CO + $CH_3C(O)$ + $HOCH_2CHO$	j_HPALD*0.6*0.5	Sander et al. (2019), Jenkin et al. (2015), Peeters et al. (2014)
J45026c	TrGJC	LZCODC23DBCOOH + hν → OH + CO + HMAC + OH	j_HPALD*0.4*0.5	Sander et al. (2019), Jenkin et al. (2015), Peeters et al. (2014)
J45026d	TrGJC	LZCODC23DBCOOH + hν → OH + CO + CO + CH_3COCH_2OH + HO_2	j_HPALD*0.4*0.5	Sander et al. (2019), Jenkin et al. (2015), Peeters et al. (2014)

Table 2: Photolysis reactions (... continued)

#	labels	reaction	rate coefficient	reference
J45027	TrGJC	LZCO3HC23DBCOD + hν → .62 EZCH3CO2CHCHO + .38 EZCHOCCH3CHO2 + OH + CO_2	j_HPALD	Sander et al. (2019)
J45028a	TrGJC	C1OOHC2OOHC4OD + hν → $CH_3COCH_2O_2H$ + OH + 2 CO + HO_2	2.77*jx(ip_HOCH2CHO)	Sander et al. (2019)
J45028b	TrGJC	C1OOHC2OOHC4OD + hν → .5 $CH_3COCH_2O_2H$ + .5 HOCHCHO + .5 CO2H3CHO + .5 HCHO + 1.5 OH	2.*jx(ip_CH3OOH)	Sander et al. (2019)
J45029	TrGC	DB1OOH + hν → DB1O2 + OH	jx(ip_CH3OOH)	Sander et al. (2019)
J45030	TrGC	DB2OOH + hν → .48 CH_3COCH_2OH + .52 $HOCH_2CHO$ + .52 MGLYOX + .48 GLYOX + HO_2 + OH	jx(ip_CH3OOH)	Sander et al. (2019)
J45031a	TrGJC	C1ODC2OOHC4OD + hν → MGLYOX + HOCHCHO + OH	jx(ip_CH3OOH)	Sander et al. (2019)
J45031b	TrGJC	C1ODC2OOHC4OD + hν → CO2H3CHO + CO + HO_2 + OH	2.*2.77*jx(ip_HOCH2CHO)	Sander et al. (2019)
J45032	TrGJC	C4MDIAL + hν → .5 $CH_3COCHCO$ + .5 $HCOCCH_3CO$ + CO + HO_2 + OH	jx(ip_NO2)*0.1*0.5	Sander et al. (2019)*
J45033	TrGCN	DB1NO3 + hν → DB1O2 + NO_2	j_IC3H7NO3	Sander et al. (2019)
J45034	TrGJTerC	CHOC3COOOH + hν → CHOC3COO2 + CO_2 + OH	jx(ip_CH3OOH)+jx(ip_HOCH2CHO) +j_ACETOL	Rickard and Pascoe (2009)
J45200a	TrGJTerC	LMBOABOOH + hν → $HOCH_2CHO$ + CH_3COCH_3 + HO_2 + OH	jx(ip_CH3OOH)*.67	Rickard and Pascoe (2009), Sander et al. (2019)
J45200b	TrGJTerC	LMBOABOOH + hν → IBUTALOH + HCHO + HO_2 + OH	jx(ip_CH3OOH)*.33	Rickard and Pascoe (2009), Sander et al. (2019)
J45201	TrGJTerC	MBOACO + hν → HCHO + HO_2 + IPRHOCO3	j_ACETOL	Rickard and Pascoe (2009)
J45202	TrGJTerC	MBOCOCO + hν → CO + HO_2 + IPRHOCO3	jx(ip_MGLYOX)	Rickard and Pascoe (2009)
J45203a	TrGJTerCN	LNMBOABOOH + hν → $NO_3CH2CHO$ + CH_3COCH_3 + HO_2 + OH	jx(ip_CH3OOH)*.65	Rickard and Pascoe (2009), Sander et al. (2019)
J45203b	TrGJTerCN	LNMBOABOOH + hν → IBUTALOH + HCHO + NO_2 + OH	jx(ip_CH3OOH)*.35	Rickard and Pascoe (2009), Sander et al. (2019)
J45204	TrGJTerCN	NC4OHCO3H + hν → IBUTALOH + CO_2 + NO_2 + OH	jx(ip_CH3OOH)	Rickard and Pascoe (2009)
J45400	TrGJAroC	C54CO + hν → HO_2 + CO + CO + CO + $CH_3C(O)$	jx(ip_MGLYOX)+2.15*jx(ip_MGLYOX) *2.	Rickard and Pascoe (2009)
J45401	TrGJAroC	C5134CO2OH + hν → $CH_3COCOCHO$ + HO_2 + CO + HO_2	jx(ip_HOCH2CHO)+2.15*jx(ip_ MGLYOX)	Rickard and Pascoe (2009)

Table 2: Photolysis reactions (... continued)

#	labels	reaction	rate coefficient	reference
J45402	TrGJAroC	C5DIALOOH + hν → MALDIAL + CO + HO_2 + OH	jx(ip_CH3OOH)+jx(ip_MACR)	Rickard and Pascoe (2009)*
J45406	TrGJAroC	C5CO14OH + hν → $CH_3C(O)$ + $HCOCO_2H$ + HO_2 + CO	jx(ip_MVK)	Rickard and Pascoe (2009)
J45407	TrGJAroC	C5DICARB + hν → .6 C5CO14O2 + .6 HO_2 + .4 TLFUONE	jx(ip_NO2)*0.2	Rickard and Pascoe (2009)*
J45408	TrGJAroC	MC3ODBCO2H + hν → CH_3COCO_2H + HO_2 + CO + HO_2 + CO	jx(ip_MACR)	Rickard and Pascoe (2009)
J45409	TrGJAroC	ACCOMECHO + hν → MECOACETO2 + HO_2 + CO	jx(ip_HOCH2CHO)	Rickard and Pascoe (2009)
J45410	TrGJAroC	MMALNHYOOH + hν → CO2H3CO3 + CO_2 + OH	jx(ip_CH3OOH)	Rickard and Pascoe (2009)*
J45411	TrGJAroC	C5DICAROOH + hν → MGLYOX + GLYOX + HO_2 + OH	jx(ip_CH3OOH)+jx(ip_HOCH2CHO) +j_ACETOL	Rickard and Pascoe (2009)*
J45412	TrGJAroCN	NTLFUOOH + hν → ACCOMECHO + NO_2 + OH	jx(ip_CH3OOH)	Rickard and Pascoe (2009)*
J45414	TrGJAroC	C5CO14OOH + hν → .83 MALANHY + .83 CH_3 + .17 MGLYOX + .17 HO_2 + .17 CO + .17 CO_2 + OH	jx(ip_CH3OOH)	Rickard and Pascoe (2009)*
J45415	TrGJAroC	TLFUOOH + hν → ACCOMECHO + HO_2 + OH	jx(ip_CH3OOH)	Rickard and Pascoe (2009)*
J45417	TrGJAroC	ACCOMECO3H + hν → MECOACETO2 + CO_2 + OH	jx(ip_CH3OOH)	Rickard and Pascoe (2009)
J45418	TrGJAroC	C5DIALCO + hν → MALDIALCO3 + CO + HO_2	jx(ip_MGLYOX)+jx(ip_MACR)	Rickard and Pascoe (2009)
J46200	TrGJTerCN	C614NO3 + hν → CO23C4CHO + HCHO + HO_2 + NO_2	2.15*jx(ip_MGLYOX)	Rickard and Pascoe (2009)
J46201	TrGJTerC	C614OOH + hν → CO23C4CHO + HCHO + HO_2 + OH	jx(ip_CH3OOH)+2.15*jx(ip_MGLYOX)	Rickard and Pascoe (2009)
J46202	TrGJTerC	CO235C5CHO + hν → CO23C4CO3 + CO + HO_2	jx(ip_MGLYOX)	Rickard and Pascoe (2009)
J46203	TrGJTerC	CO235C6OOH + hν → CO23C4CO3 + HCHO + OH	jx(ip_CH3OOH)+2.15*jx(ip_MGLYOX)	Rickard and Pascoe (2009)
J46400	TrGJAroC	PHENOOH + hν → .71 MALDALCO2H + .71 GLYOX + .29 PBZQONE + HO_2 + OH	jx(ip_CH3OOH)	Rickard and Pascoe (2009)*
J46401	TrGJAroC	C6CO4DB + hν → C4CO2DBCO3 + HO_2 + CO	jx(ip_MGLYOX)*2.	Rickard and Pascoe (2009)
J46402	TrGJAroC	C5CO2DCO3H + hν → $CH_3C(O)$ + HCOCOCHO + CO_2 + OH	jx(ip_CH3OOH)+jx(ip_MGLYOX)	Rickard and Pascoe (2009)
J46403	TrGJAroCN	NDNPHENOOH + hν → NC4DCO2H + HNO_3 + CO + CO + NO_2 + OH	jx(ip_CH3OOH)	Rickard and Pascoe (2009)*
J46404	TrGJAroCN	BZBIPERNO3 + hν → GLYOX + HO_2 + .5 BZFUONE + .5 BZFUONE + NO_2	j_IC3H7NO3	Rickard and Pascoe (2009)*
J46405	TrGJAroCN	HOC6H4NO2 + hν → HONO + CPDKETENE	jx(ip_HOC6H4NO2)	Chen et al. (2011)*
J46406	TrGJAroC	CPDKETENE + hν → CO_2 + CO + 2 HO_2 + MALDIAL	j_ketene	see note*

Table 2: Photolysis reactions (... continued)

#	labels	reaction	rate coefficient	reference
J46407	TrGJAroC	C5COOHCO3H + hν → HOCOC4DIAL + HO_2 + CO + CO_2 + OH	jx(ip_CH3OOH)	Rickard and Pascoe (2009)
J46408	TrGJAroC	BZEPOXMUC + hν → .5 C5DIALO2 + 1.5 HO_2 + 1.5 CO + .5 MALDIAL	4.E3*jx(ip_MVK)*0.1	Rickard and Pascoe (2009)
J46409	TrGJAroCN	NPHEN1OOH + hν → NPHEN1O + OH	jx(ip_CH3OOH)	Rickard and Pascoe (2009)
J46410	TrGJAroC	BZEMUCCO + hν → HCOCOHCO3 + C3DIALO2	jx(ip_HOCH2CHO)*2.+j_ACETOL	Rickard and Pascoe (2009)
J46411	TrGJAroC	BZEMUCCO2H + hν → C5DIALO2 + CO_2 + HO_2	jx(ip_MACR)	Rickard and Pascoe (2009)
J46412	TrGJAroCN	NNCATECOOH + hν → NC4DCO2H + $HCOCO_2H$ + NO_2 + OH	jx(ip_CH3OOH)	Rickard and Pascoe (2009)*
J46413	TrGJAroC	C615CO2OOH + hν → C5DICARB + CO + HO_2 + OH	jx(ip_MVK)+jx(ip_CH3OOH)	Rickard and Pascoe (2009)
J46414	TrGJAroCN	NPHENOOH + hν → MALDALCO2H + GLYOX + OH + NO_2	j_IC3H7NO3 + jx(ip_CH3OOH)	Rickard and Pascoe (2009)
J46415	TrGJAroCN	NCATECOOH + hν → NC4DCO2H + $HCOCO_2H$ + HO_2 + OH	jx(ip_CH3OOH)	Rickard and Pascoe (2009)*
J46416	TrGJAroC	PBZQOOH + hν → C5CO2OHCO3 + OH	jx(ip_CH3OOH)	Rickard and Pascoe (2009)*
J46417	TrGJAroC	BZOBIPEROH + hν → MALDIALCO3 + GLYOX + HO_2	j_ACETOL	Rickard and Pascoe (2009)
J46418	TrGJAroC	BZBIPEROOH + hν → GLYOX + HO_2 + .5 BZFUONE + .5 BZFUONE + OH	jx(ip_CH3OOH)	Rickard and Pascoe (2009)*
J46419	TrGJAroCN	NBZQOOH + hν → C6CO4DB + NO_2 + OH	jx(ip_CH3OOH)	Rickard and Pascoe (2009)*
J46420	TrGJAroC	CATEC1OOH + hν → CATEC1O + OH	jx(ip_CH3OOH)	Rickard and Pascoe (2009)
J46421	TrGJAroC	C6125CO + hν → C5CO14O2 + CO + HO_2	jx(ip_MGLYOX)+jx(ip_MVK)	Rickard and Pascoe (2009)
J46422	TrGJAroCN	DNPHENOOH + hν → NC4DCO2H + $HCOCO_2H$ + NO_2 + OH	jx(ip_CH3OOH)	Rickard and Pascoe (2009)*
J46423	TrGJAroC	BZEMUCCO3H + hν → C5DIALO2 + CO_2 + OH	jx(ip_CH3OOH)+jx(ip_MACR)	Rickard and Pascoe (2009)
J46424	TrGJAroC	C6H5OOH + hν → C6H5O + OH	jx(ip_CH3OOH)	Rickard and Pascoe (2009)
J46425	TrGJAroC	BZEMUCOOH + hν → .5 EPXC4DIAL + .5 GLYOX + .5 HO_2 + .5 C3DIALO2 + .5 C32OH13CO + OH	jx(ip_CH3OOH)+jx(ip_HOCH2CHO)*2.	Rickard and Pascoe (2009)*
J46427	TrGJAroCN	BZEMUCNO3 + hν → EPXC4DIAL + NO_2 + GLYOX + HO_2	2.77*jx(ip_HOCH2CHO)	Rickard and Pascoe (2009)
J46428	TrGJAroCN	DNPHEN + hν → HONO + NCPDKETENE	jx(ip_HOC6H4NO2)	Sander et al. (2019)
J46429	TrGJAroCN	NCPDKETENE + hν → CO_2 + CO + 2 HO_2 + NC4DCO2H	j_ketene	see note*
J47200	TrGJTerC	CO235C6CHO + hν → CHOC3COCO3 + $CH_3C(O)$	2.15*jx(ip_MGLYOX)	Rickard and Pascoe (2009)
J47201	TrGJTerC	C235C6CO3H + hν → CO235C6O2 + CO_2 + OH	jx(ip_CH3OOH)+2.15*jx(ip_MGLYOX)	Rickard and Pascoe (2009)
J47202	TrGJTerC	C716OOH + hν → CO13C4CHO + $CH_3C(O)$ + OH	jx(ip_CH3OOH)+jx(ip_HOCH2CHO)	Rickard and Pascoe (2009)
J47203	TrGJTerC	C721OOH + hν → C722O2 + OH	jx(ip_CH3OOH)	Rickard and Pascoe (2009)

Table 2: Photolysis reactions (... continued)

#	labels	reaction	rate coefficient	reference
J47204	TrGJTerC	C722OOH + hν → CH_3COCH_3 + C44O2 + OH	jx(ip_CH3OOH)	Rickard and Pascoe (2009)
J47400	TrGJAroC	TLEPOXMUC + hν → .5 C615CO2O2 + HO_2 + CO + .5 EPXC4DIAL + .5 $CH_3C(O)$	4.E3*jx(ip_MVK)*0.1	Rickard and Pascoe (2009)
J47401	TrGJAroC	C6H5CH2OOH + hν → BENZAL + HO_2 + OH	jx(ip_CH3OOH)	Rickard and Pascoe (2009)*
J47402	TrGJAroCN	C6H5CH2NO3 + hν → BENZAL + HO_2 + NO_2	0.59*j_IC3H7NO3	Rickard and Pascoe (2009)*
J47403	TrGJAroC	BENZAL + hν → HO_2 + CO + C6H5O2	jx(ip_BENZAL)	Wallington et al. (2018)
J47404	TrGJAroC	TLBIPEROOH + hν → .6 GLYOX + .4 MGLYOX + HO_2 + .2 C4MDIAL + .2 C5DICARB + .2 TLFUONE + .2 BZFUONE + .2 MALDIAL + OH	jx(ip_CH3OOH)	Rickard and Pascoe (2009)*
J47405	TrGJAroCN	TLBIPERNO3 + hν → .6 GLYOX + .4 MGLYOX + HO_2 + .2 C4MDIAL + .2 C5DICARB + .2 TLFUONE + .2 BZFUONE + .2 MALDIAL + NO_2	j_IC3H7NO3	Rickard and Pascoe (2009)*
J47406	TrGJAroC	TLOBIPEROH + hν → C5CO14O2 + GLYOX + HO_2	j_ACETOL	Rickard and Pascoe (2009)
J47407	TrGJAroC	CRESOOH + hν → .68 C5CO14OH + .68 GLYOX + HO_2 + .32 PTLQONE + OH	jx(ip_CH3OOH)	Rickard and Pascoe (2009)*
J47408a	TrGJAroCN	NCRESOOH + hν → .68 C5CO14OH + .68 GLYOX + HO_2 + .32 PTLQONE + OH + NO_2	j_IC3H7NO3	Rickard and Pascoe (2009)*
J47408b	TrGJAroCN	NCRESOOH + hν → C5CO14OH + GLYOX + NO_2 + OH	jx(ip_CH3OOH)	Rickard and Pascoe (2009)*
J47409	TrGJAroCN	TOL1OHNO2 + hν → HONO + MCPDKETENE	jx(ip_HOPh3Me2NO2)	see note*
J47410	TrGJAroC	TLEMUCCO2H + hν → C615CO2O2 + CO_2 + HO_2	jx(ip_MACR)	Rickard and Pascoe (2009)
J47411	TrGJAroC	TLEMUCCO3H + hν → C615CO2O2 + CO_2 + OH	jx(ip_CH3OOH)+jx(ip_MACR)	Rickard and Pascoe (2009)
J47412	TrGJAroC	TLEMUCOOH + hν → .5 C3DIALO2 + .5 CO2H3CHO + .5 EPXC4DIAL + .5 MGLYOX + .5 HO_2 + OH	jx(ip_CH3OOH)+2.77*jx(ip_HOCH2CHO)+j_ACETOL	Rickard and Pascoe (2009)*
J47413	TrGJAroCN	TLEMUCNO3 + hν → EPXC4DIAL + NO_2 + $CH_3C(O)$ + CO + HO_2	2.77*jx(ip_HOCH2CHO)+j_ACETOL	Rickard and Pascoe (2009)
J47414	TrGJAroC	TLEMUCCO + hν → $CH_3C(O)$ + EPXC4DIAL + CO + HO_2	2.77*jx(ip_HOCH2CHO)+2.15*jx(ip_MGLYOX)	Rickard and Pascoe (2009)
J47415	TrGJAroC	C6H5CO3H + hν → C6H5O2 + CO_2 + OH	jx(ip_CH3OOH)	Rickard and Pascoe (2009)
J47416	TrGJAroC	OXYL1OOH + hν → TOL1O + OH	jx(ip_CH3OOH)	Rickard and Pascoe (2009)
J47417	TrGJAroCN	MNCATECH + hν → HONO + MCPDKETENE	jx(ip_HOPh3Me2NO2)	see note*
J47418	TrGJAroC	MCPDKETENE + hν → CO_2 + CO + 2 HO_2 + C4MDIAL	j_ketene	see note*
J47419	TrGJAroCN	DNCRES + hν → HONO + MNCPDKETENE	jx(ip_HOPh3Me2NO2)	see note*

Table 2: Photolysis reactions (... continued)

#	labels	reaction	rate coefficient	reference
J47420	TrGJAroCN	MNCPDKETENE + hν → CO_2 + CO + 2 HO_2 + NC4MDCO2HN	j_ketene	see note*
J47421	TrGJAroC	MCATEC1OOH + hν → MCATEC1O + OH	jx(ip_CH3OOH)	Rickard and Pascoe (2009)
J47422	TrGJAroCN	NPTLQOOH + hν → C7CO4DB + NO_2 + OH	jx(ip_CH3OOH)	Rickard and Pascoe (2009)*
J47423	TrGJAroC	PTLQOOH + hν → C6CO2OHCO3 + OH	jx(ip_CH3OOH)	Rickard and Pascoe (2009)*
J47424	TrGJAroCN	NCRES1OOH + hν → NCRES1O + OH	jx(ip_CH3OOH)	Rickard and Pascoe (2009)
J47425	TrGJAroCN	MNNCATCOOH + hν → NC4MDCO2HN + $HCOCO_2H$ + NO_2 + OH	jx(ip_CH3OOH)	Rickard and Pascoe (2009)*
J47426	TrGJAroCN	MNCATECOOH + hν → NC4MDCO2HN + $HCOCO_2H$ + HO_2 + OH	jx(ip_CH3OOH)	Rickard and Pascoe (2009)*
J47427	TrGJAroC	C7CO4DB + hν → C5CO2DBCO3 + HO_2 + CO	jx(ip_MGLYOX)*2.	Rickard and Pascoe (2009)
J47428	TrGJAroCN	NDNCRESOOH + hν → NC4MDCO2HN + HNO_3 + CO + CO + NO_2 + OH	jx(ip_CH3OOH)	Rickard and Pascoe (2009)*
J47429	TrGJAroCN	DNCRESOOH + hν → NC4MDCO2HN + $HCOCO_2H$ + NO_2 + OH	jx(ip_CH3OOH)	Rickard and Pascoe (2009)*
J47430	TrGJAroC	C6COOHCO3H + hν → C5134CO2OH + HO_2 + CO + CO_2 + OH	jx(ip_CH3OOH)	Rickard and Pascoe (2009)
J48200	TrGJTerC	C86OOH + hν → C511O2 + CH_3COCH_3 + OH	jx(ip_CH3OOH)+ jx(ip_HOCH2CHO)	Rickard and Pascoe (2009)
J48201	TrGJTerC	C812OOH + hν → C813O2 + OH	jx(ip_CH3OOH)	Rickard and Pascoe (2009)
J48202	TrGJTerC	C813OOH + hν → CH_3COCH_3 + C512O2 + OH	jx(ip_CH3OOH)+jx(ip_MGLYOX)	Rickard and Pascoe (2009)
J48203	TrGJTerC	C721CHO + hν → C721O2 + CO + HO_2	jx(ip_HOCH2CHO)	Rickard and Pascoe (2009)
J48204	TrGJTerC	C721CO3H + hν → C721O2 + CO_2 + OH	jx(ip_CH3OOH)	Rickard and Pascoe (2009)
J48205	TrGJTerC	C8BCOOH + hν → C89O2 + OH	jx(ip_CH3OOH)	Rickard and Pascoe (2009)
J48206	TrGJTerC	C89OOH + hν → C810O2 + OH	jx(ip_CH3OOH)+jx(ip_HOCH2CHO)	Rickard and Pascoe (2009)
J48207	TrGJTerCN	C89NO3 + hν → C810O2 + NO_2	jx(ip_CH3OOH)+jx(ip_HOCH2CHO)	Rickard and Pascoe (2009)
J48208	TrGJTerC	C810OOH + hν → CH_3COCH_3 + C514O2 + OH	jx(ip_CH3OOH)+jx(ip_HOCH2CHO)	Rickard and Pascoe (2009)
J48209	TrGJTerCN	C810NO3 + hν → CH_3COCH_3 + C514O2 + NO_2	2.84*j_IC3H7NO3+jx(ip_HOCH2CHO)	Rickard and Pascoe (2009)
J48210	TrGJTerCN	C8BCNO3 + hν → C89O2 + NO_2	j_IC3H7NO3	Rickard and Pascoe (2009)
J48211	TrGJTerC	C85OOH + hν → C86O2 + OH	jx(ip_CH3OOH)+j_ACETOL	Rickard and Pascoe (2009)
J48400	TrGJAroC	STYRENOOH + hν → HO_2 + HCHO + BENZAL + OH	jx(ip_CH3OOH)	Rickard and Pascoe (2009)*
J49200	TrGJTerC	C96OOH + hν → C97O2 + OH	jx(ip_CH3OOH)+j_ACETOL	Rickard and Pascoe (2009)
J49201	TrGJTerC	C97OOH + hν → C98O2 + OH	jx(ip_CH3OOH)+j_ACETOL	Rickard and Pascoe (2009)

Table 2: Photolysis reactions (... continued)

#	labels	reaction	rate coefficient	reference
J49202	TrGJTerC	C98OOH + hν → C614O2 + CH_3COCH_3 + OH	(jx(ip_CH3OOH)+2.15*jx(ip_MGLYOX))	Rickard and Pascoe (2009)
J49203a	TrGJTerC	NORPINAL + hν → C85O2 + CO + HO_2	jx(ip_PINAL2HCO)	Rickard and Pascoe (2009), Sander et al. (2019)
J49203b	TrGJTerC	NORPINAL + hν → NORPINENOL	jx(ip_PINAL2ENOL)	Sander et al. (2019), Andrews et al. (2012)
J49204	TrGJTerC	C85CO3H + hν → C85O2 + CO_2 + OH	jx(ip_CH3OOH)+j_ACETOL	Rickard and Pascoe (2009)
J49205	TrGJTerC	C89CO2H + hν → .8 C811CO3 + .2 C89O2 + .2 CO_2 + HO_2	jx(ip_HOCH2CHO)	Rickard and Pascoe (2009)
J49206	TrGJTerC	C89CO3H + hν → .8 C811CO3 + .2 C89O2 + .2 CO_2 + OH	jx(ip_CH3OOH)+jx(ip_HOCH2CHO)	Rickard and Pascoe (2009)
J49207	TrGJTerC	C811CO3H + hν → C811O2 + CO_2 + OH	jx(ip_CH3OOH)	Rickard and Pascoe (2009)
J49208	TrGJTerC	NOPINDOOH + hν → C89CO3 + OH	jx(ip_CH3OOH)	Rickard and Pascoe (2009)
J40200	TrGJTerC	LAPINABOOH + hν → PINAL + HO_2 + OH	jx(ip_CH3OOH)	Rickard and Pascoe (2009)
J40201	TrGJTerC	MENTHEN6ONE + hν → RO6R1O2 + OH	jx(ip_CH3OOH)	Vereecken et al. (2007)
J40202	TrGJTerC	2OHMENTHEN6ONE + hν → 10 LCARBON + OH	jx(ip_CH3OOH)	Vereecken et al. (2007)
J40203a	TrGJTerC	PINAL + hν → C96O2 + CO + HO_2	jx(ip_PINAL2HCO)	Rickard and Pascoe (2009)
J40203b	TrGJTerC	PINAL + hν → PINEOL	jx(ip_PINAL2ENOL)	Sander et al. (2019), Andrews et al. (2012)*
J40204	TrGJTerC	PERPINONIC + hν → C96O2 + CO_2 + OH	jx(ip_CH3OOH)+j_ACETOL	Rickard and Pascoe (2009)
J40205	TrGJTerC	PINALOOH + hν → C106O2 + OH	jx(ip_CH3OOH)+jx(ip_HOCH2CHO)	Rickard and Pascoe (2009)
J40206	TrGJTerCN	PINALNO3 + hν → C106O2 + NO_2	j_IC3H7NO3+jx(ip_HOCH2CHO)	Rickard and Pascoe (2009)
J40207	TrGJTerC	C106OOH + hν → C716O2 + CH_3COCH_3 + OH	jx(ip_CH3OOH)+jx(ip_HOCH2CHO)	Rickard and Pascoe (2009)
J40208	TrGJTerCN	C106NO3 + hν → C716O2 + CH_3COCH_3 + NO_2	j_IC3H7NO3+ jx(ip_HOCH2CHO)	Rickard and Pascoe (2009)
J40209	TrGJTerC	C109OOH + hν → C89CO3 + HCHO + OH	jx(ip_CH3OOH)+jx(ip_HOCH2CHO)	Rickard and Pascoe (2009)
J40210	TrGJTerC	C109CO + hν → C89CO3 + CO + HO_2	jx(ip_MGLYOX)+jx(ip_HOCH2CHO)	Rickard and Pascoe (2009)
J40211	TrGJTerCN	LNAPINABOOH + hν → PINAL + NO_2 + OH	jx(ip_CH3OOH)	Rickard and Pascoe (2009)
J40212	TrGJTerC	BPINAOOH + hν → NOPINONE + HCHO + HO_2 + OH	jx(ip_CH3OOH)	Rickard and Pascoe (2009)
J40213	TrGJTerCN	LNBPINABOOH + hν → NOPINONE + HCHO + NO_2 + OH	jx(ip_CH3OOH)	Rickard and Pascoe (2009)
J40214	TrGJTerCN	ROO6R1NO3 + hν → ROO6R3O2 + CH_3COCH_3 + NO_2	2.84*j_IC3H7NO3+jx(ip_CH3OOH)	Sander et al. (2019)
J40215	TrGJTerCN	RO6R1NO3 + hν → 9 LCARBON + HCHO + HO_2 + NO_2	2.84*j_IC3H7NO3	Sander et al. (2019)
J6000	StTrGJCl	Cl_2 + hν → Cl + Cl	jx(ip_Cl2)	Sander et al. (2014)
J6100	StTrGJCl	Cl_2O_2 + hν → 2 Cl	jx(ip_Cl2O2)	Sander et al. (2014)
J6101	StTrGJCl	OClO + hν → ClO + O(^{3}P)	jx(ip_OClO)	Sander et al. (2014)
J6200	StGJCl	HCl + hν → Cl + H	jx(ip_HCl)	Sander et al. (2014)
J6201	StTrGJCl	HOCl + hν → OH + Cl	jx(ip_HOCl)	Sander et al. (2014)

Table 2: Photolysis reactions (... continued)

#	labels	reaction	rate coefficient	reference
J6300	TrGJClN	$ClNO_2 + h\nu \rightarrow Cl + NO_2$	jx(ip_ClNO2)	Sander et al. (2014)
J6301a	StTrGJClN	$ClNO_3 + h\nu \rightarrow Cl + NO_3$	jx(ip_ClNO3)	Sander et al. (2014)
J6301b	StTrGJClN	$ClNO_3 + h\nu \rightarrow ClO + NO_2$	jx(ip_ClONO2)	Sander et al. (2014)
J6400	StGJCl	$CH_3Cl + h\nu \rightarrow Cl + CH_3$	jx(ip_CH3Cl)	Sander et al. (2014)
J6401	StGJCl	$CCl_4 + h\nu \rightarrow$ LCARBON + 4 Cl	jx(ip_CCl4)	Sander et al. (2014)
J6402	StGJCCl	$CH_3CCl_3 + h\nu \rightarrow$ 2 LCARBON + 3 Cl	jx(ip_CH3CCl3)	Sander et al. (2014)
J6500	StGJClF	$CFCl_3 + h\nu \rightarrow$ LCARBON + LFLUORINE + 3 Cl	jx(ip_CFCl3)	Sander et al. (2014)*
J6501	StGJClF	$CF_2Cl_2 + h\nu \rightarrow$ LCARBON + 2 LFLUORINE + 2 Cl	jx(ip_CF2Cl2)	Sander et al. (2014)*
J7000	StTrGJBr	$Br_2 + h\nu \rightarrow Br + Br$	jx(ip_Br2)	Sander et al. (2014)
J7100	StTrGJBr	$BrO + h\nu \rightarrow Br + O(^3P)$	jx(ip_BrO)	Sander et al. (2014)
J7200	StTrGJBr	$HOBr + h\nu \rightarrow Br + OH$	jx(ip_HOBr)	Sander et al. (2014)
J7300	TrGJBrN	$BrNO_2 + h\nu \rightarrow Br + NO_2$	jx(ip_BrNO2)	Sander et al. (2014)
J7301	StTrGJBrN	$BrNO_3 + h\nu \rightarrow$ .85 Br + .85 NO_3 + .15 BrO + .15 NO_2	jx(ip_BrNO3)	Sander et al. (2014)*
J7400	StGJBr	$CH_3Br + h\nu \rightarrow Br + CH_3$	jx(ip_CH3Br)	Sander et al. (2014)
J7401	TrGJBr	$CH_2Br_2 + h\nu \rightarrow$ LCARBON + 2 Br	jx(ip_CH2Br2)	Sander et al. (2014)
J7402	TrGJBr	$CHBr_3 + h\nu \rightarrow$ LCARBON + 3 Br	jx(ip_CHBr3)	Sander et al. (2014)
J7500	StGJBrF	$CF_3Br + h\nu \rightarrow$ LCARBON + 3 LFLUORINE + Br	jx(ip_CF3Br)	Sander et al. (2014)
J7600	StTrGJBrCl	$BrCl + h\nu \rightarrow Br + Cl$	jx(ip_BrCl)	Sander et al. (2014)
J7601	StGJBrClF	$CF_2ClBr + h\nu \rightarrow$ LCARBON + 2 LFLUORINE + Br + Cl	jx(ip_CF2ClBr)	Sander et al. (2014)
J7602	TrGJBrCl	$CH_2ClBr + h\nu \rightarrow$ LCARBON + Br + Cl	jx(ip_CH2ClBr)	Sander et al. (2014)
J7603	TrGJBrCl	$CHCl_2Br + h\nu \rightarrow$ LCARBON + Br + 2 Cl	jx(ip_CHCl2Br)	Sander et al. (2014)
J7604	TrGJBrCl	$CHClBr_2 + h\nu \rightarrow$ LCARBON + 2 Br + Cl	jx(ip_CHClBr2)	Sander et al. (2014)
J8000	TrGJI	$I_2 + h\nu \rightarrow I + I$	jx(ip_I2)	Sander et al. (2014)
J8100	TrGJI	$IO + h\nu \rightarrow I + O(^3P)$	jx(ip_IO)	Sander et al. (2014)
J8200	TrGJI	$HOI + h\nu \rightarrow I + OH$	jx(ip_HOI)	Sander et al. (2014)
J8300	TrGJIN	$INO_2 + h\nu \rightarrow I + NO_2$	jx(ip_INO2)	Sander et al. (2014)
J8301	TrGJIN	$INO_3 + h\nu \rightarrow I + NO_3$	jx(ip_INO3)	Sander et al. (2014)
J8400	TrGJI	$CH_2I_2 + h\nu \rightarrow$ 2 I + 2 HO_2 + CO	jx(ip_CH2I2)	Sander et al. (2014)
J8401	TrGJI	$CH_3I + h\nu \rightarrow I + CH_3$	jx(ip_CH3I)	Sander et al. (2014)
J8402	TrGJCI	$CH_3CHICH_3 + h\nu \rightarrow$ 2 LCARBON + I + CH_3	jx(ip_C3H7I)	Sander et al. (2014)
J8403	TrGJClI	$CH_2ClI + h\nu \rightarrow I + Cl +$ 2 HO_2 + CO	jx(ip_CH2ClI)	Sander et al. (2014)
J8600	TrGJClI	$ICl + h\nu \rightarrow I + Cl$	jx(ip_ICl)	Sander et al. (2014)
J8700	TrGJBrI	$IBr + h\nu \rightarrow I + Br$	jx(ip_IBr)	Sander et al. (2014)
PH (aqueous)				

Table 2: Photolysis reactions (... continued)

#	labels	reaction	rate coefficient	reference
PH2100_a01	TrAa01ScJ	$H_2O_2(aq) + h\nu \rightarrow 2\ OH(aq)$	2.33*xaer(01)*jx(ip_H2O2)	see note*
PH3200_a01	TrAa01JN	$NO_3^-(aq) + h\nu \rightarrow NO_2(aq) + OH(aq) + OH^-(aq)$	xaer(01)*jx(ip_NO2) * 1.4E-4	see note*
PH4100_a01	TrAa01J	$HOCH_2OOH(aq) + h\nu \rightarrow HCOOH(aq) + OH(aq) + HO_2(aq)$	2.33*xaer(01)*jx(ip_CH3OOH)	Sander et al. (2014)
PH4101_a01	TrAa01J	$CH_3OOH(aq) + h\nu \rightarrow HCHO(aq) + OH(aq) + HO_2(aq)$	2.33*xaer(01)*jx(ip_CH3OOH)	Sander et al. (2014)
PH4200_a01	TrAa01JC	$C2H5OOH(aq) + h\nu \rightarrow CH_3CHO(aq) + HO_2(aq) + OH(aq)$	2.33*xaer(01)*jx(ip_CH3OOH)	von Kuhlmann (2001)*
PH4201_a01	TrAa01JC	$HOOCH2CO2H(aq) + h\nu \rightarrow HCHO(aq) + CO_2(aq) + HO_2(aq) + OH(aq)$	2.33*xaer(01)*jx(ip_CH3OOH)	Rickard and Pascoe (2009)*
PH4202_a01	TrAa01JC	$CH_2OOHCO_2^-(aq) + h\nu \rightarrow CHOHOOCOO_2^-(aq) + OH(aq)$	2.33*xaer(01)*jx(ip_CH3OOH)	see note*
PH4203_a01	TrAa01JC	$CH_3C(O)OOH(aq) + h\nu \rightarrow CH_3OO(aq) + CO_2(aq) + OH(aq)$	2.33*xaer(01)*jx(ip_CH3CO3H)	Sander et al. (2014)
PH4204_a01	TrAa01JC	$HOCH_2CO_3H(aq) + h\nu \rightarrow HCHO(aq) + OH(aq) + HO_2(aq) + CO_2(aq)$	2.33*xaer(01)*jx(ip_CH3OOH)	Rickard and Pascoe (2009)
PH4205_a01	TrAa01JC	$CH_3CHO(aq) + h\nu \rightarrow CH_3OO(aq) + HO_2(aq) + CO(aq)$	2.33*xaer(01)*jx(ip_CH3CHO)	Sander et al. (2014)
PH4206_a01	TrAa01JC	$CH_2OOHCHO(aq) + h\nu \rightarrow OH(aq) + HCHO(aq) + CO(aq) + HO_2(aq)$	2.33*xaer(01)*(jx(ip_CH3OOH) +jx(ip_HOCH2CHO))	Sander et al. (2019)
PH4207a_a01	TrAa01JC	$CH_2OHCHO(aq) + h\nu \rightarrow HCHO(aq) + 2\ HO_2(aq) + CO(aq)$	2.33*xaer(01)*jx(ip_HOCH2CHO) *0.83	Sander et al. (2014)*
PH4207b_a01	TrAa01JC	$CH_2OHCHO(aq) + h\nu \rightarrow OH(aq) + .6\ HCHO(aq) + .6\ CO(aq) + .6\ HO_2(aq) + .2\ GLYOX(aq) + .2\ CH_2OHCHO(aq)$	2.33*xaer(01)*jx(ip_HOCH2CHO) *0.07	Sander et al. (2014)*
PH4207c_a01	TrAa01JC	$CH_2OHCHO(aq) + h\nu \rightarrow CH_3OH(aq) + CO(aq)$	2.33*xaer(01)*jx(ip_HOCH2CHO) *0.10	Sander et al. (2014)*
PH4208_a01	TrAa01JC	$CHOCOOH(aq) + h\nu \rightarrow 2\ HO_2(aq) + CO(aq) + CO_2(aq)$	2.33*xaer(01)*jx(ip_MGLYOX)	Rickard and Pascoe (2009)
PH4209_a01	TrAa01JC	$GLYOX(aq) + h\nu \rightarrow 2\ CO(aq) + 2\ HO_2(aq)$	2.33*xaer(01)*jx(ip_GLYOX)	Sander et al. (2014)
PH4210a_a01	TrAa01JC	$HOOCCOOH(aq) + h\nu \rightarrow CO_2(aq) + HCOOH(aq)$	2.33*xaer(01)*0.72*jx(ip_ HOOCCOOH)	Yamamoto and Back (1985)
PH4210b_a01	TrAa01JC	$HOOCCOOH(aq) + h\nu \rightarrow CO_2(aq) + CO(aq) + H_2O(aq)$	2.33*xaer(01)*0.28*jx(ip_ HOOCCOOH)	Yamamoto and Back (1985)
PH4211_a01	TrAa01JC	$CHOCHOHOH(aq) + h\nu \rightarrow HCOOH(aq) + 2\ HO_2(aq) + CO(aq)$	2.33*xaer(01)*jx(ip_HOCH2CHO)	Sander et al. (2014)*
PH4300_a01	TrAa01JC	$CH_3COCH_2O_2H(aq) + h\nu \rightarrow CH_3COOO(aq) + HCHO(aq) + OH(aq)$	2.33*xaer(01)*(jx(ip_CH3OOH) +0.65*0.11*jx(ip_CHOH))	see note*
PH4301_a01	TrAa01JC	$iC_3H_7OOH(aq) + h\nu \rightarrow CH_3COCH_3(aq) + HO_2(aq) + OH(aq)$	2.33*xaer(01)*jx(ip_CH3OOH)	see note*
PH4302_a01	TrAa01JC	$CH_3COCH_2OH(aq) + h\nu \rightarrow .5\ OH(aq) + .5\ HCHO(aq) + .5\ CO(aq) + .5\ HCHO(aq) + .5\ HO_2(aq) + .5\ CH_2OHCO3(aq) + .5\ CH_3OO(aq)$	2.33*xaer(01)*0.65*0.11*jx(ip_ CHOH)	Sander et al. (2014)*

Table 2: Photolysis reactions (... continued)

#	labels	reaction	rate coefficient	reference
PH4303_a01	TrAa01JC	$CH_3C(O)CHO(aq) + h\nu \rightarrow OH(aq) + HCHO(aq) + CO(aq) + CO(aq) + HO_2(aq)$	2.33*xaer(01)*jx(ip_MGLYOX)	Sander et al. (2014)*
PH10200_a01	TrAa01JHg	$Hg(OH)_2(aq) + h\nu \rightarrow Hg(aq)$	xaer(01)*6E-5*jx(ip_NO2)	see note*
PH11200_a01	TrAa01JFe	$FeOH^{2+}(aq) + h\nu \rightarrow Fe^{2+}(aq) + OH(aq)$	xaer(01)*4.51E-3*0.312	Herrmann et al. (2000)
PH11201_a01	TrAa01JFe	$Fe(OH)_2^+(aq) + h\nu \rightarrow Fe^{2+}(aq) + OH(aq) + OH^-(aq)$	xaer(01)*5.77E-3*0.255	Herrmann et al. (2000)
PH11800_a01	TrAa01JFeS	$FeSO_4^+(aq) + h\nu \rightarrow Fe^{2+}(aq) + SO_4^-(aq)$	xaer(01)*6.43E-3*7.9E-3	Herrmann et al. (2000)

General notes

j-values are calculated with an external module (e.g., JVAL) and then supplied to the MECCA chemistry.

Values that originate from the Master Chemical Mechanism (MCM) by Rickard and Pascoe (2009) are translated according in the following way:
j(11) → jx(ip_COH2)
j(12) → jx(ip_CHOH)
j(15) → jx(ip_HOCH2CHO)
j(18) → jx(ip_MACR)
j(22) → jx(ip_ACETOL)
j(23)+j(24) → jx(ip_MVK)
j(31)+j(32)+j(33) → jx(ip_GLYOX)
j(34) → jx(ip_MGLYOX)
j(41) → jx(ip_CH3OOH)
j(53) → j(isopropyl nitrate)
j(54) → j(isopropyl nitrate)
j(55) → j(isopropyl nitrate)
j(56)+j(57) → jx(ip_NOA)

Specific notes

J41003: CH_3- and CH_2-channels are considered only and with their branching ratios being 0.42 and 0.48, respectively (Gans et al., 2011). CH-production is neglected. CH_2 is assumed to react only with O2 yielding 1.44 H_2 + 0.18 HCHO + 0.18 $O(^3P)$ + 0.33 OH + 0.33 HO_2 + 0.44 CO_2 + 0.38 CO + 0.05 H_2O as assumed in the WACCM model by J. Orlando (Doug Kinnison, pers. comm. with D. Taraborrelli).

J41006: product distribution as for HNO4

J42004: Quantum yields from Burkholder et al. (2015).

J42005a: Quantum yields from Burkholder et al. (2015).

J42005b: Quantum yields from Burkholder et al. (2015).

J42005c: Quantum yields from Burkholder et al. (2015).

J42007: It is assumed that J(PHAN) is the same as J(PAN).

J42017: Enhancement of j according to Müller et al. (2014).

J42020: It is assumed that j(NO_3CH2CHO) is the same as j(PAN).

J42021: In analogy to what is assumed for $CH_3O_2NO_2$ photolysis as in (Sander et al., 2014).

J43002: Following von Kuhlmann et al. (2003), we use j(CH_3COCH_2OH) = 0.11*jx(ip_CHOH). As an additional factor, the quantum yield of 0.65 is taken from Orlando et al. (1999a).

J43006: Following von Kuhlmann et al. (2003), we use J($iC_3H_7ONO_2$) = 3.7*jx(ip_PAN).

J43018: One third of the acetaldehyde channel is considered to be CH2CHOH according to Hjorth (2002) EUPHORE Report.

J43024: Assuming J($C_3H_7ONO_2$) = 0.59 × J($iC_3H_7ONO_2$), consistent with the photolysis rate coefficients used in the MCM (Rickard and Pascoe, 2009).

J43025a: Photolysis frequencies very similar to the ones of CH_3CHO.

J43025b: Photolysis frequencies very similar to the ones of CH_3CHO.

J43400: KDEC C3DIALO → GLYOX + CO + HO2

J44004: It is assumed that J(BIACET) is 2.15 times larger than J(MGLYOX), consistent with the photolysis rate coefficients used in the MCM (Rickard and Pascoe, 2009).

J44005a: It is assumed that J(LC4H9NO3) is the same as J($iC_3H_7ONO_2$).

J44005b: It is assumed that J(LC4H9NO3) is the same as J($iC_3H_7ONO_2$).

J44006: It is assumed that J(MPAN) is the same as J(PAN).

J44009: It is assumed that J(MACROOH) is 2.77 times larger than J($HOCH_2CHO$), consistent with the photolysis rate coefficients used in the MCM (Rickard and Pascoe, 2009).

J44010: It is assumed that J(MACROH) is 2.77 times larger than J($HOCH_2CHO$), consistent with the photolysis rate coefficients used in the MCM (Rickard and Pascoe, 2009).

J44015: It is assumed that J(BIACETOH) is 2.15 times larger than J(MGLYOX), consistent with the photolysis rate coefficients used in the MCM (Rickard and Pascoe, 2009).

J44017a: CO-channel yielding CH_3COCH which upon reaction with O_2 produces an excited Criegee Intermediate assumed to be similar to MGLOOA in MCM. MGLOOA is produced also in other reactions and is substituted by its decomposition products. Furthermore, the stabilized Criegge Intermediate is assumed to solely react with water.

J44025: J values only for the secondary nitrate.

J44026: Like for LMEKNO3 photolysis

J44027: 2.84*J_IC3H7NO3 like for other tertiary alkyl nitrates (see J4505). Enhancement of J according to Müller et al. (2014).

J44037b: Channel which produces just vinyl alcohol and not a larger enol via keto-enol phototautomerization.

J44043: The resulting vinyl peroxy radical is assumed to mostly form with HO_2 a labile hydroperoxide (see ketene formation). The products are further simplified.

J44044: 1,5-H-shift for the resulting vinyl peroxy radical assumed to be dominant.

J44046a: Simplified oxidation.

J44400b: KDEC MALDIALO → GLYOX + GLYOX + HO2

J44401: KDEC BZFUO → CO14O3CHO + HO2

J44403: KDEC NBZFUO → 0.5 CO14O3CHO + 0.5 NO2 + 0.5 NBZFUONE + 0.5 HO2

J44404b: KDEC MALDIALCO2 → 0.6 MALANHY + HO2 + 0.4 GLYOX + 0.4 CO

J44407: KDEC MALANHYO → HCOCOHCO3

J44414: KDEC MECOACETO → CH3CO3 + HCHO

J45003: It is assumed that J(LISOPACNO3) = 0.59 × J($iC_3H_7ONO_2$), consistent with the photolysis rate coefficients used in the MCM (Rickard and Pascoe, 2009).

J45005: It is assumed that J(ISOPBNO3) = 2.84 × J($iC_3H_7ONO_2$), consistent with the photolysis rate coefficients used in the MCM (Rickard and Pascoe, 2009).

J45007: It is assumed that J(ISOPDNO3) is the same as J($iC_3H_7ONO_2$).

J45009: 0.59*J_IC3H7NO3 like for other primary alkyl nitrates (see J4503). Enhancement of J according to Müller et al. (2014).

J45015: Consistent with the MCM (Rickard and Pascoe, 2009), we assume that J(HCOC5) is half as large as J(MVK). With exeption of HOCH2CO the products of MACO2 decomposition without CO_2.

J45032: approximation with 4-oxo-pentenal photolysis combining results of Thner et al(2004) and Xiang et al(2007)

J45402: KDEC C5DIALO → MALDIAL + CO + HO2

J45407: KDEC TLFUONE → 0.6 C5CO14O2 + 0.6 HO2 + 0.4 TLFUONE

J45410: KDEC MMALANHYO → CO2H3CO3

J45411: KDEC C5DICARBO → MGLYOX + GLYOX + HO2

J45412: KDEC NTLFUO → ACCOMECHO + NO2

J45414: KDEC C5CO14CO2 → 0.83 MALANHY + 0.83 CH3 + .17 MGLYOX + .17 HO2 + .17 CO + .17 CO2

J45415: KDEC TLFUO → ACCOMECHO + HO2

J46400: KDEC PHENO → 0.71 MALDALCO2H + 0.71 GLYOX + 0.29 PBZQONE + HO2

J46403: KDEC NDNPHENO → NC4DCO2H + HNO3 + CO + CO + NO2

J46404: KDEC BZBIPERO → GLYOX + HO2 + 0.5 BZFUONE + 0.5 BZFUONE

J46405: new channel created for nitrophenol decomposition

J46406: new channel created for nitrophenol decomposition

J46412: KDEC NNCATECO → NC4DCO2H + HCOCO2H + NO2

J46415: KDEC NCATECO → NC4DCO2H + HCOCO2H + HO2

J46416: KDEC PBZQO → C5CO2OHCO3

J46418: KDEC BZBIPERO → GLYOX + HO2 + 0.5 BZFUONE + 0.5 BZFUONE

J46419: KDEC NBZQO → C6CO4DB + NO2

J46422: KDEC DNPHENO → NC4DCO2H + HCOCO2H + NO2

J46425: KDEC BZEMUCO → 0.5 EPXC4DIAL + .5 GLYOX + .5 HO2 + .5 C3DIALO2 + .5 C32OH13CO

J46429: new channel

J47401: KROPRIM*O2 fast reaction C6H5CH2O = BENZAL + HO2

J47402: KROPRIM*O2 fast reaction C6H5CH2O = BENZAL + HO2

J47404: KDEC TLBIPERO → 0.6 GLYOX + 0.4 MGLYOX + HO2 + 0.2 C4MDIAL + 0.2 C5DICARB + 0.2 TLFUONE + 0.2 BZFUONE + 0.2 MALDIAL

J47405: KDEC TLBIPERO → 0.6 GLYOX + 0.4 MGLYOX + HO2 + 0.2 C4MDIAL + 0.2 C5DICARB + 0.2 TLFUONE + 0.2 BZFUONE + 0.2 MALDIAL

J47407: KDEC CRESO → 0.68 C5CO14OH + 0.68 GLYOX + HO2 + 0.32 PTLQONE

J47408a: KDEC CRESO → 0.68 C5CO14OH + 0.68 GLYOX + HO2 + 0.32 PTLQONE

J47408b: KDEC NCRESO → C5CO14OH + GLYOX + NO2

J47409: Using J for 3-methyl-2-nitrophenol.

J47412: KDEC TLEMUCO → 0.5 C3DIALO2 + 0.5 CO2H3CHO + 0.5 EPXC4DIAL + 0.5 MGLYOX + 0.5 HO2

J47417: Using J for 3-methyl-2-nitrophenol.

J47418: new channel

J47419: Using J for 3-methyl-2-nitrophenol.

J47420: new channel

J47422: KDEC NPTLQO → C7CO4DB + NO2

J47423: KDEC PTLQO → C6CO2OHCO3

J47425: KDEC MNNCATECO → NC4MDCO2H + HCOCO2H + NO2

J47426: KDEC MNCATECO → NC4MDCO2H + HCOCO2H + HO2

J47428: KDEC NDNCRESO → NC4MDCO2H + HNO3 + CO + CO + NO2

J47429: KDEC DNCRESO → NC4MDCO2H + HCOCO2H + NO2

J48400: KDEC STYRENO → HO2 + HCHO + BENZAL

J40203b: Substituted vinyl alcohol in analogy to CH_3CHO photolysis.

J6500: Even though the elementary reaction produces only 1 Cl atom (Felder and Demuth, 1993), it is assumed here that eventually all Cl atoms are released in secondary reactions.

J6501: Even though the elementary reaction probably produces only 1 Cl atom (as for $CFCl_3$), it is assumed here that eventually all Cl atoms are released in secondary reactions.

J7301: The quantum yields are recommended by Burkholder et al. (2015) for $\lambda > 300$nm and used here for the entire spectrum.

PH2100_a01: 2.33 times the gas-phase value

PH3200_a01: Scaled to $J(NO_2)$ so that its lifetime is about 10.5 days, as suggested by Zellner et al. (1990).

PH4200_a01: CH3CHOHO2 is assumed to directly decompose into CH3CHO + HO2

PH4201_a01: COOHOO is not formed but directly dissociates into CO2 + HO2

PH4202_a01: assumed to be the same as C2H5OOH + hv

PH4207a_a01: Quantum yields from Burkholder et al. (2015).

PH4207b_a01: Quantum yields from Burkholder et al. (2015). HCOCH2O2 decomposes directly to .6 HCHO + .6 CO + .6 HO2 + .2 GLYOX + .2 HOCH2CHO

PH4207c_a01: Quantum yields from Burkholder et al. (2015).

PH4211_a01: Assumed in analogy to the main channel for j(HOCH2CHO).

PH4300_a01: 2.33* k from the gas-phase reaction, CH3CO directly reacts with O2 to form CH3CO3

PH4301_a01: 2.33 * k from the gas-phase reaction,

PH4302_a01: Following von Kuhlmann et al. (2003), we use $j(CH_3COCH_2OH)$ = `0.11*jx(ip_CHOH)`. As an additional factor, the quantum yield of 0.65 is taken from Orlando et al. (1999a). CH3CO reacts with O2 to form OH + HCHO + CO. HOCH2CO reacts with O2 to form HOCH2CO3

PH4303_a01: CH3CO reacts with O2 to form OH + HCHO + CO

PH10200_a01: Scaled to $J(NO_2)$ so that it produces about 3.0×10^{-7}.

Table 3: Reversible (Henry's law) equilibria and irreversible ("heterogenous") uptake

#	labels	reaction	rate coefficient	reference
H10000f_a01	TrAa01Sc	$O_2 \rightarrow O_2(aq)$	k_exf(01,ind_O2)	see general notes*
H10000b_a01	TrAa01Sc	$O_2(aq) \rightarrow O_2$	k_exb(01,ind_O2)	see general notes*
H10001f_a01	TrAa01MblScScm	$O_3 \rightarrow O_3(aq)$	k_exf(01,ind_O3)	see general notes*
H10001b_a01	TrAa01MblScScm	$O_3(aq) \rightarrow O_3$	k_exb(01,ind_O3)	see general notes*
H21000f_a01	TrAa01Sc	$OH \rightarrow OH(aq)$	k_exf(01,ind_OH)	see general notes*
H21000b_a01	TrAa01Sc	$OH(aq) \rightarrow OH$	k_exb(01,ind_OH)	see general notes*
H21001f_a01	TrAa01Sc	$HO_2 \rightarrow HO_2(aq)$	k_exf(01,ind_HO2)	see general notes*
H21001b_a01	TrAa01Sc	$HO_2(aq) \rightarrow HO_2$	k_exb(01,ind_HO2)	see general notes*
H21002f_a01	TrAa01MblScScm	$H_2O_2 \rightarrow H_2O_2(aq)$	k_exf(01,ind_H2O2)	see general notes*
H21002b_a01	TrAa01MblScScm	$H_2O_2(aq) \rightarrow H_2O_2$	k_exb(01,ind_H2O2)	see general notes*
H31000f_a01	TrAa01ScN	$NO \rightarrow NO(aq)$	k_exf(01,ind_NO)	see general notes*
H31000b_a01	TrAa01ScN	$NO(aq) \rightarrow NO$	k_exb(01,ind_NO)	see general notes*
H31001f_a01	TrAa01ScN	$NO_2 \rightarrow NO_2(aq)$	k_exf(01,ind_NO2)	see general notes*
H31001b_a01	TrAa01ScN	$NO_2(aq) \rightarrow NO_2$	k_exb(01,ind_NO2)	see general notes*
H31002f_a01	TrAa01ScN	$NO_3 \rightarrow NO_3(aq)$	k_exf(01,ind_NO3)	see general notes*
H31002b_a01	TrAa01ScN	$NO_3(aq) \rightarrow NO_3$	k_exb(01,ind_NO3)	see general notes*
H32000f_a01	TrAa01MblScScmN	$NH_3 \rightarrow NH_3(aq)$	k_exf(01,ind_NH3)	see general notes*
H32000b_a01	TrAa01MblScScmN	$NH_3(aq) \rightarrow NH_3$	k_exb(01,ind_NH3)	see general notes*
H32001_a01	TrAa01MblScScmN	$N_2O_5 \rightarrow HNO_3(aq) + HNO_3(aq)$	k_exf_N2O5(01)*C(ind_H2O_a01)	Behnke et al. (1994), Behnke et al. (1997)
H32002f_a01	TrAa01ScN	$HONO \rightarrow HONO(aq)$	k_exf(01,ind_HONO)	see general notes*
H32002b_a01	TrAa01ScN	$HONO(aq) \rightarrow HONO$	k_exb(01,ind_HONO)	see general notes*
H32003f_a01	TrAa01MblScScmN	$HNO_3 \rightarrow HNO_3(aq)$	k_exf(01,ind_HNO3)	see general notes*
H32003b_a01	TrAa01MblScScmN	$HNO_3(aq) \rightarrow HNO_3$	k_exb(01,ind_HNO3)	see general notes*
H32004f_a01	TrAa01ScN	$HNO_4 \rightarrow HNO_4(aq)$	k_exf(01,ind_HNO4)	see general notes*
H32004b_a01	TrAa01ScN	$HNO_4(aq) \rightarrow HNO_4$	k_exb(01,ind_HNO4)	see general notes*
H41000f_a01	TrAa01MblScScm	$CO_2 \rightarrow CO_2(aq)$	k_exf(01,ind_CO2)	see general notes*
H41000b_a01	TrAa01MblScScm	$CO_2(aq) \rightarrow CO_2$	k_exb(01,ind_CO2)	see general notes*
H41001f_a01	TrAa01ScScm	$HCHO \rightarrow HCHO(aq)$	k_exf(01,ind_HCHO)	see general notes*
H41001b_a01	TrAa01ScScm	$HCHO(aq) \rightarrow HCHO$	k_exb(01,ind_HCHO)	see general notes*
H41002f_a01	TrAa01Sc	$CH_3O_2 \rightarrow CH_3OO(aq)$	k_exf(01,ind_CH3O2)	see general notes*
H41002b_a01	TrAa01Sc	$CH_3OO(aq) \rightarrow CH_3O_2$	k_exb(01,ind_CH3O2)	see general notes*
H41003f_a01	TrAa01ScScm	$HCOOH \rightarrow HCOOH(aq)$	k_exf(01,ind_HCOOH)	see general notes*
H41003b_a01	TrAa01ScScm	$HCOOH(aq) \rightarrow HCOOH$	k_exb(01,ind_HCOOH)	see general notes*

Table 3: Reversible (Henry's law) equilibria and irreversible ("heterogenous") uptake

#	labels	reaction	rate coefficient	reference
H41004f_a01	TrAa01ScScm	$CH_3OOH \rightarrow CH_3OOH(aq)$	k_exf(01,ind_CH3OOH)	see general notes*
H41004b_a01	TrAa01ScScm	$CH_3OOH(aq) \rightarrow CH_3OOH$	k_exb(01,ind_CH3OOH)	see general notes*
H41005f_a01	TrAa01Sc	$CH_3OH \rightarrow CH_3OH(aq)$	k_exf(01,ind_CH3OH)	see general notes*
H41005b_a01	TrAa01Sc	$CH_3OH(aq) \rightarrow CH_3OH$	k_exb(01,ind_CH3OH)	see general notes*
H41006f_a01	TrAa01	$HOCH_2OH \rightarrow HOCH_2OH(aq)$	k_exf(01,ind_HOCH2OH)	see general notes*
H41006b_a01	TrAa01	$HOCH_2OH(aq) \rightarrow HOCH_2OH$	k_exb(01,ind_HOCH2OH)	see general notes*
H41007f_a01	TrAa01	$HOCH_2OOH \rightarrow HOCH_2OOH(aq)$	k_exf(01,ind_HOCH2OOH)	see general notes*
H41007b_a01	TrAa01	$HOCH_2OOH(aq) \rightarrow HOCH_2OOH$	k_exb(01,ind_HOCH2OOH)	see general notes*
H41008f_a01	TrAa01	$CO \rightarrow CO(aq)$	k_exf(01,ind_CO)	see general notes*
H41008b_a01	TrAa01	$CO(aq) \rightarrow CO$	k_exb(01,ind_CO)	see general notes*
H42000f_a01	TrAa01ScScmC	$CH_3COOH \rightarrow CH_3COOH(aq)$	k_exf(01,ind_CH3CO2H)	see general notes*
H42000b_a01	TrAa01ScScmC	$CH_3COOH(aq) \rightarrow CH_3COOH$	k_exb(01,ind_CH3CO2H)	see general notes*
H42001f_a01	TrAa01ScC	$CH_3CHO \rightarrow CH_3CHO(aq)$	k_exf(01,ind_CH3CHO)	see general notes*
H42001b_a01	TrAa01ScC	$CH_3CHO(aq) \rightarrow CH_3CHO$	k_exb(01,ind_CH3CHO)	see general notes*
H42002f_a01	TrAa01ScCN	$PAN \rightarrow PAN(aq)$	k_exf(01,ind_PAN)	see general notes*
H42002b_a01	TrAa01ScCN	$PAN(aq) \rightarrow PAN$	k_exb(01,ind_PAN)	see general notes*
H42003f_a01	TrAa01C	$C_2H_5OH \rightarrow CH_3CH_2OH(aq)$	k_exf(01,ind_C2H5OH)	see general notes*
H42003b_a01	TrAa01C	$CH_3CH_2OH(aq) \rightarrow C_2H_5OH$	k_exb(01,ind_C2H5OH)	see general notes*
H42004f_a01	TrAa01C	$ETHGLY \rightarrow ETHGLY(aq)$	k_exf(01,ind_ETHGLY)	see general notes*
H42004b_a01	TrAa01C	$ETHGLY(aq) \rightarrow ETHGLY$	k_exb(01,ind_ETHGLY)	see general notes*
H42006f_a01	TrAa01C	$CH_3C(O)OO \rightarrow CH_3COOO(aq)$	k_exf(01,ind_CH3CO3)	see general notes*
H42006b_a01	TrAa01C	$CH_3COOO(aq) \rightarrow CH_3C(O)OO$	k_exb(01,ind_CH3CO3)	see general notes*
H42007f_a01	TrAa01C	$HOCH_2CHO \rightarrow CH_2OHCHO(aq)$	k_exf(01,ind_HOCH2CHO)	see general notes*
H42007b_a01	TrAa01C	$CH_2OHCHO(aq) \rightarrow HOCH_2CHO$	k_exb(01,ind_HOCH2CHO)	see general notes*
H42008f_a01	TrAa01C	$GLYOX \rightarrow GLYOX(aq)$	k_exf(01,ind_GLYOX)	see general notes*
H42008b_a01	TrAa01C	$GLYOX(aq) \rightarrow GLYOX$	k_exb(01,ind_GLYOX)	see general notes*
H42009f_a01	TrAa01C	$CH_3C(O)OOH \rightarrow CH_3C(O)OOH(aq)$	k_exf(01,ind_CH3CO3H)	see general notes*
H42009b_a01	TrAa01C	$CH_3C(O)OOH(aq) \rightarrow CH_3C(O)OOH$	k_exb(01,ind_CH3CO3H)	see general notes*
H42010f_a01	TrAa01C	$HOCH_2CO_3H \rightarrow HOCH_2CO_3H(aq)$	k_exf(01,ind_HOCH2CO3H)	see general notes*
H42010b_a01	TrAa01C	$HOCH_2CO_3H(aq) \rightarrow HOCH_2CO_3H$	k_exb(01,ind_HOCH2CO3H)	see general notes*
H42011f_a01	TrAa01C	$C_2H_5OOH \rightarrow C2H5OOH(aq)$	k_exf(01,ind_C2H5OOH)	see general notes*
H42011b_a01	TrAa01C	$C2H5OOH(aq) \rightarrow C_2H_5OOH$	k_exb(01,ind_C2H5OOH)	see general notes*
H42012f_a01	TrAa01C	$HOOCCOOH \rightarrow HOOCCOOH(aq)$	k_exf(01,ind_HOOCCOOH)	see general notes*
H42012b_a01	TrAa01C	$HOOCCOOH(aq) \rightarrow HOOCCOOH$	k_exb(01,ind_HOOCCOOH)	see general notes*
H42013f_a01	TrAa01C	$HOOCH2CO2H \rightarrow HOOCH2CO2H(aq)$	k_exf(01,ind_HOOCH2CO2H)	see general notes*

Table 3: Reversible (Henry's law) equilibria and irreversible ("heterogenous") uptake

#	labels	reaction	rate coefficient	reference
H42013b_a01	TrAa01C	HOOCH2CO2H(aq) → HOOCH2CO2H	k_exb(01,ind_HOOCH2CO2H)	see general notes*
H42014f_a01	TrAa01C	$HOCH_2CO_2H$ → $HOCH_2CO_2H$(aq)	k_exf(01,ind_HOCH2CO2H)	see general notes*
H42014b_a01	TrAa01C	$HOCH_2CO_2H$(aq) → $HOCH_2CO_2H$	k_exb(01,ind_HOCH2CO2H)	see general notes*
H42015f_a01	TrAa01C	$HCOCO_2H$ → CHOCOOH(aq)	k_exf(01,ind_HCOCO2H)	see general notes*
H42015b_a01	TrAa01C	CHOCOOH(aq) → $HCOCO_2H$	k_exb(01,ind_HCOCO2H)	see general notes*
H42017f_a01	TrAa01CN	$C_2H_5ONO_2$ → $C_2H_5ONO_2$(aq)	k_exf(01,ind_C2H5NO3)	see general notes*
H42017b_a01	TrAa01CN	$C_2H_5ONO_2$(aq) → $C_2H_5ONO_2$	k_exb(01,ind_C2H5NO3)	see general notes*
H42018f_a01	TrAa01CN	CH_3CN → CH_3CN(aq)	k_exf(01,ind_CH3CN)	see general notes*
H42018b_a01	TrAa01CN	CH_3CN(aq) → CH_3CN	k_exb(01,ind_CH3CN)	see general notes*
H42019f_a01	TrAa01C	$HOCH_2CHOHOH$ → $CH_2OHCHOHOH$(aq)	k_exf(01,ind_HOCH2CHOHOH)	see general notes*
H42019b_a01	TrAa01C	$CH_2OHCHOHOH$(aq) → $HOCH_2CHOHOH$	k_exb(01,ind_HOCH2CHOHOH)	see general notes*
H42020f_a01	TrAa01C	$CH_3CHOHOH$ → $CH_3CHOHOH$(aq)	k_exf(01,ind_CH3CHOHOH)	see general notes*
H42020b_a01	TrAa01C	$CH_3CHOHOH$(aq) → $CH_3CHOHOH$	k_exb(01,ind_CH3CHOHOH)	see general notes*
H42021f_a01	TrAa01C	CHOHOHCOOH → CHOOHOHCOOH(aq)	k_exf(01,ind_CHOHOHCOOH)	see general notes*
H42021b_a01	TrAa01C	CHOOHOHCOOH(aq) → CHOHOHCOOH	k_exb(01,ind_CHOHOHCOOH)	see general notes*
H42022f_a01	TrAa01C	CHOHOHCHOHOH → CHOHOHCHOHOH(aq)	k_exf(01,ind_CHOHOHCHOHOH)	see general notes*
H42022b_a01	TrAa01C	CHOHOHCHOHOH(aq) → CHOHOHCHOHOH	k_exb(01,ind_CHOHOHCHOHOH)	see general notes*
H42023f_a01	TrAa01C	HOOCH2CHO → $CH_2OOHCHO$(aq)	k_exf(01,ind_HOOCH2CHO)	see general notes*
H42023b_a01	TrAa01C	$CH_2OOHCHO$(aq) → HOOCH2CHO	k_exb(01,ind_HOOCH2CHO)	see general notes*
H42024f_a01	TrAa01C	CHOCHOHOH → CHOCHOHOH(aq)	k_exf(01,ind_CHOCHOHOH)	see general notes*
H42024b_a01	TrAa01C	CHOCHOHOH(aq) → CHOCHOHOH	k_exb(01,ind_CHOCHOHOH)	see general notes*
H42025f_a01	TrAa01C	$HOOCH_2CHOHOH$ → $HOOCH_2CHOHOH$(aq)	k_exf(01,ind_HOOCH2CHOHOH)	see general notes*
H42025b_a01	TrAa01C	$HOOCH_2CHOHOH$(aq) → $HOOCH_2CHOHOH$	k_exb(01,ind_HOOCH2CHOHOH)	see general notes*
H42026f_a01	TrAa01C	CH2CO → CH2CO(aq)	k_exf(01,ind_CH2CO)	see general notes*
H42026b_a01	TrAa01C	CH2CO(aq) → CH2CO	k_exb(01,ind_CH2CO)	see general notes*
H42027f_a01	TrAa01C	CH3CHOHOOH → CH3CHOHOOH(aq)	k_exf(01,ind_CH3CHOHOOH)	see general notes*
H42027b_a01	TrAa01C	CH3CHOHOOH(aq) → CH3CHOHOOH	k_exb(01,ind_CH3CHOHOOH)	see general notes*
H42028f_a01	TrAa01CN	ETHOHNO3 → ETHOHNO3(aq)	k_exf(01,ind_ETHOHNO3)	see general notes*
H42028b_a01	TrAa01CN	ETHOHNO3(aq) → ETHOHNO3	k_exb(01,ind_ETHOHNO3)	see general notes*
H42029f_a01	TrAa01C	$HCOCO_3H$ → $HCOCO_3H$(aq)	k_exf(01,ind_HCOCO3H)	see general notes*
H42029b_a01	TrAa01C	$HCOCO_3H$(aq) → $HCOCO_3H$	k_exb(01,ind_HCOCO3H)	see general notes*

Table 3: Reversible (Henry's law) equilibria and irreversible ("heterogenous") uptake

#	labels	reaction	rate coefficient	reference
H42030f_a01	TrAa01C	HOOCH2CO3H → HOOCH2CO3H(aq)	k_exf(01,ind_HOOCH2CO3H)	see general notes*
H42030b_a01	TrAa01C	HOOCH2CO3H(aq) → HOOCH2CO3H	k_exb(01,ind_HOOCH2CO3H)	see general notes*
H42031f_a01	TrAa01C	HYETHO2H → HYETHO2H(aq)	k_exf(01,ind_HYETHO2H)	see general notes*
H42031b_a01	TrAa01C	HYETHO2H(aq) → HYETHO2H	k_exb(01,ind_HYETHO2H)	see general notes*
H42032f_a01	TrAa01CN	PHAN → PHAN(aq)	k_exf(01,ind_PHAN)	see general notes*
H42032b_a01	TrAa01CN	PHAN(aq) → PHAN	k_exb(01,ind_PHAN)	see general notes*
H43000f_a01	TrAa01ScC	CH_3COCH_3 → CH_3COCH_3(aq)	k_exf(01,ind_CH3COCH3)	see general notes*
H43000b_a01	TrAa01ScC	CH_3COCH_3(aq) → CH_3COCH_3	k_exb(01,ind_CH3COCH3)	see general notes*
H43001f_a01	TrAa01C	MGLYOX → $CH_3C(O)CHO$(aq)	k_exf(01,ind_MGLYOX)	see general notes*
H43001b_a01	TrAa01C	$CH_3C(O)CHO$(aq) → MGLYOX	k_exb(01,ind_MGLYOX)	see general notes*
H43002f_a01	TrAa01C	CH_3COCO_2H → $CH_3COCOOH$(aq)	k_exf(01,ind_CH3COCO2H)	see general notes*
H43002b_a01	TrAa01C	$CH_3COCOOH$(aq) → CH_3COCO_2H	k_exb(01,ind_CH3COCO2H)	see general notes*
H43003f_a01	TrAa01C	$CH_3COCHOHOH$ → $CH_3COCHOHOH$(aq)	k_exf(01,ind_CH3COCHOHOH)	see general notes*
H43003b_a01	TrAa01C	$CH_3COCHOHOH$(aq) → $CH_3COCHOHOH$	k_exb(01,ind_CH3COCHOHOH)	see general notes*
H43005f_a01	TrAa01C	IPROPOL → IPROPOL(aq)	k_exf(01,ind_IPROPOL)	see general notes*
H43005b_a01	TrAa01C	IPROPOL(aq) → IPROPOL	k_exb(01,ind_IPROPOL)	see general notes*
H43006f_a01	TrAa01C	$CH_3COCH_2O_2H$ → $CH_3COCH_2O_2H$(aq)	k_exf(01,ind_HYPERACET)	see general notes*
H43006b_a01	TrAa01C	$CH_3COCH_2O_2H$(aq) → $CH_3COCH_2O_2H$	k_exb(01,ind_HYPERACET)	see general notes*
H43007f_a01	TrAa01C	iC_3H_7OOH → iC_3H_7OOH(aq)	k_exf(01,ind_IC3H7OOH)	see general notes*
H43007b_a01	TrAa01C	iC_3H_7OOH(aq) → iC_3H_7OOH	k_exb(01,ind_IC3H7OOH)	see general notes*
H43008f_a01	TrAa01C	$HCOCOCH_2OOH$ → $HCOCOCH_2OOH$(aq)	k_exf(01,ind_ALCOCH2OOH)	see general notes*
H43008b_a01	TrAa01C	$HCOCOCH_2OOH$(aq) → $HCOCOCH_2OOH$	k_exb(01,ind_ALCOCH2OOH)	see general notes*
H43009f_a01	TrAa01C	C32OH13CO → C32OH13CO(aq)	k_exf(01,ind_C32OH13CO)	see general notes*
H43009b_a01	TrAa01C	C32OH13CO(aq) → C32OH13CO	k_exb(01,ind_C32OH13CO)	see general notes*
H43010f_a01	TrAa01C	HCOCOCHO → HCOCOCHO(aq)	k_exf(01,ind_C33CO)	see general notes*
H43010b_a01	TrAa01C	HCOCOCHO(aq) → HCOCOCHO	k_exb(01,ind_C33CO)	see general notes*
H43011f_a01	TrAa01C	C3DIALOOH → C3DIALOOH(aq)	k_exf(01,ind_C3DIALOOH)	see general notes*
H43011b_a01	TrAa01C	C3DIALOOH(aq) → C3DIALOOH	k_exb(01,ind_C3DIALOOH)	see general notes*
H43012f_a01	TrAa01CN	C_3PAN1 → C_3PAN1(aq)	k_exf(01,ind_C3PAN1)	see general notes*
H43012b_a01	TrAa01CN	C_3PAN1(aq) → C_3PAN1	k_exb(01,ind_C3PAN1)	see general notes*
H43013f_a01	TrAa01CN	C_3PAN2 → C_3PAN2(aq)	k_exf(01,ind_C3PAN2)	see general notes*
H43013b_a01	TrAa01CN	C_3PAN2(aq) → C_3PAN2	k_exb(01,ind_C3PAN2)	see general notes*
H43014f_a01	TrAa01C	CH3CHCO → CH3CHCO(aq)	k_exf(01,ind_CH3CHCO)	see general notes*
H43014b_a01	TrAa01C	CH3CHCO(aq) → CH3CHCO	k_exb(01,ind_CH3CHCO)	see general notes*

Table 3: Reversible (Henry's law) equilibria and irreversible ("heterogenous") uptake

#	labels	reaction		rate coefficient	reference
H43015f_a01	TrAa01CN	$CH_3COCH_2OONO_2$	→	k_exf(01,ind_CH3COCH2O2NO2)	see general notes*
		$CH_3COCH_2OONO_2$(aq)			
H43015b_a01	TrAa01CN	$CH_3COCH_2OONO_2$(aq)	→	k_exb(01,ind_CH3COCH2O2NO2)	see general notes*
		$CH_3COCH_2OONO_2$			
H43016f_a01	TrAa01C	CH_3COCO_3H → CH_3COCO_3H(aq)		k_exf(01,ind_CH3COCO3H)	see general notes*
H43016b_a01	TrAa01C	CH_3COCO_3H(aq) → CH_3COCO_3H		k_exb(01,ind_CH3COCO3H)	see general notes*
H43017f_a01	TrAa01C	HCOCH2CHO → HCOCH2CHO(aq)		k_exf(01,ind_HCOCH2CHO)	see general notes*
H43017b_a01	TrAa01C	HCOCH2CHO(aq) → HCOCH2CHO		k_exb(01,ind_HCOCH2CHO)	see general notes*
H43018f_a01	TrAa01C	HCOCH2CO2H → HCOCH2CO2H(aq)		k_exf(01,ind_HCOCH2CO2H)	see general notes*
H43018b_a01	TrAa01C	HCOCH2CO2H(aq) → HCOCH2CO2H		k_exb(01,ind_HCOCH2CO2H)	see general notes*
H43019f_a01	TrAa01C	HCOCH2CO3H → HCOCH2CO3H(aq)		k_exf(01,ind_HCOCH2CO3H)	see general notes*
H43019b_a01	TrAa01C	HCOCH2CO3H(aq) → HCOCH2CO3H		k_exb(01,ind_HCOCH2CO3H)	see general notes*
H43020f_a01	TrAa01C	$HCOCOCH_2OOH$ → $HCOCOCH_2OOH$(aq)		k_exf(01,ind_HCOCOCH2OOH)	see general notes*
H43020b_a01	TrAa01C	$HCOCOCH_2OOH$(aq) → $HCOCOCH_2OOH$		k_exb(01,ind_HCOCOCH2OOH)	see general notes*
H43021f_a01	TrAa01C	HCOCOHCO3H → HCOCOHCO3H(aq)		k_exf(01,ind_HCOCOHCO3H)	see general notes*
H43021b_a01	TrAa01C	HCOCOHCO3H(aq) → HCOCOHCO3H		k_exb(01,ind_HCOCOHCO3H)	see general notes*
H43022f_a01	TrAa01CN	HCOCOHPAN → HCOCOHPAN(aq)		k_exf(01,ind_HCOCOHPAN)	see general notes*
H43022b_a01	TrAa01CN	HCOCOHPAN(aq) → HCOCOHPAN		k_exb(01,ind_HCOCOHPAN)	see general notes*
H43023f_a01	TrAa01C	HOC2H4CO2H → HOC2H4CO2H(aq)		k_exf(01,ind_HOC2H4CO2H)	see general notes*
H43023b_a01	TrAa01C	HOC2H4CO2H(aq) → HOC2H4CO2H		k_exb(01,ind_HOC2H4CO2H)	see general notes*
H43024f_a01	TrAa01C	HOC2H4CO3H → HOC2H4CO3H(aq)		k_exf(01,ind_HOC2H4CO3H)	see general notes*
H43024b_a01	TrAa01C	HOC2H4CO3H(aq) → HOC2H4CO3H		k_exb(01,ind_HOC2H4CO3H)	see general notes*
H43025f_a01	TrAa01C	HOCH2COCH2OOH	→	k_exf(01,ind_HOCH2COCH2OOH)	see general notes*
		HOCH2COCH2OOH(aq)			
H43025b_a01	TrAa01C	HOCH2COCH2OOH(aq)	→	k_exb(01,ind_HOCH2COCH2OOH)	see general notes*
		HOCH2COCH2OOH			
H43026f_a01	TrAa01C	HOCH2COCHO → HOCH2COCHO(aq)		k_exf(01,ind_HOCH2COCHO)	see general notes*
H43026b_a01	TrAa01C	HOCH2COCHO(aq) → HOCH2COCHO		k_exb(01,ind_HOCH2COCHO)	see general notes*
H43027f_a01	TrAa01C	HYPROPO2H → HYPROPO2H(aq)		k_exf(01,ind_HYPROPO2H)	see general notes*
H43027b_a01	TrAa01C	HYPROPO2H(aq) → HYPROPO2H		k_exb(01,ind_HYPROPO2H)	see general notes*
H43028f_a01	TrAa01C	METACETHO → METACETHO(aq)		k_exf(01,ind_METACETHO)	see general notes*
H43028b_a01	TrAa01C	METACETHO(aq) → METACETHO		k_exb(01,ind_METACETHO)	see general notes*
H43029f_a01	TrAa01CN	NOA → NOA(aq)		k_exf(01,ind_NOA)	see general notes*
H43029b_a01	TrAa01CN	NOA(aq) → NOA		k_exb(01,ind_NOA)	see general notes*
H43030f_a01	TrAa01CN	PR2O2HNO3 → PR2O2HNO3(aq)		k_exf(01,ind_PR2O2HNO3)	see general notes*

Table 3: Reversible (Henry's law) equilibria and irreversible ("heterogenous") uptake

#	labels	reaction	rate coefficient	reference
H43030b_a01	TrAa01CN	PR2O2HNO3(aq) → PR2O2HNO3	k_exb(01,ind_PR2O2HNO3)	see general notes*
H43031f_a01	TrAa01CN	PROPOLNO3 → PROPOLNO3(aq)	k_exf(01,ind_PROPOLNO3)	see general notes*
H43031b_a01	TrAa01CN	PROPOLNO3(aq) → PROPOLNO3	k_exb(01,ind_PROPOLNO3)	see general notes*
H43032f_a01	TrAa01C	$CH_3COCH_2OH \rightarrow CH_3COCH_2OH(aq)$	k_exf(01,ind_ACETOL)	see general notes*
H43032b_a01	TrAa01C	$CH_3COCH_2OH(aq) \rightarrow CH_3COCH_2OH$	k_exb(01,ind_ACETOL)	see general notes*
H44000f_a01	TrAa01C	MACR → MACR(aq)	k_exf(01,ind_MACR)	see general notes*
H44000b_a01	TrAa01C	MACR(aq) → MACR	k_exb(01,ind_MACR)	see general notes*
H44001f_a01	TrAa01C	MVK → MVK(aq)	k_exf(01,ind_MVK)	see general notes*
H44001b_a01	TrAa01C	MVK(aq) → MVK	k_exb(01,ind_MVK)	see general notes*
H44002f_a01	TrAa01C	$CH_3COCOCH_2O_2 \rightarrow CH_3COCOCH_2O_2(aq)$	k_exf(01,ind_BIACETO2)	see general notes*
H44002b_a01	TrAa01C	$CH_3COCOCH_2O_2(aq) \rightarrow CH_3COCOCH_2O_2$	k_exb(01,ind_BIACETO2)	see general notes*
H44003f_a01	TrAa01C	BIACETOH → BIACETOH(aq)	k_exf(01,ind_BIACETOH)	see general notes*
H44003b_a01	TrAa01C	BIACETOH(aq) → BIACETOH	k_exb(01,ind_BIACETOH)	see general notes*
H44004f_a01	TrAa01C	$CH_3COCOCH_2OOH \rightarrow CH_3COCOCH_2OOH(aq)$	k_exf(01,ind_BIACETOOH)	see general notes*
H44004b_a01	TrAa01C	$CH_3COCOCH_2OOH(aq) \rightarrow CH_3COCOCH_2OOH$	k_exb(01,ind_BIACETOOH)	see general notes*
H44005f_a01	TrAa01C	BUT2OLO → BUT2OLO(aq)	k_exf(01,ind_BUT2OLO)	see general notes*
H44005b_a01	TrAa01C	BUT2OLO(aq) → BUT2OLO	k_exb(01,ind_BUT2OLO)	see general notes*
H44006f_a01	TrAa01C	BUT2OLOOH → BUT2OLOOH(aq)	k_exf(01,ind_BUT2OLOOH)	see general notes*
H44006b_a01	TrAa01C	BUT2OLOOH(aq) → BUT2OLOOH	k_exb(01,ind_BUT2OLOOH)	see general notes*
H44007f_a01	TrAa01C	BZFUCO → BZFUCO(aq)	k_exf(01,ind_BZFUCO)	see general notes*
H44007b_a01	TrAa01C	BZFUCO(aq) → BZFUCO	k_exb(01,ind_BZFUCO)	see general notes*
H44008f_a01	TrAa01C	BZFUOOH → BZFUOOH(aq)	k_exf(01,ind_BZFUOOH)	see general notes*
H44008b_a01	TrAa01C	BZFUOOH(aq) → BZFUOOH	k_exb(01,ind_BZFUOOH)	see general notes*
H44009f_a01	TrAa01C	C312COCO3H → C312COCO3H(aq)	k_exf(01,ind_C312COCO3H)	see general notes*
H44009b_a01	TrAa01C	C312COCO3H(aq) → C312COCO3H	k_exb(01,ind_C312COCO3H)	see general notes*
H44010f_a01	TrAa01CN	C312COPAN → C312COPAN(aq)	k_exf(01,ind_C312COPAN)	see general notes*
H44010b_a01	TrAa01CN	C312COPAN(aq) → C312COPAN	k_exb(01,ind_C312COPAN)	see general notes*
H44011f_a01	TrAa01C	C413COOOH → C413COOOH(aq)	k_exf(01,ind_C413COOOH)	see general notes*
H44011b_a01	TrAa01C	C413COOOH(aq) → C413COOOH	k_exb(01,ind_C413COOOH)	see general notes*
H44012f_a01	TrAa01C	C44OOH → C44OOH(aq)	k_exf(01,ind_C44OOH)	see general notes*
H44012b_a01	TrAa01C	C44OOH(aq) → C44OOH	k_exb(01,ind_C44OOH)	see general notes*
H44013f_a01	TrAa01C	C4CODIAL → C4CODIAL(aq)	k_exf(01,ind_C4CODIAL)	see general notes*
H44013b_a01	TrAa01C	C4CODIAL(aq) → C4CODIAL	k_exb(01,ind_C4CODIAL)	see general notes*

Table 3: Reversible (Henry's law) equilibria and irreversible ("heterogenous") uptake

#	labels	reaction	rate coefficient	reference
H44014f_a01	TrAa01CN	C4PAN5 → C4PAN5(aq)	k_exf(01,ind_C4PAN5)	see general notes*
H44014b_a01	TrAa01CN	C4PAN5(aq) → C4PAN5	k_exb(01,ind_C4PAN5)	see general notes*
H44015f_a01	TrAa01C	$CH_3COCHCO \rightarrow CH_3COCHCO(aq)$	k_exf(01,ind_CH3COCHCO)	see general notes*
H44015b_a01	TrAa01C	$CH_3COCHCO(aq) \rightarrow CH_3COCHCO$	k_exb(01,ind_CH3COCHCO)	see general notes*
H44016f_a01	TrAa01C	CH3COCOCO2H → CH3COCOCO2H(aq)	k_exf(01,ind_CH3COCOCO2H)	see general notes*
H44016b_a01	TrAa01C	CH3COCOCO2H(aq) → CH3COCOCO2H	k_exb(01,ind_CH3COCOCO2H)	see general notes*
H44017f_a01	TrAa01C	$CH_3COOHCHCHO \rightarrow CH_3COOHCHCHO(aq)$	k_exf(01,ind_CH3COOHCHCHO)	see general notes*
H44017b_a01	TrAa01C	$CH_3COOHCHCHO(aq) \rightarrow CH_3COOHCHCHO$	k_exb(01,ind_CH3COOHCHCHO)	see general notes*
H44018f_a01	TrAa01C	CHOC3COO2 → CHOC3COO2(aq)	k_exf(01,ind_CHOC3COO2)	see general notes*
H44018b_a01	TrAa01C	CHOC3COO2(aq) → CHOC3COO2	k_exb(01,ind_CHOC3COO2)	see general notes*
H44019f_a01	TrAa01C	CO14O3CHO → CO14O3CHO(aq)	k_exf(01,ind_CO14O3CHO)	see general notes*
H44019b_a01	TrAa01C	CO14O3CHO(aq) → CO14O3CHO	k_exb(01,ind_CO14O3CHO)	see general notes*
H44020f_a01	TrAa01C	CO14O3CO2H → CO14O3CO2H(aq)	k_exf(01,ind_CO14O3CO2H)	see general notes*
H44020b_a01	TrAa01C	CO14O3CO2H(aq) → CO14O3CO2H	k_exb(01,ind_CO14O3CO2H)	see general notes*
H44021f_a01	TrAa01C	$CH_3COCOCHO \rightarrow CH_3COCOCHO(aq)$	k_exf(01,ind_CO23C3CHO)	see general notes*
H44021b_a01	TrAa01C	$CH_3COCOCHO(aq) \rightarrow CH_3COCOCHO$	k_exb(01,ind_CO23C3CHO)	see general notes*
H44022f_a01	TrAa01C	CO2C3CHO → CO2C3CHO(aq)	k_exf(01,ind_CO2C3CHO)	see general notes*
H44022b_a01	TrAa01C	CO2C3CHO(aq) → CO2C3CHO	k_exb(01,ind_CO2C3CHO)	see general notes*
H44023f_a01	TrAa01C	CO2C4DIAL → CO2C4DIAL(aq)	k_exf(01,ind_CO2C4DIAL)	see general notes*
H44023b_a01	TrAa01C	CO2C4DIAL(aq) → CO2C4DIAL	k_exb(01,ind_CO2C4DIAL)	see general notes*
H44024f_a01	TrAa01C	CO2H3CHO → CO2H3CHO(aq)	k_exf(01,ind_CO2H3CHO)	see general notes*
H44024b_a01	TrAa01C	CO2H3CHO(aq) → CO2H3CHO	k_exb(01,ind_CO2H3CHO)	see general notes*
H44025f_a01	TrAa01C	CO2H3CO2H → CO2H3CO2H(aq)	k_exf(01,ind_CO2H3CO2H)	see general notes*
H44025b_a01	TrAa01C	CO2H3CO2H(aq) → CO2H3CO2H	k_exb(01,ind_CO2H3CO2H)	see general notes*
H44026f_a01	TrAa01C	CO2H3CO3H → CO2H3CO3H(aq)	k_exf(01,ind_CO2H3CO3H)	see general notes*
H44026b_a01	TrAa01C	CO2H3CO3H(aq) → CO2H3CO3H	k_exb(01,ind_CO2H3CO3H)	see general notes*
H44027f_a01	TrAa01C	EPXC4DIAL → EPXC4DIAL(aq)	k_exf(01,ind_EPXC4DIAL)	see general notes*
H44027b_a01	TrAa01C	EPXC4DIAL(aq) → EPXC4DIAL	k_exb(01,ind_EPXC4DIAL)	see general notes*
H44028f_a01	TrAa01C	EPXDLCO2H → EPXDLCO2H(aq)	k_exf(01,ind_EPXDLCO2H)	see general notes*
H44028b_a01	TrAa01C	EPXDLCO2H(aq) → EPXDLCO2H	k_exb(01,ind_EPXDLCO2H)	see general notes*
H44029f_a01	TrAa01C	EPXDLCO3H → EPXDLCO3H(aq)	k_exf(01,ind_EPXDLCO3H)	see general notes*
H44029b_a01	TrAa01C	EPXDLCO3H(aq) → EPXDLCO3H	k_exb(01,ind_EPXDLCO3H)	see general notes*

Table 3: Reversible (Henry's law) equilibria and irreversible ("heterogenous") uptake

#	labels	reaction		rate coefficient	reference
H44030f_a01	TrAa01C	$HCOCCH_3CHOOH$ $HCOCCH_3CHOOH(aq)$	→	k_exf(01,ind_HCOCCH3CHOOH)	see general notes*
H44030b_a01	TrAa01C	$HCOCCH_3CHOOH(aq)$ $HCOCCH_3CHOOH$	→	k_exb(01,ind_HCOCCH3CHOOH)	see general notes*
H44031f_a01	TrAa01C	$HCOCCH_3CO \rightarrow HCOCCH_3CO(aq)$		k_exf(01,ind_HCOCCH3CO)	see general notes*
H44031b_a01	TrAa01C	$HCOCCH_3CO(aq) \rightarrow HCOCCH_3CO$		k_exb(01,ind_HCOCCH3CO)	see general notes*
H44032f_a01	TrAa01C	HMAC → HMAC(aq)		k_exf(01,ind_HMAC)	see general notes*
H44032b_a01	TrAa01C	HMAC(aq) → HMAC		k_exb(01,ind_HMAC)	see general notes*
H44033f_a01	TrAa01C	HO12CO3C4 → HO12CO3C4(aq)		k_exf(01,ind_HO12CO3C4)	see general notes*
H44033b_a01	TrAa01C	HO12CO3C4(aq) → HO12CO3C4		k_exb(01,ind_HO12CO3C4)	see general notes*
H44034f_a01	TrAa01C	HOCOC4DIAL → HOCOC4DIAL(aq)		k_exf(01,ind_HOCOC4DIAL)	see general notes*
H44034b_a01	TrAa01C	HOCOC4DIAL(aq) → HOCOC4DIAL		k_exb(01,ind_HOCOC4DIAL)	see general notes*
H44035f_a01	TrAa01C	HVMK → HVMK(aq)		k_exf(01,ind_HVMK)	see general notes*
H44035b_a01	TrAa01C	HVMK(aq) → HVMK		k_exb(01,ind_HVMK)	see general notes*
H44036f_a01	TrAa01C	IBUTALOH → IBUTALOH(aq)		k_exf(01,ind_IBUTALOH)	see general notes*
H44036b_a01	TrAa01C	IBUTALOH(aq) → IBUTALOH		k_exb(01,ind_IBUTALOH)	see general notes*
H44037f_a01	TrAa01C	IBUTDIAL → IBUTDIAL(aq)		k_exf(01,ind_IBUTDIAL)	see general notes*
H44037b_a01	TrAa01C	IBUTDIAL(aq) → IBUTDIAL		k_exb(01,ind_IBUTDIAL)	see general notes*
H44038f_a01	TrAa01C	IBUTOLBOOH → IBUTOLBOOH(aq)		k_exf(01,ind_IBUTOLBOOH)	see general notes*
H44038b_a01	TrAa01C	IBUTOLBOOH(aq) → IBUTOLBOOH		k_exb(01,ind_IBUTOLBOOH)	see general notes*
H44039f_a01	TrAa01C	IPRHOCO2H → IPRHOCO2H(aq)		k_exf(01,ind_IPRHOCO2H)	see general notes*
H44039b_a01	TrAa01C	IPRHOCO2H(aq) → IPRHOCO2H		k_exb(01,ind_IPRHOCO2H)	see general notes*
H44040f_a01	TrAa01C	IPRHOCO3H → IPRHOCO3H(aq)		k_exf(01,ind_IPRHOCO3H)	see general notes*
H44040b_a01	TrAa01C	IPRHOCO3H(aq) → IPRHOCO3H		k_exb(01,ind_IPRHOCO3H)	see general notes*
H44041f_a01	TrAa01C	LBUT1ENOOH → LBUT1ENOOH(aq)		k_exf(01,ind_LBUT1ENOOH)	see general notes*
H44041b_a01	TrAa01C	LBUT1ENOOH(aq) → LBUT1ENOOH		k_exb(01,ind_LBUT1ENOOH)	see general notes*
H44042f_a01	TrAa01C	LHMVKABOOH → LHMVKABOOH(aq)		k_exf(01,ind_LHMVKABOOH)	see general notes*
H44042b_a01	TrAa01C	LHMVKABOOH(aq) → LHMVKABOOH		k_exb(01,ind_LHMVKABOOH)	see general notes*
H44043f_a01	TrAa01C	LMEKOOH → LMEKOOH(aq)		k_exf(01,ind_LMEKOOH)	see general notes*
H44043b_a01	TrAa01C	LMEKOOH(aq) → LMEKOOH		k_exb(01,ind_LMEKOOH)	see general notes*
H44044f_a01	TrAa01C	MACO2H → MACO2H(aq)		k_exf(01,ind_MACO2H)	see general notes*
H44044b_a01	TrAa01C	MACO2H(aq) → MACO2H		k_exb(01,ind_MACO2H)	see general notes*
H44045f_a01	TrAa01C	MACO3H → MACO3H(aq)		k_exf(01,ind_MACO3H)	see general notes*
H44045b_a01	TrAa01C	MACO3H(aq) → MACO3H		k_exb(01,ind_MACO3H)	see general notes*
H44046f_a01	TrAa01C	MACROH → MACROH(aq)		k_exf(01,ind_MACROH)	see general notes*

Table 3: Reversible (Henry's law) equilibria and irreversible ("heterogenous") uptake

#	labels	reaction	rate coefficient	reference
H44046b_a01	TrAa01C	MACROH(aq) → MACROH	k_exb(01,ind_MACROH)	see general notes*
H44047f_a01	TrAa01C	MACROOH → MACROOH(aq)	k_exf(01,ind_MACROOH)	see general notes*
H44047b_a01	TrAa01C	MACROOH(aq) → MACROOH	k_exb(01,ind_MACROOH)	see general notes*
H44048f_a01	TrAa01C	MALANHYOOH → MALANHYOOH(aq)	k_exf(01,ind_MALANHYOOH)	see general notes*
H44048b_a01	TrAa01C	MALANHYOOH(aq) → MALANHYOOH	k_exb(01,ind_MALANHYOOH)	see general notes*
H44049f_a01	TrAa01C	MALDALCO2H → MALDALCO2H(aq)	k_exf(01,ind_MALDALCO2H)	see general notes*
H44049b_a01	TrAa01C	MALDALCO2H(aq) → MALDALCO2H	k_exb(01,ind_MALDALCO2H)	see general notes*
H44050f_a01	TrAa01C	MALDALCO3H → MALDALCO3H(aq)	k_exf(01,ind_MALDALCO3H)	see general notes*
H44050b_a01	TrAa01C	MALDALCO3H(aq) → MALDALCO3H	k_exb(01,ind_MALDALCO3H)	see general notes*
H44051f_a01	TrAa01C	MALDIAL → MALDIAL(aq)	k_exf(01,ind_MALDIAL)	see general notes*
H44051b_a01	TrAa01C	MALDIAL(aq) → MALDIAL	k_exb(01,ind_MALDIAL)	see general notes*
H44052f_a01	TrAa01C	MALDIALOOH → MALDIALOOH(aq)	k_exf(01,ind_MALDIALOOH)	see general notes*
H44052b_a01	TrAa01C	MALDIALOOH(aq) → MALDIALOOH	k_exb(01,ind_MALDIALOOH)	see general notes*
H44053f_a01	TrAa01C	MALNHYOHCO → MALNHYOHCO(aq)	k_exf(01,ind_MALNHYOHCO)	see general notes*
H44053b_a01	TrAa01C	MALNHYOHCO(aq) → MALNHYOHCO	k_exb(01,ind_MALNHYOHCO)	see general notes*
H44054f_a01	TrAa01C	MECOACEOOH → MECOACEOOH(aq)	k_exf(01,ind_MECOACEOOH)	see general notes*
H44054b_a01	TrAa01C	MECOACEOOH(aq) → MECOACEOOH	k_exb(01,ind_MECOACEOOH)	see general notes*
H44055f_a01	TrAa01CN	MVKNO3 → MVKNO3(aq)	k_exf(01,ind_MVKNO3)	see general notes*
H44055b_a01	TrAa01CN	MVKNO3(aq) → MVKNO3	k_exb(01,ind_MVKNO3)	see general notes*
H44056f_a01	TrAa01CN	NBZFUOOH → NBZFUOOH(aq)	k_exf(01,ind_NBZFUOOH)	see general notes*
H44056b_a01	TrAa01CN	NBZFUOOH(aq) → NBZFUOOH	k_exb(01,ind_NBZFUOOH)	see general notes*
H44057f_a01	TrAa01CN	NC4DCO2H → NC4DCO2H(aq)	k_exf(01,ind_NC4DCO2H)	see general notes*
H44057b_a01	TrAa01CN	NC4DCO2H(aq) → NC4DCO2H	k_exb(01,ind_NC4DCO2H)	see general notes*
H45000f_a01	TrAa01C	ACCOMECHO → ACCOMECHO(aq)	k_exf(01,ind_ACCOMECHO)	see general notes*
H45000b_a01	TrAa01C	ACCOMECHO(aq) → ACCOMECHO	k_exb(01,ind_ACCOMECHO)	see general notes*
H45001f_a01	TrAa01C	ACCOMECO3H → ACCOMECO3H(aq)	k_exf(01,ind_ACCOMECO3H)	see general notes*
H45001b_a01	TrAa01C	ACCOMECO3H(aq) → ACCOMECO3H	k_exb(01,ind_ACCOMECO3H)	see general notes*
H45002f_a01	TrAa01C	C1ODC2O2C4OOH → C1ODC2O2C4OOH(aq)	k_exf(01,ind_C1ODC2O2C4OOH)	see general notes*
H45002b_a01	TrAa01C	C1ODC2O2C4OOH(aq) → C1ODC2O2C4OOH	k_exb(01,ind_C1ODC2O2C4OOH)	see general notes*
H45003f_a01	TrAa01C	C1ODC2OOHC4OD → C1ODC2OOHC4OD(aq)	k_exf(01,ind_C1ODC2OOHC4OD)	see general notes*
H45003b_a01	TrAa01C	C1ODC2OOHC4OD(aq) → C1ODC2OOHC4OD	k_exb(01,ind_C1ODC2OOHC4OD)	see general notes*

Table 3: Reversible (Henry's law) equilibria and irreversible ("heterogenous") uptake

#	labels	reaction		rate coefficient	reference
H45004f_a01	TrAa01C	C1ODC3O2C4OOH C1ODC3O2C4OOH(aq)	→	k_exf(01,ind_C1ODC3O2C4OOH)	see general notes*
H45004b_a01	TrAa01C	C1ODC3O2C4OOH(aq) C1ODC3O2C4OOH	→	k_exb(01,ind_C1ODC3O2C4OOH)	see general notes*
H45005f_a01	TrAa01C	C1OOHC2OOHC4OD C1OOHC2OOHC4OD(aq)	→	k_exf(01,ind_C1OOHC2OOHC4OD)	see general notes*
H45005b_a01	TrAa01C	C1OOHC2OOHC4OD(aq) C1OOHC2OOHC4OD	→	k_exb(01,ind_C1OOHC2OOHC4OD)	see general notes*
H45006f_a01	TrAa01C	C24O3CCO2H → C24O3CCO2H(aq)		k_exf(01,ind_C24O3CCO2H)	see general notes*
H45006b_a01	TrAa01C	C24O3CCO2H(aq) → C24O3CCO2H		k_exb(01,ind_C24O3CCO2H)	see general notes*
H45007f_a01	TrAa01C	C4CO2DBCO3 → C4CO2DBCO3(aq)		k_exf(01,ind_C4CO2DBCO3)	see general notes*
H45007b_a01	TrAa01C	C4CO2DBCO3(aq) → C4CO2DBCO3		k_exb(01,ind_C4CO2DBCO3)	see general notes*
H45008f_a01	TrAa01CN	C4CO2DBPAN → C4CO2DBPAN(aq)		k_exf(01,ind_C4CO2DBPAN)	see general notes*
H45008b_a01	TrAa01CN	C4CO2DBPAN(aq) → C4CO2DBPAN		k_exb(01,ind_C4CO2DBPAN)	see general notes*
H45009f_a01	TrAa01C	C4CO2DCO3H → C4CO2DCO3H(aq)		k_exf(01,ind_C4CO2DCO3H)	see general notes*
H45009b_a01	TrAa01C	C4CO2DCO3H(aq) → C4CO2DCO3H		k_exb(01,ind_C4CO2DCO3H)	see general notes*
H45010f_a01	TrAa01CN	C4MCONO3OH → C4MCONO3OH(aq)		k_exf(01,ind_C4MCONO3OH)	see general notes*
H45010b_a01	TrAa01CN	C4MCONO3OH(aq) → C4MCONO3OH		k_exb(01,ind_C4MCONO3OH)	see general notes*
H45011f_a01	TrAa01C	C511OOH → C511OOH(aq)		k_exf(01,ind_C511OOH)	see general notes*
H45011b_a01	TrAa01C	C511OOH(aq) → C511OOH		k_exb(01,ind_C511OOH)	see general notes*
H45012f_a01	TrAa01C	C512OOH → C512OOH(aq)		k_exf(01,ind_C512OOH)	see general notes*
H45012b_a01	TrAa01C	C512OOH(aq) → C512OOH		k_exb(01,ind_C512OOH)	see general notes*
H45013f_a01	TrAa01C	C5134CO2OH → C5134CO2OH(aq)		k_exf(01,ind_C5134CO2OH)	see general notes*
H45013b_a01	TrAa01C	C5134CO2OH(aq) → C5134CO2OH		k_exb(01,ind_C5134CO2OH)	see general notes*
H45014f_a01	TrAa01C	C513CO → C513CO(aq)		k_exf(01,ind_C513CO)	see general notes*
H45014b_a01	TrAa01C	C513CO(aq) → C513CO		k_exb(01,ind_C513CO)	see general notes*
H45015f_a01	TrAa01C	C513OOH → C513OOH(aq)		k_exf(01,ind_C513OOH)	see general notes*
H45015b_a01	TrAa01C	C513OOH(aq) → C513OOH		k_exb(01,ind_C513OOH)	see general notes*
H45016f_a01	TrAa01CN	C514NO3 → C514NO3(aq)		k_exf(01,ind_C514NO3)	see general notes*
H45016b_a01	TrAa01CN	C514NO3(aq) → C514NO3		k_exb(01,ind_C514NO3)	see general notes*
H45017f_a01	TrAa01C	C514OOH → C514OOH(aq)		k_exf(01,ind_C514OOH)	see general notes*
H45017b_a01	TrAa01C	C514OOH(aq) → C514OOH		k_exb(01,ind_C514OOH)	see general notes*
H45018f_a01	TrAa01C	C54CO → C54CO(aq)		k_exf(01,ind_C54CO)	see general notes*
H45018b_a01	TrAa01C	C54CO(aq) → C54CO		k_exb(01,ind_C54CO)	see general notes*
H45019f_a01	TrAa01C	C59OOH → C59OOH(aq)		k_exf(01,ind_C59OOH)	see general notes*

Table 3: Reversible (Henry's law) equilibria and irreversible ("heterogenous") uptake

#	labels	reaction	rate coefficient	reference
H45019b_a01	TrAa01C	C59OOH(aq) → C59OOH	k_exb(01,ind_C59OOH)	see general notes*
H45020f_a01	TrAa01C	C5CO14OH → C5CO14OH(aq)	k_exf(01,ind_C5CO14OH)	see general notes*
H45020b_a01	TrAa01C	C5CO14OH(aq) → C5CO14OH	k_exb(01,ind_C5CO14OH)	see general notes*
H45021f_a01	TrAa01C	C5CO14OOH → C5CO14OOH(aq)	k_exf(01,ind_C5CO14OOH)	see general notes*
H45021b_a01	TrAa01C	C5CO14OOH(aq) → C5CO14OOH	k_exb(01,ind_C5CO14OOH)	see general notes*
H45022f_a01	TrAa01C	C5DIALCO → C5DIALCO(aq)	k_exf(01,ind_C5DIALCO)	see general notes*
H45022b_a01	TrAa01C	C5DIALCO(aq) → C5DIALCO	k_exb(01,ind_C5DIALCO)	see general notes*
H45023f_a01	TrAa01C	C5DIALOOH → C5DIALOOH(aq)	k_exf(01,ind_C5DIALOOH)	see general notes*
H45023b_a01	TrAa01C	C5DIALOOH(aq) → C5DIALOOH	k_exb(01,ind_C5DIALOOH)	see general notes*
H45024f_a01	TrAa01C	C5DICARB → C5DICARB(aq)	k_exf(01,ind_C5DICARB)	see general notes*
H45024b_a01	TrAa01C	C5DICARB(aq) → C5DICARB	k_exb(01,ind_C5DICARB)	see general notes*
H45025f_a01	TrAa01C	C5DICAROOH → C5DICAROOH(aq)	k_exf(01,ind_C5DICAROOH)	see general notes*
H45025b_a01	TrAa01C	C5DICAROOH(aq) → C5DICAROOH	k_exb(01,ind_C5DICAROOH)	see general notes*
H45026f_a01	TrAa01CN	C5PAN9 → C5PAN9(aq)	k_exf(01,ind_C5PAN9)	see general notes*
H45026b_a01	TrAa01CN	C5PAN9(aq) → C5PAN9	k_exb(01,ind_C5PAN9)	see general notes*
H45027f_a01	TrAa01C	CHOC3COOOH → CHOC3COOOH(aq)	k_exf(01,ind_CHOC3COOOH)	see general notes*
H45027b_a01	TrAa01C	CHOC3COOOH(aq) → CHOC3COOOH	k_exb(01,ind_CHOC3COOOH)	see general notes*
H45028f_a01	TrAa01CN	CHOC3COPAN → CHOC3COPAN(aq)	k_exf(01,ind_CHOC3COPAN)	see general notes*
H45028b_a01	TrAa01CN	CHOC3COPAN(aq) → CHOC3COPAN	k_exb(01,ind_CHOC3COPAN)	see general notes*
H45029f_a01	TrAa01C	CO13C4CHO → CO13C4CHO(aq)	k_exf(01,ind_CO13C4CHO)	see general notes*
H45029b_a01	TrAa01C	CO13C4CHO(aq) → CO13C4CHO	k_exb(01,ind_CO13C4CHO)	see general notes*
H45030f_a01	TrAa01C	CO23C4CHO → CO23C4CHO(aq)	k_exf(01,ind_CO23C4CHO)	see general notes*
H45030b_a01	TrAa01C	CO23C4CHO(aq) → CO23C4CHO	k_exb(01,ind_CO23C4CHO)	see general notes*
H45031f_a01	TrAa01C	CO23C4CO3H → CO23C4CO3H(aq)	k_exf(01,ind_CO23C4CO3H)	see general notes*
H45031b_a01	TrAa01C	CO23C4CO3H(aq) → CO23C4CO3H	k_exb(01,ind_CO23C4CO3H)	see general notes*
H45032f_a01	TrAa01CN	DB1NO3 → DB1NO3(aq)	k_exf(01,ind_DB1NO3)	see general notes*
H45032b_a01	TrAa01CN	DB1NO3(aq) → DB1NO3	k_exb(01,ind_DB1NO3)	see general notes*
H45033f_a01	TrAa01C	DB1OOH → DB1OOH(aq)	k_exf(01,ind_DB1OOH)	see general notes*
H45033b_a01	TrAa01C	DB1OOH(aq) → DB1OOH	k_exb(01,ind_DB1OOH)	see general notes*
H45034f_a01	TrAa01C	DB2OOH → DB2OOH(aq)	k_exf(01,ind_DB2OOH)	see general notes*
H45034b_a01	TrAa01C	DB2OOH(aq) → DB2OOH	k_exb(01,ind_DB2OOH)	see general notes*
H45035f_a01	TrAa01C	ISOPAOH → ISOPAOH(aq)	k_exf(01,ind_ISOPAOH)	see general notes*
H45035b_a01	TrAa01C	ISOPAOH(aq) → ISOPAOH	k_exb(01,ind_ISOPAOH)	see general notes*
H45036f_a01	TrAa01CN	ISOPBNO3 → ISOPBNO3(aq)	k_exf(01,ind_ISOPBNO3)	see general notes*
H45036b_a01	TrAa01CN	ISOPBNO3(aq) → ISOPBNO3	k_exb(01,ind_ISOPBNO3)	see general notes*

Table 3: Reversible (Henry's law) equilibria and irreversible ("heterogenous") uptake

#	labels	reaction	rate coefficient	reference
H45037f_a01	TrAa01C	ISOPBOH → ISOPBOH(aq)	k_exf(01,ind_ISOPBOH)	see general notes*
H45037b_a01	TrAa01C	ISOPBOH(aq) → ISOPBOH	k_exb(01,ind_ISOPBOH)	see general notes*
H45038f_a01	TrAa01C	ISOPBOOH → ISOPBOOH(aq)	k_exf(01,ind_ISOPBOOH)	see general notes*
H45038b_a01	TrAa01C	ISOPBOOH(aq) → ISOPBOOH	k_exb(01,ind_ISOPBOOH)	see general notes*
H45039f_a01	TrAa01CN	ISOPDNO3 → ISOPDNO3(aq)	k_exf(01,ind_ISOPDNO3)	see general notes*
H45039b_a01	TrAa01CN	ISOPDNO3(aq) → ISOPDNO3	k_exb(01,ind_ISOPDNO3)	see general notes*
H45040f_a01	TrAa01C	ISOPDOH → ISOPDOH(aq)	k_exf(01,ind_ISOPDOH)	see general notes*
H45040b_a01	TrAa01C	ISOPDOH(aq) → ISOPDOH	k_exb(01,ind_ISOPDOH)	see general notes*
H45041f_a01	TrAa01C	ISOPDOOH → ISOPDOOH(aq)	k_exf(01,ind_ISOPDOOH)	see general notes*
H45041b_a01	TrAa01C	ISOPDOOH(aq) → ISOPDOOH	k_exb(01,ind_ISOPDOOH)	see general notes*
H45042f_a01	TrAa01C	LC578OOH → LC578OOH(aq)	k_exf(01,ind_LC578OOH)	see general notes*
H45042b_a01	TrAa01C	LC578OOH(aq) → LC578OOH	k_exb(01,ind_LC578OOH)	see general notes*
H45043f_a01	TrAa01CN	LC5PAN1719 → LC5PAN1719(aq)	k_exf(01,ind_LC5PAN1719)	see general notes*
H45043b_a01	TrAa01CN	LC5PAN1719(aq) → LC5PAN1719	k_exb(01,ind_LC5PAN1719)	see general notes*
H45044f_a01	TrAa01C	LHC4ACCHO → LHC4ACCHO(aq)	k_exf(01,ind_LHC4ACCHO)	see general notes*
H45044b_a01	TrAa01C	LHC4ACCHO(aq) → LHC4ACCHO	k_exb(01,ind_LHC4ACCHO)	see general notes*
H45045f_a01	TrAa01C	LHC4ACCO2H → LHC4ACCO2H(aq)	k_exf(01,ind_LHC4ACCO2H)	see general notes*
H45045b_a01	TrAa01C	LHC4ACCO2H(aq) → LHC4ACCO2H	k_exb(01,ind_LHC4ACCO2H)	see general notes*
H45046f_a01	TrAa01C	LHC4ACCO3H → LHC4ACCO3H(aq)	k_exf(01,ind_LHC4ACCO3H)	see general notes*
H45046b_a01	TrAa01C	LHC4ACCO3H(aq) → LHC4ACCO3H	k_exb(01,ind_LHC4ACCO3H)	see general notes*
H45047f_a01	TrAa01C	LIEPOX → LIEPOX(aq)	k_exf(01,ind_LIEPOX)	see general notes*
H45047b_a01	TrAa01C	LIEPOX(aq) → LIEPOX	k_exb(01,ind_LIEPOX)	see general notes*
H45048f_a01	TrAa01CN	LISOPACNO3 → LISOPACNO3(aq)	k_exf(01,ind_LISOPACNO3)	see general notes*
H45048b_a01	TrAa01CN	LISOPACNO3(aq) → LISOPACNO3	k_exb(01,ind_LISOPACNO3)	see general notes*
H45049f_a01	TrAa01C	LISOPACOOH → LISOPACOOH(aq)	k_exf(01,ind_LISOPACOOH)	see general notes*
H45049b_a01	TrAa01C	LISOPACOOH(aq) → LISOPACOOH	k_exb(01,ind_LISOPACOOH)	see general notes*
H45050f_a01	TrAa01CN	LMBOABNO3 → LMBOABNO3(aq)	k_exf(01,ind_LMBOABNO3)	see general notes*
H45050b_a01	TrAa01CN	LMBOABNO3(aq) → LMBOABNO3	k_exb(01,ind_LMBOABNO3)	see general notes*
H45051f_a01	TrAa01C	LMBOABOOH → LMBOABOOH(aq)	k_exf(01,ind_LMBOABOOH)	see general notes*
H45051b_a01	TrAa01C	LMBOABOOH(aq) → LMBOABOOH	k_exb(01,ind_LMBOABOOH)	see general notes*
H45052f_a01	TrAa01CN	LNMBOABOOH → LNMBOABOOH(aq)	k_exf(01,ind_LNMBOABOOH)	see general notes*
H45052b_a01	TrAa01CN	LNMBOABOOH(aq) → LNMBOABOOH	k_exb(01,ind_LNMBOABOOH)	see general notes*
H45053f_a01	TrAa01C	MBO → MBO(aq)	k_exf(01,ind_MBO)	see general notes*
H45053b_a01	TrAa01C	MBO(aq) → MBO	k_exb(01,ind_MBO)	see general notes*
H45054f_a01	TrAa01C	MBOACO → MBOACO(aq)	k_exf(01,ind_MBOACO)	see general notes*

Table 3: Reversible (Henry's law) equilibria and irreversible ("heterogenous") uptake

#	labels	reaction	rate coefficient	reference
H45054b_a01	TrAa01C	MBOACO(aq) → MBOACO	k_exb(01,ind_MBOACO)	see general notes*
H45055f_a01	TrAa01C	MBOCOCO → MBOCOCO(aq)	k_exf(01,ind_MBOCOCO)	see general notes*
H45055b_a01	TrAa01C	MBOCOCO(aq) → MBOCOCO	k_exb(01,ind_MBOCOCO)	see general notes*
H45056f_a01	TrAa01C	MC3ODBCO2H → MC3ODBCO2H(aq)	k_exf(01,ind_MC3ODBCO2H)	see general notes*
H45056b_a01	TrAa01C	MC3ODBCO2H(aq) → MC3ODBCO2H	k_exb(01,ind_MC3ODBCO2H)	see general notes*
H45057f_a01	TrAa01C	3METHYLFURAN → 3METHYLFURAN(aq)	k_exf(01,ind_ME3FURAN)	see general notes*
H45057b_a01	TrAa01C	3METHYLFURAN(aq) → 3METHYLFURAN	k_exb(01,ind_ME3FURAN)	see general notes*
H45058f_a01	TrAa01C	MMALNHYOOH → MMALNHYOOH(aq)	k_exf(01,ind_MMALNHYOOH)	see general notes*
H45058b_a01	TrAa01C	MMALNHYOOH(aq) → MMALNHYOOH	k_exb(01,ind_MMALNHYOOH)	see general notes*
H45059f_a01	TrAa01CN	NC4MDCO2HN → NC4MDCO2HN(aq)	k_exf(01,ind_NC4MDCO2H)	see general notes*
H45059b_a01	TrAa01CN	NC4MDCO2HN(aq) → NC4MDCO2HN	k_exb(01,ind_NC4MDCO2H)	see general notes*
H45060f_a01	TrAa01CN	NC4OHCO3H → NC4OHCO3H(aq)	k_exf(01,ind_NC4OHCO3H)	see general notes*
H45060b_a01	TrAa01CN	NC4OHCO3H(aq) → NC4OHCO3H	k_exb(01,ind_NC4OHCO3H)	see general notes*
H45061f_a01	TrAa01CN	NC4OHCPAN → NC4OHCPAN(aq)	k_exf(01,ind_NC4OHCPAN)	see general notes*
H45061b_a01	TrAa01CN	NC4OHCPAN(aq) → NC4OHCPAN	k_exb(01,ind_NC4OHCPAN)	see general notes*
H45062f_a01	TrAa01CN	NISOPOOH → NISOPOOH(aq)	k_exf(01,ind_NISOPOOH)	see general notes*
H45062b_a01	TrAa01CN	NISOPOOH(aq) → NISOPOOH	k_exb(01,ind_NISOPOOH)	see general notes*
H45063f_a01	TrAa01CN	NMBOBCO → NMBOBCO(aq)	k_exf(01,ind_NMBOBCO)	see general notes*
H45063b_a01	TrAa01CN	NMBOBCO(aq) → NMBOBCO	k_exb(01,ind_NMBOBCO)	see general notes*
H45064f_a01	TrAa01CN	NTLFUOOH → NTLFUOOH(aq)	k_exf(01,ind_NTLFUOOH)	see general notes*
H45064b_a01	TrAa01CN	NTLFUOOH(aq) → NTLFUOOH	k_exb(01,ind_NTLFUOOH)	see general notes*
H45065f_a01	TrAa01C	TLFUOOH → TLFUOOH(aq)	k_exf(01,ind_TLFUOOH)	see general notes*
H45065b_a01	TrAa01C	TLFUOOH(aq) → TLFUOOH	k_exb(01,ind_TLFUOOH)	see general notes*
H45066f_a01	TrAa01C	LZCO3HC23DBCOD → LZCO3HC23DBCOD(aq)	k_exf(01,ind_LZCO3HC23DBCOD)	see general notes*
H45066b_a01	TrAa01C	LZCO3HC23DBCOD(aq) → LZCO3HC23DBCOD	k_exb(01,ind_LZCO3HC23DBCOD)	see general notes*
H45067f_a01	TrAa01C	C4MDIAL → C4MDIAL(aq)	k_exf(01,ind_C4MDIAL)	see general notes*
H45067b_a01	TrAa01C	C4MDIAL(aq) → C4MDIAL	k_exb(01,ind_C4MDIAL)	see general notes*
H46000f_a01	TrAa01CN	BZBIPERNO3 → BZBIPERNO3(aq)	k_exf(01,ind_BZBIPERNO3)	see general notes*
H46000b_a01	TrAa01CN	BZBIPERNO3(aq) → BZBIPERNO3	k_exb(01,ind_BZBIPERNO3)	see general notes*
H46001f_a01	TrAa01C	BZBIPEROOH → BZBIPEROOH(aq)	k_exf(01,ind_BZBIPEROOH)	see general notes*
H46001b_a01	TrAa01C	BZBIPEROOH(aq) → BZBIPEROOH	k_exb(01,ind_BZBIPEROOH)	see general notes*

Table 3: Reversible (Henry's law) equilibria and irreversible ("heterogenous") uptake

#	labels	reaction	rate coefficient	reference
H46002f_a01	TrAa01C	BZEMUCCO → BZEMUCCO(aq)	k_exf(01,ind_BZEMUCCO)	see general notes*
H46002b_a01	TrAa01C	BZEMUCCO(aq) → BZEMUCCO	k_exb(01,ind_BZEMUCCO)	see general notes*
H46003f_a01	TrAa01C	BZEMUCCO2H → BZEMUCCO2H(aq)	k_exf(01,ind_BZEMUCCO2H)	see general notes*
H46003b_a01	TrAa01C	BZEMUCCO2H(aq) → BZEMUCCO2H	k_exb(01,ind_BZEMUCCO2H)	see general notes*
H46004f_a01	TrAa01C	BZEMUCCO3H → BZEMUCCO3H(aq)	k_exf(01,ind_BZEMUCCO3H)	see general notes*
H46004b_a01	TrAa01C	BZEMUCCO3H(aq) → BZEMUCCO3H	k_exb(01,ind_BZEMUCCO3H)	see general notes*
H46005f_a01	TrAa01CN	BZEMUCNO3 → BZEMUCNO3(aq)	k_exf(01,ind_BZEMUCNO3)	see general notes*
H46005b_a01	TrAa01CN	BZEMUCNO3(aq) → BZEMUCNO3	k_exb(01,ind_BZEMUCNO3)	see general notes*
H46006f_a01	TrAa01C	BZEMUCOOH → BZEMUCOOH(aq)	k_exf(01,ind_BZEMUCOOH)	see general notes*
H46006b_a01	TrAa01C	BZEMUCOOH(aq) → BZEMUCOOH	k_exb(01,ind_BZEMUCOOH)	see general notes*
H46007f_a01	TrAa01C	BZEPOXMUC → BZEPOXMUC(aq)	k_exf(01,ind_BZEPOXMUC)	see general notes*
H46007b_a01	TrAa01C	BZEPOXMUC(aq) → BZEPOXMUC	k_exb(01,ind_BZEPOXMUC)	see general notes*
H46008f_a01	TrAa01C	BZOBIPEROH → BZOBIPEROH(aq)	k_exf(01,ind_BZOBIPEROH)	see general notes*
H46008b_a01	TrAa01C	BZOBIPEROH(aq) → BZOBIPEROH	k_exb(01,ind_BZOBIPEROH)	see general notes*
H46009f_a01	TrAa01CN	C5CO2DBPAN → C5CO2DBPAN(aq)	k_exf(01,ind_C5CO2DBPAN)	see general notes*
H46009b_a01	TrAa01CN	C5CO2DBPAN(aq) → C5CO2DBPAN	k_exb(01,ind_C5CO2DBPAN)	see general notes*
H46010f_a01	TrAa01C	C5CO2DCO3H → C5CO2DCO3H(aq)	k_exf(01,ind_C5CO2DCO3H)	see general notes*
H46010b_a01	TrAa01C	C5CO2DCO3H(aq) → C5CO2DCO3H	k_exb(01,ind_C5CO2DCO3H)	see general notes*
H46011f_a01	TrAa01CN	C5CO2OHPAN → C5CO2OHPAN(aq)	k_exf(01,ind_C5CO2OHPAN)	see general notes*
H46011b_a01	TrAa01CN	C5CO2OHPAN(aq) → C5CO2OHPAN	k_exb(01,ind_C5CO2OHPAN)	see general notes*
H46012f_a01	TrAa01C	C5COOHCO3H → C5COOHCO3H(aq)	k_exf(01,ind_C5COOHCO3H)	see general notes*
H46012b_a01	TrAa01C	C5COOHCO3H(aq) → C5COOHCO3H	k_exb(01,ind_C5COOHCO3H)	see general notes*
H46013f_a01	TrAa01C	C6125CO → C6125CO(aq)	k_exf(01,ind_C6125CO)	see general notes*
H46013b_a01	TrAa01C	C6125CO(aq) → C6125CO	k_exb(01,ind_C6125CO)	see general notes*
H46014f_a01	TrAa01C	C614CO → C614CO(aq)	k_exf(01,ind_C614CO)	see general notes*
H46014b_a01	TrAa01C	C614CO(aq) → C614CO	k_exb(01,ind_C614CO)	see general notes*
H46015f_a01	TrAa01CN	C614NO3 → C614NO3(aq)	k_exf(01,ind_C614NO3)	see general notes*
H46015b_a01	TrAa01CN	C614NO3(aq) → C614NO3	k_exb(01,ind_C614NO3)	see general notes*
H46016f_a01	TrAa01C	C614OOH → C614OOH(aq)	k_exf(01,ind_C614OOH)	see general notes*
H46016b_a01	TrAa01C	C614OOH(aq) → C614OOH	k_exb(01,ind_C614OOH)	see general notes*
H46017f_a01	TrAa01C	C615CO2OOH → C615CO2OOH(aq)	k_exf(01,ind_C615CO2OOH)	see general notes*
H46017b_a01	TrAa01C	C615CO2OOH(aq) → C615CO2OOH	k_exb(01,ind_C615CO2OOH)	see general notes*
H46018f_a01	TrAa01C	C6CO4DB → C6CO4DB(aq)	k_exf(01,ind_C6CO4DB)	see general notes*
H46018b_a01	TrAa01C	C6CO4DB(aq) → C6CO4DB	k_exb(01,ind_C6CO4DB)	see general notes*
H46019f_a01	TrAa01C	C6H5O → C6H5O(aq)	k_exf(01,ind_C6H5O)	see general notes*

Table 3: Reversible (Henry's law) equilibria and irreversible ("heterogenous") uptake

#	labels	reaction	rate coefficient	reference
H46019b_a01	TrAa01C	C6H5O(aq) → C6H5O	k_exb(01,ind_C6H5O)	see general notes*
H46020f_a01	TrAa01C	C6H5OOH → C6H5OOH(aq)	k_exf(01,ind_C6H5OOH)	see general notes*
H46020b_a01	TrAa01C	C6H5OOH(aq) → C6H5OOH	k_exb(01,ind_C6H5OOH)	see general notes*
H46021f_a01	TrAa01C	CATEC1O → CATEC1O(aq)	k_exf(01,ind_CATEC1O)	see general notes*
H46021b_a01	TrAa01C	CATEC1O(aq) → CATEC1O	k_exb(01,ind_CATEC1O)	see general notes*
H46022f_a01	TrAa01C	CATEC1OOH → CATEC1OOH(aq)	k_exf(01,ind_CATEC1OOH)	see general notes*
H46022b_a01	TrAa01C	CATEC1OOH(aq) → CATEC1OOH	k_exb(01,ind_CATEC1OOH)	see general notes*
H46023f_a01	TrAa01C	CATECHOL → CATECHOL(aq)	k_exf(01,ind_CATECHOL)	see general notes*
H46023b_a01	TrAa01C	CATECHOL(aq) → CATECHOL	k_exb(01,ind_CATECHOL)	see general notes*
H46024f_a01	TrAa01C	CO235C5CHO → CO235C5CHO(aq)	k_exf(01,ind_CO235C5CHO)	see general notes*
H46024b_a01	TrAa01C	CO235C5CHO(aq) → CO235C5CHO	k_exb(01,ind_CO235C5CHO)	see general notes*
H46025f_a01	TrAa01C	CO235C6OOH → CO235C6OOH(aq)	k_exf(01,ind_CO235C6OOH)	see general notes*
H46025b_a01	TrAa01C	CO235C6OOH(aq) → CO235C6OOH	k_exb(01,ind_CO235C6OOH)	see general notes*
H46026f_a01	TrAa01CN	DNPHEN → DNPHEN(aq)	k_exf(01,ind_DNPHEN)	see general notes*
H46026b_a01	TrAa01CN	DNPHEN(aq) → DNPHEN	k_exb(01,ind_DNPHEN)	see general notes*
H46027f_a01	TrAa01CN	DNPHENOOH → DNPHENOOH(aq)	k_exf(01,ind_DNPHENOOH)	see general notes*
H46027b_a01	TrAa01CN	DNPHENOOH(aq) → DNPHENOOH	k_exb(01,ind_DNPHENOOH)	see general notes*
H46028f_a01	TrAa01CN	NBZQOOH → NBZQOOH(aq)	k_exf(01,ind_NBZQOOH)	see general notes*
H46028b_a01	TrAa01CN	NBZQOOH(aq) → NBZQOOH	k_exb(01,ind_NBZQOOH)	see general notes*
H46029f_a01	TrAa01CN	NCATECHOL → NCATECHOL(aq)	k_exf(01,ind_NCATECHOL)	see general notes*
H46029b_a01	TrAa01CN	NCATECHOL(aq) → NCATECHOL	k_exb(01,ind_NCATECHOL)	see general notes*
H46030f_a01	TrAa01CN	NCATECOOH → NCATECOOH(aq)	k_exf(01,ind_NCATECOOH)	see general notes*
H46030b_a01	TrAa01CN	NCATECOOH(aq) → NCATECOOH	k_exb(01,ind_NCATECOOH)	see general notes*
H46031f_a01	TrAa01CN	NDNPHENOOH → NDNPHENOOH(aq)	k_exf(01,ind_NDNPHENOOH)	see general notes*
H46031b_a01	TrAa01CN	NDNPHENOOH(aq) → NDNPHENOOH	k_exb(01,ind_NDNPHENOOH)	see general notes*
H46032f_a01	TrAa01CN	NNCATECOOH → NNCATECOOH(aq)	k_exf(01,ind_NNCATECOOH)	see general notes*
H46032b_a01	TrAa01CN	NNCATECOOH(aq) → NNCATECOOH	k_exb(01,ind_NNCATECOOH)	see general notes*
H46033f_a01	TrAa01CN	NPHENOOH → NPHENOOH(aq)	k_exf(01,ind_NPHENOOH)	see general notes*
H46033b_a01	TrAa01CN	NPHENOOH(aq) → NPHENOOH	k_exb(01,ind_NPHENOOH)	see general notes*
H46034f_a01	TrAa01C	PBZQCO → PBZQCO(aq)	k_exf(01,ind_PBZQCO)	see general notes*
H46034b_a01	TrAa01C	PBZQCO(aq) → PBZQCO	k_exb(01,ind_PBZQCO)	see general notes*
H46035f_a01	TrAa01C	PBZQOOH → PBZQOOH(aq)	k_exf(01,ind_PBZQOOH)	see general notes*
H46035b_a01	TrAa01C	PBZQOOH(aq) → PBZQOOH	k_exb(01,ind_PBZQOOH)	see general notes*
H46036f_a01	TrAa01C	PHENOL → PHENOL(aq)	k_exf(01,ind_PHENOL)	see general notes*
H46036b_a01	TrAa01C	PHENOL(aq) → PHENOL	k_exb(01,ind_PHENOL)	see general notes*

Table 3: Reversible (Henry's law) equilibria and irreversible ("heterogenous") uptake

#	labels	reaction	rate coefficient	reference
H46037f_a01	TrAa01C	PHENOOH → PHENOOH(aq)	k_exf(01,ind_PHENOOH)	see general notes*
H46037b_a01	TrAa01C	PHENOOH(aq) → PHENOOH	k_exb(01,ind_PHENOOH)	see general notes*
H47000f_a01	TrAa01C	C235C6CO3H → C235C6CO3H(aq)	k_exf(01,ind_C235C6CO3H)	see general notes*
H47000b_a01	TrAa01C	C235C6CO3H(aq) → C235C6CO3H	k_exb(01,ind_C235C6CO3H)	see general notes*
H47001f_a01	TrAa01CN	C6CO2OHPAN → C6CO2OHPAN(aq)	k_exf(01,ind_C6CO2OHPAN)	see general notes*
H47001b_a01	TrAa01CN	C6CO2OHPAN(aq) → C6CO2OHPAN	k_exb(01,ind_C6CO2OHPAN)	see general notes*
H47002f_a01	TrAa01C	C6COOHCO3H → C6COOHCO3H(aq)	k_exf(01,ind_C6COOHCO3H)	see general notes*
H47002b_a01	TrAa01C	C6COOHCO3H(aq) → C6COOHCO3H	k_exb(01,ind_C6COOHCO3H)	see general notes*
H47003f_a01	TrAa01C	C6H5CH2OOH → C6H5CH2OOH(aq)	k_exf(01,ind_C6H5CH2OOH)	see general notes*
H47003b_a01	TrAa01C	C6H5CH2OOH(aq) → C6H5CH2OOH	k_exb(01,ind_C6H5CH2OOH)	see general notes*
H47004f_a01	TrAa01C	C6H5CO3H → C6H5CO3H(aq)	k_exf(01,ind_C6H5CO3H)	see general notes*
H47004b_a01	TrAa01C	C6H5CO3H(aq) → C6H5CO3H	k_exb(01,ind_C6H5CO3H)	see general notes*
H47005f_a01	TrAa01C	C716OOH → C716OOH(aq)	k_exf(01,ind_C716OOH)	see general notes*
H47005b_a01	TrAa01C	C716OOH(aq) → C716OOH	k_exb(01,ind_C716OOH)	see general notes*
H47006f_a01	TrAa01C	C721OOH → C721OOH(aq)	k_exf(01,ind_C721OOH)	see general notes*
H47006b_a01	TrAa01C	C721OOH(aq) → C721OOH	k_exb(01,ind_C721OOH)	see general notes*
H47007f_a01	TrAa01C	C722OOH → C722OOH(aq)	k_exf(01,ind_C722OOH)	see general notes*
H47007b_a01	TrAa01C	C722OOH(aq) → C722OOH	k_exb(01,ind_C722OOH)	see general notes*
H47008f_a01	TrAa01C	C7CO4DB → C7CO4DB(aq)	k_exf(01,ind_C7CO4DB)	see general notes*
H47008b_a01	TrAa01C	C7CO4DB(aq) → C7CO4DB	k_exb(01,ind_C7CO4DB)	see general notes*
H47009f_a01	TrAa01CN	C7PAN3 → C7PAN3(aq)	k_exf(01,ind_C7PAN3)	see general notes*
H47009b_a01	TrAa01CN	C7PAN3(aq) → C7PAN3	k_exb(01,ind_C7PAN3)	see general notes*
H47010f_a01	TrAa01C	CO235C6CHO → CO235C6CHO(aq)	k_exf(01,ind_CO235C6CHO)	see general notes*
H47010b_a01	TrAa01C	CO235C6CHO(aq) → CO235C6CHO	k_exb(01,ind_CO235C6CHO)	see general notes*
H47011f_a01	TrAa01C	CRESOL → CRESOL(aq)	k_exf(01,ind_CRESOL)	see general notes*
H47011b_a01	TrAa01C	CRESOL(aq) → CRESOL	k_exb(01,ind_CRESOL)	see general notes*
H47012f_a01	TrAa01C	CRESOOH → CRESOOH(aq)	k_exf(01,ind_CRESOOH)	see general notes*
H47012b_a01	TrAa01C	CRESOOH(aq) → CRESOOH	k_exb(01,ind_CRESOOH)	see general notes*
H47013f_a01	TrAa01CN	DNCRES → DNCRES(aq)	k_exf(01,ind_DNCRES)	see general notes*
H47013b_a01	TrAa01CN	DNCRES(aq) → DNCRES	k_exb(01,ind_DNCRES)	see general notes*
H47014f_a01	TrAa01CN	DNCRESOOH → DNCRESOOH(aq)	k_exf(01,ind_DNCRESOOH)	see general notes*
H47014b_a01	TrAa01CN	DNCRESOOH(aq) → DNCRESOOH	k_exb(01,ind_DNCRESOOH)	see general notes*
H47015f_a01	TrAa01C	MCATEC1O → MCATEC1O(aq)	k_exf(01,ind_MCATEC1O)	see general notes*
H47015b_a01	TrAa01C	MCATEC1O(aq) → MCATEC1O	k_exb(01,ind_MCATEC1O)	see general notes*
H47016f_a01	TrAa01C	MCATEC1OOH → MCATEC1OOH(aq)	k_exf(01,ind_MCATEC1OOH)	see general notes*

Table 3: Reversible (Henry's law) equilibria and irreversible ("heterogenous") uptake

#	labels	reaction	rate coefficient	reference
H47016b_a01	TrAa01C	MCATEC1OOH(aq) → MCATEC1OOH	k_exb(01,ind_MCATEC1OOH)	see general notes*
H47017f_a01	TrAa01C	MCATECHOL → MCATECHOL(aq)	k_exf(01,ind_MCATECHOL)	see general notes*
H47017b_a01	TrAa01C	MCATECHOL(aq) → MCATECHOL	k_exb(01,ind_MCATECHOL)	see general notes*
H47018f_a01	TrAa01CN	MNCATECH → MNCATECH(aq)	k_exf(01,ind_MNCATECH)	see general notes*
H47018b_a01	TrAa01CN	MNCATECH(aq) → MNCATECH	k_exb(01,ind_MNCATECH)	see general notes*
H47019f_a01	TrAa01CN	MNCATECOOH → MNCATECOOH(aq)	k_exf(01,ind_MNCATECOOH)	see general notes*
H47019b_a01	TrAa01CN	MNCATECOOH(aq) → MNCATECOOH	k_exb(01,ind_MNCATECOOH)	see general notes*
H47020f_a01	TrAa01CN	MNNCATCOOH → MNNCATCOOH(aq)	k_exf(01,ind_MNNCATCOOH)	see general notes*
H47020b_a01	TrAa01CN	MNNCATCOOH(aq) → MNNCATCOOH	k_exb(01,ind_MNNCATCOOH)	see general notes*
H47021f_a01	TrAa01CN	NCRESOOH → NCRESOOH(aq)	k_exf(01,ind_NCRESOOH)	see general notes*
H47021b_a01	TrAa01CN	NCRESOOH(aq) → NCRESOOH	k_exb(01,ind_NCRESOOH)	see general notes*
H47022f_a01	TrAa01CN	NDNCRESOOH → NDNCRESOOH(aq)	k_exf(01,ind_NDNCRESOOH)	see general notes*
H47022b_a01	TrAa01CN	NDNCRESOOH(aq) → NDNCRESOOH	k_exb(01,ind_NDNCRESOOH)	see general notes*
H47023f_a01	TrAa01C	OXYL1OOH → OXYL1OOH(aq)	k_exf(01,ind_OXYL1OOH)	see general notes*
H47023b_a01	TrAa01C	OXYL1OOH(aq) → OXYL1OOH	k_exb(01,ind_OXYL1OOH)	see general notes*
H47024f_a01	TrAa01C	PHCOOH → PHCOOH(aq)	k_exf(01,ind_PHCOOH)	see general notes*
H47024b_a01	TrAa01C	PHCOOH(aq) → PHCOOH	k_exb(01,ind_PHCOOH)	see general notes*
H47025f_a01	TrAa01C	TLBIPEROOH → TLBIPEROOH(aq)	k_exf(01,ind_TLBIPEROOH)	see general notes*
H47025b_a01	TrAa01C	TLBIPEROOH(aq) → TLBIPEROOH	k_exb(01,ind_TLBIPEROOH)	see general notes*
H47026f_a01	TrAa01C	TLEMUCCO → TLEMUCCO(aq)	k_exf(01,ind_TLEMUCCO)	see general notes*
H47026b_a01	TrAa01C	TLEMUCCO(aq) → TLEMUCCO	k_exb(01,ind_TLEMUCCO)	see general notes*
H47027f_a01	TrAa01C	TLEMUCCO2H → TLEMUCCO2H(aq)	k_exf(01,ind_TLEMUCCO2H)	see general notes*
H47027b_a01	TrAa01C	TLEMUCCO2H(aq) → TLEMUCCO2H	k_exb(01,ind_TLEMUCCO2H)	see general notes*
H47028f_a01	TrAa01C	TLEMUCCO3H → TLEMUCCO3H(aq)	k_exf(01,ind_TLEMUCCO3H)	see general notes*
H47028b_a01	TrAa01C	TLEMUCCO3H(aq) → TLEMUCCO3H	k_exb(01,ind_TLEMUCCO3H)	see general notes*
H47029f_a01	TrAa01CN	TLEMUCNO3 → TLEMUCNO3(aq)	k_exf(01,ind_TLEMUCNO3)	see general notes*
H47029b_a01	TrAa01CN	TLEMUCNO3(aq) → TLEMUCNO3	k_exb(01,ind_TLEMUCNO3)	see general notes*
H47030f_a01	TrAa01C	TLEMUCOOH → TLEMUCOOH(aq)	k_exf(01,ind_TLEMUCOOH)	see general notes*
H47030b_a01	TrAa01C	TLEMUCOOH(aq) → TLEMUCOOH	k_exb(01,ind_TLEMUCOOH)	see general notes*
H47031f_a01	TrAa01C	TLOBIPEROH → TLOBIPEROH(aq)	k_exf(01,ind_TLOBIPEROH)	see general notes*
H47031b_a01	TrAa01C	TLOBIPEROH(aq) → TLOBIPEROH	k_exb(01,ind_TLOBIPEROH)	see general notes*
H47032f_a01	TrAa01C	TOL1O → TOL1O(aq)	k_exf(01,ind_TOL1O)	see general notes*
H47032b_a01	TrAa01C	TOL1O(aq) → TOL1O	k_exb(01,ind_TOL1O)	see general notes*
H48000f_a01	TrAa01C	C721CHO → C721CHO(aq)	k_exf(01,ind_C721CHO)	see general notes*
H48000b_a01	TrAa01C	C721CHO(aq) → C721CHO	k_exb(01,ind_C721CHO)	see general notes*

Table 3: Reversible (Henry's law) equilibria and irreversible ("heterogenous") uptake

#	labels	reaction	rate coefficient	reference
H48001f_a01	TrAa01C	C721CO3H → C721CO3H(aq)	k_exf(01,ind_C721CO3H)	see general notes*
H48001b_a01	TrAa01C	C721CO3H(aq) → C721CO3H	k_exb(01,ind_C721CO3H)	see general notes*
H48002f_a01	TrAa01CN	C721PAN → C721PAN(aq)	k_exf(01,ind_C721PAN)	see general notes*
H48002b_a01	TrAa01CN	C721PAN(aq) → C721PAN	k_exb(01,ind_C721PAN)	see general notes*
H48003f_a01	TrAa01CN	C810NO3 → C810NO3(aq)	k_exf(01,ind_C810NO3)	see general notes*
H48003b_a01	TrAa01CN	C810NO3(aq) → C810NO3	k_exb(01,ind_C810NO3)	see general notes*
H48004f_a01	TrAa01C	C810OOH → C810OOH(aq)	k_exf(01,ind_C810OOH)	see general notes*
H48004b_a01	TrAa01C	C810OOH(aq) → C810OOH	k_exb(01,ind_C810OOH)	see general notes*
H48005f_a01	TrAa01C	C812OOH → C812OOH(aq)	k_exf(01,ind_C812OOH)	see general notes*
H48005b_a01	TrAa01C	C812OOH(aq) → C812OOH	k_exb(01,ind_C812OOH)	see general notes*
H48006f_a01	TrAa01C	C813OOH → C813OOH(aq)	k_exf(01,ind_C813OOH)	see general notes*
H48006b_a01	TrAa01C	C813OOH(aq) → C813OOH	k_exb(01,ind_C813OOH)	see general notes*
H48007f_a01	TrAa01C	C85OOH → C85OOH(aq)	k_exf(01,ind_C85OOH)	see general notes*
H48007b_a01	TrAa01C	C85OOH(aq) → C85OOH	k_exb(01,ind_C85OOH)	see general notes*
H48008f_a01	TrAa01C	C86OOH → C86OOH(aq)	k_exf(01,ind_C86OOH)	see general notes*
H48008b_a01	TrAa01C	C86OOH(aq) → C86OOH	k_exb(01,ind_C86OOH)	see general notes*
H48009f_a01	TrAa01CN	C89NO3 → C89NO3(aq)	k_exf(01,ind_C89NO3)	see general notes*
H48009b_a01	TrAa01CN	C89NO3(aq) → C89NO3	k_exb(01,ind_C89NO3)	see general notes*
H48010f_a01	TrAa01C	C89OOH → C89OOH(aq)	k_exf(01,ind_C89OOH)	see general notes*
H48010b_a01	TrAa01C	C89OOH(aq) → C89OOH	k_exb(01,ind_C89OOH)	see general notes*
H48011f_a01	TrAa01C	C8BC → C8BC(aq)	k_exf(01,ind_C8BC)	see general notes*
H48011b_a01	TrAa01C	C8BC(aq) → C8BC	k_exb(01,ind_C8BC)	see general notes*
H48012f_a01	TrAa01C	C8BCCO → C8BCCO(aq)	k_exf(01,ind_C8BCCO)	see general notes*
H48012b_a01	TrAa01C	C8BCCO(aq) → C8BCCO	k_exb(01,ind_C8BCCO)	see general notes*
H48013f_a01	TrAa01CN	C8BCNO3 → C8BCNO3(aq)	k_exf(01,ind_C8BCNO3)	see general notes*
H48013b_a01	TrAa01CN	C8BCNO3(aq) → C8BCNO3	k_exb(01,ind_C8BCNO3)	see general notes*
H48014f_a01	TrAa01C	C8BCOOH → C8BCOOH(aq)	k_exf(01,ind_C8BCOOH)	see general notes*
H48014b_a01	TrAa01C	C8BCOOH(aq) → C8BCOOH	k_exb(01,ind_C8BCOOH)	see general notes*
H48015f_a01	TrAa01C	NORPINIC → NORPINIC(aq)	k_exf(01,ind_NORPINIC)	see general notes*
H48015b_a01	TrAa01C	NORPINIC(aq) → NORPINIC	k_exb(01,ind_NORPINIC)	see general notes*
H48016f_a01	TrAa01C	STYRENOOH → STYRENOOH(aq)	k_exf(01,ind_STYRENOOH)	see general notes*
H48016b_a01	TrAa01C	STYRENOOH(aq) → STYRENOOH	k_exb(01,ind_STYRENOOH)	see general notes*
H49000f_a01	TrAa01C	C811CO3H → C811CO3H(aq)	k_exf(01,ind_C811CO3H)	see general notes*
H49000b_a01	TrAa01C	C811CO3H(aq) → C811CO3H	k_exb(01,ind_C811CO3H)	see general notes*
H49001f_a01	TrAa01CN	C811PAN → C811PAN(aq)	k_exf(01,ind_C811PAN)	see general notes*

Table 3: Reversible (Henry's law) equilibria and irreversible ("heterogenous") uptake

#	labels	reaction	rate coefficient	reference
H49001b_a01	TrAa01CN	C811PAN(aq) → C811PAN	k_exb(01,ind_C811PAN)	see general notes*
H49002f_a01	TrAa01C	C85CO3H → C85CO3H(aq)	k_exf(01,ind_C85CO3H)	see general notes*
H49002b_a01	TrAa01C	C85CO3H(aq) → C85CO3H	k_exb(01,ind_C85CO3H)	see general notes*
H49003f_a01	TrAa01C	C89CO2H → C89CO2H(aq)	k_exf(01,ind_C89CO2H)	see general notes*
H49003b_a01	TrAa01C	C89CO2H(aq) → C89CO2H	k_exb(01,ind_C89CO2H)	see general notes*
H49004f_a01	TrAa01C	C89CO3H → C89CO3H(aq)	k_exf(01,ind_C89CO3H)	see general notes*
H49004b_a01	TrAa01C	C89CO3H(aq) → C89CO3H	k_exb(01,ind_C89CO3H)	see general notes*
H49005f_a01	TrAa01CN	C89PAN → C89PAN(aq)	k_exf(01,ind_C89PAN)	see general notes*
H49005b_a01	TrAa01CN	C89PAN(aq) → C89PAN	k_exb(01,ind_C89PAN)	see general notes*
H49006f_a01	TrAa01CN	C96NO3 → C96NO3(aq)	k_exf(01,ind_C96NO3)	see general notes*
H49006b_a01	TrAa01CN	C96NO3(aq) → C96NO3	k_exb(01,ind_C96NO3)	see general notes*
H49007f_a01	TrAa01C	C96OOH → C96OOH(aq)	k_exf(01,ind_C96OOH)	see general notes*
H49007b_a01	TrAa01C	C96OOH(aq) → C96OOH	k_exb(01,ind_C96OOH)	see general notes*
H49008f_a01	TrAa01C	C97OOH → C97OOH(aq)	k_exf(01,ind_C97OOH)	see general notes*
H49008b_a01	TrAa01C	C97OOH(aq) → C97OOH	k_exb(01,ind_C97OOH)	see general notes*
H49009f_a01	TrAa01C	C98OOH → C98OOH(aq)	k_exf(01,ind_C98OOH)	see general notes*
H49009b_a01	TrAa01C	C98OOH(aq) → C98OOH	k_exb(01,ind_C98OOH)	see general notes*
H49010f_a01	TrAa01CN	C9PAN2 → C9PAN2(aq)	k_exf(01,ind_C9PAN2)	see general notes*
H49010b_a01	TrAa01CN	C9PAN2(aq) → C9PAN2	k_exb(01,ind_C9PAN2)	see general notes*
H49011f_a01	TrAa01C	NOPINDCO → NOPINDCO(aq)	k_exf(01,ind_NOPINDCO)	see general notes*
H49011b_a01	TrAa01C	NOPINDCO(aq) → NOPINDCO	k_exb(01,ind_NOPINDCO)	see general notes*
H49012f_a01	TrAa01C	NOPINDOOH → NOPINDOOH(aq)	k_exf(01,ind_NOPINDOOH)	see general notes*
H49012b_a01	TrAa01C	NOPINDOOH(aq) → NOPINDOOH	k_exb(01,ind_NOPINDOOH)	see general notes*
H49013f_a01	TrAa01C	NOPINONE → NOPINONE(aq)	k_exf(01,ind_NOPINONE)	see general notes*
H49013b_a01	TrAa01C	NOPINONE(aq) → NOPINONE	k_exb(01,ind_NOPINONE)	see general notes*
H49014f_a01	TrAa01C	NOPINOO → NOPINOO(aq)	k_exf(01,ind_NOPINOO)	see general notes*
H49014b_a01	TrAa01C	NOPINOO(aq) → NOPINOO	k_exb(01,ind_NOPINOO)	see general notes*
H49015f_a01	TrAa01C	NORPINAL → NORPINAL(aq)	k_exf(01,ind_NORPINAL)	see general notes*
H49015b_a01	TrAa01C	NORPINAL(aq) → NORPINAL	k_exb(01,ind_NORPINAL)	see general notes*
H49016f_a01	TrAa01C	NORPINENOL → NORPINENOL(aq)	k_exf(01,ind_NORPINENOL)	see general notes*
H49016b_a01	TrAa01C	NORPINENOL(aq) → NORPINENOL	k_exb(01,ind_NORPINENOL)	see general notes*
H49017f_a01	TrAa01C	PINIC → PINIC(aq)	k_exf(01,ind_PINIC)	see general notes*
H49017b_a01	TrAa01C	PINIC(aq) → PINIC	k_exb(01,ind_PINIC)	see general notes*
H410000f_a01	TrAa01CN	BPINANO3 → BPINANO3(aq)	k_exf(01,ind_BPINANO3)	see general notes*
H410000b_a01	TrAa01CN	BPINANO3(aq) → BPINANO3	k_exb(01,ind_BPINANO3)	see general notes*

Table 3: Reversible (Henry's law) equilibria and irreversible ("heterogenous") uptake

#	labels	reaction	rate coefficient	reference
H410001f_a01	TrAa01C	BPINAOOH → BPINAOOH(aq)	k_exf(01,ind_BPINAOOH)	see general notes*
H410001b_a01	TrAa01C	BPINAOOH(aq) → BPINAOOH	k_exb(01,ind_BPINAOOH)	see general notes*
H410002f_a01	TrAa01CN	C106NO3 → C106NO3(aq)	k_exf(01,ind_C106NO3)	see general notes*
H410002b_a01	TrAa01CN	C106NO3(aq) → C106NO3	k_exb(01,ind_C106NO3)	see general notes*
H410003f_a01	TrAa01C	C106OOH → C106OOH(aq)	k_exf(01,ind_C106OOH)	see general notes*
H410003b_a01	TrAa01C	C106OOH(aq) → C106OOH	k_exb(01,ind_C106OOH)	see general notes*
H410004f_a01	TrAa01C	C109CO → C109CO(aq)	k_exf(01,ind_C109CO)	see general notes*
H410004b_a01	TrAa01C	C109CO(aq) → C109CO	k_exb(01,ind_C109CO)	see general notes*
H410005f_a01	TrAa01C	C109OOH → C109OOH(aq)	k_exf(01,ind_C109OOH)	see general notes*
H410005b_a01	TrAa01C	C109OOH(aq) → C109OOH	k_exb(01,ind_C109OOH)	see general notes*
H410006f_a01	TrAa01CN	C10PAN2 → C10PAN2(aq)	k_exf(01,ind_C10PAN2)	see general notes*
H410006b_a01	TrAa01CN	C10PAN2(aq) → C10PAN2	k_exb(01,ind_C10PAN2)	see general notes*
H410007f_a01	TrAa01CN	LAPINABNO3 → LAPINABNO3(aq)	k_exf(01,ind_LAPINABNO3)	see general notes*
H410007b_a01	TrAa01CN	LAPINABNO3(aq) → LAPINABNO3	k_exb(01,ind_LAPINABNO3)	see general notes*
H410008f_a01	TrAa01C	LAPINABOOH → LAPINABOOH(aq)	k_exf(01,ind_LAPINABOOH)	see general notes*
H410008b_a01	TrAa01C	LAPINABOOH(aq) → LAPINABOOH	k_exb(01,ind_LAPINABOOH)	see general notes*
H410009f_a01	TrAa01CN	LNAPINABOOH → LNAPINABOOH(aq)	k_exf(01,ind_LNAPINABOOH)	see general notes*
H410009b_a01	TrAa01CN	LNAPINABOOH(aq) → LNAPINABOOH	k_exb(01,ind_LNAPINABOOH)	see general notes*
H410010f_a01	TrAa01CN	LNBPINABOOH → LNBPINABOOH(aq)	k_exf(01,ind_LNBPINABOOH)	see general notes*
H410010b_a01	TrAa01CN	LNBPINABOOH(aq) → LNBPINABOOH	k_exb(01,ind_LNBPINABOOH)	see general notes*
H410011f_a01	TrAa01C	MENTHEN6ONE → MENTHEN6ONE(aq)	k_exf(01,ind_MENTHEN6ONE)	see general notes*
H410011b_a01	TrAa01C	MENTHEN6ONE(aq) → MENTHEN6ONE	k_exb(01,ind_MENTHEN6ONE)	see general notes*
H410012f_a01	TrAa01C	2OHMENTHEN6ONE → 2OHMENTHEN6ONE(aq)	k_exf(01,ind_OH2MENTHEN6ONE)	see general notes*
H410012b_a01	TrAa01C	2OHMENTHEN6ONE(aq) → 2OHMENTHEN6ONE	k_exb(01,ind_OH2MENTHEN6ONE)	see general notes*
H410013f_a01	TrAa01C	PERPINONIC → PERPINONIC(aq)	k_exf(01,ind_PERPINONIC)	see general notes*
H410013b_a01	TrAa01C	PERPINONIC(aq) → PERPINONIC	k_exb(01,ind_PERPINONIC)	see general notes*
H410014f_a01	TrAa01C	PINAL → PINAL(aq)	k_exf(01,ind_PINAL)	see general notes*
H410014b_a01	TrAa01C	PINAL(aq) → PINAL	k_exb(01,ind_PINAL)	see general notes*
H410015f_a01	TrAa01CN	PINALNO3 → PINALNO3(aq)	k_exf(01,ind_PINALNO3)	see general notes*
H410015b_a01	TrAa01CN	PINALNO3(aq) → PINALNO3	k_exb(01,ind_PINALNO3)	see general notes*
H410016f_a01	TrAa01C	PINALOOH → PINALOOH(aq)	k_exf(01,ind_PINALOOH)	see general notes*
H410016b_a01	TrAa01C	PINALOOH(aq) → PINALOOH	k_exb(01,ind_PINALOOH)	see general notes*
H410017f_a01	TrAa01C	PINEOL → PINEOL(aq)	k_exf(01,ind_PINENOL)	see general notes*

Table 3: Reversible (Henry's law) equilibria and irreversible ("heterogenous") uptake

#	labels	reaction	rate coefficient	reference
H410017b_a01	TrAa01C	PINEOL(aq) → PINEOL	k_exb(01,ind_PINENOL)	see general notes*
H410018f_a01	TrAa01C	PINONIC → PINONIC(aq)	k_exf(01,ind_PINONIC)	see general notes*
H410018b_a01	TrAa01C	PINONIC(aq) → PINONIC	k_exb(01,ind_PINONIC)	see general notes*
H410019f_a01	TrAa01CN	RO6R1NO3 → RO6R1NO3(aq)	k_exf(01,ind_RO6R1NO3)	see general notes*
H410019b_a01	TrAa01CN	RO6R1NO3(aq) → RO6R1NO3	k_exb(01,ind_RO6R1NO3)	see general notes*
H410020f_a01	TrAa01CN	ROO6R1NO3 → ROO6R1NO3(aq)	k_exf(01,ind_ROO6R1NO3)	see general notes*
H410020b_a01	TrAa01CN	ROO6R1NO3(aq) → ROO6R1NO3	k_exb(01,ind_ROO6R1NO3)	see general notes*
H60000f_a01	TrAa01MblScCl	$Cl_2 \rightarrow Cl_2(aq)$	k_exf(01,ind_Cl2)	see general notes*
H60000b_a01	TrAa01MblScCl	$Cl_2(aq) \rightarrow Cl_2$	k_exb(01,ind_Cl2)	see general notes*
H62000f_a01	TrAa01MblScScmCl	$HCl \rightarrow HCl(aq)$	k_exf(01,ind_HCl)	see general notes*
H62000b_a01	TrAa01MblScScmCl	$HCl(aq) \rightarrow HCl$	k_exb(01,ind_HCl)	see general notes*
H62001f_a01	TrAa01MblScCl	$HOCl \rightarrow HOCl(aq)$	k_exf(01,ind_HOCl)	see general notes*
H62001b_a01	TrAa01MblScCl	$HOCl(aq) \rightarrow HOCl$	k_exb(01,ind_HOCl)	see general notes*
H63000_a01	TrAa01MblClN	$N_2O_5 + Cl^-(aq) \rightarrow ClNO_2 + NO_3^-(aq)$	k_exf_N2O5(01) * 5.E2	Behnke et al. (1994), Behnke et al. (1997)
H63001_a01	TrAa01MblClN	$ClNO_3 \rightarrow HOCl(aq) + HNO_3(aq)$	k_exf_ClNO3(01) * C(ind_H2O_a01)	see general notes*
H63002_a01	TrAa01MblClN	$ClNO_3 + Cl^-(aq) \rightarrow Cl_2(aq) + NO_3^-(aq)$	k_exf_ClNO3(01) * 5.E2	see general notes*
H70000f_a01	TrAa01MblScBr	$Br_2 \rightarrow Br_2(aq)$	k_exf(01,ind_Br2)	see general notes*
H70000b_a01	TrAa01MblScBr	$Br_2(aq) \rightarrow Br_2$	k_exb(01,ind_Br2)	see general notes*
H72000f_a01	TrAa01MblScScmBr	$HBr \rightarrow HBr(aq)$	k_exf(01,ind_HBr)	see general notes*
H72000b_a01	TrAa01MblScScmBr	$HBr(aq) \rightarrow HBr$	k_exb(01,ind_HBr)	see general notes*
H72001f_a01	TrAa01MblScBr	$HOBr \rightarrow HOBr(aq)$	k_exf(01,ind_HOBr)	see general notes*
H72001b_a01	TrAa01MblScBr	$HOBr(aq) \rightarrow HOBr$	k_exb(01,ind_HOBr)	see general notes*
H73000_a01	TrAa01MblBrN	$N_2O_5 + Br^-(aq) \rightarrow BrNO_2 + NO_3^-(aq)$	k_exf_N2O5(01) * 3.E5	Behnke et al. (1994), Behnke et al. (1997)
H73001_a01	TrAa01MblBrN	$BrNO_3 \rightarrow HOBr(aq) + HNO_3(aq)$	k_exf_BrNO3(01) * C(ind_H2O_a01)	see general notes*
H73002_a01	TrAa01MblBrN	$BrNO_3 + Br^-(aq) \rightarrow Br_2(aq) + NO_3^-(aq)$	k_exf_BrNO3(01) * 3.E5	see general notes*
H76000f_a01	TrAa01MblScBrCl	$BrCl \rightarrow BrCl(aq)$	k_exf(01,ind_BrCl)	see general notes*
H76000b_a01	TrAa01MblScBrCl	$BrCl(aq) \rightarrow BrCl$	k_exb(01,ind_BrCl)	see general notes*
H76001_a01	TrAa01MblBrClN	$ClNO_3 + Br^-(aq) \rightarrow BrCl(aq) + NO_3^-(aq)$	k_exf_ClNO3(01) * 3.E5	see general notes*
H76002_a01	TrAa01MblBrClN	$BrNO_3 + Cl^-(aq) \rightarrow BrCl(aq) + NO_3^-(aq)$	k_exf_BrNO3(01) * 5.E2	see general notes*
H80000f_a01	TrAa01ScI	$I_2 \rightarrow I_2(aq)$	k_exf(01,ind_I2)	see general notes*
H80000b_a01	TrAa01ScI	$I_2(aq) \rightarrow I_2$	k_exb(01,ind_I2)	see general notes*
H81000f_a01	TrAa01MblScI	$IO \rightarrow IO(aq)$	k_exf(01,ind_IO)	see general notes*

Table 3: Reversible (Henry's law) equilibria and irreversible ("heterogenous") uptake

#	labels	reaction	rate coefficient	reference
H81000b_a01	TrAa01MblScI	IO(aq) → IO	k_exb(01,ind_IO)	see general notes*
H81001_a01	TrAa01I	OIO → HOI(aq) + HO_2(aq)	k_exf(01,ind_OIO)	see general notes*
H81002_a01	TrAa01I	I_2O_2 → HOI(aq) + H^+(aq) + IO_2^-(aq)	k_exf(01,ind_I2O2)	see general notes*
H82000f_a01	TrAa01MblScI	HOI → HOI(aq)	k_exf(01,ind_HOI)	see general notes*
H82000b_a01	TrAa01MblScI	HOI(aq) → HOI	k_exb(01,ind_HOI)	see general notes*
H82001_a01	TrAa01MblScI	HI → H^+(aq) + I^-(aq)	$k_{\mathrm{mt}}(\mathrm{HI}) \cdot lwc$	see general notes*
H82002_a01	TrAa01ScI	HIO_3 → IO_3^-(aq) + H^+(aq)	$k_{\mathrm{mt}}(\mathrm{HIO_3}) \cdot lwc$	see general notes*
H83000_a01	TrAa01IN	INO_2 → HOI(aq) + HONO(aq)	k_exf(01,ind_INO2)	see general notes*
H83001_a01	TrAa01MblIN	INO_3 → HOI(aq) + HNO_3(aq)	k_exf(01,ind_INO3)	see general notes*
H86000f_a01	TrAa01MblScClI	ICl → ICl(aq)	k_exf(01,ind_ICl)	see general notes*
H86000b_a01	TrAa01MblScClI	ICl(aq) → ICl	k_exb(01,ind_ICl)	see general notes*
H87000f_a01	TrAa01MblScBrI	IBr → IBr(aq)	k_exf(01,ind_IBr)	see general notes*
H87000b_a01	TrAa01MblScBrI	IBr(aq) → IBr	k_exb(01,ind_IBr)	see general notes*
H91000f_a01	TrAa01MblScScmS	SO_2 → SO_2(aq)	k_exf(01,ind_SO2)	see general notes*
H91000b_a01	TrAa01MblScScmS	SO_2(aq) → SO_2	k_exb(01,ind_SO2)	see general notes*
H92000_a01	TrAa01MblScScmS	H_2SO_4 → H_2SO_4(aq)	xnom7sulf*k_exf(01,ind_H2SO4)	see general notes*
H94000f_a01	TrAa01CS	DMSO → DMSO(aq)	k_exf(01,ind_DMSO)	see general notes*
H94000b_a01	TrAa01CS	DMSO(aq) → DMSO	k_exb(01,ind_DMSO)	see general notes*
H94001_a01	TrAa01MblS	CH_3SO_3H → $CH_3SO_3^-$(aq) + H^+(aq)	k_exf(01,ind_CH3SO3H)	see general notes*
H94002f_a01	TrAa01CS	DMS → DMS(aq)	k_exf(01,ind_DMS)	see general notes*
H94002b_a01	TrAa01CS	DMS(aq) → DMS	k_exb(01,ind_DMS)	see general notes*
H100000f_a01	TrAa01Hg	Hg → Hg(aq)	k_exf(01,ind_Hg)	see general notes*
H100000b_a01	TrAa01Hg	Hg(aq) → Hg	k_exb(01,ind_Hg)	see general notes*
H100100f_a01	TrAa01Hg	HgO → HgO(aq)	k_exf(01,ind_HgO)	see general notes*
H100100b_a01	TrAa01Hg	HgO(aq) → HgO	k_exb(01,ind_HgO)	see general notes*
H100600f_a01	TrAa01ClHg	$HgCl_2$ → $HgCl_2$(aq)	k_exf(01,ind_HgCl2)	see general notes*
H100600b_a01	TrAa01ClHg	$HgCl_2$(aq) → $HgCl_2$	k_exb(01,ind_HgCl2)	see general notes*
H100700f_a01	TrAa01BrHg	$HgBr_2$ → $HgBr_2$(aq)	k_exf(01,ind_HgBr2)	see general notes*
H100700b_a01	TrAa01BrHg	$HgBr_2$(aq) → $HgBr_2$	k_exb(01,ind_HgBr2)	see general notes*
H100701f_a01	TrAa01BrClHg	ClHgBr → ClHgBr(aq)	k_exf(01,ind_ClHgBr)	see general notes*
H100701b_a01	TrAa01BrClHg	ClHgBr(aq) → ClHgBr	k_exb(01,ind_ClHgBr)	see general notes*
H100702f_a01	TrAa01BrHg	BrHgOBr → BrHgOBr(aq)	k_exf(01,ind_BrHgOBr)	see general notes*
H100702b_a01	TrAa01BrHg	BrHgOBr(aq) → BrHgOBr	k_exb(01,ind_BrHgOBr)	see general notes*
H100703f_a01	TrAa01BrClHg	ClHgOBr → ClHgOBr(aq)	k_exf(01,ind_ClHgOBr)	see general notes*
H100703b_a01	TrAa01BrClHg	ClHgOBr(aq) → ClHgOBr	k_exb(01,ind_ClHgOBr)	see general notes*

General notes

The forward (`k_exf`) and backward (`k_exb`) rate coefficients are calculated in subroutine `mecca_aero_calc_k_ex` in the file `messy_mecca_aero.f90` using accommodation coefficients and Henry's law constants from chemprop (see `chemprop.pdf`).

For uptake of X (X = N_2O_5, $ClNO_3$, or $BrNO_3$) and subsequent reaction with H_2O, Cl^-, and Br^- in H3201, H6300, H6301, H6302, H7300, H7301, H7302, H7601, and H7602, we define:

$$k_{\mathrm{exf}}(\mathrm{X}) = \frac{k_{\mathrm{mt}}(\mathrm{X}) \times \mathrm{LWC}}{[\mathrm{H_2O}] + 5 \times 10^2 [\mathrm{Cl^-}] + 3 \times 10^5 [\mathrm{Br^-}]}$$

Here, k_{mt} = mass transfer coefficient, and LWC = liquid water content of the aerosol. The total uptake rate of X is only determined by k_{mt}. The factors only affect the branching between hydrolysis and the halide reactions. The factor $5{\times}10^2$ was chosen such that the chloride reaction dominates over hydrolysis at about $[Cl^-] > 0.1$ M (see Fig. 3 in Behnke et al. (1997)), i.e. when the ratio $[H_2O]/[Cl^-]$ is less than $5{\times}10^2$. The ratio $5{\times}10^2/3{\times}10^5$ was chosen such that the reactions with chloride and bromide are roughly equal for sea water composition (Behnke et al., 1994). These ratios were measured for uptake of N_2O_5. Here, they are also used for $ClNO_3$ and $BrNO_3$.

Table 4: Heterogeneous reactions

#	labels	reaction	rate coefficient	reference
HET300	StHetN	$N_2O_5 + H_2O \rightarrow 2\ HNO_3$	khet_St(ihs_N2O5_H2O)	see general notes*
HET301	TrHetN	$N_2O_5 \rightarrow 2\ NO_3^-(cs) + 2\ H^+(cs)$	khet_Tr(iht_N2O5)	see general notes*
HET610	StHetCl	$HOCl + HCl \rightarrow Cl_2 + H_2O$	khet_St(ihs_HOCl_HCl)	see general notes*
HET620	StHetClN	$ClNO_3 + HCl \rightarrow Cl_2 + HNO_3$	khet_St(ihs_ClNO3_HCl)	see general notes*
HET621	StHetClN	$ClNO_3 + H_2O \rightarrow HOCl + HNO_3$	khet_St(ihs_ClNO3_H2O)	see general notes*
HET622	StHetClN	$N_2O_5 + HCl \rightarrow ClNO_2 + HNO_3$	khet_St(ihs_N2O5_HCl)	see general notes*
HET710	StHetBr	$HOBr + HBr \rightarrow Br_2 + H_2O$	khet_St(ihs_HOBr_HBr)	see general notes*
HET720	StHetBrN	$BrNO_3 + H_2O \rightarrow HOBr + HNO_3$	khet_St(ihs_BrNO3_H2O)	see general notes*
HET740	StHetBrClN	$ClNO_3 + HBr \rightarrow BrCl + HNO_3$	khet_St(ihs_ClNO3_HBr)	see general notes*
HET741	StHetBrClN	$BrNO_3 + HCl \rightarrow BrCl + HNO_3$	khet_St(ihs_BrNO3_HCl)	see general notes*
HET742	StHetBrCl	$HOCl + HBr \rightarrow BrCl + H_2O$	khet_St(ihs_HOCl_HBr)	see general notes*
HET743	StHetBrCl	$HOBr + HCl \rightarrow BrCl + H_2O$	khet_St(ihs_HOBr_HCl)	see general notes*
HET1001	StTrHetHg	$Hg \rightarrow Hg(cs)$	khet_Tr(iht_Hg) + khet_St(ihs_Hg)	see general notes*
HET1002	StTrHetHg	$HgO \rightarrow Hg(cs)$	khet_Tr(iht_RGM) + khet_St(ihs_RGM)	see general notes*
HET1003	StTrHetClHg	$HgCl \rightarrow Hg(cs) + LCHLORINE$	khet_Tr(iht_RGM) + khet_St(ihs_RGM)	see general notes*
HET1004	StTrHetClHg	$HgCl_2 \rightarrow Hg(cs) + 2\ LCHLORINE$	khet_Tr(iht_RGM) + khet_St(ihs_RGM)	see general notes*
HET1005	StTrHetBrHg	$HgBr \rightarrow Hg(cs) + LBROMINE$	khet_Tr(iht_RGM) + khet_St(ihs_RGM)	see general notes*
HET1006	StTrHetBrHg	$HgBr_2 \rightarrow Hg(cs) + 2\ LBROMINE$	khet_Tr(iht_RGM) + khet_St(ihs_RGM)	see general notes*
HET1007	StTrHetBrClHg	$ClHgBr \rightarrow Hg(cs) + LCHLORINE + LBROMINE$	khet_Tr(iht_RGM) + khet_St(ihs_RGM)	see general notes*
HET1008	StTrHetBrHg	$BrHgOBr \rightarrow Hg(cs) + 2\ LBROMINE$	khet_Tr(iht_RGM) + khet_St(ihs_RGM)	see general notes*
HET1009	StTrHetBrClHg	$ClHgOBr \rightarrow Hg(cs) + LCHLORINE + LBROMINE$	khet_Tr(iht_RGM) + khet_St(ihs_RGM)	see general notes*

General notes

Heterogeneous reaction rates are calculated with an external module (e.g., MECCA_KHET) and then supplied to the MECCA chemistry (see www.messy-interface.org for details)

Table 5: Acid-base and other equilibria

#	labels	reaction	$K_0[M^{m-n}]$	$-\Delta H/R[K]$	reference
EQ2100_a01	TrAa01Sc	$HO_2 \rightleftharpoons O_2^- + H^+$	1.6E-5		Weinstein-Lloyd and Schwartz (1991)
EQ2101_a01	TrAa01MblScScm	$H_2O \rightleftharpoons H^+ + OH^-$	1.0E-16	-6716	Chameides (1984)
EQ2102_a01	TrAa01Sc	$HO_3 \rightleftharpoons O_3^- + H^+$	4.4E-9		Staehelin et al. (1984)
EQ3200_a01	TrAa01MblScScmN	$NH_4^+ \rightleftharpoons H^+ + NH_3$	5.88E-10	-2391	Chameides (1984)
EQ3201_a01	TrAa01ScN	$HONO \rightleftharpoons H^+ + NO_2^-$	5.1E-4	-1260	Schwartz and White (1981)
EQ3202_a01	TrAa01MblScScmN	$HNO_3 \rightleftharpoons H^+ + NO_3^-$	15	8700	Davis and de Bruin (1964)
EQ3203_a01	TrAa01ScN	$HNO_4 \rightleftharpoons NO_4^- + H^+$	1.E-5		Warneck (1999)
EQ4100_a01	TrAa01MblScScm	$CO_2 \rightleftharpoons H^+ + HCO_3^-$	4.3E-7	-913	Chameides (1984)*
EQ4101_a01	TrAa01ScScm	$HCOOH \rightleftharpoons H^+ + HCOO^-$	1.8E-4		Weast (1980)
EQ4150_a01	TrAa01Sc	$HCHO \rightleftharpoons HOCH_2OH$	4.11E-3	-3769	see note*
EQ4151_a01	TrAa01Sc	$HCO_3 \rightleftharpoons HCOHOHO_2$	1.08E1	-2936	see note*
EQ4200_a01	TrAa01ScScmC	$CH_3COOH \rightleftharpoons H^+ + CH_3COO^-$	1.754E-5		Fisher and Barnes (1972)*
EQ4201_a01	TrAa01C	$CH_3C(O)OOH \rightleftharpoons CH_3COOO^- + H^+$	6.3E-9		Schuchmann and von Sonntag (1988)
EQ4202_a01	TrAa01C	$HOCH_2CO_3H \rightleftharpoons CH_2OHCO_2O^- + H^+$	6.3E-9		Schuchmann and von Sonntag (1988)*
EQ4203_a01	TrAa01C	$HOOCCOOH \rightleftharpoons H^+ + HOOCCOO^-$	5.6E-2		Martell (1977)
EQ4204_a01	TrAa01C	$HOOCCOO^- \rightleftharpoons H^+ + C_2O_4^{2-}$	5.4E-5		Martell (1977)
EQ4205_a01	TrAa01C	$HOOCH2CO2H \rightleftharpoons H^+ + CH_2OOHCO_2^-$	1.754E-5		Fisher and Barnes (1972)*
EQ4206_a01	TrAa01C	$CH_2OOCOOH \rightleftharpoons H^+ + CH_2OOCO_2^-$	1.754E-5		Fisher and Barnes (1972)*
EQ4207_a01	TrAa01C	$CHOOHOOCOOH \rightleftharpoons H^+ + CHOOHOOCO_2^-$	1.754E-5		Fisher and Barnes (1972)*
EQ4208_a01	TrAa01C	$HOCH_2CO_2H \rightleftharpoons H^+ + CH_2OHCO_2^-$	1.5E-4		Rumble (2020)
EQ4209_a01	TrAa01C	$CHOHOOCOOH \rightleftharpoons H^+ + CHOHOOCOO_2^-$	1.5E-4		Rumble (2020)*
EQ4210_a01	TrAa01C	$CHOCOOH \rightleftharpoons H^+ + CHOCOO^-$	1.754E-5		Fisher and Barnes (1972)
EQ4211_a01	TrAa01C	$COOHCO_3 \rightleftharpoons H^+ + CO_2^-CO_3$	1.754E-5		Fisher and Barnes (1972)
EQ4250_a01	TrAa01ScC	$CH_3CHO \rightleftharpoons CH_3CHOHOH$	1.22		Tur'yan (2000)
EQ4251_a01	TrAa01C	$CHOHOOCHO \rightleftharpoons CHOHOOCHOHOH$	1.57E1		see note*
EQ4252_a01	TrAa01C	$CH_2OHCHO \rightleftharpoons CH_2OHCHOHOH$	1.56E1		Doussin and Monod (2013)
EQ4253_a01	TrAa01C	$GLYOX \rightleftharpoons CHOCHOHOH$	3.5E2		Ervens and Volkamer (2010)
EQ4254_a01	TrAa01C	$CHOCHOHOH \rightleftharpoons CHOHOHCHOHOH$	2.0E2		Ervens and Volkamer (2010)
EQ4255_a01	TrAa01C	$CHOCOOH \rightleftharpoons CHOOHOHCOOH$	1.1E3		Doussin and Monod (2013)
EQ4256_a01	TrAa01C	$CHOCOO^- \rightleftharpoons CHOHOHCO_2^-$	6.6E1		Doussin and Monod (2013)
EQ4257_a01	TrAa01C	$CO_2^-CO_3 \rightleftharpoons CO2^-COHOHO_2$	6.6E1		see note*
EQ4258_a01	TrAa01C	$CH_2OOHCHO \rightleftharpoons HOOCH_2CHOHOH$	1.56E1		see note*
EQ4300_a01	TrAa01C	$CH_3COCOOH \rightleftharpoons H^+ + CH_3COCO2^-$	4.1E-3		Rumble (2020)

Table 5: Acid-base and other equilibria

#	labels	reaction	$K_0[M^{m-n}]$	$-\Delta H/R[K]$	reference
EQ4350_a01	TrAa01C	$CH_3C(O)CHO \rightleftharpoons CH_3COCHOHOH$	1.98E3		Doussin and Monod (2013)
EQ6000_a01	TrAa01Cl	$Cl_2^- \rightleftharpoons Cl + Cl^-$	7.3E-6		Yu (2004)
EQ6200_a01	TrAa01MblScScmCl	$HCl \rightleftharpoons H^+ + Cl^-$	1.7E6	6896	Marsh and McElroy (1985)
EQ6201_a01	TrAa01ScCl	$HOCl \rightleftharpoons H^+ + ClO^-$	3.2E-8		Lax (1969)
EQ7000_a01	TrAa01Br	$Br_2^- \rightleftharpoons Br + Br^-$	2.54E-6	-2256	Liu et al. (2002)
EQ7200_a01	TrAa01MblScScmBr	$HBr \rightleftharpoons H^+ + Br^-$	1.0E9		Lax (1969)
EQ7201_a01	TrAa01ScBr	$HOBr \rightleftharpoons H^+ + BrO^-$	2.3E-9	-3091	Kelley and Tartar (1956)*
EQ7600_a01	TrAa01MblBrCl	$BrCl + Cl^- \rightleftharpoons BrCl_2^-$	3.8	1191	Wang et al. (1994)
EQ7601_a01	TrAa01MblBrCl	$BrCl + Br^- \rightleftharpoons Br_2Cl^-$	1.8E4	7457	Wang et al. (1994)
EQ7602_a01	TrAa01MblBrCl	$Br_2 + Cl^- \rightleftharpoons Br_2Cl^-$	1.3	0	Wang et al. (1994)
EQ7603_a01	TrAa01MblBrCl	$Br^- + Cl_2 \rightleftharpoons BrCl_2^-$	4.2E6	14072	Wang et al. (1994)
EQ8600_a01	TrAa01MblScClI	$ICl + Cl^- \rightleftharpoons ICl_2^-$	7.7E1		Wang et al. (1989)
EQ8700_a01	TrAa01MblScBrI	$IBr + Br^- \rightleftharpoons IBr_2^-$	2.9E2		Troy and Margerum (1991)
EQ8701_a01	TrAa01MblScBrClI	$ICl + Br^- \rightleftharpoons IBr + Cl^-$	3.3E2		see note*
EQ9200_a01	TrAa01MblScScmS	$SO_2 \rightleftharpoons H^+ + HSO_3^-$	1.7E-2	2090	Chameides (1984)
EQ9201_a01	TrAa01MblScScmS	$HSO_3^- \rightleftharpoons H^+ + SO_3^{2-}$	6.0E-8	1120	Chameides (1984)
EQ9202_a01	TrAa01MblScScmS	$HSO_4^- \rightleftharpoons H^+ + SO_4^{2-}$	1.2E-2	2720	Seinfeld and Pandis (1998)
EQ9203_a01	TrAa01MblScScmS	$H_2SO_4 \rightleftharpoons H^+ + HSO_4^-$	1.0E3		Seinfeld and Pandis (1998)
EQ10200_a01	TrAa01Hg	$Hg^{2+} + OH^- \rightleftharpoons HgOH^+$	4.0E10		Ammann and Pöschl (2007)
EQ10201_a01	TrAa01Hg	$HgOH^+ + OH^- \rightleftharpoons Hg(OH)_2$	1.58E11		Ammann and Pöschl (2007)
EQ10600_a01	TrAa01ClHg	$Hg^{2+} + Cl^- \rightleftharpoons HgCl^+$	5.8E6		Ammann and Pöschl (2007)
EQ10601_a01	TrAa01ClHg	$HgCl^+ + Cl^- \rightleftharpoons HgCl_2$	2.5E6		Ammann and Pöschl (2007)
EQ10602_a01	TrAa01ClHg	$HgOH^+ + Cl^- \rightleftharpoons Hg(OH)Cl$	2.69E7		Ammann and Pöschl (2007)
EQ10700_a01	TrAa01BrHg	$Hg^{2+} + Br^- \rightleftharpoons HgBr^+$	1.1E9		Raofie and Ariya (2004)
EQ10701_a01	TrAa01BrHg	$HgBr^+ + Br^- \rightleftharpoons HgBr_2$	2.5E8		Raofie and Ariya (2004)
EQ10800_a01	TrAa01HgS	$Hg^{2+} + SO_3^{2-} \rightleftharpoons HgSO_3$	2.E13		van Loon et al. (2001)
EQ10801_a01	TrAa01HgS	$HgSO_3 + SO_3^{2-} \rightleftharpoons Hg(SO_3)_2^{2-}$	1.E10		van Loon et al. (2001)
EQ11200_a01	TrAa01Fe	$Fe^{3+} \rightleftharpoons FeOH^{2+} + H^+$	2.34E-3		de Laat and Le (2006)*
EQ11201_a01	TrAa01Fe	$FeOH^{2+} \rightleftharpoons Fe(OH)_2^+ + H^+$	2E-4		de Laat and Le (2006)*
EQ11202_a01	TrAa01Fe	$Fe^{3+} + H_2O_2 \rightleftharpoons FeHO_2^{2+} + H^+$	3.1E-3		de Laat and Le (2006)
EQ11203_a01	TrAa01Fe	$FeOH^{2+} + H_2O_2 \rightleftharpoons Fe(OH)(HO_2)^+ + H^+$	2E-4		de Laat and Le (2006)
EQ11600_a01	TrAa01ClFe	$Fe^{3+} + Cl^- \rightleftharpoons FeCl^{2+}$	6.61		de Laat and Le (2006)*
EQ11601_a01	TrAa01ClFe	$FeCl^{2+} + Cl^- \rightleftharpoons FeCl_2^+$	1.6		de Laat and Le (2006)*
EQ11800_a01	TrAa01FeS	$Fe^{3+} + SO_4^{2-} \rightleftharpoons FeSO_4^+$	120		Brand and van Eldik (1995)*

Table 5: Acid-base and other equilibria

#	labels	reaction	$K_0[M^{m-n}]$	$-\Delta H/R[K]$	reference
EQ11801_a01	TrAa01FeS	$FeOH^{2+} + HSO_3^- \rightleftharpoons FeSO_3^+$	8.25E2		Warneck (2018)*
EQ11802_a01	TrAa01FeS	$Fe^{2+} + SO_3^- \rightleftharpoons FeSO_3^+$	1.6E7		Warneck (2018)

Specific notes

EQ4100_a01: For $pK_a(CO_2)$, see also Dickson and Millero (1987).

EQ4150_a01: Hydration from Winkelman et al. (2000) and dehydration from Winkelman et al. (2002). Bell and Evans (1966) found that acid catalysis is negligible.

EQ4151_a01: Assumed to be the same as for HCHO.

EQ4200_a01: The pK_A has a minimum near 298 K, the temperature dependence is therefore small.

EQ4202_a01: Same as for CH3CO3H.

EQ4205_a01: Same as for CH3CO2H.

EQ4206_a01: Same as for CH3CO2H.

EQ4207_a01: Same as for CH3CO2H.

EQ4209_a01: Same as HOCH2CO2H.

EQ4251_a01: Calculated as K_{eq} * k(dehydration) where dehydration is assumed to be the same as for acetaldehyde.

EQ4257_a01: Assumed to be equal to CHOCO2m.

EQ4258_a01: Same as for $HOCH_2CHO$.

EQ7201_a01: For pK_a(HOBr), see also Keller-Rudek et al. (1992).

EQ8701_a01: Thermodynamic calculations on the IBr/ICl equilibrium according to the data tables from Wagman et al. (1982):

ICl	+	Br^-	$\rightleftharpoons$	IBr	+	Cl^-
-17.1		-103.96	=	-4.2		-131.228

$$\frac{\Delta G}{[\text{kJ/mol}]} = -4.2 - 131.228 - (-17.1 - 103.96) = -14.368$$

$$K = \frac{[\text{IBr}] \times [\text{Cl}^-]}{[\text{ICl}] \times [\text{Br}^-]} = \exp\left(\frac{-\Delta G}{RT}\right) = \exp\left(\frac{14368}{8.314 \times 298}\right) = 330$$

This means we have equal amounts of IBr and ICl when the $[Cl^-]/[Br^-]$ ratio equals 330.

EQ11200_a01: See also K values listed in Tab. 2.5 of Brand and van Eldik (1995).

EQ11201_a01: Equilibrium calculated from K_1 and K_2 in Tab. 1 of de Laat and Le (2006). k for back reaction assumed. See also K values listed in Tab. 2.5 of Brand and van Eldik (1995).

EQ11600_a01: See also K values listed in Tab. 2.5 of Brand and van Eldik (1995).

EQ11601_a01: Equilibrium calculated from K_{29} and K_{30} in Tab. 2 of de Laat and Le (2006). k for forward reaction assumed. See also K values listed in Tab. 2.5 of Brand and van Eldik (1995).

EQ11800_a01: Equilibrium at $I = 1$ M. k for back reaction assumed.

EQ11801_a01: Rate of equilibration assumed.

Table 6: Aqueous phase reactions

#	labels	reaction	k_0 $[M^{1-n}s^{-1}]$	$-E_a/R[K]$	reference
A10000_a01	TrAa01Sc	$O_3 + O_2^- \rightarrow O_3^- + O_2$	1.50E9		Staehelin et al. (1984)
A21000_a01	TrAa01Sc	$OH + O_2^- \rightarrow OH^-$	1.0E10		Sehested et al. (1968)
A21001_a01	TrAa01Sc	$OH + OH \rightarrow H_2O_2$	5.5E9		Buxton et al. (1988)
A21002_a01	TrAa01Sc	$HO_2 + O_2^- \rightarrow H_2O_2 + OH^-$	1.0E8	-900	Christensen and Sehested (1988)
A21003_a01	TrAa01Sc	$HO_2 + OH \rightarrow H_2O$	7.1E9		Sehested et al. (1968)
A21004_a01	TrAa01Sc	$HO_2 + HO_2 \rightarrow H_2O_2$	9.7E5	-2500	Christensen and Sehested (1988)
A21005_a01	TrAa01Sc	$H_2O_2 + OH \rightarrow HO_2$	2.7E7	-1684	Christensen et al. (1982)
A21006_a01	TrAa01Sc	$O_3 + OH \rightarrow HO_4$	1.10E8		Staehelin et al. (1984)
A21007_a01	TrAa01Sc	$O_3 + OH^- \rightarrow HO_2 + O_2^-$	7.00E1		Staehelin et al. (1984)
A21008_a01	TrAa01Sc	$HO_3 \rightarrow OH + O_2$	1.10E5		Staehelin et al. (1984)
A21009_a01	TrAa01Sc	$HO_4 \rightarrow HO_2 + O_2$	2.80E4		Staehelin et al. (1984)
A21010_a01	TrAa01Sc	$HO_4 + HO_4 \rightarrow H_2O_2 + 2\ O_3$	5.00E9		Staehelin et al. (1984)
A21011_a01	TrAa01Sc	$HO_4 + HO_3 \rightarrow H_2O_2 + O_3 + O_2$	5.00E9		Staehelin et al. (1984)
A31000_a01	TrAa01ScN	$NO_2^- + O_3 \rightarrow NO_3^-$	5.0E5	-6950	Damschen and Martin (1983)
A31001_a01	TrAa01ScN	$NO_2 + NO_2 \rightarrow HNO_3 + HONO$	1.0E8		Lee and Schwartz (1981)
A31002_a01	TrAa01ScN	$NO_4^- \rightarrow NO_2^-$	8.0E1		Warneck (1999)
A32000_a01	TrAa01ScN	$NO_2 + HO_2 \rightarrow HNO_4$	1.8E9		Warneck (1999)
A32001_a01	TrAa01ScN	$NO_2^- + OH \rightarrow NO_2 + OH^-$	1.0E10		Wingenter et al. (1999)
A32002_a01	TrAa01ScN	$NO_3^- + OH^- \rightarrow NO_3^- + OH$	8.2E7	-2700	Exner et al. (1992)
A32003_a01	TrAa01ScN	$HONO + OH \rightarrow NO_2$	1.0E10		Barker et al. (1970)
A32004_a01	TrAa01ScN	$HONO + H_2O_2 + H^+ \rightarrow HNO_3 + H^+$	4.6E3	-6800	Damschen and Martin (1983)
A41000_a01	TrAa01Sc	$CO_3^- + O_2^- \rightarrow HCO_3^- + OH^-$	6.5E8		Ross et al. (1992)
A41001_a01	TrAa01Sc	$CO_3^- + H_2O_2 \rightarrow HCO_3^- + HO_2$	4.3E5		Ross et al. (1992)
A41002_a01	TrAa01Sc	$HCOO^- + CO_3^- \rightarrow 2\ HCO_3^- + HO_2$	1.5E5		Ross et al. (1992)
A41003_a01	TrAa01Sc	$HCOO^- + OH \rightarrow O_2^- + H_2O + CO_2$	3.1E9	-1240	Chin and Wine (1994)
A41004_a01	TrAa01ScN	$HCOO^- + NO_3 \rightarrow NO_3^- + H^+ + O_2^- + CO_2$	5.1E7	-2200	Exner et al. (1994)*
A41005_a01	TrAa01Sc	$HCOO^- + O_3 \rightarrow OH + O_2^- + CO_2$	1.00E2		Hoigné and Bader (1983)
A41006_a01	TrAa01Sc	$HCO_3^- + OH \rightarrow CO_3^-$	8.5E6		Ross et al. (1992)
A41007_a01	TrAa01Sc	$HCHO + OH \rightarrow HCOOH + HO_2$	7.7E8	-1020	Chin and Wine (1994)
A41008_a01	TrAa01Sc	$HCOOH + OH \rightarrow HO_2 + CO_2$	1.1E8	-991	Chin and Wine (1994)
A41009_a01	TrAa01ScN	$HCOOH + NO_3 \rightarrow NO_3^- + H^+ + HO_2 + CO_2$	3.8E5	-3400	Exner et al. (1994)*
A41010_a01	TrAa01Sc	$CH_3OO + HO_2 \rightarrow CH_3OOH$	4.3E5		Jacob (1986)
A41011_a01	TrAa01Sc	$CH_3OO + O_2^- \rightarrow CH_3OOH + OH^-$	5.0E7		Jacob (1986)
A41012a_a01	TrAa01Sc	$CH_3OO + CH_3OO \rightarrow 2\ HCHO + H_2O_2$	0.20 × 1.96E8	-2165	Herrmann et al. (1999b)*

Table 6: Aqueous phase reactions (...continued)

#	labels	reaction	k_0 $[M^{1-n}s^{-1}]$	$-E_a/R[K]$	reference
A41012b_a01	TrAa01Sc	$CH_3OO + CH_3OO \rightarrow 2\ HOCH_2O_2$	0.80 × 1.96E8	-2165	Herrmann et al. (1999b)*
A41013a_a01	TrAa01Sc	$CH_3OH + OH \rightarrow HOCH_2O_2 + H_2O$	0.93 × 9.70E8	-600	Elliot and McCracken (1989)*
A41013b_a01	TrAa01Sc	$CH_3OH + OH \rightarrow HCHO + HO_2 + H_2O$	0.07 × 9.70E8	-600	Elliot and McCracken (1989)
A41014_a01	TrAa01ScN	$CH_3OH + NO_3 \rightarrow HOCH_2O_2 + NO_3^- + H^+$	5.40E5	-4300	Ervens et al. (2003a)
A41015_a01	TrAa01Sc	$CH_3OH + CO_3^- \rightarrow HOCH_2O_2 + HCO_3^-$	5.8E3	-3079	Clifton and Huie (1993)
A41016a_a01	TrAa01Sc	$CH_3OOH + OH \rightarrow CH_3OO + H_2O$	0.25 × 6.30E8		Monod et al. (2007)*
A41016b_a01	TrAa01Sc	$CH_3OOH + OH \rightarrow HCHO + OH + H_2O$	0.75 × 6.30E8		Monod et al. (2007)*
A41017a_a01	TrAa01ScN	$CH_3OOH + NO_3 \rightarrow CH_3OO + NO_3^- + H^+$	0.25 × 4.90E6	-2000	see note*
A41017b_a01	TrAa01ScN	$CH_3OOH + NO_3 \rightarrow HCHO + HO_2 + NO_3^- + H^+$	0.75 × 4.90E6	-2000	see note*
A41018a_a01	TrAa01Sc	$CH_3OOH + CO_3^- \rightarrow CH_3OO + HCO_3^-$	0.25 × 4.30E5		see note*
A41018b_a01	TrAa01Sc	$CH_3OOH + CO_3^- \rightarrow HCHO + HO_2 + HCO_3^-$	0.75 × 4.30E5		see note*
A41019a_a01	TrAa01	$HOCH_2OOH + OH \rightarrow HOCH_2O_2 + H_2O$	0.25 × 6.30E8		see note*
A41019b_a01	TrAa01	$HOCH_2OOH + OH \rightarrow CHOOOH + HO_2 + H_2O$	0.75 × 6.30E8		see note*
A41020a_a01	TrAa01N	$HOCH_2OOH + NO_3 \rightarrow HOCH_2O_2 + NO_3^- + H^+$	0.25 × 4.90E6	-2000	see note*
A41020b_a01	TrAa01N	$HOCH_2OOH + NO_3 \rightarrow CHOOOH + HO_2 + NO_3^- + H^+$	0.75 × 4.90E6	-2000	see note*
A41021_a01	TrAa01Sc	$HOCH_2O_2 \rightarrow HCHO + HO_2$	1.00E1		see note*
A41022_a01	TrAa01Sc	$HOCH_2O_2 + HO_2 \rightarrow HOCH_2OOH + O_2$	9.7E5	-2500	see note*
A41023_a01	TrAa01Sc	$HOCH_2O_2 + O_2^- \rightarrow HOCH_2OOH + O_2 + OH^-$	1.0E8	-900	see note*
A41024_a01	TrAa01Sc	$HOCH_2O_2 + HOCH_2O_2 \rightarrow 2\ HCOOH + H_2O_2$	7.4E8	-1395	Huie and Clifton (1993)
A41025_a01	TrAa01Sc	$HCOOH + H_2O_2 + H^+ \rightarrow CHOOOH + H_2O + H^+$	3.1E-4	-5235	De Filippis et al. (2009)
A41026a_a01	TrAa01Sc	$CHOOOH + H^+ \rightarrow HCOOH + H_2O_2 + H^+$	3.8E-4	-5235	De Filippis et al. (2009)
A41026b_a01	TrAa01Sc	$CHOOOH + H^+ \rightarrow CO_2 + H_2O + H^+$	1.2E-3	-8735	De Filippis et al. (2009)
A41027_a01	TrAa01Sc	$HOCH_2OH + OH \rightarrow HCOHOHO_2 + H_2O$	7.70E8	-1000	Chin and Wine (1994)
A41028_a01	TrAa01Sc	$HOCH_2OH + CO_3^- \rightarrow HCO_3^- + HCOHOHO_2$	1.30E4		Zellner et al. (1996)
A41029_a01	TrAa01ScN	$HOCH_2OH + NO_3 \rightarrow NO_3^- + H^+ + HCOHOHO_2$	1.0E6	-4500	Exner et al. (1993)
A41030_a01	TrAa01Sc	$HCOHOHO_2 \rightarrow HCOOH + HO_2$	1.00E6		see note*
A42000a_a01	TrAa01C	$CH_3CH_2OH + OH \rightarrow CH_3CHO + HO_2 + H_2O$	0.90 × 2.1E9	-830	Monod et al. (2005)*
A42000b_a01	TrAa01C	$CH_3CH_2OH + OH \rightarrow CH_2OHCH_2OO + H_2O$	0.10 × 2.1E9	-830	Monod et al. (2005)
A42001a_a01	TrAa01CN	$CH_3CH_2OH + NO_3 \rightarrow CH_3CHO + HO_2 + NO_3^- + H^+$	0.90 × 2.2E6	-3300	Ervens et al. (2003a)*
A42001b_a01	TrAa01CN	$CH_3CH_2OH + NO_3 \rightarrow CH_2OHCH_2OO + NO_3^- + H^+$	0.10 × 2.2E6	-3300	Ervens et al. (2003a)
A42002a_a01	TrAa01C	$CH_2OHCH_2OO + CH_2OHCH_2OO \rightarrow CH_2OHCHO + CH_2OHCHO + H_2O_2$	0.50 × 1.00E8		Piesiak et al. (1984)

Table 6: Aqueous phase reactions (...continued)

#	labels	reaction	k_0 $[M^{1-n}s^{-1}]$	$-E_a/R[K]$	reference
A42002b_a01	TrAa01C	$CH_2OHCH_2OO + CH_2OHCH_2OO \rightarrow CH_2OHCHO + ETHGLY$	0.33 × 1.00E8		Piesiak et al. (1984)
A42002c_a01	TrAa01C	$CH_2OHCH_2OO + CH_2OHCH_2OO \rightarrow 2\ HOCH_2O_2 + 2\ HCHO$	0.17 × 1.00E8		Piesiak et al. (1984)
A42003_a01	TrAa01C	$CH_2OHCH_2OO + O_2^- \rightarrow HYETHO2H + OH^-$	1.0E8	-900	see note*
A42004_a01	TrAa01C	$CH_2OHCH_2OO + HO_2 \rightarrow HYETHO2H$	9.7E5	-2500	see note*
A42005_a01	TrAa01C	$HYETHO2H + OH \rightarrow CH_2OHCHO$	1.10E9		see note*
A42006_a01	TrAa01C	$ETHGLY + OH \rightarrow CH_2OHCHO + HO_2 + H_2O$	1.7E9	-1191	Hoffmann et al. (2009)*
A42007_a01	TrAa01CN	$ETHGLY + NO_3 \rightarrow CH_2OHCHO + HO_2 + NO_3^- + H^+$	5.8E6	-2117	Hoffmann et al. (2009)*
A42008_a01	TrAa01C	$CH_3CHO + OH \rightarrow CH_3COOO + H_2O$	3.60E9		Schuchmann and von Sonntag (1988)
A42009_a01	TrAa01CN	$CH_3CHO + NO_3 \rightarrow CH_3COOO + NO_3^- + H^+$	3.10E6		Rousse and George (2004)
A42010_a01	TrAa01C	$CH_3COOO + CH_3COOO \rightarrow CH_3OO + CH_3OO + CO_2 + CO_2$	1.9E8	1563	see note*
A42011_a01	TrAa01C	$CH_3COOO + O_2^- \rightarrow CH_3COOO^- + O_2$	1.00E9		Schuchmann and von Sonntag (1988)
A42012_a01	TrAa01C	$CH_3CHOHOH + OH \rightarrow CH_3COHOHOO + H_2O$	1.20E9		Schuchmann and von Sonntag (1988)
A42013_a01	TrAa01CN	$CH_3CHOHOH + NO_3 \rightarrow CH_3COHOHOO + NO_3^- + H^+$	1.10E6		Rousse and George (2004)
A42014_a01	TrAa01C	$CH_3COHOHOO \rightarrow CH_3COOH + HO_2$	1.00E6		see note*
A42015a_a01	TrAa01C	$CH_2OHCHO + OH \rightarrow CH_2OHCO3 + H_2O$	0.77 × 1.40E9		Doussin and Monod (2013)
A42015b_a01	TrAa01C	$CH_2OHCHO + OH \rightarrow CHOHOOCHO + H_2O$	0.23 × 1.40E9		Doussin and Monod (2013)
A42016a_a01	TrAa01CN	$CH_2OHCHO + NO_3 \rightarrow CH_2OHCO3 + NO_3^- + H^+$	0.77 × 3.10E6		see note*
A42016b_a01	TrAa01CN	$CH_2OHCHO + NO_3 \rightarrow CHOHOOCHO + NO_3^- + H^+$	0.23 × 3.10E6		see note*
A42017_a01	TrAa01C	$CH_2OHCO3 + O_2^- \rightarrow CH_2OHCO_2O^-$	1.00E9		see note*
A42018_a01	TrAa01C	$CH_2OHCOHOHO_2 \rightarrow HOCH_2CO_2H + HO_2$	1.00E6		see note*
A42019_a01	TrAa01C	$CHOHOOCHO \rightarrow GLYOX + HO_2$	1.90E2		see note*
A42020_a01	TrAa01C	$CHOHOOCHOHOH \rightarrow CHOCHOHOH + HO_2$	1.90E2		see note*
A42021a_a01	TrAa01C	$CH_2OHCHOHOH + OH \rightarrow CH_2OHCOHOHO_2 + H_2O$	0.33 × 1.10E9		Doussin and Monod (2013)
A42021b_a01	TrAa01C	$CH_2OHCHOHOH + OH \rightarrow CHOHOOCHOHOH + H_2O$	0.28 × 1.10E9		Doussin and Monod (2013)

Table 6: Aqueous phase reactions (...continued)

#	labels	reaction	k_0 $[M^{1-n}s^{-1}]$	$-E_a/R[K]$	reference
A42021c_a01	TrAa01C	$CH_2OHCHOHOH + OH \rightarrow HCOOH + HOCH_2O_2 + H_2O$	0.39 × 1.10E9		Doussin and Monod (2013)
A42022a_a01	TrAa01CN	$CH_2OHCHOHOH + NO_3 \rightarrow CH_2OHCOHOHO_2 + NO_3^- + H^+$	0.33 × 1.10E6		see note*
A42022b_a01	TrAa01CN	$CH_2OHCHOHOH + NO_3 \rightarrow CHOHOOCHOHOH + NO_3^- + H^+$	0.28 × 1.10E6		see note*
A42022c_a01	TrAa01CN	$CH_2OHCHOHOH + NO_3 \rightarrow HCOOH + HOCH_2O_2 + NO_3^- + H^+$	0.39 × 1.10E6		see note*
A42023a_a01	TrAa01C	$CHOHOHCHOHOH + OH \rightarrow CHOHOHCOHOHO_2 + H_2O$	0.27 × 1.1E9	-1516	Buxton et al. (1997)
A42023b_a01	TrAa01C	$CHOHOHCHOHOH + OH \rightarrow HCOOH + HCOHOHO_2 + HO_2 + H_2O$	0.73 × 1.1E9	-1516	Buxton et al. (1997)*
A42024a_a01	TrAa01CN	$CHOHOHCHOHOH + NO_3 \rightarrow CHOHOHCOHOHO_2 + NO_3^- + H^+$	0.27 × 1.00E6		see note*
A42024b_a01	TrAa01CN	$CHOHOHCHOHOH + NO_3 \rightarrow HCOOH + HCOHOHO_2 + HO_2 + NO_3^- + H^+$	0.73 × 1.00E6		see note*
A42025_a01	TrAa01C	$CHOHOHCOHOHO_2 \rightarrow CHOOHOHCOOH + HO_2$	0.77 × 1.00E6		see note*
A42026_a01	TrAa01C	$CH_3COOH + OH \rightarrow CH_2OOCOOH + H_2O$	1.50E7	-1330	Chin and Wine (1994)
A42027_a01	TrAa01CN	$CH_3COOH + NO_3 \rightarrow CH_2OOCOOH + NO_3^- + H^+$	1.4E4	-3800	Exner et al. (1994)*
A42028_a01	TrAa01C	$CH_3COO^- + OH \rightarrow CH_2OOCO_2^- + H_2O$	1.00E8	-1800	Fisher and Hamill (1973)
A42029_a01	TrAa01CN	$CH_3COO^- + NO_3 \rightarrow CH_2OOCO_2^- + NO_3^- + H^+$	2.9E6	-3800	Exner et al. (1994)*
A42030a_a01	TrAa01C	$C2H5OOH + OH \rightarrow C2H5OO + H_2O$	0.80 × 5.80E8		Monod et al. (2007)
A42030b_a01	TrAa01C	$C2H5OOH + OH \rightarrow CH_3COOH + HO_2 + H_2O$	0.20 × 5.80E8		Monod et al. (2007)*
A42031a_a01	TrAa01C	$C2H5OO + C2H5OO \rightarrow CH_3CHO + CH_3CHO + H_2O_2$	0.20 × 1.9E8	1563	Herrmann et al. (1999b)*
A42031b_a01	TrAa01C	$C2H5OO + C2H5OO \rightarrow 2\ CH_3CHO + 2\ HO_2$	0.80 × 1.9E8	1563	Herrmann et al. (1999b)*
A42032_a01	TrAa01C	$C2H5OO + O_2^- \rightarrow C2H5OOH + OH^-$	1.0E8	-900	see note*
A42033_a01	TrAa01C	$C2H5OO + HO_2 \rightarrow C2H5OOH$	9.7E5	-2500	see note*
A42034_a01	TrAa01C	$CH_2OOCOOH + HO_2 \rightarrow HOOCH2CO2H$	9.7E5	-2500	see note*
A42035_a01	TrAa01C	$CH_2OOCOOH + O_2^- + H^+ \rightarrow HOOCH2CO2H$	1.0E8	-900	see note*
A42036a_a01	TrAa01C	$CH_2OOCOOH + CH_2OOCOOH \rightarrow CHOCOOH + CHOCOOH + H_2O_2$	0.30 × 7.50E7		Schuchmann et al. (1985)
A42036b_a01	TrAa01C	$CH_2OOCOOH + CH_2OOCOOH \rightarrow 2\ HCHO + 2\ CO_2 + H_2O_2$	0.30 × 7.50E7		Schuchmann et al. (1985)

Table 6: Aqueous phase reactions (...continued)

#	labels	reaction	k_0 $[M^{1-n}s^{-1}]$	$-E_a/R[K]$	reference
A42036c_a01	TrAa01C	$CH_2OOCOOH + CH_2OOCOOH \rightarrow CHOCOOH + HOCH_2CO_2H$	0.30 × 7.50E7		Schuchmann et al. (1985)
A42036d_a01	TrAa01C	$CH_2OOCOOH + CH_2OOCOOH \rightarrow CHOHOOCOOH + CHOHOOCOOH$	0.10 × 7.50E7		Schuchmann et al. (1985)
A42037_a01	TrAa01C	$CH_2OOCO_2^- + HO_2 \rightarrow CH_2OOHCO_2^- + O_2$	9.7E5	-2500	see note*
A42038_a01	TrAa01C	$CH_2OOCO_2^- + O_2^- + H^+ \rightarrow CH_2OOHCO_2^-$	1.0E8	-900	see note*
A42039a_a01	TrAa01C	$CH_2OOCO_2^- + CH_2OOCO_2^- \rightarrow CHOCOO^- + CHOCOO^- + H_2O_2$	0.30 × 7.50E7		Schuchmann et al. (1985)
A42039b_a01	TrAa01C	$CH_2OOCO_2^- + CH_2OOCO_2^- \rightarrow 2\ HCHO + 2\ CO_2 + H_2O_2 + 2\ OH^-$	0.30 × 7.50E7		Schuchmann et al. (1985)
A42039c_a01	TrAa01C	$CH_2OOCO_2^- + CH_2OOCO_2^- \rightarrow CHOCOO^- + CH_2OHCO_2^-$	0.30 × 7.50E7		Schuchmann et al. (1985)
A42039d_a01	TrAa01C	$CH_2OOCO_2^- + CH_2OOCO_2^- \rightarrow 2\ CHOHOOCOO_2^-$	0.10 × 7.50E7		Schuchmann et al. (1985)
A42040_a01	TrAa01C	$CH_2OOCO_2^- + O_3 \rightarrow O_3^- + HOCH_2OOH + CO_2$	2.00E9		Sehested et al. (1984)
A42141_a01	TrAa01C	$HOOCCOO^- + OH \rightarrow C_2O_4^- + H_2O$	2.3E8	-2766	Ervens et al. (2003b)*
A42142_a01	TrAa01C	$C_2O_4^{2-} + OH \rightarrow C_2O_4^- + OH^-$	2.25E8	-4330	Ervens et al. (2003b)*
A42143_a01	TrAa01C	$C_2O_4^- + O_2 \rightarrow 2\ CO_2 + O_2^-$	2.40E9		Hislop and Bolton (1999)
A42144a_a01	TrAa01C	$HOOCH2CO2H + OH \rightarrow CH_2OOCOOH + H_2O$	0.80 × 5.80E8		see note*
A42144b_a01	TrAa01C	$HOOCH2CO2H + OH \rightarrow CHOOHOOCOOH + H_2O$	0.20 × 5.80E8		see note*
A42145a_a01	TrAa01CN	$HOOCH2CO2H + NO_3 \rightarrow CH_2OOCOOH + NO_3^- + H^+$	0.80 × 1.70E6		Herrmann et al. (2005)
A42145b_a01	TrAa01CN	$HOOCH2CO2H + NO_3 \rightarrow CHOOHOOCOOH + NO_3^- + H^+$	0.20 × 1.70E6		Herrmann et al. (2005)
A42146a_a01	TrAa01C	$CH_2OOHCO_2^- + OH \rightarrow CH_2OOCO_2^- + H_2O$	0.80 × 5.80E8		see note*
A42146b_a01	TrAa01C	$CH_2OOHCO_2^- + OH \rightarrow CHOOHOOCO_2^- + H_2O$	0.20 × 5.80E8		see note*
A42147a_a01	TrAa01CN	$CH_2OOHCO_2^- + NO_3 \rightarrow CH_2OOCO_2^- + NO_3^- + H^+$	0.80 × 7.10E6		Herrmann et al. (2005)
A42147b_a01	TrAa01CN	$CH_2OOHCO_2^- + NO_3 \rightarrow CHOOHOOCO_2^- + NO_3^- + H^+$	0.20 × 7.10E6		Herrmann et al. (2005)
A42148_a01	TrAa01C	$CHOOHOOCOOH \rightarrow HOOCCOOH + HO_2$	1.90E2		see note*
A42149_a01	TrAa01C	$CHOOHOOCO_2^- \rightarrow HOOCCOO^- + HO_2$	1.90E2		see note*
A42150a_a01	TrAa01C	$HOCH_2CO_2H + OH \rightarrow CHOHOOCOOH + H_2O$	0.62 × 6.00E8		see note*
A42150b_a01	TrAa01C	$HOCH_2CO_2H + OH \rightarrow HCHO + CO_2 + HO_2 + H_2O$	0.38 × 6.00E8		see note*

Table 6: Aqueous phase reactions (...continued)

#	labels	reaction	k_0 $[M^{1-n}s^{-1}]$	$-E_a/R[K]$	reference
A42151a_a01	TrAa01CN	$HOCH_2CO_2H + NO_3 \rightarrow CHOHOOCOOH + NO_3^- + H^+$	0.62 × 7.4E5	-3969	Gaillard de Sémainville et al. (2007)*
A42151b_a01	TrAa01CN	$HOCH_2CO_2H + NO_3 \rightarrow HCHO + CO_2 + HO_2 + NO_3^- + H^+$	0.38 × 7.4E5	-3969	Gaillard de Sémainville et al. (2007)*
A42152_a01	TrAa01C	$CHOHOOCOOH \rightarrow CHOCOOH + HO_2$	1.90E2		von Sonntag (1987)
A42153a_a01	TrAa01C	$CH_2OHCO_2^- + OH \rightarrow CHOHOOCOO_2^- + H_2O$	0.60 × 8.60E8		Buxton et al. (1988)
A42153b_a01	TrAa01C	$CH_2OHCO_2^- + OH \rightarrow HCHO + CO_2 + O_2^- + H_2O$	0.19 × 8.60E8		Buxton et al. (1988)
A42153c_a01	TrAa01C	$CH_2OHCO_2^- + OH \rightarrow HOCH_2O_2 + CO_2 + OH^-$	0.21 × 8.60E8		Buxton et al. (1988)
A42154a_a01	TrAa01CN	$CH_2OHCO_2^- + NO_3 \rightarrow CHOHOOCOO_2^- + NO_3^- + H^+$	0.76 × 7.5E6	-3007	Gaillard de Sémainville et al. (2007)*
A42154b_a01	TrAa01CN	$CH_2OHCO_2^- + NO_3 \rightarrow HCHO + CO_2 + O_2^- + NO_3^- + H^+$	0.24 × 7.5E6	-3007	Gaillard de Sémainville et al. (2007)*
A42155_a01	TrAa01C	$CHOHOOCOO_2^- \rightarrow CHOCOO^- + HO_2$	1.90E2		von Sonntag (1987)
A42156a_a01	TrAa01C	$CHOOHOHCOOH + OH \rightarrow COOHCOHOHO_2 + H_2O$	0.15 × 3.2E8	-962	Ervens et al. (2003b)*
A42156b_a01	TrAa01C	$CHOOHOHCOOH + OH \rightarrow HCOOH + CO_2 + HO_2 + H_2O$	0.85 × 3.2E8	-962	Ervens et al. (2003b)*
A42157a_a01	TrAa01CN	$CHOOHOHCOOH + NO_3 \rightarrow COOHCOHOHO_2 + NO_3^- + H^+$	0.15 × 1.00E6		see note*
A42157b_a01	TrAa01CN	$CHOOHOHCOOH + NO_3 \rightarrow HCOOH + CO_2 + HO_2 + NO_3^- + H^+$	0.85 × 1.00E6		see note*
A42158a_a01	TrAa01C	$CHOHOHCO_2^- + OH \rightarrow CO2^-COHOHO_2 + H_2O$	0.26 × 2.9E9	-4330	Ervens et al. (2003b)*
A42158b_a01	TrAa01C	$CHOHOHCO_2^- + OH \rightarrow HCOOH + CO_2 + O_2^- + H_2O$	0.74 × 2.9E9	-4330	Ervens et al. (2003b)*
A42159a_a01	TrAa01CN	$CHOHOHCO_2^- + NO_3 \rightarrow CO2^-COHOHO_2 + NO_3^- + H^+$	0.26 × 1.80E5		Herrmann et al. (2005)
A42159b_a01	TrAa01CN	$CHOHOHCO_2^- + NO_3 \rightarrow HCOOH + CO_2 + O_2^- + NO_3^- + H^+$	0.74 × 1.80E5		Herrmann et al. (2005)
A42160_a01	TrAa01C	$CHOHOHCO_2^- + H_2O_2 \rightarrow HCOO^- + CO_2 + H_2O + H_2O$	1.10E-1		Schöne and Herrmann (2014)
A42161_a01	TrAa01C	$COOHCOHOHO_2 \rightarrow HOOCCOOH + HO_2$	1.00E6		see note*
A42162_a01	TrAa01C	$CO2^-COHOHO_2 \rightarrow HOOCCOO^- + HO_2$	1.00E6		see note*
A42163a_a01	TrAa01C	$CH_2OOHCHO + OH \rightarrow HCHO + CO + OH + H_2O$	0.77 × 1.40E9		see note*
A42163b_a01	TrAa01C	$CH_2OOHCHO + OH \rightarrow GLYOX + HO_2 + H_2O$	0.23 × 1.40E9		see note*

Table 6: Aqueous phase reactions (...continued)

#	labels	reaction	k_0 $[M^{1-n}s^{-1}]$	$-E_a/R[K]$	reference
A42164a_a01	TrAa01CN	$CH_2OOHCHO + NO_3 \rightarrow HCHO + CO + NO_3 + H_2O$	0.77 × 3.10E6		see note*
A42164b_a01	TrAa01CN	$CH_2OOHCHO + NO_3 \rightarrow GLYOX + NO_3^- + H_2O + H^+$	0.23 × 3.10E6		see note*
A42165a_a01	TrAa01C	$HOOCH_2CHOHOH + OH \rightarrow HOOCH2CO2H + HO_2 + H_2O$	0.33 × 1.10E9		see note*
A42165b_a01	TrAa01C	$HOOCH_2CHOHOH + OH \rightarrow CHOCHOHOH + OH + H_2O$	0.28 × 1.10E9		see note*
A42165c_a01	TrAa01C	$HOOCH_2CHOHOH + OH \rightarrow HCOOH + HCHO + OH + H_2O$	0.39 × 1.10E9		see note*
A42166a_a01	TrAa01CN	$HOOCH_2CHOHOH + NO_3 \rightarrow HOOCH2CO2H + NO_3^- + H_2O + H^+$	0.33 × 1.10E6		see note*
A42166b_a01	TrAa01CN	$HOOCH_2CHOHOH + NO_3 \rightarrow CHOCHOHOH + NO_3 + H_2O$	0.28 × 1.10E6		see note*
A42166c_a01	TrAa01CN	$HOOCH_2CHOHOH + NO_3 \rightarrow HCOOH + HCHO + NO_3 + H_2O$	0.39 × 1.10E6		see note*
A42167_a01	TrAa01ScC	$HOCH_2OH + HOCH_2OH \rightarrow MG2 + H_2O$	see note	see note	Hahnenstein et al. (1995)*
A42168_a01	TrAa01C	$MG2 + H_2O \rightarrow HOCH_2OH + HOCH_2OH$	see note	see note	Hahnenstein et al. (1995)
A42169_a01	TrAa01C	$MG2 + OH \rightarrow HMF + HO_2$	1.54E9	-1000	see note*
A42470_a01	TrAa01C	$CH_3COOO + H_2O \rightarrow CH_3COOH + HO_2$	7.0E5		Villalta et al. (1996)
A42471_a01	TrAa01C	$CH_2OHCO3 + H_2O \rightarrow HOCH_2CO_2H + HO_2$	7.0E5		see note*
A42472_a01	TrAa01C	$CHOCO_3 + H_2O \rightarrow CHOCOOH + HO_2$	7.0E5		see note*
A42473_a01	TrAa01C	$COOHCO_3 + H_2O \rightarrow HOOCCOOH + HO_2$	7.0E5		see note*
A43000a_a01	TrAa01C	$CH_3COCHOHOH + OH \rightarrow CH_3COCOOH + HO_2$	0.29 × 9.2E8	-1235	Schaefer et al. (2015)*
A43000b_a01	TrAa01C	$CH_3COCHOHOH + OH \rightarrow HCOOH + CH_3COOO$	0.71 × 9.2E8	-1235	Schaefer et al. (2015)
A43001_a01	TrAa01CN	$CH_3COCHOHOH + NO_3 \rightarrow CH_3COCOOH + NO_3^- + H^+$	4.5E6	-4213	Schaefer et al. (2015)*
A43002_a01	TrAa01C	$CH_3COCOOH + OH \rightarrow CH_3COOH + HO_2 + CO_2$	2.6E8	-1804	Schaefer et al. (2012)*
A43003_a01	TrAa01CN	$CH_3COCOOH + NO_3 \rightarrow CH_3COOH + NO_3^- + CO_2 + H^+$	2.8E6	-1804	Gaillard de Sémainville et al. (2007)*
A43004_a01	TrAa01C	$CH_3COCO2^- + OH \rightarrow CH_3COO^- + HO_2 + CO_2$	6.2E8	-3007	Schaefer et al. (2012)*
A43005_a01	TrAa01CN	$CH_3COCO2^- + NO_3 \rightarrow CH_3COO^- + NO_3^- + CO_2 + H^+$	2.3E7	-2887	Gaillard de Sémainville et al. (2007)*
A43006_a01	TrAa01C	$CH_3COCH_3 + OH \rightarrow CH_3COCH_2O_2$	1.80E8		Gligorovski et al. (2009)
A43007_a01	TrAa01CN	$CH_3COCH_3 + NO_3 \rightarrow CH_3COCH_2O_2 + NO_3^- + H^+$	4.4E3	-4332	Herrmann et al. (1994)*

Table 6: Aqueous phase reactions (...continued)

#	labels	reaction	k_0 $[M^{1-n}s^{-1}]$	$-E_a/R[K]$	reference
A43008a_a01	TrAa01C	$CH_3COCH_2O_2 + CH_3COCH_2O_2 \rightarrow CH_3COCH_2OH + CH_3C(O)CHO$	0.20 × 4.00E8		Zegota et al. (1986)
A43008b_a01	TrAa01C	$CH_3COCH_2O_2 + CH_3COCH_2O_2 \rightarrow 2.0\ CH_3C(O)CHO + H_2O_2$	0.45 × 4.00E8		Zegota et al. (1986)
A43009c_a01	TrAa01C	$CH_3COCH_2O_2 + CH_3COCH_2O_2 \rightarrow 2.0\ HCHO + 2.0\ CH_3COOO$	0.15 × 4.00E8		Zegota et al. (1986)
A43009d_a01	TrAa01C	$CH_3COCH_2O_2 + CH_3COCH_2O_2 \rightarrow 2.0\ CH_3C(O)CHO + 2.0\ HO_2$	0.20 × 4.00E8		Zegota et al. (1986)
A43010a_a01	TrAa01C	$CH_3COCH_2OH + OH \rightarrow CH_3COCHOHO_2$	0.85 × 5.10E8		Doussin and Monod (2013)*
A43010b_a01	TrAa01C	$CH_3COCH_2OH + OH \rightarrow HCHO + CH_3COOO$	0.15 × 5.10E8		Doussin and Monod (2013)
A43011_a01	TrAa01CN	$CH_3COCH_2OH + NO_3 \rightarrow CH_3COCHOHO_2 + NO_3^- + H^+$	2.1E7	-1564	Gaillard de Sémainville et al. (2007)*
A43012_a01	TrAa01C	$CH_3COCHOHO_2 \rightarrow CH_3C(O)CHO + HO_2$	1.90E2		von Sonntag (1987)
A43013_a01	TrAa01C	$IPROPOL + OH \rightarrow CH_3COCH_3 + HO_2$	1.90E9		see note*
A43014_a01	TrAa01CN	$IPROPOL + NO_3 \rightarrow CH_3COCH_3 + NO_3^- + H^+ + HO_2$	3.70E6		see note*
A43015a_a01	TrAa01C	$CH_3COCH_2O_2H + OH \rightarrow CH_3C(O)CHO + OH$	1.80E8		see note*
A43015b_a01	TrAa01C	$CH_3COCH_2O_2H + OH \rightarrow CH_3COCH_2O_2$	4.70E8		see note*
A43016_a01	TrAa01CN	$CH_3COCH_2O_2H + NO_3 \rightarrow CH_3COCH_2O_2 + NO_3^- + H^+$	4.50E6		see note*
A43017_a01	TrAa01C	$CH_3COCH_2O_2 + HO_2 \rightarrow CH_3COCH_2O_2H$	4.30E5		see note*
A43018_a01	TrAa01C	$CH_3COCH_2O_2 + O_2^- \rightarrow CH_3COCH_2O_2H + O_2 + OH^-$	5.00E7		see note*
A43019a_a01	TrAa01C	$iC_3H_7OOH + OH \rightarrow CH_3COCH_3 + OH$	9.90E8		see note*
A43019b_a01	TrAa01C	$iC_3H_7OOH + OH \rightarrow iC_3H_7O_2$	1.80E8		see note*
A43020_a01	TrAa01CN	$iC_3H_7OOH + NO_3 \rightarrow iC_3H_7O_2 + NO_3^- + H^+$	4.50E6		see note*
A43021_a01	TrAa01C	$iC_3H_7O_2 + HO_2 \rightarrow iC_3H_7OOH$	4.30E5		see note*
A43022_a01	TrAa01C	$iC_3H_7O_2 + O_2^- \rightarrow iC_3H_7OOH + O_2 + OH^-$	5.00E7		see note*
A43023_a01	TrAa01C	$HOCH_2OH + MG2 \rightarrow MG3 + H_2O$	see note	see note	Hahnenstein et al. (1995)*
A43024_a01	TrAa01C	$MG3 + H_2O \rightarrow HOCH_2OH + MG2$	see note	see note	Hahnenstein et al. (1995)
A43025_a01	TrAa01C	$MG3 + OH \rightarrow HM2F + HO_2$	1.54E9	-1000	see note*
A44000_a01	TrAa01ScC	$MACR + OH \rightarrow CH_2OHCO_2CH_3CHO$	9.9E9	-1203	Schöne et al. (2014)*
A44001_a01	TrAa01ScC	$CH_2OHCO_2CH_3CHO + CH_2OHCO_2CH_3CHO \rightarrow CH_3C(O)CHO + CH_3COCH_2OH + HOCH_2O_2 + HCOHOHO_2$	4.00E8		see note*

Table 6: Aqueous phase reactions (...continued)

#	labels	reaction	k_0 $[M^{1-n}s^{-1}]$	$-E_a/R[K]$	reference
A44002_a01	TrAa01ScC	MVK + OH → $CH_3COCHO_2CH_2OH$	7.1E9	-1443	Schöne et al. (2014)*
A44003_a01	TrAa01ScC	$CH_3COCHO_2CH_2OH$ + $CH_3COCHO_2CH_2OH$ → 1.1 BIACETOH + .8 LCARBON + .35 CH_2OHCHO + .35 $CH_3C(O)CHO$ + .35 $HOCH_2O_2$ + .35 CH_3COOO + .45 H_2O_2	4.00E8		see note*
A44004_a01	TrAa01C	GLYOX + CHOCHOHOH → GOLIG1 + H_2O	1.00E2		Ervens and Volkamer (2010)
A44005_a01	TrAa01C	GOLIG1 + H_2O → GLYOX + CHOCHOHOH	1.00E-1		Ervens and Volkamer (2010)
A44006_a01	TrAa01C	CHOCHOHOH + CHOCHOHOH → GOLIG2 + H_2O	1.00E2		Ervens and Volkamer (2010)
A44007_a01	TrAa01C	GOLIG2 + H_2O → CHOCHOHOH + CHOCHOHOH	1.00E-1		Ervens and Volkamer (2010)
A44008_a01	TrAa01C	CHOHOHCHOHOH + CHOCHOHOH → GOLIG3 + H_2O	1.00E2		Ervens and Volkamer (2010)
A44009_a01	TrAa01C	GOLIG3 + H_2O → CHOHOHCHOHOH + CHOCHOHOH	1.00E-1		Ervens and Volkamer (2010)
A44010_a01	TrAa01C	GOLIG1 + OH → GOLIGO1 + HO_2	2.2E9	-1516	see note*
A44011_a01	TrAa01C	GOLIG2 + OH → GOLIGO2 + HO_2	2.2E9	-1516	see note*
A44012_a01	TrAa01C	GOLIG3 + OH → GOLIGO3 + HO_2	2.2E9	-1516	see note*
A46000_a01	TrAa01C	$CH_3C(O)CHO$ + $CH_3COCHOHOH$ → $CH_3COCHOHOCHOHCOCH_3$ + H_2O	1.00E2		Ervens and Volkamer (2010)*
A46001_a01	TrAa01C	$CH_3COCHOHOCHOHCOCH_3$ + H_2O → $CH_3COCHOHOH$ + $CH_3C(O)CHO$	1.00E-1		Ervens and Volkamer (2010)*
A46002_a01	TrAa01C	$CH_3COCHOHOCHOHCOCH_3$ + OH → $CH_3COCOHOCOHCOCH_3$ + HO_2	1.84E9	-1235	see note*
A46003_a01	TrAa01C	$CH_3COCHOHOH$ + $CH_3COCHOHOH$ → $CH_3COCHOHOCOHC_3CHOHOH$ + H_2O	1.00E2		Ervens and Volkamer (2010)*
A46004_a01	TrAa01C	$CH_3COCHOHOCOHC_3CHOHOH$ + H_2O → 2 $CH_3COCHOHOH$	1.00E-1		Ervens and Volkamer (2010)*
A46005_a01	TrAa01C	$CH_3COCHOHOCOHC_3CHOHOH$ + OH → $CH_3COCOHOCOHC_3COHOH$ + HO_2	1.84E9	-1235	see note*
A60000_a01	TrAa01Cl	Cl + Cl → Cl_2	8.8E7		Wu et al. (1980)
A60001_a01	TrAa01Cl	Cl_2^- + Cl_2^- → Cl_2 + 2 Cl^-	3.5E9		Yu (2004)
A61000_a01	TrAa01Cl	Cl^- + O_3 → ClO^-	3.0E-3		Hoigné et al. (1985)
A61001_a01	TrAa01Cl	Cl_2 + O_2^- → Cl_2^-	1.0E9		Bjergbakke et al. (1981)
A61002_a01	TrAa01Cl	Cl_2^- + O_2^- → 2 Cl^-	1.0E9		Jacobi (1996)*

Table 6: Aqueous phase reactions (...continued)

#	labels	reaction	k_0 $[M^{1-n}s^{-1}]$	$-E_a/R[K]$	reference
A62000_a01	TrAa01Cl	$Cl \rightarrow H^+ + ClOH^-$	1.8E5		Yu (2004)
A62001_a01	TrAa01Cl	$Cl + H_2O_2 \rightarrow HO_2 + Cl^- + H^+$	2.7E7	-1684	Christensen et al. (1982)
A62002_a01	TrAa01Cl	$Cl^- + OH \rightarrow ClOH^-$	4.2E9		Yu (2004)
A62003_a01	TrAa01Cl	$Cl_2 + HO_2 \rightarrow Cl_2^- + H^+$	1.0E9		Bjergbakke et al. (1981)
A62004_a01	TrAa01MblCl	$Cl_2 \rightarrow Cl^- + HOCl + H^+$	21.8	-8012	Wang and Margerum (1994)
A62005_a01	TrAa01Cl	$Cl_2^- + HO_2 \rightarrow 2\ Cl^- + H^+$	1.3E10		Jacobi (1996)
A62006_a01	TrAa01Cl	$HOCl + O_2^- \rightarrow Cl + OH^-$	7.5E6		Long and Bielski (1980)
A62007_a01	TrAa01Cl	$HOCl + HO_2 \rightarrow Cl$	7.5E6		Long and Bielski (1980)
A62008_a01	TrAa01MblCl	$HOCl + Cl^- + H^+ \rightarrow Cl_2$	2.2E4	-3508	Wang and Margerum (1994)
A62009_a01	TrAa01Cl	$ClOH^- \rightarrow Cl^- + OH$	6.0E9		Yu (2004)
A62010_a01	TrAa01Cl	$ClOH^- + H^+ \rightarrow Cl$	2.4E10		Yu (2004)
A63000_a01	TrAa01ClN	$Cl + NO_3^- \rightarrow NO_3 + Cl^-$	1.0E8		Buxton et al. (1999b)
A63001_a01	TrAa01ClN	$Cl^- + NO_3 \rightarrow NO_3^- + Cl$	3.4E8		Buxton et al. (1999b)*
A63002_a01	TrAa01ClN	$Cl_2^- + NO_2^- \rightarrow 2\ Cl^- + NO_2$	6.0E7		Jacobi et al. (1996)
A64000_a01	TrAa01ScCl	$Cl_2^- + CH_3OOH \rightarrow 2\ Cl^- + H^+ + CH_3OO$	6.20E5		see note*
A70000_a01	TrAa01Br	$Br_2^- + Br_2^- \rightarrow 2\ Br^- + Br_2$	1.9E9		Ross et al. (1992)
A71000_a01	TrAa01Br	$Br^- + O_3 \rightarrow BrO^-$	2.1E2	-4450	Haag and Hoigné (1983)
A71001_a01	TrAa01Br	$Br_2 + O_2^- \rightarrow Br_2^-$	5.6E9		Sutton and Downes (1972)
A71002_a01	TrAa01Br	$Br_2^- + O_2^- \rightarrow 2\ Br^-$	1.7E8		Wagner and Strehlow (1987)
A72000_a01	TrAa01Br	$Br^- + OH \rightarrow BrOH^-$	1.1E10		Zehavi and Rabani (1972)
A72001_a01	TrAa01Br	$Br_2 + HO_2 \rightarrow Br_2^- + H^+$	1.1E8		Sutton and Downes (1972)
A72002_a01	TrAa01MblBr	$Br_2 \rightarrow Br^- + HOBr + H^+$	9.7E1	-7457	Beckwith et al. (1996)
A72003_a01	TrAa01Br	$Br_2^- + HO_2 \rightarrow Br_2 + H_2O_2 + OH^-$	4.4E9		Matthew et al. (2003)
A72004_a01	TrAa01Br	$Br_2^- + H_2O_2 \rightarrow 2\ Br^- + H^+ + HO_2$	1.0E5		Jacobi (1996)
A72005_a01	TrAa01Br	$HOBr + O_2^- \rightarrow Br + OH^-$	3.5E9		Schwarz and Bielski (1986)
A72006_a01	TrAa01Br	$HOBr + HO_2 \rightarrow Br$	1.0E9		Herrmann et al. (1999a)
A72007_a01	TrAa01Br	$HOBr + H_2O_2 \rightarrow Br^- + H^+$	1.2E6		Bichsel and von Gunten (1999)
A72008_a01	TrAa01MblBr	$HOBr + Br^- + H^+ \rightarrow Br_2$	1.6E10		Beckwith et al. (1996)
A72009a_a01	TrAa01Br	$BrOH^- \rightarrow Br^- + OH$	3.3E7		Zehavi and Rabani (1972)
A72009b_a01	TrAa01Br	$BrOH^- \rightarrow Br + OH^-$	4.2E6		Zehavi and Rabani (1972)
A72010_a01	TrAa01Br	$BrOH^- + H^+ \rightarrow Br$	4.4E10		Zehavi and Rabani (1972)
A73000_a01	TrAa01BrN	$Br^- + NO_3 \rightarrow Br + NO_3^-$	4.0E9		Neta and Huie (1986)
A73001_a01	TrAa01BrN	$Br_2^- + NO_2^- \rightarrow 2\ Br^- + NO_2$	1.7E7	-1720	Shoute et al. (1991)
A74000_a01	TrAa01Br	$Br_2^- + CH_3OOH \rightarrow 2\ Br^- + H^+ + CH_3OO$	1.0E5		Jacobi (1996)*

Table 6: Aqueous phase reactions (...continued)

#	labels	reaction	k_0 $[M^{1-n}s^{-1}]$	$-E_a/R[K]$	reference
A76001_a01	TrAa01BrCl	$Br^- + ClO^- + H^+ \rightarrow BrCl + OH^-$	3.7E10		Kumar and Margerum (1987)
A76002_a01	TrAa01MblBrCl	$Br^- + HOCl + H^+ \rightarrow BrCl$	1.32E6		Kumar and Margerum (1987)
A76003_a01	TrAa01MblBrCl	$HOBr + Cl^- + H^+ \rightarrow BrCl$	2.3E10		Liu and Margerum (2001)*
A76004_a01	TrAa01MblBrCl	$BrCl \rightarrow Cl^- + HOBr + H^+$	3.0E6		Liu and Margerum (2001)
A81000_a01	TrAa01MblI	$I^- + O_3 \rightarrow HOI + OH^-$	4.2E9	-9311	Magi et al. (1997)
A81001_a01	TrAa01MblI	$IO + IO \rightarrow HOI + IO_2^- + H^+$	1.5E9		Buxton et al. (1986)
A82000_a01	TrAa01MblI	$IO_2^- + H_2O_2 \rightarrow IO_3^-$	6.0E1		Furrow (1987)
A82001_a01	TrAa01I	$HOI + IO_2^- \rightarrow IO_3^- + I^- + H^+$	6.0E2		Chinake and Simoyi (1996)
A82002_a01	TrAa01MblI	$HOI + I^- + H^+ \rightarrow I_2$	4.4E12		Eigen and Kustin (1962)
A82003_a01	TrAa01MblI	$IO_2^- + I^- + H^+ \rightarrow 2\ HOI + OH^-$	2.0E10		Edblom et al. (1987)
A86000_a01	TrAa01MblClI	$ICl \rightarrow HOI + Cl^- + H^+$	2.4E6		Wang et al. (1989)
A86001_a01	TrAa01MblClI	$I^- + HOCl + H^+ \rightarrow ICl$	3.5E11		Nagy et al. (1988)
A86002_a01	TrAa01ClI	$IO_2^- + HOCl \rightarrow IO_3^- + Cl^- + H^+$	1.5E3		Lengyel et al. (1996)
A86003_a01	TrAa01MblClI	$HOI + Cl^- + H^+ \rightarrow ICl$	2.9E10		Wang et al. (1989)
A86004_a01	TrAa01ClI	$HOI + Cl_2 \rightarrow IO_2^- + 2\ Cl^- + 3H^+$	1.0E6		Lengyel et al. (1996)
A86005_a01	TrAa01ClI	$HOI + HOCl \rightarrow IO_2^- + Cl^- + 2\ H^+$	5.0E5		Citri and Epstein (1988)
A86006_a01	TrAa01ClI	$ICl + I^- \rightarrow I_2 + Cl^-$	1.1E9		Margerum et al. (1986)
A87000_a01	TrAa01MblBrI	$IBr \rightarrow HOI + H^+ + Br^-$	8.0E5		Troy et al. (1991)
A87001_a01	TrAa01MblBrI	$I^- + HOBr \rightarrow IBr + OH^-$	5.0E9		Troy and Margerum (1991)
A87002_a01	TrAa01BrI	$IO_2^- + HOBr \rightarrow IO_3^- + Br^- + H^+$	1.0E6		Chinake and Simoyi (1996)
A87003_a01	TrAa01MblBrI	$HOI + Br^- + H^+ \rightarrow IBr$	3.3E12		Troy et al. (1991)
A87004_a01	TrAa01BrI	$HOI + HOBr \rightarrow IO_2^- + Br^- + 2\ H^+$	1.0E6		Chinake and Simoyi (1996)
A87005_a01	TrAa01BrI	$IBr + I^- \rightarrow I_2 + Br^-$	2.0E9		Faria et al. (1993)
A91000_a01	TrAa01ScS	$SO_3^- + O_2 \rightarrow SO_5^-$	1.5E9		Huie and Neta (1987)
A91001_a01	TrAa01MblScScmS	$SO_3^{2-} + O_3 \rightarrow SO_4^{2-}$	1.5E9	-5300	Hoffmann (1986)
A91002_a01	TrAa01ScS	$SO_4^- + O_2^- \rightarrow SO_4^{2-}$	3.5E9		Jiang et al. (1992)
A91003_a01	TrAa01ScS	$SO_4^- + SO_3^{2-} \rightarrow SO_3^- + SO_4^{2-}$	4.6E8		Huie and Neta (1987)
A91004_a01	TrAa01ScS	$SO_5^- + O_2^- \rightarrow HSO_5^- + OH^-$	2.3E8		Buxton et al. (1996)
A91005_a01	TrAa01S	$SO_5^- + SO_3^{2-} \rightarrow .72\ SO_4^- + .72\ SO_4^{2-} + .28\ SO_3^- + .28\ HSO_5^- + .28\ OH^-$	1.3E7		Huie and Neta (1987), Deister and Warneck (1990)*
A91006_a01	TrAa01S	$SO_5^- + SO_5^- \rightarrow O_2 + SO_4^{2-} + LSULFUR$	1.0E8		Ross et al. (1992)*
A92000_a01	TrAa01ScS	$SO_3^{2-} + OH \rightarrow SO_3^- + OH^-$	5.5E9		Buxton et al. (1988)
A92001_a01	TrAa01ScS	$SO_4^- + OH \rightarrow HSO_5^-$	1.0E9		Jiang et al. (1992)
A92002_a01	TrAa01ScS	$SO_4^- + HO_2 \rightarrow SO_4^{2-} + H^+$	3.5E9		Jiang et al. (1992)

Table 6: Aqueous phase reactions (...continued)

#	labels	reaction	k_0 $[M^{1-n}s^{-1}]$	$-E_a/R[K]$	reference
A92003_a01	TrAa01ScS	$SO_4^- + H_2O \rightarrow SO_4^{2-} + H^+ + OH$	1.1E1	-1110	Herrmann et al. (1995)
A92004_a01	TrAa01ScS	$SO_4^- + H_2O_2 \rightarrow SO_4^{2-} + H^+ + HO_2$	1.2E7		Wine et al. (1989)
A92005_a01	TrAa01ScS	$HSO_3^- + O_2^- \rightarrow SO_4^{2-} + OH$	3.0E3		see note*
A92006_a01	TrAa01MblScScmS	$HSO_3^- + O_3 \rightarrow SO_4^{2-} + H^+$	3.7E5	-5500	Hoffmann (1986)
A92007_a01	TrAa01ScS	$HSO_3^- + OH \rightarrow SO_3^-$	4.5E9		Buxton et al. (1988)
A92008_a01	TrAa01ScS	$HSO_3^- + HO_2 \rightarrow SO_4^{2-} + OH + H^+$	3.0E3		see note*
A92009_a01	TrAa01MblScScmS	$HSO_3^- + H_2O_2 \rightarrow SO_4^{2-} + H^+$	5.2E6	-3650	Martin and Damschen (1981)
A92010_a01	TrAa01ScS	$HSO_3^- + SO_4^- \rightarrow SO_3^- + SO_4^{2-} + H^+$	8.0E8		Huie and Neta (1987)
A92011_a01	TrAa01S	$HSO_3^- + SO_5^- \rightarrow .75\ SO_4^- + .75\ SO_4^{2-} + .75\ H^+ + .25\ SO_3^- + .25\ HSO_5^-$	1.0E5		Huie and Neta (1987)
A92012_a01	TrAa01ScS	$HSO_3^- + HSO_5^- + H^+ \rightarrow 2\ HSO_4^- + H^+$	7.1E6		Betterton and Hoffmann (1988)
A93001_a01	TrAa01ScNS	$SO_4^- + NO_3^- \rightarrow SO_4^{2-} + NO_3$	5.0E4		Exner et al. (1992)
A93002_a01	TrAa01ScNS	$SO_4^{2-} + NO_3 \rightarrow NO_3^- + SO_4^-$	1.0E5		Løgager et al. (1993)
A93004_a01	TrAa01ScNS	$HSO_3^- + NO_3 \rightarrow SO_3^- + NO_3^- + H^+$	1.4E9	-2000	Exner et al. (1992)
A93005_a01	TrAa01ScNS	$HSO_3^- + HNO_4 \rightarrow HSO_4^- + NO_3^- + H^+$	3.1E5		Warneck (1999)
A94100_a01	TrAa01ScS	$SO_3^{2-} + HCHO \rightarrow CH_2OHSO_3^- + OH^-$	1.4E4		Boyce and Hoffmann (1984)*
A94101_a01	TrAa01ScS	$SO_3^{2-} + CH_3OOH + H^+ \rightarrow SO_4^{2-} + H^+ + CH_3OH$	1.6E7	-3800	Lind et al. (1987)
A94102_a01	TrAa01ScS	$HSO_3^- + HCHO \rightarrow CH_2OHSO_3^-$	4.3E-1		Boyce and Hoffmann (1984)*
A94103_a01	TrAa01ScS	$HSO_3^- + CH_3OOH + H^+ \rightarrow HSO_4^- + H^+ + CH_3OH$	1.6E7	-3800	Lind et al. (1987)
A94104_a01	TrAa01ScS	$HSO_3^- + CH_3OO \rightarrow SO_3^- + CH_3OOH$	5.00E5		Herrmann et al. (1999b)
A94105_a01	TrAa01ScS	$SO_4^- + HCOO^- \rightarrow SO_4^{2-} + CO_2 + HO_2$	1.7E8	-1500	Jacob (1986)
A94106_a01	TrAa01ScS	$SO_4^- + HCOOH \rightarrow SO_4^{2-} + CO_2 + H^+ + HO_2$	1.7E8	-1500	Jacob (1986)
A94107_a01	TrAa01ScS	$SO_4^- + CH_3OH \rightarrow SO_4^{2-} + HOCH_2O_2 + H^+$	9.0E6	-2190	Clifton and Huie (1989)
A94108a_a01	TrAa01ScS	$SO_4^- + CH_3OOH \rightarrow SO_4^{2-} + CH_3OO + H^+$	0.25 × 1.20E7		see note*
A94108b_a01	TrAa01ScS	$SO_4^- + CH_3OOH \rightarrow SO_4^{2-} + HCHO + HO_2 + H^+$	0.75 × 1.20E7		see note*
A94109_a01	TrAa01ScS	$SO_4^- + HOCH_2OH \rightarrow SO_4^{2-} + HCOHOHO_2 + H^+$	1.40E7	-1300	Buxton et al. (1990)
A94110_a01	TrAa01ScS	$SO_5^- + HCOO^- \rightarrow HSO_5^- + CO_2 + O_2^-$	1.4E4	-4000	Jacob (1986)
A94111_a01	TrAa01ScS	$CH_2OHSO_3^- + OH^- \rightarrow SO_3^{2-} + HCHO$	3.6E3		Seinfeld and Pandis (1998)
A94200_a01	TrAa01ScCS	$HSO_3^- + CH_2OOCOOH \rightarrow SO_3^- + HOOCH2CO2H$	5.00E5		see note*
A94201_a01	TrAa01ScCS	$HSO_3^- + CH_2OOCO_2^- \rightarrow SO_3^- + CH_2OOHCO_2^-$	5.00E5		see note*
A94202a_a01	TrAa01ScCS	$SO_4^- + CH_3CH_2OH \rightarrow SO_4^{2-} + CH_3CHO + HO_2 + H^+$	0.90 × 4.1E7	-1750	Clifton and Huie (1989)*
A94202b_a01	TrAa01ScCS	$SO_4^- + CH_3CH_2OH \rightarrow SO_4^{2-} + CH_2OHCH_2OO + H^+$	0.10 × 4.1E7	-1750	Clifton and Huie (1989)

Table 6: Aqueous phase reactions (...continued)

#	labels	reaction	k_0 $[M^{1-n}s^{-1}]$	$-E_a/R[K]$	reference
A94203a_a01	TrAa01ScCS	$SO_4^- + CHOHOHCHOHOH \rightarrow SO_4^{2-} + CHOHOHCOHOHO_2 + H^+$	0.27 × 2.40E7		George et al. (2001)
A94203b_a01	TrAa01ScCS	$SO_4^- + CHOHOHCHOHOH \rightarrow SO_4^{2-} + HCOHOHO_2 + HCOOH + HO_2 + H^+$	0.73 × 2.40E7		George et al. (2001)*
A94204_a01	TrAa01ScCS	$SO_4^- + CH_3COO^- \rightarrow SO_4^{2-} + CH_2OOCO_2^- + H^+$	5.10E6		Huie and Clifton (1990)
A94205_a01	TrAa01ScCS	$SO_4^- + HOOCCOO^- \rightarrow SO_4^{2-} + C_2O_4^- + H^+$	1.70E6		Grgić et al. (2007)
A94206_a01	TrAa01ScCS	$SO_4^- + C_2O_4^{2-} \rightarrow SO_4^{2-} + C_2O_4^-$	1.30E7		Grgić et al. (2007)
A96000_a01	TrAa01ClS	$SO_3^{2-} + Cl_2^- \rightarrow SO_3^- + 2\ Cl^-$	6.2E7		Jacobi et al. (1996)
A96001_a01	TrAa01MblClS	$SO_3^{2-} + HOCl \rightarrow Cl^- + HSO_4^-$	7.6E8		Fogelman et al. (1989)
A96002_a01	TrAa01ClS	$SO_4^- + Cl^- \rightarrow SO_4^{2-} + Cl$	2.5E8		Buxton et al. (1999a)
A96003_a01	TrAa01ClS	$SO_4^{2-} + Cl \rightarrow SO_4^- + Cl^-$	2.1E8		Buxton et al. (1999a)
A96004_a01	TrAa01ClS	$HSO_3^- + Cl_2^- \rightarrow SO_3^- + 2\ Cl^- + H^+$	4.7E8	-1082	Shoute et al. (1991)
A96005_a01	TrAa01MblClS	$HSO_3^- + HOCl \rightarrow Cl^- + HSO_4^- + H^+$	7.6E8		see note*
A96006_a01	TrAa01ClS	$HSO_5^- + Cl^- \rightarrow HOCl + SO_4^{2-}$	1.8E-3	-7352	Fortnum et al. (1960)
A97000_a01	TrAa01BrS	$SO_3^{2-} + Br_2^- \rightarrow 2\ Br^- + SO_3^-$	2.2E8	-649	Shoute et al. (1991)
A97001_a01	TrAa01BrS	$SO_3^{2-} + BrO^- \rightarrow Br^- + SO_4^{2-}$	1.0E8		Troy and Margerum (1991)
A97002_a01	TrAa01MblBrS	$SO_3^{2-} + HOBr \rightarrow Br^- + HSO_4^-$	5.0E9		Troy and Margerum (1991)
A97003_a01	TrAa01BrS	$SO_4^- + Br^- \rightarrow Br + SO_4^{2-}$	2.1E9		Jacobi (1996)
A97004_a01	TrAa01BrS	$HSO_3^- + Br_2^- \rightarrow 2\ Br^- + H^+ + SO_3^-$	6.3E7	-782	Shoute et al. (1991)
A97005_a01	TrAa01MblBrS	$HSO_3^- + HOBr \rightarrow Br^- + HSO_4^- + H^+$	5.0E9		see note*
A97006_a01	TrAa01BrS	$HSO_5^- + Br^- \rightarrow HOBr + SO_4^{2-}$	1.0E0	-5338	Fogelman et al. (1989)
A98000_a01	TrAa01IS	$HSO_3^- + I_2 \rightarrow 2\ I^- + HSO_4^- + 2\ H^+$	1.7E9		Yiin and Margerum (1990)
A101000_a01	TrAa01Hg	$Hg + O_3 \rightarrow HgO + O_2$	4.7E7		Munthe (1992)
A102000_a01	TrAa01Hg	$HgO + H^+ \rightarrow Hg^{2+} + OH^-$	1.0E10		Pleijel and Munthe (1995)
A102001_a01	TrAa01Hg	$Hg + OH \rightarrow Hg^+ + OH^-$	2.0E9		Lin and Pehkonen (1997)
A102002_a01	TrAa01Hg	$Hg^+ + OH \rightarrow Hg^{2+} + OH^-$	1.0E10		Lin and Pehkonen (1997)
A102003_a01	TrAa01Hg	$Hg^{2+} + HO_2 \rightarrow Hg^+ + O_2 + H^+$	1.7E4		Enami et al. (2007)
A102004_a01	TrAa01Hg	$Hg^+ + HO_2 \rightarrow Hg + O_2 + H^+$	1.0E10		Lin and Pehkonen (1997)
A106000_a01	TrAa01ClHg	$Hg + HOCl \rightarrow Hg^{2+} + Cl^- + OH^-$	2.09E6		Lin and Pehkonen (1998)
A106001_a01	TrAa01ClHg	$Hg + ClO^- \rightarrow Hg^{2+} + Cl^- + 2\ OH^-$	1.99E6		Lin and Pehkonen (1998)
A107000_a01	TrAa01BrHg	$Hg + HOBr \rightarrow Hg^{2+} + Br^- + OH^-$	0.279		Wang and Pehkonen (2004)
A107001_a01	TrAa01BrHg	$Hg + BrO^- \rightarrow Hg^{2+} + Br^- + 2\ OH^-$	0.273		Wang and Pehkonen (2004)
A107002_a01	TrAa01BrHg	$Hg + Br_2 \rightarrow Hg^{2+} + 2\ Br^-$	0.196		Wang and Pehkonen (2004)
A109000_a01	TrAa01HgS	$HgSO_3 \rightarrow Hg + HSO_4^- + H^+$	0.0106		van Loon et al. (2000)

Table 6: Aqueous phase reactions (...continued)

#	labels	reaction	k_0 $[M^{1-n}s^{-1}]$	$-E_a/R[K]$	reference
A111001_a01	TrAa01Fe	$Fe^{2+} + O_2^- \rightarrow Fe^{3+} + HO2^- + OH^-$	1E7		de Laat and Le (2006)
A111002_a01	TrAa01Fe	$Fe^{3+} + O_2^- \rightarrow O_2 + Fe^{2+}$	5E7		de Laat and Le (2006)
A111003_a01	TrAa01Fe	$Fe^{2+} + O_3 \rightarrow FeO^{2+} + O_2$	8.2E5		Løgager et al. (1992)
A112001a_a01	TrAa01Fe	$Fe^{2+} + OH \rightarrow Fe^{3+} + OH^-$	2.7E8		de Laat and Le (2006)
A112001b_a01	TrAa01Fe	$FeOH^+ + OH \rightarrow Fe^{3+} + 2\ OH^-$	2.7E8		de Laat and Le (2006)
A112002a_a01	TrAa01Fe	$Fe^{2+} + H_2O_2 \rightarrow Fe^{3+} + OH + OH^-$	5.5E1		de Laat and Le (2006)
A112002b_a01	TrAa01Fe	$FeOH^+ + H_2O_2 \rightarrow Fe^{3+} + OH + 2\ OH^-$	5.9E6		de Laat and Le (2006)
A112003_a01	TrAa01Fe	$FeHO_2^{2+} \rightarrow Fe^{2+} + HO_2$	2.3E-3		de Laat and Le (2006)
A112004_a01	TrAa01Fe	$Fe(OH)(HO_2)^+ \rightarrow Fe^{2+} + HO_2 + OH^-$	2.3E-3		de Laat and Le (2006)
A112006_a01	TrAa01Fe	$Fe^{2+} + HO_2 \rightarrow Fe^{3+} + HO2^-$	1.2E6		de Laat and Le (2006)
A112008a_a01	TrAa01Fe	$FeOH^{2+} + O_2^- \rightarrow Fe^{2+} + O_2 + OH^-$	1.5E8		Rush and Bielski (1985)
A112008b_a01	TrAa01Fe	$Fe(OH)_2^+ + O_2^- \rightarrow Fe^{2+} + O_2 + 2\ OH^-$	1.5E8		Rush and Bielski (1985)
A112009_a01	TrAa01Fe	$Fe^{2+} + O_2^- \rightarrow Fe^{3+} + H_2O_2 + 2\ OH^-$	1.0E7		Rush and Bielski (1985)
A112010_a01	TrAa01Fe	$Fe^{2+} + OH \rightarrow FeOH^{2+}$	4.3E8		Christensen and Sehested (1981)
A112011_a01	TrAa01Fe	$FeO^{2+} + H_2O_2 \rightarrow Fe^{3+} + HO_2 + OH^-$	9.5E3		Løgager et al. (1992)
A112012_a01	TrAa01Fe	$FeO^{2+} \rightarrow Fe^{3+} + OH + OH^-$	1.3E-2		Løgager et al. (1992)
A112013_a01	TrAa01Fe	$FeO^{2+} + HO_2 \rightarrow Fe^{3+} + O_2 + OH^-$	2.0E6		Løgager et al. (1992)
A112014_a01	TrAa01Fe	$FeO^{2+} + OH \rightarrow Fe^{3+} + HO2^-$	1.0E7		Løgager et al. (1992)
A112015_a01	TrAa01Fe	$FeO^{2+} + Fe^{2+} \rightarrow 2\ Fe^{3+} + 2\ OH^-$	1.4E5		Løgager et al. (1992)
A112016_a01	TrAa01Fe	$FeO^{2+} + Fe^{2+} \rightarrow Fe(OH)_2Fe^{4+}$	1.8E4		Jacobsen et al. (1997)
A112017_a01	TrAa01Fe	$Fe(OH)_2Fe^{4+} + H^+ \rightarrow 2\ Fe^{3+} + OH^-$	2.0		Jacobsen et al. (1997)
A112018_a01	TrAa01Fe	$Fe(OH)_2Fe^{4+} \rightarrow 2\ Fe^{3+} + 2\ OH^-$	0.49		Jacobsen et al. (1997)
A113001_a01	TrAa01FeN	$FeO^{2+} + HONO \rightarrow Fe^{3+} + NO_2 + OH^-$	1.1E4		Jacobsen et al. (1998)
A113002_a01	TrAa01FeN	$Fe^{2+} + NO_3 \rightarrow Fe^{3+} + NO_3^-$	8.0E6		Herrmann et al. (2000)
A116001_a01	TrAa01ClFe	$Fe^{2+} + Cl \rightarrow Fe^{3+} + Cl^-$	5.9E9		Jayson et al. (1973)
A116002a_a01	TrAa01ClFe	$Fe^{2+} + Cl_2^- \rightarrow Fe^{3+} + 2\ Cl^-$	1E7		Thornton and Laurence (1973)
A116002b_a01	TrAa01ClFe	$Fe^{2+} + Cl_2^- \rightarrow FeCl^{2+} + Cl^-$	4E6		Thornton and Laurence (1973)
A116003a_a01	TrAa01ClFe	$FeCl^+ + HO_2 \rightarrow Fe^{3+} + Cl^- + HO2^-$	1.2E6		de Laat and Le (2006)
A116003b_a01	TrAa01ClFe	$FeCl^+ + O_2^- \rightarrow Fe^{3+} + Cl^- + HO2^- + OH^-$	1E7		de Laat and Le (2006)
A116004a_a01	TrAa01ClFe	$FeCl^{2+} + HO_2 \rightarrow Fe^{2+} + Cl^- + O_2 + H^+$	2E4		de Laat and Le (2006)
A116004b_a01	TrAa01ClFe	$FeCl_2^+ + HO_2 \rightarrow Fe^{2+} + 2\ Cl^- + O_2 + H^+$	2E4		de Laat and Le (2006)
A116004c_a01	TrAa01ClFe	$FeCl^{2+} + O_2^- \rightarrow Fe^{2+} + Cl^- + O_2$	5E7		de Laat and Le (2006)
A116004d_a01	TrAa01ClFe	$FeCl_2^+ + O_2^- \rightarrow Fe^{2+} + 2\ Cl^- + O_2$	5E7		de Laat and Le (2006)
A116005_a01	TrAa01ClFe	$FeO^{2+} + Cl^- \rightarrow Fe^{3+} + Cl + 2\ OH^-$	1E2		Jacobsen et al. (1998)*

Table 6: Aqueous phase reactions (...continued)

#	labels	reaction	k_0 $[M^{1-n}s^{-1}]$	$-E_a/R[K]$	reference
A117001_a01	TrAa01BrFe	$Fe^{2+} + Br_2^- \rightarrow Fe^{3+} + 2\ Br^-$	3.6E6		Thornton and Laurence (1973)
A119001_a01	TrAa01FeS	$FeO^{2+} + SO_2 \rightarrow Fe^{3+} + SO_3^-$	4.5E5		Jacobsen et al. (1998)*
A119002_a01	TrAa01FeS	$FeO^{2+} + HSO_3^- \rightarrow Fe^{3+} + SO_3^- + OH^-$	2.5E5		Jacobsen et al. (1998)*
A119003_a01	TrAa01FeS	$FeOH^{2+} + HSO_3^- \rightarrow Fe^{2+} + SO_3^- + H_2O$	30		Ziajka et al. (1994)
A119004_a01	TrAa01FeS	$Fe^{2+} + SO_5^- \rightarrow FeOH^{2+} + HSO_5^-$	8E5		Ziajka et al. (1994)*
A119005_a01	TrAa01FeS	$Fe^{2+} + HSO_5^- \rightarrow FeOH^{2+} + SO_4^-$	3.0E4		Gilbert and Stell (1990)
A119006_a01	TrAa01FeS	$Fe^{2+} + SO_4^- \rightarrow FeSO_4^+$	3.6E7		McElroy and Waygood (1990)*
A119007_a01	TrAa01FeS	$FeOH^{2+} + SO_3^- \rightarrow Fe^{2+} + HSO_4^-$	3E7		Warneck (2018)
A119008_a01	TrAa01FeS	$FeSO_3^+ + SO_3^- \rightarrow Fe^{2+} + SO_4^{2-} + SO_2$	2.16E6		Warneck (2018)*

Specific notes

A41004_a01: We use the values A and E_A from $k_2(T)$ of Exner et al. (1994), which is different from k at 298 K listed in Table II of the same study.

A41009_a01: We use the values A and E_A from $k_1(T)$ of Exner et al. (1994), which is different from k at 298 K listed in Table I of the same study.

A41012a_a01: We use the values A and E_A from Table 1 of Herrmann et al. (1999b), which is different from k at 298 K listed in the same table.

A41012b_a01: See branch a.

A41013a_a01: Branching ratios taken from Asmus et al. (1973)

A41016a_a01: Branching ratio explaining the HCOOH-yield by Monod et al. (2007) who originally assigned it to the channel for the methylic H-abstraction. However, Monod et al. (2007), differently from Herrmann et al. (1999b), assumed that the self-reaction of CH_3O_2 would only produce 2 CH_3O radicals and thus HCHO + HO_2. Instead, the latter reaction has a 0.8 yield of $HOCH_2O_2$, which is a precursor of hydroxymethyl hydroperoxide and thus HCOOH.

A41016b_a01: The CH_2OOH radical has a lifetime of 10^{-9} s in the gas phase decomposing to HCHO and OH. O_2-addition in the aqueous-phase seems unlikely. It is hard to imagine how the $HOOHCH_2O_2$ radical would decompose into HCOOH and HO_2.

A41017a_a01: $k(H_2O_2+NO_3)$, branching ratio as for CH_3OOH + OH

A41017b_a01: See branch a.

A41018a_a01: $k(H_2O_2+CO_3^-)$, branching ratio as for CH_3OOH + OH

A41018b_a01: See branch a.

A41019a_a01: Branching ratio as for CH_3OOH + OH

A41019b_a01: $HOCHOOHO_2$ is assumed to directly decompose into CHOOOH and HO_2

A41020a_a01: $k(H_2O_2+NO_3)$, branching ratio as for CH_3OOH + OH

A41020b_a01: $HOCHOOHO_2$ is assumed to directly decompose into CHOOOH and HO_2

A41021_a01: HO_2 elimination

A41022_a01: $k(HO_2+HO_2)$

A41023_a01: $k(HO_2+O_2^-)$

A41030_a01: HO_2 elimination

A42000a_a01: CH_3CHOHO_2 is assumed to directly decompose into CH_3CHO + HO_2

A42001a_a01: CH_3CHOHO_2 is assumed to directly decompose into CH_3CHO + HO_2

A42003_a01: $k(HO_2+O_2^-)$

A42004_a01: $k(HO_2+HO_2)$

A42005_a01: k approximated from ($k(CH_3OOH+OH)$ /$k(CH_3OH+OH)$)

A42006_a01: $CH_2OHCHOHO_2$ is assumed to directly decompose into $HOCH_2CHO$ + HO_2

A42007_a01: We use the values A and E_A from Table 3 of Hoffmann et al. (2009), which is different from k at 298 K listed in Tables 1 and 2 of the same study. $CH_2OHCHOHO_2$ is assumed to directly decompose into $HOCH_2CHO$ + HO_2.

A42010_a01: k based on Monod et al. (2005): k=k(2 $CH_3CH_2(OO)$)

A42014_a01: HO_2 elimination

A42016a_a01: k assumed to be the same as for CH_3CHO + NO_3

A42016b_a01: See branch a.

A42017_a01: $k(CH_3CHOHOH+O_2^-)$

A42018_a01: HO_2 elimination

A42019_a01: k based on von Sonntag (1987)

A42020_a01: k based on von Sonntag (1987)

A42022a_a01: $k(CH_3CHOHOH+NO_3)$

A42022b_a01: See branch a.

A42022c_a01: See branch a.

A42023b_a01: $CHOHOHO_2$ directly decomposes into HCOOH + HO_2

A42024a_a01: k based on Neta and Huie (1986)

A42024b_a01: $CHOHOHO_2$ directly decomposes into HCOOH + HO_2

A42025_a01: HO_2 elimination

A42027_a01: We use the values A and E_A from $k_3(T)$ of Exner et al. (1994), which is different from k at 298 K listed in Table IV of the same study.

A42029_a01: We use the values A and E_A from $k_4(T)$ of Exner et al. (1994), which is different from k at 298 K listed in Table V of the same study.

A42030b_a01: $CH_3CHOOHO_2$ is assumed to directly decompose into CH_3CO_2H and HO_2

A42031a_a01: We use the values A and E_A from Table 1 of Herrmann et al. (1999b), which is different from k at 298 K listed in the same table.

A42031b_a01: See branch a. CH_3CHOHO_2 is assumed to directly decompose into CH_3CHO + HO_2.

A42032_a01: $k(HO_2+O_2^-)$

A42033_a01: $k(HO_2+HO_2)$

A42034_a01: $k(HO_2+HO_2)$

A42035_a01: $k(HO_2+O_2^-)$

A42037_a01: $k(HO_2+HO_2)$

A42038_a01: $k(HO_2+O_2^-)$

A42141_a01: We use the values A and E_A from the abstract of Ervens et al. (2003b), which is different from k at 298 K listed in abstract and Table 11 of the same study.

A42142_a01: We use the values A and E_A from the abstract of Ervens et al. (2003b), which is different from k at 298 K listed in the abstract and Table 11 of the same study.

A42144a_a01: k assumed to be the same as C_2H_5OOH + OH based on Monod et al. (2007)

A42144b_a01: See branch a.

A42146a_a01: k assumed to be the same as C_2H_5OOH + OH based on Monod et al. (2007)

A42146b_a01: See branch a.

A42148_a01: HO_2 elimination

A42149_a01: HO_2 elimination

A42150a_a01: COOHOO is not formed but directly dissociates into CO_2 + HO_2. Rate coefficient based on Buxton et al. (1988)

A42150b_a01: See branch a.

A42151a_a01: We use the values A and E_A from Table 2 of Gaillard de Sémainville et al. (2007), which is different from k at 298 K listed in the same Table. COOHOO is not formed but directly dissociates into CO_2 + HO_2.

A42151b_a01: See branch a.

A42154a_a01: We use the values A and E_A from Table 2 of Gaillard de Sémainville et al. (2007), which is different from k at 298 K listed in the same table.

A42154b_a01: See branch a.

A42156a_a01: We use the values A and E_A from the abstract of Ervens et al. (2003b), which is different from k at 298 K listed in the abstract and Table 10 of the same study.

A42156b_a01: See branch a. COOHOO is not formed but directly dissociates into CO_2 + HO_2.

A42157a_a01: $k(CHOHOHCHOHOH+NO_3)$

A42157b_a01: COOHOO is not formed but directly dissociates into CO_2 + HO_2

A42158a_a01: We use the values A and E_A from the abstract of Ervens et al. (2003b), which is different from k at 298 K listed in the abstract and Table 10 of the same study.

A42158b_a01: See branch a.

A42161_a01: HO_2 elimination

A42162_a01: HO_2 elimination

A42163a_a01: $k(HOCH_2CHO$ +OH)

A42163b_a01: See branch a.

A42164a_a01: $k(HOCH_2CHO+NO_3)$

A42164b_a01: See branch a.

A42165a_a01: $k(HOCH_2CHOHOH+OH)$

A42165b_a01: See branch a.

A42165c_a01: See branch a.

A42166a_a01: $k(HOCH_2CHOHOH+NO_3)$

A42166b_a01: See branch a.

A42166c_a01: See branch a.

A42167_a01: pH-dependent

A42169_a01: $k = 2 \times k(HOCH_2OH+OH)$

A42471_a01: Assumed to be the same as CH3CO3 + H2O, following Villalta et al. (1996)

A42472_a01: Assumed to be the same as CH3CO3 + H2O, following Villalta et al. (1996)

A42473_a01: Assumed to be the same as CH3CO3 + H2O, following Villalta et al. (1996)

A43000a_a01: Intermidate reaction with O_2^- and $CH(OH)_2COCH_2O_2$ neglected

A43001_a01: $CH(OH)_2COCH_2O_2$ neglected

A43002_a01: We use the values A and E_A from Table 3 of Schaefer et al. (2012), which is different from k at 298 K listed in the same table. CO_2 added for mass balance intermediate reactions neglected.

A43003_a01: We use the values A and E_A from $k_{pyruvic\ acid}(T)$ (Reaction 11) of Gaillard de Sémainville et al. (2007), which is different from k at 298 K listed in Table 2 in the same study.

A43004_a01: We use the values A and E_A from Table 3 of Schaefer et al. (2012), which is different from k at 298 K listed in the same table. CO_2 added for mass balance intermediate reactions neglected.

A43005_a01: We use the values A and E_A from Table 2 of Gaillard de Sémainville et al. (2007), which is different from k at 298 K listed in the same table.

A43007_a01: Temperature dependence from Herrmann et al. (2005)

A43010a_a01: $CH_2(OH)COCH_2O_2$ was negected with a branching ratio 0.16 added to $CH_3COCHOHO_2$

A43011_a01: We use the values A and E_A from Table 2 of Gaillard de Sémainville et al. (2007), which is different from k at 298 K listed in the same table.

A43013_a01: There is an intermediate reaction with branching ratio 0.87 and 0.13, the minor compound is neglected (Monod et al., 2005)

A43014_a01: There is an intermediate reaction with branching ratio 0.87 and 0.13, the minor compound is neglected (Herrmann et al., 1994)

A43015a_a01: k calculated comparing the rates ($CH_3OH + OH$/$CH_3OOH + OH$) and (ACETOL + OH/HYPERACET + OH)

A43015b_a01: k from $CH_3OOH + OH \rightarrow HCHO$.

A43016_a01: k taked from the reaction of the hydrated form of MGLYOX and NO_3

A43017_a01: k from $CH_3O_2 + HO_2$

A43018_a01: k from $CH_3O_2 + O_2^-$

A43019a_a01: k calculated comparing $CH_3OH + OH$ / $CH_3OOH + OH$ with IPROPL + OH

A43019b_a01: k calculated comparing CH3OH + OH / CH3OOH + OH with ACETOL + OH / HYPERCET + OH

A43020_a01: k taken from the reaction of the hydrated form of MGLYOX and NO_3

A43021_a01: k from $CH_3O_2 + HO_2$

A43022_a01: k from $CH_3O_2 + O_2^-$

A43023_a01: pH-dependent

A43025_a01: $k = 2 \times k(HOCH_2OH{+}OH)$

A44000_a01: We use the values A and E_A from Table 3 of Schöne et al. (2014), which is different from k at 298 K listed in Table 2 of the same study.

A44001_a01: $k = k(2\ CH_3COCH_2O_2)$

A44002_a01: We use the values A and E_A from Table 3 of Schöne et al. (2014), which is different from k at 298 K listed in Table 2 of the same study.

A44003_a01: $k = k(2\ CH_3COCH_2O_2)$. Originally, .2 $CH_2OHCHOHCOCH_3$ is produced by this reaction. However, the oxidation or the phase-transfer of $CH_2OHCHOHCOCH_3$ is not represented. Thus, lumped carbon (.8 LCARBON) is used to represent .2 $CH_2OHCHOHCOCH_3$.

A44010_a01: $k = 2 \times k$(CHOHOHCHOHOH+OH)

A44011_a01: $k = 2 \times k$(CHOHOHCHOHOH+OH)

A44012_a01: $k = 2 \times k$(CHOHOHCHOHOH+OH)

A46000_a01: Assumed to be the same as for glyoxal

A46001_a01: Assumed to be the same as for glyoxal

A46002_a01: $k = 2 \times k(CH_3COCHOHOH{+}OH)$

A46003_a01: Assumed to be the same as for glyoxal

A46004_a01: Assumed to be the same as for glyoxal

A46005_a01: $k = 2 \times k(CH_3COCHOHOH{+}OH)$

A61002_a01: Jacobi (1996) found an upper limit of 6E9 and cite an upper limit from another study of 2E9. Here, we set the rate coefficient to 1E9.

A63001_a01: There is also an earlier study by Exner et al. (1992) which found a smaller rate coefficient but did not consider the back reaction.

A64000_a01: k taken from $H_2O_2{+}Cl_2^-$ (Yu, 2004).

A74000_a01: Assumed to be the same as for Br_2^- + H_2O_2.

A76003_a01: The rate coefficient is defined as backward reaction divided by equilibrium constant.

A91005_a01: The rate coefficient for the sum of the paths (leading to either HSO_5^- or SO_4^{2-}) is from Huie and Neta (1987), the ratio 0.28/0.72 is from Deister and Warneck (1990).

A91006_a01: See also: (Huie and Neta, 1987; Warneck, 1991). If this reaction produces a lot of SO_4^-, it will have an effect. However, we currently assume only the stable $S_2O_8^{2-}$ as product. Since $S_2O_8^{2-}$ is not treated explicitly in the mechanism, SO_4^{2-} is used as a proxy and the second sulfur atom is put into the lumped LSULFUR.

A92005_a01: D. Sedlak, pers. comm. (1993).

A92008_a01: D. Sedlak, pers. comm. (1993).

A94100_a01: $2.48 \times 10^7 \times 5.5 \times 10^{-4}$, considering the hydrated form of HCHO.

A94102_a01: $790 \times 5.5 \times 10^{-4}$, considering the hydrated form of HCHO.

A94108a_a01: $k(H_2O_2{+}SO_4^-)$, branching ratio as for CH_3OOH + OH

A94108b_a01: See branch a.

A94200_a01: $k(CH_3OO+HSO_3^-)$

A94201_a01: $k(CH_3OO+HSO_3^-)$

A94202a_a01: CH_3CHOHO_2 is assumed to directly decompose into CH_3CHO + HO_2

A94203b_a01: $CHOHOHO_2$ directly decomposes into HCOOH + HO_2

A96005_a01: Assumed to be the same as for SO_3^{2-} + HOCl.

A97005_a01: Assumed to be the same as for SO_3^{2-} + HOBr.

A116005_a01: products assumed

A119001_a01: products assumed

A119002_a01: products assumed

A119004_a01: Assumed. Note that CAPRAM 2.4 lists k=4.3E7 from Herrmann Air Pollution Research Report 57 and it also lists k= 2.65E7 from Williams PhD 1996 http://lib.leeds.ac.uk/record=b1835184~S5. Brand and van Eldik (1995) also list k=3.56E4 from Waygood EUROTRAC 1992 report.

A119006_a01: 3E8*6500/(48000+6500)

A119008_a01: Assuming that the intermediate $S_2O_6^{2-}$ dissociates quickly.

References

Albaladejo, J., Jiménez, E., Notario, A., Cabañas, B., and Martínez, E.: CH_3O yield in the $CH_3 + O_3$ reaction using the LP/LIF technique at room temperature, J. Phys. Chem. A, 106, 2512–2519, doi:10.1021/jp012249o, 2002.

Amedro, D., Berasategui, M., Bunkan, A. J. C., Pozzer, A., Lelieveld, J., and Crowley, J. N.: Kinetics of the $OH + NO_2$ reaction: effect of water vapour and new parameterization for global modelling, Atmos. Chem. Phys., 20, 3091–3105, doi:10.5194/acp-20-3091-2020, 2020.

Ammann, M. and Pöschl, U.: Kinetic model framework for aerosol and cloud surface chemistry and gas-particle interactions - Part 2: exemplary practical applications and numerical simulations, Atmos. Chem. Phys., 7, 6025–6045, doi:10.5194/ACP-7-6025-2007, 2007.

Anderson, L. C. and Fahey, D. W.: Studies with $ClONO_2$: Thermal dissociation rate and catalytic conversion to NO using an NO/O_3 chemiluminescence detector, J. Phys. Chem., 94, 644–652, doi:10.1021/J100365A027, 1990.

Andrews, D. U., Heazlewood, B. R., Maccarone, A. T., Conroy, T., Payne, R. J., Jordan, M. J. T., and Kable, S. H.: Photo-tautomerization of acetaldehyde to vinyl alcohol: a potential route to tropospheric acids, Science, 337, 1203–1206, doi:10.1126/science.1220712, 2012.

Ariya, P. A., Khalizov, A., and Gidas, A.: Reactions of gaseous mercury with atomic and molecular halogens: Kinetics, product studies, and atmospheric implications, J. Phys. Chem. A, 106, 7310–7320, doi:10.1021/JP020719O, 2002.

Aschmann, S. M., Nishino, N., Arey, J., and Atkinson, R.: Products of the OH radical-initiated reactions of furan, 2- and 3-methylfuran, and 2,3- and 2,5-dimethylfuran in the presence of NO, J. Phys. Chem. A, 118, 457–466, doi:10.1021/jp410345k, 2014.

Asmus, K. D., Moeckel, H., and Henglein, A.: Pulse radiolytic study of the site of hydroxyl radical attack on aliphatic alcohols in aqueous solution, J. Phys. Chem., 77, 1218–1221, doi:10.1021/j100629a007, 1973.

Atkinson, R.: Gas-phase tropospheric chemistry of volatile organic compounds: 1. Alkanes and alkenes, J. Phys. Chem. Ref. Data, 26, 215–290, doi:10.1063/1.556012, 1997.

Atkinson, R.: Kinetics of the gas-phase reactions of OH radicals with alkanes and cycloalkanes, Atmos. Chem. Phys., 3, 2233–2307, doi:10.5194/ACP-3-2233-2003, 2003.

Atkinson, R. and Arey, J.: Atmospheric degradation of volatile organic compounds, Chem. Rev., 103, 4605–4638, doi:10.1021/cr0206420, 2003.

Atkinson, R., Baulch, D. L., Cox, R. A., Crowley, J. N., Hampson, R. F., Hynes, R. G., Jenkin, M. E., Rossi, M. J., and Troe, J.: Evaluated kinetic and photochemical data for atmospheric chemistry: Volume I – gas phase reactions of O_x, HO_x, NO_x and SO_x species, Atmos. Chem. Phys., 4, 1461–1738, doi:10.5194/ACP-4-1461-2004, 2004.

Atkinson, R., Baulch, D. L., Cox, R. A., Crowley, J. N., Hampson, R. F., Hynes, R. G., Jenkin, M. E., Rossi, M. J., Troe, J., and IUPAC Subcommittee: Evaluated kinetic and photochemical data for atmospheric chemistry: Volume II – gas phase reactions of organic species, Atmos. Chem. Phys., 6, 3625–4055, doi:10.5194/ACP-6-3625-2006, 2006.

Atkinson, R., Baulch, D. L., Cox, R. A., Crowley, J. N., Hampson, R. F., Hynes, R. G., Jenkin, M. E., Rossi, M. J., and Troe, J.: Evaluated kinetic and photochemical data for atmospheric chemistry: Volume III – gas phase reactions of inorganic halogens, Atmos. Chem. Phys., 7, 981–1191, doi:10.5194/ACP-7-981-2007, 2007.

Baeza-Romero, M. T., Glowacki, D. R., Blitz, M. A., Heard, D., Pilling, M. J., Rickard, A. R., and Seakins, P. W.: A combined experimental and theoretical study of the reaction between methylglyoxal and OH/OD radical: OH regeneration, Phys. Chem. Chem. Phys., 9, 4114–4128, doi:10.1039/b702916k, 2007.

Bailey, S. M., Barth, C. A., and Solomon, S. C.: A model of nitric oxide in the lower thermosphere, J. Geophys. Res., 107, doi:10.1029/2001JA000258, 2002.

Bale, C. S. E., Canosa-Mas, C. E., Shallcross, D. E., and Wayne, R. P.: A discharge-flow study of the kinetics of the reactions of IO with CH_3O_2 and CF_3O_2, Phys. Chem. Chem. Phys., 7, 2164–2172, doi:10.1039/B501903F, 2005.

Banic, C. M., Beauchamp, S. T., Tordon, R. J., Schroeder, W. H., Steffen, A., Anlauf, K. A., and Wong, H. K. T.: Vertical distribution of gaseous elemental mercury in Canada, J. Geophys. Res., 108D, 4264, doi:10.1029/2002JD002116, 2003.

Barker, G. C., Fowles, P., and Stringer, B.: Pulse radiolytic induced transient electrical conductance in liquid solutions, Trans. Faraday Soc., 66, 1509–1519, doi:10.1039/TF9706601509, 1970.

Barnes, I., Becker, K. H., Fink, E. H., Reimer, A., Zabel, F., and Niki, H.: FTIR spectroscopic study of the gas-phase reaction of HO_2 with H_2CO, Chem. Phys. Lett., 115, 1–8, doi:10.1016/0009-2614(85)80091-9, 1985.

Barnes, I., Becker, K. H., and Zhu, T.: Near UV absorption-spectra and photolysis products of difunctional organic nitrates – possible importance as NO_x reservoirs, J. Atmos. Chem., 17, 353–373, doi:10.1007/BF00696854, 1993.

Barone, S. B., Turnipseed, A. A., and Ravishankara, A. R.: Role of adducts in the atmospheric oxidation of dimethyl sulfide, Faraday Discuss., 100, 39–54, doi:10.1039/FD9950000039, 1995.

Barth, C. A.: Nitric oxide in the lower thermosphere, Planet. Space Sci., 40, 315–336, doi:10.1016/0032-0633(92)90067-X, 1992.

Bates, K. H., Crounse, J. D., St. Clair, J. M., Bennett, N. B., Nguyen, T. B., Seinfeld, J. H., Stoltz, B. M., and Wennberg, P. O.: Gas phase production and loss of isoprene epoxydiols, J. Phys. Chem. A, 118, 1237–1246, doi:10.1021/jp4107958, 2014.

Baulch, D. L., Bowman, C. T., Cobos, C. J., Cox, R. A., Just, T., Kerr, J. A., Pilling, M. J., Stocker, D., Troe, J., Tsang, W., Walker, R. W., and Warnatz, J.: Evaluated kinetic data for combustion modeling: Supplement II, J. Phys. Chem. Ref. Data, 34, 757–1397, doi:10.1063/1.1748524, 2005.

Becker, K. H., Kurtenbach, R., Schmidt, F., and Wiesen, P.: Kinetics of the NCO radical reacting with atoms and selected molecules, Combust. Flame, 120, 570–577, doi:10.1016/S0010-2180(99)00108-X, 2000.

Beckwith, R. C., Wang, T. X., and Margerum, D. W.: Equilibrium and kinetics of bromine hydrolysis, Inorg. Chem., 35, 995–1000, doi:10.1021/IC950909W, 1996.

Bedjanian, Y., Le Bras, G., and Poulet, G.: Kinetic study of the Br + IO, I + BrO and Br + I_2 reactions. Heat of formation of the BrO radical, Chem. Phys. Lett., 266, 233–238, doi:10.1016/S0009-2614(97)01530-3, 1997.

Bedjanian, Y., Laverdet, G., and Le Bras, G.: Low-pressure study of the reaction of Cl atoms with isoprene, J. Phys. Chem. A, 102, 953–959, doi:10.1021/JP973336C, 1998.

Behnke, W., Scheer, V., and Zetzsch, C.: Production of $BrNO_2$, Br_2 and $ClNO_2$ from the reaction between sea spray aerosol and N_2O_5, J. Aerosol Sci., 25, S277–S278, doi:10.1016/0021-8502(94)90369-7, 1994.

Behnke, W., George, C., Scheer, V., and Zetzsch, C.: Production and decay of $ClNO_2$ from the reaction of gaseous N_2O_5 with NaCl solution: Bulk and aerosol experiments, J. Geophys. Res., 102D, 3795–3804, doi:10.1029/96JD03057, 1997.

Bell, R. P. and Evans, P. G.: Kinetics of the dehydration of methylene glycol in aqueous solution, Proc. R. Soc. Lond. A, 291, 297–323, doi:10.1098/rspa.1966.0097, 1966.

Betterton, E. A. and Hoffmann, M. R.: Oxidation of aqueous SO_2 by peroxymonosulfate, J. Phys. Chem., 92, 5962–5965, doi:10.1021/J100332A025, 1988.

Beyersdorf, A. J., Blake, D. R., Swanson, A., Meinardi, S., Rowland, F. S., and Davis, D.: Abundances and variability of tropospheric volatile organic compounds at the South Pole and other Antarctic locations, Atmos. Environ., 44, 4565–4574, doi:10.1016/j.atmosenv.2010.08.025, 2010.

Bichsel, Y. and von Gunten, U.: Oxidation of iodide and hypoiodous acid in the disinfection of natural waters, Environ. Sci. Technol., 33, 4040–4045, doi:10.1021/ES990336C, 1999.

Birdsall, A. W., Andreoni, J. F., and Elrod, M. J.: Investigation of the role of bicyclic peroxy radicals in the oxidation mechanism of toluene, J. Phys. Chem. A, 114, 10 655–10 663, doi:10.1021/jp105467e, 2010.

Bjergbakke, E., Navartnam, S., Parsons, B. J., and Swallow, A. J.: Reaction between $HO_2\cdot$ and chlorine in aqueous solution, J. Am. Chem. Soc., 103, 5926–5928, doi:10.1021/JA00409A059, 1981.

Bossolasco, A., Faragó, E. P., Schoemaecker, C., and Fittschen, C.: Rate constant of the reaction between CH_3O_2 and OH radicals, Chem. Phys. Lett., 593, 7–13, doi:10.1016/j.cplett.2013.12.052, 2014.

Boyce, S. D. and Hoffmann, M. R.: Kinetics and mechanism of the formation of hydroxymethanesulfonic acid at low pH, J. Phys. Chem., 88, 4740–4746, doi:10.1021/j150664a059, 1984.

Brand, C. and van Eldik, R.: Transition metal-catalyzed oxidation of sulfur(IV)oxides. Atmospheric relevant processes and mechanisms, Chem. Rev., 95, 119–190, doi:10.1021/cr00033a006, 1995.

Buras, Z. J., Elsamra, R. M. I., and Green, W. H.: Direct determination of the simplest Criegee intermediate (CH_2OO) self reaction rate, J. Phys. Chem. Lett., 5, 2224–2228, doi:10.1021/jz5008406, 2014.

Burkholder, J. B., Sander, S. P., Abbatt, J., Barker, J. R., Huie, R. E., Kolb, C. E., Kurylo, M. J., Orkin,

V. L., Wilmouth, D. M., and Wine, P. H.: Chemical Kinetics and Photochemical Data for Use in Atmospheric Studies, Evaluation No. 18, JPL Publication 15-10, Jet Propulsion Laboratory, Pasadena, http://jpldataeval.jpl.nasa.gov, 2015.

Butkovskaya, N., Kukui, A., and Le Bras, G.: Pressure and temperature dependence of ethyl nitrate formation in the $C_2H_5O_2$ + NO reaction, J. Phys. Chem. A, 114, 956–964, doi:10.1021/jp910003a, 2010.

Butkovskaya, N., Kukui, A., and Le Bras, G.: Pressure and temperature dependence of methyl nitrate formation in the CH_3O_2 + NO reaction, J. Phys. Chem. A, 116, 5972–5980, doi:10.1021/jp210710d, 2012.

Buxton, G. V., Kilner, C., and Sellers, R. M.: Pulse radiolysis of HOI and IO^- in aqueous solution. Formation and characterization of I(II), Proc. Tihany Symp. Radiat. Chem., 6, 155–159, 1986.

Buxton, G. V., Greenstock, C. L., Helman, W. P., and Ross, A. B.: Critical review of rate constants for reactions of hydrated electrons, hydrogen atoms and hydroxyl radicals ($\cdot OH/\cdot O^-$) in aqueous solution, J. Phys. Chem. Ref. Data, 17, 513–886, doi:10.1063/1.555805, 1988.

Buxton, G. V., Salmon, G. A., and Wood, N. D.: A pulse radiolysis study of the chemistry of oxysulphur radicals in aqueous solution, in: Physico-Chemical Behaviour of Atmospheric Pollutants, pp. 245–250, Springer, 1990.

Buxton, G. V., McGowan, S., Salmon, G. A., Williams, J. E., and Wood, N. D.: A study of the spectra and reactivity of oxysulphur-radical anions involved in the chain oxidation of S(IV): A pulse and γ-radiolysis study, Atmos. Environ., 30, 2483–2493, doi:10.1016/1352-2310(95)00473-4, 1996.

Buxton, G. V., Malone, T. N., and Salmon, G. A.: Oxidation of glyoxal initiated by OH in oxygenated aqueous solution, J. Chem. Soc. Faraday Trans., 93, 2889–2891, doi:10.1039/A701468F, 1997.

Buxton, G. V., Bydder, M., and Salmon, G. A.: The reactivity of chlorine atoms in aqueous solution: Part II. The equilibrium $SO_4^{\cdot-} + Cl^- \rightleftharpoons Cl^\cdot + SO_4^{2-}$, Phys. Chem. Chem. Phys., 1, 269–273, doi:10.1039/A807808D, 1999a.

Buxton, G. V., Salmon, G. A., and Wang, J. Q.: The equilibrium $NO_3^\cdot + Cl^- \rightleftharpoons NO_3^- + Cl^\cdot$: A laser flash photolysis and pulse radiolysis study of the reactivity of $NO_3^\cdot$ with chloride ion in aqueous solution, Phys. Chem. Chem. Phys., 1, 3589–3593, doi:10.1039/A903286J, 1999b.

Calvert, J. G. and Lindberg, S. E.: A modeling study of the mechanism of the halogen-ozone-mercury homogeneous reactions in the troposphere during the polar spring, Atmos. Environ., 37, 4467–4481, doi:10.1016/J.ATMOSENV.2003.07.001, 2003.

Canosa-Mas, C. E., King, M. D., Lopez, R., Percival, C. J., Wayne, R. P., Shallcross, D. E., Pyle, J. A., and Daele, V.: Is the reaction between $CH_3(O)O_2$ and NO_3 important in the night-time troposphere?, J. Chem. Soc. Faraday Trans., 92, 2211–2222, doi:10.1039/FT9969202211, 1996.

Capouet, M., Müller, J.-F., Ceulemans, K., Compernolle, S., Vereecken, L., and Peeters, J.: Modeling aerosol formation in alpha-pinene photo-oxidation experiments, J. Geophys. Res., 113D, doi:10.1029/2007JD008995, 2008.

Carl, S. A. and Crowley, J. N.: 298 K rate coefficients for the reaction of OH with i$-C_3H_7I$, n$-C_3H_7I$ and C_3H_8, Atmos. Chem. Phys., 1, 1–7, doi:10.5194/acp-1-1-2001, 2001.

Chai, J., Hu, H., Dibble, T. S., Tyndall, G. S., and Orlando, J. J.: Rate constants and kinetic isotope effects for methoxy radical reacting with NO_2 and O_2, J. Phys. Chem. A, 118, 3552–3563, doi:10.1021/jp501205d, 2014.

Chameides, W. L.: The photochemistry of a remote marine stratiform cloud, J. Geophys. Res., 89D, 4739–4755, doi:10.1029/JD089ID03P04739, 1984.

Chao, W., Hsieh, J.-T., Chang, C.-H., and Lin, J. J.-M.: Direct kinetic measurement of the reaction of the simplest Criegee intermediate with water vapor, Science, 347, 751–754, doi:10.1126/science.1261549, 2015.

Chen, J., Wenger, J. C., and Venables, D. S.: Near-ultraviolet absorption cross sections of nitrophenols and their potential influence on tropospheric oxidation capacity, J. Phys. Chem. A, 115, 12 235–12 242, doi:10.1021/jp206929r, 2011.

Chin, M. and Wine, P. H.: A temperature-dependent competitive kinetics study of the aqueous-phase reactions of OH radicals with formate, formic acid, acetate, acetic acid, and hydrated formaldehyde, in: Aquatic and Surface Photochemistry, edited by Helz, G. R., Zepp, R. G., and Crosby, D. G., pp. 85–96, A. F. Lewis, NY, 1994.

Chinake, C. R. and Simoyi, R. H.: Kinetics and mechanism of the complex bromate-iodine reaction, J. Phys. Chem., 100, 1643–1656, doi:10.1021/JP951956C, 1996.

Christensen, H. and Sehested, K.: Pulse radiolysis at high temperatures and high pressures,

Radiat. Phys. Chem., 18, 723–231, doi:10.1016/0146-5724(81)90195-3, 1981.

Christensen, H. and Sehested, K.: HO_2 and O_2^- radicals at elevated temperatures, J. Phys. Chem., 92, 3007–3011, doi:10.1021/J100321A060, 1988.

Christensen, H., Sehested, K., and Corfitzen, H.: Reactions of hydroxyl radicals with hydrogen peroxide at ambient and elevated temperatures, J. Phys. Chem., 86, 1588–1590, doi:10.1021/J100206A023, 1982.

Citri, O. and Epstein, I. R.: Mechanistic study of a coupled chemical oscillator: the bromate-chlorite-iodide reaction, J. Phys. Chem., 92, 1865–1871, doi:10.1021/J100318A034, 1988.

Clifton, C. L. and Huie, R. E.: Rate constants for hydrogen abstraction reactions of the sulfate radical, SO_4^-. Alcohols, Int. J. Chem. Kinet., 21, 677–687, doi:10.1002/kin.550210807, 1989.

Clifton, C. L. and Huie, R. E.: Rate constants for some hydrogen abstraction reactions of the carbonate radical, Int. J. Chem. Kinet., 25, 199–203, doi:10.1002/kin.550250308, 1993.

Clubb, A. E., Jordan, M. J. T., Kable, S. H., and Osborn, D. L.: Phototautomerization of acetaldehyde to vinyl alcohol: a primary process in UV-irradiated acetaldehyde from 295 to 335 nm, J. Phys. Chem. Lett., 3, 3522–3526, doi:10.1021/jz301701x, 2012.

Clyne, M. A. A. and Cruse, H. W.: Atomic resonance fluorescence spectrometry for the rate constants of rapid bimolecular reactions. Part 2. Reactions Cl + BrCl, Cl + Br_2, Cl + ICl, Br + IBr, Br + ICl, J. Chem. Soc. Faraday Trans. 2, 68, 1377–1387, doi:10.1039/F29726801377, 1972.

Conn, J. B., Kistiakowsky, G. B., Roberts, R. M., and Smith, E. A.: Heats of organic reactions. XIII. Heats of hydrolysis of some acid anhydrides, Journal of the American Chemical Society, 64, 1747–1752, doi:10.1021/ja01260a001, 1942.

da Silva, G.: Carboxylic acid catalyzed keto-enol tautomerizations in the gas phase, Angew. Chem., 122, 7685–7687, doi:10.1002/ange.201003530, 2010.

Damschen, D. E. and Martin, L. R.: Aqueous aerosol oxidation of nitrous acid by O_2, O_3 and H_2O_2, Atmos. Environ., 17, 2005–2011, doi:10.1016/0004-6981(83)90357-8, 1983.

Davis, D., Chen, G., Kasibhatla, P., Jefferson, A., Tanner, D., Eisele, F., Lenschow, D., Neff, W., and Berresheim, H.: DMS oxidation in the Antarctic marine boundary layer: Comparison of model simulations and field observations of DMS, DMSO, $DMSO_2$, H_2SO_4(g), MSA(g), and MSA(p), J. Geophys. Res., 103D, 1657–1678, doi:10.1029/97JD03452, 1998.

Davis, Jr., W. and de Bruin, H. J.: New activity coefficients of 0-100 per cent aqueous nitric acid, J. Inorg. Nucl. Chem., 26, 1069–1083, doi:10.1016/0022-1902(64)80268-2, 1964.

De Filippis, P., Scarsella, M., and Verdone, N.: Peroxyformic acid formation: a kinetic study, Ind. Eng. Chem. Res., 48, 1372–1375, doi:10.1021/ie801163j, 2009.

de Laat, J. and Le, T. G.: Effects of chloride ions on the iron(III)-catalyzed decomposition of hydrogen peroxide and on the efficiency of the Fenton-like oxidation process, Appl. Catal. B: Environ., 66, 137–146, doi:10.1016/j.apcatb.2006.03.008, 2006.

Deister, U. and Warneck, P.: Photooxidation of SO_3^{2-} in aqueous solution, J. Phys. Chem., 94, 2191–2198, doi:10.1021/J100368A084, 1990.

Dickson, A. G. and Millero, F. J.: A comparison of the equilibrium constants for the dissociation of carbonic acid in seawater media, Deep-Sea Res. A, 34, 1733–1743, 1987.

Dillon, T. J., Karunanandan, R., and Crowley, J. N.: The reaction of IO with CH_3SCH_3: Products and temperature dependent rate coefficients by laser induced fluorescence, Phys. Chem. Chem. Phys., 8, 847–855, doi:10.1039/B514718B, 2006a.

Dillon, T. J., Tucceri, M. E., and Crowley, J. N.: Laser induced fluorescence studies of iodine oxide chemistry. Part II. The reactions of IO with CH_3O_2, CF_3O_2 and O_3, Phys. Chem. Chem. Phys., 8, 5185–5198, doi:10.1039/B611116E, 2006b.

Dillon, T. J., Tucceri, M. E., Sander, R., and Crowley, J. N.: LIF studies of iodine oxide chemistry, part 3. Reactions IO + NO_3 $\rightarrow$ OIO + NO_2, I + NO_3 $\rightarrow$ IO + NO_2, and CH_2I + O_2 $\rightarrow$ (products): Implications for the chemistry of the marine atmosphere at night., Phys. Chem. Chem. Phys., 10, 1540–1554, doi:10.1039/B717386E, 2008.

Dolson, D. A. and Leone, S. R.: A reinvestigation of the laser-initiated chlorine/hydrogen bromide chain reaction: absolute rate constants and the v = 2/v = 1 ratio from chlorine atom + hydrogen bromide $\rightarrow$ hydrogen chloride(v) + bromine atom, J. Phys. Chem., 91, 3543–3550, doi:10.1021/J100297A016, 1987.

Donohoue, D. L., Bauer, D., Cossairt, B., and Hynes, A. J.: Temperature and pressure dependent rate coefficients for the reaction of Hg with Br and the reaction of Br with Br: a pulsed laser photolysis-pulsed

laser induced fluorescence study, J. Phys. Chem. A, 110, 6623–6632, doi:10.1021/JP054688J, 2006.

Doussin, J.-F. and Monod, A.: Structure-activity relationship for the estimation of OH-oxidation rate constants of carbonyl compounds in the aqueous phase, Atmos. Chem. Phys., 13, 11 625–11 641, doi:10.5194/acp-13-11625-2013, 2013.

Duff, J. W., Dothe, H., and Sharma, R. D.: On the rate coefficient of the $N(^2D)+O_2 \rightarrow NO+O$ reaction in the terrestrial thermosphere, Geophys. Res. Lett., 30, 1259–1263, 2003.

Dulitz, K., Amedro, D., Dillon, T. J., Pozzer, A., and Crowley, J. N.: Temperature (208–318 K) and pressure (18–696 Torr) dependent rate coefficients for the reaction between OH and HNO_3, Atmos. Chem. Phys., 18, 2381–2394, doi:10.5194/acp-18-2381-2018, 2018.

Edblom, E. C., Györgyi, L., Orbán, M., and Epstein, I. R.: A mechanism for dynamical behavior in the Landolt reaction with ferrocyanide, J. Am. Chem. Soc., 109, 4876–4880, doi:10.1021/JA00250A020, 1987.

Eigen, M. and Kustin, K.: The kinetics of halogen hydrolysis, J. Am. Chem. Soc., 84, 1355–1361, doi:10.1021/JA00867A005, 1962.

Elliot, A. J. and McCracken, D. R.: Effect of temperature on OH reactions and equilibria: a pulse radiolysis study, Int. J. Radiat. Appl. Instrum. C, 33, 69–74, doi:10.1016/1359-0197(89)90096-9, 1989.

Enami, S., Hoshino, Y., and Kawasaki, M.: A kinetic study of the gas-phase reactions of OIO with NO, NO_2, and Cl_2, Int. J. Chem. Kinet., 39, 688–693, doi:10.1002/KIN.20283, 2007.

Ervens, B. and Volkamer, R.: Glyoxal processing by aerosol multiphase chemistry: towards a kinetic modeling framework of secondary organic aerosol formation in aqueous particles, Atmos. Chem. Phys., 10, 8219–8244, doi:10.5194/acp-10-8219-2010, 2010.

Ervens, B., George, C., Williams, J. E., Buxton, G. V., Salmon, G. A., Bydder, M., Wilkinson, F., Dentener, F., Mirabel, P., Wolke, R., and Herrmann, H.: CAPRAM 2.4 (MODAC mechanism): An extended and condensed tropospheric aqueous phase mechanism and its application, J. Geophys. Res., 108D, 4426, doi:10.1029/2002JD002202, 2003a.

Ervens, B., Gligorovski, S., and Herrmann, H.: Temperature-dependent rate constants for hydroxyl radical reactions with organic compounds in aqueous solutions, Phys. Chem. Chem. Phys., 5, 1811–1824, doi:10.1039/B300072A, 2003b.

Espinosa-Garcia, J. and Garcia-Bernáldez, J. C.: Analytical potential energy surface for the $CH_4 + O(^3P) \rightarrow CH_3 + OH$ reaction. Thermal rate constants and kinetic isotope effects, Phys. Chem. Chem. Phys., 2, 2345–2351, doi:10.1039/b001038n, 2000.

Exner, M., Herrmann, H., and Zellner, R.: Laser-based studies of reactions of the nitrate radical in aqueous solution, Ber. Bunsenges. Phys. Chem., 96, 470–477, doi:10.1002/BBPC.19920960347, 1992.

Exner, M., Herrmann, H., Michel, J. W., and Zellner, R.: Laser pulse initiated measurements of NO_3 reactions with S(IV) and organic compounds in aqueous solutions, in: Proceedings of EUROTRAC Symposium '92, edited by Borrell, P. M., Borrell, P., Cvitaš, T., and Seiler, W., pp. 615–618, SPB Academic Publishing bv, The Hague, 1993.

Exner, M., Herrmann, H., and Zellner, R.: Rate constants for the reactions of the NO_3 radical with $HCOOH/HCOO^-$ and CH_3COOH/CH_3COO^- in aqueous solution between 278 and 328 K, J. Atmos. Chem., 18, 359–378, doi:10.1007/BF00712451, 1994.

Faria, R. B., Lengyel, I., Epstein, I. R., and Kustin, K.: Combined mechanism explaining nonlinear dynamics in bromine(III) and bromine(V) oxidations of iodide ion, J. Phys. Chem., 97, 1164–1171, doi:10.1021/J100108A011, 1993.

Feierabend, K. J., Zhu, L., Talukdar, R. K., and Burkholder, J. B.: Rate coefficients for the OH + HC(O)C(O)H (glyoxal) raction between 210 and 390 K, J. Phys. Chem. A, 112, 73–82, doi:10.1021/JP0768571, 2008.

Felder, P. and Demuth, C.: Photodissociation of $CFCl_3$ at 193 nm investigated by photofragment translational spectroscopy, Chem. Phys. Lett., 208, 21–26, doi:10.1016/0009-2614(93)80070-6, 1993.

Fell, C., Steinfeld, J. I., and Miller, S.: Quenching of $N(^2D)$ by $O(^3P)$, J. Chem. Phys., 92, 4768–4777, doi:10.1063/1.457694, 1990.

Finkbeiner, M., Crowley, J. N., Horie, O., Müller, R., Moortgat, G. K., and Crutzen, P. J.: Reaction between HO_2 and ClO: Product formation between 210 and 300 K, J. Phys. Chem., 99, 16 264–16 275, doi:10.1021/J100044A011, 1995.

Fisher, J. R. and Barnes, H. L.: The ion-product constant of water to 350°, J. Phys. Chem., 76, 90–99, doi:10.1021/J100645A016, 1972.

Fisher, M. M. and Hamill, W. H.: Electronic processes in pulse-irradiated aqueous and alcoholic systems, J. Phys. Chem., 77, 171–177, doi:10.1021/j100621a006, 1973.

Flocke, F., Atlas, E., Madronich, S., Schauffler, S. M., Aikin, K., Margitan, J. J., and Bui, T. P.: Observations of methyl nitrate in the lower stratosphere during STRAT: implications for its gas phase production mechanisms, Geophys. Res. Lett., 25, 1891–1894, doi:10.1029/98GL01417, 1998.

Fogelman, K. D., Walker, D. M., and Margerum, D. W.: Non-metal redox kinetics: Hypochlorite and hypochlorous acid reactions with sulfite, Inorg. Chem., 28, 986–993, doi:10.1021/IC00305A002, 1989.

Fortnum, D. H., Battaglia, C. J., Cohen, S. R., and Edwards, J. O.: The kinetics of the oxidation of halide ions by monosubstituted peroxides, J. Am. Chem. Soc., 82, 778–782, doi:10.1021/JA01489A004, 1960.

Francisco-Marquez, M., Alvarez-Idaboy, J. R., Galano, A., and Vivier-Bunge, A.: Theoretical study of the initial reaction between OH and isoprene in tropospheric conditions, Phys. Chem. Chem. Phys., 5, 1392–1399, doi:10.1039/B211185C, 2003.

Fuller-Rowell, T. J.: Modeling the solar cycle change in nitric oxide in the thermosphere and upper mesosphere, J. Geophys. Res., 98A, 1559–1570, doi:10.1029/92JA02201, 1993.

Furrow, S.: Reactions of iodine intermediates in iodate-hydrogen peroxide oscillators, J. Phys. Chem., 91, 2129–2135, doi:10.1021/J100292A031, 1987.

Gaillard de Sémainville, P., Hoffmann, D., George, C., and Herrmann, H.: Study of nitrate radical (NO_3) reactions with carbonyls and acids in aqueous solution as a function of temperature, Phys. Chem. Chem. Phys., 9, 958–968, doi:10.1039/B613956F, 2007.

Gans, B., Boyé-Peronne, S., Broquier, M., Delsaut, M., Douin, S., Fellows, C. E., Halvick, P., Loison, J.-C., Lucchese, R. R., and Gauyacq, D.: Photolysis of methane revisited at 121.6 nm and at 118.2 nm: quantum yields of the primary products, measured by mass spectrometry, Phys. Chem. Chem. Phys., 13, 8140–8152, doi:10.1039/c0cp02627a, 2011.

Ganzeveld, L., Klemm, O., Rappenglück, B., and Valverde-Canossa, J.: Evaluation of meteorological parameters over a coniferous forest in a single-column chemistry-climate model, Atmos. Environ., 40, S21–S27, doi:10.1016/J.ATMOSENV.2006.01.061, 2006.

Garton, D. J., Minton, T. K., Troya, D., Pascual, R., and Schatz, G. C.: Hyperthermal reactions of $O(^3P)$ with alkanes: Observations of novel reaction pathways in crossed-beams and theoretical studies, J. Phys. Chem. A, 107, 4583–4587, doi:10.1021/jp0226026, 2003.

George, C., El Rassy, H., and Chovelon, J.-M.: Reactivity of selected volatile organic compounds (VOCs) toward the sulfate radical (SO_4^-), Int. J. Chem. Kinet., 33, 539–547, doi:10.1002/kin.1049, 2001.

Gilbert, B. C. and Stell, J. K.: Mechanisms of peroxide decomposition. An ESR study of the reactions of the peroxomonosulphate anion ($HOOSO3^-$) with TiIII, FeII, and α-oxygen-substituted radicals, J. Chem. Soc. Perkin Trans. 2, pp. 1281–1288, doi:10.1039/P29900001281, 1990.

Gill, K. J. and Hites, R. A.: Rate constants for the gas-phase reactions of the hydroxyl radical with isoprene, α- and β-pinene, and limonene as a function of temperature, J. Phys. Chem. A, 106, 2538–2544, doi:10.1021/jp013532q, 2002.

Gligorovski, S., Rousse, D., George, C. H., and Herrmann, H.: Rate constants for the OH reactions with oxygenated organic compounds in aqueous solution, Int. J. Chem. Kinet., 41, 309–326, doi:10.1002/kin.20405, 2009.

Glowacki, D. R., Lockhart, J., Blitz, M. A., Klippenstein, S. J., Pilling, M. J., Robertson, S. H., and Seakins, P. W.: Interception of excited vibrational quantum states by O_2 in atmospheric association reactions, Science, 337, 1066–1069, doi:10.1126/science.1224106, 2012.

Goodsite, M., Plane, J. M. C., and Skov, H.: A theoretical study of the oxidation of Hg^0 to $HgBr_2$ in the troposphere, Environ. Sci. Technol., 38, 1772–1776, doi:10.1021/ES034680S, 2004.

Grenfell, J. L., Lehmann, R., Mieth, P., Langematz, U., and Steil, B.: Chemical reaction pathways affecting stratospheric and mesospheric ozone, J. Geophys. Res., 111D, doi:10.1029/2004JD005713, 2006.

Grgić, I., Podkrajšek, B., Barzaghi, P., and Herrmann, H.: Scavenging of SO_4^- radical anions by mono-and dicarboxylic acids in the Mn(II)-catalyzed S(IV) oxidation in aqueous solution, Atmos. Environ., 41, 9187–9194, doi:10.1016/j.atmosenv.2007.07.051, 2007.

Groß, C. B. M., Dillon, T. J., Schuster, G., Lelieveld, J., and Crowley, J. N.: Direct kinetic study of OH and O_3 formation in the reaction of $CH_3C(O)O_2$ with HO_2, J. Phys. Chem. A, 1, 974–985, doi:10.1021/jp412380z, 2014.

Gruzdev, A. N., Elokhov, A. S., Makarov, O. V., and Mokhov, I. I.: Some recent results of Russian measurements of surface ozone in Antarctica. A meteorological interpretation, Tellus, 45B, 99–105, doi:10.3402/TELLUSB.V45I2.15584, 1993.

Haag, W. R. and Hoigné, J.: Ozonation of bromide-containing waters: Kinetics of formation of hypobromous acid and bromate, Environ. Sci. Technol., 17, 261–267, doi:10.1021/ES00111A004, 1983.

Hahnenstein, I., Albert, M., Hasse, H., Kreiter, C. G., and Maurer, G.: NMR spectroscopic and densimetric study of reaction kinetics of formaldehyde polymer formation in water, deuterium oxide, and methanol, Ind. Eng. Chem. Res., 34, 440–450, doi:10.1021/ie00041a003, 1995.

Hall, B.: The gas phase oxidation of elemental mercury by ozone, Water Air Soil Pollut., 80, 301–315, doi:10.1007/BF01189680, 1995.

Hatakeyama, S., Honda, S., and Akimoto, H.: Rate constants and mechanism for reactions of ketenes with OH radicals in air at 299±2 K, Bull. Chem. Soc. Jpn., 58, 2157–2162, doi:10.1246/BCSJ.58.2157, 1985.

Hermans, I., Müller, J.-F., Nguyen, T. L., Jacobs, P. A., and Peeters, J.: Kinetics of α-hydroxy-alkylperoxyl radicals in oxidation processes. HO_2·-initiated oxidation of ketones/aldehydes near the tropopause, J. Phys. Chem. A, 109, 4303–4311, doi:10.1021/jp044080v, 2005.

Herrmann, H., Exner, M., and Zellner, R.: Reactivity trends in reactions of the nitrate radical (NO_3) with inorganic and organic cloudwater constituents, Geochim. Cosmochim. Acta, 58, 3239–3244, doi:10.1016/0016-7037(94)90051-5, 1994.

Herrmann, H., Reese, A., and Zellner, R.: Time resolved UV/VIS diode array absorption spectroscopy of SO_x^- (x=3, 4, 5) radical anions in aqueous solution, J. Mol. Struct., 348, 183–186, doi:10.1016/0022-2860(95)08619-7, 1995.

Herrmann, H., Ervens, B., Nowacki, P., Wolke, R., and Zellner, R.: A chemical aqueous phase radical mechanism for tropospheric chemistry, Chemosphere, 38, 1223–1232, doi:10.1016/S0045-6535(98)00520-7, 1999a.

Herrmann, H., Reese, A., Ervens, B., Wicktor, F., and Zellner, R.: Laboratory and modelling studies of tropospheric multiphase conversions involving some C_1 and C_2 peroxyl radicals, Phys. Chem. Earth B, 24, 287–290, doi:10.1016/S1464-1909(98)00052-5, 1999b.

Herrmann, H., Ervens, B., Jacobi, H.-W., Wolke, R., Nowacki, P., and Zellner, R.: CAPRAM2.3: A chemical aqueous phase radical mechanism for tropospheric chemistry, J. Atmos. Chem., 36, 231–284, doi:10.1023/A:1006318622743, 2000.

Herrmann, H., Tilgner, A., Barzaghi, P., Majdik, Z., Gligorovski, S., Poulain, L., and Monod, A.: Towards a more detailed description of tropospheric aqueous phase organic chemistry: CAPRAM 3.0, Atmos. Environ., 39, 4351–4363, doi:10.1016/j.atmosenv.2005.02.016, 2005.

Hislop, K. A. and Bolton, J. R.: The photochemical generation of hydroxyl radicals in the UV-vis/ferrioxalate/H_2O_2 system, Environ. Sci. Technol., 33, 3119–3126, doi:10.1021/es9810134, 1999.

Hoffmann, D., Weigert, B., Barzaghi, P., and Herrmann, H.: Reactivity of poly-alcohols towards OH, NO_3 and SO_4^- in aqueous solution, Phys. Chem. Chem. Phys., 11, 9351–9363, doi:10.1039/B908459B, 2009.

Hoffmann, M. R.: On the kinetics and mechanism of oxidation of aquated sulfur dioxide by ozone, Atmos. Environ., 20, 1145–1154, doi:10.1016/0004-6981(86)90147-2, 1986.

Hoigné, J. and Bader, H.: Rate constants of reactions of ozone with organic and inorganic compounds in water-I: Non-dissociating organic compounds, Wat. Res., 17, 173–183, doi:10.1016/0043-1354(83)90098-2, 1983.

Hoigné, J., Bader, H., Haag, W. R., and Staehelin, J.: Rate constants of reactions of ozone with organic and inorganic compounds in water – III Inorganic compounds and radicals, Wat. Res., 19, 993–1004, doi:10.1016/0043-1354(85)90368-9, 1985.

Huie, R. E. and Clifton, C. L.: Temperature dependence of the rate constants for reactions of the sulfate radical, SO_4^-, with anions, J. Phys. Chem., 94, 8561–8567, doi:10.1021/j100386a015, 1990.

Huie, R. E. and Clifton, C. L.: Kinetics of the self-reaction of hydroxymethylperoxyl radicals, Chem. Phys. Lett., 205, 163–167, doi:10.1016/0009-2614(93)89222-4, 1993.

Huie, R. E. and Neta, P.: Rate constants for some oxidations of S(IV) by radicals in aqueous solutions, Atmos. Environ., 21, 1743–1747, doi:10.1016/0004-6981(87)90113-2, 1987.

Hynes, A. J. and Wine, P. H.: The atmospheric chemistry of dimethylsulfoxide (DMSO) kinetics and mechanism of the OH + DMSO reaction, J. Atmos. Chem., 24, 23–37, doi:10.1007/BF00053821, 1996.

Ingham, T., Bauer, D., Sander, R., Crutzen, P. J., and Crowley, J. N.: Kinetics and products of the reactions BrO + DMS and Br + DMS at 298 K, J. Phys. Chem. A, 103, 7199–7209, doi:10.1021/JP9905979, 1999.

Jacob, D. J.: Chemistry of OH in remote clouds and its role in the production of formic acid and peroxymonosulfate, J. Geophys. Res., 91D, 9807–9826, doi:10.1029/JD091ID09P09807, 1986.

Jacobi, H.-W.: Kinetische Untersuchungen und Modellrechnungen zur troposphärischen Chemie von Radikalanionen und Ozon in wäßriger Phase, Ph.D. thesis, Universität GH Essen, Germany, 1996.

Jacobi, H.-W., Herrmann, H., and Zellner, R.: Kinetic investigation of the Cl_2^- radical in the aqueous phase, in: Air Pollution Research Report 57: Homogeneous and heterogeneous chemical Processes in the Troposphere, edited by Mirabel, P., pp. 172–176, Office for official Publications of the European Communities, Luxembourg, 1996.

Jacobsen, F., Holcman, J., and Sehested, K.: Activation parameters of ferryl ion reactions in aqueous acid solutions, Int. J. Chem. Kinet., 29, 17–24, doi:10.1002/(SICI)1097-4601(1997)29:1⟨17::AID-KIN3⟩3.0.CO;2-O, 1997.

Jacobsen, F., Holcman, J., and Sehested, K.: Reactions of the ferryl ion with some compounds found in cloud water, Int. J. Chem. Kinet., 30, 215–221, doi:10.1002/(SICI)1097-4601(1998)30:3⟨215::AID-KIN7⟩3.0.CO;2-V, 1998.

Jagiella, S. and Zabel, F.: Reaction of phenylperoxy radicals with NO_2 at 298 K, Phys. Chem. Chem. Phys., 9, 5036–5051, doi:10.1039/B705193J, 2007.

Jayson, G. G., Parsons, B. J., and Swallow, A. J.: Some simple, highly reactive, inorganic chlorine derivatives in aqueous solution, J. Chem. Soc. Faraday Trans. 1, 69, 1597–1607, doi:10.1039/F19736901597, 1973.

Jefferson, A., Nicovich, J. M., and Wine, P. H.: Temperature-dependent kinetics studies of the reactions $Br(^2P_{3/2}) + CH_3SCH_3 \leftrightarrow CH_3SCH_2 + HBr$. Heat of formation of the CH_3SCH_2 radical, J. Phys. Chem., 98, 7128–7135, doi:10.1021/J100080A006, 1994.

Jenkin, M., Saunders, S. M., and Pilling, M. J.: The tropospheric degradation of volatile organic compounds: A protocol for mechanism development, Atmos. Environ., 31, 81–104, doi:10.1016/S1352-2310(96)00105-7, 1997.

Jenkin, M. E., Young, J. C., and Rickard, A. R.: The MCM v3.3.1 degradation scheme for isoprene, Atmos. Chem. Phys., 15, 11 433–11 459, doi:10.5194/acp-15-11433-2015, 2015.

Jiang, P.-Y., Katsumura, Y., Nagaishi, R., Domae, M., Ishikawa, K., Ishigure, K., and Yoshida, Y.: Pulse radiolysis study of concentrated sulfuric acid solutions. Formation mechanism, yield and reactivity of sulfate radicals, J. Chem. Soc. Faraday Trans., 88, 1653–1658, doi:10.1039/FT9928801653, 1992.

Kaltsoyannis, N. and Plane, J. M. C.: Quantum chemical calculations on a selection of iodine-containing species (IO, OIO, INO_3, $(IO)_2$, I_2O_3, I_2O_4 and I_2O_5) of importance in the atmosphere, Phys. Chem. Chem. Phys., 10, 1723–1733, doi:10.1039/B715687C, 2008.

Keller-Rudek, H., Koschel, D., Merlet, P., Ohms-Bredemann, U., Wagner, J., and Wietelmann, A.: Gmelin Handbook of Inorganic and Organometallic Chemistry, 8th Edition, Br, Bromine, Supplement Volume B2, Compounds with Oxygen and Nitrogen, Springer Verlag, Berlin, 1992.

Kelley, C. M. and Tartar, H. V.: On the system: bromine-water, J. Am. Chem. Soc., 78, 5752–5756, doi:10.1021/JA01603A010, 1956.

Kirchner, F., Mayer-Figge, A., Zabel, F., and Becker, K. H.: Thermal stability of peroxynitrates, Int. J. Chem. Kinet., 31, 127–144, doi:10.1002/(SICI)1097-4601(1999)31:2⟨127::AID-KIN6⟩3.0.CO;2-L, 1999.

Kleinböhl, A., Toon, G. C., Sen, B., Blavier, J.-F. L., Weisenstein, D. K., Strekowski, R. S., Nicovich, J. M., Wine, P. H., and Wennberg, P. O.: On the stratospheric chemistry of hydrogen cyanide, Geophys. Res. Lett., 33, doi:10.1029/2006GL026015, 2006.

Kohlmann, J.-P. and Poppe, D.: The tropospheric gas-phase degradation of NH_3 and its impact on the formation of N_2O and NO_x, J. Atmos. Chem., 32, 397–415, doi:10.1023/A:1006162910279, 1999.

Kondo, O. and Benson, S. W.: Kinetics and equilibria in the system $Br + CH_3OOH \rightleftharpoons HBr + CH_3OO$. An upper limit for the heat of formation of the methylperoxy radical, J. Phys. Chem., 88, 6675–6680, doi:10.1021/J150670A034, 1984.

Kumar, K. and Margerum, D. W.: Kinetics and mechanism of general-acid-assisted oxidation of bromide by hypochlorite and hypochlorous acid, Inorg. Chem., 26, 2706–2711, doi:10.1021/IC00263A030, 1987.

Lax, E.: Taschenbuch für Chemiker und Physiker, Springer Verlag, Berlin, 1969.

Lee, Y.-N. and Schwartz, S. E.: Reaction kinetics of nitrogen dioxide with liquid water at low partial pressure, J. Phys. Chem., 85, 840–848, doi:10.1021/J150607A022, 1981.

Lengyel, I., Li, J., Kustin, K., and Epstein, I. R.: Rate constants for reactions between iodine- and chlorine-containing species: A detailed mechanism of the chlorine dioxine/chlorite reaction, J. Am. Chem. Soc., 118, 3708–3719, doi:10.1021/JA953938E, 1996.

Lewis, T. R., Blitz, M. A., Heard, D. E., and Seakins, P. W.: Direct evidence for a substantive reaction between the Criegee intermediate, CH_2OO, and the

water vapour dimer, Phys. Chem. Chem. Phys., 17, 4859–4863, doi:10.1039/C4CP04750H, 2015.

Liljegren, J. A. and Stevens, P. S.: Measurements of the kinetics of the reaction of OH radicals with 3-methylfuran at low pressure, Int. J. Chem. Kinet., 45, 787–794, doi:10.1002/KIN.20814, 2013.

Lin, C.-J. and Pehkonen, S. O.: Aqueous free radical chemistry of mercury in the presence of iron oxides and ambient aerosol, Atmos. Environ., 31, 4125–4137, doi:10.1016/S1352-2310(97)00269-0, 1997.

Lin, C.-J. and Pehkonen, S. O.: Oxidation of elemental mercury by aqueous chlorine ($HOCl/OCl^-$): Implications for tropospheric mercury chemistry, J. Geophys. Res., 103D, 28 093–28 102, doi:10.1029/98JD02304, 1998.

Lind, J. A., Lazrus, A. L., and Kok, G. L.: Aqueous phase oxidation of sulfur(IV) by hydrogen peroxide, methylhydroperoxide, and peroxyacetic acid, J. Geophys. Res., 92D, 4171–4177, doi:10.1029/JD092ID04P04171, 1987.

Liu, Q. and Margerum, D. W.: Equilibrium and kinetics of bromine chloride hydrolysis, Environ. Sci. Technol., 35, 1127–1133, doi:10.1021/ES001380R, 2001.

Liu, Y., Pimentel, A. S., Antoku, Y., Giles, B. J., and Barker, J. R.: Temperature-dependent rate and equilibrium constants for $Br \cdot (aq) + Br^-(aq) \rightleftharpoons Br_2^- \cdot (aq)$, J. Phys. Chem. A, 106, 11 075–11 082, doi:10.1021/JP0255536, 2002.

Lockhart, J., Blitz, M., Heard, D., Seakins, P., and Shannon, R.: Kinetic study of the OH + glyoxal reaction: experimental evidence and quantification of direct OH recycling, J. Phys. Chem. A, 117, 11 027–11 037, doi:10.1021/jp4076806, 2013.

Lockwood, A. L., Shepson, P. B., Fiddler, M. N., and Alaghmand, M.: Isoprene nitrates: preparation, separation, identification, yields, and atmospheric chemistry, Atmos. Chem. Phys., 10, 6169–6178, doi:10.5194/acp-10-6169-2010, 2010.

Løgager, T., Holcman, J., Sehested, K., and Pedersen, T.: Oxidation of ferrous ions by ozone in acidic solutions, Inorg. Chem., 31, 3523–3529, doi:10.1021/ic00043a009, 1992.

Løgager, T., Sehested, K., and Holcman, J.: Rate constants of the equilibrium reactions $SO_4 + HNO_3 \rightleftharpoons HSO_4^- + NO_3$ and $SO_4 + NO_3 \rightleftharpoons SO_4^{2-} + NO_3$, Radiat. Phys. Chem., 41, 539–543, doi:10.1016/0969-806X(93)90017-O, 1993.

Long, C. A. and Bielski, B. H. J.: Rate of reaction of superoxide radical with chloride-containing species, J. Phys. Chem., 84, 555–557, doi:10.1021/J100442A023, 1980.

Magi, L., Schweitzer, F., Pallares, C., Cherif, S., Mirabel, P., and George, C.: Investigation of the uptake rate of ozone and methyl hydroperoxide by water surfaces, J. Phys. Chem. A, 101, 4943–4949, doi:10.1021/JP970646M, 1997.

Manion, J. A., Huie, R. E., Levin, R. D., Burgess, Jr., D. R., Orkin, V. L., Tsang, W., McGivern, W. S., Hudgens, J. W., Knyazev, V. D., Atkinson, D. B., Chai, E., Tereza, A. M., Lin, C.-Y., Allison, T. C., Mallard, W. G., Westley, F., Herron, J. T., Hampson, R. F., and Frizzell, D. H.: NIST Chemical Kinetics Database, NIST Standard Reference Database 17 (Web Version), `http://kinetics.nist.gov`, 2015.

Margerum, D. W., Dickson, P. N., Nagy, J. C., Kumar, K., Bowers, C. P., and Fogelman, K. D.: Kinetics of the iodine monochloride reaction with iodide measured by the pulsed-accelerated-flow method, Inorg. Chem., 25, 4900–4904, doi:10.1021/IC00247A025, 1986.

Marsh, A. R. W. and McElroy, W. J.: The dissociation constant and Henry's law constant of HCl in aqueous solution, Atmos. Environ., 19, 1075–1080, doi:10.1016/0004-6981(85)90192-1, 1985.

Martell, A. E.: Other organic ligands, in: Critical Stability Constants, Springer, 1977.

Martin, L. R. and Damschen, D. E.: Aqueous oxidation of sulfur dioxide by hydrogen peroxide at low pH, Atmos. Environ., 15, 1615–1621, doi:10.1016/0004-6981(81)90146-3, 1981.

Matthew, B. M., George, I., and Anastasio, C.: Hydroperoxyl radical (HO2·) oxidizes dibromide radical anion ($\cdot Br_2^-$) to bromine (Br_2) in aqueous solution: Implications for the formation of Br_2 in the marine boundary layer, Geophys. Res. Lett., 30, doi:10.1029/2003GL018572, 2003.

McCabe, D. C., Gierczak, T., Talukdar, R. K., and Ravishankara, A. R.: Kinetics of the reaction OH + CO under atmospheric conditions, Geophys. Res. Lett., 28, 3135–3138, doi:10.1029/2000GL012719, 2001.

McElroy, W. J. and Waygood, S. J.: Kinetics of the reactions of the SO_4^- radical with SO_4^-, $S_2O_8^{2-}$, H_2O and Fe^{2+}, J. Chem. Soc. Faraday Trans., 86, 2557–2564, doi:10.1039/FT9908602557, 1990.

Mellouki, A. and Mu, Y.: On the atmospheric degradation of pyruvic acid in the gas phase, J. Photochem. Photobiol. A: Chem., 157, doi:10.1016/S1010-6030(03)00070-4, 2003.

Messaadia, L., Dib, G. E., Ferhati, A., and Chakir, A.: UV-visible spectra and gas-phase rate coefficients for the reaction of 2,3-pentanedione and 2,4-pentanedione with OH radicals, Chem. Phys. Lett., 626, 73–79, doi:10.1016/j.cplett.2015.02.032, 2015.

Monod, A., Poulain, L., Grubert, S., Voisin, D., and Wortham, H.: Kinetics of OH-initiated oxidation of oxygenated organic compounds in the aqueous phase: new rate constants, structure-activity relationships and atmospheric implications, Atmos. Environ., 39, 7667–7688, doi:10.1016/j.atmosenv.2005.03.019, 2005.

Monod, A., Chevallier, E., Durand Jolibois, R., Doussin, J. F., Picquet-Varrault, B., and Carlier, P.: Photooxidation of methylhydroperoxide and ethylhydroperoxide in the aqueous phase under simulated cloud droplet conditions, Atmos. Environ., 41, 2412–2426, doi:10.1016/j.atmosenv.2006.10.006, 2007.

Müller, J.-F., Peeters, J., and Stavrakou, T.: Fast photolysis of carbonyl nitrates from isoprene, Atmos. Chem. Phys., 14, 2497–2508, doi:10.5194/acp-14-2497-2014, 2014.

Munger, J. W., Jacob, D. J., Fan, S.-M., Colman, A. S., and Dibb, J. E.: Concentrations and snow-atmosphere fluxes of reactive nitrogen at Summit, Greenland, J. Geophys. Res., 104D, 13 721–13 734, doi:10.1029/1999JD900192, 1999.

Munthe, J.: The aqueous oxidation of elemental mercury by ozone, Atmos. Environ., 26A, 1461–1468, doi:10.1016/0960-1686(92)90131-4, 1992.

Nagy, J. C., Kumar, K., and Margerum, D. W.: Non-metal redox kinetics: Oxidation of iodide by hypochlorous acid and by nitrogen trichloride measured by the pulsed-accelerated-flow method, Inorg. Chem., 27, 2773–2780, doi:10.1021/IC00289A007, 1988.

Nakanishi, H., Morita, H., and Nagakura, S.: Electronic structures and spectra of the keto and enol forms of acetylacetone, Bull. Chem. Soc. Jpn., 50, 2255–2261, doi:10.1246/bcsj.50.2255, 1977.

Nakano, Y., Ishiwata, T., and Kawasaki, M.: Rate constants of the reaction of NO_3 with CH_3I measured with use of cavity ring-down spectroscopy, J. Phys. Chem. A, 109, 6527–6531, doi:10.1021/JP051817N, 2005.

Neta, P. and Huie, R. E.: Rate constants for reactions of NO_3 radicals in aqueous solutions, J. Phys. Chem., 90, 4644–4648, doi:10.1021/J100410A035, 1986.

Nguyen, T. L., Peeters, J., and Vereecken, L.: Theoretical study of the gas-phase ozonolysis of β-pinene ($C_{10}H_{16}$), Phys. Chem. Chem. Phys., 11, 5643–5656, doi:10.1039/b822984h, 2009.

Nielsen, O. J., Sidebottom, H. W., Donlon, M., and Treacy, J.: Rate constants for the gas-phase reactions of OH radicals and Cl atoms with n-alkyl nitrites at atmospheric pressure and 298 K, Int. J. Chem. Kinet., 23, 1095–1109, doi:10.1002/kin.550231204, 1991.

O'Dowd, C. D. and Hoffmann, T.: Coastal new particle formation: a review of the current state-of-the-art, Environ. Chem., 2, 245–255, doi:10.1071/EN05077, 2005.

Ogryzlo, E. A., Paltenghi, R., and Bayes, K. D.: The rate of reaction of methyl radicals with ozone, Int. J. Chem. Kinet., 13, 667–675, doi:10.1002/kin.550130707, 1981.

Olzmann, M., Kraka, E., Cremer, D., Gutbrod, R., and Andersson, S.: Energetics, kinetics, and product distributions of the reactions of ozone with ethene and 2,3-dimethyl-2-butene, J. Phys. Chem. A, 101, 9421–9429, doi:10.1021/JP971663E, 1997.

Orlando, J. J. and Tyndall, G. S.: Rate coefficients for the thermal decomposition of $BrONO_2$ and the heat of formation of $BrONO_2$, J. Phys. Chem., 100, 19 398–19 405, doi:10.1021/JP9620274, 1996.

Orlando, J. J. and Tyndall, G. S.: The atmospheric chemistry of the HC(O)CO radical, Int. J. Chem. Kinet., 33, 149–156, doi:10.1002/1097-4601(200103)33:3⟨149::AID-KIN1008⟩3.0.CO;2-1, 2001.

Orlando, J. J. and Tyndall, G. S.: Laboratory studies of organic peroxy radical chemistry: an overview with emphasis on recent issues of atmospheric significance, Chem. Soc. Rev., 41, 6294–6317, doi:10.1039/C2CS35166H, 2012.

Orlando, J. J., Tyndall, G. S., Bilde, M., Ferronato, C., Wallington, T. J., Vereecken, L., and Peeters, J.: Laboratory and theoretical study of the oxy radicals in the OH- and Cl-initiated oxidation of ethene, J. Phys. Chem. A, 102, 8116–8123, doi:10.1021/JP981937D, 1998.

Orlando, J. J., Tyndall, G. S., Fracheboud, J. M., Estupinan, E. G., Haberkorn, S., and Zimmer, A.: The rate and mechanism of the gas-phase oxidation of hydroxyacetone, Atmos. Environ., 33, 1621–1629, doi:10.1016/S1352-2310(98)00386-0, 1999a.

Orlando, J. J., Tyndall, G. S., and Paulson, S. E.: Mechanism of the OH-initiated oxidation of methacrolein, Geophys. Res. Lett., 26, 2191–2194, doi:10.1029/1999GL900453, 1999b.

Orlando, J. J., Tyndall, G. S., Bertman, S. B., Chen, W., and Burkholder, J. B.: Rate coefficient for the reaction of OH with CH_2=C(CH_3)C(O)OONO_2 (MPAN), Atmos. Environ., 36, 1895–1900, doi:10.1016/S1352-2310(02)00090-0, 2002.

Ouyang, B., McLeod, M. W., Jones, R. L., and Bloss, W. J.: NO_3 radical production from the reaction between the Criegee intermediate CH_2OO and NO_2, Phys. Chem. Chem. Phys., 15, 17 070–17 075, doi:10.1039/c3cp53024h, 2013.

Pal, B. and Ariya, P. A.: Gas-phase HO-initiated reactions of elemental mercury: Kinetics, product studies, and atmospheric implications, Environ. Sci. Technol., 38, 5555–5566, doi:10.1021/ES0494353, 2004.

Paulot, F., Crounse, J. D., Kjaergaard, H. G., Kroll, J. H., Seinfeld, J. H., and Wennberg, P. O.: Isoprene photooxidation: new insights into the production of acids and organic nitrates, Atmos. Chem. Phys., 9, 1479–1501, doi:10.5194/ACP-9-1479-2009, 2009a.

Paulot, F., Crounse, J. D., Kjaergaard, H. G., Kürten, A., St. Clair, J. M., Seinfeld, J. H., and Wennberg, P. O.: Unexpected epoxide formation in the gas-phase photooxidation of isoprene, Science, 325, 730–733, doi:10.1126/science.1172910, 2009b.

Paulot, F., Wunch, D., Crounse, J. D., Toon, G. C., Millet, D. B., DeCarlo, P. F., Vigouroux, C., Deutscher, N. M., González Abad, G., Notholt, J., Warneke, T., Hannigan, J. W., Warneke, C., de Gouw, J. A., Dunlea, E. J., De Mazière, M., Griffith, D. W. T., Bernath, P., Jimenez, J. L., and Wennberg, P. O.: Importance of secondary sources in the atmospheric budgets of formic and acetic acids, Atmos. Chem. Phys., 11, 1989–2013, doi:10.5194/acp-11-1989-2011, 2011.

Peeters, J. and Nguyen, T. L.: Unusually fast 1,6-H shifts of enolic hydrogens in peroxy radicals: formation of the first-generation C_2 and C_3 carbonyls in the oxidation of isoprene, J. Phys. Chem. A, 116, 6134–6141, doi:10.1021/jp211447q, 2012.

Peeters, J., Müller, J.-F., Stavrakou, T., and Nguyen, V. S.: Hydroxyl radical recycling in isoprene oxidation driven by hydrogen bonding and hydrogen tunneling: the upgraded LIM1 mechanism, J. Phys. Chem. A, 118, 8625–8643, doi:10.1021/jp5033146, 2014.

Piesiak, A., Schuchmann, M. N., Zegota, H., and von Sonntag, C.: β-Hydroxyethylperoxyl radicals: a study of the γ-radiolysis and pulse radiolysis of ethylene in oxygenated aqueous solutions, Z. Naturforsch. B, 39, 1262–1267, doi:10.1515/znb-1984-0920, 1984.

Plane, J. M. C., Joseph, D. M., Allan, B. J., Ashworth, S. H., and Francisco, J. S.: An experimental and theoretical study of the reactions OIO + NO and OIO + OH, J. Phys. Chem. A, 110, 93–100, doi:10.1021/JP055364Y, 2006.

Platz, J., Nielsen, O. J., Wallington, T. J., Ball, J. C., Hurley, M. D., Straccia, A. M., Schneider, W. F., and Sehested, J.: Atmospheric chemistry of the phenoxy radical, $C_6H_5O(\cdot)$: UV spectrum and kinetics of its reaction with NO, NO_2, and O_2, J. Phys. Chem. A, 102, 7964–7974, doi:10.1021/jp982221l, 1998.

Pleijel, K. and Munthe, J.: Modelling the atmospheric mercury cycle – Chemistry in fog droplets, Atmos. Environ., 29, 1441–1457, doi:10.1016/1352-2310(94)00323-D, 1995.

Raofie, F. and Ariya, P. A.: Kinetics and products study of the reaction of BrO radicals with gaseous mercury, J. Phys. IV France, 107, 1119–1121, doi:10.1051/JP4:20030497, 2003.

Raofie, F. and Ariya, P. A.: Product study of the gas-phase BrO-initiated oxidation of Hg^0: Evidence for stable Hg^{1+} compounds, Environ. Sci. Technol., 38, 4319–4326, doi:10.1021/ES035339A, 2004.

Rickard, A. and Pascoe, S.: The Master Chemical Mechanism (MCM), `http://mcm.leeds.ac.uk`, 2009.

Rickard, A. R., Johnson, D., McGill, C. D., and Marston, G.: OH yields in the gas-phase reactions of ozone with alkenes, J. Phys. Chem. A, 103, 7656–7664, doi:10.1021/JP9916992, 1999.

Riffault, V., Bedjanian, Y., and Poulet, G.: Kinetic and mechanistic study of the reactions of OH with IBr and HOI, J. Photochem. Photobiol. A: Chem., 176, 155–161, doi:10.1016/j.jphotochem.2005.09.002, 2005.

Roble, R. G.: Energetics of the mesosphere and thermosphere, in: The upper Mesosphere and Lower Thermosphere: A Review of Experiment and Theory, Geophysical Monograph 87, edited by Johnson, R. M. and Killeen, T. L., pp. 1–23, American Geophysical Union, Washington, DC, USA, 1995.

Ross, A. B., Mallard, W. G., Helman, W. P., Bielski, B. H. J., Buxton, G. V., Cabelli, D. E., Greenstock, C. L., Huie, R. E., and Neta, P.: NDRL-NIST Solution Kinetics Database: - Ver. 1, National Institute of Standards and Technology, Gaithersburg, MD, 1992.

Roth, E., Chakir, A., and Ferhati, A.: Study of a benzoylperoxy radical in the gas phase: ultraviolet spectrum and $C_6H_5C(O)O_2$ + HO_2 reaction between 295 and 357 K, J. Phys. Chem. A, 114, 10 367–10 379, doi:10.1021/jp1021467, 2010.

Rousse, D. and George, C.: A novel long path photolysis cell-application to the reactivity of selected organic compounds toward the nitrate radical (NO_3), Phys. Chem. Chem. Phys., 6, 3408–3414, doi:10.1039/B400175C, 2004.

Rumble, J. R., ed.: CRC Handbook of Chemistry and Physics, 101st Edition, CRC Press, Boca Raton, FL, 2020.

Rush, J. D. and Bielski, B. H. J.: Pulse radiolytic studies of the reaction of HO_2/O_2^- with Fe(II)/Fe(III) ions. The reactivity of HO_2/O_2^- with ferric ions and its implication on the occurrence of the Haber-Weiss reaction, J. Phys. Chem., 89, 5062–5066, doi:10.1021/j100269a035, 1985.

Sander, R., Jöckel, P., Kirner, O., Kunert, A. T., Landgraf, J., and Pozzer, A.: The photolysis module JVAL-14, compatible with the MESSy standard, and the JVal PreProcessor (JVPP), Geosci. Model Dev., 7, 2653–2662, doi:10.5194/GMD-7-2653-2014, 2014.

Sander, R., Baumgaertner, A., Cabrera-Perez, D., Frank, F., Gromov, S., Grooß, J.-U., Harder, H., Huijnen, V., Jöckel, P., Karydis, V. A., Niemeyer, K. E., Pozzer, A., Riede, H., Schultz, M. G., Taraborrelli, D., and Tauer, S.: The community atmospheric chemistry box model CAABA/MECCA-4.0, Geosci. Model Dev., 12, 1365–1385, doi:10.5194/gmd-12-1365-2019, 2019.

Sander, S. P., Finlayson-Pitts, B. J., Friedl, R. R., Golden, D. M., Huie, R. E., Kolb, C. E., Kurylo, M. J., Molina, M. J., Moortgat, G. K., Orkin, V. L., and Ravishankara, A. R.: Chemical Kinetics and Photochemical Data for Use in Atmospheric Studies, Evaluation Number 14, JPL Publication 02-25, Jet Propulsion Laboratory, Pasadena, CA, 2003.

Schaefer, T., Schindelka, J., Hoffmann, D., and Herrmann, H.: Laboratory kinetic and mechanistic studies on the OH-initiated oxidation of acetone in aqueous solution, J. Phys. Chem. A, 116, 6317–6326, doi:10.1021/jp2120753, 2012.

Schaefer, T., van Pinxteren, D., and Herrmann, H.: Multiphase chemistry of glyoxal: revised kinetics of the alkyl radical reaction with molecular oxygen and the reaction of glyoxal with OH, NO_3, and SO_4^- in aqueous solution, Environ. Sci. Technol., 49, 343–350, doi:10.1021/es505860s, 2015.

Schöne, L. and Herrmann, H.: Kinetic measurements of the reactivity of hydrogen peroxide and ozone towards small atmospherically relevant aldehydes, ketones and organic acids in aqueous solutions, Atmos. Chem. Phys., 14, 4503–4514, doi:10.5194/acp-14-4503-2014, 2014.

Schöne, L., Schindelka, J., Szeremeta, E., Schaefer, T., Hoffmann, D., Rudzinski, K. J., Szmigielski, R., and Herrmann, H.: Atmospheric aqueous phase radical chemistry of the isoprene oxidation products methacrolein, methyl vinyl ketone, methacrylic acid and acrylic acid – kinetics and product studies, Phys. Chem. Chem. Phys., 16, 6257–6272, doi:10.1039/C3CP54859G, 2014.

Schuchmann, M. N. and von Sonntag, C.: The rapid hydration of the acetyl radical. A pulse radiolysis study of acetaldehyde in aqueous solution., J. Am. Chem. Soc., 110, 5698–5701, doi:10.1021/ja00225a019, 1988.

Schuchmann, M. N., Zegota, H., and von Sonntag, C.: Acetate peroxyl radicals, $\cdot O_2CH_2CO_2^-$: a study on the γ-radiolysis and pulse radiolysis of acetate in oxygenated aqueous solutions, Z. Naturforsch. B, 40, 215–221, doi:10.1515/znb-1985-0212, 1985.

Schwartz, S. E. and White, W. H.: Solubility equilibria of the nitrogen oxides and oxyacids in dilute aqueous solution, in: Advances in Environmental Science and Engineering, edited by Pfafflin, J. R. and Ziegler, E. N., vol. 4, pp. 1–45, Gordon and Breach Science Publishers, NY, 1981.

Schwarz, H. A. and Bielski, B. H. J.: Reactions of HO_2 and O_2^- with iodine and bromine and the I_2^- and I atom reduction potentials, J. Phys. Chem., 90, 1445–1448, doi:10.1021/J100398A045, 1986.

Scribano, Y., Goldman, N., Saykally, R. J., and Leforestier, C.: Water dimers in the atmosphere III: Equilibrium constant from a flexible potential, J. Phys. Chem. A, 110, 5411–5419, doi:10.1021/jp056759k, 2006.

Sehested, J., Christensen, L. K., Nielsen, O. J., Bilde, M., Wallington, T. J., Schneider, W. F., Orlando, J. J., and Tyndall, G. S.: Atmospheric chemistry of acetone: Kinetic study of the $CH_3C(O)CH_2O_2 + NO/NO_2$ reactions and decomposition of $CH_3C(O)CH_2O_2NO_2$, Int. J. Chem. Kinet., 30, 475–489, doi:10.1002/(SICI)1097-4601(1998)30:7⟨475::AID-KIN4⟩3.0.CO;2-P, 1998.

Sehested, K., Rasmussen, O. L., and Fricke, H.: Rate constants of OH with HO_2, O_2^-, and $H_2O_2^+$ from hydrogen peroxide formation in pulse-irradiated oxygenated water, J. Phys. Chem., 72, 626–631, doi:10.1021/J100848A040, 1968.

Sehested, K., Holcman, J., Bjergbakke, E., and Hart, E. J.: A pulse radiolytic study of the reaction OH + O_3 in aqueous medium, J. Phys. Chem., 88, 4144–4147, doi:10.1021/J150662A058, 1984.

Seinfeld, J. H. and Pandis, S. N.: Atmospheric Chemistry and Physics, John Wiley & Sons, Inc., 1998.

Shallcross, D. E., Leather, K. E., Bacak, A., Xiao, P., Lee, E. P. F., Ng, M., Mok, D. K. W., Dyke, J. M., Hossaini, R., Chipperfield, M. P., Khan, M. A. H., and Percival, C. J.: Reaction between CH_3O_2 and BrO radicals: a new source of upper troposphere lower stratosphere hydroxyl radicals, J. Phys. Chem. A, 119, 4618–4632, doi:10.1021/JP5108203, 2015.

Shoute, L. C. T., Alfassi, Z. B., Neta, P., and Huie, R. E.: Temperature dependence of the rate constants for reaction of dihalide and azide radicals with inorganic reductants, J. Phys. Chem., 95, 3238–3242, doi:10.1021/J100161A050, 1991.

Sivakumaran, V., Hölscher, D., Dillon, T. J., and Crowley, J. N.: Reaction between OH and HCHO: temperature dependent rate coefficients (202-399 K) and product pathways (298 K), Phys. Chem. Chem. Phys., 5, 4821–4827, doi:10.1039/B306859E, 2003.

So, S., Wille, U., and da Silva, G.: Atmospheric chemistry of enols: a theoretical study of the vinyl alcohol + OH + O_2 reaction mechanism, Environ. Sci. Technol., 48, 6694–6701, doi:10.1021/es500319q, 2014.

Sokolov, O., Hurley, M. D., Ball, J. C., Wallington, T. J., Nelsen, W., Barnes, I., and Becker, K. H.: Kinetics of the reactions of chlorine atoms with CH_3ONO and CH_3ONO_2, Int. J. Chem. Kinet., 31, 357–359, doi:10.1002/(SICI)1097-4601(1999)31:5⟨357::AID-KIN5⟩3.0.CO;2-6, 1999.

Solberg, S., Stordal, F., and Hov, Ø.: Tropospheric ozone at high latitudes in clean and polluted air masses, a climatological study, J. Atmos. Chem., 28, 111–123, doi:10.1023/A:1005766612853, 1997.

Staehelin, J., Buehler, R. E., and Hoigné, J.: Ozone decomposition in water studied by pulse radiolysis. 2. Hydroxyl and hydrogen tetroxide (HO_4) as chain intermediates, J. Phys. Chem., 88, 5999–6004, doi:10.1021/j150668a051, 1984.

Stone, D., Blitz, M., Daubney, L., Howes, N. U. M., and Seakins, P.: Kinetics of CH_2OO reactions with SO_2, NO_2, NO, H_2O and CH_3CHO as a function of pressure, Phys. Chem. Chem. Phys., 16, 1139–1149, doi:10.1039/c3cp54391a, 2014.

Strekowski, R. S., Nicovich, J. M., and Wine, P. H.: Kinetic and mechanistic study of the Reactions of $O(^1D_2)$ with HCN and CH_3CN, Chem. Phys. Chem., 11, 3942–3955, doi:10.1002/cphc.201000550, 2010.

Sutton, H. C. and Downes, M. T.: Reactions of the HO_2 radical in aqueous solution with bromine and related compounds, J. Chem. Soc. Faraday Trans. 1, 68, 1498–1507, doi:10.1039/F19726801498, 1972.

Swaminathan, P. K., Strobel, D. F., Kupperman, D. G., Acton, L., DeMajistre, R., Yee, J.-H., Paxton, L., Anderson, D. E., Strickland, D. J., and Duff, J. W.: Nitric oxide abundance in the mesosphere/lower thermosphere region: Roles of solar soft X rays, suprathermal $N(^4S)$ atoms, and vertical transport, J. Geophys. Res., 103A, 11 579–11 594, doi:10.1029/97JA03249, 1998.

Tao, Z. and Li, Z.: A kinetics study on reactions of C_6H_5O with C_6H_5O and O_3 at 298 K, Int. J. Chem. Kinet., 31, 65–72, doi:10.1002/(SICI)1097-4601(1999)31:1⟨65::AID-KIN8⟩3.0.CO;2-J, 1999.

Taraborrelli, D.: Isoprene oxidation and its impacts on the atmospheric composition, Ph.D. thesis, Johannes Gutenberg-Universität, Mainz, Germany, `http://d-nb.info/1003538770/34`, 2010.

Taraborrelli, D., Lawrence, M. G., Butler, T. M., Sander, R., and Lelieveld, J.: Mainz Isoprene Mechanism 2 (MIM2): an isoprene oxidation mechanism for regional and global atmospheric modelling, Atmos. Chem. Phys., 9, 2751–2777, doi:10.5194/ACP-9-2751-2009, 2009.

Thornton, A. T. and Laurence, G. S.: Kinetics of oxidation of transition-metal ions by halogen radical anions. Part I. The oxidation of iron(II) by dibromide and dichloride ions generated by flash photolysis, J. Chem. Soc. Dalton Trans., pp. 804–813, doi:10.1039/DT9730000804, 1973.

Tokos, J. J. S., Hall, B., Calhoun, J. A., and Prestbo, E. M.: Homogeneous gas-phase reaction of Hg^0 with H_2O_2, O_3, CH_3I, and $(CH_3)_2S$: Implications for atmospheric Hg cycling, Atmos. Environ., 32, 823–827, doi:10.1016/S1352-2310(97)00171-4, 1998.

Troy, R. C. and Margerum, D. W.: Non-metal redox kinetics: Hypobromite and hypobromous acid reactions with iodide and with sulfite and the hydrolysis of bromosulfate, Inorg. Chem., 30, 3538–3543, doi:10.1021/IC00018A028, 1991.

Troy, R. C., Kelley, M. D., Nagy, J. C., and Margerum, D. W.: Non-metal redox kinetics: Iodine monobromide reaction with iodide ion and the hydrolysis of IBr, Inorg. Chem., 30, 4838–4845, doi:10.1021/IC00025A030, 1991.

Tur'yan, Y. I.: Studying kinetics of the dehydration reaction of acetaldehyde in aqueous solutions using polarographic kinetic currents, Croatica Chem. Acta, 73, 657–666, `https://hrcak.srce.hr/132008`, 2000.

Tyndall, G. S., Staffelbach, T. A., Orlando, J. J., and Calvert, J. G.: Rate coefficients for the re-

actions of OH radicals with methylglyoxal and acetaldehyde, Int. J. Chem. Kinet., 27, 1009–1020, doi:10.1002/KIN.550271006, 1995.

Tyndall, G. S., Orlando, J. J., Wallington, T. J., Sehested, J., and Nielsen, O. J.: Kinetics of the reactions of acetonitrile with chlorine and fluorine atoms, J. Phys. Chem., 100, 660–668, doi:10.1021/jp9521417, 1996.

Tyndall, G. S., Cox, R. A., Granier, C., Lesclaux, R., Moortgat, G. K., Pilling, M. J., Ravishankara, A. R., and Wallington, T. J.: The atmospheric chemistry of small organic peroxy radicals, J. Geophys. Res., 106D, 12 157–12 182, doi:10.1029/2000JD900746, 2001a.

Tyndall, G. S., Orlando, J. J., Wallington, T. J., and Hurley, M. D.: Products of the chlorine-atom- and hydroxyl-radical-initiated oxidation of CH_3CN, J. Phys. Chem. A, 105, 5380–5384, doi:10.1021/jp004318p, 2001b.

van den Bergh, H. and Troe, J.: Kinetic and thermodynamic properties of INO and INO_2 intermediate complexes in iodine recombination, J. Chem. Phys., 64, 736–742, doi:10.1063/1.432220, 1976.

van Loon, L., Mader, E., and Scott, S. L.: Reduction of the aqueous mercuric ion by sulfite: UV spectrum of $HgSO_3$ and its intramolecular redox reaction, J. Phys. Chem. A, 104, 1621–1626, doi:10.1021/JP994268S, 2000.

van Loon, L. L., Mader, E. A., and Scott, S. L.: Sulfite stabilization and reduction of the aqueous mercuric ion: Kinetic determination of sequential formation constants, J. Phys. Chem. A, 105, 3190–3195, doi:10.1021/JP003803H, 2001.

Vereecken, L. and Francisco, J. S.: Theoretical studies of atmospheric reaction mechanisms in the troposphere, Chem. Soc. Rev., 41, 6259–6293, doi:10.1039/c2cs35070j, 2012.

Vereecken, L. and Peeters, J.: A theoretical study of the OH-initiated gas-phase oxidation mechanism of β-pinene ($C_{10}H_{16}$): first generation products, Phys. Chem. Chem. Phys., 14, 3802–3815, doi:10.1039/c2cp23711c, 2012.

Vereecken, L., Müller, J.-F., and Peeters, J.: Low-volatility poly-oxygenates in the OH-initiated atmospheric oxidation of α-pinene: impact of non-traditional peroxyl radical chemistry, Phys. Chem. Chem. Phys., 9, 5241–5248, doi:10.1039/b708023a, 2007.

Vereecken, L., Harder, H., and Novelli, A.: The reaction of Criegee intermediates with NO, RO_2, and SO_2, and their fate in the atmosphere, Phys. Chem. Chem. Phys., 14, 14 682–14 695, doi:10.1039/c2cp42300f, 2012.

Vereecken, L., Harder, H., and Novelli, A.: The reactions of Criegee intermediates with alkenes, ozone, and carbonyl oxides, Phys. Chem. Chem. Phys., 16, 4039–4049, doi:10.1039/c3cp54514h, 2014.

Villalta, P. W., Lovejoy, E. R., and Hanson, D. R.: Reaction probability of peroxyacetyl radical on aqueous surfaces, Geophys. Res. Lett., 23, 1765–1768, doi:10.1029/96GL01286, 1996.

von Glasow, R., Sander, R., Bott, A., and Crutzen, P. J.: Modeling halogen chemistry in the marine boundary layer, 1. Cloud-free MBL, J. Geophys. Res., 107D, 4341, doi:10.1029/2001JD000942, 2002.

von Kuhlmann, R.: Tropospheric photochemistry of ozone, its precursors and the hydroxyl radical: A 3D-modeling study considering non-methane hydrocarbons, Ph.D. thesis, Johannes Gutenberg-Universität, Mainz, Germany, 2001.

von Kuhlmann, R., Lawrence, M. G., Crutzen, P. J., and Rasch, P. J.: A model for studies of tropospheric ozone and nonmethane hydrocarbons: Model description and ozone results, J. Geophys. Res., 108D, 4294, doi:10.1029/2002JD002893, 2003.

von Sonntag, C.: The chemical basis of radiation biology, Taylor & Francis London, 1987.

Wagman, D. D., Evans, W. H., Parker, V. B., Schumm, R. H., Halow, I., Bailey, S. M., Churney, K. L., and Nuttall, R. L.: The NBS tables of chemical thermodynamic properties; Selected values for inorganic and C_1 and C_2 organic substances in SI units, J. Phys. Chem. Ref. Data, 11, suppl. 2, 1982.

Wagner, I. and Strehlow, H.: On the flash photolysis of bromide ions in aqueous solution, Ber. Bunsenges. Phys. Chem., 91, 1317–1321, doi:10.1002/BBPC.19870911203, 1987.

Wallington, T. J., Ammann, M., Cox, R. A., Crowley, J. N., Herrmann, H., Jenkin, M. E., McNeill, V., Mellouki, A., Rossi, M. J., and Troe, J.: IUPAC Task group on atmospheric chemical kinetic data evaluation: Evaluated kinetic data, `http://iupac.pole-ether.fr`, 2018.

Wang, T. X. and Margerum, D. W.: Kinetics of reversible chlorine hydrolysis: Temperature dependence and general-acid/base-assisted mechanisms, Inorg. Chem., 33, 1050–1055, doi:10.1021/IC00084A014, 1994.

Wang, T. X., Kelley, M. D., Cooper, J. N., Beckwith, R. C., and Margerum, D. W.: Equilibrium, kinetic, and UV-spectral characteristics of aqueous bromine chloride, bromine, and chlorine species, Inorg. Chem., 33, 5872–5878, doi:10.1021/IC00103A040, 1994.

Wang, Y. L., Nagy, J. C., and Margerum, D. W.: Kinetics of hydrolysis of iodine monochloride measured by the pulsed-accelerated-flow method, J. Am. Chem. Soc., 111, 7838–7844, doi:10.1021/JA00202A026, 1989.

Wang, Z. and Pehkonen, S. O.: Oxidation of elemental mercury by aqueous bromine: atmospheric implications, Atmos. Environ., 38, 3675–3688, doi:10.1016/J.ATMOSENV.2004.02.059, 2004.

Warneck, P.: Chemical reactions in clouds, Fresenius J. Anal. Chem., 340, 585–590, doi:10.1007/BF00322434, 1991.

Warneck, P.: The relative importance of various pathways for the oxidation of sulfur dioxide and nitrogen dioxide in sunlit continental fair weather clouds, Phys. Chem. Chem. Phys., 1, 5471–5483, doi:10.1039/A906558J, 1999.

Warneck, P.: The oxidation of sulfur(IV) by reaction with iron(III): a critical review and data analysis, Phys. Chem. Chem. Phys., 20, 4020–4037, doi:10.1039/c7cp07584g, 2018.

Wayne, R. P., Barnes, I., Biggs, P., Burrows, J. P., Canosa-Mas, C. E., Hjorth, J., Le Bras, G., Moortgat, G. K., Perner, D., Poulet, G., Restelli, G., and Sidebottom, H.: The nitrate radical: Physics, chemistry, and the atmosphere, Atmos. Environ., 25A, 1–203, doi:10.1016/0960-1686(91)90192-A, 1991.

Weast, R. C., ed.: CRC Handbook of Chemistry and Physics, 61st Edition, CRC Press, Inc., Boca Raton, FL, 1980.

Weinstein-Lloyd, J. and Schwartz, S. E.: Low-intensity radiolysis study of free-radical reactions in cloudwater: H_2O_2 production and destruction, Environ. Sci. Technol., 25, 791–800, doi:10.1021/ES00016A027, 1991.

Welz, O., Savee, J. D., Osborn, D. L., Vasu, S. S., Percival, C. J., Shallcross, D. E., and Taatjes, C. A.: Direct kinetic measurements of Criegee intermediate (CH_2OO) formed by reaction of CH_2I with O_2, Science, 335, 204–207, doi:10.1126/science.1213229, 2012.

Welz, O., Eskola, A. J., Sheps, L., Rotavera, B., Savee, J. D., Scheer, A. M., Osborn, D. L., Lowe, D., Booth, A. M., Xiao, P., Khan, M. A. H., Percival, C. J., Shallcross, D. E., and Taatjes, C. A.: Rate coefficients of C1 and C2 Criegee intermediate reactions with formic and acetic acid near the collision limit: Direct kinetics measurements and atmospheric implications, Angew. Chem., 126, 4635–4638, doi:10.1002/ange.201400964, 2014.

Wine, P. H., Tang, Y., Thorn, R. P., Wells, J. R., and Davis, D. D.: Kinetics of aqueous phase reactions of the SO_4^- radical with potential importance in cloud chemistry, J. Geophys. Res., 94D, 1085–1094, doi:10.1029/JD094ID01P01085, 1989.

Wingenter, O. W., Sive, B. C., Blake, N. J., and Rowland, F. S.: Atomic chlorine concentrations determined from ethane and hydroxyl measurements made over the Central Pacific Ocean, Eos, Trans. AGU (Abstract Supplement), 80, F149–F150, 1999.

Winkelman, J. G. M., Ottens, M., and Beenackers, A. A. C. M.: The kinetics of the dehydration of methylene glycol, Chem. Eng. Sci., 55, 2065–2071, doi:10.1016/S0009-2509(99)00498-4, 2000.

Winkelman, J. G. M., Voorwinde, O. K., Ottens, M., Beenackers, A. A. C. M., and Janssen, L. P. B. M.: Kinetics and chemical equilibrium of the hydration of formaldehyde, Chem. Eng. Sci., 57, 4067–4076, doi:10.1016/S0009-2509(02)00358-5, 2002.

Wu, D., Wong, D., and Di Bartolo, B.: Evolution of Cl_2^- in aqueous NaCl solutions, J. Photochem., 14, 303–310, doi:10.1016/0047-2670(80)85102-1, 1980.

Yamamoto, S. and Back, R. A.: The gas-phase photochemistry of oxalic acid, J. Phys. Chem., 89, 622–625, doi:10.1021/j100250a014, 1985.

Yiin, B. S. and Margerum, D. W.: Nonmetal redox kinetics: reactions of iodine and triiodide with sulfite and hydrogen sulfite and the hydrolysis of iodosulfate, Inorg. Chem., 29, 1559–1564, doi:10.1021/IC00333A023, 1990.

Yin, F., Grosjean, D., and Seinfeld, J. H.: Photooxidation of dimethyl sulfide and dimethyl disulfide. I: Mechanism development, J. Atmos. Chem., 11, 309–364, doi:10.1007/BF00053780, 1990.

Yoon, M.-C., Choi, Y. S., and Kim, S. K.: The OH production from the $\pi - \pi^*$ transition of acetylacetone, Chem. Phys. Lett., 300, 207–212, doi:10.1016/S0009-2614(98)01373-6, 1999.

Yu, X.-Y.: Critical evaluation of rate constants and equilibrium constants of hydrogen peroxide photolysis in acidic aqueous solutions containing chloride ions, J. Phys. Chem. Ref. Data, 33, 747–763, doi:10.1063/1.1695414, 2004.

Zegota, H., Schuchmann, M. N., Schulz, D., and von Sonntag, C.: Acetonylperoxyl radicals, $CH_3COCH_2O_2$: a study on the γ-radiolysis and pulse radiolysis of acetone in oxygenated aqueous solutions, Z. Naturforsch. B, 41, 1015–1022, doi: 10.1515/znb-1986-0815, 1986.

Zehavi, D. and Rabani, J.: The oxidation of aqueous bromide by hydroxyl radicals. A pulse radiolytic investigation, J. Phys. Chem., 76, 312–319, doi: 10.1021/J100647A006, 1972.

Zellner, R., Hartmann, D., Karthäuser, J., Rhäsa, D., and Weibring, G.: A laser photolysis/LIF study of the reactions of $O(^3P)$ atoms with CH_3 and CH_3O_2 radicals, J. Chem. Soc. Faraday Trans. 2, 84, 549–568, doi:10.1039/f29888400549, 1988.

Zellner, R., Exner, M., and Herrmann, H.: Absolute OH quantum yield in the laser photolysis of nitrate, nitrite and dissolved H_2O_2 at 308 and 351 nm in the temperature range 278-353 K, J. Atmos. Chem., 10, 411–425, doi:10.1007/BF00115783, 1990.

Zellner, R., Herrmann, H., Exner, M., Jacobi, H.-W., Raabe, G., and Reese, A.: Formation and reactions of oxidants in the aqueous phase, in: Heterogeneous and Liquid-Phase Processes, edited by Warneck, P., pp. 146–152, Springer Verlag, Berlin, 1996.

Ziajka, J., Beer, F., and Warneck, P.: Iron-catalysed oxidation of bisulphit aqueous solution: evidence for free radical chain mechanism, Atmos. Environ., 28, 2549–2552, doi:10.1016/1352-2310(94)90405-7, 1994.

CHEMPROP

A list of chemical properties for MECCA and other chemistry submodels of MESSy

created from `chemprop.tbl`

Rolf Sander et al.

2020-09-24

Table 7: Henry's law constants

KPP name	$H^{\ominus}$ [M/atm]	Reference	$\frac{\mathrm{d}\ln H^{\ominus}}{\mathrm{d}(1/T)}$ [K]	Reference
O2	1.3E-3	Wilhelm et al. (1977)	1500.	
O3	1.03E-2	Burkholder et al. (2015)	2830.	
OH	3.0E1	Hanson et al. (1992)	4300.	
HO2	3.9E3	Hanson et al. (1992)	5900.	
H2O	BIG_DP	see notes	0.	
H2O2	1.E5	Lind and Kok (1994)	6338.	
NH3	60.2	Burkholder et al. (2015)	4160.	
NO	1.9E-3	Schwartz and White (1981)	1480.	
NO2	1.2E-2	Burkholder et al. (2015)	2360.	
NO3	3.8E-2	Burkholder et al. (2015)	2000.	Berdnikov and Bazhin (1970)
N2O5	0.088	Fried et al. (1994)	3600.	
HONO	4.9E1	Schwartz and White (1981)	4780.	
HNO3	2.45E6/1.5E1	Brimblecombe and Clegg (1989)	8694.	
HNO4	1.26E4	Régimbal and Mozurkewich (1997)	6900.	
CH3O2	6.	Jacob (1986)	5600.	
CH3OH	2.20E2	Snider and Dawson (1985)	5200.	
CH3OOH	3.0E2	Lind and Kok (1994)	5322.	
CO	9.8E-4	Sander (2015)	1300.	
CO2	3.4E-2	Sander et al. (2011)	2400.	
HCHO	2.53E0	Rosanka et al. (2021)	7100.	
HCOOH	8.9E3	Burkholder et al. (2015)	6100.	
HOCH2O2	8.0E4	Leriche et al. (2000)	8200.	
HOCH2OH	1.015E4	US EPA (2012)	9870.	
HOCH2OOH	1.7E6	Sander (2015)	9870.	
CH3NO3	2.0E0	Sander (2015)	4740.	
C2H5O2	6.0E0	see notes	5600.	
C2H5OH	2.0E2	Snider and Dawson (1985)	6630.	
C2H5OOH	3.34E2	O'Sullivan et al. (1996)	6000.	
CH2CO	1.0E6	Taraborrelli (2020)		
CH3CHO	5.91E0	Rosanka et al. (2021)	5890.	
CH3CHOHOH	7633.59	US EPA (2012)		
CH3CHOHOOH	1.0E6	Taraborrelli (2020)		
CH3CO2H	4.1E3	Burkholder et al. (2015)	6200.	
CH3CO3	1.0E-1	Sander (2015)		
CH3CO3H	8.4E2	O'Sullivan et al. (1996)	5300.	
CHOCHOHOH	2583.98	US EPA (2012)		
CHOHOHCHOHOH	5.71428E6	US EPA (2012)		
CHOHOHCOOH	320513.0	US EPA (2012)		
ETHGLY	4.0E6	Bone et al. (1983)		
GLYOX	1.19E3	Rosanka et al. (2021)	7480.	
HCOCO2H	9.9	Rosanka et al. (2021)		
HCOCO3H	2.7E6	Taraborrelli (2020)		
HOCH2CHO	2.4E3	Rosanka et al. (2021)	3850.	
HOCH2CHOHOH	209205.0	US EPA (2012)		
HOCH2CO2H	2.4E4	Burkholder et al. (2015)	4030.	
HOCH2CO3H	4.8E4	see notes	6014.	
HOOCCOOH	5.0E8	Saxena and Hildemann (1996)		
HOOCH2CHO	1.0E6	Taraborrelli (2020)		
HOOCH2CHOHOH	209205.0	US EPA (2012)		
HOOCH2CO2H	1.5E6	see notes	6014.	
HOOCH2CO3H	1.0E6	Taraborrelli (2020)		

Table 7: Henry's law constants (continued...)

KPP name	$H^{\ominus}$ [M/atm]	Reference	$\frac{\mathrm{d}\ln H^{\ominus}}{\mathrm{d}(1/T)}$ [K]	Reference
HYETHO2H	4.0E6	Taraborrelli (2020)		
C2H5NO3	1.6	Sander (2015)	5400.	
CH3CN	5.27E1	Sander (2015)	4000.	
ETHOHNO3	3.9E4	Taraborrelli (2020)		
PAN	2.8	Burkholder et al. (2015)	5730.	
PHAN	4.E4	Taraborrelli (2020)		
ACETOL	4.7e2	Taraborrelli (2020)		
ALCOCH2OOH	1.0E6	Taraborrelli (2020)		
C33CO	9.0e3	Taraborrelli (2020)		
CH3CHCO	1.0E6	Taraborrelli (2020)		
CH3COCH3	27.8	Burkholder et al. (2015)	5530.	
CH3COCHOHOH	3533.57	US EPA (2012)		
CH3COCO2H	3.14E5	Burkholder et al. (2015)	5090.	
CH3COCO3H	9.0e3	Taraborrelli (2020)		
HCOCH2CHO	1.0E6	Taraborrelli (2020)		
HCOCH2CO2H	6.6E7	Taraborrelli (2020)		
HCOCH2CO3H	1.0E6	Taraborrelli (2020)		
HCOCOCH2OOH	1.0E6	Taraborrelli (2020)		
HOC2H4CO2H	4.2E7	Taraborrelli (2020)		
HOC2H4CO3H	1.0E6	Taraborrelli (2020)		
HOCH2COCH2OOH	1.0E6	Taraborrelli (2020)		
HOCH2COCHO	4.1E5	Taraborrelli (2020)		
HYPERACET	4.7E3	Taraborrelli (2020)		
HYPROPO2H	9.2E5	Taraborrelli (2020)		
IC3H7OOH	1.3E2	Taraborrelli (2020)		
IPROPOL	1.3E2	Sander (2015)	7470.	
MGLYOX	1.75	Rosanka et al. (2021)	7500.	
PROPACID	5.7E3	Khan et al. (1995)	6800.	Abraham (1984)
C32OH13CO	9.0e3	Taraborrelli (2020)		
C3DIALOOH	9.0e3	Taraborrelli (2020)		
HCOCOHCO3H	2.0e6	Taraborrelli (2020)		
METACETHO	3.7e3	Taraborrelli (2020)	7500.	
C3PAN1	1.0E6	Taraborrelli (2020)		
C3PAN2	1.0E6	Taraborrelli (2020)		
CH3COCH2O2NO2	1.0E3	Taraborrelli (2020)		
NOA	1.0E3	Taraborrelli (2020)		
PR2O2HNO3	1.1E4	Taraborrelli (2020)		
PROPOLNO3	4.5E3	Taraborrelli (2020)		
HCOCOHPAN	3.9e4	Taraborrelli (2020)	8600.	
BIACETO2	1.0E6	Taraborrelli (2020)		
BIACETOH	1.3E3	Taraborrelli (2020)		
BIACETOOH	1.0E6	Taraborrelli (2020)		
BUT2OLO	1.0E3	Taraborrelli (2020)		
BUT2OLOOH	1.0E6	Taraborrelli (2020)		
C312COCO3H	1.0E6	Taraborrelli (2020)		
C413COOOH	1.0E6	Taraborrelli (2020)		
C44OOH	1.0E6	Taraborrelli (2020)		
C4CODIAL	1.0E6	Taraborrelli (2020)		
CH3COCHCO	1.0E6	Taraborrelli (2020)		
CH3COCOCO2H	4.3E8	Taraborrelli (2020)		
CH3COOHCHCHO	1.0E6	Taraborrelli (2020)		

Table 7: Henry's law constants (continued...)

KPP name	$H^{\ominus}$ [M/atm]	Reference	$\frac{\mathrm{d}\ln H^{\ominus}}{\mathrm{d}(1/T)}$ [K]	Reference
CHOC3COO2	1.0E6	Taraborrelli (2020)		
CO23C3CHO	3.6e5	Taraborrelli (2020)		
CO2C3CHO	1.7E3	Taraborrelli (2020)		
CO2H3CHO	4.1E5	Taraborrelli (2020)		
CO2H3CO2H	1.0E6	Taraborrelli (2020)		
CO2H3CO3H	1.E6	Taraborrelli (2020)		
HCOCCH3CHOOH	1.0E6	Taraborrelli (2020)		
HCOCCH3CO	1.0E6	Taraborrelli (2020)		
HMAC	1.7E3	Taraborrelli (2020)		
HO12CO3C4	5.E7	Taraborrelli (2020)		
HVMK	1.7E3	Taraborrelli (2020)		
IBUTALOH	1.0E6	Taraborrelli (2020)		
IBUTDIAL	1.7E3	Taraborrelli (2020)		
IBUTOLBOOH	1.0E6	Taraborrelli (2020)		
IPRHOCO2H	4.2E7	Taraborrelli (2020)		
IPRHOCO3H	1.0E6	Taraborrelli (2020)		
MACO2H	2.58E3	Khan et al. (1992)	0.	
MACO3H	3.4E3	Taraborrelli (2020)		
MACR	4.9E0	Ji and Evans (2007)	4300.	
MACROH	5.E7	Taraborrelli (2020)		
MACROOH	5.E7	Taraborrelli (2020)		
MVK	2.6E1	Ji and Evans (2007)	4800.	
BZFUCO	9.0e3	Taraborrelli (2020)		
BZFUOOH	2.0e6	Taraborrelli (2020)		
CO14O3CHO	3.6e5	Taraborrelli (2020)		
CO14O3CO2H	9.0e3	Taraborrelli (2020)		
CO2C4DIAL	2.0e6	Taraborrelli (2020)		
EPXC4DIAL	3.6e5	Taraborrelli (2020)		
EPXDLCO2H	9.0e3	Taraborrelli (2020)		
EPXDLCO3H	9.0e3	Taraborrelli (2020)		
HOCOC4DIAL	3.1e5	Taraborrelli (2020)	5100.	
MALANHYOOH	2.0e6	Taraborrelli (2020)		
MALDALCO2H	9.0e3	Taraborrelli (2020)		
MALDALCO3H	9.0e3	Taraborrelli (2020)		
MALDIAL	3.6e5	Taraborrelli (2020)		
MALDIALOOH	2.0e6	Taraborrelli (2020)		
MALNHYOHCO	2.0e6	Taraborrelli (2020)		
MECOACEOOH	3.1e5	Taraborrelli (2020)	5100.	
C312COPAN	1.0E6	Taraborrelli (2020)		
C4PAN5	1.0E6	Taraborrelli (2020)		
MVKNO3	1.0E6	Taraborrelli (2020)		
NBZFUOOH	2.4e4	Taraborrelli (2020)		
NC4DCO2H	3.9e4	Taraborrelli (2020)	8600.	
LBUT1ENOOH	1.0E6	Taraborrelli (2020)		
LHMVKABOOH	5.E6	Taraborrelli (2020)		
LMEKOOH	1.E3	Taraborrelli (2020)		
C1ODC2O2C4OOH	1.0E6	Taraborrelli (2020)		
C1ODC2OOHC4OD	1.0E6	Taraborrelli (2020)		
C1ODC3O2C4OOH	1.0E6	Taraborrelli (2020)		
C1OOHC2OOHC4OD	1.0E6	Taraborrelli (2020)		
C4MDIAL	1.0E6	Taraborrelli (2020)		

Table 7: Henry's law constants (continued...)

KPP name	$H^{\ominus}$ [M/atm]	Reference	$\frac{\mathrm{d}\ln H^{\ominus}}{\mathrm{d}(1/T)}$ [K]	Reference
C511OOH	1.0E6	Taraborrelli (2020)		
C512OOH	1.0E6	Taraborrelli (2020)		
C513CO	1.0E6	Taraborrelli (2020)		
C513OOH	1.0E6	Taraborrelli (2020)		
C514OOH	1.0E6	Taraborrelli (2020)		
C59OOH	3.E11	Taraborrelli (2020)		
CHOC3COOOH	1.0E6	Taraborrelli (2020)		
CO13C4CHO	1.0E6	Taraborrelli (2020)		
CO23C4CHO	1.0E6	Taraborrelli (2020)		
CO23C4CO3H	1.0E6	Taraborrelli (2020)		
DB1OOH	1.0E6	Taraborrelli (2020)		
DB2OOH	1.0E6	Taraborrelli (2020)		
ISOPAOH	4.E6	Taraborrelli (2020)		
ISOPBOH	3.E6	Taraborrelli (2020)		
ISOPBOOH	3.E6	Taraborrelli (2020)		
ISOPDOH	3.E6	Taraborrelli (2020)		
ISOPDOOH	3.E6	Taraborrelli (2020)		
MBO	1.0E6	Taraborrelli (2020)		
MBOACO	1.0E6	Taraborrelli (2020)		
MBOCOCO	1.0E6	Taraborrelli (2020)		
ME3FURAN	1.0E6	Taraborrelli (2020)		
ACCOMECHO	3.7e3	Taraborrelli (2020)	7500.	
ACCOMECO3H	3.1e5	Taraborrelli (2020)	5100.	
C24O3CCO2H	3.1e5	Taraborrelli (2020)	5100.	
C4CO2DBCO3	9.0e3	Taraborrelli (2020)		
C4CO2DCO3H	2.0e6	Taraborrelli (2020)		
C5134CO2OH	3.1e5	Taraborrelli (2020)	5100.	
C54CO	3.6e5	Taraborrelli (2020)		
C5CO14OH	2.2e3	Taraborrelli (2020)	6583.	
C5CO14OOH	3.1e5	Taraborrelli (2020)	5100.	
C5DIALCO	9.0e3	Taraborrelli (2020)		
C5DIALOOH	3.6e5	Taraborrelli (2020)		
C5DICARB	3.7e3	Taraborrelli (2020)	7500.	
C5DICAROOH	2.0e6	Taraborrelli (2020)		
MC3ODBCO2H	2.2e3	Taraborrelli (2020)	6583.	
MMALNHYOOH	2.0e6	Taraborrelli (2020)		
TLFUOOH	2.0e6	Taraborrelli (2020)		
C4MCONO3OH	1.0E6	Taraborrelli (2020)		
C514NO3	1.0E6	Taraborrelli (2020)		
C5PAN9	1.0E6	Taraborrelli (2020)		
CHOC3COPAN	1.0E6	Taraborrelli (2020)		
DB1NO3	1.0E4	Taraborrelli (2020)		
ISOPBNO3	8.9E3	Taraborrelli (2020)		
ISOPDNO3	8.9E3	Taraborrelli (2020)		
NC4OHCO3H	1.0E6	Taraborrelli (2020)		
NC4OHCPAN	1.0E6	Taraborrelli (2020)		
NISOPOOH	2.E4	Taraborrelli (2020)		
NMBOBCO	1.0E6	Taraborrelli (2020)		
C4CO2DBPAN	3.9e4	Taraborrelli (2020)	8600.	
NC4MDCO2H	9.0e3	Taraborrelli (2020)		
NTLFUOOH	9.0e3	Taraborrelli (2020)		

Table 7: Henry's law constants (continued...)

KPP name	$H^{\ominus}$ [M/atm]	Reference	$\frac{\mathrm{d}\ln H^{\ominus}}{\mathrm{d}(1/T)}$ [K]	Reference
LC578OOH	3.E11	Taraborrelli (2020)		
LHC4ACCHO	4.E5	Taraborrelli (2020)		
LHC4ACCO2H	6.6E7	Taraborrelli (2020)		
LHC4ACCO3H	2.2E5	Taraborrelli (2020)		
LIEPOX	1.0E6	Taraborrelli (2020)		
LISOPACOOH	4.E6	Taraborrelli (2020)		
LMBOABOOH	1.0E6	Taraborrelli (2020)		
LZCO3HC23DBCOD	1.0E6	Taraborrelli (2020)		
LC5PAN1719	6.E4	Taraborrelli (2020)		
LISOPACNO3	2.E4	Taraborrelli (2020)		
LMBOABNO3	1.0E6	Taraborrelli (2020)		
LNMBOABOOH	1.0E6	Taraborrelli (2020)		
C614CO	1.0E6	Taraborrelli (2020)		
C614OOH	1.0E6	Taraborrelli (2020)		
CO235C5CHO	1.0E6	Taraborrelli (2020)		
CO235C6OOH	1.0E6	Taraborrelli (2020)		
BZBIPEROOH	2.0e6	Taraborrelli (2020)		
BZEMUCCO	9.0e3	Taraborrelli (2020)		
BZEMUCCO2H	9.0e3	Taraborrelli (2020)		
BZEMUCCO3H	9.0e3	Taraborrelli (2020)		
BZEMUCOOH	2.0e6	Taraborrelli (2020)		
BZEPOXMUC	3.6e5	Taraborrelli (2020)		
BZOBIPEROH	9.0e3	Taraborrelli (2020)		
C5CO2DCO3H	2.0e6	Taraborrelli (2020)		
C5COOHCO3H	2.0e6	Taraborrelli (2020)		
C6125CO	3.7e3	Taraborrelli (2020)	7500.	
C615CO2OOH	3.1e5	Taraborrelli (2020)	5100.	
C6CO4DB	2.0e6	Taraborrelli (2020)		
C6H5O	2.9e3	Taraborrelli (2020)	6800.	
C6H5OOH	2.9e3	Taraborrelli (2020)	6800.	
CATEC1O	4.6e3	Taraborrelli (2020)		
CATEC1OOH	4.6e3	Taraborrelli (2020)		
CATECHOL	4.6e3	Taraborrelli (2020)		
PBZQCO	4.6e3	Taraborrelli (2020)		
PBZQOOH	2.0e6	Taraborrelli (2020)		
PHENOL	2.9e3	Taraborrelli (2020)	6800.	
PHENOOH	2.0e6	Taraborrelli (2020)		
C614NO3	1.0E6	Taraborrelli (2020)		
BZBIPERNO3	2.9e3	Taraborrelli (2020)	6800.	
BZEMUCNO3	3.9e4	Taraborrelli (2020)	8600.	
C5CO2DBPAN	3.7e3	Taraborrelli (2020)	7500.	
C5CO2OHPAN	3.9e4	Taraborrelli (2020)	8600.	
DNPHEN	2.3e3	Taraborrelli (2020)		
DNPHENOOH	2.3e3	Taraborrelli (2020)		
NBZQOOH	2.4e4	Taraborrelli (2020)		
NCATECHOL	4.6e3	Taraborrelli (2020)		
NCATECOOH	2.0e6	Taraborrelli (2020)		
NDNPHENOOH	2.3e3	Taraborrelli (2020)		
NNCATECOOH	2.3e3	Taraborrelli (2020)		
NPHENOOH	4.6e3	Taraborrelli (2020)		
C235C6CO3H	1.0E6	Taraborrelli (2020)		

Table 7: Henry's law constants (continued...)

KPP name	$H^{\ominus}$ [M/atm]	Reference	$\frac{\mathrm{d}\ln H^{\ominus}}{\mathrm{d}(1/T)}$ [K]	Reference
C716OOH	1.0E6	Taraborrelli (2020)		
C721OOH	1.0E6	Taraborrelli (2020)		
C722OOH	1.0E6	Taraborrelli (2020)		
CO235C6CHO	1.0E6	Taraborrelli (2020)		
C6COOHCO3H	2.0e6	Taraborrelli (2020)		
C6H5CH2OOH	2.9e3	Taraborrelli (2020)	6800.	
C6H5CO3H	2.4e4	Taraborrelli (2020)		
C7CO4DB	3.7e3	Taraborrelli (2020)	7500.	
CRESOL	2.9e3	Taraborrelli (2020)	6800.	
CRESOOH	2.0e6	Taraborrelli (2020)		
MCATEC1O	2.0e6	Taraborrelli (2020)		
MCATEC1OOH	4.6e3	Taraborrelli (2020)		
MCATECHOL	4.6e3	Taraborrelli (2020)		
OXYL1OOH	2.9e3	Taraborrelli (2020)	6800.	
PHCOOH	1.4E4	Goldstein (1982)	6500.	
TLBIPEROOH	2.0e6	Taraborrelli (2020)		
TLEMUCCO	3.1e5	Taraborrelli (2020)	5100.	
TLEMUCCO2H	2.2e3	Taraborrelli (2020)	6583.	
TLEMUCCO3H	2.2e3	Taraborrelli (2020)	6583.	
TLEMUCOOH	2.0e6	Taraborrelli (2020)		
TLOBIPEROH	3.9e4	Taraborrelli (2020)	8600.	
TOL1O	2.9e3	Taraborrelli (2020)	6800.	
C7PAN3	1.0E6	Taraborrelli (2020)		
C6CO2OHPAN	3.9e4	Taraborrelli (2020)	8600.	
DNCRES	2.3e3	Taraborrelli (2020)		
DNCRESOOH	2.3e3	Taraborrelli (2020)		
MNCATECH	4.6e3	Taraborrelli (2020)		
MNCATECOOH	2.0e6	Taraborrelli (2020)		
MNNCATCOOH	2.3e3	Taraborrelli (2020)		
NCRESOOH	4.6e3	Taraborrelli (2020)		
NDNCRESOOH	2.3e3	Taraborrelli (2020)		
TLEMUCNO3	3.9e4	Taraborrelli (2020)	8600.	
C721CHO	1.0E6	Taraborrelli (2020)		
C721CO3H	1.0E6	Taraborrelli (2020)		
C810OOH	1.0E6	Taraborrelli (2020)		
C812OOH	1.0E6	Taraborrelli (2020)		
C813OOH	1.0E6	Taraborrelli (2020)		
C85OOH	1.0E6	Taraborrelli (2020)		
C86OOH	1.0E6	Taraborrelli (2020)		
C89OOH	1.0E6	Taraborrelli (2020)		
C8BC	1.0E6	Taraborrelli (2020)		
C8BCCO	1.0E6	Taraborrelli (2020)		
C8BCOOH	1.0E6	Taraborrelli (2020)		
NORPINIC	4.E13	Taraborrelli (2020)		
STYRENOOH	2.4e4	Taraborrelli (2020)		
C721PAN	1.0E6	Taraborrelli (2020)		
C810NO3	1.0E6	Taraborrelli (2020)		
C89NO3	1.0E6	Taraborrelli (2020)		
C8BCNO3	1.0E6	Taraborrelli (2020)		
C811CO3H	1.0E6	Taraborrelli (2020)		
C85CO3H	1.0E6	Taraborrelli (2020)		

Table 7: Henry's law constants (continued...)

KPP name	$H^{\ominus}$ [M/atm]	Reference	$\frac{\mathrm{d}\ln H^{\ominus}}{\mathrm{d}(1/T)}$ [K]	Reference
C89CO2H	6.6E7	Taraborrelli (2020)		
C89CO3H	1.0E6	Taraborrelli (2020)		
C96OOH	1.0E6	Taraborrelli (2020)		
C97OOH	1.0E6	Taraborrelli (2020)		
C98OOH	1.0E6	Taraborrelli (2020)		
NOPINDCO	1.0E6	Taraborrelli (2020)		
NOPINDOOH	1.0E6	Taraborrelli (2020)		
NOPINONE	1.0E6	Taraborrelli (2020)		
NOPINOO	1.0E6	Taraborrelli (2020)		
NORPINAL	1.0E6	Taraborrelli (2020)		
NORPINENOL	1.0E6	Taraborrelli (2020)		
PINIC	4.E13	Taraborrelli (2020)		
C811PAN	1.0E6	Taraborrelli (2020)		
C89PAN	1.0E6	Taraborrelli (2020)		
C96NO3	1.0E6	Taraborrelli (2020)		
C9PAN2	1.0E6	Taraborrelli (2020)		
BPINAOOH	1.0E6	Taraborrelli (2020)		
C106OOH	1.0E6	Taraborrelli (2020)		
C109CO	1.0E6	Taraborrelli (2020)		
C109OOH	1.0E6	Taraborrelli (2020)		
MENTHEN6ONE	1.0E6	Taraborrelli (2020)		
OH2MENTHEN6ONE	1.0E6	Taraborrelli (2020)		
PERPINONIC	7.4E5	Taraborrelli (2020)		
PINAL	1.0E6	Taraborrelli (2020)		
PINALOOH	1.0E6	Taraborrelli (2020)		
PINENOL	1.0E6	Taraborrelli (2020)		
PINONIC	7.4E5	Taraborrelli (2020)		
BPINANO3	1.0E6	Taraborrelli (2020)		
C106NO3	1.0E6	Taraborrelli (2020)		
C10PAN2	1.0E6	Taraborrelli (2020)		
PINALNO3	1.0E6	Taraborrelli (2020)		
RO6R1NO3	1.0E6	Taraborrelli (2020)		
ROO6R1NO3	1.0E6	Taraborrelli (2020)		
LAPINABNO3	1.0E6	Taraborrelli (2020)		
LAPINABOOH	1.0E6	Taraborrelli (2020)		
LNAPINABOOH	1.0E6	Taraborrelli (2020)		
LNBPINABOOH	1.0E6	Taraborrelli (2020)		
Cl2	9.3E-2	Sander et al. (2011)	2000.	
ClNO3	BIG_DP	see notes	0.	
HCl	2./1.7	Brimblecombe and Clegg (1989)	9000.	
HOCl	6.6E2	Burkholder et al. (2015)	5880.	
Br2	7.25E-1	Burkholder et al. (2015)	4390.	
BrCl	9.4E-1	Bartlett and Margerum (1999)	5600.	
BrNO3	BIG_DP	see notes	0.	
HBr	1.3	Brimblecombe and Clegg (1989)	10000.	
HOBr	1.3E3	Blatchley et al. (1992)	5862.	
HI	BIG_DP	see notes	0.	
HIO3	BIG_DP	see notes	0.	
HOI	4.5E2	Chatfield and Crutzen (1990)	5862.	
I2	3.	Palmer et al. (1985)	4431.	
I2O2	BIG_DP	see notes	0.	

Table 7: Henry's law constants (continued...)

KPP name	$H^{\ominus}$ [M/atm]	Reference	$\frac{\mathrm{d}\ln H^{\ominus}}{\mathrm{d}(1/T)}$ [K]	Reference
IBr	2.4E1	see notes	5600.	
ICl	1.1E2	see notes	5600.	
INO2	BIG_DP	see notes	0.	
INO3	BIG_DP	see notes	0.	
IO	4.5E2	see notes	5862.	
OIO	BIG_DP	see notes	0.	
CH3SO3H	BIG_DP	see notes	0.	
DMS	5.4E-1	Burkholder et al. (2015)	3460.	
DMSO	9.5E4	Watts and Brimblecombe (1987)	1300.	
H2SO4	1.E11	see notes	0.	
SO2	1.3	Burkholder et al. (2015)	2900.	
Hg	0.13	Andersson et al. (2008)	2700.	
HgO	3.2E6	Shon et al. (2005)	0.	
HgCl	2.4E7	see notes	0.	
HgCl2	2.4E7	Shon et al. (2005)	0.	
HgBr	2.4E7	see notes	0.	
HgBr2	2.4E7	see notes	0.	
ClHgBr	2.4E7	see notes	0.	
BrHgOBr	2.4E7	see notes	0.	
ClHgOBr	2.4E7	see notes	0.	
OXL	3.2E6	Brimblecombe et al. (1992)	7285.	

Table 8: Accommodation coefficients

KPP name	$\alpha^{\ominus}$	Reference	α-T-dep	Reference
O1D	0.1	see notes	0.	
O3P	0.1	see notes	0.	
O2	0.01	see notes	2000.	
O3	0.002	DeMore et al. (1997)	0.	
H	0.1	see notes	0.	
H2	0.1	see notes	0.	
OH	0.01	Takami et al. (1998)	0.	
HO2	0.5	Thornton and Abbatt (2005)	0.	
H2O	0.0	see notes	0.	
H2O2	0.077	Worsnop et al. (1989)	3127.	
H2OH2O	0.1	see notes	0.	
N	0.1	see notes	0.	
N2D	0.1	see notes	0.	
N2	0.1	see notes	0.	
NH3	0.06	DeMore et al. (1997)	0.	
N2O	0.1	see notes	0.	
NO	5.0E-5	Saastad et al. (1993)	0.	
NO2	0.0015	Ponche et al. (1993)	0.	
NO3	0.04	Rudich et al. (1996)	0.	
N2O5	0.1	see notes	0.	
HONO	0.04	DeMore et al. (1997)	0.	
HOONO	0.1	see notes	0.	
HNO3	0.5	Abbatt and Waschewsky (1998)	0.	
HNO4	0.1	see notes	0.	
NH2	0.1	see notes	0.	
HNO	0.1	see notes	0.	
NHOH	0.1	see notes	0.	
NH2O	0.1	see notes	0.	
NH2OH	0.1	see notes	0.	
LNITROGEN	0.1	see notes	0.	
CH2OO	0.1	see notes	0.	
CH2OOA	0.1	see notes	0.	
CH3	0.1	see notes	0.	
CH3O	0.1	see notes	0.	
CH3O2	0.01	see notes	2000.	
CH3OH	0.1	see notes	0.	
CH3OOH	0.0046	Magi et al. (1997)	3273.	
CH4	0.1	see notes	0.	
CO	0.1	see notes	0.	
CO2	0.01	see notes	2000.	
HCHO	0.04	DeMore et al. (1997)	0.	
HCOOH	0.014	DeMore et al. (1997)	3978.	
HOCH2O2	0.1	see notes	0.	
HOCH2OH	0.1	see notes	0.	
HOCH2OOH	0.1	see notes	0.	
CH3NO3	0.1	see notes	0.	
CH3O2NO2	0.1	see notes	0.	
CH3ONO	0.1	see notes	0.	
CN	0.1	see notes	0.	
HCN	0.1	see notes	0.	
HOCH2O2NO2	0.1	see notes	0.	
NCO	0.1	see notes	0.	
LCARBON	0.1	see notes	0.	
C2H2	0.1	see notes	0.	

Table 8: Accommodation coefficients (continued...)

KPP name	$\alpha^{\ominus}$	Reference	α-T-dep	Reference
C2H4	0.1	see notes	0.	
C2H5O2	0.1	see notes	0.	
C2H5OH	9.E-3		0.	
C2H5OOH	0.1	see notes	0.	
C2H6	0.1	see notes	0.	
CH2CHOH	0.1	see notes	0.	
CH2CO	0.1	see notes	0.	
CH3CHO	3.0E-2	see notes	0.	
CH3CHOHO2	0.1	see notes	0.	
CH3CHOHOH	0.1	see notes	0.	
CH3CHOHOOH	0.1	see notes	0.	
CH3CO	0.1	see notes	0.	
CH3CO2H	2.0E-2	Davidovits et al. (1995)	4079.	
CH3CO3	0.1	see notes	0.	
CH3CO3H	0.1	see notes	0.	
CHOCHOHOH	0.1	see notes	0.	
CHOHOHCHOHOH	0.1	see notes	0.	
CHOHOHCOOH	0.1	see notes	0.	
ETHGLY	0.1	see notes	0.	
GLYOX	0.1	see notes	0.	
HCOCH2O2	0.1	see notes	0.	
HCOCO	0.1	see notes	0.	
HCOCO2H	0.1	see notes	0.	
HCOCO3	0.1	see notes	0.	
HCOCO3H	0.1	see notes	0.	
HOCH2CH2O	0.1	see notes	0.	
HOCH2CH2O2	0.1	see notes	0.	
HOCH2CHO	0.1	see notes	0.	
HOCH2CHOHOH	0.1	see notes	0.	
HOCH2CO	0.1	see notes	0.	
HOCH2CO2H	0.1	see notes	0.	
HOCH2CO3	0.1	see notes	0.	
HOCH2CO3H	0.1	see notes	0.	
HOCHCHO	0.1	see notes	0.	
HOOCCOOH	0.1	see notes	0.	
HOOCH2CHO	0.1	see notes	0.	
HOOCH2CHOHOH	0.1	see notes	0.	
HOOCH2CO2H	0.1	see notes	0.	
HOOCH2CO3	0.1	see notes	0.	
HOOCH2CO3H	0.1	see notes	0.	
HYETHO2H	0.1	see notes	0.	
C2H5NO3	0.1	see notes	0.	
C2H5O2NO2	0.1	see notes	0.	
CH3CN	0.1	see notes	0.	
ETHOHNO3	0.1	see notes	0.	
NCCH2O2	0.1	see notes	0.	
NO3CH2CHO	0.1	see notes	0.	
NO3CH2CO3	0.1	see notes	0.	
NO3CH2PAN	0.1	see notes	0.	
PAN	0.1	see notes	0.	
PHAN	0.1	see notes	0.	
ACETOL	0.1	see notes	0.	
ALCOCH2OOH	0.1	see notes	0.	
C2H5CHO	0.1	see notes	0.	

Table 8: Accommodation coefficients (continued...)

KPP name	$\alpha^{\ominus}$	Reference	α-T-dep	Reference
C2H5CO3	0.1	see notes	0.	
C33CO	0.1	see notes	0.	
C3H6	0.1	see notes	0.	
C3H8	0.1	see notes	0.	
CH3CHCO	0.1	see notes	0.	
CH3COCH2O2	0.1	see notes	0.	
CH3COCH3	3.72E-3	Davidovits et al. (1995)	6395.	
CH3COCHOHOH	0.1	see notes	0.	
CH3COCO2H	0.1	see notes	0.	
CH3COCO3	0.1	see notes	0.	
CH3COCO3H	0.1	see notes	0.	
CHOCOCH2O2	0.1	see notes	0.	
HCOCH2CHO	0.1	see notes	0.	
HCOCH2CO2H	0.1	see notes	0.	
HCOCH2CO3	0.1	see notes	0.	
HCOCH2CO3H	0.1	see notes	0.	
HCOCOCH2OOH	0.1	see notes	0.	
HOC2H4CO2H	0.1	see notes	0.	
HOC2H4CO3	0.1	see notes	0.	
HOC2H4CO3H	0.1	see notes	0.	
HOCH2COCH2O2	0.1	see notes	0.	
HOCH2COCH2OOH	0.1	see notes	0.	
HOCH2COCHO	0.1	see notes	0.	
HYPERACET	0.1	see notes	0.	
HYPROPO2	0.1	see notes	0.	
HYPROPO2H	0.1	see notes	0.	
IC3H7O2	0.1	see notes	0.	
IC3H7OOH	0.1	see notes	0.	
IPROPOL	0.1	see notes	0.	
MGLYOX	0.1	see notes	0.	
NC3H7O2	0.1	see notes	0.	
NC3H7OOH	0.1	see notes	0.	
NPROPOL	0.1	see notes	0.	
PERPROACID	0.1	see notes	0.	
PROPACID	0.1	see notes	0.	
PROPENOL	0.1	see notes	0.	
C32OH13CO	0.1	see notes	0.	
C3DIALO2	0.1	see notes	0.	
C3DIALOOH	0.1	see notes	0.	
HCOCOHCO3	0.1	see notes	0.	
HCOCOHCO3H	0.1	see notes	0.	
METACETHO	0.1	see notes	0.	
C3PAN1	0.1	see notes	0.	
C3PAN2	0.1	see notes	0.	
CH3COCH2O2NO2	0.1	see notes	0.	
IC3H7NO3	0.1	see notes	0.	
NC3H7NO3	0.1	see notes	0.	
NOA	0.1	see notes	0.	
PPN	0.1	see notes	0.	
PR2O2HNO3	0.1	see notes	0.	
PRONO3BO2	0.1	see notes	0.	
PROPOLNO3	0.1	see notes	0.	
HCOCOHPAN	0.1	see notes	0.	
BIACET	0.1	see notes	0.	

Table 8: Accommodation coefficients (continued...)

KPP name	$\alpha^{\ominus}$	Reference	α-T-dep	Reference
BIACETO2	0.1	see notes	0.	
BIACETOH	0.1	see notes	0.	
BIACETOOH	0.1	see notes	0.	
BUT1ENE	0.1	see notes	0.	
BUT2OLO	0.1	see notes	0.	
BUT2OLO2	0.1	see notes	0.	
BUT2OLOOH	0.1	see notes	0.	
BUTENOL	0.1	see notes	0.	
C312COCO3	0.1	see notes	0.	
C312COCO3H	0.1	see notes	0.	
C3H7CHO	0.1	see notes	0.	
C413COOOH	0.1	see notes	0.	
C44O2	0.1	see notes	0.	
C44OOH	0.1	see notes	0.	
C4CODIAL	0.1	see notes	0.	
CBUT2ENE	0.1	see notes	0.	
CH3COCHCO	0.1	see notes	0.	
CH3COCHO2CHO	0.1	see notes	0.	
CH3COCOCO2H	0.1	see notes	0.	
CH3COOHCHCHO	0.1	see notes	0.	
CHOC3COO2	0.1	see notes	0.	
CO23C3CHO	0.1	see notes	0.	
CO2C3CHO	0.1	see notes	0.	
CO2H3CHO	0.1	see notes	0.	
CO2H3CO2H	0.1	see notes	0.	
CO2H3CO3	0.1	see notes	0.	
CO2H3CO3H	0.1	see notes	0.	
EZCH3CO2CHCHO	0.1	see notes	0.	
EZCHOCCH3CHO2	0.1	see notes	0.	
HCOCCH3CHOOH	0.1	see notes	0.	
HCOCCH3CO	0.1	see notes	0.	
HCOCO2CH3CHO	0.1	see notes	0.	
HMAC	0.1	see notes	0.	
HO12CO3C4	0.1	see notes	0.	
HVMK	0.1	see notes	0.	
IBUTALOH	0.1	see notes	0.	
IBUTDIAL	0.1	see notes	0.	
IBUTOLBO2	0.1	see notes	0.	
IBUTOLBOOH	0.1	see notes	0.	
IC4H10	0.1	see notes	0.	
IC4H9O2	0.1	see notes	0.	
IC4H9OOH	0.1	see notes	0.	
IPRCHO	0.1	see notes	0.	
IPRCO3	0.1	see notes	0.	
IPRHOCO2H	0.1	see notes	0.	
IPRHOCO3	0.1	see notes	0.	
IPRHOCO3H	0.1	see notes	0.	
MACO2	0.1	see notes	0.	
MACO2H	0.1	see notes	0.	
MACO3	0.1	see notes	0.	
MACO3H	0.1	see notes	0.	
MACR	0.1	see notes	0.	
MACRO	0.1	see notes	0.	
MACRO2	0.1	see notes	0.	

Table 8: Accommodation coefficients (continued...)

KPP name	$\alpha^{\ominus}$	Reference	α-T-dep	Reference
MACROH	0.1	see notes	0.	
MACROOH	0.1	see notes	0.	
MBOOO	0.1	see notes	0.	
MEK	0.1	see notes	0.	
MEPROPENE	0.1	see notes	0.	
MPROPENOL	0.1	see notes	0.	
MVK	0.1	see notes	0.	
NC4H10	0.1	see notes	0.	
PERIBUACID	0.1	see notes	0.	
TBUT2ENE	0.1	see notes	0.	
TC4H9O2	0.1	see notes	0.	
TC4H9OOH	0.1	see notes	0.	
BZFUCO	0.1	see notes	0.	
BZFUO2	0.1	see notes	0.	
BZFUONE	0.1	see notes	0.	
BZFUOOH	0.1	see notes	0.	
CO14O3CHO	0.1	see notes	0.	
CO14O3CO2H	0.1	see notes	0.	
CO2C4DIAL	0.1	see notes	0.	
EPXC4DIAL	0.1	see notes	0.	
EPXDLCO2H	0.1	see notes	0.	
EPXDLCO3	0.1	see notes	0.	
EPXDLCO3H	0.1	see notes	0.	
HOCOC4DIAL	0.1	see notes	0.	
MALANHY	0.1	see notes	0.	
MALANHYO2	0.1	see notes	0.	
MALANHYOOH	0.1	see notes	0.	
MALDALCO2H	0.1	see notes	0.	
MALDALCO3H	0.1	see notes	0.	
MALDIAL	0.1	see notes	0.	
MALDIALCO3	0.1	see notes	0.	
MALDIALO2	0.1	see notes	0.	
MALDIALOOH	0.1	see notes	0.	
MALNHYOHCO	0.1	see notes	0.	
MECOACEOOH	0.1	see notes	0.	
MECOACETO2	0.1	see notes	0.	
BUT2OLNO3	0.1	see notes	0.	
C312COPAN	0.1	see notes	0.	
C4PAN5	0.1	see notes	0.	
IBUTOLBNO3	0.1	see notes	0.	
IC4H9NO3	0.1	see notes	0.	
MACRNO3	0.1	see notes	0.	
MPAN	0.1	see notes	0.	
MVKNO3	0.1	see notes	0.	
PIPN	0.1	see notes	0.	
TC4H9NO3	0.1	see notes	0.	
EPXDLPAN	0.1	see notes	0.	
MALDIALPAN	0.1	see notes	0.	
NBZFUO2	0.1	see notes	0.	
NBZFUONE	0.1	see notes	0.	
NBZFUOOH	0.1	see notes	0.	
NC4DCO2H	0.1	see notes	0.	
LBUT1ENO2	0.1	see notes	0.	
LBUT1ENOOH	0.1	see notes	0.	

Table 8: Accommodation coefficients (continued...)

KPP name	$\alpha^{\ominus}$	Reference	α-T-dep	Reference
LC4H9O2	0.1	see notes	0.	
LC4H9OOH	0.1	see notes	0.	
LHMVKABO2	0.1	see notes	0.	
LHMVKABOOH	0.1	see notes	0.	
LMEKO2	0.1	see notes	0.	
LMEKOOH	0.1	see notes	0.	
LBUT1ENNO3	0.1	see notes	0.	
LC4H9NO3	0.1	see notes	0.	
LMEKNO3	0.1	see notes	0.	
C1ODC2O2C4OD	0.1	see notes	0.	
C1ODC2O2C4OOH	0.1	see notes	0.	
C1ODC2OOHC4OD	0.1	see notes	0.	
C1ODC3O2C4OOH	0.1	see notes	0.	
C1OOHC2O2C4OD	0.1	see notes	0.	
C1OOHC2OOHC4OD	0.1	see notes	0.	
C1OOHC3O2C4OD	0.1	see notes	0.	
C4MDIAL	0.1	see notes	0.	
C511O2	0.1	see notes	0.	
C511OOH	0.1	see notes	0.	
C512O2	0.1	see notes	0.	
C512OOH	0.1	see notes	0.	
C513CO	0.1	see notes	0.	
C513O2	0.1	see notes	0.	
C513OOH	0.1	see notes	0.	
C514O2	0.1	see notes	0.	
C514OOH	0.1	see notes	0.	
C59O2	0.1	see notes	0.	
C59OOH	0.1	see notes	0.	
C5H8	0.1	see notes	0.	
CHOC3COCO3	0.1	see notes	0.	
CHOC3COOOH	0.1	see notes	0.	
CO13C4CHO	0.1	see notes	0.	
CO23C4CHO	0.1	see notes	0.	
CO23C4CO3	0.1	see notes	0.	
CO23C4CO3H	0.1	see notes	0.	
DB1O	0.1	see notes	0.	
DB1O2	0.1	see notes	0.	
DB1OOH	0.1	see notes	0.	
DB2O2	0.1	see notes	0.	
DB2OOH	0.1	see notes	0.	
HCOC5	0.1	see notes	0.	
ISOPAOH	0.1	see notes	0.	
ISOPBO2	0.1	see notes	0.	
ISOPBOH	0.1	see notes	0.	
ISOPBOOH	0.1	see notes	0.	
ISOPDO2	0.1	see notes	0.	
ISOPDOH	0.1	see notes	0.	
ISOPDOOH	0.1	see notes	0.	
MBO	0.1	see notes	0.	
MBOACO	0.1	see notes	0.	
MBOCOCO	0.1	see notes	0.	
ME3FURAN	0.1	see notes	0.	
ACCOMECHO	0.1	see notes	0.	
ACCOMECO3	0.1	see notes	0.	

Table 8: Accommodation coefficients (continued...)

KPP name	$\alpha^{\ominus}$	Reference	α-T-dep	Reference
ACCOMECO3H	0.1	see notes	0.	
C24O3CCO2H	0.1	see notes	0.	
C4CO2DBCO3	0.1	see notes	0.	
C4CO2DCO3H	0.1	see notes	0.	
C5134CO2OH	0.1	see notes	0.	
C54CO	0.1	see notes	0.	
C5CO14O2	0.1	see notes	0.	
C5CO14OH	0.1	see notes	0.	
C5CO14OOH	0.1	see notes	0.	
C5DIALCO	0.1	see notes	0.	
C5DIALO2	0.1	see notes	0.	
C5DIALOOH	0.1	see notes	0.	
C5DICARB	0.1	see notes	0.	
C5DICARBO2	0.1	see notes	0.	
C5DICAROOH	0.1	see notes	0.	
MC3ODBCO2H	0.1	see notes	0.	
MMALANHY	0.1	see notes	0.	
MMALANHYO2	0.1	see notes	0.	
MMALNHYOOH	0.1	see notes	0.	
TLFUO2	0.1	see notes	0.	
TLFUONE	0.1	see notes	0.	
TLFUOOH	0.1	see notes	0.	
C4MCONO3OH	0.1	see notes	0.	
C514NO3	0.1	see notes	0.	
C5PAN9	0.1	see notes	0.	
CHOC3COPAN	0.1	see notes	0.	
DB1NO3	0.1	see notes	0.	
ISOPBDNO3O2	0.1	see notes	0.	
ISOPBNO3	0.1	see notes	0.	
ISOPDNO3	0.1	see notes	0.	
NC4CHO	0.1	see notes	0.	
NC4OHCO3	0.1	see notes	0.	
NC4OHCO3H	0.1	see notes	0.	
NC4OHCPAN	0.1	see notes	0.	
NISOPO2	0.1	see notes	0.	
NISOPOOH	0.1	see notes	0.	
NMBOBCO	0.1	see notes	0.	
ACCOMEPAN	0.1	see notes	0.	
C4CO2DBPAN	0.1	see notes	0.	
C5COO2NO2	0.1	see notes	0.	
NC4MDCO2H	0.1	see notes	0.	
NTLFUO2	0.1	see notes	0.	
NTLFUOOH	0.1	see notes	0.	
LC578O2	0.1	see notes	0.	
LC578OOH	0.1	see notes	0.	
LDISOPACO	0.1	see notes	0.	
LDISOPACO2	0.1	see notes	0.	
LHC4ACCHO	0.1	see notes	0.	
LHC4ACCO2H	0.1	see notes	0.	
LHC4ACCO3	0.1	see notes	0.	
LHC4ACCO3H	0.1	see notes	0.	
LIEPOX	0.1	see notes	0.	
LISOPAB	0.1	see notes	0.	
LISOPACO	0.1	see notes	0.	

Table 8: Accommodation coefficients (continued...)

KPP name	$\alpha^{\ominus}$	Reference	α-T-dep	Reference
LISOPACO2	0.1	see notes	0.	
LISOPACOOH	0.1	see notes	0.	
LISOPCD	0.1	see notes	0.	
LISOPEFO	0.1	see notes	0.	
LISOPEFO2	0.1	see notes	0.	
LMBOABO2	0.1	see notes	0.	
LMBOABOOH	0.1	see notes	0.	
LME3FURANO2	0.1	see notes	0.	
LZCO3C23DBCOD	0.1	see notes	0.	
LZCO3HC23DBCOD	0.1	see notes	0.	
LZCODC23DBCOOH	0.1	see notes	0.	
LC5PAN1719	0.1	see notes	0.	
LISOPACNO3	0.1	see notes	0.	
LISOPACNO3O2	0.1	see notes	0.	
LMBOABNO3	0.1	see notes	0.	
LNISO3	0.1	see notes	0.	
LNISOOH	0.1	see notes	0.	
LNMBOABO2	0.1	see notes	0.	
LNMBOABOOH	0.1	see notes	0.	
LZCPANC23DBCOD	0.1	see notes	0.	
C614CO	0.1	see notes	0.	
C614O2	0.1	see notes	0.	
C614OOH	0.1	see notes	0.	
CO235C5CHO	0.1	see notes	0.	
CO235C6O2	0.1	see notes	0.	
CO235C6OOH	0.1	see notes	0.	
BENZENE	0.1	see notes	0.	
BZBIPERO2	0.1	see notes	0.	
BZBIPEROOH	0.1	see notes	0.	
BZEMUCCO	0.1	see notes	0.	
BZEMUCCO2H	0.1	see notes	0.	
BZEMUCCO3	0.1	see notes	0.	
BZEMUCCO3H	0.1	see notes	0.	
BZEMUCO2	0.1	see notes	0.	
BZEMUCOOH	0.1	see notes	0.	
BZEPOXMUC	0.1	see notes	0.	
BZOBIPEROH	0.1	see notes	0.	
C5CO2DBCO3	0.1	see notes	0.	
C5CO2DCO3H	0.1	see notes	0.	
C5CO2OHCO3	0.1	see notes	0.	
C5COOHCO3H	0.1	see notes	0.	
C6125CO	0.1	see notes	0.	
C615CO2O2	0.1	see notes	0.	
C615CO2OOH	0.1	see notes	0.	
C6CO4DB	0.1	see notes	0.	
C6H5O	0.1	see notes	0.	
C6H5O2	0.1	see notes	0.	
C6H5OOH	0.1	see notes	0.	
CATEC1O	0.1	see notes	0.	
CATEC1O2	0.1	see notes	0.	
CATEC1OOH	0.1	see notes	0.	
CATECHOL	0.1	see notes	0.	
CPDKETENE	0.1	see notes	0.	
PBZQCO	0.1	see notes	0.	

Table 8: Accommodation coefficients (continued...)

KPP name	$\alpha^{\ominus}$	Reference	α-T-dep	Reference
PBZQO2	0.1	see notes	0.	
PBZQONE	0.1	see notes	0.	
PBZQOOH	0.1	see notes	0.	
PHENO2	0.1	see notes	0.	
PHENOL	0.1	see notes	0.	
PHENOOH	0.1	see notes	0.	
C614NO3	0.1	see notes	0.	
BZBIPERNO3	0.1	see notes	0.	
BZEMUCNO3	0.1	see notes	0.	
BZEMUCPAN	0.1	see notes	0.	
C5CO2DBPAN	0.1	see notes	0.	
C5CO2OHPAN	0.1	see notes	0.	
DNPHEN	0.1	see notes	0.	
DNPHENO2	0.1	see notes	0.	
DNPHENOOH	0.1	see notes	0.	
HOC6H4NO2	0.1	see notes	0.	
NBZQO2	0.1	see notes	0.	
NBZQOOH	0.1	see notes	0.	
NCATECHOL	0.1	see notes	0.	
NCATECO2	0.1	see notes	0.	
NCATECOOH	0.1	see notes	0.	
NCPDKETENE	0.1	see notes	0.	
NDNPHENO2	0.1	see notes	0.	
NDNPHENOOH	0.1	see notes	0.	
NNCATECO2	0.1	see notes	0.	
NNCATECOOH	0.1	see notes	0.	
NPHEN1O	0.1	see notes	0.	
NPHEN1O2	0.1	see notes	0.	
NPHEN1OOH	0.1	see notes	0.	
NPHENO2	0.1	see notes	0.	
NPHENOOH	0.1	see notes	0.	
C235C6CO3H	0.1	see notes	0.	
C716O2	0.1	see notes	0.	
C716OOH	0.1	see notes	0.	
C721O2	0.1	see notes	0.	
C721OOH	0.1	see notes	0.	
C722O2	0.1	see notes	0.	
C722OOH	0.1	see notes	0.	
CO235C6CHO	0.1	see notes	0.	
CO235C6CO3	0.1	see notes	0.	
MCPDKETENE	0.1	see notes	0.	
ROO6R3O	0.1	see notes	0.	
ROO6R3O2	0.1	see notes	0.	
ROO6R5O2	0.1	see notes	0.	
BENZAL	0.1	see notes	0.	
C6CO2OHCO3	0.1	see notes	0.	
C6COOHCO3H	0.1	see notes	0.	
C6H5CH2O2	0.1	see notes	0.	
C6H5CH2OOH	0.1	see notes	0.	
C6H5CO3	0.1	see notes	0.	
C6H5CO3H	0.1	see notes	0.	
C7CO4DB	0.1	see notes	0.	
CRESO2	0.1	see notes	0.	
CRESOL	0.1	see notes	0.	

Table 8: Accommodation coefficients (continued...)

KPP name	$\alpha^{\ominus}$	Reference	α-T-dep	Reference
CRESOOH	0.1	see notes	0.	
MCATEC1O	0.1	see notes	0.	
MCATEC1O2	0.1	see notes	0.	
MCATEC1OOH	0.1	see notes	0.	
MCATECHOL	0.1	see notes	0.	
OXYL1O2	0.1	see notes	0.	
OXYL1OOH	0.1	see notes	0.	
PHCOOH	0.1	see notes	0.	
PTLQCO	0.1	see notes	0.	
PTLQO2	0.1	see notes	0.	
PTLQONE	0.1	see notes	0.	
PTLQOOH	0.1	see notes	0.	
TLBIPERO2	0.1	see notes	0.	
TLBIPEROOH	0.1	see notes	0.	
TLEMUCCO	0.1	see notes	0.	
TLEMUCCO2H	0.1	see notes	0.	
TLEMUCCO3	0.1	see notes	0.	
TLEMUCCO3H	0.1	see notes	0.	
TLEMUCO2	0.1	see notes	0.	
TLEMUCOOH	0.1	see notes	0.	
TLEPOXMUC	0.1	see notes	0.	
TLOBIPEROH	0.1	see notes	0.	
TOL1O	0.1	see notes	0.	
TOLUENE	0.1	see notes	0.	
C7PAN3	0.1	see notes	0.	
C6CO2OHPAN	0.1	see notes	0.	
C6H5CH2NO3	0.1	see notes	0.	
DNCRES	0.1	see notes	0.	
DNCRESO2	0.1	see notes	0.	
DNCRESOOH	0.1	see notes	0.	
MNCATECH	0.1	see notes	0.	
MNCATECO2	0.1	see notes	0.	
MNCATECOOH	0.1	see notes	0.	
MNCPDKETENE	0.1	see notes	0.	
MNNCATCOOH	0.1	see notes	0.	
MNNCATECO2	0.1	see notes	0.	
NCRES1O	0.1	see notes	0.	
NCRES1O2	0.1	see notes	0.	
NCRES1OOH	0.1	see notes	0.	
NCRESO2	0.1	see notes	0.	
NCRESOOH	0.1	see notes	0.	
NDNCRESO2	0.1	see notes	0.	
NDNCRESOOH	0.1	see notes	0.	
NPTLQO2	0.1	see notes	0.	
NPTLQOOH	0.1	see notes	0.	
PBZN	0.1	see notes	0.	
TLBIPERNO3	0.1	see notes	0.	
TLEMUCNO3	0.1	see notes	0.	
TLEMUCPAN	0.1	see notes	0.	
TOL1OHNO2	0.1	see notes	0.	
C721CHO	0.1	see notes	0.	
C721CO3	0.1	see notes	0.	
C721CO3H	0.1	see notes	0.	
C810O2	0.1	see notes	0.	

Table 8: Accommodation coefficients (continued...)

KPP name	$\alpha^{\ominus}$	Reference	α-T-dep	Reference
C810OOH	0.1	see notes	0.	
C811O2	0.1	see notes	0.	
C812O2	0.1	see notes	0.	
C812OOH	0.1	see notes	0.	
C813O2	0.1	see notes	0.	
C813OOH	0.1	see notes	0.	
C85O2	0.1	see notes	0.	
C85OOH	0.1	see notes	0.	
C86O2	0.1	see notes	0.	
C86OOH	0.1	see notes	0.	
C89O2	0.1	see notes	0.	
C89OOH	0.1	see notes	0.	
C8BC	0.1	see notes	0.	
C8BCCO	0.1	see notes	0.	
C8BCO2	0.1	see notes	0.	
C8BCOOH	0.1	see notes	0.	
NORPINIC	0.1	see notes	0.	
EBENZ	0.1	see notes	0.	
STYRENE	0.1	see notes	0.	
STYRENO2	0.1	see notes	0.	
STYRENOOH	0.1	see notes	0.	
C721PAN	0.1	see notes	0.	
C810NO3	0.1	see notes	0.	
C89NO3	0.1	see notes	0.	
C8BCNO3	0.1	see notes	0.	
NSTYRENO2	0.1	see notes	0.	
NSTYRENOOH	0.1	see notes	0.	
LXYL	0.1	see notes	0.	
C811CO3	0.1	see notes	0.	
C811CO3H	0.1	see notes	0.	
C85CO3	0.1	see notes	0.	
C85CO3H	0.1	see notes	0.	
C89CO2H	0.1	see notes	0.	
C89CO3	0.1	see notes	0.	
C89CO3H	0.1	see notes	0.	
C96O2	0.1	see notes	0.	
C96OOH	0.1	see notes	0.	
C97O2	0.1	see notes	0.	
C97OOH	0.1	see notes	0.	
C98O2	0.1	see notes	0.	
C98OOH	0.1	see notes	0.	
NOPINDCO	0.1	see notes	0.	
NOPINDO2	0.1	see notes	0.	
NOPINDOOH	0.1	see notes	0.	
NOPINONE	0.1	see notes	0.	
NOPINOO	0.1	see notes	0.	
NORPINAL	0.1	see notes	0.	
NORPINENOL	0.1	see notes	0.	
PINIC	0.1	see notes	0.	
C811PAN	0.1	see notes	0.	
C89PAN	0.1	see notes	0.	
C96NO3	0.1	see notes	0.	
C9PAN2	0.1	see notes	0.	
LTMB	0.1	see notes	0.	

Table 8: Accommodation coefficients (continued...)

KPP name	$\alpha^{\ominus}$	Reference	α-T-dep	Reference
APINAOO	0.1	see notes	0.	
APINBOO	0.1	see notes	0.	
APINENE	0.1	see notes	0.	
BPINAO2	0.1	see notes	0.	
BPINAOOH	0.1	see notes	0.	
BPINENE	0.1	see notes	0.	
C106O2	0.1	see notes	0.	
C106OOH	0.1	see notes	0.	
C109CO	0.1	see notes	0.	
C109O2	0.1	see notes	0.	
C109OOH	0.1	see notes	0.	
C96CO3	0.1	see notes	0.	
CAMPHENE	0.1	see notes	0.	
CARENE	0.1	see notes	0.	
MENTHEN6ONE	0.1	see notes	0.	
OH2MENTHEN6ONE	0.1	see notes	0.	
OHMENTHEN6ONEO2	0.1	see notes	0.	
PERPINONIC	0.1	see notes	0.	
PINAL	0.1	see notes	0.	
PINALO2	0.1	see notes	0.	
PINALOOH	0.1	see notes	0.	
PINENOL	0.1	see notes	0.	
PINONIC	0.1	see notes	0.	
RO6R1O2	0.1	see notes	0.	
RO6R3O2	0.1	see notes	0.	
ROO6R1O2	0.1	see notes	0.	
SABINENE	0.1	see notes	0.	
BPINANO3	0.1	see notes	0.	
C106NO3	0.1	see notes	0.	
C10PAN2	0.1	see notes	0.	
PINALNO3	0.1	see notes	0.	
RO6R1NO3	0.1	see notes	0.	
ROO6R1NO3	0.1	see notes	0.	
LAPINABNO3	0.1	see notes	0.	
LAPINABO2	0.1	see notes	0.	
LAPINABOOH	0.1	see notes	0.	
LNAPINABO2	0.1	see notes	0.	
LNAPINABOOH	0.1	see notes	0.	
LNBPINABO2	0.1	see notes	0.	
LNBPINABOOH	0.1	see notes	0.	
LHAROM	0.1	see notes	0.	
LFLUORINE	0.1	see notes	0.	
CHF3	0.1	see notes	0.	
CHF2CF3	0.1	see notes	0.	
CH3CF3	0.1	see notes	0.	
CH2F2	0.1	see notes	0.	
CH3CHF2	0.1	see notes	0.	
CCl4	0.1	see notes	0.	
CF2Cl2	0.1	see notes	0.	
CF2ClCF2Cl	0.1	see notes	0.	
CF2ClCFCl2	0.1	see notes	0.	
CF3CF2Cl	0.1	see notes	0.	
CFCl3	0.1	see notes	0.	
CH2Cl2	0.1	see notes	0.	

Table 8: Accommodation coefficients (continued...)

KPP name	$\alpha^{\ominus}$	Reference	α-T-dep	Reference
CH2FCF3	0.1	see notes	0.	
CH3CCl3	0.1	see notes	0.	
CH3CFCl2	0.1	see notes	0.	
CH3Cl	0.1	see notes	0.	
CHCl3	0.1	see notes	0.	
CHF2Cl	0.1	see notes	0.	
Cl	0.1	see notes	0.	
Cl2	0.038	Hu et al. (1995)	6546.	
Cl2O2	0.1	see notes	0.	
ClNO2	0.1	see notes	0.	
ClNO3	0.108	Deiber et al. (2004)	0.	
ClO	0.1	see notes	0.	
HCl	0.074	Schweitzer et al. (2000)	3072.	
HOCl	0.5	see notes	0.	
OClO	0.1	see notes	0.	
LCHLORINE	0.1	see notes	0.	
Br	0.1	see notes	0.	
Br2	0.038	Hu et al. (1995)	6546.	
BrCl	0.038	see notes	6546.	
BrNO2	0.1	see notes	0.	
BrNO3	0.063	Deiber et al. (2004)	0.	
BrO	0.1	see notes	0.	
CF2ClBr	0.1	see notes	0.	
CF3Br	0.1	see notes	0.	
CH2Br2	0.1	see notes	0.	
CH2ClBr	0.1	see notes	0.	
CH3Br	0.1	see notes	0.	
CHBr3	0.1	see notes	0.	
CHCl2Br	0.1	see notes	0.	
CHClBr2	0.1	see notes	0.	
HBr	0.032	Schweitzer et al. (2000)	3940.	
HOBr	0.5	Abbatt and Waschewsky (1998)	0.	
LBROMINE	0.1	see notes	0.	
C3H7I	0.1	see notes	0.	
CH2ClI	0.1	see notes	0.	
CH2I2	0.1	see notes	0.	
CH3I	0.1	see notes	0.	
HI	0.036	Schweitzer et al. (2000)	4130.	
HIO3	0.01	see notes	0.	
HOI	0.5	see notes	0.	
I	0.1	see notes	0.	
I2	0.01	see notes	2000.	
I2O2	0.1	see notes	2000.	
IBr	0.018	see notes	2000.	
ICl	0.018	Braban et al. (2007)	2000.	
INO2	0.1	see notes	2000.	
INO3	0.1	see notes	2000.	
IO	0.5	see notes	2000.	
IPART	0.1	see notes	0.	
OIO	0.01	see notes	0.	
CH3SO2	0.1	see notes	0.	
CH3SO3	0.1	see notes	0.	
CH3SO3H	0.076	De Bruyn et al. (1994)	1762.	
DMS	0.1	see notes	0.	

Table 8: Accommodation coefficients (continued...)

KPP name	$\alpha^{\ominus}$	Reference	α-T-dep	Reference
DMSO	0.048	De Bruyn et al. (1994)	2578.	
H2SO4	0.65	Pöschl et al. (1998)	0.	
OCS	0.1	see notes	0.	
S	0.1	see notes	0.	
SF6	0.1	see notes	0.	
SH	0.1	see notes	0.	
SO	0.1	see notes	0.	
SO2	0.11	DeMore et al. (1997)	0.	
SO3	0.1	see notes	0.	
LSULFUR	0.1	see notes	0.	
Hg	0.1	see notes	0.	
HgO	0.1	see notes	0.	
HgCl	0.1	see notes	0.	
HgCl2	0.1	see notes	0.	
HgBr	0.1	see notes	0.	
HgBr2	0.1	see notes	0.	
ClHgBr	0.1	see notes	0.	
BrHgOBr	0.1	see notes	0.	
ClHgOBr	0.1	see notes	0.	
RGM	0.1	see notes	0.	
LTERP	0.1	see notes	0.	
LALK4	0.1	see notes	0.	
LALK5	0.1	see notes	0.	
LARO1	0.1	see notes	0.	
LARO2	0.1	see notes	0.	
LOLE1	0.1	see notes	0.	
LOLE2	0.1	see notes	0.	
LfPOG02	0.1	see notes	0.	
LfPOG03	0.1	see notes	0.	
LfPOG04	0.1	see notes	0.	
LfPOG05	0.1	see notes	0.	
LbbPOG02	0.1	see notes	0.	
LbbPOG03	0.1	see notes	0.	
LbbPOG04	0.1	see notes	0.	
LfSOGsv01	0.1	see notes	0.	
LfSOGsv02	0.1	see notes	0.	
LbbSOGsv01	0.1	see notes	0.	
LbbSOGsv02	0.1	see notes	0.	
LfSOGiv01	0.1	see notes	0.	
LfSOGiv02	0.1	see notes	0.	
LfSOGiv03	0.1	see notes	0.	
LfSOGiv04	0.1	see notes	0.	
LbbSOGiv01	0.1	see notes	0.	
LbbSOGiv02	0.1	see notes	0.	
LbbSOGiv03	0.1	see notes	0.	
LbSOGv01	0.1	see notes	0.	
LbSOGv02	0.1	see notes	0.	
LbSOGv03	0.1	see notes	0.	
LbSOGv04	0.1	see notes	0.	
LbOSOGv01	0.1	see notes	0.	
LbOSOGv02	0.1	see notes	0.	
LbOSOGv03	0.1	see notes	0.	
LaSOGv01	0.1	see notes	0.	
LaSOGv02	0.1	see notes	0.	

Table 8: Accommodation coefficients (continued...)

KPP name	$\alpha^{\ominus}$	Reference	α-T-dep	Reference
LaSOGv03	0.1	see notes	0.	
LaSOGv04	0.1	see notes	0.	
LaOSOGv01	0.1	see notes	0.	
LaOSOGv02	0.1	see notes	0.	
LaOSOGv03	0.1	see notes	0.	
ISO2	0.1	see notes	0.	
ISON	0.1	see notes	0.	
ISOOH	0.1	see notes	0.	
LHOC3H6O2	0.1	see notes	0.	
LHOC3H6OOH	0.1	see notes	0.	
MVKO2	0.1	see notes	0.	
MVKOOH	0.1	see notes	0.	
NACA	0.1	see notes	0.	
ONE	0.1	see notes	0.	
O	0.1	see notes	0.	
C	0.1	see notes	0.	
OXL	0.1	see notes	0.	
O2m	0.1	see notes	0.	
OHm	0.1	see notes	0.	
Hp	0.1	see notes	0.	
NH4p	0.1	see notes	0.	
NO2m	0.1	see notes	0.	
NO3m	0.1	see notes	0.	
NO4m	0.1	see notes	0.	
CO3m	0.1	see notes	0.	
CO3mm	0.1	see notes	0.	
HCO3m	0.1	see notes	0.	
HCOOm	0.1	see notes	0.	
CH3COOm	0.1	see notes	0.	
HOCH2CO2m	0.1	see notes	0.	
OXLm	0.1	see notes	0.	
OXLmm	0.1	see notes	0.	
CH3COCO2Hm	0.1	see notes	0.	
Clm	0.1	see notes	0.	
Cl2m	0.1	see notes	0.	
ClOm	0.1	see notes	0.	
ClOHm	0.1	see notes	0.	
Brm	0.1	see notes	0.	
Br2m	0.1	see notes	0.	
BrOm	0.1	see notes	0.	
BrOHm	0.1	see notes	0.	
BrCl2m	0.1	see notes	0.	
Br2Clm	0.1	see notes	0.	
Im	0.1	see notes	0.	
IO2m	0.1	see notes	0.	
IO3m	0.1	see notes	0.	
ICl2m	0.1	see notes	0.	
IBr2m	0.1	see notes	0.	
IClBrm	0.1	see notes	0.	
SO3m	0.1	see notes	0.	
SO3mm	0.1	see notes	0.	
SO4m	0.1	see notes	0.	
SO4mm	0.1	see notes	0.	
SO5m	0.1	see notes	0.	

Table 8: Accommodation coefficients (continued...)

KPP name	$\alpha^{\ominus}$	Reference	α-T-dep	Reference
HSO3m	0.1	see notes	0.	
HSO4m	0.1	see notes	0.	
HSO5m	0.1	see notes	0.	
CH3SO3m	0.1	see notes	0.	
CH2OHSO3m	0.1	see notes	0.	
Nap	0.1	see notes	0.	
Kp	0.1	see notes	0.	
Mgpp	0.1	see notes	0.	
Capp	0.1	see notes	0.	
Fepp	0.1	see notes	0.	
Feppp	0.1	see notes	0.	

Notes

Henry's law constants

- BIG_DP is a large number that represents infinite solubility in the code.
- The temperature dependence of the Henry constants is:

$$K_{\mathrm{H}} = K_{\mathrm{H}}^{\ominus} \times \exp\left(\frac{-\Delta_{\mathrm{soln}}H}{R}\left(\frac{1}{T} - \frac{1}{T^{\ominus}}\right)\right)$$

  where $\Delta_{\mathrm{soln}}H$ = molar enthalpy of dissolution [J/mol] and $R = 8.314$ J/(mol K).
- **HNO3:** Calculated using the acidity constant from Davis and de Bruin (1964).
- **CH3O2:** This value was estimated by Jacob (1986).
- **C2H5O2:** Assumed to be the same as for CH3O2.
- **HOCH2CO3H:** Estimate.
- **HOOCH2CO2H:** Estimate.
- **HBr:** Calculated using the acidity constant from Lax (1969).
- **HOBr:** Twice the value of HOCl, according to Blatchley et al. (1992). Same temperature dependence as for HOCl assumed.
- **IO:** Assumed to be the same as for HOI.
- **HOI:** Lower limit.
- **ICl:** Calculated using thermodynamic data from Wagman et al. (1982).
- **IBr:** Calculated using thermodynamic data from Wagman et al. (1982).
- **H2SO4:** To account for the very high Henry's law coefficient of H2SO4, a very high value was chosen arbitrarily.
- **DMSO:** Lower limit cited from another reference.
- **HgCl:** Assumed to be the same as for HgCl2.
- **HgBr:** Assumed to be the same as for HgCl2.
- **HgBr2:** Assumed to be the same as for HgCl2.
- **ClHgBr:** Assumed to be the same as for HgCl2.
- **BrHgOBr:** Assumed to be the same as for HgCl2.
- **ClHgOBr:** Assumed to be the same as for HgCl2.

Accommodation coefficients

- If the accommodation coefficient is not known, a value of $\alpha = 0.1$ is assumed.
- The temperature dependence of the accommodation coefficients is given by (Jayne et al., 1991):

$$\begin{aligned}\frac{\alpha}{1-\alpha} &= \exp\left(\frac{-\Delta_{\mathrm{obs}}G}{RT}\right) \\ &= \exp\left(\frac{-\Delta_{\mathrm{obs}}H}{RT} + \frac{\Delta_{\mathrm{obs}}S}{R}\right)\end{aligned}$$

where $\Delta_{\mathrm{obs}}G$ is the Gibbs free energy barrier of the transition state toward solution (Jayne et al., 1991), and $\Delta_{\mathrm{obs}}H$ and $\Delta_{\mathrm{obs}}S$ are the corresponding enthalpy and entropy, respectively. The equation can be rearranged to:

$$\ln\left(\frac{\alpha}{1-\alpha}\right) = \frac{-\Delta_{\mathrm{obs}}H}{R} \times \frac{1}{T} + \frac{-\Delta_{\mathrm{obs}}S}{R}$$

and further:

$$\mathrm{d}\ln\left(\frac{\alpha}{1-\alpha}\right) \Big/ \mathrm{d}\left(\frac{1}{T}\right) = \frac{-\Delta_{\mathrm{obs}}H}{R}$$

- **O2:** Estimate.
- **O3:** Value measured at 292 K.
- **OH:** Value measured at 293 K.
- **HO2:** Value for aqueous salts at 293 K.
- **NH3:** Value measured at 295 K.
- **NO:** Value measured between 193 and 243 K.
- **NO2:** Value measured at 298 K.
- **NO3:** Value is a lower limit, measured at 273 K.
- **N2O5:** Value for sulfuric acid, measured between 195 and 300 K.
- **HONO:** Value measured between 247 and 297 K.
- **HNO3:** Value measured at room temperature. Abbatt and Waschewsky (1998) say $\gamma > 0.2$. Here $\alpha = 0.5$ is used.
- **HNO4:** Value measured at 200 K for water ice.
- **CH3O2:** Estimate.
- **CO2:** Estimate.
- **HCHO:** Value measured between 260 and 270 K.
- **PAN:** Estimate.
- **C2H5O2:** Estimate.
- **CH3CHO:** Using the same estimate as in the CAPRAM 2.4 model (Ervens et al., 2003).
- **HCl:** Temperature dependence derived from published data at 2 different temperatures
- **HOCl:** Assumed to be the same as α(HOBr).
- **ClNO3:** Value measured at 274.5 K.
- **HBr:** Temperature dependence derived from published data at 2 different temperatures
- **HOBr:** Value measured at room temperature. Abbatt and Waschewsky (1998) say $\gamma > 0.2$. Here $\alpha = 0.5$ is used.
- **BrNO3:** Value measured at 273 K.
- **BrCl:** Assumed to be the same as α(Cl2).
- **I2:** Estimate.
- **IO:** Estimate.

- **OIO:** Estimate.
- **I2O2:** Estimate.
- **HI:** Temperature dependence derived from published data at 2 different temperatures
- **HOI:** Assumed to be the same as α(HOBr). See also Mössinger and Cox (2001) and Holmes et al. (2001).
- **HIO3:** Estimate.
- **INO2:** Estimate.
- **INO3:** Estimate.
- **ICl:** Estimate.
- **IBr:** Assumed to be the same as α(ICl).
- **H2SO4:** Value measured at 303 K.
- **Hg:** Estimate.
- **HgO:** Estimate.
- **HgCl2:** Estimate.
- **HgBr2:** Estimate.
- **ClHgBr:** Estimate.
- **BrHgOBr:** Estimate.
- **ClHgOBr:** Estimate.

Acid/base constants

- **pinic acid:** The same R_K_acid and R_K_acid2 values as for succinic acid from Haynes (2014) are used.
- **norpinic acid:** The same R_K_acid and R_K_acid2 values as for succinic acid from Haynes (2014) are used.
- **H2SO4:** From Wikipedia.

References

Abbatt, J. P. D. and Waschewsky, G. C. G.: Heterogeneous interactions of HOBr, HNO_3, O_3, and NO_2 with deliquescent NaCl aerosols at room temperature, J. Phys. Chem. A, 102, 3719–3725, doi:10.1021/JP980932D, 1998.

Abraham, M. H.: Thermodynamics of solution of homologous series of solutes in water, J. Chem. Soc. Faraday Trans. 1, 80, 153–181, doi:10.1039/F19848000153, 1984.

Andersson, M. E., Gårdfeldt, K., Wängberg, I., and Strömberg, D.: Determination of Henry's law constant for elemental mercury, Chemosphere, 73, 587–592, doi:10.1016/J.CHEMOSPHERE.2008.05.067, 2008.

Bartlett, W. P. and Margerum, D. W.: Temperature dependencies of the Henry's law constant and the aqueous phase dissociation constant of bromine chloride, Environ. Sci. Technol., 33, 3410–3414, doi:10.1021/ES990300K, 1999.

Berdnikov, V. M. and Bazhin, N. M.: Oxidation-reduction potentials of certain inorganic radicals in aqueous solutions, Russ. J. Phys. Chem., 44, 395–398, 1970.

Blatchley, III, E. R., Johnson, R. W., Alleman, J. E., and McCoy, W. F.: Effective Henry's law constants for free chlorine and free bromine, Wat. Res., 26, 99–106, doi:10.1016/0043-1354(92)90117-M, 1992.

Bone, R., Cullis, P., and Wolfenden, R.: Solvent effects on equilibria of addition of nucleophiles to acetaldehyde and the hydrophilic character of diols, J. Am. Chem. Soc., 105, 1339–1343, doi:10.1021/ja00343a044, 1983.

Braban, C. F., Adams, J. W., Rodriguez, D., Cox, R. A., Crowley, J. N., and Schuster, G.: Heterogeneous reactions of HOI, ICl and IBr on sea salt and sea salt proxies, Phys. Chem. Chem. Phys., 9, 3136–3148, doi:10.1039/B700829E, 2007.

Brimblecombe, P. and Clegg, S. L.: Erratum, J. Atmos. Chem., 8, 95, doi:10.1007/BF00053818, 1989.

Brimblecombe, P., Clegg, S. L., and Khan, I.: Thermodynamic properties of carboxylic acids relevant to their solubility in aqueous solutions, J. Aerosol Sci., 23, S901–S904, doi:10.1016/0021-8502(92)90557-C, 1992.

Burkholder, J. B., Sander, S. P., Abbatt, J., Barker, J. R., Huie, R. E., Kolb, C. E., Kurylo, M. J., Orkin, V. L., Wilmouth, D. M., and Wine, P. H.: Chemical Kinetics and Photochemical Data for Use in Atmospheric Studies, Evaluation No. 18, JPL Publication 15-10, Jet Propulsion Laboratory, Pasadena, `http://jpldataeval.jpl.nasa.gov`, 2015.

Chatfield, R. B. and Crutzen, P. J.: Are there interactions of iodine and sulfur species in marine air photochemistry?, J. Geophys. Res., 95D, 22 319–22 341, doi:10.1029/JD095ID13P22319, 1990.

Davidovits, P., Hu, J. H., Worsnop, D. R., Zahniser, M. S., and Kolb, C. E.: Entry of gas molecules into liquids, Faraday Discuss., 100, 65–81, doi:10.1039/FD9950000065, 1995.

Davis, Jr., W. and de Bruin, H. J.: New activity coefficients of 0-100 per cent aqueous nitric acid, J. Inorg. Nucl. Chem., 26, 1069–1083, doi:10.1016/0022-1902(64)80268-2, 1964.

De Bruyn, W. J., Shorter, J. A., Davidovits, P., Worsnop, D. R., Zahniser, M. S., and Kolb, C. E.: Uptake of gas-phase sulfur species methanesulfonic acid, dimethylsulfoxide, and dimethyl sulfone by aqueous surfaces, J. Geophys. Res., 99D, 16 927–16 932, doi:10.1029/94JD00684, 1994.

Deiber, G., George, C., Le Calvé, S., Schweitzer, F., and Mirabel, P.: Uptake study of $ClONO_2$ and $BrONO_2$ by halide containing droplets, Atmos. Chem. Phys., 4, 1291–1299, doi:10.5194/ACP-4-1291-2004, 2004.

DeMore, W. B., Sander, S. P., Golden, D. M., Hampson, R. F., Kurylo, M. J., Howard, C. J., Ravishankara, A. R., Kolb, C. E., and Molina, M. J.: Chemical kinetics and photochemical data for use in stratospheric modeling. Evaluation number 12, JPL Publication 97-4, Jet Propulsion Laboratory, Pasadena, CA, 1997.

Dong, H., Du, H., and Qian, X.: Theoretical prediction of pKa values for methacrylic acid oligomers using combined quantum mechanical and continuum solvation methods, J. Phys. Chem. A, 112, 12 687–12 694, doi:10.1021/jp807315p, 2008.

Ervens, B., George, C., Williams, J. E., Buxton, G. V., Salmon, G. A., Bydder, M., Wilkinson, F., Dentener, F., Mirabel, P., Wolke, R., and Herrmann, H.: CAPRAM 2.4 (MODAC mechanism): An extended and condensed tropospheric aqueous phase mechanism and its application, J. Geophys. Res., 108D, 4426, doi:10.1029/2002JD002202, 2003.

Fried, A., Henry, B. E., Calvert, J. G., and Mozurkewich, M.: The reaction probability of N_2O_5 with sulfuric acid aerosols at stratospheric temperatures and compositions, J. Geophys. Res., 99D, 3517–3532, doi:10.1029/93JD01907, 1994.

Goldstein, D. J.: Air and steam stripping of toxic pollutants, Tech. Rep. EPA-68-03-002, Industrial Environmental Research Laboratory, Cincinnati, OH, USA, 1982.

Hanson, D. R., Burkholder, J. B., Howard, C. J., and Ravishankara, A. R.: Measurement of OH and HO_2 radical uptake coefficients on water and sulfuric acid surfaces, J. Phys. Chem., 96, 4979–4985, doi:10.1021/J100191A046, 1992.

Haynes, W. M., ed.: CRC Handbook of Chemistry and Physics, 95th Edition (Internet Version 2015), Taylor and Francis Group, 2014.

Holmes, N. S., Adams, J. W., and Crowley, J. N.: Uptake and reaction of HOI and $IONO_2$ on frozen and dry NaCl/NaBr surfaces and H_2SO_4, Phys. Chem. Chem. Phys., 3, 1679–1687, doi:10.1039/B100247N, 2001.

Hu, J. H., Shi, Q., Davidovits, P., Worsnop, D. R., Zahniser, M. S., and Kolb, C. E.: Reactive uptake of Cl_2(g) and Br_2(g) by aqueous surfaces as a function of Br^- and I^- ion concentration: The effect of chemical reaction at the interface, J. Phys. Chem., 99, 8768–8776, doi:10.1021/J100021A050, 1995.

Jacob, D. J.: Chemistry of OH in remote clouds and its role in the production of formic acid and peroxymonosulfate, J. Geophys. Res., 91D, 9807–9826, doi:10.1029/JD091ID09P09807, 1986.

Jayne, J. T., Duan, S. X., Davidovits, P., Worsnop, D. R., Zahniser, M. S., and Kolb, C. E.: Uptake of gas-phase alcohol and organic acid molecules by water surfaces, J. Phys. Chem., 95, 6329–6336, doi:10.1021/J100169A047, 1991.

Ji, C. and Evans, E. M.: Using an internal standard method to determine Henry's law constants, Environ. Toxicol. Chem., 26, 231–236, doi:10.1897/06-339R.1, 2007.

Khan, I., Brimblecombe, P., and Clegg, S. L.: The Henry's law constants of pyruvic and methacrylic acids, Environ. Technol., 13, 587–593, doi:10.1080/09593339209385187, 1992.

Khan, I., Brimblecombe, P., and Clegg, S. L.: Solubilities of pyruvic acid and the lower (C_1-C_6) carboxylic acids. Experimental determination of equilibrium vapour pressures above pure aqueous and salt solutions, J. Atmos. Chem., 22, 285–302, doi:10.1007/BF00696639, 1995.

Lax, E.: Taschenbuch für Chemiker und Physiker, Springer Verlag, Berlin, 1969.

Leriche, M., Voisin, D., Chaumerliac, N., Monod, A., and Aumont, B.: A model for tropospheric multiphase chemistry: application to one cloudy event during the CIME experiment, Atmos. Environ., 34, 5015–5036, doi:10.1016/S1352-2310(00)00329-0, 2000.

Lide, D. R., ed.: CRC Handbook of Chemistry and Physics, 88th Edition (Internet Version 2008), CRC Press/Taylor and Francis, Boca Raton, FL, 2008.

Lind, J. A. and Kok, G. L.: Correction to "Henry's law determinations for aqueous solutions of hydrogen peroxide, methylhydroperoxide, and peroxyacetic acid" by John A. Lind and Gregory L. Kok, J. Geophys. Res., 99D, 21 119, 1994.

Magi, L., Schweitzer, F., Pallares, C., Cherif, S., Mirabel, P., and George, C.: Investigation of the uptake rate of ozone and methyl hydroperoxide by water surfaces, J. Phys. Chem. A, 101, 4943–4949, doi:10.1021/JP970646M, 1997.

Mössinger, J. C. and Cox, R. A.: Heterogeneous reaction of HOI with sodium halide salts, J. Phys. Chem. A, 105, 5165–5177, doi:10.1021/JP0044678, 2001.

O'Sullivan, D. W., Lee, M., Noone, B. C., and Heikes, B. G.: Henry's law constant determinations for hydrogen peroxide, methyl hydroperoxide, hydroxymethyl hydroperoxide, ethyl hydroperoxide, and peroxyacetic acid, J. Phys. Chem., 100, 3241–3247, doi:10.1021/JP951168N, 1996.

Palmer, D. A., Ramette, R. W., and Mesmer, R. E.: The hydrolysis of iodine: Equilibria at high temperatures, J. Nucl. Mater., 130, 280–286, doi:10.1016/0022-3115(85)90317-4, 1985.

Pandis, S. N. and Seinfeld, J. H.: Sensitivity analysis of a chemical mechanism for aqueous-phase atmospheric chemistry, J. Geophys. Res., 94D, 1105–1126, doi:10.1029/JD094ID01P01105, 1989.

Ponche, J. L., George, C., and Mirabel, P.: Mass transfer at the air/water interface: Mass accommodation coefficients of SO_2, HNO_3, NO_2 and NH_3, J. Atmos. Chem., 16, 1–21, doi:10.1007/BF00696620, 1993.

Pöschl, U., Canagaratna, M., Jayne, J. T., Molina, L. T., Worsnop, D. R., Kolb, C. E., and Molina, M. J.: Mass accommodation coefficient of H_2SO_4 vapor on aqueous sulfuric acid surfaces and gaseous diffusion coefficient of H_2SO_4 in N_2/H_2O, J. Phys. Chem. A, 102, 10 082–10 089, doi:10.1021/JP982809S, 1998.

Régimbal, J.-M. and Mozurkewich, M.: Peroxynitric acid decay mechanisms and kinetics at low pH, J. Phys. Chem. A, 101, 8822–8829, doi:10.1021/JP971908N, 1997.

Rosanka, S., Sander, R., Wahner, A., and Taraborrelli, D.: Oxidation of low-molecular weight organic compounds in cloud droplets: development of the JAMOC chemical mechanism in CAABA/MECCA (version 4.5.0gmdd), Geosci. Model Dev. Discuss., doi:10.5194/gmd-2020-337, 2021.

Rudich, Y., Talukdar, R. K., Imamura, T., Fox, R. W., and Ravishankara, A. R.: Uptake of NO_3 on KI solutions: Rate coefficient for the $NO_3 + I^-$ reaction and gas-phase diffusion coefficients for NO_3, Chem. Phys. Lett., 261, 467–473, doi:10.1016/0009-2614(96)00980-3, 1996.

Saastad, O. W., Ellermann, T., and Nielsen, C. J.: On the adsorption of NO and NO_2 on cold H_2O/H_2SO_4 surfaces, Geophys. Res. Lett., 20, 1191–1193, doi:10.1029/93GL01621, 1993.

Sander, R.: Compilation of Henry's law constants (version 4.0) for water as solvent, Atmos. Chem. Phys., 15, 4399–4981, doi:10.5194/acp-15-4399-2015, 2015.

Sander, S. P., Abbatt, J., Barker, J. R., Burkholder, J. B., Friedl, R. R., Golden, D. M., Huie, R. E., Kolb, C. E., Kurylo, M. J., Moortgat, G. K., Orkin, V. L., and Wine, P. H.: Chemical Kinetics and Photochemical Data for Use in Atmospheric Studies, Evaluation No. 17, JPL Publication 10-6, Jet Propulsion Laboratory, Pasadena, `http://jpldataeval.jpl.nasa.gov`, 2011.

Saxena, P. and Hildemann, L. M.: Water-soluble organics in atmospheric particles: A critical review of the literature and application of thermodynamics to identify candidate compounds, J. Atmos. Chem., 24, 57–109, doi:10.1007/BF00053823, 1996.

Schwartz, S. E. and White, W. H.: Solubility equilibria of the nitrogen oxides and oxyacids in dilute aqueous solution, in: Advances in Environmental Science and Engineering, edited by Pfafflin, J. R. and Ziegler, E. N., vol. 4, pp. 1–45, Gordon and Breach Science Publishers, NY, 1981.

Schweitzer, F., Mirabel, P., and George, C.: Uptake of hydrogen halides by water droplets, J. Phys. Chem. A, 104, 72–76, doi:10.1021/JP992621O, 2000.

Shon, Z.-H., Kim, K.-H., Kim, M.-Y., and Lee, M.: Modeling study of reactive gaseous mercury in the urban air, Atmos. Environ., 39, 749–761, doi:10.1016/J.ATMOSENV.2004.09.071, 2005.

Snider, J. R. and Dawson, G. A.: Tropospheric light alcohols, carbonyls, and acetonitrile: Concentrations in the southwestern United States and Henry's law data, J. Geophys. Res., 90D, 3797–3805, doi:10.1029/JD090ID02P03797, 1985.

Takami, A., Kato, S., Shimono, A., and Koda, S.: Uptake coefficient of OH radical on aqueous surface, Chem. Phys., 231, 215–227, doi:10.1016/S0301-0104(98)00004-4, 1998.

Taraborrelli, D.: Estimated value, unpublished, 2020.

Thornton, J. and Abbatt, J. P. D.: Measurements of HO_2 uptake to aqueous aerosol: Mass accommodation coefficients and net reactive loss, J. Geophys. Res., 110D, doi:10.1029/2004JD005402, 2005.

US EPA: Estimation Programs Interface Suite™ for Microsoft® Windows, `https://www.epa.gov/tsca-screening-tools/epi-suitetm-estimation-program-interface`, Washington, DC, USA, 2012.

Wagman, D. D., Evans, W. H., Parker, V. B., Schumm, R. H., Halow, I., Bailey, S. M., Churney, K. L., and Nuttall, R. L.: The NBS tables of chemical thermodynamic properties; Selected values for inorganic and C_1 and C_2 organic substances in SI units, J. Phys. Chem. Ref. Data, 11, suppl. 2, 1982.

Warneck, P.: The relative importance of various pathways for the oxidation of sulfur dioxide and nitrogen dioxide in sunlit continental fair weather clouds, Phys. Chem. Chem. Phys., 1, 5471–5483, doi:10.1039/A906558J, 1999.

Watts, S. F. and Brimblecombe, P.: The Henry's law constant of dimethyl sulphoxide, Environ. Technol. Lett., 8, 483–486, doi:10.1080/09593338709384509, 1987.

Wilhelm, E., Battino, R., and Wilcock, R. J.: Low-pressure solubility of gases in liquid water, Chem. Rev., 77, 219–262, doi:10.1021/CR60306A003, 1977.

Worsnop, D. R., Zahniser, M. S., Kolb, C. E., Gardner, J. A., Watson, L. R., van Doren, J. M., Jayne, J. T., and Davidovits, P.: The temperature dependence of mass accommodation of SO_2 and H_2O_2 on aqueous surfaces, J. Phys. Chem., 93, 1159–1172, doi:10.1021/J100340A027, 1989.

Bibliography

This bibliography list includes all references used within the main text of this PhD thesis. For references within each manuscript and their supplemental material, please consult their respective reference lists.

Akagi, S. K., Yokelson, R. J., Wiedinmyer, C., Alvarado, M. J., Reid, J. S., Karl, T., Crounse, J. D., and Wennberg, P. O.: Emission factors for open and domestic biomass burning for use in atmospheric models, Atmospheric Chemistry and Physics, 11, 4039–4072, https://doi.org/10.5194/acp-11-4039-2011, 2011.

Arey, J., Aschmann, S. M., Kwok, E. S. C., and Atkinson, R.: Alkyl Nitrate, Hydroxyalkyl Nitrate, and Hydroxycarbonyl Formation from the NO_x-Air Photooxidations of C_5-C_8 n-Alkanes, The Journal of Physical Chemistry A, 105, 1020–1027, https://doi.org/10.1021/jp003292z, 2001.

Atkinson, R.: A structure-activity relationship for the estimation of rate constants for the gas-phase reactions of OH radicals with organic compounds, International Journal of Chemical Kinetics, 19, 799–828, https://doi.org/10.1002/kin.550190903, 1987.

Atkinson, R., Baulch, D. L., Cox, R. A., Crowley, J. N., Hampson, R. F., Hynes, R. G., Jenkin, M. E., Rossi, M. J., Troe, J., and Subcommittee, I.: Evaluated kinetic and photochemical data for atmospheric chemistry: Volume II – gas phase reactions of organic species, Atmospheric Chemistry and Physics, 6, 3625–4055, https://doi.org/10.5194/acp-6-3625-2006, 2006.

Barnes, I., Becker, K. H., and Zhu, T.: Near UV absorption spectra and photolysis products of difunctional organic nitrates: Possible importance as NOxreservoirs, Journal of Atmospheric Chemistry, 17, 353–373, https://doi.org/10.1007/BF00696854, 1993.

Barnes, I., Solignac, G., Mellouki, A., and Becker, K. H.: Aspects of the Atmospheric Chemistry of Amides, ChemPhysChem, 11, 3844–3857, https://doi.org/10.1002/cphc.201000374, 2010.

Behar, D.: Pulse radiolysis study of aqueous hydrogen cyanide and cyanide solutions, The Journal of Physical Chemistry, 78, 2660–2663, https://doi.org/10.1021/j100619a005, 1974.

Bejan, I., Abd El Aal, Y., Barnes, I., Benter, T., Bohn, B., Wiesen, P., and Kleffmann, J.: The photolysis of ortho-nitrophenols: a new gas phase source of HONO, Phys. Chem. Chem. Phys., 8, 2028–2035, https://doi.org/10.1039/B516590C, 2006.

Blando, J. D. and Turpin, B. J.: Secondary organic aerosol formation in cloud and fog droplets: a literature evaluation of plausibility, Atmospheric Environment, 34, 1623 – 1632, https://doi.org/10.1016/S1352-2310(99)00392-1, 2000.

Bloss, C., Wagner, V., Jenkin, M. E., Volkamer, R., Bloss, W. J., Lee, J. D., Heard, D. E., Wirtz, K., Martin-Reviejo, M., Rea, G., Wenger, J. C., and Pilling, M. J.: Development of a detailed chemical mechanism (MCMv3.1) for the atmospheric oxidation of aromatic hydrocarbons, Atmospheric Chemistry and Physics, 5, 641–664, https://doi.org/10.5194/acp-5-641-2005, 2005.

Borduas, N., Place, B., Wentworth, G. R., Abbatt, J. P. D., and Murphy, J. G.: Solubility and reactivity of HNCO in water: insights into HNCO's fate in the atmosphere, Atmospheric Chemistry and Physics, 16, 703–714, https://doi.org/10.5194/acp-16-703-2016, 2016.

Bott, A. and Zdunkowski, W.: Electromagnetic energy within dielectric spheres, J. Opt. Soc. Am. A, 4, 1361–1365, https://doi.org/10.1364/JOSAA.4.001361, 1987.

Bunkan, A. J. C., Mikoviny, T., Nielsen, C. J., Wisthaler, A., and Zhu, L.: Experimental and Theoretical Study of the OH-Initiated Photo-oxidation of Formamide, The Journal of Physical Chemistry A, 120, 1222–1230, https://doi.org/10.1021/acs.jpca.6b00032, PMID: 26859252, 2016.

Cabrera Perez, C. D.: Simple monocyclic aromatic compounds from a global scale perspective, Ph.D. thesis, University Mainz, URL `https://openscience.ub.uni-mainz.de/handle/20.500.12030/880`, 2017.

Cabrera-Perez, D., Taraborrelli, D., Sander, R., and Pozzer, A.: Global atmospheric budget of simple monocyclic aromatic compounds, Atmospheric Chemistry and Physics, 16, 6931–6947, https://doi.org/10.5194/acp-16-6931-2016, 2016.

Calvert, J., Mellouki, A., and Orlando, J.: Mechanisms of atmospheric oxidation of the oxygenates, OUP USA, 2011.

Calvert, J. G., Derwent, R. G., Orlando, J. J., Wallington, T. J., and Tyndall, G. S.: Mechanisms of atmospheric oxidation of the alkanes, OUP USA, 2008.

Capouet, M., Müller, J.-F., Ceulemans, K., Compernolle, S., Vereecken, L., and Peeters, J.: Modeling aerosol formation in alpha-pinene photo-oxidation experiments, Journal of Geophysical Research: Atmospheres, 113, https://doi.org/10.1029/2007JD008995, 2008.

Chang, D., Lelieveld, J., Tost, H., Steil, B., Pozzer, A., and Yoon, J.: Aerosol physicochemical effects on CCN activation simulated with the

chemistry-climate model EMAC, Atmospheric Environment, 162, 127 – 140, https://doi.org/10.1016/j.atmosenv.2017.03.036, 2017.

Chen, J., Wenger, J. C., and Venables, D. S.: Near-Ultraviolet Absorption Cross Sections of Nitrophenols and Their Potential Influence on Tropospheric Oxidation Capacity, The Journal of Physical Chemistry A, 115, 12 235–12 242, https://doi.org/10.1021/jp206929r, PMID: 21958133, 2011.

Cheng, S.-B., Zhou, C.-H., Yin, H.-M., Sun, J.-L., and Han, K.-L.: OH produced from o-nitrophenol photolysis: A combined experimental and theoretical investigation, The Journal of Chemical Physics, 130, 234 311, https://doi.org/10.1063/1.3152635, 2009.

Clerbaux, C., Boynard, A., Clarisse, L., George, M., Hadji-Lazaro, J., Herbin, H., Hurtmans, D., Pommier, M., Razavi, A., Turquety, S., Wespes, C., and Coheur, P.-F.: Monitoring of atmospheric composition using the thermal infrared IASI/MetOp sounder, Atmospheric Chemistry and Physics, 9, 6041–6054, https://doi.org/10.5194/acp-9-6041-2009, 2009.

Cooper, O. R., Parrish, D. D., Ziemke, J., Balashov, N. V., Cupeiro, M., Galbally, I. E., Gilge, S., Horowitz, L., Jensen, N. R., Lamarque, J.-F., Naik, V., Oltmans, S. J., Schwab, J., Shindell, D. T., Thompson, A. M., Thouret, V., Wang, Y., and Zbinden, R. M.: Global distribution and trends of tropospheric ozone: An observation-based review, Elementa Sci. Anthropocene, 2, 000 029, https://doi.org/10.12952/journal.elementa.000029, 2014.

Crounse, J. D., Knap, H. C., Ørnsø, K. B., Jørgensen, S., Paulot, F., Kjaergaard, H. G., and Wennberg, P. O.: Atmospheric Fate of Methacrolein. 1. Peroxy Radical Isomerization Following Addition of OH and O2, The Journal of Physical Chemistry A, 116, 5756–5762, https://doi.org/10.1021/jp211560u, PMID: 22452246, 2012.

Crutzen, P.: A discussion of the chemistry of some minor constituents in the stratosphere and troposphere, Pure and Applied Geophysics, 106, 1385–1399, https://doi.org/10.1007/BF00881092, 1973.

Deckert, R., Jöckel, P., Grewe, V., Gottschaldt, K.-D., and Hoor, P.: A quasi chemistry-transport model mode for EMAC, Geoscientific Model Development, 4, 195–206, https://doi.org/10.5194/gmd-4-195-2011, 2011.

Deguillaume, L., Leriche, M., Monod, A., and Chaumerliac, N.: The role of transition metal ions on HO_x radicals in clouds: a numerical evaluation of its impact on multiphase chemistry, Atmospheric Chemistry and Physics, 4, 95–110, https://doi.org/10.5194/acp-4-95-2004, 2004.

Dietmüller, S., Jöckel, P., Tost, H., Kunze, M., Gellhorn, C., Brinkop, S., Frömming, C., Ponater, M., Steil, B., Lauer, A., and Hendricks, J.: A new radiation infrastructure for the Modular Earth Submodel System (MESSy, based on version 2.51),

Geoscientific Model Development, 9, 2209–2222, https://doi.org/10.5194/gmd-9-2209-2016, 2016.

Eddingsaas, N. C., VanderVelde, D. G., and Wennberg, P. O.: Kinetics and Products of the Acid-Catalyzed Ring-Opening of Atmospherically Relevant Butyl Epoxy Alcohols, The Journal of Physical Chemistry A, 114, 8106–8113, https://doi.org/10.1021/jp103907c, PMID: 20684583, 2010.

Emmons, L. K., Walters, S., Hess, P. G., Lamarque, J.-F., Pfister, G. G., Fillmore, D., Granier, C., Guenther, A., Kinnison, D., Laepple, T., Orlando, J., Tie, X., Tyndall, G., Wiedinmyer, C., Baughcum, S. L., and Kloster, S.: Description and evaluation of the Model for Ozone and Related chemical Tracers, version 4 (MOZART-4), Geoscientific Model Development, 3, 43–67, https://doi.org/10.5194/gmd-3-43-2010, 2010.

Epstein, S. A. and Nizkorodov, S. A.: A comparison of the chemical sinks of atmospheric organics in the gas and aqueous phase, Atmospheric Chemistry and Physics, 12, 8205–8222, https://doi.org/10.5194/acp-12-8205-2012, 2012.

Ervens, B.: Modeling the Processing of Aerosol and Trace Gases in Clouds and Fogs, Chemical Reviews, 115, 4157–4198, https://doi.org/10.1021/cr5005887, 2015.

Ervens, B. and Volkamer, R.: Glyoxal processing by aerosol multiphase chemistry: towards a kinetic modeling framework of secondary organic aerosol formation in aqueous particles, Atmospheric Chemistry and Physics, 10, 8219–8244, https://doi.org/10.5194/acp-10-8219-2010, 2010.

Ervens, B., Turpin, B. J., and Weber, R. J.: Secondary organic aerosol formation in cloud droplets and aqueous particles (aqSOA): a review of laboratory, field and model studies, Atmospheric Chemistry and Physics, 11, 11 069–11 102, https://doi.org/10.5194/acp-11-11069-2011, 2011.

Fowler, D., Amann, M., Anderson, R., Ashmore, M., Cox, P., Depledge, M., Derwent, D., Grennfelt, P., Hewitt, N., Hov, O., Jenkin, M., Kelly, F., Liss, P. S., Pilling, M., Pyle, J., Slingo, J., and Stevenson, D.: Ground-level ozone in the 21st century: Future trends, impacts and policy implications, vol. 15 (08), Royal Society Science Policy Report, URL `https://ueaeprints.uea.ac.uk/id/eprint/25413/`, 2008.

Fowler, D., Pilegaard, K., Sutton, M., Ambus, P., Raivonen, M., Duyzer, J., Simpson, D., Fagerli, H., Fuzzi, S., Schjoerring, J., Grainer, C., Neftel, A., Isaksen, I., Laj, P., Maione, M., Monks, P., Burkhardt, J., Daemmgen, U., Neirynck, J., Personne, E., Wichink-Kruit, R., Butterbach-Bahl, K., Flechard, C., Tuovinen, J., Coyle, M., Gerosa, G., Loubet, B., Altimir, N., Gruenhage, L., Ammann, C., Cieslik, S., Paoletti, E., Mikkelsen, T., Ro-Poulsen, H., Cellier, P., Cape, J., Horvath, L., Loreto, F., Niinemets, U., Palmer, P., Rinne, J., Misztal, P., Nemitz, E., Nilsson, D., Pryor, S., Gallagher, M., Vesala, T., Skiba, U., Brueggemann, N., Zechmeister-Boltenstern, S., Williams, J., O'Dowd, C., Facchini, M., de Leeuw,

G., Flossman, A., Chaumerliac, N., and Erisman, J.: Atmospheric Composition Change: Ecosystems-Atmosphere interactions, Atmospheric Environment, 43, 5193–5267, https://doi.org/10.1016/j.atmosenv.2009.07.068, 2009.

Franco, B., Clarisse, L., Stavrakou, T., Müller, J.-F., Van Damme, M., Whitburn, S., Hadji-Lazaro, J., Hurtmans, D., Taraborrelli, D., Clerbaux, C., and Coheur, P.-F.: A General Framework for Global Retrievals of Trace Gases From IASI: Application to Methanol, Formic Acid, and PAN, Journal of Geophysical Research: Atmospheres, 123, 13,963–13,984, https://doi.org/10.1029/2018JD029633, 2018.

Gromov, S., Jöckel, P., Sander, R., and Brenninkmeijer, C. A. M.: A kinetic chemistry tagging technique and its application to modelling the stable isotopic composition of atmospheric trace gases, Geoscientific Model Development, 3, 337–364, https://doi.org/10.5194/gmd-3-337-2010, 2010.

Guenther, A., Karl, T., Harley, P., Wiedinmyer, C., Palmer, P. I., and Geron, C.: Estimates of global terrestrial isoprene emissions using MEGAN (Model of Emissions of Gases and Aerosols from Nature), Atmospheric Chemistry and Physics, 6, 3181–3210, https://doi.org/10.5194/acp-6-3181-2006, 2006.

Guenther, A. B., Jiang, X., Heald, C. L., Sakulyanontvittaya, T., Duhl, T., Emmons, L. K., and Wang, X.: The Model of Emissions of Gases and Aerosols from Nature version 2.1 (MEGAN2.1): an extended and updated framework for modeling biogenic emissions, Geoscientific Model Development, 5, 1471–1492, https://doi.org/10.5194/gmd-5-1471-2012, 2012.

Hagemann, S. and Stacke, T.: Impact of the soil hydrology scheme on simulated soil moisture memory, Climate Dynamics, 44, 1731–1750, https://doi.org/10.1007/s00382-014-2221-6, 2015.

Hahnenstein, I., Albert, M., Hasse, H., Kreiter, C. G., and Maurer, G.: NMR Spectroscopic and Densimetric Study of Reaction Kinetics of Formaldehyde Polymer Formation in Water, Deuterium Oxide, and Methanol, Industrial & Engineering Chemistry Research, 34, 440–450, https://doi.org/10.1021/ie00041a003, 1995.

Heil, A., Kaiser, J. W., Van der Werf, G. R., Wooster, M. J., Schultz, M. G., and van der Gon, H. D.: Assessment of the real-time fire emissions (GFASv0) by MACC, European Centre for Medium-Range Weather Forecasts, 2010.

Hems, R. F. and Abbatt, J. P. D.: Aqueous Phase Photo-oxidation of Brown Carbon Nitrophenols: Reaction Kinetics, Mechanism, and Evolution of Light Absorption, ACS Earth and Space Chemistry, 2, 225–234, https://doi.org/10.1021/acsearthspacechem.7b00123, 2018.

Herrmann, H.: Kinetics of Aqueous Phase Reactions Relevant for Atmospheric Chemistry, Chemical Reviews, 103, 4691–4716, https://doi.org/10.1021/cr020658q, 2003.

Herrmann, H., Schaefer, T., Tilgner, A., Styler, S. A., Weller, C., Teich, M., and Otto, T.: Tropospheric Aqueous-Phase Chemistry: Kinetics, Mechanisms, and Its Coupling to a Changing Gas Phase, Chemical Reviews, 115, 4259–4334, https://doi.org/10.1021/cr500447k, PMID: 25950643, 2015.

Huang, G., Brook, R., Crippa, M., Janssens-Maenhout, G., Schieberle, C., Dore, C., Guizzardi, D., Muntean, M., Schaaf, E., and Friedrich, R.: Speciation of anthropogenic emissions of non-methane volatile organic compounds: a global gridded data set for 1970–2012, Atmospheric Chemistry and Physics, 17, 7683–7701, https://doi.org/10.5194/acp-17-7683-2017, 2017.

Hurtmans, D., Coheur, P.-F., Wespes, C., Clarisse, L., Scharf, O., Clerbaux, C., Hadji-Lazaro, J., George, M., and Turquety, S.: FORLI radiative transfer and retrieval code for IASI, Journal of Quantitative Spectroscopy and Radiative Transfer, 113, 1391 – 1408, https://doi.org/10.1016/j.jqsrt.2012.02.036, three Leaders in Spectroscopy, 2012.

Jagiella, S. and Zabel, F.: Reaction of phenylperoxy radicals with NO2 at 298 K, Phys. Chem. Chem. Phys., 9, 5036–5051, https://doi.org/10.1039/B705193J, 2007.

Jenkin, M. E., Saunders, S. M., and Pilling, M. J.: The tropospheric degradation of volatile organic compounds: a protocol for mechanism development, Atmospheric Environment, 31, 81 – 104, https://doi.org/10.1016/S1352-2310(96)00105-7, 1997.

Jenkin, M. E., Shallcross, D. E., and Harvey, J. N.: Development and application of a possible mechanism for the generation of cis-pinic acid from the ozonolysis of α- and β-pinene, Atmospheric Environment, 34, 2837 – 2850, https://doi.org/10.1016/S1352-2310(00)00087-X, 2000.

Jenkin, M. E., Saunders, S. M., Wagner, V., and Pilling, M. J.: Protocol for the development of the Master Chemical Mechanism, MCM v3 (Part B): tropospheric degradation of aromatic volatile organic compounds, Atmospheric Chemistry and Physics, 3, 181–193, https://doi.org/10.5194/acp-3-181-2003, 2003.

Jenkin, M. E., Young, J. C., and Rickard, A. R.: The MCM v3.3.1 degradation scheme for isoprene, Atmospheric Chemistry and Physics, 15, 11 433–11 459, https://doi.org/10.5194/acp-15-11433-2015, 2015.

Jiang, X., Guenther, A., Potosnak, M., Geron, C., Seco, R., Karl, T., Kim, S., Gu, L., and Pallardy, S.: Isoprene emission response to drought and the impact on global atmospheric chemistry, Atmospheric Environment, 183, 69 – 83, https://doi.org/10.1016/j.atmosenv.2018.01.026, 2018.

Jöckel, P., Sander, R., Kerkweg, A., Tost, H., and Lelieveld, J.: Technical Note: The Modular Earth Submodel System (MESSy) - a new approach towards Earth System Modeling, Atmospheric Chemistry and Physics, 5, 433–444, https://doi.org/10.5194/acp-5-433-2005, 2005.

Jöckel, P., Tost, H., Pozzer, A., Brühl, C., Buchholz, J., Ganzeveld, L., Hoor, P., Kerkweg, A., Lawrence, M. G., Sander, R., Steil, B., Stiller, G., Tanarhte, M., Taraborrelli, D., van Aardenne, J., and Lelieveld, J.: The atmospheric chemistry general circulation model ECHAM5/MESSy1: consistent simulation of ozone from the surface to the mesosphere, Atmospheric Chemistry and Physics, 6, 5067–5104, https://doi.org/10.5194/acp-6-5067-2006, 2006.

Jöckel, P., Kerkweg, A., Buchholz-Dietsch, J., Tost, H., Sander, R., and Pozzer, A.: Technical Note: Coupling of chemical processes with the Modular Earth Submodel System (MESSy) submodel TRACER, Atmospheric Chemistry and Physics, 8, 1677–1687, https://doi.org/10.5194/acp-8-1677-2008, 2008.

Jöckel, P., Kerkweg, A., Pozzer, A., Sander, R., Tost, H., Riede, H., Baumgaertner, A., Gromov, S., and Kern, B.: Development cycle 2 of the Modular Earth Submodel System (MESSy2), Geoscientific Model Development, 3, 717–752, https://doi.org/10.5194/gmd-3-717-2010, 2010.

Jöckel, P., Tost, H., Pozzer, A., Kunze, M., Kirner, O., Brenninkmeijer, C. A. M., Brinkop, S., Cai, D. S., Dyroff, C., Eckstein, J., Frank, F., Garny, H., Gottschaldt, K.-D., Graf, P., Grewe, V., Kerkweg, A., Kern, B., Matthes, S., Mertens, M., Meul, S., Neumaier, M., Nützel, M., Oberländer-Hayn, S., Ruhnke, R., Runde, T., Sander, R., Scharffe, D., and Zahn, A.: Earth System Chemistry integrated Modelling (ESCiMo) with the Modular Earth Submodel System (MESSy) version 2.51, Geoscientific Model Development, 9, 1153–1200, https://doi.org/10.5194/gmd-9-1153-2016, 2016.

Jülich Supercomputing Centre: JURECA: Modular supercomputer at Jülich Supercomputing Centre, Journal of large-scale research facilities, 4, https://doi.org/10.17815/jlsrf-4-121-1, 2018.

Jülich Supercomputing Centre: JUWELS: Modular Tier-0/1 Supercomputer at the Jülich Supercomputing Centre, Journal of large-scale research facilities, 5, https://doi.org/10.17815/jlsrf-5-171, 2019.

Kaiser, J. W., Heil, A., Andreae, M. O., Benedetti, A., Chubarova, N., Jones, L., Morcrette, J.-J., Razinger, M., Schultz, M. G., Suttie, M., and van der Werf, G. R.: Biomass burning emissions estimated with a global fire assimilation system based on observed fire radiative power, Biogeosciences, 9, 527–554, https://doi.org/10.5194/bg-9-527-2012, 2012.

Kaufman, Y. J., Justice, C. O., Flynn, L. P., Kendall, J. D., Prins, E. M., Giglio, L., Ward, D. E., Menzel, W. P., and Setzer, A. W.: Potential global fire monitoring from EOS-MODIS, Journal of Geophysical Research: Atmospheres, 103, 32 215–32 238, https://doi.org/10.1029/98JD01644, 1998.

Kerkweg, A., Buchholz, J., Ganzeveld, L., Pozzer, A., Tost, H., and Jöckel, P.: Technical Note: An implementation of the dry removal processes DRY DEPosition and SEDImentation in the Modular Earth Submodel System (MESSy), Atmospheric

Chemistry and Physics, 6, 4617–4632, https://doi.org/10.5194/acp-6-4617-2006, 2006a.

Kerkweg, A., Sander, R., Tost, H., and Jöckel, P.: Technical note: Implementation of prescribed (OFFLEM), calculated (ONLEM), and pseudo-emissions (TNUDGE) of chemical species in the Modular Earth Submodel System (MESSy), Atmospheric Chemistry and Physics, 6, 3603–3609, https://doi.org/10.5194/acp-6-3603-2006, 2006b.

Kerkweg, A., Sander, R., Tost, H., Jöckel, P., and Lelieveld, J.: Technical Note: Simulation of detailed aerosol chemistry on the global scale using MECCA-AERO, Atmospheric Chemistry and Physics, 7, 2973–2985, https://doi.org/10.5194/acp-7-2973-2007, 2007.

Koss, A. R., Sekimoto, K., Gilman, J. B., Selimovic, V., Coggon, M. M., Zarzana, K. J., Yuan, B., Lerner, B. M., Brown, S. S., Jimenez, J. L., Krechmer, J., Roberts, J. M., Warneke, C., Yokelson, R. J., and de Gouw, J.: Non-methane organic gas emissions from biomass burning: identification, quantification, and emission factors from PTR-ToF during the FIREX 2016 laboratory experiment, Atmospheric Chemistry and Physics, 18, 3299–3319, https://doi.org/10.5194/acp-18-3299-2018, 2018.

Kumar, V., Chandra, B. P., and Sinha, V.: Large unexplained suite of chemically reactive compounds present in ambient air due to biomass fires, Scientific Reports, 8, 626, https://doi.org/10.1038/s41598-017-19139-3, 2018.

Kwok, E. S. and Atkinson, R.: Estimation of hydroxyl radical reaction rate constants for gas-phase organic compounds using a structure-reactivity relationship: An update, Atmospheric Environment, 29, 1685 – 1695, https://doi.org/10.1016/1352-2310(95)00069-B, 1995.

Landgraf, J. and Crutzen, P. J.: An Efficient Method for Online Calculations of Photolysis and Heating Rates, Journal of the Atmospheric Sciences, 55, 863–878, https://doi.org/10.1175/1520-0469(1998)055<0863:AEMFOC>2.0.CO;2, 1998.

Leslie, M. D., Ridoli, M., Murphy, J. G., and Borduas-Dedekind, N.: Isocyanic acid (HNCO) and its fate in the atmosphere: a review, Environ. Sci.: Processes Impacts, 21, 793–808, https://doi.org/10.1039/C9EM00003H, 2019.

Leuenberger, C., Ligocki, M. P., and Pankow, J. F.: Trace organic compounds in rain. 4. Identities, concentrations, and scavenging mechanisms for phenols in urban air and rain, Environmental Science & Technology, 19, 1053–1058, https://doi.org/10.1021/es00141a005, PMID: 22288749, 1985.

Lin, S.-J. and Rood, R. B.: Multidimensional Flux-Form Semi-Lagrangian Transport Schemes, Monthly Weather Review, 124, 2046–2070, 1996.

Liu, T., Mickley, L. J., Marlier, M. E., DeFries, R. S., Khan, M. F., Latif, M. T., and Karambelas, A.: Diagnosing spatial biases and uncertainties in global fire

emissions inventories: Indonesia as regional case study, Remote Sensing of Environment, 237, 111 557, https://doi.org/10.1016/j.rse.2019.111557, 2020.

Loreto, F. and Velikova, V.: Isoprene Produced by Leaves Protects the Photosynthetic Apparatus against Ozone Damage, Quenches Ozone Products, and Reduces Lipid Peroxidation of Cellular Membranes, Plant Physiology, 127, 1781–1787, https://doi.org/10.1104/pp.010497, 2001.

Loreto, F., Mannozzi, M., Maris, C., Nascetti, P., Ferranti, F., and Pasqualini, S.: Ozone Quenching Properties of Isoprene and Its Antioxidant Role in Leaves, Plant Physiology, 126, 993–1000, https://doi.org/10.1104/pp.126.3.993, 2001.

Madronich, S. and Calvert, J. G.: Permutation reactions of organic peroxy radicals in the troposphere, Journal of Geophysical Research: Atmospheres, 95, 5697–5715, https://doi.org/10.1029/JD095iD05p05697, 1990.

Mayer, B. and Madronich, S.: Actinic flux and photolysis in water droplets: Mie calculations and geometrical optics limit, Atmospheric Chemistry and Physics, 4, 2241–2250, https://doi.org/10.5194/acp-4-2241-2004, 2004.

Mellouki, A., Wallington, T. J., and Chen, J.: Atmospheric Chemistry of Oxygenated Volatile Organic Compounds: Impacts on Air Quality and Climate, Chemical Reviews, 115, 3984–4014, https://doi.org/10.1021/cr500549n, 2015.

Mertens, J. D., Chang, A. Y., Hanson, R. K., and Bowman, C. T.: A shock tube study of reactions of atomic oxygen with isocyanic acid, International Journal of Chemical Kinetics, 24, 279–295, https://doi.org/10.1002/kin.550240306, 1992.

Messaadia, L., El Dib, G., Ferhati, A., and Chakir, A.: UV–visible spectra and gas-phase rate coefficients for the reaction of 2,3-pentanedione and 2,4-pentanedione with OH radicals, Chemical Physics Letters, 626, 73 – 79, https://doi.org/10.1016/j.cplett.2015.02.032, 2015.

Minerath, E. C. and Elrod, M. J.: Assessing the Potential for Diol and Hydroxy Sulfate Ester Formation from the Reaction of Epoxides in Tropospheric Aerosols, Environmental Science & Technology, 43, 1386–1392, https://doi.org/10.1021/es8029076, PMID: 19350908, 2009.

Mouchel-Vallon, C., Deguillaume, L., Monod, A., Perroux, H., Rose, C., Ghigo, G., Long, Y., Leriche, M., Aumont, B., Patryl, L., Armand, P., and Chaumerliac, N.: CLEPS 1.0: A new protocol for cloud aqueous phase oxidation of VOC mechanisms, Geoscientific Model Development, 10, 1339–1362, https://doi.org/10.5194/gmd-10-1339-2017, 2017.

Müller, J.-F., Peeters, J., and Stavrakou, T.: Fast photolysis of carbonyl nitrates from isoprene, Atmospheric Chemistry and Physics, 14, 2497–2508, https://doi.org/10.5194/acp-14-2497-2014, 2014.

Myhre, G., Shindell, D., Bréon, F., Collins, W., Fuglestvedt, J., Huang, J., Koch, D., Lamarque, J., Lee, D., Mendoza, B., et al.: Anthropogenic and Natural Radiative Forcing, in: Climate Change 2013 – The Physical Science Basis: Working Group I Contribution to the Fifth Assessment Report of the Intergovernmental Panel on Climate Change, p. 659–740, Cambridge University Press, https://doi.org/10.1017/CBO9781107415324.018, 2014.

Nakanishi, H., Morita, H., and Nagakura, S.: Electronic Structures and Spectra of the Keto and Enol Forms of Acetylacetone, Bulletin of the Chemical Society of Japan, 50, 2255–2261, https://doi.org/10.1246/bcsj.50.2255, 1977.

Nguyen, T. L., Peeters, J., and Vereecken, L.: Theoretical study of the gas-phase ozonolysis of β-pinene ($C_{10}H_{16}$), Phys. Chem. Chem. Phys., 11, 5643–5656, https://doi.org/10.1039/B822984H, 2009.

Nielsen, C. J., Herrmann, H., and Weller, C.: Atmospheric chemistry and environmental impact of the use of amines in carbon capture and storage (CCS), Chem. Soc. Rev., 41, 6684–6704, https://doi.org/10.1039/C2CS35059A, 2012.

Novelli, A., Vereecken, L., Bohn, B., Dorn, H.-P., Gkatzelis, G. I., Hofzumahaus, A., Holland, F., Reimer, D., Rohrer, F., Rosanka, S., Taraborrelli, D., Tillmann, R., Wegener, R., Yu, Z., Kiendler-Scharr, A., Wahner, A., and Fuchs, H.: Importance of isomerization reactions for OH radical regeneration from the photo-oxidation of isoprene investigated in the atmospheric simulation chamber SAPHIR, Atmospheric Chemistry and Physics, 20, 3333–3355, https://doi.org/10.5194/acp-20-3333-2020, 2020.

Nölscher, A., Butler, T., Auld, J., Veres, P., Muñoz, A., Taraborrelli, D., Vereecken, L., Lelieveld, J., and Williams, J.: Using total OH reactivity to assess isoprene photooxidation via measurement and model, Atmospheric Environment, 89, 453 – 463, https://doi.org/10.1016/j.atmosenv.2014.02.024, 2014.

Orlando, J. J., Tyndall, G. S., and Paulson, S. E.: Mechanism of the OH-initiated oxidation of methacrolein, Geophysical Research Letters, 26, 2191–2194, https://doi.org/10.1029/1999GL900453, 1999.

Pan, X., Ichoku, C., Chin, M., Bian, H., Darmenov, A., Colarco, P., Ellison, L., Kucsera, T., da Silva, A., Wang, J., Oda, T., and Cui, G.: Six global biomass burning emission datasets: intercomparison and application in one global aerosol model, Atmospheric Chemistry and Physics, 20, 969–994, https://doi.org/10.5194/acp-20-969-2020, 2020.

Paulot, F., Crounse, J. D., Kjaergaard, H. G., Kürten, A., St. Clair, J. M., Seinfeld, J. H., and Wennberg, P. O.: Unexpected Epoxide Formation in the Gas-Phase Photooxidation of Isoprene, Science, 325, 730–733, https://doi.org/10.1126/science.1172910, 2009.

Peeters, J., Boullart, W., Pultau, V., Vandenberk, S., and Vereecken, L.: Structure-Activity Relationship for the Addition of OH to (Poly)alkenes: Site-Specific and Total Rate Constants, The Journal of Physical Chemistry A, 111, 1618–1631, https://doi.org/10.1021/jp066973o, PMID: 17298042, 2007.

Peeters, J., Nguyen, T. L., and Vereecken, L.: HOx radical regeneration in the oxidation of isoprene, Phys. Chem. Chem. Phys., 11, 5935–5939, https://doi.org/10.1039/B908511D, 2009.

Peeters, J., Müller, J.-F., Stavrakou, T., and Nguyen, V. S.: Hydroxyl Radical Recycling in Isoprene Oxidation Driven by Hydrogen Bonding and Hydrogen Tunneling: The Upgraded LIM1 Mechanism, The Journal of Physical Chemistry A, 118, 8625–8643, https://doi.org/10.1021/jp5033146, PMID: 25010574, 2014.

Pozzer, A., Jöckel, P., Sander, R., Williams, J., Ganzeveld, L., and Lelieveld, J.: Technical Note: The MESSy-submodel AIRSEA calculating the air-sea exchange of chemical species, Atmospheric Chemistry and Physics, 6, 5435–5444, https://doi.org/10.5194/acp-6-5435-2006, 2006.

Prather, M. J., Holmes, C. D., and Hsu, J.: Reactive greenhouse gas scenarios: Systematic exploration of uncertainties and the role of atmospheric chemistry, Geophysical Research Letters, 39, https://doi.org/10.1029/2012GL051440, 2012.

Pringle, K. J., Tost, H., Pozzer, A., Pöschl, U., and Lelieveld, J.: Global distribution of the effective aerosol hygroscopicity parameter for CCN activation, Atmospheric Chemistry and Physics, 10, 5241–5255, https://doi.org/10.5194/acp-10-5241-2010, 2010.

Pye, H. O. T., Nenes, A., Alexander, B., Ault, A. P., Barth, M. C., Clegg, S. L., Collett Jr., J. L., Fahey, K. M., Hennigan, C. J., Herrmann, H., Kanakidou, M., Kelly, J. T., Ku, I.-T., McNeill, V. F., Riemer, N., Schaefer, T., Shi, G., Tilgner, A., Walker, J. T., Wang, T., Weber, R., Xing, J., Zaveri, R. A., and Zuend, A.: The acidity of atmospheric particles and clouds, Atmospheric Chemistry and Physics, 20, 4809–4888, https://doi.org/10.5194/acp-20-4809-2020, 2020.

Roberts, J. M., Veres, P. R., Cochran, A. K., Warneke, C., Burling, I. R., Yokelson, R. J., Lerner, B., Gilman, J. B., Kuster, W. C., Fall, R., and de Gouw, J.: Isocyanic acid in the atmosphere and its possible link to smoke-related health effects, Proceedings of the National Academy of Sciences, 108, 8966–8971, https://doi.org/10.1073/pnas.1103352108, 2011.

Roeckner, E., Bäuml, G., Bonaventura, L., Brokopf, R., Esch, M., Giorgetta, M., Hagemann, S., Kirchner, I., Kornblueh, L., Manzini, E., et al.: The atmospheric general circulation model ECHAM 5. PART I: Model description, Max-Planck-Institut für Meteorologie, 2003.

Roeckner, E., Brokopf, R., Esch, M., Giorgetta, M., Hagemann, S., Kornblueh, L., Manzini, E., Schlese, U., and Schulzweida, U.: Sensitivity of Simulated Climate to

Horizontal and Vertical Resolution in the ECHAM5 Atmosphere Model, Journal of Climate, 19, 3771–3791, https://doi.org/10.1175/JCLI3824.1, 2006.

Rosanka, S., Vu, G. H. T., Nguyen, H. M. T., Pham, T. V., Javed, U., Taraborrelli, D., and Vereecken, L.: Atmospheric chemical loss processes of isocyanic acid (HNCO): a combined theoretical kinetic and global modelling study, Atmospheric Chemistry and Physics, 20, 6671–6686, https://doi.org/10.5194/acp-20-6671-2020, 2020.

Rosanka, S., Sander, R., Wahner, A., and Taraborrelli, D.: Oxidation of low-molecular-weight organic compounds in cloud droplets: development of the Jülich Aqueous-phase Mechanism of Organic Chemistry (JAMOC) in CAABA/MECCA (version 4.5.0), Geoscientific Model Development, 14, 4103–4115, https://doi.org/10.5194/gmd-14-4103-2021, 2021a.

Rosanka, S., Sander, R., Franco, B., Wespes, C., Wahner, A., and Taraborrelli, D.: Oxidation of low-molecular-weight organic compounds in cloud droplets: global impact on tropospheric oxidants, Atmospheric Chemistry and Physics, 21, 9909–9930, https://doi.org/10.5194/acp-21-9909-2021, 2021b.

Rosanka, S., Franco, B., Clarisse, L., Coheur, P.-F., Pozzer, A., Wahner, A., and Taraborrelli, D.: The impact of organic pollutants from Indonesian peatland fires on the tropospheric and lower stratospheric composition, Atmospheric Chemistry and Physics, 21, 11 257–11 288, https://doi.org/10.5194/acp-21-11257-2021, 2021c.

Rosanka, S., Sander, R., Wahner, A., and Taraborrelli, D.: Model output from CAABA/MECCA obtained during the development of JAMOC [Data set], https://doi.org/10.26165/JUELICH-DATA/SD9F6B, 2021d.

Sander, R.: Modeling Atmospheric Chemistry: Interactions between Gas-Phase Species and Liquid Cloud/Aerosol Particles, Surveys in Geophysics, 20, 1–31, https://doi.org/10.1023/A:1006501706704, 1999.

Sander, R.: Compilation of Henry's law constants (version 4.0) for water as solvent, Atmospheric Chemistry and Physics, 15, 4399–4981, https://doi.org/10.5194/acp-15-4399-2015, 2015.

Sander, R.: The community atmospheric chemistry box model CAABA/MECCA [Data set], https://doi.org/10.5281/zenodo.4707938, 2021.

Sander, R., Jöckel, P., Kirner, O., Kunert, A. T., Landgraf, J., and Pozzer, A.: The photolysis module JVAL-14, compatible with the MESSy standard, and the JVal PreProcessor (JVPP), Geoscientific Model Development, 7, 2653–2662, https://doi.org/10.5194/gmd-7-2653-2014, 2014.

Sander, R., Baumgaertner, A., Cabrera-Perez, D., Frank, F., Gromov, S., Grooß, J.-U., Harder, H., Huijnen, V., Jöckel, P., Karydis, V. A., Niemeyer, K. E., Pozzer, A., Riede, H., Schultz, M. G., Taraborrelli, D., and Tauer, S.: The community

atmospheric chemistry box model CAABA/MECCA-4.0, Geoscientific Model Development, 12, 1365–1385, https://doi.org/10.5194/gmd-12-1365-2019, 2019.

Sandu, A. and Sander, R.: Technical note: Simulating chemical systems in Fortran90 and Matlab with the Kinetic PreProcessor KPP-2.1, Atmospheric Chemistry and Physics, 6, 187–195, https://doi.org/10.5194/acp-6-187-2006, 2006.

Saunders, S. M., Jenkin, M. E., Derwent, R. G., and Pilling, M. J.: Protocol for the development of the Master Chemical Mechanism, MCM v3 (Part A): tropospheric degradation of non-aromatic volatile organic compounds, Atmospheric Chemistry and Physics, 3, 161–180, https://doi.org/10.5194/acp-3-161-2003, 2003.

Scanza, R. A., Hamilton, D. S., Perez Garcia-Pando, C., Buck, C., Baker, A., and Mahowald, N. M.: Atmospheric processing of iron in mineral and combustion aerosols: development of an intermediate-complexity mechanism suitable for Earth system models, Atmospheric Chemistry and Physics, 18, 14 175–14 196, https://doi.org/10.5194/acp-18-14175-2018, 2018.

Schummer, C., Groff, C., Al Chami, J., Jaber, F., and Millet, M.: Analysis of phenols and nitrophenols in rainwater collected simultaneously on an urban and rural site in east of France, Science of The Total Environment, 407, 5637 – 5643, https://doi.org/10.1016/j.scitotenv.2009.06.051, 2009.

Schwartz, S. E.: Mass-Transport Considerations Pertinent to Aqueous Phase Reactions of Gases in Liquid-Water Clouds, in: Chemistry of Multiphase Atmospheric Systems, edited by Jaeschke, W., pp. 415–471, Springer Berlin Heidelberg, Berlin, Heidelberg, 1986.

Seinfeld, J. H. and Pandis, S. N.: Atmospheric chemistry and physics: from air pollution to climate change, John Wiley & Sons, 2016.

Sellers, P. J.: Canopy reflectance, photosynthesis and transpiration, International Journal of Remote Sensing, 6, 1335–1372, https://doi.org/10.1080/01431168508948283, 1985.

Sharkey, T. D. and Singsaas, E. L.: Why plants emit isoprene, Nature, 374, 769–769, https://doi.org/10.1038/374769a0, 1995.

Shi, Y. and Matsunaga, T.: Temporal comparison of global inventories of CO2 emissions from biomass burning during 2002–2011 derived from remotely sensed data, Environmental Science and Pollution Research, 24, 16 905–16 916, https://doi.org/10.1007/s11356-017-9141-z, 2017.

Sillman, S.: The relation between ozone, NOx and hydrocarbons in urban and polluted rural environments, Atmospheric Environment, 33, 1821 – 1845, https://doi.org/10.1016/S1352-2310(98)00345-8, 1999.

Staehelin, J. and Hoigné, J.: Decomposition of ozone in water in the presence of organic solutes acting as promoters and inhibitors of radical chain reactions, Environmental Science & Technology, 19, 1206–1213, https://doi.org/10.1021/es00142a012, 1985.

Staehelin, J., Buehler, R. E., and Hoigné, J.: Ozone decomposition in water studied by pulse radiolysis. 2. Hydroxyl and hydrogen tetroxide (HO4) as chain intermediates, The Journal of Physical Chemistry, 88, 5999–6004, https://doi.org/10.1021/j150668a051, 1984.

Taraborrelli, D., Lawrence, M. G., Butler, T. M., Sander, R., and Lelieveld, J.: Mainz Isoprene Mechanism 2 (MIM2): an isoprene oxidation mechanism for regional and global atmospheric modelling, Atmospheric Chemistry and Physics, 9, 2751–2777, https://doi.org/10.5194/ACP-9-2751-2009, 2009.

Taraborrelli, D., Lawrence, M. G., Crowley, J. N., Dillon, T. J., Gromov, S., Groß, C. B. M., Vereecken, L., and Lelieveld, J.: Hydroxyl radical buffered by isoprene oxidation over tropical forests, Nature Geoscience, 5, 190–193, https://doi.org/10.1038/ngeo1405, 2012.

Taylor, W. D., Allston, T. D., Moscato, M. J., Fazekas, G. B., Kozlowski, R., and Takacs, G. A.: Atmospheric photodissociation lifetimes for nitromethane, methyl nitrite, and methyl nitrate, International Journal of Chemical Kinetics, 12, 231–240, https://doi.org/10.1002/kin.550120404, 1980.

Tilgner, A., Bräuer, P., Wolke, R., and Herrmann, H.: Modelling multiphase chemistry in deliquescent aerosols and clouds using CAPRAM3.0i, Journal of Atmospheric Chemistry, 70, 221–256, https://doi.org/10.1007/s10874-013-9267-4, 2013.

Tost, H.: Global Modelling of Cloud, Convection and Precipitation Influences on Trace Gases and Aerosols, Ph.D. thesis, Rheinische Friedrich-Wilhelms-Universität Bonn, 2006.

Tost, H., Jöckel, P., Kerkweg, A., Sander, R., and Lelieveld, J.: Technical note: A new comprehensive SCAVenging submodel for global atmospheric chemistry modelling, Atmospheric Chemistry and Physics, 6, 565–574, https://doi.org/10.5194/acp-6-565-2006, 2006a.

Tost, H., Jöckel, P., and Lelieveld, J.: Influence of different convection parameterisations in a GCM, Atmospheric Chemistry and Physics, 6, 5475–5493, https://doi.org/10.5194/acp-6-5475-2006, 2006b.

Tost, H., Jöckel, P., Kerkweg, A., Pozzer, A., Sander, R., and Lelieveld, J.: Global cloud and precipitation chemistry and wet deposition: tropospheric model simulations with ECHAM5/MESSy1, Atmospheric Chemistry and Physics, 7, 2733–2757, https://doi.org/10.5194/acp-7-2733-2007, 2007a.

Tost, H., Jöckel, P., and Lelieveld, J.: Lightning and convection parameterisations - uncertainties in global modelling, Atmospheric Chemistry and Physics, 7, 4553–4568, https://doi.org/10.5194/acp-7-4553-2007, 2007b.

Tully, F. P., Perry, R. A., Thorne, L. R., and Allendorf, M. D.: Free-radical oxidation of isocyanic acid, Symposium (International) on Combustion, 22, 1101 – 1106, https://doi.org/10.1016/S0082-0784(89)80120-1, 1989.

Vereecken, L. and Peeters, J.: A theoretical study of the OH-initiated gas-phase oxidation mechanism of β-pinene ($C_{10}H_{16}$): first generation products, Phys. Chem. Chem. Phys., 14, 3802–3815, https://doi.org/10.1039/C2CP23711C, 2012.

Vereecken, L., Müller, J.-F., and Peeters, J.: Low-volatility poly-oxygenates in the OH-initiated atmospheric oxidation of α-pinene: impact of non-traditional peroxyl radical chemistry, Phys. Chem. Chem. Phys., 9, 5241–5248, https://doi.org/10.1039/B708023A, 2007.

Vereecken, L., Chakravarty, H. K., Bohn, B., and Lelieveld, J.: Theoretical Study on the Formation of H- and O-Atoms, HONO, OH, NO, and NO2 from the Lowest Lying Singlet and Triplet States in Ortho-Nitrophenol Photolysis, International Journal of Chemical Kinetics, 48, 785–795, https://doi.org/10.1002/kin.21033, 2016.

Wang, R., Balkanski, Y., Boucher, O., Bopp, L., Chappell, A., Ciais, P., Hauglustaine, D., Peñuelas, J., and Tao, S.: Sources, transport and deposition of iron in the global atmosphere, Atmospheric Chemistry and Physics, 15, 6247–6270, https://doi.org/10.5194/acp-15-6247-2015, 2015.

Wang, Z., Nicholls, S. J., Rodriguez, E. R., Kummu, O., Hörkkö, S., Barnard, J., Reynolds, W. F., Topol, E. J., DiDonato, J. A., and Hazen, S. L.: Protein carbamylation links inflammation, smoking, uremia and atherogenesis, Nature Medicine, 13, 1176–1184, https://doi.org/10.1038/nm1637, 2007.

Wennberg, P. O., Bates, K. H., Crounse, J. D., Dodson, L. G., McVay, R. C., Mertens, L. A., Nguyen, T. B., Praske, E., Schwantes, R. H., Smarte, M. D., St Clair, J. M., Teng, A. P., Zhang, X., and Seinfeld, J. H.: Gas-Phase Reactions of Isoprene and Its Major Oxidation Products, Chemical Reviews, 118, 3337–3390, https://doi.org/10.1021/acs.chemrev.7b00439, PMID: 29522327, 2018.

Wesely, M.: Parameterization of surface resistances to gaseous dry deposition in regional-scale numerical models, Atmospheric Environment (1967), 23, 1293 – 1304, https://doi.org/10.1016/0004-6981(89)90153-4, 1989.

Whitehouse, L. E., Tomlin, A. S., and Pilling, M. J.: Systematic reduction of complex tropospheric chemical mechanisms, Part I: sensitivity and time-scale analyses, Atmospheric Chemistry and Physics, 4, 2025–2056, https://doi.org/10.5194/acp-4-2025-2004, 2004a.

Whitehouse, L. E., Tomlin, A. S., and Pilling, M. J.: Systematic reduction of complex tropospheric chemical mechanisms, Part II: Lumping using a time-scale based approach, Atmospheric Chemistry and Physics, 4, 2057–2081, https://doi.org/10.5194/acp-4-2057-2004, 2004b.

Wooldridge, M. S., Hanson, R. K., and Bowman, C. T.: A shock tube study of CO + OH → CO2 + H and HNCO + OH → products via simultaneous laser absorption measurements of OH and CO2, International Journal of Chemical Kinetics, 28, 361–372, https://doi.org/10.1002/(SICI)1097-4601(1996)28:5<361::AID-KIN5>3.0.CO;2-T, 1996.

Young, P. J., Emmons, L. K., Roberts, J. M., Lamarque, J.-F., Wiedinmyer, C., Veres, P., and VandenBoer, T. C.: Isocyanic acid in a global chemistry transport model: Tropospheric distribution, budget, and identification of regions with potential health impacts, Journal of Geophysical Research: Atmospheres, 117, https://doi.org/10.1029/2011JD017393, 2012.

Young, P. J., Archibald, A. T., Bowman, K. W., Lamarque, J.-F., Naik, V., Stevenson, D. S., Tilmes, S., Voulgarakis, A., Wild, O., Bergmann, D., Cameron-Smith, P., Cionni, I., Collins, W. J., Dalsøren, S. B., Doherty, R. M., Eyring, V., Faluvegi, G., Horowitz, L. W., Josse, B., Lee, Y. H., MacKenzie, I. A., Nagashima, T., Plummer, D. A., Righi, M., Rumbold, S. T., Skeie, R. B., Shindell, D. T., Strode, S. A., Sudo, K., Szopa, S., and Zeng, G.: Pre-industrial to end 21st century projections of tropospheric ozone from the Atmospheric Chemistry and Climate Model Intercomparison Project (ACCMIP), Atmospheric Chemistry and Physics, 13, 2063–2090, https://doi.org/10.5194/acp-13-2063-2013, 2013.

Young, P. J., Naik, V., Fiore, A. M., Gaudel, A., Guo, J., Lin, M., Neu, J., Parrish, D., Rieder, H., Schnell, J., et al.: Tropospheric Ozone Assessment Report: Assessment of global-scale model performance for global and regional ozone distributions, variability, and trends, Elem Sci Anth, 6, https://doi.org/10.1525/elementa.265, 2018.

Yu, S.: Role of organic acids (formic, acetic, pyruvic and oxalic) in the formation of cloud condensation nuclei (CCN): a review, Atmospheric Research, 53, 185 – 217, https://doi.org/10.1016/S0169-8095(00)00037-5, 2000.

Personal acknowledgements

First of all, I would like to particularly thank Domenico Taraborrelli for his outstanding supervision in these three years. His support in pursuing my own ideas, sharing his knowledge of atmospheric chemistry, and his overview of many global modelling aspects shaped this thesis considerably.

I would like to especially thank Prof. Andreas Wahner for offering me the opportunity to pursue this work, all his support, and many fruitful discussions. I am also grateful to Prof. Susanne Crewell for her particular interest in my work, for accepting to act as referee, and for the evaluation of the results of this thesis.

I would like to thank Prof. Astrid Kiendler-Scharr for offering me the opportunity to pursue this work, her support, and for establishing the connection to Vaishali Naik. Here, I would like to kindly thank Vaishali Naik for acting as my external mentor and offering me a research stay at the NOAA Geophysical Fluid Dynamics Laboratory.

I would like to thank Anna Novelli and Luc Vereecken for including me in their research and for providing me a non-global modelling perspective on scientific problems.

I am very thankful to the co-authors of each study. In particular, I would like to thank Rolf Sander for all his support related to MECCA and Bruno Franco for providing the IASI retrievals and his assistance in the model comparisons.

A special thanks goes to Sabine Schröder for her support in handling the high performance computing facilities at the beginning of this work. Here, I would also like to thank Alina Zimmermann for all her administrative help.

A special thank goes to Prof. Volker Grewe for motivating me to continue my research career, making me aware of this opportunity, and for a fruitful side project.

Many thanks to my colleagues who supported this work, for many interesting discussions, and for proofreading this thesis. Very special thanks go to my friends for their motivation, support, and interest in this work.

Many thanks to my siblings Janis, Vivian, and Marie for always believing in me and my skills. I am deeply grateful to my parents Ingetraud and Manfred for their love, their encouragement, their endless support, and for inspiring me to pursue a career in Aerospace Engineering, which ultimately started this awesome journey.

And last, but surely not least, I am deeply grateful to Anne, who supported and motivated me wherever possible, for her understanding, and her rock-solid trust in me.

Erklärung

Hiermit versichere ich an Eides statt, dass ich die vorliegende Dissertation selbstständig und ohne die Benutzung anderer als der angegebenen Hilfsmittel und Literatur angefertigt habe. Alle Stellen, die wörtlich oder sinngemäß aus veröffentlichten und nicht veröffentlichten Werken dem Wortlaut oder dem Sinn nach entnommen wurden, sind als solche kenntlich gemacht. Ich versichere an Eides statt, dass diese Dissertation noch keiner anderen Fakultät oder Universität zur Prüfung vorgelegen hat; dass sie - abgesehen von unten angegebenen Teilpublikationen und eingebundenen Artikeln und Manuskripten - noch nicht veröffentlicht worden ist sowie, dass ich eine Veröffentlichung der Dissertation vor Abschluss der Promotion nicht ohne Genehmigung des Promotionsausschusses vornehmen werde. Die Bestimmungen dieser Ordnung sind mir bekannt. Darüber hinaus erkläre ich hiermit, dass ich die Ordnung zur Sicherung guter wissenschaftlicher Praxis und zum Umgang mit wissenschaftlichem Fehlverhalten der Universität zu Köln gelesen und sie bei der Durchführung der Dissertation zugrundeliegenden Arbeiten und der schriftlich verfassten Dissertation beachtet habe und verpflichte mich hiermit, die dort genannten Vorgaben bei allen wissenschaftlichen Tätigkeiten zu beachten und umzusetzen. Ich versichere, dass die eingereichte elektronische Fassung der eingereichten Druckfassung vollständig entspricht.

Teilpublikationen:

Novelli, A., Vereecken, L., Bohn, B., Dorn, H.-P., Gkatzelis, G. I., Hofzumahaus, A., Holland, F., Reimer, D., Rohrer, F., Rosanka, S., Taraborrelli, D., Tillmann, R., Wegener, R., Yu, Z., Kiendler-Scharr, A., Wahner, A., and Fuchs, H.: Importance of isomerization reactions for OH radical regeneration from the photo-oxidation of isoprene investigated in the atmospheric simulation chamber SAPHIR, Atmospheric Chemistry and Physics, 20, 3333–3355, https://doi.org/10.5194/acp-20-3333-2020, 2020.

Rosanka, S., Vu, G. H. T., Nguyen, H. M. T., Pham, T. V., Javed, U., Taraborrelli, D., and Vereecken, L.: Atmospheric chemical loss processes of isocyanic acid (HNCO): a combined theoretical kinetic and global modelling study, Atmospheric Chemistry and Physics, 20, 6671–6686, https://doi.org/10.5194/acp-20-6671-2020, 2020.

Rosanka, S., Sander, R., Wahner, A., and Taraborrelli, D.: Oxidation of low-molecular-weight organic compounds in cloud droplets: development of the Jülich Aqueous-phase Mechanism of Organic Chemistry (JAMOC) in CAABA/MECCA (version 4.5.0), Geoscientific Model Development, 14, 4103–4115, https://doi.org/10.5194/gmd-14-4103-2021, 2021a.

Rosanka, S., Sander, R., Franco, B., Wespes, C., Wahner, A., and Taraborrelli, D.: Oxidation of low-molecular-weight organic compounds in cloud droplets: global impact on tropospheric oxidants, Atmospheric Chemistry and Physics, 21, 9909–9930, https://doi.org/10.5194/acp-21-9909-2021, 2021b.

Rosanka, S., Franco, B., Clarisse, L., Coheur, P.-F., Pozzer, A., Wahner, A., and Taraborrelli, D.: The impact of organic pollutants from Indonesian peatland fires on the tropospheric and lower stratospheric composition, Atmospheric Chemistry and Physics, 21, 11 257–11 288, https://doi.org/10.5194/acp-21-11257-2021, 2021c.

Weitere Publikationen:

Franco, B., Blumenstock, T., Cho, C., Clarisse, L., Clerbaux, C., Coheur, P.-F., De Mazière, M., De Smedt, I., Dorn, H.-P., Emmerichs, T., Fuchs, H., Gkatzelis, G., Griffith, D. W. T., Gromov, S., Hannigan, J. W., Hase, F., Hohaus, T., Jones, N., Kerkweg, A., Kiendler-Scharr, A., Lutsch, E., Mahieu, E., Novelli, A., Ortega, I., Paton-Walsh, C., Pommier, M., Pozzer, A., Reimer, D., Rosanka, S., Sander, R., Schneider, M., Strong, K., Tillmann, R., Van Roozendael, M., Vereecken, L., Vigouroux, C., Wahner, A., and Taraborrelli, D.: Ubiquitous atmospheric production of organic acids mediated by cloud droplets, Nature, 593, 233–237, https://doi.org/10.1038/s41586-021-03462-x, 2021.

Frömming, C., Grewe, V., Brinkop, S., Jöckel, P., Haslerud, A. S., Rosanka, S., van Manen, J., and Matthes, S.: Influence of weather situation on non-CO_2 aviation climate effects: the REACT4C climate change functions, Atmospheric Chemistry and Physics, 21, 9151–9172, https://doi.org/10.5194/acp-21-9151-2021, 2021.

Rosanka, S., Frömming, C., and Grewe, V.: The impact of weather patterns and related transport processes on aviation's contribution to ozone and methane concentrations from NO_x emissions, Atmospheric Chemistry and Physics, 20, 12 347–12 361, https://doi.org/10.5194/acp-20-12347-2020, 2020.

Datum, Simon Henrik Rosanka